

Modern Methods for Lipid Analysis by Liquid Chromatography/Mass Spectrometry and Related Techniques

Editor

William Craig Byrdwell

Department of Chemistry and Biochemistry

Florida Atlantic University

Boca Raton, FL 33431



Urbana, Illinois

AOCS Mission Statement

To be a global forum to promote the exchange of ideas, information, and experience, to enhance personal excellence, and to provide high standards of quality among those with a professional interest in the science and technology of fats, oils, surfactants, and related materials.

AOCS Books and Special Publications Committee

M. Mossoba, Chairperson, U.S. Food and Drug Administration, College Park, Maryland
R. Adlof, USDA, ARS, NCAUR, Peoria, Illinois
M.L. Besemer, Besemer Consulting, Rancho Santa, Margarita, CA
P. Dutta, Swedish University of Agricultural Sciences, Uppsala, Sweden
T. Foglia, ARS, USDA, ERRC, Wyndmoor, Pennsylvania
V. Huang, Yuanpei University of Science and Technology, Taiwan
L. Johnson, Iowa State University, Ames, Iowa
H. Knapp, DBC Research Center, Billings, Montana
D. Kodali, Global Agritech Inc., Minneapolis, Minnesota
G. List, USDA, NCAUR, Peoria, Illinois
T. McKeon, USDA, ARS, WRRRC, Albany, California
R. Moreau, USDA, ARS, ERRC, Wyndoor, Pennsylvania
A. Sinclair, RMIT University, Melbourne, Victoria, Australia
P. White, Iowa State University, Ames, Iowa
R. Wilson, USDA, REE, ARS, NPS, CPPVS, Beltsville, Maryland

Copyright (c) 2005 by AOCS Press. All rights reserved. No part of this book may be reproduced or transmitted in any form or by any means without written permission of the publisher.

The paper used in this book is acid-free and falls within the guidelines established to ensure permanence and durability.

Library of Congress Cataloging-in-Publication Data

Modern methods for lipid analysis by liquid chromatography/mass spectrometry and related techniques / editor, William Craig Byrdwell.

p. cm.

Includes bibliographical references and index.

ISBN 1-893997-75-8 (acid-free paper)

1. Lipids--Analysis. 2. Chromatographic analysis. 3. Mass spectrometry. 4. Atmospheric ionization. I. Byrdwell, William Craig.

QP751.M595 2005

547'.77046--dc22

2004029544

Printed in the United States of America.

11 10 09 08 07 6 5 4 3 2

Preface

There has been an increasing level of interest in liquid chromatography/mass spectrometry (LC/MS) for lipid analysis as the number of commercially available instruments having atmospheric pressure ionization (API) interfaces has increased. As prices on LC/MS instruments having API sources have come down, the number of instruments installed in labs worldwide has burgeoned. Articles in the literature have now described extensive use of electrospray ionization (ESI) and atmospheric pressure chemical ionization (APCI) for analysis of most classes of lipids. The benefits of these API sources for lipid analysis are becoming widely recognized. It is this growing interest in modern API techniques for lipid analysis that has precipitated publication of this volume.

Journal articles have described many aspects of qualitative and quantitative analysis of lipids using LC/(APCI and ESI)-MS. The identities of characteristic near-molecular ions and fragment ion patterns have been reported for most lipid classes. Numerous articles are now in print that were the first reports of various aspects of lipid analysis by LC/(APCI and ESI)-MS. The number of groundbreaking new articles has now diminished, as more articles are appearing that describe applications of techniques already demonstrated. Thus, the field of lipid analysis by LC/(APCI and ESI)-MS has reached somewhat of a plateau.

Since LC with either APCI- or ESI-MS is no longer in its infancy, this is an optimal time to pause and summarize what is known to date. Such a summary will serve as a valuable reference and resource for those interested in moving into the field of lipid analysis using modern instrumentation. The goal in writing this book was to gather together writings from many of the leaders in the field who had published the first and/or numerous articles in various aspects of lipids analysis by LC/API-MS. Those who have followed the literature to date will recognize the authors writing chapters herein. They have published extensively in the field and are imminently qualified to summarize their own work and related work in their fields of expertise.

This type of volume is not meant to be read sequentially from cover to cover, like a novel. It is hoped that this book will serve as a concise reference volume that contains a record of almost all aspects known to date of LC/API-MS for lipid analysis. It is intended to be referenced a chapter at a time, depending on the lipid class and MS technique being investigated. For this reason, the authors have been encouraged to provide comprehensive reviews of their areas of emphasis, including discussion of the theory and principles of each technique. With each author being so thorough, there was some amount of overlap in the descriptions of the techniques discussed in the various chapters. This overlap has been retained to allow each chapter to stand on its own without the need for extensive references to other chapters or sources. When this volume is read in its entirety, one finds that each author emphasized the aspects of theory and principles that most applied to their own molecules of interest,

and so each chapter provides one facet of the technique used. To understand the techniques more completely, it is beneficial to see all of their facets, or aspects, as reflected in the variety of applications demonstrated herein.

It is hoped that the reader will find it valuable to read, in their own words, summaries of work from those authors who are already recognized for their leadership in the field of LC/MS for lipid analysis. This volume allows authors to present more detail than has been allowed in some journal articles. Furthermore, not only does this volume contain a wealth of previously published data; it also contains some new, unpublished data that will soon be published elsewhere. So, although this book describes the previous work that has established the foundation of the field, it also demonstrates new data that is defining a new level of “state-of-the-art.” Described herein are the methods that will be applied to lipids into the next decade and hopefully beyond. One method especially, atmospheric pressure photoionization (APPI), is still in its infancy and will undoubtedly experience dramatic growth for lipid analysis in the coming years.

William Craig Byrdwell

January 12, 2005

Acknowledgments

The Editor gratefully acknowledges my collaborator William E. Neff for his help, friendship, and cooperation over the last several years. The ongoing cooperation and collaboration with Kathleen Warner at the National Center for Agricultural Utilization Research, in Peoria, IL, is very gratefully acknowledged. The guidance and assistance of Dr. M. Cecilia Yappert over the years has also been greatly appreciated, as has the advice and collaboration from Dr. Doug Borchman and Dr. Edward A. Emken. A special thanks goes to my children, Matthew and Heather, for their patience and understanding. A very special thanks goes to my mother, I. Jean Beck, for her unwaivering support and encouragement.

Contents

| | | |
|-----------|---|-----|
| | Preface | iii |
| | Acknowledgments | v |
| Chapter 1 | Atmospheric Pressure Ionization Techniques in Modern Lipid Analysis <i>William Craig Byrdwell</i> | 1 |
| Chapter 2 | Analysis of Phospholipids by Liquid Chromatography Coupled with On-Line Electrospray Ionization Mass Spectrometry and Tandem Mass Spectrometry <i>Åsmund Larsen and Erlend Hvattum</i> | 19 |
| Chapter 3 | Electrospray Ionization with Low-Energy Collisionally Activated Dissociation Tandem Mass Spectrometry of Complex Lipids: Structural Characterization and Mechanisms of Fragmentation <i>Fong-Fu Hsu and John Turk</i> | 61 |
| Chapter 4 | Liquid Chromatography/Electrospray Ionization Mass Spectrometry for Analysis of Oxidized Lipids <i>Arnis Kuksis</i> | 179 |
| Chapter 5 | Analysis of Fatty Acids by APCI-MS <i>Tomáš Režanka and Jaroslav Votruba</i> | 242 |
| Chapter 6 | Regiospecific Analysis of Triacylglycerols using High Performance Liquid Chromatography/Atmospheric Pressure Chemical Ionization Mass Spectrometry <i>Hazel R. Mottram</i> | 276 |
| Chapter 7 | Qualitative and Quantitative Analysis of Triacylglycerols by Atmospheric Pressure Ionization (APCI and ESI) Mass Spectrometry Techniques <i>William Craig Byrdwell</i> | 298 |

| | | |
|------------|---|-----|
| Chapter 8 | Analysis of Carotenoids Using Atmospheric Pressure Chemical Ionization Mass Spectrometry <i>Natasa Pajkovic and Richard B. van Breemen</i> | 413 |
| Chapter 9 | Analysis of Molecular Species of Plant Glycolipids by HPLC/APCI-MS <i>Ryo Yamauchi</i> | 431 |
| Chapter 10 | Liquid Chromatography/Mass Spectrometry Analysis of Biosurfactant Glycolipids Secreted by Microorganisms <i>Alberto Nuñez, Robert A. Moreau, and Thomas A. Foglia</i> | 447 |
| Chapter 11 | Analysis of Steroids by Liquid Chromatography— Atmospheric Pressure Photoionization Mass Spectrometry <i>Risto Kostianen and Tiina Kauppila</i> | 472 |
| Chapter 12 | Toward Total Cellular Lipidome Analysis by ESI Mass Spectrometry from a Crude Lipid Extract <i>Xianlin Han and Richard W. Gross</i> | 488 |
| Chapter 13 | Dual Parallel Liquid Chromatography/Mass Spectrometry for Lipid Analysis <i>William Craig Byrdwell</i> | 510 |
| | Index | 577 |

Chapter 1

Atmospheric Pressure Ionization Techniques in Modern Lipid Analysis

William Craig Byrdwell

Department of Chemistry and Biochemistry, Florida Atlantic University, 777 Glades Road,
P.O. Box 3091, Boca Raton, FL 33431

Introduction

Some classes of lipids are large molecules that are not sufficiently volatile to allow gas-phase analysis by means such as gas chromatography (GC). Often, non-volatile lipids can be saponified to remove the fatty acid chains and these can be derivatized to yield volatile molecules, such as fatty acid methyl esters (FAME), pyrrolidides, picolinyl esters, and others. These derivatives may be readily analyzed by gas chromatography in combination with a variety of detectors, including mass spectrometry. FAME analysis by GC with flame ionization detection (FID) is a common analytical method that provides valuable information regarding the net fatty acid chain composition of a sample. However, GC of FA derivatives can provide only an approximation of the composition of the original intact molecules. If there is non-random distribution of the FA chains in the parent molecules, FAME analysis can provide no indication of the distribution of those chains on the original molecules. It is preferable to analyze the large lipid molecules intact.

Liquid chromatography has become the method of choice for separation of many classes of large lipid molecules. But the choice of liquid chromatography for separation inherently implies limitations in the choices available for detection. The flame ionization detector for liquid chromatography, refractive index and ultraviolet/visible (UV/vis) detectors, and more recently the evaporative light-scattering detector (ELSD) have all been employed for detection of lipids. But these two-dimensional detectors require complete chromatographic resolution to allow all molecular species to be identified. Unfortunately, even simple natural samples of lipids often contain species with the same equivalent carbon number (ECN) that overlap partially or entirely. The ECN is a measure of the overall non-polar characteristic of a fatty acid chain or molecule, given as the number of carbon atoms minus two times the number of double bonds (sites of unsaturation), $ECN = N_{\text{carb}} - (2 \times U)$. For example, a 16:0 (palmitic) acyl chain has the same ECN ($16 - 0 = 16$) as an 18:1 acyl chain ($18 - 2 = 16$). On reversed-phase chromatographic systems, molecules containing FA chains with the same ECN elute with similar retention times. Therefore, a simple two-dimensional detector often cannot differentiate

between overlapped species. Due to the highly complex nature of lipid mixtures, mass spectrometry has long been used for identification of molecular species within various lipid classes. MS is effective because lipids that are chromatographically unresolved due to acyl chains with the same ECN can usually be discriminated by their masses or fragments.

The information-rich nature of mass spectrometry makes it the most desirable detector for many applications. But, although gas chromatography is conveniently coupled to conventional ionization sources such as electron impact ionization (EI) and chemical ionization (CI) sources, the condensed mobile phase used for liquid separations is not readily compatible with high-vacuum ionization sources. Over the years, numerous approaches have been used to introduce effluent from liquid chromatographic systems into mass spectrometers. One option that has always been available is collection of fractions followed by evaporation of solvent and mass spectrometric analysis of the resultant residue by probe or desorption techniques. Such approaches are time- and labor-intensive and do not accomplish the goal of a simple, unified LC-MS analysis. Arpino (1) likened the union of the condensed phase of liquid chromatography with the high vacuum required by mass spectrometry to the difficult marriage between fish and fowl. How could the fish, confined to his liquid world, ever hope to couple with the bird, living in her rarified environment?

The Development of LC-MS Techniques

In the decade of the 1970s, several approaches were demonstrated that accomplished the union of LC with MS. Thorough discussion of all historical developments in early LC interfacing techniques is beyond the scope of this chapter, but several approaches that gained wide use and acceptance will be mentioned, because their development paralleled the development of atmospheric pressure ionization (API) techniques. Some techniques have flourished and then faded, while others are only now reaching their zeniths.

In 1968 and 1970, Dole *et al.* (2–4), at Northwestern University, demonstrated that multiply charged gas-phase macroions of polystyrene in volatile solvent could be produced by electrospray of a solution at atmospheric pressure into a mass spectrometer. Modifications of the nozzle-skimmer approach used by them [but developed previously by others (5)] are still in use today, as mentioned later. Surprisingly, the technique got off to a rather slow start. Other than those by Dole *et al.*, it seems that more review articles appeared describing the use of electrospray ionization (ESI) than research articles employing it, until the mid 1980s. The low flow rates allowed by conventional electrospray ionization, in the 5–10 $\mu\text{L}/\text{min}$ range, were a limiting factor. Yamashita and Fenn (6,7), working at Yale University, employed electrospray in the early 1980s, and in 1985 (8) were the first to describe its use as an interface with microbore liquid chromatography. This work ultimately earned Dr. Fenn a Nobel Prize in Chemistry in 2002.

Meanwhile, Iribarne and Thomson at the University of Toronto (9,10) demonstrated a technique that they referred to as ion evaporation. In their technique, a solution was pneumatically sprayed through a fine needle, and a charge was applied to the spray by an electrode placed near the sprayer. The spray was oriented orthogonally to the mass spectrometer inlet. In 1987, Bruins *et al.* (11) incorporated a concentric nitrogen sheath gas to nebulize the effluent stream that emerged from a normal electrospray needle at high voltage. They proposed the name ionspray for their technique, since it was a hybrid between ion evaporation and electrospray methods. It is also referred to as pneumatically assisted electrospray. The modification allowed higher flow rates, up to 200 $\mu\text{L}/\text{min}$, to be employed. For a period of time, the terms electrospray and ionspray, or pneumatically assisted electrospray, remained distinct. However, the popularity of pneumatically assisted electrospray has led it to become the default method, and most users now simply refer to it as electrospray. Numerous variations and modifications in the basic electrospray principles have been reported. Many of these are discussed in the thorough treatment of LC-MS by Niessen (12). The key elements that generally define modern ESI sources are (i) charged droplets are formed from a liquid sample by applying a high voltage to a needle from which the liquid is sprayed, (ii) solvent in the charged droplets evaporates to the point where the coulombic repulsion of ions in the droplet overcomes the surface tension of the droplets and causes them to break apart into smaller droplets (at the Rayleigh stability limit), and (iii) droplet size continues to diminish until gas-phase ions are ultimately released. As mentioned previously, a sheath gas is usually used at higher flow rates, to aid in solvent evaporation. In most ESI sources, no heat is necessary to aid in desolvation. Design details of a typical ESI source used for lipid analysis will be provided in Chapter 7 herein.

Discussion of electrospray ionization (ESI) is important here, because it is one of the two most popular atmospheric pressure ionization (API) sources. Most instrument manufacturers now make available both ESI and atmospheric pressure chemical ionization (APCI) sources that fit the same atmospheric pressure-to-high vacuum interface. Our group routinely employs both ionization methods for lipid analysis, as will be demonstrated in later chapters.

While ESI-MS was still in its infancy, Horning *et al.* (13), at the Institute for Lipid Research at the Baylor College of Medicine, developed another type of source capable of ionizing molecules at atmospheric pressure. In 1973 and early 1974, Horning *et al.* (13,14) reported an atmospheric pressure ionization source that used a syringe sample inlet with a carrier gas to transport the sample past a nickel-63 beta radiation source for ionization. The ions thus produced were sampled into the high-vacuum mass analyzer through a 25 μm pinhole. Shortly thereafter, Horning *et al.* (15) showed the first example of the new API source as an online detector for LC. They increased the size of the reaction chamber, which was reported to accommodate flow rates up to 2.0 mL/min. In this report, they also presented data in which the beta emitter was replaced with a corona discharge elec-

trode. The corona discharge design was more fully described in 1975, and constitutes the basis for modern APCI sources (16). Atmospheric pressure ionization eventually became known as atmospheric pressure chemical ionization, to differentiate it from electrospray, which also occurred at atmospheric pressure, and to emphasize the fact that it involves a solvent-mediated process, similar to conventional CI. The key elements that define the modern APCI source are (i) a sheath gas is used to nebulize the liquid effluent stream; (ii) the nebulized spray passes down the center of a heated vaporizer, which aids in evaporation of the solvent; and (iii) the desolvated molecular mist passes by a corona discharge needle at high voltage, where ions are produced. The atmospheric gases near the tip of the corona needle, including water vapor that is ionized to hydronium ions, participate in the ionization process. Solvent vapor may also participate in the formation of ions or adducts. Specific design details of a typical APCI-MS source are shown in Chapter 7.

Around the same time that APCI and ESI were being developed, other techniques were also reported. In the late 1960s, Tal'roze *et al.* (17) demonstrated the direct introduction of a liquid mixture into a mass spectrometer through a metal leak inlet system. Then, in 1972, they showed the use of a thin glass capillary for direct liquid introduction (DLI) (18). As the name suggests, DLI is the direct introduction of a liquid stream through a capillary into the high vacuum of a mass spectrometer's ionization source. As one would expect, only a very low flow rate could be accommodated by such a simple arrangement. Even at low flow rates, the capillary DLI interface had a number of drawbacks. Primary among these was the tendency of the solvent to evaporate before reaching the end of the capillary, leading to buildup of analyte on the inside of the capillary, often plugging the capillary. To avoid this, a restrictor was placed at the end of the capillary to prevent premature evaporation and to produce a liquid jet. A number of restrictors were described by various authors. Unfortunately, plugging of the restrictors was also a consistent problem. The development of different designs of DLI interfaces, as well as applications of the technique, has been well reviewed (19,20). One advantage of DLI was that it allowed the use of conventional ionization sources, and yielded CI spectra by interaction with solvent molecules from the effluent stream (solvent-mediated CI). But the flow rates that could be accommodated were limited to a maximum of 50–100 $\mu\text{L}/\text{min}$, much lower than the typical analytical LC system. Therefore, the flow from conventional systems had to be split to deliver only a small portion of the stream to the DLI interface. Since only a portion of the analyte was being directed to the ionization source, there was a substantial loss of sensitivity. The limitation in the allowed flow rate and the plugging of the pinhole restrictors led DLI to lose favor compared to the other emerging LC-MS interfaces.

A moving wire interface was developed by Scott *et al.* (21). In this approach, the LC effluent was deposited on a moving wire, which passed through close-tolerance ruby jewel apertures into the high-vacuum source of the mass spectrometer, where the wire was heated to desorb the sample into the source. The small amount of sample deposited onto the wire and other shortcomings led McFadden *et al.* (22)

to develop a moving belt design with a wider transport medium. These techniques were reviewed by Arpino in 1989 (23). The main advantage of the moving belt interface was that one could couple it to a conventional source to obtain library-searchable EI spectra, or utilize CI. Despite this advantage, the interface has lost favor and has given way to APCI and ESI interfaces.

The thermospray (TSP) interface was first developed by Vestal and coworkers (24). It initially used a CO₂ laser to perform rapid vaporization of the effluent stream, but this was soon replaced by oxy-hydrogen flames (25), and later by electric heating elements. A key difference in the design of the thermospray source was that the nebulized, ionized effluent passed by an electrode that repelled the ions orthogonally into a sampling cone and into the high-vacuum region of the mass spectrometer. An ionizing filament or discharge electrode could be used to ionize the nebulized stream, or ionization could be accomplished simply by inclusion of a volatile buffer in the effluent. Vestal commercialized the thermospray interface under the Vestec name, and versions of the interface could be fitted to various brands of mass spectrometers. By the early 1980s, the thermospray ionization source was recognized for its versatility and ease of use. One great advantage of thermospray ionization was that it allowed high flow rates, up to 2 mL/min, to be used. Compared to other commercially available interfaces, such as DLI and electrospray, this represented a substantial benefit that allowed the thermospray interface to be applied to a much wider range of analytes. Thermospray became the LC-MS interface of choice through the late 1980s and early 1990s. TSP has been thoroughly reviewed; two of these reviews are referenced here (26,27). The popularity of this ionization source has now waned with the explosive growth in popularity of ESI and APCI methods. Drawbacks to the thermospray method include the tendency of the vaporizers to clog, the need to optimize solvent and volatile buffer compositions for each class of compounds, the need to optimize temperature and other operating parameters for each class, and the moderate sensitivity. This type of ionization is among those thoroughly discussed by Niessen (12).

One other interface that has been a competitor to the popular atmospheric pressure ionization sources will be mentioned. This is the monodisperse aerosol generation interface for chromatography (MAGIC), which combines liquid chromatography with mass spectrometry. Developed by Willoughby and Browner (28), from the Georgia Institute of Technology, this interface utilized a small-diameter glass orifice to form a fine liquid jet that was dispersed using a gas stream introduced at a right angle to the jet. This produced a fine aerosol spray with uniform droplet size that was coupled through a two-stage momentum separator to the normal EI source of the mass spectrometer. This source allowed flow rates in the 0.1 to 0.5 mL/min range, and produced spectra that were identical to conventional EI spectra, which allowed comparison of spectra to standard EI spectral libraries. Improvements in the interface were made over time, and the numerous applications of the MAGIC, or particle-beam, interface have been reviewed (29,30). Still, the low flow rates required, and the usefulness for mostly low-molecular weight com-

pounds that yield good EI spectra have caused this technique, like others, to give way to the burgeoning popularity of the API techniques. There are still cases, however, where EI spectra are highly desired for molecules separated by LC. For these situations, Cappiello and coworkers make the case that a micro- or nanoscale particle beam interface still has a valuable place in the analytical chemist's arsenal (30,31). The wide variety in the classes of lipids means that some classes, such as fatty acids (as their methyl esters, picolinyl esters, etc.), are amenable to ionization using electron impact ionization, whereas others are too large to produce definitive EI spectra. Thus, for the smaller classes, techniques such as particle-beam that produce conventional EI spectra might still be useful for automated library matching. However, the classes of larger lipid molecules require the soft ionization advantages of atmospheric pressure ionization interfaces.

ESI and APCI have shown themselves to be the two primary interfaces that have enduring advantages such as ease of use, durability, compatibility with high flow rates, interchangeability, resistance to clogging, affordability, and versatility (applicability to a wide range of analytes). Plus, they produce high-quality spectra that allow molecular weight determination with diagnostically useful fragmentation, without collision-induced dissociation (CID) in the case of APCI, and with CID in the case of ESI. These multiple benefits are the reasons that these two techniques have endured while others have risen in popularity and then fallen.

ESI and APCI have been available for some time, but there is also a new atmospheric pressure ionization source for mass spectrometry that only recently became commercially available. This newcomer to the field of liquid chromatography–mass spectrometry is atmospheric pressure photoionization (APPI). Robb, Covey, and Bruins (32) introduced APPI as a detector for LC-MS in 2000. While photoionization had been used as a detector for GC as early as the mid 1970s (33–36), and as a simple LC detector in the 1980s (37,38), it was not until very recently that photoionization has been used to produce ions for LC-MS. Because of its recent development, reports describing analyses by LC-APPI-MS are still relatively few. Raffaelli and Saba (39) reviewed applications of APPI in 2003. Applications of APPI to lipids are very limited, and extend mostly to steroids.

Like ESI and APCI, APPI is a soft ionization technique that typically produces molecular ions and protonated molecules, with minimal fragmentation. However, like APCI, APPI does usually produce some structurally diagnostic fragments. An APPI source has design similarities in common with an APCI source, in that they both employ a nebulizing gas and a vaporizer heater to aid in solvent evaporation. However, the APPI source employs a high-intensity lamp to irradiate the sample stream with photons, instead of a high-voltage corona discharge needle. Argon, krypton, or xenon lamps may be employed, depending on the desired photon energy. The APPI source developed by Syagen Technology, Inc. (Tustin, CA), called the PhotoMate[®], for use on Agilent and ThermoElectron instruments, utilizes a krypton lamp, which emits photons at 10.0 and 10.6 eV. APPI is reported to be applicable to many of the same molecules as APCI, but it is reported to have advantages over

APCI for ionization of highly non-polar molecules such as polyaromatic hydrocarbons (PAH). Syage *et al.* (40) reported detection limits for reserpine of around 1 pg for APPI, which was similar to that obtained by their APCI source (detection limit at $3\sigma = 1.2$ pg for APPI, 0.8 pg for APCI; real detection limit closer to 3 pg). Some compounds, however, responded significantly better to APPI (i.e., anthracene, benzo(a)anthracene, vitamins A and C) than they did to APCI. APPI was reported to exhibit less flow rate dependence and to give better signal at low flow rates than APCI.

Direct photoionization of most molecules occurs with a low statistical probability, so a dopant is often incorporated into the effluent prior to APPI to act as an intermediate to absorb the photon energy and produce a dopant ion, which then reacts with an analyte molecule to produce an analyte molecular ion or protonated molecule. More detail on theoretical aspects of APPI, and the specific design features of an APPI source, are given in Chapter 11, in which Kostianen and Kauppila describe APPI for steroid analysis. It is sufficient here to say that APPI is a recent addition to the lineup of commercially available API ion sources; it is applicable to many of the same molecule classes as APCI, and it is complementary to APCI for some molecules. Of course, both APCI and APPI are complementary to ESI for most classes of molecules, including lipids.

ESI and APCI are currently the most popular atmospheric pressure ionization sources, with APPI quickly gaining popularity. The popularity of APPI is being advanced by the introduction of a combination APCI/APPI source by ThermoElectron on its LC/MS⁽ⁿ⁾ instruments. Combination ionization sources for MS are discussed further in Chapter 13 on dual parallel techniques. Although there are not yet any reports of the application of LC-APPI-MS to analysis of triacylglycerols, phospholipids, or several other classes of lipids, one would expect that these gaps in data will be filled in the very near future. The classes of molecules to which the three most popular atmospheric pressure ionization sources apply are shown in Figure 1.1.

ESI-MS is well recognized for its ability to ionize large molecules, especially biomolecules, and has gained a central position in the field of proteomics. Thus Figure 1.1 reflects the ability of ESI to ionize large molecules. But ESI is not commonly known for its applicability to non-polar molecules with low proton affinities. ESI-MS is well known for its ability to ionize polar or ionic molecules (such as phospholipids, as discussed in following chapters), but many classes of lipids are non-polar and thus present a challenge to ESI-MS for analysis. Examples will be provided herein that show that ESI can ionize some classes of non-polar molecules quite effectively that were not previously thought to be amenable to ESI-MS.

Figure 1.1 also reflects the lower molecular weight ranges over which APCI and APPI are useful. The lower useful M.W. range for APCI will be seen later in this volume, but many lipids fall into the range of M.W. to which APCI is perfectly suited. Regardless of its limited applicability to large biomolecules, APCI will be shown to be a valuable tool for obtaining mass spectral data that allow conclusive

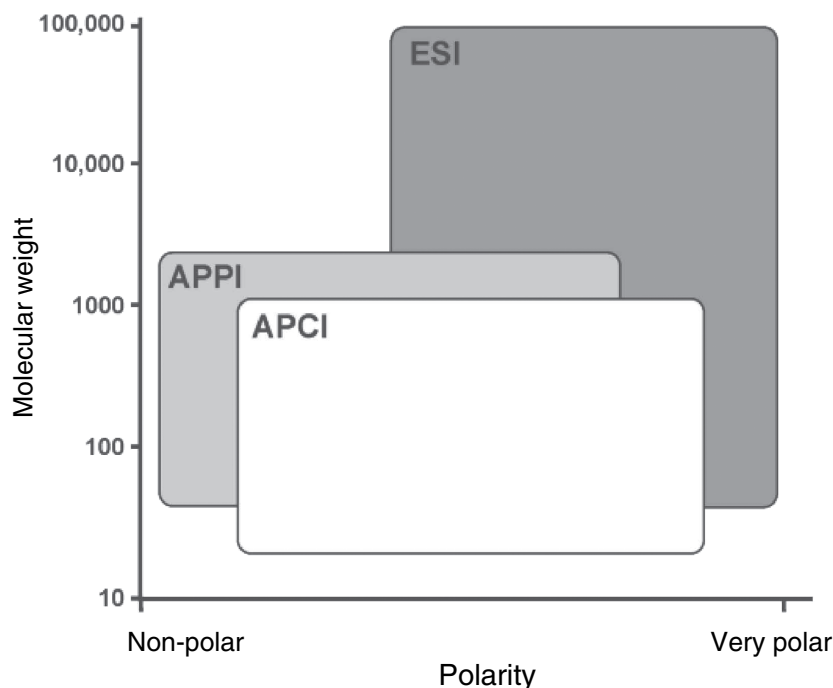


Fig. 1.1. Classes of molecules to which ESI, APPI, and APCI ionization sources apply.

identification and quantification of many lipid classes. The soft fragmentation provided by APCI will be shown to be a valuable complement to the protonated molecules and adducts observed by ESI-MS. Although APPI has been applied to lipids to only a limited extent thus far, Chapter 11 describes what is known to date. The general background of the development of API techniques has been described in the preceding section, and the API interfaces available from different manufacturers will be discussed in the next section, but the descriptions of the theory and instrumentation of the specific ionization sources (ESI, APCI, and APPI) are left to other chapters.

Experimental

API Interfaces

Coupling an LC effluent with a high-vacuum mass spectrometer requires removal of a large volume of evaporated condensed-phase solvent. Obviously it is not desirable to introduce the full volume of expanded solvent into the mass spectrometer. Instead, approaches have been developed by which the beam being sampled is enriched in analyte ions versus solvent molecules. The interface should transfer ions efficiently,

while eliminating as many neutral molecules and other “chemical noise” to the greatest extent possible. Fortunately, once ions are formed by the ionization source, electrical fields such as plate lenses or ion guides can be used to keep ions traveling in a concentric path down the center of the ion optics, while neutral molecules are pumped away. Advances in vacuum technology, which have led to turbomolecular pumps with higher pumping capacities, now allow much larger volumes of gas to be pumped away efficiently. Nevertheless, increased pumping capacity is not the key to a successful API interface. Enrichment of the sample beam by using sampling orifices, skimmers, and ion guides is the key to an efficient API interface.

Since its inception as a commercially available ionization interface, APCI has been designed to utilize the same atmospheric pressure ionization interface that is employed for ESI-MS. APCI was designed to be interchangeable with ESI. The design of the API interface determines, to a large extent, the sensitivity and detection limit for an instrument. The interface design determines the amount of chemical noise allowed to pass into the mass filter at high vacuum. Of course, the ionization source may also contribute a large amount of chemical noise. Usually APCI has higher chemical background than ESI, but this is only one of the reasons why ESI has detection limits typically 100 or more times lower than APCI.

Most first-generation API interfaces employed a linear design, in which the nebulized spray was in line with the inlet capillary. Instrument manufacturers now mount the ionization source in an orthogonal geometry, to minimize the amounts of solvent and other neutral molecules allowed to pass into the mass spectrometer. On our tandem mass spectrometer, which is an older first-generation instrument, after ions are produced at atmospheric pressure, by APCI or ESI, they are sampled into the end of the heated capillary that serves as the interface to vacuum stage one. The whole interface region, from atmospheric pressure to high vacuum, is shown in Figure 1.2 for the Finnigan MAT TSQ 700 in our lab. The exit end of the heated capillary serves as a nozzle to spray the incoming ionic effluent stream through the concentric tube lens, onto the skimmer cone. The skimmer samples the spray ~1 mm off-center from the primary ion trajectory. Then, the ions move through the octapole lens in the first high-vacuum region past two closely spaced plate lenses to the first quadrupole, which is in the second high-vacuum region.

The Thermo Finnigan LCQ Deca ion trap mass spectrometer in our laboratory is a newer instrument but also uses a first-generation API source, almost identical to the one on the TSQ 700, but the newer instrument uses a second-generation heated capillary interface. Instead of the construction shown in Figure 1.2, the LCQ Deca mass spectrometer uses an “API stack” attached to the back of the spray shield that contains the heated capillary, tube lens, and skimmer. The components in this version of the interface are shown in Figure 1.3. After the skimmer on the Deca lies a short quadrupole ion lens (non-mass-filtering) and then a short octapole lens, before the entrance lens to the trap.

A second-generation Agilent (formerly Hewlett-Packard) API interface is shown in Figure 1.4. Two important differences are that (i) the interface employs

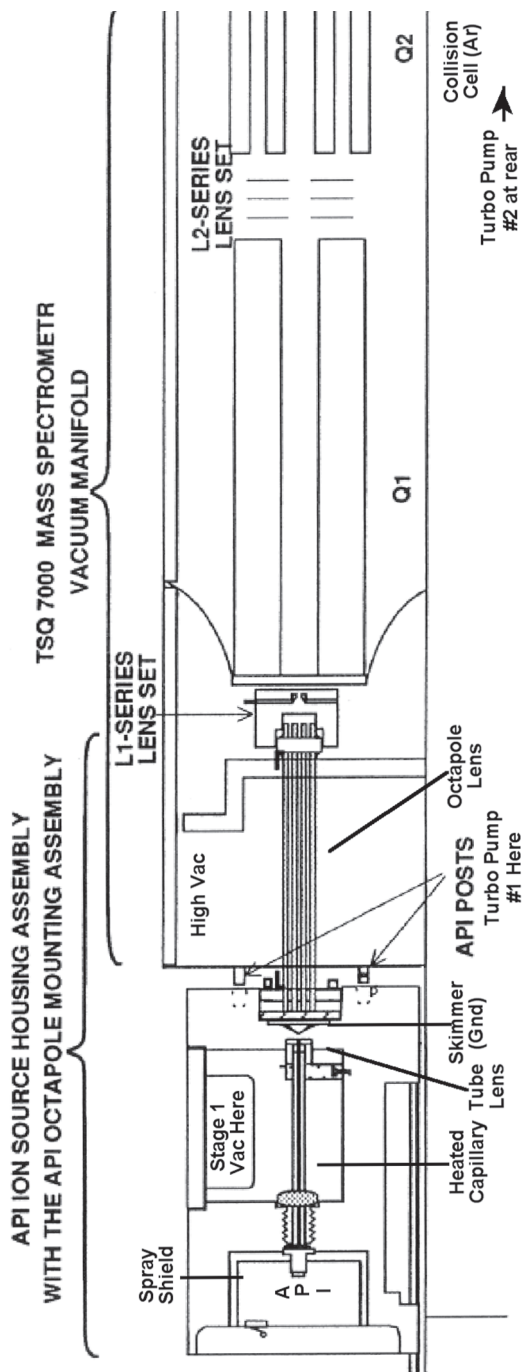


Fig. 1.2. Instrument design for Finnigan MAT TSQ 700 tandem mass spectrometer. (Figure adapted from TSQ 700 API Operator's Manual. Used by permission from ThermoElectron Corporation.)

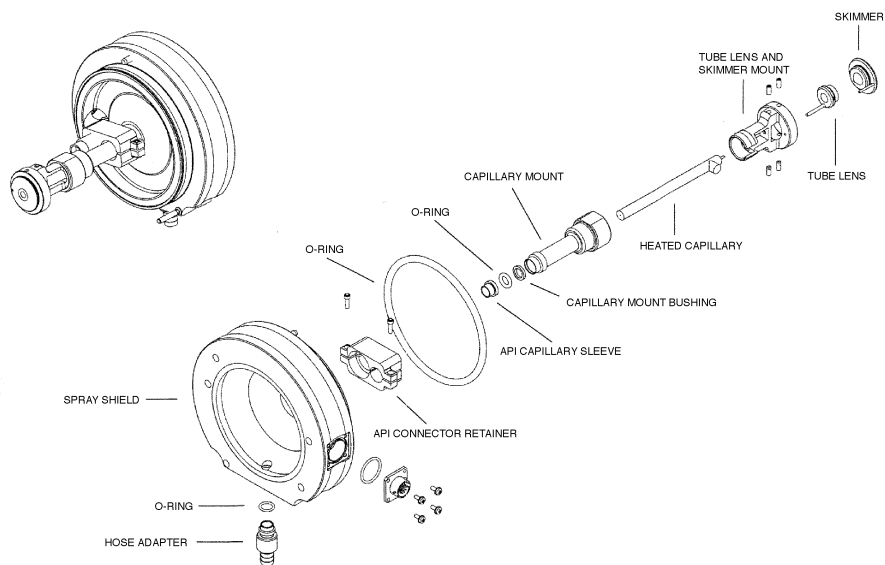


Fig. 1.3. Diagram of the “API stack” that contains heated capillary, tube lens, and skimmer in an LCQ Deca ion trap mass spectrometer. (Figure adapted from *LCQ Hardware Manual*. Used by permission from ThermoElectron Corporation.)

an orthogonal arrangement between the ESI or APCI probe and the inlet capillary to high vacuum, and (ii) the interface employs a countercurrent gas around the inlet capillary to help keep the capillary from clogging, to break up solvent-molecule clusters, and for other purposes. Most instrument makers, including ThermoElectron/Finnigan, Applied Biosystems/MDS Sciex, and others, now include both an orthogonal design and a countercurrent gas in their interface designs. Despite these modifications, the API interfaces used by several manufacturers share essential design components with the inlet capillary/skimmer design that was employed early in the history of the ESI source.

Micromass, Ltd. (formerly VG and formerly Fisons, and now part of Waters Corporation), offers ESI and APCI sources for its machines. Micromass[®] uses a unique Z-spray[™] API interface system, as shown in Figure 1.5, composed of two orthogonal sampling cones, to reduce the amount of contamination reaching the ion optics. This allows extended use with “dirty” biological or environmental samples, or allows the use of non-volatile buffers without clogging.

Applied Biosystems makes available an orthogonal API interface called the Turbo-V[™] ion source that incorporates a curtain gas, and in which the spray is orthogonal to the sampling orifice. This source has two separate nozzles that provide heated gas that aids in sample desolvation. These heated gas jets are in a V

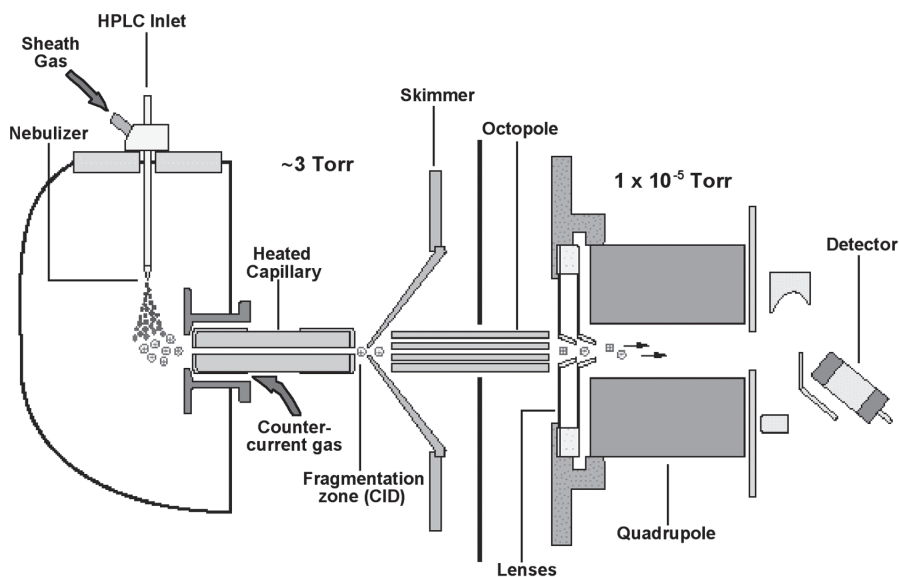


Fig. 1.4. Agilent (formerly Hewlett-Packard) quadrupole mass spectrometer employing an atmospheric pressure ionization interface, with electrospray ionization source installed. (Figure used with permission of Agilent Technologies, Inc.)

configuration (hence the name Turbo-V), coplanar with the LC spray located midway between the heated gas jets. These are coplanar and are all orthogonal to the sampling orifice. In this source, the central probe may readily be changed between ESI and APCI.

Regardless of the variety of API interface implementations, most instruments employ a capillary/skimmer approach or an orifice/skimmer approach to interface between atmospheric pressure and an area of intermediate vacuum. Then, typically behind the skimmer is an ion guide, either a nonscanning quadrupole or a multipole of some variety. After the ion focusing elements comes the mass filter, at high vacuum. Because of these common design elements, most sources are capable of performing “up-front” collision-induced dissociation (CID) of ions. Some sources have two locations at which up-front CID can be accomplished. For those instruments that employ a capillary/skimmer approach (also referred to as a nozzle/skimmer since the exit of the capillary acts as a spray nozzle), a potential may be applied between the exit of the capillary and the skimmer to increase the kinetic energy of molecules in this area of intermediate vacuum, thus producing fragment ions by energetic collisions with atmospheric gases. This is referred to as nozzle/skimmer (N/S) up-front CID. The region where this type of fragmentation occurs is labeled the “fragmentation zone” in Figure 1.4. Alternatively, a potential may be applied between the skimmer and the multipole that follows the skimmer in the ion path. Since this multipole is often a nonfiltering quadrupole, this type of

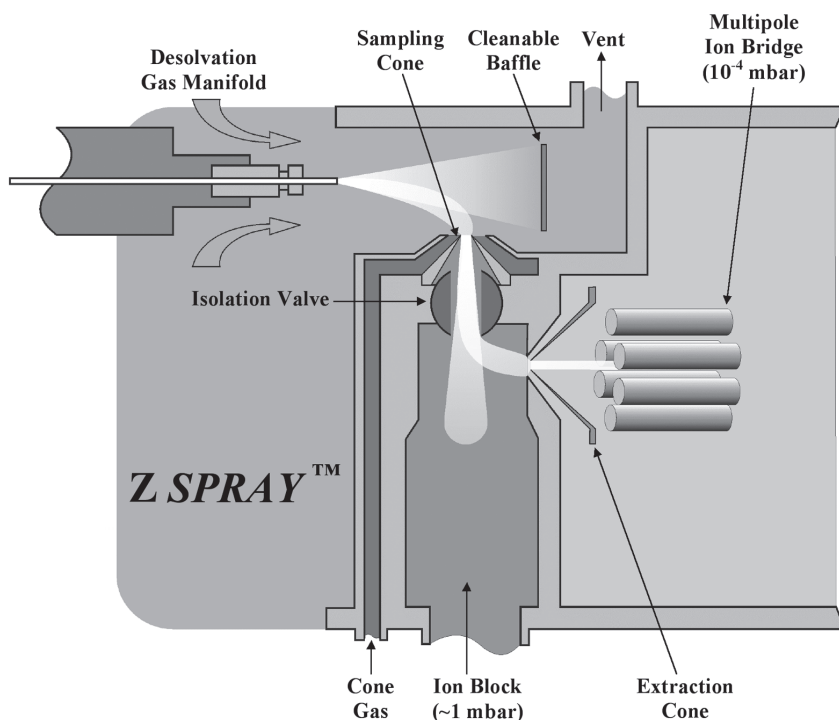


Fig. 1.5. This is the latest-generation Micromass Z-Spray™ interface. Two orthogonal sampling orifices reduce the amount of contaminants that reach the ion optics at high vacuum. The Cone Spray further acts to minimize cluster ion formation and exclude undesirable buffer ions. (Figure adapted with permission from Waters Corporation, Inc.)

up-front CID is sometimes referred to as skimmer/quadrupole (S/Q) up-front CID. For example, the octapole on the TSQ 700 shown in Figure 1.2 allows skimmer/multipole up-front CID to be performed. The Micromass Z-Spray™ source allows up-front CID in the region between the first sampling cone and the extraction cone. Again, all of these approaches use the API interface region, not the ionization source, to produce fragments so it is a misnomer to refer to these techniques as “in-source” CID; rather, the more correct term is “up-front” CID, as stated. Although CID can be helpful to increase the amount of structurally useful fragments for some compounds, not all molecules are efficiently fragmented by this approach. Thus, ESI with up-front CID is sometimes not a substitute for the gentle fragmentation brought about in an APCI source. Furthermore, since up-front CID fragmentation is nonspecific, the direct relationship between parent and daughter ions is lost if more than one compound is present in the CID region. There is no way to be certain which fragments came from which parent. Thus, MS/MS of defined precursor ions is still preferred over fragmentation by up-front CID. However, in the case

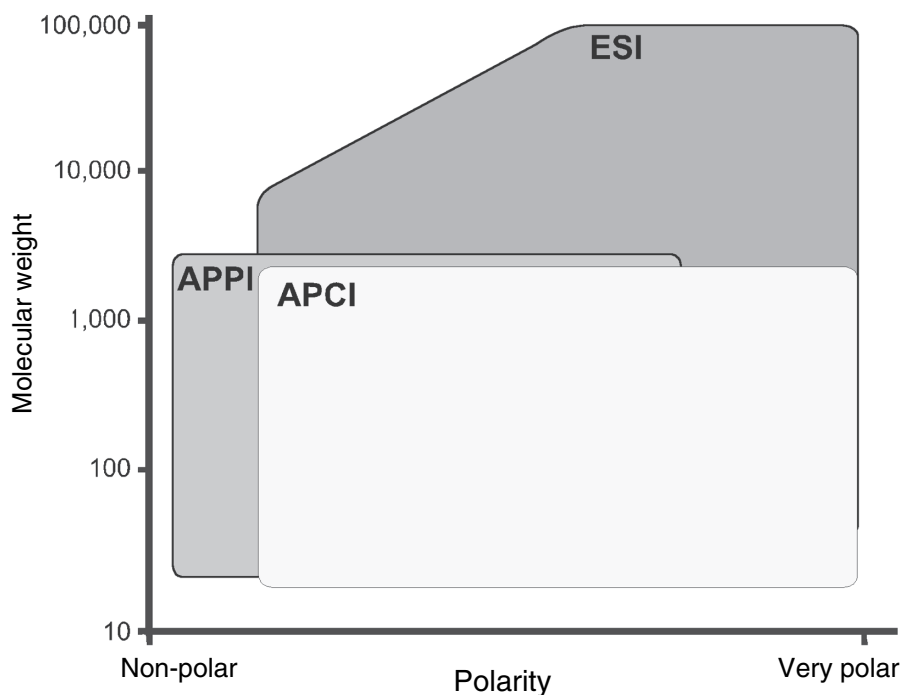


Fig. 1.6. Modified ranges of molecular weights and polarities based on applications demonstrated in this volume.

where only a single quadrupole instrument is available, up-front CID can increase the amount of structural data obtained from an LC-MS experiment. However, extra caution is required for data interpretation; the nonspecific fragmentation from up-front CID can lead to ambiguity and even misidentification of the fragments produced by up-front CID.

Data from several different instruments having different API interfaces will be presented in this volume. The ionization sources used on several of these instruments will be described in detail. Despite the differences in ion source and API interface designs, all of the work described herein employs liquid chromatography coupled with one or more mass spectrometers *via* an atmospheric pressure ionization interface with either ESI, APCI, or APPI as the ion source. In the 21st century, these three atmospheric pressure ionization techniques are the most popular methods for analysis of lipids in complex samples. It is expected that this trio of API sources will continue to be the ionization techniques of choice for at least the coming decade. ESI will continue to find ever-increasing uses in lipid analysis, in addition to its entrenched position as the dominant choice for protein analysis. Recently, an atmospheric pressure matrix-assisted laser desorption ionization (MALDI) source was introduced from ThermoElectron Corporation. Waters, Inc.,

has made a dual ion source, with interchangeable API and MALDI sources, available on its Q-TOF Ultima GLOBAL line of mass spectrometers. Researchers will watch the development of API/MALDI sources with great interest in the coming years.

APPI will be applied to an increasing number of analyte classes in the coming years. It is almost a certainty that common lipid classes will be among the subjects of investigation by APPI. Over the coming years, APCI and APPI will compete for the position of the second most popular ionization method for LC-MS. The development of combination sources will continue, as instrument manufacturers make it easier for analysts to obtain both ESI and APPI or APCI data. ThermoElectron Corporation has introduced the combination APCI/APPI source, and Applied Biosystems/MDS Sciex has introduced a combined ESI/APCI ion source.

Many of the authors who have published extensively in the area of lipid analysis by API techniques are authors in this volume. They have published extensively in the field of LC/MS for lipid analysis and have defined the state of the art for lipid analysis in the last decade. The chapters in this volume describe applications of the three popular API techniques to many lipid classes from fatty acids to triacylglycerols, and from phospholipids to carotenoids and steroids. As demonstrated in this volume, the variety of molecules to which these techniques are applied reveals that the ranges of polarities and molecular weights amenable to APCI and ESI are broader than the ranges shown in Figure 1.1. It is demonstrated herein that ESI-MS can be used for molecules that are relatively non-polar, and that are as small as triacylglycerols and diacylglycerol monomers. Yet ESI-MS can also be used for larger non-polar molecules such as high-molecular-weight triacylglycerol oxidation product oligomers.

APCI is shown to be useful both for small polar molecules (e.g., phospholipids) and for non-polar molecules (e.g., fatty acids, triacylglycerols, TAG derivatives, etc.). However the limitations of APCI-MS for analysis of larger molecules (> 2,000 amu) are demonstrated and compared to the sensitivity of ESI-MS for these same molecules. ESI-MS is shown to be useful for large non-polar molecules up to ~4,000 amu. It is assumed that the upper range of observable molecular weights of very non-polar molecules is less than the upper range of molecular weights observable from polar molecules, as represented by the sloping boundary of the area representing ESI-MS analytes in Figure 1.6. The current limit on the upper mass range of non-polar molecules (TAGOX) observed by ESI-MS is the upper mass limit (m/z 4,000) of the mass spectrometer used for this analysis.

APPI analysis has thus far been applied to very few lipid molecule classes. Chapter 11 describes the current state of the art in the application of APPI-MS to steroids. The bounded area representing the range of analytes amenable to APPI analysis in Figure 1.6 will likely be expanded over the coming years as new applications related to lipids are published. For now, APPI is still presumed to have some benefit over APCI for a few highly non-polar molecules, such as aromatic hydrocarbons, petroleum distillates and other highly aromatic molecules, and molecules that contain chromophore groups. The presence of chromophore groups on large non-polar molecules may allow APPI to be useful for some molecules slightly

larger than the range amenable to APCI analysis. By the same token, the need for a chromophore or additive for APPI can limit the lower mass range, such that APCI may be more useful for some smaller molecules.

The reports presented in this book demonstrate that the frontiers of the applicability of APPI-, APCI-, and ESI-MS to lipid analysis are being pushed steadily forward as new reports demonstrate analysis of a wider and wider range of lipid analyte molecules.

Although the separation capability of LC is extremely powerful when combined with the information-rich detection by MS, not all methods require the prior chromatographic separation of analytes. Included in this volume are alternative approaches to LC-MS. Chapter 12 describes a recently developed approach to lipidomics using direct infusion, without prior chromatographic separation. Thus, several analytical methodologies currently compete with each other in the pursuit of the best approach to a comprehensive and facile method for lipid analysis. This volume provides a complete review of the current literature, describes the latest cutting-edge research being performed across the globe, and finally provides an indication of the direction in which the field of lipid analysis by API-MS using LC and related techniques is moving.

References

1. Arpino, P.J., On-line Liquid Chromatography/Mass Spectrometry? An Odd Couple! *Trends Anal. Chem. 1*: 154–158 (1982).
2. Dole, M., R.L. Hines, L.L. Mack, R.C. Mobley, L.D. Ferguson, and M.B. Alice, Gas Phase Macroions, *Macromolecules 1*: 96–97 (1968).
3. Dole, M., L.L. Mack, and R.L. Hines, Molecular Beams of Macroions, *J. Chem. Phys. 49*: 2240–2249 (1968).
4. Mack, L.L., P. Kralik, A. Rheude, and M. Dole, Molecular Beams of Macroions II, *J. Chem. Phys. 52*: 4977–4986 (1970).
5. Kantrowitz, A., and J. Grey, A High Intensity Source for the Molecular Beam 1. Theoretical, *Rev. Sci. Instr. 22*: 328–332 (1951).
6. Yamashita, M., and J.B. Fenn, Negative Ion Production with the Electrospray Ion Source, *J. Phys. Chem. 88*: 4671–4675 (1984).
7. Yamashita, M., and J.B. Fenn, Electrospray Ion Source—Another Variation on the Free Jet Theme, *J. Phys. Chem. 88*: 4451–4459 (1984).
8. Whitehouse, C.M., R.N. Dreyer, M. Yamashita, and J.B. Fenn, Electrospray Interface for Liquid Chromatographs and Mass Spectrometers, *Anal. Chem. 57*: 675–679 (1985).
9. Iribarne, J.V., and B.A. Thomson, Evaporation of Small Ions from Charged Droplets, *J. Chem. Phys. 64*: 2287–2293 (1976).
10. Thomson, B.A., and J.V. Iribarne, Field-Induced Ion Evaporation from Liquid Surfaces at Atmospheric Pressure, *J. Chem. Phys. 71*: 4451–4463 (1979).
11. Bruins, A.P., T.R. Covey, and J.D. Henion, Ion Spray Interface for Combined Liquid Chromatography/Atmospheric Pressure Ionization Mass Spectrometry, *Anal. Chem. 59*: 2642 (1987).
12. Niessen, W.M.A., *Liquid Chromatography–Mass Spectrometry*, Chromatographic Science Series, edited by J. Cazes, Marcel Dekker, Inc., New York, 1999.

13. Horning, E.C., M.G. Horning, D.I. Carroll, I. Dzidic, and R.N. Stillwell, New Picogram Detection System Based on a Mass Spectrometer with an External Ionization Source at Atmospheric Pressure, *Anal. Chem.* 45: 936–943 (1973).
14. Carroll, D.I., I. Dzidic, R.N. Stillwell, M.G. Horning, and E.C. Horning, Subpicogram Detection System for Gas Phase Analysis Based upon Atmospheric Pressure Ionization (API) Mass Spectrometry, *Anal. Chem.* 46: 706–710 (1974).
15. Horning, E.C., D.I. Carroll, I. Dzidic, K.D. Haegele, M.G. Horning, and R.N. Stillwell, Atmospheric Pressure Ionization (API) Mass Spectrometry. Solvent-Mediated Ionization of Samples Introduced in Solution and in a Liquid Chromatographic Effluent Stream, *J. Chromatogr. Sci.* 12: 725–729 (1974).
16. Carroll, D.I., I. Dzidic, R.N. Stillwell, K.D. Haegele, and E.C. Horning, Atmospheric-Pressure Ionization Mass-Spectrometry: Corona Discharge Ion Source for Use in Liquid Chromatograph-Mass Spectrometer-Computer Analytical System, *Anal. Chem.* 47: 2369–2373 (1975).
17. Talroze, V.L., G.V. Karpov, I.G. Gorodets, and V.E. Skurat, Capillary System for Introduction of Liquid Mixtures into an Analytical Mass Spectrometer, *Russ. J. Phys. Chem.* 42: 1658–1664 (1968).
18. Talroze, V.I., V.E. Skurat, N.B. Zolotoi, and I.G. Gorodets, Glass and Quartz Capillary Nozzles for Mass Spectrometer Liquid Sample Injector, *Russ. J. Phys. Chem.* 46: 456–458 (1972).
19. Niessen, W.M.A., A Review of Direct Liquid Introduction Interfacing for LC/MS Part 1: Instrumental Aspects, *Chromatographia* 21: 277–287 (1986).
20. Niessen, W.M.A., A Review of Direct Liquid Introduction Interfacing for LC/MS Part 2: Mass Spectrometry and Applications, *Chromatographia* 21: 342–354 (1986).
21. Scott, R.P.W., C.G. Scott, M. Munroe, and J. Hess, Interface for On-line Liquid Chromatography-Mass Spectroscopy Analysis, *J. Chromatogr.* 99: 395–405 (1974).
22. McFadden, W.H., H.L. Schwartz, and S. Evans, Direct Analysis of Liquid Chromatographic Effluents, *J. Chromatogr.* 122: 389–396 (1976).
23. Arpino, P., Combined Liquid Chromatography Mass Spectrometry. Part I. Coupling by Means of a Moving Belt Interface, *Mass Spectrom. Rev.* 8: 35–55 (1989).
24. Blakely, C.R., M.J. McAdams, and M.L. Vestal, Crossed-Beam Liquid Chromatograph Mass Spectrometer Combination, *J. Chromatogr.* 158: 261–276 (1978).
25. Blakely, C.R., J.J. Carmody, and M.L. Vestal, A New Soft Ionization Technique for Mass Spectrometry of Complex Molecules, *J. Am. Chem. Soc.* 102: 5931–5933 (1980).
26. Arpino, P., Combined Liquid Chromatography Mass Spectrometry. Part II. Techniques and Mechanisms of Thermospray, *Mass Spectrom. Rev.* 9: 631–669 (1990).
27. Arpino, P., Combined Liquid Chromatography Mass Spectrometry. Part III. Applications of Thermospray, *Mass Spectrom. Rev.* 11: 3–40 (1992).
28. Willoughby, R.C., and R.F. Browner, Monodisperse Aerosol Generation Interface for Combining Liquid Chromatography with Mass Spectrometry, *Anal. Chem.* 56: 2626–2631 (1984).
29. Creaser, C.S., and J.W. Stygall, Particle-Beam Liquid-Chromatography Mass-Spectrometry—Instrumentation and Applications—A Review, *Analyst* 118: 1467–1480 (1993).
30. Cappiello, A., Is Particle Beam an Up-to-Date LC-MS Interface? State of the Art and Perspectives, *Mass Spectrom. Rev.* 15: 283–296 (1996).

31. Cappiello, A., G. Famigliani, F. Mangani, and P. Palma, New Trends in the Application of Electron Ionization to Liquid Chromatography—Mass Spectrometry Interfacing, *Mass Spectrom. Rev.* 20: 88–104 (2001).
32. Robb, D.B., T.R. Covey, and A.P. Bruins, Atmospheric Pressure Photoionization: An Ionization Method for Liquid Chromatography–Mass Spectrometry, *Anal. Chem.* 72: 3653–3659 (2000).
33. Driscoll, J.N., Application of a Photoionization Detector in Gas Chromatography, *Am. Lab.* 8: 71–75 (1976).
34. Driscoll, J.N., and F.F. Spaziani, PID Development Gives New Performance Levels, *Res. Dev.* 27: 50–54 (1976).
35. Driscoll, J.N., and J.B. Clarici, A New Photoionization Detector for Gas Chromatography, *Chromatographia* 9: 567–570 (1976).
36. Driscoll, J.N., Evaluation of a New Photoionization Detector for Organic Compounds, *J. Chromatogr.* 134: 49–55 (1977).
37. Locke, D.C., B.S. Dhingra, and A.D. Baker, Liquid Phase Detector for Liquid Chromatography, *Anal. Chem.* 54: 447–450 (1982).
38. Driscoll, J.N., D.W. Conron, P. Ferioli, I.S. Krull, and K.H. Xie, Trace Analysis of Organic Compounds by High-Performance Liquid Chromatography with Photoionization Detection, *J. Chromatogr.* 302: 43–50 (1984).
39. Raffaelli, A., and A. Saba, Atmospheric Pressure Photoionization Mass Spectrometry, *Mass Spectrom. Rev.* 22: 318–331 (2003).
40. Hanold, K.A., M.D. Evans, J.A. Syage, S.M. Fischer, and P.H. Cormia, Atmospheric Pressure Photoionization (APPI) Interface for LC/MS, *American Society for Mass Spectrometry Annual Meeting*, 2001.

Chapter 2

Analysis of Phospholipids by Liquid Chromatography Coupled with On-Line Electrospray Ionization Mass Spectrometry and Tandem Mass Spectrometry

Åsmund Larsen^a and Erlend Hvattum^b

^aGE Healthcare, Analytical Sciences R & D, Oslo, Norway, and ^bDepartment of Chemistry, Biotechnology, and Food Science, Agricultural University of Norway, N-1432 Ås, Norway

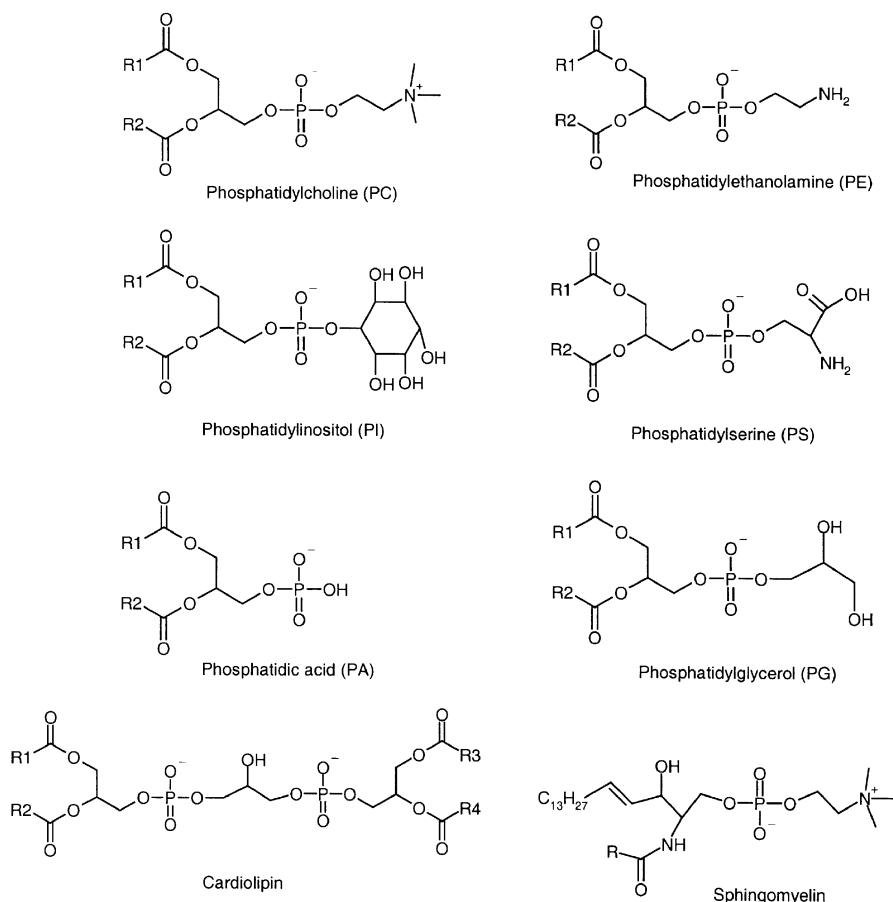
Introduction

Biological Aspects

Phospholipids (PL) are the major constituents of most cellular membranes. In addition, they play important roles in the control of many biological processes and they are gaining importance in a variety of medical, biological, biotechnological, and industrial applications. An enormous variety of phospholipid structures is found in nature, exhibiting great diversity of both the apolar and the polar moieties of the lipid molecules. The phospholipids are divided into several distinct molecular classes, distinguished by the head group attached to the phosphate moiety. The main phospholipid classes are phosphatidylcholine (PC), phosphatidylethanolamine (PE), phosphatidylinositol (PI), phosphatidylserine (PS), phosphatidylglycerol (PG), phosphatidic acid (PA), and cardiolipin (CL) (Scheme 2.1). Although sphingomyelin (SM) belongs to a separate class of lipids called sphingolipids, it is also an important constituent of plasma membranes of higher animals. Liquid chromatography-mass spectrometry (LC-MS) analysis of sphingomyelins will therefore be partly covered in this chapter.

Many molecular species are found in a single phospholipid class. They are characterized by the combination of fatty acyl residues attached to the *sn*-1 and *sn*-2 positions of the molecule and by the nature of the chemical linkage between the fatty acid (FA) chain and the *sn*-1 position of the glycerol backbone. Three types of linkage bonds are common: Acyl, ether, and vinyl-ether bonds. Ether and vinyl-ether bonds are solely found in the *sn*-1 position and are most common among PC and PE (1). Phospholipids containing ether bonds, 1-*O*-alkyl, in the *sn*-1 position are called plasmanyl-PL, while phospholipids containing vinyl-ether bonds, 1-*O*-alkyl-1'-enyl, in the *sn*-1 position are known as plasmenyl-PL (or plasmalogens). Plasmanyl and plasmenyl phospholipids are especially abundant in heart, kidney, and central nervous system (CNS) (2–4).

Phospholipids play essential structural and functional roles in most cell membranes. The only exceptions are neuronal tissues, which contain a large portion of



Scheme 2.1. Structures of the common phospholipid classes with fatty acyl substituents in the *sn*-1 and *sn*-2 positions, and sphingomyelin. Plasmanyl-PC and plasmanyl-PE (not shown) have an *O*-alkyl substituent in the *sn*-1 position, while plasmenyl-PC and plasmenyl PE have an *O*-alk-1'-enyl substituent in *sn*-1 position.

cerebrosides and gangliosides, and membranes of plant chloroplasts, which are enriched in diacylglycerolipids (5). The phospholipid content and composition of cellular membranes is highly regulated and varies from one cell type to another. The phospholipid composition of different membranes within a cell also varies. In addition to playing an essential role in membrane construction, they also anchor proteins to the membrane, modify activity of membrane-bound proteins, and serve as important second messengers (6). These functions are facilitated by an asymmetry between the two monolayer leaflets of the membrane bilayer, based on differences in the distribution of the major phospholipid classes. A fundamental property

of most biological membranes is, therefore, an asymmetric distribution of lipids across the bilayer (7,8). Early studies on lipid organization were based on measurements of the accessibility of PL to exogenous phospholipases and membrane-impermeable reagents that react with primary amines. These studies showed that the choline-containing phospholipids (phosphatidylcholine (PC) and sphingomyelin (SM)) are localized to the external leaflet of the plasma membrane, or to the topologically equivalent luminal surface of internal organelles (9–12). In contrast, the aminophospholipids (PE and PS) are enriched on the cytofacial surface of these membranes. For example, in the membranes of erythrocytes approximately 80% of SM and 75% of PC are located in the outer monolayer. The distribution of PE is similarly asymmetric, but in the opposite sense; approximately 80% of the lipid resides in the inner monolayer (13). The asymmetric distribution of PS is absolute; PS is found exclusively in the cytofacial monolayer (13). It has been proposed that the cell membranes are not only organized as a continuous fluid mosaic, but might, in addition, consist of dynamic assemblies of lipids in the exoplasmic leaflet of the bilayer (14). The most important properties of these ‘membrane rafts’ are that they can include and exclude proteins to variable extents. The membrane surrounding the lipid rafts consists mostly of phospholipids that have not been completely characterized (14).

The phospholipid composition of membranes can vary considerably with species and with the source of the tissue. The choline phospholipids, including sphingomyelin, account for more than half of the total phospholipid composition in most mammalian tissues, although the amount of sphingomyelin may vary considerably (15). The amount of choline and ethanolamine phospholipids occurring in the plasmemyl form also varies with the origin of mammalian tissue. Plasmemyl PL account for about half of the choline and ethanolamine phospholipids in heart; in neural tissues plasmemyl ethanolamine accounts for greater than half of the ethanolamine phospholipids (15). Only small amounts of plasmemyl choline are present in neural tissue (15). The inositol phospholipids of mammalian tissues consist of three different phospholipids, phosphatidylinositol, and two more highly-phosphorylated molecules, phosphatidylinositol-4-phosphate and phosphatidylinositol-4,5-biphosphate. The metabolism of inositol lipids is involved in the signal transduction pathways of many hormones, neurotransmitters, and growth factors (16–20). In the classical pathway, the membrane phospholipid phosphatidylinositol-4,5-biphosphate is hydrolyzed by phospholipase C enzymes to release the second messengers inositol-1,4,5-triphosphate and 1,2-diacylglycerol. Inositol-1,4,5-triphosphate induces intracellular Ca^{2+} release and 1,2-diacylglycerol activates the protein kinase C isozymes. Phosphatidylglycerol occurs widely in mammalian tissues, but great differences are found regarding the amounts of PG present. It is mainly located in the mitochondria of mammalian cells (21). PG is a precursor in the biosynthesis of cardiolipin (22–27) and the synthesis has been found to take place in the mitochondria of mammalian cells (22,23,26,28). A specific function of PG has been established in the lung, where this lipid is an important component of

pulmonary surfactant, representing about 10% of total phospholipids of the surfactant (29–31). As previously mentioned, PS is exclusively found in the cytofacial monolayer. However, recent studies suggest that loss of phospholipid asymmetry and exposure of PS are required for recognition and removal of apoptotic cells by macrophages and other phagocytes (32).

Various FA are distributed in phospholipids in different mammalian tissues. The fatty acyl residues of individual phospholipids appear to be under strict metabolic regulation. In general, saturated FA are esterified in the *sn*-1 position while unsaturated FA, such as arachidonic acid, are commonly found in the *sn*-2 position. The composition of the molecular species can affect membrane fluidity, which in turn will alter the activity of many membrane-bound proteins (6,33–35). Phospholipids have functions other than simply maintaining membrane integrity. The choline phospholipid, 1-alkyl-2-arachidonoyl-PC is a precursor for platelet-activating factor (PAF) (36). PAF is a biologically active glycerophospholipid (1-alkyl-2-acetyl-PC) which is assumed to act as a chemical mediator of anaphylaxis, septic shock, and various inflammatory reactions (37). Phospholipids also serve as sources of arachidonic acid and other polyunsaturated FA, which can be metabolized by various oxygenase enzymes. This leads to the formation of prostaglandins and leukotrienes (38).

Many diseases are primarily associated with the defective functioning of a given type of cell. Since the defects are often reflected in abnormalities in the structure and function of a given type of cell, membrane phospholipids are invariably involved in different diseases. Compositional alterations in brain phospholipids have been reported in patients with Alzheimer's disease (AD). The levels of PI and PE that are rich in easily oxidizable polyunsaturated FA have been shown to be diminished in AD brain (39). A decrease in plasmenyl PE has also been described in AD brain (40). The molecular species composition of PC varies from different cell types and tissues, and the perturbation of PC homeostasis in mammalian cells leads to cell death (41). Finally, there is growing evidence that the accumulation of phospholipid oxidation products may be associated with several chronic disease processes, including atherosclerosis (42). All of this leads to the conclusion that there is a growing need for reliable analytical methods for characterization of phospholipid species from various biological sources. With the recent coupling of high-performance liquid chromatography (HPLC) to mass spectrometry (MS), new detection opportunities have been opened up for the structural analysis of phospholipid species.

Medical Applications of Liposomes

Due to their amphiphilic and ionic nature, phospholipids in aqueous environments readily form organized macromolecular structures such as liposomes or vesicles (43). Research groups worldwide have developed drug delivery systems by using various liposomes. By encapsulating drugs into liposomes targeted to specific disease

areas, new therapeutic and diagnostic approaches have been discovered (44). The encapsulation by a soft lipid membrane could potentially lead to the controlled release of drugs in targeted organs or tissues. For diagnostic purposes, liposomes have been investigated for drug delivery, gene transfer, and immunodiagnostic applications (43). Liposomal contrast agents for magnetic resonance imaging, computed tomography, nuclear medicine, ultrasound, and positron emission tomography have also been investigated (44–47). Air- and gas-filled microbubbles have shown favorable acoustic properties, which make them attractive as ultrasound diagnostic agents (44,48–51). Furthermore, liposomes for gene therapy have been studied with particular attention to systems for DNA delivery (52). The approach of using self-enclosed colloidal particles to encapsulate different drugs is a relatively new field in drug development and is likely to grow. Phospholipids are normally the main lipid constituents in liposomes, together with modified synthetic phospholipids, sterols, and other lipid classes (52). The requirement for characterizing the liposome composition *in vitro* and *in vivo* necessitates specific and sensitive analytical methods like LC-MS. Furthermore, the fact that phospholipids are endogenous compounds found in all cell membranes would require that the analytical methods distinguish between endogenous and exogenous phospholipid species (i.e., species characterization). This situation is particularly challenging, since the distribution of endogenous levels of phospholipid species varies in different organs and tissues and could also vary from individual to individual and with diet. Therefore, in drug discovery, a qualitative and quantitative screening of the endogenous phospholipid composition in biological materials is often necessary. Analytical methods capable of such specificity (e.g., in pharmacokinetic and toxicokinetic studies) are essential. The diversity of medical applications of liposomes and of liposome compositions, together with an increased focus on the biological role of membrane phospholipids, is a driving force for analytical method development in the field.

Liquid Chromatography of Phospholipids in Combination with Mass Spectrometry

Normal-Phase LC-MS. Normal-phase high-performance liquid chromatography separates the phospholipids into their respective classes. This is invaluable in the process of identifying phospholipid species, especially when dealing with extracts from biological sources, where several classes are present with numerous species within each class. Several normal-phase HPLC methods have been described for this purpose. A common feature for all of these methods is that they separate the phospholipids according to their polar head groups, and almost disregard the *sn*-1 and *sn*-2 FA substituents. With such group separation, the different species within a given class elute as a single chromatographic peak. There might be slight differences in the retention times of the individual species within a given class. Nevertheless, the difference in retention times is generally less than that between the classes, enabling class determination based on retention time.

Many normal-phase HPLC methods published up until approximately 1995 were based on ultraviolet (UV) detection (53). However, the advent of atmospheric pressure ionization mass spectrometry (API-MS) techniques led rapidly to the development of more MS-compatible LC methods. In the case of phospholipids, new methods were developed to avoid the use of nonvolatile mobile-phase additives like phosphate buffers and phosphoric acids.

In the early development of API-MS, the focus was primarily on reversed-phase applications. This was used in the field of life sciences, particularly in protein research. For the first time, mass spectra of proteins with molecular weights above 10,000 Da were demonstrated by Fenn *et al.* (54). This is still a very important field of applications involving many research groups worldwide. In the years following Fenn's work, the number of publications on different reversed-phase methods compatible with on-line LC-MS exploded, with a particular focus on aqueous mobile-phase compositions with volatile additives like formic acid, acetic acid, ammonium formate, ammonium acetate, triethyl amine, and ammonia. The most commonly used organic solvents feasible for on-line LC-MS were light alcohols like methanol and isopropanol, together with acetonitrile. LC-MS became one of the most important tools in biochemical research, including metabolite identification, peptide and protein research, carbohydrate analysis, and other pharmaceutical applications (55). As the number of applications expanded from the use of proteins to smaller molecules, the variety of mobile-phase solvents that proved to be compatible with API mass spectrometry increased. This included normal-phase applications, like phospholipid class separations using more nonpolar solvents like chloroform, dichloromethane, and hexane.

The stationary phases used with normal-phase chromatography are either based on plain silica (56–58) or chemically modified silica particles like diol groups (59–61) and amine groups (62). The organic modifiers commonly used for normal-phase LC-MS of phospholipids are chloroform, methanol, hexane, 1-propanol, isopropanol, and acetonitrile. In addition, most methods contain some kind of additive: a buffer, an acid or a base to adjust pH, or an ion-pair reagent. The methods are usually based on gradient elution from two reservoirs. The additives are included to improve the chromatographic peak shape and to change the retention time for a given phospholipid class. These effects are probably due to the ionic or zwitterionic nature of the phospholipid classes. PI, PG, and PA are anionic phospholipids; PS is zwitterionic and anionic; while PC and PE are zwitterionic and neutral. The exact mechanism of how different additives affect retention behavior or peak shape does not seem to be clear. However, different mobile-phase additives clearly give different elution orders of phospholipid classes. One example illustrating this is the use of the same diol column and mobile-phase compositions, except for the addition of 0.05% triethylamine (TEA) (59,60). The addition of 0.05% TEA (60) changed the elution order from PC < PE < PG < PA < PI < PS (59) (Fig. 2.1) to PG < PC < PE < PI < PS (60) (Fig. 2.2). The LC-MS method described by A. Karlsson *et al.* in 1996 (61) made use of hexane/1-propanol/

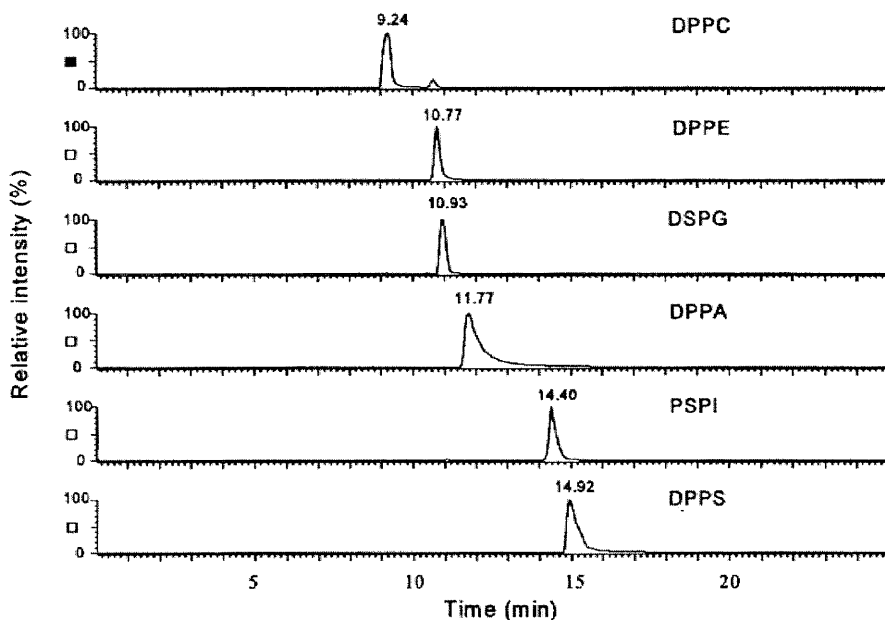


Fig. 2.1. Negative-ion HPLC-ESI-MS analysis of a phospholipid mixture, with SIM of the following phospholipids (approx. 8 $\mu\text{g/mL}$ of each): DPPC, DPPE, DSPG, DPPA, PSPI, and DPPS. *Source:* Reference 59. Reproduced with permission from the publisher (Elsevier).

formic acid/triethylamine as mobile-phase constituents, which gave the elution order $\text{PG} < \text{PE} < \text{PC} < \text{PS} < \text{PI}$ using the same diol stationary phase as in the preceding example (Fig. 2.3). Comparing the method used by Uran *et al.* (60) with the method from Karlsson *et al.* (61), both PE/PC and PS/PI switched elution orders in spite of using the same column and TEA mobile-phase additive. The organic mobile-phase composition, however, was different for the two methods.

The many variables within each LC method make it difficult to pinpoint exactly which additive, stationary phase or organic modifier, is responsible for the specific elution order or retention behavior. A systematic approach to these questions has not been found in the literature. Furthermore, many LC-MS methods found in the literature cover only one or two specific phospholipid classes. Nevertheless, the different normal-phase LC-MS methods have demonstrated class separations enabling the identification of phospholipid species from many different biological sources.

A common characteristic feature of most published LC-MS methods for normal-phase phospholipid class separation is the low amount of water present. Still, these methods have proven to produce intact molecule-related ions of phospho-

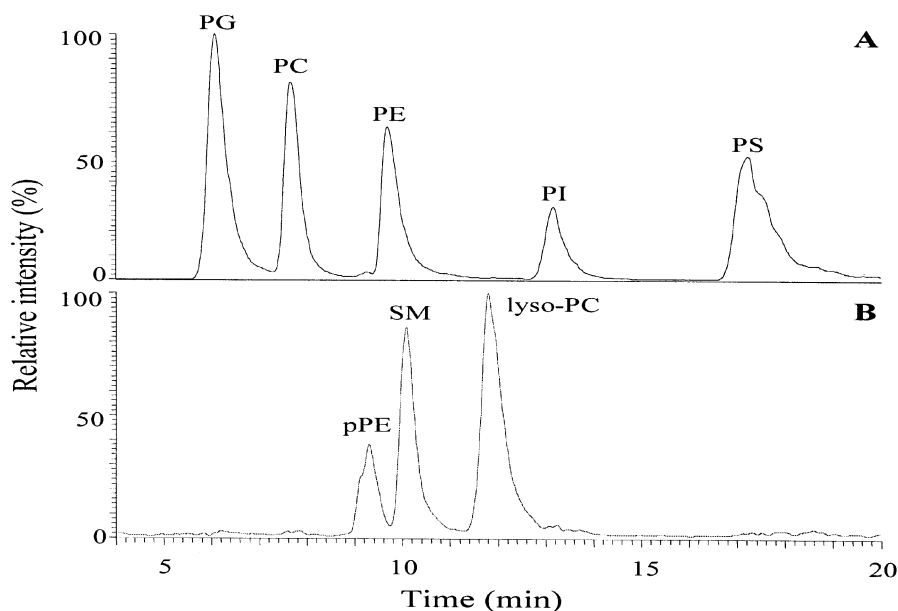


Fig. 2.2. Negative-ion HPLC-ESI-MS analysis of a phospholipid mixture (approx. 10 $\mu\text{g/mL}$ of each), obtained in the scanning mode. (A) The sum of mass chromatograms of DSPG, DSPC, POPE, PI, and PPS. (B) The sum of mass chromatograms of pPE, SM, and lyso-PC. *Source:* Reference 60. Reproduced with permission from the publisher (Elsevier).

lipids for API-MS. This could be related to the ionic nature of phospholipids, which makes the ionization/desolvation process in API-MS suitable for the production of ions in the gas phase.

In the case of a general screening for phospholipid species in biological materials, all classes and species are equally important and they occur in different absolute amounts. For on-line LC-MS, the chromatography necessary to obtain class identification do not always require baseline separation. Soft ionization techniques like electrospray ionization (ESI) or atmospheric pressure chemical ionization (APCI) produce mostly molecule-related ions from phospholipids. From a mass measurement point of view, their molecule-related ions (their protonated, deprotonated, or cation adduct ions) will be even-electron ions. This is in contrast to ionization methods based on electron ionization (EI), which gives almost exclusively odd-electron radical cations (M^+) in the positive-ion mode, to the extent that they give molecular ions. The practical consequence of dealing with even-electron molecule-related ions is that amine classes like PC, PE, and PS, which have odd molecular weights, will have even m/z values for their molecule-related ions. Due to the nitrogen rule, the non-amine-containing phospholipids (PA, PI, PG), which have even molecular weights,

will have odd molecule-related ions. Note that the nitrogen rule is based on the use of integer values for the atoms. This simple rule is particularly useful when amine and non-amine containing classes are only partially separated. This is indeed the case for the normal-phase LC method described by Hvattum *et al.* in 1998 (59), in which PE and PG are separated by only 0.16 minutes (Fig. 2.1). The even/odd molecule-related ions make it easier to distinguish the classes even if they elute closely. The report by Hvattum *et al.* also gives an example of how the structural specificity offered by MS can compensate for not always having sufficient chromatographic resolution between the compounds of interest. In many ways, this is the strength of combining the two dimensions represented by separation in time (LC) and molecular mass (MS). Furthermore, upon performing product-ion scans of each molecule-related ion, the species composition can be determined, allowing verification of the correct class assignment. The product-ion scan of a specific precursor gives ions that are unique for each particular species. The phospholipid class can be verified by comparison to calculated theoretical masses of molecule-related ions, since all classes have different molecular masses (of their ^{12}C isotope) for each given species. This ability to verify that a particular phospholipid species belongs to a specific class is an important feature of the LC-MS approach to phospholipid analysis, compared to other methods. Polar lipid extracts from biological materials would normally contain cholesterol species, and di- and triglycerides, together with sphingomyelins and other polar lipids, which could potentially interfere with the phospholipid class assignments. Hence, the ability to verify with MS/MS that a specific m/z value obtained in full-scan MS mode actually originates from a specific phospholipid species, and not from other polar lipids, is invaluable in phospholipid species characterization. The low detection limits obtained by MS detection also make it possible to determine the identities of phospholipid species that occur at low levels in a biological extract.

In most cases, the approach of using a class separation of complex biological extracts prior to MS detection would simplify the identification process. The alternative of doing direct infusion into the electrospray source of the mass spectrometer without prior separation would bring along some challenges; class determination would have to be obtained through diagnostic class-specific product ions. The presence of highly abundant ^{13}C molecule-related ions also undoubtedly complicates phospholipid class and species identification in complex biological extracts, when based solely on mass spectrometry. However, when dealing with a mixture of synthetic phospholipids, where the class and species complexity is dramatically reduced, direct mass spectrometric determination could be a time-saving and specific approach to species identification.

Reversed-Phase LC-MS. In contrast to normal-phase HPLC methods, reversed-phase chromatography can separate phospholipids according to the FA composition in the *sn*-1 and *sn*-2 positions. This approach is orthogonal to normal-phase LC methods. A reversed-phase LC-MS approach could be useful for the identification or quantification of synthetic phospholipids, where only one or a few specific

classes and species are involved. In such cases, it also opens the possibility for the use of other detectors like UV or evaporative light scattering detection.

For biological extracts, one possible approach is to do a class separation with isolation of the individual classes by normal-phase LC, followed by an orthogonal separation according to their FA compositions using reversed-phase LC-MS. This would allow identification of isobaric species within the same class. Phospholipid molecule-related ions exhibit isotopic patterns that are mainly due to the number of ^{13}C isotopes; for example, the m/z value of the ^{12}C molecule-related ion for 18:0/18:0 PS would be the same as that for the $2 \times ^{13}\text{C}$ isotope ion of 18:0/18:1 PS. This can be a challenge with normal-phase LC-MS, and particularly with direct infusion into electrospray ionization MS in cases where such isobaric overlap of isotopic masses occurs (60).

Many reversed-phase LC methods for phospholipids are described in the literature. However, as with normal-phase LC, many methods are not readily compatible with on-line electrospray ionization mass spectrometry or they involve derivatization, either pre- or post-column. LC-MS methods for PS species separations have been obtained by the use of C18, C30, and polystyrene/divinylbenzene LC columns (63). The mobile phase was adjusted to separate three synthetic PS species with MS and evaporative light scattering detection. Bovine brain PS species were also separated using the polystyrene/divinylbenzene LC column with the same mobile-phase (Fig. 2.4).

Temperature gradient elution using a 0.5 mm ID column has also been reported for improved sensitivity of PS species (64). Separation of isobaric PS species was obtained using this approach. Furthermore, an improvement in sensitivity by a factor of 20 was gained, compared to previously reported numbers obtained with conventional columns (64).

An HPLC separation of PC species has been reported by Vernooij *et al.* (65,66) using two different columns and mobile phases. A C8 column with a mobile phase consisting of methanol/water/formic acid gave partial separation of the main PC species (65). Another method, using electrospray ionization together with isocratic elution from a C18 column with a mobile phase consisting of methanol/acetonitrile/triethylamine, appeared to give improved peak shapes and resolution (66) (Fig. 2.5).

Another LC method was reported by Isaac *et al.* (67) using capillary chromatography with a mobile phase of methanol/tetrahydrofuran/0.1% formic acid for the separation of PC and sphingomyelin species from brain extracts. The use of capillary chromatography offers better sensitivity when only small amounts of tissues and cells are available.

Separation of oxidatively stressed PC species was done by Spickett *et al.* (68) by using a methanol/hexane/ammonium acetate mobile phase with isocratic elution. The column was a Luna Phenomenex C8, 1.0×150 mm and detection was by positive-ion ESI-MS. The oxidized PC species were detected as their monohydroperoxides and the LC separation was found to be essential for the detection of oxidized phospholipids, compared to direct infusion, for an extract of U937 cells.

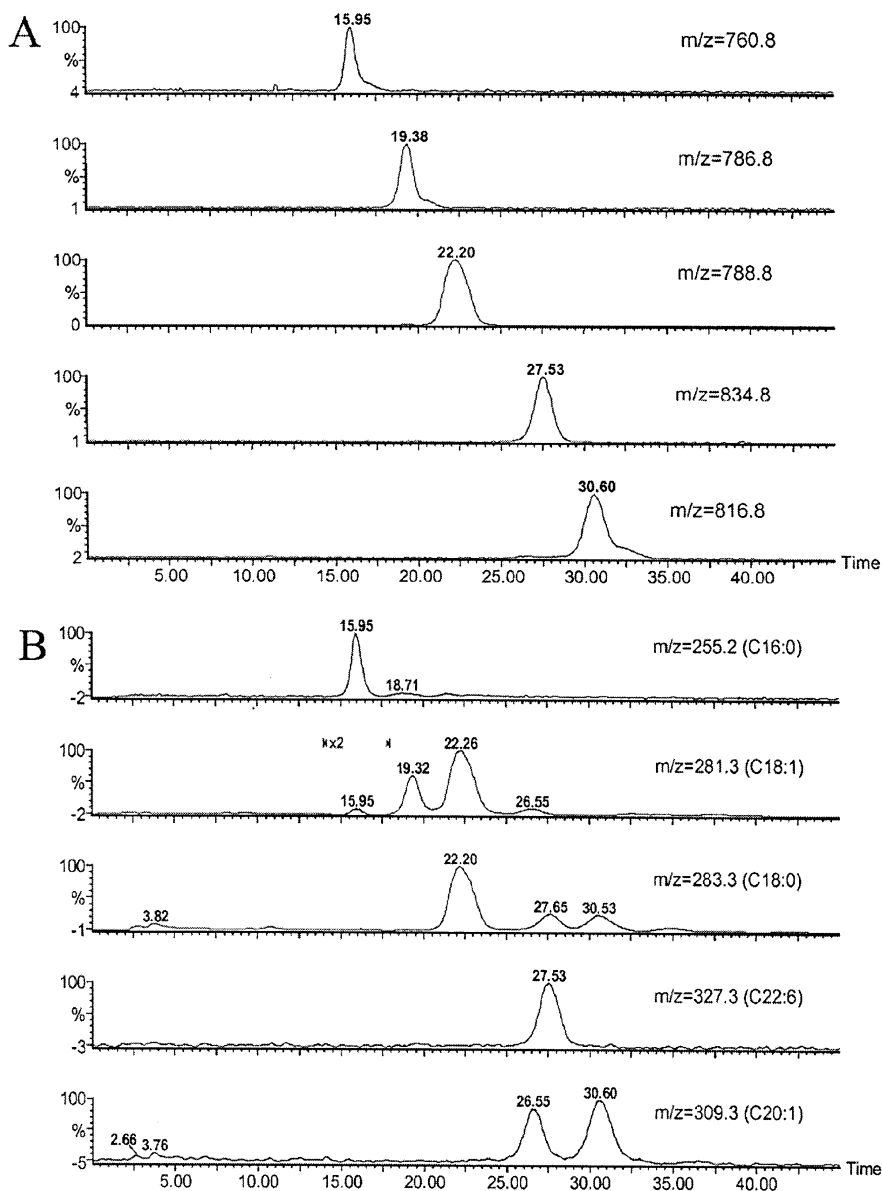


Fig. 2.4. HPLC-ESI-MS of bovine brain PS in negative-ion mode, using the PS/DVB column. Traces in (A): Mass chromatograms of deprotonated molecules (low cone voltage). Traces in (B): Mass chromatograms of the carboxylate anion fragments (high cone voltage). (A) and (B) were obtained in the same run alternating between high and low cone voltages. *Source:* Reference 63. Reproduced with permission from the publisher (Elsevier).

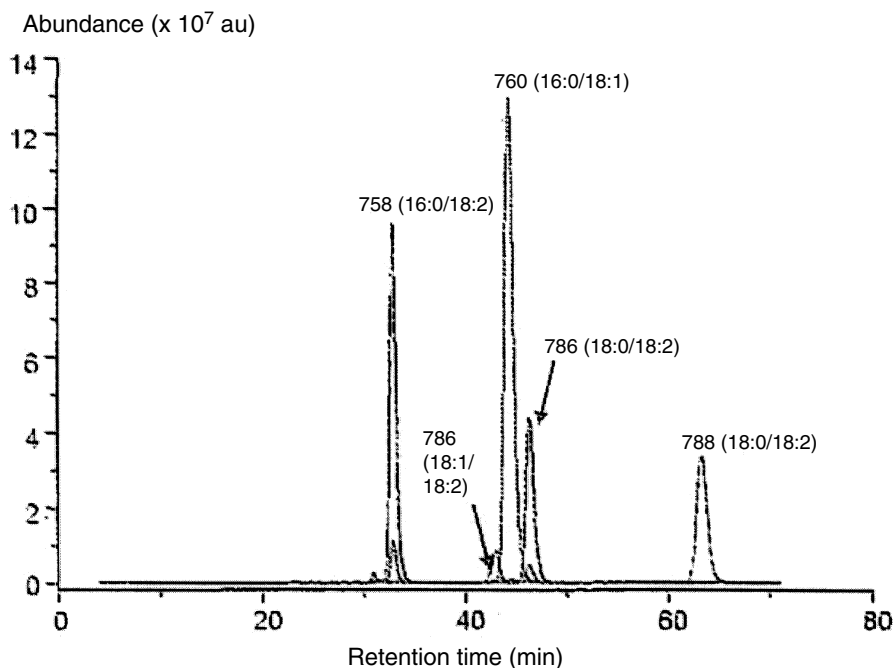


Fig. 2.5. Reconstituted ion chromatograms of $[M + H]^+$ ions of four representative molecule-related ions in egg phosphatidylcholine with RP-HPLC in combination with positive-ion ESI-MS. *Source:* Reference 66. Reproduced with permission from the publisher (John-Wiley & Sons, Ltd.).

Separation of PG species using negative-ion ESI detection has also been reported. However, the PG species were separated and detected as their *bis* (3,5-dinitrophenylurethane) derivatives (69). An octadecylsilane (ODS) LC column was used with a mobile phase consisting of methanol/water/ammonium hydroxide, with isocratic elution, for the separation of PG species in spinach leaves and *Escherichia coli*. One reported advantage of the derivatization method was that sensitive UV detection was possible together with species identification by LC-MS.

Species separations of PC, PE, and PI have been reported by Lee *et al.* and Kim *et al.* using positive- and negative-ion electrospray ionization MS detection (70,71). Both methods make use of C18 columns and ammonium hydroxide as a mobile-phase additive. While Kim *et al.* (71) report the use of a methanol/hexane/ammonium hydroxide mobile phase and gradient elution, the LC method described by Lee *et al.* (70) makes use of methanol/acetonitrile/ammonium acetate/ammonium hydroxide. From the determination of hydrogenated lecithin phospholipids in positive-ion mode, extensive sodiated molecule ions were detected. In negative-ion mode using collision-induced dissociation, deprotonated molecules with species-

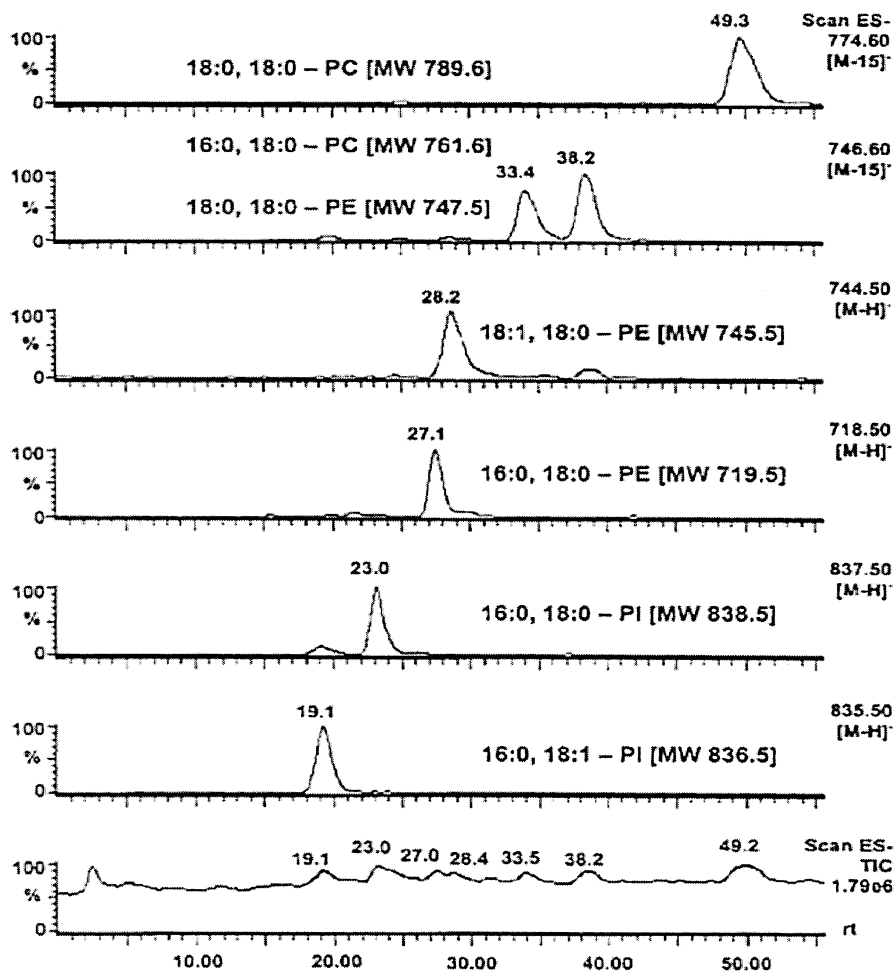


Fig. 2.6. Negative-ion chromatograms obtained from lecithin (2 μ g) by selectively monitoring deprotonated molecules or molecular adduct ions (CV=60 V). *Source:* Reference 70. Reproduced with kind permission from the publisher (John Wiley & Sons, Ltd.).

diagnostic carboxylate anions were reported (70). Both LC methods gave partial species separations of PC, PE, and PI species. However, as with the reversed-phase LC methods for PS, partial LC separation in combination with electrospray ionization MS detection proved to be sufficient for species determination (Fig. 2.6). The elution order for the phospholipid species separation appears to be the same for all methods. A species' retention time within a given class is determined by the FA chain lengths and the degree(s) of unsaturation; the more saturated the FA and the

longer their carbon chains, the longer the retention time of the species. However, if the sample contains more than one class, a mixture of class and species separation would potentially make the species identification more complicated than with the normal-phase class separation and LC-MS.

Electrospray Ionization Mass Spectrometry of Phospholipids

Electrospray Ionization Mass Spectrometry. The preferred atmospheric pressure ionization technique for phospholipids has emerged to be electrospray ionization (ESI) (72). Atmospheric pressure chemical ionization (APCI) has also been used to some extent, but the gentle formation of intact molecule-related ions facilitated by electrospray ionization has made ESI the preferred technique. Modern ion sources for ESI can accommodate chromatographic flow rates up to 1.0 mL/min. With these flow rates, post-column splitting is no longer essential, and both narrow-bore and standard columns can be used. ESI is a soft ionization technique and usually provides protonated or deprotonated molecules, depending on whether the analysis is carried out in positive- or negative-ion mode. In addition, molecular adducts usually provided by cations like Na^+ , K^+ , or NH_4^+ are fairly common. Other types of adducts might also appear, depending on the mobile phase used to introduce the compounds into the mass spectrometer. Due to the soft ionization with ESI-MS, little structural information is generally obtained. In-source fragmentation can be achieved and thus detected by single-stage MS. However, MS/MS is normally required for complex mixtures of classes and species. There are several MS/MS configurations available but the most frequently used are triple quadrupole and ion-trap instruments. In addition, quadrupole time-of-flight (Q-TOF), magnetic sector instruments, and Fourier transformed ion cyclotron resonance (FT-ICR) instruments are all available with electrospray ionization sources. The cost of the latter instruments prohibits them from yet becoming standard in most laboratories.

ESI-MS of Phosphatidylcholine. Phosphatidylcholine (PC) is the major phospholipid class in mammalian membranes. PC contains a quaternary nitrogen atom with a fixed positive charge and more readily forms positive than negative ions by electrospray ionization. It therefore provides substantial $[\text{M} + \text{H}]^+$ ions. The fragmentation of protonated molecules of PC, either through in-source fragmentation or collision-induced dissociation (CID), is dominated by a prominent ion at m/z 184, representing the protonated phosphocholine head group, $[(\text{CH}_3)_3\text{N}^+\text{C}_2\text{H}_4\text{OP}(\text{OH})_2\text{O}]^+$ (70,73–76) (Fig. 2.7A). The m/z 184 fragment ion is a diagnostic ion for protonated phosphatidylcholine species (70). Ions yielding structural information of the molecular species are, however, of low abundance in the product-ion spectra of protonated phosphatidylcholines (75). The pathway for the formation of the fragment ion at m/z 184 has been extensively studied. Using perdeuterated fatty acyl substituents, it has been found that the hydrogen participating in the formation of the m/z 184 most likely arises from the α -hydrogens of the fatty acyl chains (75).

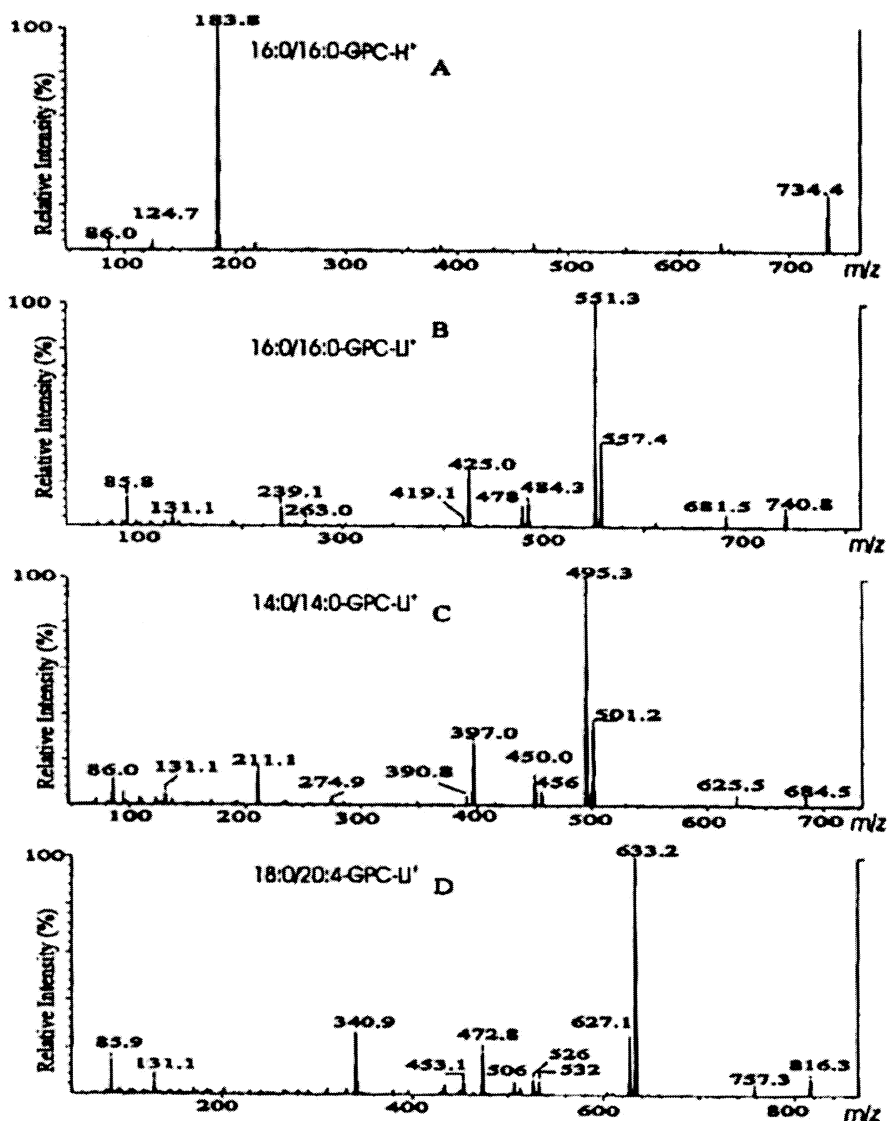


Fig. 2.7. Positive-ion ESI tandem mass spectra of cationic adducts of standard phosphatidylcholine species. The panels are tandem mass spectra obtained from CID of the $[M + H]^+$ ion of dipalmitoyl-PC (panel A), the $[M + Li]^+$ ion of dipalmitoyl-PC (panel B), the $[M + Li]^+$ ion of dimyristoyl-PC (panel C), or the $[M + Li]^+$ ion of (1-stearoyl, 2-arachidonoyl)-PC (panel D). Using panel D as an example, the production spectrum shows ions at m/z 757 ($[M + Li - 59]^+$); m/z 633 ($[M + Li - 183]^+$); m/z 473 ($[M + Li - 59 - R_1COOH]^+$), and m/z 453 ($[M + Li - 59 - R_2COOH]^+$). Source: Reference 74. Reproduced with kind permission from the publisher (Elsevier).

In contrast to the protonated molecules of phosphatidylcholines, the product ion spectra generated by CID of lithiated adducts of PC species ($[M + Li]^+$) yield fragment ions that permit assignment of the identities and positions of FA substituents (58,74,75,77) (Fig. 2.7B–D). Hsu *et al.* have extensively studied the CID fragmentation of lithiated adducts of PC (74,75). The suggested fragmentation pathway starts with a neutral loss of trimethylamine ($[M + Li - 59]^+$) followed by an additional loss of *O,O'*-dimethylenephosphoric acid or lithium *O,O'*-dimethylenephosphate to yield prominent diglyceride-like fragment ions at $[M + Li - 183]^+$ and $[M + Li - 189]^+$, respectively. Corresponding fragment ions have also been found for sodiated PC (78).

The $[M + Li]^+$ ions of PC are also fragmented by the neutral losses of the FA moieties in either the *sn*-1 or *sn*-2 positions. These fragments identify the FA substituents in a given PC species. Among the ions that permit the structural identification are $[M + Li - R_xCOOH]^+$ and $[M + Li - 59 - R_xCOOH]^+$ ($x = 1,2$) ions (74,75). However, they appear as minor fragment ions in the product-ion spectra of PC species when using triple quadrupole MS, and they may therefore be difficult to detect when analyzing PC species of low abundance (Fig. 2.7D). Fragments representing the neutral losses of the lithium salts of the free FA ($[M + Li - R_xCOOLi]^+$) from both the *sn*-1 and *sn*-2 positions are also observed from lithiated PC species (74,75). With a polyunsaturated *sn*-2 substituent, fragment ions consistent with the net elimination of the lithiated polar head group and loss of the *sn*-2 substituent as a substituted ketene have also been shown (74). The relative abundances of the ions reflecting neutral losses of the FA substituents from lithiated PC species have been used as an indication of the positions of these substituents. Positional isomers of PC standards have been examined and the results indicate that the abundances of the ions reflecting a loss of the *sn*-1 substituent ($[M + Li - R_1COOH]^+$ and $[M + Li - 59 - R_1COOH]^+$) exceed those of the ions reflecting a loss of the *sn*-2 substituent ($[M + Li - R_2COOH]^+$ and $[M + Li - 59 - R_2COOH]^+$) (74). Using deuterium labeled analogs of PC, it has been shown that the α -hydrogens of the FA substituents participate in the fragmentation process leading to the $[M + Li - R_xCOOH]^+$ and $[M + Li - 59 - R_xCOOH]^+$ ions (75). The preferential loss of the *sn*-1 substituent has been ascribed to the α -hydrogens of the *sn*-2 fatty acyl chain being more labile than those at *sn*-1. Thus, an α -hydrogen of the *sn*-2 fatty acyl chain has been suggested to preferentially participate in the fragmentation process leading to a favored neutral loss of the *sn*-1 substituent (75).

PC can also appear as plasmanyl-PCs (1-*O*-alkyl-2-acyl-*sn*-glycero-3-phosphocholines) and plasmenyl-PCs (1-*O*-alk-1'-enyl-2-acyl-*sn*-glycero-3-phosphocholines). Hsu *et al.* (79) have characterized the fragmentation of these ether phospholipids by ESI-MS. Protonated plasmanyl- and plasmenyl-PC species yield mainly the protonated phosphocholine head group at m/z 184 from CID (i.e., the same fragment as found from protonated diacyl-PC). Consequently, structural characterization of the ether phospholipids from the protonated adducts is not feasible. As with the diacyl-PCs, one has to turn to the lithiated adducts of the ether

phospholipids for structural characterization of these compounds in the positive-ion mode (79). The product-ion spectra of the $[M + Li]^+$ ions of plasmanyl- and plasmenyl-PCs show no ions corresponding to $[M + Li - R_2COOH]^+$, and the $[M + Li - 59 - R_2COOH]^+$ ions are of low abundance. This, together with an increased abundance of the $[M + Li - 59]^+$ ion, readily distinguishes the plasmanyl- and plasmenyl-PCs from the diacyl-PCs. The FA substituent at *sn*-2 is identified by fragment ions corresponding to $[M + Li - R_2COOHLi]^+$ for both plasmanyl- and plasmenyl-PC. The product-ion spectra of lithiated plasmenyl-PCs also contain a prominent ion corresponding to $[M + Li - 183 - R_2COOH]^+$, which permits their differentiation from plasmanyl PCs (75,79).

Scanning for parents that undergo losses of the head-group or a component of the head-group will identify PC (or sphingomyelin) species as lithiated adducts by ESI-MS/MS in a crude phospholipid extract. The combination of three neutral loss scans, (i.e., neutral loss of 189, 183, and 59 amu), identifies both glycerolipid and sphingolipid parents that contain the phosphocholine head-group in a phospholipid mixture (74). After determination of the phosphocholine-containing species, product-ion scans of the individual species yield fragment ions that facilitate the assignment of the FA composition of the PC species. Finally, the position of the FA substituents can be determined as suggested above; i.e., based on the relative intensities of the fragment ions resulting from the neutral losses of R_1COOH and R_2COOH .

Using positive-ion ESI-MS/MS, structural information of the PC species appears to be best achieved with lithiated adducts of the species. In order to form these adducts, a LiOH solution (or other Li^+ -containing solution) must be added to the phospholipid extract prior to infusion of the mixture into the ESI source. In order to perform HPLC separation of the phospholipid classes prior to on-line MS analysis, the LiOH solution must therefore be added to the mobile phase either pre- or post-column. Examples in the literature of on-line LC-MS/MS analysis of lithiated PC species are, as far as the authors know, not available.

Many classes of phospholipids possess a net negative charge at neutral pH. Accordingly, negative-ion ESI mass spectra of these phospholipids can be efficiently obtained, which exhibit primarily $[M - H]^-$ ions. However, phosphatidylcholine, phosphatidylethanolamine, and sphingomyelin are zwitterionic molecules and, therefore, both positive- and negative-ion mass spectra of these phospholipid classes are accessible through ESI-MS. However, phosphatidylcholines and sphingomyelins are more efficiently analyzed in the positive-ion mode as the sodiated ion complex under normal analysis conditions (80). Negative-ion ESI-MS analysis of PC yields mass spectra containing different molecule-related ions of PC. Some report a chlorine adduct of PCs (i.e., $[M + Cl]^-$) as the base peak, especially when excess chloride is added to an infusion solution (78,81,82). Another abundant PC molecule-related ion is $[M - 15]^-$, which is due to a loss of CH_3 from the choline head group (60,76,78,83,84). Furthermore, if formic acid is used as a mobile-phase additive, the PC species can form formate adducts; i.e., $[M + 45]^-$ (60,85). It has

been reported that CID of the $[M + Cl]^-$ and $[M + 45]^-$ adduct ions produces the $[M - 15]^-$ product ion (60,78,81,82). When HPLC is coupled on-line with electro-spray ionization MS, most mobile phases readily give rise to either the $[M - 15]^-$ or the $[M + 45]^-$ molecule-related ions (60,61,70,76,82–84). Normal-phase LC separation of a phospholipid mixture offers the advantage of phospholipid class separation prior to MS determination of the individual species. The PC species are generally identified by their retention times in the chromatogram. CID of individual molecule-related ions of PC yields product ions that readily identify the species. Following CID, the $[M - 15]^-$ ions of PC yield three major series of fragments: (i) neutral losses of the *sn*-1 and *sn*-2 substituents as FA ($[M - 15 - R_1COOH]^-$ and $[M - 15 - R_2COOH]^-$); (ii) neutral losses of the *sn*-1 and *sn*-2 substituents as ketenes ($[M - 15 - R_1'CH=C=O]^-$ and $[M - 15 - R_2'CH=C=O]^-$); and (iii) the *sn*-1 and *sn*-2 carboxylate anions (R_1COO^- and R_2COO^-) (78) (Fig. 2.8a). Both the lysophospholipid-like fragments and the carboxylate anions might be used for species determination. Using triple quadrupole mass spectrometers, the carboxylate anions are abundant fragments in the product-ion spectra of the diacyl-PC species (78,82,83). However, the lysophospholipid-like fragments are preferred for species determination with ion-trap MS, due to the lower abundance of the car-

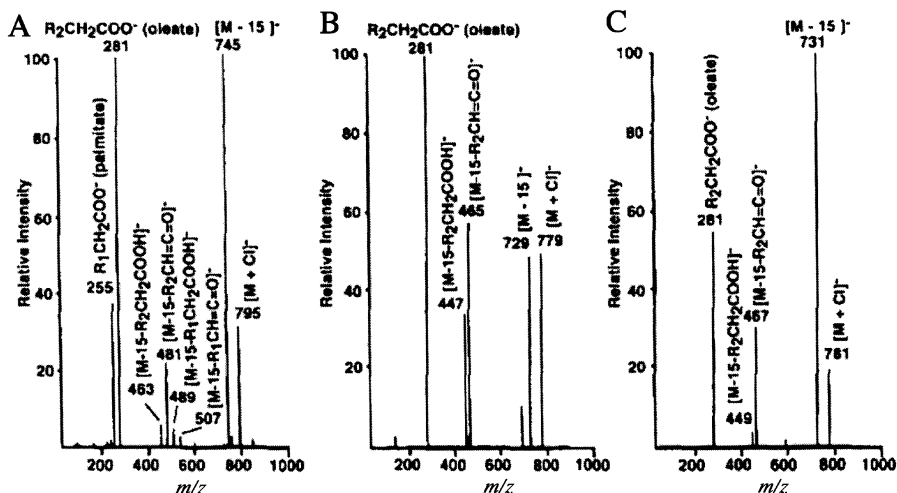


Fig. 2.8. Negative-ion ESI tandem mass spectra of the chlorine adducts of phosphatidylcholines. (A) ESI-MS/MS of the chlorine adduct of 1-hexadecanoyl-2-octadec-9'-enyl-*sn*-glycero-3-phosphocholine. (B) ESI-MS/MS of the chlorine adduct of 1-*O*-(*Z*)-hexadec-1'-enyl-2-octadec-9'-enyl-*sn*-glycero-3-phosphocholine (plasmenyl-PC). (C) ESI-MS/MS of the chlorine adduct of 1-*O*-hexadecyl-2-octadec-9'-enyl-*sn*-glycero-3-phosphocholine (plasmanyl-PC). Each phosphatidylcholine (1 pmol/mL) was dissolved in 1:2 chloroform-methanol with the addition of 1 μ mol/mL of NaCl. *Source:* Reference 78. Reproduced with kind permission from the publisher (Elsevier).

boxylate anions (60,82). The relative abundances of the carboxylate anions obtained after CID have been used for regiospecific assignment of the acyl moieties in asymmetrical PC species.

It has been reported that the intensity of the carboxylate anion derived from the *sn*-2 acyl substituent is greater than the corresponding carboxylate anion from the *sn*-1 acyl substituent (76,78) (Fig. 2.8a). However, this is very much dependent on the collision energy and on the chain length and degree of unsaturation of the fatty acyl substituent in the *sn*-2 position (83,84). Therefore, the regiospecificity of the acyl chains, determined from the relative intensities of the carboxylate anions, should be treated with some caution. For a positive determination of the regiospecific position based on the carboxylate ion intensities, the use of regiospecific standards is recommended.

The plasmanyl-PCs (1-*O*-alkyl-2-acyl-*sn*-glycero-3-phosphocholines) and plasmenyl-PCs (1-*O*-alk-1'-enyl-2-acyl-*sn*-glycero-3-phosphocholines) can also readily be determined with negative-ion ESI-MS. The molecule-related ions are similar to those reported for diacyl-PC. The product-ion spectra of both plasmanyl- and plasmenyl-PC contain product ions that identify the FA in the *sn*-2 position; i.e., product ions corresponding to $[M - 15 - R_2COOH]^-$, $[M - 15 - R'_2CH=C=O]^-$, and R_2COO^- (78) (Fig. 2.8b-c). However, the relative abundances of these product ions have been reported to be different from those observed for the diacyl-PC species (78).

ESI-MS of Sphingomyelins. Sphingomyelins (SM, ceramide phosphocholines) are significant components of many mammalian membranes and are important constituents of nervous tissue and blood. They consist of an *N*-acyl FA linked to a long-chain hydrocarbon and have a phosphorylcholine head group. The base peaks in the mass spectra of sphingomyelins, analyzed with positive-ion ESI-MS, have been reported to be both $[M + H]^+$ ions (85,86) and $[M + Na]^+$ ions (78). As with PC, the major fragment ion after CID of protonated sphingomyelins is the protonated phosphocholine ion at m/z 184 (85,86). With ESI-MS in the negative-ion mode, the $[M - CH_3]^-$ ion was reported to be the major ion (86). However, when the negative-ion ESI-MS analysis was performed in the presence of chloride ions, a predominant chlorine adduct ion ($[M + Cl]^-$) was obtained (78). However, very little structural information from the sphingomyelins is obtained with ESI-MS. Atmospheric pressure chemical ionization (APCI) in the positive-ion mode has been reported to be more useful for the structural characterization of these compounds (86). The reason is that APCI yields more extensive in-source fragmentation of the sphingomyelins, to give ceramide-like product ions. With the ceramide ions as precursors, fragment ions representative of the long-chain base and the FA parts are detected in the product-ion spectra (86). Sphingomyelin species have also been characterized as their lithiated adducts using ESI-MS in the positive-ion mode (87). Under low-energy CID, the product-ion spectra have been reported to give abundant fragment ions representative of both the long-chain base and the FA, which permit determination of the structure (87).

ESI-MS of Phosphatidylethanolamine (PE). The phosphatidylethanolamine (PE) molecule is zwitterionic, and thus positive- and negative-ion mass spectra are both accessible through ESI-MS. Negative-ion ESI-MS mass spectra of PE contain only the $[M - H]^-$ ion and are stated to be far more sensitive than positive-ion spectra of PE by ESI-MS (80). The main molecule-related ion of PE by positive-ion ESI-MS is reported to be the $[M + H]^+$ ion (85). Sodiated adducts of PE have also been reported (78). Lithiated adducts of PE similar to the lithiated adducts of PC can be obtained by addition of LiOH to the infusion solution (88). The protonated molecules of PE species yield major fragment ions of $[M + H - 141]^+$, by loss of the polar head group after CID (85,89) (Fig. 2.9A). In addition, a fragment ion at $[M + H - 181]^+$ and a corresponding m/z 181 ion have also been reported (85). For protonated PE species, structural information is not available regarding the identities of the FA moieties and their positions in the glycerol backbone (89).

Han and Gross (78) reported the characterization of PE as its sodiated molecular species ($[M + Na]^+$) by ESI-MS/MS. CID of the sodiated adduct yielded multiple product ions, including: neutral loss of the vinyl amine to form the sodiated phosphatidic acid ($[M + Na - 43]^+$); neutral loss of the five-member amidophosphane ($[M + Na - 123]^+$); and two fragments reported to be diglyceride-like ions; i.e., $[M + Na - 141]^+$ and $[M + Na - 163]^+$ (78). The fragment ion at $[M + Na - 163]^+$ was reported to be equivalent to the fragment ion at $[M + H - 141]^+$, found after CID of protonated PE species. In addition to fragment ions resulting from neutral loss of the polar head group (or parts of it), fragment ions arising from neutral losses of the acyl groups were also found, although at low abundances. The neutral losses of the acyl groups were believed to arise from the sodiated phosphatidic acid fragment ion at $[M + Na - 43]^+$, via formation of a five- or six-member phosphodiester (78). The resulting fragment ions were consequently either $[M + Na - 43 - R_1COOH]^+$ or $[M + Na - 43 - R_2COOH]^+$. These two product ions provide information about the regioselectivity of *sn*-1 and *sn*-2 constituents of PE. However, the relative abundances of these ions were fairly low and no report on the optimization of the MS parameters (e.g., increasing the collision energy to increase the relative abundances of these fragment ions) was given.

The characterization of PE species as their lithiated adducts by ESI-MS/MS has been extensively studied by Hsu and Turk (88). Upon adding LiOH (or LiOAc) to the infusion solution, PE generated both a monolithiated molecular adduct ion, $[M + Li]^+$, and a dilithiated molecular adduct ion, $[M - H + 2Li]^+$, by ESI. The abundances of these two ions were dependent on the concentration of the lithium salt added.

Both monolithiated and dilithiated PE were reported to give fragment ions elucidating the structures of the PE species. Only the fragmentation of monolithiated PE will be covered in this text. CID of the $[M + Li]^+$ ion yields fragment ions that are indicative of the phosphoethanolamine head group and are thus characteristic for the PE class. The fragment ions are $[M + Li - 43]^+$, $[M + Li - 141]^+$, and $[M + Li - 147]^+$, representing neutral losses of ethylenimine (CH_2CH_2NH), $(HO)_2P(O)$

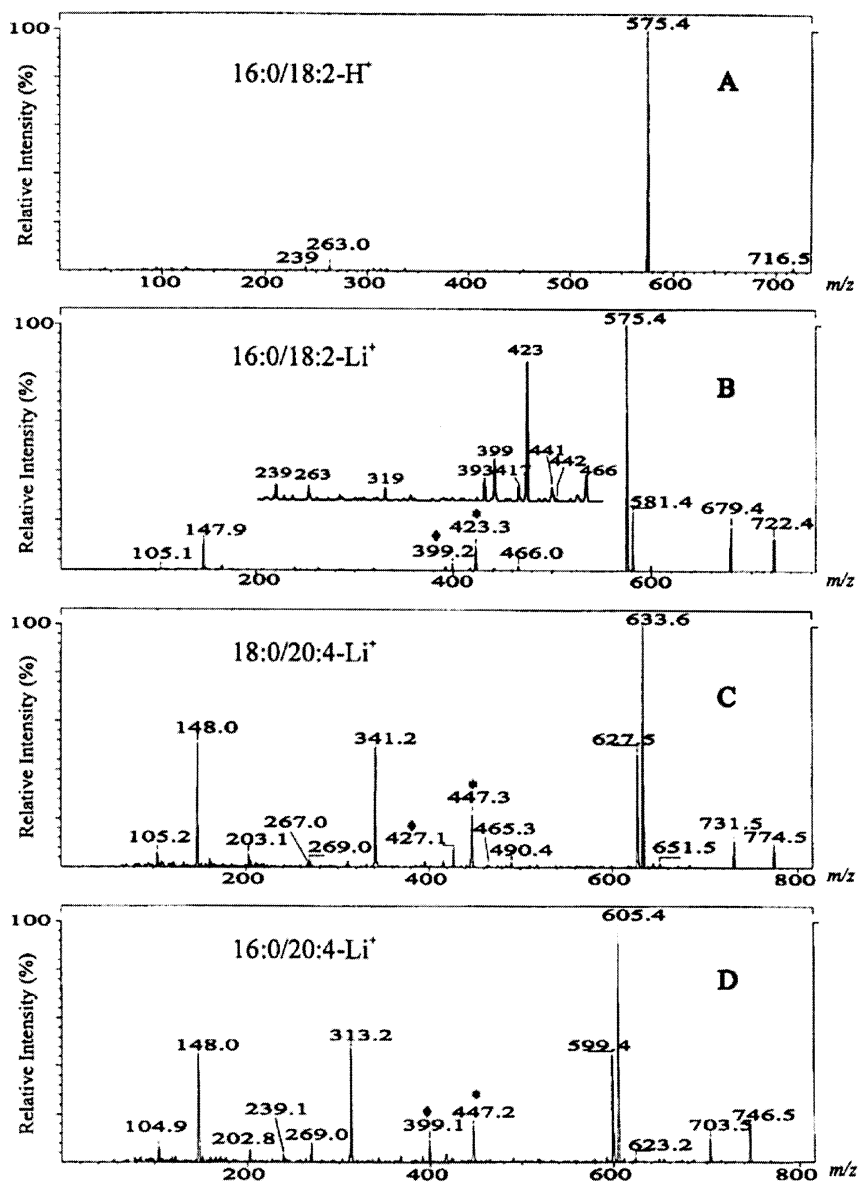


Fig. 2.9. Positive-ion ESI tandem mass spectra of (A) protonated 16:0/18:2-PE, (B) lithiated 16:0/18:2-PE, (C) lithiated 18:0/20:4-PE, and (D) lithiated 16:0/20:4-PE. * $[M + Li - 43 - R_1COOH]^+$ ion, reflecting loss of the FA at *sn*-1; \blacklozenge $[M + Li - 43 - R_2COOH]^+$ ion, reflecting loss of the FA at *sn*-2. The abundance of the former ion is higher than that of the latter, resulting in structural identification. *Source:* Reference 88. Reproduced with permission from the publisher (John Wiley & Sons, Ltd.).

$(\text{OCH}_2\text{CH}_2\text{NH}_2)$, and $(\text{LiO})(\text{HO})\text{P}(\text{O})(\text{OCH}_2\text{CH}_2\text{NH}_2)$, respectively (88) (Fig. 2.9B–D). The two latter ions are consequently diglyceride-like ions and the fragment ions arising from different losses of the polar head group of lithiated PE are similar to those obtained with sodiated PE (see above). The product-ion spectrum of $[\text{M} + \text{Li}]^+$ also contains ions representing the neutral losses of the *sn*-1 and *sn*-2 FA, at $[\text{M} + \text{Li} - \text{R}_1\text{COOH}]^+$ and $[\text{M} + \text{Li} - \text{R}_2\text{COOH}]^+$, respectively, although at low abundances. Under the given conditions, ions arising from the combined losses of ethylenimine and *sn*-1 and *sn*-2 FA, at $[\text{M} + \text{Li} - 43 - \text{R}_1\text{COOH}]^+$ and $[\text{M} + \text{Li} - 43 - \text{R}_2\text{COOH}]^+$, respectively, were also observed and were more abundant than the fragment ions representing the losses of *sn*-1 and *sn*-2 fatty acids from lithiated PE (Fig. 2.9B–D). The ions arising from the combined losses of ethylenimine and *sn*-1 and *sn*-2 FA seem, therefore, more favorable for structural assignment of the PE species. In addition, the relative abundances of the two ions differ such that the ion arising from the loss of ethylenimine and the *sn*-1 FA was more abundant than the similar ion arising from the loss of ethylenimine and the *sn*-2 FA. This suggests that the relative abundances of these ions may indicate the positions of the FA substituents under the given conditions (88). In addition to the above-mentioned fragment ions from lithiated PE, the product-ion spectrum also exhibited ions arising from the combined losses of ethylenimine and the FA as ketenes and a relatively abundant ion at *m/z* 148, representing a lithiated ethanolaminephosphate (Fig. 2.9B–D). The latter fragment ion is, therefore, also characteristic for PE species. The authors also reported a specific fragment ion for PE species containing arachidonic acid in the *sn*-2 position, namely a fragment ion arising from the neutral loss of 433 amu, which is equivalent to the combined losses of $(\text{LiO})(\text{HO})\text{P}(\text{O})(\text{OCH}_2\text{CH}_2\text{NH}_2)$ and the *sn*-2 arachidonic acid as a ketene (88). This ion was prominent for PE species containing arachidonic acid in the *sn*-2 position. It was not reported whether or not equivalent fragment ions were found for PE species containing other long-chain unsaturated FA in the *sn*-2 position. Based on the above-mentioned fragments for lithiated PE, the authors proposed a scheme for identification of PE molecular species *via* constant neutral loss scans. Specifically, constant neutral loss scans of 147 amu and 43 amu identify the PE species and, in addition, constant neutral loss scanning of 433 amu identifies the PE species containing arachidonic acid in the *sn*-2 position.

The advantages of using lithiated adducts of PE for structural characterization by ESI-MS have been reported to include increased abundances of the $[\text{M} + \text{Li}]^+$ ions, compared to the low abundances of the $[\text{M} + \text{Na}]^+$ ions, and abundant fragment ions after CID of the $[\text{M} + \text{Li}]^+$, compared to the limited structural information obtained from sodiated adducts (88). However, the use of transition metal ion complexes for structural analysis of PE species has also been reported (90). These PE metal ion complexes gave the same neutral losses as those reported with lithiated PE. Particularly, the cobalt (II) ion complex of PE yielded abundant lysophospholipid-like fragment ions that allowed straightforward assignment of the FA moieties of PE (90).

Lithiated adducts of plasmeyl-PEs (1-*O*-alk-1'-enyl-2-acyl-*sn*-glycero-3-phosphoethanolamines) have also been characterized by ESI-MS/MS (88). In addition to fragment ions arising from the neutral loss of the phosphoethanolamine head group (or parts of it), the product-ion spectrum also shows two fragment ions that confirm the identities of the plasmeyl-PE species. One of these fragment ions arises from the combined losses of ethylenimine and the *sn*-1 alk-1'-enyl chain as an alcohol. The other arises from the combined losses of (LiO)(HO)P(O)(OCH₂CH₂NH₂) and the *sn*-2 FA. Based on these fragment ions, the identities of the alkenyl ether at *sn*-1 and the FA at *sn*-2 can be determined (88). As far as we know, structural characterization of PE species as their lithiated adducts in combination with LC-ESI/MS has not been reported.

As reported by Han and Gross (80), negative-ion ESI-MS mass spectra of PE contain mainly the [M - H]⁻ ion. Moreover, there are several reports on the combination of on-line HPLC and negative-ion ESI-MS for determination of PE species (60,61,82–84). According to Han and Gross (78) and as illustrated in Figure 2.10, the most abundant product ions in negative-ion ESI-MS/MS of deprotonated PE are the carboxylate anions. This has also been observed by other authors (82). In addition to the carboxylate anions, lysophospholipid-like product ions can also be observed. These correspond to the neutral loss of the fatty acyl ketene and/or the FA from the *sn*-1 and *sn*-2 positions (78,82) (Fig. 2.10).

The dominating product ions after CID with ion-trap mass spectrometry are the lysophospholipid-like ions. This is in contrast to CID with a triple quadrupole mass spectrometer, where the dominating product ions are the carboxylate anions, and lysophospholipid-like ions are virtually undetectable (82). The carboxylate anions and the lysophospholipid-like ions can, accordingly, be used for structural assignment of the PE species (60,78,81–85). Identification of the PE phospholipid class can be provided with on-line normal-phase chromatography prior to MS detection (60,82–84), or by using low-mass, class-characteristic product ions (78,81,82). For deprotonated PE, these product ions have been observed at *m/z* 214 (82), *m/z* 196 (78,81,82), and *m/z* 140 (81,82); i.e., product ions corresponding to [CH₂(OH)CH(OH)CH₂PO₄CH₂CH₂NH₂]⁻, [CH₂C(OH)CH₂PO₄CH₂CH₂NH₂]⁻, and [HPO₄CH₂CH₂NH₂]⁻, respectively. These product ions of deprotonated PE are, however, only found at very low abundances using a triple quadrupole instrument (Fig. 2.10).

The abundance ratio of the *sn*-1 to *sn*-2 carboxylate anions has been used for regiospecific assignment of the acyl moieties of PE species (78,81). However, this abundance ratio is very much dependent on the collision energy, and on the chain length and degree of unsaturation of the *sn*-2 FA (83,84). Therefore, for a positive determination of the regiospecific position based on the carboxylate ion intensities, the use of regiospecific standards is recommended.

Negative-ion ESI-MS of plasmeyl-PE also yields prominent [M - H]⁻ ions (58). The product-ion spectrum, obtained after CID of deprotonated plasmeyl-PE, has been reported to contain a prominent carboxylate anion arising from the *sn*-2

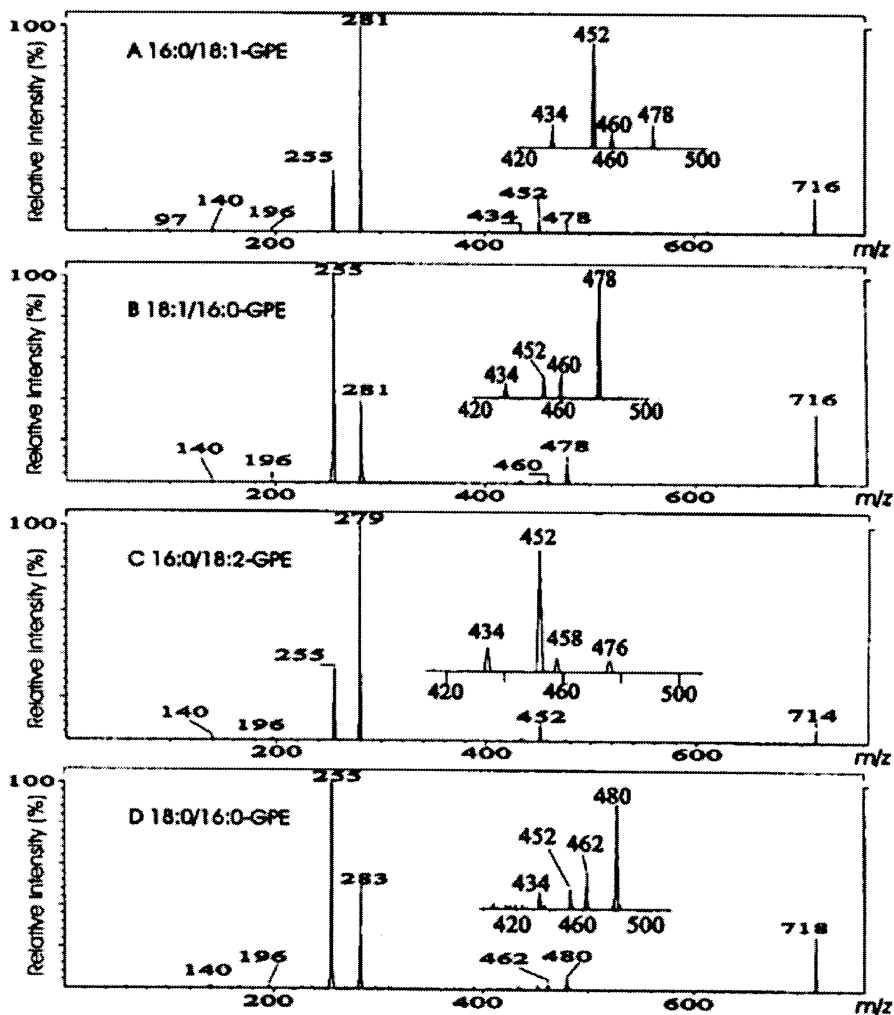


Fig. 2.10. Negative-ion ESI tandem mass spectra of $[M - H]^-$ ions of (A) 16:0/18:1-PE, (B) 18:1/16:0-PE, (C) 16:0/18:2-PE, and (D) 18:0/16:0-PE. Using panel (A) as an example, the product-ion spectrum shows ions at m/z 478 ($[M - H - R'_1CH=C=O]^-$); m/z 452 ($[M - H - R'_2CH=C=O]^-$); m/z 281 ($[R_2COO]^-$), and m/z 255 ($[R_1COO]^-$). Source: Reference 95. Reproduced with permission from the publisher (Elsevier).

fatty acyl group. In addition, ions reflecting the neutral loss of the *sn*-2 fatty acyl chain as a free FA or as a ketene are also reported (58). However, it has been stated that since negative-ion ESI-MS/MS analysis of plasmeyl-PE only gives information of the *sn*-2 carboxylate anion, confirmation of the structure should be verified by a comparison of the PE mass spectra before and after the removal of the plas-

menyl-PEs by acid treatment (58,88). The reason for this is that differentiation between plasmenyl-PE and 1-*O*-alkyl-ether PE species is not possible based solely on the product-ion spectrum, and mild acid hydrolysis will selectively hydrolyze the labile 1-*O*-alk-1'-enyl bond, thereby reducing the abundance of the plasmenyl-PE species (58,89).

ESI-MS of Phosphatidylinositol (PI). Phosphatidylinositols (PI) are phospholipids with an inositol head group and are widely distributed in nature. In addition to PI, two more highly phosphorylated molecules, phosphatidylinositol-4-phosphate and phosphatidylinositol-4,5-bisphosphate, are common in animal tissues. However, only ESI-MS of PI will be described in this text. Kerwin *et al.* (85) reported that positive ESI-MS yielded both sodium and proton adducts of PI; however, they found that the negative ESI-MS mass spectra were easier to interpret. Consequently, PI are mainly characterized by negative-ion ESI-MS. Hsu and Turk (91) have extensively studied the fragmentation processes of PI using ESI-MS with a triple quadrupole instrument. Negative-ion ESI-MS yields abundant $[M - H]^-$ ions of PI species. Following CID, the $[M - H]^-$ ions yield three major series of fragment ions that reflect: (i) neutral losses of the *sn*-1 and *sn*-2 substituents as FA ($[M - H - R_1COOH]^-$ and $[M - H - R_2COOH]^-$); (ii) neutral loss of the *sn*-1 and *sn*-2 substituents as ketenes ($[M - H - R_1'CH=C=O]^-$ and $[M - H - R_2'CH=C=O]^-$); and (iii) *sn*-1 and *sn*-2 fatty carboxylate anions (R_1COO^- and R_2COO^-) (Fig. 2.11). The ions reflecting neutral losses of the *sn*-2 substituents (as a FA and a ketene) are more abundant than those ions reflecting neutral losses of the analogous substituents at the *sn*-1 position. This has been proposed to permit assignment of the positions of the FA moieties (91). However, these diagnostic ions are not very abundant (Fig. 2.11).

PIs also exhibit abundant fragment ions representing the loss of the inositol group from the lysophospholipid-like ions; i.e., $[M - H - R'_xCH=C=O - \text{inositol}]^-$ (or at the same *m/z* value, $[M - H - R_xCOOH - (\text{inositol} - H_2O)]^-$). Furthermore, CID of the $[M - H]^-$ ion of PI yields several product ions that reflect the inositol polar head group; e.g., at *m/z* 223, 241, 259, 297 and 315 (Fig. 2.11). The detailed mechanisms for the formation of these product ions have been studied by Hsu and Turk (91) and will not be discussed in this text. In contrast to the other class-specific ions, the product ion at *m/z* 241 is especially abundant in the product-ion spectra of PI. Precursor ion scanning of *m/z* 241 or the other ions representing the inositol polar head group, can be utilized to selectively identify PI species in a phospholipid mixture or, when using normal-phase class separation prior to ESI-MS detection, to confirm the retention time of the PI species.

At the collision energies used in the study of Hsu and Turk, the product ions representing the carboxylate anions were the two most prominent ions in the tandem spectrum (91) (Fig. 2.11). The carboxylate anions can therefore readily be used for assignment of the PI species present in a phospholipid mixture (61,83,84). However, studies of the relative abundances of the *sn*-1 and *sn*-2 carboxylate

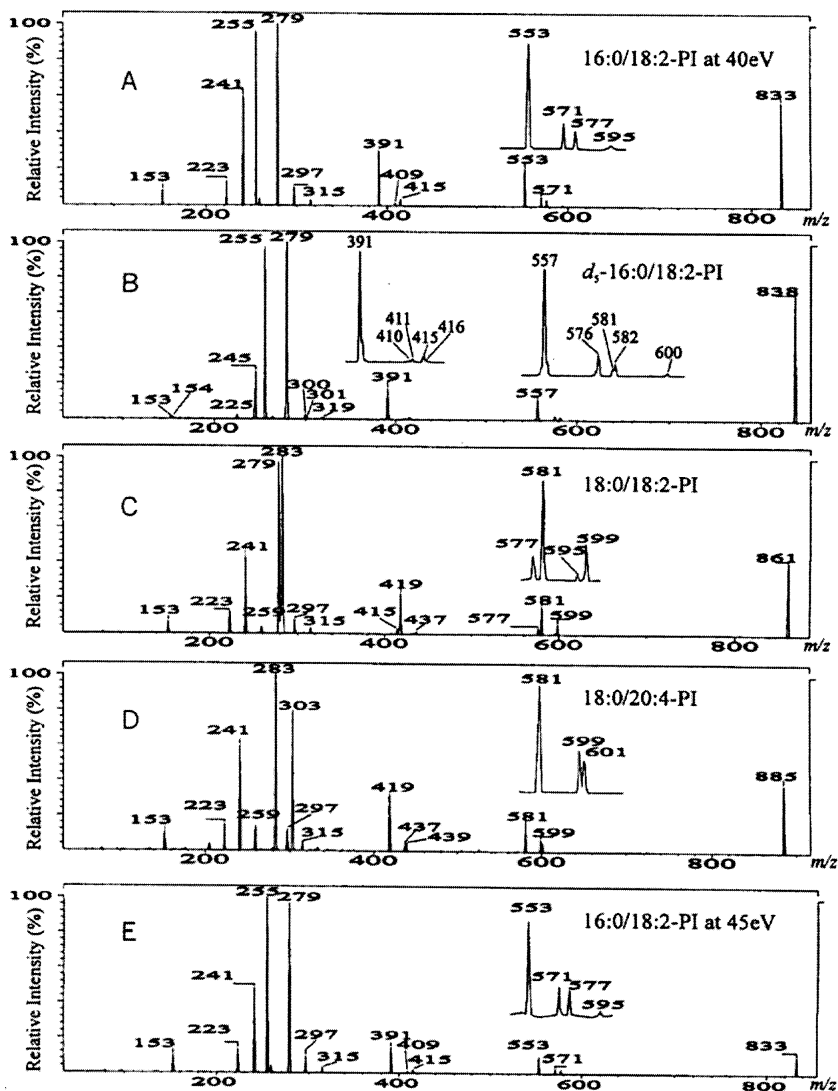


Fig. 2.11. Negative-ion ESI tandem mass spectra (collision energy of 40 eV) of $[M - H]^-$ ions of (A) 16:0/18:2-PI, (B) d_5 -16:0/18:2-PI, where deuteriums were labelled on the 5 hydroxy hydrogen atoms of the inositol by H-D exchange, (C) 18:0/18:2-PI, and (D) 18:0/20:4-PI. (E) Tandem mass spectrum of 16:0/18:2-PI obtained at 45 eV. Using panel (A) as an example, the product ion spectrum shows ions at m/z 577 and 553, representing neutral losses of the *sn*-1 and *sn*-2 substituents as fatty acids, respectively; at m/z 595 and 571, representing neutral losses of the *sn*-1 and *sn*-2 substituents as ketenes, respectively; at m/z 279 ($[R_2COO]^-$) and at m/z 255 ($[R_1COO]^-$). *Source:* Reference 91. Reproduced with permission from the publisher (Elsevier).

anions did not support a straightforward correlation of the position of esterification. This is because the intensities of the carboxylate anions are almost equal at collision energies between 20 – 40 eV (84,91). However, the intensity ratio of *sn*-1/*sn*-2 of the carboxylate anions increases with increasing collision energy (84,91). It has been suggested that this is due to an increased fragmentation of the lysophospholipid-like product ions, since the lyso *sn*-1 product ions ($[M - H - R_2COOH]^-$ and the $[M - H - R'_2CH=C=O - \text{inositol}]^-$) are more favorably formed than their lyso *sn*-2 counterparts. Further decomposition of the former ions to the *sn*-1 carboxylate anions might explain the increased *sn*-1/*sn*-2 abundance ratio observed at higher collision energies (91). In addition, the carboxylate anions might undergo further fragmentation after they are formed. The degree of fragmentation depends on the unsaturation of the molecules. Hsu and Turk reported that polyunsaturated fatty anions (e.g., the 4,7,10,13,16,19-docosahexenoate (C22:6) anion (*m/z* 327)), undergo fragmentation to give *m/z* 283 by loss of CO₂. The same has been observed in our laboratory (Larsen and Hvattum, unpublished results) and might be confused with the carboxylate anion of C18:0 with the same *m/z* value. Although the product ions obtained by neutral losses of the FA or the ketenes are low in abundance compared to the carboxylate anions, they might be more reliable for determination of the regioselectivity of PI species (91). However, positional determination without the use of regioselective standards should be a subject for further research. The vast number of biologically occurring PI species would make it impractical to synthesize all regioselective species. Therefore, a generic method proven to be independent of the FA composition and experimental conditions would be a valuable contribution to phospholipid characterization by mass spectrometry.

ESI-MS of Phosphatidylserine (PS). Phosphatidylserine (PS) is an important phospholipid class and is predominantly found expressed on the inner leaflet of membranes, e.g., erythrocyte membranes (11,12). It has been shown that the loss of phospholipid asymmetry and surface exposure of PS are required for recognition and removal of apoptotic cells by macrophages and other phagocytes (32). Electrospray ionization of PS results in the formation of both positive and negative ions. However, it has been shown that negative ion formation tends to dominate in this class of phospholipids (92). In the positive-ion mode, mainly sodium adducts of PS have been found (92), although protonated molecules are also encountered (85). In the negative-ion mode, the $[M - H]^-$ ion dominates (83,85). Characterization of PS species by ESI-MS/MS has predominantly been carried out in the negative-ion mode. CID of the $[M - H]^-$ ion yields product ions arising from the neutral loss of the serine group ($[M - H - 87]^-$), neutral losses of the serine group and the acyl ketenes ($[M - H - 87 - R'_xCH=C=O]^-$), and neutral losses of the serine group and the FA ($[M - H - 87 - R_xCOOH]^-$) (Fig. 2.12).

In contrast to most other phospholipid classes, the lysophospholipid-like fragments from PS are relatively abundant (82,84). The intensity ratio of these fragments is such that $[M - 87 - R_2COOH]^- > [M - 87 - R_1COOH]^-$. Consequently,

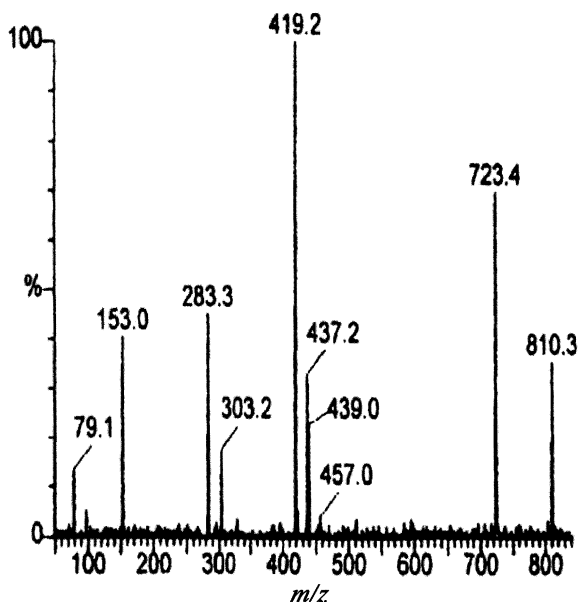


Fig. 2.12. Negative-ion ESI tandem mass spectrum of deprotonated C18:0/C20:4-PS. The collision energy was 25 eV. The product-ion spectrum shows ions at m/z 439 ($[M - H - 87 - R_1COOH]^-$); m/z 419 ($[M - H - 87 - R_2COOH]^-$); m/z 457 ($[M - H - 87 - R'_1CH=C=O]^-$); m/z 437 ($[M - H - 87 - R'_2CH=C=O]^-$); m/z 303 ($[R'_2COO]^-$); and m/z 283 ($[R_1COO]^-$). Source: Reference 84. Reproduced with permission from the publisher (John Wiley & Sons, Ltd.).

these abundant fragment ions could be used for positional determination of the FA moiety. When using ion-trap MS, the lyso PA-like fragments are the most prominent ions for MS² and MS³ product-ion scans, while MS⁴ product-ion scans gave the carboxylate anions (82). Hence, MS³ product-ion scans were used for species characterization in a recent study (60). Product ions representing the *sn*-1 and *sn*-2 carboxylate anions are also found at high abundance from PS species (78,82–85) (Fig. 2.12). It seems that for PS species, in contrast to most other phospholipid classes, the carboxylate anion arising from the *sn*-1 FA is always more prominent than the carboxylate anion arising from the *sn*-2 FA (78,82–84). The same applies for phosphatidic acid (PA) species (93). It has been explained by Hsu and Turk that this phenomenon for PA species is due to an initial sterically more favorable formation of $[M - H - R_2COOH]^- > [M - H - R_1COOH]^-$ ions from the PA $[M - H]^-$ ions (93). The $[M - H - R_xCOOH]^-$ ions might then undergo further fragmentation resulting in an increased *sn*-1/*sn*-2 abundance ratio at higher collision energies (93).

Likewise, as for PA species, the carboxylate anions of PS might also arise from the lyso-PA product ions (i.e., the $[M - H - 87 - R_xCOOH]^-$ ions) and since the abundance of $[M - H - 87 - R_2COOH]^- > [M - H - 87 - R_1COOH]^-$, this will yield a preferential formation of R_1COO^- over R_2COO^- . It has also been suggested that the carboxylate anions form directly from PS by nucleophilic attack of the phosphate anion on either the C-1 or C-2 site of the glycerol backbone, through loss of a 5- or 6-member ring system (84). Studies have shown that the carboxylate anion abundance ratio changes significantly with collision energy (84). However,

the *sn*-1/*sn*-2 abundance ratio was always greater than two for collision energies greater than 15 eV, indicating that positional determination is possible without regiospecific standards. PS appears to be the only phospholipid class showing an abundant product ion due to the neutral loss of the polar head group ($[M - H - 87]^-$). Neutral loss scans of 87 amu could therefore be used for class-specific detection of PS in a mixture or for verification of the retention times of PS species when performing on-line LC-MS.

ESI-MS of Phosphatidic Acid (PA). Phosphatidic acid (PA), the simplest phospholipid, is one of the building units for phospholipid biosynthesis (94). PA contains a phosphate group at the *sn*-3 position and, as in the other phospholipids, acyl groups in the *sn*-1 and *sn*-2 positions. This anionic phospholipid is preferentially studied in the negative-ion mode. Hsu and Turk have reported a detailed mechanistic study of PA by CID with ESI-MS/MS (93). In the negative-ion mode, the $[M - H]^-$ ion dominates in the mass spectrum of PA. Three major series of product ions are found following CID of deprotonated PA. Similar to CID of PS, these are product ions arising from: (i) the neutral loss of a free FA ($[M - H - R_x\text{COOH}]^-$); (ii) neutral loss of a ketene ($[M - H - R'_x\text{CH}=\text{C}=\text{O}]^-$); and (iii) the carboxylate anions ($R_x\text{COO}^-$) (Fig. 2.13). The neutral losses of the free FA and of the fatty acyl ketene at *sn*-2 were found to be more favorable than the analogous losses at *sn*-1 (93). This is consistent with the results reported for deprotonated PE, in which pathways leading to analogous losses at *sn*-2 also were sterically more favorable (95). However, the relative abundances of the fragment ions from deprotonated PA were such that $[M - H - R_1\text{COOH}]^- > ([M - H - R'_1\text{CH}=\text{C}=\text{O}]^-$ and $[M - H - R_2\text{COOH}]^- > ([M - H - R'_2\text{CH}=\text{C}=\text{O}]^-$ (Fig. 2.13). This suggests that the neutral loss of the free FA was a more facile process than the corresponding ketene loss. This is the opposite of what has been observed for deprotonated PE (95). Therefore, pathways leading to the formation of the product ions, arising from the neutral losses of the free FA from deprotonated PA, may be different from those of deprotonated PE. The $[M - H]^-$ ion of PE is reported to undergo charge-remote fragmentation to yield these ions (95), while fragmentation of the $[M - H]^-$ ion of PA by CID is suggested to follow charge-driven processes that are initiated by the phosphate anionic charge site (93).

The relative intensities of the FA carboxylate anion fragments arising from CID of PA are such that $R_1\text{COO}^- > R_2\text{COO}^-$ (84). This is the same as observed for PS species. As explained previously, the major pathway for the formation of the carboxylate anions is through a further fragmentation of $[M - H - R_x\text{COOH}]^-$ ions by a neutral loss of 136 amu. Since the abundances of these ions are such that $[M - H - R_2\text{COOH}]^- > [M - H - R_1\text{COOH}]^-$, further fragmentation of these ions yields more of the *sn*-1 carboxylate anion than the *sn*-2 carboxylate anion (93). The differential formation of the carboxylate anions would therefore permit accurate assignment of the regiospecificity of the FA substituents of PA molecules by tandem mass spectrometry.

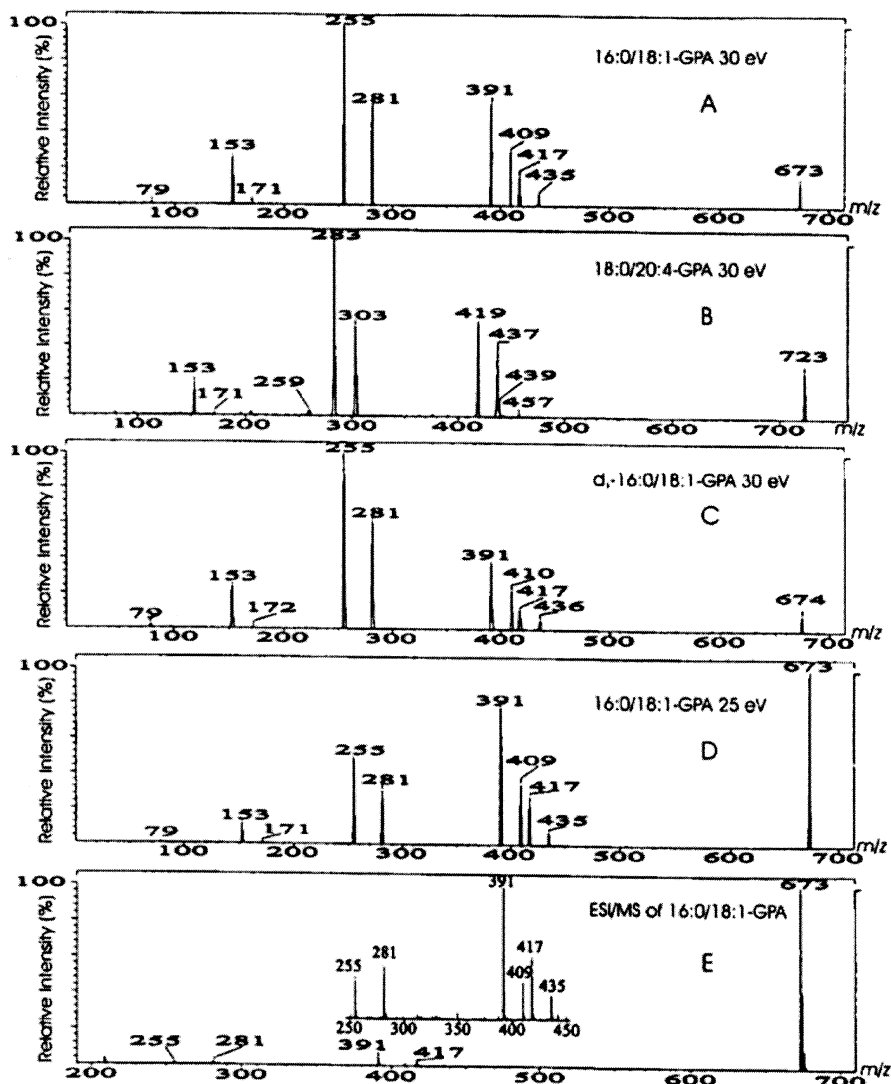


Fig. 2.13. Negative-ion ESI tandem mass spectra (collision energy 30 eV) of $[M - H]^-$ ions of (A) 16:0/18:1-PA, (B) 18:0/20:4-PA, (C) H-D exchanged-16:0/18:1-PA, (D) the tandem mass spectrum of 16:0/18:1-PA obtained at 25 eV, and (E) the ESI mass spectrum of 16:0/18:1-PA. Using panel (A) as an example, the product ion spectrum shows ions at m/z 417 and m/z 391, corresponding to neutral losses of the fatty acid moieties at sn -1 and sn -2, respectively; at m/z 435 and m/z 409, corresponding to neutral losses of the fatty acyl ketenes at sn -1 and sn -2, respectively; and at m/z 281 ($[R_2COO]^-$), and at m/z 255 ($[R_1COO]^-$). *Source:* Reference 93. Reproduced with permission from the publisher (Elsevier).

ESI-MS of Phosphatidylglycerol (PG). Phosphatidylglycerol (PG) occurs widely in most cells, but is less abundant than most of the other phospholipids. It is mainly found in the mitochondria of animal cells and is a precursor of more complex phospholipids, including the cardiolipins (96). This acidic phospholipid is preferentially analyzed in the negative-ion mode by ESI-MS. PG has been reported to form sodium adducts with ESI in the positive-ion mode (92), but detailed studies of PG by ESI-MS have been carried out in the negative-ion mode (82,97). In the negative-ion mode, PG yields abundant $[M - H]^-$ ions. CID of the $[M - H]^-$ ions yields similar fragment ions as described for the other phospholipid classes; i.e., product ions arising from: (i) the neutral losses of free FA ($[M - H - R_x\text{COOH}]^-$); (ii) neutral losses of ketenes ($[M - H - R'_x\text{CH}=\text{C}=\text{O}]^-$); and (iii) the carboxylate anion fragments ($R_x\text{COO}^-$) (Fig. 2.14). In addition, PG class-specific ions are also found; i.e., ions of the glycerol polar head group. These ions (e.g., at m/z 245 (probably [glycero phosphoglycerol - H] $^-$) and m/z 227 (probably [glycero phosphoglycerol - H - H₂O] $^-$) are found at low abundances with tandem quadrupole instruments (97) but are relatively more abundant after multiple collisions with ion-trap instruments (82).

The relative abundances of the PG lysophospholipid-like fragment ions show a similar pattern as the other phospholipid classes; i.e., the $[M - H - R_2\text{COOH}]^-$ and $[M - H - R'_2\text{CH}=\text{C}=\text{O}]^-$ ions are more abundant than their counterpart $[M - H - R_1\text{COOH}]^-$ and $[M - H - R'_1\text{CH}=\text{C}=\text{O}]^-$ ions. This confirms the notion that neutral loss of the *sn*-2 FA or ketene is sterically more favorable than the analogous losses at *sn*-1. The identity and position of the fatty acyl substituents can thus be assigned by comparing the differential formation of the *sn*-1 and *sn*-2 lysophospholipid-like ions. However, these fragment ions are low in abundance compared to the carboxylate fragment ions ($R_x\text{COO}^-$) and may be difficult to detect (Fig. 2.14). The fragmentation of PG species to the carboxylate anions is proposed to occur through a nucleophilic attack of the anionic phosphate on the C-1 or the C-2 of the glycerol to which the fatty acyl chains are attached, thus expelling the *sn*-1 or the *sn*-2 carboxylate anions (82,97). This fragmentation process leads to the preferential formation of $R_2\text{COO}^-$ over that of $R_1\text{COO}^-$ at the conditions applied (97). At the given conditions, the relative abundances of the carboxylate anions can thus be used to assign the positions and identities of the fatty acyl substituents of the PG species, and are probably more reliable, due to the higher intensities of these fragment ions in the product-ion spectra of PG species.

ESI-MS of Cardiolipin (CL). Cardiolipin is a unique phospholipid with a dimeric structure carrying four acyl groups and two negative charges. It is exclusively found in bacterial and mitochondrial membranes and is most abundant in mammalian heart tissue (96). Cardiolipin has two negatively-charged phosphodiester groups and would therefore generate abundant negative ions, including the doubly charged $[M - 2H]^{2-}$ ion. Bovine heart cardiolipin was analyzed by negative-ion

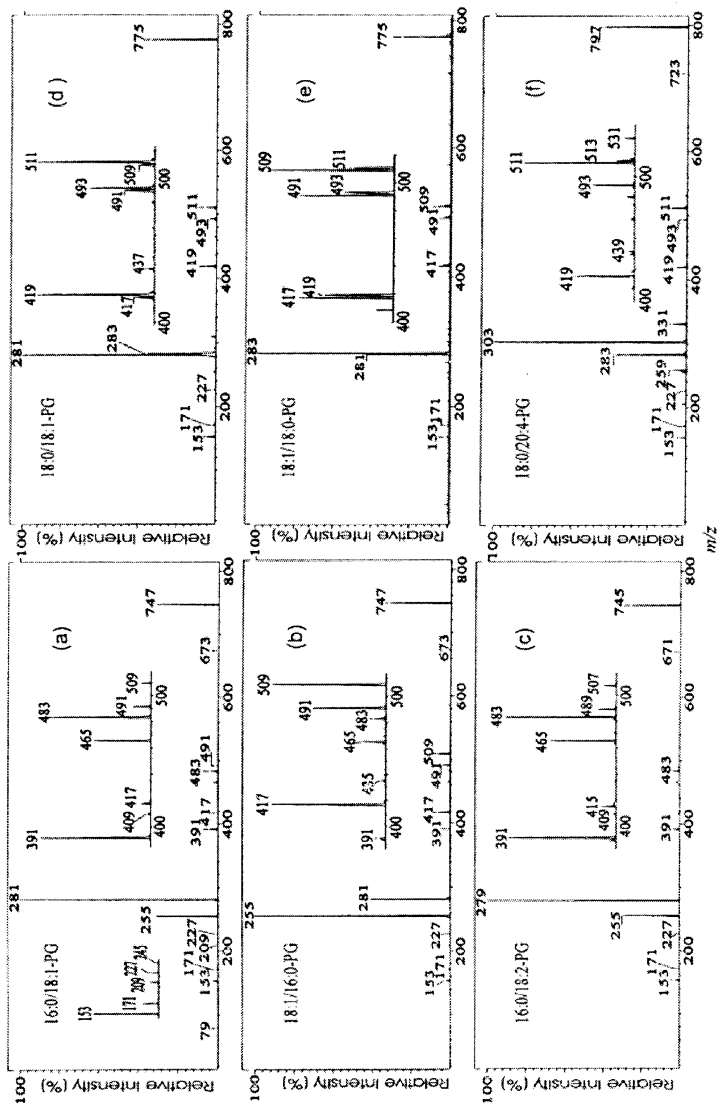


Fig. 2.14. Negative-ion ESI tandem mass spectra of $[M - H]^-$ ions of (a) 16:0/18:1-PG (m/z 747), (b) 18:1/16:0-PG (m/z 747), (c) 16:0/18:2-PG (m/z 745), (d) 18:0/18:1-PG (m/z 775), (e) 18:1/18:0-PG (m/z 775), and (f) 18:0/20:4-PG (m/z 797). Using panel (a) as an example, the product-ion spectrum shows ions at m/z 491 and m/z 465, reflecting neutral losses of the fatty acids at *sn*-1 and *sn*-2, respectively; at m/z 509 and m/z 483, reflecting neutral losses of the acyl ketenes at *sn*-1 and *sn*-2, respectively; at m/z 281 ($[R_2COO]^-$), and at m/z 255 ($[R_1COO]^-$). Source: Reference 97. Reproduced with permission from the publisher (Elsevier).

ESI-MS and several structurally informative product ions were found after CID of the $[M - 2H]^{2-}$ ion (78). A dominating product ion was found to be the carboxylate anion, indicating the FA composition of the cardiolipin. Cardiolipin in rabbit heart mitochondria has also been characterized by a combination of normal-phase HPLC isolation followed by reversed-phase HPLC coupled with ESI-MS (98). Using ion-trap mass spectrometry, the individual molecular species of cardiolipin were characterized by a data-dependent multistage MS fragmentation. Hoischen *et al.* used ESI-MS and collision induced dissociation tandem mass spectrometry for analysis of cardiolipin and lysocardiolipin in cytoplasmic membranes of bacteria (99).

Quantification of Phospholipids using ESI-MS

The ultimate goal in LC-ESI-MS analysis of phospholipids is to obtain a reasonable quantitative estimation of the molecular species identified in a given sample. In general, the widespread approach for quantification with LC-MS has been to use stable isotope-labeled internal standards. This is feasible when there are a limited number of compounds to be analyzed. However, in a cell-membrane extract, several hundred different phospholipid species might be present and it is neither practical nor possible to obtain stable isotope-labeled internal standards for each of the phospholipid species of interest.

There are several examples of quantification of phospholipids using direct infusion into the ESI chamber by a syringe pump. Han *et al.* determined individual molecular species of human platelet phospholipids during thrombin stimulation (100). They examined the intensities of the molecule-related ions of different PC species using positive-ion ESI-MS. Saturated versus unsaturated phospholipids from different subclasses were found to give identical ion intensities. The quantification of the molecular species from different phospholipid classes was obtained using nonbiological phospholipid species as internal standards (100). Several other studies have used a representative nonbiological internal standard for each phospholipid class for quantification of the different species (101–103), while others have used a representative isotope-labeled internal standard for quantification of the phospholipid species (76,104). However, other studies have shown that, in ESI-MS, the instrument response for phospholipids can vary depending on—apart from the structure of the polar head group—factors like acyl chain length, acyl chain unsaturation, and total lipid concentration (92). Consequently, in some studies several nonbiological internal standards for each phospholipid class have been used in order to compensate for the variation of instrument response depending on, for example, the identity of the fatty acyl chain (105–107). Zacarias *et al.* (108) have proposed a general method for relating negative-ion ESI-MS intensities to concentration, when analyzing samples having a complex mixture of phospholipids. They suggested the development of a response factor based on a calibration curve that relates the log of the intensity of the observed molecular species to the log of the concentration (108).

Absolute quantification of specific phospholipid species has been carried out by LC-ESI-MS using either an internal standard containing stable isotopes (56) or nonbiological phospholipid species as the internal standard (59).

In many cases, it is sufficient to estimate the relative abundances of the molecular species within a particular phospholipid class. This has been used both for estimating the relative distribution of phospholipid species in different biological samples (58,60,77,85) and for assessing changes in the relative species distribution under specific experimental conditions (77,83). In these cases, the relative distribution of the phospholipid species is probably not correct. Nevertheless, estimation of the relative distribution is probably sufficient for at least observing changes in the phospholipid species composition in biological systems, after application of various stimuli to these systems.

To this day, there is no specific method for accurately determining the amount of all phospholipid species in a biological sample. A minimum of three internal standards, preferably (di)unsaturated standards, for each head group class has been recommended (92). Although quantification has been done by direct infusion of a biological phospholipid extract, it is probably wise to perform a pre-separation of the phospholipid classes prior to ESI-MS, either on-line or off-line. This is especially important with samples containing high concentrations of lipids or other impurities that might interfere with the ionization process. Pre-separation of the phospholipid classes is most conveniently done by using LC-MS on-line, which also allows a more straightforward class determination of the phospholipid species. Nonetheless, quantification of individual phospholipid species is not straightforward because intensity is not necessarily a strict linear function of the concentration over a broad concentration range.

Concluding Remarks

Liquid chromatography coupled with electrospray ionization and tandem mass spectrometry has proven to be a valuable analytical technique for phospholipid species determination in complex biological extracts. The identification of phospholipid class-specific diagnostic ions offers the advantage of using the unique features of tandem quadrupole mass spectrometers to assign different phospholipid species to a given phospholipid class, by either neutral-loss or precursor-ion scanning. The detailed mechanistic studies of the fragmentation of the phospholipid molecule-related ions generated by electrospray ionization have provided specific product ions for structural characterization of the phospholipid species. At the present time, LC-ESI-MS analysis does not provide information about the position of the double bonds in unsaturated fatty acyl substituents. In addition, there is still a lot to be done regarding absolute quantification of the phospholipid species in a given sample. In spite of this, it is fair to say that LC-ESI-MS has nicely replaced the previously time-consuming multistep approach for phospholipid species determination. Since new phospholipid molecules continue to be discovered, some with

profound action on cellular biochemistry, the area of quantification appears to be an important application for biology and medicine.

References

1. Snyder, F., The Ether Lipid Trail: A Historical Perspective, *Biochim. Biophys. Acta* 1436: 265–278 (1999).
2. Ansell, G.B., Phospholipids and the Nervous System, in *Form and Function of Phospholipids*, edited by G.B. Ansell, J.N. Hawthorne, and R.M.C. Dawson, Elsevier, New York, 1973, pp. 377–422.
3. Panganamala, R.V., L.A. Horrocks, J.C. Geer, and D.G. Cornwell, Positions of Double Bonds in the Monounsaturated Alk-1-Enyl Groups from the Plasmalogens of Human Heart and Brain, *Chem. Phys. Lipids* 6: 97–102 (1971).
4. Druilhet, R.E., M.L. Overturf, and W.M. Kirkendall, Structure of Neutral Glycerides and Phosphoglycerides of Human Kidneys, *Int. J. Biochem.* 6: 893–901 (1975).
5. Thompson, G.A., Phospholipids in the Regulation of Membrane Lipid Metabolism, CRC Press, Boca Raton, 1980, pp. 175–175.
6. Spector, A.A., and M.A. Yorek, Membrane Lipid Composition and Cellular Function, *J. Lipid Res.* 26: 1015–1035 (1985).
7. Bretscher, M.S., Asymmetrical Lipid Bilayer Structure for Biological Membranes, *Nature New Biol.* 236: 11–12 (1972).
8. Bretscher, M.S., Membrane Structure—Some General Principles, *Science* 181: 622–629 (1973).
9. Bretscher, M.S., Phosphatidyl-ethanolamine—Differential Labelling in Intact Cells and Cell Ghosts of Human Erythrocytes by a Membrane-Impermeable Reagent, *J. Mol. Biol.* 71: 523–528 (1972).
10. Verkleij, A.J., R.F.A. Zwaal, B. Roelofsen, P. Comfurius, D. Kastelijn, and L.L.M. Van Deenen, The Asymmetric Distribution of Phospholipids in the Human Red Cell Membrane. A Combined Study using Phospholipases and Freeze-Etch Electron Microscopy, *Biochim. Biophys. Acta* 323: 178–193 (1973).
11. Rothman, J.E., and J. Lenard, Membrane Asymmetry, *Science* 195: 743–753 (1977).
12. Op Den Kamp, J.A.F., Lipid Asymmetry in Membranes, *Annu. Rev. Biochem.* 48: 47–71 (1979).
13. Daleke, D.L., and J.V. Lyles, Identification and Purification of Aminophospholipid Flippases, *Biochim. Biophys. Acta* 1486: 108–127 (2000).
14. Simons, K., and D. Toomre, Lipid Rafts and Signal Transduction, *Nat. Rev. Mol. Cell Biol.* 1: 31–39 (2000).
15. Yorek, M.A., Biological Distribution, in *Phospholipids Handbook*, edited by G. Cevc, Marcel Dekker, Inc., New York, 1993, pp. 745–775.
16. Berridge, M.J., Cell Signalling: A Tale of Two Messengers, *Nature* 365: 388–389 (1993).
17. Liscovitch, M., and L.C. Cantley, Lipid Second Messengers, *Cell* 77: 329–334 (1994).
18. Quest, A.F.G., S. Ghosh, W.Q. Xie, and R.M. Bell, DAG Second Messengers: Molecular Switches and Growth Control, *Adv. Exp. Med. Biol.* 400: 297–303 (1997).
19. Strum, J.C., S. Ghosh, and R.M. Bell, Lipid Second Messengers. A Role in Cell Growth Regulation and Cell Cycle Progression, *Adv. Exp. Med. Biol.* 407: 421–431 (1997).
20. Ashcroft, S.J.H., Intracellular Second Messengers, *Adv. Exp. Med. Biol.* 426: 73–80 (1997).

21. Vance, D.E. Phospholipid Metabolism in Eucaryotes, in *Biochemistry of Lipids and Membranes*, edited by D.E. Vance, and J.E. Vance, The Benjamin/Cummings Publishing Company, Inc., Menlo Park, 1985, pp. 242–270.
22. Hostetler, K.Y., H. Van Den Bosch, and L.L.M. Van Deenen, Biosynthesis of Cardiolipin in Liver Mitochondria, *Biochim. Biophys. Acta* 239: 113–119 (1971).
23. Hostetler, K.Y., H. Van Den Bosch, and L.L.M. Van Deenen, The Mechanism of Cardiolipin Biosynthesis in Liver Mitochondria, *Biochim. Biophys. Acta* 260: 507–513 (1972).
24. Short, S.A., and D.C. White, Biosynthesis of Cardiolipin from Phosphatidylglycerol in *Staphylococcus Aureus*, *J. Bacteriol.* 109: 820–826 (1972).
25. Burritt, M.F., and T.O. Henderson, Properties of a Membrane-Bound Cardiolipin Synthase from *Lactobacillus Plantarum*, *J. Bacteriol.* 123: 972–977 (1975).
26. Stuhne-Sekalec, L., and N.Z. Stanacev, Mechanism and Localization of Cardiolipin Biosynthesis Revisited: Evidence for the Identical Mechanism and Different Localization in Mitochondrial and Submitochondrial Membranes Isolated from Guinea Pig and Rat Liver, *Biochem. Cell Biol.* 68: 922–935 (1990).
27. Tamai, K.T., and M.L. Greenberg, Biochemical Characterization and Regulation of Cardiolipin Synthase in *Saccharomyces Cerevisae*, *Biochim. Biophys. Acta* 1046: 214–222 (1990).
28. Hostetler, K.Y., and H. Van Den Bosch, Subcellular and Submitochondrial Localization of Biosynthesis of Cardiolipin and Related Phospholipids in Rat-Liver, *Biochim. Biophys. Acta* 260: 380–386 (1972).
29. Pflieger, R.C., R.F. Henderson, and J.Waide, Phosphatidyl Glycerol—A Major Component of Pulmonary Surfactant, *Chem. Phys. Lipids* 9: 51–68 (1972).
30. Rooney, S.A., B.A. Page-Roberts, and E.K. Motoyama, Role of Lamellar Inclusions in Surfactant Production: Studies on Phospholipid Composition and Biosynthesis in Rat and Rabbit Lung Subcellular Fractions, *J. Lipid Res.* 16: 418–425 (1975).
31. Sanders, R.L., and W.J. Longmore, Phosphatidylglycerol in Rat Lung. II. Comparison of Occurrence, Composition, and Metabolism in Surfactant and Residual Lung Fractions, *Biochemistry* 14: 835–840 (1975).
32. Fadok, V.A., A. De Cathelineau, D.L. Daleke, P.M Henson, and D.L. Bratton, Loss of Phospholipid Asymmetry and Surface Exposure of Phosphatidylserine is Required for Phagocytosis of Apoptotic Cells by Macrophages and Fibroblasts, *J. Biol. Chem.* 276: 1071–1077 (2001).
33. Stubbs, C.D., and A.D. Smith, The Modification of Mammalian Membrane Polyunsaturated Fatty Acid Composition in Relation to Membrane Fluidity and Function, *Biochim. Biophys. Acta* 779: 89–137 (1984).
34. Muderhwa, J.M., and H.L. Brockman, Lateral Lipid Distribution is a Major Regulator of Lipase Activity: Implications for Lipid-Mediated Signal Transduction, *J. Biol. Chem.* 267: 24184–24192 (1992).
35. Zakim, D., J. Kavecansky, and S.Scarlata, Are Membrane Enzymes Regulated by the Viscosity of the Membrane Environment?, *Biochemistry* 31: 11589–11594 (1992).
36. Wykle, R.L., B. Malone, and F. Snyder, Enzymatic Synthesis of 1-Alkyl-2-Acetyl-*sn*-Glycero-3-Phosphocholine, A Hypertensive and Platelet-Aggregating Lipid, *J. Biol. Chem.* 255: 10256–10260 (1980).
37. Yamashita, A., T. Sugiura, and K. Waku, Acyltransferases and Transacylases Involved in Fatty Acid Remodeling of Phospholipids and Metabolism of Bioactive Lipids in Mammalian Cells, *J. Biochem.* 122: 1–16 (1997).

38. Funk, C.D., Prostaglandins and Leukotrienes: Advances in Eicosanoid Biology, *Science* 294: 1871–1875 (2001).
39. Prasad, M.R., M.A. Lovell, M. Yatin, H. Dhillon, and W.R. Markesbery, Regional Membrane Phospholipid Alterations in Alzheimer's Disease, *Neurochem. Res.* 23: 81–88 (1998).
40. Guan, Z.Z., Y.A. Wang, N.J. Cairns, P.L. Lantos, G. Dallner, and P.J. Sindelar, Decrease and Structural Modifications of Phosphatidylethanolamine Plasmalogen in the Brain with Alzheimer Disease, *J. Neuropathol. Exp. Neurol.* 58: 740–747 (1999).
41. Cui, Z., and M. Houweling, Phosphatidylcholine and Cell Death, *Biochim. Biophys. Acta* 1585: 87–96 (2002).
42. Berliner, J.A., G. Subbanagounder, N. Leitinger, A.D. Watson, and D. Vora, Evidence for a Role of Phospholipid Oxidation Products in Atherogenesis, *Trends Cardiovasc. Med.* 11: 142–147 (2001).
43. Litzinger, D.C., and L. Huang, Phosphatidylethanolamine Liposomes—Drug Delivery, Gene-Transfer and Immunodiagnostic Applications, *Biochim. Biophys. Acta* 1113: 201–227 (1992).
44. Tilcock, C., Delivery of Contrast Agents for Magnetic Resonance Imaging, Computed Tomography, Nuclear Medicine and Ultrasound, *Adv. Drug Deliv. Rev.* 37: 33–51 (1999).
45. McDannold, N., S.L. Fossheim, H. Rasmussen, H. Martin, N. Vykhodtseva, and K. Hynynen, Heat-Activated Liposomal MR Contrast Agent: Initial In Vivo Results in Rabbit Liver and Kidney, *Radiology* 230: 743–752 (2004).
46. Krause, W., Delivery of Diagnostic Agents in Computed Tomography, *Adv. Drug Deliv. Rev.* 37: 159–173 (1999).
47. Oku, N., Delivery of Contrast Agents for Positron Emission Tomography Imaging by Liposomes, *Adv. Drug Deliv. Rev.* 37: 53–61 (1999).
48. Christiansen, C., H. Kryvi, P.C. Sontum, and T. Skotland, Physical and Biochemical-Characterization of Albunex™, A New Ultrasound Contrast Agent Consisting of Air-Filled Albumin Microspheres Suspended in a Solution of Human Albumin, *Biotechnol. Appl. Biochem.* 19: 307–320 (1994).
49. Bjercknes, K., P.C. Sontum, G. Smistad, and I. Agerkvist, Preparation of Polymeric Microbubbles: Formulation Studies and Product Characterisation, *Int. J. Pharm.* 158: 129–136 (1997).
50. Dolan, M.S., J. Dent, C. Defilippi, T. Christopher, J.H. Wible, and A.J. Labovitz, Increasing the Dose and Rate of Albunex Infusion Leads to Superior Left Ventricular Contrast Effect, *J. Am. Soc. Echocardiogr.* 11: 426–432 (1998).
51. Sontum, P.C., J. Ostensen, K. Dyrstad, and L. Hoff, Acoustic Properties of NC100100 and Their Relation with the Microbubble Size Distribution, *Invest. Radiol.* 34: 268–275 (1999).
52. Lasic, D.D., and N.S. Templeton, Liposomes in Gene Therapy, *Adv. Drug Deliv. Rev.* 20: 221–266 (1996).
53. Christie, W.W., Separation of Phospholipid Classes by High-Performance Liquid Chromatography, in *Advances In Lipid Methodology*, Vol. 3, edited by W.W. Christie, The Oily Press, Ayr, Bridgwater, UK, 1996. pp. 77–107.
54. Fenn, J.B., M Mann, C.K. Meng, S.F. Wong, and C.M. Whitehouse, Electrospray Ionization For Mass-Spectrometry of Large Biomolecules, *Science* 246: 64–71 (1989).
55. Hoke II, S.H., K.L. Morand, K.D. Greis, T.R. Baker, K.L. Harbol, and R.L.M. Dobson, Transformations in Pharmaceutical Research and Development, Driven by

- Innovations in Multidimensional Mass Spectrometry-Based Technologies, *Int. J. Mass Spectrom.* 212: 135–196 (2001).
56. Harrison, K.A., K.L. Clay, and R.C. Murphy, Negative Ion Electrospray and Tandem Mass Spectrometric Analysis of Platelet Activating Factor (PAF) (1-Hexadecyl-2-Acetyl-Glycerophosphocholine, *J. Mass Spectrom.* 34: 330–335 (1999).
 57. Taguchi, R., J. Hayakawa, Y. Takeuchi, and M. Ishida, Two-Dimensional Analysis of Phospholipids by Capillary Liquid Chromatography/Electrospray Ionization Mass Spectrometry, *J. Mass Spectrom.* 35: 953–966 (2000).
 58. Ramanadham, S., F.F. Hsu, A. Bohrer, W. Nowatzke, Z.M. Ma, and J. Turk, Electrospray Ionization Mass Spectrometric Analyses of Phospholipids from Rat and Human Pancreatic Islets and Subcellular Membranes: Comparison to Other Tissues and Implications for Membrane Fusion in Insulin Exocytosis, *Biochemistry* 37: 4553–4567 (1998).
 59. Hvattum, E., A. Larsen, S. Uran, P.M. Michelsen, and T. Skotland, Specific Detection and Quantification of Palmitoyl-Stearoyl-Phosphatidylserine in Human Blood using Normal-Phase Liquid Chromatography Coupled with Electrospray Mass Spectrometry, *J. Chromatogr. B* 716: 47–56 (1998).
 60. Uran, S., A. Larsen, P.B. Jacobsen, and T. Skotland, Analysis of Phospholipid Species in Human Blood using Normal-Phase Liquid Chromatography Coupled with Electrospray Ionization Ion-Trap Tandem Mass Spectrometry, *J. Chromatogr. B* 758: 265–275 (2001).
 61. Karlsson, A.A., P. Michelsen, A. Larsen, and G. Odham, Normal-Phase Liquid Chromatography Class Separation and Species Determination of Phospholipids Utilizing Electrospray Mass Spectrometry Tandem Mass Spectrometry, *Rapid Commun. Mass Spectrom.* 10: 775–780 (1996).
 62. Byrdwell, W.C., Dual Parallel Liquid Chromatography/Dual Mass Spectrometry (LC2/MS2) of Bovine Brain Total Lipid Extract, *J. Liq. Chromatogr. & Rel. Technol.* 26: 3147–3181 (2003).
 63. Larsen, A., E. Mokastet, E. Lundanes, and E. Hvattum, Separation and Identification of Phosphatidylserine Molecular Species using Reversed-Phase High-Performance Liquid Chromatography with Evaporative Light Scattering and Mass Spectrometric Detection, *J. Chromatogr. B* 774: 115–120 (2002).
 64. Larsen, A., and P. Molander, Temperature Optimization for Improved Determination of Phosphatidylserine Species by Micro Liquid Chromatography with Electrospray Tandem Mass Spectrometric Detection, *J. Sep. Sci.* 27: 297–303 (2004).
 65. Vernooij, E.A.A.M., J.J. Kettenes-Van Den Bosch, and D.J.A. Crommelin, Rapid Determination of Acyl Chain Position in Egg Phosphatidylcholine by High Performance Liquid Chromatography Electrospray Mass Spectrometry, *Rapid Commun. Mass Spectrom.* 12: 83–86 (1998).
 66. Vernooij, E.A.A.M., J.F.H.M. Brouwers, J.J. Kettenes-Van Den Bosch, and D.J.A. Crommelin, RP-HPLC/ESI MS Determination of Acyl Chain Positions in Phospholipids, *J. Sep. Sci.* 25: 285–289 (2002).
 67. Isaac, G., D. Bylund, J.E. Mansson, K.E. Markides, and J. Bergquist, Analysis of Phosphatidylcholine and Sphingomyelin Molecular Species from Brain Extracts using Capillary Liquid Chromatography Electrospray Ionization Mass Spectrometry, *J. Neurosci. Methods* 128: 111–119 (2003).
 68. Spickett, C.M., N. Rennie, H. Winter, L. Zamboni, L. Landi, A. Jerlich, R.J. Schaur, and A.R. Pitt, Detection of Phospholipid Oxidation in Oxidatively Stressed Cells by

- Reversed-Phase HPLC Coupled with Positive-Ionization Electrospray MS, *Biochem. J.* 355: 449–457 (2001).
69. Ishioka, S., Y. Taoka, and Y. Itabashi, Molecular Species Analysis of Phosphatidylglycerols by Reversed-Phase HPLC/ESI-MS, *Bunseki Kagaku* 52: 795–803 (2003).
 70. Lee, M.H., J.S. Yoo, and G.H. Lee, Analysis of Lecithin in Cosmetics by Reversed-Phase Liquid Chromatography Electrospray Tandem Mass Spectrometry, *Rapid Commun. Mass Spectrom.* 12: 1709–1714 (1998).
 71. Kim, H.Y., T.C.L. Wang, and Y.C. Ma, Characterization of Polyunsaturated Phospholipid Remodeling in Mammalian Cells by High-Performance Liquid Chromatography Electrospray Ionization Mass Spectrometry, *ACS Symp. Ser.* 619: 267–280 (1996).
 72. Pulfer, M., and R.C. Murphy, Electrospray Mass Spectrometry of Phospholipids, *Mass Spectrom. Rev.* 22: 332–364 (2003).
 73. Kim, H.Y., T.C.L. Wang, and Y.C. Ma, Liquid-Chromatography Mass-Spectrometry of Phospholipids using Electrospray-Ionization, *Anal. Chem.* 66: 3977–3982 (1994).
 74. Hsu, F.F., A. Bohrer, and J. Turk, Formation of Lithiated Adducts of Glycerophosphocholine Lipids Facilitates Their Identification by Electrospray Ionization Tandem Mass Spectrometry, *J. Am. Soc. Mass Spectrom.* 9: 516–526 (1998).
 75. Hsu, F.F., and J. Turk, Electrospray Ionization/Tandem Quadrupole Mass Spectrometric Studies on Phosphatidylcholines: The Fragmentation Processes, *J. Am. Soc. Mass Spectrom.* 14: 352–363 (2003).
 76. Fang, J.S., and M.J. Barcelona, Structural Determination and Quantitative Analysis of Bacterial Phospholipids using Liquid Chromatography Electrospray Ionization Mass Spectrometry, *J. Microbiol. Methods* 33: 23–35 (1998).
 77. Ramanadham, S., F.F. Hsu, S. Zhang, A. Bohrer, Z.M. Ma, and J. Turk, Electrospray Ionization Mass Spectrometric Analyses of Phospholipids from INS-1 Insulinoma Cells: Comparison to Pancreatic Islets and Effects of Fatty Acid Supplementation on Phospholipid Composition and Insulin Secretion, *Biochim. Biophys. Acta* 1484: 251–266 (2000).
 78. Han, X.L., and R.W. Gross, Structural Determination of Picomole Amounts of Phospholipids via Electrospray Ionization Tandem Mass Spectrometry, *J. Am. Soc. Mass Spectrom.* 6: 1202–1210 (1995).
 79. Hsu, F.F., J. Turk, A.K. Thukkani, M.C. Messner, K.R. Wildsmith, and D.A. Ford, Characterization of Alkylacyl, Alk-1-Enylacyl and Lyso Subclasses of Glycerophosphocholine by Tandem Quadrupole Mass Spectrometry with Electrospray Ionization, *J. Mass Spectrom.* 38: 752–763 (2003).
 80. Han, X.L., and R.W. Gross, Electrospray-Ionization Mass Spectroscopic Analysis of Human Erythrocyte Plasma-Membrane Phospholipids, *Proc. Natl. Acad. Sci. U. S. A.* 91: 10635–10639 (1994).
 81. Smith, P.B.W., A.P. Snyder, and C.S. Harden, Characterization of Bacterial Phospholipids by Electrospray-Ionization Tandem Mass-Spectrometry, *Anal. Chem.* 67: 1824–1830 (1995).
 82. Larsen, A., S. Uran, P.B. Jacobsen, and T. Skotland, Collision-Induced Dissociation of Glycerol Phospholipids using Electrospray Ion-Trap Mass Spectrometry, *Rapid Commun. Mass Spectrom.* 15: 2393–2398 (2001).
 83. Hvattum, E., C. Rosjo, T. Gjoen, G. Rosenlund, and B. Ruyter, Effect of Soybean Oil and Fish Oil on Individual Molecular Species of Atlantic Salmon Head Kidney Phospholipids Determined by Normal-Phase Liquid Chromatography Coupled to Negative Ion Electrospray Tandem Mass Spectrometry, *J. Chromatogr. B* 748: 137–149 (2000).

84. Hvattum, E., G. Hagelin, and A. Larsen, Study of Mechanisms Involved in the Collision-Induced Dissociation of Carboxylate Anions from Glycerophospholipids using Negative Ion Electrospray Tandem Quadrupole Mass Spectrometry, *Rapid Commun. Mass Spectrom.* 12: 1405–1409 (1998).
85. Kerwin, J.L., A.R. Tuininga, and L.H. Ericsson, Identification of Molecular-Species of Glycerophospholipids and Sphingomyelin using Electrospray Mass-Spectrometry, *J. Lipid Res.* 35: 1102–1114 (1994).
86. Karlsson, A.A., P. Michelsen, and G. Odham, Molecular Species of Sphingomyelin: Determination by High-Performance Liquid Chromatography Mass Spectrometry with Electrospray and High-Performance Liquid Chromatography Tandem Mass Spectrometry with Atmospheric Pressure Chemical Ionization, *J. Mass Spectrom.* 33: 1192–1198 (1998).
87. Hsu, F.F., and J. Turk, Structural Determination of Sphingomyelin by Tandem Mass Spectrometry with Electrospray Ionization, *J. Am. Soc. Mass Spectrom.* 11: 437–449 (2000).
88. Hsu, F.F., and J. Turk, Characterization of Phosphatidylethanolamine as a Lithiated Adduct by Triple Quadrupole Tandem Mass Spectrometry with Electrospray Ionization, *J. Mass Spectrom.* 35: 596–606 (2000).
89. Kayganich, K.A., and R.C. Murphy, Fast-Atom-Bombardment Tandem Mass-Spectrometric Identification of Diacyl, Alkylacyl, and Alk-1-Enylacyl Molecular-Species of Glycerophosphoethanolamine in Human Polymorphonuclear Leukocytes, *Anal. Chem.* 64: 2965–2971 (1992).
90. Ho, Y.P., P.C. Huang, and K.H. Deng, Metal Ion Complexes in the Structural Analysis of Phospholipids by Electrospray Ionization Tandem Mass Spectrometry, *Rapid Commun. Mass Spectrom.* 17: 114–121 (2003).
91. Hsu, F.F., and J. Turk, Characterization of Phosphatidylinositol, Phosphatidylinositol-4-Phosphate, and Phosphatidylinositol-4,5-Bisphosphate by Electrospray Ionization Tandem Mass Spectrometry: A Mechanistic Study, *J. Am. Soc. Mass Spectrom.* 11: 986–999 (2000).
92. Koivusalo, M., P. Haimi, L. Heikinheimo, R. Kostiaainen, and P. Somerharju, Quantitative Determination of Phospholipid Compositions by ESI-MS: Effects of Acyl Chain Length, Unsaturation, and Lipid Concentration on Instrument Response, *J. Lipid Res.* 42: 663–672 (2001).
93. Hsu, F.F., and J. Turk, Charge-Driven Fragmentation Processes in Diacyl Glycerophosphatidic Acids Upon Low-Energy Collisional Activation. A Mechanistic Proposal, *J. Am. Soc. Mass Spectrom.* 11: 797–803 (2000).
94. Scherphof, G.L., Phospholipid Metabolism in Animal Cells, in *Phospholipids Handbook*, edited by G. Cevc, Marcel Dekker, Inc., New York, 1993, pp. 777–800.
95. Hsu, F.F., and J. Turk, Charge-Remote and Charge-Driven Fragmentation Processes in Diacyl Glycerophosphoethanolamine Upon Low-Energy Collisional Activation: A Mechanistic Proposal, *J. Am. Soc. Mass Spectrom.* 11: 892–899 (2000).
96. Schlame, M., D. Rua, and M.L. Greenberg, The Biosynthesis and Functional Role of Cardiolipin, *Prog. Lipid Res.* 39: 257–288 (2000).
97. Hsu, F.F., and J. Turk, Studies on Phosphatidylglycerol with Triple Quadrupole Tandem Mass Spectrometry with Electrospray Ionization: Fragmentation Processes and Structural Characterization, *J. Am. Soc. Mass Spectrom.* 12: 1036–1043 (2001).
98. Lesnefsky, E.J., M.S.K. Stoll, P.E. Minkler, and C.L. Hoppel, Separation and Quantitation of Phospholipids and Lysophospholipids by High-Performance Liquid Chromatography, *Anal. Biochem.* 285: 246–254 (2000).

99. Hoischen, C., W. Ihn, K. Gura, and J. Gumpert, Structural Characterization of Molecular Phospholipid Species in Cytoplasmic Membranes of the Cell Wall-Less *Streptomyces hygroscopicus* L Form by Use of Electrospray Ionization Coupled with Collision-Induced Dissociation Mass Spectrometry, *J. Bacteriol.* 179: 3437–3442 (1997).
100. Han, X.L., R.A. Gubitsoklug, B.J. Collins, and R.W. Gross, Alterations in Individual Molecular Species of Human Platelet Phospholipids During Thrombin Stimulation: Electrospray Ionization Mass Spectrometry-Facilitated Identification of the Boundary Conditions for the Magnitude and Selectivity of Thrombin-Induced Platelet Phospholipid Hydrolysis, *Biochemistry* 35: 5822–5832 (1996).
101. Pike, L.J., X.L. Han, K.N. Chung, and R.W. Gross, Lipid Rafts are Enriched in Arachidonic Acid and Plasmenylethanolamine and Their Composition is Independent of Caveolin-1 Expression: A Quantitative Electrospray Ionization/Mass Spectrometric Analysis, *Biochemistry* 41: 2075–2088 (2002).
102. Duffin, K., M. Obukowicz, A. Raz, and J.J. Shieh, Electrospray/Tandem Mass Spectrometry for Quantitative Analysis of Lipid Remodeling in Essential Fatty acid Deficient Mice, *Anal. Biochem.* 279: 179–188 (2000).
103. Ivanova, P.T., B.A. Cerda, D.M. Horn, J.S. Cohen, F.W. Mclafferty, and H.A. Brown, Electrospray Ionization Mass Spectrometry Analysis of Changes in Phospholipids in RBL-2H3 Mastocytoma Cells During Degranulation, *Proc. Natl. Acad. Sci. U.S.A.* 98: 7152–7157 (2001).
104. Garcia, M.C., G. Ward, Y.C. Ma, N. Salem, and H.Y. Kim, Effect of Docosahexaenoic Acid on the Synthesis of Phosphatidylserine in Rat Brain Microsomes and C6 Glioma Cells, *J. Neurochem.* 70: 24–30 (1998).
105. Brugger, B., G. Erben, R. Sandhoff, F.T. Wieland, and W.D. Lehmann, Quantitative Analysis of Biological Membrane Lipids at the Low Picomole Level by Nano-Electrospray Ionization Tandem Mass Spectrometry, *Proc. Natl. Acad. Sci. U.S.A.* 94: 2339–2344 (1997).
106. Blom, T.S., M. Koivusalo, E. Kuismanen, R. Kostianen, P. Somerharju, and E. Ikonen, Mass Spectrometric Analysis Reveals an Increase in Plasma Membrane Polyunsaturated Phospholipid Species Upon Cellular Cholesterol Loading, *Biochemistry* 40: 14635–14644 (2001).
107. Kakela, R., P. Somerharju, and J. Tynnela, Analysis of Phospholipid Molecular Species in Brains from Patients with Infantile and Juvenile Neuronal-Ceroid Lipofuscinosis Using Liquid Chromatography-Electrospray Ionization Mass Spectrometry, *J. Neurochem.* 84: 1051–1065 (2003).
108. Zacarias, A., D. Bolanowski, and A. Bhatnagar, Comparative Measurements of Multicomponent Phospholipid Mixtures by Electrospray Mass Spectroscopy: Relating Ion Intensity to Concentration, *Anal. Biochem.* 308: 152–159 (2002).

Chapter 3

Electrospray Ionization with Low-Energy Collisionally Activated Dissociation Tandem Mass Spectrometry of Complex Lipids: Structural Characterization and Mechanisms of Fragmentation

Fong-Fu Hsu and John Turk

Mass Spectrometry Resource, Division of Endocrinology, Diabetes, Metabolism, and Lipid Research, Department of Internal Medicine, Washington University School of Medicine, St. Louis, MO 63110

Introduction

The development of the desorption technique of fast atom bombardment (FAB) combined with mass spectrometry (MS) has permitted direct analyses of intact complex lipid molecules (1–4). One of the earliest applications of the technique to achieve structural characterization of complex lipids was the analysis of long-chain fatty acids by using tandem magnetic sector/high-energy collisionally activated dissociation (CAD) (5,6). These studies led to the discovery of charge-remote fragmentation (CRF), which yields ions informative for locating the position(s) of double bonds within the fatty acyl chains (7–10). The product ions from FAB-generated molecular ions of phospholipids, following CAD with high- or low-energy, could also identify the head groups and the positions of fatty acid substituents on the glycerol backbones. Many of the structurally informative ions generated by CAD are thought to derive from CRF processes (1–10).

Although FAB is powerful and, with MS/MS, can yield rich structural information, its sensitivity is limited. As a result, tremendous effort is required to obtain sufficient quantities of biological specimens to yield informative FAB mass spectra (11,12). However, the recent introduction of electrospray ionization (ESI) MS (13,14) to analyze intact complex lipids has further advanced the research in this field to a new level (15,16). ESI-MS analyses of phospholipids are 2 to 3 orders of magnitude more sensitive than those achieved by FAB/MS (17–19). The superb sensitivity and ease of continuous sample introduction with ESI, coupled with tandem MS, provide opportunities to explore the structures and fragmentation processes of complex lipids in greater detail. The ions generated by ESI have also minimized some of the problems associated with FAB/MS, such as the complication of spectra with matrix ions.

In contrast, only a few studies on lipids using matrix-assisted laser desorption/ionization (MALDI) (20–23), another current ionization method particularly suitable in the analysis of proteins (24,25), are reported. This ionization technique for

lipid analysis is generally hampered by the abundance of the matrix-derived noise in the mass range of interest, by a lack of reproducibility, by complications stemming from formation of various adduct ions, by dissociation of the pseudomolecular ion species during ionization, and by the lack of universal matrices for sensitive detection. The lack of sensitivity is particularly apparent in the context of current expectations of sub-picomole detection in the ESI-MS era. However, with the recent development of MALDI-TOF/TOF (26), MALDI quadrupole-TOF (Q-TOF) (27,28), and MALDI FT-ICR (29) instruments, it is expected that more research on complex lipids will be performed with this ionization method, and that sensitivity will be increased by introduction of new matrices.

In this chapter, we will describe the current state of knowledge about the mechanisms involved in the formation of various product ions following collisional activation of pseudomolecular ion species generated by ESI in the positive-ion and/or negative-ion modes. Mechanisms of fragmentation of common glycerophospholipids, including glycerophosphocholine (GPCho), glycerophosphoethanolamine (GPEtn), glycerophosphoserine (GPSer), glycerophosphatidic acid (GPA), glycerophosphoinositol (GPIno), glycerophosphoglycerol (GPGro), and cardiolipin (CL), as well as sphingolipids including sphingomyelin (SM), glycosphingolipids (GSL), and sulfatides will be described. Additionally, fragmentation mechanisms of ceramide (Cer) and triacylglycerols (TAG) will be discussed. Phospholipid classes that undergo similar fragmentation processes will be grouped together, starting with their positive pseudomolecular ions in the order of $[M + H]^+$, $[M + Alk]^+$, and $[M - H + 2Alk]^+$ (if applicable), and followed by negative-ion pseudomolecular-ion species in the order of $[M - H]^-$, $[M - 2H]^{2-}$ and $[M - 2H + Alk]^-$ (if applicable), (where Alk = Li, Na).

Techniques and Methods

Tandem Mass Spectrometry

The ESI source is compatible with nearly all tandem mass spectrometers, including tandem sector, tandem quadrupole, ion-trap (IT), ion-cyclotron resonance (ICR), TOF/TOF, and hybrid instruments such as the quadrupole-time-of-flight (Q-TOF). However, most structural characterizations and studies on the fragmentation processes of complex lipids have been achieved mainly with a triple-stage quadrupole (TSQ) mass spectrometer (15–18), because of its early development with ESI, its high efficiency in collection of fragment ions in the rf-only collision cell, its ease of operation, and its relatively low cost. Recently, studies on lipids also have been carried out by ion-trap MS (ITMS) (15,16,30,31), and more complicated instruments, such as Q-TOF (32) and FT-ICR (33) MS coupled with ESI.

Structural characterization achieved by magnetic sector instruments, which involve high-energy CAD by using translational energies in the keV range (34,35), may yield additional structural information (36), but the sensitivity is poor, compared to that obtained by TSQ MS, which is usually operated with collision energies

below 100 eV (37). In addition, the relative ease of applying skimmer CAD (“in-source CAD”) allows pseudo-MS/MS/MS experiments to be carried out by TSQ instruments, to reveal the fragmentation processes in greater detail. Similarly, one reason ITMS is particularly attractive is because MS^n spectra ($n = 2, 3, \dots$) can be obtained in series by time (38). However, its sensitivity has been limited by the number of ions that can be trapped; the low-mass cutoff nature of the instrument (38) also restrains its application in structural characterizations that require information from low-mass ions.

Fragment ions generated by high-energy CAD with sector instruments and by low-energy CAD with TSQ or ITMS instruments are similar. The gas-phase ion chemistry and the mechanisms underlying the fragmentation processes are generally interchangeable among the various methods applied, although differences may exist. The mechanisms of fragmentation of lipids described in this chapter are based primarily on the studies in the authors’ laboratory, where the experiments were carried out mainly with a Finnigan TSQ 7000 triple quadrupole mass spectrometer operated at unit resolution, and a Finnigan LCQ DECA ITMS, with which MS^n -spectra ($n = 2, 3$) were obtained. Samples were infused continuously at a flow rate of 1 $\mu\text{L}/\text{min}$ into the mass spectrometers. Tandem mass spectra were acquired in profile mode at 3 s per scan, and were accumulated for a period of time that was determined by the quality of the spectra, typically 3–10 min.

Preparation of Deuterium-Labeled Lipid Standards

Tandem mass spectra from deuterium-labeled analogs were often acquired to confirm the fragmentation pathways. Labeled analogs deuterated at both exchangeable hydrogens and at nonexchangeable hydrogens were used. The former compounds were obtained *via* hydrogen-deuterium (H-D) exchange with CH_3OD . Samples were dissolved in CH_3OD , and were blown to dryness under nitrogen and reconstituted in CH_3OD , before being subjected to ESI-MS. In studies requiring $[M + D]^+$ precursors, samples were dissolved in CH_3OD and acidified with $\text{CH}_3\text{CO}_2\text{D}$. The syringe and the transfer line of the capillary to the ESI source were washed thoroughly with CH_3CN before H-D exchanged samples were infused. The labeled compounds deuterated at non-exchangeable hydrogens were purchased from vendors.

The designations and abbreviations that are recommended by the International Union of Pure and Applied Chemistry (IUPAC) (<http://www.chem.qmul.ac.uk/iupac/lipid/>) are used. Glycerophospholipid nomenclatures fall into three categories: diacyl-, 1-*O*-alkyl-2-acyl- (plasmanyl-), and 1-*O*-alk-1'-enyl-2-acyl (plasmalogen). Examples of three types of phosphocholines are: the dipalmitoyl-, 1-*O*-hexadecyl-2-palmitoyl-, and 1-*O*-hexadec-1'-enyl-2-palmitoyl-*sn*-glycero-3-phosphocholines, designated as 16:0/16:0-PC, *a*16:0/16:0-PC, and *p*16:0/16:0-PC, respectively. The designation of sphingolipids such as sphingomyelin, sulfatide, and ceramide is in the form of d(or t)LCB/FA, with d denoting a dihydroxy and t denoting a trihydroxy long chain base (LCB), and a fatty acid (FA). The sphingosine

(sphing-4-enine) and sphinganine LCB, for example, are designated as d18:1, and d18:0, respectively. Fatty acyl moieties with or without α -hydroxyl substituents are denoted as hFA or nFA, respectively. Therefore, d18:1/16:0-SM, d18:1/16:0-Cer, and d18:1/16:0-sulfatide represent 1-phosphocholine-*N*-palmitoyl-sphingosine, *N*-palmitoyl-sphingosine, and 3-sulfogalactosyl-*N*-palmitoyl-sphingosine (3-sulfogalactosylceramide), respectively.

Molecular Species Formed by Electrospray Ionization

Nearly all phospholipids are readily ionizable, when subjected to ESI. However, ion formation for phospholipids under ESI is governed by the polar head groups that distinguish the various classes. Early studies with ESI-MS analyses of the phospholipid “platelet activating factor” (PAF) demonstrated that choline glycerophospholipids could be successfully analyzed as protonated ($[M + H]^+$) and alkali metal ($[M + \text{Alk}]^+$) adducts in the positive-ion mode or as chloride adducts ($[M + \text{Cl}]^-$) in the negative-ion mode (17). Adduct ions of GPCho in the forms of $[M + \text{CH}_3\text{CO}_2]^-$, $[M - 15]^-$ (18,39,40), $[M + \text{Alk}]^+$ (Alk = Li, Na, K) (18, 41), and $[M + \text{CF}_3\text{CO}_2\text{H} + \text{K}]^+$ (31) were later reported. However, the sensitivity of GPCho in positive-ion mode was two orders of magnitude (10^2) greater than that in the negative-ion mode, attributable to the fact that GPCho contains a quaternary nitrogen with a fixed positive charge and more readily forms positive than negative ions by ESI. Adduct formation with Cl^- or CH_3CO_2^- was also observed for ceramide (42), sphingomyelin (43), and glycosphingolipids (44).

In the negative-ion mode, GPEtn, GPSer, GPGro, GPINo, and GPA all yield prominent $[M - H]^-$ ions. GPSer also forms the $[M - 2H + \text{Alk}]^-$ adduct ion in the presence of Alk^+ . In the positive-ion mode, GPEtn, GPSer, GPGro, GPINo, and GPA all form $[M + H]^+$ ions or alkali metal adduct ions in the form of $[M + \text{Alk}]^+$, or $[M + 2\text{Alk} - H]^+$, depending on the concentration of alkali metal or H^+ ions present in the samples. The sensitivity in the positive-ion mode, in general, is at least 1 order of magnitude less than that observed in the negative-ion mode.

Ions in the forms of $[M - 2H + \text{Na} + \text{Co}]^+$ and $[M - 2H + \text{Na} + \text{Ni}]^+$ were recently reported for phospholipid classes of GPEtn, GPGro, and of GPSer (45), but the sensitivity was not as great as that observed for $[M - H]^-$ ions. Sulfatides contain an anionic sulfate charge site and readily form $[M - H]^-$ ions in the negative-ion mode (43,46). Other phospholipid species, such as cardiolipin (CL) and phosphatidylinositol polyphosphates (PIP), which bear multiple phosphoric acid charge sites, form $[M - H]^-$, $[M + \text{Na} - 2H]^-$, and $[M - 2H]^{2-}$ ions in the negative-ion mode. The formation of these pseudomolecular species is strictly affected by the presence or absence of metal ions such as Na^+ and Li^+ , and by the pH of the solution in which the electrospray ionization events take place. The $[M - 2H]^{2-}$ ion is the major species observed for phosphatidylinositol bisphosphate (PIP_2), which possesses three phosphoric acid charge sites. However, ions in the form of $[M - 3H]^{3-}$ are not observed, indicating that the charge state of the ion formed did not

reflect the number of phosphoric charge sites (47). Beckedorf *et al.* (32) reported that $[M - 2H + Na]^-$ and $[M - 3H + Na]^{2-}$ ions were the major ions observed for D-glucopyranosylcardiolipin using a QTOF instrument equipped with a nanospray ESI source. The less intense $[M - 2H + 3Na]^+$ ions were observed in the positive-ion mode (32). Dimeric molecular species are often formed, if high concentrations of phospholipid solution are ionized.

Structural characterization of phospholipids relies on the rich pattern of fragment ions generated by CAD of the precursor ions. Ions formed by ESI under different conditions for various classes of phospholipids vary greatly. The mechanisms described in this chapter are written based on the premise that the molecular species subjected to CAD tandem MS for structural characterization are readily ionized by ESI, in the positive-ion and/or negative-ion mode(s). Mechanistic studies and structural characterization of the molecular species that formed adducts with multiple atoms, ions, or molecules, such as the $[M - 2H + Na + Ni]^+$ and $[M + CF_3CO_2H + K]^+$, will not be described here.

Structural Characterization by Tandem Mass Spectrometry and Fragmentation Processes

Fragmentation Processes of the $[M + H]^+$ Ions

Glycerophosphocholine (GPCho). The protonated molecular species ($[M + H]^+$) are readily formed by GPCho and SM, which possess a positive charge site on the quaternary nitrogen of the choline head group. The product-ion spectra arising from the $[M + H]^+$ ions are often simple, and therefore are less applicable, although not completely unusable, for structural characterization (48). For example, the product-ion spectrum of the $[M + H]^+$ ion of 16:0/18:1-PC at m/z 760.6 (Fig. 3.1A) is dominated by m/z 184, representing a phosphocholine ion; ions relating to the structural information are of low abundance. Studies on the product-ion spectra of various GPCho, including deuterium-labeled analogs, indicate that formation of the m/z 184 ion involves participation of an α -hydrogen, mainly of the fatty acyl chain at *sn*-2 (Scheme 3.1) (47). The studies also reveal that the α -hydrogen of the fatty acyl chain at *sn*-2 is more labile than that at *sn*-1, and results in the more favorable formation of the $[M + H - R'_2CH=CO]^+$ ion, reflecting loss of the *sn*-2 fatty acyl group as a ketene, than the $[M + H - R_1CH=CO]^+$ ion, reflecting the analogous loss at *sn*-1. Therefore, assignment of the fatty acyl moieties in the glycerol backbone can be achieved. However, the abundances of the ions arising from losses of the fatty acyl moieties as acids at *sn*-1 ($[M + H - R_1CO_2H]^+$) and at *sn*-2 ($[M + H - R_2CO_2H]^+$) are nearly identical, attributable to the fact that the acid losses, which involve the H^+ that protonated the molecule in the gas phase, are not regioselective.

Glycerophosphoethanolamine (GPEtn). In contrast to GPCho, the product-ion spectra of GPEtn are dominated by the $[M + H - 141]^+$ ion (**a** ion, Scheme 3.2),

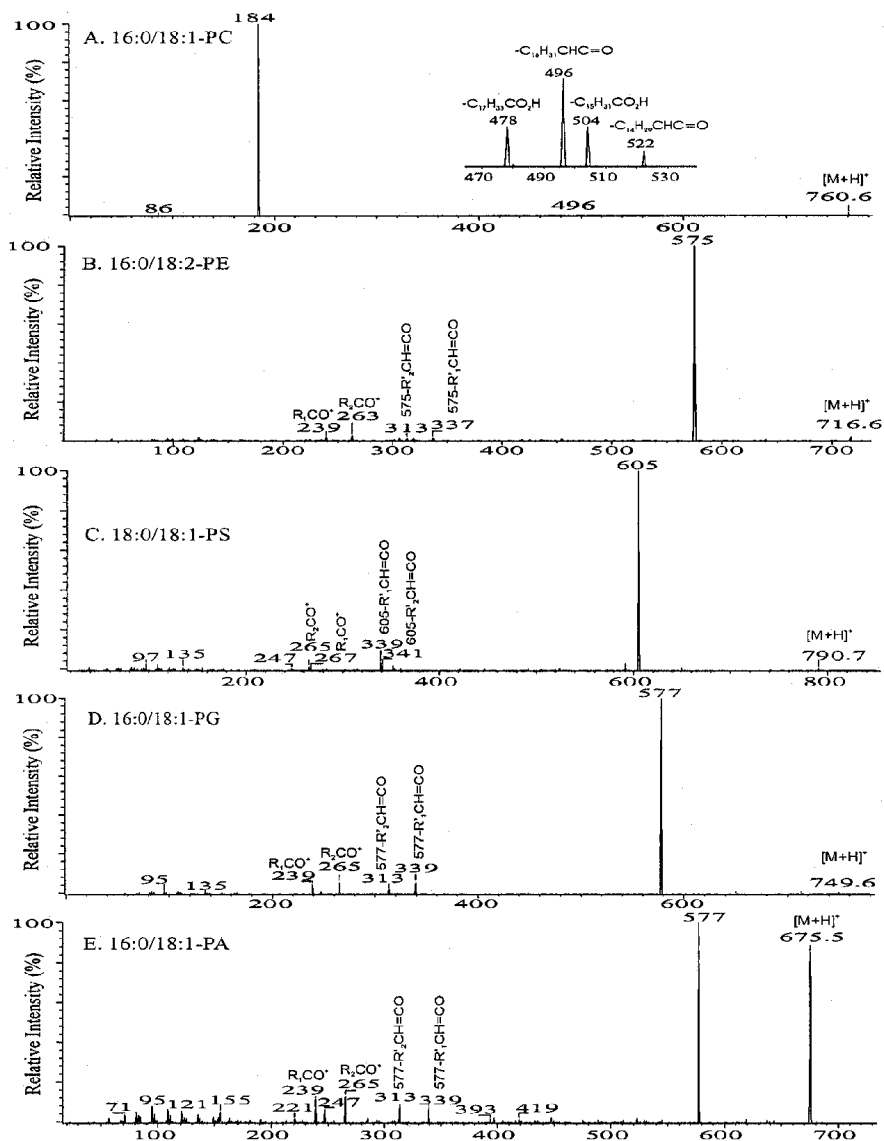
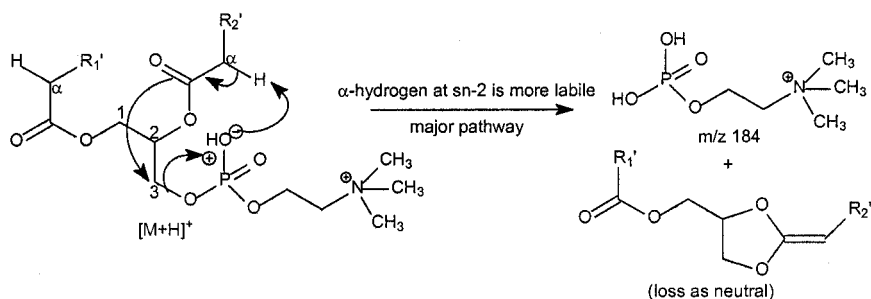
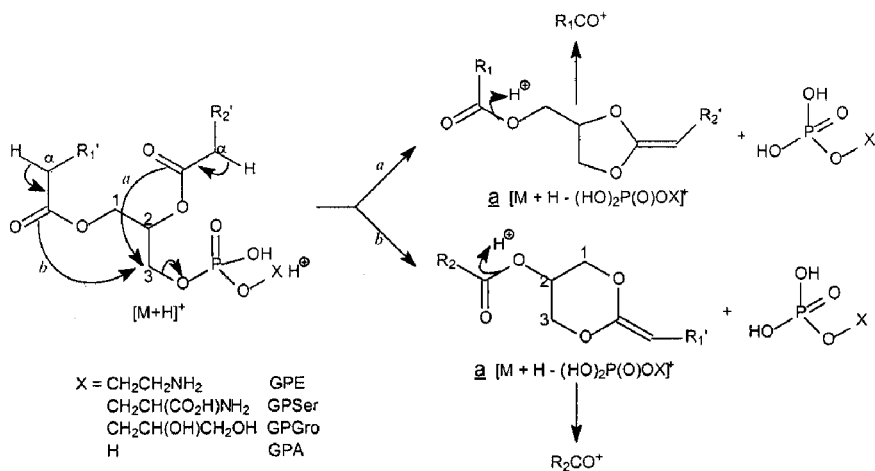


Fig. 3.1. The product-ion spectra of the $[M + H]^+$ ions of (A) 16:0/18:1-PC at m/z 760; (B) 16:0/18:2-PE at m/z 716; (C) 18:0/18:1-PS at m/z 790; (D) 16:0/18:1-PG at m/z 749; and of (E) 16:0/18:1-PA at m/z 675.



Scheme 3.1. Proposed mechanism of fragment formation from GPCCho.

arising from elimination of the phosphoethanolamine moiety *via* the same bond cleavage involving an α -hydrogen as described previously. As shown in Figure 3.1B, the product-ion spectrum of the $[M + H]^+$ ion of 16:0/18:2-PE at m/z 716 is dominated by the m/z 575 ($[M + H - 141]^+$) ion, which dissociates to yield 16:0-, and 18:2-acylium ions at m/z 239 (R_1CO^+) and 263 (R_2CO^+), respectively (Scheme 3.2) (49). Following CAD, both the phosphoethanolamine head group and the $[M - 141]^+$ moiety arising from the CAD cleavage compete for the protons that lead to ion formation. The observation of $[M + H - 141]^+$, rather than a protonated phosphoethanolamine, indicates that the phosphoethanolamine is less competitive for the proton.



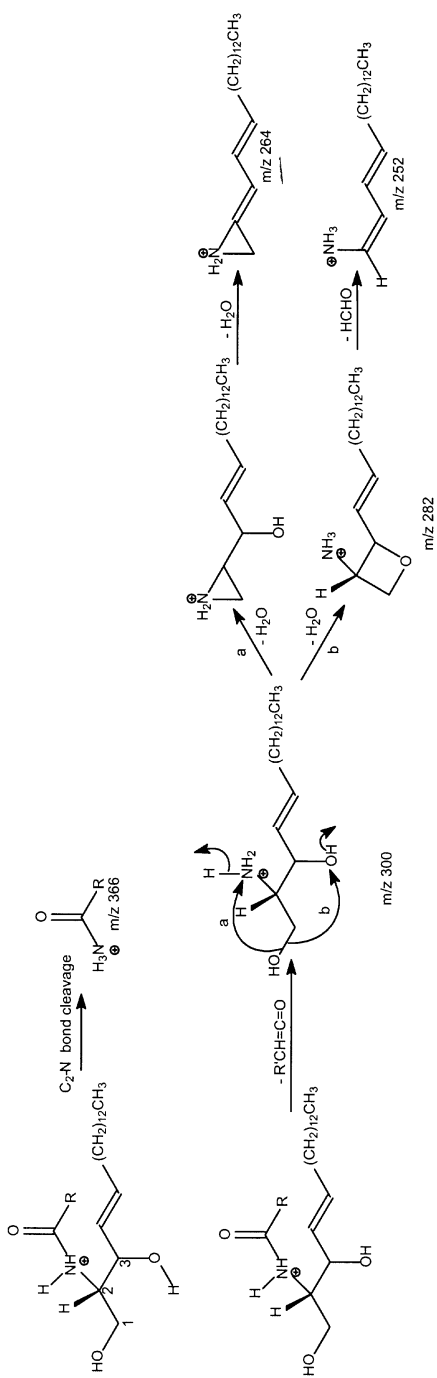
Scheme 3.2. Proposed mechanisms of fragmentation of glycerophospholipids.

In contrast, the gas-phase phosphocholine formed by CAD of GPCho is more basic, and formation of the protonated phosphocholine ion of m/z 184 is a more facile process. The fragmentation process leading to the $[M + H - 141]^+$ ion of GPEtn, again, involves the participation of the α -hydrogen of the fatty acyl substituent, mainly at *sn*-2.

Glycerophosphoserine (GPSer). The striking similarities in the product-ion spectra of the $[M + H]^+$ ions arising from GPSer and GPEtn indicate that the fragmentation processes and the gas phase basicities of phosphoserine and phosphoethanolamine are similar. The product-ion spectrum of the $[M + H]^+$ ion of 18:0/18:1-PS at m/z 790 (Fig. 3.1C) is dominated by m/z 605 ($[M + H - 185]^+$), arising from expulsion of phosphoserine *via* the same pathway as that of GPEtn (Scheme 3.2). The protonated phosphoserine ion expected at m/z 186 is not present. The spectrum also contains ions at m/z 339 and 341, arising from further dissociation of m/z 605, by losses of the fatty acyl substituents at *sn*-1 and *sn*-2 as ketenes, respectively. The acylium ions are observed at m/z 265 (R_2CO^+) and 267 (R_1CO^+).

Glycerophosphoglycerol (GPGro) and Glycerophosphoric Acid (GPA). The product-ion spectra of the $[M + H]^+$ ions of both 16:0/18:1-PG at m/z 749 (Fig. 3.1D) and 16:0/18:1-PA (Fig. 3.1E) at m/z 675 are dominated by ions at m/z 577, representing the $[M + H - (HO)_2P(O)OX]^+$ ions (where X = H or $CH_2CH_2(OH)CH_2OH$) arising from losses of phosphoglycerol and of phosphate, respectively. The spectra are also similar to those arising from GPEtn and GPSer. Both the gas-phase phosphoglycerol and the phosphate residues are acidic and are therefore less competitive for the proton necessary to form a protonated $(HO)_2P(O)OX$ ion, and formation of the $[M + H - (HO)_2P(O)OX]^+$ ions (**a** ion, Scheme 3.2) prevails. The identities of the fatty acyl substituents are again reflected by the acylium ions (R_xCO^+) at m/z 265 (18:1) and 239 (16:0), and by the ions at m/z 339 and 313, arising from losses of the fatty acyl substituents at *sn*-1 and at *sn*-2 as ketenes, respectively. However, the above ions are of low abundance and the difference in the abundances of the analogous ion pairs is not substantial; thus, the positions of fatty acyl substituents on the glycerol backbones cannot be easily assigned.

Ceramide (Cer) and Sphingomyelin (SM). The $[M + H]^+$ ion of ceramide readily eliminates H_2O to form an $[M + H - H_2O]^+$ ion, when subjected to ESI (50). The product-ion spectra arising from both $[M + H]^+$ and $[M + H - H_2O]^+$ are similar, indicating that loss of H_2O is the primary step leading to further dissociation. Figure 3.2A illustrates that the product-ion spectrum of the $[M + H]^+$ of d18:1/24:1-Cer at m/z 648 contains a major ion at m/z 264, which is diagnostic for ceramide containing a d18:1 long chain base (50). The ion reflecting the fatty acyl substituent is observed at m/z 366, arising from cleavage of the C2-N bond of the LCB to form a protonated amide ion (Scheme 3.3). The primary loss of the fatty



Scheme 3.3. Proposed mechanisms of fragment formation from ceramide.

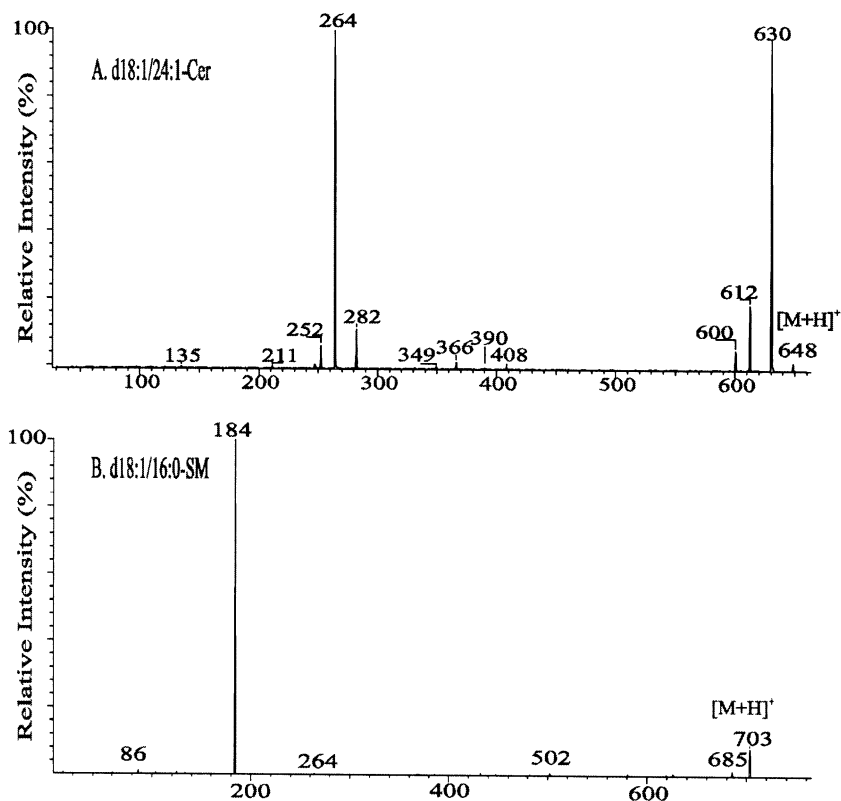


Fig. 3.2. The product-ion spectra of the $[M + H]^+$ ions of (A) d18:1/24:1-Cer at m/z 648, and of (B) d18:1/16:0-SM at m/z 703.

acyl substituent as a ketene gives rise to a protonated LCB at m/z 300, which dissociates to an azirium cation at m/z 264 by consecutive losses of two H_2O (see Scheme 3.4).

Although sphingomyelin (SM) also possesses a ceramide nucleus, the production spectrum of the $[M + H]^+$ ion of d18:1/16:0-SM at m/z 703.6 (Fig. 3.2B) is dominated by a protonated phosphocholine ion at m/z 184 (51), which is also observed in the product-ion spectra of GPCho. The ions similar to those observed for ceramide are not present. This is consistent with the notion that the gas-phase phosphocholine readily receives a proton to form a phosphocholine cation. In contrast, the product-ion spectra of the $[M + Li]^+$ ions of SM contain fragment ions reflecting both the fatty acyl substituents and LCB, which are readily usable for structural identification.

The product-ion spectra arising from the $[M + H]^+$ ions described above are simple and contain only a few prominent ions that are unique to the individual lipid classes. Therefore, precursor-ion scans of m/z 184 and of m/z 264, which are unique to the GPCho and ceramide classes, respectively, have been used to achieve simultaneous qualitative and semiquantitative identification of the individual molecular species in biological specimens (50,52). Tandem mass spectrometric analyses of GPEtn and GPSer using neutral loss scans of 141 and 185, respectively, have also been previously described (4). Although product-ion spectra from the $[M + H]^+$ ions permit structural identification, fragment ions informative for structural characterization are often of low abundance, and thus are less useful for complete structural determination. In contrast, fragment ions arising from alkali metal adduct ions, and in particular the $[M + Li]^+$ ions, as well as those arising from the $[M - H]^-$ ions in negative-ion mode, are more abundant and permit unambiguous structural identification.

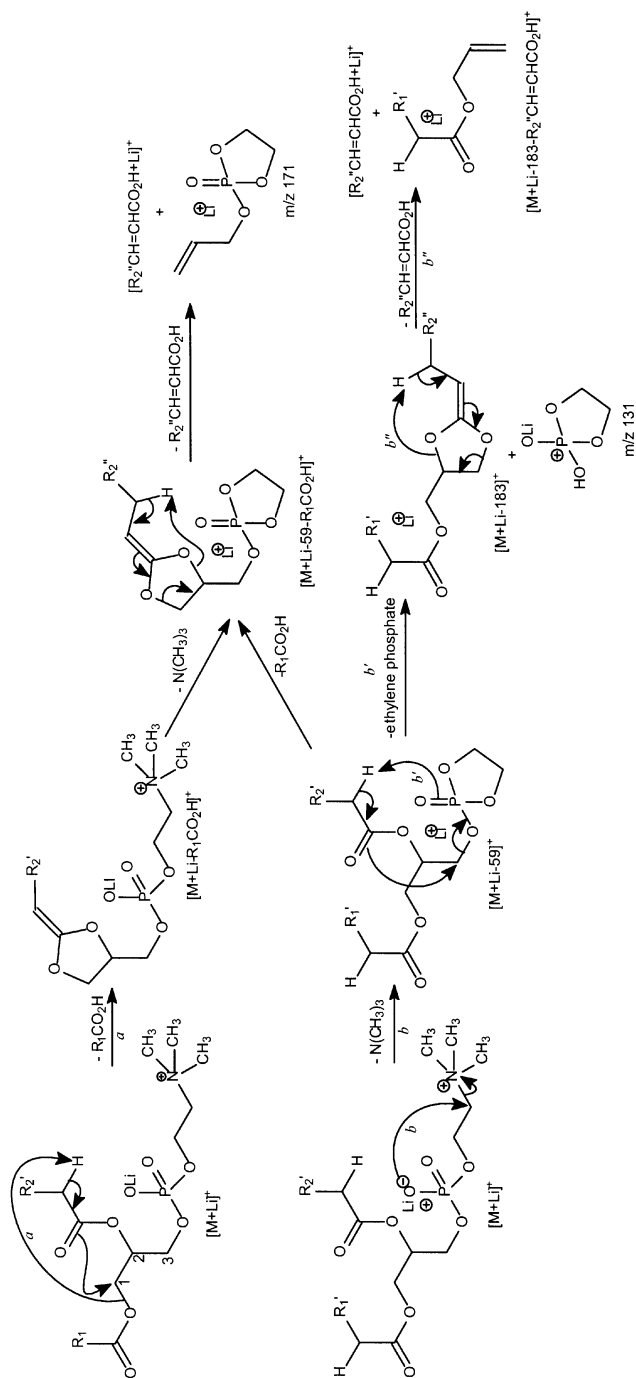
Fragmentation Processes of Lithiated Adduct Ions ($[M + Li]^+$ and $[M - H + 2Li]^+$ Ions)

Formation of Li^+ and other metal adduct ions as a means of tailoring fragmentation of biomolecules dates to the 1980s (7–10). Among the earlier observations in the study of phospholipids by tandem MS with ESI are that fragment ions arising from the $[M + Li]^+$ adduct ions of GPCho lipids are abundant, and structural identification and distinction among isomers can be achieved (41). In contrast, product-ion spectra from the $[M + Na]^+$, $[M + K]^+$, or $[M + H]^+$ ions yield little information about the fatty-acid substituents. The $[M + Li]^+$ adduct ions generated by ESI have been successfully employed in the structural characterization of GPEtn (49), GPSer, GPGro, GPA, TAG (53), SM (54), GSL (55–57), ceramides (58), and lysophosphatidylcholines (59) by tandem MS following CAD.

GPEtn (49), long-chain fatty acids (60), GPSer, GPGro, GPIIno, and GPA also form dilithiated adduct ions ($[M + 2Li - H]^+$), which yield unique tandem mass spectra that are useful for structural identification.

GPCho

1,2-Diacyl-sn-glycero-3-phosphocholines. Charge-remote fragmentation is the major fragmentation process leading to ion formation from the $[M + Li]^+$ ions of GPCho under low-energy CAD (48). An α -hydrogen of one fatty acyl chain is involved in the elimination of the adjacent fatty acyl substituent as an acid. The α -hydrogens of the fatty acyl chain at *sn*-2 are more labile than those at *sn*-1. This results in preferential loss of R_1CO_2H to yield a more prominent $[M + Li - R_1CO_2H]^+$ ion than the $[M + Li - R_2CO_2H]^+$ ion arising from R_2CO_2H loss (route *a*, Scheme 3.4). Loss of trimethylamine leads to the $[M + Li - 59]^+$ ion, which preferentially eliminates R_1CO_2H by using the α -hydrogens of the fatty acyl group



Scheme 3.4. Proposed mechanisms of fragmentation of lithiated GPCho.

at *sn*-2 to produce $[M + Li - 59 - R_1CO_2H]^+$. This is preferred over elimination of R_2CO_2H to yield $[M + Li - 59 - R_2CO_2H]^+$, which involves the participation of the α -hydrogens of the *sn*-1 fatty acyl substituent (route *b*). The disparity in the formation of the above ion pairs not only results in the structural identification of GPCho, but also its positional isomers such as 16:0/18:1-PC (Fig. 3.3A) and 18:1/16:0-PC (Fig. 3.3B) can be differentiated (41,48).

Studies from source CAD tandem MS indicate that loss of trimethylamine (giving $[M + Li - 59]^+$) is a primary step leading to formation of the major ions observed in the product-ion spectra of the $[M + Li]^+$ of GPCho (48). The $[M + Li - 59]^+$ ion at m/z 707 (Fig. 3.3A) further dissociates to $[M + Li - 183]^+$ at m/z 583 and to $[M + Li - 189]^+$ at m/z 577, *via* losses of ethylene phosphate and of lithium ethylene phosphate, respectively (route *b'*). The m/z 577 is more abundant than m/z 583, but the abundances of the analogous ion pair at m/z 605 ($[M + Li - 183]^+$) and m/z 599 ($[M + Li - 189]^+$) are reversed for lithiated 16:0/20:4-PC (Fig. 3.2C), which contains a highly unsaturated fatty acyl chain at *sn*-2. Similar results were observed for the analogous ions arising from GPETn.

The $[M + Li - 183]^+$ ions at m/z 583 in Figure 3.3A and B are lithiated species. The m/z 583 ion arising from 16:0/18:1-PC gives m/z 303 by further elimination of the 18:1-fatty acyl substituent at *sn*-2 as an α,β -unsaturated fatty acid (lost as an 18:2-fatty acid, route *b'*, Scheme 3.4). A similar ion at m/z 329 ($583 - 254$), reflecting loss of a 16:1-fatty acid is also present in the product-ion spectrum of 18:1/16:0-PC (Fig. 3.3B), but the analogous ion arising from a similar loss from *sn*-1 is not observed. These results provide additional information to confirm the structure. The $[M + Li - 189]^+$ ion at m/z 577 is a protonated ion, which is similar to the **a** ion depicted in Scheme 3.2, and is the precursor of the acylium ions observed at m/z 239 and 265.

The product-ion spectrum of 16:0/20:4-PC (Fig. 3.3C) contains a unique ion at m/z 313, arising from loss of the 20:4-fatty acyl chain as a ketene from m/z 599 ($[M + Li - 189]^+$). This fragmentation process is only observed for phospholipid classes consisting of a highly unsaturated fatty acyl moiety at *sn*-2, including diacyl GPCho and GPETn.

The abundance ratio of the $[M + Li - R_1CO_2Li]^+$ and $[M + Li - R_2CO_2Li]^+$ ions is close to one (Fig. 3.3A–C), indicating that there was no preference in the losses of the lithium carboxylate moieties (loss of R_xCO_2Li , $x = 1, 2$) involving the Li^+ ion that cationizes the molecule. This is consistent with the earlier notion that the H^+ that protonates GPCho molecules to form the $[M + H]^+$ ion results in nonregiospecific losses of free acids, and thus ions at $[M + H - R_1CO_2H]^+$ and $[M + H - R_2CO_2H]^+$ are of nearly equal abundance in the product-ion spectra of the $[M + H]^+$ ions of diacyl-PC.

1-O-alkyl-2-acyl-sn-glycero-3-phosphocholines (Plasmanylocholines) and 1-O-alk-1'-enyl-2-acyl-sn-glycero-3-phosphocholines (Plasmalogens). The product-ion spectra of the $[M + Li]^+$ ions of 1-*O*-hexadecyl-2-oleoyl-*sn*-glycero-3-

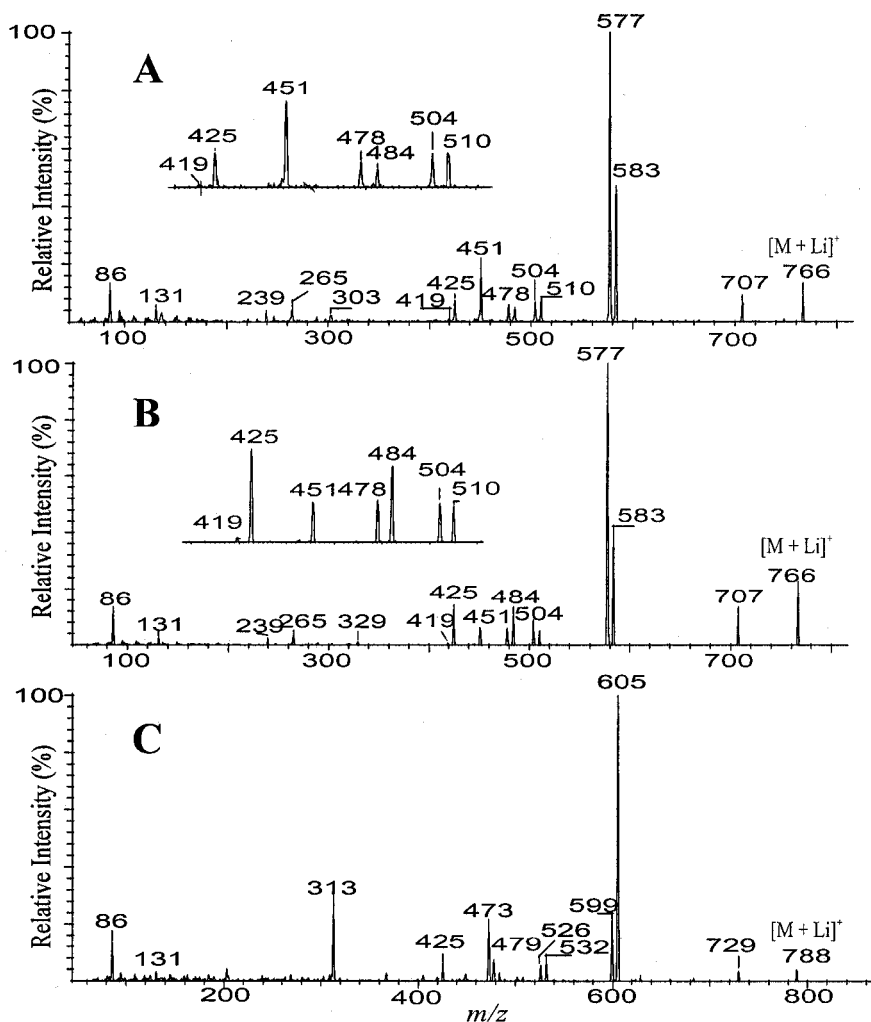


Fig. 3.3. The product-ion spectra of the $[M + Li]^+$ ions of (A) 16:0/18:1-PC; (B) 18:1/16:0-PC at m/z 766; and of (C) 16:0/20:4-PC at m/z 788.

phosphocholines (*a*16:0/18:1-PC) at m/z 752 (Fig. 3.4A) is dominated by the $[M + Li - 59]^+$ ion at m/z 693, while the $[M + Li - 59 - R_xCO_2H]^+$ ion at m/z 411 is of low abundance, and the $[M + Li - R_xCO_2H]^+$ ion expected at m/z 470 is not present. This is attributable to the fact that the 1-*O*-alkyl moiety at *sn*-1 does not contain labile α -hydrogens that are required for the R_2CO_2H loss, and thus, the pathways

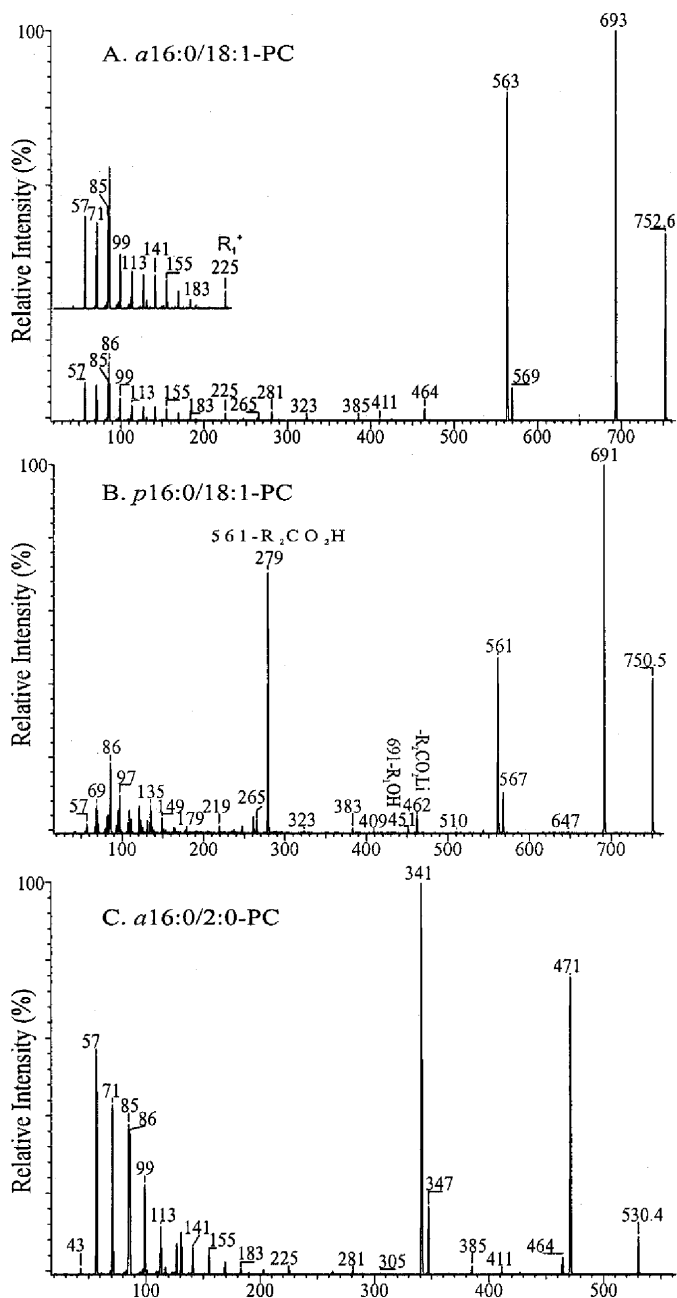


Fig. 3.4. The product-ion spectra of the $[M + Li]^+$ ions of (A) a16:0/18:1-PC at m/z 752; (B) p16:0/18:1-PC at m/z 750, and of (C) the a16:0/2:0-PC at m/z 530.

leading to the formation of the $[M + Li - R_2CO_2H]^+$ and $[M + Li - 59 - R_2CO_2H]^+$ ions are not operative. The ions at m/z 510 ($[M + Li - R_1OH]^+$) and 451 ($[M + Li - 59 - R_1OH]^+$) that would reflect the loss of the 1-*O*-alkyl substituent at *sn*-1 are also absent, because expulsion of an alcohol via this fragmentation process occurs less readily than loss of an acid. The lack of an α -hydrogen at *sn*-1 also accounts for the rise of the $[M + Li - 59]^+$ ions, which would have been significantly decreased by the further dissociation process that utilizes an α -hydrogen at *sn*-1.

The product-ion spectrum of the $[M + Li]^+$ ion of *p*16:0/18:1-PC at m/z 750.5 (Fig. 3.4B), which is a plasménylcholine (plasmalogen GPCho) with a 1-alk-1-enyl moiety, is similar to that of *a*16:0/18:1-PC. The spectrum contains a prominent ion at m/z 279 ($561 - C_{17}H_{33}CO_2H$), corresponding to further loss of the 18:1-fatty acyl moiety at *sn*-2 from m/z 561 ($[M + Li - 189]^+$). The prominence of the m/z 279 ion ($[M + Li - 189 - R_2CO_2H]^+$), along with the decline of the $[M + Li - 189]^+$ ion at m/z 561 resulting from the further dissociation, facilitates identification of plasmalogen GPCho by tandem MS and permits its differentiation from a plasmanylyl GPCho (59).

Another spectral feature that distinguishes these two subclasses is that the spectrum of the plasmanylyl GPCho also contains the R_1^+ ion arising from cleavage of the C-O ether bond of the 1-*O*-alkyl moiety at *sn*-1. This unique ion gives rise to a series of $(CH_2)_nH^+$ (where $n = 4, 5, \dots, 13$) ions at m/z 57, 71, ..., and 183 (Fig. 3.4A, inset), whereas the ion series from plasmalogen GPCho is not present (Fig. 3.4B). Similar results are observed for 1-*O*-alkyl-2-acetyl-*sn*-glycero-3-phosphocholine (platelet activating factor, Fig. 3.4C), a subclass of plasmanylylcholine. Furthermore, plasmanyethanolamine produced similar results.

The intensities of the $[M + Li - R_xCO_2Li]^+$ ions observed for diacyl- (Fig. 3.3A and B, m/z 504 and 478), plasmanylyl- (Fig. 3.4A, m/z 464) and plasménylyl- (Fig. 3.4B, m/z 462) GPCho are similar. This is consistent with the earlier suggestion that the pathways leading to the R_xCO_2Li loss, which involve the Li^+ ion that cationizes the molecule to $[M + Li]^+$, are similar and are not regioselective. This is regardless of the fact that the three different classes of lithiated PC molecules possess either one or two fatty acyl groups.

Lysophosphatidylcholines. The ions reflecting losses of fatty acid substituents (i.e., $[M + Li - R_xCO_2H]^+$ and $[M + Li - 59 - R_xCO_2H]^+$ ions) are not present in the product-ion spectra of the $[M + Li]^+$ ions of 2- and 1-lysophosphatidylcholines, in which either the *sn*-1 or *sn*-2 moiety is substituted by a hydroxyl group. This is because an α -hydrogen is not present in either one of the radyl groups. The product-ion spectrum of the $[M + Li]^+$ ion of lyso1/18:1-PC at m/z 528 (Fig. 3.5A) is similar to that of *a*16:0/18:1-PC (Fig. 3.3D). The abundances of the ions at m/z 345 ($[M + Li - 183]^+$) and 339 ($[M + Li - 189]^+$) are close to those of the corresponding ions observed in the spectrum of diacyl-PC. However, the $[M + Li - 59]^+$ ion at m/z 469 becomes abundant, and the m/z 246 ($[M + Li - R_2CO_2H]^+$) and m/z 187 ($[M + Li - 59 - R_2CO_2H]^+$) ions are not present.

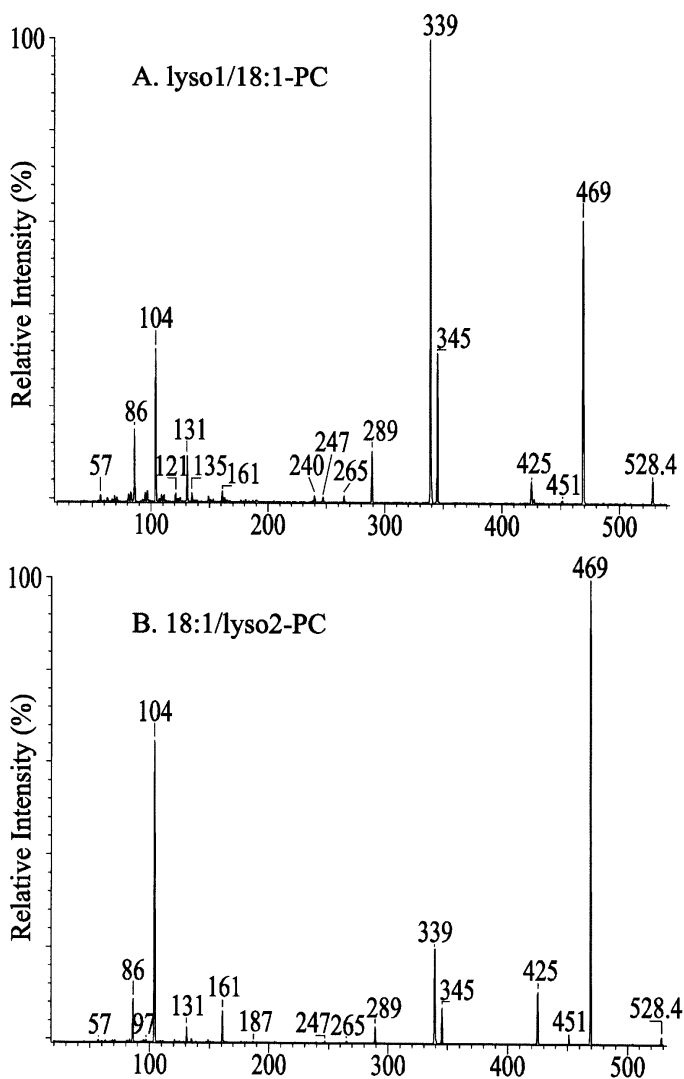


Fig. 3.5. The product-ion spectra of the $[M + Li]^+$ ions of (A) lyso1/18:1-PC at m/z 528, and of (B) 18:1/lyso2-PC at m/z 528.

Both the lyso1/18:1-PC and *a*16:0/18:1-PC share a structure that consists of a pair of α -hydrogens at the *sn*-2 fatty acyl chain, while the α -hydrogens at *sn*-1 are not present. Therefore, the resemblance between the two spectra is partially attributed to the fact that the major pathways leading to ion formations are initiated by

releasing the α -hydrogen of the fatty acyl chain at *sn*-2. In contrast, pathways leading to dissociation of 18:1/lyso2-PC are initiated by the less labile α -hydrogens of the fatty acyl chain at *sn*-1. This fragmentation process results in a distinct production spectrum featuring a prominent ion at m/z 469 ($[M + Li - 59]^+$), and less prominent ions at m/z 345 ($[M + Li - 183]^+$) and 339 ($[M + Li - 189]^+$) (Fig. 3.5B). The consecutive dissociation processes differentiated by the origins of the α -hydrogen lead to the prominence of m/z 339 and 345 and to the decline of m/z 469 for lyso1/18:1-PC (Fig. 3.5A). This can be easily distinguished from the 18:1/lyso2-PC isomer that contains a prominent ion at m/z 469, and less prominent ions at m/z 339 and 345 (59). The distinction between the product-ion spectra of the $[M + Na]^+$ ions of 1- and of 2-lysophosphatidyl isomers of GPEtn or of GPCho is also substantial. The utility of CAD tandem MS of $[M + Na]^+$ adduct ions for distinction among lysophospholipid isomers has been previously described (59,61).

Lysoplasmanyl- and Lysoplasmenylphosphocholines. Both the $[M + Li]^+$ ions of *a*16:0/lyso2-PC at m/z 488.4 (Fig. 3.6A) and of *p*16:0/lyso2-PC at m/z 486.4 (Fig. 3.6B) yield product-ion spectra similar to that observed for 18:1/lyso2-PC (Fig. 3.5B). However, the $[M + Li - 189]^+$ ions at m/z 299 ($[488 - 189]^+$) and m/z 297 ($[486 - 189]^+$) are absent in the product-ion spectra of *a*16:0/lyso2-PC and *p*16:0/lyso2-PC, respectively. The $[M + Li - 183]^+$ ions at m/z 305 ($[488 - 183]^+$) for *a*16:0/lyso2-PC, and at m/z 303 ($[486 - 183]^+$) for *p*16:0/lyso2-PC, are of low abundance.

These results are consistent with the notion that the α -hydrogens of the fatty acyl chain must be present to participate in the formation of the above ions. The lack of α -hydrogens in both the *sn*-1 and *sn*-2 moieties, as seen for the two compounds, hampers the dissociation process leading to $[M + Li - 189]^+$, and results in the drastic decline of the $[M + Li - 189]^+$ ion and in the prominence of the $[M + Li - 59]^+$ ion.

GPEtn

When ionized in the presence of Li^+ , GPEtn forms both monolithiated ($[M + Li]^+$) and dilithiated ($[M - H + 2Li]^+$) adduct ions. The intensities of the $[M + Li]^+$ and the $[M - H + 2Li]^+$ ions are dependent on the concentration of the Li^+ ion. The monolithiated adduct ion is the major species when 1 nmol/ μ L LiOAc was present in the solution. The dilithiated ion becomes the exclusive adduct ion when Li^+ (as LiOH in methanol) exceeds 2 nmol/ μ L (49).

[M + Li]⁺ Ions of Diacyl GPEtn. The profiles of the product-ion spectra and the fragmentation processes of the $[M + Li]^+$ ions of GPEtn are similar to those of GPCho. Figure 3.7A illustrates that the product-ion spectrum of the $[M + Li]^+$ ion of 16:0/18:2-PE at m/z 722 contains an abundant ion at m/z 679 ($[M + Li - 43]^+$) (**a**), arising from loss of aziridine to give an equivalent to a monolithiated 16:0/18:2-PA, which can then eliminate LiH_2PO_4 and H_3PO_4 to yield m/z 575 ($[M + Li - 147]^+$) (**c**) and m/z 581 ($[M + Li - 141]^+$) (**d**), respectively (Scheme 3.5). These ions, along with

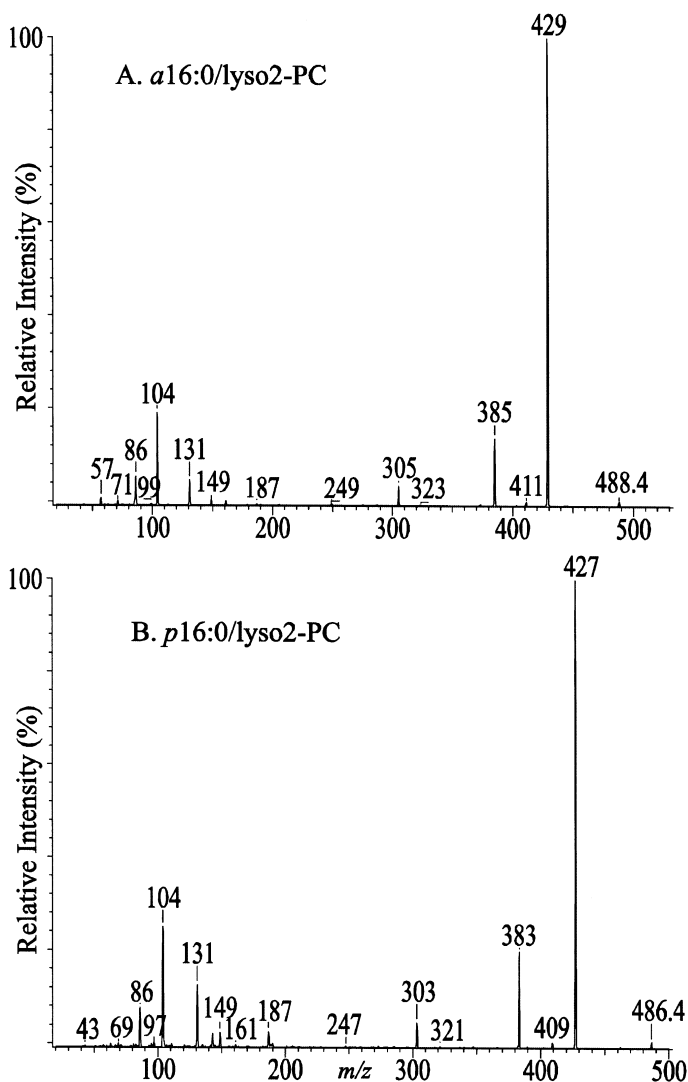


Fig. 3.6. The product-ion spectra of the $[M + Li]^+$ ions of (A) *a*16:0/lyso2-PC at m/z 488, and of (B) *p*16:0/lyso2-PC at m/z 486.

m/z 148 (**b**) and 105, respectively, representing a lithiated ethanolaminephosphate ($[(HO)_2PO_2(CH_2)_2NH_2Li]^+$) ion and a lithiated phosphoric acid ($[(HO)_3POLi]^+$) ion, are indicative of the phosphoethanolamine head group and are characteristic of GPEtn. Ions at m/z 423 ($[M + Li - 43 - R_1CO_2H]^+$) and 441 ($[M + Li - 43 - C_{14}H_{29}CH=CO]^+$) arise from the combined loss of the ethylamine moiety as an aziridine and

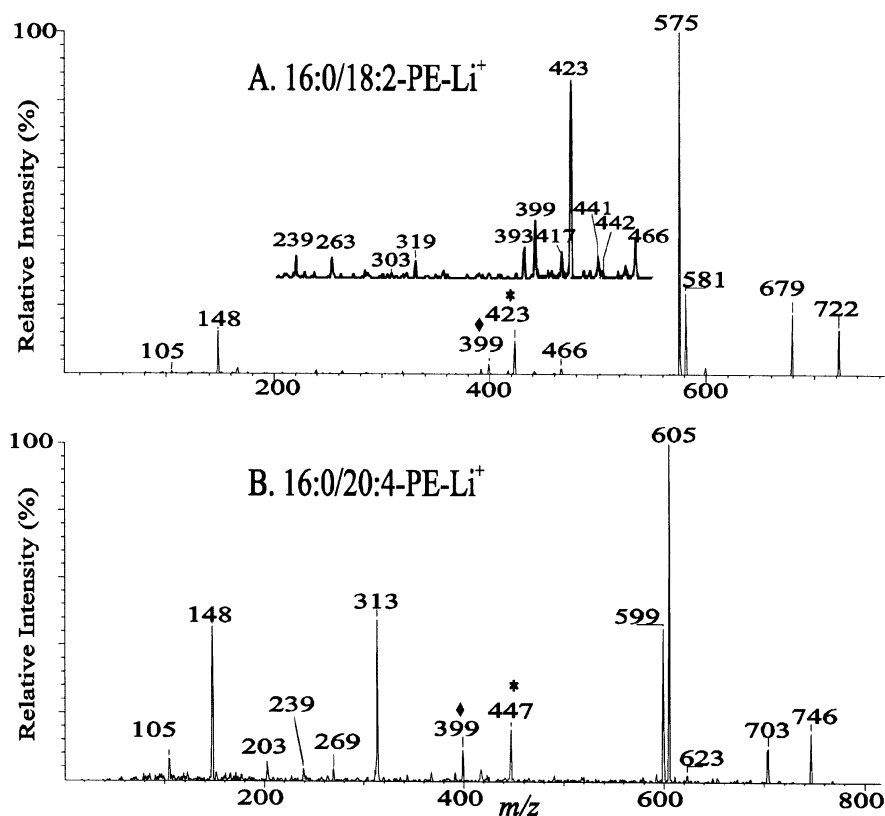


Fig. 3.7. The product-ion spectra of the $[M + Li]^+$ ions of (A) 16:0/18:2-PE at m/z 722 and of (B) 16:0/20:4-PE at m/z 746.

palmitic acid, and from the loss of the ethylamine moiety as an aziridine and of palmitic ketene, respectively. The analogous losses at *sn*-2 result in m/z 399 ($[M + Li - 43 - R_2CO_2H]^+$) and m/z 417 ($[M + Li - 43 - R_2'CH=CO]^+$), respectively. Because the m/z 423 ion is more abundant than the m/z 399 ion, the positions of the fatty acid substituents on the glycerol backbone can be determined.

The m/z 466 ($[M + Li - R_1CO_2H]^+$) ion arising from loss of the 16:0-fatty acid at *sn*-1 is more abundant than the m/z 442 ($[M + Li - R_2CO_2H]^+$) ion arising from loss of the 18:2-fatty acid at *sn*-2. This is consistent with the finding that loss of the fatty acyl substituent at *sn*-1 as an acid is more favorable than the analogous loss at *sn*-2, similar to that described for GPCho. The $[M + Li - 147]^+$ ion at m/z 575 is a protonated ion, which is equal to an $[M + Li - 189]^+$ ion as described for GPCho. This ion further dissociates to the 18:2 and 16:0 acylium ions at m/z 263 and m/z 239, respectively (Fig. 3.7A, inset). Similar results are observed for 16:0/20:4-PE

at m/z 746 (Fig. 3.7B), but that spectrum also contains a prominent ion at m/z 313, arising from further dissociation of the $[M + Li - 147]^+$ ion at m/z 599 to eliminate the *sn*-2 fatty acid as a ketene. This fragmentation process has also been observed for GPCho species possessing a polyunsaturated fatty acyl substituent at *sn*-2, as described earlier.

The abundance of the $[M + Li - 141]^+$ ion relative to the $[M + Li - 147]^+$ ion increases as the number of double bonds of the *sn*-2 fatty acyl chain increases (Fig. 3.7A and B). This is similar to the trend observed for GPCho, as described earlier. These results suggest that the gaseous Li^+ ion may preferentially associate with the polyunsaturated, rather than the saturated, fatty acyl chains.

[M + Li]⁺ Ions of Plasmalogen GPEtn and Plasmanyl GPEtn

As shown in Figure 3.8A, the product-ion spectrum of the $[M + Li]^+$ ion of *p*18:0/18:1-PE at m/z 736 contains a prominent ion at m/z 693 ($[M + Li - 43]^+$), along with ions at m/z 595 ($[M + Li - 141]^+$), 589 ($[M + Li - 147]^+$), and m/z 148 that are commonly observed for GPEtn. The product-ion spectrum also contains ions at m/z 613 ($[M + Li - 123]^+$), and 607 ($[M + Li - 129]^+$), arising from losses of (HO)P(O)(OCH₂CH₂NH), and (LiO)P(O)(OCH₂CH₂NH), respectively (as in Scheme 3.6, route *a*). The ion at m/z 425, representing loss of aziridine and loss of the *sn*-1 alk-1'-enyl as an alcohol (C₁₆H₃₃CH=CHOH), as well as the ion at m/z 307, arising from m/z 589 ($[M + Li - 147]^+$) *via* further loss of the *sn*-2 substituent as a fatty acid (C₁₇H₃₃CO₂H), are also present. Therefore, the identities of the alkenyl ether at *sn*-1 and the fatty acid at *sn*-2 can be determined. The identity of the fatty acid at *sn*-2 is further recognized by the acylium ion at m/z 265 ($[C_{17}H_{33}CO]^+$). The spectrum also contains abundant ions with m/z values below 200. Although these ions do not provide specific structural information, they appear to be characteristic of both plasmalogen GPEtn and plasmalogen GPCho, and provide information to differentiate them from the plasmanyl subclasses. The product-ion spectrum of the $[M + Li]^+$ ion of *p*18:0/22:6-PE at m/z 782 (Fig. 3.8B) contains the analogous ions, but the expected acylium ion at m/z 311, arising from the 22:6 fatty acid at *sn*-2, is not present. This is consistent with the fact that the acylium ion is formed by consecutive dissociation of the protonated species of the $[M + Li - 147]^+$ ion at m/z 635, which is of low abundance in the spectrum.

The presence of the ions that reflect both the *sn*-1 and *sn*-2 substituents in the product-ion spectra of the $[M + Li]^+$ ions of plasmalogen GPEtn species permits confident differentiation among isomeric structures. This is illustrated by the product-ion spectrum of the precursor ion at m/z 758 from a bovine brain lipid extract (Fig. 3.8C), which clearly shows the m/z 447/307 and m/z 475/279 ion pairs arising from *p*18:0/20:4-PE and *p*16:0/22:4-PE, respectively. In contrast, product-ion spectra of plasmalogen GPEtn obtained in the negative-ion mode would yield only the *sn*-2 carboxylate anion. Therefore, confirmation of the structure requires a comparison of the two mass spectra of the GPEtn obtained before and after

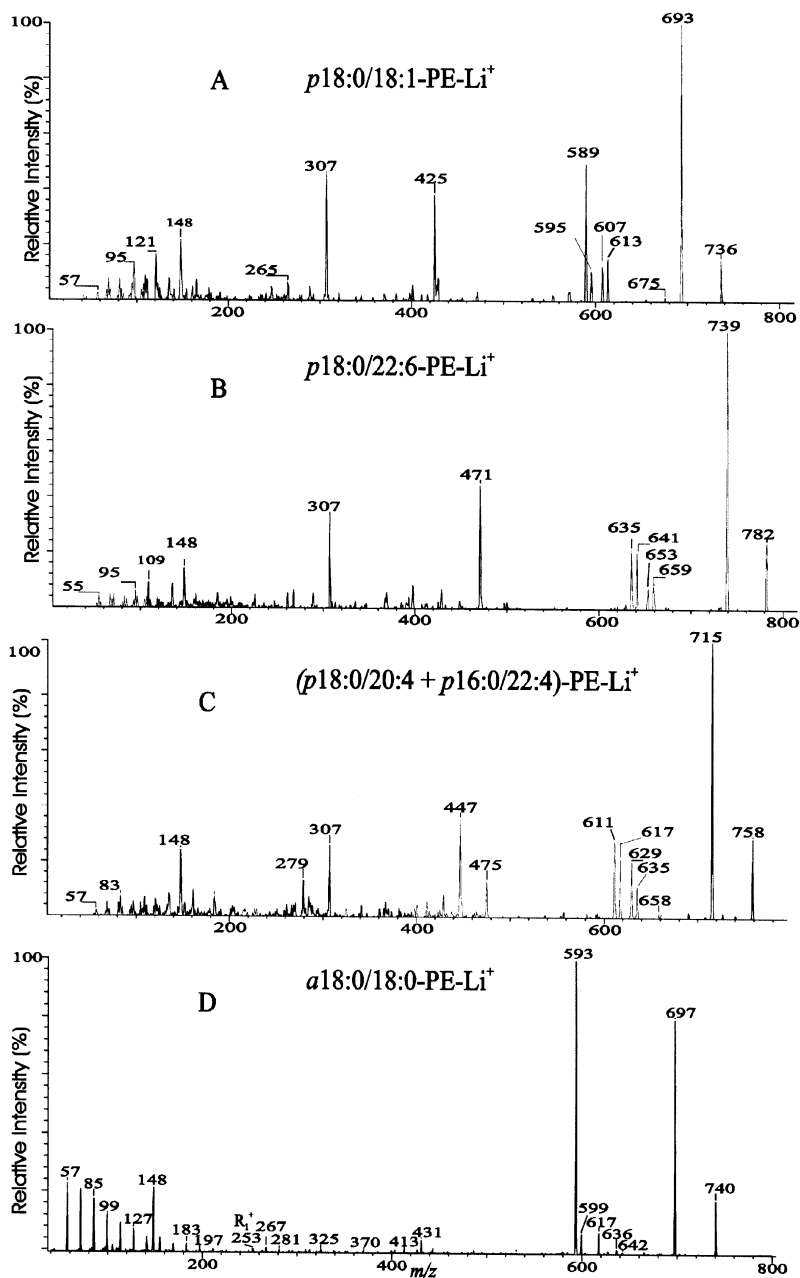


Fig. 3.8. The product-ion spectra of the $[M + \text{Li}]^+$ ions of (A) $p18:0/18:1\text{-PE}$ at m/z 736; (B) $p18:0/22:6\text{-PE}$ at m/z 782; (C) $(p18:0/20:4 + p16:0/22:4)\text{-PE}$; and of (D) $a18:0/18:0\text{-PE}$ at m/z 740.

destructive removal of plasmalogen GPEtn by acid treatment, which results in severe sample losses (62,63). The presence of the ion pairs also permits differentiation of a plasmalogen GPEtn from a plasmanyl-GPEtn, which lacks these ion pairs in its product-ion spectrum, as shown in Figure 3.8D.

The product-ion spectrum of *a*18:0/18:0-PE at m/z 740 (Fig. 3.8D) is also dominated by the $[M + Li - 43]^+$ ion at m/z 697. The spectrum also contains ions at m/z 617 ($[M + Li - 123]^+$), m/z 599 ($[M + Li - 141]^+$), m/z 593 ($[M + Li - 147]^+$), and m/z 148, similar to those observed in the spectrum of plasmalogen GPEtn. Since the ion pairs similar to those observed for plasmalogen GPEtn are absent, identification of the moieties at *sn*-1 and *sn*-2 would rely on the ions at m/z 431 ($[M + Li - 43 - R_2'CH=CO]^+$), arising from the loss of the ethylamine moiety as an aziridine combined with the loss of the *sn*-2 acyl chain as a ketene, as well as the ion at m/z 253 (R_1^+). The m/z 253 ion (R_1^+) is similar to that arising from plasmanyl-GPCho and gives rise to a series of $(CH_2)_nH^+$ ions that are diagnostic of the plasmanyl-GPEtn subclass. The spectrum also contains m/z 267 (R_2CO^+), which confirms the *sn*-2 fatty acyl moiety.

$[M - H + 2Li]^+$ Ions of GPEtn

In contrast, the product-ion spectrum of the $[M - H + 2Li]^+$ ion of 16:0/18:2-PE at m/z 728 (Fig. 3.9A) is dominated by m/z 599 ($[M - H + 2Li - 129]^+$) (**f** ion, Scheme 3.6) and m/z 136 ($[(LiO)_2P^+OCH_2CH_2NH]^+$) (**e**) ions, arising from cleavage of the C3O-P bond of the polar head group. The spectrum also contains a m/z 154 ion (**h**), arising from cleavage of the C3-OP bond, probably involving the participation of the hydrogen at C-2 of the glycerol backbone. Ions at m/z 685 ($[M - H + 2Li - 43]^+$) and 605 ($[M - H + 2Li - (HO)PO(OCH_2CH_2NH)^+$) are of low abundance, and the $[M - H + 2Li - 141]^+$ and $[M - H + 2Li - 147]^+$ ions are not present. The m/z 472 ion ($[M - H + 2Li - R_1CO_2H]^+$) is more abundant than the m/z 448 ion ($[M - H + 2Li - R_2CO_2H]^+$), consistent with the notion that the α -hydrogen of the fatty acyl substituent at *sn*-2, which participates in the R_1CO_2H loss, is more labile than that at *sn*-1. Ions at m/z 429 ($[M - H + 2Li - 43 - R_1CO_2H]^+$) and m/z 405 ($[M - H + 2Li - 43 - R_2CO_2H]^+$) arise from m/z 685 *via* further losses of the 16:0- and 18:1-fatty acids, respectively. The formation of these two ions involves the participation of the exchangeable hydrogen at the phosphate of the dilithiated 16:0/18:2-PA-like intermediate (Scheme 3.6, **g** ion), as evidenced by the product-ion spectra of deuterium-labeled analogs. The similar losses of the fatty acids as the lithium salts give rise to m/z 423 ($[M - H + 2Li - 43 - R_1CO_2Li]^+$) and m/z 399 ($[M - H + 2Li - 43 - R_2CO_2Li]^+$), respectively. The spectrum also contains ions at m/z 343 ($599 - R_1CO_2H$) and m/z 319 ($599 - R_2CO_2H$), arising from further losses of the fatty acids at *sn*-1 and *sn*-2 from m/z 599, respectively, as well as ions at m/z 337 ($599 - R_1CO_2Li$) and m/z 313 ($599 - R_2CO_2Li$), arising from the corresponding losses of the fatty acids as lithium salts. These ions reflecting the acid losses at *sn*-1 are about 2 times more abundant than those reflecting the analogous losses at *sn*-2. Therefore,

the identity and the regiospecificity of the fatty acyl substituents of the molecule can be easily determined. An ion corresponding to a lithiated 18:2 fatty acid from *sn*-2 was observed at m/z 287, but an analogous ion deriving from the *sn*-1 fatty acid was not observed. This provides direct assignment of the *sn*-2 fatty acid substituent.

Similar to dilithiated diacyl GPEtn, the product-ion spectrum of the dilithiated *p*16:0/20:4-PE at m/z 736 (Fig. 3.9C), is also dominated by the $[M - H + 2Li - 129]^+$ (m/z 607) and $[(LiO)_2P^+OCH_2CH_2NH]$ (m/z 136) ions, arising from cleavage of the CO-P bond as described in Scheme 3.6. However, ions that indicate the akenyl ether at *sn*-1 or the fatty acid at *sn*-2 are not present.

GPSer, GPGro, GPIno, and GPA

The similarities among the GPEtn, GPSer, and GPGro classes observed by ESI-MS lie not only in the formation of the molecular species, but also in their tandem mass spectra. The fragmentation pathways underlying the ion formation under low-energy CAD are nearly identical. The fragment ion species analogous to those arising from GPEtn for the $[M + Li]^+$ ions of GPSer, GPGro, and of GPA, as well as for the $[M - H + 2Li]^+$ ions of GPSer, GPGro, GPIno, and of GPA are listed in Table 1 and Table 2, respectively. The sensitivity of GPSer, GPGro, and GPA observed as $[M + Li]^+$ and $[M - H + 2Li]^+$ adduct ions, and of GPIno observed as the $[M - H + 2Li]^+$ ion, is significantly poorer than that observed in negative-ion mode, when ionized in the presence of Li^+ .

$[M + Li]^+$ Ions of GPSer and GPGro

The product-ion spectrum of the $[M + Li]^+$ ion of 18:0/18:1-PS at m/z 796 (Fig. 3.10A) contains ions at m/z 605 ($[M + Li - 191]^+$) and m/z 611 ($[M + Li - 185]^+$),

TABLE 3.1

Head Group-Related Ions Observed in the Product-Ion Spectra of the $[M + Li]^+$ Ions

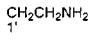
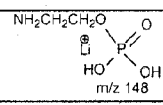
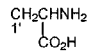
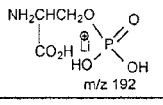
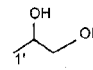
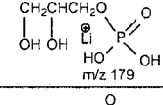
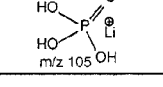

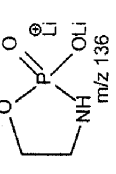
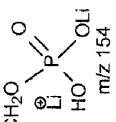
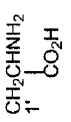
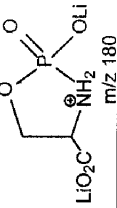
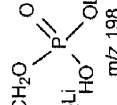
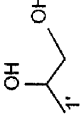
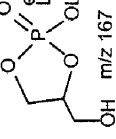
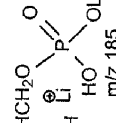
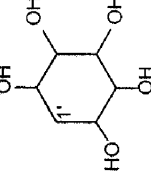
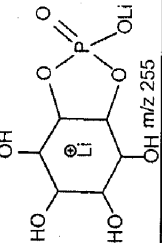
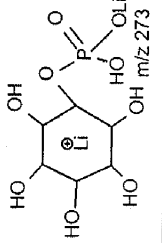
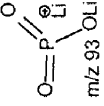
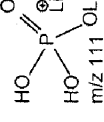
| Phospholipid | Head group (YH) | <u>a</u> | <u>a</u> - LiH_2PO_4 | <u>a</u> - H_3PO_4 | <u>b</u> |
|--------------|---|-------------------|------------------------|----------------------|--|
| PE |  | $[M + Li - 43]^+$ | $[M + Li - 147]^+$ | $[M + Li - 141]^+$ |  |
| PS |  | $[M + Li - 87]^+$ | $[M + Li - 191]^+$ | $[M + Li - 185]^+$ |  |
| PG |  | $[M + Li - 74]^+$ | $[M + Li - 178]^+$ | $[M + Li - 172]^+$ |  |
| PA | H | $[M + Li]^+$ | $[M + Li - 104]^+$ | $[M + Li - 98]^+$ |  |

TABLE 3.2
Head Group-Related Ions Observed in the Product-Ion Spectra of the $[M + 2Li]^+$ Ions

| Phospholipid | Head group (YH) | g | f | e | h |
|--------------|---|-------------------------|-------------------------|--|--|
| PE |  | $[M + 2Li - H - 43]^+$ | $[M + 2Li - H - 129]^+$ |  m/z 136 |  m/z 154 |
| PS |  | $[M + 2Li - H - 87]^+$ | - |  m/z 180 |  m/z 198 |
| PG |  | $[M + 2Li - H - 74]^+$ | $[M + 2Li - H - 160]^+$ |  m/z 167 |  m/z 185 |
| PI |  | $[M + 2Li - H - 162]^+$ | $[M + 2Li - H - 248]^+$ |  m/z 255 |  m/z 273 |
| PA | H | $[M + 2Li - H]^+$ | $[M + 2Li - H - 86]^+$ |  m/z 93 |  m/z 111 |

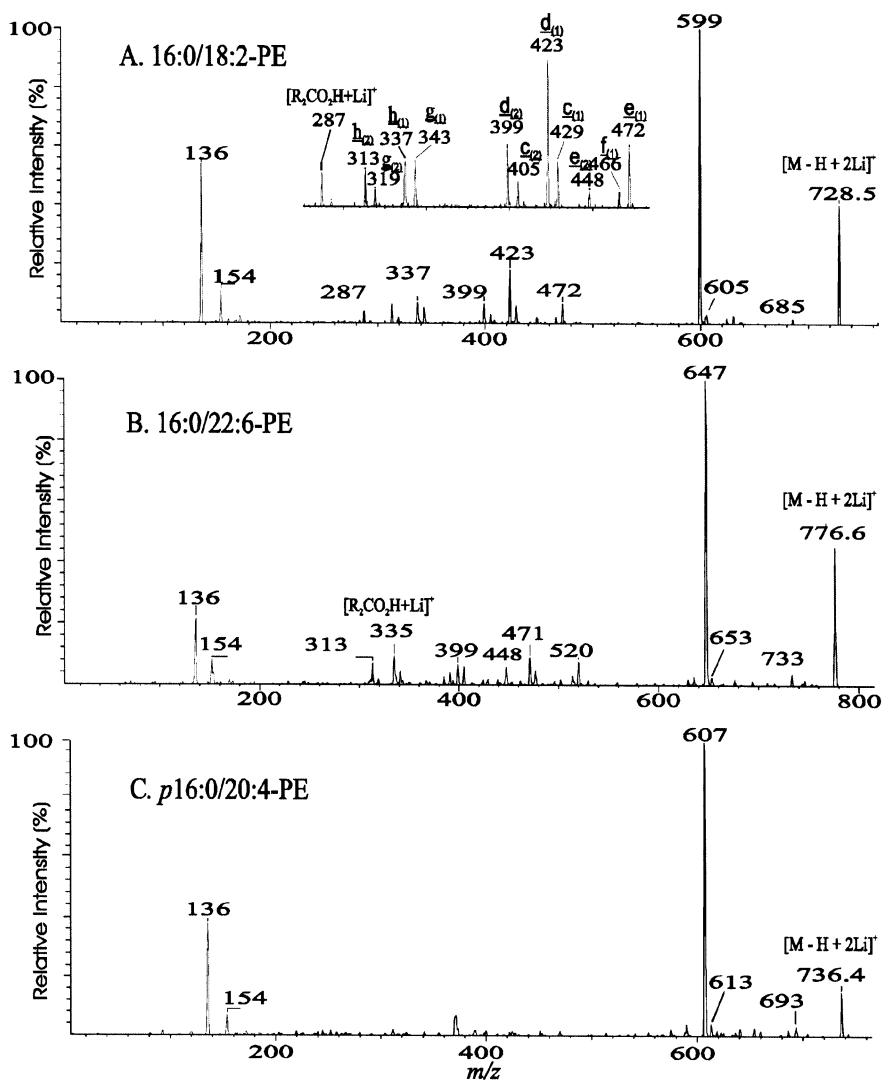


Fig. 3.9. The product-ion spectra of the $[M + 2Li - H]^+$ ions of (A) 16:0/18:1-PE at m/z 728; (B) 16:0/22:6-PE at m/z 776; and of (C) p16:0/20:4-PE at m/z 736.

arising from losses of phosphoserine as a lithium salt and as an acid, respectively, along with the lithiated phosphoserine at m/z 192 (Table 3.1, **b** ion). An ion arising from loss of the [serine - H_2O] moiety ($[M + Li - 87]^+$) is observed at m/z 709, which yields m/z 425 ($[M + Li - 87 - R_1CO_2H]^+$) and m/z 427 ($[M + Li - 87 - R_2CO_2H]^+$) via losses of the fatty acyl substituents at *sn*-1 and *sn*-2, respectively.

The m/z 425 ion is more abundant than the m/z 427 ion, similar to the behavior described for GPCho and GPETn, and this permits assignment of the location of the fatty acyl substituent on the glycerol backbone. The spectrum also contains a unique ion at m/z 698, arising from internal loss of phosphoric acid (98 Da) probably *via* a prior rearrangement process, as well as the acylium ions at m/z 267 (R_1CO^+) and m/z 265 (R_2CO^+). The m/z 698 is the most prominent ion in the MS²-spectrum obtained by an ITMS instrument (Fig. 3.10B), indicating that this rearrangement occurs as a more facile process in ITMS.

The $[M + Li]^+$ ion of 16:0/18:1-PG at m/z 755 undergoes similar fragmentation that results in a product-ion spectrum (Fig. 3.10C) with the feature that the $[M + Li - R_1CO_2H]^+$ ion at m/z 499 is more abundant than the $[M + Li - R_2CO_2H]^+$ ion at m/z 473. The spectrum also contains prominent ions at m/z 577 and 179 (Table 3.1), arising from the loss of the GPGro head group and from the lithiated head group ion. Analogous losses were observed for GPSer.

The major fragmentation processes observed for the $[M + Li]^+$ ion of 16:0/18:1-PA at m/z 681 (Fig. 3.10D) arise from loss of H_3PO_4 and LiH_2PO_4 , which give rise to m/z 577 and 583, respectively. The lithiated phosphoric acid ion expected at m/z 105 is not present. The product-ion spectrum of GPA is similar to that of GPETn, consistent with the notion that loss of ethylamine to give a GPA-like ion is the primary step leading to further dissociation of GPETn.

[M + 2Li - H]^+ Ions of GPSer, GPGro, GPIno, and GPA. ESI-MS/MS of the dilithiated adduct ion of 18:0/18:1-PS at m/z 802 (Fig. 3.11A) yields a major ion at m/z 715, arising from loss of serine ($[(M + 2Li - H) - 87]^+$) to form a dilithiated GPA-like ion. This ion undergoes further dissociation to form the ions at m/z 431 ($715 - R_1CO_2H$) and 433 ($715 - R_2CO_2H$), by eliminating the fatty acyl substituents at *sn*-1 and *sn*-2, respectively.

The additional Li^+ in the $[M + 2Li - H]^+$ ion species stabilizes the remote charge site, and CRF processes leading to acid losses that give ions of m/z 431 and 433 prevail. The preferential formation of the m/z 431 ion over the m/z 433 ion is due to the greater lability of the α -hydrogens of the *sn*-2 fatty acyl substituent, similar to the cases mentioned above. The cleavage of C3-OP bond to eliminate a dilithium salt of phosphoserine ($[(M + 2Li - H) - 197]^+$) gives rise to the m/z 605 ion, along with the head group ion at m/z 198 (Scheme 3.6, route *c*) (Table 3.2).

Similarly, MS/MS of the dilithiated adduct ion of 16:0/18:1-PG at m/z 761 (Fig. 3.11B) yields ions arising from the same fragmentation processes as described for GPSer. The spectrum has features at: m/z 505 ($761 - R_1CO_2H$) > 479 ($761 - R_2CO_2H$); and m/z 431 ($761 - 74 - R_1CO_2H$) > 405 ($761 - 74 - R_2CO_2H$). However, the ion at m/z 167, arising from cleavage of the C3O-P bond (Scheme 3.6, route *a*), rather than of the C3-OP bond as observed for GPSer, is the most prominent. The ions at m/z 601 and 607 resulting from losses of the phosphoglycerol head group are of low abundance. The preferential formation of m/z 167 from cleavage of the C3O-P bond over formation of m/z 601 suggests that the gas-phase

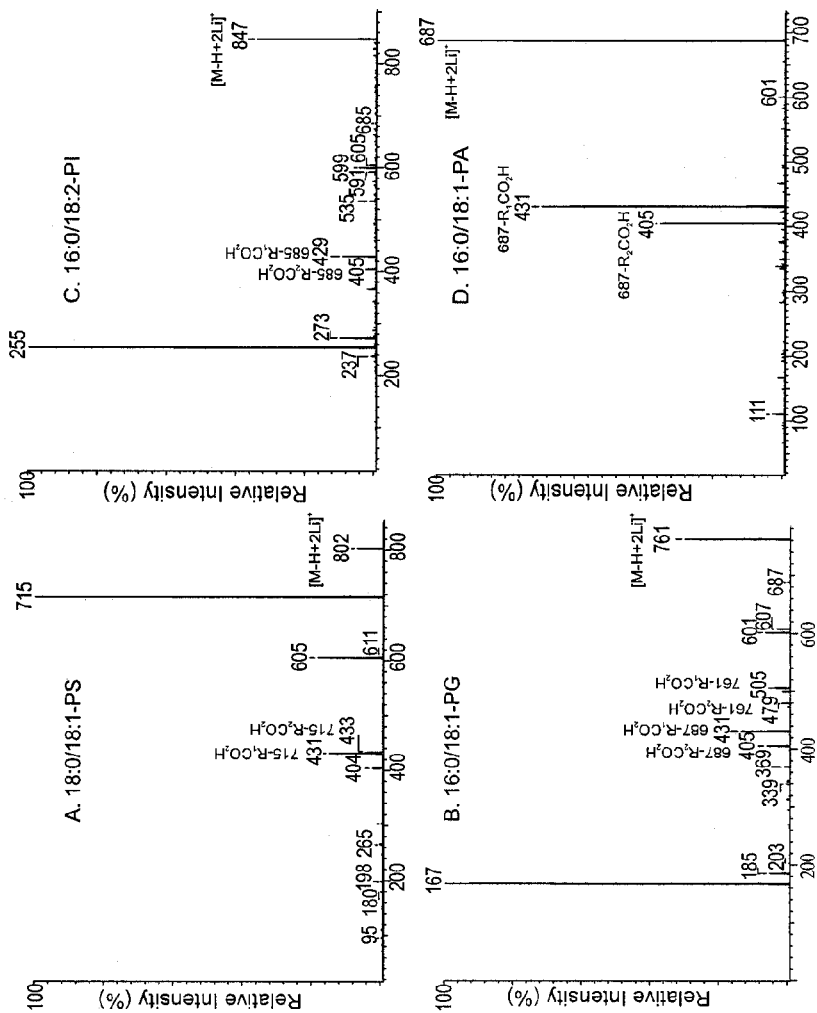


Fig. 3.11. The production-ion spectra of the $[M + 2Li - H]^+$ ions of (A) 18:0/18:1-PS at m/z 802; (B) 16:0/18:1-PG at m/z 761; (C) 16:0/18:2-PI at m/z 847; and of (D) 16:0/18:1-PA at m/z 687.

(LiO)(HO)P=O(OX) moiety (where X = glycerol - H₂O) is more competitive than the diacylglycerol moiety for Li⁺. Similar results are also observed for the [M + 2Li - H]⁺ ion of 16:0/18:2-PI at *m/z* 847 (Fig. 3.11C), which gives rise to a prominent [(LiO)(HO)P=O(OX) + Li]⁺ (where X = inositol - H₂O) (**e** ion) ion at *m/z* 255, and the lithiated diacylglycerol ion (**f** ion) at *m/z* 599 is of low abundance.

In contrast, the product-ion spectrum of the [M + 2Li - H]⁺ ion of 16:0/18:1-PA (Fig. 3.11D) at *m/z* 687 is rather simple. The *m/z* 431 (687 - R₁CO₂H) ion is more abundant than the *m/z* 405 (687 - R₂CO₂H) ion in the spectrum, and this difference is readily applicable for locating the fatty acyl substituents on the glycerol backbone.

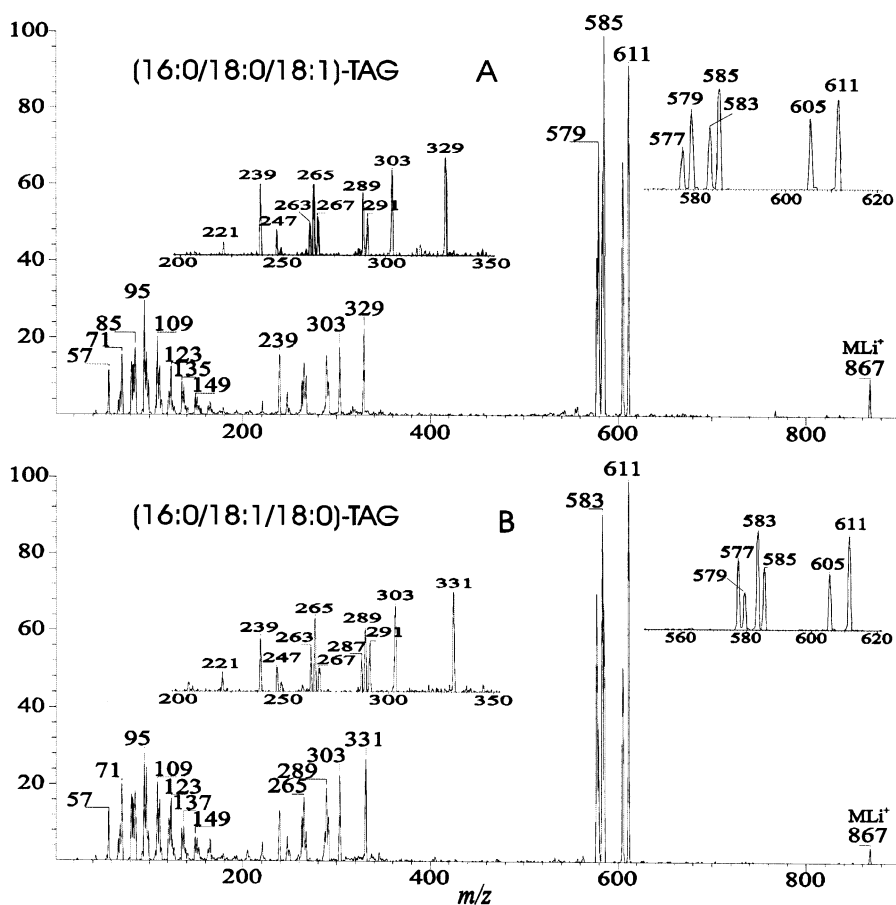


Fig. 3.12. The product-ion spectra of the [M + Li]⁺ ions of (16:0/18:0/18:1)-TAG (A) and of (16:0/18:1/18:0)-TAG at *m/z* 867 (B).

Triacylglycerols

The $[M + Li]^+$ ions of TAG are particularly important for structural characterization, because TAG molecules do not readily form $[M + H]^+$ or $[M - H]^-$ ions when ionized by ESI. Ions formed from low-energy CAD of $[M + Na]^+$ and of $[M + NH_4]^+$ ions also contain limited structural information. Thus, structural details such as the position of the fatty acyl moieties on the glycerol backbone, cannot be determined (64). However, high-energy CAD tandem MS of the $[M + NH_4]^+$ and $[M + Na]^+$ adduct ions generated by ESI, as well as by FAB, has been previously reported (65). The product-ion spectra contain abundant fragment ions, including ions arising from fragmentation of the fatty acyl substituents, but the spectra are rather complicated (65).

In contrast, low-energy CAD product-ion spectra of the $[M + Li]^+$ ions of TAG contain abundant fragment ions that are applicable for structural identification and differentiation of regioisomers (53). For example, the product-ion spectra of the lithiated adducts of isomers of (16:0/18:0/18:1)-TAG (Fig. 3.12A) and (16:0/18:1/18:0)-TAG at m/z 867 (Fig. 3.12B) contain ions at m/z 611, 583, and 585, reflecting losses of the 16:0, 18:0, and 18:1 fatty acids, respectively, and ions at m/z 605, 577, and 579, reflecting losses of the above fatty acids as lithium salts. The identities of the fatty acid substituents are also reflected in the $[R_nCO_2H + Li]^+$ ions at m/z 291, 289, and 263, for 18:0, 18:1, and 16:0-fatty acids, respectively. The spectra also contain acylium (R_nCO^+) ions at m/z 267 (18:0), 265 (18:1), and 239 (16:0), mainly arising from the secondary fragmentation of the $[M + Li - R_xCO_2Li]^+$ ion, a protonated ion species. Finally, the $[R_nCO^+ - 18]$ ions can be seen at m/z 249, 247, and 221 arising from the 18:0, 18:1, and 16:0-fatty acids, respectively. Therefore, the identities of fatty acyl moieties can be easily determined.

The ions at m/z 585 and m/z 611 in Figure 3.12A have similar abundances and are about 1.5-fold more abundant than the m/z 583 ion, which arises from loss of the 18:0-acid at *sn*-2. The abundances of the ions at m/z 579 and m/z 605 are also very similar and are more prominent than that of m/z 577, arising from loss of the 18:0-acid at *sn*-2 as a lithium salt. The above results suggest that the loss of the fatty acid at *sn*-2 as an acid or a lithium salt is a less favorable pathway than the analogous losses at *sn*-1 or *sn*-3, and that this provides information to locate the fatty acyl substituents on the glycerol backbone. The preferential formation of the ions corresponding to the fatty acyl moiety losses at *sn*-1 or at *sn*-3 over the ions arising from similar losses at *sn*-2 is consistent with the notion that the α -hydrogens of the fatty acyl chain at *sn*-2 are more labile and provide a proton for the neighboring fatty acyl substituents to promote the acid losses, as described earlier. Similar results are also observed for (16:0/18:1/18:0)-TAG (Fig. 3.12B), in which the ions at m/z 611 and m/z 583, arising from 16:0- (*sn*-1) and 18:0-fatty acid (*sn*-3) losses, respectively, are more abundant than m/z 585, arising from loss of the 18:1-acid at *sn*-2. Because the two spectra show substantial differences that are dependent on the positions of the fatty acid substituents, positional isomers can be easily distinguished.

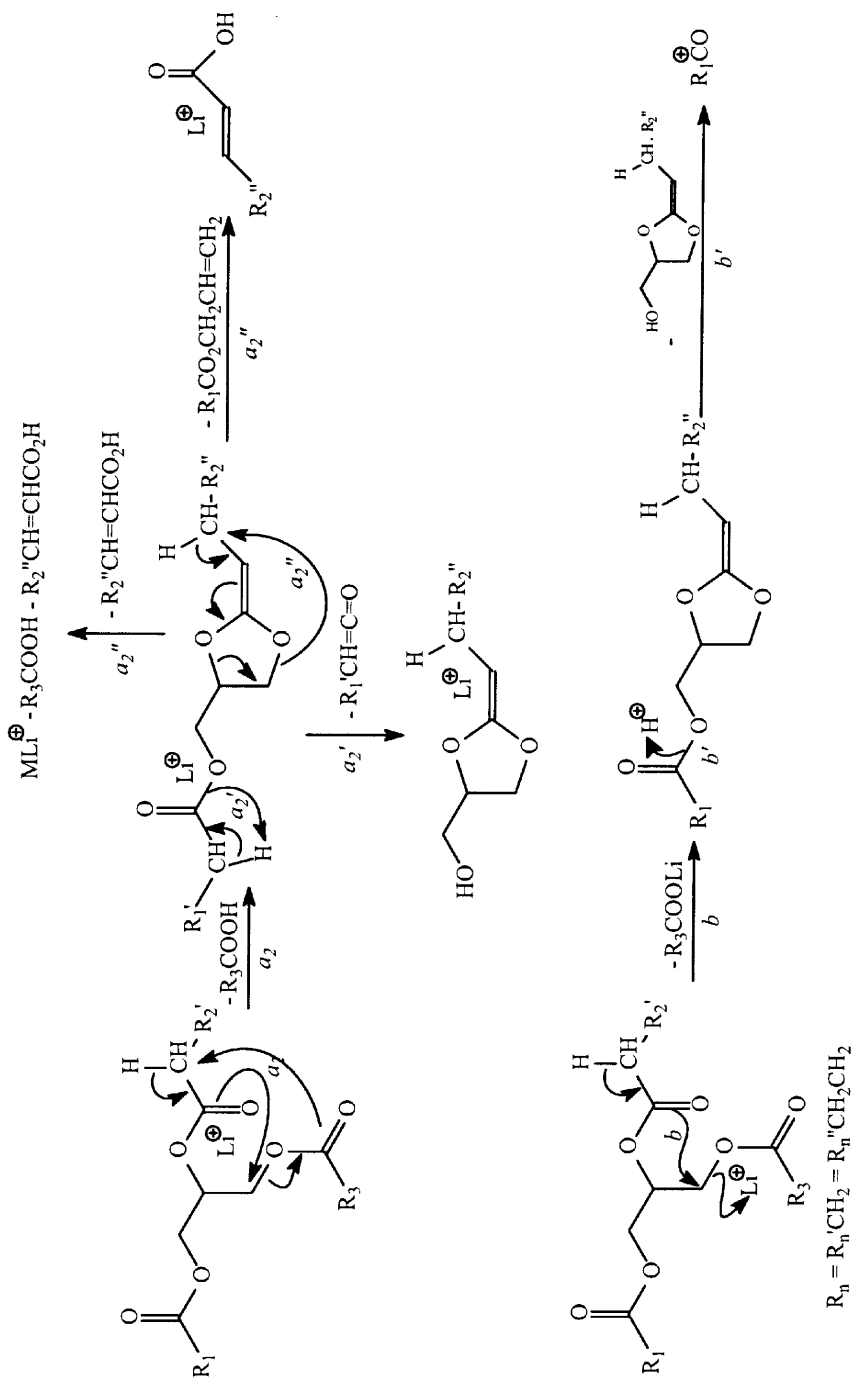
Two other characteristic ions that provide structural identification of (16:0/18:0/18:1)-TAG (Fig. 3.12A) are observed at m/z 329 and 303, arising from initial losses of the 16:0- (*sn*-1) and 18:1-fatty acids (*sn*-3), respectively, followed by loss of the *sn*-2 18:0-fatty acyl chain as an α,β -unsaturated fatty acid. The loss of the fatty acyl substituent at *sn*-2 as an α,β -unsaturated fatty acid was previously observed for GPCho and GPEtn. These pathways have been confirmed by the use of deuterium-labeled TAG analogs that give rise to the corresponding ions with the expected mass shifts (53). These results demonstrate that the $[M + Li - R_1CO_2H \text{ (or } R_3CO_2H)]^+$ is equivalent to the $[M + Li - 183]^+$ ion observed for lithiated GPCho, and the $[M + Li - 141]^+$ ion observed for lithiated GPEtn. This ion can then undergo consecutive elimination of the *sn*-2 fatty acyl substituent as an α,β -unsaturated fatty acid (Scheme 3.7).

Under low-energy CAD, the fragmentation processes for $[M + Li]^+$ ions of the glycerolipid classes of GPCho, GPEtn, GPSer, GPGro, and of TAG are similar. The α -hydrogens of the fatty acyl substituents participate in the losses of the adjacent fatty acyl moieties as free acids. The α -hydrogens of the fatty acyl substituent at *sn*-2 are more labile than those at *sn*-1 (and at *sn*-3 for TAG), leading to the preferential loss of R_1CO_2H (or R_3CO_2H) *via* CRF, over the similar loss at *sn*-2 (loss of R_2CO_2H). This fragmentation process results in an informative spectrum that permits assignment of the position and the identity of the fatty acyl substituents.

Ceramide

More than 30 ceramide (Cer) molecular species in nine subclasses have recently been analyzed as the $[M + Li]^+$ adduct ions by CAD tandem quadrupole MS with ESI (58). Both the FAB high-energy CAD (66–68) and the ESI low-energy CAD (58) product-ion spectra of the $[M + Li]^+$ adduct ions of ceramides contain structurally informative ions. All ceramides share similar fragmentation processes, but each individual ceramide subclass exhibits unique fragmentation processes that are useful for structural characterization.

N-Acylsphingosine (*d*18:1/*n*FA-Cer). The product-ion spectrum of the $[M + Li]^+$ ion of *d*18:1/24:1-Cer at m/z 654 (Fig. 3.13A) contains a prominent ion at m/z 636, arising from the loss of H_2O , and ions at m/z 618 and 606, arising from further losses of H_2O and HCHO, respectively. These losses are typical of lithiated *d*18:1/*n*FA-Cer. The analogous *d*₃-*d*18:1/24:1-Cer at m/z 657 (Fig. 3.13B), prepared by H-D exchange, gives two analogous ions at m/z 637 (loss of D_2O) and 638 (loss of DHO), which involve two and one losses of the exchangeable hydrogens, respectively. The source-CAD MS²-spectra of m/z 636, 637, and 638, generated by source CAD of the *d*18:1/24:1-Cer or *d*₃-*d*18:1/24:1-Cer, are also distinguishable, suggesting that the m/z 636 ion consists of several isomers (Scheme 3.8, ions **a**₁, **b**₁, **b**₁'). Loss of HCHO to give m/z 606, and further dissociation to yield a lithiated amide at m/z 372 (**d**_{1a}, Scheme 3.8A), are the major processes that were followed by the ion at m/z 636. The HCHO loss is consistent with the obser-



Scheme 3.7. Proposed fragmentation mechanisms of triacylglycerol lithium adducts.

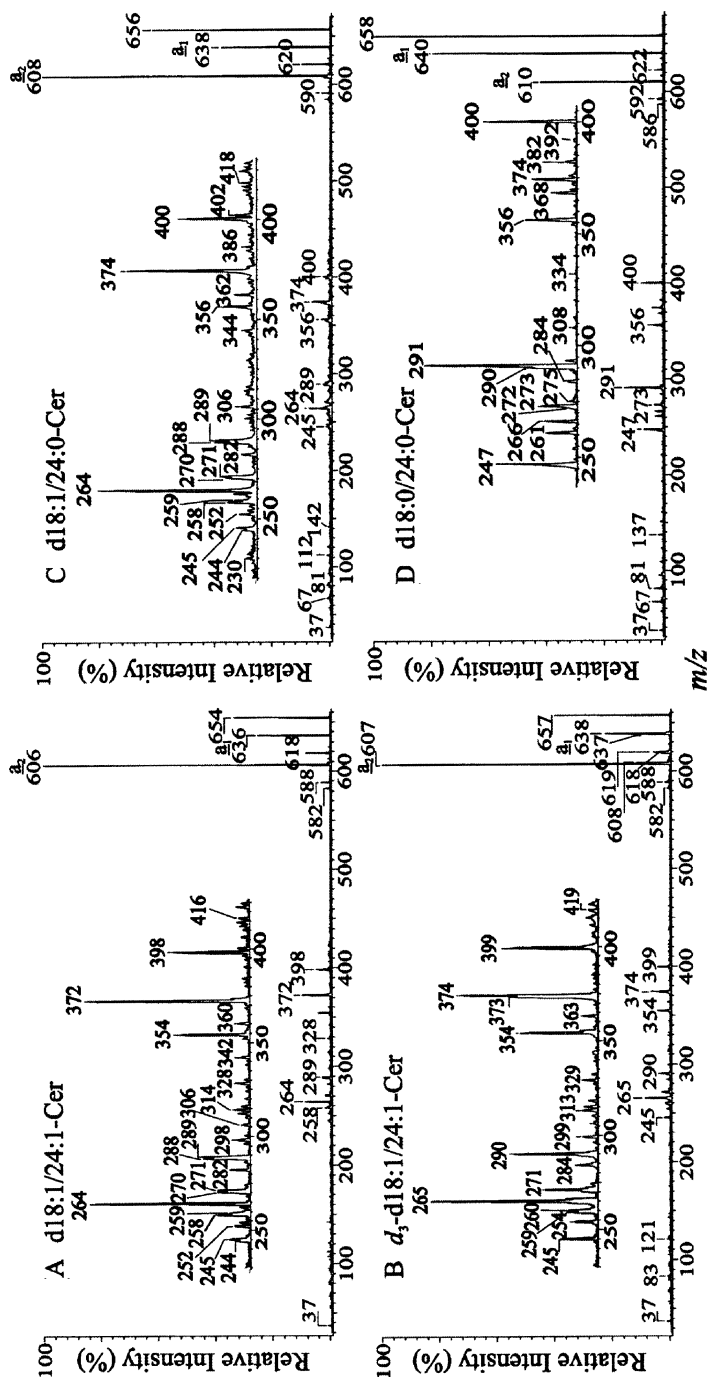
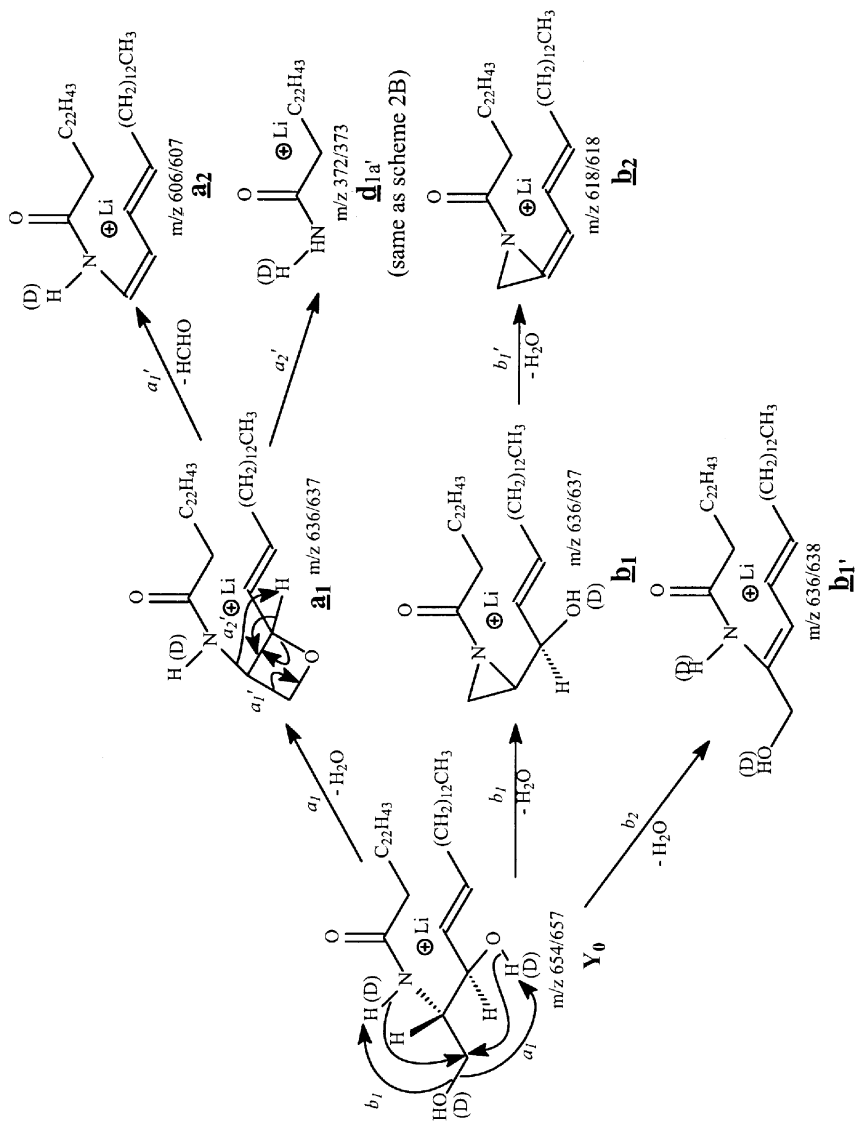


Fig. 3.13. The product-ion spectra of the $[M + Li]^+$ ions of (A) d18:1/24:1-Cer at m/z 654; (B) d_1 -d18:1/24:1-Cer at m/z 657; (C) d18:1/24:0-Cer at m/z 656; and of (D) d18:0/24:0-Cer at m/z 658.



Scheme 3.8. Proposed mechanisms of fragment formation from d18:1/24:1-Ceramide lithium adducts.

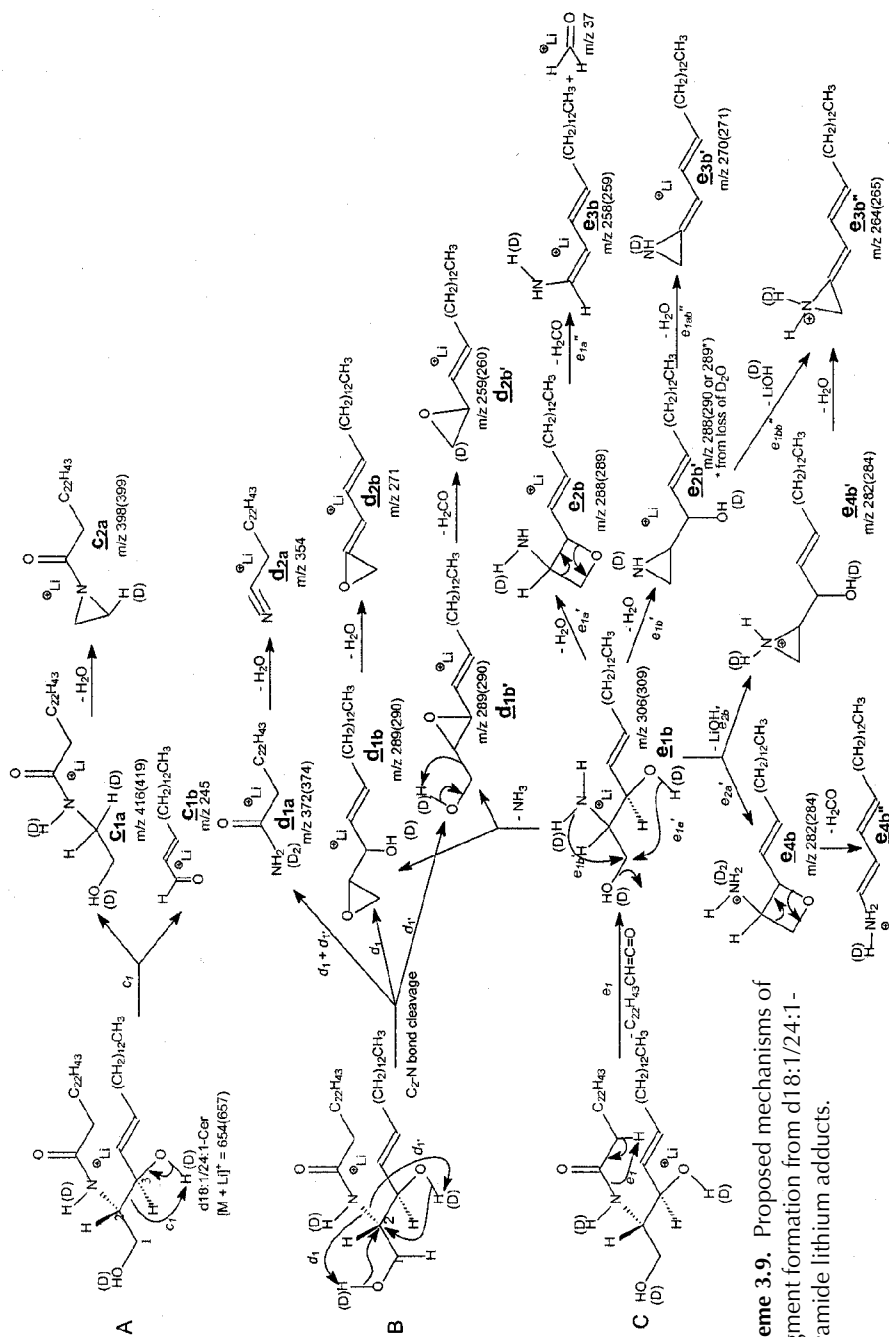
vation of the $[\text{HCHO} + \text{Li}]^+$ ion at m/z 37 (56). Similar fragmentation pathways are also observed for SM (54) and glycosphingolipids (56,57), which contain a ceramide nucleus.

Fragment ions arising from cleavages involving the LCB are essential for structural characterization. Some of the ions are of low abundance and thus are of less diagnostic value; nevertheless they appear to be the precursors of many prominent ions that lead to structural identification. The cleavage of the C2-C3 bond of the LCB (Scheme 3.9A) results in a lithiated aldehyde ion at m/z 245 ($[\text{CH}_3(\text{CH}_2)_{12}\text{CH}=\text{CH}-\text{CHO} + \text{Li}^+]$ (\mathbf{c}_{1b}), along with m/z 416 (\mathbf{c}_{1a}), which further dissociates to a prominent ion at m/z 398 (\mathbf{c}_{2a}) by loss of H_2O . The direct cleavage of the C2-N bond (Scheme 3.9B) gives rise to the m/z 372 ion (\mathbf{d}_{1a}), and an ion at m/z 289, representing a lithiated oxirane (\mathbf{d}_{1b}) or a lithiated epoxide ion ($\mathbf{d}_{1b'}$), respectively. The proposed structure of the m/z 289 ion is supported by the findings that both the m/z 271 (\mathbf{d}_{2b}) and m/z 259 ($\mathbf{d}_{2b'}$) ions are generated by the ion at m/z 289.

This leads to the assumption that m/z 271 arises from loss of H_2O from an oxirane intermediate of the m/z 289 ion (\mathbf{d}_{1b}), which is primarily formed by cleavage of the C2-N bond (route d_1) with the participation of the 1-hydroxy hydrogen. At the same time, the m/z 259 ($\mathbf{d}_{2b'}$) ion is formed by loss of HCHO from the lithiated epoxide intermediate of m/z 289 ($\mathbf{d}_{1b'}$), which arises from the same cleavage involving the 3-hydroxy hydrogen (route $d_{1'}$) of the LCB. The m/z 372 ion can also eliminate an H_2O to form an ion at m/z 354 (\mathbf{d}_{2a}).

The formation of m/z 306 (\mathbf{e}_{1b}) from m/z 654 *via* loss of the fatty acyl group as a ketene (loss of $\text{C}_{22}\text{H}_{43}\text{CH}=\text{C}=\text{O}$) (Scheme 3.9C) is another important fragmentation pathway, because the m/z 306 ion is a precursor of several ions that reflect the identity of 18:1-LCB, and it is the most prominent ion in the product-ion spectra of *N*- α -hydroxyacylsphingosines. The m/z 306 ion is equivalent to a lithiated sphingosine, and dissociates to form m/z 289 by loss of NH_3 (Scheme 3.9B) or to form m/z 288 by loss of H_2O (Scheme 3.9C). It is also the precursor leading to m/z 282 (\mathbf{e}_{4b}), 258, 270, 252, and 264, which are all characteristic of ceramides with a d18:1-LCB (Scheme 3.9C). The analogous ions are observed for ceramide subclasses with various LCB, including d16:1- and d18:0-LCB. The m/z 264 ($\mathbf{e}_{3b'}$) is the most prominent ion in the product-ion spectra of the $[\text{M} + \text{H}]^+$ ions of d18:1/nFA-Cer (47). The source-CAD product-ion spectrum of m/z 264 contains a prominent ion at m/z 82, possibly corresponding to a stable conjugated aziridine ion, and therefore the m/z 264 probably represents an alkenylaziridine ion (Scheme 3.3 and Scheme 3.9C, $\mathbf{e}_{3b''}$ ion) (56). The fatty acid moiety of the molecule is reflected by a major ion at m/z 372 (\mathbf{d}_{1a}). Therefore, the m/z 264 and m/z 372 ion pairs are indicative of a d18:1/24:1-Cer. The analogous ion pairs are observed at m/z 374 and m/z 264 for d18:1/24:0-Cer (from MS/MS of m/z 656, Fig. 3.13C), and at m/z 374 and m/z 266 for d18:0/24:0-Cer (from MS/MS of m/z 658, Fig. 3.13D), along with the other aforementioned ions deriving from various cleavages.

The product-ion spectrum of d18:0/nFA-Cer can be distinguished from that of d18:1/nFA-Cer by the fact that the $[\text{M} + \text{Li} - \text{H}_2\text{O} - \text{HCHO}]^+$ (\mathbf{a}_2) ions are the



most prominent for d18:1/nFA-Cer (Fig. 3.13A–C), while the $[M + Li - H_2O]^+$ (**a**₁) ions are the most abundant for d18:0/nFA-Cer (Fig. 3.13D), when the spectra are obtained at the same collision energy (50 eV). Ceramides with an 18:0-LCB yield analogous ions at m/z 266 (**e**_{3b}^o), and 272 (**e**_{3b}^v), as expected, but these are less prominent than in the spectra of the 18:1 LCB. The expected ion at m/z 260 is not present, attributable to the fact that these ions are less conjugated and less stable than those arising from d18:1/nFA-Cer. The product-ion spectrum of d18:0/24:0-Cer (Fig. 3.13D) contains a prominent ion at m/z 291 (**d**_{1b} + **d**_{1b}^v), and a protonated amide ion at m/z 368 ($C_{23}H_{47}CONH_3^+$). The prominence of the m/z 291 ion is due to the fact that C2–N bond cleavage (Scheme 3.9B) leading to the formation of this ion is the dominant pathway for the d18:0/nFA-Cer, while loss of the acyl moiety as a ketene and the consecutive dissociation to the m/z 264 ion is the major fragmentation pathway for d18:1/nFA-Cer.

N- α -Hydroxyacylsphing-4-enines (d18:1/hFA-Cer) and *N*- ω -hydroxyacylsphing-4-enines (d18:1/ ω FA-Cer). The lithiated *N*- α -hydroxyacylsphingenines undergo more extensive fragmentations than their *N*-acylsphingenine counterparts at the same collision energy. The product-ion spectrum of the lithiated d18:1/h24:0-Cer ion at m/z 672 (Fig. 3.14A) contains characteristic ions at m/z 654 ($[M + Li - H_2O]^+$) (**a**₁), m/z 636 ($[M + Li - 2H_2O]^+$) (**a**₁ – H₂O), and m/z 624 ($[M + Li - H_2O - HCHO]^+$) (**a**₂). However, cleavages initiated by the α -hydroxyl group of the *N*-acyl chain become the major fragmentation pathways (54–56,66,67) (Scheme 3.10A), which result in a lithiated *N*-formylsphingosine at m/z 334 (**f**_{1b}) and a lithiated aldehyde at m/z 345 ($[C_{22}H_{45}CHO + Li]^+$) (**c**_{3a}^v). The m/z 334 (**f**_{1b}) ion undergoes consecutive losses of H₂O or HCHO *via* the similar pathways as described in Scheme 3.8 to give m/z 316 (334 – H₂O), m/z 298 (334 – 2H₂O), and m/z 286 (334 – H₂O – HCHO). The α -hydroxyl group of the *N*-acyl chain also facilitates the formation of the ion at m/z 306, which is diagnostic for the d18:1/hFA-Cer subclass and arises from the same mechanism (Scheme 3.10B, route *e*₁).

Ions at m/z 416 (**c**_{2a}) and m/z 390 (**d**_{1a}) identify the h24:0 fatty acyl substituent. These are formed by the same pathways as observed for *N*-acylsphingosines but are less abundant, due to further dissociation initiated by the α -hydroxyl group leading to the m/z 345 ion, and to a lithiated aziridine ($[HNCH_2CH_2 + Li]^+$) ion at m/z 50 that becomes the major fragmentation process (Scheme 3.10C). The unique pattern observed in the product-ion spectrum of d18:0/nFA-Cer also occurs in the spectrum of *N*- α -hydroxyacylsphinganine (d18:0/hFA-Cer). This is demonstrated by the product-ion spectrum of d18:0/h16:0-Cer at m/z 562 (Fig. 3.14B), in which ions at m/z 514 ($[M + Li - H_2O - HCHO]^+$) and m/z 260 are of low abundance and ions at m/z 266 (**e**_{3b}^o) and m/z 272 (**e**_{3b}^v) indicative of a saturated LCB are absent, permitting its distinction from the d18:1/hFA-Cer subclass.

The pattern of the product-ion spectrum of d18:1/ ω 30:0-Cer at m/z 756 (Fig. 3.14C) is similar to that of d18:1/nFA-Cer (Fig. 3.13A–C), suggesting that frag-

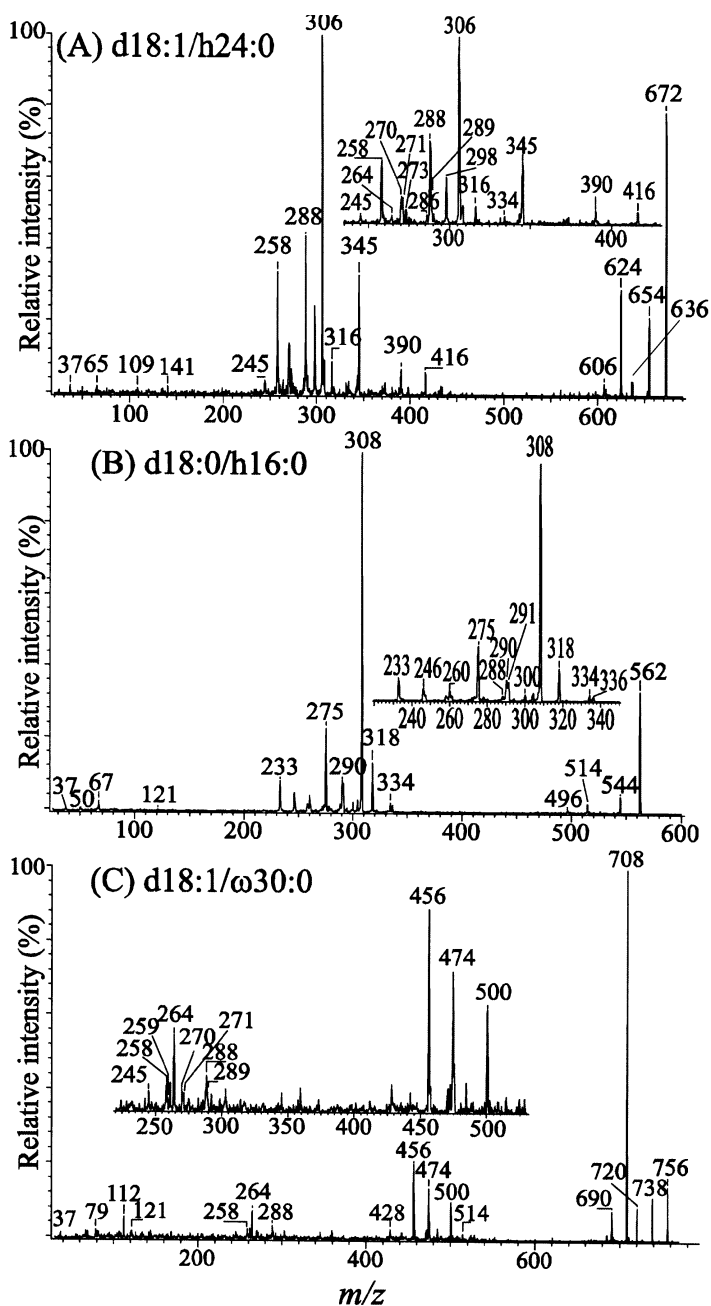


Fig. 3.14. The product-ion spectra of the $[M + Li]^+$ ions of (A) d18:1/h24:0-Cer at m/z 672; (B) d18:0/h16:0-Cer at m/z 562; and of (C) d18:1/ω30:0-Cer at m/z 756.

mentation processes for d18:1/nFA-Cer and d18:1/ ω FACer are similar. However, ions reflecting the ω -hydroxy fatty acyl substituent are prominent at m/z 500 (**e**_{2a}), m/z 474 (**d**_{1a}) and m/z 456 (**d**_{2a}). The ions that reflect the d18:1-LCB, for example, at m/z 264 (**e**_{3b'}), m/z 288 (**e**_{2b} + **e**_{2b'} + **e**_{2b''}), and m/z 258 (**e**_{3b}) are less abundant than the same ions observed for d18:1/nFA-Cer. Therefore, it can be concluded that the ω -hydroxyl group enhances the formation of the ions that reflect the fatty acyl substituents, while the α -hydroxyl group induces fragmentation.

N-Acyl-4-hydroxysphinganine (*N*-Acylphytosphingosine) and *N*- α -hydroxyacyl-4-hydroxysphinganine (*N*- α -Hydroxyacylphytosphingosine). The production spectrum of *N*-acylphytosphingosine distinguishes itself from that of other subclasses. As shown in Figure 3.15A, the product-ion spectrum of the $[M + Li]^+$ ion of *N*-tetradodecanoylphytosphingosine (t18:0/24:0-Cer) at m/z 674 is dominated by the m/z 656 ($674 - H_2O$) (**a**₁), m/z 626 ($656 - HCHO$) (**a**₂), m/z 638 (**a**₁ - H_2O), and m/z 608 (**a**₂ - H_2O) ions. However, the m/z 626 is less prominent than its precursor ion of m/z 656, representing a reversal from what was observed in Fig. 13A–C, which arose from d18:1/nFA-Cer. This reflects the fact that the **a**₂ ion at m/z 626 is less conjugated than the analogous ion arising from d18:1/nFA-Cer. This is consistent with the prominence of the (**a**₂ - H_2O) ion at m/z 608, arising from further loss of H_2O with the participation of the hydroxyl group at C-4 of the LCB to form a stable conjugated ion, which is equivalent to the **a**₂ ion observed in the product-ion spectrum of d18:1/nFA-Cer.

The prominent ion pairs at m/z 428 (**b**_{1a}) and m/z 416 (**b**_{1b}) are unique to this subclass. The m/z 428 ion (**b**_{1a}) may arise from the lithiated aziridine intermediate of m/z 656 (**b**₁) via cleavage of the C-C bond of the 3,4-diol of the LCB (Scheme 3.11). This cleavage also results in a weak ion at m/z 233, corresponding to a lithiated aldehyde ($[C_{14}H_{29}CHO + Li]^+$). Another proposed pathway for formation of the m/z 428 ion involves a primary cleavage of the same bond from m/z 674 via combined losses of an aldehyde and H_2 to yield to a m/z 446 intermediate, which further dissociates to m/z 428 or m/z 416 by loss of an H_2O or HCHO (Scheme 3.11). The observation of these two ions, plus the ions at m/z 400 (**c**_{2a}), m/z 374 (**d**_{1a}), and m/z 356 (**d**_{2a}) (Scheme 3.9B), commonly observed for 24:0-FA, easily identifies the fatty acyl constituent of the molecule. The phytosphingosine LCB can be identified by the m/z 288 (**e**_{3b'}), 289 (**d**_{2b}), 263 (**c**_{1b}), 307 (**d**_{1b} + **d**_{1b'}), and 306 (**e**_{2b} + **e**_{2b'} + **e**_{2b''}) ions.

In the same spectrum, a set of ions at m/z 442, 430, 414, 388, and 370, which reflect the 25:0-FA (the masses are 14-Da higher than the corresponding ions arising from a 24:0-FA) are also observed, along with ions at m/z 274 (**e**_{3b}), m/z 275 (**d**_{2b}), m/z 293 (**d**_{1b} + **d**_{1b'}), and m/z 249 (**c**_{1b}), arising from t17:0-LCB. These ions clearly demonstrate that the lithiated molecular species of m/z 674 also contains a t17:0/25:0-Cer isomer. A minor t16:0/26:0-Cer isomer is also present in the spectrum. This is revealed by the masses of m/z 456, 444, 428 (overlapped with the ions from t18:0/24:0-Cer), 402, and 384, which reflect the 26:0-FA, as well as the

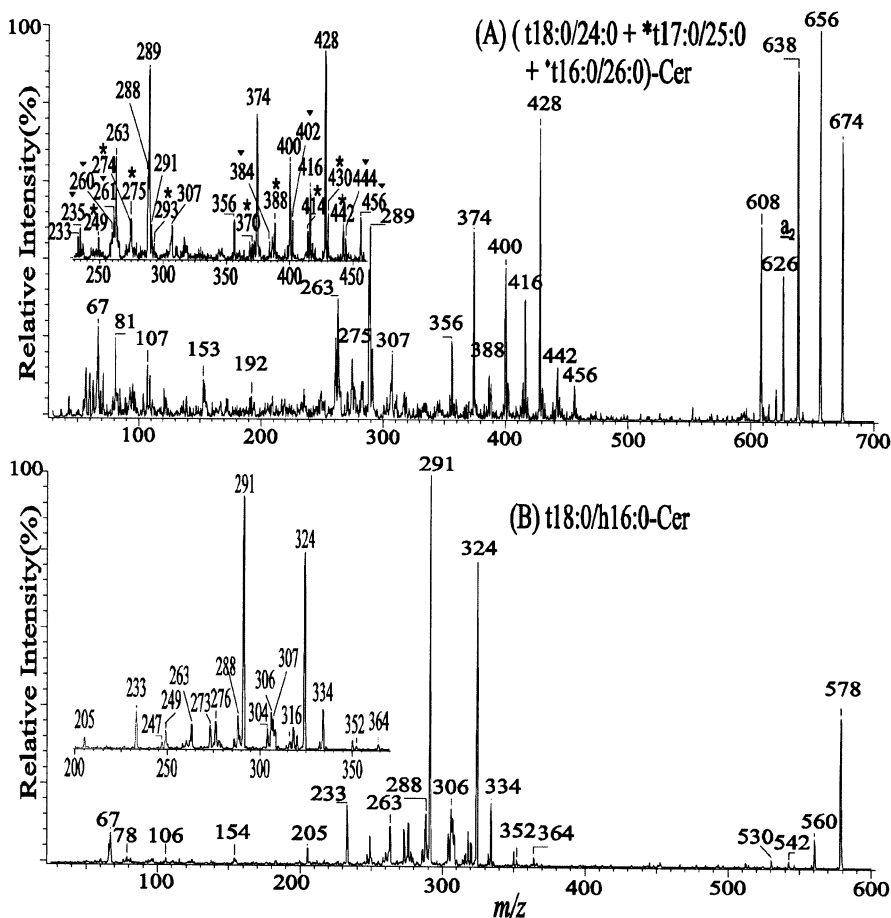
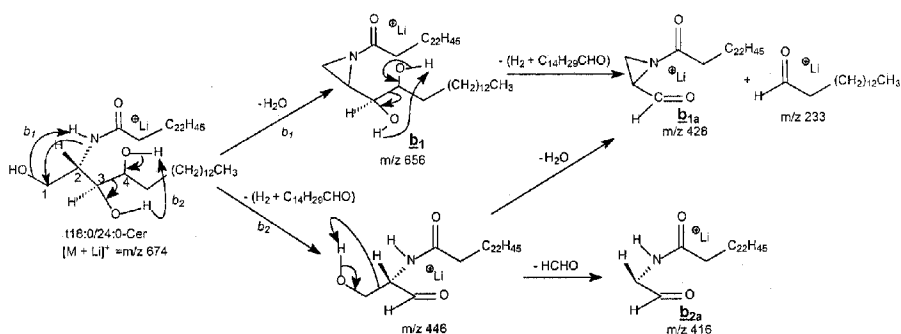


Fig. 3.15. The product-ion spectra of the $[M + Li]^+$ ions of (A) (t18:0/24:0 + t17:0/25:0 + t16:0/26:0)-Cer at m/z 674, and of (B) t18:0/h16:0-Cer at m/z 578.

masses at m/z 235 (**c_{1b}**), m/z 260 (**e_{3b}**), and m/z 261 (**d_{2b}**) that reflect the t16:0-LCB.

The fact that an α -hydroxyl group in the *N*-acyl chain facilitates the decomposition of ceramides is also reflected by the product-ion spectra of *N*- α -hydroxyacylphosphingosines. Figure 3.15B illustrates that the product-ion spectrum of the $[M + Li]^+$ ion of t18:0/h16:0-Cer at m/z 578 contains weak ions at m/z 560 ($[M + Li - H_2O]^+$) (**a₁**), m/z 542 ($[M + Li - 2H_2O]^+$) (**a₁ - H₂O**), and m/z 530 ($[M + Li - H_2O - HCHO]^+$) (**a₂**). The m/z 304 (**c_{2a}**) and m/z 233 (**c_{3a}**) ions that reflect the t16:0-FA are of low abundance. However, the analogous ions at m/z 656 (**a₁**), 638



Scheme 3.11. Proposed mechanisms of fragment formation from ceramide lithium adducts.

(**a**₁ – H₂O), and 608 (**a**₂) observed in the spectrum of t18:0/24:0-Cer are among the most prominent (Fig. 3.15A).

Again, the cleavage of the amide N-CO bond initiated by the α -hydroxyl group is the major fragmentation process for the lithiated t18:0/h16:0-Cer. This fragmentation process leads to a prominent ion at m/z 324 ($[M + Li]^+ - CO - C_{14}H_{29}CHO$) (**e**_{1b}), which undergoes an H₂O loss to yield an aziridine (**e**_{2b}) or an oxetane (**e**_{2b}) ion at m/z 306, followed by elimination of an H₂O or HCHO to form the m/z 288 (**e**_{3b}) or m/z 276 (**e**_{3b}) ion, respectively. The ions at m/z 352 ($[M + Li]^+ - C_{14}H_{29}CHO$) (**f**_{1b}), m/z 334 (**f**_{1b} – H₂O) (**f**_{2b} + **f**_{2b}'), m/z 316 (**f**_{2b} – H₂O) (**f**_{3b}), and m/z 304 (**f**_{2b}' – HCHO) (**f**_{3b}) arise from the same pathways as described for *N*- α -hydroxyacylsphingosines (Scheme 3.10A).

The apparent distinction between the product-ion spectra of the lithiated *N*- α -hydroxyacylsphingosine and of the lithiated *N*- α -hydroxyacylphytosphingosine lies in the fact that the **d**_{3b} series ion at m/z 273 in the former spectrum (Fig. 3.14A) is of low abundance, while the analogous ion at m/z 291 in the spectrum of t18:0/h16:0-Cer (Fig. 3.15B) is the most prominent. The prominence of the **d**_{3b} ions observed for the *N*- α -hydroxyacylphytosphingosines, but not for the *N*- α -hydroxyacylsphingosines, may indicate that further dissociation of the **d**_{3b} ion from the *N*- α -hydroxyacylphytosphingosines is thermodynamically less favorable than that from the *N*- α -hydroxyacylsphingosines, which possess an unsaturated LCB. This notion is consistent with the prominence of the analogous ion of m/z 275 in the product-ion spectrum of d18:0/h16:0-Cer (Fig. 3.14B), which consists of a saturated LCB.

N- ω -Hydroxyacyl-6-hydroxysphing-4-ene (t18:1/ ω FA-Cer) and *N*- α -hydroxy-6-hydroxysphing-4-ene (t18:1/hFA-Cer). *N*- ω -Hydroxyacyl-6-hydroxy-4-sphingenine (t18:1/ ω FA-Cer) is a protein-bound ceramide found in human stratum corneum, whereas *N*- α -hydroxy-6-hydroxysphing-4-ene

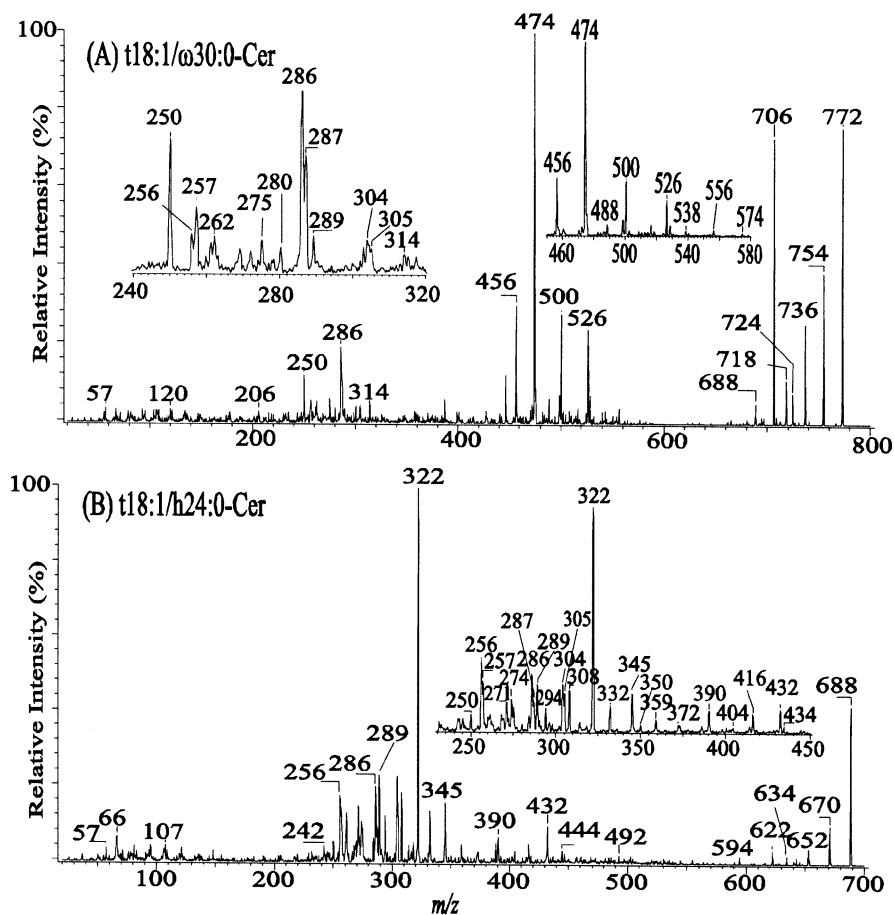


Fig. 3.16. The product-ion spectra of the $[M + Li]^+$ ions of (A) t18:1/ ω 30:0-Cer at m/z 772, and of (B) t18:1/h24:0-Cer at m/z 688.

(t18:1/hFA-Cer) is not protein bound (69). The major species of t18:1/ ω FA-Cer found in human stratum corneum is t18:1/ ω 30:0-Cer, which gives an $[M + Li]^+$ ion at m/z 772. Upon CAD, the m/z 772 ion yields intense fragment ions at m/z 754 ($772 - H_2O$), m/z 736 ($772 - 2H_2O$), and m/z 718 ($772 - 3H_2O$), by consecutive losses of H_2O , and ions at m/z 724 ($754 - HCHO$), m/z 706 ($736 - HCHO$), and m/z 688 ($716 - HCHO$) generated by loss of HCHO (Fig. 3.16A). The m/z 688 ion can also arise from additional loss of H_2O from m/z 706, involving the ω -hydroxyl group of the fatty acid substituent. The ω -hydroxytriacontanoic acid moiety (ω 30:0) was identified by the presence of the prominent ions at m/z 500 (c_{2a}), 526

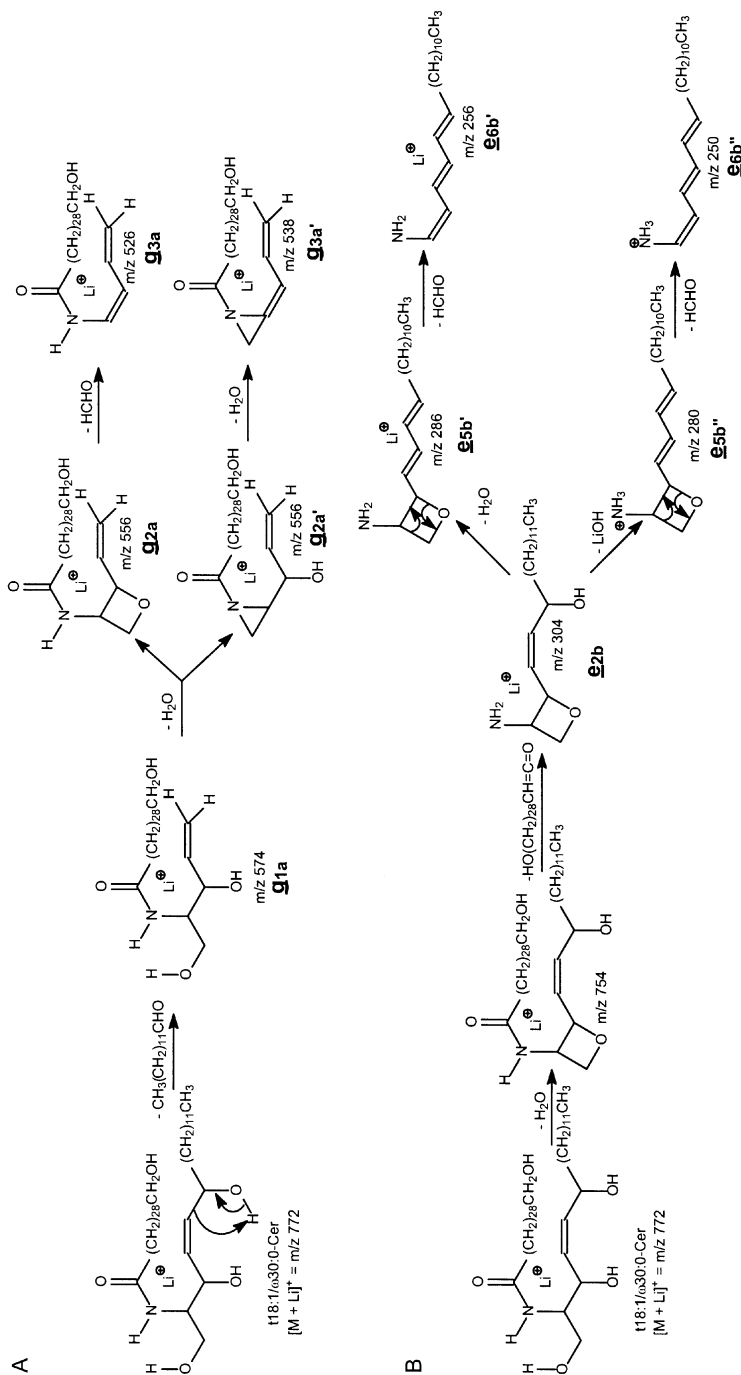
(**g**_{3a}), 474 (**d**_{1a}), and 456 (**d**_{2a}), which are also abundant in the spectrum of d18:1/ω30:0-Cer (Fig. 3.14C).

The ions specific to this subclass arise from the decompositions initiated by cleavage of the C5-C6 bond of the LCB to eliminate an aldehyde to yield an ion at *m/z* 574 (**g**_{1a}) (Scheme 3.12A). This is followed by a water loss step as described earlier, to yield both lithiated oxetane (**g**_{2a}) and aziridine (**g**_{2a'}) intermediates at *m/z* 556, which dissociate to *m/z* 526 (**g**_{3a}) and *m/z* 538 (**g**_{3a'}) by expulsion of HCHO and H₂O, respectively. The t18:1-LCB is recognized by the prominent **e**_{3b'} ion at *m/z* 286, which arises from *m/z* 754 ([M + Li - H₂O]⁺) (**a**₁) by initial loss of the ω-hydroxyl fatty acid as a ketene (loss of HO(CH₂)₂₈CH=C=O) to yield the *m/z* 304 ion, probably as a lithiated oxetane. This is followed by loss of an H₂O or a LiOH to yield the *m/z* 286 (**e**_{5b'}) or *m/z* 280 (**e**_{5b''}) ion, respectively (Scheme 3.12B). These fragmentation processes also result in the *m/z* 256 (**e**_{6b'}) and *m/z* 250 (**e**_{6b''}) ions by further expulsion of HCHO, and are consistent with the idea that a lithiated oxetane intermediate was primarily formed. Therefore, ceramides with a t18:1-LCB can be easily recognized by the presence of ions at *m/z* 250, 256, 280, and 286, in addition to ions at *m/z* 305 (**d**_{1b} + **d**_{1b'}), 287 (**d**_{2b}), 304 (**e**_{2b} + **e**_{2b'}), 275 (**d**_{2b'}), and 289 (**d**_{3b}).

The subclass of t18:1/hFA-Cer found in human stratum corneum is mainly composed of t18:1/h24:0-Cer and t18:1/h26:0-Cer (69). The [M + Li]⁺ ion of t18:1/h24:0-Cer at *m/z* 688 (Fig. 3.16B) undergoes vigorous fragmentation when subjected to CAD, attributable to the presence of the α-hydroxyl group in the fatty acyl substituent. The major ions arise from the same fragmentation pathways as described in Scheme 3.10A and B. The product-ion spectrum is dominated by a peak at *m/z* 322 (**e**_{1b}), and also contains ions at *m/z* 289 (**d**_{3b}), *m/z* 304 (**e**_{2b} + **e**_{2b'} + **e**_{2b''}), and *m/z* 286 (**e**_{3b'} + **e**_{5b'}) that reflect the 6-hydroxysphing-4-enine LCB. The ions at *m/z* 345 (**c**_{3a'}), *m/z* 416 (**c**_{2a}), and *m/z* 390 (**d**_{1a}) reflect the h24:0 fatty acyl substituent, but are of low abundance. In contrast, the [M + Li]⁺ ions of t18:1/ωFA-Cer (Fig. 3.16A) undergo less fragmentation, and the product-ion spectra are dominated by ions reflecting the fatty acyl substituent.

Glycosphingolipids

The use of tandem MS with ESI in the studies of GSL as lithiated adducts has been reported by several groups (55–57). The product-ion spectra of glycosphingolipids contain common ions similar to those observed for ceramides and ions arising from the sugar moieties, indicating that loss of the sugar moiety is the primary step leading to further fragmentations. As shown in Figure 3.17A, the product-ion spectrum of the [M + Li]⁺ ion of d18:1/24:0-GalCer at *m/z* 818 contains the ion series of *m/z* 656, 638, 620, and 608, which are characteristic ions of d18:1/24:0-Cer. The ions reflecting the fatty acyl substituent and LCB are also identical to those observed for d18:1/24:0-Cer (Fig. 3.13C). The sugar moiety is reflected by ions at *m/z* 187, 169 (187 - H₂O), 127, and 97 (Scheme 3.13). The product-ion spectra of both d18:1/24:0-GluCer and



Scheme 3.12. Proposed mechanisms of fragment formation from $t18:1/\omega30:0$ -Ceramide lithium adducts.

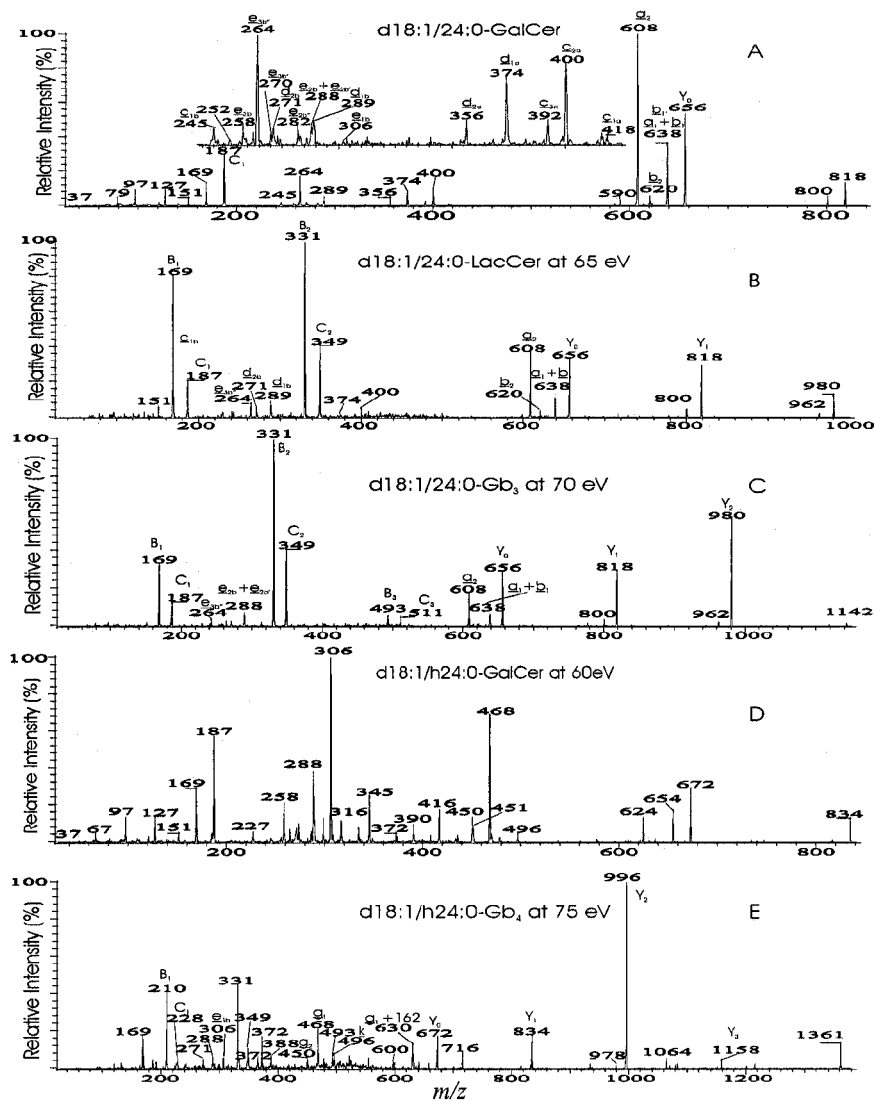
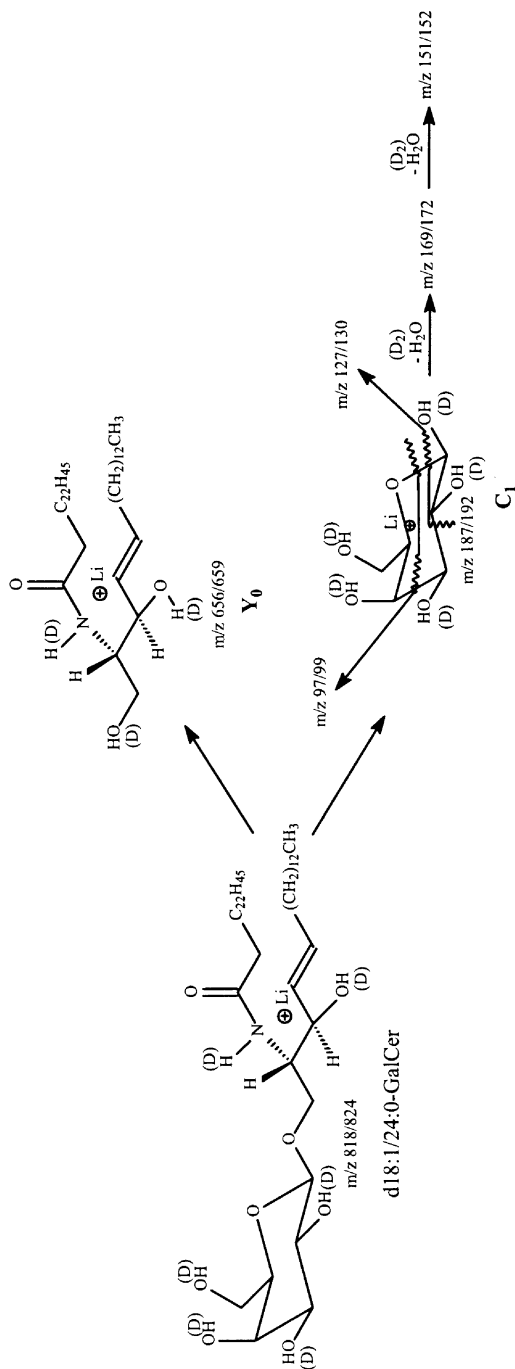


Fig. 3.17. The product-ion spectra of the $[M + Li]^+$ ions of (A) d16:1/24:0-GalCer at m/z 818; (B) d18:1/24:0-LacCer at m/z 980; (C) d18:1/24:0-Gb₃ at m/z 1142; (D) d18:1/h24:0-GalCer at m/z 834; and of (E) d18:1/h24:0-Gb₄ at m/z 1361.

d18:1/24:0-GalCer, which give the same $[M + H]^+$ at m/z 818, are identical. The product-ion spectra of d18:1/24:0-LacCer (Fig. 3.17B), which consists of a disaccharide, and of d18:1/24:0-Gb₃ (Fig. 3.17C), an analog containing a trihexose, are also similar.



Scheme 3.13. Proposed mechanisms of fragment formation from lithium adducts of galactosylceramide.

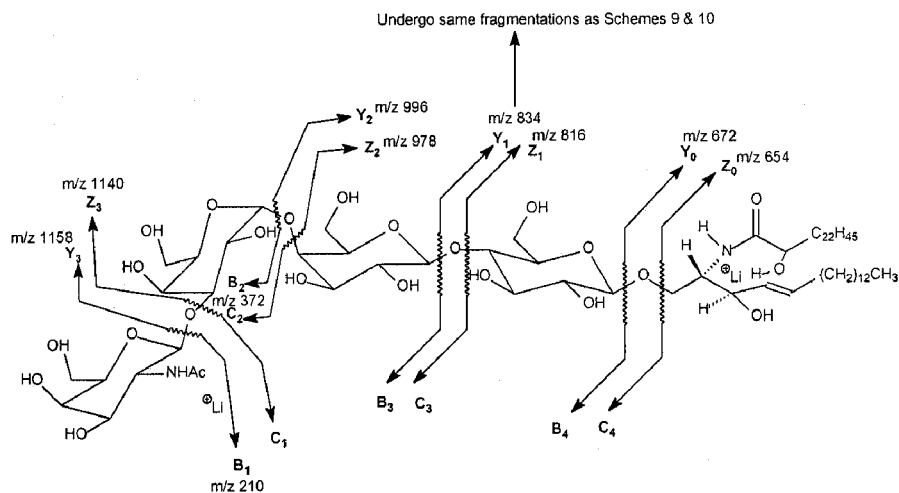
This is consistent with the notion that loss of the sugar moiety is the primary fragmentation process. It is interesting to note that the ions reflecting the sugar moieties become more prominent as the size of the sugar moiety increases.

The product-ion spectrum of the $[M + Li]^+$ ion of d18:1/h24:0-GalCer (Fig. 3.17D) contains ions similar to those observed for d18:1/h24:0-Cer (Fig. 3.14A), but the spectrum is dominated by m/z 468, arising from cleavage of the C-C bond between the carbonyl and the α -hydroxyl group of the fatty acyl chain *via* the same fragmentation pathway as described in Scheme 3.10B. The spectrum also contains ions at m/z 306 and m/z 288, arising from further losses of a dehydrated hexose (162 Da) and hexose (180 Da) from m/z 468, respectively. The product-ion spectrum of d18:1/h24:0-Gb₄ at m/z 1361 (Fig. 3.17E) also contains ions that are characteristic of d18:1/hFA-GluCer, but the spectrum is dominated by m/z 996, deriving from loss of the Gal-NAcGal moiety (Scheme 3.14). The spectrum also contains ions that are typical of d18:1/hFA-ceramide and ions from various losses of the sugar moiety (70).

Sphingomyelin

The major fragment ions observed for sphingomyelin (SM), ceramide, and GSL under low-energy CAD are similar. The product-ion spectrum of the lithiated 18:1/24:1-SM at m/z 819 (Fig. 3.18A) is dominated by m/z 636 ($[M + Li]^+ - 183$), arising from primary loss of the trimethylamine to give m/z 760, followed by elimination of an ethylene phosphate [(HO)P(O)(OCH₂CH₂O)] to give rise to a dehydrated ceramide ion. The loss of lithium ethylene phosphate [(LiO)P(O)(OCH₂CH₂O)] from m/z 760 gives rise to m/z 630 ($[M + Li]^+ - 189$). These fragmentation processes are identical to those described for GPCho (Scheme 3.15). Further losses of HCHO and of H₂O from m/z 636 give rise to ions at m/z 606 and m/z 618, respectively. The m/z 630 is a protonated ion and undergoes a loss of H₂O to another protonated species of *N*-acyl aziridine at m/z 612 (**a'**), which gives rise to m/z 390 (**a**) and m/z 264 (**b**), by loss of the LCB as a conjugated diene and by loss of the fatty acyl group as a ketene, respectively (Scheme 3.15).

The m/z 264 ion is diagnostic of a d18:1-LCB, while the m/z 390 (**a**) ion reflects the 24:1-fatty acyl moiety. The m/z 390 ion is also present in the product-ion spectrum of the $[M + H]^+$ ion of d18:1/24:1-Cer (Fig. 3.2A), but not in the spectra of the $[M + Li]^+$ ions of d18:1/24:1-Cer (Fig. 3.13A) and of d18:1/24:1-GalCer (Fig. 3.17A). This confirms that the m/z 390 arises from a protonated precursor ion of m/z 612, which originates from a protonated precursor of m/z 630. The analogous ions reflecting the 16:0-fatty acyl chain and 18:1-LCB are respectively observed at m/z 280 (compared to m/z 390 for d18:1/24:1-Cer) and m/z 264 in the product-ion spectrum of d18:1/16:0-SM (Fig. 3.18B), in which the m/z 264 ion is less abundant than m/z 280. This information, along with the presence of the m/z 131 (lithiated ethylene phosphate) and 86 (CH₂=CH-N(CH₃)₃⁺) ions, reflecting the phosphocholine head group, permit unambiguous structural determination of SM (43,54).



Scheme 3.14. Proposed mechanisms of fragment formation from lithium adducts of glycosphingolipids.

The product-ion spectrum of d18:0/16:0-SM at m/z 711 (Fig. 3.18C), a typical sphingolipid containing the saturated d18:0-LCB, is dominated by m/z 528, arising from loss of the phosphocholine head group. The ion at m/z 498, arising from further loss of HCHO, has a low abundance. The ions reflecting the fatty acyl substituent and 18:0-LCB are observed at m/z 280 and m/z 266, respectively, along with m/z 291, which is the characteristic ion previously observed in the product-ion spectra of ceramides and GSLs consisting of a d18:0-LCB.

Multiple ions reflecting the fatty acyl substituents and LCB are shared by Cer, SM, and GSL, and are readily applicable to structural identification. Formation of a ceramide precursor ion by elimination of the phosphocholine head group or sugar moiety, respectively, is the primary fragmentation step for SM and GSL. This is followed by the consecutive dissociation processes that are identical to those proposed for ceramide. However, the \underline{a} and \underline{a}' ions (Scheme 3.15) are unique to SM.

Fragmentation Processes Observed in Negative-Ion Mode

GPCho

One of the most interesting findings in the earlier studies on phospholipids by FAB/MS in the negative-ion mode was that a set of three ion species arises from GPCho due to losses of methyl ($[M - 15]^-$), trimethylamine ($[M - 60]^-$), and of choline ($[M - 86]^-$), respectively (1). The $[M - 15]^-$, $[M - 60]^-$, and $[M - 86]^-$ ions yield distinguishable product-ion spectra upon high-energy CAD (1). When subjected to ESI, GPCho also forms various $[M + X]^-$ adduct ions (where $X = Cl^-$;

acetate, CH_3CO_2^- ; or formate, HCO_2^-), along with the $[\text{M} - 15]^-$ ($[\text{M} + \text{X} - \text{CH}_3\text{X}]^-$) ions (17,18,39,40). Interestingly, adduct ions in the form of $[\text{M} + \text{CF}_3\text{CO}_2]^-$ are also observed along with the $[\text{M} - 15]^-$, $[\text{M} - 60]^-$, and $[\text{M} - 86]^-$ ions, when GPC₁₀ is ionized in the presence of CF_3CO_2^- . The low-energy CAD product-ion spectra of the m/z 744 ($[\text{M} - 15]^-$) ion (Fig. 3.19A), of the m/z 699 ($[\text{M} - 60]^-$) ion (Fig. 3.19B), and of the m/z 673 ($[\text{M} - 86]^-$) ion (Fig. 3.19C) arising from 16:0/18:1-PC are readily distinguishable. Furthermore, the spectra are similar to those obtained by FAB/MS/MS (1), indicating that the fragmentation processes

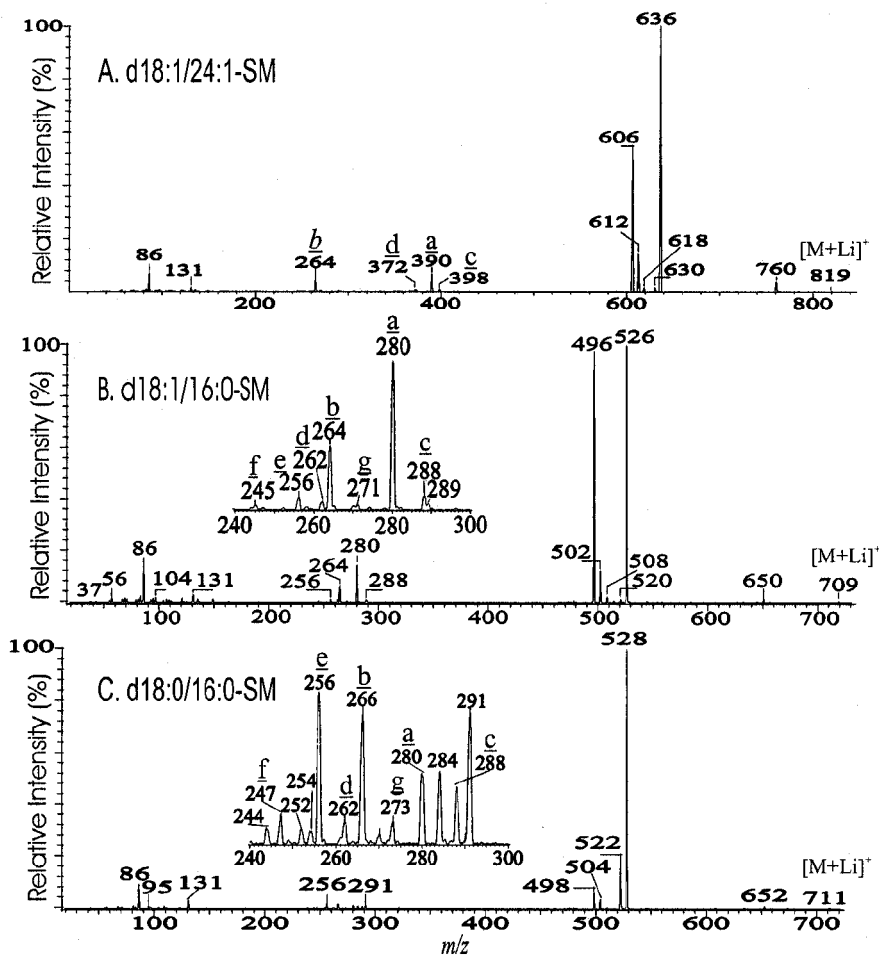
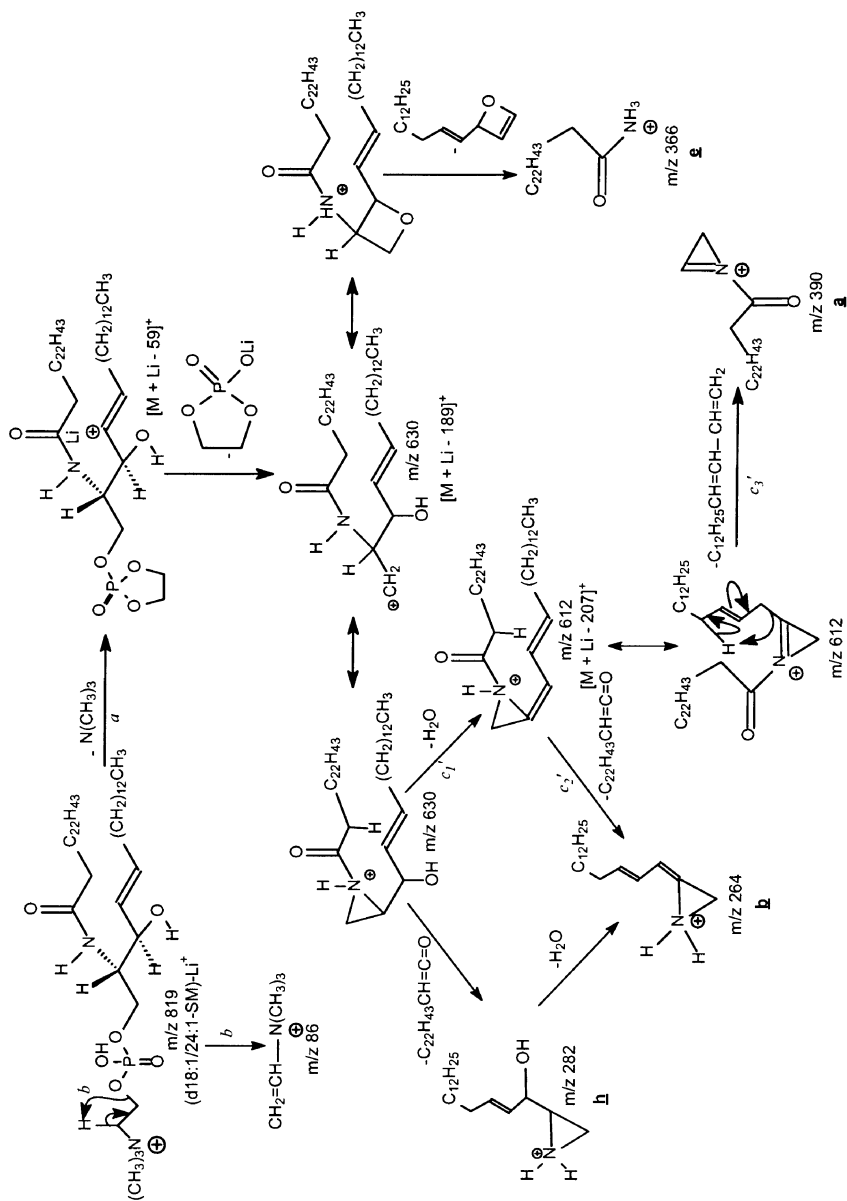


Fig. 3.18. The product-ion spectra of the $[\text{M} + \text{Li}]^+$ ions of (A) d18:1/24:1-SM at m/z 819; (B) d18:1/16:0-SM at m/z 709; and of (C) d18:0/16:0-SM at m/z 711.



Scheme 3.15. Proposed mechanisms of fragmentation of sphingomyelin lithium adducts.

that occur with FAB- and ESI-generated species, under high- or low-energy CAD, are similar.

The negative-ion product-ion spectra of all phospholipid classes mainly consist of four series of ions that correspond to: (i) $[M - H - R_xCO_2H]^-$ (loss of the fatty acyl substituents as free fatty acids); (ii) $[M - H - R'_xCH=C=O]^-$ (loss of the fatty acyl substituents as ketenes); (iii) $[R_xCO_2]^-$ (fatty carboxylate anions) (where $x = 1, 2$; $R_x = R'_xCH_2$); and (iv) ions that reflect the polar head group. The relative abundances of fragment ions from these series are affected by differences in the polar head groups of the various phospholipid classes that govern their gas-phase basicities.

As shown in Figure 3.19A–C, all the spectra are dominated by the carboxylate anions at m/z 255 ($R_1CO_2^-$) and 281 ($R_2CO_2^-$). The m/z 281 ion is more abundant than m/z 255 in the product-ion spectra of $[M - 15]^-$ (Fig. 3.19A) and of $[M - 60]^-$ (Fig. 3.19B), while the abundances of the two ions are reversed in the product-ion spectrum of $[M - 86]^-$ (Fig. 3.19C). The greater abundances of $R_2CO_2^-$ ions than $R_1CO_2^-$ ions in the product-ion spectra of the $[M - 15]^-$ ions of GPCho has been used to assign the positions of the fatty acyl substituents on the glycerol backbone (1). However, the relative abundances of the carboxylate anions are influenced by the chain length and by the number of double bonds in the fatty acyl substituents, so this can result in unreliable assignment (71). In contrast, fragment ions reflecting the losses of the fatty acid at *sn*-2, as either an acid or as a ketene, are always more abundant than the ions arising from the analogous losses at *sn*-1 ($[M - 86 - R_2CO_2H]^- > [M - 86 - R_1CO_2H]^-$; $[M - 86 - R'_2CHC=O]^- > [M - 86 - R'_1CHC=O]^-$), respectively, arising from $[M - 86]^-$, which is equivalent to a deprotonated GPA ion. This observation leads to the suggestion that structural assignments based on the relative abundances of the $[M - 86 - R_xCO_2H]^-$ ions are more reliable than those based on the relative abundances of the $R_xCO_2^-$ ions (71).

The product-ion spectrum of the $[M - 86]^-$ ion of 16:0/18:1-PC generated by ESI (Fig. 3.19C) is, indeed, identical to that of the $[M - H]^-$ ion of 16:0/18:1-PA at m/z 673 (Fig. 3.20A), as shown below, where the mechanisms for ion formation will be described. The fragmentation mechanisms for the $[M - 15]^-$ ion at m/z 744 and for the $[M - 60]^-$ ion at m/z 699 under low-energy CAD are also similar to those observed for the $[M - H]^-$ ion of GPEn.

GPA

The major pathways of ion formation from the $[M - H]^-$ ion of GPA are charge-driven fragmentation (CDF) processes, by which the prominent ions at $[M - H - R_xCO_2H]^-$ and $[M - H - R'_xCH=C=O]^-$ ($R_x = R'_xCH_2$, $x = 1, 2$), arising from losses of the fatty acyl substituents as acids and as ketenes, respectively, are formed with the participation of the exchangeable hydrogen of the phosphate head group (72). The preferential formation of the $[M - H - R_2CO_2H]^-$ ion at m/z 391 over the $[M - H - R_1CO_2H]^-$ ion at m/z 417, and the greater abundance of the $[M - H - R'_2CH=C=O]^-$ ion at m/z 409 than the $[M - H - R'_1CH=C=O]^-$ ion at m/z 435 observed in Figure 3.20A, are due to

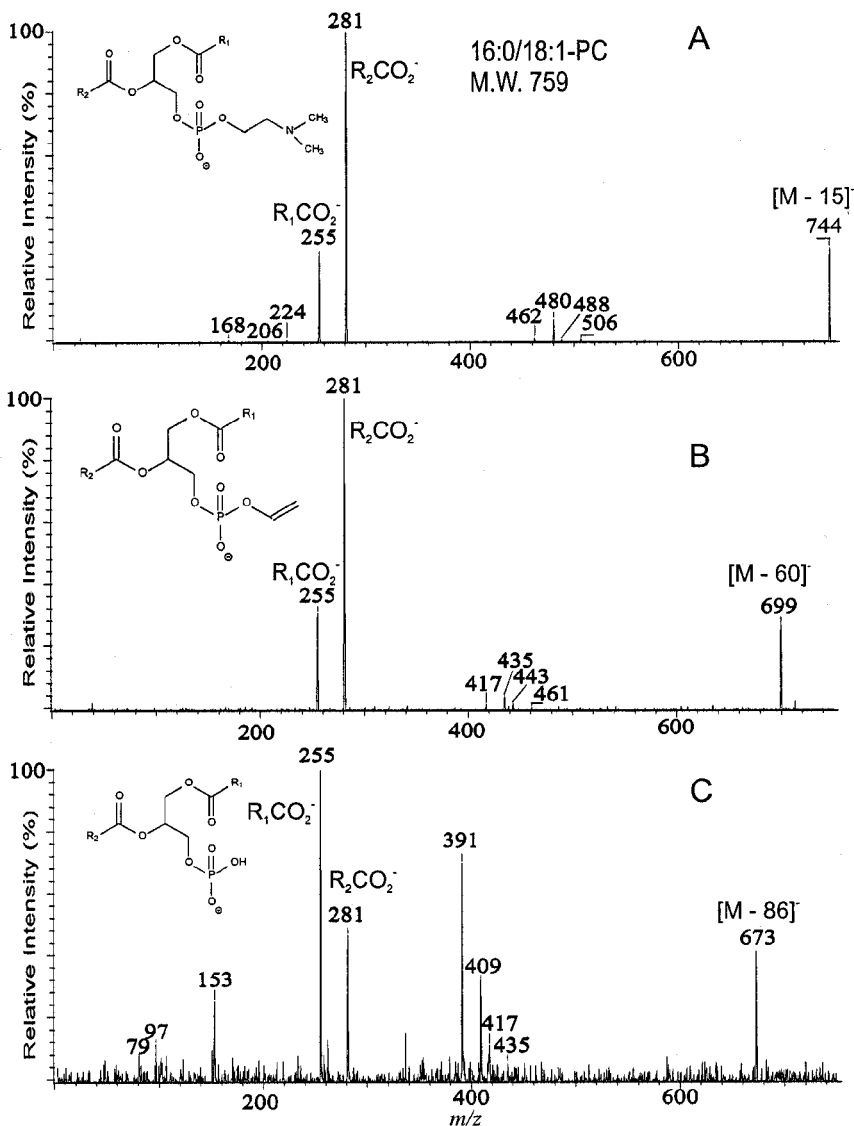


Fig. 3.19. The product-ion spectra of the (A) $[M - 15]^-$ ion at m/z 744; the (B) $[M - 60]^-$ ion at m/z 699; and of the (C) $[M - 86]^-$ ion at m/z 673. The ions are generated from 16:0/18:1-PC by ESI in the presence of $CF_3CO_2^-$ in negative-ion mode.

the fact that loss of the fatty acyl substituent at *sn*-2 as an acid or as a ketene is sterically more favorable than the analogous loss at *sn*-1. This agrees with the notion that the phosphate charge site, which initiates the fragmentation process by CDF, is in closer

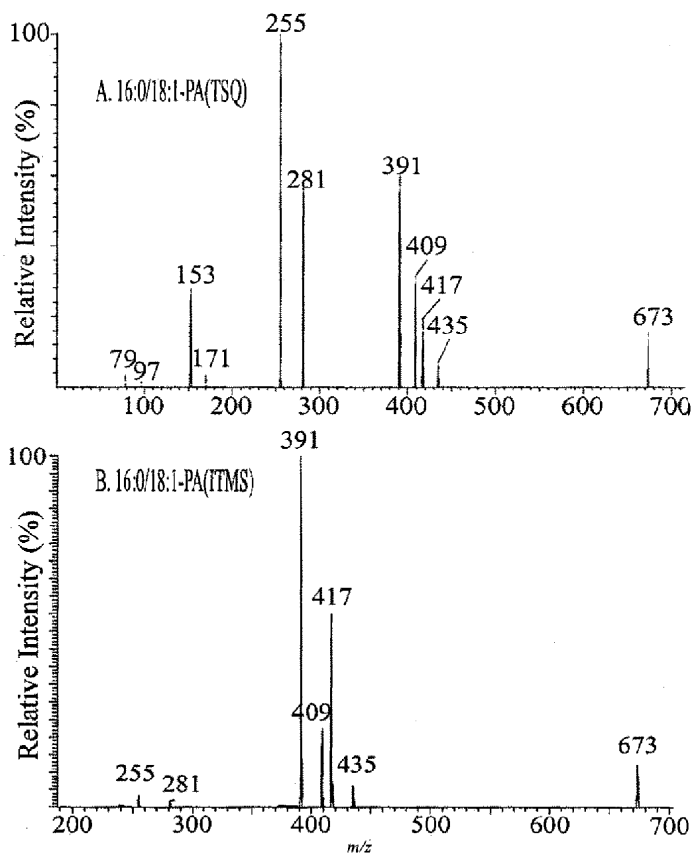
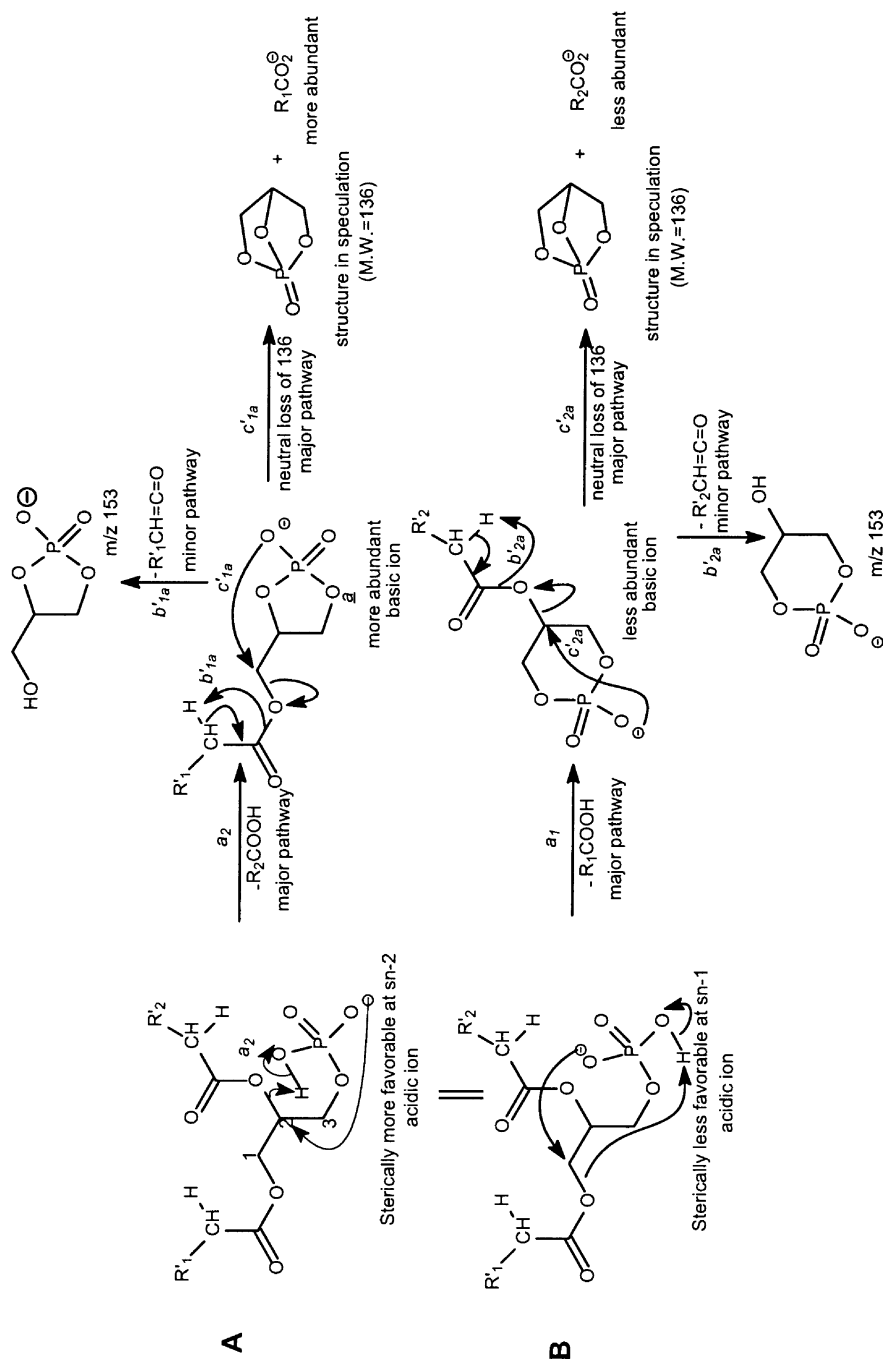
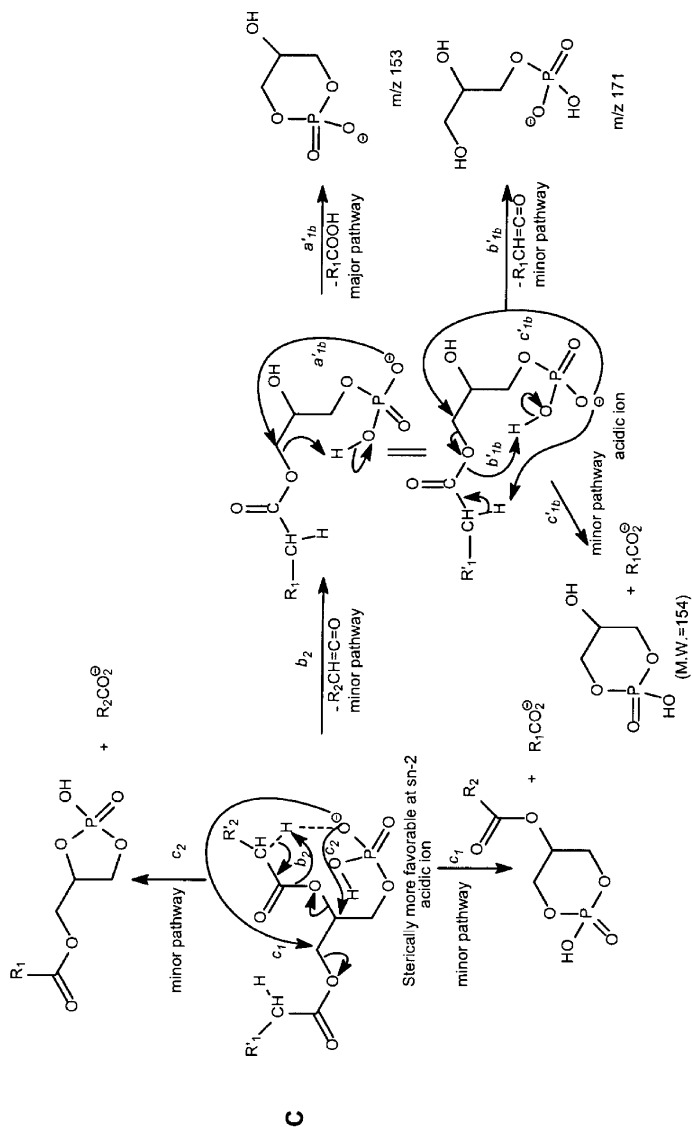


Fig. 3.20. The product-ion spectra of the $[M - 15]^-$ ion at m/z 673 by a triple stage quadrupole (TSQ) MS (A) and by ion trap mass spectrometry (ITMS) (B).

proximity to the fatty acyl moiety at *sn*-2 than to that at *sn*-1 (73). The respective greater abundances of the $[M - H - R_x \text{CO}_2\text{H}]^-$ ions at m/z 391 and m/z 417, than the $[M - H - R_x \text{CH}=\text{C}=\text{O}]^-$ ions at m/z 409 and m/z 435, are attributable to the fact that the gaseous $[M - H]^-$ of GPA is an acidic ion, which undergoes more facile acid loss than ketene loss (Scheme 3.16). Tandem mass spectrometric studies on phospholipids using ITMS have been previously reported (30). The MS^2 -spectrum of 16:0/18:1-PA (Fig. 3.20B) obtained with ITMS is dominated by the $[M - H - R_x \text{CO}_2\text{H}]^-$ ions at m/z 391 and m/z 417. The $[M - H - R_x \text{CH}=\text{C}=\text{O}]^-$ ions at m/z 407 and m/z 433, and the $R_x \text{CO}_2^-$ ions at m/z 255 and m/z 281, are of low abundance.

Collisional activation that occurs in TSQ instruments involves multiple collisions that result in consecutive fragmentation processes. In contrast, resonance excitation is the major process in ITMS, and ions arising from consecutive fragmentation steps are





Scheme 3.16. Proposed mechanisms of fragmentation of phosphatidic acid (PA) in negative-ion mode.

minimal. The decline of the $[M - H - R_xCO_2H]^-$ ions at m/z 391 and m/z 417 in the product-ion spectrum obtained with the TSQ instrument is in accord with the rise of the $R_xCO_2^-$ ions of m/z 255 and m/z 281. These latter ions are attributable to the consecutive dissociations of the ions at m/z 391 ($[M - H - R_2CO_2H]^-$) (Scheme 3.16A, route c_{1a}') and m/z 417 ($[M - H - R_1CO_2H]^-$) (Scheme 3.16A, route c_{2a}') to ions at m/z 255 and m/z 281, respectively, *via* loss of 136. These pathways are supported by source-CAD MS²- and MS³-spectra of both the $[M - H - R_2CO_2H]^-$ ion at m/z 391 (Fig. 3.21A) and the $[M - H - R_1CO_2H]^-$ ion at m/z 417 (Fig. 3.21B). In these spectra, the third generation ions at m/z 255 (Fig. 3.21A) and at m/z 281 (Fig. 3.21B) are prominent. The consecutive fragmentation pathways involving the nucleophilic attack of the anionic charge site of the $[M - H - R_xCO_2H]^-$ precursors on the C2 or C3 of the glycerol to expel $R_xCO_2^-$ are also consistent with the notion that the $[M - H - R_xCO_2H]^-$ ions become basic ions. Conversely, the $[M - H - R_xCH=C=O]^-$ ions at m/z 409 and m/z 435 become more acidic than their precursor $[M - H]^-$ ions. This is due to gaining protons from loss of the ketene, and then undergoing further acid loss to form the ion at m/z 153 ($[M - H - R_{1 \text{ (or } 2)}CH=C=O - R_{2 \text{ (or } 1)}CO_2H]^-$) (Fig. 3.21C and D) (Scheme 3.16C, route a_{1b}). The m/z 391 ($[M - H - R_2CO_2H]^-$) ion is more favorably formed than the m/z 417 ($[M - H - R_1CO_2H]^-$) ion due to the steric proximity of the *sn*-2 acyl chain to the charge site in the primary fragmentation step. Therefore, the m/z 255 ($R_1CO_2^-$) ion is more abundant than the m/z 281 ($R_2CO_2^-$) ion, resulting from secondary dissociation of the $[M - H - R_xCO_2H]^-$ ion to give $R_xCO_2^-$.

GPSer

When subjected to ESI in the negative-ion mode, GPSer forms the $[M - H]^-$ ion along with a prominent ion of $[M - H - 87]^-$ arising from in-source fragmentation that causes the loss of serine. Thus, the major fragmentation processes for GPSer under low-energy CAD mainly reflect secondary dissociation of the $[M - H - 87]^-$ ion. As illustrated in Figure 3.22A, the product-ion spectrum of the $[M - H]^-$ ion of 16:0/18:1-PS at m/z 760 is dominated by the $[M - H - 87]^-$ ion at m/z 673 ion, which is equivalent to the $[M - H]^-$ ion of 16:0/18:1-PA, and gives rise to a source-CAD product-ion spectrum (m/z 760 \rightarrow m/z 673) identical to that displayed in Figure 3.20A.

GPSer also forms $[M - 2H + Alk]^-$ (Alk = Na, Li) ions when subjected to ESI in the presence of Alk^+ ions, due to the fact that it possesses two anionic charge sites at which an Alk^+ can attach. The product-ion spectrum of the $[M - 2H + Li]^-$ ion of 16:0/18:1-PS at m/z 766 (Fig. 3.22B) contains major ions at m/z 502 and m/z 528, arising from losses of the fatty acyl substituents as ketenes. The spectrum also contains the ions at m/z 484 and m/z 510, arising from losses of the fatty acyl substituents as acids, but these ions are of low abundance. These results suggest that the gaseous ion of $[M - 2H + Li]^-$ becomes more basic than that of $[M - H]^-$ after a proton at an anionic site is replaced by Li^+ . The m/z 502 ($[M - 2H + Li - R'_2CH=CO]^-$) ion, reflecting loss of the fatty acyl ketene at *sn*-2, is more abundant than m/z 528 ($[M - 2H + Li - R'_1CH=CO]^-$), corresponding to the similar loss at *sn*-1. This is con-

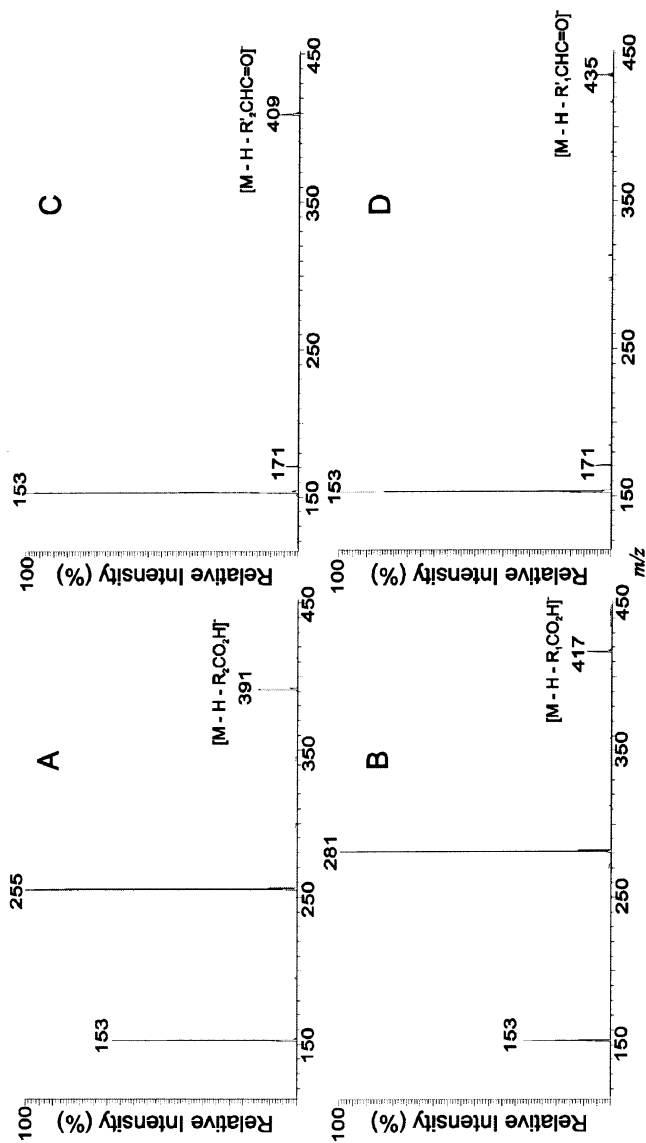


Fig. 3.21. The ITMS MS³-spectra of the (A) m/z 391 ($[M - H - R_2CO_2H]^-$) ($673 \rightarrow 391$); (B) the m/z 417 ($[M - H - R_1CO_2H]^-$) ($673 \rightarrow 417$); (C) the m/z 409 ($[M - H - R'_2CHC=O]^-$) ($673 \rightarrow 409$); and (D) the m/z 435 ($[M - H - R'_1CHC=O]^-$) ($673 \rightarrow 435$) ions, from the MS²-spectrum of 16:0/18:1-PA at m/z 673.

sistent with the notion that loss of fatty acid substituents as ketenes is the favored pathway for basic precursor ions and the process is sterically more favorable at *sn*-2 than at *sn*-1.

GPETn

Both charge-remote and charge-driven processes are the major fragmentation pathways that lead to ion formation from GPETn. The gas-phase $[M - H]^-$ ion of GPETn is basic

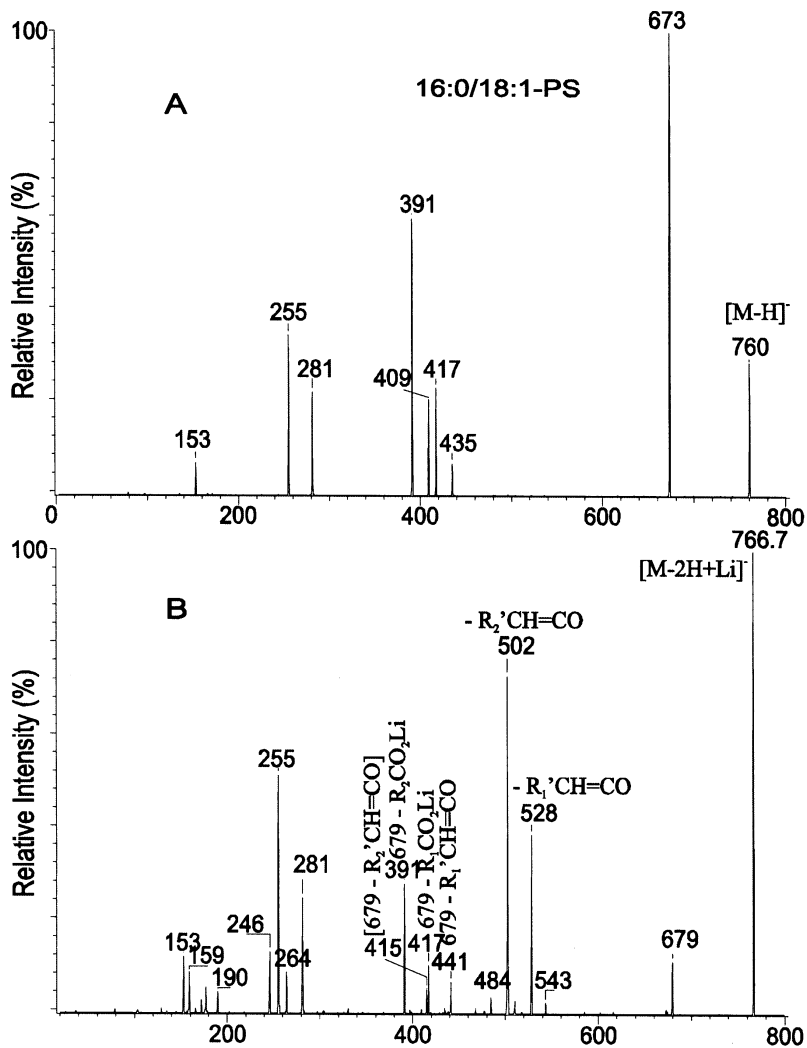


Fig. 3.22. The product-ion spectra of (A) the $[M - H]^-$ ion of m/z 760, and of (B) the $[M - 2H + Li]^-$ ion at m/z 766, from 16:0/18:1-PS.

and undergoes preferential losses of fatty acyl substituents as ketenes ($[M - H - R_X'CH=C=O]^-$) rather than as acids ($[M - H - R_XCO_2H]^-$) (74). This feature is demonstrated by the product-ion spectra of 16:0/18:1-PE (Fig. 3.23A), and 18:1/16:0-PE (Fig. 3.23B) isomers at m/z 716, obtained with a TSQ instrument. The anionic charge site initiates nucleophilic attack either on the α -hydrogen of the fatty acyl substituent or on

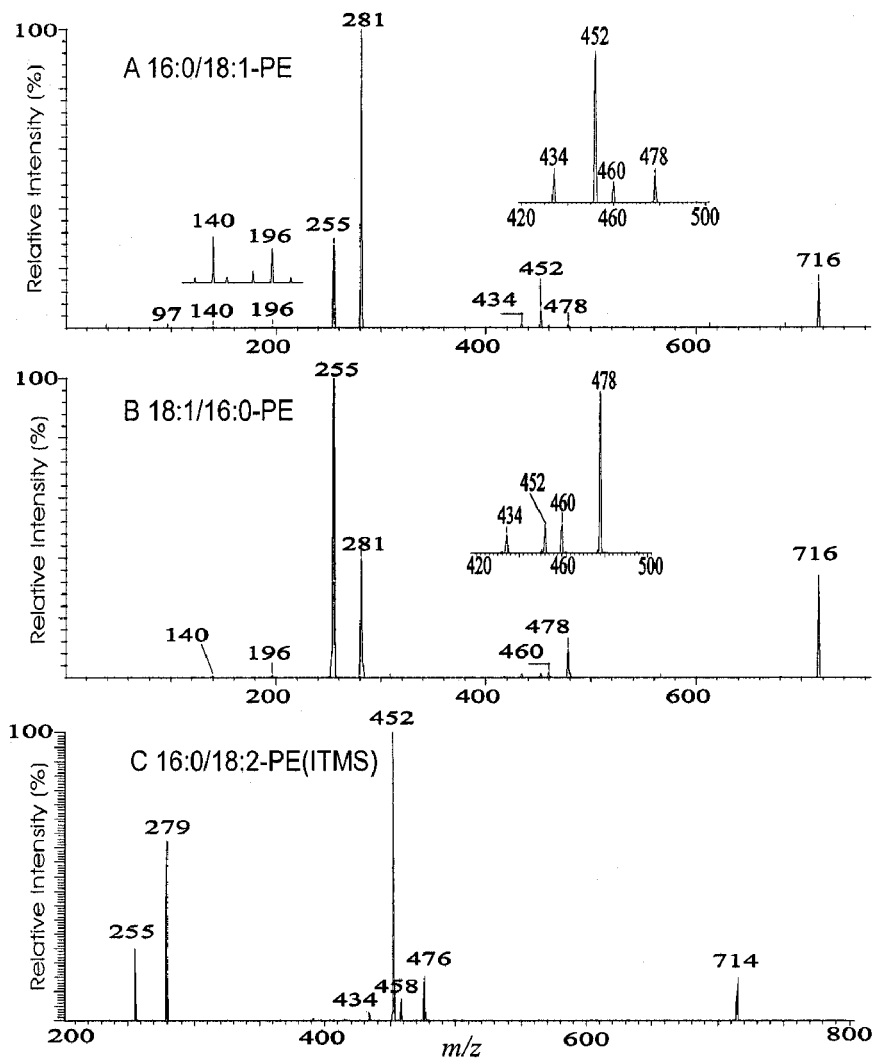


Fig. 3.23. The TSQ product-ion spectra of the $[M - H]^-$ ions of (A) 16:0/18:1-PE, and of (B) 18:1/16:0-PE at m/z 716. The ITMS MS^2 -spectrum of 16:0/18:2-PE at m/z 714 is shown in (C).

the carbon of the glycerol to which the substituent attached. The attack on the α -hydrogens of the fatty acyl chain results in the $[M - H - R_x'CH=C=O]^-$ ion series at m/z 478 and m/z 452 (Scheme 3.17A), whereas attack on the glycerol hydrogens leads to formation of $R_xCO_2^-$ ions at m/z 281 and m/z 255 by charge-transfer (Scheme 3.17B).

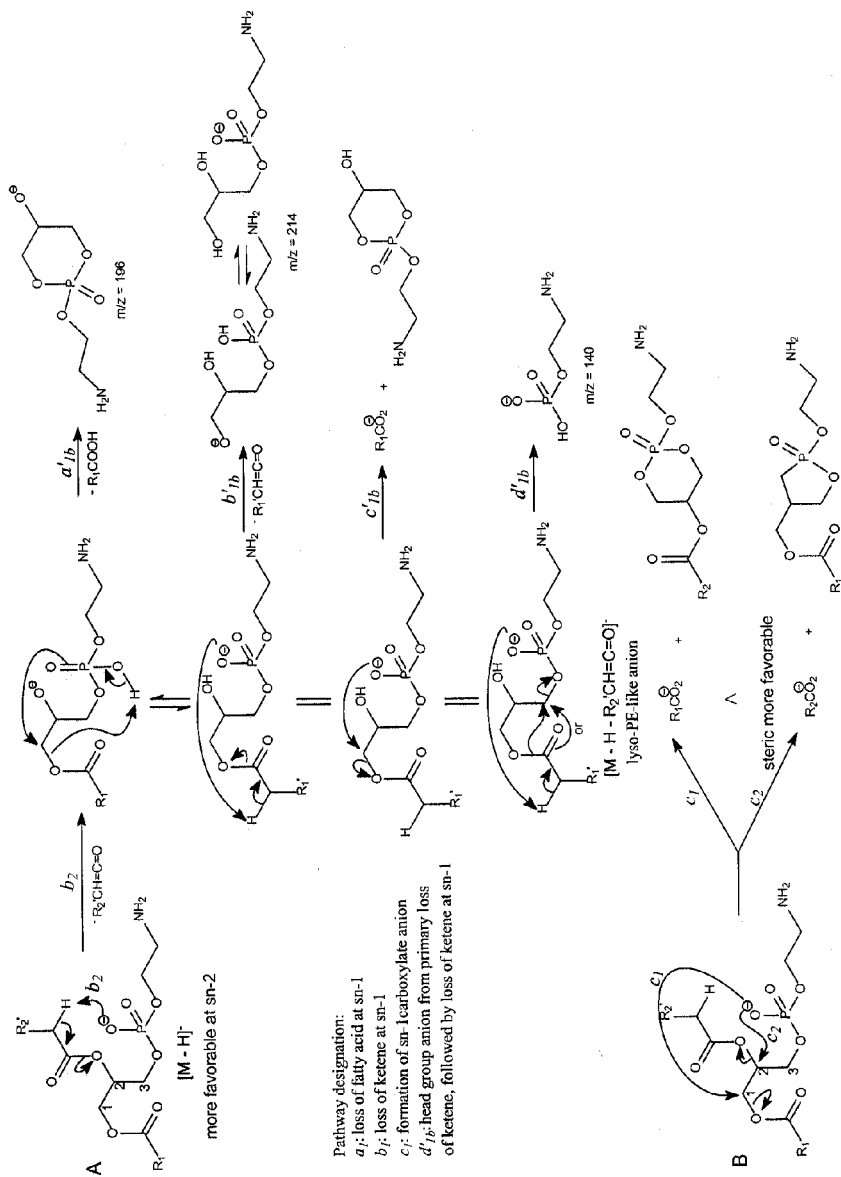
Both of the fragmentation processes are sterically more favorable at *sn*-2 than at *sn*-1, and result in the observation that the m/z 452 ion ($[M - H - R_2'CH=C=O]^-$) is more abundant than m/z 478 ($[M - H - R_1'CH=C=O]^-$); and the m/z 281 ion ($R_2CO_2^-$) is more abundant than the m/z 255 ion ($R_1CO_2^-$) for the 16:0/18:1-PE isomer (Fig. 3.23A). In contrast, the abundances of these ion pairs are reversed in the product-ion spectrum of 18:1/16:0-PE (Fig. 3.23B).

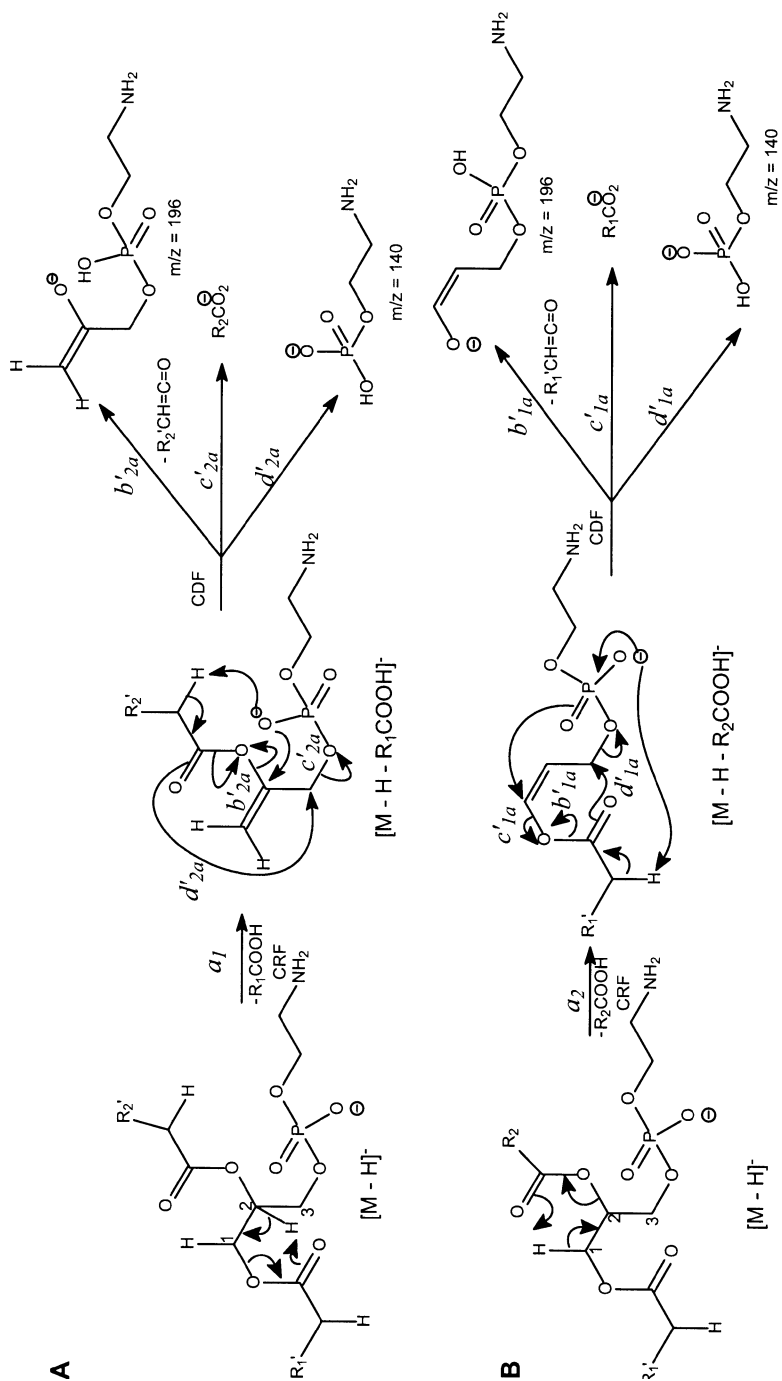
The formation of the $[M - H - R_xCO_2H]^-$ ions involves participation of the hydrogens attached to the glycerol backbone. The methine hydrogen at C-2 of the glycerol backbone participates in the loss of R_1CO_2H (Scheme 3.18A), while the methylene hydrogens at C-1 are involved in the loss of R_2CO_2H (Scheme 3.18B). These fragmentation pathways are CRF processes; the result is that the $[M - H - R_2CO_2H]^-$ ion at m/z 434 is slightly more abundant than the $[M - H - R_1CO_2H]^-$ ion at m/z 460 (Fig. 3.23A).

This is probably because there is only one hydrogen, the methine hydrogen, that participates in the loss of R_1CO_2H , whereas two hydrogens at C-1, the methylene hydrogens, can participate in the loss of R_2CO_2H . The ions reflecting the polar head group are observed at m/z 140 and 196 (Table 3), which are 43 Da (ethylamine) higher than the analogous ions at m/z 97 and 153 observed for GPA, indicating that these ions arise from similar fragmentation processes.

The MS²-spectrum of 16:0/18:2-PE at m/z 714 (Fig. 3.23C) obtained with an ITMS instrument is dominated by the $[M - H - R_2'CH=C=O]^-$ ion at m/z 452, arising from loss of the *sn*-2 fatty acyl substituent as a ketene, and by the $R_2CO_2^-$ ion at m/z 279. Smaller peaks are seen at m/z 476 and m/z 255, corresponding to the $[M - H - R_1'CH=C=O]^-$ ion and the $R_1CO_2^-$ ion, respectively. In contrast, ions at m/z 458 and m/z 434, arising from losses of the fatty acyl moieties as free fatty acids, are of low abundance. This is consistent with the idea that losses of the fatty acyl substituents as ketenes and formation of carboxylate anions are the major fragmentation processes for basic phospholipid classes such as GPEtn; whereas losses of the fatty acyl substituents as acids are the major pathways for acidic precursors such as GPA, as described earlier.

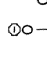


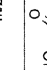
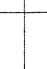
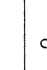

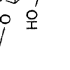
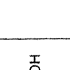
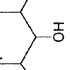
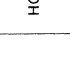

The profiles of both the product-ion spectra of the $[M - 15]^-$ ion at m/z 744 (Fig. 3.19A) and of the $[M - 60]^-$ ion at m/z 709 (Fig. 3.19B) observed for 16:0/18:1-PC are nearly identical to those arising from the $[M - H]^-$ ion of 16:0/18:1-PE, indicating that the gas-phase basicities of the former two ions are close to that of the $[M - H]^-$ ion of GPEtn. This is consistent with the suggestion that the $[M - 15]^-$ and $[M - 60]^-$ ions represent a deprotonated phosphatidyl-ethanol-*N,N'*-dimethylamine ion and a deprotonated phosphatidylethylene ion, respectively (1,4). The phosphatidyl-ethanol-*N,N'*-dimethylamine polar head group is also revealed by the presence of the ions at m/z 224, m/z 206, and m/z 168 (Fig. 3.19A) (Table 3).





Scheme 3.18. Proposed mechanisms of fragment formation from GPEtn in negative-ion mode.

TABLE 3.3
Proposed Configurations of the Polar Head Group-Related Ions Observed for the $[M - H]^-$ Ions of the Major Phospholipid Classes

| Phospholipid | Head group | $[M - H - R_2(H - R_1)_2(CH=CO)]^-$ | $[M - H - R_2CO_2H - R_1CO_2H]^-$ | |
|--------------|---|--|--|--|
| PE | $CH_2CH_2NH_2$ 1' |  $m/z = 196$ |  $m/z = 140$ |  $m/z = 168$ |
| PC(M - 15) | $CH_2CH_2N(CH_3)_2$ 1' |  $m/z = 224$ |  $m/z = 171$ |  $m/z = 259$ |
| PG |  1' |  $m/z = 209$ |  $m/z = 237$ | |
| PI |  1' |  $m/z = 315$ | | |
| PA | H |  $m/z = 153$ | | |
| PS | CH_2CHNH_2 1' CO_2H | Same as PA | | |

GPGro and Acylphosphatidylglycerol (Acyl-PG)

GPGro

GPGro is a weakly acidic phospholipid (75), and the gas-phase basicity of the $[M - H]^-$ ion is between that of GPEtn and GPA. This notion is consistent with the observation that the $[M - H - R'_2CH=C=O]^-$ ion at m/z 483 in the product-ion spectrum of 16:0/18:1-PG at m/z 747 (Fig. 3.24A) obtained by a TSQ instrument is more abundant than the $[M - H - R_2CO_2H]^-$ ion at m/z 465. On the other hand, the $[M - H - R_1CO_2H]^-$ ion at m/z 491 is more abundant than the $[M - H - R'_1CH=C=O]^-$ ion at m/z 509. The spectrum features ions at m/z 465 ($[M - H - R_2CO_2H]^-$) and m/z 483 ($[M - H - R'_2CH=C=O]^-$) that are respectively more abundant than the analogous ions at m/z 491 ($[M - H - R_1CO_2H]^-$) and m/z 509 ($[M - H - R'_1CH=C=O]^-$) because of the preferential losses at *sn*-2, similar to those described for GPA and GPEtn. Similarly, the m/z 391 ion arising from the combined losses of the *sn*-2 fatty acid substituent and the polar head group ($[M - H - R_2CO_2H - 74]^-$) is more abundant than the m/z 417 ion arising from the analogous losses at *sn*-1 ($[M - H - R_1CO_2H - 74]^-$). The above-mentioned spectral features, along with the observation that the $R_2CO_2^-$ at m/z 281 is more abundant than the m/z 255 ion ($R_1CO_2^-$), permit the differentiation of this molecule from the 18:1/16:0-PG isomer (Fig. 3.24B). Ions that are indicative of the polar head group are observed at m/z 227, 209, 171, and 153 (Table 3.3), arising from the similar processes as described for GPA and GPEtn.

Both CRF and CDF contribute to the fragmentation processes underlying the formation of the $[M - H - R_xCO_2H]^-$ ions for GPGro. Evidence for this lies in the studies of the *d*-labeled d_2 -16:0/18:1-PG analog (Fig. 3.24C). The deuterium-labeled molecules showed two separate processes: the first process involves the formation of the m/z 466 ($[M - H - R_2CO_2D]^-$) and m/z 492 ($[M - H - R_1CO_2D]^-$) ions *via* CDF, which involves the participation of the exchangeable hydrogen of the glycerol head group; the second process involves a CRF mechanism that requires the participation of a non-exchangeable hydrogen on the glycerol backbone to form the m/z 467 ($[M - H - R_2CO_2H]^-$) and m/z 493 ($[M - H - R_1CO_2H]^-$) ions (76). The occurrence of both CRF and CDF processes in the fragmentation of GPGro further supports the concept that acid loss from an acidic precursor, such as GPA, is a CDF process, which involves the exchangeable hydrogen; whereas the similar loss from a basic phospholipid class, such as GPEtn, is a CRF process that involves the hydrogen at the glycerol backbone.

In contrast, the fragmentation processes that occur in ITMS are mainly CDF, which requires lower energy. This is reflected by the MS²-spectrum of 16:0/18:1-PG (Fig. 3.24D), in which the $[M - H - R_xCO_2H]^-$ ions at m/z 491 and m/z 465 are, respectively, more abundant than the $[M - H - R'_xCH=CO]^-$ ions at m/z 509 and m/z 483. These results also indicate that the gas-phase $[M - H]^-$ ion of GRGro is slightly acidic. The influences of the gas-phase basicities of the precursor ions on the fragmentation processes are also observed for other phospholipid classes, including CL and GPINo.

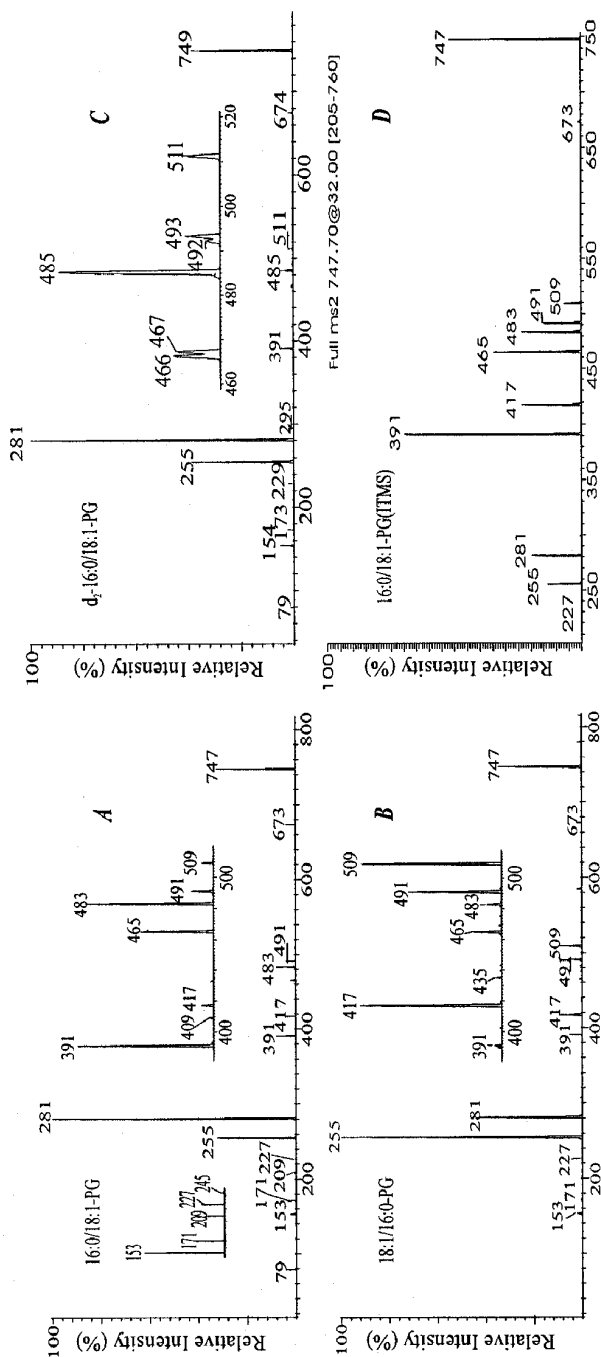


Fig. 3.24. The TSQ production spectra of the $[M - H]^-$ ions of (A) 16:0/18:1-PG; and of (B) 18:1/16:0-PG; and at (C) m/z 747, and of d_2 -16:0/18:1-PG at m/z 749. (D) is the ITMS MS^2 -spectrum of 16:0/18:2-PG at m/z 714.

Acylphosphatidylglycerol

Acylphosphatidylglycerols (acyl-PG) that occur in nature possess a GPGro nucleus in which the *sn*-3' carbon atom of the glycerol head group is esterified by another fatty acid substituent. This extra acyl chain yields an additional ion set upon CAD (77–80). The MS²- and MS³-spectra generated by TSQ and ITMS instruments have recently been used to characterize complex structures of acyl-PG in mixtures (80). As described below, the product-ion spectrum of 1-palmitoyl-2-palmitoleoyl-*sn*-glycero-3-phospho-(3'-myristoleoyl)-1'-*sn*-glycerol (14:1-16:0/16:1)-PG at *m/z* 927 obtained with a TSQ instrument (Fig. 3.25A, *m/z* 927) is dominated by the carboxylate anions at *m/z* 255 (16:0), *m/z* 253 (16:1), and *m/z* 225 (14:1). The abundances of the carboxylate anions are in the order: *m/z* 253 (R₂CO₂⁻) > *m/z* 225 (R₃'CO₂⁻) > *m/z* 255 (R₁CO₂⁻), and the abundance ratio of *m/z* 253 to *m/z* 255 is close to 2, similar to that observed for 16:0/16:1-PG. The different abundances observed in the formation of the R_xCO₂⁻ ions provide an explicit method to assign the 16:0-, 16:1, and 14:1-fatty acyl moieties at *sn*-1, *sn*-2, and *sn*-3', respectively. The fatty acyl substituents are also reflected by the fragment ions at *m/z* 719 ([M - H - C₁₂H₂₃CHC=O]⁻), *m/z* 691 ([M - H - C₁₄H₂₇CHC=O]⁻), and *m/z* 689 ([M - H - C₁₄H₂₉CHC=O]⁻), arising from losses of the 14:1, 16:1, and 16:0-fatty acyl ketenes from *m/z* 927, respectively. Similarly, ions at *m/z* 701, *m/z* 673, and *m/z* 671 arise from losses of the 14:1, 16:1, and 16:0-fatty acids, respectively. The *m/z* 691 ion is more abundant than the *m/z* 673 ion, and these ions are the most prominent among the ion series (panel A, subset). In contrast, the abundances of the *m/z* 701 and *m/z* 671 ions are respectively greater than those of the *m/z* 719 and *m/z* 689 ions. The preferential formation of the *m/z* 691 ion, by loss of 16:1-ketene, over formation of the *m/z* 673 ion, *via* loss of 16:1-acid, is similar to the trend observed for GPGro (Fig. 3.24). Thus, the assignment of the 16:1 and 16:0-fatty acyl substituents at *sn*-2 and at *sn*-1 of the glycerol backbone, respectively, can be confirmed; whereas the remaining 14:1-fatty acyl substituent is attached to the 3' position of the glycerol head group. A unique ion at *m/z* 379, which represents a 14:1-acyl glycerophosphate ion and signifies a 14:1-fatty acyl moiety at *sn*-3', was also observed (Scheme 3.18). The ions at *m/z* 719 ([M - H - R'₃CH=CO]⁻) and *m/z* 701 ([M - H - R₃CO₂H]⁻), arising from loss of a 14:1-ketene and of a 14:1-acid at *sn*-3', respectively, are also more abundant than the ions at *m/z* 689 and *m/z* 671, respectively, which arose from the analogous losses of the 16:0-fatty acyl moiety at *sn*-1. This is consistent with the observation that the R₃CO₂⁻ ion at *m/z* 225 is more abundant than the R₁CO₂⁻ ion at *m/z* 255. These results indicate that the gas-phase basicity and the fragmentation mechanisms of the [M - H]⁻ ion of acyl-PG may be close to those of GPGro. The product-ion spectrum of the [M - H]⁻ ion at *m/z* 929 (Fig. 3.25B) contains a similar ion profile that reflects the presence of the 14:0-, 16:0-, and 16:1-fatty acyl moieties and therefore represents a 14:0-16:0/16:1-PG structure.

The identities of the fatty acyl moieties and their positions on the glycerol backbone or in the glycerol head group can also be assigned by the [M - H -

$R'_2CH=C=O - R_xCO_2H - 74]^-$ ion series, which is the most prominent in the MS²-spectrum obtained by ITMS. As shown in Figure 3.25C, the 14:1-16:0/16:1-PG is dominated by ions at m/z 391, 389, and 361. The m/z 391 ion ($[M - H - R'_2CH=CO - 74 - R_3CO_2H]^-$) is the most prominent and is slightly more abundant than m/z 361 ($[M - H - R'_{2(or\ 1)}CH=CO - 74 - R_{1(or\ 2)}CO_2H]^-$), which is much more abundant than m/z 389 ($[M - H - R'_3CH=C=O - 74 - R_2CO_2H]^-$). The profile of the m/z 391 and m/z 389 ions is also similar to that observed for 16:0/16:1-PG obtained with ITMS under the same condition, suggesting that the m/z 927 ion possesses 16:0- and 16:1-acyl substituents at *sn*-1 and *sn*-2, respectively. The observation of the abundances of m/z 391 > m/z 361 >> m/z 389 in the MS²-spectrum obtained with ITMS provides another unambiguous method to locate the fatty acyl substituents. More than 30 species of acyl-PG, including complex configurational isomers isolated from *salmonella* bacteria, were identified without having to use traditional laborious analytical methods (80).

Cardiolipin

Cardiolipin (CL, 1,3-bisphosphatidyl-*sn*-glycerol) is a phosphoglyceride that contains a phosphatidylglycerol linked to a phosphoglyceride unit to make it a diphosphatidylglycerol. CL possesses two phosphate charge sites and forms both $[M - H]^-$ and $[M - 2H]^{2-}$ ions when subjected to ESI. The major species of CL found in mammalian heart cells is (18:2/18:2)(18:2/18:2)-CL, the simplest form of CL. It contains four identical 18:2-acyl substituents residing at *sn*-1, -2, -1', and -2', respectively. The compound gives an $[M - H]^-$ ion at m/z 1447 and an $[M - 2H]^{2-}$ ion at m/z 723.6. Selection and CAD of the $[M - 2H]^{2-}$ ion at m/z 723 (Fig. 3.26A) at a collision energy of 22 eV yields the 18:2-carboxylate anion at m/z 279, reflecting the uniform fatty acyl moiety of the molecule. The product-ion spectrum also contains the m/z 592 ion, a doubly-charged fragment ion arising from loss of an 18:2-fatty acyl group as a ketene (723 - 262/2). However, ions reflecting loss of the fatty acyl substituents as acids are not observed, indicating that the $[M - 2H]^{2-}$ ion, which contains one less proton, is a basic precursor ion and undergoes more facile ketene than acid loss. The $R_xCO_2^-$ ion at m/z 279 arises from nucleophilic attack of an anionic phosphate charge site onto C2 or C2' of a glycerol backbone (Scheme 3.19A). This fragmentation process also gives rise to m/z 1167 (723 × 2 - 279). In contrast, the $[M - H]^-$ ion at m/z 1447 (Fig. 3.26B) is an acidic ion, which yields m/z 1167 by loss of an 18:2-fatty acid, and m/z 695 (**a** ion) by cleavage of the O-C bond (**d**), along with m/z 751 (**b** + 56) and m/z 831 (**b** + 136) (Scheme 3.19B).

The carboxylate anion arising from the fatty acyl substituent at *sn*-1 (or *sn*-1') is more abundant than that arising from *sn*-2 (or *sn*-2') in the product-ion spectrum of the $[M - H]^-$ precursors, while the abundances of these two ions are reversed in the product-ion spectrum arising from the corresponding $[M - 2H]^{2-}$ precursors. This is shown in Figure 3.26, which illustrates the product-ion spectra of the $[M - 2H]^{2-}$ ion of (16:0/16:1)(16:0/16:1)-CL at m/z 673.6 (panel C) and of its $[M - H]^-$ ion at m/z 1347 (panel D), obtained with the TSQ instrument.

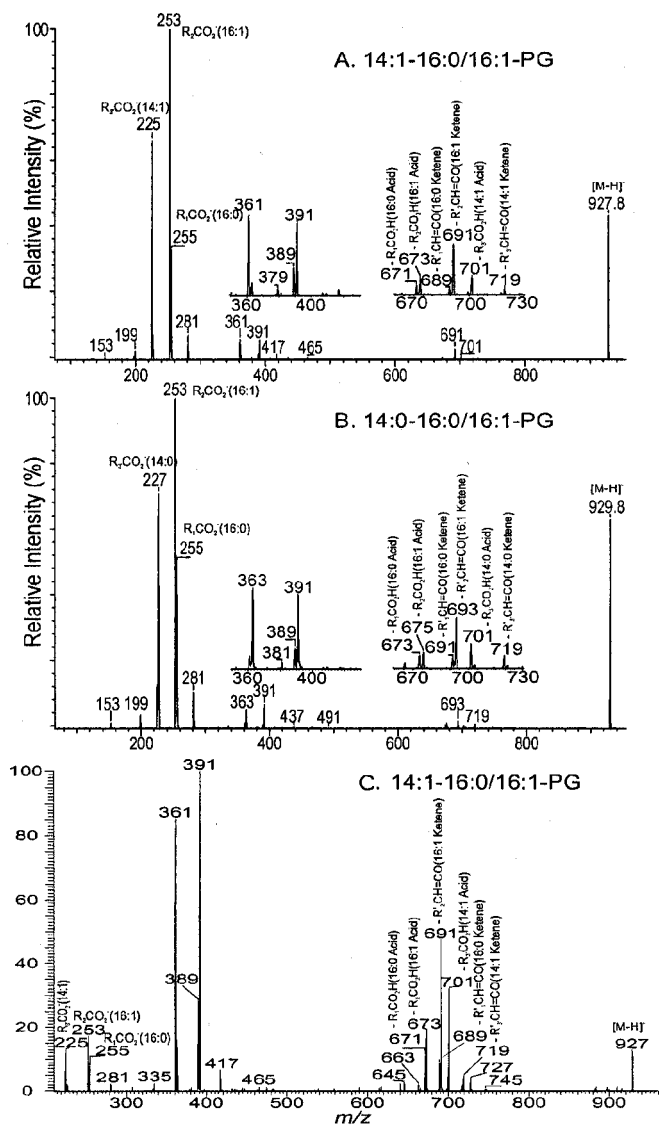


Fig. 3.25. The TSQ product-ion spectra of the $[M - H]^-$ ions of (A) 14:1-16:0/16:1-PG at m/z 927; of (B) 14:0-16:0/16:1-PG at m/z 929. The ITMS MS^2 -spectrum of 14:1-16:0/16:1-PG at m/z 927 is shown in (C).

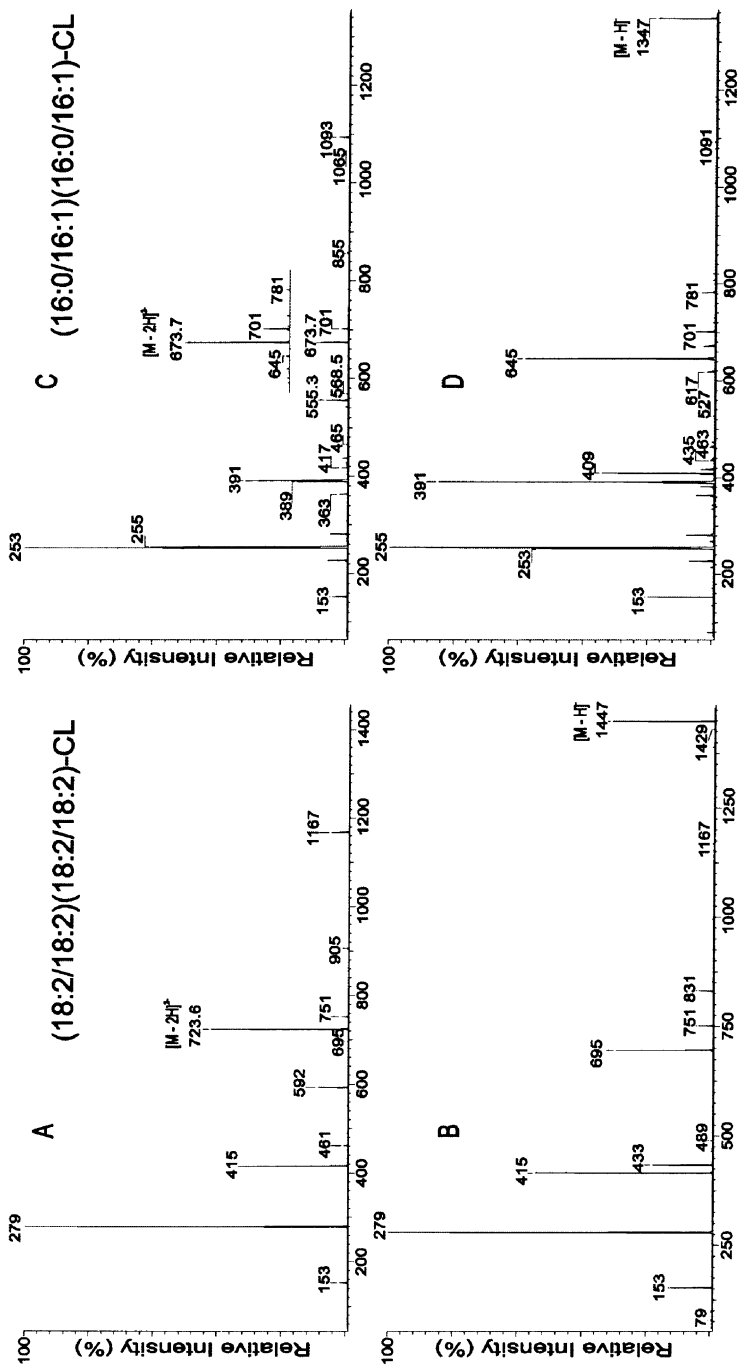
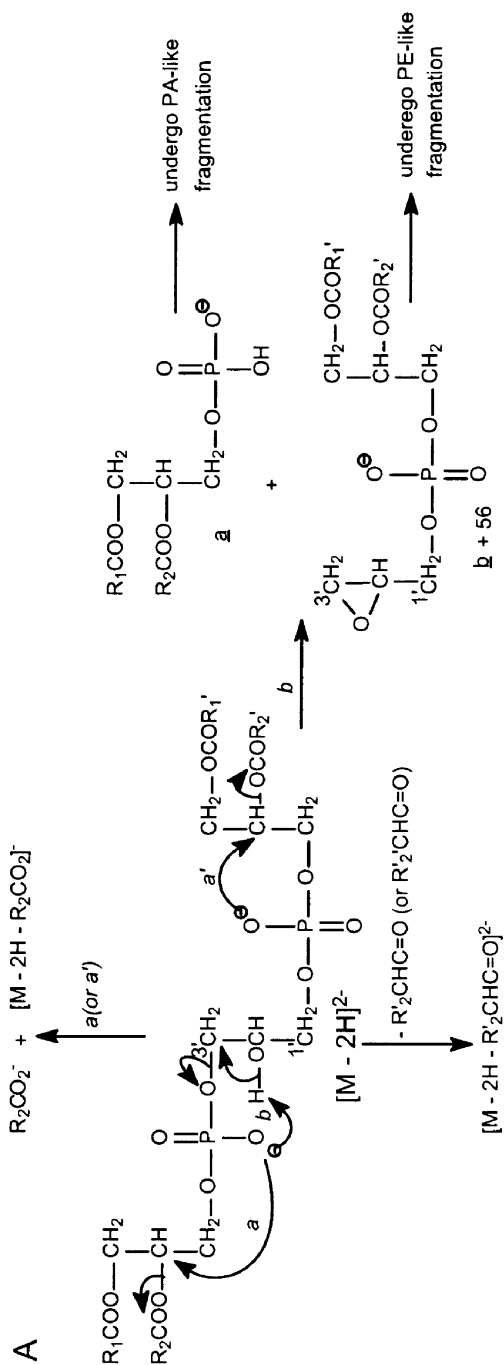


Fig. 3.26. The production spectra of the (A) $[M - 2H]^{2-}$ ions of m/z 723.6, and the (B) $[M - H]^{-}$ ions of m/z 1447, from (18:2/18:2)(18:2/18:2)-CL. (C) and (D) are the production spectra of the $[M - 2H]^{2-}$ (m/z 673.7) and of the $[M - H]^{-}$ (m/z 1347) ions from (16:0/16:1)(16:0/16:1)-CL, respectively.



The m/z 255 ion is more abundant than the m/z 253 ion in the latter spectrum, but the abundances of the two ions are reversed in the product-ion spectrum of m/z 673.6 (Fig. 3.26C), which is a basic $[M - 2H]^{2-}$ ion. This reversal in abundances of the carboxylate anions obtained from precursors with different charge states provides complementary information to confirm the positions of fatty acyl substituents.

Figure 3.26C also shows ions at m/z 645 (**a**) and m/z 701 (**b** + 56), deriving from nucleophilic attack of the anionic charge site on the remaining exchangeable hydrogen of the glycerol head group (Scheme 3.19A, route *b*). The nucleophilic attack on the fatty acyl substituent at *sn*-2 or *sn*-2' also results in simultaneous formation of m/z 1093 ($673 \times 2 - 253$) and the 16:1-carboxylate anion at m/z 253. The similar attack on the 16:0 fatty acyl substituent at *sn*-1 or *sn*-1' results in simultaneous generation of ions at m/z 1091 ($673 \times 2 - 255$) and m/z 255 (16:0-carboxylate). The m/z 253 is more abundant than the m/z 255, consistent with the idea that the fragmentation processes leading to ion formation are sterically more favorable at *sn*-2 than at *sn*-1.

The loss of the fatty acyl ketene at *sn*-2 or *sn*-2' leads to a doubly-charged fragment ion at m/z 555 ($673 - 236/2$), which is also more abundant than m/z 554 ($673 - 238/2$), another doubly-charged fragment ion arising from loss of the ketene at *sn*-1 or *sn*-1'. This preferential formation of the ions reflecting the ketene loss at *sn*-2 or *sn*-2' over that at *sn*-1 or *sn*-1' is consistent with the concept described earlier and permits structural determination of complex CL molecules, including configurational isomers and positional isomers.

The MS²-spectrum of the $[M - H]^-$ ion at m/z 1347 obtained with an ITMS instrument (Fig. 3.27A) contains similar ions, but the spectrum is dominated by m/z 645 (**a** ion), along with m/z 701 (**b** + 56) and m/z 781 (**b** + 136) (Scheme 3.19B). The m/z 645 ion is equivalent to a deprotonated ion of 16:0/16:1-PA and gives an MS³-spectrum containing major fragment ions at m/z 389 and m/z 391 via further loss of palmitic (16:0) acid at *sn*-1, and of palmitoleic (16:1) acid at *sn*-2, respectively (Fig. 3.27B). These results confirm the structural assignments made for characterization of 16:0/16:1-16:0/16:1-CL. The MS³-spectrum of the m/z 781 ion (Fig. 3.27C) contains a major ion at m/z 645 and fragment ions similar to those observed in the MS³-spectrum of m/z 645, indicating that m/z 781 undergoes neutral loss of 136 to yield m/z 645 ($781 - 136$), similar to that described in Scheme 3.16A.

GPI_{no}, Glycerophosphoinositol Monophosphate (PIP), and Glycerophatylinositol Bisphosphate (PIP₂)

GPI_{no}

GPI_{no} is a strong acid (75) and this fact is consistent with the features of the product-ion spectra of the $[M - H]^-$ ion of 16:0/18:2-PI at m/z 833 obtained by

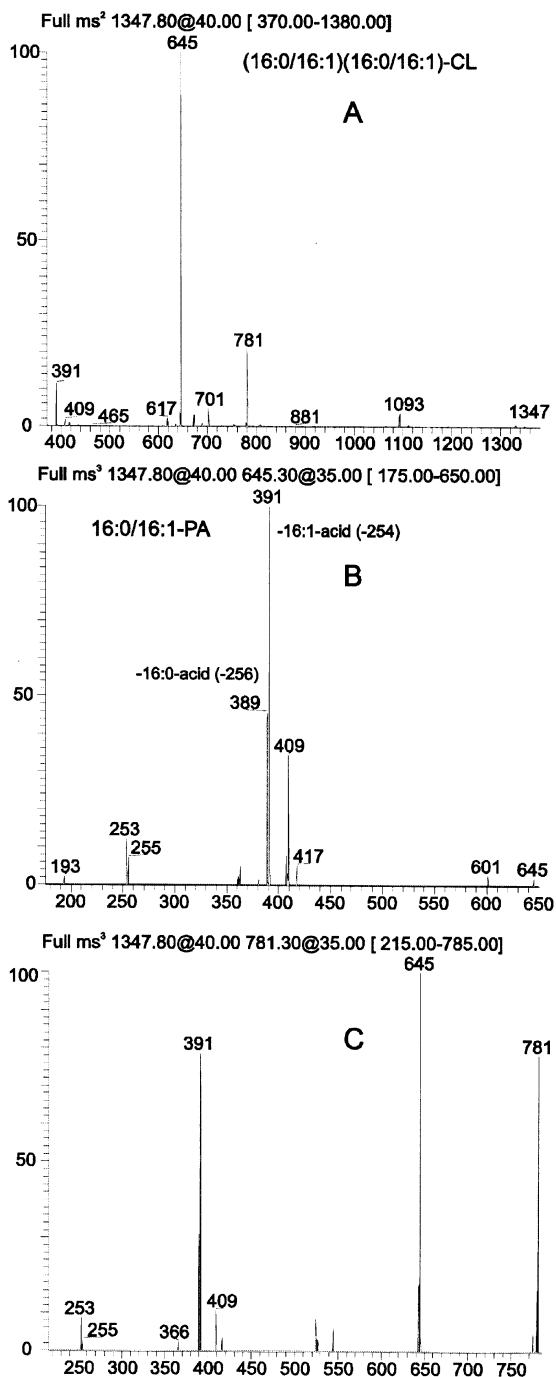


Fig. 3.27. (A) The ITMS MS²-spectrum of the $[M - H]^-$ ion (m/z 1347) of (16:0/16:1)(16:0/16:1)-CL. The ITMS MS³-spectra of m/z 645 ($1347 \rightarrow 645$) and of m/z 781 ($1347 \rightarrow 781$) are shown in (B) and (C), respectively.

low-energy CAD with a TSQ instrument (Fig. 3.28A) and with an ITMS instrument (Fig. 3.28B). The spectral features include the findings that the m/z 553 ($[M - H - R_2CO_2H]^-$) is more abundant than m/z 571 ($[M - H - R'_2CH=C=O]^-$), and the m/z 577 ($[M - H - R_1CO_2H]^-$) is more abundant than m/z 595 ($[M - H - R'_2CH=C=O]^-$). Also, the m/z 391 ($[M - H - R_2CO_2H - (\text{inositol} - H_2O)]^-$ (or $[M - H - R'_2CH=C=O - \text{inositol}]^-$)) ion, formed from consecutive loss of the inositol head group, is more abundant than the m/z 417 ($[M - H - R_1CO_2H - (\text{inositol} - H_2O)]^-$ (or $[M - H - R'_1CH=C=O - \text{inositol}]^-$) ion (Scheme 3.20). These trends are due to the fact that fragment ions reflecting the losses that arise from charge-driven processes occur preferentially at the *sn*-2 position (47).

Figure 3.28A illustrates that the relative intensity of the $R_2CO_2^-$ ion at m/z 279 is close to that of the $R_1CO_2^-$ ion at m/z 255. This represents an appreciable difference from the trend observed for the other phospholipid classes that yield two car-

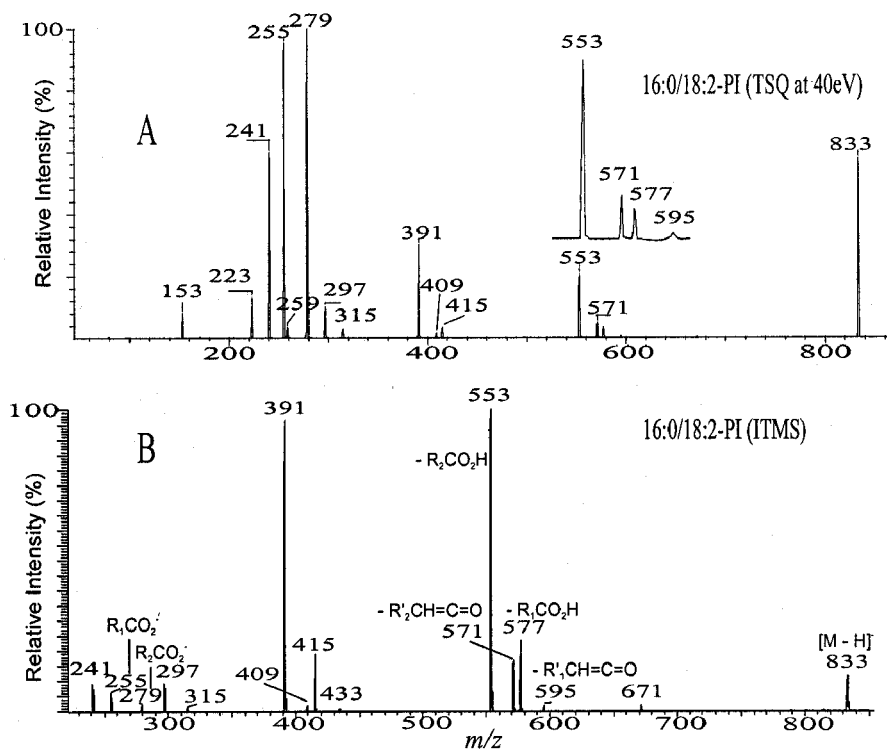
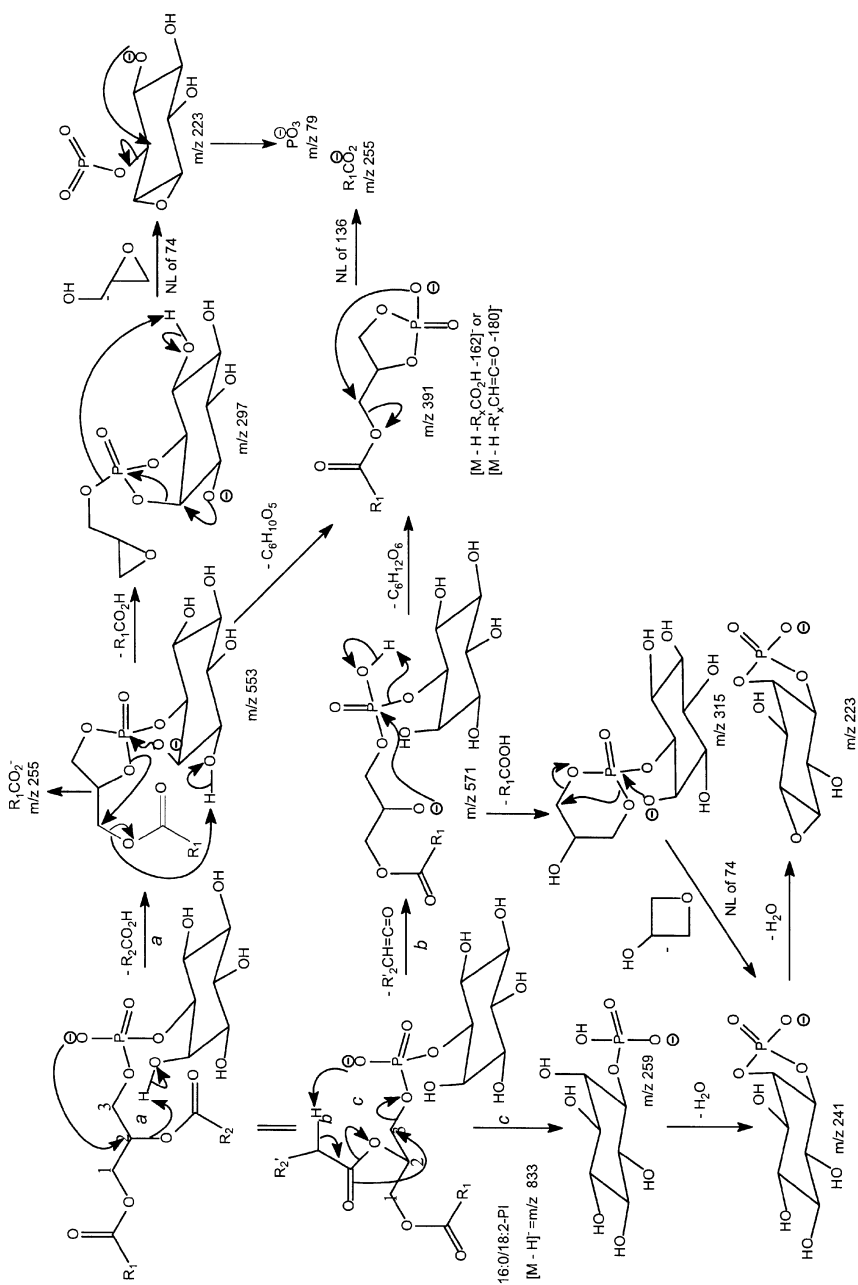


Fig. 3.28. The product-ion spectrum of the $[M - H]^-$ ion of 16:0/18:2-PI at m/z 833 obtained with (A) TSQ, and with (B) ITMS instruments.



Scheme 3.20. Proposed fragmentation mechanisms from glycerophosphoinositol in negative-ion mode.

boxylate anions with substantially different intensities. Three pathways lead to formation of the $R_x\text{CO}_2^-$ ions for GPIIno.

The predominant pathway arises from nucleophilic attack of the phosphate anionic charge site to expel the *sn*-1 or *sn*-2 fatty acyl substituents to give $R_1\text{CO}_2^-$ or $R_2\text{CO}_2^-$. This pathway is a CDF process, which is sterically more favorable at *sn*-2 than at *sn*-1 under low-energy CAD, and results in the abundance of m/z 279 ($R_2\text{CO}_2^-$) > m/z 255 ($R_1\text{CO}_2^-$). However, the $R_1\text{CO}_2^-$ ion at m/z 255 can also arise from further decomposition of the $[\text{M} - \text{H} - \text{R}'_2\text{CH}=\text{C}=\text{O} - \text{inositol}]^-$ (same m/z value as $[\text{M} - \text{H} - \text{R}_2\text{CO}_2\text{H} - (\text{inositol} - \text{H}_2\text{O})]^-$) ion at m/z 391, the $[\text{M} - \text{H} - \text{R}_2\text{CO}_2\text{H}]^-$ ion at m/z 553, and of the $[\text{M} - \text{H} - \text{R}'_2\text{CH}=\text{C}=\text{O}]^-$ ion at m/z 571 (Scheme 3.20). Similarly, the m/z 279 ($R_2\text{CO}_2^-$) can also arise from the $[\text{M} - \text{H} - \text{R}'_1\text{CH}=\text{C}=\text{O} - \text{inositol}]^-$ (same m/z value as $[\text{M} - \text{H} - \text{R}_1\text{CO}_2\text{H} - (\text{inositol} - \text{H}_2\text{O})]^-$) ion at m/z 415, the $[\text{M} - \text{H} - \text{R}_1\text{CO}_2\text{H}]^-$ ion at m/z 577, and of the $[\text{M} - \text{H} - \text{R}'_1\text{CH}=\text{C}=\text{O}]^-$ ion at m/z 595. These secondary fragmentation processes that yield $R_x\text{CO}_2^-$ ions prevail as the collision energy increases, resulting in the abundance of m/z 255 ($R_1\text{CO}_2^-$) > m/z 279 ($R_2\text{CO}_2^-$). This is because ions at m/z 391, 553, and 571 are preferentially formed by the elimination steps that were related to the fatty acyl moiety at *sn*-2. In contrast, the analogous ions at m/z 415, 577, and 595, arising from the similar losses at *sn*-1, are respectively less abundant. Therefore, at a higher collision energy ($\geq 45\text{eV}$), the m/z 255 ion is more abundant than the m/z 279 ion, whereas the abundances of the two ions are reversed when the MS/MS spectrum of the $[\text{M} - \text{H}]^-$ ion of 16:0/18:2-PI is obtained at a lower collision energy ($\leq 35\text{eV}$).

Within the range of the collision energies optimized for the analysis of GPIIno by tandem MS with a TSQ instrument, the carboxylate anions undergo various degrees of fragmentation after their formation, dependent on the degree of unsaturation of the fatty acyl moieties. Thus, the relative intensities of the carboxylate anions from GPIIno vary with the collision energy. Consequently, assignment of the positions of the fatty acid substituents on the glycerol backbone based on the abundances of the carboxylate anions observed in the product-ion spectra is not reliable. In contrast, the consecutive fragmentation processes observed by using an ITMS instrument are minimal and the fragment ions mainly derive from the primary fragmentation processes. Thus, the $R_x\text{CO}_2^-$ ions at m/z 255 and m/z 279 are of low abundance in the product-ion spectrum of 16:0/18:2-PI obtained with ITMS (Fig. 3.28B).

The ions reflecting the inositol head group are observed at m/z 315, 297, 279, 259, 241, and 223. The m/z 297 ion ($[\text{M} - \text{H} - \text{R}_1\text{CO}_2\text{H} - \text{R}_2\text{CO}_2\text{H}]^-$) arises from consecutive losses of the fatty acyl substituents as acids. The first acid loss involves an exchangeable hydrogen of the inositol head group, while the subsequent loss of the other fatty acid substituent involves both the exchangeable hydrogen on the inositol head group and the non-exchangeable hydrogen on the glycerol backbone, suggesting that both CDF and CRF processes contribute to formation of m/z 297, at optimal collision energy.

Phosphatidylinositol Monophosphate (PIP) and Phosphatidylinositol Bisphosphate (PIP₂)

The phosphatidylinositol-4-phosphates (PI-4-P) have two anionic charge sites and form both $[M - H]^-$ and $[M - 2H]^{2-}$ ions when subjected to ESI. The product-ion spectrum of the $[M - H]^-$ ion of 18:0/20:4-PI-4-P at m/z 965 (Fig. 3.29A) contains ions at m/z 661 and m/z 679, corresponding to $[M - H - R_2COOH]^-$ and $[M - H - R_2CH=C=O]^-$ ions, respectively. The former ion is 5 times more abundant than the latter, indicating that the gaseous $[M - H]^-$ ion of 18:0/20:4-PI-4-P is an acidic precursor, which preferentially undergoes acid loss versus ketene loss. This is further evidenced by the observation of the greater abundance of m/z 681 ($[M - H - R_1COOH]^-$) than m/z 699 ($[M - H - R_1CH=C=O]^-$). The intensities of the m/z 661 and the m/z 679 ions are also greater than those of their respective counterpart ions at m/z 681 and m/z 699. This is consistent with the notion that neutral losses of the fatty acyl chain as a ketene and as an acid at *sn*-2 are sterically more favorable than the same losses from *sn*-1. Ions at m/z 785 ($[M - H - \text{inositol}]^-$) and m/z 803 ($[M - H - (\text{inositol} - H_2O)]^-$) correspond to losses of inositol and (inositol - H₂O) moieties, respectively. The formation of these two ions involves a rearrangement process, in which the anionic phosphate charge site at C4' of the phosphoinositol head group attacks the glycerophosphate to eliminate inositol or (inositol - H₂O) (Scheme 3.21). These pathways are in accord with the presence of the m/z 159 and m/z 177 ions, corresponding to $(PO_3)(HPO_3)^-$ and $(H_2PO_3)(OPO_3H)^-$, respectively. This unusual loss of an internal hexose residue was also observed for sulfatide, which is described below.

Several ions arising from water loss are observed at m/z 947 ($965 - H_2O$), m/z 663 ($681 - H_2O$), and m/z 643 ($661 - H_2O$). The spectrum also contains ions at m/z 885 and m/z 867, arising from losses of HPO₃ and H₃PO₄, respectively. The former ion undergoes fragmentation identical to that of the $[M - H]^-$ ion of 18:0/20:4-PI. The spectrum also displays the same common ions at m/z 259, 241, 223, 153, 97, and 79 that occurred from GPI_{no}. The spectrum also contains the m/z 321 ion (Scheme 3.21), arising from loss of the diacylglycerol moiety to form a dehydrated inositol bisphosphate, which gives the m/z 303 ion by loss of H₂O. The m/z 321 and m/z 303 ions reflect the additional phosphate substitution in the head group and are observed in the product-ion spectra of the $[M - H]^-$ ions of both PI-4-P and PI-3-P.

The $[M - 2H]^{2-}$ ion of 18:0/20:4-PI-4-P at m/z 482.4 (Fig. 3.29B) yields the m/z 885 ($482 \times 2 - 79$) ion by loss of PO₃⁻. At the same time, the phosphate anionic charge site in the $[M - 2H]^{2-}$ attacks the C-2 of the glycerol backbone to expel the R₂CO₂⁻, and this results in the formation of the m/z 661 ($[M - 2H]^{2-} - R_2CO_2^-$) ($482 \times 2 - 303$) and the m/z 303 (R₂CO₂⁻) ions, simultaneously. The phosphate anionic site also attacks the C-1 to expel the R₁CO₂⁻, giving rise to m/z 681 ($[M - 2H]^{2-} - R_1CO_2^-$) ($482 \times 2 - 283$) and m/z 283 (R₁CO₂⁻). The intensities of the m/z 661 and m/z 303 (R₂CO₂⁻) ions are respectively more abundant than the m/z 681 and the m/z 283

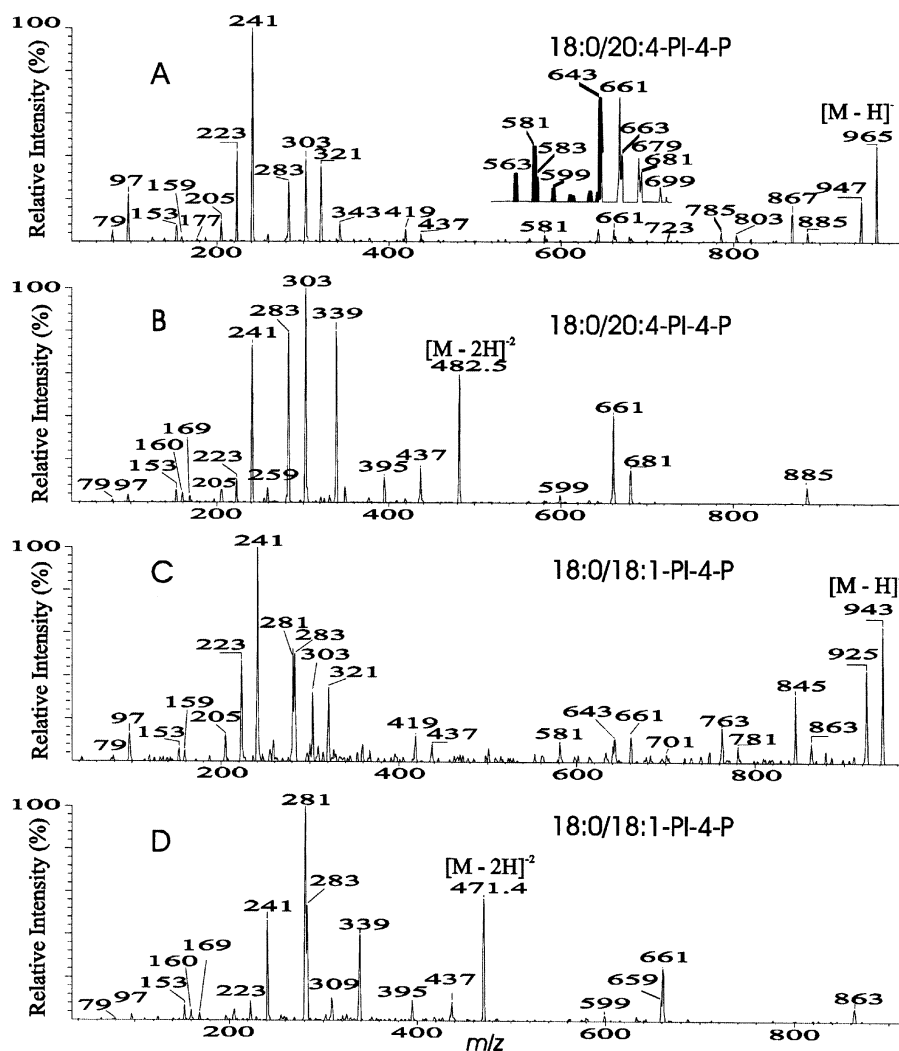
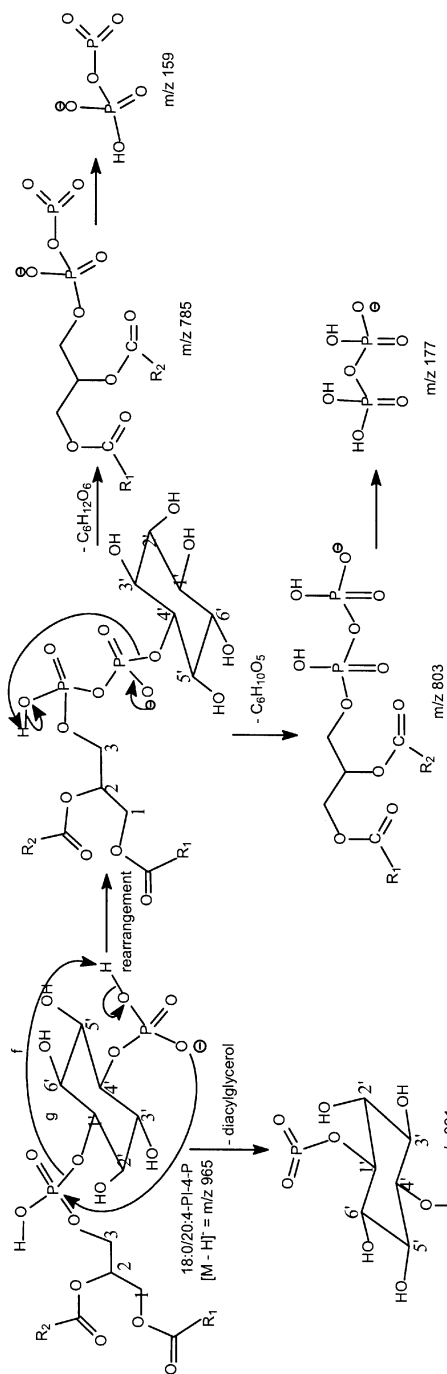


Fig. 3.29. The product-ion spectra of the (A) $[M - H]^-$ ion at m/z 965, and of the (B) $[M - 2H]^{2-}$ ion at m/z 482.4 from 18:0/20:4-PI-4-P. (C) and (D) are the spectra of the $[M - H]^-$ (m/z 943) and $[M - 2H]^{2-}$ (m/z 471.4) ions from 18:0/18:1-PI-4-P, respectively.

($R_1CO_2^-$) ions. The ions reflecting losses of the fatty acyl substituents as acids are not present. This is consistent with the notion that the $[M - 2H]^{2-}$ ion, which contains one less proton than the $[M - H]^-$ ion, becomes a basic precursor ion and undergoes CDF processes through the attack of the anionic charge site onto C-1 or C-2 of the glycerol to form $R_XCO_2^-$ and $([M - 2H]^{2-} - R_XCO_2^-)$ ions, simultaneously. The anionic charge



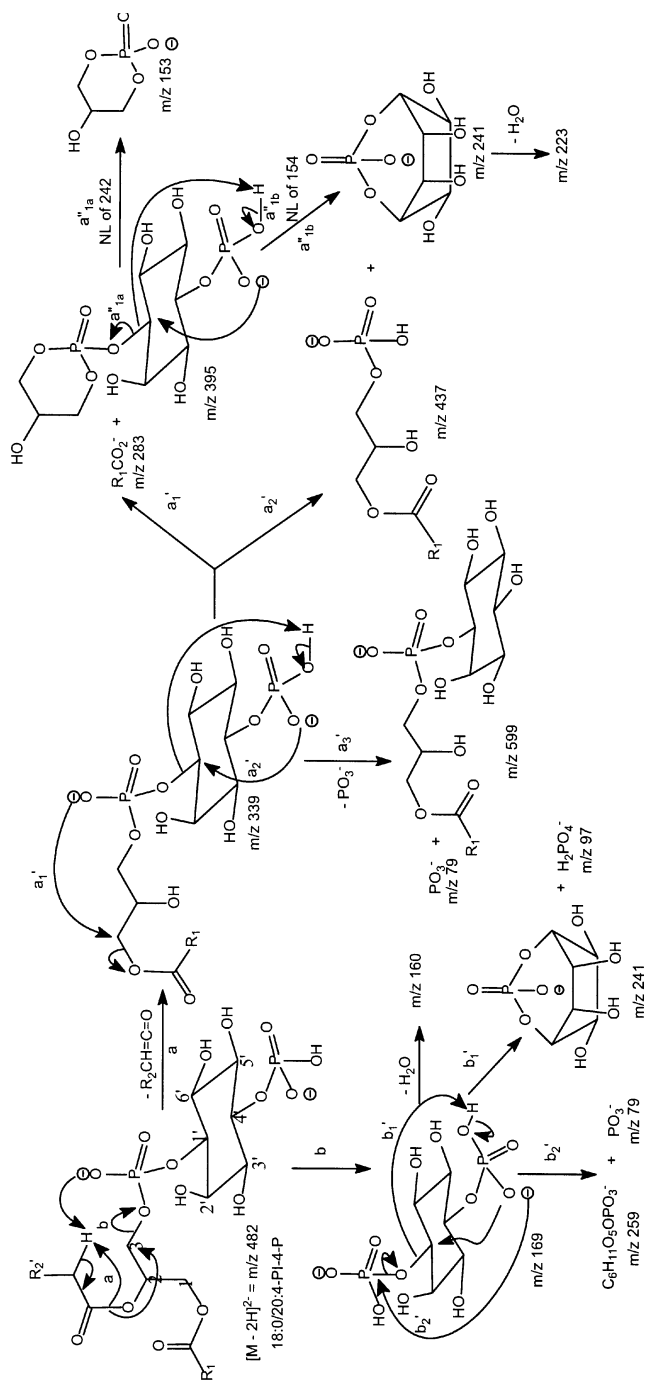
Scheme 3.21. Proposed mechanisms of fragment formation from glycerophosphoinositol monophosphate ($[M-H]^-$ ion) in negative-ion mode.

site also attacks the α -hydrogen of a fatty acid substituent to eliminate a ketene. This latter process results in the m/z 339 ($[M - 2H - R_2CH=C=O]^{2-}$) ($482 - 286/2$) ion, a doubly-charged fragment ion that arises from loss of the 20:4-fatty acyl chain at *sn*-2 as a ketene. An analogous ion arising from loss of the *sn*-1 substituent (the m/z 349 ion) is not observed. These results are consistent with the idea that the CDF processes are more sterically favorable at *sn*-2 than at *sn*-1. The spectrum also contains the m/z 395 ion ($339 \times 2 - 283$), arising from expulsion of the 18:0 carboxylate anion (m/z 283) at *sn*-1 from the m/z 339 ion (Scheme 3.22, route a_1'), which also gives the m/z 599 ion ($339 \times 2 - 79$), by loss of PO_3^- (route a_3'), and ions at m/z 241 ($339 \times 2 - 437$) and m/z 437 (route a_2'). The m/z 241 ion can also arise from m/z 395 by neutral loss of 154 (route a'_{1b}). This latter process also results in m/z 153 by loss of 242 (a'_{1a}). The preceding fragmentation pathways and the proposed ion configurations are also supported by the source-CAD tandem mass spectra of the m/z 339 and the m/z 395 ions, and by the product-ion spectrum of the $[M - 2H]^{2-}$ ion of 18:0/18:1-PI-4-P (Fig. 3.29D) at m/z 471.4.

The additional phosphate in the inositol head group is indicated by the presence of the m/z 169 and m/z 160 ions, representing the doubly-charged ions of inositol bisphosphate ($[C_6H_{10}O_4(OPO_3H)_2]^{2-}$) and of dehydrated inositol bisphosphate ($[C_6H_{10}O_4(OPO_3H)_2 - H_2O]^{2-}$), respectively (Scheme 3.22, route *b*). The m/z 169 ion, again, undergoes further dissociation to yield the singly-charged ions at m/z 241 and m/z 97 ($H_2PO_4^-$) (route b_1') or at m/z 259 and m/z 79 (PO_3^-) (route b_2'), simultaneously. The m/z 169 and m/z 160 ions plus ions at m/z 259, 241, and 223, which reflect the polar head group of the molecule, permit identification of PIPs, and classification of the phosphorylation state of the inositol head group.

The product-ion spectrum of the $[M - H]^-$ ion of 18:0/20:4-PI-4-P at m/z 965 (Fig. 3.29A) contains abundant carboxylate anions at m/z 303 ($R_2CO_2^-$) and m/z 283 ($R_1CO_2^-$). The former ion is more abundant than the latter. However, the m/z 281 ($R_2CO_2^-$) and m/z 283 ($R_1CO_2^-$) ions in the product-ion spectrum of 18:0/18:1-PI-4-P at m/z 943 (Fig. 3.29C) are nearly equally abundant, similar to what was observed in the CAD spectrum of GPIIno. This reflects the fact, as described earlier, that the m/z 321 ion undergoes an H_2O loss to give m/z 303 ($[PO_3C_6H_3O_3-OPO_3H]^-$), which overlaps with the 20:4-carboxylate anion at m/z 303 ($C_{19}H_{31}COO^-$), because the two ions are not resolvable by a quadrupole mass spectrometer. Therefore, pathways for the formation of the carboxylate anions from PI-4-Ps are similar to those for GPIIno, which is also acidic. The $[M - 2H]^{2-}$ ion of 18:0/20:4-PI-4-P at m/z 482.5 undergoes GPETn-like fragmentation and the $R_2CO_2^-$ ion at m/z 303 is more abundant than the $R_1CO_2^-$ ion at m/z 283 (Fig. 3.29B). Similarly, the $R_2CO_2^-$ at m/z 281 is more abundant than the $R_1CO_2^-$ at m/z 283, in the product-ion spectrum of the $[M - 2H]^{2-}$ ion of 18:0/18:1-PI-4-P at m/z 471.4 (Fig. 3.29D).

Both the $[M - H]^-$ and $[M - 2H]^{2-}$ ions of phosphatidylinositol-3-phosphate (PI-3-P) generated by ESI yield product-ion spectra similar to those of PI-4-P. However, the $[M - H - H_3PO_4]^-$ ion is much more abundant in the product-ion



Scheme 3.22. Proposed mechanisms of fragmentation of glycerophosphoinositol monophosphate ($[M - 2H]^{2-}$ ion) in negative-ion mode.

spectra of the $[M - H]^-$ ions arising from PI-4-P than from PI-3-P, permitting distinction between the two isomers (47).

Phosphatidylinositol-4,5-Bisphosphate (PI-4,5-P₂) and Phosphatidylinositol-3,4-Bisphosphate (PI-3,4-P₂)

Phosphatidylinositol bisphosphates also form both $[M - H]^-$ and $[M - 2H]^{2-}$ ions by ESI. The product-ion spectrum of the $[M - H]^-$ ion of 18:0/20:4-PI-4,5-P₂ at m/z 1045 (Fig. 3.30A) contains abundant fragment ions similar to those observed in the spectrum of 18:0/20:4-PI-4-P. Ions at m/z 965, 947, and 929 correspond to losses of HPO₃, H₃PO₄, and (H₃PO₄ + H₂O), respectively. The expulsion of one HPO₃, followed by elimination of the inositol and of the (inositol - H₂O) moieties, yields the m/z 785 ($[M - H - HPO_3 - \text{inositol}]^-$) and m/z 803 ($[M - H - HPO_3 - (\text{inositol} - H_2O)]^-$) ions, respectively. This fragmentation process gives rise to m/z 177 and m/z 159, representing (H₂PO₃)(OPO₃H)⁻ and (PO₃)(HPO₃)⁻ ions, respectively, and has also been observed in the CAD spectrum of PIP. The product-ion spectra of PIP₂ are similar to those of PIP. Therefore, it appears that an HPO₃ moiety is eliminated from PIP₂ to yield a PIP-like ion, which then undergoes fragmentation processes that are similar to those of PIP.

In addition to the ions at m/z 321, 303, 241, 223, and so on, reflecting the polar head groups commonly seen in the spectra of the PI-4-P and PI-3-P classes, a prominent ion at m/z 401, reflecting a dehydrated inositol trisphosphate anion as a singly-charged species is also present. This is consistent with the earlier finding that PIPs yield an ion at m/z 321, representing a dehydrated inositol bisphosphate anion (Scheme 3.21). The m/z 401 ion also yields an ion at m/z 383 *via* loss of H₂O. These ions permit identification of the phosphorylation state of the head group and assignment of the parent species as a PIP₂ isomer.

The doubly-charged precursor ion of 18:0/20:4-PI-4,5-P₂ (m/z 522.4, Fig. 3.0B) also undergoes fragmentations similar to those of the $[M - 2H]_2^{2-}$ ion of PI-4-P described earlier. Again, the preferential loss of R₂CO₂⁻ over R₁CO₂⁻ leads to the formation of m/z 741 ($522 \times 2 - 303$) > m/z 761 ($522 \times 2 - 283$). However, doubly-charged fragment ions expected at m/z 379, reflecting a ketene loss ($[M - 2H - R_2CH=C=O]^{2-}$), and ions at m/z 169 and m/z 160, representing an inositol bisphosphate ($[C_6H_{10}O_4(OPO_3H)_2]^{2-}$) anion and a dehydrated inositol bisphosphate ($[C_6H_{10}O_4(OPO_3H)_2 - H_2O]^{2-}$) anion, respectively, are absent.

The gaseous $[M - 2H]_2^{2-}$ ion of 18:0/20:4-PI-4,5-P₂ is more acidic than that of 18:0/20:4-PI-4-P due to the attachment of an additional phosphate moiety, which may deter the nucleophilic attack of the anionic charge site on C-1 and on C-2 of the glycerol backbone to form the carboxylate anions, or on the α -hydrogen of the fatty acyl moieties to expel ketenes. Therefore, ions at m/z 303 (R₂CO₂⁻) and m/z 283 (R₁CO₂⁻) are also less prominent than those arising from 18:0/20:4-PI-4-P (Fig. 3.29B). It is interesting to note that the m/z 370 ($[M - 2H - R_2COOH]^{2-}$) ion, arising from an acid loss, is also absent.

Studies of 16:0/16:0-PI-3,4-P₂ reveal that its fragmentation processes are similar to those of PI-4,5-P₂. Distinction between these two isomeric subclasses cannot be achieved by their tandem mass spectra, although isomers between PI-3-P and PI-4-P can be distinguished from each other. These findings are consistent with the notion that distinction among inositol polyphosphates isomers becomes more difficult as the number of phosphate substituents increases (81).

In conclusion, the [M – H][–] ions of GPI_{no}, PIP, and PIP₂ are acidic precursors and undergo fragmentation processes similar to those for GPA upon CAD. However, the doubly-charged ([M – 2H]^{2–}) ions of PIP and PIP₂ undergo fragmentation processes that are typical of those of the [M – H][–] ions of GPETns, which are basic. These results suggest that gaseous [M – 2H]^{2–} ions of PIP and PIP₂, from which two protons have been removed from the neutral molecules, are basic precursors, and in this way are similar to the doubly-charged ions of CL.

Lysophospholipids, Plasmenyolphospholipids (Plasmalogens), and Plasmanyolphospholipids

The product-ion spectra of both lyso1/18:1-PE (Fig. 3.31A) and 18:1/lyso2-PE (Fig. 3.31B) are dominated by the sole carboxylate anion at *m/z* 281 that identifies the 18:1-fatty acyl moiety of the molecules. In the spectrum from 1-lysophosphatidylethanolamine, the *m/z* 214 ion, which reflects loss of the 18:1-fatty acyl chain as a ketene ([M – H – R₁CH=C=O][–]), is more abundant than the *m/z* 196 ion, which corresponds to loss of the 18:1-fatty acyl chain as an acid ([M – H – R₁CO₂H][–]). The abundances of the two ions are reversed in the spectrum from 2-lysophosphatidylethanolamine. This is consistent with the notion that the gas-phase [M – H][–] ions of 1- and of 2-lysophosphatidylethanolamine are weakly basic ions and undergo more facile loss of the fatty acyl substituent as a ketene at *sn*-2 than at *sn*-1. Thus, positional isomers of 1- and 2-lyso-PE can be differentiated. However, acidic lysophospholipids such as the [M – H][–] ions of 1- and 2-lysophosphatic acids undergo mainly acid loss *via* CDF processes. This is evidenced by the MS³-spectrum of the *m/z* 409 ion (Fig. 3.21C), which is equivalent to the [M – H][–] ion of 16:0/lyso-PA. The spectrum is nearly identical to that arising from *m/z* 435 (Fig. 3.21D), which is equivalent to a lyso1/18:1-PA ion, indicating that differentiation between 1- and 2-lysophosphatic acid isomers by their product-ion spectra may not be feasible. Similarly, distinction between acidic isomers of 1- and 2-lysophosphatidylinositol is also not possible.

Both the product-ion spectra of plasmeryl (*p*16:0/18:2-PE, Fig. 3.31C) and plasmanyl (*a*16:0/18:0-PE, Fig. 3.31D) GPETn are dominated by a single set of ions of RCO₂[–], [M – H – RCO₂H][–] and [M – H – R'CH=CO][–] that identify the fatty acid substituent but not its location in the glycerol backbone. Ions reflecting the 1-*O*-alkyl or the 1-*O*-alk-1'-enyl moiety are not present, and therefore complete structural characterization, and in particular, differentiation between plasmanyl- and plasmeryl phospholipid subclasses, is not possible. However, product-ion spectra arising from the [M + Li]⁺ ions of these two subclasses as described previously do distinguish these two ether phospholipid subclasses.

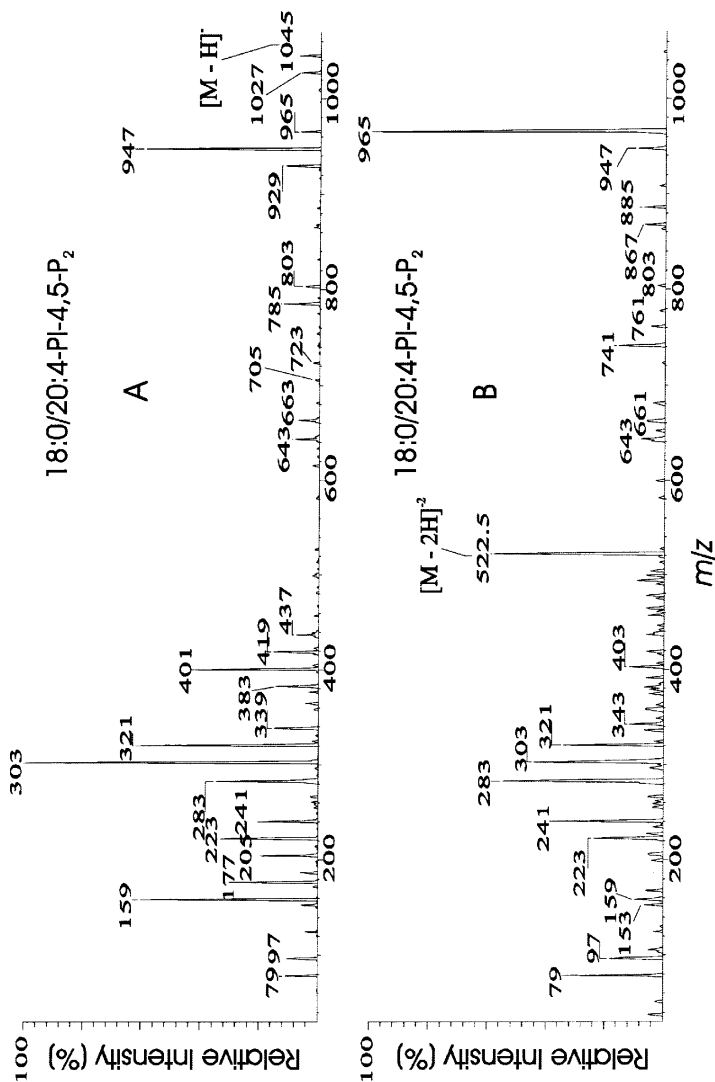


Fig. 3.30. The product-ion spectra of the (A) $[M - H]^-$ ion at 1045, and of the (B) $[M - 2H]^{2-}$ ion at m/z 522.5 from 18:0/20:4-PI-4,5-P₂.

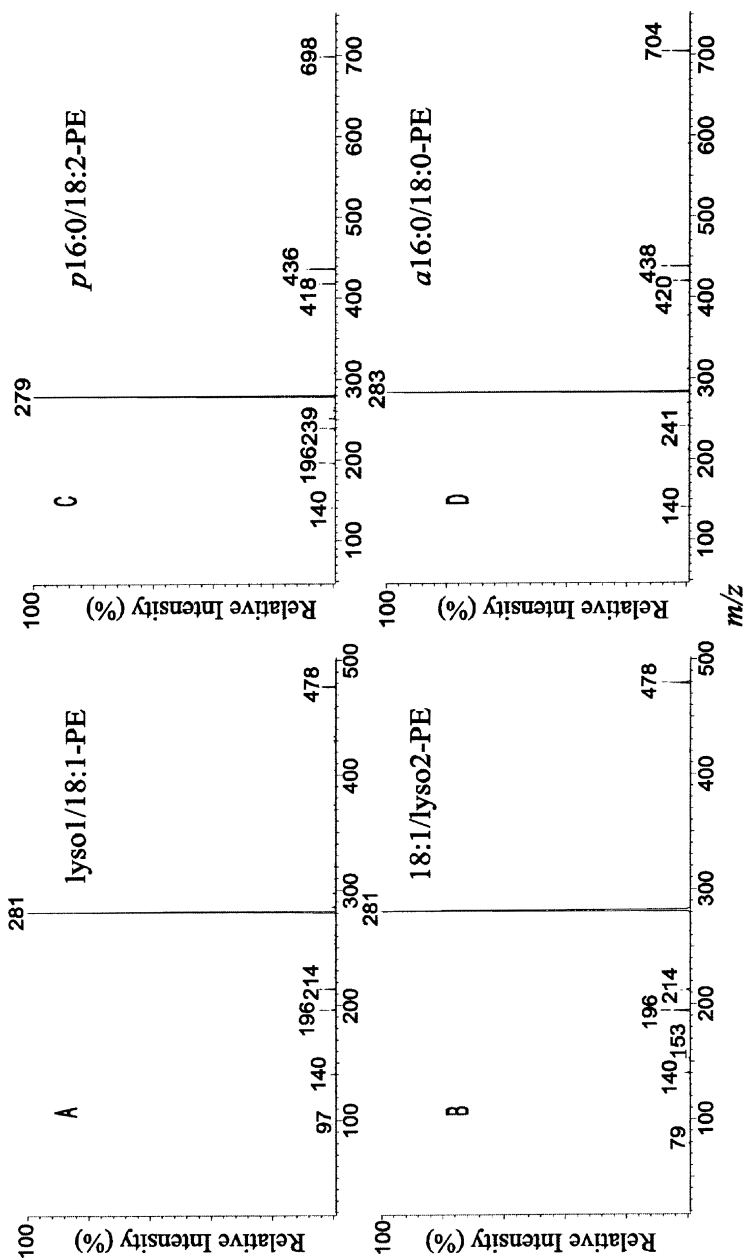


Fig. 3.31. The production spectra of the $[M - H]^-$ ions of lyso1/18:1-PE at m/z 478 (A), of the 18:1/lyso2-PE at m/z 478 (B), of *p*16:0/18:0-PE at 698 (C), and of α 16:0/18:0-PE at m/z 704 (D).

Phospholipids Consisting of Polyunsaturated Fatty Acid Substituents

The unique features in the product-ion spectra of phospholipids consisting of polyunsaturated fatty acyl substituents can be observed not only in the positive-ion CAD of $[M + Li]^+$ ions, but also in the negative-ion CAD of $[M - H]^-$ ions. Following CAD, polyunsaturated carboxylate anions arising from phospholipids undergo secondary fragmentation (82). The 4,7,10,13,16,19-docosahexenoate (4,7,10,13,16,19-22:6) anion at m/z 327 dissociates to a major ion of m/z 283 by loss of CO_2 and only 10% ($\Sigma\%$) of the $R_xCO_2^-$ ions survive at a collision energy of 35 eV. The 5,8,11,14-eicosatetraenoic (20:4) anion at m/z 303 also decomposes to m/z 259 by the same loss, and only 20% ($\Sigma\%$) of the m/z 303 ions survive. In contrast, saturated carboxylate anions, such as the stearate carboxylate anion (18:0) at m/z 283, undergo little dissociation at the same collision energy, and 99% of these ions survive (47).

Secondary dissociation of the carboxylate anions affects the abundance ratio of the fragment ions of $R_2CO_2^-/R_1CO_2^-$ drastically (71). As shown in Figure 3.32A, the product-ion spectrum of the 16:0/20:4-PE contains ions at m/z 303 and m/z 255, representing 20:4- and 16:0-carboxylate anions, respectively, but the spectrum also contains the m/z 259 ion generated by CO_2 loss from the m/z 303 ion. The product-ion spectrum of 16:0/22:6-PE (Fig. 3.32B) contains carboxylate ions at m/z 255 and m/z 327, along with an abundant ion at m/z 283 ($327 - CO_2$).

The largest effect of CO_2 loss on the ratio of abundances of $R_2CO_2^-/R_1CO_2^-$ is observed for 18:0/22:6-PE (Fig. 3.32C), which gives ions at m/z 283 ($R_1CO_2^-$) and m/z 327 ($R_2CO_2^-$), respectively. The 22:6 anion at m/z 327 also gives rise to m/z 283 ($C_{21}H_{31}^-$, F.W. = 283.242) by loss of CO_2 . This m/z 283 ion is isobaric with the 18:0-carboxylate anion ($C_{17}H_{35}CO_2^-$, F.W. = 283.264) arising from the acyl chain at *sn*-1, and results in an increase in the abundance of the m/z 283 ion and in a marked decline of the $R_2CO_2^-/R_1CO_2^-$ ratio, because the $C_{21}H_{31}^-$ and $C_{17}H_{35}CO_2^-$ ions are not resolved by the quadrupole mass spectrometer. This phenomenon is also illustrated by the product-ion spectrum of 22:6/22:6-PG (Fig. 3.32D), which exhibits the 22:6-carboxylate ion at m/z 327 and an ion at m/z 283 ($327 - CO_2$), arising from loss of CO_2 from m/z 327 rather than a 18:0-carboxylate ion. In contrast, the abundance ratio of $R_2CO_2^-/R_1CO_2^-$ is close to 3/1 for 16:0/18:2-PE (Fig. 3.23A) and 16:0/18:1-PG (Fig. 3.24A), because CO_2 elimination does not readily occur and so the apparent $R_2CO_2^-/R_1CO_2^-$ ratio is much closer to the actual relative abundances of the carboxylate anions.

In negative-ion mode, fragment ions arising from the loss of the fatty acyl substituent as an acid or as a ketene at *sn*-2 are consistently more abundant than those arising from the corresponding losses at *sn*-1. Thus, the position of the fatty acyl substituents of phospholipids on the glycerol backbone can be determined. In this respect, structural characterization using ITMS is attractive, because the ions reflecting loss of the carboxylate anions in the MS^2 -spectra are often prominent and the ions rarely undergo secondary degradation. In contrast, the product-ion spectra obtained with

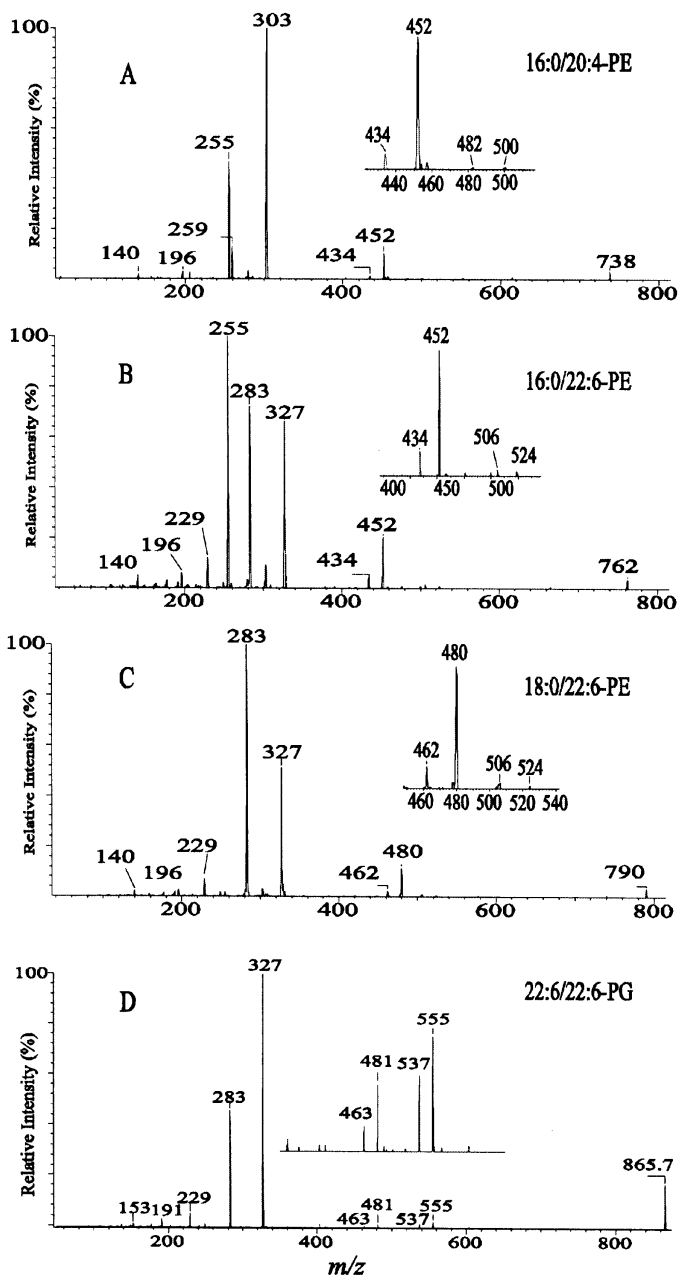


Fig. 3.32. The product-ion spectra of the $[M - H]^-$ ions of (A) 16:0/20:4-PE at m/z 738; of (B) 16:0/22:6-PE at m/z 762; of (C) 18:0/22:6-PE at m/z 790; and of (D) 22:6/22:6-PG at m/z 865.

TSQ instruments are dominated by the $R_x\text{CO}_2^-$ ions, of which the abundances are affected by the collision energy and by the various polar head groups that dictate the fragmentation processes. The marked change in the abundance ratio of $R_2\text{CO}_2^-/R_1\text{CO}_2^-$ in the product-ion spectra of the $[\text{M} - \text{H}]^-$ ions for the phospholipids consisting of a highly unsaturated fatty acyl moiety at *sn*-2 or *sn*-1 is mainly attributable to the further dissociation of the polyunsaturated $R_x\text{CO}_2^-$ ion. An altered abundance ratio of $R_2\text{CO}_2^-/R_1\text{CO}_2^-$ is also observed for phospholipids that contain very short-chain fatty acyl substituents ($<C_{10}$). The abundance of the short-chain carboxylate anions also decreases as the collision energy increases.

The relative abundances of $R_x\text{CO}_2^-$ ions in the product-ion spectra of phospholipids can reflect the position of the fatty acyl substituents on the glycerol backbone, if the carboxylate anions are stable. This method for structural determination is convenient because $R_x\text{CO}_2^-$ ions are often prominent in the product-ion spectra obtained with TSQ instruments. However, understanding the mechanisms underlying the fragmentation processes for various phospholipids is required to avoid misinterpretation. This awareness has facilitated structural identification of complicated phospholipid species such as acyl-PG, cardiolipins, and PIP, as described before.

Ceramide

Characterization and quantitation of ceramides in negative-ion mode by tandem MS have been achieved with FAB-tandem-sector MS (66,67), ESI-ITMS (83,84), and ESI-TSQ MS instruments (42,85). Results from these studies indicate that fragment ions arising from high-energy and low-energy CAD are similar, and that CDF is the major pathway leading to ion formation, although CRF processes can also be observed with high-energy CAD (66,67). The product-ion spectrum of the $[\text{M} + \text{Cl}]^-$ adduct ion of ceramide contains little structural information, but product-ion spectra arising from both the $[\text{M} + \text{CH}_3\text{CO}_2]^-$ and $[\text{M} - \text{H}]^-$ ions are informative and are nearly identical (42). The spectra contain multiple ions reflecting both fatty acyl and LCB substituents.

As shown in Figure 3.33A, the $[\text{M} - \text{H}]^-$ ion of d18:1/18:1-Cer at m/z 562 yields a weak ion at m/z 544 (**c**₁), corresponding to loss of H_2O , followed by HCHO loss to give rise to the m/z 514 ion (**c**₄), which dissociates to m/z 250 (**b**₇) by loss of the fatty acyl moiety as a ketene (loss of $\text{C}_{16}\text{H}_{31}\text{CH}=\text{C}=\text{O}$). The m/z 544 ion also gives rise to the m/z 263 ion (**b**₆) by eliminating the fatty acyl moiety as an amide (loss of $\text{C}_{17}\text{H}_{33}\text{CONH}_2$, 281 Da). The H_2O loss leading to the m/z 544 ion from m/z 562 involves participation of an exchangeable hydrogen *via* several fragmentation pathways similar to those proposed for the $[\text{M} + \text{Li}]^+$ ion in the positive-ion mode (Scheme 3.8) (58).

Two interesting ions at m/z 532 ($[\text{M} - \text{H} - 30]^-$) and m/z 530 ($[\text{M} - \text{H} - 32]^-$) arise from losses of HCHO and $[\text{H}_2 + \text{HCHO}]$, respectively, and these ions are also present in the spectrum obtained by high-energy CAD (66,67). The mechanism(s) of ion formation are proposed in Scheme 3.23. The suggested structure of the m/z

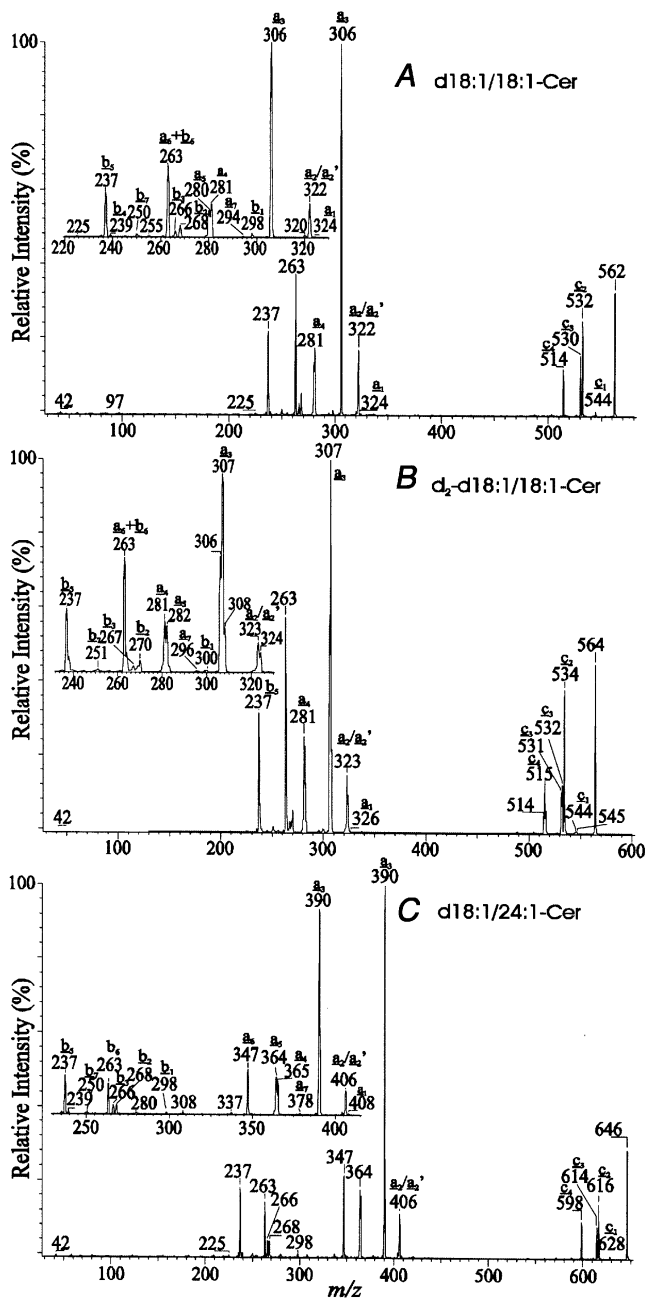
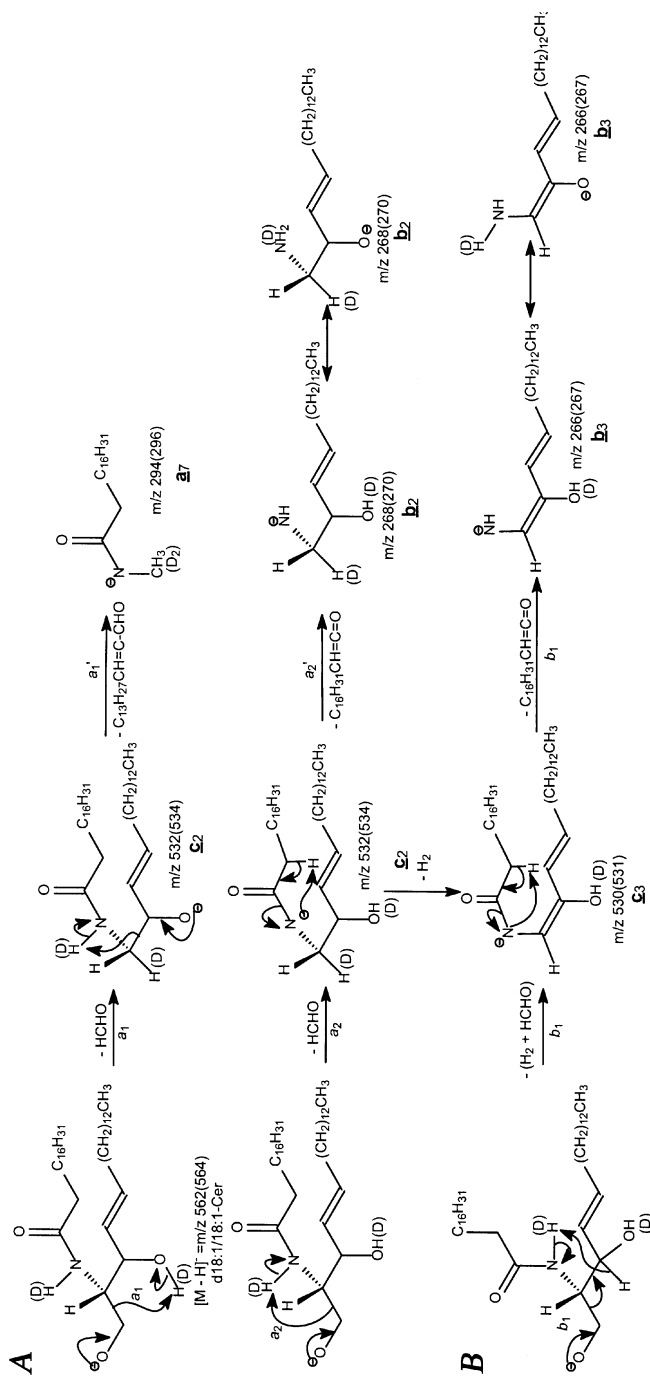


Fig. 3.33. The product-ion spectra of the $[M - H]^-$ ions of (A) d18:1/18:1-Cer at m/z 562; (B) d_2 -d18:1/18:1-Cer at m/z 564; and of (C) d18:1/24:1-Cer at m/z 646.



Scheme 3.23. Proposed mechanisms of ceramide fragment formation from ceramide in negative-ion mode. (A) Ion designation: symbols with script **a** are fatty acid-related ions; symbols with script **b** are long-chain base-related ions; symbols with script **c** are common ions. (B) Masses in parentheses arise from d-labeled analogs. In some cases multiple masses were observed, probably due to hydrogen scrambling, which may account for a few mass discrepancies.

532 ion is consistent with the observation of the m/z 268 (**b**₂) and m/z 294 (**a**₇) ions in the source-CAD product-ion spectrum of the m/z 532 ion (42). The m/z 268 ion (**b**₂) arises from further loss of the fatty acyl moiety as a ketene, and the m/z 294 ion (**a**₇) arises from loss of the LCB as an aldehyde (Scheme 3.23A).

The m/z 530 ion has been suggested to arise from m/z 562 by a direct loss of CH₃OH (67,68). However, the product-ion spectrum of the H-D exchanged d_2 -d18:1/18:1-Cer (Fig. 3.33B) contains two analogous ions at m/z 531 and m/z 532, suggesting that the m/z 531/532 ions arise from loss of HCHO along with loss of HD/H₂, involving the exchangeable/non-exchangeable hydrogen (Scheme 3.23B). This mechanism is supported by the product-ion spectra of m/z 531 and m/z 532 generated by source-CAD of d_2 -d18:1/18:1-Cer. The two spectra are identical, indicating that the two ions have the same structure (42).

A unique ion at m/z 281 (**a**₄) corresponding to the oleate carboxylate anion is observed in the product-ion spectra of d18:1/18:1-Cer (Fig. 3.33A) and of d_2 -d18:1/18:1-Cer (Fig. 3.33B). An analogous ion at m/z 365 (**a**₄), reflecting a 24:1-fatty acyl substituent is also observed for d18:1/24:1-Cer (Fig. 3.33C). The ion may originate from initial cleavage of the C2-C3 bond to form an *N*-oleoylaminoethanol anion (C₁₇H₃₃CONHCH₂CH₂O⁻) at m/z 324 (**a**₁, Scheme 3.24A) by loss of the LCB as an aldehyde (CH₃(CH₂)₁₂CH=CHCHO, 238 Da). This bond cleavage also gives rise to m/z 237 ([CH₃(CH₂)₁₂CH=CHCHO - H]⁻) (**b**₅, Scheme 3.24B), representing a deprotonated aldehyde ion that can be used to identify the d18:1-LCB. An analogous ion at m/z 239 reflecting the 18:0-LCB is observed for d18:0/nFA (Fig. 3.34A and B). Further loss of H₂ from m/z 324 gives rise to a deprotonated *N*-oleoylaminoethylen-1-ol ion at m/z 322 (C₁₇H₃₃CONHCH=CHO⁻) (**a**₂), followed by a rearrangement process to yield a carboxyethenolamine anion (C₁₇H₃₃COOCH=CHNH⁻) (**a**₂), which results in a carboxylate ion at m/z 281 (C₁₇H₃₃CO₂⁻) (**a**₄) by eliminating azirine (41 Da) (Scheme 3.24A, route *a*). This fragmentation pathway is supported by studies of authentic *N*-oleoylaminoethanol (42).

The m/z 306 (**a**₃) arises from several consecutive dissociation steps, in which an *N*-acylaminoethanol arising from loss of the LCB as an aldehyde is primarily formed, followed by loss of an H₂O (Scheme 3.24A). These fragmentation processes are supported by the product-ion spectrum from d_2 -18:1/18:1-Cer (Fig. 3.33b). The proposed configuration of the m/z 306 is consistent with the presence of the m/z 279 and m/z 263, resulting from CAD of the m/z 306 ion.

The product-ion spectrum of *N*-acylsphinganine (Fig. 3.34A) differs from that of *N*-acylsphingosine by the absence of the [M - H - HCHO]⁻ ion, when spectra are acquired at optimal collision energy. This permits structural differentiation between these two subclasses of ceramides (42,66,67). Figure 3.34A illustrates that the product-ion spectrum of the [M - H]⁻ ion of d18:0/18:0-Cer at m/z 566 contains the m/z 534 ion (**c**₃), reflecting loss of (H₂ + HCHO), but an ion at m/z 536 arising from HCHO loss is absent. However, the m/z 536 ion is present in the spectra obtained at low collision energy, indicating that the m/z 536 ion is unstable and eliminates H₂, with the participation of an exchangeable hydrogen, to form a more

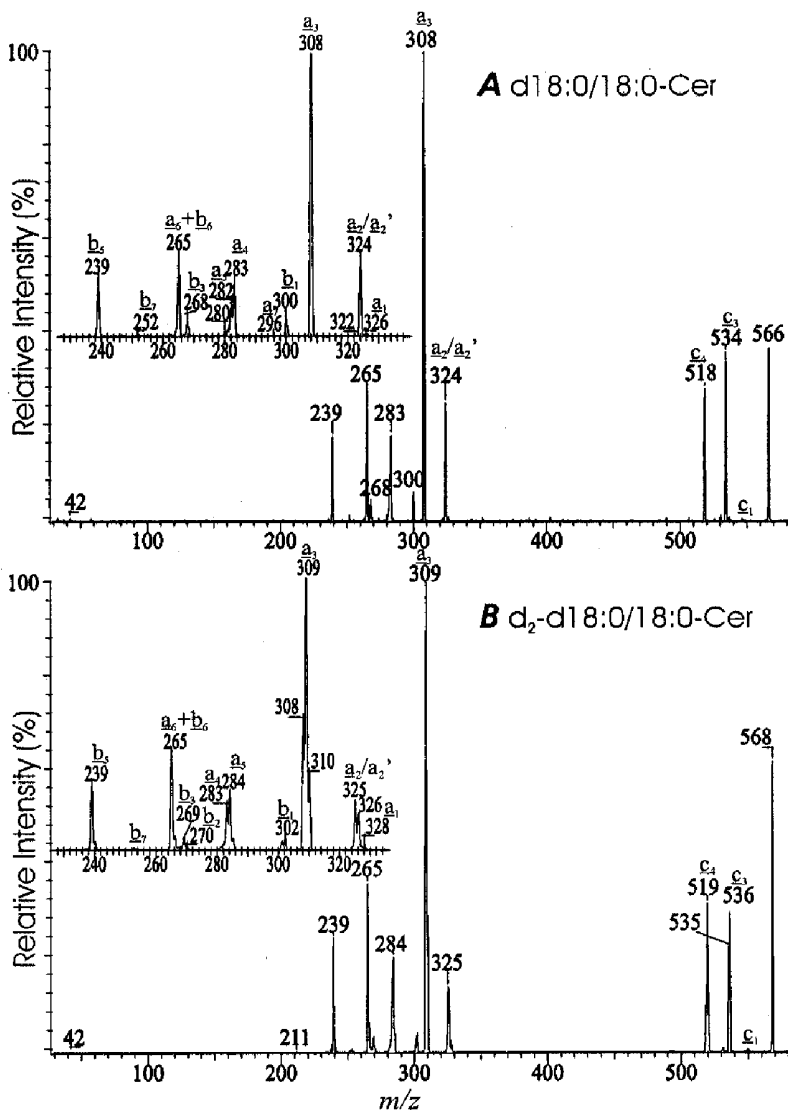


Fig. 3.34. The product-ion spectra of the $[M - H]^-$ ions of (A) d18:0/18:0-Cer at m/z 566, and of (B) d₂-d18:0/18:0-Cer at m/z 568.

stable ion of m/z 534 $([566 - (H_2 + HCHO)]^-)$. This is supported by the product-ion spectrum of d₂-d18:0/18:0-Cer (Fig. 3.34B), which contains ions at m/z 536 and 535 that reflect the loss of $(H_2 + HCHO)$ and $(HD + HCHO)$, respectively.

Sphingomyelin and Glycosphingolipids

As observed for GPCho, the $[M + Cl]^-$ or $[M + CH_3CO_2]^-$ adduct ion of SM gives rise to $[M - 15]^-$ by eliminating CH_3Cl or $CH_3CO_2CH_3$, respectively. Upon CAD, the $[M - 15]^-$ ion yields a prominent ion at m/z 168, representing a phosphoethanol-*N*-dimethylamine anion (Scheme 3.25). In contrast, the product-ion spectrum of GPCho is dominated by $R_xCO_2^-$ and the m/z 168 ion is of low abundance (Fig. 19A). Figure 3.35A illustrates that the product-ion spectrum of the $[M - 15]^-$ ion of d18:1/16:0-SM at m/z 687 is dominated by m/z 168, and the ion at m/z 449, arising from loss of 16:0-fatty acyl ketene, and ions at m/z 616 and m/z 598, reflecting loss of the ethanol-*N*-dimethylamine head group, are of low abundance.

The CAD product-ion spectrum of the $[M - H]^-$ ion of d18:1/24:0-GlcCer at m/z 810 (Fig. 3.35B), obtained with a TSQ instrument, is informative for structural characterization, and the fragment ions are similar to those observed in high-energy CAD spectra (85). The major fragmentation process involves cleavage of the sugar moiety to yield a deprotonated d18:1/24:0-Cer at m/z 648, which then undergoes consecutive dissociation steps similar to those observed for ceramide.

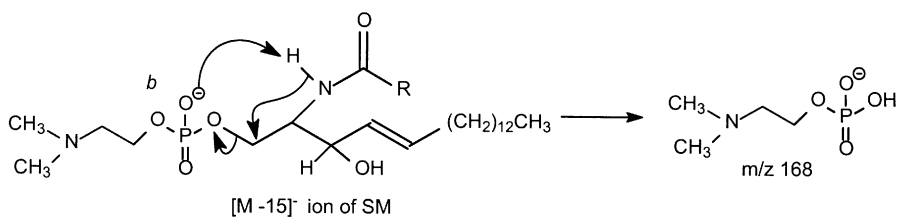
Sulfatide

The sphingolipid sulfatide (3-sulfogalactosylceramide) is a ceramide galactoside 3-sulfate, which gives superb sensitivity in negative-ion mode by ESI. FAB in combination with tandem sector and with TSQ instruments has been used for structural elucidation of sulfatides (87). ESI coupled with TSQ or ITMS instruments has recently been used to characterize sulfatides and for determination of their fragmentation patterns (43,46,88).

Common Fragmentation Processes of Sulfatides Observed by TSQ and ITMS.

The product-ion spectrum of the $[M - H]^-$ ion, as exemplified by the d18:1/24:1-sulfatide at m/z 888 (Fig. 3.36A) obtained with a TSQ instrument, is dominated by an $HOSO_3^-$ ion at m/z 97 (43,46,87,88), and ions at m/z 259, 257, and 241 that reflect the 3-sulfogalactosyl moiety are also abundant. In contrast, ions with masses smaller than 200 Da are not observed in the MS^2 -spectrum of m/z 888 obtained with an ITMS (Fig. 3.36B) because of the low-mass cutoff (14). The m/z 259 and m/z 257 ions arise from the fragmentation processes identical to those for the m/z 390 ion, *via* cleavage of the C2–C3 bond of the LCB (Scheme 3.26). Further loss of H_2O from m/z 259 gives rise to m/z 241, probably representing several isomers of an anhydro galactosylpyranose 3-sulfate (**c3**) anion. Alternatively, the m/z 241 ion could arise from loss of ceramide (Scheme 3.26C, route *a*).

In addition to the previously mentioned ions reflecting the sugar moiety of the molecule, the spectra (Fig. 3.36A and B) also contain the m/z 650 ion (**a2**) ($888 - 238$), arising from loss of the d18:1-LCB as an α,β -unsaturated aldehyde ($HCOCH=CH(CH_2)_{12}CH_3$, 238 Da) (Scheme 3.27A, route *a*), as well as the m/z 648 ion (**a3**) arising from the losses of the aldehyde and H_2 , simultaneously ($888 - (238 + 2)$) (route *b*).



Scheme 3.25. Proposed mechanism of fragmentation of the [M-15]⁻ fragment of SM in negative-ion mode.

The direct loss of the fatty acyl moiety as a ketene from [M - H]⁻ *via* cleavage of the NH-CO bond results in the ion at *m/z* 540 (**b1**), which undergoes a water loss to yield the *m/z* 522 ion (**b2** + **b2'**), *via* two separate pathways as shown in Scheme 3.27B. The frag-

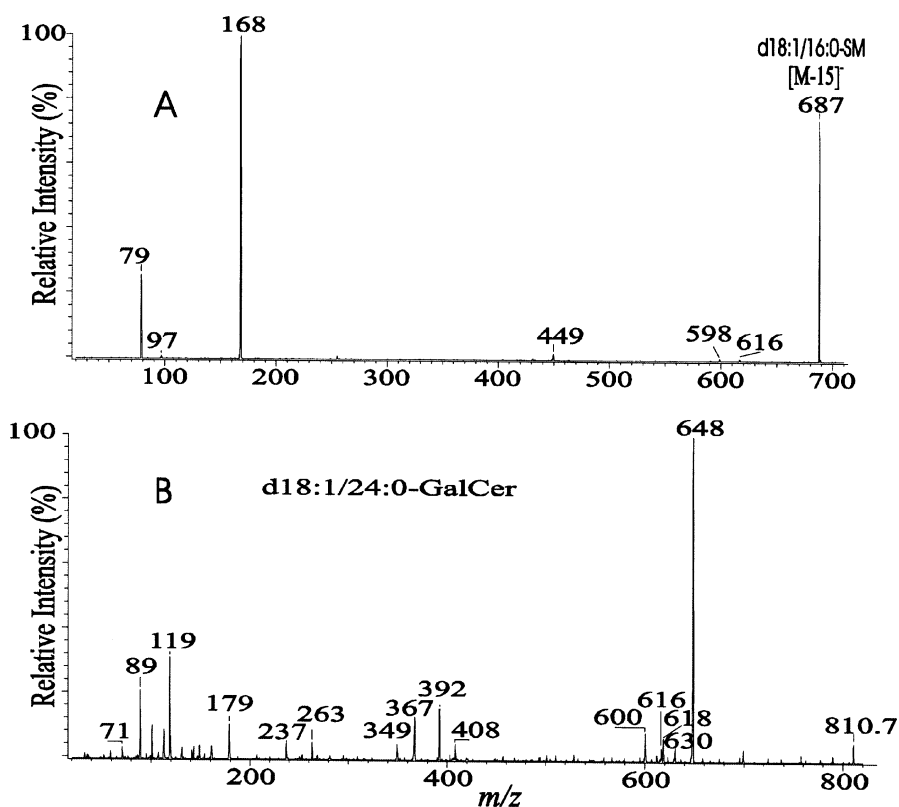


Fig. 3.35. The product-ion spectra of the [M - 15]⁻ ion of (A) d18:1/16:0-SM at *m/z* 687, and of the (B) [M - H]⁻ ion of d18:1/24:0-GalCer at *m/z* 810 (B).

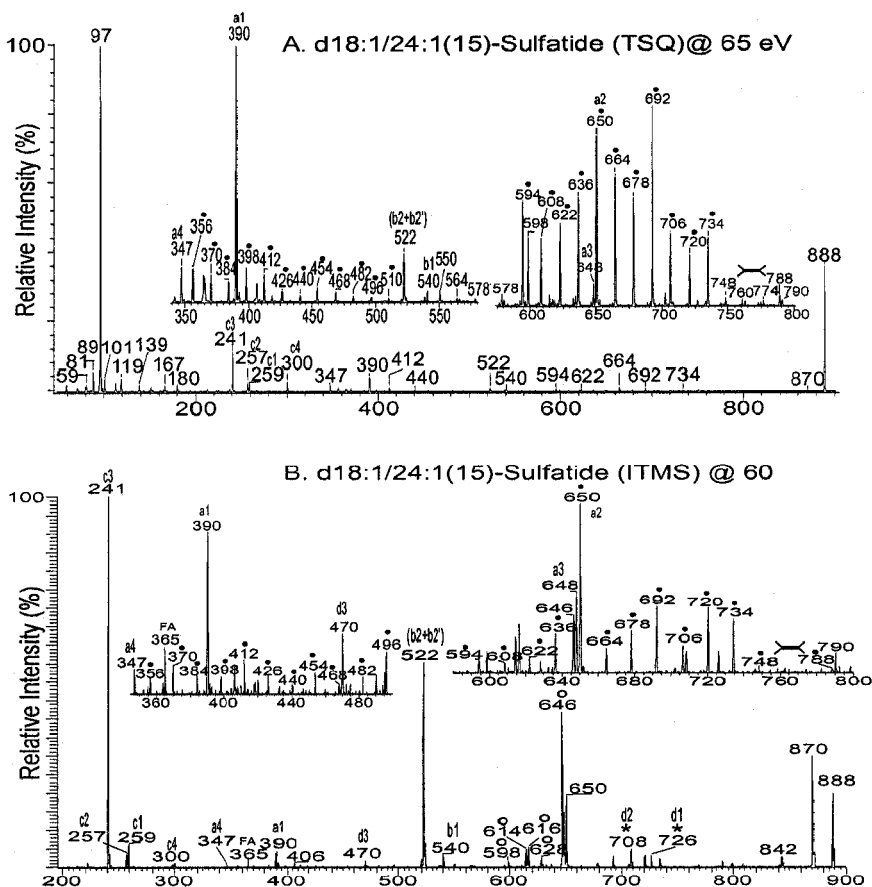


Fig. 3.36. The product-ion spectra of the $[M - H]^-$ ions of d18:1/h24:1-sulfatide at m/z 904 obtained with (A) TSQ and with (B) ITMS instruments. (C) The ITMS MS²-spectrum of the $[M - H]^-$ ion of d_5 -d18:1/24:1-sulfatide at m/z 893. (Continued) →

mentation processes are based on the findings that the product-ion spectrum of the H-D exchanged d_5 -d18:1/h24:1-sulfatide at m/z 893 (Fig. 3.36C) contains the analogous ions at m/z 527 and 526, by losses of HDO and D₂O, respectively. The m/z 540 ion also forms a 1-*O*-2'-aminoethenyl galactosyl 3-sulfate ion (m/z 300, c4), via the combined losses of the LCB as an aldehyde and H₂ [loss of 240 (H₂ + HCOCH=CH(CH₂)₁₂CH₃)] (Scheme 3.27B, route c). This fragmentation process is supported by the MS³-spectrum of m/z 540 (888 → 540) (87). The anionic charge sites of the ions herein described probably reside at the sulfate at C-3 of the galactosylpyranoside.

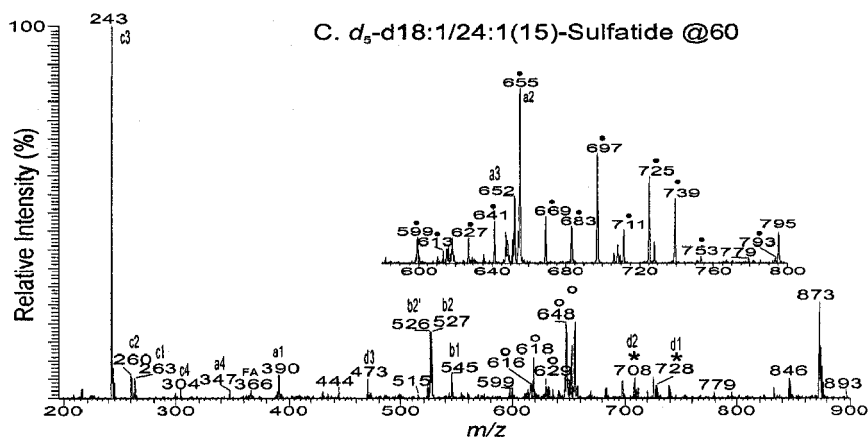
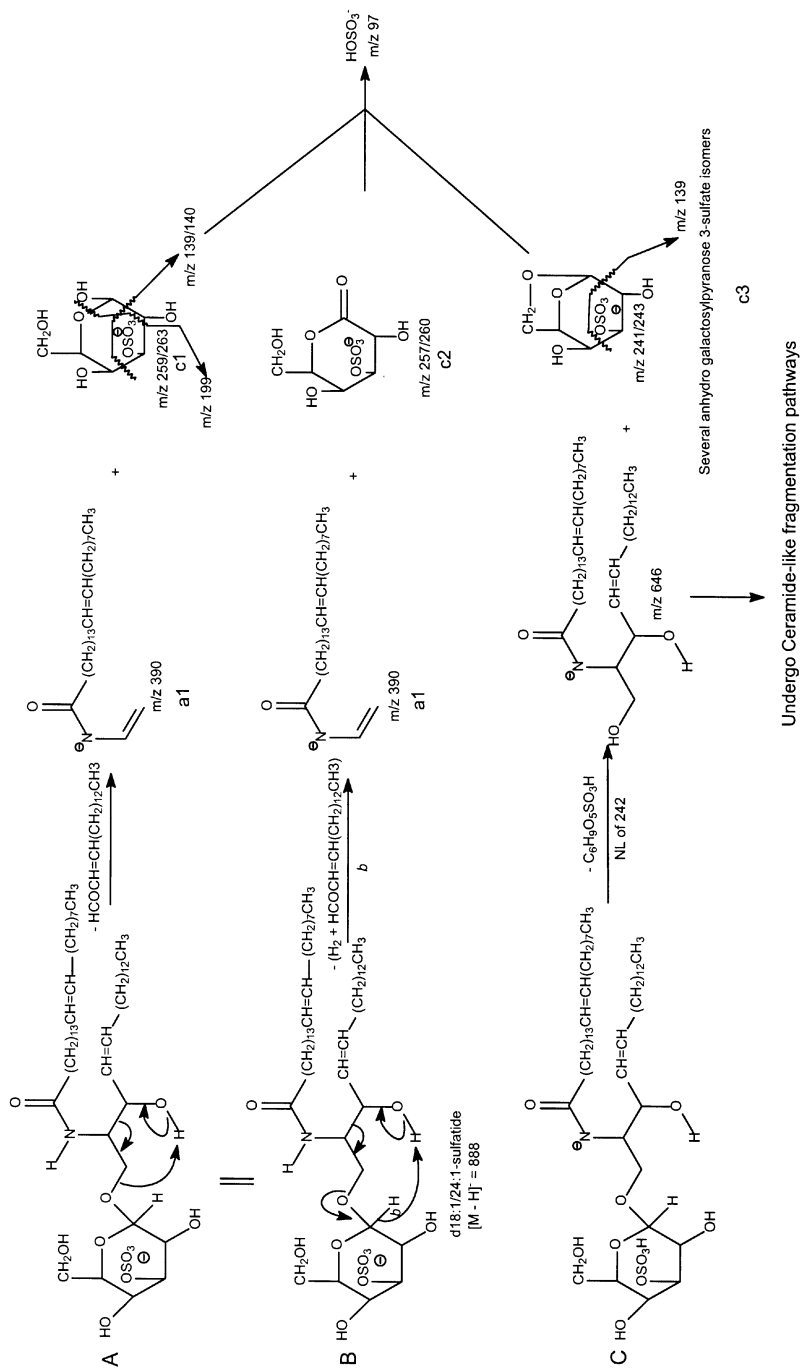


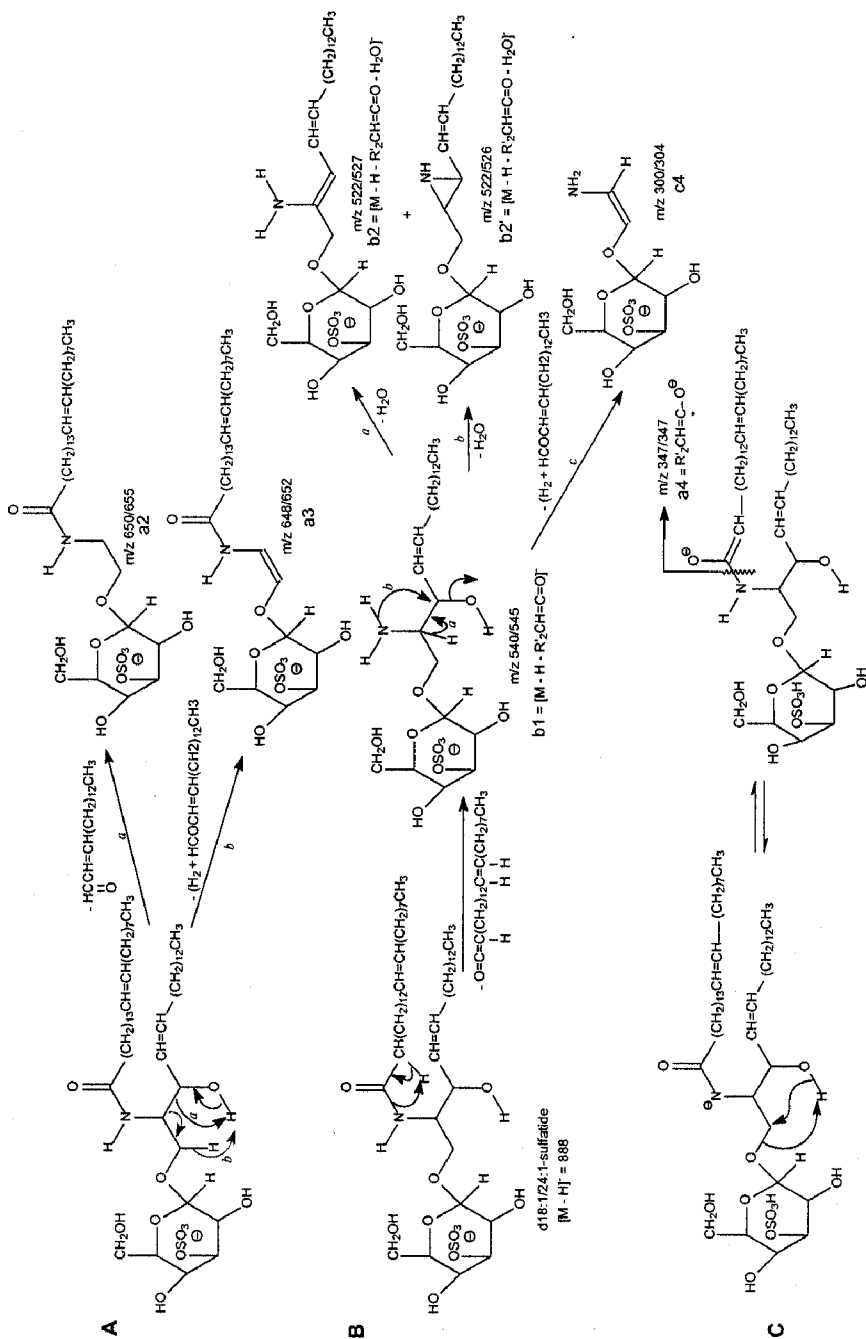
Fig. 3.36. (Continued).

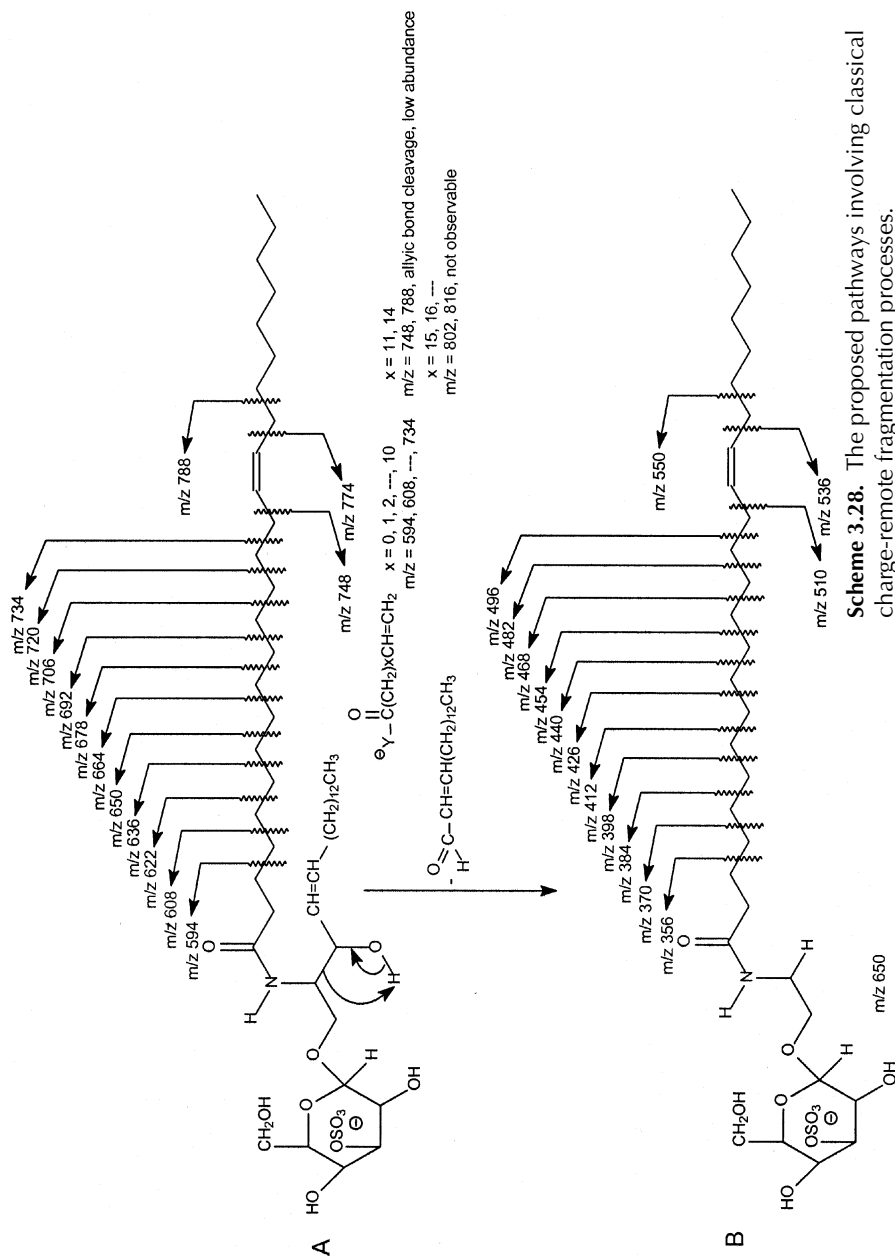
Alternatively, the charge site could reside on the nitrogen or oxygen of the amide. This proposal is based on the presence of the m/z 646 ion ($888 - 242$) that arises from expulsion of an anhydro galactosylpyranose 3-sulfate (242 Da) to yield an ion equivalent to a deprotonated d18:1/24:1-Cer, which undergoes further dissociation to yield ions at m/z 628 ($646 - \text{H}_2\text{O}$), m/z 616 ($646 - \text{HCHO}$), m/z 614 [$646 - (\text{H}_2 + \text{HCHO})$], m/z 598 [$646 - (\text{H}_2\text{O} + \text{HCHO})$], m/z 408 [$646 - 238 (\text{HCOCH}=\text{CH}[\text{CH}_2]_{12}\text{CH}_3)$], m/z 406 [$646 - 240 (238 + \text{H}_2)$], m/z 390 (**a3**) ($408 - \text{H}_2\text{O}$), m/z 365 ($\text{C}_{23}\text{H}_{45}\text{CO}_2^-$), m/z 364, 298, and 263, identical to those ions observed in the spectrum of d18:1/24:1-Cer (42). The m/z 347 ion (**a4**) may derive from homolytic cleavage of the NH-CO bond, where the anionic charge resides on the oxygen (Scheme 3.27C).

“Classical Charge-Remote Fragmentation Processes” Observed by Low-Energy CAD Tandem MS. One of the most interesting findings in the MS²-spectra of sulfatides under low-energy CAD obtained with a TSQ (Fig. 3.36A, inset) or an ITMS (Fig. 3.36B, inset) instrument is that ions resembling those reported at high energy (keV) *via* CRF (7–10) are also present. One series of ions ($-\text{YCO}(\text{CH}_2)_x\text{CH}=\text{CH}_2$, $x = 0, 1, 2, \dots$) with an increment of 14 daltons (CH_2) is observed at m/z 594, 608, 622, 636, 650, 664, ..., 734, and 748. The ions are of low abundance at m/z 748 and 788, resulting from cleavages of the inner side of the allylic C-C bond and the outer allylic C-C bond, respectively. The ion series is interrupted between these two ions and terminates at m/z 788 (Scheme 3.28A). These results suggest that the double bond on the 24:1-fatty acid substituent is located at C-15, counting from the carbonyl carbon of the fatty acid, and is in agreement with the finding reported by high-energy CAD (87). Another series of ions that exhibits similar features is observed at m/z 356, 370, 384,



Scheme 3.26. Proposed mechanisms of fragmentation of sulfatide in negative-ion mode.

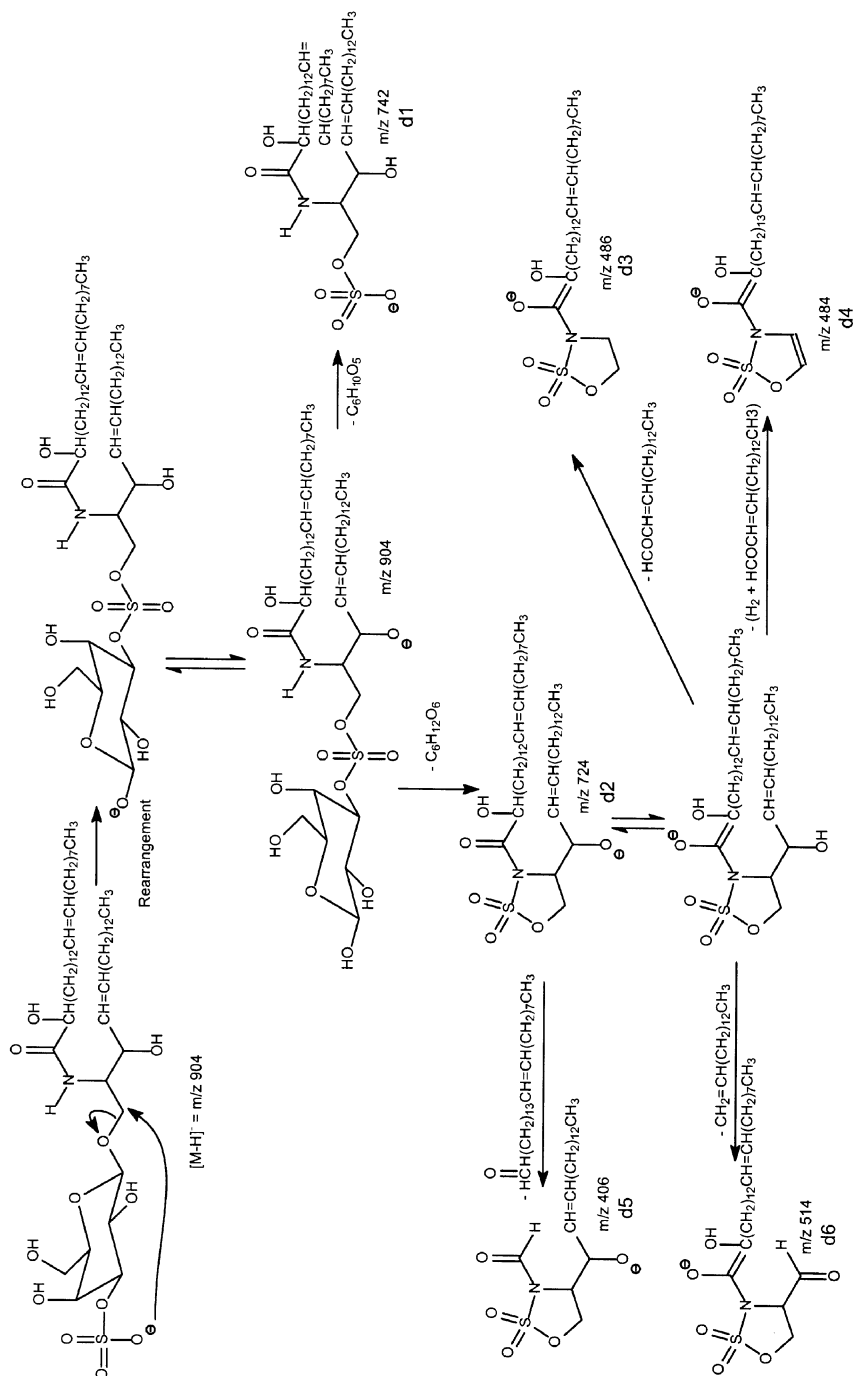




398, ..., 496, 510, and 550. The ions between m/z 510 and 550, where the double bond is located, are absent. This ion series likely arises from further dissociation of the m/z 650 ion (**a2**) via similar CRF processes (Scheme 3.28B). The proposed fragmentation pathways are also supported by the product-ion spectrum of d_5 -d18:1/24:1-sulfatide at m/z 893 (Fig. 3.36C), in which a 5-Da mass shift is observed for the analogous ions arising from CRF (Schemes 26 to 30, deuterium-labeling is denoted by D, and the observed m/z values are shown after the /).

The apparent difference between the ion series described previously and that observed in the high-energy CAD product-ion spectrum is that the latter spectrum also contains ions at m/z 788, 802, 816, etc., that are nearly equally abundant. These ions continue the series past the absent ions caused by the unsaturated bond. This is attributable to the fact that in high-energy CAD, internal energy transfer by collision can be varied to a much smaller degree, the range of average energies deposited into the ion is wide, and the energy deposition curve can extend to high energies. As a result, fragment ions deriving from fragmentation reactions requiring high critical energy can be observed, and spectra with an even distribution of fragment ions can be obtained. In contrast, the internal energy deposition during the low-energy CAD process is much narrower than in high-energy collisions, and so fragmentation processes requiring a large critical energy are not observed (89). This unique pattern of ions arising from CRF processes permits determination of the position of the double bond of the fatty acid substituent.

Unusual "Internal Galactose Residue Loss" Observed by Quadrupole Ion-Trap Tandem MS. Ions at m/z 726 and m/z 708, reflecting losses of a dehydrated galactose moiety (162 Da) and a galactose moiety (180 Da), respectively, are also present in the MS²-spectrum of m/z 888 (Fig. 3.36B). The analogous ions from the similar losses are also observed at m/z 742 and m/z 724 for d18:1/h24:1-sulfatide at m/z 904 (Fig. 3.37A), and are more prominent. However, this internal galactose loss is not observed in the product-ion spectrum of d18:1/24:1-sulfatide (Fig. 3.36A) and d18:1/h24:1-sulfatide (Fig. 3.37B) obtained with a TSQ mass spectrometer. The galactose residue loss may arise from a rearrangement process (Scheme 3.29), which involves the nucleophilic attack of the charge-site at C1 of the LCB to yield a galactose-sulfuryl-ceramide intermediate (Scheme 3.29, **d** ion), which then eliminates C₆H₁₀O₅ or C₆H₁₂O₆ to yield a 1-sulfo-ceramide (**d1**) or a five-member ring anion (**d2**), respectively. The corresponding ions with the expected mass shifts are observed at m/z 728 and m/z 708 in the MS²-spectrum of d_5 -d18:1/24:1-sulfatide at m/z 893 (Fig. 3.36C), prepared by H-D exchange. The loss of an internal hexose residue is observed for PIP as discussed earlier and has been previously reported for various compounds, mainly as the protonated species under low- and high-energy CAD (90–94). The finding that the internal galactose loss from [M – H][–] ions of sulfatides occurs in ITMS, but not in TSQ instruments, is consistent with the fact that the dissociation reaction to eliminate galactose involves a rearrangement process, which requires low activation energy. However,



Scheme 3.29. The proposed pathways involving an "internal hexose dose" via rearrangement.

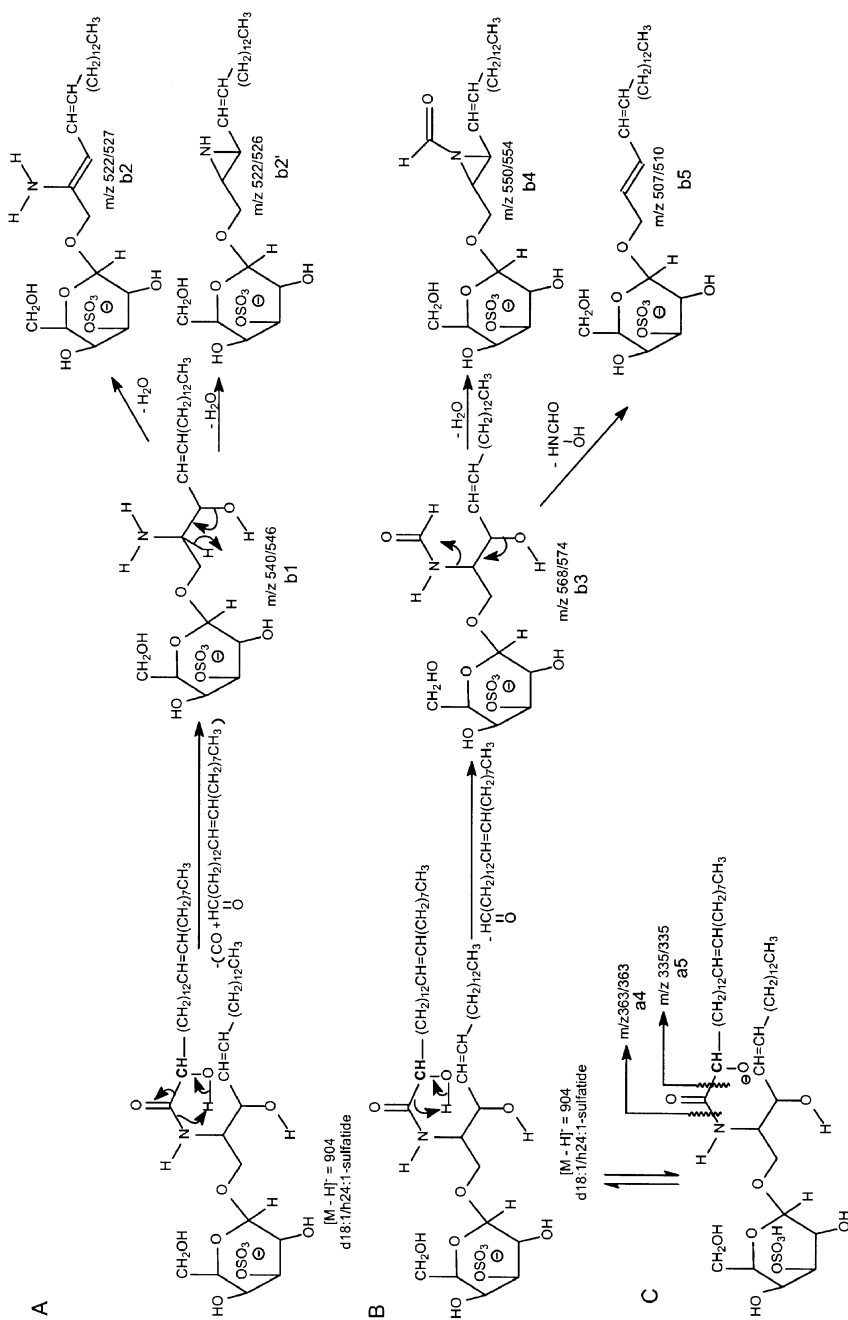
the configuration of the charged precursor ion, such that it is favorable for the rearrangement process, may also play a role in the ion formation (90–93).

Structural Characterization of the Sulfatide Subclasses with α -Hydroxy Fatty Acyl Substituents (d18:1/hFA-Sulfatides) and with Sphinganine LCB (d18:0/FA-Sulfatide). Along with the aforementioned common ions that identify the LCB, sugar, and fatty acid moieties, tandem mass spectra of sulfatides consisting of an α -hydroxy fatty acid substituent and a d18:1-LCB (d18:1/hFA-sulfatide) contain a unique set of ions. These include prominent ions at m/z 568, 540, and 522, and less abundant ions at m/z 550 and 507. These features are demonstrated by the product-ion spectrum of the d18:1/h24:1-sulfatide ion at m/z 904 obtained with an ITMS (Fig. 3.37A) and with a TSQ (Fig. 3.37B) instrument. The m/z 540 ion (**b1**) derives from cleavage of the C-C bond between the carbonyl and the α -hydroxy carbon (OC-CH(OH)) of the fatty acid to expel both a CO and the fatty acyl moiety as an aldehyde (loss of $(\text{CO} + \text{HCO}(\text{CH}_2)_{12}\text{CH}=\text{CH}(\text{CH}_2)_7\text{CH}_3)$, 364 Da).

The cleavage is consistent with the notion that the α -hydroxyl group of the fatty acyl substituent accelerates the fragmentation processes, as was described for ceramide. The m/z 540 ion also dissociates to m/z 522 (**b2** + **b2'**) by eliminating an H_2O (Scheme 3.30A). These fragmentation pathways are similar to those described earlier for the d18:1/nFA-sulfatides (Scheme 3.30B). The cleavage of the same OC-CH(OH) bond, to expel the fatty acyl moiety as an aldehyde, gives rise to the m/z 568 ion (**b3**), which yields the m/z 550 ($568 - 18$) (**b4**) ion by loss of H_2O (Scheme 3.30B). Further dissociation of the ion at m/z 568 also gives rise to m/z 507 (**b5**), which is not present in the product-ion spectrum of d18:1/nFA-sulfatide, in which the precursor ion (**b3** type) leading to such a loss is not available. The homolytic cleavage of the same bond also yields the m/z 335 ion (**a5**). The presence of this ion, together with the m/z 363 ion (**a4**), resulting from homolytic cleavage of the NH-CO bond (Scheme 3.30C), indicates that the anionic charge site resides on the α -hydroxyl group of the fatty acid substituent. These observations further support the proposal that fragmentation pathways for sulfatides under low-energy CAD involve more than one charge site. The proposed fragmentation pathways (Scheme 3.30) are supported by the MS^2 -spectrum of the m/z 908 ion that arises from d18:0/h24:0-sulfatide (Fig. 3.38a), prepared by hydrogenation of d18:1/h24:1-sulfatide. The spectrum contains the analogous ions at m/z 570 (**b3**), m/z 552 (**b4**), m/z 542 (**b1**), m/z 524 (**b2** + **b2'**), and m/z 509 (**b5**), which exhibit a mass shift of 2Da, reflecting the d18:0-LCB.

The ion series deriving from classical CRF is also observed in the ITMS MS^2 spectra of sulfatides containing an α -hydroxy fatty acid substituent (LCB/hFA-sulfatide) and provides information to identify the position of the double bond of the fatty acyl substituent.

As shown in Figure 3.37A, the MS^2 spectrum of the d18:1/h24:1-sulfatide (inset) gives the ion clusters at m/z 610, 624, 638, 652, 666, 680, 694, 708, 722, 736, 750, and 764, with the last (m/z 764) being the least abundant. This information clearly demonstrates that the double bond of the fatty acyl substituent resides



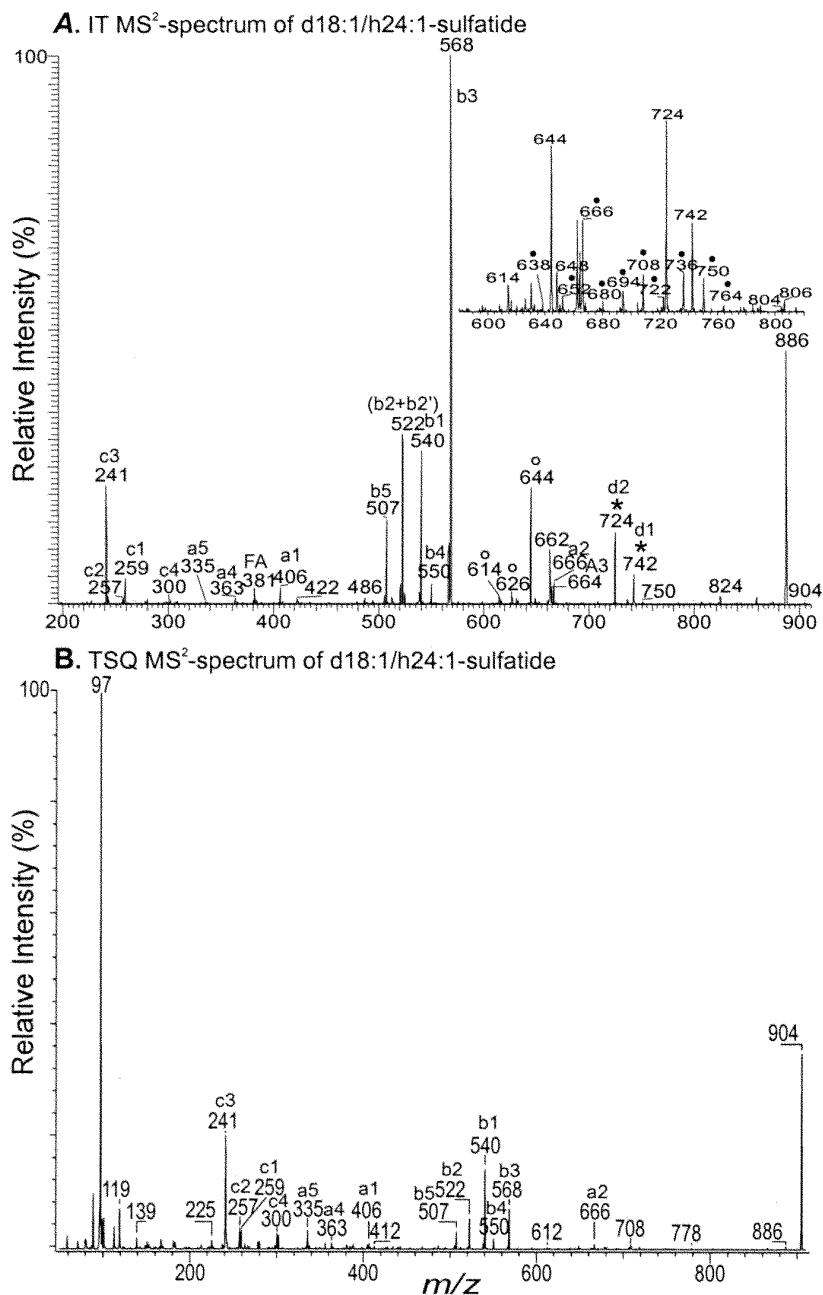


Fig. 3.37. The product-ion spectra of the $[M - H]^-$ ions of d18:1/h24:1-sulfatide at m/z 904 obtained with (A) ITMS and with (B) TSQ instruments.

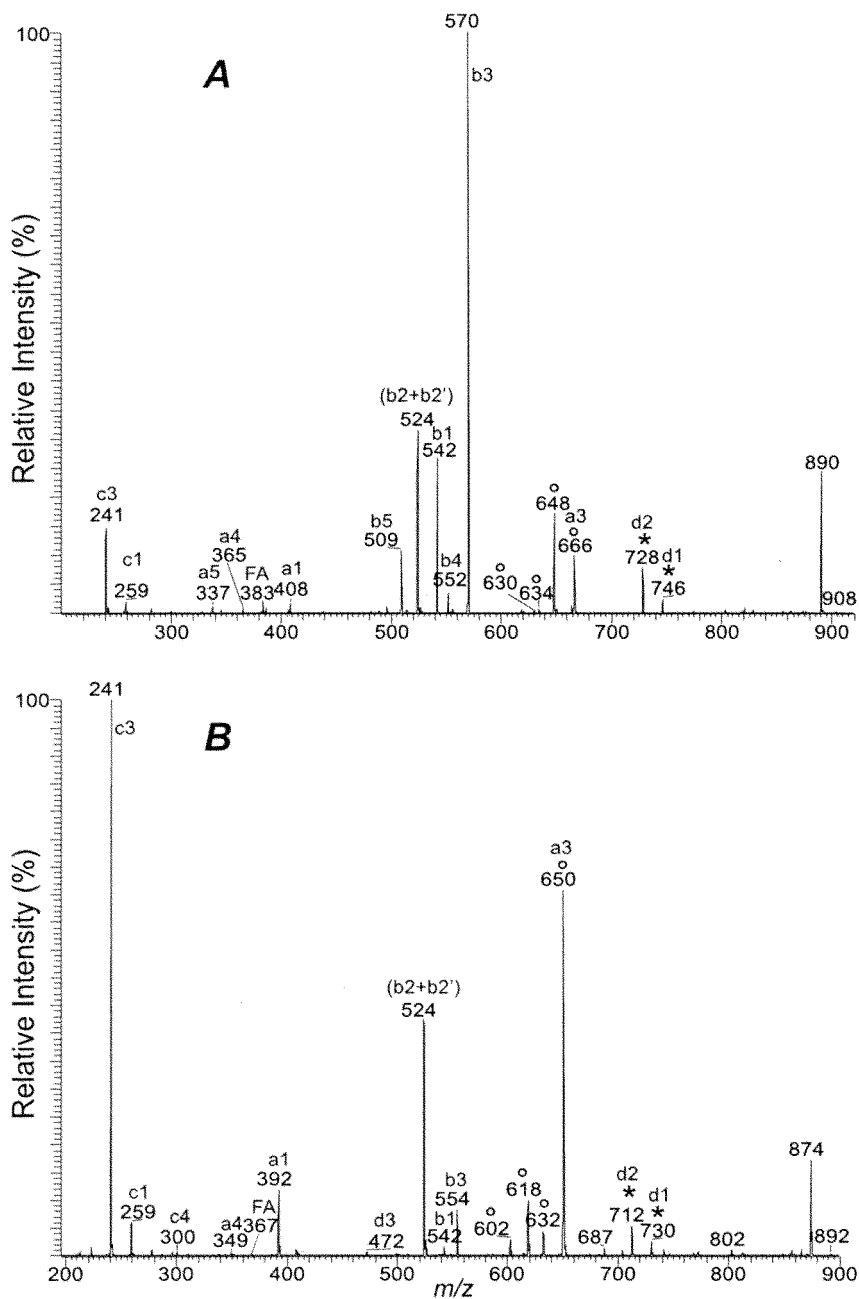


Fig. 3.38. The ITMS MS²-spectra of the [M – H][–] ions of (A) d18:0/h24:0-sulfatide at m/z 908, and of the (B) d18:0/24:0-sulfatide at m/z 892.

at C-15, although the ion series is of low abundance. In contrast, this ion series is not present in the TSQ product-ion spectrum of d18:1/h24:1-sulfatide (Fig. 3.37B). These results may indicate that the compound type (d18:1/nFA-sulfatide vs. d18:1/hFA-sulfatide), the mass of the collision target (He vs. Ar), and the target gas pressure (0.7 mtorr vs. 2.3 mtorr) used in the CAD processes (ITMS vs. TSQ MS) may be more crucial than the energy required for CRF (9). Collisional activation in a TSQ instrument is a multiple-collision process that results in consecutive fragmentation processes, while resonance excitation is the major process underlying the fragmentation in ITMS. The OC-CH(OH) bond of the fatty acyl substituent may be sufficiently labile that it is preferentially cleaved by the multiple-collision processes that occur in the TSQ, and thus CRF processes that require a stable charge site on the precursor do not readily occur (8). This is also consistent with the observation of the internal galactose loss (*via* rearrangement) in the MS² spectra obtained with an ITMS machine but not observed in the spectra acquired with a TSQ instrument.

As described previously, expulsion of an anhydro galactosylpyranose 3-sulfate (242 Da) yields a deprotonated ceramide anion that undergoes consecutive dissociation steps to produce the ion series that identifies the ceramide moiety. The ion series for d18:0/24:0-sulfatide (Fig. 3.38B) includes an ion at m/z 650, which is equivalent to a deprotonated d18:0/24:0-Cer ion, together with ions at m/z 632 ($650 - \text{H}_2\text{O}$), m/z 618 [$650 - (\text{H}_2 + \text{HCHO})$], and m/z 602 [$650 - (\text{H}_2\text{O} + \text{HCHO})$]. However, the ion at m/z 620 ($650 - \text{HCHO}$), reflecting loss of HCHO, is not present. Similar results are also observed for the d18:0/h24:0-sulfatide at m/z 908 (Fig. 3.38A). These findings indicate that the molecule contains a sphinganine rather than a sphingosine LCB, consistent with the observations from the ceramides possessing a sphinganine LCB (42). This feature in the ion series provides a simple means to distinguish a d18:0/FA-sulfatide from a d18:1/FA-sulfatide. The tandem mass spectra thus provide sufficient information to identify the sugar moiety, the fatty acyl substituent, and the LCB of the sulfatide subclass containing a sphinganine LCB (d18:0/FA-sulfatide).

Acknowledgments

The authors acknowledge the support of U.S. Public Health Service Grants P41-RR-00954, R37-DK-34388, P60-DK-20579, P30-DK56341, and P01-HL-57-278 and a grant (No.996003) from the Juvenile Diabetes Foundation. The authors also thank Dr. William Craig Byrdwell for his critical comments on the manuscript.

References

1. Jensen, N.J., K.B. Tomer, and M.L. Gross, Fast Atom Bombardment and Tandem Mass Spectrometry of Phosphatidylserine and Phosphatidylcholine, *Lipids* 21: 580–588 (1986).
2. Jensen, N.J., K.B. Tomer, and M.L. Gross, FAB MS/MS for Phosphatidylinositol, -Glycerol, -Ethanolamine and Other Complex Phospholipids, *Lipids* 22: 480–489 (1987).

3. Jensen, N.J., and M.L. Gross, A Comparison of Mass Spectrometry Methods for Structural Determination and Analysis of Phospholipids, *Mass Spectrom. Rev.* 7: 41–69 (1988).
4. Murphy, R.C., and K.A. Harrison, Fast Atom Bombardment Mass Spectrometry of Phospholipids, *Mass Spectrom. Rev.* 13: 57–75 (1994).
5. Adams, J., and M.L. Gross, Structural Determination of Modified Fatty Acids by Collisional Activation of Cationized Molecules, *Org. Mass Spectrom.* 23: 307–316 (1988).
6. Jensen, N.J., K.B. Tomer, and M.L. Gross, Gas Phase Ion Decomposition Occurring Remote to a Charge Site, *J. Am. Chem. Soc.* 107: 1863–1868 (1985).
7. Adams, J., Charge-Remote Fragmentations: Analytical Applications and Fundamental Studies, *Mass Spectrom. Rev.* 9: 141–186 (1990).
8. Gross, M.L., Charge-Remote Fragmentations: Method, Mechanism and Applications, *Int. J. Mass Spectrom. Ion Proc.* 118–119: 137–165 (1992).
9. Wysocki, V.H., and M.M. Ross, Charge-Remote Fragmentation of Gas-Phase Ions: Mechanistic and Energetic Considerations in the Dissociation of Long-Chain Functionalized Alkanes and Alkenes, *Int. J. Mass Spectrom. Ion Proc.* 104: 179–211 (1991).
10. Cheng, C., and M.L. Gross, Applications and Mechanisms of Charge-Remote Fragmentation, *Mass Spectrom. Rev.* 19: 398–420 (2000).
11. Ramanadham, S., A. Bohrer, R. Gross, and J. Turk, Mass Spectrometric Characterization of Arachidonate-Containing Plasmalogens in Human Pancreatic Islets and in Rat Islet Beta Cells and Subcellular Membranes, *Biochemistry* 32: 13499–13509 (1993).
12. Hazen, S.L., C.R. Hall, D.A. Ford, and R.W. Gross, Isolation of a Human Myocardial Cytosolic Phospholipase A2 Isoform. Fast Atom Bombardment Mass Spectroscopic and Reverse-Phase High Pressure Liquid Chromatography Identification of Choline and Ethanolamine Glycerophospholipid Substrates, *J. Clin. Invest.* 91: 2513–2522 (1993).
13. Fenn, J.B., M. Mann, C.K. Meng, S.F. Wong, and C.M. Whitehouse, Electrospray Ionization for Mass Spectrometry of Large Biomolecules, *Science* 246: 64–71 (1989).
14. Yamashita, M., and J.B. Fenn, Electrospray Ion Source. Another Variation on the Free-Jet Theme, *J. Phys. Chem.* 88: 4451–4459 (1984).
15. Pulfer, M., and R.C. Murphy, Electrospray Mass Spectrometry of Phospholipids, *Mass Spectrom. Rev.* 22: 332–364 (2003).
16. Griffiths, W.J., Tandem Mass Spectrometry in the Study of Fatty Acids, Bile Acids, and Steroids, *Mass Spectrom. Rev.* 22: 81–152 (2003).
17. Weintraub, S.T., R.N. Pinckard, and M. Hail, Electrospray Ionization for Analysis of Platelet-Activating Factor, *Rapid Commun. Mass Spectrom.* 5: 309–311 (1991).
18. Han, X., and R.W. Gross, Structural Determination of Picomole Amounts of Phospholipids via Electrospray Ionization Tandem Mass Spectrometry, *J. Am. Soc. Mass Spectrom.* 6: 1202–1210 (1995).
19. Kim, H.Y., T.C. Wang, and Y.C. Ma, Liquid Chromatography/Mass Spectrometry of Phospholipids Using Electrospray Ionization, *Anal. Chem.* 66: 3977–3982 (1994).
20. Harvey, D.J., Matrix-Assisted Laser Desorption/Ionization Mass Spectrometry of Phospholipids, *J. Mass Spectrom.* 30: 1333–1346 (1995).

21. Schiller, J., J. Arnhold, S. Benard, M. Muller, S. Reichl, and K. Arnold, Lipid Analysis by Matrix-Assisted Laser Desorption and Ionization Mass Spectrometry: A Methodological Approach, *Anal. Biochem.* 267: 46–56 (1999).
22. Ho, Y.P., and C. Fenselau, Applications of 1.06- μm IR Laser Desorption on a Fourier Transform Mass Spectrometer, *Anal. Chem.* 70: 4890–4895 (1998).
23. Ishida, Y., O. Nakanishi, S. Hirao, S. Tsuge, J. Urabe, T. Sekino, M. Nakanishi, T. Kimoto, and H. Ohtani, Direct Analysis of Lipids in Single Zooplankton Individuals by Matrix-Assisted Laser Desorption/Ionization Mass Spectrometry, *Anal. Chem.* 75: 4514–4518 (2003).
24. Karas, M., and F. Hillenkamp, Laser Desorption Ionization of Proteins with Molecular Masses Exceeding 10,000 Daltons, *Anal. Chem.* 60: 2299–2301 (1988).
25. Karas, M., D. Bachmann, U. Bahr, and F. Hillenkamp, Matrix Assisted Ultraviolet Laser Desorption of Non-Volatile Compounds, *Int. J. Mass Spectrom. Ion Proc.* 78: 53–68 (1987).
26. Medzihradszky, K.F., J.M. Campbell, M.A. Baldwin, A.M. Falick, P. Juhasz, M.L. Vestal, A.L. Burlingame, The Characteristics of Peptide Collision-Induced Dissociation Using a High-Performance MALDI-TOF/TOF Tandem Mass Spectrometer, *Anal. Chem.* 72: 552–558 (2000).
27. Morris, H.R., T. Paxton, A. Dell, J. Langhorne, M. Berg, R.S. Bordoli, J. Hoyes, R.H. Bateman, High Sensitivity Collisionally-Activated Decomposition Tandem Mass Spectrometry on a Novel Quadrupole/Orthogonal-Acceleration Time-of-Flight Mass Spectrometer, *Rapid Commun. Mass Spectrom.* 10: 889–896 (1996).
28. Hunnam, V., D.J. Harvey, D.A. Priestman, R.H. Bateman, R.S. Bordoli, and R. Tyldesley, Ionization and Fragmentation of Neutral and Acidic Glycosphingolipids with a Q-TOF Mass Spectrometer Fitted with a MALDI Ion Source, *J. Am. Soc. Mass Spectrom.* 12: 1220–1225 (2001).
29. Marto, J.A., F.M. White, S. Seldomridge, and A.G. Marshall, Structural Characterization of Phospholipids by Matrix-Assisted Laser Desorption/Ionization Fourier Transform Ion Cyclotron Resonance Mass Spectrometry, *Anal. Chem.* 67: 3979–3984 (1995).
30. Larsen, A., S. Uran, P.B. Jacobsen, and T. Skotland, Collision Induced Dissociation of Glycero Phospholipids Using Electrospray Ion-Trap Mass Spectrometry, *Rapid Commun. Mass Spectrom.* 15: 2393–2398 (2001).
31. Ho, Y.P., and P.C. Huang, A Novel Structural Analysis of Glycerophosphocholines as TFA/ K^+ Adducts by Electrospray Ionization Ion Trap Tandem Mass Spectrometry, *Rapid Commun. Mass Spectrom.* 16: 1582–1589 (2002).
32. Beckedorf, A.I., C. Schaffer, P. Messner, and J. Peter-Katalinic, Mapping and Sequencing of Cardiolipins from *Geobacillus stearothermophilus* NRS 2004/3a by Positive and Negative Ion NanoESI-QTOF-MS and MS/MS, *J. Mass Spectrom.* 37: 1086–1094 (2002).
33. Fridriksson, E.K., P.A. Shipkova, E.D. Sheets, D. Holowka, B. Baird, and F.W. McLafferty, Quantitative Analysis of Phospholipids in Functionally Important Membrane Domains from RBL-2H3 Mast Cells Using Tandem High-Resolution Mass Spectrometry, *Biochemistry* 38: 8056–8063 (1999).

34. Jennings, K.R., Collision-Induced Decomposition of Aromatic Molecular Ions, *Int. J. Mass Spectrom. Ion Phys.* 1: 227–235 (1968).
35. McLafferty, F.W., *Tandem Mass Spectrometry*, John Wiley & Sons, New York, 1983.
36. Gross, M.L., Mass Spectrometry Research: An Interplay Between Ion Chemistry, Instrumental Development, and Applications, *Mass Spectrom. Rev.* 8: 165–167 (1989).
37. Yost, R.A., and C.G. Enke, Selected Ion Fragmentation with a Tandem Quadrupole Mass Spectrometer, *J. Am. Chem. Soc.* 100: 2274–2275 (1978).
38. Louris, J.N., R.G. Cooks, J.E.P. Syka, P.E. Kelley, G.C. Stafford, Jr., and J.F.J. Todd, Instrumentation, Applications and Energy Deposition in Quadrupole Ion-Trap Tandem Mass Spectrometry, *Anal. Chem.* 59: 1677–1685 (1987).
39. Kerwin, J.L., A.R. Tuininga, and L.H. Ericsson, Identification of Molecular Species of Glycerophospholipids and Sphingomyelin Using Electrospray Mass Spectrometry, *J. Lipid Res.* 35: 1102–1114 (1994).
40. Harrison, K.A., and R.C. Murphy, Negative Electrospray Ionization of Glycerophosphocholine Lipids. Formation of $[M-15]^-$ Ions Occur via a Collision Decomposition of Adduct Anions, *J. Mass Spectrom.* 30: 1772–1773 (1995).
41. Hsu, F.F., A. Bohrer, and J. Turk, Formation of Lithiated Adducts of Glycerophosphocholine Lipids Facilitates Their Identification by Electrospray Ionization Tandem Mass Spectrometry, *J. Am. Soc. Mass Spectrom.* 9: 516–526 (1998).
42. Hsu, F.F., and J. Turk, Characterization of Ceramides by Low Energy Collisional-Activated Dissociation Tandem Mass Spectrometry with Negative-Ion Electrospray Ionization, *J. Am. Soc. Mass Spectrom.* 13: 558–570 (2002).
43. Hsu, F.F., and J. Turk, Tandem Quadrupole Mass Spectrometry of Sphingomyelin and Sulfatides, in *The Encyclopedia of Mass Spectrometry: Applications in Biochemistry, Biology, and Medicine, Part A*, edited by R. Caprioli and M.L. Gross, Elsevier Science, New York, in press.
44. Zhu, J., and R.B. Cole, Formation and Decomposition of Chloride Adduct Ions, *J. Am. Soc. Mass Spectrom.* 11: 932–941 (2000).
45. Ho, Y.P., P.C. Huang, and K.H. Deng, Metal Ion Complexes in the Structural Analysis of Phospholipids by Electrospray Ionization Tandem Mass Spectrometry, *Rapid Commun. Mass Spectrom.* 17: 114–121 (2003).
46. Hsu, F.F., A. Bohrer, and J. Turk, Electrospray Ionization Tandem Mass Spectrometric Analysis of Sulfatide. Determination of Fragmentation Patterns and Characterization of Molecular Species Expressed in Brain and Pancreatic Islets, *Biochim. Biophys. Acta* 1392: 202–216 (1998).
47. Hsu, F.F., and J. Turk, Characterization of Phosphatidylinositol, Phosphatidylinositol-4-Phosphate and Phosphatidylinositol-4,5-Bisphosphate by Electrospray Ionization Tandem Mass Spectrometry: A Mechanistic Study, *J. Am. Soc. Mass Spectrom.* 11: 986–999 (2000).
48. Hsu, F.F., and J. Turk, Electrospray Ionization/Tandem Quadrupole Mass Spectrometric Studies on Phosphatidylcholines: The Fragmentation Processes, *J. Am. Soc. Mass Spectrom.* 14: 352–363 (2003).
49. Hsu, F.F., and J. Turk, Characterization of Phosphatidylethanolamine as a Lithiated

- Adduct by Triple Quadrupole Tandem Mass Spectrometry with Electrospray Ionization, *J. Mass Spectrom.* 35: 595–606 (2000).
50. Gu, M., J.L. Kerwin, J.D. Watts, and R. Aebersold, Ceramide Profiling of Complex Lipid Mixtures by Electrospray Ionization Mass Spectrometry, *Anal. Biochem.* 244: 347–356 (1997).
 51. Karlsson, A.A., P. Michelsen, and G. Odham, Molecular Species of Sphingomyelin: Determination by High-Performance Liquid Chromatography/Mass Spectrometry with Electrospray and High-Performance Liquid Chromatography/Tandem Mass Spectrometry with Atmospheric Pressure Chemical Ionization, *J. Mass Spectrom.* 33: 1192–1198 (1998).
 52. Brugger, B., G. Erben, R. Sandhoff, F.T. Wieland, and W.D. Lehmann, Quantitative Analysis of Biological Membrane Lipids at the Low Picomole Level by Nano-Electrospray Ionization Tandem Mass Spectrometry, *Proc. Natl. Acad. Sci. USA* 94: 2339–2344 (1997).
 53. Hsu, F.F., and J. Turk, Structural Characterization of Triacylglycerols as Lithiated Adducts by Electrospray Ionization Mass Spectrometry Using Low-Energy Collisionally Activated Dissociation on a Triple Stage Quadrupole Instrument, *J. Am. Soc. Mass Spectrom.* 10: 587–599 (1999).
 54. Hsu, F.F., and J. Turk, Structural Determination of Sphingomyelin by Tandem Mass Spectrometry with Electrospray Ionization, *J. Am. Soc. Mass Spectrom.* 11: 437–449 (2000).
 55. Levery, S.B., M.S. Toledo, R.L. Doong, A.H. Straus, and H.K. Takahashi, Comparative Analysis of Ceramide Structural Modification Found in Fungal Cerebrosides by Electrospray Tandem Mass Spectrometry with Low Energy Collision-Induced Dissociation of Li⁺ Adduct Ions, *Rapid Commun. Mass Spectrom.* 14: 551–563 (2000).
 56. Hsu, F.F., and J. Turk, Structural Determination of Glycosphingolipids as Lithiated Adducts by Electrospray Ionization Mass Spectrometry Using Low Energy Collisional-Activated Dissociation on a Triple Stage Quadrupole Instrument, *J. Am. Soc. Mass Spectrom.* 12: 61–79 (2001).
 57. Olling, A., M.E. Breimer, E. Peltomaa, B.E. Samuelsson, and S. Ghardashkhani, Electrospray Ionization and Collision-Induced Dissociation Time-of-Flight Mass Spectrometry of Neutral Glycosphingolipids, *Rapid Commun. Mass Spectrom.* 12: 637–645 (1998).
 58. Hsu, F.F., J. Turk, M.E. Stewart, and D.T. Downing, Structural Studies on Ceramides as Lithiated Adducts by Low Energy Collisional-Activated Dissociation Tandem Mass Spectrometry with Electrospray Ionization, *J. Am. Soc. Mass Spectrom.* 13: 680–695 (2002).
 59. Hsu, F.F., J. Turk, A.K. Thukkani, M.C. Messner, K.R. Wildsmith, and D.A. Ford, Characterization of Alkylacyl, Alk-1-enylacyl and Lyso Subclasses of Glycerophosphocholine by Tandem Quadrupole Mass Spectrometry with Electrospray Ionization, *J. Mass Spectrom.* 38: 752–763 (2003).
 60. Hsu, F.F., and J. Turk, Distinction Among Isomeric Unsaturated Fatty Acids as Lithiated Adducts by Electrospray Ionization Mass Spectrometry Using Low Energy Collisionally

- Activated Dissociation on a Triple Stage Quadrupole Instrument, *J. Am. Soc. Mass Spectrom.* 10: 600–612 (1999).
61. Han, X., and R.W. Gross, Structural Determination of Lysophospholipid Regioisomers by Electrospray Ionization Tandem Mass Spectrometry, *J. Am. Chem. Soc.* 118: 451–458 (1996).
 62. Kayganich, K.A., and R.C. Murphy, Fast Atom Bombardment Tandem Mass Spectrometric Identification of Diacyl, Alkylacyl, and Alk-1-enylacyl Molecular Species of Glycerophosphoethanolamine in Human Polymorphonuclear Leukocytes, *Anal. Chem.* 64: 2965–2971 (1992).
 63. Ramanadham, S., F.F. Hsu, A. Bohrer, W. Nowatzke, Z. Ma, and J. Turk, Electrospray Ionization Mass Spectrometric Analyses of Phospholipids from Rat and Human Pancreatic Islets and Subcellular Membranes: Comparison to Other Tissues and Implications for Membrane Fusion in Insulin Exocytosis, *Biochemistry* 37: 4553–4567 (1998).
 64. Duffin, K.L., J.D. Henion, and J.J. Shieh, Electrospray and Tandem Mass Spectrometric Characterization of Acylglycerol Mixtures that are Dissolved in Nonpolar Solvents, *Anal. Chem.* 63: 1781–1788 (1991).
 65. Cheng, C., M.L. Gross, and E. Pittenauer, Complete Structural Elucidation of Triacylglycerols by Tandem Sector Mass Spectrometry, *Anal. Chem.* 70: 4417–4426 (1998).
 66. Ann, Q., and J. Adams, Structural Determination of Ceramides and Neutral Glycosphingolipids by Collisional Activation of $[M + Li]^+$ Ions, *J. Am. Soc. Mass Spectrom.* 3: 260–263 (1992).
 67. Ann, Q., and J. Adams, Structural-Specific Collision-Induced Fragmentations of Ceramides Cationized with Alkaline-Metal Ions, *Anal. Chem.* 65: 7–13 (1993).
 68. Rubino, F.A., L. Zecca, and S. Sonnino, Characterization of a Complex Mixture of Ceramides by Fast Atom Bombardment and Precursor and Fragment Analysis Tandem Mass Spectrometry, *Biol. Mass Spectrom.* 23: 82–90 (1994).
 69. Steward, M.E., and D.T. Downing, A New 6-Hydroxy-4-Sphingenine-Containing Ceramide in Human Skin, *J. Lipid Res.* 40: 1434–1439 (1999).
 70. Costello, C.E., and J.E. Vath, Tandem Mass Spectrometry of Glycolipids, *Methods Enzymol.* 193: 738–768 (1990).
 71. Huang, Z.H., D.A. Gage, and C.C. Sweeley, Characterization of Diacylglycerophosphocholine Molecular Species by FAB-CAD-MS/MS: A General Method Not Sensitive to the Nature of the Fatty Acyl Groups, *J. Am. Soc. Mass Spectrom.* 3: 71–78 (1992).
 72. Hsu, F.F., and J. Turk, Charge-Driven Fragmentation Processes in Diacyl Glycerophosphatidic Acids upon Low-Energy Collisional Activation. A Mechanistic Proposal, *J. Am. Soc. Mass Spectrom.* 11: 797–803 (2000).
 73. Hitchcock, P.B., R. Mason, K.M. Thomas, and G.G. Shipley, Structural Chemistry of 1,2-Dilauroyl-DL-Phosphatidylethanolamine: Molecular Conformation and Intermolecular Packing of Phospholipids, *Proc. Natl. Acad. Sci. USA* 71: 3036–3040 (1974).
 74. Hsu, F.F., and J. Turk, Charge-Driven and Charge-Remote Fragmentation Processes in Diacyl Glycerophosphoethanolamine upon Low-Energy Collisional Activation. A Mechanistic Proposal, *J. Am. Soc. Mass Spectrom.* 11: 892–899 (2000).

75. Christie, W.W., Isolation, Separation, Identification, and Structural Analysis of Lipids, in *Lipid Analysis*, 2nd ed., Pergamon Press, New York, 1982, pp.1–16.
76. Hsu, F.F., and J. Turk, Studies on Phosphatidylglycerol with Triple Quadrupole Tandem Mass Spectrometry with Electrospray Ionization: Fragmentation Processes and Structural Characterization, *J. Am. Soc. Mass Spectrom.* 12: 1036–1043 (2001).
77. Holmback, J., A.A. Karlsson, and K.C. Arnoldsson, Characterization of N-Acylphosphatidylethanolamine and Acylphosphatidylglycerol in Oats, *Lipids* 36: 153–165 (2001).
78. Niepel, T., H. Meyer, V. Wray, and W.R. Abraham, Intraspecific Variation of Unusual Phospholipids from *Corynebacterium Spp.* Containing a Novel Fatty Acid, *J. Bacteriol.* 180: 4650–4657 (1998).
79. Costello, C.E., D.H. Beach, and B.N. Singh, Acidic Glycerol Lipids of *Trichomonas vaginalis* and *Tritrichomonas foetus*, *Biol. Chem.* 382: 275–281 (2001).
80. Hsu, F.F., J. Turk, Y. Shi, and E.A. Groisman, Characterization of Acylphosphatidylglycerols from *Salmonella typhimurium* by Tandem Mass Spectrometry with Electrospray Ionization, *J. Am. Soc. Mass Spectrom.* 15: 1–11 (2004).
81. Hsu, F.F., J. Turk, and M.L. Gross, Structural Distinction Among Inositol Phosphate Isomers Using High-Energy and Low-Energy Collisional-Activated Dissociation Tandem Mass Spectrometry with Electrospray Ionization, *J. Mass Spectrom.* 38: 447–457 (2003).
82. Kerwin, J.L., A.M. Wiens, and L.H. Ericsson, Identification of Fatty Acids by Electrospray Mass Spectrometry and Tandem Mass Spectrometry, *J. Mass Spectrom.* 31: 184–192 (1996).
83. Raith, K., and R.H.H. Neubert, Structural Studies on Ceramides by Electrospray Tandem Mass Spectrometry, *Rapid Commun. Mass Spectrom.* 12: 935–938 (1998).
84. Vietzke, J.P., O. Brandt, D. Abeck, C. Rapp, M. Strassner, V. Schreiner, and U. Hintze, Comparative Investigation of Human Stratum Corneum Ceramides, *Lipids* 36: 299–304 (2001).
85. Han, X., Characterization and Direct Quantitation of Ceramide Molecular Species from Lipid Extracts of Biological Samples by Electrospray Ionization Tandem Mass Spectrometry, *Anal. Biochem.* 302: 199–212 (2002).
86. Ann, Q., and J. Adams, Collision-Induced Decomposition of Sphingomyelins for Structural Elucidation, *Biol. Mass Spectrom.* 22: 285–294 (1993).
87. Ohashi, Y., and Y. Nagai, Fast-Atom-Bombardment Chemistry of Sulfatide (3-Sulfogalactosylceramide), *Carbohydr. Res.* 221: 235–243 (1991).
88. Hsu, F.F., and J. Turk, Studies on Sulfatides by Quadrupole Ion-Trap Mass Spectrometry with Electrospray Ionization: Structural Characterization and the Fragmentation Processes that Include an Unusual Internal Galactose Residue Loss and the Classical Charge-Remote Fragmentations, *J. Am. Soc. Mass Spectrom.* 15: 536–546 (2004).
89. Vekey, K., Internal Energy Effects in Mass Spectrometry, *J. Mass Spectrom.* 31: 445–463 (1996).
90. Brull, L.P., W. Heerma, J. Thomas-Oates, J. Haverkamp, V. Kovacik, and P. Kovac, Loss of Internal 1 → 6 Substituted Monosaccharide Residues from Underivatized and per-O-Methylated Trisaccharides, *J. Am. Soc. Mass Spectrom.* 8: 43–49 (1997).

91. Warrack, B.M., M.E. Hail, A. Triolo, F. Animati, R. Seraglia, and P. Traldi, Observation of Internal Monosaccharide Losses in the Collisionally Activated Dissociation Mass Spectra of Anthracycline Aminodisaccharides, *J. Am. Soc. Mass Spectrom.* *9*: 710–715 (1998).
92. Ma, Y.L., I. Vedernikova, H. Van den Heuvel, and M. Claeys, Internal Glucose Residue Loss in Protonated *O*-Diglycosyl Flavonoids Upon Low-Energy Collision-Induced Dissociation, *J. Am. Soc. Mass Spectrom.* *11*: 136–144 (2000).
93. Harvey, D.J., T.S. Mattu, M.R. Wormald, L. Royle, R.A. Dwek, and P.M. Rudd, “Internal Residue Loss” Rearrangements Occuring During the Fragmentation of Carbohydrates Derivatized at the Reducing Terminus, *Anal. Chem.* *74*: 734–740 (2002).
94. Tadano-Aritomi, K., T. Hikita, M. Kubota, T. Kasama, K. Toma, S. Hakomori, and I. Ishizuka, Internal Residue Loss Produced by Rearrangement of a Novel Cationic Glycosphingolipid, Glyceroplasmalopsychosine, in Collision-Induced Dissociation, *J. Mass Spectrom.* *38*: 715–722 (2003).W

Chapter 4

Liquid Chromatography/Electrospray Ionization Mass Spectrometry for Analysis of Oxidized Lipids

Arnīs Kuksis

Banting and Best Department of Medical Research, University of Toronto, Toronto,
ON M5G 1L6, Canada

Introduction

The analysis of oxidized lipids has become increasingly popular in recent years due to the widespread recognition of the importance of lipid autoxidation in the food industry, biology, and medicine. With few exceptions, autoxidation affects all lipid classes, although some lipids are more susceptible to it than others. Tissue lipid oxidation products have been difficult to identify until recently, when ultrasensitive detectors and improved chromatographic techniques have become available.

The significance of oxidation arises from the specific physicochemical, chemical, and biological activities of the oxidized lipids, which are peculiar to each lipid class. In addition to the long established adverse metabolic effects of oxocholesterol, recent work has identified adverse metabolic effects of the hydroperoxides, isoprostanes, aldehydes, and ozonides of the glycerolipids. Less specifically, analyses of oxolipids have provided an indication of a degenerating environment, food spoilage, aging, and disease. Various analytical techniques have been employed in the isolation and identification of the oxolipids and in describing their functionality. High-performance liquid chromatography (HPLC) in combination with electrospray ionization-(ESI) mass spectrometry (ESI-MS) has been especially well suited for this purpose and forms the subject matter of this chapter.

Following a brief consideration of the specialized methodology required for reliable oxolipid analyses, including extraction, derivatization, and LC/ESI-MS analysis, the chapter follows an orderly discussion of the analysis of hydroperoxides, epoxides and hydroxides, and isoprostanes and neuroprostanes, followed by core aldehydes and ozonides, generated from the major neutral and polar lipid classes. The chapter concludes with a call for maximum control of autoxidation and chemical oxidation during isolation, derivatization, and analysis of oxolipids to guard against artifact formation.

Specialized Methodology

Since oxolipids are formed by mere exposure to air, a critical methodological issue is the use of techniques that prevent any significant artifact formation by oxidation during sample preparation, purification by chromatography, as well as

sample analysis. Early workers attributed the loss of polyunsaturated fatty acids (FA) on thin-layer chromatography (TLC) to iodination during staining with iodine vapor (1), whereas later workers recognized the general oxidative hazards of TLC itself. Lipid peroxidation on chromatographic columns, however, has been recognized only recently (2,3) and has led to the elimination of the chromatographic step in tandem mass spectrometric (MS/MS) analyses (4). Conventional techniques are barely useful for the analysis of oxidation products formed from complex biological lipid sources, and new, more appropriate methods are being constantly sought (5–7).

Extraction and Purification

To minimize autoxidation of unsaturated lipids during isolation, it is necessary to exclude air from the extraction solvents and transition metals from chromatographic adsorbents. This may be accomplished by conducting the extraction with inert solvents (e.g., $\text{CHCl}_3/\text{MeOH}$, but not Et_2O , which readily forms hydroperoxides) under an inert gas (e.g., oxygen-free N_2 , Ar) in the presence of appropriate antioxidants (e.g., butylated hydroxytoluene, BHT). The adsorbents for TLC and column cartridges must be washed with chelating agents to remove such divalent ions as Cu^{2+} and Fe^{2+} . It is also good practice to complete the extraction as quickly as possible and, if necessary, to store the extracts at as low a temperature as possible (e.g., -80°C). Iodine must be avoided as a staining agent because it acts as an oxidant and adds to the double bonds of the resolved compounds. It is recommended to rinse all aqueous solvents with Chelex-100 before use (2,4). Furthermore, all columns and filters are to be prerinsed with diethylenetriamine-pentaacetic acid (DTPA)-containing solvents (at neutral pH). The washing may be done *in situ*, at the normal flow rate of the column. As an example (2), lipids are initially extracted three times by the method of Bligh and Dyer (8) from tissue homogenates [generated using a ratio of 1 g tissue:10 mL 50 mM sodium phosphate (pH 7.0)] and supplemented with 2 mM DTPA or 100 μM BHT under an Ar atmosphere. The combined extracts are rapidly dried under N_2 , resuspended in $\text{MeOH}/\text{H}_2\text{O}$ (98:2, vol/vol), and diluted with a known amount of dimyristoyl GroPCho internal standard, which also prevents losses on adsorptive surfaces and vessel walls. The neutral lipids in the lipid extracts were removed by passage through a C_{18} minicolumn (Supelcoclean LC-18 SPE tubes, 3 mL). The recovered polar phospholipids were dried under nitrogen and stored in the dark under an Ar atmosphere at -80°C until analysis within 24 h. In independent studies the overall recoveries of each synthetic lipid (when analyzed at the trace levels observed in biological samples with palmitoyloleoyl GroPCho carrier) was confirmed to be in excess of 80% under the conditions described. The phospholipid hydroxyalkenals are unlikely to persist during preparation of hydroperoxides and core aldehydes by chemical oxidation in the presence of strong hydroperoxides.

In other instances, tolerable recoveries of oxolipids have been obtained by using the Folch *et al.* (9) method of extraction under an inert atmosphere (glove box) and in the presence of BHT. The synthetic antioxidant, S20478 (50 μM), was capable of inhibiting the initiation and propagation of copper-mediated low-density lipoprotein (LDL) oxidation as determined by the time- and dose-dependent inhibition of the formation of conjugated dienes and thiobarbituric acid-reactive substances (TBARS) (10). Yasuda and Narita (11) extracted lipid hydroperoxides quantitatively from human plasma with a mixture of *n*-hexane/EtAc (1:1, vol/vol).

Total lipid extracts containing oxophospholipids are commonly purified by TLC or minicolumns to remove the neutral lipids. This also must be done under inert atmosphere. Kenar *et al.* (12) stored phosphate-buffered saline (PBS; pH 7.4, 50 mM) over Chelex-100 at least 24 h to remove transition metal contaminants. Detailed procedures for isolation, quantification, and structural determination of lipid-derived mediators have been described by Gronert *et al.* (13).

Derivatization

Although many oxolipids may be subjected to HPLC in the free form, a preparation of derivatives is desirable for ease of detection and stabilization of the oxolipids for chromatographic and MS identification. Thus, fluorescent derivatives of hydroperoxides have been prepared to increase the specificity and sensitivity of detection (11). The hydroperoxides may be reduced to hydroxides by reaction with triphenylphosphine (TPP), with the result that the more stable hydroxides may be further derivatized for specific identification (9). For NaBH_4 reduction, oxidized phospholipids are treated with NaBH_4 (50 mmol/L) in PBS or MeCN for 30 min to achieve 90% reduction (14). Di-unsaturated oxolipids may be subjected to hydrogenation or deuteration, resulting in a specific molecular weight change as well as a lesser change in the chromatographic properties. The hydrazones of core aldehydes and ketones have been prepared by reaction with 2,4-dinitrophenylhydrazine (DNPH) (15,16) and 1-methyl-1-DNPH (17). Harrison *et al.* (18) have described various microreactions for the derivatization of oxolipids, including preparation of trimethylsilyl (TMS), *tert*-butyldimethylsilyl (TBDMS), and oxime derivatives. The ultimate derivatization results in the release of the oxo-fatty chain from the glycerolipid or cholesteryl ester molecule, which may be completed by enzymatic or chemical methods. Lee *et al.* (19) recommend the use of pentafluorobenzoate (PFB) derivatives of hydroxy FA for sensitive targeted lipidomics analysis with electron capture. Oxidized phospholipids may be treated with phospholipases A_1 , A_2 , C, and D in PBS containing 5 mmol/L CaCl_2 at pH 5.6, 7.0, 7.3, and 5.6, respectively, to release primary and secondary FA, diacylglycerols, or phosphatidic acids (14). The samples were incubated at 37°C for 1 h for phospholipase A_2 , or overnight for phospholipases A_1 , C, and D, to achieve 70–100% hydrolysis.

Chemical peroxidation and ozonization of cholesterol and other lipids may be performed as a means of preparation of reference compounds and as part of the analytical routine in aiding oxolipid identification (15,16).

For assessment of 9-H(P)ODE, 9-H(P)ETE, and F₂-isoprostanes in reaction mixtures, hydroperoxides in the reaction mixture may be reduced to their corresponding hydroxides during extraction by using a modified Dole procedure in which the reducing agent, TPP, is present (20,21). These conditions also inhibit artificial formation of isoprostanes and oxidized lipids.

Resolution and Peak Detection

Component resolution by HPLC is a critical part in LC/ESI-MS when the MS analysis is performed with a single-quadrupole instrument. In tandem MS, HPLC may serve as a convenient method of sample introduction. Usually normal- or reversed-phase HPLC is used, but chiral phase HPLC and silver-ion HPLC have also been employed in specific instances. Normal-phase HPLC is performed on compressed silica gel columns, although ion-exchange resins may also be used as supports. Reversed-phase HPLC separations are performed on siliconized C₁₈ silica columns, which may be further modified by end-capping, but C₅ and C₈ columns have also been employed. The HPLC separations may be conducted with isocratic or gradient solvent mixtures, which are delivered at precise rates and concentrations. The separations may be done at ambient, subambient, or elevated temperatures.

Frequently, HPLC provides the unknown compound in a pure state for mass spectrometric fragmentation. Simple LC-MS, however, is not sufficient to establish the exact composition of all molecular species, especially glycerolipids, which requires the identification of the component FA in each parent molecule. More complete identification may be obtained by MS/MS, which is based on the specific mass spectrometric fragmentation of primary ions. LC/ESI-MS with a single-quadrupole instrument can be used to produce collision-induced dissociation (CID) spectra of singly charged species with greater sensitivity than can be achieved with flow ESI-MS/MS (22,23). If a low voltage of 50–120 V is applied to the capillary exit, the pseudomolecular ion remains intact and the molecular weight of the analyte is obtained. If higher voltages are applied (e.g., 200–300 V) to the capillary exit, extensive and reproducible fragmentation of the molecular adduct ion is realized (pseudo-MS/MS) (22,24). Recent reviews of LC/ESI-MS applications to lipid analyses are available (5,7,24).

Quantification

Comparisons of total ion current peak areas may be used to obtain relative quantification of components in an HPLC profile, but precise quantification of HPLC peaks as well as peak components requires the use of internal standards. A molecu-

lar species of a mass different from those of the measured members of the homologous series usually suffices, but stable isotope-labeled derivatives of the measured species may provide greater accuracy because homologs may differ in their ionization response.

Dzeletovic *et al.* (25) have developed an isotope-dilution-MS/MS method for the determination of nine cholesterol oxidation products in human plasma. A corresponding deuterium-labeled internal standard, containing three to six deuterium atoms, was synthesized for each cholesterol oxidation product, except 5 β ,6 β -epoxycholesterol, which was determined by using the internal standard, 5 α ,6 α -epoxycholesterol. It was found that separation of oxysterols from cholesterol by HPLC was very laborious and some potentially interesting oxysterols were not determined. Instead of HPLC, the authors used solid-phase extraction. A 100-mg silica cartridge (International Sorbent Technology, Mid Glamorgan, UK) was conditioned with 2 mL of hexane and the sample (in 1 mL of toluene) was applied to it. After a 1-mL hexane wash, cholesterol was eluted with 8 mL of 0.5% 2-propanol in hexane. Oxysterols were then eluted with 5 mL of 30% 2-propanol in hexane. The recovery of cholesterol was 96.5–97.4% as determined by the use of [^{14}C]-cholesterol. Detailed identification of the cholesterol oxides was performed by gas chromatography/MS (GC/MS). Dzeletovic *et al.* (25) used the above method based on isotope dilution–MS/MS to determine the kinetics of formation of oxysterols during oxidation of LDL by cupric ions or soybean lipoxygenase. During oxidation, preferentially esterified cholesterol was consumed and consumption of polyunsaturated FA and formation of conjugated dienes preceded the appearance of oxysterols.

Schmitt *et al.* (21) quantified F₂-isoprostanes by stable isotope-dilution-MS with 8-epi-[$^2\text{H}_4$]-PDG_{2 α} as a standard. LC/ESI-MS/MS analyses were performed on a Quattro II triple-quadrupole mass spectrometer (Micromass, Inc.) interfaced with an HP 1100 HPLC (Hewlett-Packard). The 9-hydroxy-10,12-octadecadienoic acid (9-HODE), 9-hydroxy-5,7,11,14-eicosatetraenoic acid (9-HETE), and F₂-isoprostanes in column effluents were determined in the negative-ion mode with multiple reaction monitoring (MRM) using the transitions m/z 295 to 171 for 9-HODE, m/z 319 to 151 for 9-HETE, m/z 353 to 309 for F₂-isoprostanes, and m/z 357 to 313 for [$^2\text{H}_4$]-PDG_{2 α} . The endogenous content of 9-hydroperoxy-10,12-octadecadienoic acid [9-H(P)ODE] and 9-hydroperoxy-5,7,11,14-eicosatetraenoic acid [9-H(P)ETE] in samples was initially determined by the method of standard addition, utilizing known amounts of authentic 9-HODE and 9-HETE added to samples.

Serhan *et al.* (26) used lipidomics methodology and extracted lipid-derived mediators generated from ω -3 FA with deuterium-labeled internal standards (15-HETE and 20:4) for LC-MS/MS analysis using a Finnigan LCQ equipped with a LUNA C18-2 (150 \times 2 mm; 5 μm) column and a rapid spectra scanning UV/vis detector. Serhan *et al.* (26) suspended the compounds in mobile phase and injected them into the HPLC component (SpectraSystem P4000, Thermoseparation Products, San Jose, CA). The

column was eluted isocratically with MeOH/H₂O/AcOH (65/34.99/0.01 by vol) at 0.2 mL/min into the electrospray probe. Full scan mass spectra were recorded in the negative ion mode in the range m/z 330–360. For further identification of the analytes, product ion mass spectra were obtained for m/z 317, m/z 299, m/z 273, and m/z 255. In special instances, electron capture by TFA derivatives may be used to enhance the sensitivity of detection of both unknowns and standards (19).

Sterols

Hydroperoxides, Epoxides, and Hydroxides

Sevanian *et al.* (27) compared separation of several oxidation products of sterols by GC/EI-MS and HPLC with particle beam ionization (PBI) or thermospray ionization (TSI) mass spectrometry (LC/PBI-MS or LC/TSI-MS) under isocratic conditions. The HPLC method used an Ultrasphere-Si 250 column (250 × 4.6 mm; Altex) and a mobile phase composed of hexane/2-propanol (96:4, vol/vol) at a flow rate of 0.4 mL/min. The PBI interface was set with 30 psi of helium nebulizing gas and with a desolvation chamber temperature of 45°C. Under these conditions, isomeric 7-hydroxycholesterols and 7-hydroperoxycholesterols were readily separated. Whereas LC/MS analysis of cholesterol oxides provided less resolution and lower sensitivity than GC/EI-MS, a distinct advantage was evident for direct measurements of cholesterol-7-hydroperoxides and 7-ketocholesterol. These two cholesterol oxides are particularly sensitive to storage in solvents, derivatization procedures, and analytical conditions used in GC analysis, which are minimized or avoided by using the LC/MS conditions.

Osada *et al.* (28) used LC/ESI-MS to identify cholesterol oxidation products in various oxidation mixtures. Figure 4.1 shows the total positive-ion current profile and mass spectra of a standard mixture of the major oxidized cholesterol derivatives. The column was eluted with a mixture of MeOH/MeCN (40:60, vol/vol) at a flow rate of 0.8 mL/min. The column effluent was mixed at a postcolumn mixing joint with a mobile phase containing 0.5% NH₄OH pumped at 0.3 mL/min by another HPLC pump.

Positive-ion spectra were taken in the m/z range 300–500. Selected ion mass chromatograms were retrieved from the computer. The oxocholesterol standards gave the following characteristic ions: 25-hydroxycholesterol (peak 1), m/z 367, 385, 413, 425, and 441; 26-hydroxycholesterol (peak 2), m/z 367, 385, 413, 425, and 441; cholestanetriol (peak 3), m/z 367, 385, 413, 438, and 441; 7 α -hydroxycholesterol (peak 4), 367, 385, 413, 425, 441; 7 β -hydroxycholesterol (peak 5), m/z 367, 385, 413, 425, and 441; 7-ketocholesterol (peak 6), m/z 401 and 439; 5 α -epoxycholesterol (peak 7), m/z 367, 385, 413, 425, and 441; 5 β -epoxycholesterol (peak 8), m/z 367, 385, 413, 425, and 441; 3,5-cholestadiene-7-one (peak 9), m/z 383, 405, and 421; and 4,6-cholestadiene-3-one (peak 10), m/z 383, 405, and 421. The identification of the 25- and 26-hydroxycholesterols, as well as 7 α - and 7 β -

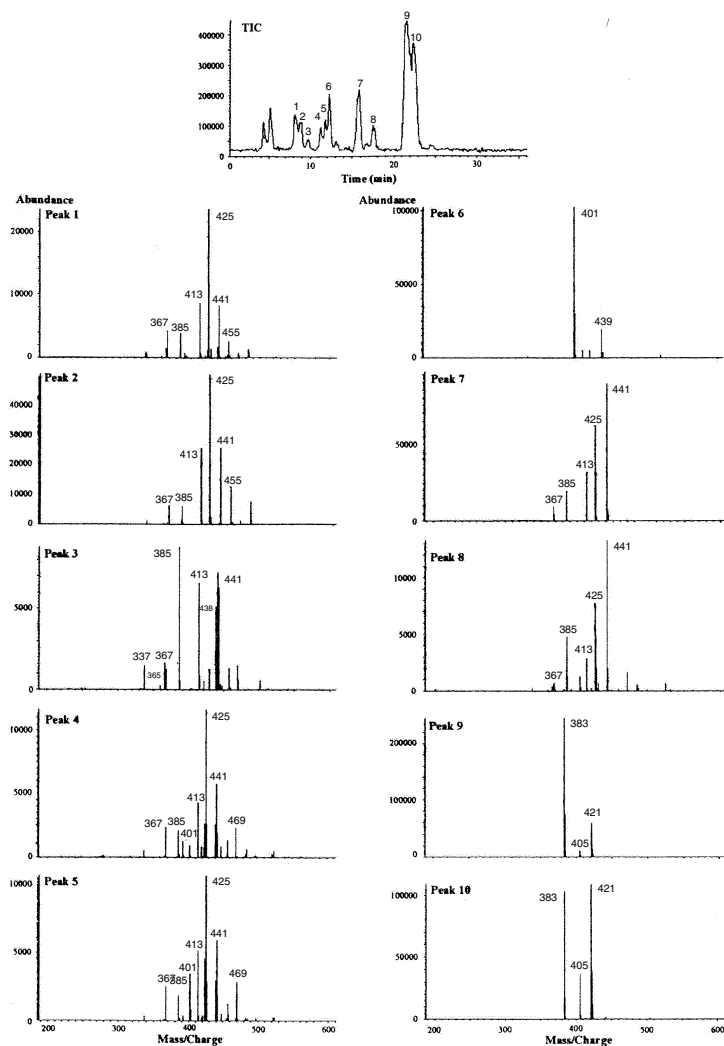


Fig. 4.1. Reversed-phase LC/ESI-MS mass spectra of mixed oxidized cholesterol standards. Peak identification: (1) 25-Hydroxycholesterol; (2) 26-hydroxycholesterol; (3) cholestanetriol; (4) 7α -hydroxycholesterol; (5) 7β -hydroxycholesterol; (6) 7-ketocholesterol; (7) α -epoxycholesterol; (8) 5β -epoxycholesterol; (9) 3,5-cholestadien-7-one; and (10) 4,6-cholestadien-3-one. HPLC conditions: column, Supelcosil LC-18 (25 cm \times 4.6 mm, i.d., 5 μ m); mobile phase, isocratic MeOH/ MeCN (60:40, vol/vol) over 30 min; detector, UV from 190 to 290 nm. ESI-MS, Hewlett-Packard Model 5988B single-quadrupole mass spectrometer. Positive ionization spectra were taken over the mass range 300 to 500. Postcolumn addition of 0.5% NH_4OH at 0.3 mL/min. *Source:* Osada *et al.* (28).

hydroxycholesterols and the 5 α - and 5 β -epoxycholesterols, relied on the differences in the HPLC retention times of the oxosterol derivatives, since they possessed identical masses and gave identical fragmentation patterns. Osada *et al.* (28) employed this LC/ESI-MS method for the demonstration of the presence of cholestanetriol, 7 α - and 7 β -hydroxycholesterols, 7-ketocholesterol, and 5 α - and 5 β -epoxycholesterols in heated tallow and in photo-oxidized cholesterol.

Schmitt *et al.* (21) used reversed-phase HPLC with on-line atmospheric pressure chemical ionization (APCI)-MS to determine the production of 7-hydroperoxy-cholesterol as well as other oxysterols following exposure of LDL to a myeloperoxidase (MPO)/H₂O₂/NO₂ system. Specifically, 7-hydroxycholesterol, 7-ketocholesterol, and 7-hydroperoxycholesterol were resolved on an Ultrasphere ODS C₁₈ column (4.6 mm \times 250 mm, 5 μ m, Beckman Instruments). The column was eluted at a rate of 1.5 mL/min with MeCN/H₂O (91:9, vol/vol) and 0.1% formate (vol/vol). The column was washed between runs with MeCN and 0.1% formate. The effluent was split to deliver 900 μ L/min to the UV detector and 100 μ L/min to the mass detector and APCI in the positive-ion mode with selected ion monitoring. Identification of 7-hydroxycholesterol was performed by demonstrating comigration of ions at m/z 385.3 ([M-H₂O]⁺) and m/z 367.3 ([M-2H₂O]⁺) with the same retention time as the authentic standard. Identification of 7-hydroperoxycholesterol was achieved by demonstrating comigration of ions at m/z 401.3 ([M-H₂O]⁺), m/z 383.3 ([M-2H₂O]⁺), and m/z 367.3 ([M-H₂O-H₂O₂]⁺) with the same retention time as the authentic standard. Identification of 7-ketocholesterol was achieved by demonstrating comigration of ions at m/z 401.3 ([M+H]⁺) and m/z 383 ([M-H₂O]⁺) with the same retention time as the authentic standard. The retention times for 25-hydroxycholesterol, 5,6 α - and β -epoxides, and triol were determined by LC/MS analysis of authentic standards.

Ozonides

Ozonides of cholesterol have been analyzed as an aid in identifying the structure of the lipid molecules and because of interest in identifying biomolecules that can be used to measure exposure to inhaled ozone in smog. Ozone adds rapidly to carbon-carbon double bonds to form an initial 1,2,3-trioxolane (molozone), which undergoes rearrangement to the more stable 1,2,4-trioxolane (Criegee ozonide) *via* a carbonyl oxide and aldehyde intermediates (29). The structures of cholesterol ozonization products have not been completely elucidated, despite the fact that ozone toxicity is of great importance in the biosphere and that ozone is used as a sterilizing agent in the food industry. The action of ozone on cholesterol in organic solvents has received the most attention, and there is general agreement that 5,6-secoosterols result (30). Solvent participation occurs in ozonizations of cholesterol conducted in protic solvents. In halocarbons containing methanol, 5 ϵ ,6 ϵ -epidioxy-6 ϵ -methoxy-5,6-secocholestane-3 β ,5 ϵ -diol result. Cholesterol in water dispersion is rapidly and completely oxidized by ozone at room temperature to the major peroxidic

product 5 ϵ ,6 ϵ -epidioxy-5,6-secocholestane-3 β ,5 ϵ ,6 ϵ -triol and to such minor products as secoaldehyde, isomeric 5,6-epoxides, and 3 β ,10-dihydroxy-6-oxo-5,6,10-disecocholestan-5-oic acid lactone.

Cholesterol ozonization products were originally identified by direct GC/MS (30,31), with the major ozonization product being 3 β -hydroxy-5-oxo-5,6-secocholestan-6-al. High-resolution mass spectrometric measurements were made with a CEC 21-110B instrument at 30 eV. More recently, LC/ESI-MS has been used because it avoids heat decomposition and eliminates the need for chemical stabilization of the oxidation products.

In the past, cholesterol ozonides have been analyzed as indicators of the progress of food sterilization by ozonization. Wentworth *et al.* (32) have provided evidence for the formation of ozone and ozonolysis products in human atherosclerotic arteries. They have also proposed the trivial designation "atheronals" for the ozonolysis products of cholesterol demonstrated to be formed in inflammatory human disease and in atherosclerosis (32). Using the procedure developed by Wang *et al.* (33), the "atheronals" were isolated and identified in homogenized plaque material as the 2,4-DNPH derivatives of ozonolysis products of 5,6-secocholesterol, for example, ketoaldehyde and its aldolization product.

Steryl Esters

Hydroperoxides, Epoxides, and Hydroxides

Kritharides *et al.* (34) described an HPLC system for the identification of some of the lipid oxidation products of LDL oxidized by copper. Using a reversed-phase C₁₈ column (5 μ m, 25 cm \times 0.46 cm i.d. with 5-cm guard column) and an isocratic solvent system of MeCN/2-propanol/H₂O (44:54:2, by vol), the oxolipids were resolved into a number of oxidized lipid moieties that were initially detected simply by their absorbance at 234 nm. The nature of several of these compounds was determined by chromatographic criteria, chemiluminescence, and MS/MS (Finnigan TSQ 700 equipped with a direct chemical insertion probe).

Havrilla *et al.* (6) reported the coupling of silver coordination ion spray (CIS)-MS (Ag⁺CIS-MS) to normal-phase HPLC by postcolumn addition of AgBF₄, which greatly improved the power of such techniques as selected ion monitoring (SIM) and selected reaction monitoring (SRM). The separated cholesteryl linoleate oxidation products were characterized by conversion to the corresponding methyl esters and comparing with samples of known structures (9). The autoxidation products of cholesteryl linoleate were prepared by using the free radical initiator di-tert-butylhyponitrite (DTBN), which was synthesized before use and treated with Chelex-100 resin for 24 h to remove transition metal contaminants. Analytical HPLC was conducted on a Waters model 600 HPLC instrument with an HP 1050 Multiwavelength detector and an HP 3396 Series III integrator. For cholesteryl linoleate and cholesteryl arachidonate hydroperoxide analysis, the HPLC was

equipped with two tandem Beckman Ultrasphere 5- μm silica columns (4.6 mm \times 25 cm), and 0.5% 2-propanol in hexane at a delivery rate of 0.1 mL/min. For analytical determination of the more polar cyclic peroxides, HPLC was conducted on a Waters model 600E pump with a Waters 717plus Autosampler and a Waters 996 Photodiode array detector. A single Beckman Ultrasphere 5- μm silica column (4.6 mm \times 25 cm) with a flow rate of 1.0 mL/min of 1.0% 2-propanol in hexane was utilized. Analytical HPLC of the cholesteryl linoleate hydroperoxides resolved four major components in the mixture: a *trans,cis*-conjugated diene with peroxide substitution on carbon 13 of the linoleate chain (15.0 min) was followed by the *trans,trans*-substituted geometric isomer (17.5 min), with the partly resolved hydroperoxides at the 9-position of the linoleate chain eluted later, at 20.1 and 20.5 min. The hydroperoxides were identified by CIS-MS. CID experiments of the $^{107}\text{Ag}^+$ and $^{109}\text{Ag}^+$ complexes gave characteristic fragment ions. The spectra of the C-13-substituted hydroperoxides and the C-9-substituted isomers were essentially identical except for differences in the CID fragments.

The oxidation products of cholesteryl arachidonate on analytical HPLC gave six major fractions (6), which were identified as cholesteryl 15-hydroxy-5(Z), 8(Z), 11(Z), 13(E)-eicosatetraenoate (11.44 min), cholesteryl 12-hydroxy-5(Z), 8(Z), 10(E), 14(Z)-eicosatetraenoate (12.14 min), cholesteryl 11-hydroxy-5(Z), 8(Z), 12(E), 14(Z)-eicosatetraenoate (13.12 min), cholesteryl 9-hydroxy-5(Z), 7(Z), 11(Z), 14(Z)-eicosatetraenoate (16.97 min), cholesteryl 8-hydroxy-5(Z), 9(E), 11(Z), 14(Z)-eicosatetraenoate (17.29 min), and cholesteryl 5-hydroxy-6(E), 8(Z), 11(Z), 14(Z)-eicosatetraenoate (22.57 min). HPLC/ Ag^+ CIS-MS of the oxidation mixture of cholesteryl arachidonate provided support for the assigned structures (Fig. 4.2). Panel A shows the UV absorption profile. SRM analysis of the parent $^{107}\text{Ag}^+$ adduct at m/z 811 gives fragments that identify the position of substitution on the arachidonate chain. Thus, Hock fragmentation of cholesterol-15-HPETE gives a fragment at m/z 343 (panel C). The 11- and 12-hydroperoxides of cholesteryl arachidonate give identical Hock fragmentation ions, and panel D shows the sum of signals detected from SRM for m/z 303. Cholesteryl-8-HPETE and cholesteryl-9-HPETE both give the same Hock fragmentation product. Panel E shows the SRM for this ion at m/z 263, and the corresponding fragmentation of the cholesteryl-5-HPETE gives m/z 327 (Panel F) (6).

Isoprostanes, Neuroprostanes, and Dinorprostanes

Cyclic peroxidation products of arachidonic acid esters were first recognized in the early 1990s (20). Since that time cyclic peroxidation products have been obtained also from linolenic and docosenoic acid esters. Cyclic peroxidation products of cholesteryl arachidonate were later isolated by Kenar *et al.* (12) and Havrilla *et al.* (6). Yin *et al.* (35) have described the details of the formation of bicyclic endoperoxides from autoxidation of cholesteryl arachidonate. Only the isoprostane bicyclic endoperoxides of cholesteryl-15-HPETE (type IV) were specifically characterized.

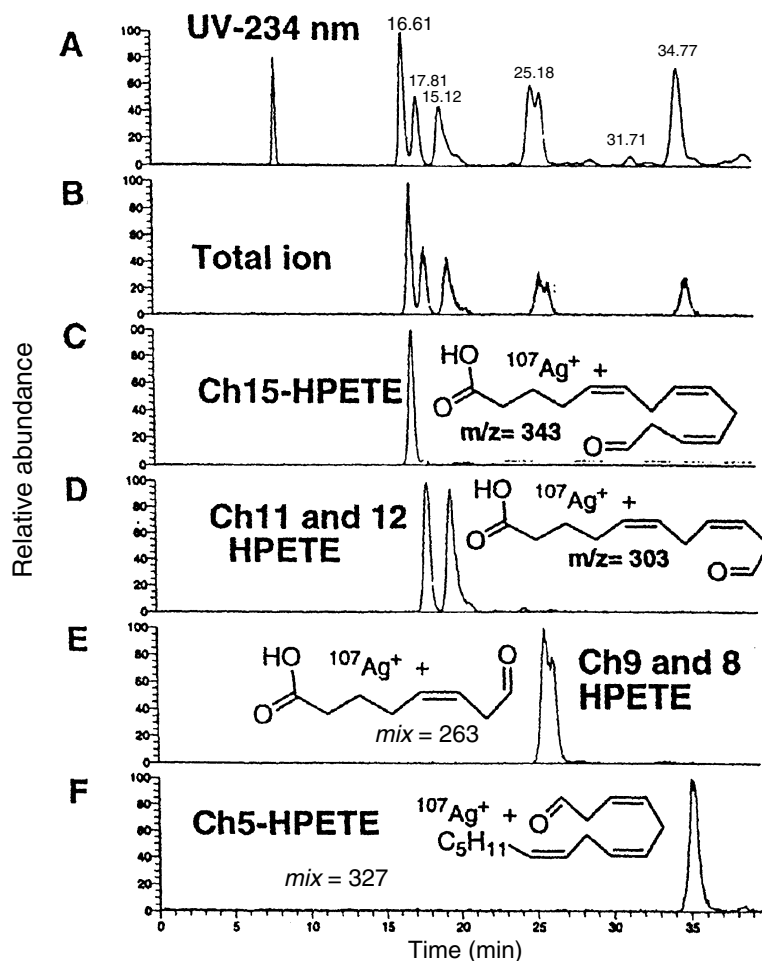


Fig. 4.2. HPLC/CIS-MS of a cholesteryl arachidonate oxidation mixture formed by co-oxidation with cyclohexadiene. UV detection at 234 nm (A); HPLC/CIS-MS total ion current (B); HPLC/CIS-MS in selected reaction monitoring mode for $m/z = 787$ to 343 (C); HPLC/CIS-MS in selected reaction monitoring mode for $m/z = 787$ to 303 (D); HPLC/CIS-MS in selected reaction monitoring mode for $m/z = 787$ to 263 (E); HPLC/CIS-MS in selected reaction monitoring mode for $m/z = 787$ to 327 (F). HPLC conditions: two tandem Beckman Ultrasphere narrow-bore 5- μm silica columns (2.0 mm \times 25 cm) operated in isocratic mode with 35% 2-propanol in hexane. Si columns, 0.5% 2-propanol in hexane at 150 $\mu\text{L}/\text{min}$. Column effluent was passed through an Applied Biosystems 785A programmable absorbance UV detector, with detection at 234 nm. An Upchurch PEEK high-pressure mixing tee was connected next in series for the postcolumn addition of the silver salts (Applied Biosystems, Boston, Massachusetts). The silver tetrafluoroborate (AgBF_4) solution (0.25 mM in 2-propanol) was added via a Harvard Apparatus syringe pump at a flow rate of 75 $\mu\text{L}/\text{min}$. A section of PEEK tubing (1.04 m, 0.25 mm i.d.) allowed time for the complexation of the silver to the lipid while delivering effluent to the mass spectrometer. Source: Havrilla *et al.* (6).

Analytical HPLC was performed with a Waters model 600E pump and a Waters 996 Photodiode array detector. Cyclic peroxide analysis by analytical HPLC used a single Beckman Ultrasphere 5- μm (4.6 mm \times 25 cm) silica column. A flow rate of 1 mL/min was used for analytical normal-phase HPLC. Preparative normal-phase HPLC was performed with a Dynamax-60 A (83-121-C) silica column (21.4 mm \times 25 cm \times 8 μm particles) with a flow rate of 10 mL/min. Narrow-bore HPLC for MS analysis used a single Beckman Ultrasphere 5- μm (2.0 mm \times 25 cm) silicic acid column for analysis of cyclic peroxides and two Beckman Ultrasphere 5- μm (2.0 mm \times 25 cm) silica columns for acyclic hydroperoxide analysis. The flow rate for the LC/MS separations and analysis was 150 $\mu\text{L}/\text{min}$. For HPLC sample introduction into the mass spectrometer, a Hewlett-Packard 1090 HPLC system was used. The AgBF_4 solution (0.25 mM in 2-propanol) was added *via* a Harvard Apparatus syringe pump at a flow rate of 75 $\mu\text{L}/\text{min}$. A long section of PEEK tubing (1.04 m, 0.25 mm i.d.) allowed time for the complexation of the silver to the lipid while delivering effluent to the mass spectrometer. SRM was performed by coupling HPLC to Ag^+ CIS-MS. The SRM chromatogram from the parent ion m/z 843 to the characteristic endoperoxide fragment, m/z 375, is shown in Figure 4.3.

Chromatography of the oxidation mixture from cholesteryl-15-HPETE monitored at UV 234 nm and 207 nm gave the same profile. The endoperoxides do not have conjugated diene structures and they are therefore not detected at 234 nm. Other products formed from the reaction of arachidonate hydroperoxides include serial cyclic and monocyclic peroxide compounds that contain a conjugated diene substructure. These compounds can be detected at 234 nm as peaks in the HPLC/UV chromatogram. They have been identified previously as having a serial cyclic structure (6).

Since 22:5n3 and 22:6n3 also occur in the form of cholesteryl esters, it would be anticipated that neuroprostane-containing cholesteryl esters would also be formed. In current studies, the cholesteryl ester peroxidation products are discarded along with the peroxidation products of other neutral lipids, which generally contain only limited amounts of 22:6. Furthermore, the neuroprostanes would not be released from the cholesteryl esters by phospholipases, which are commonly used to obtain the neuroprostanes in the free form.

Core Aldehydes

Kuksis (36) and Kamido *et al.* (15) recognized the presence of both lipid ester hydroperoxides and core aldehydes among the cholesteryl ester and triacylglycerol (TAG) peroxidation products isolated from liposomal and LDL preparations, and set out to examine the *tert*-BOOH/ Fe^{2+} combination as a possible means for preparing for biochemical and metabolic studies larger amounts of oxo-TAGs than provided by autoxidation.

Kamido *et al.* (15,37,38) used reversed-phase HPLC to isolate and identify cholesteryl ester core aldehydes (aldehydes still bound to the cholesterol ring) following copper-catalyzed peroxidation of human LDL. The core aldehydes were isolated as

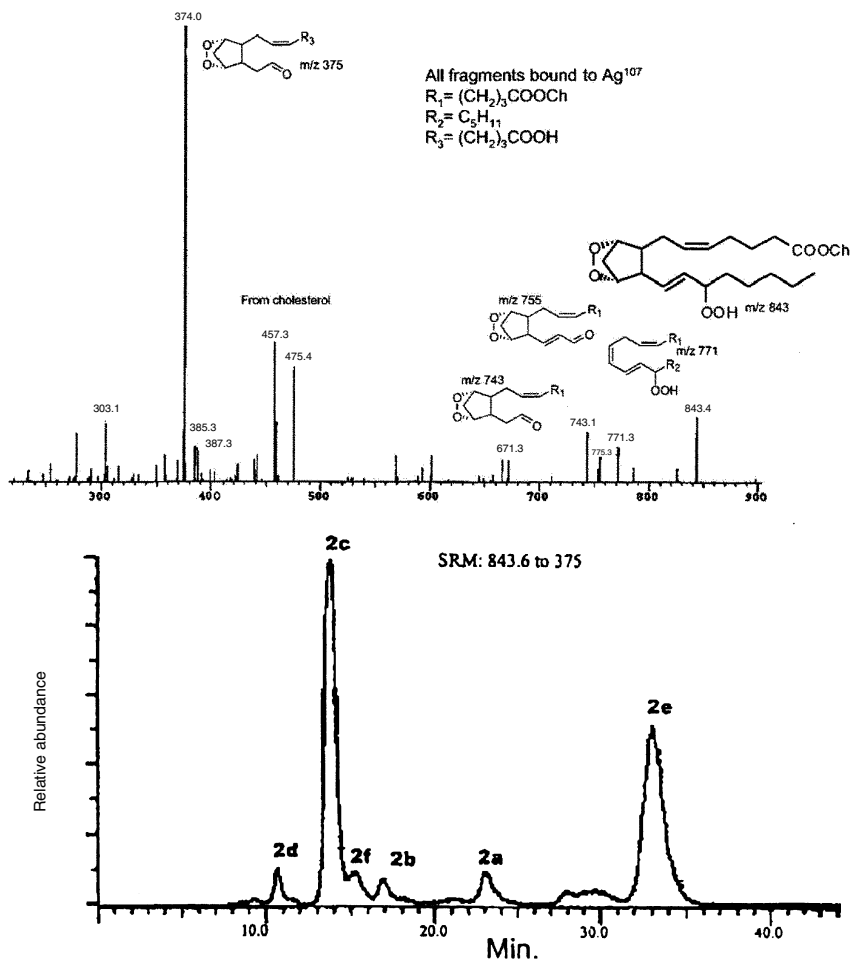


Fig. 4.3. Identification of type IV bicyclic endoperoxide **2** by using a triple-quadrupole mass spectrometer. (A) CID spectrum of the parent ion m/z 843.4; an apparent fragment with m/z 771 is obtained by the loss of malonaldehyde, a well-known process for endoperoxides. The fragments with m/z 753 and 385 result from dehydration of the fragment at m/z 771. (B) Selective reaction monitoring was carried out by coupling HPLC to Ag^+ CIS-MS. The chromatogram shows the SRM reaction from the parent ion m/z 843 to the characteristic endoperoxide fragment, m/z 375. LC/CIS-MS conditions: A single Beckman Ultrasphere 5- μ m (4.6 mm \times 25 cm) silica column operated in isocratic mode with 1% 2-propanol in hexane at flow rate of 1 mL/min. *Source:* Yin *et al.* (35).

the DNPH derivatives and were identified by reversed-phase HPLC with TSI-MS. The major components were the C_4 – C_{10} oxoalkanoyl esters of cholesterol and 7-keto-cholesterol, and they accounted for 1–2% of the cholesteryl linoleate and arachidonate consumed. The DNPH derivatives of the core aldehydes were purified and isolated by

TLC, where they appeared as yellow zones corresponding to the 5-oxovaleroyl (R_f 0.26) and 9-oxononanoyl (R_f 0.33) cholesterol, when subjected to a double development with CH_2Cl_2 and toluene. The DNPH derivatives were recovered from the TLC plates with $\text{CHCl}_3/\text{MeOH}$ (2:1, vol/vol). The core aldehydes of 7-ketocholesteryl esters, which remained near the origin (R_f 0.10), were recovered in a similar manner. HPLC separations were performed on a Supelcosil LC-18 column (250 \times 4.6 mm, Supelco Inc., Mississauga, Ontario) using $\text{MeCN}/2\text{-propanol}$ 4:1 (vol/vol) or a linear gradient of 30–90% EtCN in MeCN as the eluting solvents. The column was installed in a Hewlett-Packard model 1084B liquid chromatograph and was operated at a flow rate of 1.0–1.5 mL/min. The peaks were monitored at 358 nm. In a parallel study, Kamido *et al.* (37) used $\text{MeCN}/2\text{-propanol}$ 80:20 (vol/vol) for the isocratic HPLC resolution of the cholesteryl and 7-ketocholesteryl ester core aldehydes as the DNPH derivatives. About 1% of the HPLC column effluent was admitted to a Hewlett-Packard model 5985B single-quadrupole mass spectrometer *via* a direct liquid inlet (DLI) interface. Negative chemical ionization (NCI) mass spectra were taken every 5 s over the entire chromatograms in the mass range 200–900. Figure 4.4 shows the reversed-phase LC/MS chromatograms of the cholesteryl and 7-ketocholesteryl ester core aldehydes. The individual core aldehydes are identified on the basis of the retention times and SIM. The molecular species range from C_4 to C_{10} in chain lengths, with the C_9 species accounting for the bulk of the aldehydes. Hoppe *et al.* (39) used this HPLC method to demonstrate the production of cholesteryl ester core aldehydes along with the core acids during peroxidation of the cholesteryl linoleate.

In the negative-ion mode tentatively identified were 7 α -hydroxycholesteryl 9-carboxynonanoate, 7 β -hydroxycholesteryl-9-carboxynonanoate, 5,6-epoxycholesteryl 8-carboxyoctanoate, 5,6-epoxycholesteryl 9-carboxynonanoate, 7 α -hydroxycholesteryl 9-oxononanoate DNPH, 7 β -hydroxycholesteryl 9-oxononanoate DNPH, 7-ketocholesteryl 9-carboxy nonanoate DNPH, cholesteryl 9-carboxynonanoate, cholesteryl 8-oxo-octanoate DNPH, and cholesteryl 9-oxononanoate DNPH.

Recently, Kawai *et al.* (40) reported the covalent binding of oxidized cholesteryl esters to protein. Figure 4.5 demonstrates the reaction of lysine with 9-oxononanoyl cholesterol. The figure shows (A) loss of amino acids in the 9-oxononanoyl cholesterol-treated bovine serum albumen (BSA); (B) reaction of N^α -benzoyl-glycyl-lysine with 9-oxononanoyl cholesterol as indicated by single-ion monitoring at m/z 832 and (C) UV absorption at 240 nm; (D) shows the full mass spectrum of the peak eluted at 21 min in the HPLC profile.

Ozonides

Smith *et al.* (41) reported the structures of cholesterol 3 β -acyl ester ozonides formed by reaction with ozone in participating alcoholic solvents, as established by proton and ^{13}C spectra, as a 3 β -acyloxy-7 α -alkoxy(5*R*,7*R*)-5 α -B-homo-6-oxa-

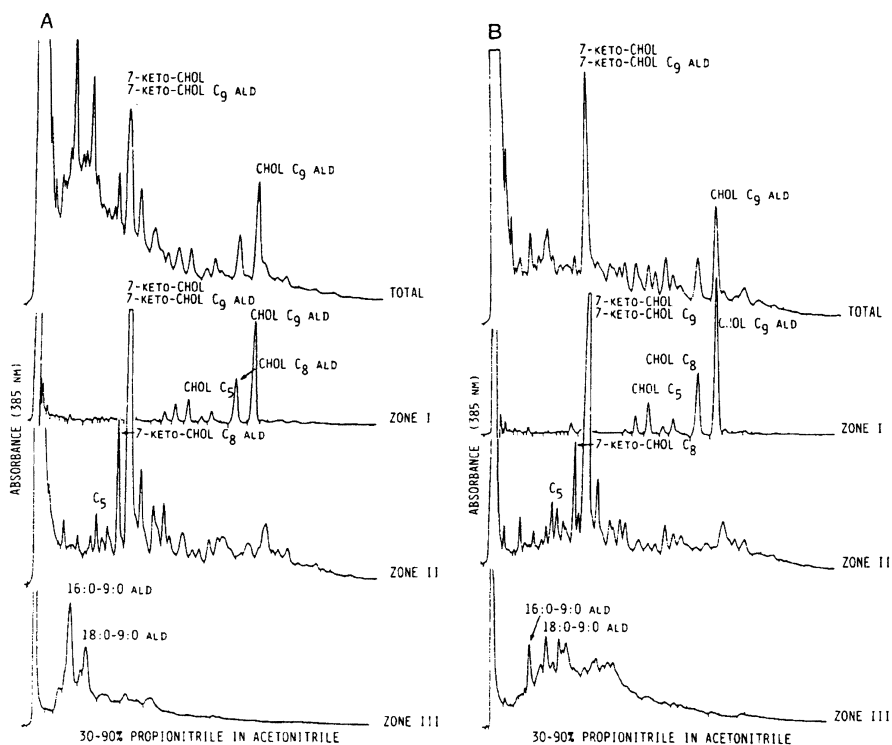


Fig. 4.4. Reversed-phase HPLC of TLC fractions of the DNPH derivatives of lipid ester core aldehydes from oxidized human LDL (A) and HDL (B). Peak identification: total, DNPH of total lipid extract; zone I, DNPH of cholesteryl ester core aldehydes; zone II, DNPH of 7-ketocholesteryl ester core aldehydes; zone III, DNPH of diacylglycerol core aldehydes derived from glycerophospholipids. HPLC conditions: Supelco LC-18 column (250 mm \times 4.6 mm, Supelco Inc.; mobile phase, linear gradient of 30 to 90% EtCN in MeCN in 30 min; detection, UV at 358 nm. *Source:* Kamido *et al.* (37).

cholestane-5-hydroxyperoxides. The structure of the dimeric cholesterol ozonide formed in nonparticipating solvents with cholesterol, acting as an alcohol, was established as 7α -cholest-5'-en-3'-yloxy- 3β -hydroxy-($5R,7R$)- 5α -B-homo-6-oxo-cholestane-5-hydroperoxide. This constituted a revision of an earlier proposed structure based on a less complete chemical characterization and lower resolution nuclear magnetic resonance (NMR) data.

Herrera *et al.* (42) showed that the ozonization products of cholesteryl acetate can be resolved into one major and one minor pair of peaks by reversed-phase HPLC (Fig. 4.6). The two peaks of the major pair give the same molecular ion at m/z 495 and presumably represent a resolution of the $7\alpha/7\beta$ isomers of the major product identified by Jaworski and Smith (43) as (5,7 ξ -epidioxy-5 ξ -B-homo-6-

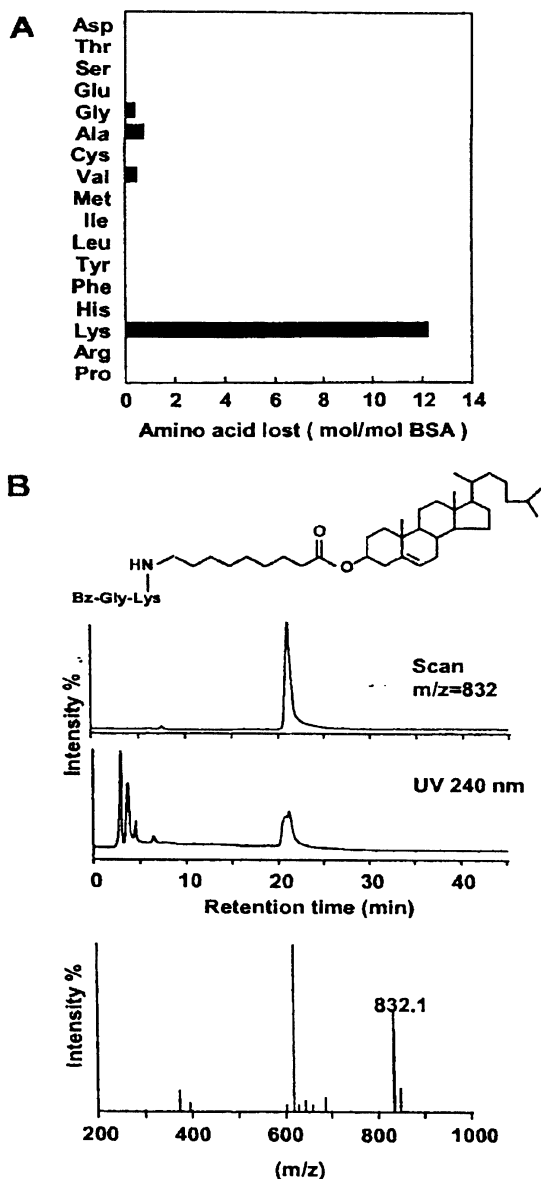


Fig. 4.5. Reaction of 9-oxononyl cholesterol with lysine. (A) Loss of amino acids in the 9-oxononyl cholesterol-treated BSA. (B) Reaction of N^α -benzoyl-glycyl-lysine with 9-oxononyl cholesterol. The products were stabilized with NaCBH_3 and characterized by LC/MS. Top: Selected ion current chromatogram of m/z 832 obtained from LC/MS analysis. Middle: HPLC profile of the reaction mixture. Bottom: Mass spectrum of the peak eluted at 21 min in the HPLC profile. LC/MS conditions: Develosil ODS-HG-5 column (4.6×250 mm; Nomura Chemicals, Aichi, Japan) using a linear gradient from 90% aqueous MeCN to 100% MeCN for 30 min (UV detection at 240 nm) or with a linear gradient of 2-propanol/MeOH (2:8, vol/vol) to 2-propanol/MeOH (8:2, vol/vol) for 45 min at a flow rate of 0.8 mL/min (LC/MS detection). For the LC/MS measurement with a Jasco PlatformII-LC instrument, 0.5% NH_4OH was added to the mobile phase. Source: Kawai *et al.* (40).

oxacholestan)- 3β -acetate. Another major peak of an m/z 479, which was eluted much earlier, was assigned to (5-oxo-5,6-secocholestan-6- α l)- 3β -acetate. It had been previously reported to result from reaction of cholesterol with ozone in hexane dispersion at room temperature. The structure had been earlier deduced from NMR, EI-MS, and CI-MS analysis (43). The reversed-phase HPLC (Supelcosil C-18,

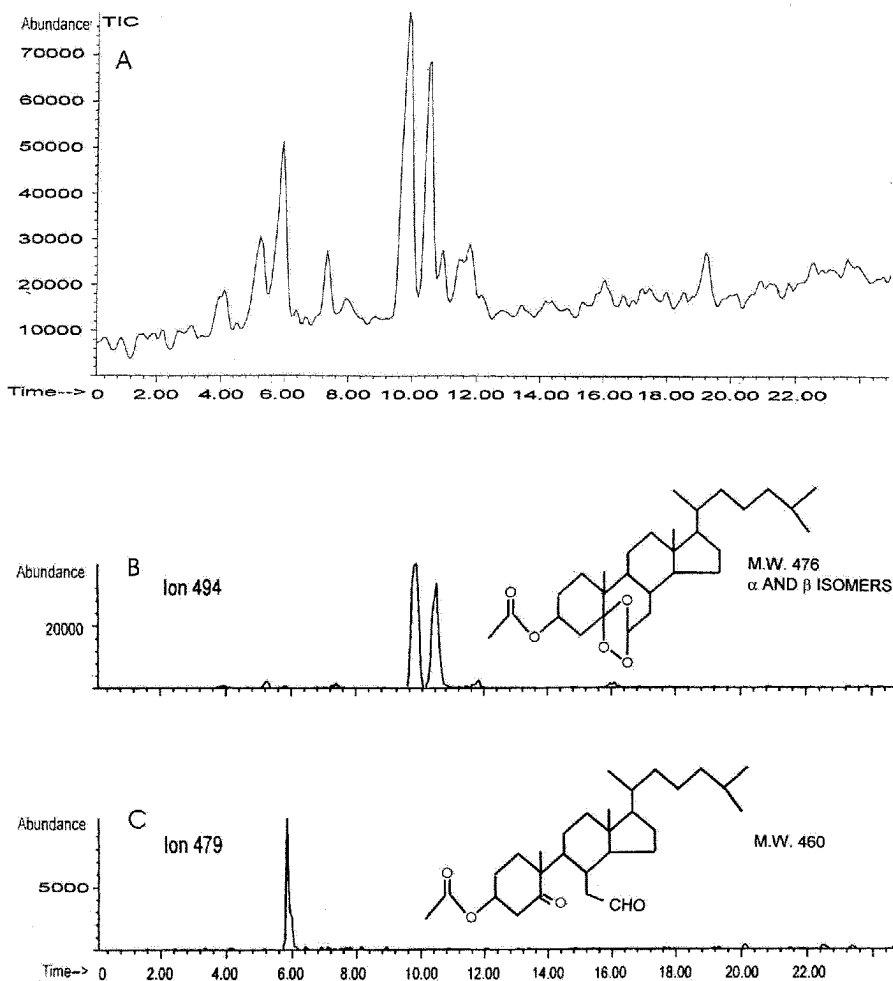


Fig. 4.6. Total positive-ion current profile of ozonized cholesteryl acetate (A), Ion m/z 495 ($[476+18]^+$), (isomeric 5,7 ξ -epidioxy-5 ξ -B-homo-6-oxacholestan)-3 β -acetate (B); and ion m/z 479 ($[460+18]^+$), (5-oxo-5,6-secocholestan-6-al)-3 β -acetate (C). The tentative structures of the ions are given in the figure. HPLC/ESI-MS conditions: columns, Supelcosil LC-18 (250 mm \times 4.6 mm i.d.); mobile phase, linear gradient of 20–80% 2-propanol in MeOH over 30 min. ESI-MS, positive-ion mode over the mass range of 300 to 1200 Da; exit voltage set to 120 V. Post-column addition of 0.5% NH_4OH in MeOH at 0.3 mL/min. ξ , unknown configuration. *Source:* Herrera *et al.* (42).

250 mm × 4.6 mm i.d.) was performed using a gradient of 20–80% 2-propanol in MeOH over a period of 30 min.

In cholesteryl linoleate, the oxidation of the ring and the linoleate ester chain proceed independently. Herrera *et al.* (42) used reversed-phase HPLC to examine the sequence of events leading to the ozonization of both the ring and the fatty chain. The cholesteryl linoleate (1 mg) was dissolved in 1 mL of hexane and cooled in a dry ice-acetone bath for 5 min. O₂ gas containing 3–4% ozone was then bubbled through the solution at a rate of 150 mL/min. When the blue color persisted, the hexane was evaporated to dryness and the cholesteryl ester ozonides were redissolved in CHCl₃/MeOH and subjected to purification by TLC (250 μm thick layer, 20 × 20 cm glass plate) on silica gel H by using an apolar solvent system made up of heptane/2-propyl ether/HOAc (60:40:4, by vol) for the development.

A total of four bands were visualized under UV light, recovered from the silica gel by extraction with CHCl₃/MeOH (2:1, vol/vol) and examined by LC/ESI-MS. Figure 4.7 shows the single-ion mass chromatograms for the initial products of ozonization of cholesteryl linoleate as obtained by reversed-phase LC/ESI-MS, along with the postulated tentative structures. On the basis of common notions about the role of polarity in determining the elution order, the retention time of the linoleate ester of epoxycholesterol would appear to be out of place and must be compared to that of an authentic standard. The reversed-phase HPLC separation of cholesteryl linoleate ozonides was performed on a Supelco LC-18 (250 mm × 4.6 mm i.d) column installed into a Hewlett-Packard model 1050 liquid chromatograph connected to an evaporative light-scattering detector (ELSD) (Model ELSD II; Varex, Rockville, MD). The column was eluted with a gradient of 20–80% 2-propanol in MeOH over 40 min with a flow rate set at 1 mL/min. Figure 4.8 shows the reversed-phase HPLC/ESI-MS analysis of the major products of ozonization of cholesteryl linoleate. The total positive-ion current profile of cholesteryl linoleate (A) is compared to the single-ion mass chromatograms of the major oxidation products in Figure 4.8 (B, C, D, and E). The ozonization products are tentatively identified in the figure. In addition to the simple hydroperoxides and core aldehydes, complex products of alkylation of the sterol ring were observed, with a nine-carbon mono-ozonide as the alkoxy group.

Neutral Glycerolipids

Hydroperoxides, Epoxides, and Hydroxides

Kuksis *et al.* (16) used reversed-phase HPLC to identify mixed hydroperoxide and core aldehyde derivatives of synthetic and natural TAG following reaction with the *tert*-BOOH/Fe²⁺ reagent. The oxidation products were extracted with CHCl₃/MeOH, reacted with DNPH, and resolved by normal-phase TLC into fractions, depending on the number of hydrazone derivatives formed. The individual TLC bands were examined by reversed-phase HPLC with on-line TSI-MS. The HPLC sep-

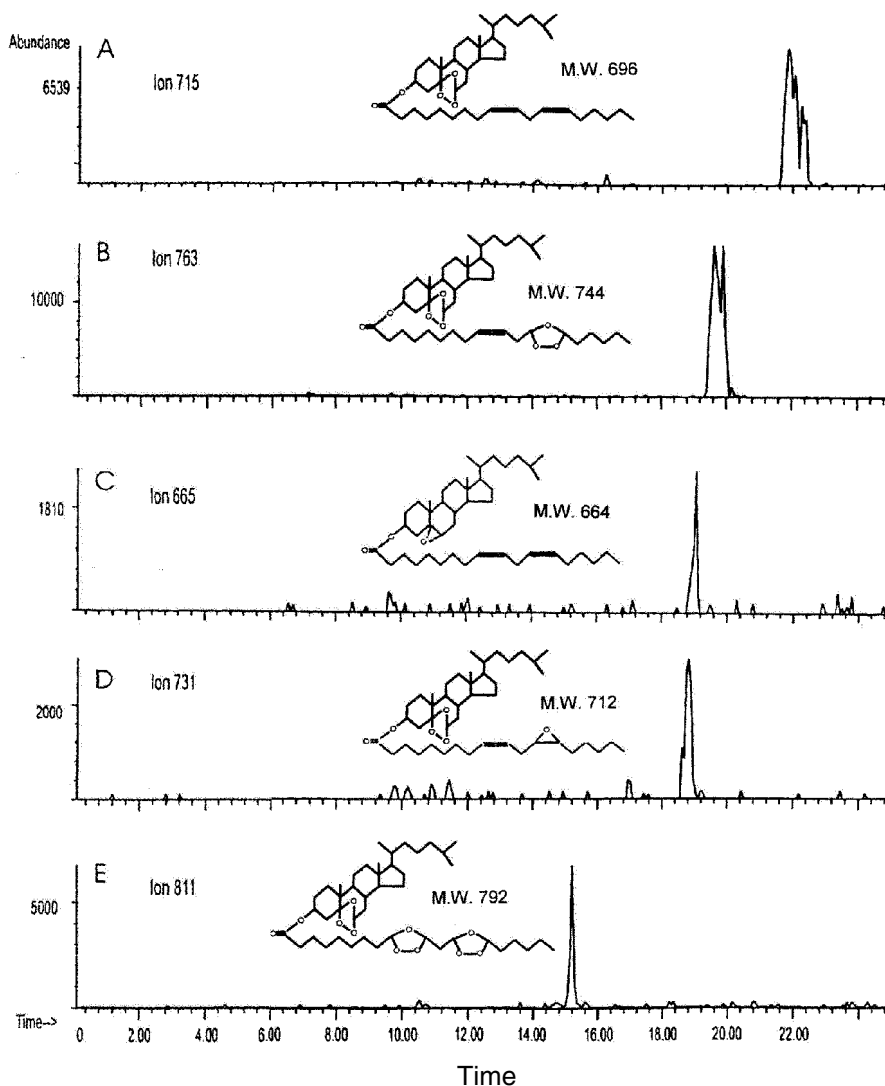


Fig. 4.7. Total positive-ion current profile of initial ozonization products of cholesterol linoleate: Ion m/z 715 ($[696+18]^+$), (5,7 ξ -epidioxy-5 ξ -B-homo-6-oxacholestan)-3 β -linoleate (A); ion m/z 763 ($[744+18]^+$), (B); ion m/z 665 ($[664+11]^+$), 5,6-epoxy-cholesteryl-3 β -linoleate (C); ion m/z 731 ($[712+18]^+$), (5,7 ξ -epidioxy-5 ξ -B-homo-6-oxacholestan)-3 β -linoleate mono-epoxide (D); ion m/z 811 ($[792+18]^+$), (5,7 ξ -epidioxy-5 ξ -B-homo-6-oxacholestan)-3 β -linoleate diozonide (E). The tentative structures of the ions are given in the figure. HPLC/ESI-MS conditions are as in Figure 4.6. *Source:* Herrera *et al.* (42).

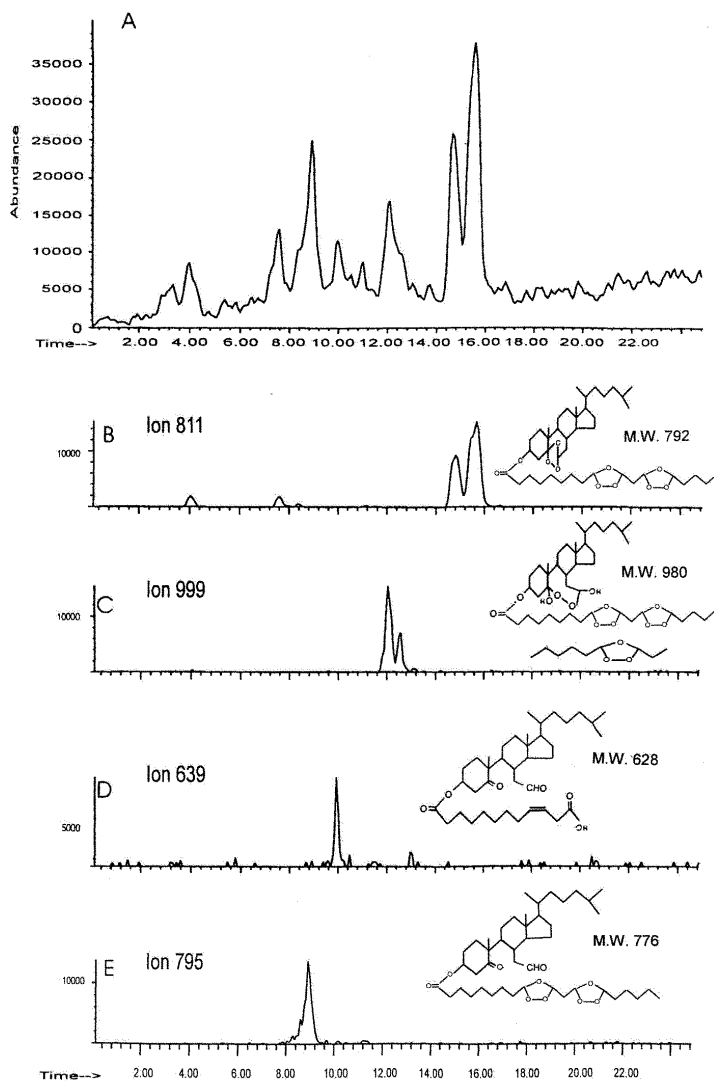


Fig. 4.8. Reversed-phase LC/ESI-MS of the major products of ozonization of cholesterol linoleate. Total positive-ion current profile of cholesterol linoleate (A); single-ion mass chromatograms of the four major $[M+H]^+$ ions (B–E). Peak identification: m/z 811 ($[792+18]^+$), (5,7 ξ -epidioxy-5 ξ -B-homo-6-oxacholestan)-3 β -linoleate diozonide (B); ion m/z 999 ($[980+18]^+$), (6-alkoxy-5,6-epidioxy-5-hydroxy-5,6-secocholesterlyl)-3 β -linoleate diozonide with a monounsaturated nine carbon ozonide as the alkoxy group (C); ion m/z 647 ($[620+18]^+$), (5-oxo-5,6-secocholestan-6-al)-3 β -dodecadienoate (D); ion m/z 795 ($[776+18]^+$) (5-oxo-5,6-secocholestan-6-al)-3 β -linoleate diozonide (E). The tentative structures of the ions are given in the figure. HPLC/ESI-MS conditions are as in Figure 4.6. Source: Herrera *et al.* (42).

arations were performed on an HP-1090 liquid chromatograph equipped with a reversed-phase C₁₈ Supelcosil column (4.6 mm × 250 mm), which was eluted with a gradient of 20–80% 2-propanol in MeOH over 30 min. The oxo-TAG were identified by LC/TSI-MS. A solution of 0.2 M NH₄Ac/MeOH 1:1 (vol/vol) was added to the postcolumn flow at a rate of 0.2 mL/min. The oxo-TAG were identified on the basis of the single-ion mass chromatograms for the major peroxidation products of 18:2/18:1/16:0 present in specific TLC bands.

Kusaka *et al.* (44) reported compositional analysis of normal plant TAG (corn, olive, and perilla) and hydroperoxidized *rac*-1-stearoyl-2-oleoyl-3-linoleoyl-*sn*-glycerols by HPLC in combination with APCI-MS (LC/APCI-MS). TAG irradiated with a tungsten lamp (40 W) gave characteristic fragment ions [M–H₂O₂+H]⁺, [M–H₂O+H]⁺, and [M–R₁(R₃)COOH–H₂O+H]⁺, which could be used to discriminate between FA in *sn*-1- (or *sn*-3-) and *sn*-2-positions. The analyses were performed on a Hitachi (Tokyo, Japan) M-2000 double-focusing mass spectrometer equipped with a Hitachi L-6200 HPLC instrument and a Hitachi APCI interface system. A Cosmosil ₅C₁₈-packed column with 5-μm particles (250 × 4.6 mm i.d.) was used with hexane/MeCN/2-propanol (10:80:10, by vol) as a mobile phase. LC/APCI-MS of the plant TAG gave mass spectra with peaks of [M+H]⁺ and [M–R₁(R₃)COOH+H]⁺ ions, in which [M+H]⁺ and R₁(R₃)COOH represented, respectively, the protonated molecule and FA at the *sn*-1- (or *sn*-3-) position of the TAG. It was possible to discriminate between FA in *sn*-1- (or *sn*-3-) and 2-positions. LC/APCI-MS of hydroperoxidized TAG gave characteristic fragment ions [M–H₂O₂+H]⁺, [M–H₂O+H]⁺, and [M–R₁(R₃)COOH–H₂O+H]⁺.

The *tert*-BOOH/Fe²⁺ oxidation products of unsaturated TAG contained high molecular weight derivatives other than hydroperoxides and core aldehydes, which could not be readily identified in the absence of synthetic standards. Sjovalld *et al.* (45) reported the conversion of synthetic TAG of known structure to hydroperoxides, hydroxides, epoxides, and core aldehydes and their DNPH derivatives by published procedures. The oxo-TAG standards were resolved by normal-phase HPLC, and the identities of the oxo-TAG confirmed by LC/ESI-MS. Elution factors of oxo-TAG were determined in relation to a homologous series of saturated TAG, ranging from 24 to 54 acyl carbons, as analyzed by reversed-phase HPLC, using a Supelcosil LC-18 column (250 mm × 4.6 mm i.d.) and a gradient of 20–80% 2-propanol in MeOH as the eluting solvent (0.85 mL/min) and an ELSD. A total of 31 incremental elution factors were calculated from the chromatography of 33 oxygenated and nonoxygenated TAG species, ranging in carbon number from 36 to 54 and in double bond number from 0 to 6. Sjovalld *et al.* (45) used plots of theoretical carbon numbers (TCN) versus retention times of reference compounds along with a series of saturated monoacid TAG as an aid in the peak identification. TCN and correction factors were calculated for oxo-TAG and unsaturated TAG using saturated TAG to provide a reference curve. Unsaturated and oxo-TAG were coinjected individually or in small sets with the series of saturated TAG. Sjovalld *et al.* (46) used the elution factors to tentatively identify the lipid ester hydroperoxides and

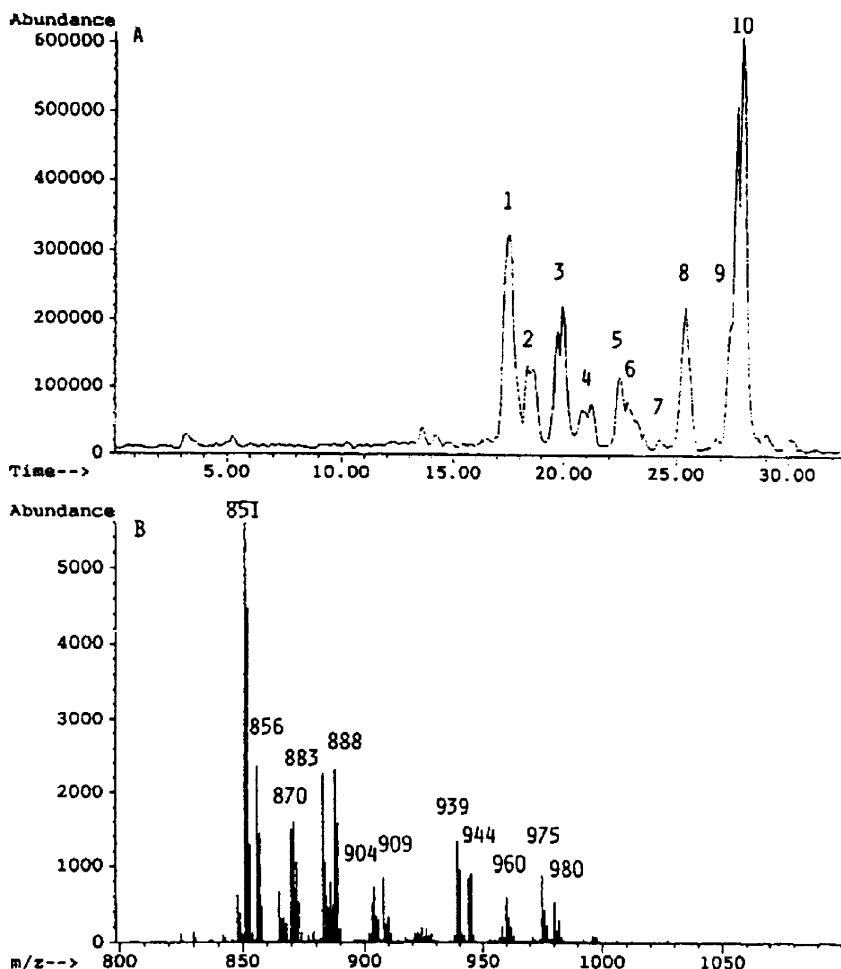


Fig. 4.9. (A) Reversed-phase LC/ESI-MS profile of the oxidation products of 18:1/16:0/16:0 following a 30-h exposure at 37°C to 7.2 M *tert*-BOOH. (B) Average mass spectrum over the elution time (13.314–30.720 min) of the oxotriacylglycerol derivatives. (C) Single-ion chromatograms for the major ions (nominal masses) m/z 882, 902, 864, 1026, 938, and 850, tentatively identified as shown in the figure. Peak identification: 1, 18:1/16:0/16:0, OOH; 2, 18:0/ 16:0/16:0, OOH, epoxy; 3, 18:1/16:0/16:0, epoxy; 4, 18:1/16:0/16:0, epoxy; 5, 18:0/ 16:0/16:0, epoxy; 6, 18:1/16:0/16:0, TBHP (tert-butylhydroperoxide); 7, 18:2/16:0/16:0, diTBHP; 8, 18:1/16:0/18:0, TBHP; 9, 18:1/16:0/18:0, TBHP; 10, 18:1/16:0/16:0. LC/ESI-MS conditions: Column, Supelcosil LC-18 (250 × 4.6 mm i.d.); mobile phase, linear gradient of 20–80% 2-propanol in MeOH (0.85 mL/min) in 30 min; instrumentation, HP model 1090 liquid chromatograph interfaced with a nebulizer-assisted ESI source connected to an HP model 5989A quadrupole mass spectrometer. *Source:* Sjovall *et al.* (47). (continued)

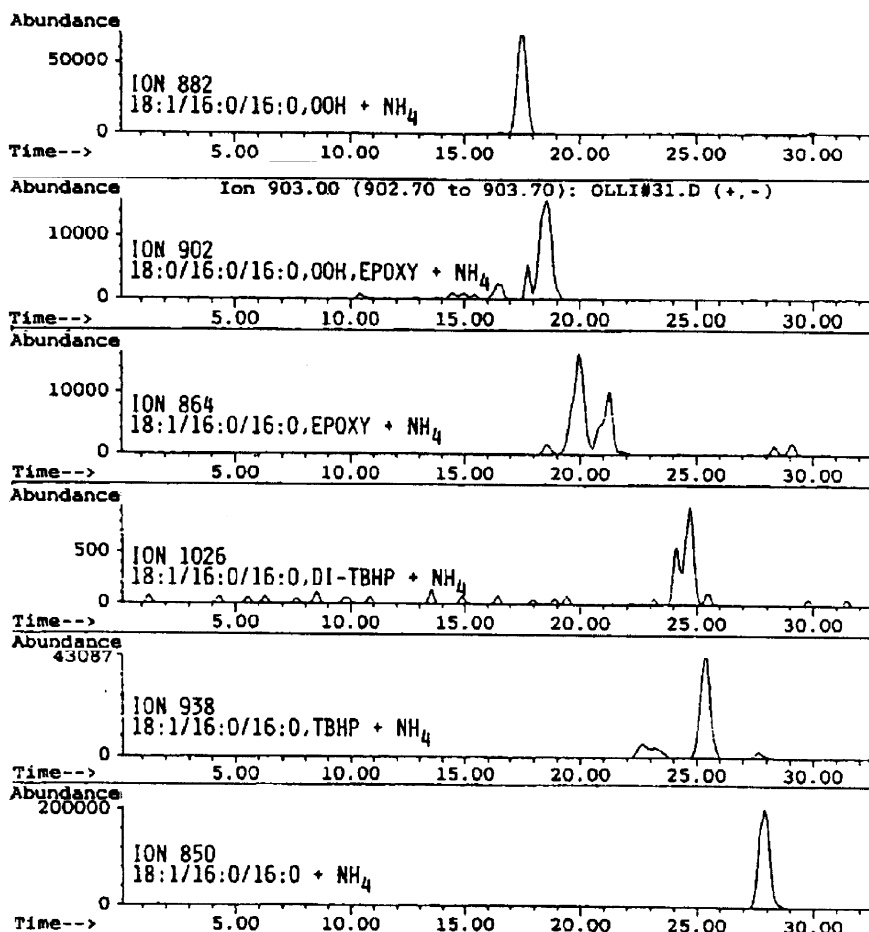


Fig. 4.9. (continued)

core aldehydes resolved by HPLC from oxidized triacylglycerols of Baltic herring oil. Later Sjovall *et al.* (47) used reversed-phase HPLC to separate and tentatively identify the oxidation products based on relative retention times of standards and the estimated elution factors for functional groups and their positional distribution in *tert*-BOOH/Fe²⁺-treated corn oil. Hydroperoxides, diepoxides, and hydroxides were the major components of the oxidation mixture (50–95% of total). Previously unidentified peroxide-bridged *tert*-butyl adducts were present in significant amounts (5–50% of total oxidation products) in all preparations. The tentative reversed-phase HPLC identification of the adducts was confirmed by determining the molecular mass of each component by on-line ESI-MS. Figure 4.9 shows the reversed-phase LC/ESI-MS profile of the *tert*-BOOH oxidation products of

18:1/16:0/16:0 (Fig. 4.9A), along with the full mass spectrum (Fig. 4.9B) averaged over the elution range of the oxoacylglycerols. The chromatogram is complex and in contrast to the relatively simple full mass spectrum, which includes both ammonia and sodium adducts. Figure 4.9C shows the single-ion mass chromatograms for the major ions (as ammonia adducts) at m/z 882, 902, 864, 1026, 938, and 850 arranged in order of increasing retention time (47). The figure includes the tentative structures that best correspond to the chromatographic and mass spectrometric properties of the oxidized 16:0/16:0/18:1. Reduction of the oxidized 16:0/16:0/18:1 with NaCNBH_3 led to the conversion of the monohydroperoxides into the monohydroxides (m/z 866) and of the mono- and di-*tert*-BOOH derivatives into the corresponding mono- and dihydroxide derivatives (m/z 866 and 882, respectively).

Figure 4.10 shows the reversed-phase LC/ESI-MS profile of the products for the more extensively oxidized 18:0/18:0/18:2 (Fig. 4.10A), along with the full mass spectrum (Fig. 4.10B) averaged over the elution time (13.59–33.36 min) of the oxoacylglycerol derivatives. Figure 4.10C shows the single-ion mass chromatograms for the major ions as ammonia adducts at m/z 1058, 952, 1024, 936, and 1114 arranged in order of increasing HPLC elution time. Figure 4.10D shows the single-ion mass chromatograms for the remaining major ions as the ammonia adducts (m/z 918, 1080, 992, 1170, and 904) in the total mass spectrum of the 18:0/18:0/18:2 oxidation products (47). The figures show the tentative structures that best correspond to the chromatographic and mass spectrometric properties of the oxo-TAG. Reduction of the oxidized 18:0/18:0/18:2 with NaCNBH_3 led to the conversion of the hydroperoxides and diepoxides to the corresponding monohydroxides (m/z 920, as ammonia adduct), dihydroxides (m/z 936, as ammonia adduct), and hydroxy epoxides (m/z 936, as ammonia adduct). The *tert*-BOOH bridges were also reduced to the corresponding hydroxides as indicated by the increase in the proportion of the hydroxides.

Figure 4.11 shows the total positive-ion current profile of the *tert*-BOOH adducts of *tert*-BOOH oxidized corn oil (Fig. 4.11A) as obtained by reversed-phase LC/ESI-MS, along with the full mass spectrum (m/z 700–1400) averaged over the entire elution profile (Fig. 4.11B). The total ion current profile of native corn oil overlaps partly with that of the total oxidized corn oil, suggesting the presence of residual TAG. Figure 4.11C shows the single-ion mass chromatograms for the six major residual TAG masses (48). In order of decreasing retention time they are: m/z 933 (18:0/18:1/20:1), m/z 931 (a, 18:1/18:1/20:1; b, 20:0/18:2/18:1), m/z 929 (20:0/18:2/18:2), m/z 877 (a, 16:0/18:1/18:1; b, 16:0/18:2/18:0), m/z 875 (16:0/18:2/18:1), and m/z 873 (16:0/18:2/18:2). Figure 4.11D shows the single-ion mass chromatograms for the mono-*tert*-BOOH adducts of the six major residual TAG shown in Figure 4.11C, while Figure 4.11E shows the single-ion mass chromatograms for the di-*tert*-BOOH adducts of the six major residual TAG shown in Figure 4.11C (48). The peaks were identified by combining the data from TLC, HPLC with ELSD, and the masses provided by ESI-MS. It was concluded that stable adduct formation is an unavoidable complication of preparing TAG by oxidation with strong *tert*-BOOH solutions.

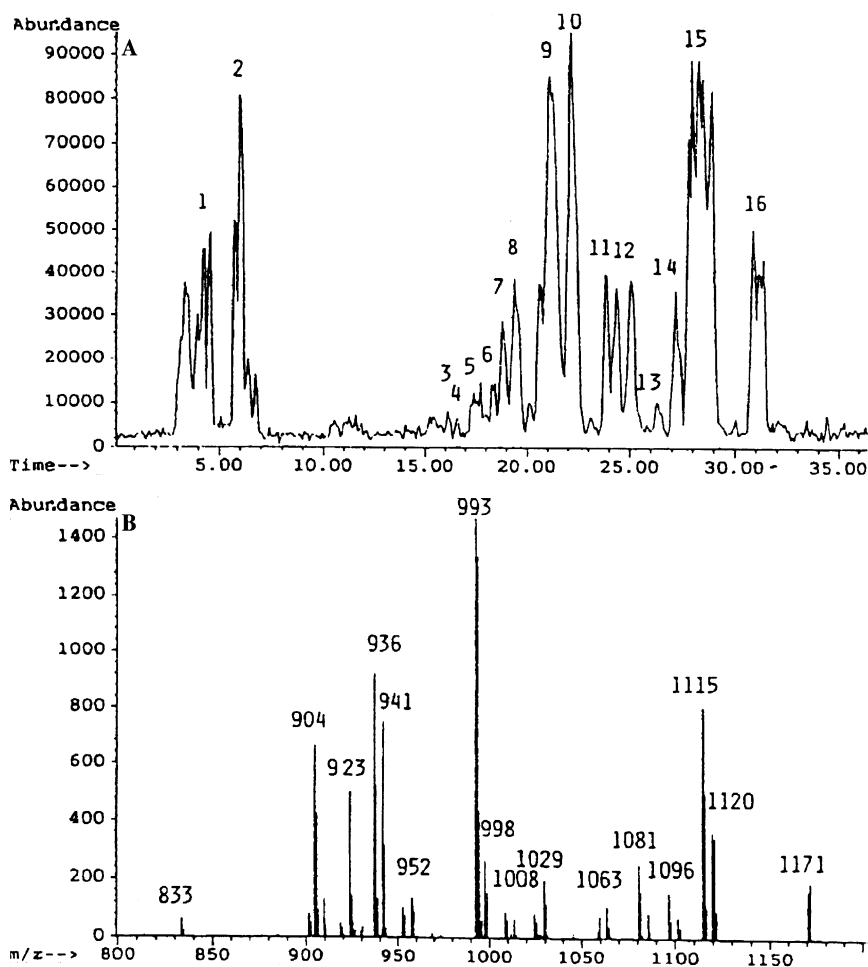


Fig. 4.10. Reversed-phase LC/ESI-MS (A) profile of the oxidation products of 18:0/18:0/18:2 following a 45-min exposure at 37°C to 7.2 M *tert*-BOOH (TBHP) along with the full mass spectrum (B) averaged over the elution time (13.587–33.362 min) of the oxo-TAG derivatives. Peaks were identified by combined TLC, reversed-phase HPLC retention factors of standards, and LC/ESI-MS as follows: 1–5, free FA and mono- and diacylglycerol derivatives; 6, 18:0/18:0/18:1, OOH,O-O,TBHP adduct; 7, 18:0/18:0/18:1,OOH,epoxy; 8, 18:0/18:0/18:2,OOH,THBP adduct; 9, 18:0/18:0/18:1,OOH; 10, 18:0/18:0/18:1,O-O, di-TBHP adduct; 11, 18:0/18:0/18:3,epoxy; 14, 18:0/18:0/18:2, di-TBHP adduct; 15, 18:0/18:0/18:2,TBHP adduct; 15, 18:0/18:0/18:1,tri-TBHP adduct; 16, 18:0/18:0/18:2. OOH, hydroperoxide; O-O, cyclic peroxide. All ion masses are rounded values. Other LC/ESI-MS conditions were as given in Figure 4.9. *Source: Sjovall et al. (47).*

(continued)

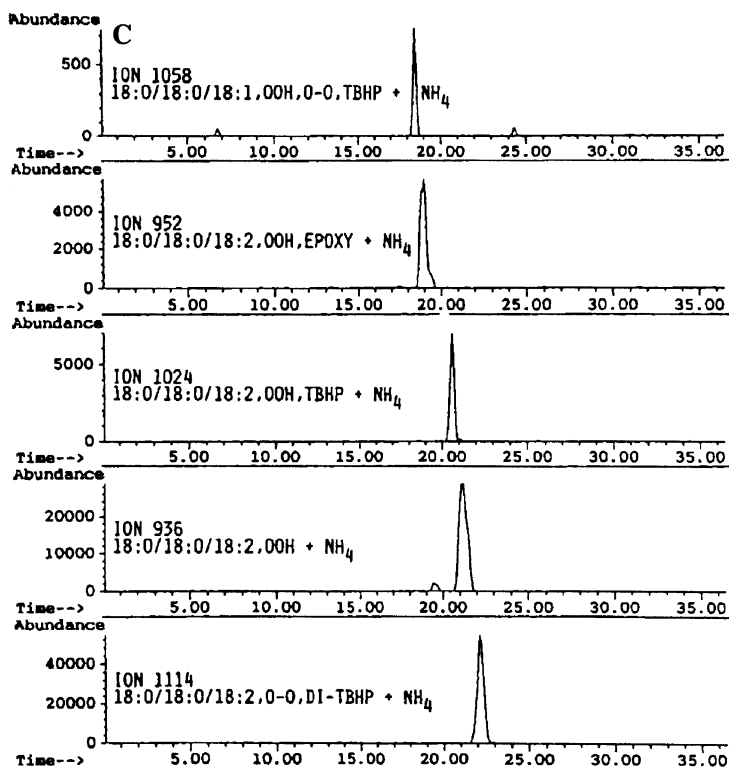


Fig. 4.10. (C) Single-ion mass chromatograms for the major ions m/z 1058, 952, 1024, 936, and 1114. (continued)

Kozak *et al.* (49) used LC/ESI-MS/MS to demonstrate that 2-arachidonoyl-glycerol (2-AG) is a substrate for cyclooxygenase 2 (COX-2), which provides the novel lipid prostaglandin H₂ glycerol ester (PGH₂-G) *in vitro* and in cultured macrophages. LC/MS was conducted with a Waters 2690 Separations Module with a Zorbax RX-C18 narrow-bore column (15 cm × 2.1 mm, 5 μm) interfaced to a Finnigan TSQ-7000 triple-quadrupole mass spectrometer. Sodiated analytes were eluted with increasing concentrations of MeCN in 0.001% aqueous NaOAc. Selected ion monitoring and quantification was accomplished by using pentadeuterated glyceryl prostaglandin standards. CID was accomplished with Ar as the collision gas.

Isoprostanes, Neuroprostanes, and Dinorprostanes

The polyunsaturated FA 20:4n6, 20:5n3, and 22:6n3 are predominantly incorporated into glycerophospholipids, but 11–18% of 22:6n3 may be found to be taken up

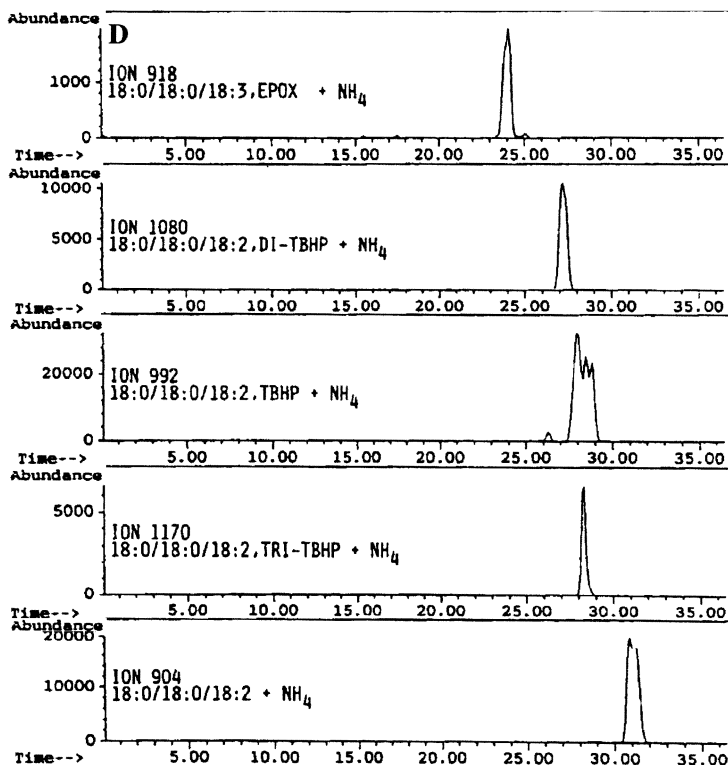
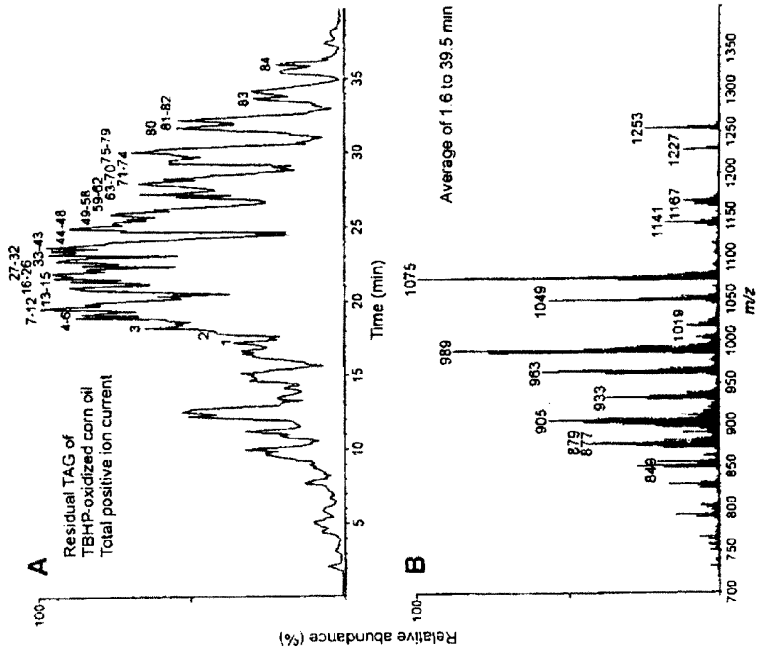
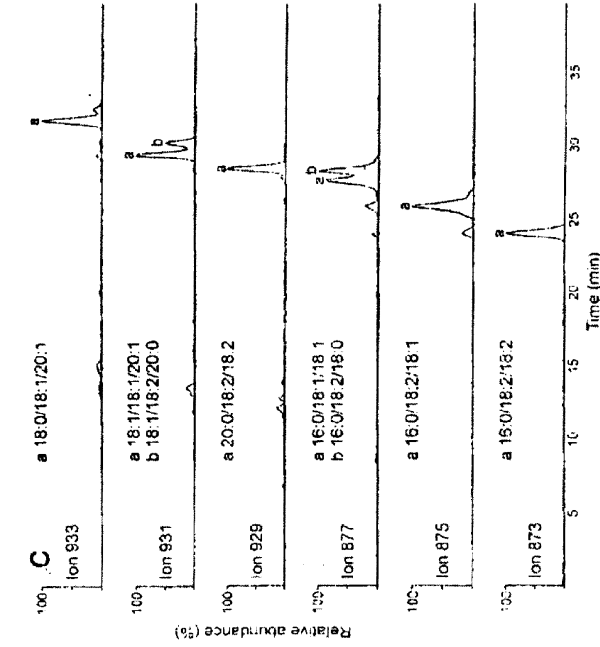


Fig. 4.10. (D) Single-ion mass chromatograms for the major ions m/z 918, 1080, 992, 1170, and 904.

into neutral lipid pools of the brain (50). These acids in their various ester forms would be anticipated to be subject to the oxidative influences demonstrated for the polyunsaturated glycerophospholipids (20). However, no specific reports of isoprostane or neuroprostane containing cholesteryl esters or triacylglycerols would appear to have been reported. Likewise, the 18:3 n 3 containing TAG of plant tissues would be expected to yield dinorprostane-containing acylglycerols, which also have not been reported, although the corresponding glycerophospholipids are known (51).

Core Aldehydes

Since the core aldehydes retain the core structure of corresponding oxidized polyunsaturated fatty acid esters, the HPLC methods for their analysis are essentially those developed for the separation of their parent compounds. Due to the high natural abundance and ready oxidation, the linoleate and arachidonate esters of cholesterol and GroPCho constitute the main sources of the 9-oxononanoyl and 5-oxopentanoyl core aldehydes, respectively.



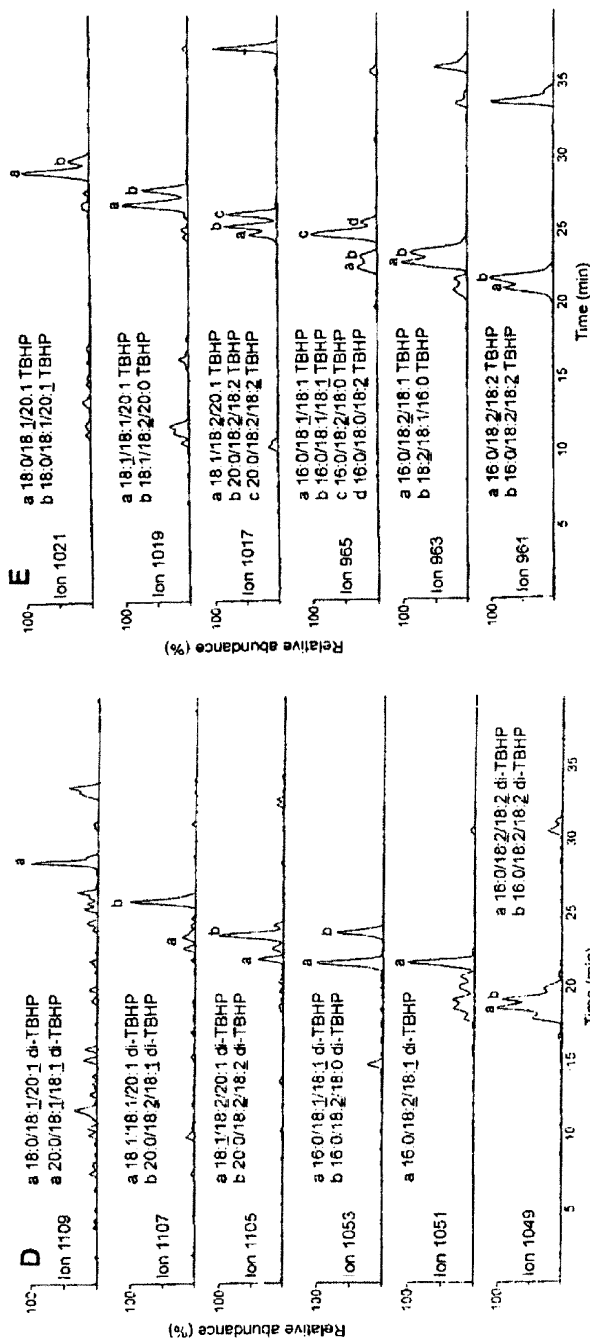


Fig. 4.11. Total positive-ion current profile of TLC Band 10 as obtained by reversed-phase LC/ESI-MS (A) along with the full mass spectrum (m/z 700–1400) averaged over the entire elution profile (B); single-ion mass chromatograms for the six major residual TAG masses (C); single-ion mass chromatograms for the mono-TBHP adducts of the six major residual TAG in C (D); single-ion mass chromatograms for the di-TBHP adducts of the six major residual TAG shown in C (E). Other LC/ESI-MS conditions were as given in Figure 4.9. Source: Sjovall *et al.* (48).

Kuksis *et al.* (16) used reversed-phase HPLC to identify mixed hydroperoxide and core aldehyde derivatives of synthetic and natural TAG following reaction with the *tert*-BOOH/Fe²⁺ reagent. The oxidation products were extracted with CHCl₃/MeOH, reacted with DNPH, and resolved by normal-phase TLC into fractions depending on the number of hydrazone derivatives formed. The individual TLC bands were examined by reversed-phase HPLC with on-line TSI-MS. The HPLC separations were performed on an HP-1090 liquid chromatograph equipped with a reversed-phase C-18 Supelcosil column (4.6 × 250 mm), which was eluted with a gradient of 20–80% 2-propanol in MeOH over 30 min. A solution of 0.2 M NH₄Ac/MeOH 1:1 (vol/vol) was added to the postcolumn flow at a rate of 0.2 mL/min.

Ravandi *et al.* (52) used reductive ozonolysis to prepare synthetic TAG containing one, two, and three core aldehyde groups per TAG molecule. These core aldehydes were isolated by TLC as the DNPH derivatives and their structures were confirmed by HPLC with on-line TSI-MS. Single-ion mass chromatograms and full mass spectra showed the presence of TAG containing one and two aldehyde groups per TAG molecule. The HPLC separations were obtained using a gradient of the 20–80% 2-propanol/MeOH system described by Kuksis *et al.* (16). Kurvinen *et al.* (53) used comparable HPLC methods to prepare and characterize the core aldehydes of monoacylglycerol (MAG) molecules as the DNPH derivatives. Figure 4.12 shows the total positive-ion current chromatogram obtained by reversed-phase LC/ESI-MS for the reduced Schiff base of triglycine (GGG) and 2-MAG-ALD (A) and the full mass spectrum averaged over the Schiff base peak (B). The Schiff base adduct of GGG eluted at the beginning of the run (2.2 min), but not with the solvent front. The adducts of GGH and GHK eluted at 2.0 and 2.1 min, respectively. The total mass spectrum averaged over the NaCNBH₃-reduced Schiff base peak of GGG and 2-MAG-ALD showed the [M+1]⁺ protonated molecule to be the major ion of reaction products at *m/z* 420. The monosodium adduct of the reduced Schiff base was detected at *m/z* 442 with approximately half the intensity of the protonated molecule, whereas the intensity of the ion for the disodiated adduct at *m/z* 464 was even smaller. Ions representing the unreacted triglycine were *m/z* 190, 212, and 234, corresponding to [M+1]⁺, [M+Na]⁺, and [M+2Na]⁺ ions, respectively. Kurvinen *et al.* (53) used similar LC/ESI-MS methods to demonstrate the formation of the 2-MAG-ALD adducts of valine, lysine, as well as phosphatidylethanolamine (PtdEtn), in addition to the three tripeptides.

Steenhorst-Slikkerveer *et al.* (54) analyzed the nonvolatile lipid oxidation products in vegetable oils by normal-phase LC/MS. This resulted in a separation into classes of TAG oxidation products, such as epoxy-, oxo-, hydroperoxy-, hydroxy-, and “2¹/₂” glycerides, which were identified by SIM. LC-MS was performed on an HP 1100 LC/MSD, which was operated using a binary high-pressure pump, an autoinjector, a thermostated column, and a diode-array detector. Downstream of the diode-array detector, 0.15 mM NaI in EtOH/MeOH 1:1 (vol/vol) was added at 100 μL/min to the eluant flow by means of another HPLC pump. The HPLC separations were performed on a Waters Diol column (200 × 3 mm i.d.). The mobile phase gradient started with hexane and proceeded to a mixture of hexane/methyl

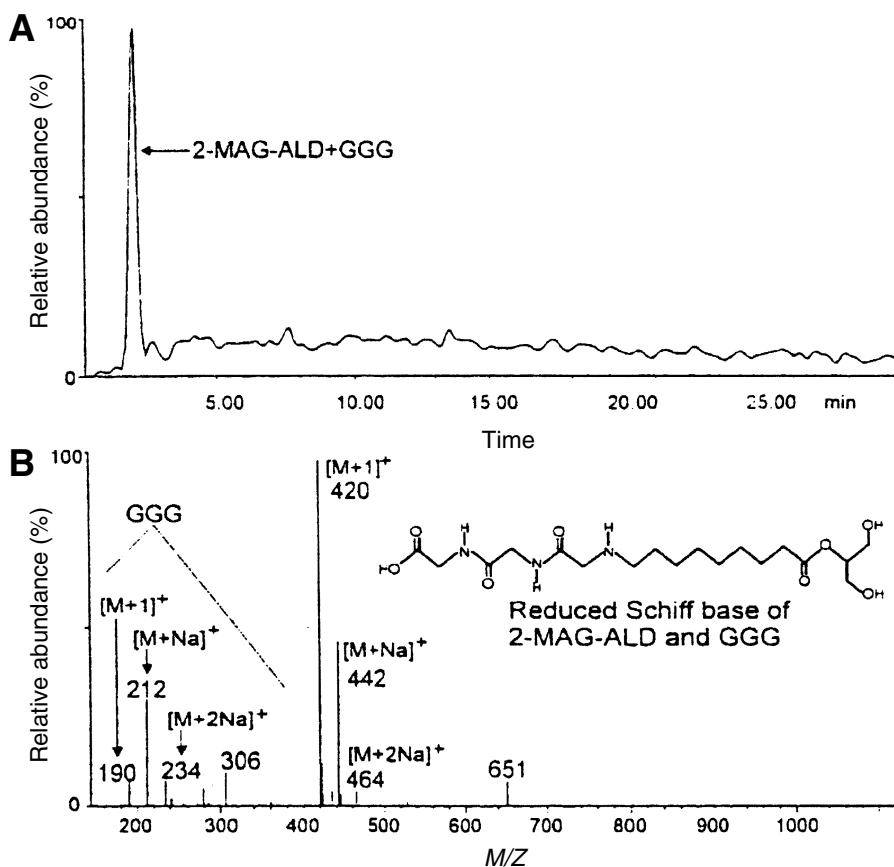


Fig. 4.12. Reversed-phase LC/ESI-MS of sodium cyanoborohydride-reduced Schiff base of 2-MAG-ALD and triglycine (GGG). Total positive-ion current chromatogram (A) and total mass spectrum of Schiff base peak (B). Ions are identified in figures and discussed further in text. LC/ESI-MS instrumentation: HP Liquid chromatograph 1090 equipped with a silica column (Supelcosil LC-Si, 5 μ m, 250 \times 4.6 mm i.d.) and connected to an HP 5989A quadrupole mass spectrometer equipped with a nebulizer-assisted ESI interface; mobile phase, a linear gradient from 5% NH_4OH in $\text{H}_2\text{O}/\text{MeOH}/\text{hexane}$ (12:88:0, by vol, to 0:88:12, by vol) in 17 min after holding the starting composition for 3 min. *Source:* Kurvinen *et al.* (53).

tert-butyl ether (MTBE) or hexane/isopropyl alcohol (IPA). When these non-volatile lipid oxidation products were analyzed by reversed-phase HPLC, the various species present were separated according to class [OOH-TAG, hydroxy-TAG (OH-TAG), epoxy-TAG, etc.] and size [OOH-18:2/18:2/18:2, OOH18:1/18:2/18:2, OOH-18:1/18:1/18:2, etc.] (55). For the analysis of oxidation products originating from a single polyunsaturated parent TAG species, the reversed-phase HPLC yielded

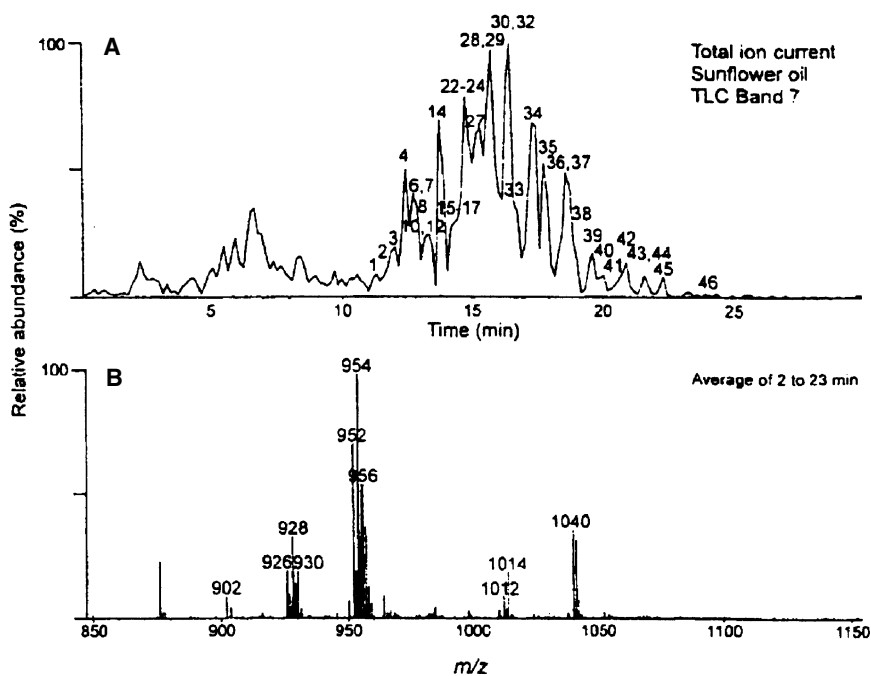


Fig. 4.13. (A) Total negative-ion current profile of TLC band 7 of the DNPH derivatives of oxidized sunflower seed oil. (B) The full mass spectrum averaged over the core aldehyde elution range (2–23 min). (C) The mass chromatograms of major ions of (9-oxo)nonanoyl acylglycerols as DNPH derivatives from TLC band 7 of oxidized sunflower oil. The numbered peaks in (A) represent TAG that contain a least one core aldehyde function per molecule along with some TBHP adducts. Unnumbered early peaks in (A) represent hydrazones of short-chain aldehydes. LC/ESI-MS conditions were as given in Figure 4.9. *Source:* Sjovall *et al.* (56).

(continued)

excellent separations, while oxidation products of mixed TAG gave complex chromatograms.

Kuksis (36) and Kamido *et al.* (15,37) recognized the presence of lipid ester hydroperoxides and core aldehydes among the TAG peroxidation products isolated from liposomal and LDL preparations. Kuksis *et al.* (16) identified mixed hydroperoxide and core aldehyde derivatives of synthetic and natural TAG following reaction with *tert*-BOOH and Fe^{2+} ions. The oxidation products were extracted with $\text{CHCl}_3/\text{MeOH}$, resolved by normal-phase TLC, and identified by reversed-phase LC/ESI-MS with negative chemical ionization. The major TAG from 2–4 h of peroxidation of 18:2/18:1/16:0 and corn oil TAG contained one unmodified FA in combination with 9-oxononanoic acid and 9- or 13-hydroperoxy derivatives of

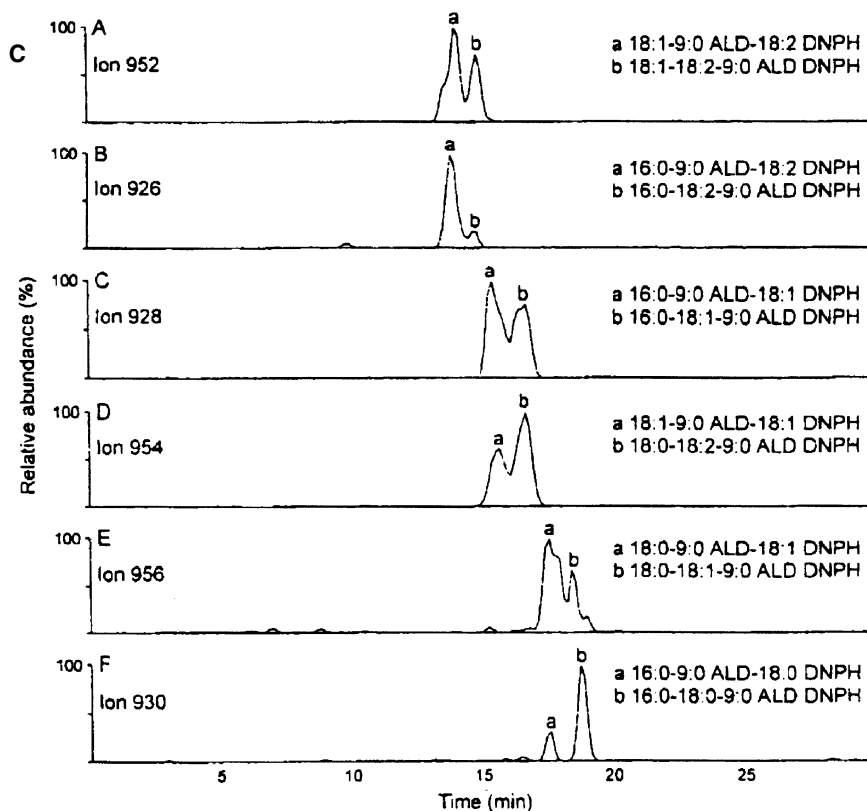


Fig. 4.13. (C) Single-ion mass chromatograms of major ions in Figure 4.13B.

linoleic acid. Molecular species containing combinations of one unmodified acid and two [9-oxo]nonanoic or two hydroperoxy acids were also present in significant amounts in peroxidized corn oil. The core aldehydes were identified as the DNPH derivatives, with the 1-(9-oxo)nonanoyl-2,3-dipalmitoyl-*sn*-glycerol giving a major ion at m/z 901 ($[M-1]^-$ for DNPH) by reversed-phase LC/TSI-MS. A minor ion at m/z 961 was due to an acetate adduct $[M+59]^-$ and another one at m/z 983 was due to the deprotonated adduct of sodium acetate $[M+82-1]^-$. A reversed-phase LC/TSI-MS spectrum of 1,2-di-(9-oxo)nonanoyl-3-palmitoyl-*sn*-glycerol gave an m/z 997 ($[M-1]^-$ for DNPH) as the sole significant ion.

Sjovall *et al.* (56) reported the use of reversed-phase HPLC to investigate the formation of TAG core aldehydes during rapid oxidation of corn and sunflower oils with *tert*-BOOH/ Fe^{2+} . The core aldehydes were isolated as DNPH derivatives by preparative TLC and identified by reversed-phase HPLC with on-line ESI-MS and by reference standards. Using the reversed-phase HPLC system developed earlier (45), a total of 113 species of TAG core aldehydes were specifically identified, accounting for

32–53% of the DNPH-reactive material of high molecular weight (M.W.), representing 25–33% of the total oxidation products. The major core aldehyde species (50–60% of total TAG core aldehydes) were the mono[9-oxo]nonanoyl- and mono[12-oxo]-9,10-epoxy dodecenoyl- or [12-oxo]-9-hydroxy-10,11-dodecenoyl-DAG. Sjovalld *et al.* have since used the above reversed-phase HPLC system to demonstrate significant formation of core aldehydes during rapid oxidation of corn and sunflower oils by *tert*-BOOH/Fe²⁺ reagent (48,55) and during autoxidation of sunflower oil (57). The presence of TAG core aldehydes among the peroxidation products of vegetable oils has been demonstrated using APCI by Byrdwell and Neff (58).

Sjovalld *et al.* (56) determined the core aldehydes of natural TAG as the DNPH derivatives by reversed-phase LC/ESI-MS. The total negative-ion elution profile of the DNPH derivatives of oxidized sunflower oil TAG showed several clusters of peaks. These clusters were resolved by normal-phase TLC and, after elution from the silica gel, were subjected to reversed-phase LC/ESI-MS. Figure 4.13 shows the total negative-ion current profile of TLC band 7 (Fig. 4.13A) and the full mass spectrum (Fig. 4.13B) averaged over the core aldehyde elution range (2–23 min). The complex profile of the chromatogram is deceptive in view of the relative simplicity of the total mass spectrum, which shows major ions at *m/z* 928, 952, 954, and 956, with minor ions at *m/z* 876, 1014, and 1040. The peak complexity is due to the chromatographic resolution of the regio- and geometric isomers of the DNPH derivatives of the core aldehydes, which possess identical molecular masses, as shown in Figure 4.13C for simple core aldehyde peaks eluted over the period of 14.2–18.8 min. The ion identification is given in the figure. In addition to 9:0 core aldehydes, a series of compounds was found to correspond to 8:0 core aldehydes. However, there were no masses corresponding to the 13:2 and 12:1 core aldehydes in TLC band 7. Recently, Sjovalld *et al.* (57) have reported the tentative identification and quantification of TAG core aldehydes as DNPH derivatives in autoxidized sunflower seed oil by using reversed-phase LC/ESI-MS. In contrast to the samples oxidized by *tert*-BOOH, the autoxidized samples of sunflower oil contained both 12:1 and 13:2 core aldehydes. Under the selected experimental conditions, the single-ion mass chromatograms of the DNPH derivatives of the monoaldehydes representing *sn*-2- and *sn*-1(3)-isomers were fully or partially resolved. Sjovalld *et al.* (57) provided extensive tabulations of the oxo-TAG of autoxidized sunflower oil. Quantitatively the core aldehydes made up 2–12 g/kg of oil by UV detection and 2–9 g/kg of oil by ESI-MS detection, whereas the hydroperoxides measured in the unreduced state by HPLC with ELSD were estimated at 200 g/kg after 18 days of autoxidation (57).

Ozonides

The preparation of ozonides and core aldehydes from the unsaturated TAG was originally used for the characterization of TAG structures by TLC. For this purpose the ozonides were reduced with TPP to yield the TAG and GroPCho containing short-chain aldehyde functions (core aldehyde groups).

Ravandi *et al.* (52) used both normal- and reversed-phase LC/ESI-MS for the separation and identification of the lipid ester ozonides and aldehydes. They have reported the normal-phase HPLC retention times of the mono-, di-, and triozone prepared from unsaturated TAG by partial ozonization (52). The isocratic solvent system for the resolution of TAG ozonides was made up of heptane/2-propyl ether/HOAc 60:40:4, by vol. The ozonides of the TAG migrate more slowly than the parent molecules and are resolved according to the number of substitutions introduced. The HPLC resolution was monitored by ELSD. The identification of the ozonides was confirmed by LC/ESI-MS. Ozonized sunflower oil TAG have been prepared for topical application (OLEOZON) as a registered drug [cited in the study by Jardines *et al.* (59)].

Polar Glycerolipids

Hydroperoxides, Epoxides, and Hydroxides

Porter *et al.* (60) reported the separation of the oxidation products of 1-palmitoyl-2-linoleoyl-GroPCho and of 1-stearoyl-2-arachidonoyl-GroPCho, produced by exposure of the unoxidized phospholipids to a stream of air by using reversed-phase HPLC. A reversed-phase μ Bondapak C₁₈ column was eluted with MeOH/H₂O/CHCl₃ (100:10:10, by vol) to obtain a diene hydroperoxide fraction and an unidentified decomposition product of the diene hydroperoxide fraction. The diene hydroperoxide fraction was shown, by reduction with TPP, hydrolysis with snake venom, and HPLC of the methyl hydroxylinoleates, to be made up of the 13-*cis/trans*-, 13-*trans/trans*-, 9-*trans/cis*-, and 9-*trans/trans*-isomers. The oxidation of 1-stearoyl-2-arachidonoyl-GroPCho yielded several products. Separation of the various oxidation products by HPLC followed by TPP reduction, snake venom hydrolysis, and HPLC analysis of the hydroxy arachidonate methyl esters led to the conclusion that a major fraction containing arachidonic acid ester hydroperoxides as primary products was obtained along with another fraction containing secondary degradation products. With the techniques based on those of Porter *et al.* (60), Hughes *et al.* (61) developed a method for the isolation, identification, and quantification of individual lipid hydroxy acids and have applied this methodology to determine whether lipid hydroxy acids are formed in mouse liver PtdCho following treatment of the animals *in vivo* with CCl₄. Hydroxylated derivatives of 18:2n6, 20:4n6, and 22:6n3 acids were formed as demonstrated by HPLC analyses. HPLC was carried out with a Glenco model HPLPS-1 pumping system, Waters U6K loop injector, and Waters model 450 variable wavelength detector. Two silica gel columns (30 cm \times 3.9 mm i.d., Porasil; Waters) were used in series with hexane/2-propanol/HOAc (995:4:1, by vol) and a flow rate of 2.4 mL/min. The peaks were detected by measuring absorbance at 235 nm. The peaks were identified by determining the fatty acid components by GLC. The hydroperoxide was reduced to the hydroxy acid with TPP. Zhang *et al.* (62) reported the first method to analyze intact hydroxy-

eicosatrienoyl-GroPCho species by fast atom bombardment-MS (FAB-MS). Subsequently, Zhang *et al.* (63) described an LC/TSI-MS technique for the analysis of phospholipid hydroperoxides. Myher *et al.* (23), Kamido *et al.* (37), and Ravandi *et al.* (52,64,65) used on-line TSI-MS and ESI-MS in combination with normal-phase HPLC for the identification of the major hydroperoxides and core aldehydes of PtdCho from oxidized plasma lipoproteins and atheroma. The hydroperoxides and core aldehydes were resolved by normal-phase HPLC using a gradient of $\text{CHCl}_3/\text{MeOH}/\text{NH}_4\text{OH}$ (see previous discussion).

The presence of PtdCho containing hydroxy FA in tissue lipid extracts is frequently attributed to free radical-initiated mechanisms. Ponchaut *et al.* (66) used FAB-MS/MS to identify the molecular species of PtdCho of heart mitochondria. Detailed analysis of the negative-ion mass spectra revealed the presence of six carboxylate ions at m/z 267, 269, 271, 295, 297, and 299, which corresponded to the hydroxyhexadecadienoate, hydroxyhexadecenoate, hydroxyhexadecanoate, hydroxyoctadecadienoate, hydroxyoctadecenoate, and hydroxyoctadecanoate, respectively, as indicated by their fragmentation patterns.

Milne and Porter (67) have reported an improved method for the separation of phospholipid hydroperoxides by reversed-phase HPLC, which, for the first time, separates some of the hydroperoxide isomers along with CIS-MS. CIS-MS can be coupled with reversed-phase HPLC by the addition of AgBF_4 to the mobile phase or to the effluent postcolumn, thus allowing powerful LC/MS techniques to be used to identify complex mixtures of phospholipid hydroperoxides. The HPLC separations were performed with a Discovery C-18 (ODS) column (4.6×250 mm, $5 \mu\text{m}$, Supelco) and operated with a mobile phase of $\text{MeOH}/\text{H}_2\text{O}$ (95:5, vol/vol) at a rate of 1 mL/min. From LC/CIS-MS experiments, the hydroperoxides were isolated from the unoxidized phospholipid using analytical HPLC ($\text{MeOH}/\text{H}_2\text{O}$, 95:5, vol/vol) containing no ion-pairing agent. Under optimal conditions, two resolved hydroperoxide peaks with retention times of 14.04 and 14.97 min were observed by UV detection at 234 nm. To determine the elution order of the four isomeric hydroperoxides of linoleoyl GroPCho, compounds eluting in these peaks were isolated. The collected PtdCho hydroperoxides in each peak were converted to the corresponding hydroperoxyoctadecadienoic (HPDE) methyl esters by reduction with TPP and transesterification. The methyl esters were identified by normal-phase HPLC as described by Porter and Wujek (68). The first peak (14.04 min) was found to contain both the 13-substituted hydroperoxides and the 9-*cis,trans*-hydroperoxide. The second peak (14.97 min) contained only the 9-*trans,trans*-hydroperoxide. The oxidized fraction of 16:0/18:2 GroPCho (13.5–15.5 min) or 16:0/20:4 GroPCho (20–28 min) was collected, concentrated, and analyzed.

After developing a chromatographic method that resolved some of the 16:0/18:2 GroPCho-OOH isomers, Milne and Porter (67) explored the possibility of identifying oxidized PtdCho molecular species without conversion or derivatization, for example, by using CIS-MS, which had proven successful in identifying cholesteryl hydroperoxides. Coupling of HPLC and LC/CIS-MS was achieved either by postcolumn mixing

of 0.50 mM AgBF_4 in MeOH with the HPLC effluent or by adding AgBF_4 to the HPLC mobile phase to yield a 0.15 mM solution. Chromatography was performed using the Supelco Discovery C1-18 analytical column with a mobile phase of MeOH/ H_2O (95:5, vol/vol) at a flow rate of 1 mL/min. Characteristic chromatograms were obtained for a mixture of 16:0/18:2 GroPCho-OOH. The peaks were identified by MS in the SRM mode. In this mode, a specific precursor-to-product mass conversion produced at a characteristic energy in the collision cell is monitored. SRM separates the differently substituted hydroperoxides based on the difference in their Hock fragments. LC/CIS-MS experiments were also used to identify the 11-substituted hydroperoxide of 16:0/18:2 GroPCho. Milne and Porter (67) applied similar methods to the study of 18:0/20:4 GroPCho. A UV profile obtained for the six hydroperoxides of 18:0/20:4 GroPCho was compared with a chromatogram of the corresponding alcohols obtained by reduction of the hydroperoxides with TPP. The elution order of the alcohols was identical to that of the hydroperoxides. The various hydroperoxides were identified by SRM because their Hock fragments were either unique or similar for specific structures. These hydroperoxides were distinguished from each other by monitoring unique minor fragments. When natural phospholipids are oxidized to the hydroperoxides, diastereomers are formed because oxygen addition can occur to either face of the pentadienyl radical and unoxidized phospholipids have a chiral center at C_2 of the glycerol backbone, with a configuration of *R*. Surprisingly, the separation of the diastereomers was seen only for the 9-hydroperoxyeicosatetraenoyl-GroPCho (9-HPETE-GroPCho) and not for the other HPETE-GroPCho isomers (Fig. 4.14).

Since the polyunsaturated FA become hydroxylated following their release from the glycerophospholipids by phospholipase A_2 , the hydroxy FA have been identified by LC/ESI-MS/MS in the free form. Nakamura *et al.* (69) used LC/ESI-MS/MS to analyze epoxyeicosatrienoic (EET) acids and monohydroxyeicosatetraenoic acids (HETE) isolated from human red blood cell (RBC) membranes following base hydrolysis. ESI resulted in the formation of an abundant isobaric carboxylate anion at m/z 319 for both of these oxidized metabolites of arachidonic acid. The product ion spectra from the collision-induced dissociation of this carboxylate anion could be used to identify each of the isomeric eicosanoids from the unique fragment ions of each eicosanoid. The observed product ion spectra were identical with those previously obtained by FAB-MS, but ESI required less EET and HETE for analysis. Both EET and HETE phospholipids were present in human RBC; their abundances could be substantially increased by treatment under conditions that would induce free radical oxidation of membrane phospholipids. Thus, following incubation of human RBC with *tert*-BOOH, phospholipids were extracted and purified by normal-phase HPLC to yield PtdEtn, phosphatidylserine (PtdSer), and phosphatidylcholine (PtdCho). Each class of phospholipid was hydrolyzed to yield the free carboxylic acid before on-line LC/ESI-MS/MS. Figure 4.15 shows the ESI-MS/MS analysis of EET, HETE (m/z 319), and $[^{18}\text{O}_2]_{12}$ -HETE (m/z 323) standards *via* reversed-phase HPLC (69).

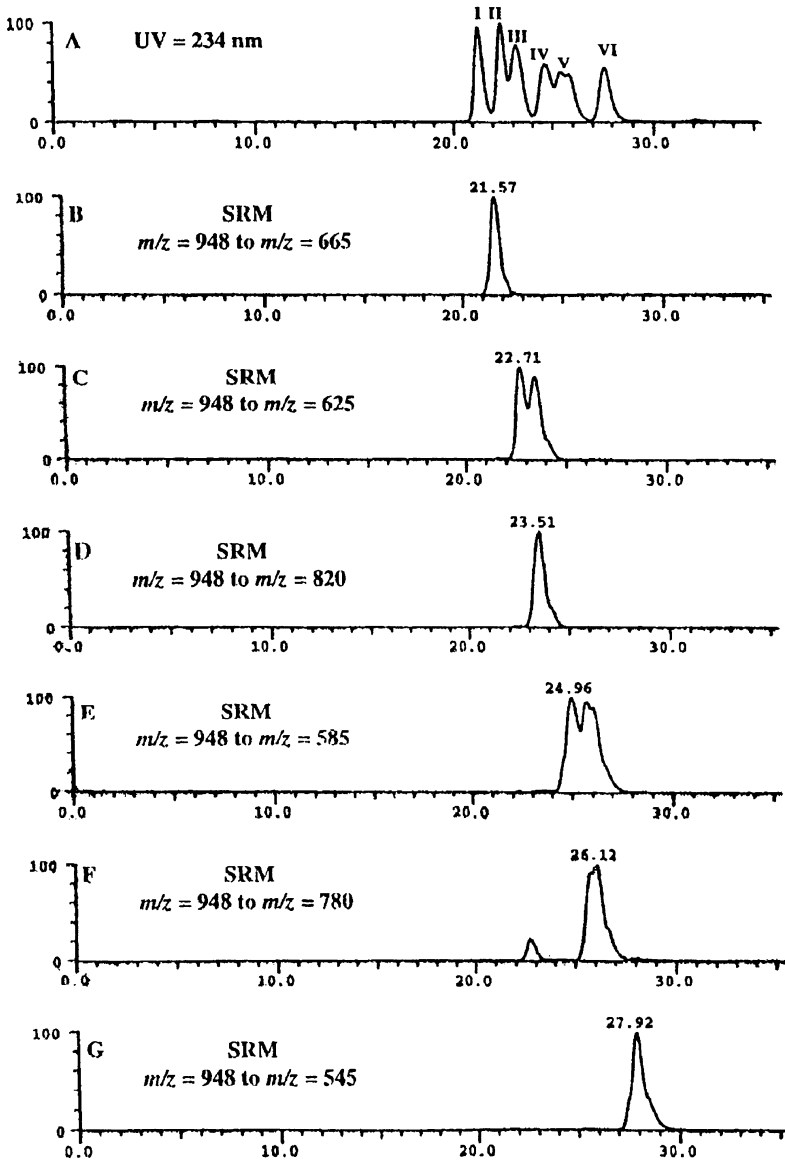


Fig. 4.14. Chromatograms of the product mixture obtained from a 24-h oxidation of 1-stearoyl-2-arachidoyl-*sn*-glycero-3-phosphocholine containing 0.1 equivalents of pentamethylchromanol (mobile phase, MeOH/H₂O, 95:5, vol/vol; Discovery C18 analytical column, Supelco), (A) UV detection at 234 nm: I = 15-HPETE PC; II = 11-HPETE PC; III = 12-HPETE PC; IV = 8-HPETE PC; V = 9-HETE PC; VI = 5-HPETE PC; B–G, HPLC/CIS-MS in SRM mode. HPETE, hydroperoxyeicosatetraenoic acid; PC, PtdCho. *Source:* Milne and Porter (67).

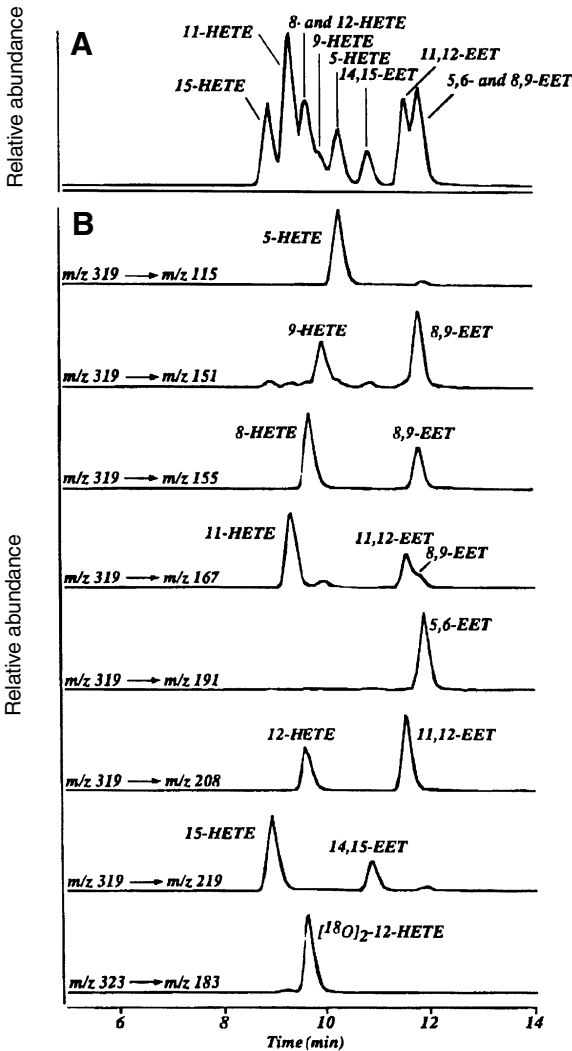


Fig. 4.15. LC/ESI-MS/MS analysis of EET, HETE (m/z 319), and [$^{18}\text{O}_2$]-12-HETE (m/z 323) standards via reversed-phase HPLC. A mixture of each standard (2 ng per component) was injected and then eluted from a 250×1.0 -mm i.d. ODS column under a gradient of 20% 6.5 mM NH_4Ac (pH 5.7) programmed to 100% MeOH/MeCN (35:65, vol/vol) over 15 min at a flow rate of 50 $\mu\text{L}/\text{min}$, as described in detail elsewhere (70). The mass spectrometer was operated in the multiple reaction monitoring mode. (A) Summation of all ion current transitions of m/z 319 to m/z 115, 151, 155, 167, 191, 208, and 219 and m/z 323 to m/z 183. (B) Transitions specific to each EET and HETE isomer are indicated above each trace and individually normalized. Peak identification is explained in the text. *Source:* Nakamura *et al.* (69).

Serhan *et al.* (26) used LC/ESI-MS/MS to demonstrate that inflammatory tissue exudates from mice treated with ω -3 polyunsaturated FA and aspirin generate a novel array of bioactive lipid signals. Thus, human endothelial cells with upregulated COX-2 treated with aspirin converted 20:5n3 to 18R-hydroxyeicosapentaenoic acid (HEPE) and 15R-HEPE. Each was used by polymorphonuclear leukocytes to generate separate classes of novel trihydroxy-containing mediators, including 5-series 15R-LX5 and 5,12,18R-triHEPE. Figure 4.16 shows the reversed-phase LC/ESI-MS/MS identification of the mono- and triHEPE generated from EPA (eicosapentaenoic acid) in the presence of aspirin in TNF α -induced leukocyte exudates (26). LC

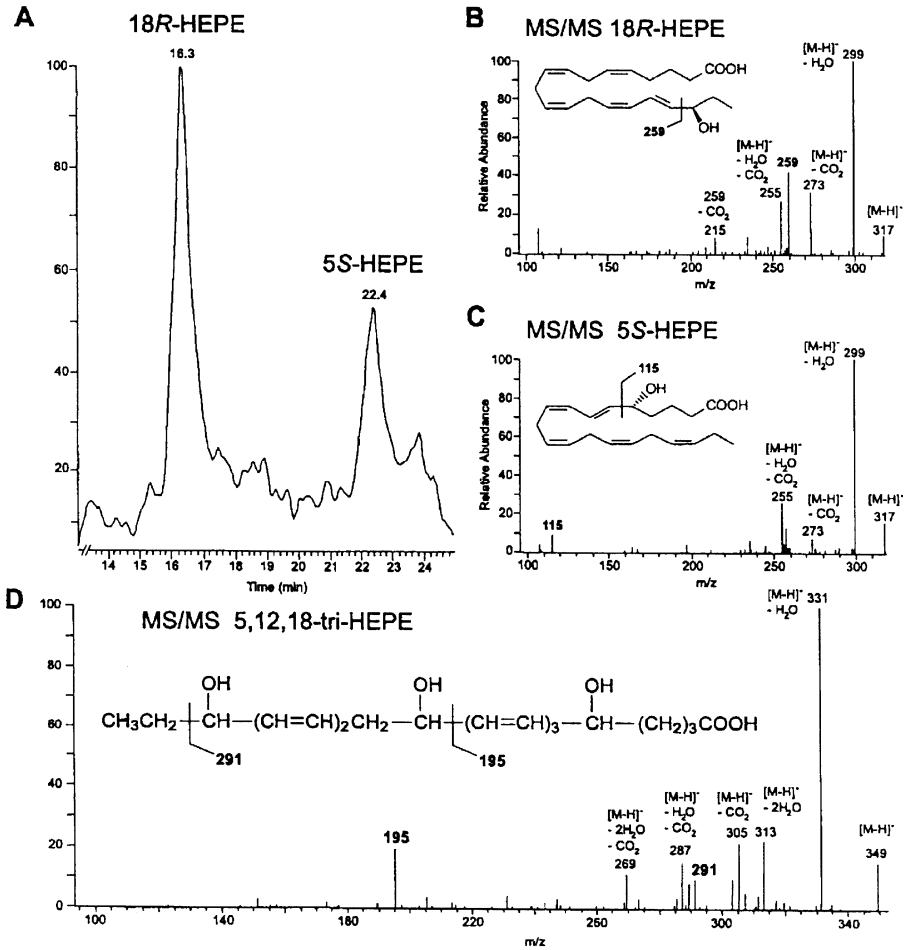


Fig. 4.16. Chiral phase LC/ESI-MS/MS identification of novel polyunsaturated hydroxy FA in inflammatory exudates from murine dorsal pouches treated with aspirin. Selected ion chromatogram of monoHEPE (A); MS/MS of 18R-HEPE (B); MS/MS of 5S-HEPE (C); MS/MS of 12,15,18-triHEPE (D). Chiral phase LC/ESI-MS/MS conditions: Finnigan LCQ equipped with a Chiralcel OB-H (J.T. Baker) column was used to determine R and S alcohol configurations of monohydroxy-polyunsaturated FA using isocratic (hexane/2-propanol, 96:4, vol/vol) as described in detail elsewhere (13). *Source:* Serhan *et al.* (26).

retention times and MS/MS spectra (Fig. 4.16A, B, and C) gave product ions consistent with structures shown in respective insets. Subsequently, Hong *et al.* (50) used the lipidomic methodology to recognize a novel series of endogenous mediators in blood, leukocytes, brain, and glial cells as 17S-hydroxy-containing docosanoids

denoted as docosatrienes (the main bioactive member of the series was 10,17S-docosatriene) and 17S-series resolvins. In a parallel study, Marcheselli *et al.* (70) identified stereospecific messengers from 22:6n3-oxygenation pathways in a mouse stroke model. The newly discovered brain messenger 10,17S-docosatriene potently inhibited leukocyte infiltration. Figure 4.17 shows the reversed-phase LC/ESI-MS/MS quantitative analysis of 10,17S-docosatriene and docosahexaenoic acid (DHA) levels in mouse hippocampus after 1 h of middle cerebral artery occlusion (MCA-O) and 6 h of reperfusion. The data support the hypothesis that endogenously infused 22:6n3 is being utilized for the synthesis of the bioactive docosanoid, 10,17S-docosatriene.

Isoprostanes, Neuroprostanes, and Dinorprostanes

Morrow *et al.* (71) and Morrow and Roberts (20) have reported the formation of isoprostanes during peroxidation of esters of 20:4n6, while Roberts *et al.* have reported the formation of isoprostane-like compounds, termed neuroprostanes, during peroxidation of esters of 22:5n3 and 22:6n3. The formation of neuroprostanes is similar to the formation of isoprostanes from 20:4n6 and proceeds *via* generation of highly unstable endoperoxide intermediates (35). There is evidence that the neuroprostanes like isoprostanes are formed in significant amounts *in vitro* and *in vivo* from the free radical-catalyzed peroxidation of the 22:6n3-containing phospholipids, and are presumably released in the free form by a phospholipase (73).

Morrow *et al.* (74) demonstrated that on normal-phase HPLC, the F₂-isoprostane containing phospholipids exhibited many more polar characteristics than nonoxidized phospholipids. Normal-phase HPLC analysis of lipid extracts from livers of CCl₄-treated rats was performed on a 25-cm × 4.6-mm Econosil SI column with 5-μm particles (Alltech Associates), using an isocratic solvent system of hexane/2-propanol/H₂O (4:6:1, by vol) at a flow rate of 1 mL/min. UV absorbance was monitored continuously at 205 nm. Aliquots of fractions eluted were collected, subjected to alkaline hydrolysis, and the free F₂-isoprostanes identified and quantified by GC. Kayganich-Harrison *et al.* (75) confirmed that the F₂-isoprostane is esterified to the GroPCho backbone, by CID of [M-CH₃]⁻ ions from oxidized phospholipids. CID of the [M-CH₂CHN(CH₃)₃]⁻ ion revealed that F₂-isoprostanes were primarily esterified to the *sn*-2-position of the PtdCho. The isoprostane formation is a facile process, which has been subsequently found to take place *in vivo* (75) and includes the formation of the D₂/E₂ isoprostanes. Normal-phase HPLC analysis of lipid extracts was performed on a 25-cm × 4.6-mm i.d. Econosil SI column (Alltech) with 5-μm particles using an isocratic solvent system of hexane/2-propanol/H₂O 4:6:1 (by vol) at a flow rate of 1 mL/min. UV absorbance was monitored continuously at 205 nm. Aliquots of fractions were subjected to hydrolysis using bee venom phospholipase A₂ and then analyzed for free D₂/E₂-isoprostanes. Waugh *et al.* (76) identified and quantified the F₂-isoprostane regioisomers formed *in vivo* in the rat (Fig. 4.18). The above systems may be suitable for the resolution and quantification of the isoprostanes that are commonly analyzed by GC, including their urinary metabolites (77).

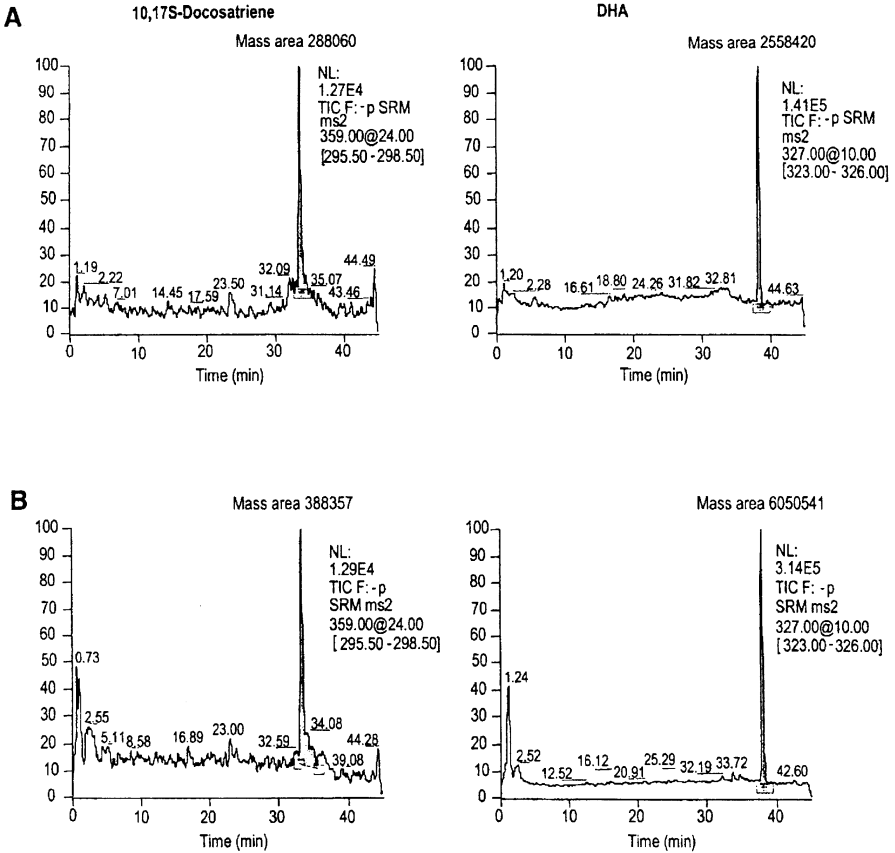


Fig. 4.17. LC/ESI-MS/MS quantitative analysis of 10,17S-docosatriene and DHA levels in mouse hippocampus after 1 h of MCA-O and 6 h of reperfusion. Shown are representative chromatograms of 10,17S-docosatriene selected reaction monitoring for the parent ion m/z 359 on quadrupole 1 and the daughter ion m/z 297 on quadrupole 3. Also shown are the DHA for parent ion m/z 327 and daughter ion m/z 325 on quadrupole 1 and quadrupole 3, respectively. (A) Animals treated by cerebroventricular perfusion of cerebrospinal fluid vehicle for 6 h produced consistent endogenous amounts of 10,17S-docosatriene and DHA. (B) Animals that were perfused with DHA (20 μ g) exhibited greater formation of 10,17S-docosatriene and at least a threefold increase in DHA levels. LC/ESI-MS/MS conditions: Samples were loaded into a Surveyor MS pump (Thermo-Finnigan) equipped with a C18 Discovery column (Supelco), 10 cm \times 2.1 mm i.d., 5 μ m. Samples were eluted with a linear gradient [100% solution A (MeOH/H₂O/HOAc, 60:40:0.01, by vol) to 100% solution B (MeOH/ HOAc, 99.99:0.01, vol/vol)] and run at a flow rate of 300 μ L/min for 45 min. LC effluents were diverted to the ESI probe on a TSQ Quantum (Thermo-Finnigan) triple-quadrupole mass spectrometer running in negative-ion detection mode. *Source:* Marcheselli *et al.* (70).

Later, Ravandi *et al.* (78) used on-line ESI-MS to demonstrate the formation of isoprostane-containing PtdCho during copper catalyzed oxidation of LDL, while Ahmed *et al.* (79–82), using similar LC/ESI-MS methods, reported the formation of PtdCho isoprostanes during peroxidation of high-density lipoprotein (HDL) with a peroxyinitrite generating system. The latter authors reported different experimental conditions under which the isoprostanes accumulated in the glycerophospholipid fraction of HDL.

Reich *et al.* (73) have isolated D₄/E₄-neuroprostanes esterified to glycerophospholipids from rat and human brain and have released them by hydrolysis with phospholipase A₂ from *A. mellifera* venom. The D₄/E₄-neuroprostanes were purified by HPLC and analyzed by LC/ESI-MS/MS. HPLC was performed on a 25-cm × 4.6-mm Econosil C-18 column (5 μm particles) by using an isocratic solvent system of H₂O/MeCN/HOAc (68:32:0.1, by vol) at a flow rate of 1 mL/min. D₄/E₄-neuroprostanes eluted at a retention volume of 25–55 mL. Fractions were then analyzed with LC/ESI-MS/MS by using either a 15-cm × 2.1-mm Econosil C-18 column or a 15-cm × 1-mm Zorbax C-18 column. The solvent system employed in each case was a gradient consisting of 20 mM NH₄Ac/MeCN/HOAc (90:10:0.1, by vol) to 20 mM NH₄Ac/MeCN/HOAc (10:90:0.1, by vol) over the course of 10 min at a flow rate of 0.2 mL/min or 50 μL/min, respectively.

Eicosanoids with E/D-type prostane rings are unstable and dehydrate to cyclopentenone-containing compounds possessing A-type and J-type prostane rings, respectively. Fam *et al.* (83), therefore, explored the A₄/J₄-neuroprostanes from dehydration of E₄/D₄-neuroprostanes and demonstrated that oxidation of 22:6 yielded the anticipated compounds (Fig. 4.19). Esterified A₄/J₄-neuroprostanes in glycerophospholipids were hydrolyzed using chemical saponification with KOH (83), following treatment with methoxylamine HCl in CHCl₃/MeOH (2:1, vol/vol) for 1 h at room temperature. The A₄/J₄-neuroprostanes were conjugated with an excess of glutathione (GSH) and the adducts were purified using a C₁₈ Sep-Pak cartridge preconditioned with MeCN and 0.1 M NH₄Ac (pH 3.4). The neuroprostanes were eluted with 10 mL of 95% EtOH and were identified by LC-MS. HPLC was performed using a MAGIC 2002 LC system (Michrom BioResources, Auburn, CA) operating in the isocratic mode with the mobile phase of H₂O/acetone/HOAc (77:22:9:0.1, by vol). Individual components were separated on an Eclipse XDB-C18 column (2.1 × 50 mm, 5-μm particle size, Agilent, Palo Alto, CA) at a flow rate of 75 μL/min. The compounds were identified by on-line ESI-MS (83).

γ-Ketoaldehydes (isoketals) have been reported as products of the isoprostane pathway of free radical-induced peroxidation of 20:4n6 (35). Utilizing LC-MS analyses, Bernoud-Hubac *et al.* (84) found that neuroketals were formed in abundance *in vitro* during oxidation of 22:6n3, and were formed in greater abundance than isoketals during oxidation of 20:4n6. The neuroketals were analyzed by HPLC as the lysyl adducts formed during oxidation of 22:6n3 in the presence of lysine (Fig. 4.20). Youssef *et al.* (85) have recently measured brain levels of F₂-isoprostanes and F₄-neuroprostanes and their precursors as sensitive and reliable

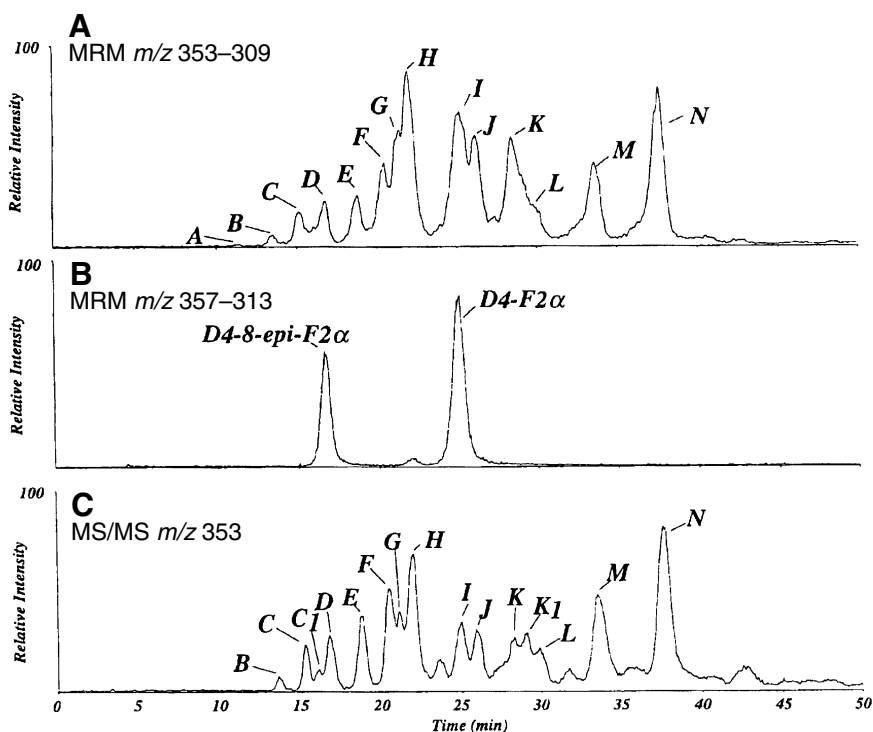


Fig. 4.18. Reversed-phase HPLC separation of F₂-isoprostanes extracted from the liver of rat treated with CCl₄ analyzed by direct ESI-MS. (A) Multiple reaction monitoring (MRM) of the loss of 44 amu from the molecular anion of the F₂-isoprostanes at m/z 353. (B) Multiple reaction monitoring of the loss of 44 amu of the molecular anion of D4-8-epi-PGF_{2α} and D4-PGF_{2α} at m/z 357. C, Reconstructed total ion current of all product ions obtained following CID and MS/MS of the carboxylate anion of F₂-isoprostanes, m/z 353. LC/ESI-MS conditions: column, Phenomenox Ultracarb ODS 5 μm 4.6 mm × 25 cm (Torrance, CA); mobile phase, linear gradient starting with 25% solvent B (MeCN/MeOH, 95:5, vol/vol) increasing to 30% solvent B in 50 min. Mobile phase system A consisted of 0.05% HOAc adjusted to pH 5.7 with NH₄OH. For on-line LC-MS/MS, a postcolumn splitter yielding 15 μL/min flow into mass spectrometer and the remaining 985 μL/min diverted to a fraction collector. For some experiments, [²H₄]PGF_{2α} and [²H₄]8-epi-PGF_{2α} (10 ng each) were added to an aliquot of F₂-isoprostane extract prior to reversed-phase HPLC analysis. The peaks represent various regioisomers of F₂-isoprostanes as discussed in text. Source: Waugh *et al.* (76).

indicators of oxidative injury. Since comparable levels were observed in all animal age groups, it was concluded that aging is not accompanied by enhanced brain susceptibility to oxidative stress.

Parchmann and Mueller (51) have described HPLC analysis of dinor-isoprostanes E₁ in plants. Aqueous samples containing dinor-isoprostane PE₁ were

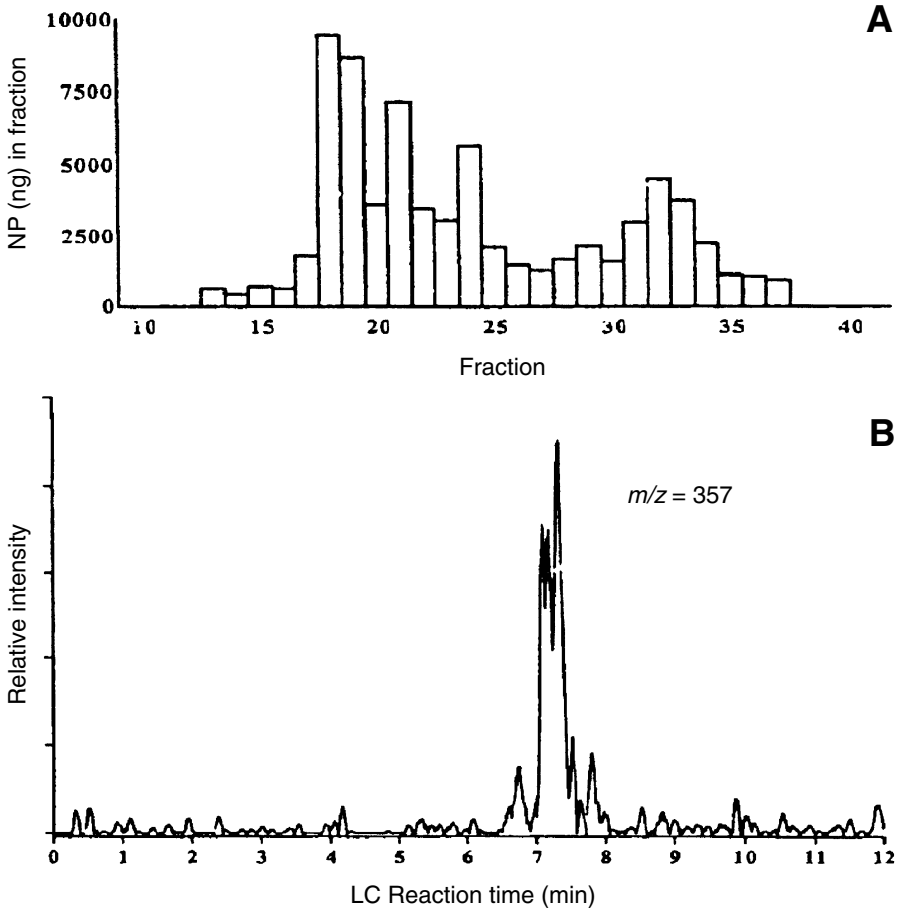


Fig. 4.19. (A) Normal-phase HPLC analysis of A_4/I_4 -neuroprostanes generated from the oxidation of DHA *in vitro*. Normal-phase HPLC was performed using a 25-cm \times 4.6-mm Econosil Si column employing an isocratic solvent system of hexane-2-propanol/HOAc (97:3:0.1, by vol) at 1 mL/min. Quantities of A_4/I_4 in neuroprostanes in HPLC fractions were measured by GC/MS. Material eluted in fraction 18 is shown in B and C. (B) Selected ion monitoring chromatogram of the [parent molecule-H]⁻ (M) ion at m/z 357 from LC/ESI-MS analysis of putative A_4/I_4 -neuroprostanes obtained from prior HPLC purification of oxidized DHA *in vitro*. Reversed-phase HPLC was carried out using a 5-cm \times 2.1-mm Zorbax C-18 column (Agilent). The solvent system was a gradient of 5 mM $NH_4Ac/MeCN/HOAc$ (90:10:0.1, by vol) to 5 mM $NH_4Ac/MeCN/HOAc$ (10:90:0.1, by vol) over the course of 10 min at a flow rate of 200 μ L/min. (C) LC/ESI-MS spectrum of A_4/I_4 -neuroprostanes generated *in vitro*. Material represented in the m/z 357 chromatogram in B was subject to CID at 25 eV, and daughter ions were scanned from m/z 50 to 400. Source: Fam *et al.* (83).

(continued)

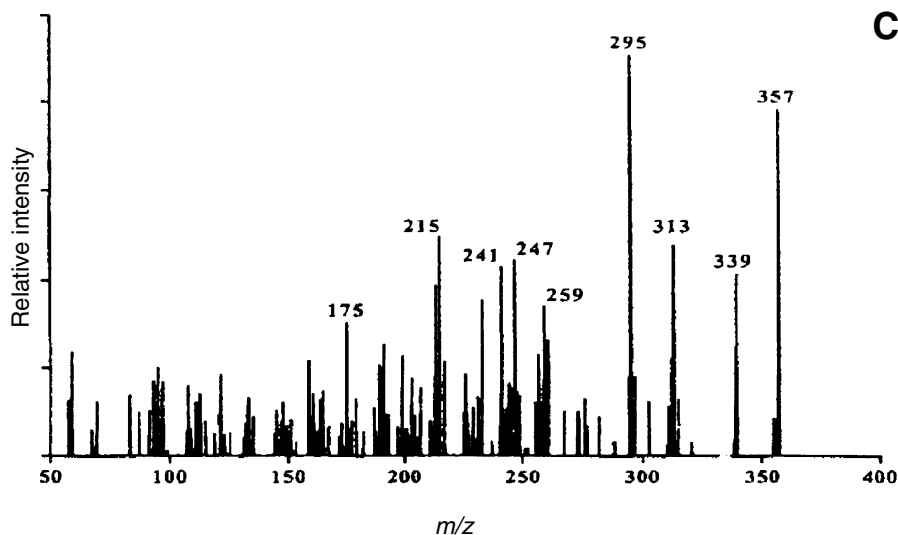


Fig. 4.19. (continued)

obtained from autoxidation of 18:3 (5 mg) in MeOH/H₂O or lipoxygenase (LOX)-catalyzed oxidation of 18:3 (5 mg) in borate buffer. For HPLC analysis, samples were spiked with 5 µg of prostaglandin PGE₁ as internal standard. After addition of 0.05% BHT (wt/vol), the incubation mixture was acidified with citric acid to pH 3 and extracted with Et₂O. The ether phase was taken to dryness under a stream of N₂ and reconstituted in CHCl₃. The sample was incubated with 20 mg of TPP for 5 min to reduce peroxides to their corresponding hydroxy derivatives and applied to a silica solid-phase extraction column (500 mg). The column was washed with 9 mL of Et₂O/HOAc (98:2, vol/vol) and 3 mL of CHCl₃/acetone/HOAc (8:2:0.1, by vol), thereby removing remaining FA and their monohydroperoxides. Dinor-isoprostane PE₁ compounds were eluted with 6 mL of Et₂O/acetone/HOAc (6:4:0.1, by vol). The eluate was taken to dryness, reconstituted in 100 µL of a solution of 0.25% BHT in MeOH, and treated with 400 µL of 1 M KOH for 10 min at 40°C, which converted the dinor-isoprostane PE₁, and PGE₁ to the corresponding B₁-ring compounds.

The incubation mixture was acidified with citric acid to pH 3 and extracted with Et₂O. The Et₂O phase was taken to dryness and analyzed by HPLC on a Lichrospher 100 reversed-phase C₁₈ end-capped column (5 µm, 250 × 4 mm i.d., Merck) using a mixture of MeCN/MeOH/H₂O/HOAc (24:28:48:0.01, by vol) for 15 min and then with 30:35:35:0.01 (by vol) as eluting solvents at a flow rate of 1 mL/min. The chromatogram showed the presence of three strongly UV-absorbing compounds at 278 nm, representing dinor-isoprostane PB₁ type I and type II and the derivative of the internal standard.

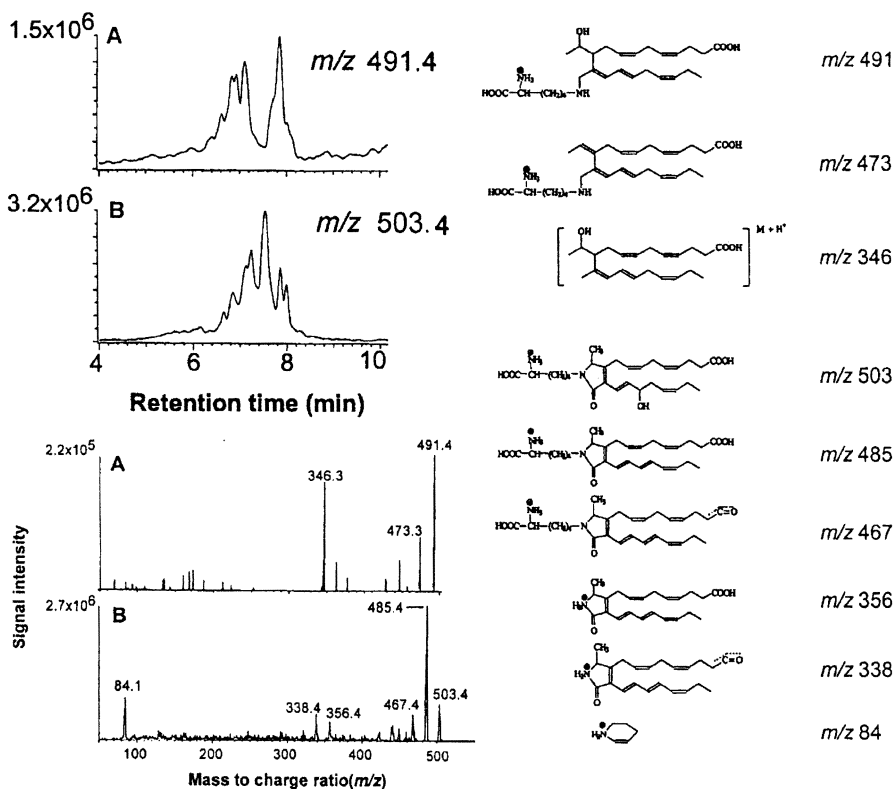


Fig. 4.20. LC/ESI-MS/MS analysis of neuroketal (NK)-lysyl adducts formed during oxidation of 22:6n3 in the presence of lysine. (A) Selected ion current chromatogram of the $[MH]^+$ ions m/z 491 for the dehydrated reduced Schiff base adducts; (B) $[MH]^+$ ions m/z 503 for the lactam adducts; (C) CID (at -25 eV) products of A scanned from m/z 50 to m/z 550; (D) CID (at -25 eV) products of B scanned from m/z 50 to m/z 550. The proposed structures of individual ions are shown in the right side panel of the figure. LC/ESI-MS conditions: HPLC column, Waters 2.1×150 -mm C_{18} column; mobile phase, $H_2O/MeCN$ gradient (3%/min; hold 5 min) at 0.2 mL/min. Parent ions were scanned from m/z 400 to m/z 500 in the positive-ion mode. CID of molecular ions was performed as indicated above. Source: Bernoud-Hubac *et al.* (84).

Core Aldehydes

Lipid hydroperoxides, the primary products of lipid peroxidation, are degraded into aldehydes, the secondary products of oxidation. When polyunsaturated glycerophospholipids and cholesteryl esters are oxidized, both water-soluble short-chain aliphatic aldehydes and lipid-soluble core aldehydes (aldehydes still bound to parent molecules) are generated in stoichiometric amounts. While the water-soluble aldehydes are well characterized by various chromatographic methods in both free and derivatized

form, the chromatographic methods for the isolation and resolution of the core aldehydes have been established only recently (14,86).

When polyunsaturated glycerophospholipids and cholesteryl esters are oxidized, both water-soluble short-chain aliphatic aldehydes and lipid-soluble core aldehydes are generated in stoichiometric amounts. The core aldehydes were obtained by ozonization followed by reduction with TPP (reductive ozonolysis). Later, 1-stearoyl-2-[5-oxo]valeroyl (core aldehyde)-GroPCho was synthesized as a substrate for acetyl platelet activating factor (PAF) acetylhydrolase (87). A core aldehyde of a galactoglycerolipid had been isolated from an alga (88).

Kamido *et al.* (38) used LC/TSI-MS to resolve and identify GroPCho core aldehydes generated by OsO_4 oxidation of egg yolk PtdCho followed by NaIO_4 cleavage. Both 16:0/9:0ALD and 18:0/9:0ALD GroPCho were generated. The core aldehydes were purified by TLC before LC/TSI-MS. The core aldehydes were identified as the hydrazones of the diacylglycerols (DAG) released by phospholipase C. Myher *et al.* (23) used normal-phase HPLC with on-line ESI-MS for a sensitive detection and identification of the PtdCho core aldehydes and core acids among the oxygenated PtdCho recovered from copper-oxidized LDL. Kayganich-Harrison and Murphy (89) reported a detailed characterization of chain-shortened oxidized GroPCho lipids using FAB-MS and tandem MS.

Ou *et al.* (90) reported the normal-phase LC/ESI-MS total ion profile of oxidized soybean PtdCho along with the $[\text{M}+1]^+$ or $[\text{M}+\text{Na}]^+$ mass chromatograms of the major core aldehyde species. The total ion current profile shows a major peak for the unoxidized PtdCho (PC) along with smaller peaks for the core aldehydes (PC-ALD) and core acids (PC-ACID). The major core aldehyde species are 16:0/9:0ALD (m/z 650), 18:0/9:0ALD (m/z 678), 16:0/13:1ALD (m/z 704), 18:1/9:0ALD (m/z 676), and the sodiated 16:0/9:0ALD (m/z 672), as expected from the known composition of the molecular species of soybean PtdCho. The PC-ACID peak consisted of the ω -carboxy homologs corresponding to the core aldehydes, as indicated by their chromatographic migration and the presence of an extra oxygen (16 mass units) in the molecule. Ou *et al.* (90,91) have also reported the identification and quantification of PtdCho that contain aldehyde residues by fluorimetric HPLC.

Ravandi *et al.* (52,78) showed that during normal-phase HPLC of phospholipids, the PtdCho core aldehydes and core acids are eluted as clearly resolved peaks following elution of PtdCho. Using the linear gradient of 100% A ($\text{CHCl}_3/\text{MeOH}/\text{NH}_4\text{OH}$, 80:19.5:0.5, by vol) to 100% B ($\text{CHCl}_3/\text{MeOH}/\text{H}_2\text{O}/\text{NH}_4\text{OH}$, 60:34.5:5.5:0.5, by vol) in 14 min, then at 100% B for 10 min (72), the PtdCho core aldehyde is eluted between PtdCho and the first peak of sphingomyelin, while the core acid overlaps with the second peak of sphingomyelin.

Bergqvist and Kuksis (92) reported the normal-phase LC/ESI-MS profile of commercial bovine heart cardiolipin after treatment with *tert*-BOOH. There was no significant resolution between native cardiolipin and its hydroperoxides on the normal-phase HPLC column. Among the specifically identified peaks were m/z 1448, $[\text{M}-1]^-$ (LLLL); m/z 1480, $[\text{M}-1]^-$ (LLLL-OOH); m/z 1482, $[\text{M}-1]^-$ (LLLO-

OOH); m/z 1512, $[M-1]^-$ (LLLL-di-OOH); m/z 1514, $[M-1]^-$ (LLLO-di-OOH); m/z 1544, $[M-1]^-$ (LLLL-tri-OOH); m/z 1576, $[M-1]^-$ (LLLL-tetra-OOH). Instrumentation and operating conditions were as described by Ravandi *et al.* (52).

The LC/ESI-MS methods of isolation and chromatographic separation of PtdCho hydroperoxides, isoprostanes, and core aldehydes described by Ravandi *et al.* (52) have been utilized extensively by Ahmed *et al.* (79–82) in studies of peroxy-nitrite oxidation of HDL.

Itabe *et al.* (93) have reported the preparation of the core aldehydes using ^{14}C -labeled and nonlabeled 16:0/18:1 and 16:0/18:2 and 16:0/20:4 GroPCho, which yielded the 16:0/9:0ALD and 16:0/5:0ALD GroPCho, respectively. PtdCho containing an unsaturated fatty acyl chain was treated with osmium tetroxide followed by sodium periodate at room temperature; see also the study by Kamido *et al.* (15). The TLC-purified C_9 and C_5 core aldehydes were separated by reversed-phase HPLC (Lichrosorb RP-18, Merck) and eluted with a gradient of solvent A (MeOH/MeCN/ H_2O , 616:264:120, by vol) and solvent B (MeOH/MeCN, 7:30, vol/vol). The structures of the synthetic compounds were confirmed by FAB-MS spectra recorded for the $[M+H]^+$ and $[M+Na]^+$ ions.

Khaselev and Murphy (94) employed HPLC in their investigation of the oxidation of 20:4n6-containing plasmenyl GroPCho. The plasmenyl PCho was oxidized by AAPH [2,2'-azobis(2-amidopropane)hydrochloride]. The oxidation products were extracted with $\text{CHCl}_3/\text{MeOH}$ (1:1, vol/vol) and the CHCl_3 layer was analyzed by on-line reversed-phase LC-MS/MS using a 5- μm Columbus C-18 100A (1.0 \times 150 mm) column (Phenomenex, Torrance, CA) connected to a UV monitor (photodiode array) on-line just before the ESI interface. The HPLC was performed at a flow rate of 50 $\mu\text{L}/\text{min}$ with the mobile phase consisting of MeOH/ $\text{H}_2\text{O}/\text{MeCN}$ (60:20:20, by vol) containing 1 mM NH_4Ac as solvent A, and 1 mM NH_4Ac in MeOH as solvent B eluting 0% B to 100% in 40 min followed by isocratic elution of 100% B for 20 min. Several major as well as minor GroPCho species were observed when 1-*O*-hexadecyl-1 ϵ -enyl-2-20:4-GroPCho was oxidized for 3 h in the presence of AAPH: 1-lyso/20:4 GroPCho (19.3 min), 1:0acyl/20:4 GroPCho (21.1 min), 16:0p/5:0(carbonyl) GroPCho (27.3 min), 16:0p/5HPETE-GroPCho (40.2 min), 16:0p/5ETE-GroPCho (42.8 min), 16:0p-OH/20:4 GroPCho (44.6 min), and 16:0p/20:4 GroPCho (starting material) (491.1 min). Thus, the reaction products included 1,2-diacyl lipids, a lysophospholipid, oxidation products involving the *sn*-1-position alone, oxidation products involving the *sn*-2-position alone, chain-shortened ω -aldehyde radical substituents (core aldehydes), as well as products that were oxidized both at the *sn*-1- and *sn*-2-positions.

Podrez *et al.* (2,3) and Hoff *et al.* (95) have recently reported the characterization of a conserved family of oxidized PtdCho that serve as novel high-affinity ligands for cells stably transfected with CD36, mediating recognition of multiple oxidized forms of LDL. Specifically, four major structurally related phospholipids with CD36 binding activity were identified from oxidized 1-hexadecanoyl-2-eicosatetra-5',8',11',14'-enyl-GroPCho and four corresponding structural analogs with CD36

binding activity were identified from oxidized 1-hexadecanoyl-2-octadecadi-9',12'-enoyl-GroPCho. Each was synthetically prepared, its structure confirmed by multi-lamellar NMR and high resolution MS. LC/ESI-MS/MS studies demonstrated that oxidized PtdCho are formed during LDL oxidation by multiple distinct pathways (2,3,95). LDL modified by MPO-generated nitrating intermediates (NO₂-LDL) was formed by incubating LDL (0.2 mg of protein/mL) at 37°C in 50 mM sodium phosphate, pH 7.0, 100 μM DTPA, 30 nM MPO, 100 μg/mL glucose, 20 ng/mL glucose oxidase, and 0.5 mM NaNO₂ for 8 h. The lipids were resolved by using a ternary (MeCN/MeOH/H₂O) gradient generated by a Waters 600 E multisolvent system HPLC and monitored using ELSD. Lipids, both free and derivatized, were resolved on a Luna C₁₈ column (250 mm × 4.6 mm i.d., 5 μm, Phenomenex). A discontinuous gradient was used by mixing solvent A (MeOH/H₂O, 85:15, vol/vol) with solvent B (MeOH). MS analyses were performed on a Quatro II triple-quadrupole mass spectrometer (Micromass, Inc.) equipped with an ESI probe and interfaced with an HP 1100 HPLC. Quantification of the various oxidized PtdCho species was performed with LC/ESI-MS/MS in positive-ion mode using MRM. HCOOH (0.1%) was included in the mobile phase (Fig. 4.21) (95). The phospholipid hydroxyalkenals derived from arachidonoyl and linoleoyl GroPCho were found to be enriched in fresh atherosclerotic lesions from the aorta of Watanabe heritable hyperlipidemic rabbits (95). The phospholipid hydroxyalkenals were isolated by LC/ESI-MS/MS as described by Podrez *et al.* (2). It should be noted that the [9-oxo]nonanoyl GroPCho described by Kamido *et al.* (15,37) has the same mass and HPLC properties as the monohydroxides of [8-oxo]octenoyl GroPCho.

More recently, Kamido *et al.* (96) and Ravandi *et al.* (97) have reported the HPLC isolation and identification of PtdCho core aldehydes from human atherosclerotic lesions of various stages of development. While the [5-oxo]valeroyl- and [9-oxo]nonanoyl-esters of the palmitoyl and stearoyl lysoGroPCho could readily be recognized, the corresponding hydroxyalkenals could not be demonstrated. These compounds either had not been formed under the autoxidation conditions of the human atheromas or had decomposed to the stable final saturated core aldehydes during preparation and storage of the lipid extracts as suggested by Podrez *et al.* (2).

Ozonides

Ravandi *et al.* (52) used both normal- and reversed-phase LC/ESI-MS for the separation and identification of TAG, PtdCho, and cholesteryl ester ozonides and aldehydes obtained by ozonization. Santrock *et al.* (98) used FAB-MS to study the reaction of ozone with 1-palmitoyl-2-palmitoleoyl-GroPCho and to demonstrate that the decomposition of the ozonide led to 9'-oxononanoyl- and 9'-carboxynonoyl acyl esters at the *sn*-2-position (core aldehydes). The ozone addition products were not observed. Squadrito *et al.* (99) described the production of the *cis*- and *trans*-Criegee ozonides during the ozonization of 1-palmitoyl 2-oleoyl GroPCho

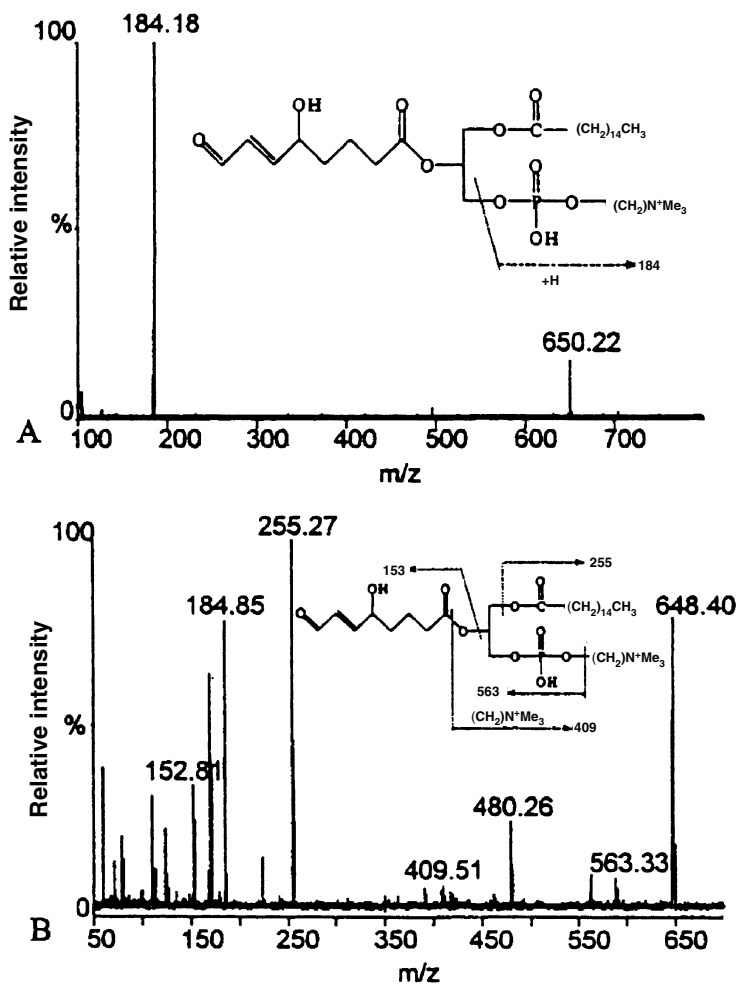


Fig. 4.21. Unbound 5-hydroxy-8-oxo-6-octenoyl-GroPCcho (HOOA-PC) is detected in human atherosclerotic lesions and in Cu^{2+} -oxidized LDL. Authentic PC-HOOA was subjected to LC/ESI-MS/MS in the positive- (A) and negative- (B) ion modes. Assignment of multiple characteristic ions is consistent with the proposed structure shown in insert. (C) LC/ESI-MS/MS in the positive-ion mode of a phospholipid fraction derived from extracts of human atherosclerotic lesions. MRM transitions from $m/z = 650$ to 184 were monitored. (D) LC/ESI-MS/MS in the positive-ion mode of PC-HOOA in oxLDL (upper scan) and LDL (lower scan). MRM transitions (parent ion at $m/z = 650$, daughter ion at $m/z = 184$) were monitored. The detection of PC-OOHA in tissues and in oxLDL was performed as previously described (2,3). The analyses were performed on a Quatro II triple-quadrupole mass spectrometer (Micromass, Inc., UK) equipped with an ESI probe and interfaced with an HP 1100 HPLC (Hewlett-Packard). Lipids were resolved on a Luna C18 (250×4.6 mm, $5 \mu\text{m}$) column (Phenomenex)

(continued)

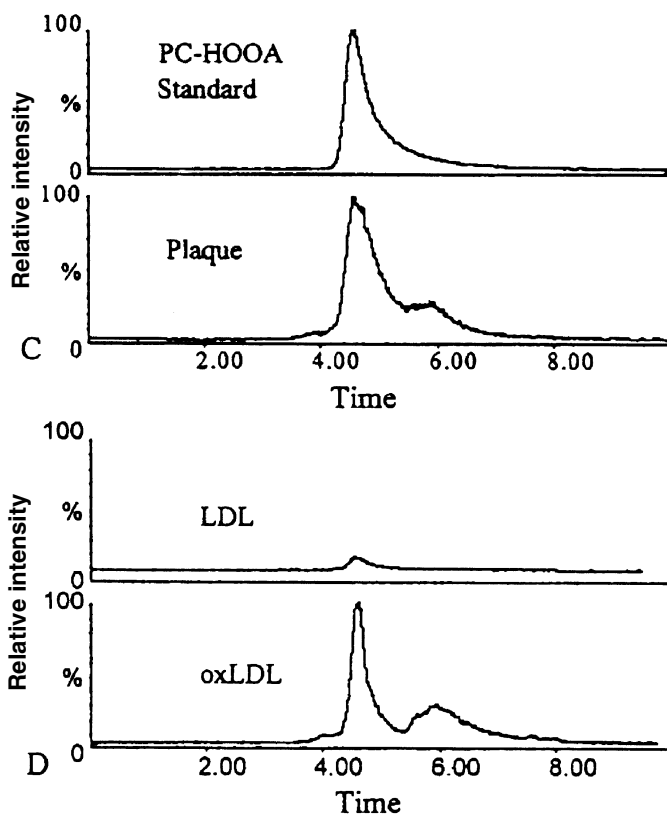


Fig. 4.21. (continued) using a discontinuous gradient obtained by mixing solvent A (MeOH/H₂O, 85:15, vol/vol) with solvent B (MeOH). Quantification of various oxidized PtdCho species was performed using LC/ESI-MS/MS in positive-ion mode using MRM. Formic acid (0.1%) was added in the mobile phase. *Source:* Hoff *et al.* (95).

liposomes. These ozonides were isolated by solid-phase extraction and purified by HPLC with a reversed-phase Hypersil ODS (200 × 4.6 mm) column using a mobile phase consisting of 0.05 M choline in MeOH/H₂O (95.5, vol/vol) at a flow rate of 1.5 mL/min. The absorbance of the eluant was monitored at 212 nm. The ozonides were identified by two-dimensional ¹H-NMR.

Ravandi *et al.* (52) utilized normal-phase HPLC with on-line ESI-MS to identify the ozonides formed from unsaturated PtdCho. Figure 4.22 shows the single-ion mass chromatograms recorded for the PtdCho of egg yolk (52). Normal-phase HPLC separation of both native and ozonized phospholipids was obtained on Spherisorb (3 μm, 100 mm × 4.6 mm i.d., Altech) column. The column was eluted with a linear gradient of 100% A [CHCl₃/MeOH/NH₄OH, 80:19.5:0.5 (by vol)] to 100% B [CHCl₃/MeOH/H₂O/NH₄OH, 60:34.5:5.5:0.5 (by vol)] in 14 min, then at 100% B for 120 min.

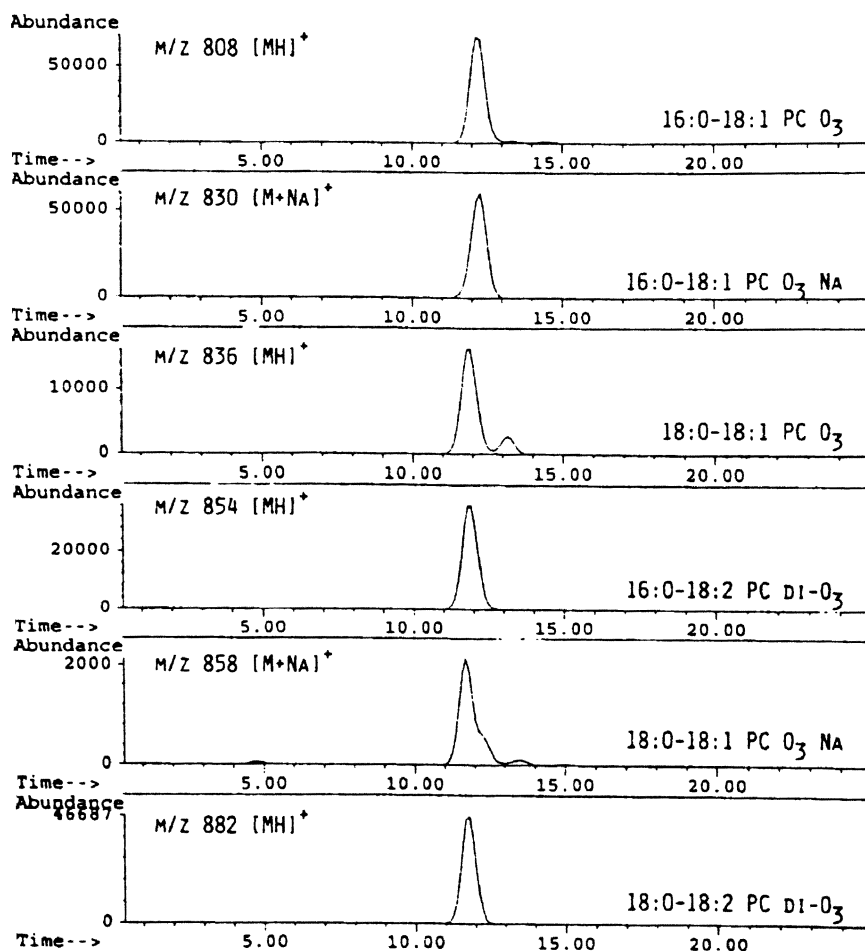


Fig. 4.22. Single-ion plots for the ozonides of intact egg yolk PtdCho as obtained by normal-phase HPLC with on-line ESI-MS. LC/ESI-MS conditions: column, Spherisorb, 3 μ m, 100 mm \times 4.6 mm i.d.; mobile phase, linear gradient of 100% A ($\text{CHCl}_3/\text{MeOH}/\text{NH}_4\text{OH}$, 80:19.5:0.5, by vol) to 100% B ($\text{CHCl}_3/\text{MeOH}/\text{H}_2\text{O}/\text{NH}_4\text{OH}$, 60:34.5:5.5:0.5, by vol) in 14 min, then 100% B for 10 min. ESI-MS, Hewlett-Packard Model 5985 Quadrupole mass spectrometer; 0.2 M $\text{NH}_4\text{Ac}/\text{MeOH}$ (1:1, vol/vol) was added postcolumn at a rate of 0.2 mL/min. Mass spectra were recorded over the mass range 200–1200. The ions shown in the figure represent rounded masses. *Source:* Ravandi *et al.* (52).

With this normal-phase HPLC system the ozonides of PtdCho overlap with the parent molecules. The molecules were distinguished by positive ESI-MS spectra, which were recorded in the mass range 200–1200. Both palmitoyl and stearoyl homologs were obtained for each of the ozonides.

The masses represent the $[M+1]^+$ and $[M+Na]^+$ ions. The ozonide peaks are eluted over a period of 12–13 min, with the monoozonides emerging slightly earlier. The distribution of the ozonide peaks corresponded to the distribution of the unsaturated species of egg yolk PtdCho, which is high in mono- and diunsaturated species, such as 16:0/18:1 and 16:0/18:2.

Harrison and Murphy (100), subjected the ozonides of unsaturated GroPCho to direct MS as either positive or negative molecular species generated by ESI. Polyunsaturated fatty acyl groups esterified to GroPCho yielded a mixture of ozonide species with the maximum number of ozone molecules added equal to the total number of double bonds. Ozonide decomposition resulted in ω -aldehyde and ω -carboxylic acid products as revealed by ESI-MS.

Bergqvist and Kuksis (92) performed HPLC analyses on the ozonides of cardiolipin. Figure 4.23 shows a total negative-ion profile of bovine heart cardiolipin following 2 h (A) and 6 h (B) of post-ozonization degradation as obtained by LC/ESI-MS. Detailed examination of the mass spectra of the separate LC/MS peaks revealed an orderly sequence of elution of the oxidized species of each series of the octa-, hepta-, hexa-, penta-, tetra-, tri-, and diozonide series. Peak A1 yielded (see inset) a major ion at m/z 1832 (octaozonide of 18:2/18:2/18:2/18:2) and a minor ion at m/z 1786 (heptaozonide of 18:2/18:2/18:2/18:1). Peak A2 gave several major ions, including m/z 1832, m/z 1660 (unknown), m/z 1628 (hexaozonide-9ALD), m/z 1690 (unknown), m/z 1486 (unknown), m/z 1424 (tetraozonide-di-9ALD), and m/z 1031 (tri-9ALD, 9CA). Peaks B4 and B5 yielded (see insert) a major ion at m/z 1645 (hexaozonide-9CA), m/z 1441 (tetraozonide 9ALD, 9CA), m/z 1665 (pentaazonide, LLOP), m/z 1598 (pentaazonide 9CA), m/z 1732 (heptaozonide 12CA), and others.

Peak B6 contained m/z 1456 (tetraozonide, di-9CA), m/z 1544 (pentaazonide, 9CA, 12CA), m/z 1478 (triozonide, 9ALD, 9CA, 12CA), and others, where ALD stands for core aldehyde and CA for core carboxylic acid. Instrumentation and operating conditions were as given above (52).

Tagiri-Endo *et al.* (101) used HPLC with chemiluminescence detection to analyze the product of ozonolysis of 1-palmitoyl-2-oleoyl glycerophosphocholine in ethanol-containing solvent. The reaction yielded a large amount of a novel ethoxyhydroperoxide compound (1-palmitoyl-2-[9-ethoxy-9-hydroperoxynonanoyl]-GroPCho). Soybean PtdCho yielded 1-palmitoyl (and stearoyl) 2-[9-ethoxy-9-hydro-peroxynonanoyl]-GroPCho, which were resolved by reversed-phase HPLC with a binary gradient consisting of A, MeOH/H₂O (1:1, vol/vol) then EtOH/hexane (1:9, vol/vol), and B, MeOH. The ethoxyhydroperoxides were identified by on-line ESI-time of flight (TOF)-MS.

Summary and Conclusions

Lipid peroxidation takes place inside and outside of cells. It is often difficult to distinguish between products of enzymatic oxidation and products of autoxidation resulting from free radical action. Lipid oxidation induces membrane disturbance

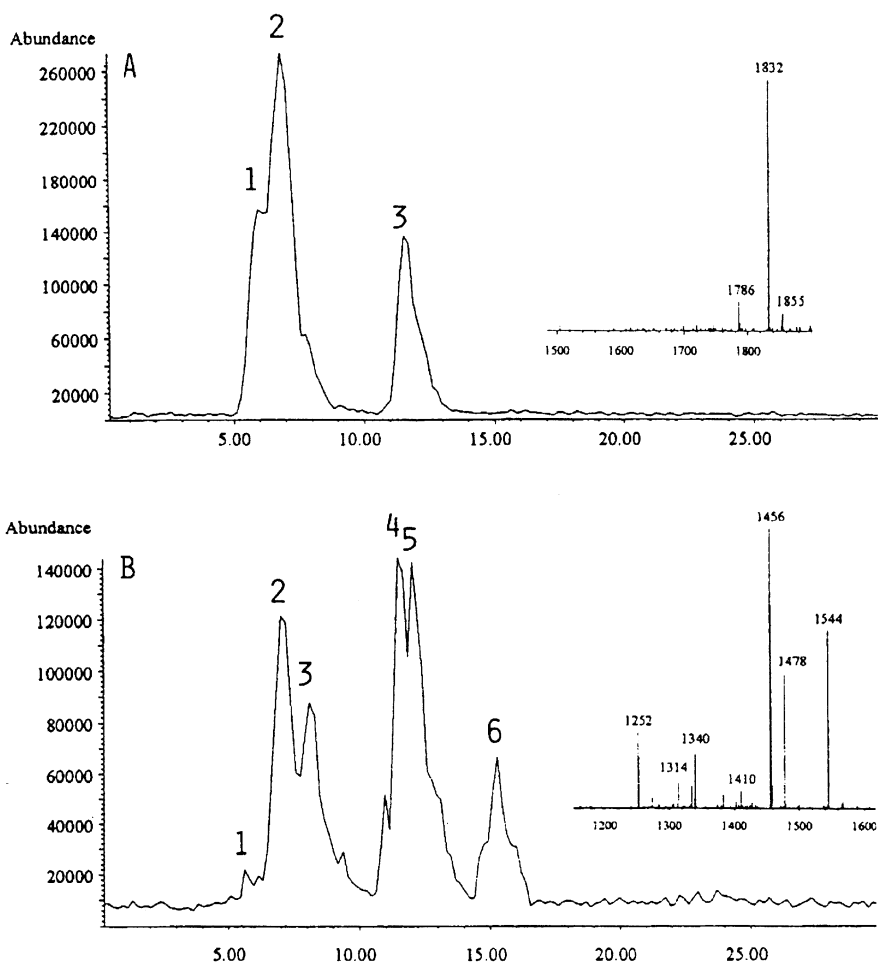


Fig. 4.23. Total negative-ion profile of bovine heart cardiolipin following 2 h (A) and 6 h (B) of post-ozonization degradation as obtained by normal-phase HPLC/ESI-MS. Peak A1, ozonides; peak A2, mixed ozonides/aldehydes; peak A3, mixed ozonides/aldehydes/monocarboxylates. Peak B1, ozonides; peaks B2 and B3, mixed ozonides/aldehydes. Peaks B4 and B5, mixed ozonides/aldehydes/monocarboxylates; peak B6, mixed ozonides/aldehydes/dicarboxylates; inset A, full mass spectrum averaged over peak A1 and peak A2; inset B, full mass spectrum averaged over peaks B4, B5, and B6. LC/ESI-MS conditions were as given in Figure 4.21. *Source:* Bergqvist and Kuksis (92).

and damage, and its products are known to induce the generation of various cytokines and cell signaling. The eicosanoids and their metabolites have now been joined in biological activity by the docosanoids and their metabolites. Recently, convincing arguments have been advanced for a comprehensive study of the lipid

composition of plasma and other tissues to take full advantage of the sequencing of the genome and the isolation and identification of the protein molecules encoded by it and the identification of their functions. The need for targeted quantitative lipidomics is exemplified by recent studies of endogenous bioactive lipids produced in cells transfected with COX-2. Until recently, dioxygen has been the sole form of oxygen thought to be biologically relevant. The recent discovery that tri-oxygen species (ozone) occur in biology changes the oxidation chemistry *in vivo* and is likely to lead to the discovery of new reaction pathways and products not unlike those generated by lipid ozonization *in vitro*. Establishing a basal level of plasma and tissue oxolipids that fluctuates with dietary and environmental influences, with liver function, and with the state of health would be desirable. The highest specificity for oxolipid analysis can be obtained by using methodologies based on electrospray or atmospheric pressure chemical ionization coupled with liquid chromatography/tandem mass spectrometry.

Analysis of oxolipids, however, requires special care. Sterols and polyunsaturated FA appear to be notably prone to artifact formation during isolation, purification, and storage, although other oxolipids are also subject to alteration. An estimate of the extent of oxolipid artifact formation may be obtained by the use of isotope-labeled lipids added to the test sample. In the absence of such controls for artifact formation, measurements of plasma and tissue oxolipid levels may very well be overestimated. This frequently overlooked issue is of real importance, because traces of oxolipids and unidentified metabolites may have unexpected physiological activity. It may be helpful to remember that the same sophisticated methodology that serves to identify the true oxolipids and their metabolites is also ideal for immortalizing artifacts.

References

1. Nachman, M.Z., C.C. Sweeley, N.M. Oldham, and R.E. Olsen, Changes in Fatty Acid Composition During Preparative Thin-Layer Chromatography, *J. Lipid Res.* 4: 484–485 (1963).
2. Podrez, E.A., E. Poliakov, Z. Shen, R. Zhang, Y. Deng, M. Sun, *et al.*, Identification of a Novel Family of Oxidized Phospholipids that Serve as Ligands for the Macrophage Scavenger Receptor CD36, *J. Biol. Chem.* 277: 38503–38516 (2002).
3. Podrez, E.A., E. Poliakov, Z. Shen, R. Zhang, Y. Deng, M. Sun, *et al.*, A Novel Family of Atherogenic Oxidized Phospholipids Promotes Macrophage Foam Cell Formation via the Scavenger Receptor CD36 and Is Enriched in Atherosclerotic Lesions, *J. Biol. Chem.* 277: 38517–38523 (2002).
4. Han, X., and R.W. Gross, Global Analyses of Cellular Lipidomes Directly from Crude Extracts of Biological Samples by ESI Mass Spectrometry: A Bridge to Lipidomics, *J. Lipid Res.* 44: 1071–1079 (2003).
5. Murphy, R.C., J. Fiedler, and J. Hevko, Analysis of Non-Volatile Lipids by Mass Spectrometry, *Chem. Rev.* 101: 479–526 (2001).
6. Havrilla, C.M., D.L. Hachey, and N.A. Porter, Coordination (Ag⁺) Ion Spray Mass Spectrometry of Peroxidation Products of Cholesterol Linoleate and Cholesterol Arachidonate: High-Performance Liquid Chromatography-Mass Spectrometry

- Analysis of Peroxide Products from Polyunsaturated Lipid Autoxidation, *J. Am. Chem. Soc.* 122: 8042–8055 (2000).
- Byrdwell, W.C., Dual Parallel Liquid Chromatography/Dual Mass Spectrometry (LC2/MS2) of Bovine Brain Total Lipid Extract, *J. Liquid Chromatogr. Relat. Technol.* 26: 3147–3181 (2003).
 - Bligh, E.G., and W.J. Dyer, A Rapid Method of Total Lipid Extraction and Purification, *Can. J. Biochem. Physiol.* 37: 911–917 (1959).
 - Folch, J., M. Lees, and G.H. Sloane-Stanley, A Simple Method for the Isolation and Purification of Total Lipids from Animal Tissues, *J. Biol. Chem.* 226: 497–509 (1957).
 - Arborati, M., D. Benchorba, I. Lesieur, J.G. Bizot-Esiard, B. Guardiola-Lemaitre, M.J. Chapman, *et al.*, Oxidative Degradation of Cholesteryl Esters in Low Density Lipoproteins: Analysis by Liquid Chromatography—Light Scattering and Protection by a New Synthetic Antioxidant, S20478, *Fund. Clin. Pharmacol.* 11: 68–77 (1997).
 - Yasuda, M., and S. Narita, Simultaneous Determination of Phospholipid Hydroperoxides and Cholesteryl Ester Hydroperoxides in Human Plasma by High-Performance Liquid Chromatography with Chemiluminescence Detection, *J. Chromatogr. B* 693: 211–217 (1997).
 - Kenar, J.A., C.M. Havrilla, N.A. Porter, J.R. Guyton, S.A. Brown, K.R. Klemp, *et al.*, Identification and Quantification of the Regioisomeric Cholesteryl Linoleate Hydroperoxides in Oxidized Human Low Density Lipoprotein and High Density Lipoprotein, *Chem. Res. Toxicol.* 9: 737–744 (1996).
 - Gronert, K., C.B. Clish, M. Romano, and C.N. Serhan, Transcellular Regulation of Eicosanoid Biosynthesis, in *Eicosanoid Protocols*, edited by E.A., Lianos, Humana Press, Totowa, NJ, 1999, pp. 119–144.
 - Kuksis, A., H. Kamido, and A. Ravandi, Glycerophospholipid Core Aldehydes: Mechanism of Formation, Methods of Detection, Natural Occurrence, and Biological Significance, in *Lipid Oxidation Pathways*, edited by A. Kamal-Eldin, AOCS Press, Champaign, IL, 2003, pp. 138–189.
 - Kamido, H., A. Kuksis, L. Marai, J.J. Myher, and H. Pang, Preparation, Chromatography and Mass Spectrometry of Cholesteryl Ester and Glycerolipid-Bound Aldehydes, *Lipids* 27: 645–650 (1992).
 - Kuksis, A., J.J. Myher, L. Marai, and K. Geher, Analysis of Hydroperoxides and Core Aldehydes of Triacylglycerols, in 17th Nordic Lipid Symposium, *Lipidforum*, edited by Y. Malkki, Bergen, Norway, 1993, pp. 230–238.
 - Buldt, A., and U. Karst, 1-Methyl-1-(2,4-Dinitrophenyl)hydrazine as a New Reagent for the HPLC Determination of Aldehydes, *Anal. Chem.* 69: 3617–3622 (1997).
 - Harrison, K.A., S.S. Davies, G.K. Marathe, T. McIntyre, S. Prescott, K.M. Reddy, *et al.*, Analysis of Oxidized Glycerophosphocholine Lipids Using Electrospray Ionization Mass Spectrometry and Microderivatization Techniques, *J. Mass Spectrom.* 35: 224–236 (2000).
 - Lee, S.H., M.V. Williams, R.N. DuBois, and I.A. Blair, Targeted Lipidomics Using Electron Capture Atmospheric Pressure Chemical Ionization Mass Spectrometry, *Rapid Commun. Mass Spectrom.* 17: 2168–2176 (2003).
 - Morrow, J.D., and L.J. Roberts, The Isoprostanes: Unique Bioactive Products of Lipid Peroxidation, *Prog. Lipid Res.* 36: 1–21 (1997).
 - Schmitt, D., Z. Shen, R. Zhang, S.M. Colles, W. Wu, R.G. Salomon, *et al.*, Leukocytes Utilize Myeloperoxidase-Generated Nitrating Intermediates as Physiological Catalysts

- for the Generation of Biologically Active Oxidized Lipids and Sterols in Serum, *Biochemistry* 38: 16904–16915 (1999).
22. Voyksner, R.D., and T. Pack, Investigation of Collision-Activation Decomposition Process and Spectra in the Transport Region of an Electrospray Single-Quadrupole Mass Spectrometer, *Rapid Commun. Mass Spectrom.* 5: 1263–1268 (1991).
 23. Myher, J.J., A. Kuksis, A. Ravandi, and N. Cocks, Normal Phase Liquid Chromatography/Mass Spectrometry with Electrospray for Sensitive Detection of Oxygenated Glycerophospholipids, *INFORM* 5: 478, Abstract No. 13E (1994).
 24. Kuksis, A., and J.J. Myher, Application of Tandem Mass Spectrometry for the Analysis of Long-Chain Carboxylic Acids, *J. Chromatogr. B* 671: 35–70 (1995).
 25. Dzeletovic, S., O. Breuer, E. Lund, and U. Diczfalusy, Determination of Cholesterol Oxidation Products in Human Plasma by Isotope Dilution-Mass Spectrometry, *Anal. Biochem.* 225: 73–80 (1995).
 26. Serhan, C.N., C.B. Clish, J. Brannon, S.P. Colgan, N. Chiang, and K. Gronert, Novel Functional Sets of Lipid Derived Mediators with Anti-Inflammatory Actions Generated from Omega-3 Fatty Acids via Cyclooxygenase 2-Nonsteroidal Anti-Inflammatory Drugs and Transcellular Processing, *J. Exp. Med.* 192: 1197–1204 (2000).
 27. Sevanian, A., R. Seraglia, P. Traldi, P. Rossato, F. Ursini, and H. Hodis, Analysis of Plasma Cholesterol Oxidation Products Using Gas- and High Performance Liquid Chromatography/Mass Spectrometry, *Free Rad. Biol. Med.* 17: 397–409 (1994).
 28. Osada, K., A. Ravandi, and A. Kuksis, Rapid Analysis of Oxidized Cholesterol Derivatives by High-Performance Liquid Chromatography Combined with Diode-Array Ultraviolet and Evaporative Laser Light Scattering Detection, *J. Am. Oil Chem. Soc.* 76: 863–871 (1999).
 29. Harrison, K.A., and R.C. Murphy, Direct Mass Spectrometric Analysis of Ozonides: Application to Unsaturated Glycerophosphocholine Lipids, *Anal. Chem.* 68: 3224–3230 (1996).
 30. Smith, L.L., Review of Progress in Sterol Oxidations: 1987–1995, *Lipids* 31: 453–487 (1996).
 31. Osada, K., and A. Sevanian, Cholesterol Photodynamic Oxidation by Ultraviolet Irradiation and Cholesterol Ozonization by Ozone Exposure, *Methods Enzymol.* 319: 188–196 (2000).
 32. Wentworth, P., Jr., J. Nieva, C. Takeuchi, R. Galve, A.D. Wentworth, R.B. Dilley, et al., Evidence for Ozone Formation in Human Atherosclerotic Arteries, *Science* 302: 1053–1056 (2003).
 33. Wang, K., E. Bermudez, and W.A. Pryor, The Ozonization of Cholesterol: Separation and Identification of 2,4-Dinitrophenylhydrazine Derivatization Products of 3 β -Hydroxy-5-Oxo-5,6-Seco-Cholestan-6-Al, *Steroids* 58: 225–228 (1993).
 34. Kritharides, L., W. Jessup, J. Gifford, and R.T. Dean, A Method for Defining the Stages of Low Density Lipoprotein Oxidation by the Separation of Cholesterol- and Cholesterol Ester-Oxidation Products Using HPLC, *Anal. Biochem.* 213: 79–89 (1993).
 35. Yin, H., C.M. Havrilla, J.D. Morrow, and N.A. Porter, Formation of Isoprostane Bicyclic Endoperoxides from the Autoxidation of Cholesteryl Arachidonate, *J. Am. Chem. Soc.* 124: 7745–7754 (2002).
 36. Kuksis, A., Core Aldehydes—Neglected Products of Lipid Peroxidation, *INFORM* 1: 1055–1058 (1990).

37. Kamido, H., A. Kuksis, L. Marai, and J.J. Myher, Lipid Ester-Bound Aldehydes Among Copper-Catalyzed Peroxidation Products of Human Plasma Lipoproteins, *J. Lipid Res.* 36: 1876–1886 (1995).
38. Kamido, H., A. Kuksis, L. Marai, and J.J. Myher, Identification of Cholesterol-Bound Aldehydes in Copper Oxidized Low Density Lipoproteins, *FEBS Lett.* 304: 269–272 (1992).
39. Hoppe, G., A. Ravandi, D. Herrera, A. Kuksis, and H.F. Hoff, Oxidation Products of Cholesteryl Linoleate Are Resistant to Hydrolysis in Macrophages, Form Complexes with Proteins, and Are Present in Human Atherosclerotic Lesions, *J. Lipid Res.* 38: 1347–1360 (1997).
40. Kawai, Y., A. Saito, N. Shibata, M. Kobayashi, S. Yamada, T. Osawa, *et al.*, Covalent Binding of Oxidized Cholesteryl Esters to Protein: Implications for Oxidative Modification of Low Density Lipoprotein and Atherosclerosis, *J. Biol. Chem.* 278: 21040–21049 (2003).
41. Smith, L.L., E.L. Ezell, and K. Jaworski, On the Ozonization of Cholesterol 3-Acyl Esters in Protic Media, *Steroids* 61: 401–406 (1996).
42. Herrera, D., A. Ravandi, and A. Kuksis, Reversed-Phase LC/MS Identification of Some Ozonization Products of Cholesteryl Linoleate, in *Abstracts, 94th AOCS Annual Meeting & Expo*, AOCS Press, 2003, p. 10.
43. Jaworski, K., and L.L. Smith, Ozonization of Cholesterol in Non-participating Solvents, *J. Org. Chem.* 53: 545–554 (1988).
44. Kusaka, T., S. Ishihara, M. Sakaida, A. Mifune, Y. Nakano, K. Tsuda, *et al.*, Composition Analysis of Normal Plant Triacylglycerols and Hydroperoxidized *Rac*-1-Stearoyl-2-Oleoyl-3-Linoleoyl-*sn*-Glycerols by Liquid Chromatography-Atmospheric Pressure Chemical Ionization Mass Spectrometry, *J. Chromatogr. A* 730: 1–7 (1996).
45. Sjoval, O., A. Kuksis, L. Marai, and J.J. Myher, Elution Factors of Synthetic Oxotriacylglycerols as an Aid in Identification of Peroxidized Natural Triacylglycerols by Reversed Phase High Performance Liquid Chromatography with Electrospray Mass Spectrometry, *Lipids* 32: 1211–1218 (1997).
46. Sjoval, O., J.-P. Kurvinen, and H. Kallio, Lipid Ester Hydroperoxides and Core Aldehydes in Oxidized Triacylglycerols of Baltic Herring Oil, in *Proceedings of 19th Nordic Lipid Symposium*, Scandinavian Forum for Lipid Research and Technology, Ronneby, Sweden, 1997, p. 57.
47. Sjoval, O., A. Kuksis, and H. Kallio, Reversed Phase High-Performance Liquid Chromatographic Separation of *tert*-Butyl Hydroperoxide Oxidation Products of Unsaturated Triacylglycerols, *J. Chromatogr. A* 905: 119–132 (2001).
48. Sjoval, O., A. Kuksis, and H. Kallio, Analysis of Molecular Species of Peroxide Adducts of Triacylglycerols Following Treatment of Corn Oil with *tert*-Butyl Hydroperoxide, *Lipids* 36: 1347–1356 (2001).
49. Kozak, K.R., S.W. Rowlinson, and L.J. Marnett, Oxygenation of the Endocannabinoid, 2-Arachidonoylglycerol, to Glyceryl Prostaglandins by Cyclooxygenase-2, *J. Biol. Chem.* 275: 33744–33749 (2000).
50. Hong, S., K. Gronert, P.R. Devchand, R.-L. Moussignac, and C.N. Serhan, Novel Docosatrienes and 17S-Resolvins Generated from Docosahexaenoic Acid in Murine Brain, Human Blood, and Glial Cells, *J. Biol. Chem.* 278: 14677–14687 (2003).
51. Pachmann, S., and M.J. Mueller, Evidence for the Formation of Dinor Isoprostanes E1 from α -Linolenic Acid in Plants, *J. Biol. Chem.* 273: 32650–32655 (1998).

52. Ravandi, A., A. Kuksis, J.J. Myher, and L. Marai, Determination of Lipid Ester Ozonides and Core Aldehydes by High Performance Liquid Chromatography with On-Line Mass Spectrometry, *J. Biochem. Biophys. Methods* 30: 271–285 (1995).
53. Kurvinen, J.-P., A. Kuksis, A. Ravandi, O. Sjoval, and H. Kallio, Rapid Complexing of Oxoacylglycerols with Amino Acids, Peptides and Aminophospholipids, *Lipids* 34: 299–305 (1999).
54. Steenhorst-Slikkeveer, L., A. Louter, H.-G. Janssen, and C. Bauer-Plank, Analysis of Non-Volatile Lipid Oxidation Products in Vegetable Oils by Normal-Phase High Performance Liquid Chromatography with Mass Spectrometric Detection, *J. Am. Oil Chem. Soc.* 77: 837–845 (2000).
55. Bauer-Plank, C., and L. Steenhorst-Slikkeveer, Analysis of Triacylglycerol Hydroperoxides in Vegetable Oils by Non-Aqueous Reversed-Phase High Performance Liquid Chromatography with Ultraviolet Detection, *J. Am. Oil Chem. Soc.* 77: 477–482 (2000).
56. Sjoval, O., A. Kuksis, and H. Kallio, Formation of Triacylglycerol Core Aldehydes During Rapid Oxidation of Corn and Sunflower Oils with *tert*-Butyl Hydroperoxide/Fe²⁺, *Lipids* 37: 81–94 (2002).
57. Sjoval, O., A. Kuksis, and H. Kallio, Tentative Identification and Quantification of TAG Core Aldehydes as Dinitrophenylhydrazones in Autoxidized Sunflowerseed Oil Using Reversed Phase HPLC with Electrospray Ionization MS, *Lipids* 38: 1179–1190 (2003).
58. Byrdwell, W.C., and W.E. Neff, Autoxidation Products of Normal and Genetically Modified Canola Oil Varieties Determined Using Liquid Chromatography with Mass Spectrometric Detection, *J. Chromatogr.* 905: 85–102 (2001).
59. Jardines, D., T. Correa, O. Ledea, Z. Zamora, A. Rosado, and J. Molerio, Gas-Chromatography-Mass Spectrometry Profile of Urinary Organic Acids of Wistar Rats Orally Treated with Ozonized Unsaturated Triglycerides and Ozonized Sunflower Oil, *J. Chromatogr. B* 783: 517–525 (2003).
60. Porter, N.A., R.A. Wolf, and H. Weenen, The Free Radical Oxidation of Polyunsaturated Lecithins, *Lipids* 15: 163–167 (1980).
61. Hughes, H., C.V. Smith, E.C. Horning, and J.R. Mitchell, High Performance Liquid Chromatography and Gas Chromatography-Mass Spectrometry Determination of Specific Lipid Peroxidation Products *In Vivo*, *Anal. Biochem.* 130: 431–436 (1983).
62. Zhang, J.Y., B.J. Nobes, J. Wang, and I.A. Blair, Characterization of Hydroxyeicosatetraenoic Acids and Hydroxyeicosatetraenoic Acid Phosphatidylcholines by Liquid Secondary Ion Tandem Mass Spectrometry, *Biol. Mass Spectrom.* 23: 399–405 (1994).
63. Zhang, J.-R., A.R. Cazars, B.S. Lutzke, and E.D. Hall, HPLC-Chemiluminescence and Thermospray LC/MS Study of Hydroperoxides Generated from Phosphatidylcholine, *Free Rad. Biol. Med.* 18: 1–10 (1995).
64. Ravandi, A., A. Kuksis, N. Shaikh, and G. Jackowski, Preparation of Schiff Base Adducts of Phosphatidylcholine Core Aldehydes and Aminophospholipids, Amino Acids, and Myoglobin, *Lipids* 32: 989–1001 (1997).
65. Ravandi, A., A. Kuksis, L. Marai, J.J. Myher, H. Kamido, G. Steiner, *et al.*, Isolation and Identification of Glycated Aminophospholipids from Red Blood Cells of Diabetics, *FEBS Lett.* 381: 77–81 (1995).
66. Ponchaut, S., K. Veitch, R. Libert, F. Van Hoof, L. Hue, and E. de Hoffman, Analysis by Fast-Atom Bombardment Tandem Mass Spectrometry of Phosphatidylcholine Isolated from Heart Mitochondrial Fractions: Evidence of Incorporation of Monohydroxylated Fatty Acyl Moieties, *J. Am. Soc. Mass Spectrom.* 7: 50–58 (1996).

67. Milne, G.L., and N.A. Porter, Separation and Identification of Phospholipid Peroxidation Products, *Lipids* 36: 1265–1275 (2001).
68. Porter, N.A., and D.G. Wujek, Autoxidation of Polyunsaturated Fatty Acids, an Expanded Mechanistic Study, *J. Am. Chem. Soc.* 106: 2626–2629 (1984).
69. Nakamura, T., D.L. Bratton, and R.C. Murphy, Analysis of Epoxyeicosatrienoic and Monohydroxyeicosatetraenoic Acids Esterified to Phospholipids in Human Red Blood Cells by Electrospray Tandem Mass Spectrometry, *J. Mass Spectrom.* 32: 888–896 (1997).
70. Marcheselli, V.L., S. Hong, W.J. Lukiw, X.H. Tian, K. Gronert, A. Musto, *et al.*, Novel Docosanoids Inhibit Brain Ischemia-Reperfusion-Mediated Leukocyte Infiltration and Pro-Inflammatory Gene Expression, *J. Biol. Chem.* 278: 43807–43817 (2003).
71. Morrow, J.D., T.M. Harris, and L.J. Roberts, II, Non-cyclooxygenase Oxidative Formation of a Series of Novel Prostaglandins: Analytical Ramifications for Measurement of Eicosanoids, *Anal. Biochem.* 184: 1–10 (1990).
72. Roberts, L.J. II, T.J. Montine, W.R. Markesbery, A.R. Tapper, P. Hardy, S. Chemtob, *et al.*, Formation of Novel D-Ring and E-Ring Isoprostane-Like Compounds (D₄/E₄-Neuroprostanes) *In Vivo* from Docosahexaenoic Acid, *J. Biol. Chem.* 273: 13605–13612 (1998).
73. Reich, E.E., W.E. Zackert, C.J. Brame, Y. Chen, L.J. Roberts II, D.L. Hachey, *et al.*, Formation of Novel D-Ring and E-Ring Isoprostane-Like Compounds (D₄/E₄-Neuroprostanes) *In Vivo* from Docosahexaenoic Acid, *Biochemistry* 39: 2376–2383 (2000).
74. Morrow, J.D., J.A. Awad, H.J. Hollis, I.A. Blair, and L.J. Roberts II, Non-Cyclooxygenase-Derived Prostanoids (F₂-Isoprostanes) are Formed *In Situ* on Phospholipids, *Proc. Natl. Acad. Sci. USA* 89: 10721–10725 (1992).
75. Kayganich-Harrison, K.A., D.M. Rose, R.C. Murphy, J.D. Morrow, and L.J. Roberts II, Collision-Induced Dissociation of F₂-Isoprostane-Containing Phospholipids, *J. Lipid Res.* 34: 1229–1235 (1993).
76. Waugh, R.J., J.D. Morrow, L.J. Roberts II, and R.C. Murphy, Identification and Relative Quantitation of F₂-Isoprostane Regioisomers Formed *In Vivo* in the Rat, *Free Rad. Biol. Med.* 23: 943–954 (1997).
77. Morrow, J.D., W.E. Zackert, J.P. Yang, E.H. Kurhts, D. Callewaert, R. Dworski, *et al.*, Quantification of the Urinary Metabolite of 15-F_{2t}-Isoprostane (8-iso-PGF_{2α}) by a Stable Isotope Dilution Mass Spectrometric Assay, *Anal. Biochem.* 269: 326–331 (1999).
78. Ravandi, A., A. Kuksis, N. Shaikh, and G. Jackowski, Glucosylated Glycerophosphoethanolamines Are the Major LDL Glycation Products and Increase LDL Susceptibility to Oxidation, *Arterioscler. Thromb. Vasc. Biol.* 20: 467–477 (2000).
79. Ahmed, Z., A. Ravandi, G.F. Maguire, A. Emili, D. Draganov, B. La Du, *et al.*, Apolipoprotein A-I Promotes the Formation of Phosphatidylcholine Core Aldehydes that are Hydrolyzed by Paraoxonase (PON-1) During High Density Lipoprotein Oxidation with Peroxynitrite Donor, *J. Biol. Chem.* 276: 24473–24481 (2001).
80. Ahmed, Z., A. Ravandi, G.F. Maguire, A. Emili, D. Draganov, B. La Du, *et al.*, Multiple Substrates for Paraoxonase-1 During Oxidation of Phosphatidylcholine by Peroxynitrite, *Biochem. Biophys. Res. Commun.* 290: 391–396 (2002).
81. Ahmed, Z., A. Ravandi, G.F. Maguire, A. Kuksis, and P.W. Connelly, Formation of Apolipoprotein A-I-Phosphatidylcholine Core Aldehyde Schiff Base Adducts Promotes Uptake by THP-1-Macrophages, *Cardiovasc. Res.* 58: 712–720 (2003).
82. Ahmed, Z., S. Babaei, G.F. Maguire, D. Draganov, A. Kuksis, B.N. La Du, *et al.*, Paraoxonase-1 Reduces Monocyte Chemotaxis and Adhesion to Endothelial Cells due

- to Oxidation of Palmitoyl, Linoleoyl Glycerophosphocholine, *Cardiovasc. Res.* 57: 225–231 (2003).
83. Fam, S.S., L.J. Murphey, E.S. Terry, W.E. Zackert, Y. Chen, L. Gao, *et al.*, Formation of Highly Reactive A-Ring and J-Ring Isoprostane-Like Compounds (A4/J4-Neuroprostanes) *In Vivo* from Docosahexaenoic Acid, *J. Biol. Chem.* 277: 36076–36084 (2002).
 84. Bernoud-Hubac, N., S.S. Davies, O. Boutaud, T.J. Montine, and L.J. Roberts II, Formation of Highly Reactive γ -Ketoaldehydes (Neuroketals) as Products of the Neuroprostane Pathway, *J. Biol. Chem.* 276: 30964–30970 (2001).
 85. Youssef, J.A., L.S. Birnbaum, L.L. Swift, J.D. Morrow, and M.Z. Badr, Age-Independent, Grey Matter-Localized, Brain-Enhanced Oxidative Stress in Male Fischer 344 Rats: Brain Levels of F₂-Isoprostanes and F₄-Neuroprostanes, *Free Rad. Biol. Med.* 34: 1631–1635 (2003).
 86. Brame, C.J., R.G. Salomon, J.D. Morrow, and L.J. Roberts II, Identification of Extremely Reactive γ -Ketoaldehydes (Isolevuglandins) as Products of the Isoprostane Pathway and Characterization of their Lysyl Protein Adducts, *J. Biol. Chem.* 274: 13139–13146 (1999).
 87. Stremmler, K.E., D.M. Stafforini, S.M. Prescott, G.A. Zimmerman, and T.M. McIntyre, An Oxidized Derivative of Phosphatidylcholine Is a Substrate for Platelet Activating Factor Acetylhydrolase from Human Plasma, *J. Biol. Chem.* 264: 5331–5334 (1989).
 88. Jiang, Z.D., and W.H. Gerwick, An Aldehyde-Containing Galactolipid from the Red Alga *Gracilariopsis lemaneiformis*, *Lipids* 26: 960–963 (1991).
 89. Kayganich-Harrison, A., and R.C. Murphy, Characterization of Chain-Shortened Oxidized Glycerophosphocholine Lipids Using Fast Atom Bombardment and Tandem Mass Spectrometry, *Anal. Biochem.* 221: 16–24 (1994).
 90. Ou, Z., A. Ogamo, L. Guo, and Y. Konda, Identification and Quantification of Choline Glycerophospholipids that Contain Aldehyde Residues by Fluorometric High Performance-Liquid Chromatography, *Anal. Biochem.* 227: 289–294 (1995).
 91. Ou, Z., A. Ogamao, Y. Kawai, and Y. Nakagawa, Quantification of Choline Glycerophospholipids that Contain Carboxylate Residues by Fluorometric High-Performance Liquid Chromatography, *J. Chromatogr. A* 724: 131–136 (1996).
 92. Bergqvist, M., and A. Kuksis, Liquid Chromatography with On-Line Electrospray Mass Spectrometry of Oxidized Diphosphatidylglycerol, in *New Techniques and Applications in Lipid Analysis*, edited by R.E. McDonald and M.M. Mossoba, AOCS Press, Champaign, IL, 1997, pp. 81–99.
 93. Itabe, H., K. Suzuki, R. Hosoya, M. Mori, Y. Higashi, Y. Fujimoto, *et al.*, Preparation of Radioactive Aldehyde-Containing Phosphatidylcholine, *Anal. Biochem.* 285: 151–155 (2000).
 94. Khaselev, N., and R.C. Murphy, Structural Characterization of Oxidized Phospholipid Products Derived from Arachidonate-Containing Plasmemyl Glycerophosphocholine, *J. Lipid Res.* 41: 564–572 (2000).
 95. Hoff, H.F., J. O'Neil, Z. Wu, G. Hoppe, and R.L. Salomon, Phospholipid Hydroxylalkenals: Biological and Chemical Properties of Specific Oxidized Lipids Present in Atherosclerotic Lesions, *Arterioscler. Thromb. Vasc. Biol.* 23: 275–282 (2003).
 96. Kamido, H., H. Eguchi, H. Ikeda, T. Imaizumi, K. Yamana, K. Hartvigsen, *et al.*, Core Aldehydes of Alkyl Glycerophosphocholines in Atheroma Induce Platelet Aggregation and Inhibit Endothelium-Dependent Arterial Relaxation, *J. Lipid Res.* 43: 158–166 (2002).

97. Ravandi, A., S. Babaei, R. Leung, G. Hoppe, H. Hoff, H. Kamido, *et al.*, Phospholipids and Oxophospholipids in Atherosclerotic Plaques at Different Stages of Plaque Development, *Lipids* 39: 97–109 (2004).
98. Santrock, J., R.A. Gorski, and J.F. O’Gara, Products and Mechanism of the Reaction of Ozone with Phospholipids in Unilamellar Phospholipid Vesicles, *Chem. Res. Toxicol.* 5: 134–141 (1992).
99. Squadrito, G.L., R.M. Uppu, R. Cueto, and W.A. Pryor, Production of the Criegee Ozonide During the Ozonization of 1-Palmitoyl-2-Oleoyl-*sn*-Glycero-3-Phosphocholine Liposomes, *Lipids* 27: 955–958 (1992).
100. Harrison, K.A., and R.C. Murphy, Direct Mass Spectrometric Analysis of Ozonides: Application to Unsaturated Glycerophosphocholine Lipids, *Anal. Chem.* 68: 3224–3230 (1996).
101. Tagiri-Endo, M., K. Ono, K. Nakagawa, M. Yotsu-Yamashita, and T. Miyazawa, Ozonization of PC in Ethanol: Separation and Identification of a Novel Ethoxyhydroperoxide, *Lipids* 37: 1007–1012 (2002).

Chapter 5

Analysis of Fatty Acids by APCI-MS

Tomáš Řezanka and Jaroslav Votruba

Institute of Microbiology, Videnska 1083, 14220 Prague, Czech Republic

Introduction

The integration of chromatographic and spectroscopic analytical techniques now represents the mainstream in advanced analysis of natural compounds. Usually, this approach can be described as a two-step procedure. In the first step, the mixture of compounds is separated by a suitable technique such as gas chromatography (GC) or high-performance liquid chromatography (HPLC). Second, a specific detection method, for example, mass spectrometry (MS), is used to obtain structural information about individual substances. In an ideal case, this approach makes it possible to identify simultaneously the individual compounds in the sample, or at least estimate their chemical structures.

A combination of GC and MS techniques is currently widely used. This approach links together in one measurement the separation, with high efficiency, of individual chemical species by GC, plus the identification of their chemical structures. However, the GC-MS technique is limited to the identification of volatile compounds. In the case of poorly volatile compounds, chemical derivatization of the sample must be performed before using GC-MS. The inherent limitation of direct measurement by the volatility, as well as the thermal degradation of labile compounds, stimulated research into a more sophisticated combination of techniques, that is, LC-MS, but the two techniques show low compatibility. In general, MS operates at a high vacuum in the range of 10^{-3} to 10^{-5} Pa, whereas the output from HPLC is a liquid phase with a flow rate between 0.5 and 2 mL/min at atmospheric pressure. The feasibility of LC-MS coupling thus depends on the fast and efficient evaporation of the liquid phase from HPLC and reduction of superfluous mobile phase in the input flow to the mass spectrometer. Various devices have been designed for this purpose.

Materials and Methods

Atmospheric Pressure Chemical Ionization

Recently, new “soft” ionization techniques such as electrospray ionization (ESI) and atmospheric pressure chemical ionization (APCI) were developed to integrate HPLC

with MS. The application of these techniques permits us to evaluate the molecular masses of detected compounds. However, the use of these methods can pose problems in determining chemical structures, because of the relatively small amount of fragments formed. If necessary, this disadvantage can be overcome by the use of tandem MS (LC-MS/MS).

APCI is a method that makes it possible to produce ions by means of a gas discharge electrode. The electrode is installed near the end of an HPLC capillary that is equipped with a pneumatic sprayer located in a small heated chamber. In this way, the liquid mobile phase can be evaporated and preheated to a very high temperature of a few hundred degrees. The high voltage on the discharge electrode produces a corona arc that ionizes the molecules of evaporated mobile phase, which are in excess when compared with the analyte. Subsequently, the ions formed from the mobile phase ionize the molecules of the analyte in the same way as in the classical chemical ionization.

APCI, when used in LC-MS, permits the use of water and organic mobile phases at flow rates of up to 2 mL/min. Such performance permits the use of both conventional and micro columns with normal or reversed phases. However, the method has some limits when applied to the analysis of fatty acid (FA); for example, the mobile phase must contain volatile electrolytes such as formic or trifluoroacetic acids or ammonium acetate.

Determination of the molecular mass by APCI-MS is based either on the presence of the protonated molecule, $[M+H]^+$, or on the existence of molecular adducts with sodium, $[M+Na]^+$, or potassium ions, $[M+K]^+$, when positive ions are detected. When negative ions are detected, the molecular mass determination can be based on the occurrence of the deprotonated molecule ions $[M-H]^-$. Occasionally, one can observe the existence of ions of adducts with very different intensities that originate from the solvents of the mobile phase, such as $[M+H+MeOH]^+$ or $[M+H+ACN]^+$.

Generally, a higher voltage applied to the inlet capillary gives rise to a higher degree of fragmentation of analyte molecules. The proper interpretation of the fragmentation patterns in APCI-MS mass spectra provides information on the chemical structures of unknown compounds, or confirms the presence of a target compound. The APCI-MS technique can be employed in the analysis of a wide spectrum of compounds in the whole polarity range from nonpolar compounds to compounds that exhibit an ionic character.

Results and Discussion

Several articles concerning APCI applications in LC-MS have been published recently. The technique is becoming widely used for the analysis of lipids and their derivatives. As shown in other chapters of this book, the LC-MS technique was successfully used in analytical systems with reversed phases (RP) for the analysis of miscellaneous natural lipid products.

FA were one of the first classes of natural products to be analyzed using GC-MS. The use of LC-MS has opened new possibilities in analyzing complex mixtures of compounds that are commonly found in biological samples. One of the most exciting advantages that LC-MS has over GC-MS is that LC-MS permits the separation and structural elucidation of compounds without purification or derivatization steps, and it also permits the identification of nonvolatile and thermally labile substances. Several ionization and detection modes, including ESI or APCI, can be used for FA analysis by LC-MS. The major advantages of LC/APCI-MS analysis of FA are the fast separation and identification of FA in natural samples, the use of high flow rates (0.1–2.0 mL/min), and that it is not necessary to derivatize the FA. Using APCI, ions can be monitored in negative or positive modes, with AcOH, HCOOH, or AcONH₄ being usually added to the mobile phase to facilitate FA ionization. In LC-MS analysis of FA using APCI ionization mode, one of the main factors that affects the generation of ions is the orifice voltage (see the examples herein). Further possible uses of APCI include MS-MS analysis, in which a precursor ion is mass-selected by a first mass analyzer, focused into a collision region, and then the fragments are analyzed in the second mass analyzer. This provides a more specific detection of FA and their derivatives, which makes it possible to determine the double-bond positions or branched points in the FA chains.

Surprisingly, Murphy and colleagues (1) in their extensive review mentioned only one application of the LC/APCI-MS technique for detection of FA derivatives, that is, eicosanoids in biological extracts.

APCI-MS of FAME

The APCI-MS mass spectra of FA are relatively simple and typically show a protonated molecule, $[M+H]^+$, the adduct, and some fragments that make it possible to conclusively identify positional isomers, but not double-bond positions.

FA with unusually long chain lengths and higher numbers of double bonds in the chain are extremely sensitive to thermal degradation. The GC-MS method allows the analysis of very-long-chain polyunsaturated FA up to 30:7, whereas the identification of longer chain acids has not been possible (2).

Typical fatty acid methyl esters (FAME) containing from 16 to 22 carbon atoms have been analyzed by means of LC/APCI-MS (3). The effects of orifice voltage and the total number of carbon atoms versus the number of double bonds in each homolog on mass spectra were discussed and the correction coefficients for FA homologs from saturated to hexaenoic were also mentioned.

Although it is commonly accepted that APCI gives very little fragmentation, it was possible to obtain very fragment-rich spectra by changing the cone voltage (see Fig. 5.1). At low collision energy (5 eV), the positive-ion APCI-MS mass spectrum of eicosatrienoic acid methyl ester shows the $[M+H]^+$ ion at m/z 321 as practically the only peak. Already at a moderate collision energy (50 eV), where most sample ions would survive, the $[M+H]^+$ ion is converted into fragments:

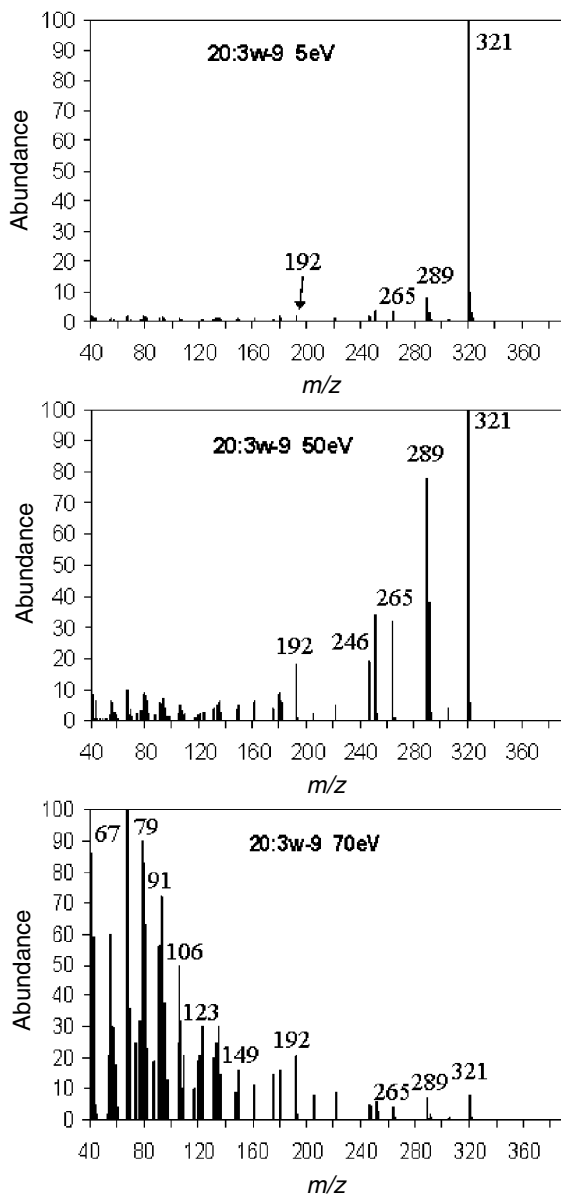


Fig. 5.1. The APCI-MS mass spectra of 20:3 ω -9 methyl esters at different cone voltages.

[M-29]⁺ or [M-C₂H₅]⁺, [M-31]⁺ or [M-MeO]⁺, [M-56]⁺ or [M-C₄H₈]⁺, and [M-69]⁺ or [M-C₅H₉]⁺, at m/z 292, m/z 289, m/z 265, and m/z 252, respectively. At the highest collision energy (70 eV), the largest number of fragments are observed, especially peaks in the low region of m/z , that is, at m/z 67, 79, 93, 95, 108, 121, and so on.

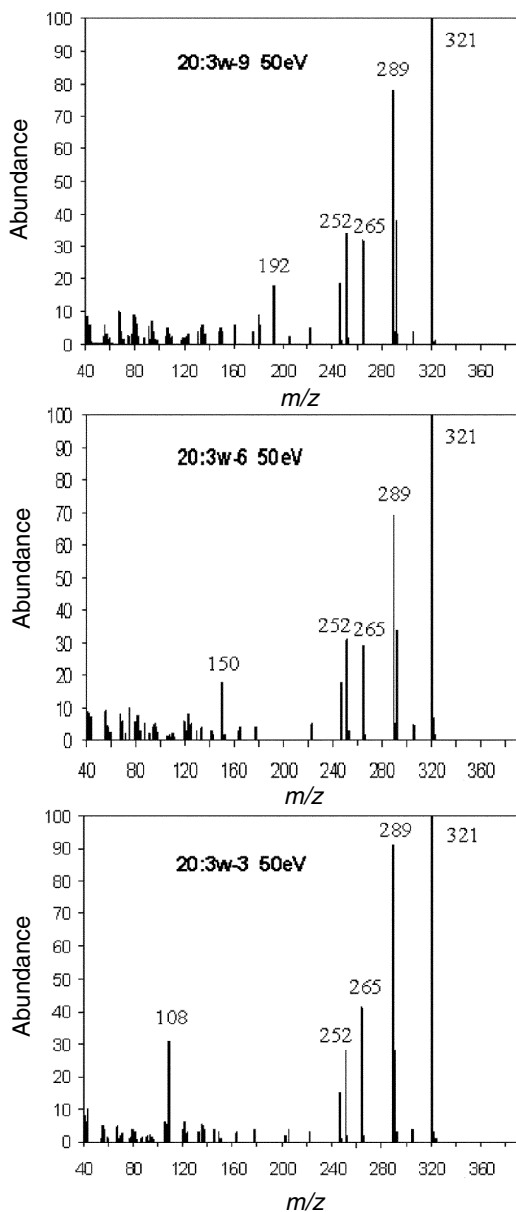


Fig. 5.2. APCI-MS mass spectra of positional isomers of eicosatrienoic fatty acid methyl esters at 50 eV.

Figure 5.2 shows mass spectra recorded at 50 eV of all three commercially available methyl esters of eicosatrienoic acid. On the basis of the well-known rule that methyl esters of several different fatty acids of the ω -3 family give a characteristic fragment at m/z 108 whereas those of the ω -6 series give a prominent ion at m/z 150

and the ω -9 family would therefore be expected to have an abundant ion at m/z 192, we were able to determine the positions of double bonds in methyl esters of polyunsaturated fatty acids (PUFA) from the abundances of mentioned ions in their APCI mass spectra.

The theoretical aspects of optimal performance of a suitable interface and selection of appropriate limiting parameters for interfacing supercritical fluid chromatography with MS were presented in the study by Sjoberg and Markides (4). The effects of different instrumental and chemical parameters were investigated to optimize the ion current signal and stability of ions in ESI and APCI modes (Fig. 5.3). Besides other analyzed compounds, the detection of stearic and pentacosanoic acid methyl esters was optimized and the detection limit in single-ion monitoring mode, based on a $S/N = 3$, was found to be 1.1 pg (APCI) or 1.0 pg (ESI) for stearic, and 0.3 pg (APCI) or 0.2 pg (ESI) for pentacosanoic acid methyl esters, respectively.

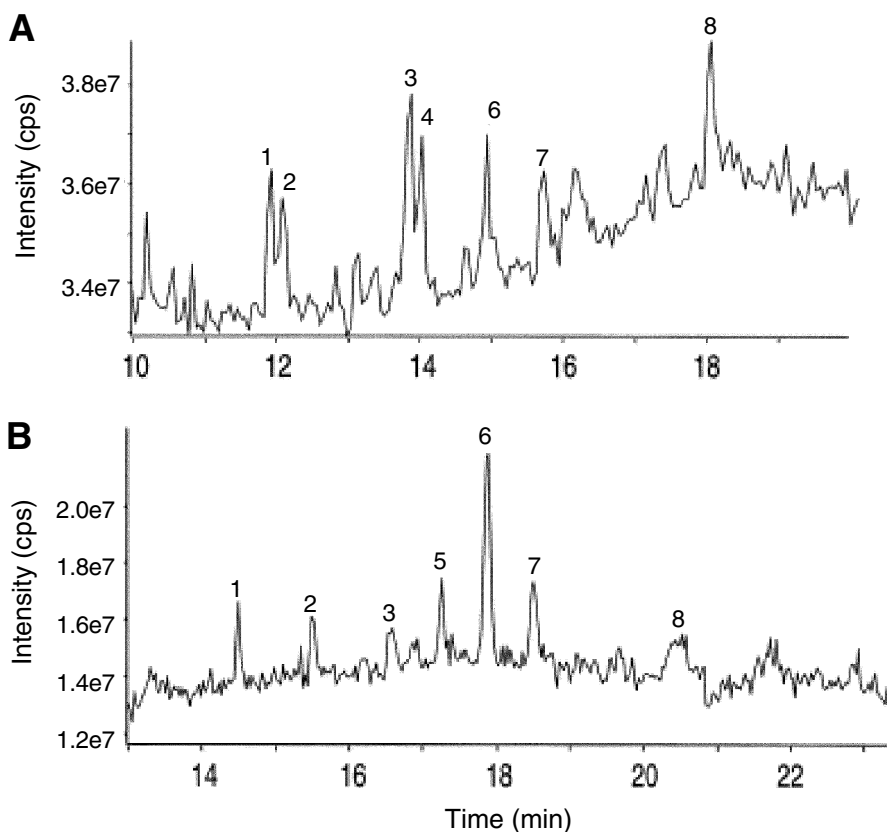


Fig. 5.3. Supercritical-fluid chromatography MS total ion chromatograms of full scans obtained in APCI mode (A) and ESI mode (B). Peaks: 1, stearic acid methyl ester; 3, pentacosanoic acid methyl ester.

Partially hydrogenated fat of commercial origin was analyzed for fatty acids that contained conjugated dienes (5). The peaks eluted from the HPLC and having the conjugated diene chromophore were analyzed by MS. Protonated molecular species, $[M+H]^+$, and ammoniated molecular species, $[M+NH_4]^+$, were detected for all analytes. The molecular mass of each FAME could be determined, but the use of a single quadrupole instrument with a soft ionization source precluded determination of the geometry and position of the double bonds in the fatty chains. For instance, a molecular mass of 294 was obtained for the methyl esters of linoleic acid and for esters of a conjugated linoleic acid (Fig. 5.4). Similarly, a molecular mass of 296 was obtained for the methyl esters of both oleic and elaidic acids (Fig. 5.5).

LC/APCI-MS of Very-Long-Chain Polyunsaturated Fatty Acids (VLCPUFA)

The presence and identity of very-long-chain PUFA from three freshwater crustacean species, *Bathynella natans*, *B. baicalensis*, and *Baicalobathynella magna* from Lake Baikal and caves of Central Europe were determined by means of LC/APCI-MS (6). This method permitted the identification of more than 50 very-long-chain PUFA. These acids, predominantly 26:5 ω -6, 28:7 ω -6, 30:7 ω -3, and 40:7 ω -6, were described in the crustaceans for the first time. The mass spectrum of 40:8 ω -3, including diagnostic ions, is shown in Figure 5.6.

More recently, the very-long-chain PUFA *allZ*-4,7,10,13,16,19,22,25,28-tetra-triacontanoenoic acid was determined and identified in the freshwater crustacean species *Bathynella natans* living in caves of central Europe by means of LC/APCI-MS (7). The APCI mass spectrum of VLCPUFA had characteristic ions consistent with 34:9 FAME. The pseudomolecular ion $[M+42]^+$ is conventionally taken to be mainly characteristic for PUFA, but in fact it also arises by the addition of acetonitrile from the mobile phase.

However, the determination of position of double bonds was unsuccessful on the basis of the cleavage of nitrogen derivatives (i.e., 4,4-dimethyloxazoline or picolinyl ester; data not shown). Nevertheless, this method was described as successful either for substances with equal chain lengths, but having only one double bond, or for shorter chain compounds having a maximum of eight double bonds and only 28 carbon atoms. In our case, this technique failed, or its results were ambiguous. Therefore, we used the method based on the ratios of ions at m/z 109 and 151. The m/z 109/151 ratio is near unity and hence the presumed structure is ω -6 (see Fig. 5.7). This was the first time that a FA with nine double bonds was reported as a natural or synthetic product.

The method of enrichment of very-long-chain fatty acids (VLCFA) from total FA of a heterotrophically cultivated green freshwater alga *Chlorella kessleri* and of their identification as picolinyl esters by means of LC/APCI-MS was described by Řezanka (8). This method is based on the use of preparative RP-HPLC of hundred-milligram amounts and their subsequent identification by microbore LC/APCI-MS. A combination of these two techniques was used to identify unusual VLCFA of up

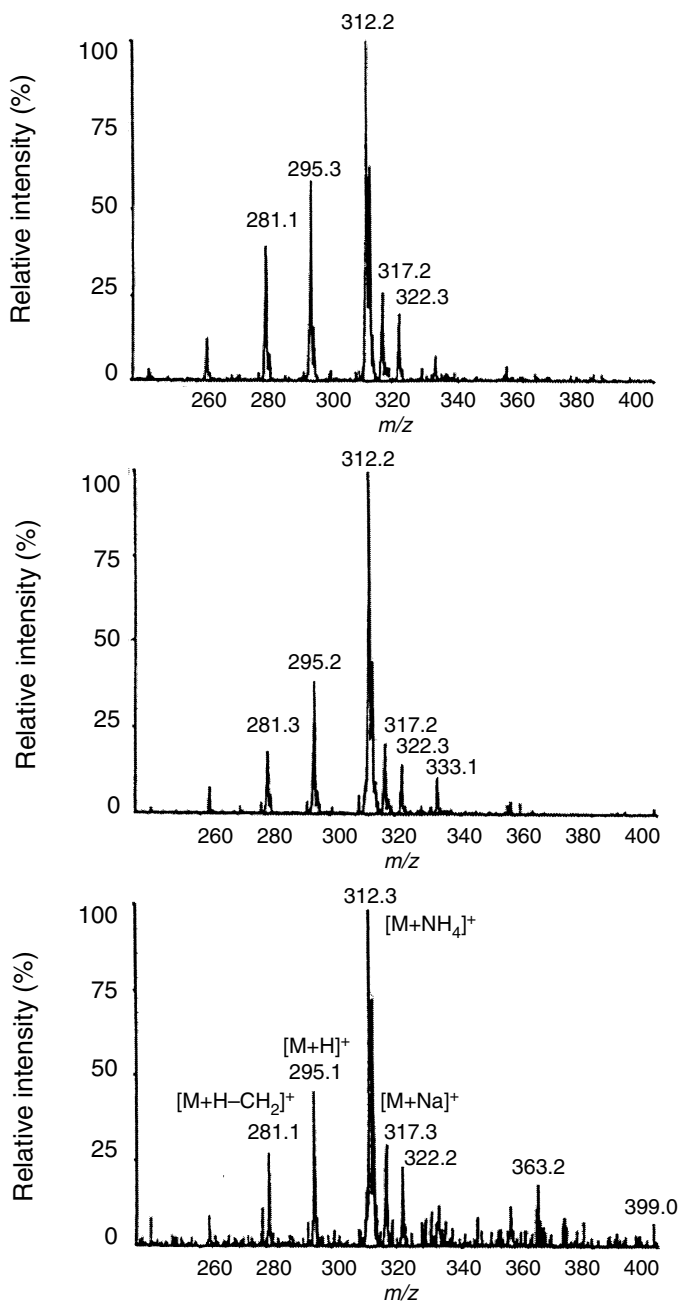


Fig. 5.4. APCI-MS mass spectra of methyl linoleate (upper), and methyl esters of linoleic acid isomers with conjugated dienes (middle and lower).

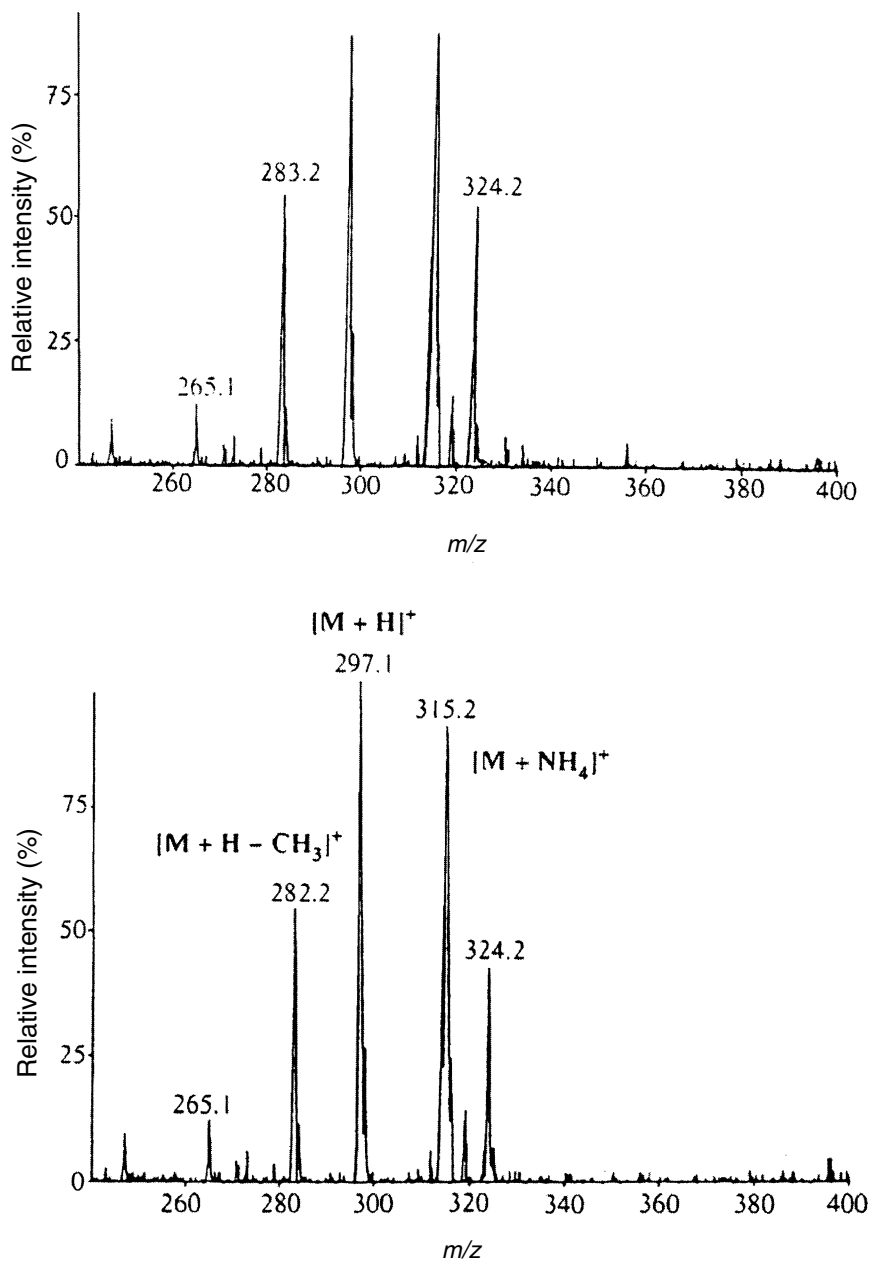


Fig. 5.5. APCI-MS mass spectra of methyl oleate (upper) and methyl elaidate (lower).

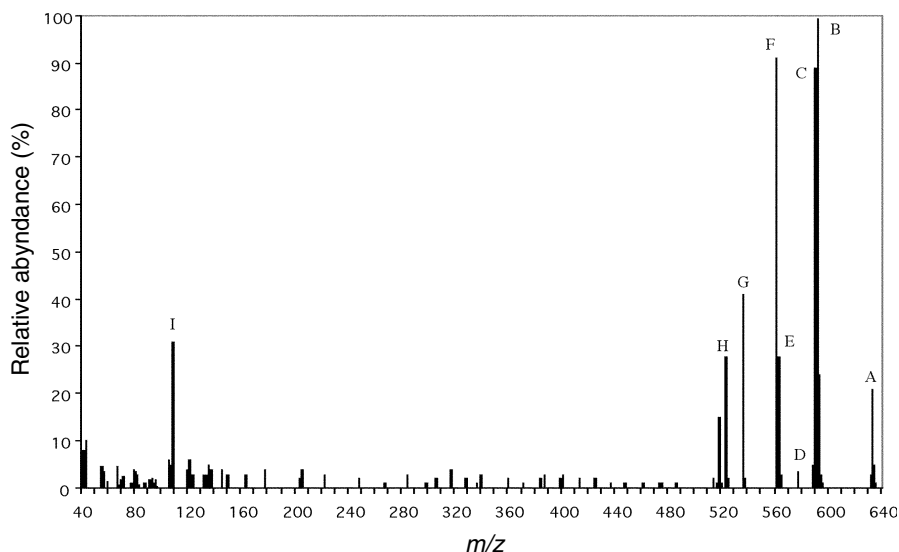


Fig. 5.6. LC-MS (APCI) of 40:8 ω 3 FAME from *Bathynella natans*. Ions: A $[M+H+ACN]^+$, B $[M+H]^+$, C $[M-H]^+$, D $[M+H-Me]^+$, E $[M+H-Et]^+$, F $[M+H-MeO]^+$, G $[M+H-Bu]^+$, H $[M+H-pentyl]^+$, I m/z 109 (diagnostic ion).

to 47 carbons, both saturated and monounsaturated, having two positional isomers (ω -9 and ω -26).

In contrast to EI ionization, in which the mass spectra of the picolinyl esters of straight-chain saturated FA show the most abundant ions in the lower part of mass spectra, that is, ions at m/z 92, 108, 151, and 164, these ions are in the minority in APCI, as shown in Figure 5.8 (e.g., 43:0). Even-numbered ions differing by 14 amu and representing the products of cleavage between methylene groups also have low intensities. A different situation can be found in the M^+ region. Here we can observe the formation of two abundant ions: $[M-H]^+$ and $[M+H]^+$, as well as the generation of adducts with the mobile phase such as $[M+40]^+$ or $[M+C_2H_2N]^+$ and $[M+54]^+$ or $[M+C_3H_4N]^+$. In all investigated VLCFA spectra, the ion $[M+H]^+$ is the most abundant.

In the case of monoenoic derivatives, the ions $[M-H]^+$, $[M+H]^+$, $[M+40]^+$, and $[M+54]^+$ were also very abundant in the M^+ region. A large difference in ion distribution was found with the $[M-H]^+$ ion, which exhibited a threefold higher intensity in monoenoic VLCFA than in saturated VLCFA. The 38:1 FA, the mass spectrum which is shown in Figure 5.9, represents a mixture of two positional isomers in a ratio of approximately 1:1. Detection of ions at m/z 262, 276, and 302 and at 500, 514, and 540 pointed to the presence of a mixture of two positional isomers, ω -9 and ω -26.

The study reported by Holcapek and colleagues (9) concerned the identification by LC/APCI-MS of the individual compounds after partial reesterification of plant oil used as a biofuel. The pseudomolecular ions, $[M+H]^+$, were observed for

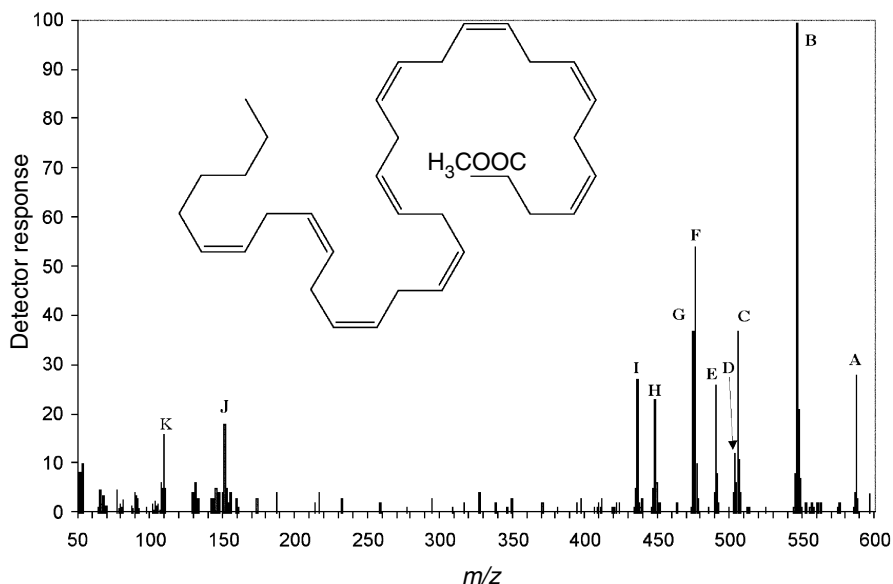


Fig. 5.7. LC/APCI-MS of 34:9 ω 6 FAME from *Bathynella natans*. Ions (abundance): (A) $[M+H+2\times CH_3CN]^+$, m/z 587 (28); (B) $[M+H+CH_3CN]^+$, m/z 546 (100); (C) $[M+H]^+$, m/z 505 (37); (D) $[M-H]^+$, m/z 503 (12); (E) $[M+H-CH_3]^+$, m/z 490 (26); (F) $[M+H-C_2H_5]^+$, m/z 476 (54); (G) $[M+H-CH_3O]^+$, m/z 474 (37); (H) $[M+H-C_4H_9]^+$, m/z 448 (23); (I) $[M+H-C_5H_9]^+$, m/z 436 (27); (J) m/z 151 (18) (diagnostic ion); (K) m/z 109 (16) (diagnostic ion).

all eluted compounds. In addition to these ions, a series of aliphatic ions similar to those obtained by conventional EI-MS were observed in the spectra of FAME under the ionization conditions used.

LC/APCI-MS of Fatty Acids and Resin Acids

LC-MS-based methods were developed for the analysis of 10 resin acids and five FA in process waters from paper industries (10). No fragmentation of target compounds was observed using APCI with negative ionization. The $[M-H]^-$ ions permitted the individual quantification of fatty and aromatic resin acids. Limits of detection were ~ 0.1 ng for all compounds. Changes in parameters that were common for the two interfaces, such as the drying gas temperature, nebulizer pressure, capillary voltage, and cone voltage, caused only insignificant differences in the mass spectra. In contrast, an increase in the corona current from 4 to 10 μA increased the response and a value of 8 μA was selected, which led to slightly higher sensitivities for most compounds. Once the MS parameters had been optimized for each interface, the responses obtained for the target compounds under the optimal conditions were compared.

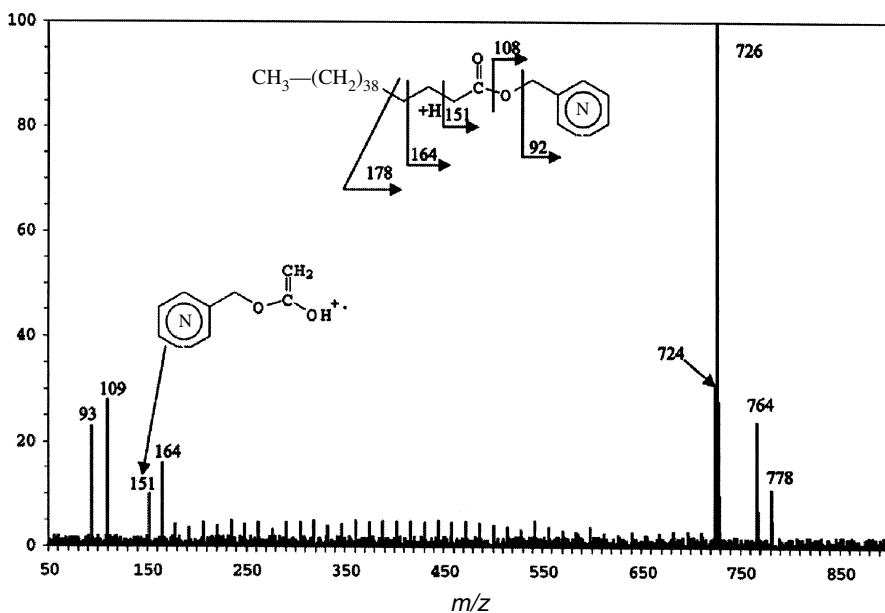


Fig. 5.8. APCI-MS mass spectrum of the picolinyl ester of 43:0 acid; the structures of major ions are shown.

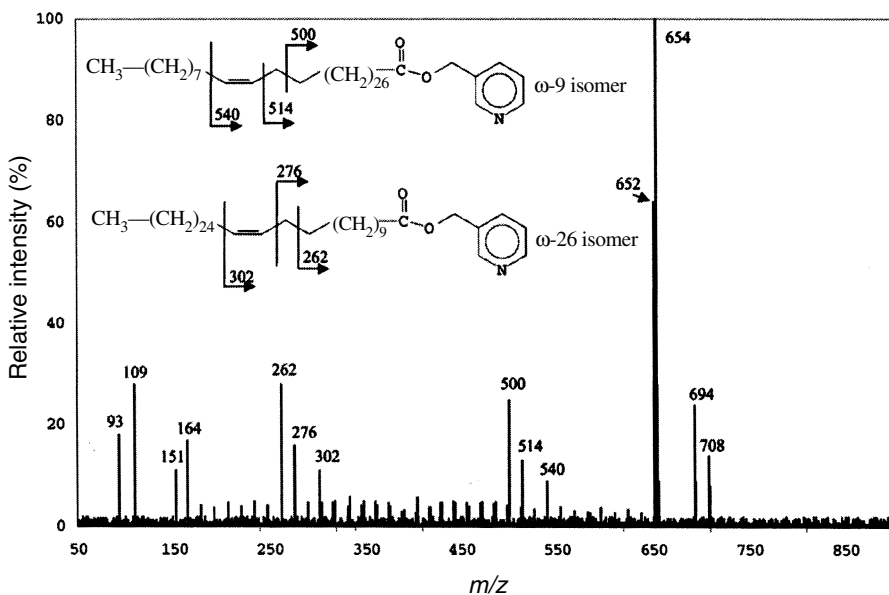


Fig. 5.9. APCI-MS mass spectrum of the picolinyl ester of a 38:1 fatty acid mixture; the structures of major ions are shown.

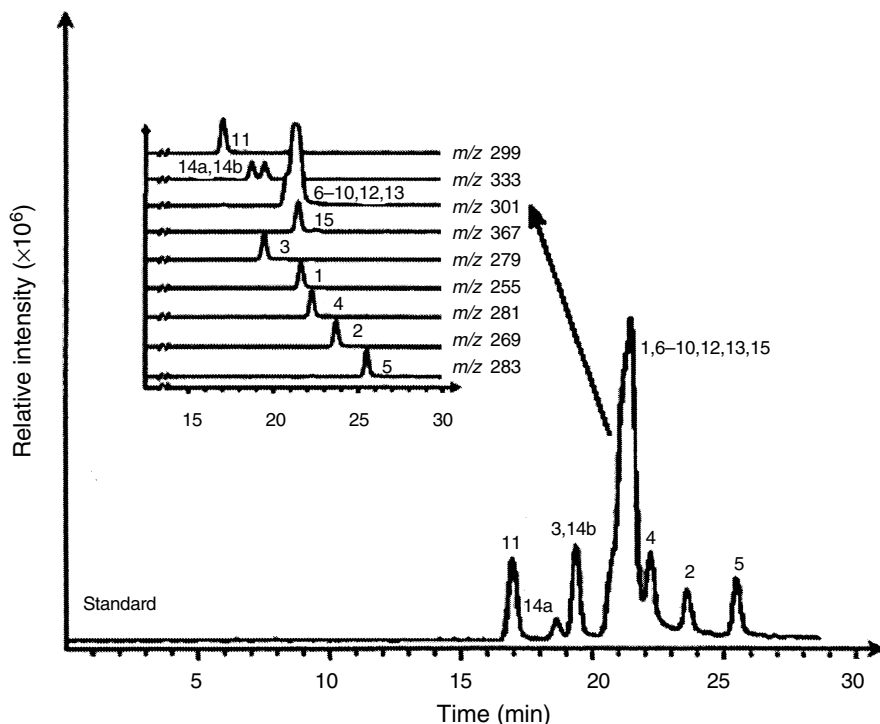


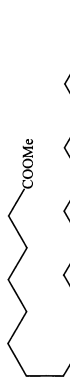
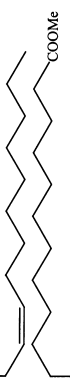

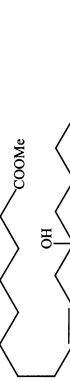
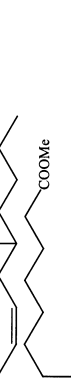


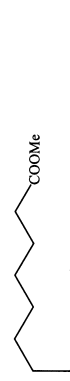
Fig. 5.10. Total-ion chromatogram from LC/APCI-MS in SIM mode of the five fatty acids and the 10 resin acids (16 ng injected). Acids: 1 = palmitic; 2 = margaric; 3 = linoleic; 4 = oleic; 5 = stearic; 6–15 resins' acids.

A comparative study (11) of the performance of LC/APCI-MS and GC-MS for the determination of resin and fatty acids from paper mill process waters (Fig. 5.10) also reported the limits of detection, recoveries, reproducibility, linearity, and precision of both methods. Although LC/APCI-MS involved coelution of the nonaromatic resin acids, it also showed good sensitivity (limits of detection $\sim 3 \mu\text{g/L}$) and permitted the detection of resin and fatty acids at the $\mu\text{g/L}$ level.

LC/APCI-MS for Oxidized FA

The FA and FAME commonly encountered in commercial vegetable oils were tested as substrates for immobilized peroxygenase enzyme from oat (*Avena sativa*) seeds, and the epoxide products were characterized by LC/APCI-MS (12). All reaction products were examined by using MS coupled with LC or GC, and the authors were able to demonstrate that the oat seed peroxygenase exhibited specificity for epoxide formation with no other products being detected (Table 5.1). It was evident that all spectral data included the following ions: $[\text{M}+\text{H}+\text{ACN}]^+$, $[\text{M}+\text{H}]^+$, $[\text{M}+\text{H}-\text{H}_2\text{O}]^+$, $[\text{M}+\text{H}-\text{MeOH}]^+$, and $[\text{M}+\text{H}^+-\text{H}_2\text{O}-\text{MeOH}]^+$.

TABLE 5.1
Tabulated Mass Spectra of Epoxides

| Substrate | RT (min) | APCI-MS | Product |
|---|----------|--|-------------------------|
|  | 30.50 | m/z 354 [M+42 (+H ⁺ +ACN)], 313 [M+1], 295 [M+1-18 (+H ⁺ -H ₂ O)], 263 [M-49, (+H ⁺ -H ₂ O-MeOH)] | 2a |
|  | 43.50 | m/z 410 [M+42], 369 [M+1], 351 [M-17], 337 [M-31, (+H ⁺ -MeOH)], 319 [M-49] | 3a |
|  | 12.16 | m/z 370 [M+42], 329 [M+1], 311 [M-17], 293 [M-35, (+H ⁺ -2H ₂ O)], 279 [M-49] | 4a |
|  | 27.18 | m/z 352 [M+42], 311 [M+1], 293 [M-17], 279 [M-31], 262 [M-49] | 5a (9,10-epoxy) |
|  | 27.42 | m/z 352 [M+42], 311 [M+1], 293 [M-17], 279 [M-31], 261 [M-49] | 5b (12,13-epoxy) |
|  | 18.07 | m/z 368 [M+42], 327 [M+1], 309 [M-17], 296 [M-31], 222 [M-49] | 5c (diepoxy) |
|  | 23.28 | m/z 350 [M+42], 309 [M+1], 291 [M-17], 277 [M-31], 259 [M-49] | 7a (monoepoxy) |
|  | 12.54 | m/z 366 [M+42], 325 [M+1], 307 [M-17], 293 [M-31], 275 [M-49] | 7b (9,10-15,16-diepoxy) |

LC/APCI-MS was developed (13) as an alternative method for characterization of hydroxylated metabolites of oleic and elaidic acids in rat and human liver microsomes.

Oxidation of oleic and elaidic acids led to the formation of two main metabolites, which were identified as ω - and (ω -1)-hydroxylated (or 17-OH and 18-OH) fatty acids on the basis of their pseudomolecular ions and their fragmentation. The assay was accurate and reproducible, with a detection limit of 25 ng per injection. LC/APCI-MS offers considerable advantages since the method does not require the use of a radioactive molecule, completely separates the two hydroxymetabolites, confirms the identification of each metabolite, and is as sensitive as radiometric analysis.

The corresponding mass spectra of OH-FA and the elaidic acid are shown in Figure 5.11. The OH-FA were characterized by a deprotonated molecule ion, $[M-H]^-$, at m/z 297; elaidic acid also exhibited a deprotonated molecule ion at m/z 281.

LC/APCI-MS of FA Amide Derivatives

A useful method for analyzing FA by LC/APCI-MS has been developed (14). The sensitivity of determination of six kinds of palmitamide derivatives monitored by

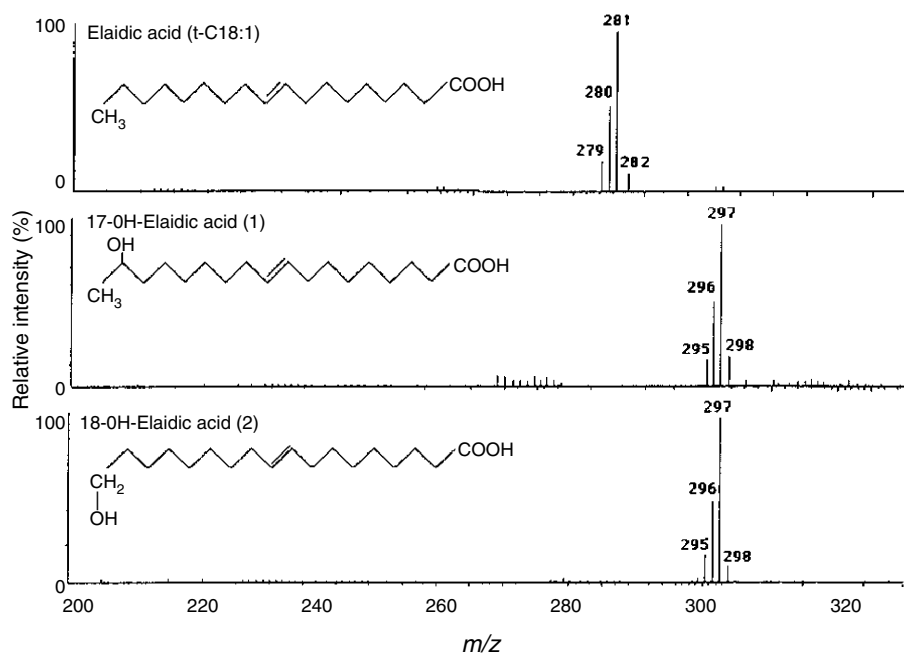


Fig. 5.11. APCI-MS mass spectra (negative ion mode) of elaidic acid and its hydroxylated metabolites.

the single $[M+H]^+$ ion was, in decreasing order: *N-n*-propylamide > anilide > *N,N*-diethylamide ~ *N,N*-diphenylamide > *N*-1-naphthylamide. This method was used to detect both hydroxy and nonhydroxy FA (e.g., from 16:0 to 30:0). Many kinds of FA, including hydroxy FA of the rat brain, were detected in a single run.

N,N-propylamide derivatives exhibited a single and intense $[M+H]^+$ ion. In the mass spectra of *N,N*-diethylamide, $[M+H]^+$ ions were also observed as the base peaks. The mass spectra of *N*-1-naphthylamide or *N,N*-diphenylamide derivatives contained, in addition to $[M+H]^+$ ions, ions at m/z 144 $[(C_6H_5)_2NH_2+H]^+$ and m/z 170 $[(C_6H_5)_2NH+H]^+$, respectively, arising from cleavage of the amide group. The mass spectra of 2-hydroxy FAs showed intense $[M+H]^+$ ions as base peaks, whereas those of 12-hydroxy FA showed $[M+H]^+$ ions but had $[M+H-H_2O]^+$ ions as base peaks (Fig. 5.12).

A simple and selective LC/APCI-MS method was developed (15) for the determination of anandamide (arachidonylethanolamide), an endogenous cannabinoid

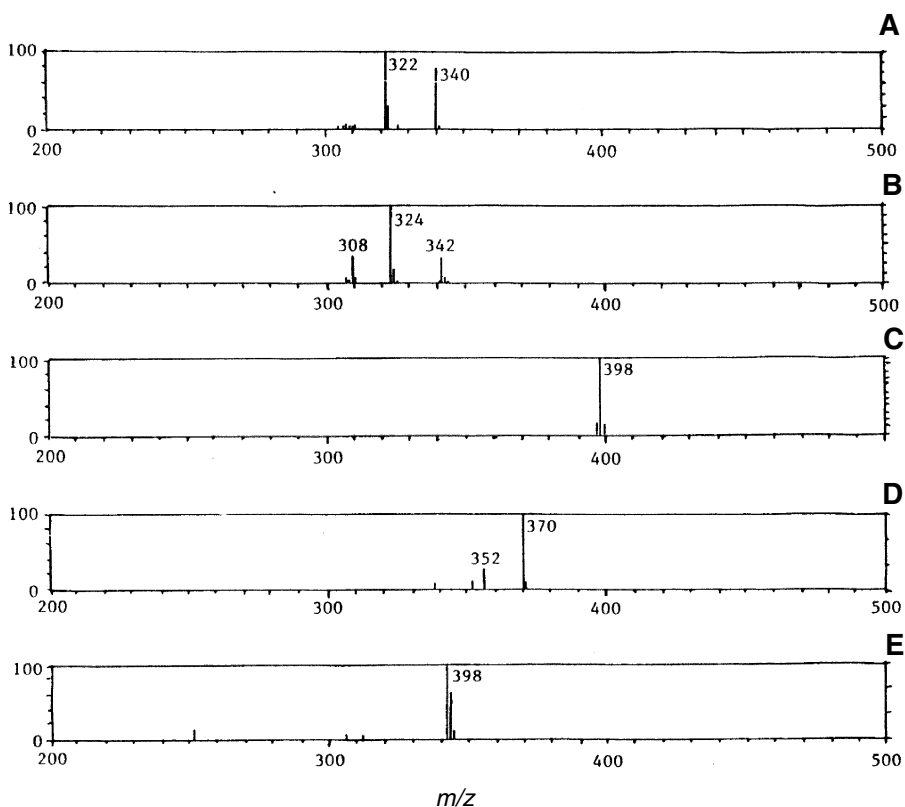


Fig. 5.12. APCI-MS mass spectra of different *N-n*-propylamide derivatives: (A) 12-OH-18:1, (B) 12-OH-18:0, (C) 2-OH-22:0, (D) 2-OH-20:0, (E) 2-OH-18:0.

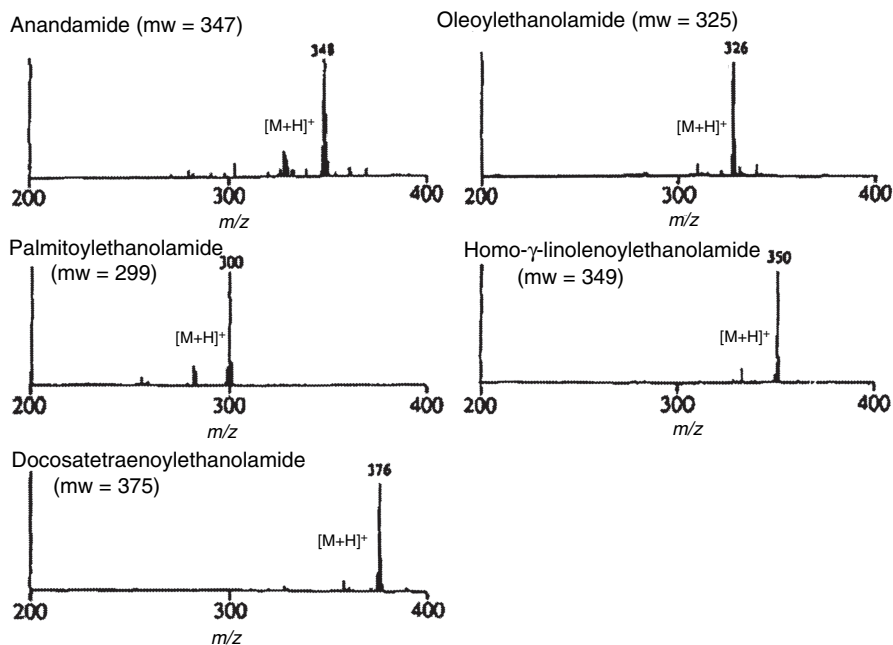


Fig. 5.13. APCI-MS mass spectra of anandamide and its analogs.

receptor ligand, and its analogs. The calibration curve for standard anandamide was linear over the range of 625 fmol to 125 pmol and the detection limit was 200 fmol per injection at a signal-to-noise ratio of 2. The mass spectra obtained from anandamide and its analogs are shown in Figure 5.13. All of them produced protonated molecule ions as the base-peak ions at m/z 348 (anandamide), m/z 300 (palmitoylethanolamide), m/z 326 (oleoylethanolamide), m/z 350 (homo- γ -linolenylethanolamide), and m/z 376 (docosatetraenylethanolamide). To optimize APCI conditions, the effects of the drift voltage and the nebulizer temperature on anandamide ion production were examined. The intensity of $[M+H]^+$ decreased as the drift voltage increased, while the intensity of $[M+H-H_2O]^+$ increased. The maximum intensity of $[M+H]^+$ was observed when the drift voltage was set at 20 V. The temperature for which the $[M+H]^+$ intensity was at a maximum was around 200°C. Similar results were obtained for anandamide analogs.

Other Applications of LC/APCI-MS to PUFA

LC/APCI-MS analysis proved to be a method superior to GC-MS in the identification of PUFA chain length and degree of unsaturation (16). Based on the unequivocal presence of the protonated molecule ion and characteristic acyl daughter ions, 20:5 was clearly identified from *Shewanella pealeana* (Fig. 5.14). LC/APCI-MS analysis also resulted in the detection of previously unidentified unsaturated com-

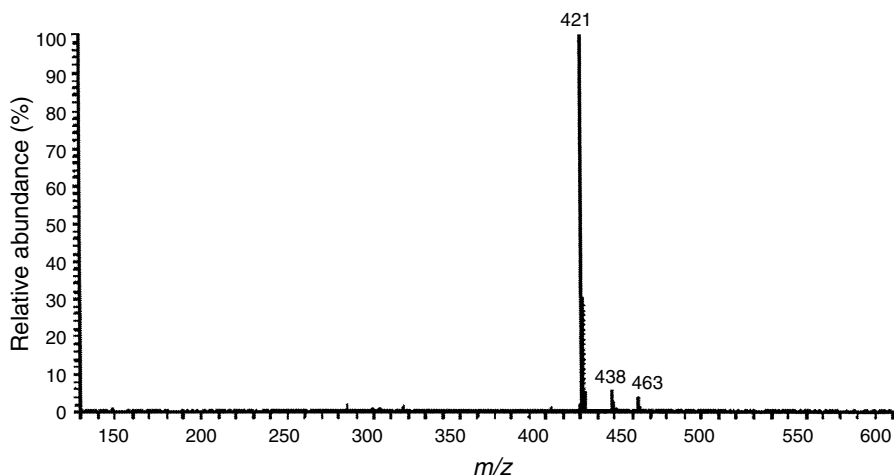


Fig. 5.14. APCI-MS mass spectrum of 20:5 2-oxo-phenylethyl ester from *S. pealeana*.

ponents. A 16:4 PUFA was detected and identified from the characteristic protonated molecule at m/z 367. Further PUFA components (18:4 and 22:5) were also clearly identified by LC-MS analysis from the presence of the characteristic protonated parent and MS-MS daughter ions.

The LC retention times also provided confirmatory support for the assignment of these and other rare or novel PUFA. The correlation of retention time with unsaturation for the C_{22} chain series from menhaden oil demonstrated the powerful ability of the LC/APCI-MS system to directly identify PUFA by the protonated molecules (Fig. 5.15). The correlations based on both chain length and degree of unsaturation were also demonstrated for another series of PUFA from menhaden oil including 28:8, 28:7, 28:6, 26:7, 26:6, 26:5, 26:4, 24:6, and 24:5. Any potential ambiguity for FA of the same molecular mass (e.g., 27:1 and 28:8) was eliminated by observation of retention times.

Ionization and detection of PUFA by LC/APCI-MS provided a significant benefit in detection ability when compared to ultraviolet (UV) detection (approximately 20 to 30 times stronger response relative to 16:0). Analysis of a menhaden oil standard containing the unsaturation series 16:0 to 16:4 demonstrated that the degree of enhanced detection was approximately proportional to the number of double bonds, in addition to a small effect of chain length (Table 5.2). Tests with a pure DHA phenacyl ester standard gave an absolute detection limit in full-scan mode of 200 pg, comparable with UV detection of the pure standard. In the selected reaction-monitoring mode, the detection limit for docosahexaenoic phenacyl ester based on the acyl daughter ion at m/z 311, derived from the molecular ion, was 5 pg. This limit is essentially independent of whether the sample is a standard or a complex mixture of FA.

LC/APCI-MS was used to analyze FA split off from lecithins after phospholipase A treatment and also some hydroperoxy FA split off from photo-oxidized

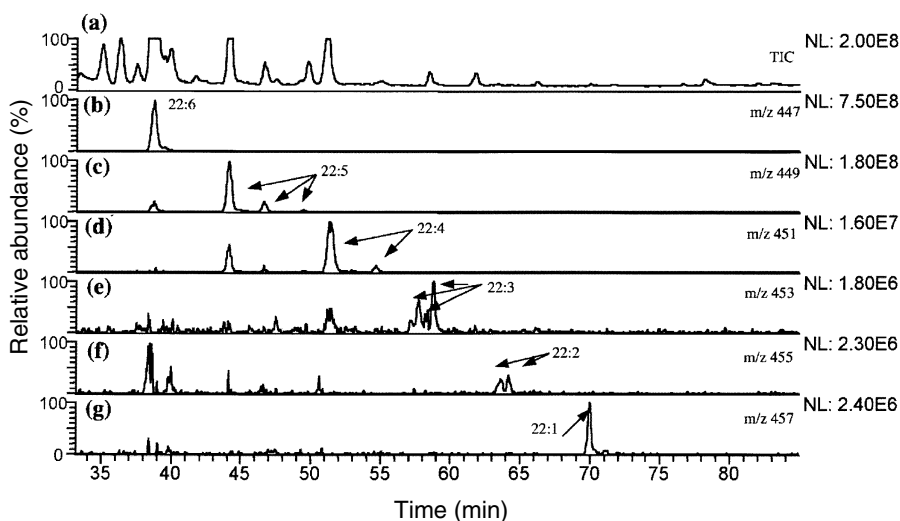


Fig. 5.15. Total ion chromatogram (a) and mass chromatograms (b–f) of the $[M+H]^+$ ions for the C_{22} 2-oxo-phenylethyl esters of menhaden oil.

lecithin. The pseudomolecular ions $[M+H]^+$ in 7-methoxy-1,4-benzoxazin-2-one-3-methyl derivatives (MB; see Fig. 5.16) were the base peaks. Ions observed at m/z 231 in mass spectra of these MB derivatives are assumed to be ions of $(MB+ACN)$ (17). No significant difference was observed between the spectra of saturated and unsaturated FA.

TABLE 5.2

Relative Response Factors (Relative to the Detection of 16:0) for APCI-MS Detection Versus UV Detection of Fatty Acid 2-oxo-Phenylethyl Esters from a Menhaden Oil Standard and *S. pealeana*

| Fatty acid | Response factor |
|------------|-----------------|
| 16:4 | 19.5 |
| 16:3 | 23.6 |
| 16:2 | 2.7 |
| 16:1 | 3.6 |
| 16:0 | 1.0 |
| 18:4 | 23.2 |
| 20:5 | 23.2 |
| 22:5 | 31.6 |
| 22:6 | 25.7 |
| 18:0 | 1.04 |
| 16:0 | 1.00 |
| 14:0 | 0.88 |

An $[M+H-H_2O]^+$ ion (base peak) accompanying a smaller pseudomolecular ion $[M+H]^+$ was observed in the mass spectrum of the 12-OH-18:0 MB (Fig. 5.17). The spectrum of the 2-OH-18:0 MB derivative was similar. The sensitivity of the palmitic acid MB derivative was determined by monitoring the single $[M+H]^+$ ion and amounts as low as 5 ng of palmitic acid could be detected.

FA esters of 3-(*N*-phenylamino)-1,2-propanediol were considered the best chemical markers of toxic oils related to the Spanish toxic oil syndrome (18). Their analysis was based on solid-phase extraction using strong anion-exchange cartridges, followed by LC/APCI-MS-MS quantification. Quantitative measurements were performed by two different internal standards (Table 5.3): compound 4 for quantification of the monoesters and compound 9 for the diesters of compound 1. Analyses were performed in the precursor-ion scan mode. $[M+H]^+$ ions at m/z 432, 420, 684.5, 692.5, 694.5, and 696.5 (for compounds 3, 4, 9, 5, 6, and 8, respectively) were selected in the first quadrupole and the common product ion at m/z 132 was monitored in the second analyzer (Fig. 5.18).

In a sphingomyelin-enriched sample of polar lipids from bovine milk, molecular species of intact sphingomyelin were separated by LC-MS (19). In-source fragmentation of sphingomyelin ions by positive APCI led to the formation of ceramide ions. With the ceramide ions as precursors, ions representative of both the long-chain base parts and the FA parts were detected in APCI-MS-MS. By using this procedure, it was possible to determine the sphingomyelin molecular mass and then the respective long-chain base (LCB)-FA combination(s) by using APCI(+)-MS-MS. At least 36 protonated molecules of intact sphingomyelin were detected in the bovine milk sample. The combinations found covered a range of molecular masses from 673 to 815. The 12 most common protonated molecules were composed of at least 25 different LCB-FA combinations. Saturated and unsaturated LCB and FA were detected in addition to hydroxy FA. The most common LCB were 16:1, 17:1, 18:1, and 19:1, whereas the most common FA were 16:0, 22:0, 23:0, and 24:0.

LCB-FA combinations of sphingomyelin from bovine brain, bovine erythrocytes, and chicken egg yolk were also identified. For positive-ion APCI, the mass spectra were more complex than for ESI because of extensive in-source fragmentation (Fig. 5.19). For sphingomyelin 18:1/18:0, the base peak appeared at m/z 548, corresponding to protonated molecules with a loss of phosphorylcholine, $[M+H-183]^+$ (the M-183 part is hereafter denoted Cer, ceramide).

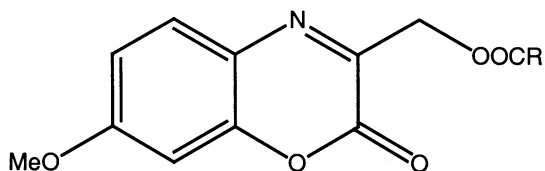


Fig. 5.16. Structure of 7-methoxy-1,4-benzoxazin-2-one-3-methyl (MB) ester of fatty acid.

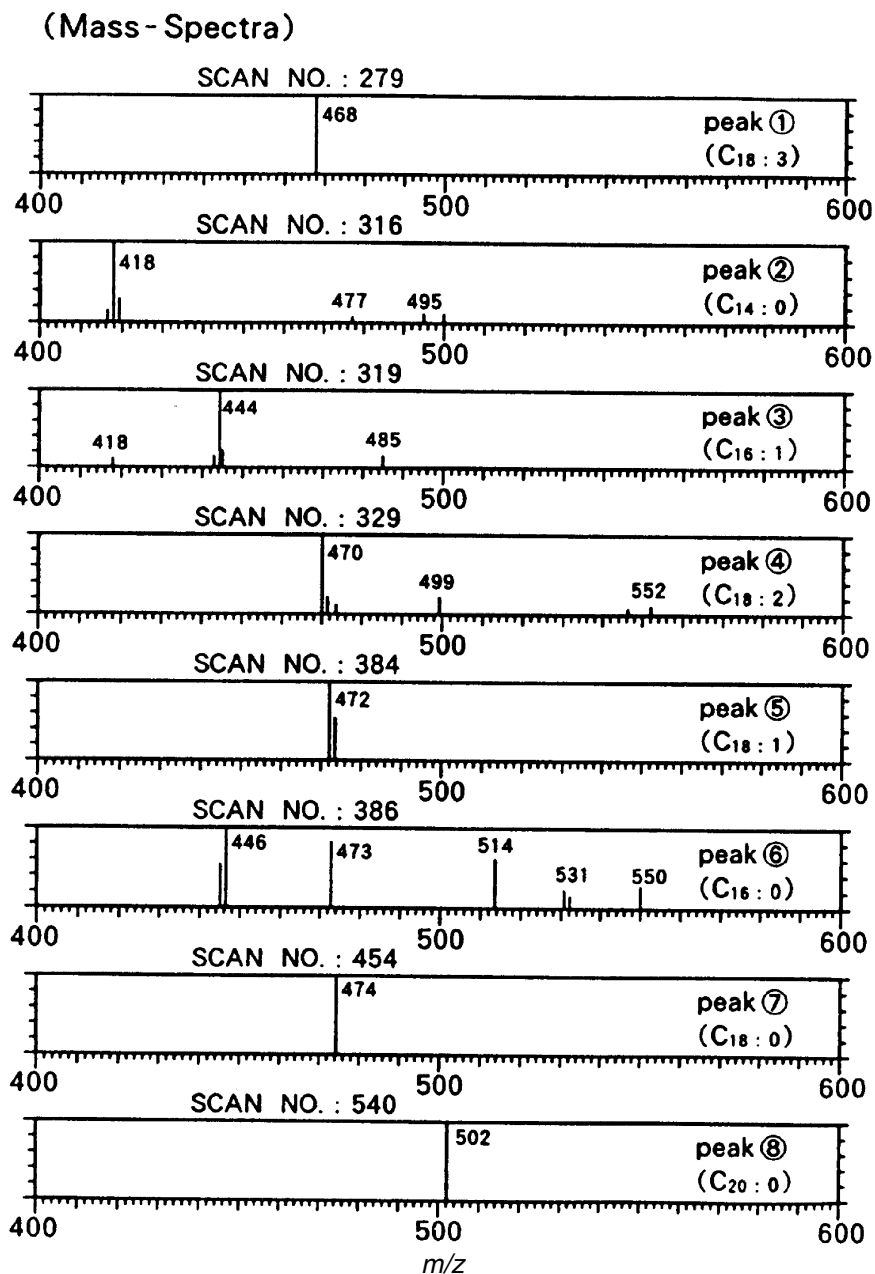
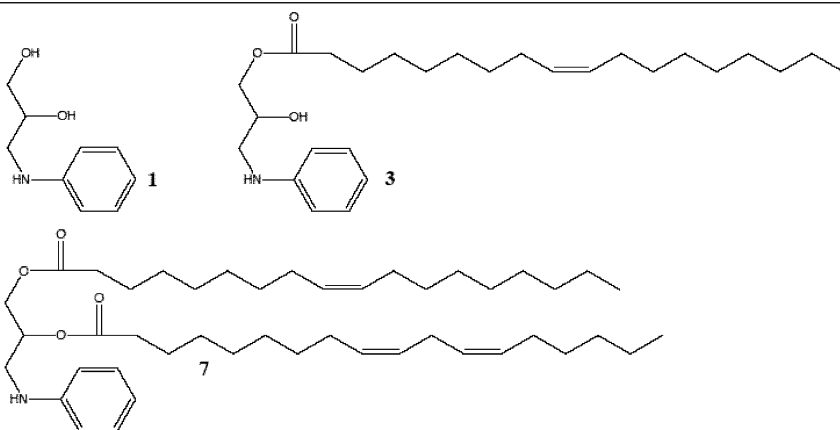


Fig. 5.17. LC-MS mass spectra of the MB derivatives of fatty acids. A mixture of eight kinds of fatty acids (approximately 10 nmol each 14:0, 16:0, 16:1, 18:0, 18:1, 18:2, 18:3, and 20:0) was used.

TABLE 5.3

Structures and Names of Different of Toxic Compounds

| Compound | Chemical name | (M+H) ⁺ |
|----------|---|--------------------|
| 1 | 3-(<i>N</i> -phenylamino)-1,2-propanediol | 168 |
| 2 | 2-hydroxy-3-(<i>N</i> -phenylamino)propyl linoleate | 430 |
| 3 | 2-hydroxy-3-(<i>N</i> -phenylamino)propyl oleate | 432 |
| 4 | 2-hydroxy-3-(<i>N</i> -phenylamino)propyl heptadecanoate | 420 |
| 5 | 2-linoleoyl-3-(<i>N</i> -phenylamino)propyl linoleate | 692 |
| 6 | 2-oleoyloxy-3-(<i>N</i> -phenylamino)propyl linoleate | 694 |
| 7 | 2-linoleoyl-3-(<i>N</i> -phenylamino)propyl oleate | 694 |
| 8 | 2-oleoyloxy-3-(<i>N</i> -phenylamino)propyl oleate | 696 |
| 9 | 2-oleoyloxy-3-(<i>N</i> -phenylamino)propyl heptadecanoate | 698 |



In addition to $[\text{Cer}+\text{H}]^+$, also $[\text{Cer}+\text{H}-\text{H}_2\text{O}]^+$, $[\text{Cer}+\text{Na}]^+$, and $[\text{Cer}+\text{K}]^+$ were abundant. In the molecular ion region, $[\text{M}+\text{H}-\text{CH}_2]^+$ ions of m/z 717 were obtained (formed presumably in a substitution reaction in which one methyl group is replaced by hydrogen). Also, $[\text{M}+\text{H}-\text{CH}_2-\text{H}_2\text{O}]^+$ and $[\text{M}-\text{CH}_2+\text{Na}]^+$ were obtained. Prominent ions of m/z 654 were tentatively assigned as $[\text{M}+\text{H}-\text{N}(\text{CH}_3)_3-\text{H}_2\text{O}]^+$ wherein one molecule of water was lost from the LCB. In the low-mass region, ions of m/z 184 corresponding to phosphorylcholine were observed, as in the positive ESI mode. Similar results were obtained for the other sphingomyelin standards. In APCI with negative-ion detection, the mass spectra (not shown) were reported to be comparable to those obtained in negative-ion ESI but with lower sensitivity.

Lipid extracts of archaeological shards from late Roman cooking pots were analyzed by using LC/APCI-MS (20). This advanced technique showed the use of beeswax through identification of the constituting alkanes and mono- and diesters. Part of the animal fat was characterized as originating from ruminants because of the presence of *trans* FA. The results illustrate how the compositions of complex mixtures can be unraveled and the original contents of ancient ceramic vessels can be determined by using specialized analytical equipment.

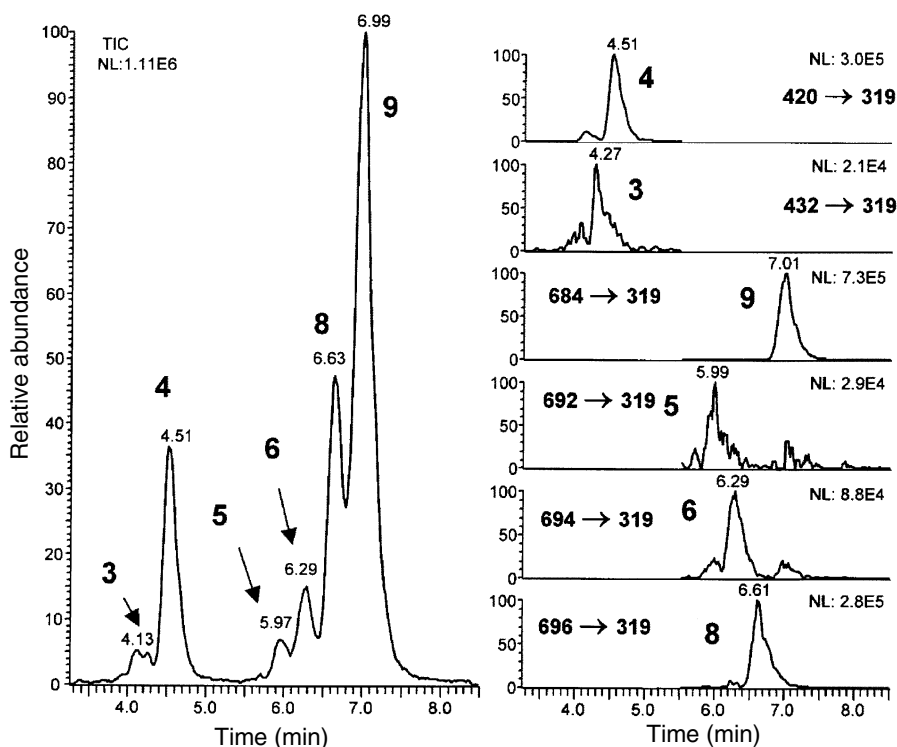


Fig. 5.18. LC-APCI-MS/MS chromatogram (left) and extracted ion chromatograms (right) corresponding to the analysis of toxic oil syndrome-related oil sample.

The saturated monoesters were the most important compounds of beeswax and consisted of long-chain alcohols (C_{24} – C_{36}) esterified with palmitic acid. The hydroxymonoesters coeluted with monoesters of a similar carbon number and the monoesters with a larger carbon number (C_{46} – C_{50}) coeluted with hydroxydiesters.

The most important fragment ions of the saturated monoesters (alkyl palmitates) were characterized by an intense hydride-extracted molecular ion $[M-H]^+$ and $[C_{15}H_{31}COOH-H]^+$ ion formed by the loss of the FA. Also, the acylium ion of palmitic acid at m/z 237, $[C_{15}H_{31}COO-H_2O]^+$, was detected. No distinction could be made between the mass spectrum of saturated and unsaturated monoesters, since unsaturated monoesters form abundant $[M+H]^+$ ions. Hydroxymonoesters eluted just after the saturated monoesters and showed hydride-extracted molecular ions, $[M-H]^+$, and the hydroxy-palmitic acid ion $[C_{15}H_{30}OHCOOH-H]^+$, formed by the loss of the FA. The diesters (C_{56} – C_{64}) showed an abundant $[M+H]^+$ ion and intense fragment ions caused by the loss of palmitic acid, $[M+H-C_{15}H_{31}COOH]^+$. Also, hydroxydiesters were detected, which showed an $[M+H]^+$ ion together with an $[M+H-C_{15}H_{30}OHCOOH]^+$ ion formed by the loss of hydroxy-palmitic acid.

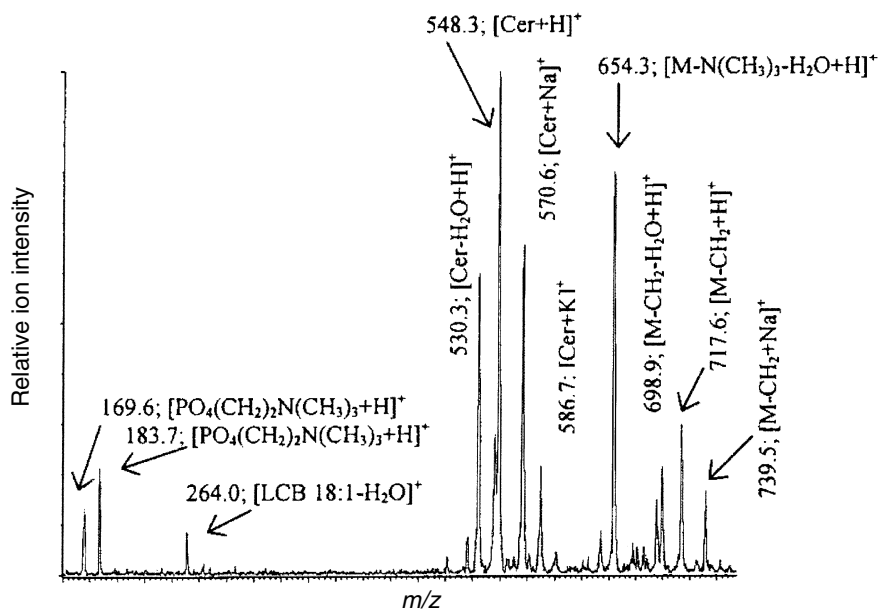


Fig. 5.19. APCI mass spectrum of *d*-18:1/18:0-sphingomyelin.

Vitamin Metabolites by LC/APCI-MS

The separation of possible metabolites of vitamin D₃, that is, 3-stearate, 3-palmitate, 3-oleate, and 3-linoleate, was performed by using LC/APCI-MS (21). The FA esters were derivatized with a Cookson-type reagent (4-phenyl-1,2,4-triazoline-

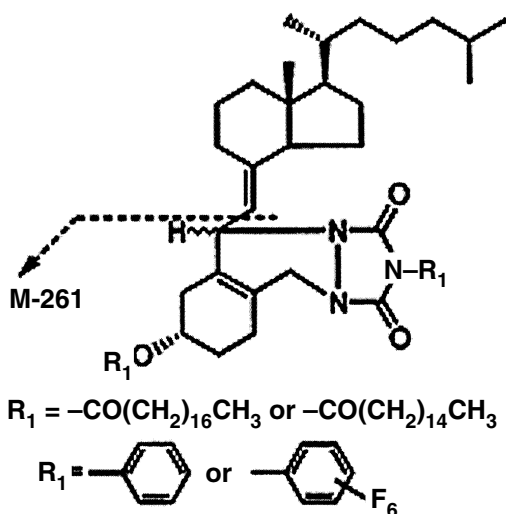


Fig. 5.20. Fragmentation of adducts of D₃ 3-fatty acid esters with Cookson-type reagents.

3,5-dione) to give stable Diels-Alder adducts (PTAD) (Fig. 5.20) and they showed a quasimolecular ion as an intense peak.

Endogenous vitamin D₃ is present mainly in urine and serum in a nonpolar esterified form. The LC/APCI-MS of these esters showed their deesterified ion (*m/z* 367) as a base peak in the positive-ion mode, but pseudomolecular ions (*m/z* 651 and 623, respectively) were also detected with weak intensity (<12%). In the negative mode, these esters did not show any characteristic ions (Table 5.4).

The adducts with PTAD showed pseudomolecular ions with relatively strong intensities (>53%), together with the corresponding [M–261]⁺ ions as base peaks in positive-ion mode. It may be postulated that these fragment ions were formed by cleavage at the C_{6–7} bond of the D skeleton and loss of the CD-ring with a side chain, which can be used to identify the FA moiety of these esters. In the negative-ion mode, PTAD adducts showed pseudomolecular ions or cluster ions, which were postulated as the addition of a Cl[–] ion derived from CHCl₃ used as an injection solvent.

Separation and characterization of 3-FA esters of pregnenolone and dehydroepiandrosterone in rat brain were performed by using LC/APCI-MS operating in the positive-ion mode (22). The FA esters obtained from the rat brain were derivatized with *O*-methyl-hydroxylamine to give the respective methyloximes, which were identified by comparing their chromatographic retention times with those of authentic samples during LC/APCI-MS.

The xanthoside composition of the crude extract of *Umbilicaria proboscidea* was characterized by using LC-UV diode array detection and LC/APCI-MS methods (23). The presence of acylated xanthone-*O*-glucosides was determined by both positive- and negative-ion LC/APCI-MS. Based on UV and MS spectral data and nuclear magnetic

TABLE 5.4

LC-APCI-MS Data on D₃ 3-Fatty Acid Esters and Their Adducts with Cookson-type Reagents

| Compound | M.W. | Observed ion (<i>m/z</i>) | |
|----------------------------|------|--|--|
| | | Positive | Negative |
| D ₃ 3-Stearate | 650 | 367.4 [M+H–C ₁₈ H ₃₆ O ₂] ⁺ (100) ^a 651.7 [M+H] ⁺ (10) | ND ^b |
| PTAD ^c | 825 | 564.5 [M–261] ⁺ (100) 826.7[M+H] ⁺ (93) | 319.1(100) 860.5 [M+35] [–] (76) |
| D ₃ 3-Palmitate | 622 | 367.4 [M+H–C ₁₆ H ₃₂ O ₂] ⁺ (100) 623.6 [M+H] ⁺ (12) | ND |
| PTAD | 797 | 536.4 [N–261] ⁺ (100) 798.8 [M+H] ⁺ (53) 886.6 [M–1] ⁺ (61) ^d | 796.9 [M–H] [–] (20) 832.6 [M+35] [–] (100) |

^aRelative intensity (%).

^bNot detected.

^cAdduct.

^dAmbiguity still remains in this ion's identification.

resonance (NMR) spectroscopy, a total of 14 compounds (6-*O*-acylated umbilicaxanthosides A and B) were identified in *U. proboscidea* for the first time. To further develop the applicability of LC-MS techniques to phytochemical characterization, the effect of different ionization energies on fragmentation was studied using APCI-MS. Optimal ionization conditions were achieved with positive-ion APCI using ammonium acetate buffer, and with negative-ion APCI by using formic acid (pH 4).

The (2,4-dinitrophenyl)hydrazones of 1-alkanals (from formaldehyde to octadecanal) and other carbonyl compounds were separated by LC/APCI-MS (24). The base peak in the negative-ion APCI mass spectrum was the $[M-H]^-$ ion $(NO_2)_2C_6H_3NN=CR_1R_2$ ($R_1=H$ for aldehydes). The report described the measurement of carbonyl compounds at the levels of 0.014–0.015 ppb in urban air and the identification of carbonyls at ppb concentrations as reaction products in laboratory studies of the atmospheric oxidation of unsaturated organic compounds.

Let us briefly mention some more details about the application of the ESI method for analyses and identification of FA and their simple derivatives.

LC/ESI-MS Methods for FA Analysis

Low-energy negative-ion ESI-MS and ESI-MS/MS were used (25) to characterize saturated and unsaturated FA. The carbon number and degree of unsaturation of FA were determined. ESI-MS/MS was used to localize double-bond positions of mono- and polyunsaturated FA. For compounds with up to two unsaturated bonds, fragmentation was dominated by the loss of H_2O from the carboxyl moiety and very low-intensity peaks were generated from bonds cleaved at carbons α or β to sites of unsaturation. There was extensive hydride migration during ESI-MS/MS of compounds with three or more double bonds and the localization of double and triple bonds was very difficult. Detection limits for negative-ion ESI-MS/MS were at or below 1 pg.

Features of MS-MS of dilithiated adduct ions of unsaturated FA, obtained by ESI-MS with low-energy collisionally activated dissociation on a triple-stage quadrupole instrument, were described (26). These spectra distinguished among isomeric unsaturated FA and permitted the assignment of double-bond location. The spectra contained radical cations reflecting cleavage of bonds between the first and second and between the second and third carbon atoms in the FA chain. These ions were followed by a closed-shell ion series with members separated by 14 units that reflected cleavage of bonds between the third and fourth and then between subsequent adjacent pairs of carbon atoms.

The use of EI and ESI for the determination of branching positions and localization of unsaturation in FA was described in a report by Vetter and colleagues (27). A new derivative of the carboxyl group, *N*-methyl-2-alkylimidazoline (MIM), was introduced with the aim of improving the control of FA fragmentation. The results obtained from saturated chains were very similar to those generated by EI. The current data do not permit us to formulate definitive rules for the fragmentation of the MIM derivatives of PUFA.

LC/ESI-MS of Dimethylaminoethyl and Trimethylaminoethyl Esters

The development of a new derivative, the dimethylaminoethyl ester (DMAE), for the analysis of FA by ESI-MS/MS was described by Johnson (28). Qualitative and quantitative analyses of long-chain to VLCFA in plasma, blood, urine, and wax were performed. Branched chain, unsaturated, dicarboxylic, hydroxy, amino, and oxo acids were also studied.

The mass spectrum of the DMAE ester of arachidic acid was dominated by an $[M+H]^+$ at m/z 384. It yielded strong product ions at m/z 339, 90, and 72. The ion at m/z 90 was identified as protonated dimethylaminoethanol that had been eliminated from the DMAE ester. The ion at m/z 72 is probably an immonium ion, $MeHC=N^+Me_2$, commonly generated from aliphatic amines.

Further, the trimethylaminoethyl (TMAE) ester iodide (29) affords between 8 and 12 times greater signal intensity than the corresponding dimethylaminoethyl ester used in the analysis of long-chain to VLCFA. It is a superior derivative for unsaturated and monohydroxylated long-chain FAs but was unsuitable for bile acids and dicarboxylic acids. The product ion spectra of the molecular cations of all TMAE derivatives of saturated FA from acetic to triacontanoic contained a $[M-C_3H_9N]^+$ ion as the most intense ion. As observed for DMAE esters, there was no difference in the mass spectra or product ion spectra of derivatives of straight-chain and multiple-branched FA of the same molecular mass.

In contrast to DMAE esters, the molecular cations of TMAE derivatives of unsaturated FA yielded $[M-C_3H_9N]^+$ product ions of similar intensity to those obtained from saturated FA with the same number of carbon atoms. Unlike GC-MS, which separates isomeric forms, the PUFA identified by ESI-MS/MS represent the total of all of the ω -3, ω -6, ω -9, and so on, series isomers.

An obvious shortcoming of the ESI-MS/MS method used for analyzing hydroxy FA is that all the isomeric forms such as 2-, 3-, and ω -hydroxy isomers are measured collectively.

LC/ESI-MS of Oxidized FA

Negative-ion ESI-MS and ESI-MS/MS were used to characterize saturated and unsaturated monohydroxy FA and FA metabolites formed by incubation with soybean lipoxygenase (30). Ions corresponding to the $[M-H]^-$ of eicosanoids were readily observed by using ESI-MS, but double-bond migration precluded the use of MS to localize double bonds or the position of hydroxyl moieties; however, by following MS analysis with negative-ion ESI-MS/MS of precursor ions, the position of oxygenation could be determined for picogram quantities of underivatized monohydroxy FA.

Two reports (31,32) describing ESI and low-energy MS-MS of polyhydroxy unsaturated FA and negative-ion ESI-MS/MS structural characterization of leukotriene B_4 -derived metabolites were published. The low-energy collision-induced dissociation (CID) of the carboxylate anions generated by ESI of leukotriene B_4 and 16 of its metabolites was studied in a tandem quadrupole mass spectrometer (31).

Negative ESI, fast atom bombardment (FAB), and low-energy MS-MS were used for the analysis of dihydroxyecosatrienoic acids containing a vicinal diol and three nonconjugated double bonds, of dihydroxyecosatetraenoic acids, which contain a conjugated triene structure, and of trihydroxyecosatetraenoic acids, which contain a vicinal diol and a conjugated tetraene structure (32).

A rapid method was described for the identification of FA hydroperoxides by LC/ESI-MS/MS without any derivatization required before analysis (33).

A new interface for capillary electrophoresis (CE-ESI) was presented (34). The liner has been evaluated for the analysis of FA and prostaglandins, all run with negative ESI.

Direct analysis (35) of intact long-chain fatty acyl CoA esters was investigated by using matrix-assisted laser desorption time-of-flight MS and ESI-MS. Decomposition of the $[M+H]^+$ ion of hexadecyl coenzyme A at m/z 1006 yielded a prominent product ion at m/z 499 characteristic for the fatty acyl portion of the molecule. Similar fatty acyl product ion fragments, corresponding to a neutral loss of m/z 609, were found for the $[M+H]^+$ species of all of the fatty acyl CoA esters investigated.

Acylcarnitines were used for determining the β -oxidation defects in patients (neonatal and prenatal inborn errors) with biochemically heterogeneous diseases (see Table 5.5) (36–49). This method was also used for detection of further metabolic disorders (50–52). Also, the structures of lipid A and further bacterial lipids were determined by ESI-MS methods (53–57).

ESI-MS/MS analyses were performed on phospholipid and cholesterol esters without any previous chromatographic separation (58). The fragmentation of cholesterol esters was shown and a fragment ion at m/z 369 was the most abundant product ion of cholesterol esters.

The study by Kerwin and colleagues (59) described the use of positive- and negative-ion ESI with MS-MS to identify glycerophospholipid and ceramide headgroups and their alkyl, alkenyl, and acyl constituents.

Conclusions

The largely unsatisfactory state of the art in APCI of simple derivatives of FA can be summarized as follows:

Fundamental studies that would contain essential details describing the effect of external parameters such as capillary voltage setting, corona current, nebulizer pressure, drying gas flow and temperature, vaporizer temperature, fragmenter settings, and so on, on FA identification have not yet been published. For instance, contradictory data exist on the addition of mobile-phase components (i.e., acetonitrile) to double bond(s) of unsaturated FA. Some authors have identified an ion at $[M+42]^+$, others have found an ion adduct at $[M+54]^+$, and still others did not detect any adduct ions. However, it is commonly known that ions of all types arise during chemical ionization (60). Therefore, all of the possibilities have been considered. For full identification of FA, it is necessary to know the value of the molecular mass, from

TABLE 5.5

Quantitative Plasma Acylcarnitine Analysis Using Electrospray Tandem Mass Spectrometry for the Diagnosis of Organic Acidemias and Fatty Acid Oxidation Defects

| Disorder | Diagnostic <i>m/z</i> ratio | Acylcarnitines ^a | Reference controls (95th centile ^b), $\mu\text{mol/L}$ | Patients (range ^d), $\mu\text{mol/L}$ |
|-----------------------|-----------------------------|--|--|---|
| SCAD/EMA | 288/274 | C ₄ /C ₃ | 0.98 ^c | 0.71–9.0 ^c |
| | 288/347 | C ₄ /C ₈ -d ₃ | 0.32 | 0.80–5.00 |
| | 302/274 | C ₅ /C ₃ | 0.80 ^c | 0.19–4.52 ^c |
| | 302/347 | C ₅ /C ₈ -d ₃ | 0.22 | 0.16–0.64 |
| MCAD | 316/347 | C ₆ /C ₈ -d ₃ | 0.12 | 0.12–2.14 |
| | 344/347 | C ₈ /C ₈ -d ₃ | 0.22 | 1.16–25.78 |
| | 370/347 | C _{10:1} /C ₈ -d ₃ | 0.22 | 0.26–2.24 |
| LCHAD/MTP | 472/459 | C ₁₆ OH/C ₁₆ -d ₃ | 0.02 | 0.12–0.60 |
| | 498/459 | C _{18:1} OH/C ₁₆ -d ₃ | 0.01 | 0.14–0.86 |
| | 500/459 | C ₁₈ OH/C ₁₆ -d ₃ | 0.04 | 0.12–0.78 |
| VLCAD | 426/459 | C _{14:1} /C ₁₆ -d ₃ | 0.18 | 0.76–13.28 |
| | 424/459 | C _{14:2} /C ₁₆ -d ₃ | 0.08 | 0.30–3.48 |
| CPT II | 456/459 | C ₁₆ /C ₁₆ -d ₃ | 0.24 | 2.06–3.94 |
| | 454/459 | C _{16:1} /C ₁₆ -d ₃ | 0.08 | 0.50–0.86 |
| | 484/459 | C ₁₈ /C ₁₆ -d ₃ | 0.10 | 0.64–1.44 |
| | 482/459 | C _{18:1} /C ₁₆ -d ₃ | 0.28 | 1.56–4.32 |
| | 480/459 | C _{18:2} /C ₁₆ -d ₃ | 0.18 | 0.54–1.66 |
| GA I | 388/347 | Glutaryl/C ₈ -d ₃ | 0.06 | 0.46–1.34 |
| GA II/MAD | 288/274 | C ₄ /C ₃ | 0.98 ^c | 2.09–12.54 ^c |
| | 302/274 | C ₅ /C ₃ | 0.80 ^c | 1.82–6.27 ^c |
| | 316/347 | C ₆ /C ₈ -d ₃ | 0.12 | 0.22–3.54 |
| | 344/347 | C ₈ /C ₈ -d ₃ | 0.22 | 0.80–7.96 |
| | 372/347 | C ₁₀ /C ₈ -d ₃ | 0.30 | 0.82–5.88 |
| HMG-CoA-lyase | 318/347 | Hydroxy-C ₅ /C ₈ -d ₃ | 0.06 | 0.08–1.42 |
| | 402/347 | Methylglutaryl/C ₈ -d ₃ | 0.02 | 0.08–0.70 |
| β -Ketothiolase | 300/347 | C _{5:1} /C ₈ -d ₃ | 0.04 | 0.14–0.72 |
| | 318/347 | Hydroxy-C ₅ /C ₈ -d ₃ | 0.06 | 0.12–0.30 |
| PA | 274/263 | C ₃ /C ₂ -d ₃ | 1.30 | 6.50–60.10 |
| MMA | 274/263 | C ₃ /C ₂ -d ₃ | 1.30 | 13.00–70.50 |
| | 374/347 | Methylmalonyl/C ₈ -d ₃ | 0.06 | 0.12–0.94 |
| IVA | 302/274 | C ₅ /C ₃ | 0.80 ^c | 52.96–60.47 ^c |
| | 302/347 | C ₅ /C ₈ -d ₃ | 0.22 | 15.52–18.38 |

^ad₃ depicts a labeled internal standard.

^bThe 95th centile of the reference range.

^cExpressed as ratio.

^dRange of values found in patient samples, not all concentrations and/or ratios were abnormal in each case. Abbreviations: SCAD, short-chain acyl-CoA dehydrogenase; MCAD, medium-chain acyl-CoA dehydrogenase; LCHAD/MTP, long-chain 3-hydroxyacyl-CoA dehydrogenase/mitochondrial trifunctional protein; VLCAD, very-long-chain acyl-CoA dehydrogenase; CPT II, carnitine palmitoyltransferase II; GA I, glutaric acidemia type I; GA II/MAD, glutaric acidemia type II/multiple acyl-CoA dehydrogenase; HMG-CoA lyase, 3-hydroxy-3-methylglutaryl-CoA dehydrogenase; BKT, β -ketothiolase; PA, propionic acidemia; MMA, methylmalonic acidemia; IVA, isovaleric acidemia.

which the chain length and number of double bonds can be deduced. However, some samples of natural origin can contain 27:1 and 28:8 FA. Although both FA have the same molecular mass, there are no problems in separating them by chromatography (16).

Unfortunately, the APCI-MS method failed in the identification of the position and configuration of double bonds (*E/Z*), as discussed herein for the case of acetonitrile addition to the C=C bond. In particular, the method fails in identification of branched (and polybranched) FA and for FA in which the main chain was substituted by a hydroxyl group or oxygen atom. One report that confirmed the feasibility of the APCI method in this field was published earlier (8).

As follows from the survey of these reports, APCI methods were applied first in cases of FA identification where classical GC-MS techniques failed. The methods provided unsatisfactory results in the identification of VLCFA and VLCPUFA in natural samples, especially those of exotic origin. As shown herein, the higher fixed and variable costs of analysis by APCI-MS methods must be considered.

Currently, the possibilities of APCI-MS methods are not fully exploited, especially in analysis of simple derivatives of FA. The technique is relatively new and is still waiting for its boom. Because of the commercial availability of LC/APCI-MS systems we would expect an increase of sophisticated APCI applications in LC-MS in the coming years. Unfortunately, the high purchase price and operating costs seem to be the main limitations in the use of LC/APCI-MS. However, the robustness and sensitivity of analyses, the possibility of simultaneous evaluation of the content of chemical compounds, estimation of their chemical structures, and determination of molecular masses all combine to make it a technique of extraordinary value.

References

1. Murphy, R.C., J. Fiedler, and J. Hevko, Analysis of Nonvolatile Lipids by Mass Spectrometry, *Chem. Rev.* 101: 479–526 (2001).
2. Rezanka, T., and V.M. Dembitsky, Very Long Chain Polyunsaturated Fatty Acids in Crustacea of the Order Bathynellacea, *Biochem. Syst. Ecol.* 27: 551–558 (1999).
3. Rezanka, T., Analysis of Polyunsaturated Fatty Acids Using High Performance Liquid Chromatography—Atmospheric Pressure Chemical Ionization Mass Spectrometry, *J. High Resol. Chromatogr.* 23: 338–342 (2000).
4. Sjoberg, P.J.R., and K.E. Markides, Capillary Column Supercritical Fluid Chromatography—Atmospheric Pressure Ionisation Mass Spectrometry-Interface Performance of Atmospheric Pressure Chemical Ionisation and Electrospray Ionization, *J. Chromatogr. A* 855: 317–327 (1999).
5. Banni, S., B.W. Day, R.W. Evans, F.P. Corongui, and B. Lombardi, Liquid Chromatographic-Mass Spectrometric Analysis of Conjugated Diene Fatty Acids in a Partially Hydrogenated Fat, *J. Am. Oil Chem. Soc.* 71: 1321–1325 (1994).
6. Rezanka, T., Analysis of Very Long Chain Polyunsaturated Fatty Acids Using High-Performance Liquid Chromatography—Atmospheric Pressure Chemical Ionization Mass Spectrometry, *Biochem. Syst. Ecol.* 28: 847–856 (2000).

7. Řezanka, T., and V.M. Dembitsky, Tetratriacontanoenoic Acid, First Natural Acid with Nine Double Bonds Isolated from a Crustacean *Bathynella natans*, *Tetrahedron* 60: 4261–4264 (2004).
8. Řezanka, T., Identification of Very Long Chain Fatty Acids by Atmospheric Pressure Chemical Ionization Liquid Chromatography-Mass Spectroscopy from Green Alga *Chlorella kessleri*, *J. Sep. Sci.* 25: 1332–1336 (2002).
9. Holcapek, M., P. Jandera, and J. Fischer, Analysis of Acylglycerols and Methyl Esters of Fatty Acids in Vegetable Oils and in Biodiesel, *Crit. Rev. Anal. Chem.* 31: 53–56 (2001).
10. Rigol, A., A. Latorre, S. Lacorte, and D. Barcelo, Direct Determination of Resin and Fatty Acids in Process Waters of Paper Industries by Liquid Chromatography/Mass Spectrometry, *J. Mass Spectrom.* 38: 417–426 (2003).
11. Latorre, A., A. Rigol, S. Lacorte, and D. Barcelo, Comparison of Gas Chromatography-Mass Spectrometry and Liquid Chromatography-Mass Spectrometry for the Determination of Fatty and Resin Acids in Paper Mill Process Waters, *J. Chromatogr. A* 991: 205–215 (2003).
12. Piazza, G.J., A. Nunez, and T.A. Foglia, Epoxidation of Fatty Acids, Fatty Methyl Esters, and Alkenes by Immobilized Oat Seed Peroxygenase, *J. Mol. Catal. B Enzymol.* 21: 143–151 (2003).
13. Adas, F., D. Picart, F. Berthou, B. Simon, and Y. Amet, Liquid Chromatography–Mass Spectrometry and Gas Chromatography–Mass Spectrometry of ω - and (ω -1)-Hydroxylated Metabolites of Elaidic and Oleic Acids in Human and Rat Liver Microsomes, *J. Chromatogr. B* 714: 133–144 (1998).
14. Ikeda, M., and T. Kusaka, Liquid Chromatography-Mass Spectrometry of Hydroxy and Non-Hydroxy Fatty Acids as Amide Derivatives, *J. Chromatogr.* 575: 197–205 (1992).
15. Koga, D., T. Santa, T. Fukushima, H. Homma, and K. Imai, Liquid Chromatographic-Atmospheric Pressure Chemical Ionization Mass Spectrometric Determination of Anandamide and Its Analogs in Rat Brain and Peripheral Tissues, *J. Chromatogr. B* 690: 7–13 (1997).
16. Nichols, D.S., and N.W. Davies, Improved Detection of Polyunsaturated Fatty Acids as Phenacyl Esters Using Liquid Chromatography-Ion Trap Mass Spectrometry, *J. Microbiol. Methods* 50: 103–113 (2002).
17. Kusaka, T., and M. Ikeda, LC-MS of Fatty Acids Including Hydroxy and Hydroperoxy Acids as Their 3-Methyl-7-methoxy-1,4-benzoxazin-2-one Derivatives, *J. Chromatogr.* 639: 165–173 (1993).
18. Calaf, R.E., J. Pena, S. Paytubi, M. Carrascal, M. Posada, and E. Gelpi, Automated Strong Cation Exchange Extraction of Fatty Acid Esters of 3-(*N*-Phenylamino)-1,2-propanediol from Oil Samples for Routine Quantification by HPLC-APCI/MS/MS, *J. Agr. Food Chem.* 49: 5085–5091 (2001).
19. Karlsson, A.A., P. Michelsen, and G. Odham, Molecular Species of Sphingomyelin: Determination by High-Performance Liquid Chromatography Mass Spectrometry with Electrospray and High-Performance Liquid Chromatography Tandem Mass Spectrometry with Atmospheric Pressure Chemical Ionization, *J. Mass Spectrom.* 33: 1192–1198 (1998).
20. Kimpe, K., P.A. Jacobs, and M. Waelkens, Mass Spectrometric Methods Prove the Use of Beeswax and Ruminant Fat in Late Roman Cooking Pots, *J. Chromatogr. A* 968: 151–160 (2002).

21. Mitamura, K., Y. Nambu, M. Tanaka, A. Kawanishi, J. Kitahori, and K. Shimada, High-Performance Liquid Chromatographic Separation of Vitamin D-3 3-Fatty Acid Esters and Their Liquid Chromatography Mass Spectrometry, *J. Liq. Chromatogr. Rel. Technol.* 22: 367–377 (1999).
22. Shimada, K., Y. Mukai, A. Nakajima, and Y. Naka, Studies on Neurosteroids, 6: Characterization of Fatty Acid Esters of Pregnenolone and Dehydroepiandrosterone in Rat Brains Using Liquid Chromatography Mass Spectrometry, *Anal. Commun.* 34: 145–146 (1997).
23. Rezanka, T., and V.M. Dembitsky, Identification of Acylated Xanthone Glycosides by Liquid Chromatography–Atmospheric Pressure Chemical Ionization Mass Spectrometry in Positive and Negative Modes from the Lichen *Umbilicaria proboscidea*, *J. Chromatogr. A* 995(1-2): 109–118 (2003).
24. Grosjean, E., P.G. Green, and D. Grosjean, Liquid Chromatography Analysis of Carbonyl (2,4-Dinitrophenyl)hydrazones with Detection by Diode Array Ultraviolet Spectroscopy and by Atmospheric Pressure Negative Chemical Ionization Mass Spectrometry, *Anal. Chem.* 7: 1851–1861 (1999).
25. Kerwin, J.L., A.L. Wiens, and L.H. Ericsson, Identification of Fatty Acids by Electrospray Mass Spectrometry and Tandem Mass Spectrometry, *J. Mass Spectrom.* 31: 184–192 (1996).
26. Hsu, F.F., and J. Turk, Distinction Among Isomeric Unsaturated Fatty Acids as Lithiated Adducts by Electrospray Ionization Mass Spectrometry Using Low Energy Collisionally Activated Dissociation on a Triple Stage Quadrupole Instrument, *J. Am. Soc. Mass Spectrom.* 10: 600–612 (1999).
27. Vetter, W., W. Meister, and G. Oesterheld, 2-Alkylimidazoline Derivative to Control Fatty Acid Fragmentation upon Electron Impact and Electrospray Ionization, *J. Mass Spectrom.* 33: 461–472 (1998).
28. Johnson, D.W., Dimethylaminoethyl Esters for Trace, Rapid Analysis of Fatty Acids by Electrospray Tandem Mass Spectrometry, *Rapid Commun. Mass Spectrom.* 13: 2388–2393 (1999).
29. Johnson, D.W., Alkyldimethylaminoethyl Ester Iodides for Improved Analysis of Fatty Acids by Electrospray Ionization Tandem Mass Spectrometry, *Rapid Commun. Mass Spectrom.* 14: 2019–2024 (2000).
30. Kerwin, J.L., and J.J. Torvik, Identification of Monohydroxy Fatty Acids by Electrospray-Mass Spectrometry and Tandem-Mass Spectrometry, *Anal. Biochem.* 237: 56–64 (1996).
31. Wheelan, P., J.A. Zirrollia, and R.C. Murphy, Negative Ion Electrospray Tandem Mass Spectrometric Structural Characterization of Leukotriene B4 (LTB4) and LTB4-Derived Metabolites, *J. Am. Soc. Mass Spectrom.* 7: 129–139 (1996).
32. Wheelan, P., J.A. Zirrolli, and R.C. Murphy, Electrospray Ionization and Low-Energy Tandem Mass Spectrometry of Polyhydroxy Unsaturated Fatty Acids, *J. Am. Soc. Mass Spectrom.* 7: 140–149 (1996).
33. Schneider, C., P. Schreier, and M. Herderich, Analysis of Lipoxygenase-Derived Fatty Acid Hydroperoxides by Electrospray Ionization Tandem Mass Spectrometry, *Lipids* 32: 331–336 (1997).
34. Petersson, M.A., G. Hulthe, and E. Fogelqvist, New Sheathless Interface for Coupling Capillary Electrophoresis to Electrospray Mass Spectrometry Evaluated by the Analysis of Fatty Acids and Prostaglandins, *J. Chromatogr. A* 854: 141–154 (1999).

35. Hankin, J.A., and R.C. Murphy, MALDI-TOF and Electrospray Tandem Mass Spectrometric Analysis of Fatty Acyl-CoA Esters, *Int. J. Mass Spectrom. Ion Processes* 165: 467–474 (1997).
36. Chace, D.H., S.L. Hillman, J.L. Van Hove, and E.W. Naylor, Rapid Diagnosis of MCAD Deficiency: Quantitative Analysis of Octanoylcarnitine and Other Acylcarnitines in Newborn Blood Spots by Tandem Mass Spectrometry, *Clin. Chem.* 43: 2106–2113 (1997).
37. Millington, D.S., N. Kodo, D.L. Norwood, and C.R. Roe, Tandem Mass Spectrometry: A New Method for Acylcarnitine Profiling with Potential for Neonatal Screening for Inborn Errors of Metabolism, *J. Inherit. Metab. Dis.* 13: 321–324 (1990).
38. Nada, M.A., C. Vianey-Saban, and C.R. Roe, Prenatal Diagnosis of Mitochondrial Fatty Acid Oxidation Defects, *Prenat. Diagn.* 16: 117–124 (1996).
39. Rashed, M.S., P.T. Luand, M.P. Bucknall, and D. Little, Diagnosis of Inborn Errors of Metabolism from Blood Spots by Acylcarnitines and Amino Acids Profiling Using Automated Electrospray Tandem Mass Spectrometry, *Pediatr. Res.* 38: 324–331 (1995).
40. Rashed, M.S., P.T. Luand, M.J. Bennett, J.J. Barnard, D.R. Govindaraju, and P. Rinaldo, Inborn Errors of Metabolism Diagnosed in Sudden Death Cases by Acylcarnitine Analysis of Postmortem Bile, *Clin. Chem.* 41: 1109–1114 (1995).
41. Rashed, M.S., M.P. Bucknall, and D. Little, Screening Blood Spots for Inborn Errors of Metabolism by Electrospray Tandem Mass Spectrometry with a Microplate Batch Process and a Computer Algorithm for Automated Flagging of Abnormal Profiles, *Clin. Chem.* 43: 1129–1141 (1997).
42. Shigematsu, Y., I. Hata, and A. Nakai, Prenatal Diagnosis of Organic Acidemias Based on Amniotic Fluid Levels of Acylcarnitines, *Pediatr. Res.* 39: 680–684 (1996).
43. Van Hove, J.L., W. Zhang, and S.G. Kahler, Medium-Chain Acyl-CoA Dehydrogenase (MCAD) Deficiency: Diagnosis by Acylcarnitine Analysis in Blood, *Am. J. Hum. Genet.* 52: 958–966 (1993).
44. Van Hove, J.L., S.L. Rutledge, M.A. Nada, S.G. Kahler, and D.S. Millington, 3-Hydroxyisovalerylcarnitine in 3-Methylcrotonyl-CoA Carboxylase Deficiency, *J. Inherit. Metab. Dis.* 18: 592–601 (1995).
45. Vreken, P., A.E.M. van Lint, A.H. Bootsma, H. Overmars, R.J.A. Wanders, and A.H. Van Gennip, Quantitative Plasma Acylcarnitine Analysis Using Electrospray Tandem Mass Spectrometry for the Diagnosis of Organic Acidemias and Fatty Acid Oxidation Defects, *J. Inherit. Metab. Dis.* 22: 302–306 (1999).
46. Giak Sim, K., K. Carpenter, J. Hammond, J. Christodoulou, and B. Wilckena, Quantitative Fibroblast Acylcarnitine Profiles in Mitochondrial Fatty Acid β -Oxidation Defects: Phenotype/Metabolite Correlations, *Mol. Genet. Metab.* 76: 327–334 (2002).
47. Ford, D.A., X.L. Han, C.C. Horner, and R.W. Gross, Accumulation of Unsaturated Acylcarnitine Molecular Species During Acute Myocardial Ischemia: Metabolic Compartmentalization of Products of Fatty Acyl Chain Elongation in the Acylcarnitine Pool, *Biochemistry* 35: 7903–7909 (1996).
48. Vreken, P., A.E.M. van Lint, A.H. Bootsma, H. Overmars, R.J.A. Wanders, and A.H. van Gennip, Rapid Diagnosis of Organic Acidemias and Fatty-Acid Oxidation Defects by Quantitative Electrospray Tandem-MS Acyl-Carnitine Analysis in Plasma, *Adv. Exp. Med. Biol.* 466: 327–337 (1999).
49. Sim, K.G., K. Carpenter, J. Hammond, J. Christodoulou, and B. Wilcken, Quantitative Fibroblast Acylcarnitine Profiles in Mitochondrial Fatty Acid β -Oxidation Defects: Phenotype/Metabolite Correlations, *Mol. Genet. Metab.* 76: 327–334 (2002).

50. Hsu, F.F., A. Bohrer, M. Wohltmann, S. Ramanadham, Z.M. Ma, K. Yarasheski, *et al.*, Electrospray Ionization Mass Spectrometric Analyses of Changes in Tissue Phospholipid Molecular Species During the Evolution of Hyperlipidemia and Hyperglycemia in Zucker Diabetic Fatty Rats, *Lipids* 35: 839–854 (2000).
51. Murthy, M., J. Hamilton, R.S. Greiner, T. Moriguchi, N. Salem, and H.Y. Kim, Differential Effects of n-3 Fatty Acid Deficiency on Phospholipid Molecular Species Composition in the Rat Hippocampus, *J. Lipid Res.* 43: 611–617 (2002).
52. Johnson, D.W., and M.U. Trinh, Analysis of Isomeric Long-Chain Hydroxy Fatty Acids by Tandem Mass Spectrometry: Application to the Diagnosis of Long-Chain 3-Hydroxyacyl CoA Dehydrogenase Deficiency, *Rapid Commun. Mass Spectrom.* 17: 171–175 (2003).
53. Corsaro, M.M., F.D. Piaz, R. Lanzetta, and M. Parrilli, Lipid A Structure of *Pseudoalteromonas haloplanktis* TAC 125: Use of Electrospray Ionization Tandem Mass Spectrometry for the Determination of Fatty Acid Distribution, *J. Mass Spectrom.* 37: 481–488 (2002).
54. Kussak, A., and A. Weintraub, Quadrupole Ion-Trap Mass Spectrometry to Locate Fatty Acids on Lipid A from Gram-Negative Bacteria, *Anal. Biochem.* 307: 131–137 (2002).
55. Vanderdrift, K.M.G.M., H.P. Spaink, G.V. Bloemberg, A.A.N. Van Brussel, B.J.J. Lugtenberg, J. Haverkamp, *et al.*, *Rhizobium leguminosarum* bv. *trifolii* Produces Lipochitin Oligosaccharides with Node-Dependent Highly Unsaturated Fatty Acyl Moieties: An Electrospray-Ionization and Collision-Induced Dissociation Tandem-Mass Spectrometric Study, *J. Biol. Chem.* 271: 22563–22569 (1996).
56. Rutters, H., H. Sass, H. Cypionka, and J. Rullkotter, Microbial Communities in a Wadden Sea Sediment Core—Clues from Analyses of Intact Glyceride Lipids, and Released Fatty Acids, *Org. Geochem.* 33: 803–816 (2002).
57. Toledo, M.S., S.B. Lavery, E. Suzuki, A.H. Straus, and H.K. Takahashi, Characterization of Cerebrosides from the Thermally Dimorphic Mycopathogen *Histoplasma capsulatum*: Expression of 2-Hydroxy Fatty N-Acyl (*E*)- δ -3-Unsaturation Correlates with the Yeast-Mycelium Phase Transition, *Glycobiology* 11: 113–124 (2001).
58. Duffin, K., M. Obukowicz, A. Raz, and J.J. Shieh, Electrospray/Tandem Mass Spectrometry for Quantitative Analysis of Lipid Remodeling in Essential Fatty Acid Deficient Mice, *Anal. Biochem.* 279: 179–188 (2000).
59. Kerwin, J.L., A.R. Tuininga, and L.H. Ericsson, Identification of Molecular Species of Glycerophospholipids and Sphingomyelin Using Electrospray MS, *J. Lipid Res.* 35: 1102–1114 (1994).
60. Moneti, G., G. Pieraccini, F. Dani, S. Turillazzi, D. Favretto, and P. Traldi, Ion-Molecule Reactions of Ionic Species from Acetonitrile with Unsaturated Hydrocarbons for the Identification of the Double-Bond Position Using an Ion Trap, *J. Mass Spectrom.* 32: 1371–1373 (1997).

Chapter 6

Regiospecific Analysis of Triacylglycerols Using High Performance Liquid Chromatography/Atmospheric Pressure Chemical Ionization Mass Spectrometry

Hazel R. Mottram

Organic Geochemistry Unit, School of Chemistry, University of Bristol, Cantock's Close, Bristol BS8 1TS, UK

Introduction

Naturally occurring mixtures of triacylglycerols (TAG) represent a considerable challenge to the analytical chemist. A typical animal fat or vegetable oil may contain in the region of 40 different TAG molecular species, while more complex mixtures such as milk fat or fish oil may comprise 150 or more individual species. The range of fatty acyl moieties present may include a wide range of carbon numbers and double bonds. In addition to determining which fatty acyl moieties are present in a TAG, it is also important to be able to determine their positions on the glycerol backbone of the molecule, since this has considerable significance from biochemical (1,2), nutritional (3,4), and biotechnological (5) points of view. However, the ability to unambiguously identify positional isomers of individual TAG, especially when they are components of complex natural mixtures, is a long-standing problem in lipid chemistry. Generally, it is not possible to directly measure the optical rotation of naturally occurring TAG since it is too weak, although in some cases, such as milk fat, the molecules are sufficiently asymmetric to allow this (6,7). Consequently, other techniques have been developed, which typically involve either the formation and separation of diacyl-*sn*-glycerols or analysis of the intact molecule.

Enzymatic Approaches

The first method for the stereospecific analysis of TAG was introduced by Brockerhoff (8) and employs pancreatic lipase (E.C. 3.1.1.3) or a Grignard reagent to partially hydrolyze TAG, giving rise to a mixture of 1,2- and 2,3-diacyl-*sn*-glycerols, which are phosphorylated to their corresponding phosphatidylphenols (Fig. 6.1). The 2-position fatty acyl moiety of the 1,2-diacylglycerol phosphatidylphenol can then be cleaved using phospholipase A₂ (E.C. 3.1.1.4) leaving a 1-monoacylglycerol lysophosphatidylphenol, which can be analyzed directly for the 1-position fatty acyl moiety, and an intact 2,3-diacylglycerol phosphatidylphenol. The 2-position fatty acyl moiety can be determined through analysis of the free fatty acids (FA) formed through

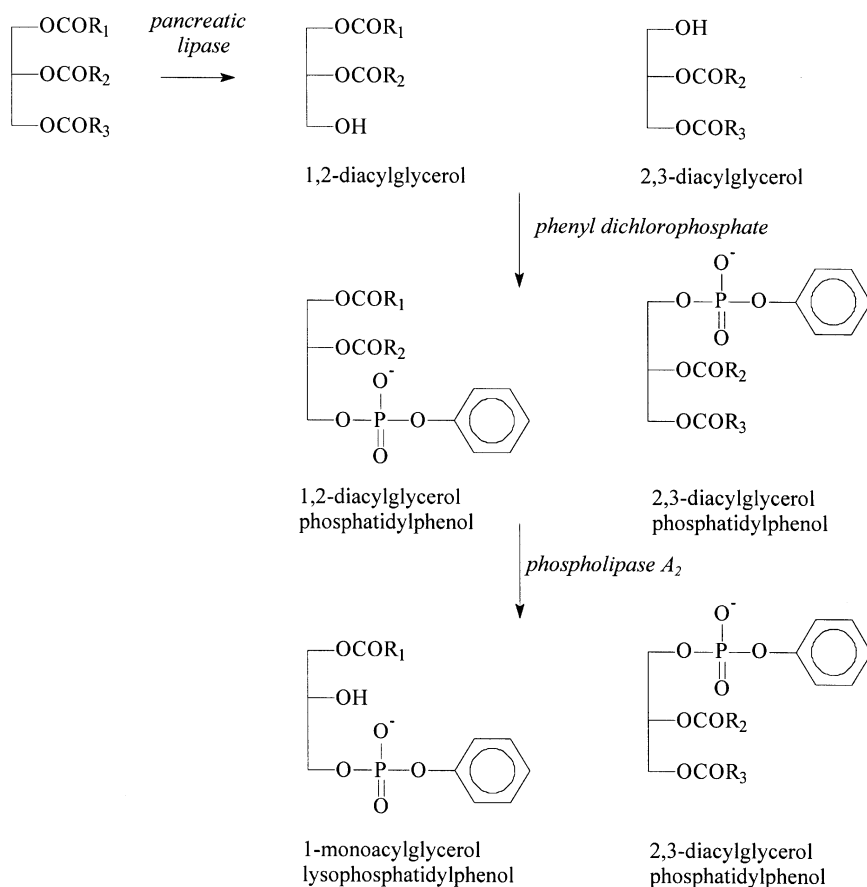


Fig. 6.1. Enzymatic method for stereospecific analysis of triacylglycerols. *Source:* Reference 8.

the action of phospholipase A_2 . The composition of the fatty acyl moiety in the *sn*-3-position cannot be determined by direct analysis, so is calculated indirectly.

A variation on this method (9) allows the FA compositions of all three positions to be determined directly. A Grignard reagent is used to prepare 1,3-diacyl-*sn*-glycerols, which are phosphorylated to phosphatidylphenols. Phospholipase A_2 is used to cleave the fatty acyl moiety at the 1-position, leaving a 3-monoacylglycerol lysophosphatidylphenol. Hence, the *sn*-1 FA is determined through analysis of the FA acids and the *sn*-3 composition through analysis of the lysophosphatidylphenols. The *sn*-2 FA composition is obtained through pancreatic lipase degradation of intact TAG. One drawback of this method is that it is difficult to obtain 1,3-diacyl-*sn*-glycerols that are representative of the original TAG owing to the problem of acyl migration, and consequently there are doubts about the accuracy.

A number of variations of the enzymatic method have been published, including a modification for the analysis of small quantities (10–40 mg) of TAG (10) and a method that relies on the rate of hydrolysis of phospholipase C being much faster for 1,2-diacyl-*sn*-glycerols than for 2,3-diacyl-*sn*-glycerols (11). All of the techniques involving enzymatic hydrolysis are subject to limitations based on the selectivity of the lipase. Studies reveal that there may be some selectivity for certain chain lengths and numbers of double bonds, as well as a possibility of acyl migration during the analysis (12), which may give a distorted distribution of 2-position FA. In addition, these methods only give information on the overall distribution of FA in each position and provide no information about individual TAG species. Assignments of the FA positions for individual components would require prior purification of individual TAG using preparative HPLC or a similar technique.

Chromatographic Methods

Derivatization Approach. Chiral stationary phases have been used to separate enantiomers of monoacyl-*sn*-glycerols and diacyl-*sn*-glycerols. Typically, mono- or diacyl-*sn*-glycerols are prepared from TAG by reaction with a Grignard reagent, and then are derivatized prior to analysis with some bulky chiral group to aid separation. Achiral stationary phases can also be employed to separate diacyl-*sn*-glycerols. Christie *et al.* (13) have developed a method in which TAG are partially hydrolyzed with ethyl magnesium bromide and derivatized to their (*S*)-(+)-1-(1-naphthyl) ethyl isocyanates prior to purification with a solid-phase octadecylsilyl extraction column (Fig. 6.2). The fatty acyl moieties at the *sn*-1- and *sn*-3-positions are determined from the gas chromatographic analysis of the total FA and of the fractions of 1,2- and 2,3-diacyl-*sn*-glycerols. The 2-position FA are calculated from the difference between these.

This technique has been applied to the analysis of a range of TAG mixtures, including vegetable oils, rat adipose tissue, egg yolk, and tallow (13,14). As with enzymatic techniques, without prefractionation such as preparative HPLC, techniques that rely on derivatization and separation of acylglycerols give no information on the positions of FA substitution in individual TAG in a mixture.

Argentation Chromatography. Using a silver ion impregnated column with polar solvents, silver ion HPLC has been demonstrated to separate ABA (e.g., 1,3-palmitoyl-2-oleoyl glycerol) and AAB (e.g., 1,2-palmitoyl-3-oleoyl glycerol) types of positional isomers (15), but gives no information on the positions of FA in an ABC type of TAG. Laakso and Voutilainen (16) used silver ion HPLC in conjunction with atmospheric pressure chemical ionization (APCI) mass spectrometry (MS) to separate and identify positional isomers of TAG present in various γ -linolenic acid-containing oils.

Nuclear Magnetic Resonance

Nuclear magnetic resonance spectroscopy (NMR) can be used to obtain both qualitative and quantitative information on the *sn*-2 FA of a TAG, with the ^{13}C reso-

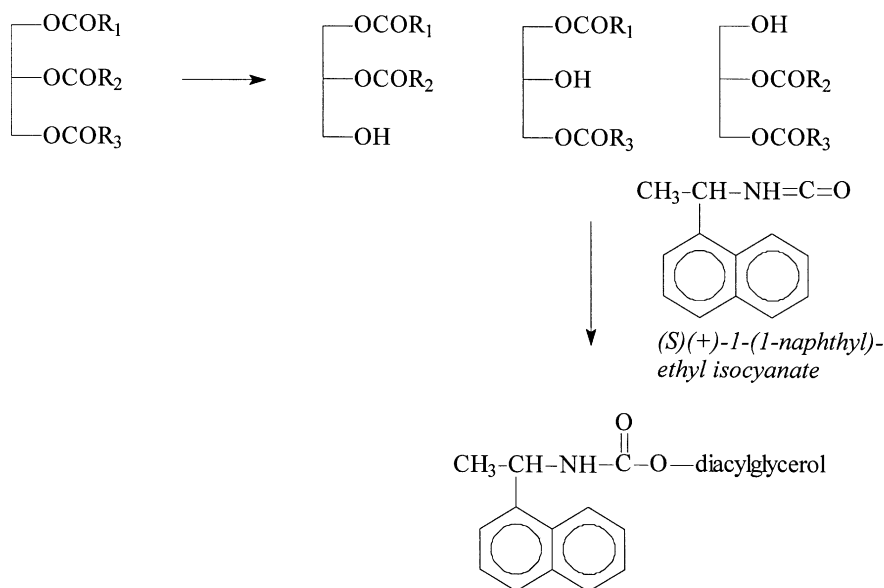


Fig. 6.2. Chemical derivatization allowing stereospecific analysis of triacylglycerols. Source: Reference 13.

nances of the carbonyl groups of *sn*-1 and *sn*-3 FA being well resolved from those of the *sn*-2 FA (17,18). Most unsaturated FA are nondegenerate and therefore, in unsaturated TAG, all three positions can be differentiated. The technique has been applied to the analysis of a range of vegetable oils (19,20), including those containing γ -linolenic acid (21,22), as well as fish oils (23). A comparison of Grignard deacylation, TLC and HPLC methods for TAG stereospecific analysis with ^{13}C -NMR showed that all three methods are valid within their acceptable error margins (24). The advantages of the NMR method are that little sample preparation is necessary and the technique is nondestructive. However, without prior fractionation, the positional distribution of individual TAG in a mixture cannot be determined.

Mass Spectrometric Methods

The application of mass spectrometric techniques to the analysis of TAG has the advantage of allowing absolute identification of the components present. Ryhage and Stenhagen (25) noted that ions corresponding to the loss of a fatty acyl chain from the TAG molecule were not observed for the 2-position acids when using electron ionization. Similarly, using negative ion chemical ionization tandem MS, the $[\text{M-H-RCO}_2\text{H}]^-$ ion corresponding to loss of the 2-position fatty acyl moiety was observed to be less abundant than that resulting from loss of the 1- and 3-position fatty acyl moieties (26). However, in order to determine the regiospecific configuration of individual TAG within a mixture, such as a vegetable oil or animal

fat, it is necessary to combine the resolution provided by HPLC with the molecular characterization afforded by MS. Although a wide range of mass spectrometric ionization techniques are available for studying TAG, only certain techniques are suitable for use in conjunction with HPLC systems. APCI is a relatively recent MS ionization technique (27), which has been shown to be particularly suited to the combined HPLC/MS analysis of TAG.

Atmospheric Pressure Chemical Ionization

APCI is a relatively “soft” ionization technique, but unlike electrospray ionization, APCI usually gives rise to some fragmentation, which facilitates structural characterization. A schematic diagram of a typical APCI source is shown in Figure 6.3.

The HPLC effluent exits the chromatographic column *via* a capillary, where it is converted into a mist of fine droplets through a combination of gentle heating and pneumatic nebulization. A make-up gas (typically nitrogen) is then used to sweep the mixture of droplets and vapor toward the ion formation region, which is held at atmospheric pressure. A corona discharge needle facilitates the ionization of trace amounts of water vapor and the resulting charged species in turn ionize the analyte molecules. Ions are then transported into the vacuum mass analyzer region *via* a pinhole entrance into an area of intermediate vacuum ($\sim 10^{-3}$ torr) followed by various ion focusing elements. To date, all APCI analyses of TAG have been carried out in the positive-ion mode.

APCI Spectra of TAG

The first RP-HPLC separation of TAG with identification by APCI-MS was demonstrated by Byrdwell and Emken (28). The APCI spectra of TAG are relatively simple (Fig. 6.4), with the most abundant ions in the spectrum generally corresponding to diacylglycerol fragment ions, $[M-RCO_2]^+$, resulting from the loss of

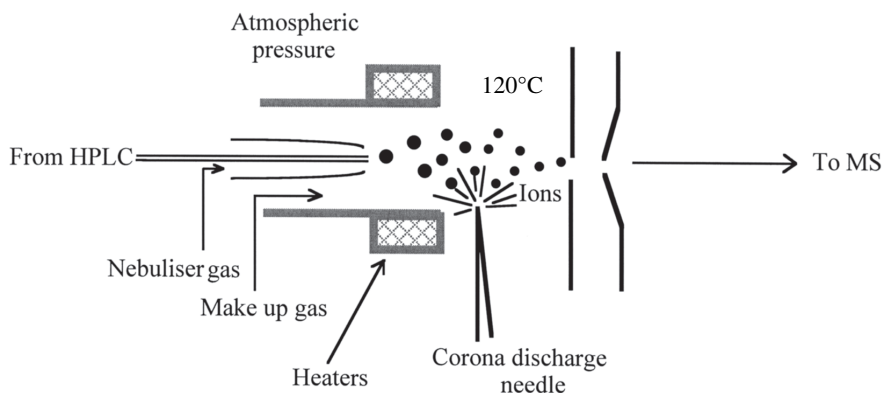


Fig. 6.3. Schematic diagram of an atmospheric pressure chemical ionization source.

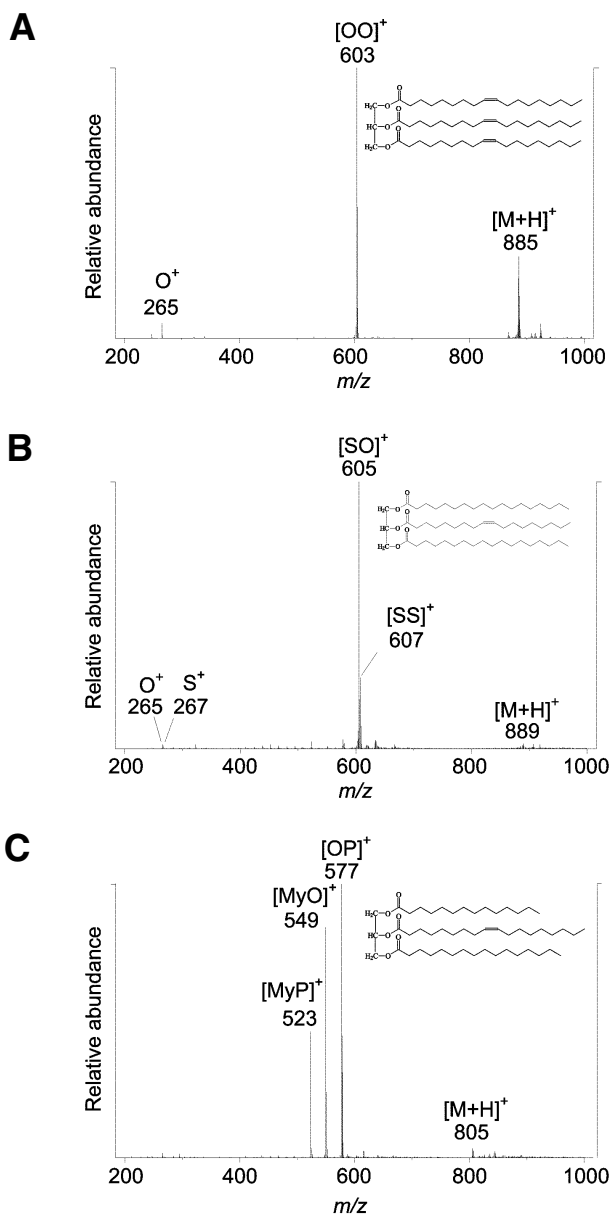


Fig. 6.4. APCI-MS mass spectra of (A) AAA (OOO), (B) ABA (SOS), and (C) ABC (MyOP) TAG. For abbreviations see Table 6.1.

fatty acyl moieties (“diacylglycerol” ions, $[DG]^+$). In conjunction with acylium ions $[RCO]^+$ corresponding to the fatty acyl moieties themselves, these allow identification of the FA present in each TAG species. A protonated molecule $[M+H]^+$ is often seen, although, since the intensity of this ion increases with the degree of

TABLE 6.1[RCO]⁺ Ions Observed in the HPLC/APCI-MS Mass Spectra of Various Vegetable Oils

| Trivial name | Abbreviation | Carbon number: degree of unsaturation | [RCO] ⁺ <i>m/z</i> |
|---------------|--------------|--|----------------------------------|
| Palmitic | P | 16:0 | 239 |
| Palmitoleic | Po | 16:1 | 237 |
| Margaric | Ma | 17:0 | 253 |
| Heptadecenoic | Mo | 17:1 | 251 |
| Stearic | S | 18:0 | 267 |
| Oleic | O | 18:1 | 265 |
| Linoleic | L | 18:2 | 263 |
| Linolenic | Ln | 18:3 | 261 |
| Stearidonic | St | 18:4 | 259 |
| Arachidic | A | 20:0 | 295 |
| Gadoleic | G | 20:1 | 293 |
| Behenic | B | 22:0 | 323 |
| Lignoceric | Li | 24:0 | 351 |

unsaturation of the molecule, it is not always detected in the spectra of highly saturated TAG (29). Adduct ions corresponding to the addition of water or HPLC solvent may also be observed.

The mass spectra of an AAA type TAG are typified by that of 1,2,3-trioleoyl glycerol (OOO, Fig. 6.4A, for abbreviations see Table 6.1), in which three clusters of ions can be seen: [M+H]⁺ at *m/z* 885; a single [M–RCO₂]⁺ ion at *m/z* 603 owing to loss of oleate; and a single [RCO]⁺ ion at *m/z* 265. In the mass spectrum of an ABA type TAG such as 1,3-distearoyl-2-oleoyl glycerol (SOS, Fig. 6.4B), two FA are present and hence two acylium ions are observed at *m/z* 265 (O⁺) and *m/z* 267 (S⁺). Likewise, two [M–RCO₂]⁺ ions are present corresponding to loss of stearate (*m/z* 605) and oleate (*m/z* 607), resulting in [SO]⁺ [AB]⁺ and ([SS]⁺) ([AA]⁺) ions, respectively. Similarly, the mass spectrum of an ABC type TAG, 1-myristoyl-2-oleoyl-3-palmitoyl glycerol (MyOP; Fig. 6.4C), shows three [M–RCO₂]⁺ ions at *m/z* 523, 549, and 577, corresponding to loss of oleate to give [MyP]⁺, loss of palmitate to give [MyO]⁺, and loss of myristate to give [PO]⁺, respectively. Tables 6.1, 6.2, and 6.3 list *m/z* values of a range of typical acylium, diacylglycerol, and protonated molecule ions seen in the APCI mass spectra of TAG.

The relatively simple mass spectra obtained from APCI, in conjunction with the separation afforded by HPLC, provide sufficient information to enable identification of the fatty acyl moieties in the individual TAG in a mixture. The technique has been applied to the analysis of TAG mixtures from a wide range of origins as summarized in Table 6.4. One major advantage of the APCI-MS process is that it enables the position of FA within the TAG to be determined; however, somewhat surprisingly, this facility has been rather underexploited.

TABLE 6.2[M-RCO₂]⁺ Ions Observed in the HPLC/APCI-MS Mass Spectra of Various Vegetable Oils

| [M-RCO ₂] ⁺ | m/z | [M-RCO ₂] ⁺ | m/z | [M-RCO ₂] ⁺ | m/z | [M-RCO ₂] ⁺ | m/z |
|------------------------------------|-----|------------------------------------|-----|------------------------------------|-----|------------------------------------|-----|
| PoPo | 547 | MaLn | 587 | SO | 605 | LB | 659 |
| PPo | 549 | MoL | 587 | PA | 607 | GG | 659 |
| PP | 551 | MaL | 589 | SS | 607 | PoLi | 661 |
| PoMo | 561 | MoO | 589 | MoG | 617 | OB | 661 |
| PMo | 563 | MaO | 591 | MaG | 619 | AG | 661 |
| PoMa | 563 | MoS | 591 | MoA | 619 | PLi | 663 |
| PMa | 565 | StSt | 591 | MaA | 621 | SB | 663 |
| PoSt | 569 | MaS | 593 | GSt | 625 | AA | 663 |
| PoLn | 571 | LnSt | 593 | LnG | 627 | MoLi | 675 |
| PSt | 571 | LnLn | 595 | ASt | 627 | MaLi | 677 |
| PLn | 573 | LSt | 595 | LG | 629 | LiSt | 683 |
| PoL | 573 | LLn | 597 | LnA | 629 | LnLi | 685 |
| MoMo | 575 | OSt | 597 | OG | 631 | LLi | 687 |
| PL | 575 | SSt | 599 | LA | 631 | GB | 689 |
| PoO | 575 | OLn | 599 | PoB | 633 | SLi | 691 |
| MaMo | 577 | LL | 599 | SG | 633 | OLi | 691 |
| PO | 577 | SLn | 601 | OA | 633 | AB | 691 |
| PoS | 577 | OL | 601 | PB | 635 | GLi | 717 |
| MaMa | 579 | PoG | 603 | SA | 635 | ALi | 719 |
| PS | 579 | SL | 603 | MoB | 647 | BB | 719 |
| MoSt | 583 | OO | 603 | MaB | 649 | BLi | 747 |
| MoLn | 585 | PG | 605 | BSt | 655 | LiLi | 775 |
| MaSt | 585 | PoA | 605 | LnB | 657 | | |

See Table 6.1 for abbreviations.

Position of FA Substitution

Mottram and Evershed (30) observed that the relative intensities of the [M-RCO₂]⁺ ions could be used to obtain information on the positions of FA within the TAG. Through loop injections of TAG standards of known regiospecific compositions into the APCI source of a Finnigan MAT TSQ 700, they noted that in the APCI-MS mass spectrum of an ABC type TAG, the least abundant [M-RCO₂]⁺ ion corresponds to loss of the FA from the *sn*-2-position (Fig. 6.5). They suggested that the reason for this is that it is energetically less favorable to lose a FA from the *sn*-2-position than from the *sn*-1- or *sn*-3-position. This effect is demonstrated in the spectrum of MyOP (Fig. 6.4C), in which the least abundant [M-RCO₂]⁺ ion is formed by the loss of oleate from the *sn*-2-position, leaving

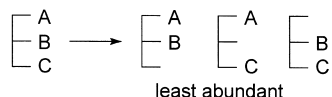


Fig. 6.5. Schematic diagram showing the possible DAG ions formed from a trifunctional ABC type TAG.

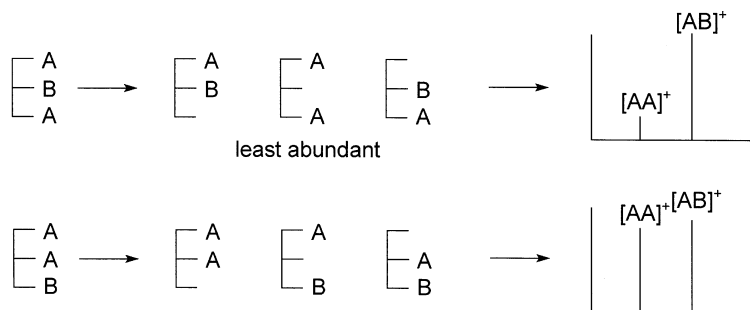
TABLE 6.3[M+H]⁺ Ions Observed in the HPLC/APCI-MS Mass Spectra of Various Vegetable Oils

| Triacylglycerol | [M+H] ⁺ <i>m/z</i> | Triacylglycerol | [M+H] ⁺ <i>m/z</i> | Triacylglycerol | [M+H] ⁺ <i>m/z</i> |
|-----------------|----------------------------------|-----------------|----------------------------------|-----------------|----------------------------------|
| PLnP | 829 | LStL | 875 | GLO | 911 |
| POPo | 831 | LnLnL | 875 | ALL | 911 |
| PLP | 831 | OLSt | 877 | PoGG | 913 |
| POP | 833 | LLLn | 877 | GOO | 913 |
| LnPLn | 851 | LnLnO | 877 | ALO | 913 |
| LnLP | 853 | LLL | 879 | AOO | 915 |
| LLP | 855 | LnLO | 879 | ALS | 915 |
| LnOP | 855 | LLO | 881 | BLP | 915 |
| LOP | 857 | OLnO | 881 | BLL | 939 |
| OOPo | 857 | LLS | 883 | GGO | 941 |
| OOP | 859 | OLO | 883 | BOL | 941 |
| PLS | 859 | OOO | 885 | BOO | 943 |
| PoSS | 861 | LOS | 885 | LPLi | 943 |
| POS | 861 | OSO | 887 | MaMoLi | 945 |
| LMoO | 869 | LAP | 887 | BOS | 945 |
| OMoO | 871 | SLS | 887 | LOLi | 965 |
| LnLnSt | 871 | OSS | 889 | LLLi | 967 |
| MaOO | 873 | AOP | 889 | LiOO | 971 |
| LnLnLn | 873 | GLL | 909 | | |

See Table 6.1 for abbreviations.

a MyP⁺ ion (*m/z* 523). The two more abundant [M-RCO₂]⁺ ions are due to loss of My (*sn*-1(3)) and P (*sn*-3(1)) giving [OP]⁺ and [MyO]⁺ ions, respectively.

In addition, Mottram and Evershed (30) determined that positional isomers of difunctional TAG can also be distinguished using the [M-RCO₂]⁺ ions. An isomeric pair of ABA and AAB type TAG will give the same [M-RCO₂]⁺ ions, i.e., [AA]⁺ and [AB]⁺. However, the ratio of [AA]⁺: [AB]⁺ is lower for the ABA isomer, since formation of the 1,2-isomer of the [AB]⁺ ion is energetically more favorable than generating the analogous 1,3-[AB]⁺ ion from the AAB isomer (Fig. 6.6). If the fragmen-

**Fig. 6.6.** The DAG ions formed from ABA and AAB type TAG.

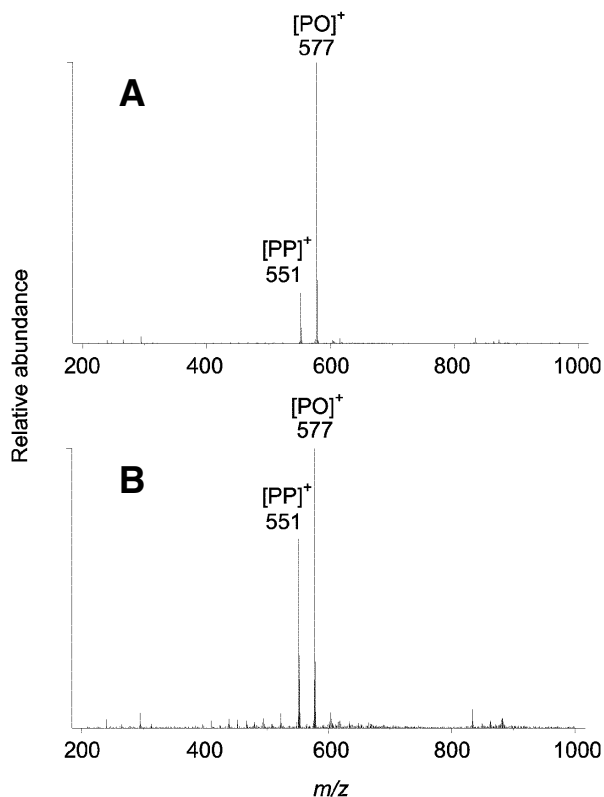


Fig. 6.7. The APCI-MS mass spectra of (A) POP and (B) PPO. For abbreviations see Table 6.1.

tations were energetically equally favorable, one would expect to observe $[AB]^+$ and $[AA]^+$ ions in a 2:1 ratio, regardless of the position of substitution of the A or B acyl moieties on the glycerol backbone. However, the $[PP]^+:[PO]^+$ ratio observed for POP (Fig. 6.7) is only 0.2, indicating that the formation of the 1,3- $[PP]^+$ ion is energetically disfavored. This is probably due to the 1,3-ion forming a resonance structure containing a five-member ring (Fig. 6.8), that is less stable than the six-member rings formed by the resonance of the 1,2- and 2,3-ions (29). Consequently, the two isomers show markedly different spectra (Fig. 6.7). The notation used to describe TAG can be used to reflect their regiospecific compositions. Hence POS refers to 1(3)-palmitoyl-2-oleoyl-3(1)stearoyl glycerol.

These observations correspond well with a report published at around the same time by Laakso and Voutilainen (16), who were investigating the application of silver ion (argentation) chromatography with APCI-MS detection using a Finnigan MAT TSQ 700 mass spectrometer for the analysis of seed oils containing both α - and γ -linolenic acids. Amongst other things, the latter authors noted that the elution order of the TAG was affected by the position of the fatty acyl moiety within the TAG. In particular, an unsaturated FA in the 2-position caused the TAG

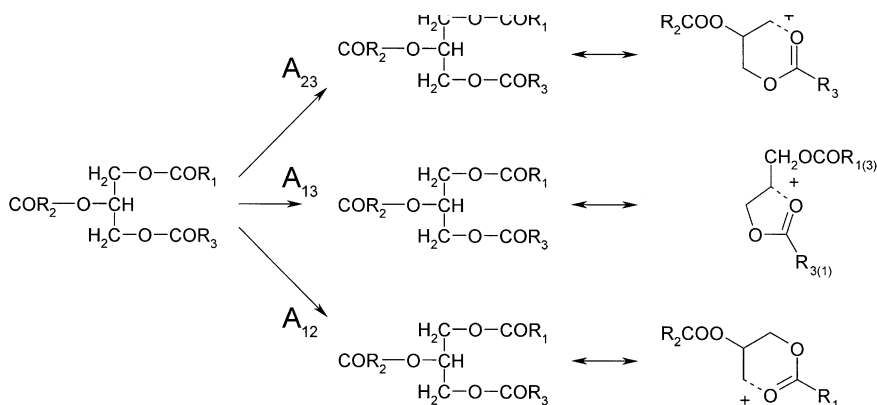


Fig. 6.8. Possible resonance structures of the diacylglycerol fragment ions formed following APCI of triacylglycerols. *Source:* Reference 29.

to elute before the TAG having the same unsaturated FA in the 1- or 3-position. Differences observed in the mass spectra of these resolved components showed that the abundance of the 1,3-DAG ion was less than that of the corresponding 1,2- or 2,3-DAG ion, indicating that the ratio of DAG fragment ions could be used to deduce the positions of the acyl chains on regioisomers.

Regiospecific Analysis of Complex Mixtures of TAG

HPLC/APCI-MS has been used to characterize a range of TAG mixtures, including vegetable, nut and seed oils, and animal and dairy fats (Table 6.4). Mottram *et al.* (31) used HPLC/APCI-MS to regiospecifically characterize nearly 40 TAG present in a soybean oil (Fig. 6.9) and found that the relative proportion of each FA in the 2-position, calculated from the quantification of the TAG according to the method by Byrdwell *et al.* (32), compared favorably with the 2-position FA composition determined from the more conventional lipase digestion method.

Mottram and Evershed subsequently analyzed a range of edible oils, namely black currant, evening primrose, hazelnut, olive, maize, and rapeseed. In general, each TAG was present as a single regio-isomer in a particular oil. However, there were some exceptions. For example, a mixture of both LLO and LOL regioisomers was observed in rapeseed oil, whereas soybean, poppy seed, maize, olive, and evening primrose seed oils were shown to contain a mixture of PLO and POL. These latter two regio-isomers can be observed in the chromatogram of maize oil by superimposing the mass chromatograms of m/z 575 (PL⁺) and 577 (PO⁺) (Fig. 6.10A). It can be seen that the left side of the peak corresponds to POL, since the least abundant DG ion is m/z 575. In contrast, on the right side of the peak, the least abundant DG ion is m/z 577 indicating that PLO is present. Comparison of the m/z 575 and 577 mass chromatograms across the chromatographic peak of POL in black currant seed oil (Fig. 6.8B) shows that a single positional isomer is present.

TABLE 6.4
Application of HPLC/APCI-MS to Analysis of TAG

| Reference | Samples analyzed | Regiospecific information recorded |
|-------------------------------------|---|------------------------------------|
| <i>TAG standards</i> | | |
| Byrdwell and Emken, 1995 (28) | SSS, OOO, LLL, LnLnLn | N |
| Mottram and Evershed, 1996 (30) | TAG standards | Y |
| <i>Plant oils</i> | | |
| Byrdwell <i>et al.</i> , 1996 (32) | Normal and interesterified soybean oils and lard | N |
| Byrdwell and Neff, 1996 (38) | Canola oils: normal and genetically modified high-stearic and high-lauric varieties | N |
| Byrdwell and Neff, 1998 (39) | Hydroxy-acid containing seed oils: castor bean oil, <i>Lesquerella fendleri</i> and <i>Lesquerella gordonii</i> | N |
| Byrdwell <i>et al.</i> , 2001 (40) | Potential margarine base stocks, including blends and interesterified mixtures | N |
| Holcapek <i>et al.</i> , 2003 (29) | Hazelnut, pistachio, poppyseed, almond, palm, brazil-nut, rapeseed, macadamia, soyabean, sunflower, linseed, <i>Draacocephalum moldavica</i> , evening primrose, corn, amaranth, <i>Silybum arianum</i> | Y |
| Jakab and Forgacs, 2002 (41) | Peanut, pumpkin seed, sesame seed, soybean, and wheat germ | Y |
| Jakab <i>et al.</i> , 2002 (33) | Almond, avocado, corn germ, grape seed, linseed, mustard seed, olive, peanut, pumpkin seed, sesame seed, soybean, sunflower, walnut, and wheat germ | Y |
| Jakab <i>et al.</i> , 2003 (34) | Grape seed, olive, pumpkin seed, soybean, sunflower, and wheat germ oils | Y |
| Kusaka <i>et al.</i> , 1996 (42) | Perilla, corn, olive | Y |
| Laakso, 1997 (43) | α - and γ -Linolenic acid-containing oils: cloudberry seed oil, evening primrose oil, borage oil, and black currant seed oil | N |
| Mottram <i>et al.</i> , 1997 (31) | Black currant, blue poppyseed, evening primrose, extra virgin olive, hazelnut, maize, rapeseed, and soybean | Y |
| Neff and Byrdwell, 1995 (44) | Soybean oils: normal and genetically modified high-stearic and high-palmitic varieties | N |
| Neff and Byrdwell, 1995 (45) | <i>Crepis alpina</i> and <i>Vernonia galamensis</i> seed oils | N |
| Neff <i>et al.</i> 2001 (46) | Highly saturated edible fats: coconut, cocoa butter, palm, randomized palm, palm olein, and randomized palm olein oils | N |
| Parcerisa <i>et al.</i> , 2000 (47) | Hazelnut and olive oil and hazelnut-olive blends | Y |
| Stubiger <i>et al.</i> , 2003 (48) | Castor oil | N |

TABLE 6.4
(Continued)

| Reference | Samples analyzed | Regiospecific information recorded |
|---|---|------------------------------------|
| <i>Animal fats</i> | | |
| Mottram and Evershed, 2001 (49) | Bovine milk fat | N |
| Mottram <i>et al.</i> , 2001 (35) | Beef, chicken, lamb, and pork | Y |
| Neff <i>et al.</i> , 2002 (50) | Animal tallow and potential food formulation fats | N |
| <i>Structured lipids and interesterified blends</i> | | |
| Lee <i>et al.</i> , 2002 (51) | Intesterified hydrogenated soybean oil and triacetin | N |
| Mangos <i>et al.</i> , 1999 (52) | Intesterified rapeseed oil and triacetin | Y |
| Mu <i>et al.</i> , 2000 (53) | Intesterified rapeseed oil and triacetin | N |
| <i>TAG oxidation products</i> | | |
| Byrdwell and Neff, 1999(54) | OOO oxidation products | N |
| Byrdwell and Neff, 2001 (55) | Oxidation products of normal, high-stearic, and high-lauric canola oils | N |
| Byrdwell and Neff, 2002 (56) | Canola oil, OOO oxidation products | Y |
| Neff and Byrdwell, 1998 (57) | OOO, LLL, and LnLnLn oxidation products | N |
| <i>Museum objects</i> | | |
| Shibamaya <i>et al.</i> , 1999 (58) | Exudate on painting and paint extracts | Y |
| <i>Archaeological samples</i> | | |
| Evershed <i>et al.</i> , 2002 (36) | Lipids from Saxon-Medieval cooking pots | Y |
| Kimpe <i>et al.</i> , 2001 (59) | Lipids from Roman oil lamps | N |
| Kimpe <i>et al.</i> , 2002 (37) | Lipids from late Roman cooking pots | Y |
| <i>Medical samples</i> | | |
| Mu and Hoy, 2000 (60) | Lymph TAG | N |

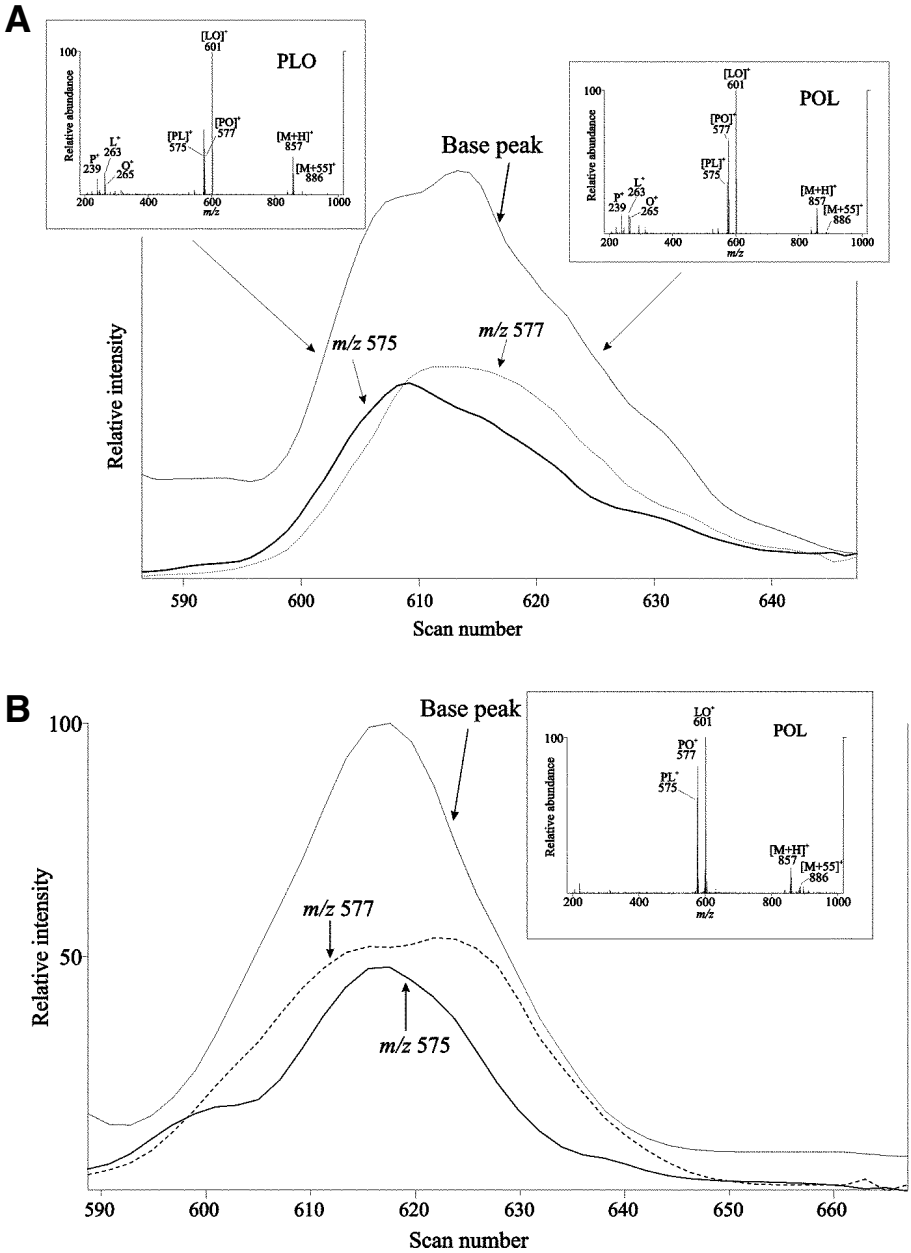


Fig. 6.10. Partial mass chromatograms and mass spectra from the PLO/POL peak in (A) maize oil and (B) black currant seed oil. For abbreviations see Table 6.1. *Source:* Reference 31.

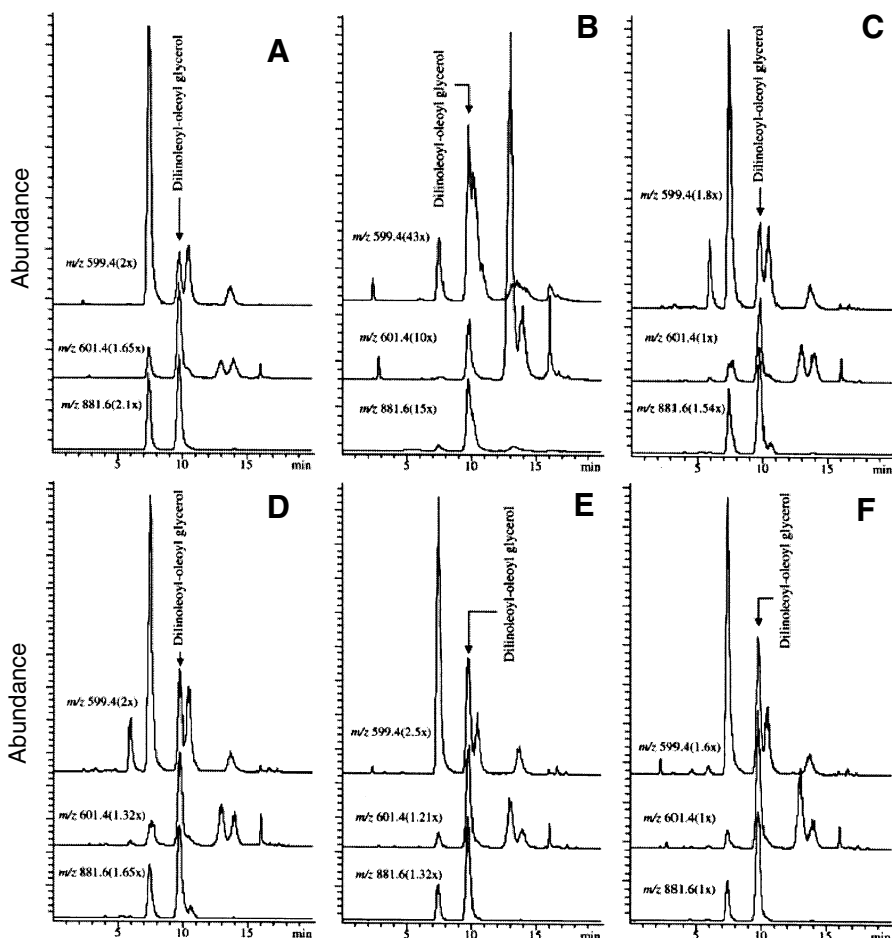


Fig. 6.11. Selected ion chromatograms of m/z 599 ($[LL]^+$), m/z 601 ($[LO]^+$) and m/z 881 ($[LOL+H]^+$ and/or $[LLO+H]^+$) ions from grape seed oil (A), olive oil (B), sunflower oil (C), soybean oil (D), pumpkin seed oil (E), and wheat germ oil (F) measured by HPLC/APCI-MS in SIM mode. *Source:* Reference 34.

and pork contained only the *cis* isomer; while the *cis*-18:1 was predominantly found in the 2-position of the TAG, the *trans*-18:1 showed a preference for the 1- and 3-position. Similarly, it was confirmed that although the 2-position of beef, chicken, and lamb fat TAG was dominated by unsaturated FA, in pork fat, a characteristically high proportion of palmitic acid was seen in this position. The compositional and regiospecific data compared well with previous TAG and FA analyses.

A more unusual application of HPLC/APCI-MS has been the analysis of fats adsorbed into archaeological pottery. Evershed *et al.* (36) used HPLC/APCI-MS to iden-

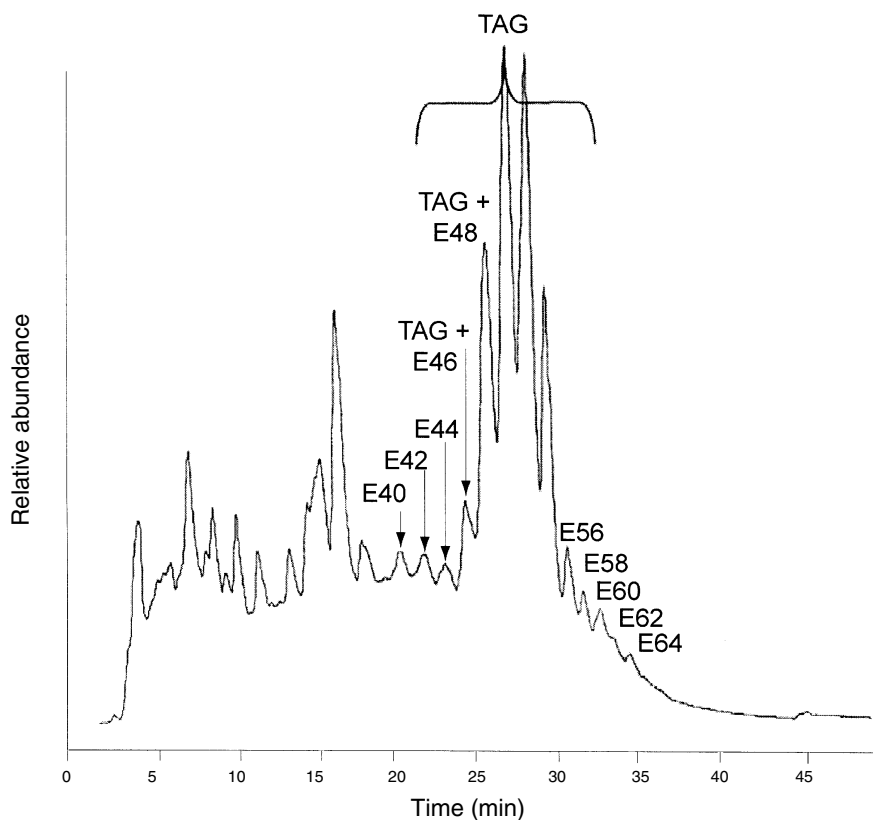


Fig. 6.12. HPLC/APCI-MS profile of an archaeological cooking pot. The monoesters with 40–50 carbon atoms and diesters with 56–64 carbon atoms are indicated by E40–E50 and E56–E64, respectively. *Source:* Kimpe *et al.* (37).

tify the regio-isomers of TAG preserved in a late Saxon–early Medieval cooking vessel. The TAG were highly saturated and the unsaturated components were shown to contain more than one isomer of the 18:1 FA, suggesting that the vessel had contained a ruminant animal fat. The ratio of palmitic to stearic acid in the 2-position of the archaeological fats was much closer to that observed in ruminant fats than in nonruminant fats. Similarly, Kimpe *et al.* (37) used the technique to analyze the fats adsorbed in a late Roman cooking vessel and were able to obtain regiospecific information for several of the TAG identified (Fig. 6.12). The saturated nature of the TAG indicated that the fat was of animal origin and the positions of the saturated fatty acyl moieties within the TAG, in conjunction with the subsequent identification of *trans* isomers of the 18:1 FA using gas chromatography, indicated that the fat was probably from a ruminant animal.

Conclusions

The complex mixtures of TAG that comprise edible oils and fats represent a considerable analytical challenge. In addition to determining which fatty acids are present in a TAG mixture, the positions at which those FA are esterified to the glycerol backbone is of considerable importance. The most efficient separations of TAG mixtures have been achieved with reversed-phase HPLC; when this is used in conjunction with APCI, relatively simple mass spectra are obtained which allow the regiospecific characterization of individual TAG in a mixture. This relatively new advance in analytical chemistry has considerable application in the field of lipid analysis.

References

1. Aoyama, T., K. Fukui, K. Taniguchi, S. Nagaoka, T. Yamamoto, and Y. Hashimoto, Absorption and Metabolism of Lipids in Rats Depends on Fatty-Acid Isomeric Position, *J. Nutr.* 126: 225–231 (1996).
2. Pufal, D.A., P.T. Quinlan, and A.M. Salter, Effect of Dietary Triacylglycerol Structure on Lipoprotein Metabolism—A Comparison of the Effects of Dioleoylpalmitoyl Glycerol in which Palmitoyl is Esterified to the 2- or the 1(3)-Position of the Glycerol, *Biochim. Biophys. Acta* 1258: 41–48 (1995).
3. Martin, J.C., P. Bougnoux, J.M. Antoine, M. Lanson, and C. Couet, Triacylglycerol Structure of Human Colostrum and Mature Milk, *Lipids* 28: 637–643 (1993).
4. Zampelas, A., C.M. Williams, L.M. Morgan, J. Wright, and T. Quinlan, The Effect of Triacylglycerol Fatty-Acid Positional Distribution on Postprandial Plasma Metabolite and Hormone Responses in Normal Adult Men, *Brit. J. Nutr.* 71: 401–410 (1994).
5. Valenzuela, A., and S. Nieto, Biotechnology of Lipids—The Use of Lipases for the Structural Modification of Fats and Oils, *Grasas Aceitas* 45: 337–343 (1994).
6. Anderson, B.A., C.A. Sutton, and M. J. Pallansch, Optical Activity of Butterfat and Vegetable Oils, *J. Am. Oil Chem. Soc.* 47: 15–16 (1970).
7. Schlenk, W., Jr., Synthesis and Analysis of Optically Active Triglycerides, *J. Am. Oil Chem. Soc.* 42: 945–957 (1965).
8. Brockerhoff, H., A Stereospecific Analysis of Triglycerides, *J. Lipid Res.* 6: 10–15 (1965).
9. Brockerhoff, H., Stereospecific Analysis of Triglycerides: An Alternative Method, *J. Lipid Res.* 8: 167–169 (1967).
10. Christie, W.W., and J.H. Moore, A Semimicro Method for the Stereospecific Analysis of Triglycerides, *Biochim. Biophys. Acta* 176: 445–452 (1969).
11. Myher, J.J., and A. Kuksis, Stereospecific Analysis of Triacylglycerols via Racemic Phosphatidyl Cholines and Phospholipase C, *Can. J. Biochem.* 57: 117–124 (1979).
12. Jensen, R.G., F.A. Dejong, and R.M. Clark, Determination of Lipase Specificity, *Lipids* 18: 239–252 (1983).
13. Christie, W.W., B. Nikolovadamyanova, P. Laakso, and B. Herslof, Stereospecific Analysis of Triacyl-*sn*-glycerols via Resolution of Diastereomeric Diacylglycerol Derivatives by High-Performance Liquid-Chromatography on Silica, *J. Am. Oil Chem. Soc.* 68: 695–701 (1991).

14. Laakso, P., and W.W. Christie, Chromatographic Resolution of Chiral Diacylglycerol Derivatives: Potential in the Stereospecific Analysis of Triacyl-*sn*-glycerols, *Lipids* 25: 349–353 (1990).
15. Adlof, R.O., Analysis of Triacylglycerol Positional Isomers by Silver Ion High Performance Liquid Chromatography, *J. High Resolut. Chromatogr. Chromatogr. Commun.* 18: 105–107 (1995).
16. Laakso, P., and P. Voutilainen, Analysis of Triacylglycerols by Silver-Ion High-Performance Liquid Chromatography-Atmospheric Pressure Chemical Ionization Mass Spectrometry, *Lipids* 31: 1311–1322 (1996).
17. Schoolery, J.N., Some Quantitative Applications of Carbon-13 NMR Spectroscopy, *Prog. Nucl. Magn. Reson. Spectrosc.* 11: 79–93 (1977).
18. Shiao, T.Y., and M.S. Shiao, Determination of Fatty Acid Compositions of Triacylglycerols by High Resolution NMR Spectroscopy, *Bot. Bull. Academica Sinica* 30: 191–199 (1989).
19. Ng, S., High Resolution ^{13}C NMR Spectra of the Carbonyl Carbons of the Triglycerides of Palm Oil, *J. Chem. Soc. Chem. Commun.*: 179–180 (1983).
20. Wallenberg, K.F., Quantitative High Resolution C-13 NMR of the Olefinic and Carbonyl Carbons of Edible Vegetable Oils, *J. Am. Oil Chem. Soc.* 67: 487–494 (1990).
21. Bergana, M.M., and T.W. Lee, Structure Determination of Long-Chain Polyunsaturated Triacylglycerols by High-Resolution ^{13}C Nuclear Magnetic Resonance, *J. Am. Oil Chem. Soc.* 73: 551–556 (1996).
22. Gunstone, F.D., The C-13 NMR Spectra of Oils Containing Gamma-Linolenic Acid, *Chem. Phys. Lipids* 56: 201–207 (1990).
23. Gunstone, F.D., High Resolution NMR Studies of Fish Oils, *Chem. Phys. Lipids* 59: 83–89 (1991).
24. Redden, P.R., X. Lin, and D.F. Horrobin, Comparison of the Grignard Deacylation TLC and HPLC Methods and High Resolution ^{13}C -NMR for the *sn*-2 Positional Analysis of Triacylglycerols Containing γ -Linolenic Acid, *Chem. Phys. Lipids* 79: 9–19 (1996).
25. Ryhage, R., and E. Stenhagen, Mass Spectrometry in Lipid Research, *J. Lipid Res.* 1: 361–390 (1960).
26. Kallio, H., and G. Currie, Analysis of Low Erucic-Acid Rapeseed Oil (*Brassica campestris*) by Negative Ion Chemical Ionization Tandem Mass Spectrometry—A Method Giving Information on the Fatty Acid Composition in Positions *sn*-2 and *sn*-1/3 of Triacylglycerols, *Lipids* 28: 207–215 (1993).
27. Covey, T.R., E.D. Lee, A.P. Bruins, and J.D. Henion, Liquid Chromatography/Mass Spectrometry, *Anal. Chem.* 58: 1451A–1461A (1986).
28. Byrdwell, W.C., and E.A. Emken, Analysis of Triglycerides Using Atmospheric-Pressure Chemical Ionization Mass-Spectrometry, *Lipids* 30: 173–175 (1995).
29. Holcapek, M., P. Jandera, P. Zderadicka, and L. Hrubá, Characterization of Triacylglycerol and Diacylglycerol Composition of Plant Oils Using High-Performance Liquid Chromatography-Atmospheric Pressure Chemical Ionization Mass Spectrometry, *J. Chromatogr. A* 1010: 195–215 (2003).
30. Mottram, H.R., and R.P. Evershed, Structure Analysis of Triacylglycerol Positional Isomers Using Atmospheric Pressure Chemical Ionisation Mass Spectrometry, *Tetrahedron Lett.* 37: 8593–8596 (1996).
31. Mottram, H.R., S.E. Woodbury, and R.P. Evershed, Identification of Triacylglycerol

- Positional Isomers Present in Vegetable Oils by High Performance Liquid Chromatography Atmospheric Pressure Chemical Ionization Mass Spectrometry, *Rapid Comm. Mass Spectrom.* 11: 1240–1252 (1997).
32. Byrdwell, W.C., E.A. Emken, W.E. Neff, and R.O. Adlof, Quantitative Analysis of Triglycerides Using Atmospheric Pressure Chemical Ionization-Mass Spectrometry, *Lipids* 31: 919–935 (1996).
 33. Jakab, A., K. Nagy, K. Heberger, K. Vekey, and E. Forgacs, Differentiation of Vegetable Oils by Mass Spectrometry Combined with Statistical Analysis, *Rapid Comm. Mass Spectrom.* 16: 2291–2297 (2002).
 34. Jakab, A., I. Jablonkai, and E. Forgacs, Quantification of the Ratio of Positional Isomer Dilinoleoyl-Oleoyl Glycerols in Vegetable Oils, *Rapid Comm. Mass Spectrom.* 17: 2295–2302 (2003).
 35. Mottram, H.R., Z.M. Crossman, and R.P. Evershed, Regiospecific Characterisation of the Triacylglycerols in Animal Fats Using High Performance Liquid Chromatography-Atmospheric Pressure Chemical Ionisation Mass Spectrometry, *Analyst* 126: 1018–1024 (2001).
 36. Evershed, R.P., S.N. Dudd, M.S. Copley, R. Berstan, A.W. Stott, H.R. Mottram, S.A. Buckley, and Z.M. Crossman, Chemistry of Archaeological Animal Fats, *Accounts of Chemical Research* 35: 660–668 (2002).
 37. Kimpe, K., P. Jacobs, and M. Waelkens, Mass Spectrometric Methods Prove the Use of Beeswax and Ruminant Fat in Late Roman Cooking Pots, *J. Chromatogr. A* 968: 151–160 (2002).
 38. Byrdwell, W.C., and W.E. Neff, Analysis of Genetically Modified Canola Varieties by Atmospheric Pressure Chemical Ionization Mass Spectrometric and Flame Ionization Detection, *J. Liq. Chrom.* 19: 2203–2225 (1996).
 39. Byrdwell, W.C., and W.E. Neff, Analysis of Hydroxy-Containing Seed Oils Using Atmospheric Pressure Chemical Ionization Mass Spectrometry, *J. Liq. Chrom.* 21: 1485–1501 (1998).
 40. Byrdwell, W.C., W.E. Neff, and G.R. List, Triacylglycerol Analysis of Potential Margarine Base Stocks by High-Performance Liquid Chromatography with Atmospheric Pressure Chemical Ionization Mass Spectrometry and Flame Ionization Detection, *J. Agric. Food Chem.* 49: 446–457 (2001).
 41. Jakab, A., and E. Forgacs, Characterization of Plant Oils on a Monolithic Silica Column by High-Performance Liquid Chromatography-Atmospheric Pressure Chemical Ionization-Mass Spectrometry, *Chromatographia* 56: Suppl. S (2002).
 42. Kusaka, T., S. Ishihara, M. Sakaida, A. Mifune, Y. Nakano, K. Tsuda, M. Ikeda, and H. Nakano, Composition Analysis of Normal Plant Triacylglycerols and Hydroperoxidized *rac*-1-Stearoyl-2-oleoyl-3-linoleoyl-*sn*-glycerols by Liquid Chromatography-Atmospheric Pressure Chemical Ionization Mass Spectrometry, *J. Chromatogr. A* 730: 1–7 (1996).
 43. Laakso, P., Characterization of α - and γ -Linolenic Acid Oils by Reversed-Phase High-Performance Liquid Chromatography-Atmospheric Pressure Chemical Ionization Mass Spectrometry, *J. Am. Oil Chem. Soc.* 74: 1291–1300 (1997).
 44. Neff, W.E., and W.C. Byrdwell, Soybean Oil Triacylglycerol Analysis by Reversed-Phase High-Performance Liquid Chromatography Coupled with Atmospheric Pressure Chemical Ionization Mass Spectrometry, *J. Am. Oil Chem. Soc.* 72: 1185–1191 (1995).
 45. Neff, W.E., and W.C. Byrdwell, Triacylglycerol Analysis by High Performance Liquid

- Chromatography-Atmospheric Pressure Chemical Ionization Mass Spectrometry: *Crepis alpina* and *Vernonia galamensis* Seed Oils, *J. Liq. Chromatogr.* 18: 4165–4181 (1995).
46. Neff, W.E., W.C. Byrdwell, and G.R. List, Triacylglycerol Structures of Food Fats High in Saturated Acids by HPLC and Mass Spectrometry, *J. Liq. Chrom.* 24: 837–854 (2001).
 47. Parcerisa, J., I. Casals, J. Boatella, R. Codony, and M. Rafecas, Analysis of Olive and Hazelnut Oil Mixtures by High-Performance Liquid Chromatography-Atmospheric Pressure Chemical Ionization Mass Spectrometry of Triacylglycerols and Gas-Liquid Chromatography of Non-Saponifiable Compounds (Tocopherols and Sterols), *J. Chromatogr. A* 881: 149–158 (2000).
 48. Stubinger, G., E. Pittenauer, and G. Allmaier, Characterisation of Castor Oil by On-Line and Off-Line Non-Aqueous Reversed-Phase High-Performance Liquid Chromatography–Mass Spectrometry (APCI and UV/MALDI), *Phytochemical Analysis* 14: 337–346 (2003).
 49. Mottram, H.R., and R.P. Evershed, Elucidation of the Composition of Bovine Milk Fat Triacylglycerols Using High-Performance Liquid Chromatography—Atmospheric Pressure Chemical Ionisation Mass Spectrometry, *J. Chromatogr. A* 926: 239–253 (2001).
 50. Neff, W.E., W.C. Byrdwell, K.R. Steidley, G.R. List, and G. Snowden, Triacylglycerol Structure of Animal Tallows, Potential Food Formulation Fats, by High Performance Liquid Chromatography Coupled with Mass Spectrometry, *J. Liq. Chrom.* 25: 985–998 (2002).
 51. Lee, K.T., K.C. Jones, and T.A. Foglia, Separation of Structured Lipids by High Performance Liquid Chromatography, *Chromatographia* 55: 197–201 (2002).
 52. Mangos, T.J., K.C. Jones, and T.A. Foglia, T.A. Normal-Phase High Performance Liquid Chromatographic Separation and Characterization of Short- and Long-Chain Triacylglycerols, *Chromatographia* 49: 363–368 (1999).
 53. Mu, H.L., H. Sillen, and C.E. Hoy, Identification of Diacylglycerols and Triacylglycerols in a Structured Lipid Sample by Atmospheric Pressure Chemical Ionization Liquid Chromatography/Mass Spectrometry, *J. Am. Oil Chem. Soc.* 77: 1049–1059 (2000).
 54. Byrdwell, W.C., and W.E. Neff, Non-Volatile Products of Triolein Produced at Frying Temperatures Characterized Using Liquid Chromatography with Online Mass Spectrometric Detection, *J. Chromatogr. A* 852: 417–432 (1999).
 55. Byrdwell, W.C., and W.E. Neff, Autoxidation Products of Normal and Genetically Modified Canola Oil Varieties Determined Using Liquid Chromatography with Mass Spectrometric Detection, *J. Chromatogr. A* 905: 85–102 (2001).
 56. Byrdwell, W.C., and W.E. Neff, Dual Parallel Electrospray Ionization and Atmospheric Pressure Chemical Ionization Mass Spectrometry (MS), MS/MS and MS/MS/MS for the Analysis of Triacylglycerols and Triacylglycerol Oxidation Products, *Rapid Commun. Mass Spectrom.* 16: 300–319 (2002).
 57. Neff, W.E., and W.C. Byrdwell, Characterization of Model Triacylglycerol (Triolein, Trilinolein and Trilinolenin) Autoxidation Products *via* High-Performance Liquid Chromatography Coupled with Atmospheric Pressure Chemical Ionization Mass Spectrometry, *J. Chromatogr. A* 818: 169–186 (1998).
 58. Shibayama, N., S.Q. Lomax, K. Sutherland, and E.R.D. La Rie, Atmospheric Pressure

Chemical Ionization Liquid Chromatography Mass Spectrometry and Its Application to Conservation: Analysis of Triacylglycerols, *Studies in Conservation* 44: 253–268 (1999).

59. Kimpe, K., P. Jacobs, and M. Waelkens, Analysis of Oil Used in Late Roman Oil Lamps with Different Mass Spectrometric Techniques Revealed the Presence of Predominantly Olive Oil Together with Traces of Animal Fat, *J. Chromatogr. A* 937: 87–95 (2001).
60. Mu, H.L., and C.E. Hoy, Application of Atmospheric Pressure Chemical Ionization Liquid Chromatography-Mass Spectrometry in Identification of Lymph Triacylglycerols, *J. Chromatogr. B* 748: 425–437 (2000).

Chapter 7

Qualitative and Quantitative Analysis of Triacylglycerols by Atmospheric Pressure Ionization (APCI and ESI) Mass Spectrometry Techniques

William Craig Byrdwell

Department of Chemistry & Biochemistry, Florida Atlantic University, 777 Glades Road, P.O. Box 3091, Boca Raton, FL 33431

Introduction

As mentioned in the introduction to this volume (Chapter 1), atmospheric pressure chemical ionization (APCI) and electrospray ionization (ESI) are the two most popular atmospheric pressure ionization (API) interfaces today. Both of these ionization sources have been used individually and in combination for analysis of a variety of lipid classes, as presented in recent reviews. Atmospheric pressure chemical ionization for analysis of most lipid classes has been reviewed by Byrdwell (1–4). Some applications of APCI mass spectrometry (APCI-MS) to triacylglycerol (TAG) analysis have been reviewed by Laakso (5). Electrospray ionization mass spectrometry for lipid analysis was reviewed in 1995 by Myher and Kuksis (6). More recently, ESI-MS for analysis of phospholipids has been reviewed by Pulfer and Murphy (7). Byrdwell (8) recently reviewed some applications of ESI-MS to lipids, but focused primarily on the publications of his group in the area (4). The rapidly growing number of applications of ESI-MS to lipid analysis makes it mandatory that ESI-MS is included as one of the “modern techniques for lipid analysis using liquid chromatography/mass spectrometry.” Similarly, the number of publications demonstrating applications of APCI to lipid analysis has also grown exponentially in recent years. Any discussion of modern analytical techniques for lipid analysis must likewise include discussion of LC/ APCI-MS techniques.

The theoretical considerations and instrument hardware for both APCI and ESI will be presented in this chapter, and applications of these two twin techniques to TAG analysis will be discussed. Applications of these techniques to other lipid classes are the subjects of other chapters in this volume. Also in this chapter will be presented data demonstrating that both APCI-MS and ESI-MS can be used to determine the identities of the most likely positional isomers present in TAG mixtures. A full treatment of APCI-MS for analysis of TAG positional isomers is found in Chapter 6, by Hazel Mottram, in this volume. This chapter will also present

data demonstrating that both APCI-MS and ESI-MS can be used to determine the identities of components in mixtures of the products formed by oxidized triacylglycerols, the TAG oxidation products (TAGOX). A full treatment of APCI-MS for analysis of TAGOX is found in Chapter 4, by Arnis Kuksis, in this volume. Next, this chapter will review the work that we and others have previously published regarding quantification of TAG in mixtures. We will present published data demonstrating our approach for calculating response factors for TAG analyzed by LC/APCI-MS. We will also present new, unpublished data that show the application of this proven technique to TAG analyzed by LC/ESI-MS. This chapter will also review the applications to TAG analysis by using techniques other than reversed-phase (RP) HPLC/(APCI/ESI)-MS, such as argentation (Ag^+) chromatography and supercritical fluid chromatography. Next, after having shown the complementary benefits of both APCI-MS and ESI-MS in their various applications, this chapter will review and present new data to show how these two techniques may be used in "dual parallel mass spectrometer" experiments to obtain both types of data simultaneously from one LC effluent (an LC1/MS2 experiment). Another dual parallel mass spectrometer experiment will be shown that employs both APCI and ESI simultaneously on two mass spectrometers attached to two different LC systems separating polar and non-polar components on two LC systems in parallel, from one injection (an LC2/MS2 experiment). An extensive presentation of dual parallel techniques is found in Chapter 13 in this volume.

Atmospheric Pressure Chemical Ionization Mass Spectrometry for TAG Analysis

Numerous methods for HPLC analysis of TAG with conventional two-dimensional detectors have been published, but unfortunately these have limitations. The complexity of most TAG mixtures does not allow complete structural analysis using a simple two-dimensional detector. Even peaks that appear sharp and distinct using a refractive index detector, UV detector, or evaporative light scattering detector can actually contain multiple overlapped components. Furthermore, some of these two-dimensional detectors do not respond equally to all TAG. Ultraviolet detection exhibits more absorbance signal from unsaturated TAG than from saturated ones. Also the short wavelengths (~205–210 nm) usually employed for UV analysis of TAG limit choices in the solvent system that can be used. The typical acetonitrile/chloroform binary solvent system used for non-aqueous RP (NARP)-HPLC of TAG obviates the use of a UV detector due to the strong absorbance by chloroform. To be certain that all TAG that make up a peak are observed, mass spectrometry is necessary. The soft ionization produced by APCI-MS makes it an ideal tool for TAG analysis.

Tyrefors *et al.* (9) appear to have been first to apply APCI-MS (with supercritical fluid chromatography, SFC) to analysis of TAG. They used SFC/APCI-MS to analyze a mixture of lipids containing stearic acid methyl ester, cholesterol, cholest-

teryl palmitate, and trilaurin. They used a custom-built SFC interface attached to a Sciex API III tandem mass spectrometer. Their interface had several design characteristics that made it different from current commercially available LC/APCI-MS sources. First, their interface used a restrictor tip that helped to establish the pressure necessary to maintain supercritical conditions. This restrictor was drawn to a diameter of less than 1 μm , from which was sprayed the CO_2 mobile phase. Also, the tip of the restrictor was heated, which is in contrast to modern LC-based APCI interfaces, in which the effluent is first sprayed pneumatically, and then passed through a heated vaporizer cylinder. The first SFC/APCI-MS mass spectrum of trilaurin showed several differences compared to the spectra that are now more commonly observed from such fully saturated TAG. Their APCI-MS mass spectrum exhibited a protonated molecule as a base peak, with a large $[\text{M}+\text{H}_2\text{O}]^+$ adduct formed due to sparging of the make-up gas through water. In most APCI-MS mass spectra, as discussed herein, the water adduct is not as large as that observed by Tyrefors *et al.* The primary fragment formed (at $\sim 18\%$ abundance) was the diacylglycerol fragment ion, $[\text{M}-\text{RCOO}]^+$, or $[\text{M}+\text{H}-\text{RCOOH}]^+$.

Byrdwell and Emken (10) demonstrated the first HPLC/APCI-MS of TAG. They used a commercially available APCI interface on a Finnigan MAT single quadrupole mass spectrometer to analyze a mixture of synthetic triacylglycerols having varying degrees of unsaturation. A mixture of monoacid (all three fatty acyl chains the same) TAG standards was separated using an analytical scale reversed-phase column from which the flow rate of 1 mL/min was split to deliver 400 $\mu\text{L}/\text{min}$ to the APCI interface, with the remaining 600 $\mu\text{L}/\text{min}$ sent to an evaporative light scattering detector. The article showed mass spectra that are now known to be typical of results produced by a variety of instruments from different manufacturers. The spectra showed that TAG with numerous sites of unsaturation produced protonated molecules as base peaks, and diacylglycerol fragment ions, $[(\text{M}+\text{H})-\text{RCOOH}]^+$, which is equivalent to $[\text{M}-\text{RCOO}]^+$, as the main fragments. Typical APCI-MS mass spectra of TAG from a synthetic mixture are shown below. In contrast to the mass spectrum shown by Tyrefors *et al.* (9), the results by Byrdwell and Emken (10) showed that TAG with no sites of unsaturation produced little or no abundance of the intact protonated molecule. The APCI-MS mass spectra exhibited diacylglycerol (DAG) fragment ions that allowed the fatty acyl chains to be determined conclusively.

The initial articles mentioned above conclusively showed the utility of APCI-MS in combination with HPLC for TAG analysis. But many important aspects of this new technique remained to be investigated and expanded. If 1995 was the infancy of HPLC/APCI-MS for TAG analysis, 1996 was when the technique really "started to walk." Several important articles were published in this year. Data demonstrating the important developments in the evolution of APCI-MS for TAG analysis are presented below in the Results and Discussion section below.

In the intervening decade, ESI and APCI have been modified and optimized, so that today they are the two most-used methods with liquid chromatography for

analysis of large nonvolatile lipids. The refinements incorporated into modern API sources have made them much more robust ionization sources than their predecessors. They now exhibit numerous benefits that include ease of use, durability, compatibility with high flow rates, resistance to clogging, affordability, and applicability to a wide range of analytes. The typical modern API interface allows ESI or APCI to be used interchangeably.

Electrospray Ionization Mass Spectrometry for TAG Analysis

Electrospray ionization mass spectrometry (ESI-MS) has become most closely associated with protein analysis because proteins are large, nonvolatile, easily ionized molecules that are ideally suited to ionization by ESI. The field of proteomics has undergone explosive growth in the past decade due in major part to the development of rugged commercially available ESI sources for interfacing liquid chromatography to mass spectrometry. The importance of ESI-MS for analysis of large biomolecules was highlighted in 2002, when John B. Fenn received half of half of the Nobel Prize in chemistry (equals one-fourth) for his contributions working with ESI-MS “for the development of methods for identification and structure analyses of biological macromolecules,” which was shared with Koichi Tanaka (also one-fourth), “for their development of soft desorption ionization methods for mass spectrometric analyses of biological macromolecules” (MALDI), and Kurt Wüthrich (one-half), “for his development of nuclear magnetic resonance spectroscopy for determining the three-dimensional structure of biological macromolecules in solution.”

But ESI-MS has also found many uses outside the field of proteomics. Phospholipids are one class of lipids that are easily charged, and so are particularly amenable to analysis by ESI-MS. For this reason, ESI-MS has been applied to phospholipids extensively in the past. Chapter 2 by Hvattum and Larsen, Chapter 3 by Hsu and Turk, and Chapter 12 by Han and Gross thoroughly describe various aspects of ESI-MS for analysis of phospholipids, from LC/MS, to mechanistic considerations, to analysis without separation. Another class of lipids to which ESI-MS has been applied is triacylglycerols (TAG). It may seem counterintuitive that neutral lipids, such as triacylglycerols, would be amenable to ESI-MS, but methods have been developed recently to allow even this non-polar class to be easily analyzed with high sensitivity.

Analysis of TAG by ESI-MS (by infusion, without chromatographic separation) was first demonstrated by Duffin *et al.* (13). Sodiated ions were formed by addition of sodium acetate and ammonium adduct ions were formed by addition of ammonium acetate. The signal obtained by non-polar lipids was observed to be proportional to the degree of polarity of the molecules. Thus, monoacylglycerols gave more response than diacylglycerols, which gave more response than triacylglycerols. TAG containing unsaturated fatty acyl chains produced more signal than saturated TAG. These authors reported low abundances of fragment

ions during MS/MS of sodiated TAG, $[M+Na]^+$, but good abundances of fragment ions and good quality MS/MS spectra from $[M+NH_4]^+$ adduct ions. In this work, the location of sites of unsaturation could not be determined from the mass spectra due to bond migration during fragmentation. In 1996, Myher *et al.* (14) showed the stereospecific analysis of triacylglycerols, but this was of dinitrophenylurethane (DNPU) derivatives of diacylglycerols from TAG, not analysis of intact TAG directly by ESI-MS. Sandra *et al.* (15) reported the use of ESI-MS for analysis of a fraction collected from capillary electrochromatography (CEC) for TAG analysis. Later, fractions from CEC following supercritical fluid chromatography (SFC) of sardine oil were analyzed by ESI-MS (16). Schuyl *et al.* (17) demonstrated online argentation (silver-ion) liquid chromatography/ESI-MS of TAG. These authors also employed sodium acetate and ammonium acetate. Signal in the presence of ammonium acetate was flow rate dependent and so sodium acetate was chosen for TAG quantification, although this precluded the acquisition of good MS/MS data. Cheng *et al.* (18) used ESI-MS/MS (with sample introduced by infusion, without chromatography) to distinguish the positions of double bonds on the fatty acyl chains from their fragmentation patterns. ESI-MS also allowed them to distinguish the positions of the acyl chains on the glycerol backbone (FAB-MS also allowed the regioisomers to be distinguished by MS/MS of $[M+Na]^+$ parent ions). Hsu and Turk (19) used infusion of standards to analyze TAG as their lithiated adducts by ESI-MS. Fragments in the MS/MS spectra of the lithiated adducts allowed determination of the *sn*-2 fatty acid (FA) substituent. Han and Gross also reported analysis of lithiated adducts of TAG (20). These authors reported identification of the *sn*-2 FA, and also showed neutral loss experiments that aided in structural elucidation. ESI-MS has been applied with non-aqueous reversed-phase liquid chromatography to TAG by Hvattum (21). Sjovald *et al.* have applied ESI-MS to TAG oxidation products (22) and dinitrophenylhydrazones of TAG oxidation products (23,24).

Yli-Jokipii *et al.* (25) reported several applications over several years of ESI-MS for analysis of regioisomers of TAG and their incorporation into chylomicron and very low density lipoprotein (VLDL) TAG. In 2001, they reported the structures of regioisomers of TAG in lard, tallow, egg yolk, chicken skin, palm oil, palm olein, palm stearin, and a transesterified blend of palm stearin and coconut oil, analyzed by ESI tandem mass spectrometry, without prior chromatographic separation. Trends in the regiospecific structures of TAG from the various sources were reported, based on the lengths and degrees of unsaturation of the FA. In the same year, the group of researchers reported the first of their reports on the effects of different types of TAG on chylomicron and VLDL TAG, and their effect on postprandial lipemia (25). The authors used ESI-MS of TAG to show that, within three hours, the chylomicron and VLDL TAG composition reflected that of the fat fed, with high levels of incorporation. TAG with palmitic acid in the *sn*-1 and *sn*-3 positions caused a larger proportion of TAG in plasma. Next, the same group used the ESI-MS method for a study of the effect of fat fed on the chylomicron TAG of

women (26). The authors used ESI-MS data to demonstrate that the TAG molecular weight, and to a lesser extent the positional distribution, affects the rates of clearance of chylomicron TAG. Next, they used ESI-MS to follow the incorporation and clearance of lard and modified lard fed to normal healthy volunteers (27). The positional isomer distribution of the fat fed was again shown to have a distinct impact on the chylomicron TAG composition formed by postprandial lipid metabolism. In 2004, Yli-Jokopii *et al.* reported the same ESI-MS approach applied to analysis of decanoic acid, a model medium-chain FA (MCFA), that was fed and then incorporated into chylomicron and VLDL TAG (28). The position of decanoic acid in the chylomicron TAG reflected its position in the TAG fed.

In 2002, Dorschel (29) used ESI-MS for identification of TAG in peanut oil. Sandra *et al.* (30) reported SFC/ESI-MS for TAG analysis that showed mass spectra in which silver ions were coordinated to TAG species. In 2003, numerous relevant articles appeared. Marzilli *et al.* (31) reported ESI-MS, MS/MS, and MS³ on an ion trap mass spectrometer for analysis of TAG standards; Fard *et al.* (32) demonstrated high-resolution Fourier transform ion cyclotron resonance mass spectrometry (FT-ICR-MS), first without prior LC separation, and then of fractions collected from an HPLC separation. Similarly, in 2004 Wu *et al.* (33) reported the use of FT-ICR-MS, without prior LC separation, for analysis of TAG in canola, olive, and soybean oils. In negative-ion mode, 3,000–4,000 distinct compounds were indicated, and the pattern of acidic components in soybean oil was easily differentiated from those of canola and olive oils. In positive-ion ESI-MS, ~2,000 compounds were indicated, and the TAG were easily identified by their characteristic [DAG]⁺ and [TAG+H]⁺ ions. The technique was used to detect the adulteration of olive oil with less expensive soybean oil.

In 2003, Han and Gross (34) demonstrated analysis of TAG as part of their technique for lipidome analysis using positive and negative ESI-MS without prior chromatographic separation. Their approach is described in detail in Chapter 12 herein. In the same year, Kalo *et al.* (35) used ESI-MS for regiospecific analysis of short-chain TAG positional isomers. The authors reported the ammonium adducts of TAG from nine mixtures, each made by interesterification of three FA, as well as three mixtures having only two FA. Most recently, the research group of William Artz reported the use of HPLC/ESI-MS for analysis of TAG in oil from the ouricuri tree (*Syagrus coronata*) (36). The oil was shown to contain a substantial proportion of short- to medium-chain FA, such as caprylic, capric, lauric, and myristic acids. Also in 2004, Malone and Evans (37) reported ESI-MS for analysis of positional isomers of several binary mixtures of TAG. They reported trends similar to those that had already been reported by others, such as the preferential loss of the FA in the *sn*-1 and *sn*-3 positions. The authors showed that the relationship between the fractional [DAG]⁺ fragment ion intensities and the regioisomeric TAG composition was linear.

In 2002, we published our first application of the dual parallel mass spectrometer arrangement to ESI-MS, MS/MS, and MS³ of canola oil TAG and of triolein

oxidation products (38). In this report we employed two mass spectrometers, utilizing ESI-MS and APCI-MS, for analysis of the column eluate from one reversed-phase liquid chromatography system (LC1/MS2). Data from the LC1/MS2 arrangement are presented below.

ESI-MS data reflect some trends that were initially observed by Duffin *et al.* (13) and by Cheng *et al.* (18), specifically that TAG containing unsaturated FA respond with higher abundances than TAG containing saturated FA by ESI-MS, and the positions of the fatty acyl chains on the glycerol backbone can be determined from the [DAG]⁺ fragment ion ratios observed in ESI-MS/MS mass spectra, as will be demonstrated herein. In fact, ESI-MS/MS mass spectra were more definitive and gave more reproducible results than APCI-MS mass spectra, which have also been shown to be useful for discriminating the positional isomers (39–41). The higher response given by unsaturated TAG under ESI-MS conditions is exactly opposite the trend that has been reported extensively for APCI-MS analysis of TAG, starting with the initial report of Byrdwell and Emken (10), and being more explicitly reflected in the response factors demonstrated by Byrdwell *et al.* (42–44) for TAG quantification by APCI-MS. Application of a similar approach to quantitative analysis by ESI-MS as that used for APCI-MS is presented herein. These data demonstrate that the response factors for saturated TAG by ESI-MS are larger than the response factors for unsaturated TAG, reflecting the lower response of saturates by ESI-MS. Overall, ESI-MS is shown to be much more sensitive for analysis of TAG, as their sodium or ammonium adducts, than is APCI-MS.

Before presenting data, it is useful to examine the principles of ESI. Two models will be mentioned that describe the steps in the ionization process of molecules of different sizes by ESI. The contributions to the development of the modern ESI source by Dole *et al.* (45–47), Yamashita and Fenn (48–50), Iribarne and Thomson (51,52), and Bruins *et al.* (53) were discussed in the introduction to this volume. Work by some of these authors to develop the two ionization models is described below. A more detailed presentation of the history of ESI-MS methods is given in the thorough treatment of liquid chromatography/mass spectrometry by Niessen (54). The theory and principles of electrospray ionization are discussed in detail in the volume by Cole (55), with a foreword by John Fenn describing personal experiences in the timeline of early developments. This chapter will focus on applications of ESI-MS (and APCI-MS) to triacylglycerols, and will show the hardware that we have used for publications from our laboratory, which is the same as (or similar to) the hardware used by several other research groups cited herein.

Experimental

Principles of APCI-MS

In 1973 and early 1974, Horning *et al.* (56,57) and Carroll *et al.* (58,59) developed a new type of source capable of ionizing molecules at atmospheric pressure. They

reported an atmospheric pressure ionization source that used a syringe sample inlet with a carrier gas to transport the sample past a nickel-63 beta radiation source that performed ionization. The ions produced by this source were sampled into the high vacuum mass analyzer through a 25- μm pinhole. In 1974, Horning *et al.* (57) showed the first example of the new API source as an online detector for LC. For this report, they increased the size of the reaction chamber, which was reported to accommodate flow rates up to 2.0 mL/min. This report also demonstrated that the beta emitter (Ni foil) could be replaced with a corona discharge electrode. The corona discharge design was described more thoroughly in 1975, and it is this

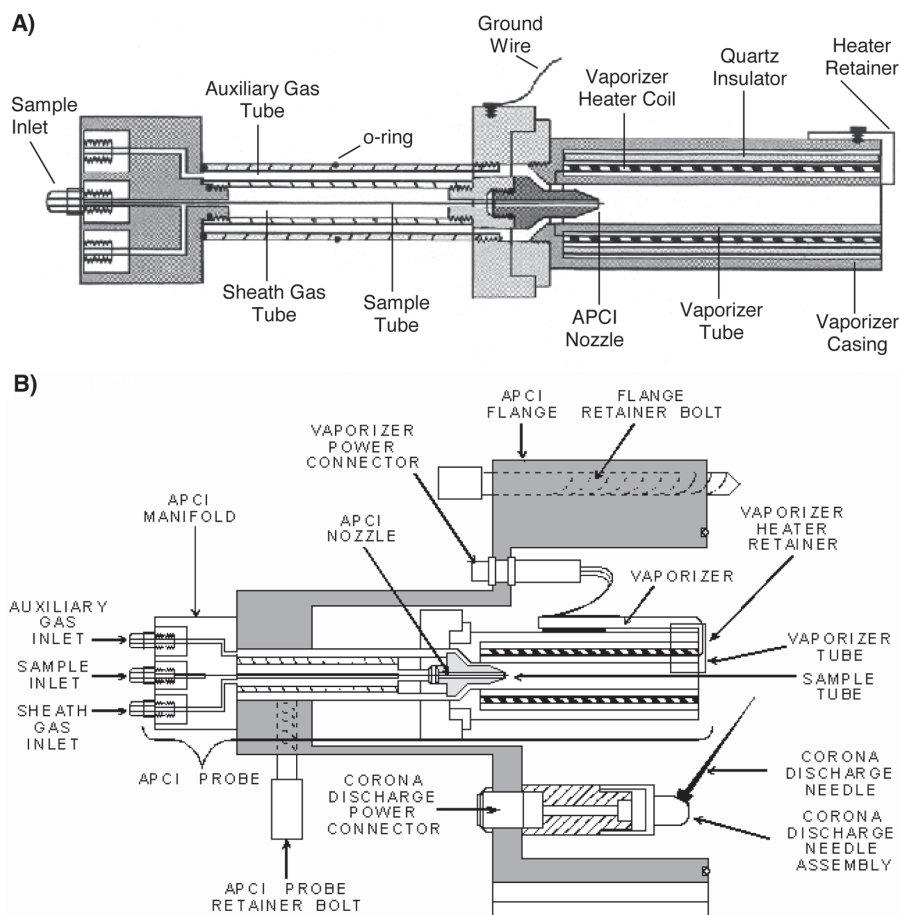
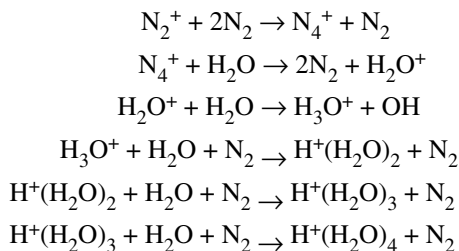


Fig. 7.1. Atmospheric pressure chemical ionization (APCI) source. (A) APCI probe. (B) APCI head. *Source: APCI Hardware Manual.* Adapted and reproduced with permission from ThermoElectron, Inc.

design that constitutes the basis for modern APCI sources (59). Atmospheric pressure ionization eventually became known as atmospheric pressure chemical ionization, to differentiate it from electrospray, which also occurs at atmospheric pressure. This name also emphasizes that APCI is similar to conventional chemical ionization in that it involves a solvent-mediated process.

An APCI source has several characteristics in common with some of the ionization methods mentioned in Chapter 1. First, APCI employs a pneumatically assisted vaporization process with heated desolvation, followed by corona discharge ionization. Figure 7.1 shows the components of the first-generation Finnigan MAT API-1 source. The components include the sample inlet capillary, spray nozzle, heated vaporizer, and corona discharge needle. In Figure 7.1, one can see that the LC effluent attaches to the sample inlet capillary (0.15 mm i.d. \times 0.39 mm o.d. \times \sim 10.2 cm long) that goes from the attachment nut to just past the end of the APCI nozzle, emerging in the bottom of the heating tube (as seen looking into the tube). Sheath gas (purified N_2) enters the ionization head and emerges out of the nozzle, concentric with the end of the sample capillary (and keeps the capillary tip "floating" in the center of the nozzle). At the end of the nozzle, a spray is produced from the sample with the nitrogen gas. The liquid mist travels down the center of the heated vaporizer tube, held at sufficient temperature to vaporize all solvent before leaving the tube. An auxiliary gas enters around the edge of the nozzle, providing additional gas flow to keep the desolvated mist from contact with the vaporizer tube walls. Then, the desolvated molecular mist passes by the tip of a corona discharge needle carrying a high voltage that produces ionization in the atmospheric chemicals around the tip. Figure 7.2 shows the process of ionization (protonation) of water clusters using purified nitrogen sheath gas plus simple atmospheric gases.

The series of reactions occurring in pure nitrogen with traces of water at pressures of 0.5 to 4 torr (thus including atmospheric pressure) were described by Good *et al.* (60) in 1970. These reactions were recognized by Horning *et al.* (61) in 1973 to apply to APCI with atmospheric gases present. The intermediates of these reactions are seen in Figure 7.2. The mechanism of $(H_2O)_nH^+$ formation is as follows:



In addition to the above reactions, any chemicals present in the source can react with each other or with the analyte, including ambient gas, sheath nitrogen, auxil-

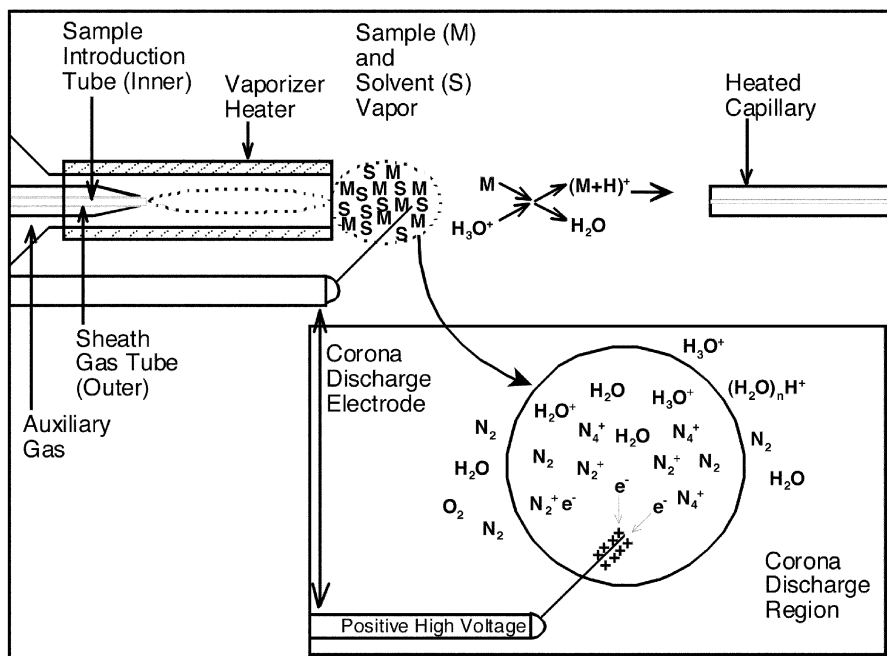


Fig. 7.2. Ionization process occurring in the APCI source. Source: *APCI Operator's Manual*. Adapted and reproduced with permission from ThermoElectron, Inc.

ary nitrogen, postcolumn additive, sparging liquid, incorporated buffer, or other additives. At atmospheric pressure these chemicals can create ions in a number of ways: either they can transfer protons, or they can attach themselves to make adduct molecules (ions), or the chemicals in the source can add together first and then react with analyte molecules to form adduct ions. Other reactions occurring at atmospheric pressure during the ionization process include soft decomposition reactions, which lead to the series of fragments that occur for each class of molecules. The fragments produced by decomposition can even act as reagents themselves and produce adducts by adding to other analyte molecules.

In APCI, the formation of adducts is often a nuisance instead of a benefit. In such cases, it is desirable to add chemical reagents to the ionization source that quench undesirable adduct formation, while promoting formation of protonated molecules. For example, when our acetonitrile/methylene chloride HPLC method for separation of TAG was transferred from the TSQ 700 tandem mass spectrometer to the LCQ Deca instrument, we noticed substantially larger amounts of acetonitrile-related adducts than had been present on the TSQ. To solve the problem, we connected a sparging bottle to bubble the sheath gas through methanol before it entered the source. Saturating the sheath gas with methanol eliminated the acetonitrile-

trile-related adducts and gave substantial abundances of protonated molecules. Previously, Manninen and Laakso (62) had compared several chemical ionization reactant molecules by sparging the sheath gas through a bottle containing one of several solvents. They compared the signal given when methanol (MeOH), isopropanol, water, or 0.5% NaOH in MeOH was used as the sparging solvent. The best signal was produced when the sheath gas was bubbled through methanol.

There are at least two convenient ways to introduce reagent chemicals into the APCI source. As just mentioned, bubbling the sheath liquid through a reagent liquid is quite effective at adding a modifier into the ionization source (make sure to use a trap bottle, also, to keep the reagent liquid from back-streaming when the gases are turned off). Alternatively, a liquid may be added to the LC eluate *via* a tee prior to the sample inlet. A syringe pump typically supplies this liquid. However, one disadvantage of providing additional chemical reagents is that the heated vaporizer coil accumulates buildup more quickly than without additives. Therefore, more frequent cleanup and maintenance of the heated vaporizer are required.

APCI often produces ample abundances of protonated molecules (Note: We refrain from the term “*protonated molecular ion*,” because “molecular ion” has a specific meaning, which is distorted by calling it “protonated,” which also has a specific meaning. A “protonated molecular ion” would be an odd-electron molecular ion $M^{\cdot+}$, plus a proton H^+ resulting in an odd electron $MH^{\cdot 2+}$. Instead, referring to the ion as a protonated molecule, which implies ionization, or a protonated molecule ion would be appropriate for an even-electron molecule, M , ionized by addition of a proton, H^+ , to form an even-electron protonated molecule, MH^+ , which is an ion.) Some classes of molecules, however, do not produce large abundances of protonated molecules. This can happen when the analyte molecule is so labile that only a small abundance of the protonated molecule remains. Examples include alcohol-containing molecules, in which the alcohol is lost quite readily by dehydration, $-H_2O$ (leaving behind a double bond). In these cases, the adducts formed from chemical reagents that are added are distinctly not a nuisance, and may be the only way that near-molecular ions are observed. In such cases, a reliable series of adduct ions with atmospheric or other gases or a reagent liquid can provide reproducible confirmation of the molecular weight, from multiple abundant ions corresponding to adducts with the analyte.

As mentioned above, atmospheric pressure chemical ionization is one of the two common atmospheric pressure ionization sources; electrospray ionization is the other. These two interfaces are interchangeable. On the ThermoFinnigan instruments used in our laboratory, both ionization sources attach to an atmospheric pressure ionization interface that is pumped down to rough vacuum (~ 1 torr) using a rotary vacuum pump, followed by an area of intermediate vacuum ($\sim 10^{-3}$ torr), and then finally high vacuum ($< 10^{-5}$ torr). A diagram of the API-1 interface on our TSQ 700 is shown in Figure 7.3. An ESI-MS source is attached to the API interface in Figure 7.3. The API interface is connected to the front of the high vacuum

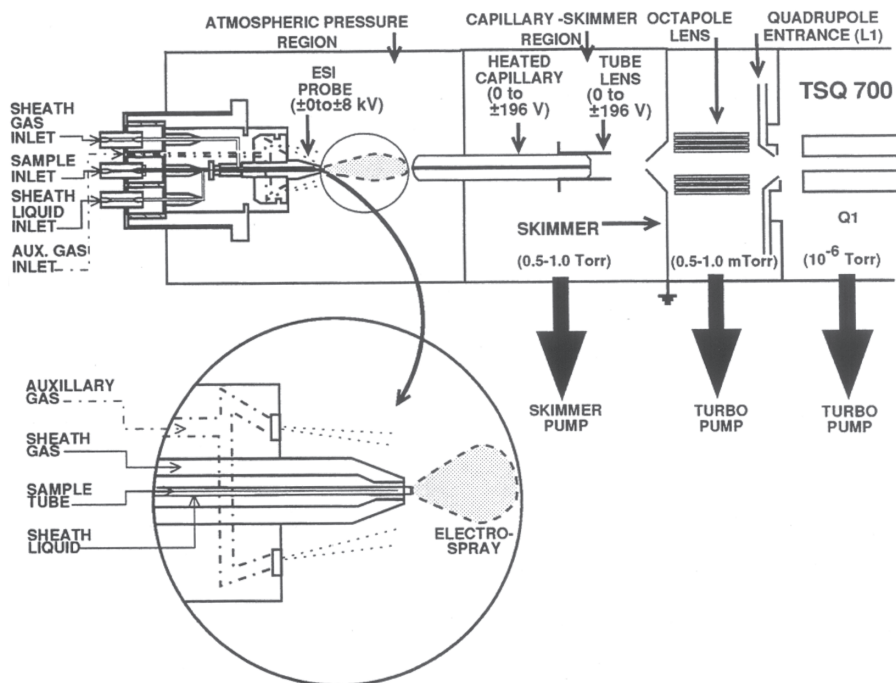


Fig. 7.3. Electro spray ionization source and atmospheric pressure ionization interface to high vacuum on ThermoElectron (formerly Finnigan MAT) TSQ 700. Adapted and reproduced with permission from ThermoElectron, Inc.

manifold, maintained at high vacuum by two turbomolecular pumps. In the API interface, most instrument manufacturers employ common elements. The spray produced by the LC eluate in the ionization source is typically sprayed either directly onto or orthogonally to a heated capillary (older ThermoFinnigan instruments sprayed directly onto the capillary; newer instruments now employ an orthogonal design). The capillary is not only heated to help keep the ions in flight, but also a potential is applied to draw the ions from the source and provide them with a defined amount of kinetic energy. We typically heat the capillary to 265°C for triacylglycerols, while a slightly higher temperature, ~275°C, is necessary for optimal ion transmission from phospholipids. The spray exiting the capillary is then focused onto one or more skimmers maintained at ground potential. In the latest generation of API interface ThermoElectron employs an orthogonal spray to minimize contamination of the heated capillary. They have also now incorporated a countercurrent gas around the capillary inlet to break up solvent clusters and to keep the capillary cleaner (this allows expanded use of inorganic buffers).

Principles of ESI-MS for TAG Analysis

While ESI-MS has found its greatest use in the burgeoning field of proteomics, its commercial availability, affordability, and ease of use as an LC detector have caused it to be applied to almost every class of molecules. Some molecules are particularly amenable to ESI-MS because they are either already ionic (such as phospholipids) or they contain easily ionizable functional groups (such as proteins). Other classes of molecules are neutral, have little functional group diversity, and do not readily form protonated molecules under normal ESI conditions. These classes of molecules require the use of an ionic reagent (electrolyte/buffer) that can produce adduct ions. Triacylglycerols are one such class of neutral molecules that are not readily ionized without the use of a reagent buffer to promote adduct formation. The special steps that must be taken for TAG analysis by ESI-MS will be described below, after discussion of the electrospray process.

The process of producing ions from electrospray of a liquid flow is as follows: LC effluent or infused liquid enters the ESI source through a small grounded inlet capillary (grounding keeps the high voltage from propagating back to the HPLC pump, especially if electrolyte is included in the solvent system). The inlet capillary is threaded down the center of a stainless steel hypodermic needle. The needle is typically maintained at 4–6 kV. The high voltage applied to the needle charges the surfaces of drops emerging from the needle, which disperse into a fine spray of charged droplets. The nebulizing gas used to spray the solution aids in evaporation of solvent from the charged droplets. There are two models for formation of gas-phase ions from an electrosprayed solution. The first model is the “ion evaporation” (or ion desorption) model by Iribarne and Thomson (51). This model was developed to describe the formation of small ions from charged droplets. In this model, solvent evaporating from droplets causes them to shrink in size while the number of charges remains constant, until the charge density on the surface overcomes the surface tension holding the drop together (at the Rayleigh stability limit). At the Rayleigh limit, the drop undergoes fission into smaller charged droplets. These smaller charged droplets again start to shrink as solvent evaporates further. Eventually the charge density in the droplet once again allows the coulomb repulsion to overcome the surface tension, causing another fission of the droplets. This sequence of steps repeats itself again and again, until the droplets are small enough (at the critical size) that they can spontaneously evaporate a cluster ion from the charged drop. Ion evaporation from evaporating charged droplets requires (1) that the electrostatic energy become large enough, (2) that the critical size (the size at which a cluster ion can evaporate from a droplet) be larger than the analyte ion residue, and (3) the critical size must also be larger than the Rayleigh limit of instability.

The competing model to explain the formation of charged ions during electrospray is the “charge residue” model put forth by Dole (46,47). Since Dole’s group was working on macromolecule polymeric ions, as mentioned in Chapter 1, their experi-

ences led them to present a different model for the process of ion formation during ESI. Their model applies to large macroions in charged droplets and is the model most often used to describe the ionization of proteins. The first steps of this model are the same as the ion evaporation model. The first stages of both models involve solvent evaporation and droplet fission at the Rayleigh limit to produce smaller and smaller charged droplets. Rather than ions evaporating out of the shrinking droplets, the charge residue model assumes that solvent evaporation and Rayleigh fission continue until there is essentially one analyte ion per droplet. At that point, the electrolyte, which is located on the droplet surface, is forced close to the analyte ion as the solvent continues to evaporate. The electrolyte is forced onto the surface of the analyte macroion by evaporating solvent and reacts with the analyte to become protonated or to produce an ionic adduct. Thus, the charge is left on the analyte as a kind of residue, by the process of solvent evaporation following droplet shrinkage by evaporation and fission. As mentioned, the ion evaporation model is applied to [and Iribarne and Thomson's (51) equations reflect] small analyte molecules, while the charge residue model was developed to describe the ionization behavior of large macroions. Thus, it is ion evaporation that is responsible for producing gas-phase triacylglycerol adduct ions from the sprayed effluent. The TAG are ionized to form adducts in solution at the tip of the electrospray needle, and then they are released from the droplet at the critical size. Even TAG oligomers, which are substantially larger, have functional groups with which the electrolyte ion reacts in solution before being released from the droplet.

Regardless of which method formed the ions, after they are formed from the charged droplets, they move in the potential field toward the entrance capillary, and some of the ions become entrained in the flow of gas that enters the mass spectrometer. A countercurrent gas, or "curtain gas," surrounds the inlet capillary in most modern instrument designs. This helps to reduce the amount of buffer allowed into the heated capillary and helps to break up solvent clusters. After passing down the heated capillary, the spray exits the rear of the heated capillary, where it undergoes supersonic free jet expansion in an area of partial vacuum (<1 torr; see Fig. 7.3). In this region, ions are focused by a tube lens onto a skimmer that samples ions off-center from the cone of spray. Once past the skimmer, ions are kept in their trajectories by ion guides. These ion guides may be plate lenses or multipoles (or a combination of these). After these ion-focusing elements, ions travel into the high vacuum region to the mass analyzer. This area between atmospheric pressure and high vacuum, which incorporates ion guides and skimmers, is the API interface, described in Chapter 1. The API interface of our TSQ 700 tandem mass spectrometer was shown in Figure 7.3. As mentioned previously, electrospray ionization is one of the two most commonly available ionization sources that attach to an API interface. The ESI source from the TSQ 700 mass spectrometer is shown in Figure 7.4. The electrospray ionization source on our LCQ Deca ion trap mass spectrometer is almost identical to that from the TSQ 700. Both instruments employ a first-generation ESI source, which uses a linear geometry, instead of the orthogonal orientation adopted in later designs. In the linear geometry, the spray direction is linear with the bore of the heated capillary inlet.

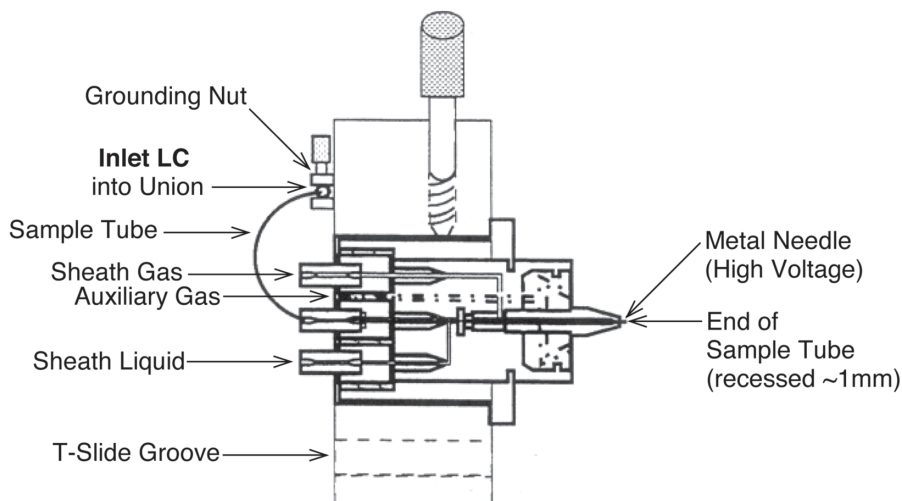


Fig. 7.4. Electrospray ionization head. *Source: API Operator's and Service Manual.* Adapted and reproduced with permission from ThermoElectron, Inc.

Very simple in its design, the electrospray ionization source produces ions from solution with little or no fragmentation. Some fragmentation may be induced in the API interface, if desired. A potential may be applied between the outlet nozzle of the heated capillary and the skimmer, which is held at ground potential (refer to Fig. 7.3). This is called “*nozzle-skimmer collision induced dissociation*” (CID). Since fragmentation occurs prior to ions entering the mass analyzer, this process is referred to as “*up-front CID*.” Alternatively, a potential may be applied between the skimmer and the first multipole ion guide. This is skimmer-multipole CID and is a more common option for up-front CID. On most machines, the voltages may be programmed to alternate between normal and CID voltages, so that mass spectra with and without up-front fragmentation may be obtained during the same run. This is especially useful in cases where the ESI interface is attached to a single quadrupole instrument from which MS/MS is not possible. Since the fragments obtained by up-front CID are often similar to those obtained by conventional MS/MS, up-front CID is often referred to as “*pseudo-MS/MS*.” However, some molecules do not fragment well with up-front CID, while others do fragment, but produce few structurally useful fragments. This is discussed further in the chapter on dual parallel techniques, Chapter 13.

As mentioned, TAG are not readily ionized under ESI-MS conditions. The references cited in the introductory section had a common characteristic: Each one used an ionic additive to form an adduct with TAG molecules. Typically, these were cations in the form of ammonium or an alkali metal (Na or Li), usually provided as acetates. The nature of the cation affected the ability of the adduct to frag-

ment and produce beneficial MS/MS spectra. The results presented below reflect the use of additives, as given in Table 7.1.

API-MS Mass Spectrometers

On our tandem instrument, after ions are produced at atmospheric pressure, by APCI or ESI, they are sampled into the end of the heated capillary that serves as the interface to vacuum stage one. The whole interface region, from atmospheric pressure to high vacuum, was shown in Figure 7.3 for the Finnigan MAT TSQ 700 in our lab. The rear of the heated capillary serves as a nozzle to spray the incoming ionic effluent stream through the concentric tube lens, onto the skimmer cone. The skimmer samples the spray ~1 mm off center from the primary ion trajectory. Then, the ions move through the octapole lens in the first high vacuum region past two closely spaced plate lenses to the first quadrupole, which is in the second high vacuum region.

The Thermo Finnigan LCQ Deca ion trap mass spectrometer in our laboratory uses a first-generation API source, almost identical to the one on the TSQ 700, but uses a second-generation heated capillary interface. Instead of the construction shown in Figure 7.3, the LCQ Deca mass spectrometer uses an “API stack” attached to the back of the spray shield that contains the heated capillary, tube lens, and skimmer. The components in this version of the interface are shown in Chapter 1, Figure 1.3. After the skimmer on the Deca lies a short quadrupole lens (non-mass-filtering) and then a short octapole lens, before the entrance lens to the trap.

As mentioned in Chapter 1, most instrument manufacturers now employ API interfaces that have (i) an orifice orthogonal to the direction of spray, and (ii) a countercurrent gas emanating from around the heated capillary inlet. The orthogonal arrangement allows increased use of buffers without contaminating the heated capillary inlet. The countercurrent gas greatly aids in solvent evaporation and reduces the amount of solvent cluster ions admitted into the mass analyzer. The newer ThermoElectron (formerly ThermoFinnigan, formerly Finnigan MAT), Agilent (formerly Hewlett-Packard), Applied Biosystems/PE Sciex, and other instruments utilize these two API interface design features. The Micromass API interface goes even a step further and has two orthogonal sampling cones to reduce chemical noise even more. This is the Z-Spray™ interface pictured in Chapter 1, Figure 1.5. The newest Micromass API source also incorporates a countercurrent gas at the first sampling orifice.

The computer interfaces have changed and improved dramatically in many ways over the last several years. The Digital Equipment Corporation (DEC) Unix clone on the original Finnigan MAT TSQ and SSQ machines has given way to Microsoft Windows-based systems with cut-and-paste graphics. In many ways cut-and-paste graphics make desktop publishing of results easier. However, some flexibility was sacrificed in the move from Instrument Command Language (ICL)-based instrument programming to Windows-based programming. In the older ICL-based instrument methods, an operator could easily change the values of parameters in real time, allowing many variables to be

TABLE 7.1
Additives Used for ESI-MS of TAG by Various Authors, and Topics Discussed in the Articles

| Author | Ref. | Adduct/source | How added | LC-MS? | MS/MS? | Positional isomers? | Rate (amount) | Other |
|----------------------|------|--|---|------------------|--------|---------------------|----------------------------------|--|
| Duffin <i>et al.</i> | 13 | [M+Na] ⁺ 10 mM NaOCOCH ₃ [M+NH ₄] ⁺ 10 mM NH ₄ OCOCH ₃ [M+H] ⁺ 2% HOCHO | In infusion solvent In infusion solvent In infusion solvent | N | N | N | 2 μL/min 2 μL/min 2 μL/min | |
| Sandra <i>et al.</i> | 15 | [M+NH ₄] ⁺ 50 mM NH ₄ OCOCH ₃ | In CEC solvent | N, CEC fractions | N | N | 1 μL inj. | |
| Cheng <i>et al.</i> | 18 | [M+NH ₄] ⁺ 10 μM NH ₄ OCOCH ₃ [M+Na] ⁺ 1 μM NaOCOCH ₃ | In infusion solvent In infusion solvent | N | Y | N | 10 μL/min 10 μL/min | |
| Schuyf <i>et al.</i> | 17 | [M+Na] ⁺ 0.1 mM NaOCOCH ₃ in MeOH | Added postcolumn | Y | N | N | 30 μL/min | Quantification, argentation chromatography |
| Hsu and Turk | 19 | [M+Li] ⁺ 2.0 mM LiOCOCH ₃ | In infusion solvent | N | Y | Y | 1 μL/min | Deuterium-labeled TAG |

| | | | | | | | | |
|------------------------|-------|--|--------------------------|--------------------|---|---------------------|---|--------------------------------|
| Dermaux <i>et al.</i> | 16 | [M+NH ₄] ⁺ 0.5% NH ₄ OCOCH ₃ | In sample solvent | N,CEC fractions | N | N | 1 µL inj. | |
| Han and Gross | 20,34 | [M+Li] ⁺ LiOH | In extraction solvent | N | N | N | 1 µL/min | Neutral loss data |
| Hvattum | 21 | [M+NH ₄] ⁺ 0.01% HCOOH w/ NH ₄ to pH 5.3 | In mobile phase | Y | Y | ~Y | 0.1 mL/min (0.8 mL/min split 1:7) | |
| Sandra <i>et al.</i> | 30 | [M+Ag] ⁺ 100 µg/ml Ag ⁺ from AgNO ₃ in MeOH | Added postcolumn | SFC | N | N (APCI only) | 1.0 mL/min | SFC |
| Fard <i>et al.</i> | 32 | [M+Na] ⁺ N.S. | N.S. | N | N | N | N.S. | High resolution ESI-FTICRMS |
| Marzilli <i>et al.</i> | 31 | [M+NH ₄] ⁺ 10 mM NH ₄ OCOCH ₃ | In infusion solvent | N | Y | Y | 2 µL/min | |
| Kalo <i>et al.</i> | 35 | [M+NH ₄] ⁺ 3% of (25% NH ₄ /H ₂ O) | In mobile phase | Y | Y | 0.06 Y | | |
| Byrdwell and Neff | 38 | [M+NH ₄] ⁺ 20 mM NH ₄ OCOCH ₃ | Sheath liquid | Y | Y | Y | 20 µL/min | Dual parallel |

optimized on the fly. In the newer Xcalibur™ software, the threshold and mass ranges are set for each segment of the chromatogram and cannot easily be varied interactively. The flexibility and real-time control of the ICL procedures allow a user to perform almost any experiment they can conceive of, as long as they can program the ICL code. Once the data are acquired, the Windows-based Xcalibur™ software does a better job of displaying the chromatogram time axes and other graphing functions. Therefore, it is useful to convert data files obtained on the TSQ system into Xcalibur™ files, to allow their more convenient graphical representation.

Results and Discussion

Triacylglycerols

TAG Qualitative Analysis by APCI-MS. Triacylglycerol analysis has always presented a difficult analytical challenge. High temperature gas chromatography (HTGC) has been used for many years, but there are drawbacks to this approach. TAG with numerous sites of unsaturation are subject to degradation at the temperatures used for HTGC. TAG with long fatty chains and/or oxygen-containing functional groups require higher temperatures that often produce substantial column bleed. Numerous methods for HPLC of TAG are available, but these, too, have limitations. The complexity of most TAG mixtures in naturally occurring fats and oils precludes complete structural analysis using a simple two-dimensional detector. Simple synthetic mixtures, such as model systems and TAG standards, can be analyzed by HPLC with two-dimensional detectors and can also be analyzed by LC/MS without separation (by infusion) to allow facile qualitative characterization of all components. For more complex samples, chromatographic separation of components coupled to the information-rich APCI and/or ESI MS detectors clearly makes qualitative and quantitative analysis easier than without separation, as will be seen.

Tyrefors *et al.* (9) showed the separation of a mixture of lipids containing stearic acid methyl ester, cholesterol, cholesteryl palmitate, and trilaurin. They reported a custom-built interface attached to a Sciex API III tandem mass spectrometer for supercritical fluid chromatography (SFC)/APCI-MS. This first report was discussed in the Introduction above. In their report, the mass spectrum of stearic acid methyl ester had a protonated molecule as the base peak, with a substantial water adduct. A spectrum of cholesterol showed the $[M-H_2O]^+$ fragment at m/z 369 as the base peak, with some abundance of water adduct, but no protonated molecule. Cholesteryl palmitate also showed the m/z 369 base peak due to the cholesterol backbone, and the $[M+H_2O]^+$ adduct, and again, no protonated molecule. In most APCI-MS mass spectra, as discussed below, the water adduct is not as large as that observed by Tyrefors *et al.* (9). The sparging of the make-up gas through water was primarily responsible for this difference.

Byrdwell and Emken (10) used a commercially available APCI interface on a Finnigan MAT single quadrupole mass spectrometer to demonstrate the first

HPLC/APCI-MS of a mixture of synthetic triacylglycerols having varying degrees of unsaturation. A mixture of monoacid (all three fatty acyl chains the same) TAG standards was separated by using an analytical scale reversed-phase column from which the flow rate of 1 mL/min was split to deliver 400 μ L/min to the APCI interface, and the remaining 600 μ L/min went to an evaporative light scattering detector. The article showed mass spectra that are now known to be typical of results produced by a variety of instruments from different manufacturers. The spectra showed that TAG with numerous sites of unsaturation produced protonated molecules as base peaks, $[M+H]^+$, and diacylglycerol fragment ions, $[(M+H)-RCOOH]^+$, which may be written as simply $[M-RCOO]^+$, as the main fragments. In contrast to the mass spectrum shown by Tyrefors *et al.* (9), the results by Byrdwell and Emken (10) showed that TAG with no sites of unsaturation produced little or no abundance of the intact protonated molecule. The APCI-MS mass spectra exhibited DAG fragment ions that conclusively allowed the fatty acyl chains to be determined.

The new HPLC/APCI-MS method was next applied by Neff and Byrdwell (11) to the natural mixtures of TAG in normal and genetically modified soybean oils. An HPLC/APCI-MS chromatogram and HPLC/evaporative light-scattering detector (ELSD) chromatogram of a typical refined, bleached, and deodorized soybean oil are shown in Figure 7.5. Typical mass spectra of soybean oil TAG are shown in Figure 7.6. Mass spectra of TAG having from six sites of unsaturation (OLnL) (see abbreviations in Fig. 7.6) to one site (POS) are shown in Figure 7.6. The spectra in this figure reflect the trends that are now known to be characteristic of APCI-MS mass spectra. TAG having more than four sites of unsaturation had the protonated molecule as the base peak in APCI-MS spectra, for example, OLnL, Figure 7.6A. TAG with fewer than three sites of unsaturation had one of the DAG fragment ions as the base peak, for example, Figure 7.6E and Figure 7.6F. TAG having three or four sites of unsaturation could have either the protonated molecule or a DAG fragment ion as the base peak, depending on how the unsaturation was distributed in the molecule. For instance, OLO contained four sites of unsaturation, and gave a DAG fragment ion as the base peak in the mass spectrum in Figure 7.6B. On the other hand, LLS also had four sites of unsaturation, but gave the protonated molecule as the base peak in the spectrum in Figure 7.6C. Most TAG with three sites of unsaturation gave a DAG fragment ion as the base peak, such as in the spectrum of SOL in Figure 7.6D. But TAG having three sites of unsaturation that contained Ln, that is, SSLn and PPLn from high stearic and high palmitic SBO, respectively, gave protonated molecules as the base peaks in the tabular data in our earlier report (11).

These natural samples contained numerous "critical pairs" [TAG having the same equivalent carbon number (ECN)] of TAG having identical masses, but different distributions of unsaturation in the fatty acyl chains, such as OOO and SOL, which both have an ECN of 48 and an isotopic molecular weight of 884.8. When the chromatographic separation is less than optimal, these could not be differentiated based on the protonated molecule peaks, so the DAG fragment ions were crucial to differentiating

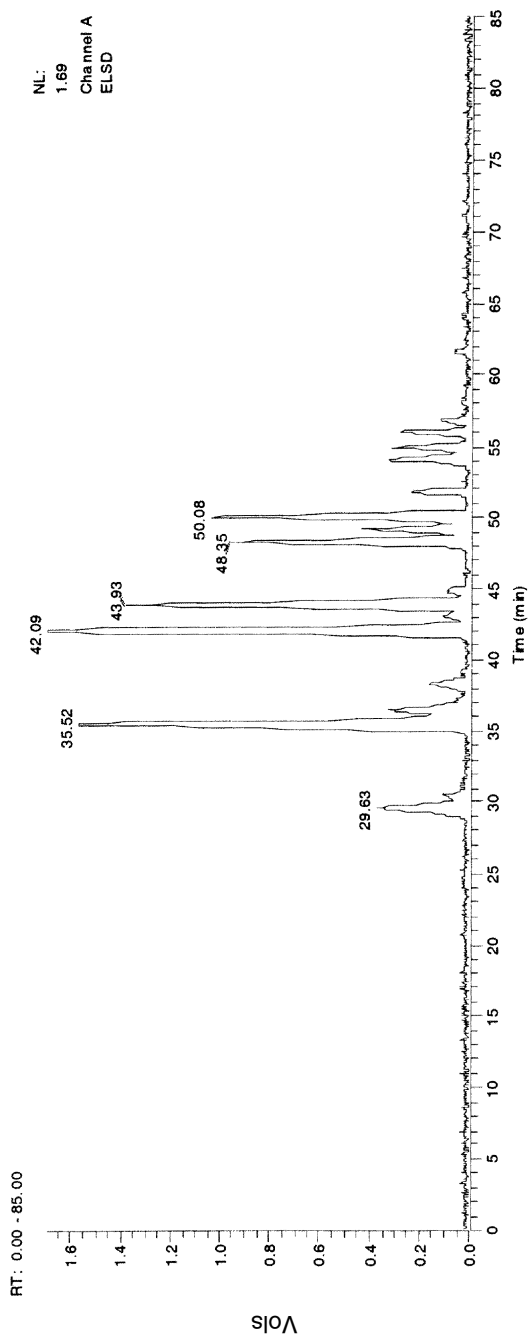


Fig. 7.5. (Continued).

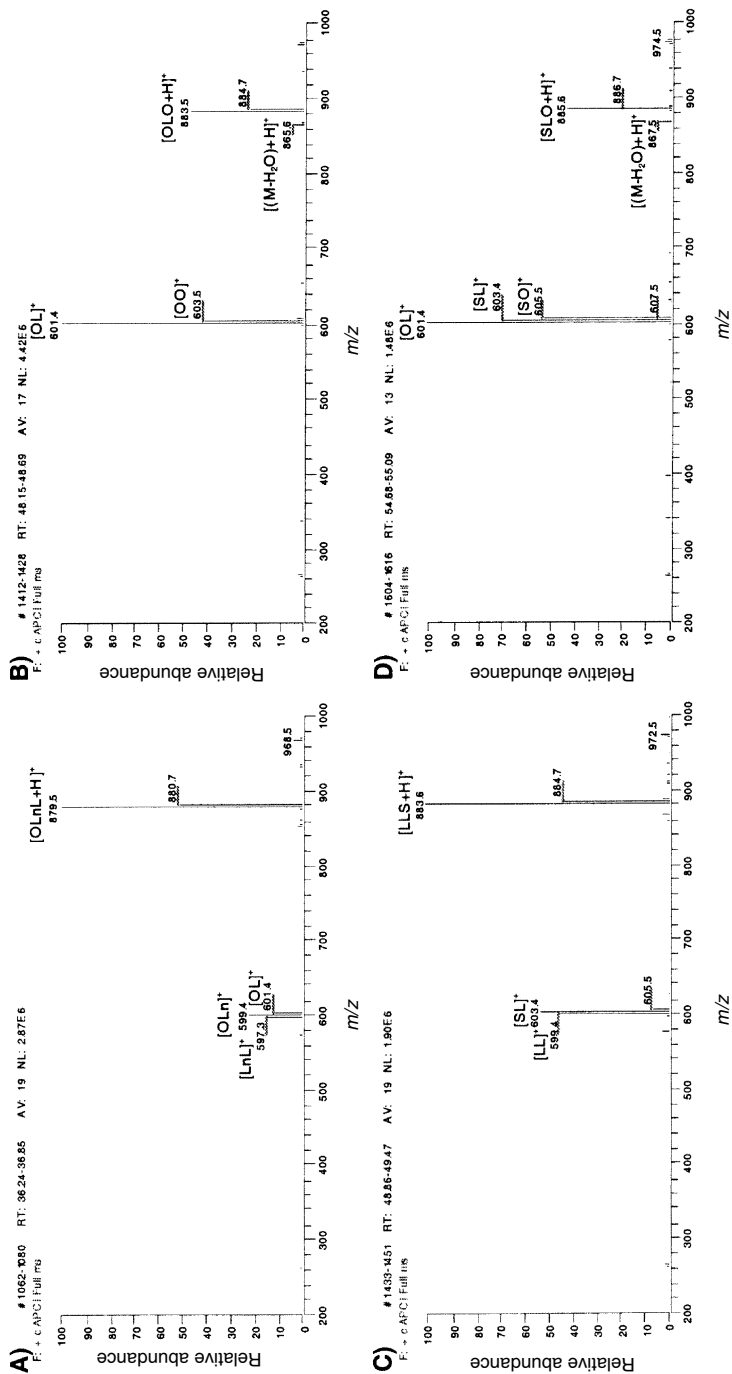


Fig. 7.6. APCI-MS mass spectra of soybean oil TAG. (A) OLnL, (B) OLO, (C) LLS, (D) SLO, (E) SLP, (F) POS, (G) expanded FA fragment region of SLP, (H) expanded FA fragment region of OLO. Abbreviations: FA, fatty acid; Ln, linolenic acyl chain (18:3); L, linoleic acyl chain (18:2); O, oleic acyl chain (18:1); S, stearic acyl chain (16:0); P, palmitic acyl chain (16:0).

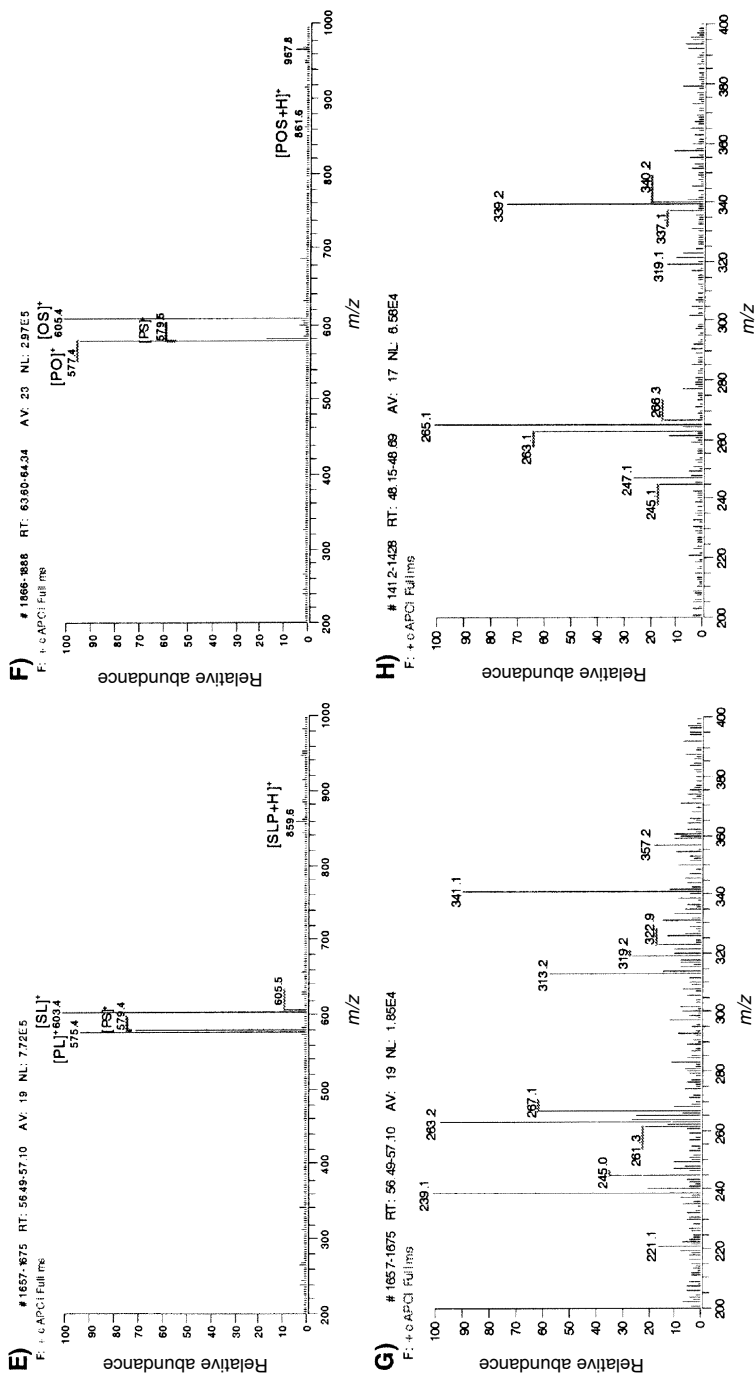


Fig. 7.6. (Continued).

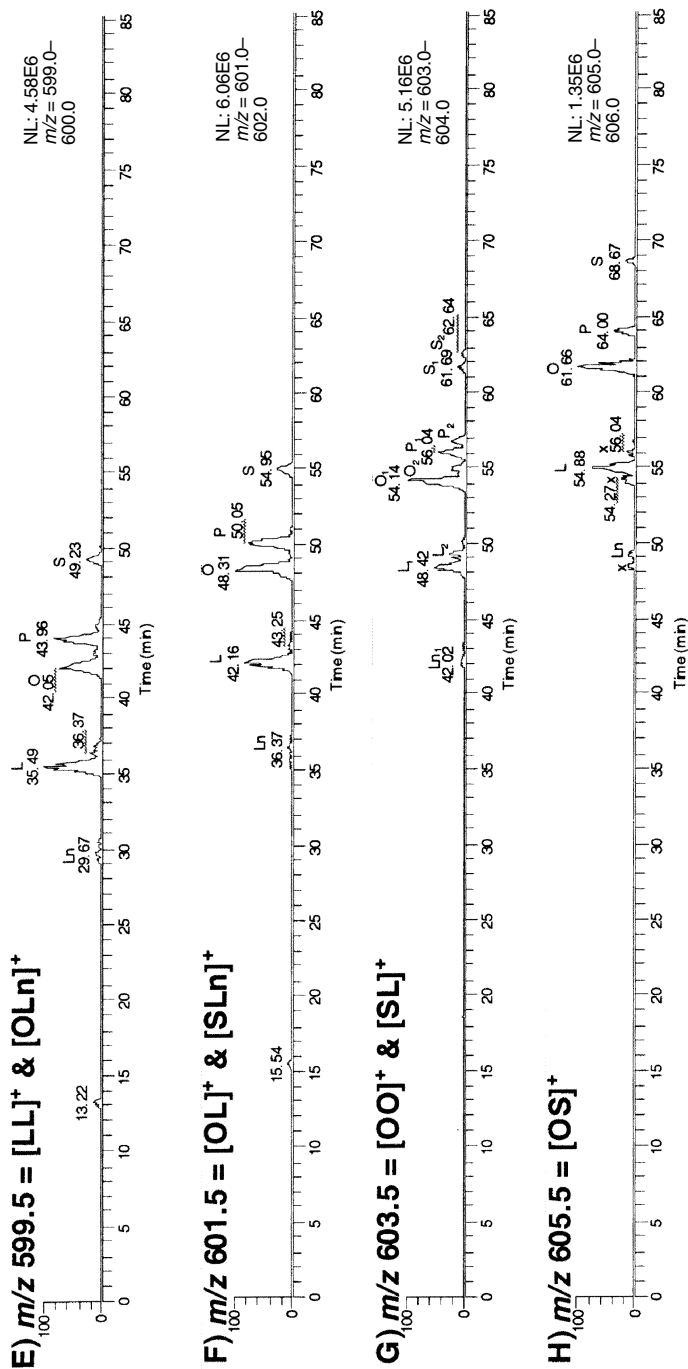
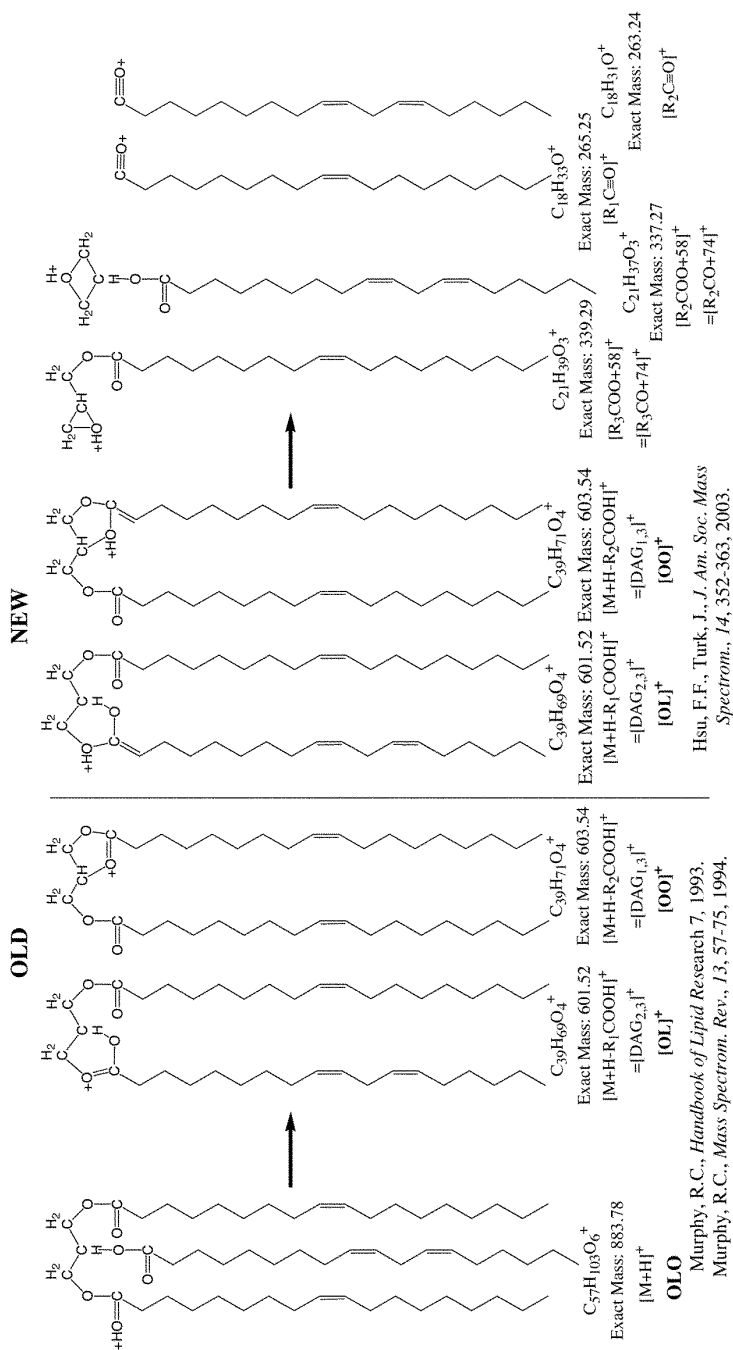


Fig. 7.7. (Continued).



Scheme 7.1. Identities of fragments formed by TAG, with references. The same fragments are formed by phospholipids.

such critical pairs. For instance, both OOO and SOL shared a fragment at m/z 603.5 (= [OO]⁺ and [SL]⁺); however, the mass spectrum of SOL had peaks at m/z 599.5 and 605.5, representing [OL]⁺ and [SO]⁺, respectively, which the mass spectrum of OOO did not have. Thus, these two TAG could be distinguished by their DAG fragment ions. However, when the chromatographic separation was good, virtually no intractable overlaps occurred, as can be seen in Figure 7.7G. Critical pair overlap was also possible from TAG having the same ECN but different lengths of fatty acyl chains, such as PLL, POL_n, OOL_n, and SLL_n (each with ECN = 44). Again, when the separation was less than optimal, these species occurred overlapped, but a good separation allowed them to be chromatographically differentiated. Whether overlapped or not, the DAG fragment ions of these TAG allowed them to be distinguished by mass. The identities of typical fragments from OLO observed under APCI-MS conditions are shown in Scheme 7.1. These fragments have been observed by EI, CI, and other ionization techniques through the years. The mechanisms of lipid fragmentation have been thoroughly discussed by Murphy (63) among others. As mentioned above, the primary fragments formed by TAG are diacylglycerol fragment ions formed by loss of one fatty acyl chain. The same fragments are formed by APCI-MS and ESI-MS, although in different relative intensities.

Scheme 7.1 shows two proposed identities (based on two different mechanisms) for the DAG fragment ions. The first possibility was that a fatty acyl chain was lost from the backbone, and the carbonyl group on a neighboring acyl chain undertook nucleophilic attack of the carbon from which the acyl chain was lost. This process gave DAG fragment ions in which one FA formed a five-member ring, having the two oxygens, one of which carried the charge, as depicted by Cheng and Gross (18) and by Murphy (63) and others. This proposed mechanism had two resonance structures leading to extra stability. The double bond and the charge could be on either of the two oxygen atoms on the fatty acyl chain. Hsu and Turk (19), on the other hand, reported a study of deuterium-labeled TAG (by ESI-MS of lithiated adducts) that demonstrated that the α -hydrogen of a neighboring FA was abstracted in the process of fragment formation. This resulted in a DAG fragment ion having an α,β site of unsaturation on the FA that formed the five-member ring. This structure is also shown in Scheme 7.1. This proposed mechanism also had two resonance structures, leading to extra stability. The proton [or deuterium or lithium (19)] could be on either of the acyl oxygens in the five-member ring. The fragments formed by TAG under APCI-MS conditions are the same as those described by Hsu and Turk (19), which were formed by ESI-MS of lithiated adducts. We expect that the mechanism shown by Hsu and Turk should become the convention in future publications.

The DAG fragments formed by TAG were completely analogous to the [DAG]⁺ that were formed by phospholipids, by loss of the polar head group. Hsu and Turk (64) recently reported a detailed study of the fragmentation processes undergone by deuterated phosphatidylcholine (PC). They performed a thorough study that demonstrated rather conclusively that the [DAG]⁺ formed by phospho-

lipids (e.g., PC) were formed with abstraction of an α -hydrogen on one of the fatty chains. Thus, Hsu and Turk (19,64) have shown that the same $[\text{DAG}]^+$ formed by both TAG and by phospholipids contained an α,β site of unsaturation on the FA that formed the five-member ring.

The DAG fragment ions in mass spectra of individual TAG can allow one to readily deduce the identity of the TAG from its $[\text{DAG}]^+$. However, when multiple TAG having the same ECN but different FA were chromatographically overlapped, it could be difficult to determine which $[\text{DAG}]^+$ came from which TAG (especially in the case of overlap of three or more TAG) from the mass spectrum alone. Therefore, a method was developed by which the identities of individual TAG were conclusively determined based first on the chromatographic behavior of $[\text{DAG}]^+$ and then confirmed by the mass spectra. Masses corresponding to DAG fragment ions were extracted out of the total ion chromatogram (these were referred to as "extracted ion chromatograms," EIC) to show the elution pattern of all TAG containing a particular DAG fragment ion. A typical set of EIC is shown in Figure 7.7. In the EIC of a DAG fragment ion, a peak appears for every TAG that underwent fragmentation to yield that DAG fragment ion. Each peak that appears represents a fatty acyl chain that was lost from the TAG to form the DAG fragment ion, $[\text{M-RCOO}]^+$. Therefore, a peak appears for every fatty acyl chain that combined with the DAG to form a TAG molecular species. Furthermore, all of the DAG fragments that were produced by fragmentation of one individual TAG molecular species had to occur at the same retention time, since they were produced by one TAG that eluted at a particular time. For instance, the TAG palmitoyloleoyllinoleoylglycerol (POL) produced three DAG fragments, $[\text{PO}]^+$, $[\text{PL}]^+$, and $[\text{OL}]^+$. Therefore, the O peak in the $[\text{PL}]^+$ EIC (Fig. 7.7B) must occur at the same time as the P peak in the $[\text{OL}]^+$ EIC (Fig. 7.7F), and this must be the same time as the L peak in the $[\text{PO}]^+$ EIC (Fig. 7.7C), and these occurred simultaneously with the peak arising from the $[\text{POL+H}]^+$ protonated molecule (EIC not shown). And because these ions all occur at the same time, since they arise from the same TAG, the areas under the peaks of each ion are proportional to the abundance of each ion at that time, so a plot of the integrated areas versus mass gives a good representation of an average mass spectrum across the peak.

Using these EIC, the DAG fragment ions from overlapped TAG can be easily attributed to the proper parent molecule. However, due to the complexity of typical TAG mixtures, some irreconcilable overlaps still occur. These will be addressed further in the section regarding quantification of TAG. For qualitative analysis, such overlaps do not present a substantial problem because the other $[\text{DAG}]^+$ formed from the same TAG can be used to identify the TAG. When the chromatographic separation is optimal, all overlaps can be avoided. The chromatography in Figure 7.5 was performed by using an Inertsil ODS-2 octadecylsilane chromatographic column. We later changed to an ODS-3 column, which was designed to have a lower backpressure, so a longer lifetime. Unfortunately, the resolution provided by the

later generation of column was not as good as the resolution given by its predecessor. In cases of inadequate chromatographic resolution, peaks must sometimes be integrated together and apportioned, as discussed below. We have recently changed back to the ODS-2 columns and have benefited from the improved resolution provided by this column.

The EIC in Figure 7.7 not only allow TAG to be identified and their retention times determined, but also intact, chromatographically resolved DAG can be identified in these EIC. For instance, the DAG oleoyl,linoleoylglycerol (OL) gave a DAG fragment ion of m/z 601.5 at 15.54 minutes in Figure 7.7F. Ion chromatograms and mass spectra of DAG are shown in Figure 7.8. In addition to the DAG fragment ions, DAG also gave intact protonated molecules. The abundance of the $[M+H]^+$ from the DAG was proportional to the number of sites of unsaturation in the DAG. The abundances of the $[DAG]^+$ and $[M+H]^+$ ions for the DAG in Figure 7.8 were as follows: **LLn**: $[LLn]^+ = m/z$ 597.3 (72.18%), $[M+H]^+ = 613.3$ (100.0%) at 11.69 min; **LL**: $[LL]^+ = m/z$ 599.4 (100.0%), $[M+H]^+ = 617.4$ (82.28%) at 13.22 min; **OL**: $[OL]^+ = m/z$ 601.4 (100.0%), $[M+H]^+ = 619.5$ (9.48%) at 15.54 min; and **OO**: $[OO]^+ = m/z$ 603.4 (100.0%), $[M+H]^+ = 621.4$ (0.70%) at 18.54 min. Note that the DAG LLn (with five sites of unsaturation) had a protonated molecule as the base peak, while DAG having fewer sites of unsaturation had the $[DAG]^+$ as the base peak.

In 1999, Holcapek *et al.* (65) showed APCI-MS mass spectra of structured DAG. They showed that the 1,3 isomer gave more $[DAG]^+$ abundance and less $[RCO+74]^+$ abundance than the 1,2 isomer. They reported that the ratio of the protonated molecule abundance to the $[RCO+74]^+$ was always higher for the 1,3-DAG than the 1,2-DAG. Although the authors stated that the mass spectra of DAG with three or more double bonds gave protonated molecules as base peaks, the mass spectra of OL that were shown had the $[DAG]^+$ as the base peak. Figure 7.8C is very similar to the mass spectrum of OL shown by Holcapek *et al.* (65). Our mass spectra in Figure 7.8 show that DAG with four or fewer double bonds gave the $[DAG]^+$ as a base peak, while it took five double bonds to produce a $[M+H]^+$ base peak. All authors report that DAG with few sites of unsaturation give the $[DAG]^+$ fragment ion as the base peak.

Shibayama *et al.* (66) reported the APCI-MS mass spectra of DAG in the exudates from an oil painting. Their mass spectra of DAG (having few or no sites of unsaturation) showed the expected $[DAG]^+$ base peaks with little to no protonated molecule. These authors reported larger abundances of $[RCO+74]^+$ and $[RCO]^+$ fragments than are shown in Figure 7.8. This may be due to the 20-V cone voltage applied by Shibayama *et al.* (66). Mu *et al.* (67) also reported mass spectra of diacylglycerols. Although they analyzed TAG as their $[M+NH_4]^+$ adducts, the mass spectra of DAG exhibited only $[DAG]^+$ and $[RCO+74]^+$ fragments, with no ammoniated molecule adduct ion. Interestingly, the maximum intensity of the $[M+NH_4]^+$ adduct ion from triolein was obtained with an up-front CID voltage of 120 V.

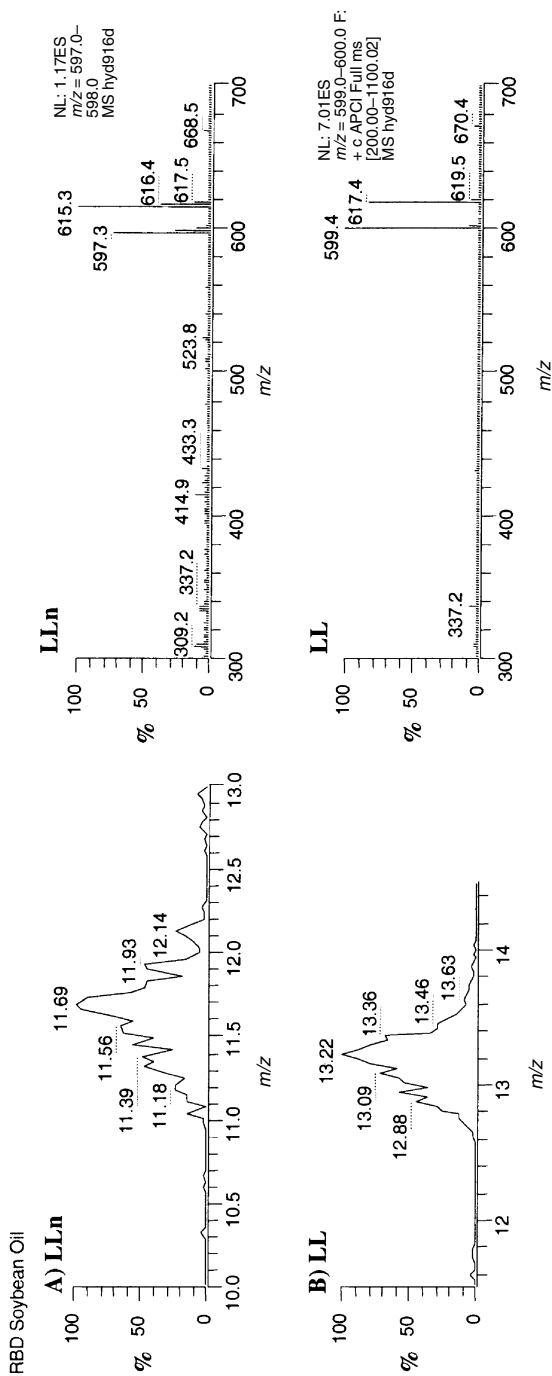


Fig. 7.8. APCI-MS ion chromatograms and mass spectra of diacylglycerols. (A) LLn: $[M+H]^+ = m/z$ 615.5, $[LLn]^+ = m/z$ 597.5; (B) LL: $[M+H]^+ = m/z$ 617.5, $[LL]^+ = m/z$ 599.5; (C) OL: $[M+H]^+ = m/z$ 619.5, $[LLn]^+ = m/z$ 601.5; (D) OO: $[M+H]^+ = m/z$ 621.5, $[LLn]^+ = m/z$ 603.5. (Calculated m/z values given.)

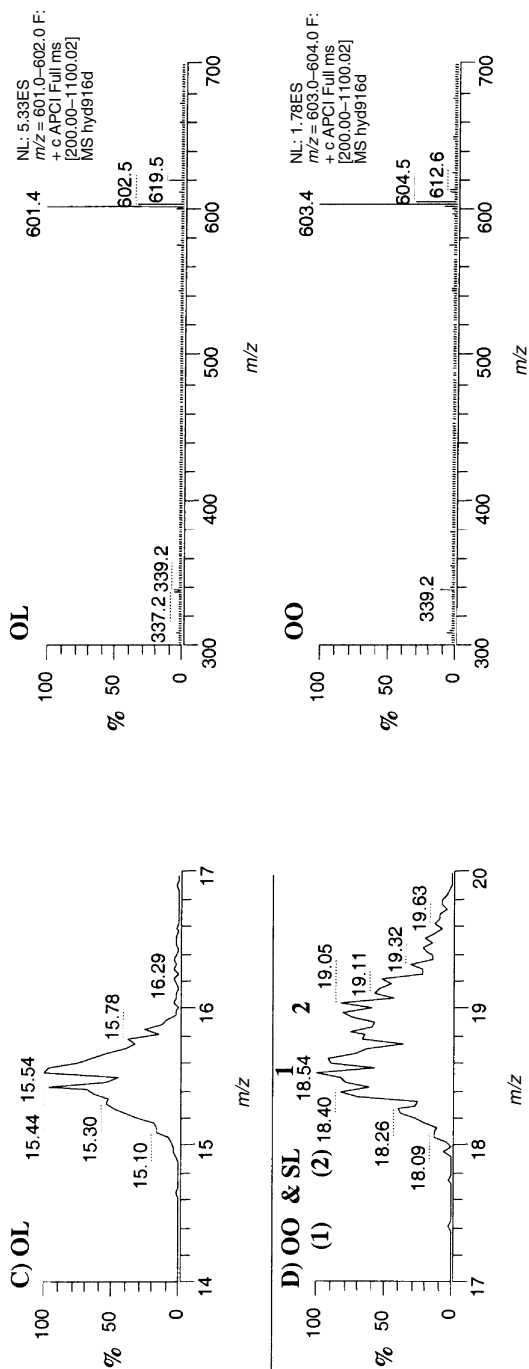


Fig. 7.8. (Continued).

Figure 7.8 and the examples cited previously demonstrate that LC/APCI-MS may be used for analysis of DAG, as well as TAG, and that some of the same trends observed for TAG (with respect to the number of sites of unsaturation) are also seen in the fragment ratios of DAG.

The EIC in Figure 7.7 allow the majority of TAG to be identified and their retention times determined. Some other TAG were also present at low levels. These were mostly TAG that included longer fatty acyl chains, specifically arachidic acid (20:0, A) and gadoleic acid (20:1, G).

Ion chromatograms and mass spectra showing TAG that contained longer FA are shown in Figure 7.9. These TAG are often not mentioned in analysis of soybean oil (SBO) because they are present at such low levels. Nevertheless, EIC and mass spectra such as those in Figure 7.9 are adequate for qualitative analysis. From the ion chromatograms in Figure 7.9, 22 to 24 TAG containing A or G can be identified. Mass spectra of these TAG containing longer FA exhibited the same trends with respect to the degree of unsaturation that has been discussed in detail previously.

The first articles by Byrdwell *et al.* (10,11) on HPLC/APCI-MS of TAG employed a hexane/propionitrile solvent system. The mass spectra demonstrated the “chemical ionization” aspect of APCI-MS because chemicals present in the chromatographic system produced small abundances of adducts with the analyte molecules, in addition to the protonated molecules. Propionitrile produced two adducts with TAG: an $[M+CH_3CH_2CN+H]^+$ ($= [M+55+1]^+$) adduct ion and an $[M+38+1]^+$ adduct. Because of the formation of adducts with propionitrile, and due to the noxious nature of this solvent, its use was phased out by us in favor of an acetonitrile/dichloromethane solvent system. Another adduct that was observed at low abundances in some mass spectra was a water adduct, $[M+H_2O]^+$. Small abundances of the adduct of water with the DAG fragment ion are also commonly observed. It is not known whether $[M-RCOO+H_2O]^+$ ions are actually adducts of the DAG fragments with water, or whether they occur due to a small percentage of fragments being formed by cleavage of the ester linkage between the oxygen and ester carbon, for ketene leaving group, followed by full protonation, $[M-RCO+2H]^+$. Both scenarios lead to the same masses. Loss of the ketene is discussed by Hsu and Turk in Chapter 3.

In addition to DAG fragment ions, typical APCI-MS mass spectra also include small abundances of reproducible fragments arising from individual FA. The two most common fragments formed from the FA present in a TAG were the acylium ions, $[R_xCO]^+$, and the $[R_xCOO+58]^+$ fragment, where x is the designation of the position on the glycerol backbone. These are also referred to as the $[R_xCO+74]^+$ peak, but we prefer the $[R_xCOO+58]^+$ designation, since it allows easier calculation from the FA mass. These fragments are also formed from DAG fragment ions during APCI-MS/MS, as we recently demonstrated (38). These fragments allow confirmation of the identities of DAG fragment ions, by allowing each FA of which the DAG are composed to be confirmed

independently. Figure 7.6G and Figure 7.6H show the region from m/z 200 to 400 in Figure 7.6E and Figure 7.6B, respectively. This m/z range encompasses the $[\text{RCO}]^+$ and the $[\text{RCOO}+58]^+$ fragments (the $[\text{RCO}-\text{H}_2\text{O}]^+$ ion is also seen). The identities and calculated masses of these common fragments are given in the table:

| FA | $[\text{RCO}]^+$ | $[\text{RCOO}+58]^+$ |
|-----------|------------------------------------|--|
| P | 239.2 | 313.3 |
| Ln | 261.2 | 335.3 |
| L | 263.2 | 337.3 |
| O | 265.3 | 339.3 |
| S | 267.3 | 341.3 |

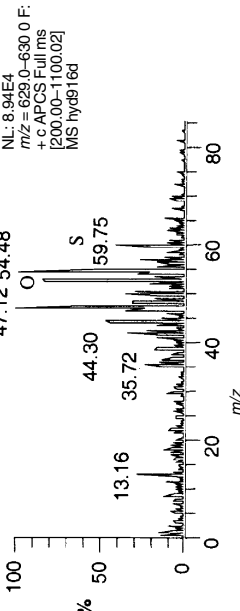
The specific structures of the $[\text{RCO}]^+$ and the $[\text{RCOO}+58]^+$ fragments from OLO are shown in Scheme 7.1. In the mass spectrum in Figure 7.6E, the m/z 239.1 peak had an abundance of 2.40% of the base peak (m/z 603.4 = 100%). In Figure 7.6G, the m/z 239.1 peak was rescaled to represent 100%, to make the peaks more apparent. In the mass spectrum in Figure 7.6B, the peak at m/z 265.1 had an abundance of 1.49% of the base peak (m/z 601.4 = 100%). In Figure 7.6H, m/z 265.1 was scaled so that this was the base peak in the m/z 200 to 400 range. Because of their low abundances in full mass spectra, we often ignore these peaks. They are very useful, however, for structural identification in MS/MS spectra, in which they exhibit larger abundances.

Other general trends observed in APCI-MS mass spectra of TAG include the tendency to form small abundances of dehydrated protonated molecules, $[(\text{M}-\text{H}_2\text{O})+\text{H}]^+$. Also, small abundances of adducts with solvents and solvent-derived molecules are common. Small abundances of water adducts are often formed. Nitriles, such as acetonitrile and propionitrile, produce small abundances of nitrile-derived adduct ions.

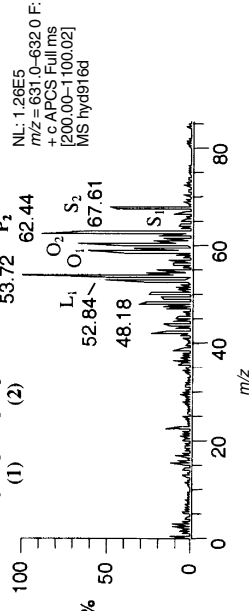
One important caveat must be mentioned in association with using EIC for qualitative analysis of intact TAG molecular species. As can be seen in Figure 7.7, the m/z values of the $[\text{DAG}]^+$ within a homologous series of carbon chain lengths (18,18 or 18,16 or 16,16) differ by 2 amu, representing varying numbers of sites of unsaturation. Every DAG fragment could be composed of all ^{12}C atoms, or could contain one or more ^{13}C atoms. As shown by a table of isotopic abundances, every carbon atom has a 1.1% probability of being a ^{13}C instead of a ^{12}C . A fragment containing 39 carbon atoms, such as an 18,18 DAG, therefore has a $39 \times 1.1\% = 42.9\%$ chance of having at least 1 ^{13}C and a smaller percentage probability of having 2 ^{13}C atoms. Of course, the hydrogen and oxygen atoms also contribute small probabilities of heavy isotopes. Thus, in any mass spectrum, isotopic abundances of ^{13}C were present. For instance, in the case of

RBD Soybean Oil

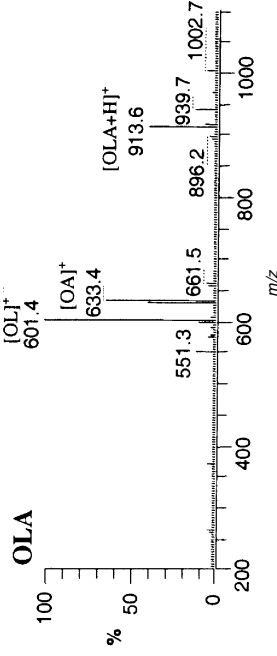
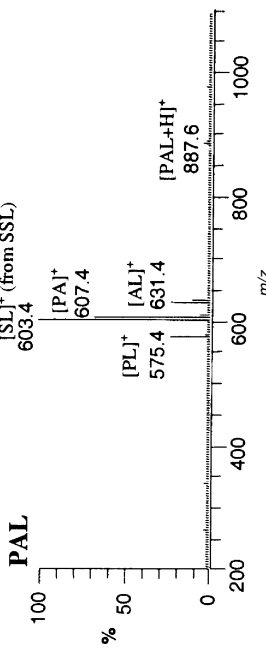
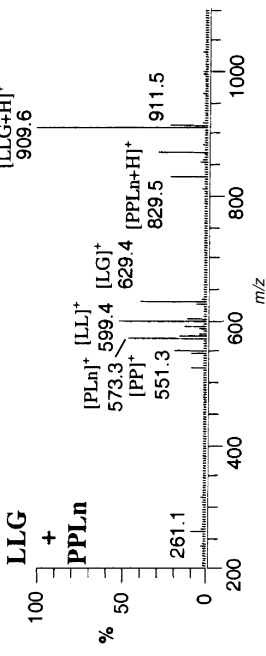
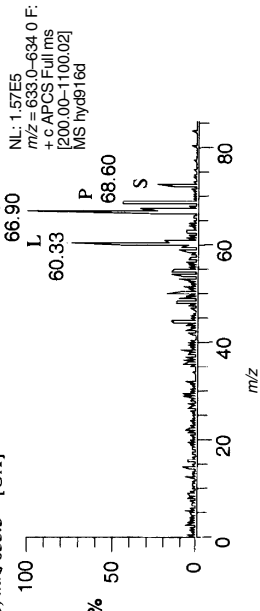
A) m/z 629.5 = [GL]⁺



B) m/z 631.5 = [OG]⁺ or [AL]⁺



C) m/z 633.5 = [OA]⁺



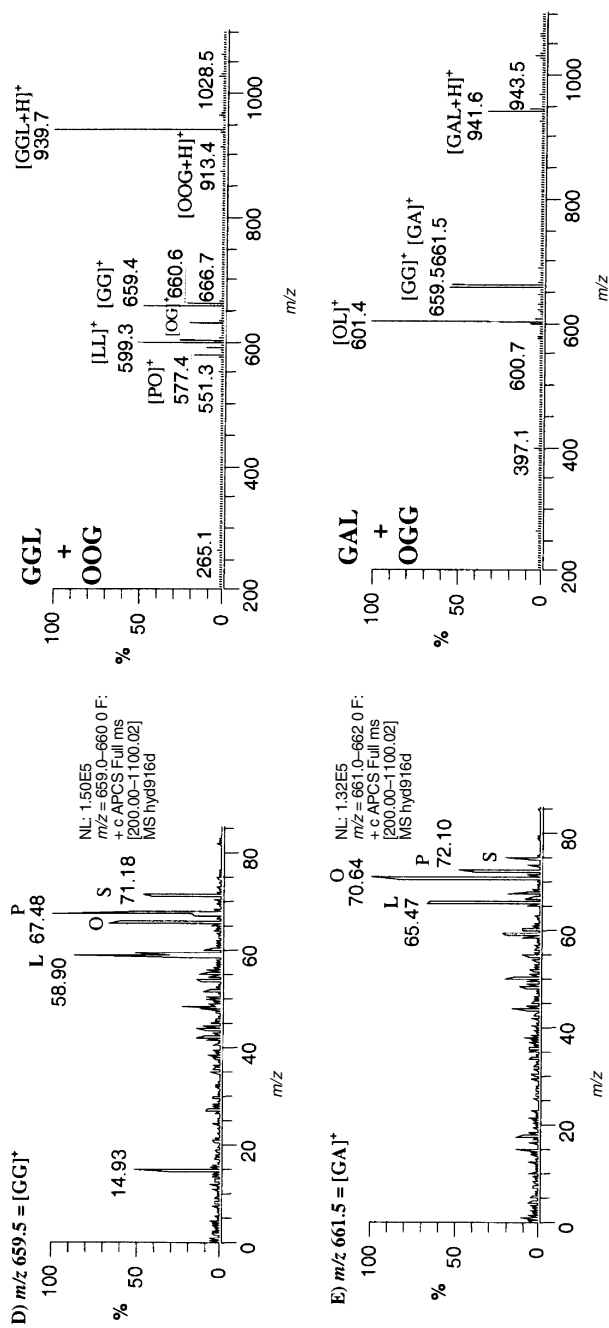


Fig. 7.9. Extracted ion chromatograms of DAG fragments containing A (arichidic acid, 20:0) and G (gadolcic acid, 20:1). Mass spectra of selected peaks in EIC. (A) EIC of m/z 629.5, = [GL]⁺; (B) EIC of m/z 631.5, = [OG]⁺ (eluted first) and [AL]⁺ (eluted second); (C) EIC of m/z 633.5, = [OA]⁺; (D) EIC of m/z 659.5, = [GG]⁺; (E) EIC of m/z 661.5, = [GA]⁺.

the OO DAG fragment ($C_{39}H_{71}O_4 = 603.5$ amu), an isotopic abundance calculator gave the following abundances for the DAG, DAG with $1\cdot^{13}C$, DAG with $2\cdot^{13}C$, and DAG with $3\cdot^{13}C$ isotopic abundances: 100%, 43.40%, 10.01%, 1.62%, respectively. So, approximately 10% of all $[OO]^+$ fragments could be expected to have $2\cdot^{13}C$ atoms, and therefore to have a mass of 605.5 instead of 603.5. These carbon-isotope-containing variants would therefore produce peaks in the chromatogram of m/z 605.5, which was the same as the mass of the normal OS DAG having only ^{12}C . All EIC of DAG fragment ions contained a contribution from the $2\cdot^{13}C$ variant of the DAG fragment having one more site of unsaturation. The m/z 605.5 EIC contained a contribution from the $2\cdot^{13}C$ variants from m/z 603.5; the m/z 603.5 EIC contained a contribution from the $2\cdot^{13}C$ variants from m/z 601.5; the m/z 601.5 EIC contained a contribution from the $2\cdot^{13}C$ variants from m/z 599.5, and so on. The degree to which the isotopic peaks present a problem depends on the relative amounts of each DAG fragment. If the (M-2) peak was less abundant than the (M) peak, the $2\cdot^{13}C$ variant of the (M-2) peak was negligible in the (M) chromatogram. On the other hand, if the (M-2) peak was much larger than the corresponding (M) peak, the $2\cdot^{13}C$ variant of the (M-2) peak was quite noticeable in the (M) chromatogram. Fortunately, the peaks from the $2\cdot^{13}C$ variant of the (M-2) peak occurred at the same retention time as the all- ^{12}C isotope variants of (M-2), for example, m/z 603.5, and these occurred at different retention times from the species having one less site of unsaturation (M), for example, m/z 605.5. With some caution, the two- ^{13}C variant peaks can be identified in affected EIC, as in Figure 7.7H. With an understanding of this caveat, use of EIC of DAG fragment ions for qualitative analysis can allow definitive identification of many more TAG molecular species than is possible by using conventional two-dimensional detectors.

The data shown above demonstrate most of the trends that have been observed in APCI-MS mass spectra for qualitative analysis of TAG. Another important aspect of TAG qualitative analysis is the determination of positional isomers from the APCI-MS data. Some discussion of TAG positional isomer determination is given below, but complete and thorough discussion of this aspect of TAG analysis by APCI-MS is given in Chapter 6, by Hazel Mottram. Before discussing positional isomers, however, it is worthwhile to examine some of the other early publications dealing with TAG analysis by APCI-MS.

TAG Oxidation Products by APCI-MS. In 1995, Neff and Byrdwell (12) described the HPLC/APCI-MS of seed oil TAG containing atypical functional groups. In the seed oil of *Crepis alpina*, numerous crepenynic acid (*cis*-9-octadecen-12-ynoic acid) containing TAG were identified. These behaved like normal polyunsaturated TAG, producing protonated molecules as base peaks, and low abundances of DAG fragment ions. In the same article, oxygen-containing TAG were identified in the seed oil of *Vernonia galamensis*. All of the primary TAG in this oil contained vernolic acid

(*cis*-12,13-epoxy-*cis*-9-octadecenoic acid). These epoxy-TAG underwent extensive fragmentation and produced complex mass spectra. The APCI-MS mass spectra of these epoxy-TAG provided definitive fragment patterns that allowed the number of oxygen functional groups and their locations on the fatty acyl chains to be determined. Two primary fragmentation mechanisms were observed in these epoxy-containing TAG. First, the epoxy groups were lost to form $[M+H-H_2O]^+$ ions from protonated molecules and from DAG fragment ions. The $[M+H-H_2O]^+$ fragments typically occurred at 40 to 100% of the $[M+H]^+$ abundance. TAG with multiple vernolic acyl chains lost multiple moles of water, $[M+H-nH_2O]^+$, where n was the number of epoxy groups. Second, the epoxy acyl chains underwent intra-annular cleavage, leaving a C12:2 chain on the TAG. The leaving fragment, a hexanal chain fragment, could then act as a reactant to form an $[M+102]^+$ adduct with another TAG molecule. TAG with multiple epoxy TAG could undergo both mechanisms to form chain-shortened and dehydrated TAG and DAG fragments. The fragments formed from the epoxy-TAG in this natural oil were later seen to be the same epoxy fragments formed by hydroperoxides and epoxides produced by autoxidation and by heated oxidation. These are discussed further herein.

Kusaka *et al.* (68) first used LC/APCI-MS for analysis of TAG oxidation products (hydroperoxides). In 1999, Neff and Byrdwell (69) employed HPLC/APCI-MS for analysis of the products formed by autoxidation of three TAG standards, triolein, trilinolein, and trilinolenin. The usual acetonitrile/methylene chloride HPLC method employed by Byrdwell *et al.* (44) was modified to elute polar functional group-containing TAG over a broad time range. The APCI-MS mass spectra were rich with fragments providing structural information regarding the oxygen functional groups and their locations within the TAG. We showed the mass spectra of hydroperoxides (from OOO, LLL, and LnLnLn), two types of epoxides (both from OOO and LLL, one type from LnLnLn), epidioxides (from LnLnLn), hydroxyl-containing species (from LnLnLn), and combinations of these (diepoxides, dihydroperoxides, etc.). Fragments in mass spectra of the different classes were used to identify numerous isomers having oxygen functional groups in different locations along the fatty chain. We then used the same method to identify the tri-acylglycerol oxidation products (TAGOX) formed from triolein at elevated temperatures (70). The autoxidation products formed by autoxidation of triolein (69) were fewer and less diverse than the oxidation products formed by heated oxidation. Hydroperoxides were a major component of autoxidation products, while these were present to a much lesser extent in oxidation products formed by extended exposure to frying temperatures.

The products produced by heated oxidation included all of the same products formed by autoxidation, plus other products formed by the more extreme oxidation conditions. Chromatograms and mass spectra of the oxidation products formed from heated triolein are shown in Figure 7.10 and Figure 7.11. In addition to the same epoxides and hydroperoxides as those formed by autoxidation, the TAGOX from heated oxidation included a ketone formed at a site of unsatu-

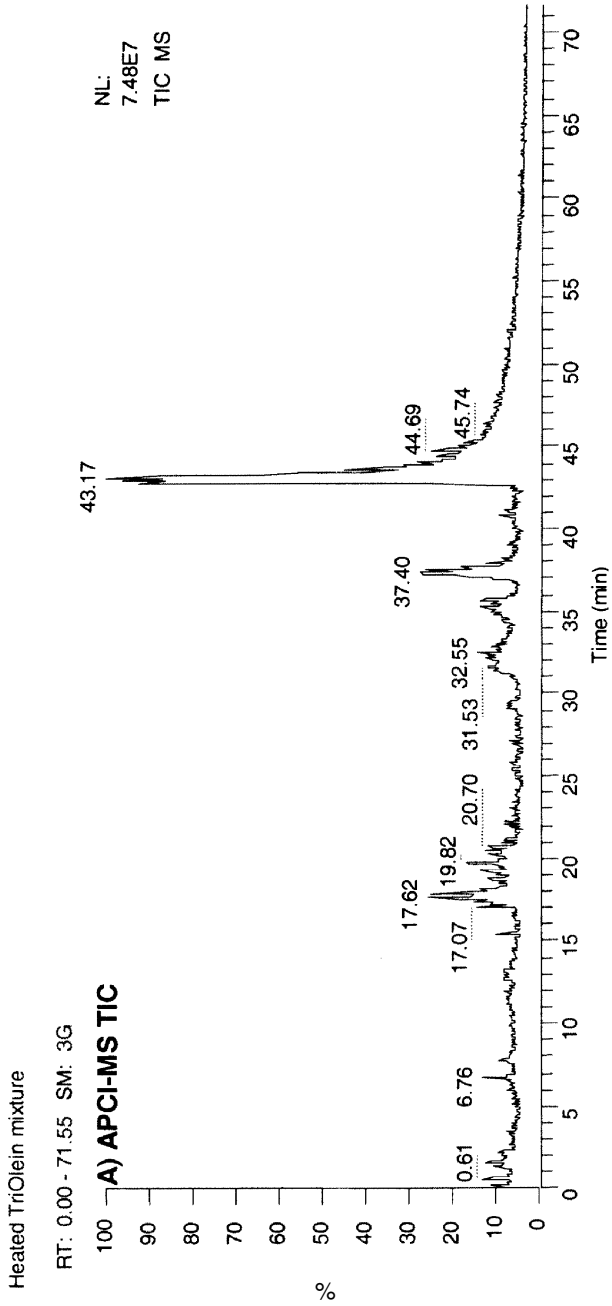


Fig. 7.10. APCI-MS and ELSD chromatograms of triolein oxidation products. (A) Total ion chromatogram. (B) Evaporative light scattering detector (ELSD) chromatogram.

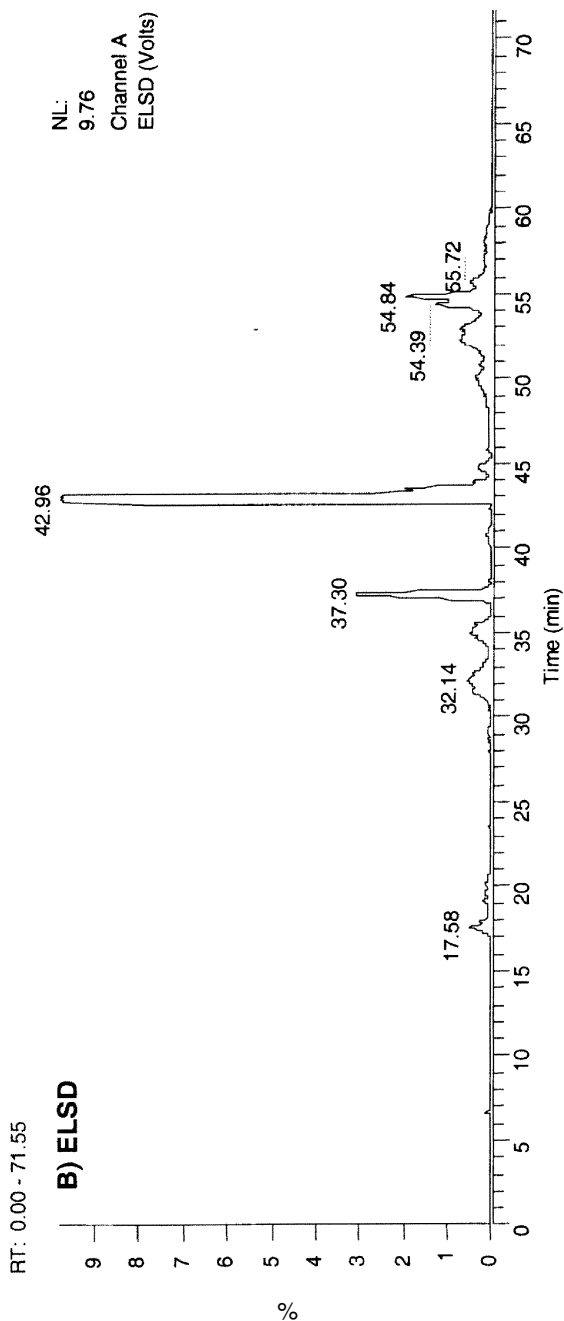


Fig. 7.10. (Continued).

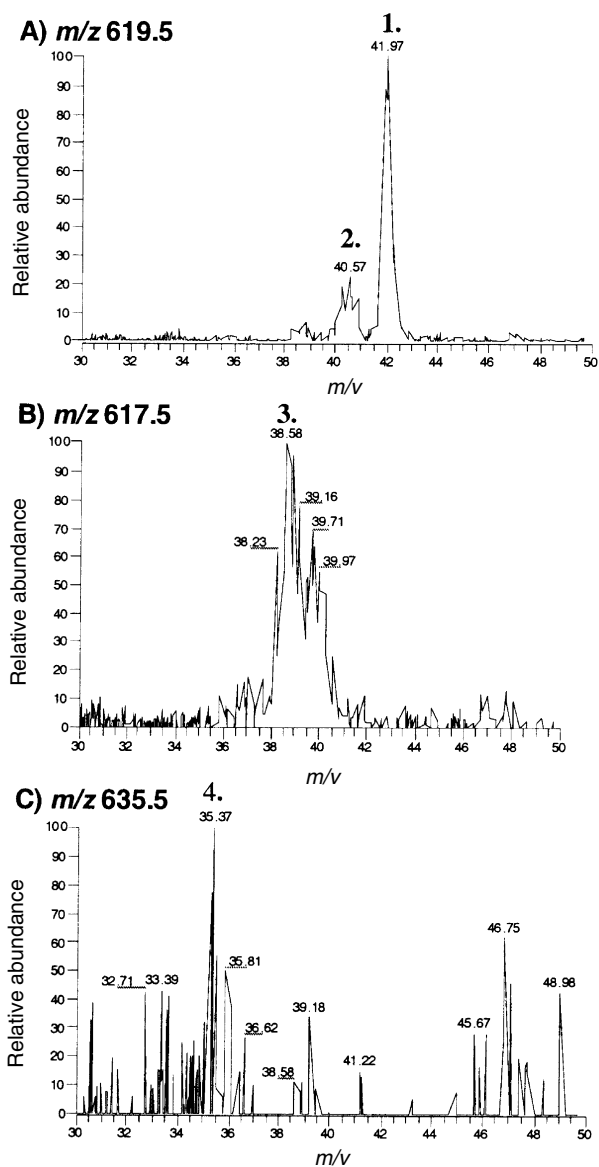


Fig. 7.11. Extracted ion chromatograms and APCI-MS mass spectra of triolein heated oxidation products. (A) EIC of m/z 619.5; (B) EIC of m/z 617.5; (C) EIC of m/z 635.5; (D) APCI-MS mass spectrum of triolein, OOO; (E) mass spectrum of OOS-epoxide; (F) mass spectrum of OO,keto-S (which eluted partially overlapped with OOO-epoxide); (G) mass spectrum of OOO-epoxide; (H) mass spectrum of OOS-epidioxide, which is isobaric with OOO-hydroperoxide (partially overlapped with OOO- $C_{11}H_{20}$); (I) mass spectrum of the chain-shortened product OOO- $C_{11}H_{20}$.

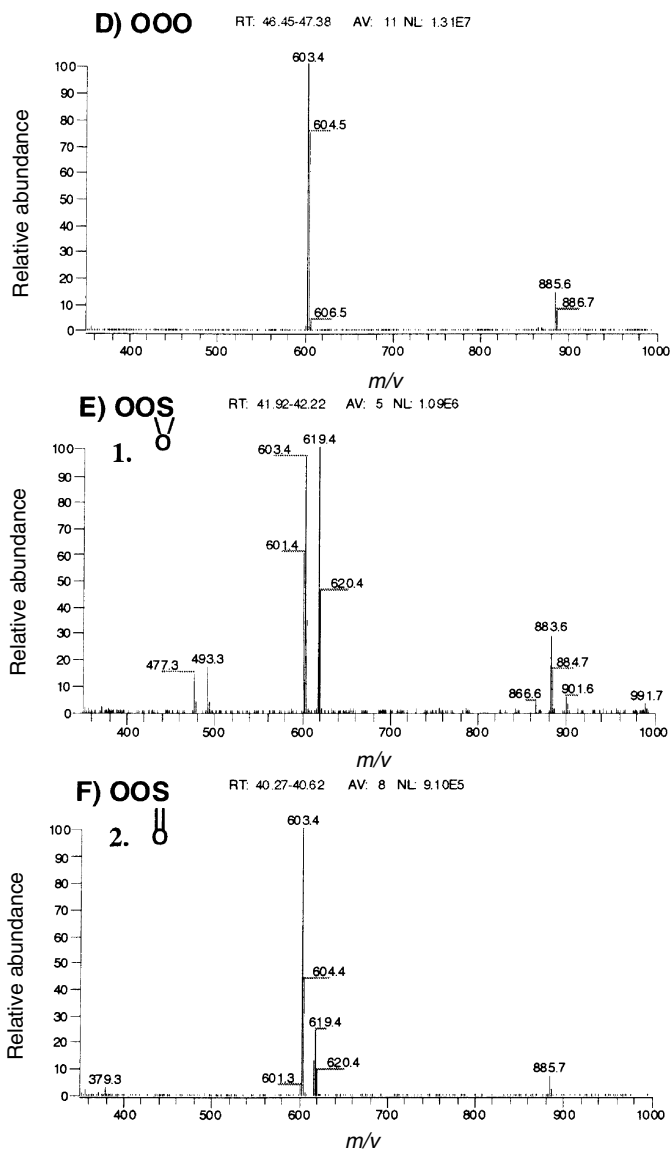


Fig. 7.11. (Continued).

ration and several chain-shortened species formed by cleavage of the oxidized fatty acyl chains. Mass spectra of the common oxidation products observed by APCI-MS are shown in Figure 7.11.

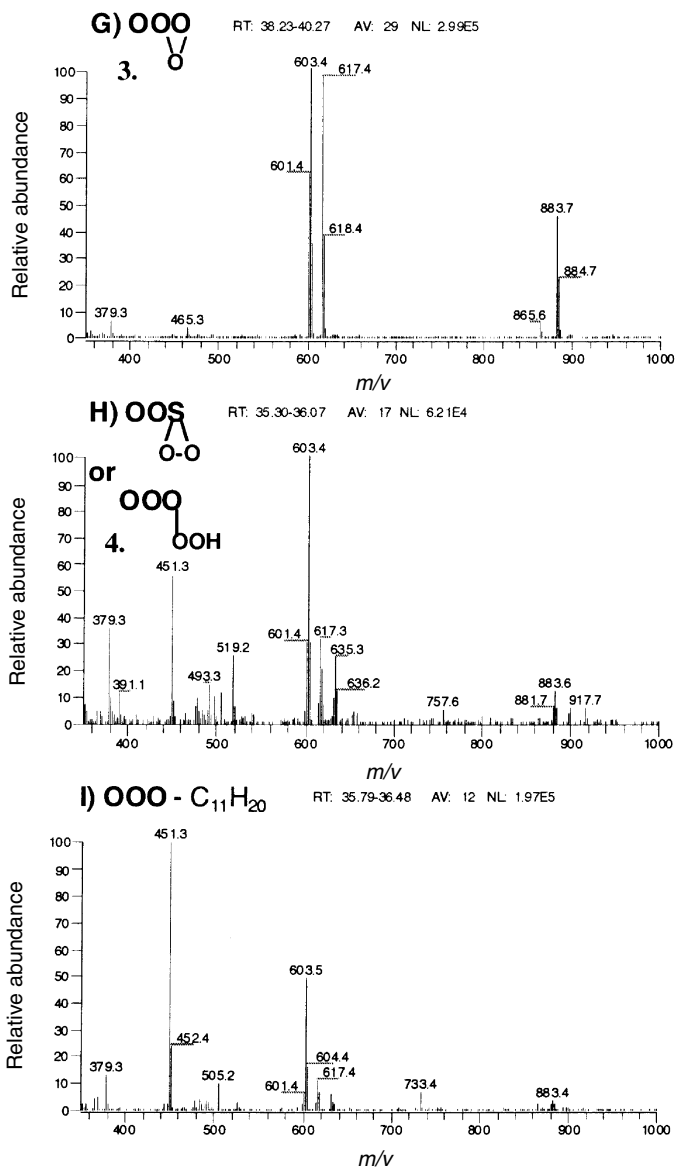
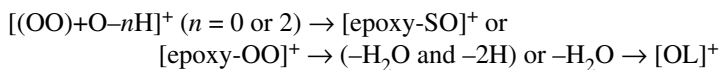


Fig. 7.11. (Continued).

Monomeric oxidation products of triolein were more polar than triolein itself, and so eluted before it on these reversed-phase columns. As we had initially shown (69), the mass spectra produced by APCI-MS allowed us to identify two epoxides: those in which the epoxide added across a double bond, and those in which it

added not across a double bond. Mass spectra of these two epoxides can be seen in Figure 7.11E and Figure 7.11G, respectively. In the mass spectra of the epoxides in which the epoxide was not formed across a double bond, fragments were present that indicated that the epoxide could be either directly adjacent to a double bond, or not adjacent. Epoxides that formed next to a double bond lost the epoxide by dehydration with stabilization from the double bond. Epoxide fragments formed by oxidized triolein in the APCI source can be described as $[\text{DAG}+\text{O}-n\text{H}]^+$ ($= [\text{epoxy-DAG}]^+$), where n is either 0 or 2, to give either an oleoyl, epoxy-stearoyl diacylglycerol fragment ion ($[\text{DAG}+\text{O}]^+ = [\text{epoxy-SO}]^+$, m/z 619.5) or an oleoyl, epoxy-oleoyl diacylglycerol fragment ion ($[\text{DAG}+\text{O}-2\text{H}]^+ = [\text{epoxy-OO}]^+$, m/z 617.5), respectively. Another fragment produced by epoxides was the $[\text{DAG}-2\text{H}]^+$ fragment ion, equivalent to $[\text{OL}]^+$. This was produced by decomposition of an epoxide by dehydration in the APCI source, summarized as follows:



The observation that the OS-epoxide gave the $[\text{OL}]^+$ fragment required Neff and Byrdwell (69) to propose the mechanism given in their report on autoxidation. By the mechanism described, we were able to posit how OOS-epoxide could have a protonated molecule and diacylglycerol fragment ion that were 2 amu higher than those from OOO-epoxide, yet these two different epoxides yielded several identical fragments upon loss of the epoxide groups. For example, the mass spectrum of OOS-epoxide in Figure 7.11E exhibited a protonated molecule ion at m/z 901.8, and gave a primary fragment at 883.8, due to dehydration ($-\text{H}_2\text{O}$). Similarly, the OS-epoxide diacylglycerol fragment ion at m/z 619.6 gave a primary fragment at m/z 601.5 (loss of 18 amu). On the other hand, OOO-epoxide (Fig. 7.11G) had a protonated molecule ion at m/z 899.8, but produced the same 883.8 primary fragment as OOS-epoxide, and the OO-epoxide DAG fragment ion had the m/z value of 617.5, but produced the same fragment ion at m/z 601.5 as OS-epoxide. The fragments produced during soft ionization of the molecules in the APCI-MS source allowed a fragmentation mechanism to be proposed that accounted for the observed behavior.

The left column of Figure 7.11 shows ion chromatograms that represent dioleoyl fragment ions containing one or two additional oxygen atoms. The EIC of m/z 619.5 represented species in which the oxygen functional group formed at the site of a double bond, leading to OO, epoxy-S or OO, keto-S. The ketone was shown to elute before the epoxide on the reversed-phase system, indicating that the ketone was more polar than the epoxide. The EIC of m/z 619.5, in Figure 7.11A, showed sharper, more distinct chromatographic peaks than species in which the oxygen was not across the double bond. These sharper peaks were due the relative structural simplicity of these species, compared to species in which the oxygen added not at the site of unsaturation. For OOS-epoxide, there was only one posi-

tion on the chain where the double bond occurred, $\Delta 9$, so there was only one position for the epoxide to form across that site of unsaturation, and therefore a narrow chromatographic peak was observed. The ketone had two possible positions, 9- or 10-keto. The ketone gave a slightly broader peak, and a very different mass spectrum, seen in Figure 7.11F. The fragment ratios in the mass spectra of the epoxides (Fig. 7.11E and 7.11G) were very different from the fragment ratios in the mass spectra of the ketone (Fig. 7.11F). The epoxy-containing TAG exhibited large [epoxy-DAG]⁺ fragments (close to the abundance of [OO]⁺) and a substantial abundance of the protonated molecule, as well as the [(M+H)-H₂O]⁺ fragment. The ketone formed a [keto-DAG]⁺ fragment with much less abundance than the [OO]⁺, and virtually no protonated molecule. Thus, these data showed that the different classes of TAGOX gave very different fragment ratios in their mass spectra, but also that the chromatographic behavior provided valuable additional information to allow classes of molecules to be identified.

In the TAGOX mixture produced by triolein at elevated temperature, hydroperoxides were present at very low levels, compared to the autoxidation mixture. It is not surprising that the hydroperoxide was less stable and long-lived at elevated temperature. Unfortunately, APCI-MS mass spectra of hydroperoxides exhibit very low abundances of the intact protonated molecule and of the hydroperoxy-DAG fragment. Identification of hydroperoxides by APCI-MS can be problematic because of excess fragmentation, and the lack of intact hydroperoxy-containing fragments. The fragments in APCI-MS mass spectra of hydroperoxides are the same as the fragments in the mass spectra of epoxides. Thus, for hydroperoxides, it may be necessary to employ ESI-MS data as an aid for identification of hydroperoxy-TAG, unless they are present in large amounts (as in the case of autoxidation products). Figure 7.11H shows the APCI-MS mass spectrum of what is believed to be OOS-epidioxide. Both epidioxides and hydroperoxides were expected to be present in the TAGOX mixture, but these cannot be differentiated by mass. Both epidioxides and hydroperoxides gave [DAG+2O]⁺ fragments at m/z 635.5, coming from [(((TAG)-H+OOH)+H⁺)-RCOOH]⁺ or [(((TAG)+2O)+H⁺)-RCOOH]⁺. However, the abundance of the intact [hydroperoxy-DAG]⁺ ion formed from OOO-hydroperoxide was small, which presented a problem for identification of the hydroperoxide. OOO-hydroperoxide readily lost H₂O to form an epoxide in the form of [(TAG)OOH-H₂O+H]⁺, which was equivalent to [epoxy-OOO+H]⁺, and this gave the abundant [epoxy-DAG]⁺ fragment ion at m/z 617.5, showing that hydroperoxides give a very abundant epoxy-DAG fragment that is similar to the epoxy-DAG fragment observed from epoxy-containing TAG. Epidioxy-SOO can give rise to the [epoxy-DAG]⁺ fragment at m/z 619.5 ion that is equivalent to [OS-epoxide]⁺. The hydroperoxide could conceivably form a hydroxide having m/z 619.5, but hydroxy groups are not stable in the APCI source and readily undergo further loss of H₂O, which would result in the net loss of H₂O₂ to form the [OL]⁺ fragment. The presence of a substantial abundance of m/z 619.5 from an abundant ion at m/z 635.5 is taken as an indication of the epidioxy species, while low abun-

dances of m/z 635.5 and m/z 619.5 with a large abundance of m/z 617.5 produced from the m/z 635.5 are taken as indications of the hydroperoxy species. Thus, both epidioxides and hydroperoxides gave the same fragments as described above for epoxides: $[\text{DAG} + \text{O}-n\text{H}]^+$ fragments ($n = 0$ or 2), and then the $[\text{DAG}-2\text{H}]^+$ fragments are formed by further loss of H_2O (or H_2O and 2H). The chromatographic behavior of the species also supports the identification of the epidioxide. It was less polar and eluted later than most hydroperoxides. The difficulty in distinguishing OOS-epidioxide from OOO-hydroperoxide by HPLC/APCI-MS alone leads one to the conclusion that identification of hydroperoxides and epidioxides should be considered tentative until additional analytical methods, such as NMR spectroscopy, are applied to the chromatographic fractions.

The oxidation products produced by heated triolein included species in which the fatty acyl chain that contained the oxygen functional group underwent scission to yield chain-shortened TAG and core aldehydes. When the oxidized fatty acyl chain was cleaved, two possibilities occurred. The first possibility was that the chain broke and took the oxygen functional group with it, leaving behind a shortened TAG with no additional oxygen functional group. The second possibility was that the chain broke and left an oxygen functional group behind on the remaining TAG core. The species formed when the oxygen was left behind were "core aldehydes." These have been studied extensively by Kuksis, using ESI-MS. In Chapter 4 in this volume, Kuksis discusses his work and that of others who have used ESI-MS for analysis of core aldehydes and their derivatives. In APCI-MS spectra, both possibilities occurred, to form both core aldehydes and simple chain-shortened TAG. The mass spectrum in Figure 7.11I represents a chain-shortened species in which the acyl chain cleaved between carbons 7 and 8, and the oxygen functional group left with the C_{11} acyl chain. The chain-shortened TAG seen in Figure 7.11I behaved like a normal TAG under APCI-MS conditions, and produced a usable abundance of the $[\text{M}+\text{H}]^+$ ion at m/z 733.4, and a strong $[\text{DAG}]^+$ fragment ion at m/z 451.3 that reflected the shortened chain. Our more recent publication (38), which employed dual parallel mass spectrometers, used a different solvent gradient that eluted the core aldehydes over a broader time range and allowed them to be identified easily. Detection was done by both ESI-MS and APCI-MS. The added sensitivity provided by ESI-MS made identification of core aldehydes by ESI-MS easier than by APCI-MS. Figure 11 in that report (38) showed that the core aldehydes eluted at shorter retention times than the normal chain-shortened TAG having the same masses. The shorter retention times of the core aldehydes reflected the fact that these aldehydes were more polar than the isobaric chain-shortened TAG.

In addition to the monomeric and chain-shortened TAG discussed above, larger TAGOX were also formed. Addition of molecular fragments to triolein molecules resulted in chromatographically resolved chain-addition products that were larger than triolein, but smaller than a triolein dimer. Addition of two or more triolein molecules together resulted in oligomers. Unfortunately, these larger TAGOX produced little response by APCI-MS. In Figure 7.10A, no high molecu-

lar weight (HMW) TAG oxidation products were observed in the APCI-MS chromatogram after triolein eluted. The ELSD, on the other hand, produced substantial signal from the HMW TAGOX that eluted after triolein. We found that collecting fractions from multiple preparative HPLC runs was necessary to increase the concentration of HMW TAGOX to the level where they could be observed by using APCI-MS (70). Thus, although APCI-MS provided very valuable data for identification of the most abundant monomeric TAGOX, it was not sufficiently sensitive to allow HMW TAGOX, or monomeric TAGOX present at low levels, to be identified. In spite of the fact that APCI-MS was less sensitive, the rich fragmentation patterns provided for TAGOX made it a valuable complementary technique to the more sensitive ESI-MS. Each class of TAGOX produced distinctly different fragmentation patterns under APCI-MS conditions, and these patterns allowed many classes to be differentiated without the need for MS/MS.

After our initial publications demonstrating LC/APCI-MS for analysis of TAGOX, we applied the approach to autoxidized normal and genetically modified canola oils (71). Normal, high stearic acid, and high lauric acid canola varieties were subjected to autoxidation and the oxidized oils analyzed. The most common products in these natural samples were hydroperoxides and the same two types of epoxides (formed either across a double bond, or not across a double bond) that were observed in autoxidized triolein (69) and in the heated TAG standards (70). Epoxides formed stable and long-lived species that eluted just before normal TAG. APCI-MS mass spectra of hydroperoxides of numerous TAG molecular species showed epoxides as the primary fragments, similar to the spectra of model TAG described previously. Oxidized FA were seen in TAG in combination with virtually every possible normal FA present.

Other applications of APCI-MS to analysis of TAG that contain oxygen functional groups include the article by Adas *et al.* (72) that reported the APCI-MS and ESI-MS analyses of hydroxylated metabolites of oleic and elaidic FA as their carboxylate anions, in negative-ion mode. The APCI-MS mass spectra shown therein appeared similar to the ESI-MS mass spectra, although the ESI-MS mass spectra seemed to show more losses of H₂O from the hydroxy FA than did the APCI-MS spectra. Bylund *et al.* (73) also reported APCI-MS and ESI-MS of hydroxy- and epoxy-containing metabolites of arachidonic and oleic acids. They reported that the spectra obtained by APCI-MS were essentially the same as those reported by ESI-MS. It appears that all of the MS/MS spectra shown were obtained using ESI.

In 1998, Mochida *et al.* (74) published a report of the APCI-MS analysis of methyl hydroperoxyoleates. The normal APCI-MS mass spectrum of the hydroperoxy-containing methyl ester of the FA oleic acid showed no protonated molecule, [M+H]⁺, but showed losses of H₂O and loss of the hydroperoxy group, H₂O₂. To solve the problem of the lack of [M+H]⁺ ion, the authors added ammonium hydroxide (ammonia water) to the ethanol mobile phase. This modification produced ammoniated molecule adduct ions as the base peaks. It also produced a rich

fragmentation pattern from losses of H_2O and loss of the hydroperoxy group, H_2O_2 . The authors also showed optimization of the nebulizer temperature and drift voltages on their Hitachi instrument.

To summarize, APCI-MS has been shown to be very valuable for analysis of monomeric TAGOX. TAG epoxides produced abundant [epoxy-DAG]⁺ and [M+H]⁺ ions. Conversely, the TAG ketone produced very small abundances of the intact protonated molecule and intact [keto-DAG]⁺. Hydroperoxides were common in mixtures produced by autoxidation, but they were present only at very low levels in TAGOX mixtures produced by heated oxidation. APCI-MS mass spectra of hydroperoxides were very similar to the mass spectra of epoxides. The lack of [M+H]⁺ and [hydroperoxy-DAG]⁺ in APCI-MS spectra made APCI-MS less than ideal for analysis of hydroperoxides. Epidioxides were similar to epoxides in the way that both classes of cyclic TAGOX produced higher abundances of [M+H]⁺ and [cyclic oxo-DAG]⁺ fragments than noncyclic TAG. APCI-MS mass spectra of epidioxides were helpful for identification of this class of molecules. There are other classes of monomeric TAGOX that appear to be present but which we have not discussed due to insufficient evidence for their conclusive identification. HMW TAGOX did not produce sufficient response by APCI-MS, without prior sample enrichment. Because not all classes of TAGOX produced either good signal response, or beneficial fragment patterns by APCI-MS, the dual parallel mass spectrometer approach will be shown to be beneficial for TAGOX analysis, since both APCI-MS and ESI-MS data are obtained simultaneously.

TAG Analysis by ESI-MS. As discussed in the introductory section, Duffin *et al.* (13) were the first to apply ESI-MS to neutral lipid analysis. And as mentioned previously, ESI-MS of neutral lipids requires an ionic additive, or reagent, of some type. Ionic adducts are formed between the neutral analyte and the ionic additive, in the ESI source. The identity of the adduct determines whether or not MS/MS can be performed. [M+Na]⁺ adducts were shown to be more reproducible and sensitive than [M+NH₄]⁺ adducts, but the [M+Na]⁺ yielded poor MS/MS spectra. Table 7.1 presented a summary of the articles published and the additives used for ESI-MS of TAG to date. Although we had been doing APCI-MS of TAG for several years, our interest in ESI-MS for TAG analysis was sparked in 1998, when we identified TAG as their [M+Na]⁺ adduct ions in the neutral bolus eluted from a total lipid extract at the beginning of a normal-phase analysis of phospholipids (75). That was our first experiment in which we obtained both ESI-MS and APCI-MS data simultaneously from the same sample injection (“dual parallel mass spectrometers,” LC1/MS2). Based on the published precedent (see Table 7.1), it had already been demonstrated that ESI-MS could be effective for TAG analysis, and that the data obtained by ESI-MS was valuable and complementary to the data obtained by APCI-MS. Since it was desirable to have data from both types of ionization sources, it seemed natural to extend our LC1/MS2 instrumental approach to TAG analysis (38). In 2002, both TAG and TAGOX were analyzed by using our

LC1/MS2 method (see Chapter 13 in this volume for further details). For our work, we used ammonium formate as the reagent additive, because we wanted the smallest, most volatile ammonium buffer that we could find. We have experienced problems with inorganic buffers clogging our heated capillary inlet, since our instrument does not employ a countercurrent gas. Also, we added the electrolyte directly into the ESI source as a sheath liquid, instead of adding it *via* a tee. With the use of the appropriate additive as a sheath liquid, the benefits of ESI-MS for TAG analysis became abundantly clear when it was compared to APCI-MS in the same run, in parallel.

The mass spectra obtained by ESI-MS typically exhibit pseudomolecular ions (adduct ions formed with the ionic additive) as base peaks, if minimal up-front CID voltage is applied. Figure 7.12 shows ESI-MS and APCI-MS chromatograms of canola TAG, similar to our recent publication (38) in which ESI-MS and APCI-MS data were obtained simultaneously. It is apparent in Figure 7.12 that ESI-MS produced better response to TAG than did APCI-MS. The APCI-MS and MS/MS mass spectra were typical of APCI-MS data presented in the preceding sections. The full-scan ESI-MS mass spectra of TAG, shown in Figure 7.13, exhibited almost exclusively $[M+NH_4]^+$ adduct ions, although small (and useful) abundances of $[DAG]^+$ fragment ions were also observed in the full-scan spectra. The ESI-MS data reflected all of the trends initially observed by Duffin *et al.* (13) and by Cheng *et al.* (18), specifically that TAG containing unsaturated TAG responded with higher abundances than saturated TAG by ESI-MS, and the position of the fatty acyl chain on the glycerol backbone could be determined from the $[DAG]^+$ fragment ion ratios observed in ESI-MS/MS mass spectra, such as those shown in Figure 7.13. In fact, ESI-MS/MS mass spectra were more definitive and gave more reproducible results than APCI-MS mass spectra, which have also been shown to be useful for discriminating the positional isomers (39–41).

The higher response given by unsaturated TAG under ESI-MS conditions was exactly opposite the trend that has been reported extensively for APCI-MS analysis of TAG, starting with the initial report of Byrdwell and Neff (10), and being more explicitly reflected in the response factors demonstrated by Byrdwell *et al.* (42–44) for TAG by APCI-MS. The higher response of unsaturated TAG is clearly seen in Figure 7.12, as shown by the larger peaks for the unsaturated TAG eluted at earlier retention times than the more saturated TAG. Application of a similar approach to quantitative analysis by ESI-MS as that used for APCI-MS (unpublished results, presented herein) demonstrates that the response factors for saturated TAG are larger than the response factors for unsaturated TAG, reflecting their lower response by ESI-MS. Overall, ESI-MS on the TSQ700 has been found to be much more sensitive (~100 times more sensitive) for analysis of all TAG (as their ammonium adducts) than was APCI-MS (as protonated molecules, with fragments), and ESI-MS on the LCQDeca was found to be another factor or 100 times more sensitive than ESI-MS on the TSQ700.

The mass spectra obtained by ESI-MS/MS of TAG were shown to appear very similar to the full-scan MS mass spectra obtained by APCI-MS. ESI-MS, MS/MS, and MS³ mass spectra of several TAG having varying degrees of unsaturation are shown in Figure 7.13. In ESI-MS/MS mass spectra, as in APCI-MS spectra, the [DAG]⁺ fragment ions were the most abundant peaks (in APCI-MS mass spectra, TAG having few sites of unsaturation gave a [DAG]⁺ as the base peak, whereas TAG having more than four sites of unsaturation gave a protonated molecule as the base peak). Furthermore, the ESI-MS³ mass spectra, such as shown in Figure 7.13, exhibited [RCO]⁺, [RCO-H₂O]⁺, [RCOO+58]⁺, and [RCOO+58-H₂O]⁺ fragments that allowed confirmation of the identities of the individual fatty acyl chains attached to the glycerol backbone. ESI-MS³ showed the same fragments as APCI-MS/MS mass spectra, as depicted in Scheme 7.1. APCI-MS/MS spectra displayed more deviation in the abundances of the fragment ions than did ESI-MS³, primarily because APCI-MS/MS data were obtained on our older tandem quadrupole instrument, whereas ESI-MS³ data were obtained on the newer ion trap machine. The ESI-MS³ spectra of polyunsaturated TAG, however, displayed a much higher degree of charge-remote fragmentation (CRF) and more complicated spectra than were observed from TAG having fewer sites of unsaturation. Comparison of Figure 7.13A and 7.13B to Figure 7.13C and 7.13D illustrates this difference. For the polyunsaturated TAG, the large number of fragments produced by CRF sometimes obscured the acyl-chain-specific fragments.

One important point should be made regarding ESI-MS data. Even though the [DAG]⁺ in ESI-MS mass spectra were small (see the left column of Fig. 7.13), they were nevertheless present at useful abundances. From these, extracted ion chromatograms could be constructed that allowed qualitative elucidation of the identities of all TAG. This is best illustrated by using the same synthetic mixture of 35 TAG that we use to demonstrate quantitative analysis. Figure 7.14 is the RP-HPLC/ESI-MS chromatogram of the mixture of 35 TAG synthesized by the interesterification of FA with glycerol (42). Figure 7.15 shows ion chromatograms of the *m/z* values of representative [DAG]⁺ fragment ions extracted from the total ion chromatogram. Figure 7.15 clearly shows that the DAG fragment ions allowed the retention times of all TAG to be determined with ease. For qualitative analysis, the ion chromatograms showed where every TAG that contained a specific DAG eluted. Just like the EIC obtained by APCI-MS, the EIC obtained by ESI-MS showed a peak for every fatty acid that combined with the [DAG]⁺ to form a TAG. The EIC such as shown in Figure 7.15 provided the quickest method for qualitative identification of TAG identities and retention times. Then, a mass spectrum of each TAG is obtained by averaging a window across each peak at each retention time.

The [DAG]⁺ fragment ions and ammoniated molecule adduct ions in the ESI-MS mass spectra, along with the MS/MS spectra at the same retention time are used to confirm the identification made based on the EIC of the [DAG]⁺ masses.

Canola Oil, 2 Col., Dual Parallel, LC/TSQ

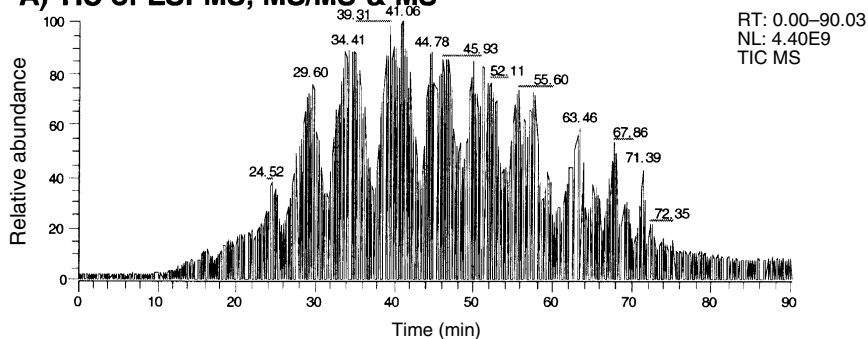
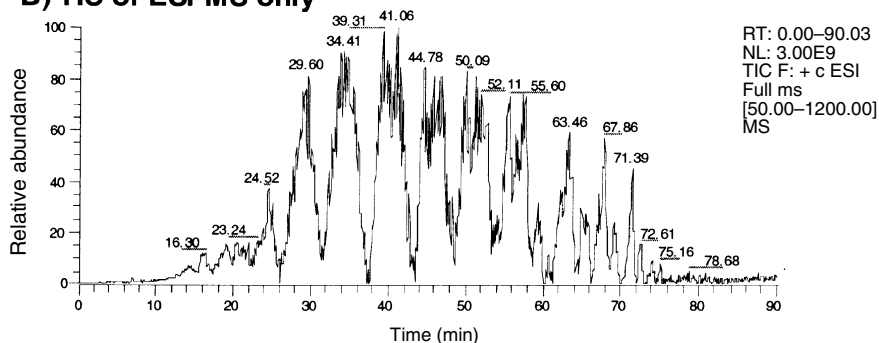
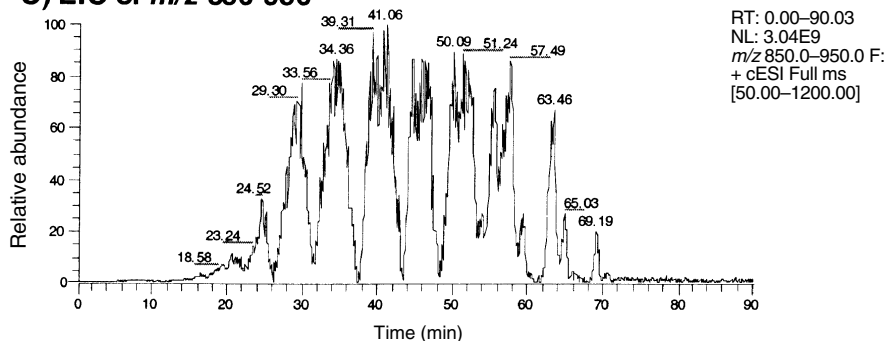
A) TIC of ESI-MS, MS/MS & MS³**B) TIC of ESI-MS only****C) EIC of *m/z* 850–950**

Fig. 7.12. Separation of canola oil triacylglycerols (TAG) by reversed-phase HPLC with detection using “dual parallel mass spectrometers” employing ESI-MS and APCI-MS. (A) Total ion chromatogram (TIC) of TAG showing MS, MS/MS, and MS³. (B) TIC showing only full-scan ESI-MS. (C) Extracted ion chromatograms (EIC) showing *m/z* range 850–950. (D) TIC showing all APCI-MS and MS/MS scans. (E) TIC showing only full-scan APCI-MS. (F) Evaporative light-scattering detector (ELSD) chromatogram.

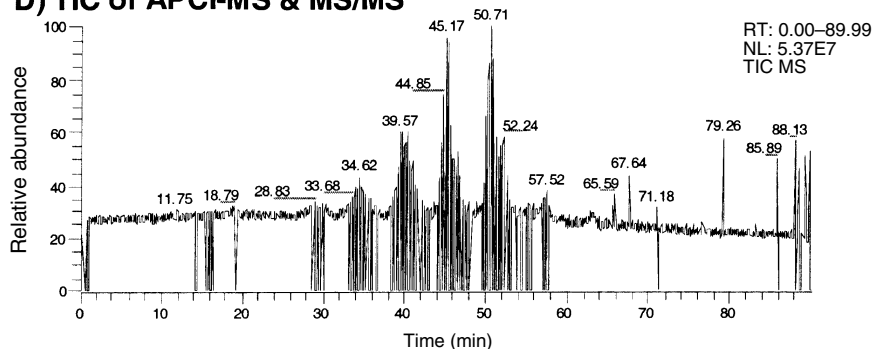
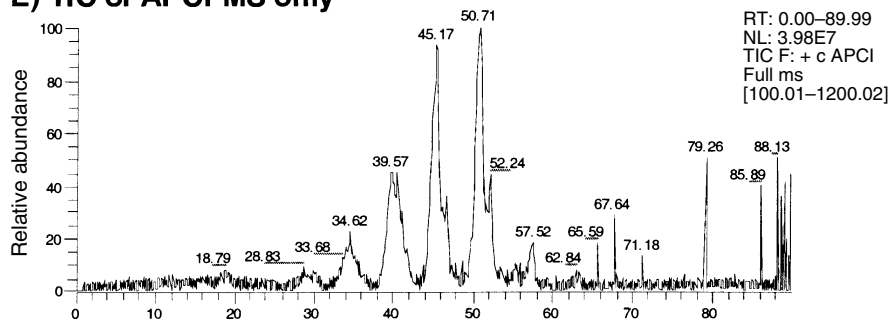
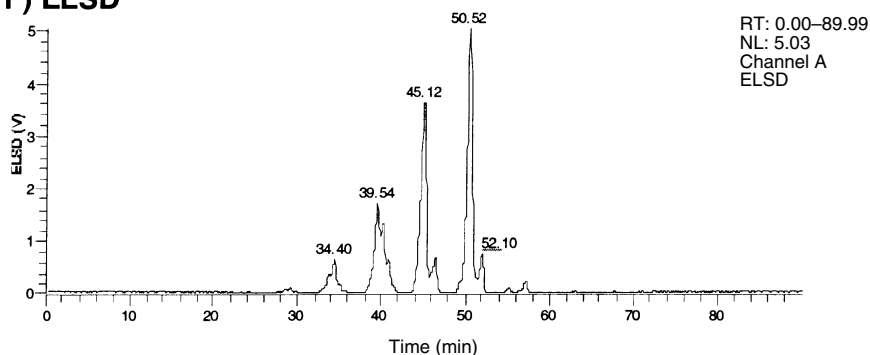
D) TIC of APCI-MS & MS/MS**E) TIC of APCI-MS only****F) ELSD**

Fig. 7.12. (Continued).

Thus, as with APCI-MS, the extracted ion chromatograms of $[\text{DAG}]^+$ serve as a valuable tool in TAG identification.

TAG Oxidation Products by ESI-MS. Work Done by Others. Early in the development of ESI-MS methods for non-polar lipid analysis (1995), Ravandi *et al.* (76)

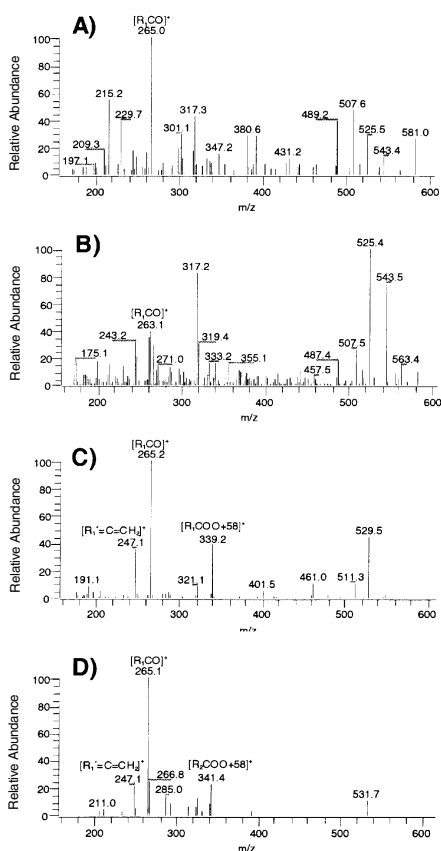


Fig. 7.13. (Continued).

group published a report by Sjovall *et al.* (77) that used HPLC with detection by ESI-MS to determine the elution factors of numerous DNPH derivatives of core aldehydes, as well as nonderivatized monomeric TAGOX, such as hydroperoxides, epoxides and hydroxides. Later, Sjovall *et al.* (78) applied their HPLC/ESI-MS approach to identification of the oxidation products formed by TAG standards after oxidation by *t*-butyl hydroperoxide (TBHP). After that article, the LC/ESI-MS approach was applied to TBHP oxidation products formed by corn and sunflower oils. These and other applications of ESI-MS to TAGOX analysis are discussed in the thorough treatment of the subject by Kuksis in Chapter 4 in this volume.

A variety of nonvolatile TAG oxidation products was examined by Steenhorst-Slikkerveer *et al.* (79). These authors employed a normal-phase HPLC system for separation of the oxidation products, followed by ESI-MS on a single quadrupole instrument. Sodium iodide was added postcolumn to act as a reagent electrolyte, so $[M+Na]^+$ adducts were observed.

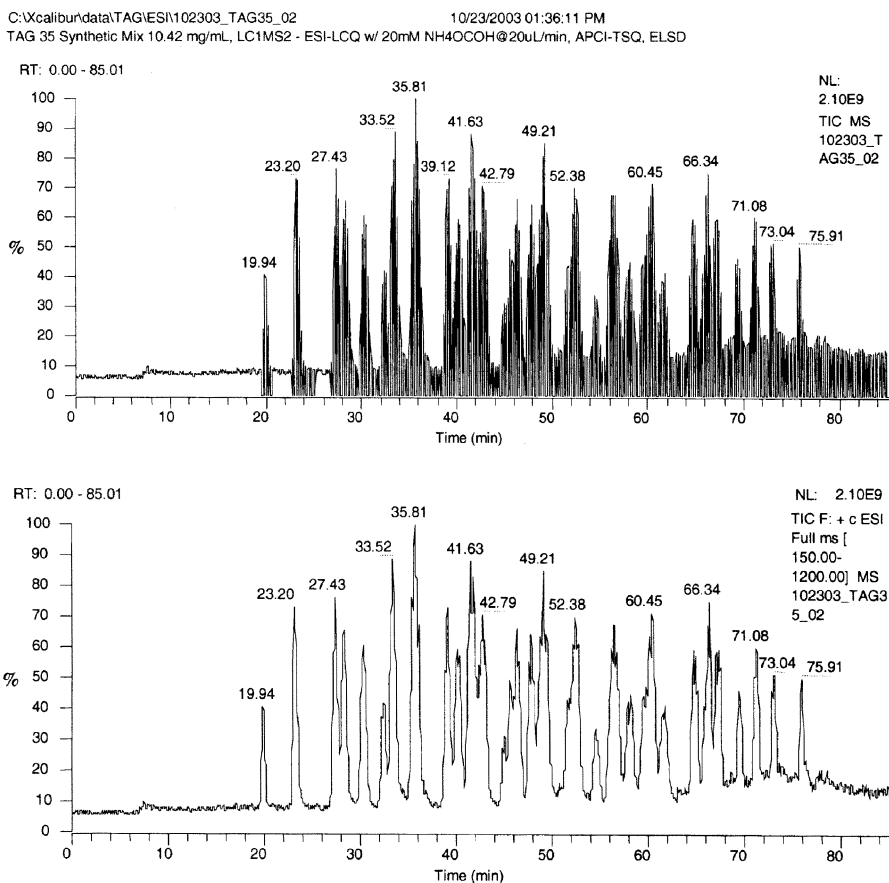


Fig. 7.14. Total ion chromatograms obtained by RP-HPLC/ESI-MSⁿ of a mixture of 35 synthetic TAG. (A) Total ion chromatogram (TIC) showing all MS, MS/MS and MS³ scans. (B) TIC showing only full-scan MS.

In 2004, Giuffrida *et al.* (80) reported the analysis of epoxidation products of TAG, cholesterol, and phytosterols by using oxidation by (i) air and (ii) ¹⁸O₂. TAGOX were separated by using NARP-HPLC and sent to the ESI source of a tandem mass spectrometer (Sciex API4000) for MS/MS experiments; in another experiment, TAGOX were infused into the ESI source of an LCQDeca ITMS. Ammonium formate was added to the infusion solvent to act as the electrolyte. The authors proposed the formation of the epoxy-stearoyl TAG, epoxy-SSS, from SSO hydroperoxide, to form an epoxide across the double bond. In the ESI-MS/MS mass spectrum of 1,2-distearoyl-3-hydroperoxyoleoyl-glycerol ([SS(¹⁸O)HpO]) reported therein, the [M+NH₄]⁺ ion is seen to arise at *m/z* 943.0 (calculated theoretical isotopic mass = 942.85). The authors reported the ion that they called [M-S]⁺ at *m/z* 641.7, which can also be

C:\xcalibur\data\TAG\ESI\102303_TAG35_02

10/23/2003 01:36:11 PM

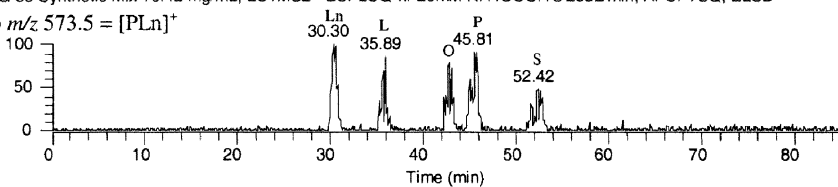
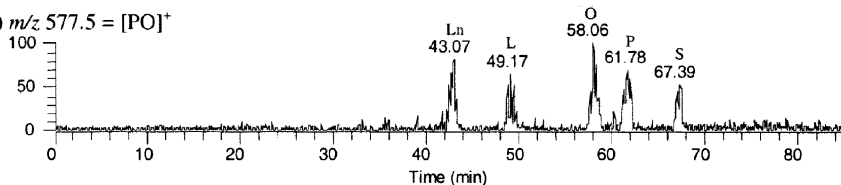
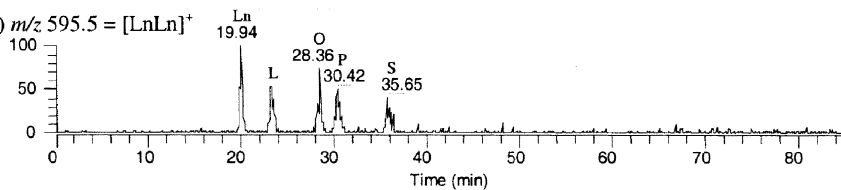
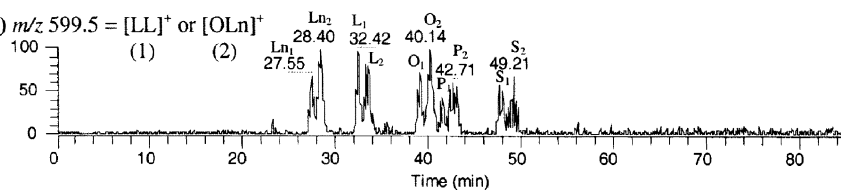
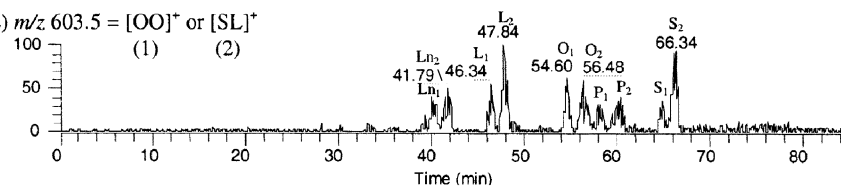
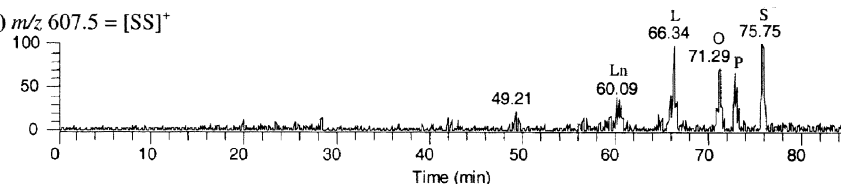
TAG 35 Synthetic Mix 10.42 mg/mL, LC1MS2 - ESI-LCQ w/ 20mM NH₄COOH@20uL/min, APCI-TSQ, ELSDA) m/z 573.5 = [PLn]⁺B) m/z 577.5 = [PO]⁺C) m/z 595.5 = [LnLn]⁺D) m/z 599.5 = [LL]⁺ or [OLn]⁺E) m/z 603.5 = [OO]⁺ or [SL]⁺F) m/z 607.5 = [SS]⁺

Fig. 7.15. Ion chromatograms of [DAG]⁺ from ESI-MS mass spectra. (A) EIC of m/z 573.5 = [PLn]⁺; (B) EIC of m/z 577.5 = [PO]⁺; (C) EIC of m/z 595.5 = [LnLn]⁺; (D) EIC of m/z 599.5 = [LL]⁺ and [OLn]⁺; (E) EIC of m/z 603.5 = [OO]⁺ and [SL]⁺; (F) EIC of m/z 607.5 = [SS]⁺.

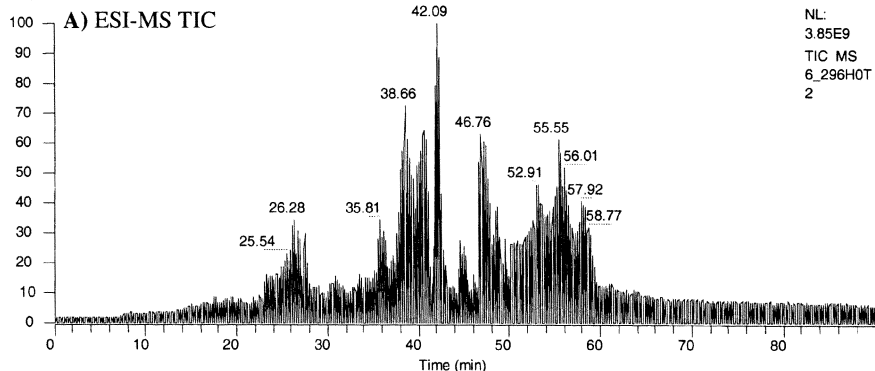
referred to as the [hydroperoxy-OS]⁺ fragment. In the ESI-MS/MS mass spectrum, they reported a fragment from the epoxide formed not across the double bond, which had an abundant peak at m/z 621.7, which they referred to as [M-S-H₂¹⁸O]⁺, which is equivalent to [epoxy-OS]⁺. An ion equivalent to [epoxy-SS]⁺, which would represent formation of the epoxide across the double bond and would have a calculated isotopic mass of 623.7, was not labeled in the ESI-MS/MS mass spectrum of the m/z 943.0 hydroperoxy parent, although the mass spectrum does show a peak at what appears to be $\sim m/z$ 623.7 that has a larger abundance than would be expected if it were only the 2-¹³C variant of m/z 621.7. Formation of epoxides both at the site of unsaturation and not at the site of unsaturation would, of course, be expected based on the earlier work of Byrdwell and Neff, using APCI-MS (69–71) and ESI-MS/MS (38). The epoxy-SSS product formed by epoxidation across the double bond would give an ammoniated molecule with a calculated isotopic mass of 924.85. The authors performed ESI-MS/MS of m/z 925.1 (mass spectrum described, not shown) and reported an ion at m/z 603.7. This is equivalent to [SL]⁺ and indicates that the epoxide that formed across a double bond underwent the same type of fragmentation mechanism reported by Byrdwell and Neff (69). The SSS-epoxide reported by these authors is also the same molecule reported by Kuksis *et al.* as 18:0-18:0-18:1 and 18:0-18:1-18:0 in their earlier report (77), with the underline indicating that the double bond occurred at the site of the double bond (molecular mass = 904.8). These epoxides are analogous to OOS-epoxide that has been reported from autoxidation and heated oxidation of triolein, OOO, by Byrdwell and Neff using APCI-MS (69–71) and ESI-MS/MS (38). Giuffrida *et al.* (81) proposed a mechanism for direct formation of epoxides from hydroperoxy radicals. Of course, such a mechanism would not apply to the ESI-MS/MS mass spectra of intact hydroperoxy parent ions, because these already have a stable hydroperoxide attached, instead of involving attack by an external hydroperoxy radical. Giuffrida *et al.* (82) went on to report ESI-MS/MS mass spectra of several epoxy sterols.

The extensive work on TAGOX monomers and core aldehydes by Kuksis *et al.*, detailed in Chapter 4 of this volume, plus our work with higher molecular weight oligomers, and the reports by other authors cited previously, have shown that HPLC/ESI-MS is currently the best available option for online LC-MS analysis of nonvolatile lipid oxidation products. In contrast, APCI-MS can serve as a valuable complementary technique for TAGOX monomers, but it does not produce sufficient ionization of HMW TAGOX.

Our Work. The increased sensitivity of ESI-MS compared to APCI-MS became especially important when examining TAG oxidation products. A total ion chromatogram obtained by ESI-MS of triolein TAGOX is shown in Figure 7.16. This chromatogram was obtained by using our dual parallel mass spectrometer arrangement in which both ESI-MS and APCI-MS data were obtained simultaneously. The TAGOX produced substantially more signal by ESI-MS than they did by APCI-MS, as clearly demonstrated by comparison of Figure 7.16 to Figure 7.10. Furthermore, the TAGOX from triolein gave more signal under ESI-MS conditions (as the ammoniated molecules) than did normal triolein (comparing the triolein peak at ~ 47 min in Fig. 7.16B to

Heated TriOlein, 6 Hr., 0 Toco., Dual Parallel, LC/TSQ

RT: 0.00 - 90.00



RT: 0.00 - 90.00

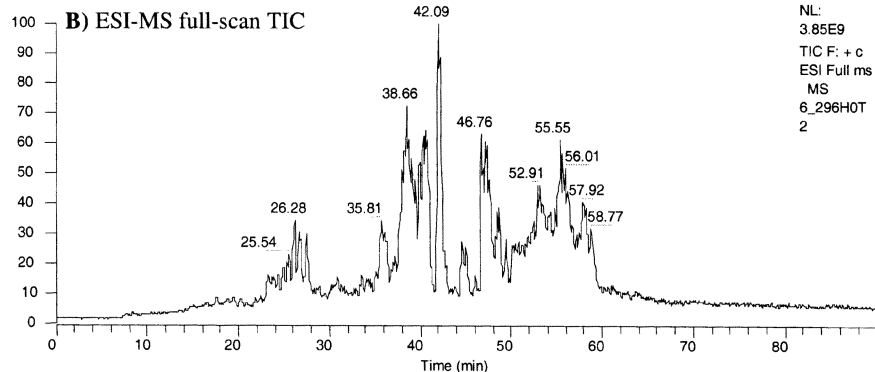


Fig. 7.16. ESI-MS total ion chromatograms (TIC) showing the separation of triolein and its oxidation products. (A) All ESI-MS, MS/MS, and MS³ scans. (B) ESI-MS TIC filtered to show only full MS scans.

the TAGOX peaks near 40 min). For all TAGOX, the ammonium adduct, $[M+NH_4]^+$, was the base peak in full-scan MS spectra obtained by ESI-MS.

ESI-MS and MS/MS mass spectra are shown in Figure 7.17. As with the normal TAG, the ESI-MS/MS mass spectra of TAGOX appeared very similar to full-scan APCI-MS mass spectra (Fig. 7.11). Since all ESI-MS mass spectra exhibited an $[M+NH_4]^+$ ion as the base peak, with very little fragmentation, MS/MS was necessary for structural elucidation. For instance, both OOS-epoxide and OOS-ketone had m/z 918.7 for the $[M+NH_4]^+$ in Figure 7.17A and Figure 7.17E, respectively. Only the differences in the fragmentation patterns in the MS/MS spectra, along with their chromatographic behavior, allowed these species to be differentiated. The trends observed in APCI-MS mass spectra of TAGOX, such as the low abundances of near-molecular ions given by the ketone, but large abundances of molecular adduct ions and fragments

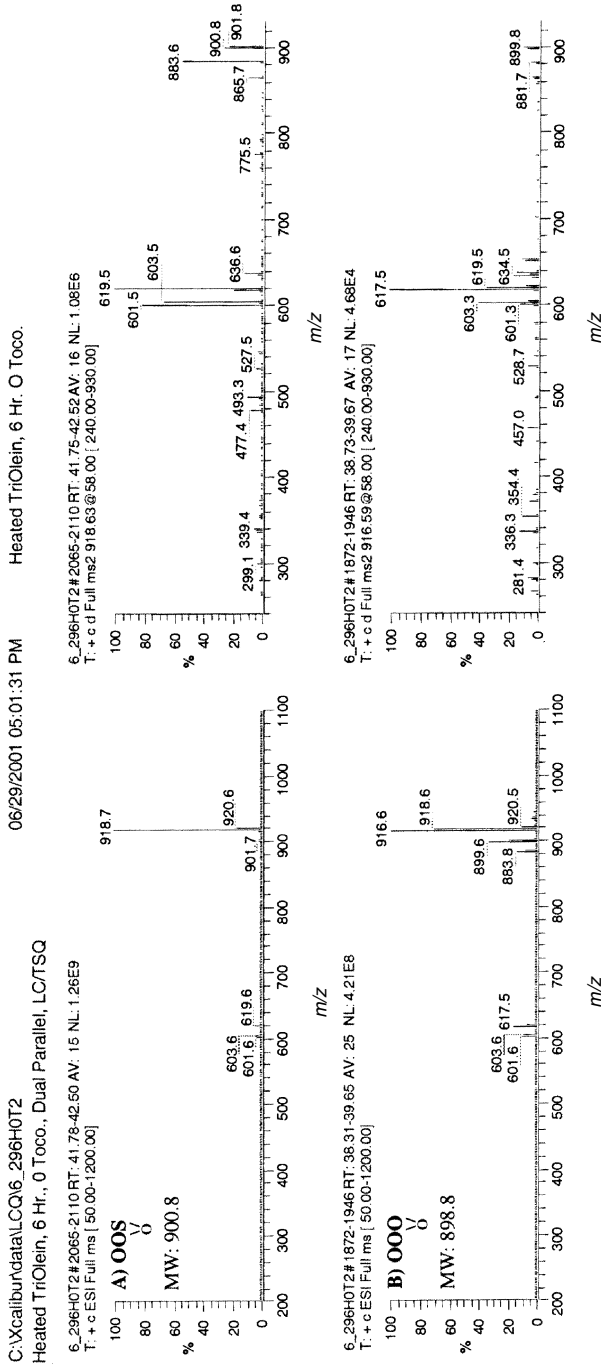


Fig. 7.17. (Part I) ESI-MS and MS/MS mass spectra of heated triolein monomeric TAG oxidation products. (A) ESI-MS and MS/MS mass spectra of OOS-epoxide. (B) Mass spectra of OOO-epoxide. (C) Mass spectra of OOO-hydroperoxide, which is isobaric with OOS-epidioxide. (D) Mass spectra of OOS-epidioxide, which is isobaric with OOO-hydroperoxide.

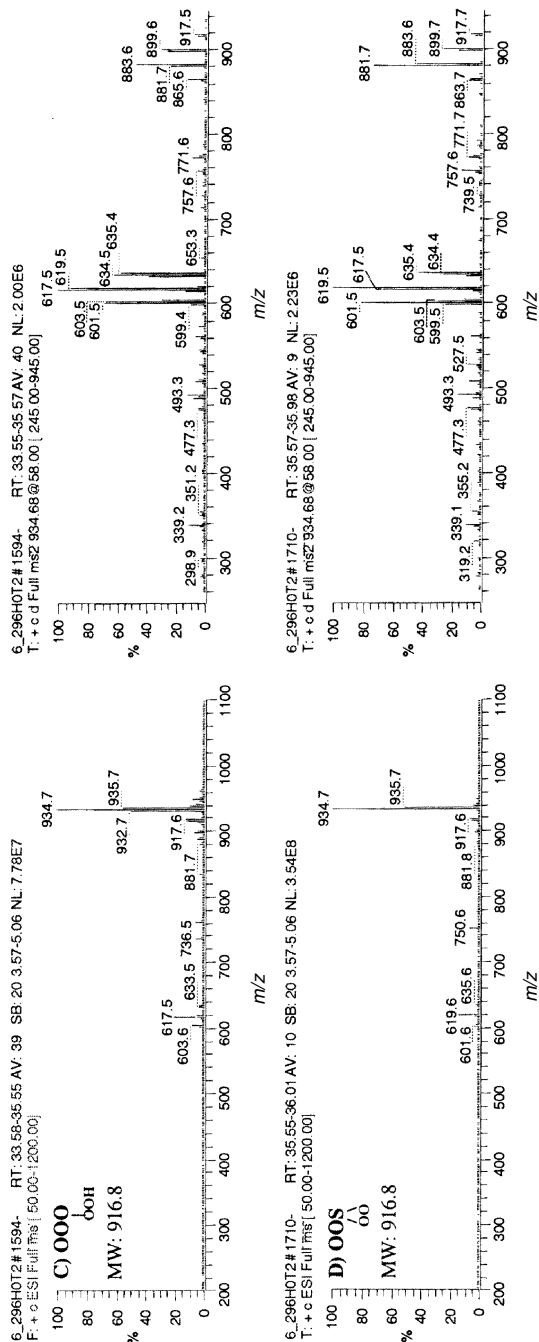


Fig. 7.17. (Part I) (Continued).

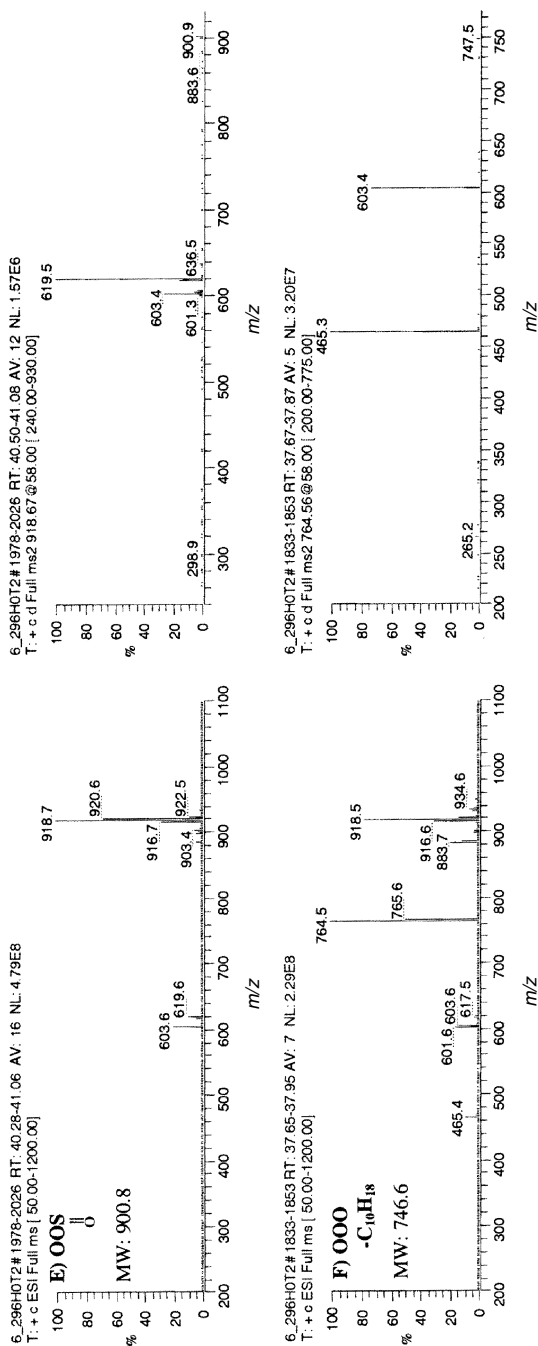


Fig. 7.17. (Part II) ESI-MS and MS/MS mass spectra of heated triolein monomeric TAG oxidation products and chain-shortened products: (E) Mass spectra of OOS-ketone. (F) Mass spectra of $OOO-C_{10}H_{18}$. (G) Mass spectra of $OOO-C_{11}H_{20}$; (H) mass spectra of OOO -epidioxide.

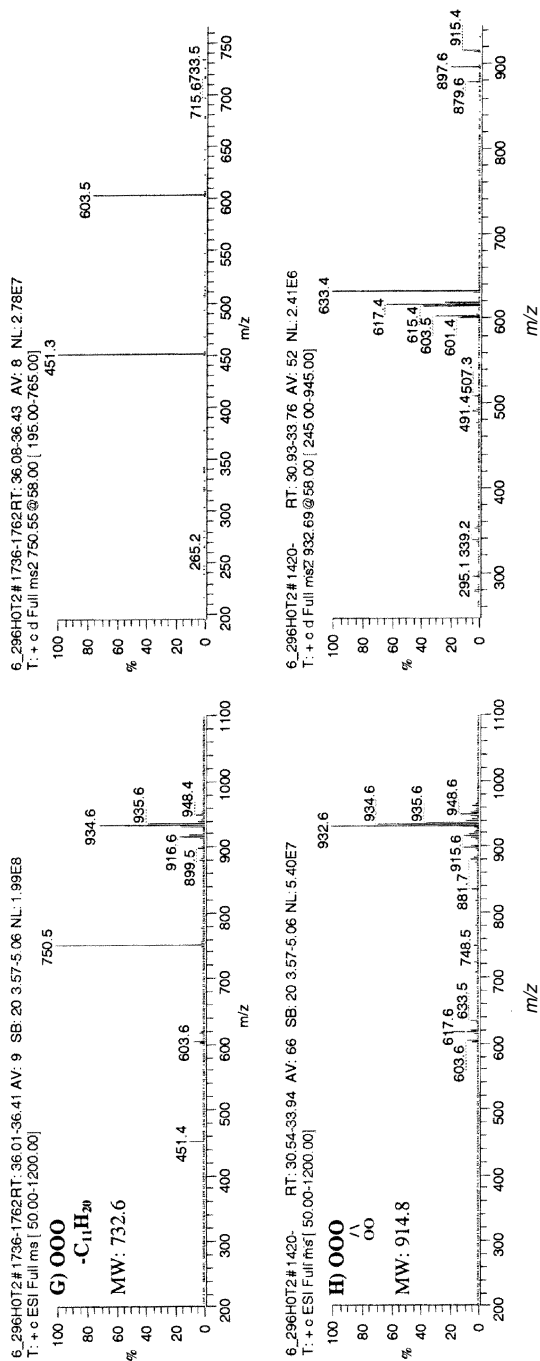


Fig. 7.17. (Part II) (Continued).

containing cyclic oxygen-containing functional groups, were also observed in the ESI-MS/MS mass spectra. Other similar trends in MS/MS spectra of TAGOX were also observed, included the proclivity of hydroperoxides to form low abundances of the intact protonated molecule (m/z 917.5 in Fig. 7.17C2) and the [(DAG)OOH]⁺ fragment.

There were some differences between the mass spectra of TAGOX obtained by ESI-MS/MS versus spectra obtained by APCI-MS, and between fragmentation processes undergone by TAGOX versus normal TAG. One important difference was that ammonium adducts of epoxides were especially stable, so ammonium-containing fragments were formed from epoxides and also from hydroperoxides that fragmented during MS/MS to form epoxides. First, the TAGOX molecules formed ammonium adducts of triacylglycerols (as mentioned above), but then these [TAG+NH₄]⁺ underwent fragmentation to lose one fatty chain. The fatty chain that was lost could either be the one that contained the ammonium group, or it could be one of the other fatty chains. Furthermore, the fatty chain that was lost could either contain the oxygen functional group or not. Thus normal [DAG]⁺, oxidized [DAG]⁺, and ammonium adducts of these fragments can be seen in ESI-MS/MS spectra. If the [M+NH₄]⁺ lost the fatty chain containing the oxygen functional group, then a normal [DAG]⁺ was formed. On the other hand, if the [M+NH₄]⁺ lost a normal FA, then an oxygen functional group-containing diacylglycerol fragment was left behind (DAGOX), and some of these remained in the form of ammonium adducts, [DAGOX+NH₄]⁺. For instance, the ESI-MS/MS mass spectrum of OOO-epoxide in Figure 7.17B2 showed a fragment at m/z 634.5, which was the [OO-epoxide + NH₄]⁺, in addition to the normal [OO-epoxide]⁺ at 617.5 and [OO]⁺ at m/z 603.3. ESI-MS/MS of normal TAG, such as those shown in Figure 7.13, did not exhibit a [DAG+NH₄]⁺ fragment. APCI-MS spectra of TAGOX, such as those shown in Figure 7.11, also did not exhibit the [DAG+NH₄]⁺ fragment.

OOS-epoxide (Figure 7.17A2) also underwent fragmentation analogous to that of OOO-epoxide, to form an [OS-epoxide]⁺ fragment ion at m/z 619.5. Furthermore, an [OS-epoxide+NH₄]⁺ was formed at m/z 636.6 under ESI-MS/MS conditions, similar to the [OO-epoxide+NH₄]⁺ formed by OOO-epoxide. The [DAG-epoxide + NH₄]⁺ fragments were not formed by normal TAG, and they were not formed under APCI-MS conditions. The hydroperoxides and epidioxides produced epoxides as fragments during ESI-MS/MS (the same fragments as those described above in the section on APCI-MS of TAGOX), and some of these epoxide fragments remained as ammonium adducts, [DAG-epoxide+NH₄]⁺. For example, OOO-hydroperoxide (Fig. 7.17C2) produced a fragment at m/z 635.4, which was the intact hydroperoxy-DAG fragment, [hydroperoxy-OO]⁺; it also produced the epoxide fragment at m/z 617.5. These were the same fragments formed by APCI-MS. But under ESI-MS/MS conditions, an ammonium adduct of the epoxide fragment was also observed. This had a m/z value of 634.5, and the abundance of this peak was larger than the abundance of the [hydroperoxy-OO]⁺ at m/z 635.4. These fragments were unique to the TAGOX under ESI-MS/MS conditions using ammonium as the reagent electrolyte.

The LC1/MS2 report on TAGOX (38) showed ESI-MS mass spectra of chain-shortened and also chain-addition products formed from triolein. These had been reported by APCI-MS (70), but the advantage of the ESI-MS data was that it allowed the chain-addition products to be identified from a single injection, without sample enrichment. ESI-MS allowed a larger variety of chain-shortened products to be identified. ESI-MS data provided both definitive molecular weight information (from the ammonium adduct ions) and structurally indicative fragments for structural elucidation (from MS/MS spectra). Mass spectra of two chain-shortened species are shown in Figure 7.17F and Figure 7.17G. The ESI-MS mass spectra exhibited the protonated molecules as base peaks, with small $[\text{DAG}]^+$. The ESI-MS/MS spectra had DAG fragment ions as the primary peaks. From direct comparison of APCI-MS to ESI-MS using a dual parallel arrangement, it appeared that ESI-MS was better for TAGOX analysis (more sensitive, while still providing structural characterization) than APCI-MS (which was much less sensitive, and did not provide intact near-molecular ions).

The sensitivity of ESI-MS to dimers and dimers containing extra oxygen atoms (38) led us to extend our chromatographic analysis of HMW TAGOX to investigate larger oligomers. These had long been reported by techniques such as size exclusion chromatography (SEC) [see Dobarganes *et al.* (83), for example], but they had never been identified as intact molecules by online LC/MS. Our recent report (84) showed that ESI-MS with ammonium formate added as a sheath liquid produced intact ammonium adducts of TAGOX oligomers, including dimers (two trioleins), trimers (three trioleins), and tetramers (four trioleins). Figure 7.18 shows ion chromatograms and mass spectra of HMW TAGOX oligomers. The extracted ion chromatograms represent the mass ranges of dimers, trimers, and tetramers containing none, one, or two additional oxygen atoms in addition to the covalently linked triolein molecules. Masses corresponding to ammonium adducts of intact molecules composed of two triolein moieties joined together, with and without additional sites of unsaturation, were observed at m/z 1783 to 1787. Molecules composed of three covalently linked triolein moieties (trimers), with and without additional sites of unsaturation, were observed at m/z 2666 to 2672. Oligomers composed of four covalently linked triolein molecules (tetramers), with and without additional sites of unsaturation, were observed at m/z 3547–3557. Previously, TAGOX up to the size of dimers had been identified by APCI-MS (70), but prior enrichment of the sample was required. Using ESI-MS, HMW TAGOX were observed from a single injection.

Because of the sensitivity of ESI-MS to HMW TAGOX, we were able to obtain MS, MS/MS, and MS^3 data from the TAGOX oligomers on the ion trap mass spectrometer. The MS/MS spectra provided valuable fragments that allowed structural subunits of the oligomers to be identified.

The masses and the MS/MS spectra allowed the nature of the linkages between oligomers to be specified and the identities of fragments to be proposed. In this first report of the LC/ESI-MS analysis of HMW TAGOX (84), the authors described how the high molecular weights of the TAGOX oligomers resulted in a distribution of isotopic abundances, and they showed that the most abundant isotope was usually not the

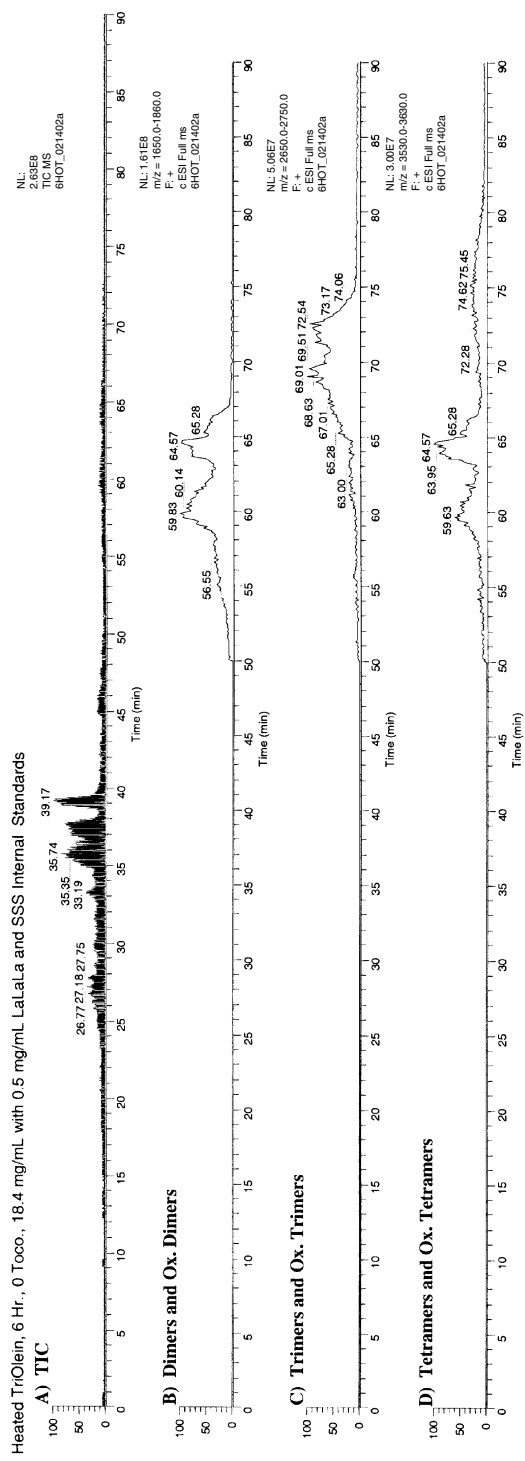


Fig. 7.18. Extracted ion chromatograms (EIC) and mass spectra of triolein high molecular weight TAG oxidation products obtained by RP-HPLC/ESI-MS. (A) Total ion chromatogram; (B) EIC of m/z range 1760–1860; (C) EIC of m/z range 2650–2750; (D) EIC of m/z range 3530–3630; (E) ESI-MS mass spectrum averaged across Dimer/Ox. Dimer peaks, right column: average 54–67 min; (F) ESI-MS mass spectrum averaged across Trimer/Ox. Trimer peaks, right column: average 64–75 min; (G) ESI-MS mass spectrum averaged across Tetramer/Ox. Tetramer/Ox. Tetramer peaks, right column: average ESI-MS spectrum from 70–80 min.

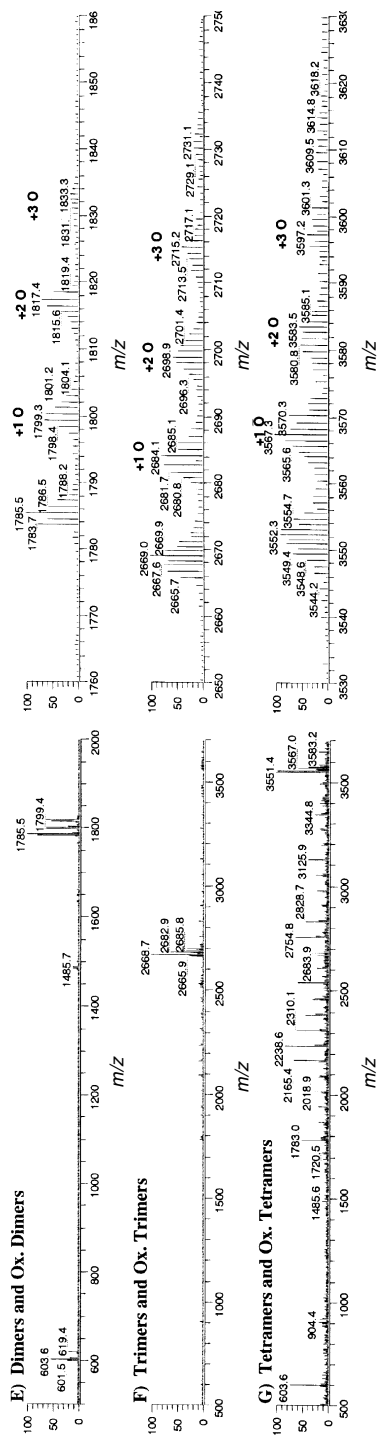


Fig. 7.18. (continued).

monoisotopic peak. The authors presented an approach by which the m/z values and abundances of the various isotopes of TAGOX oligomers might be useful to estimate the ratios of oligomers having different levels of unsaturation. In that report, it was also shown that even tristearin (SSS), which has no sites of unsaturation vulnerable to oxidation, underwent oxidation at frying temperatures. The products of tristearin oxidation were entirely analogous to the products formed by triolein. Among the TAGOX observed from SSS were monomeric SSS oxidation products (such as epoxides), dimers and oxidized dimers, chain-addition products, and chain-shortened products (both normal acyl chains and core aldehydes).

It should be mentioned that dimerization of the HMW TAGOX also occurred “on the fly” in the ESI ionization source. Therefore, the largest peak in the chromatogram in Figure 7.18D that represented the triolein tetramers was actually formed by two dimers that joined together in the ESI source to produce a molecule in the same mass range as intact, chromatographically resolved tetramers. However, it can clearly be seen that this peak occurred at the same time as the triolein dimers, and had a peak profile similar to the dimers. This was easily distinguished from the stable, long-lived tetramers formed in the oil and then chromatographically resolved from the dimers and trimers. The native, intact tetramers eluted between ~72 and 80 min. It has been our experience that almost every type of molecule can dimerize in the ESI source. Phospholipids (PL) are naturally especially susceptible to dimerization, due to their zwitterionic nature (PL dimerization can be greatly reduced by using very dilute solutions). It is a testament to the very gentle ionization process of ESI that even large, very non-polar molecules such as triolein dimers can form dimers in the ESI source.

Our goal in TAGOX analysis has always been to establish an online LC/MS method that could be applied directly to TAGOX mixtures without prior derivatization or extensive sample preparation. We have used HPLC/ESI-MS for direct analysis of intact, unaltered TAGOX in solutions that were prepared simply by dissolving the TAGOX in chloroform (or methylene chloride). While our approach has proved successful, it has the disadvantage that hydroperoxides are not easily distinguished, because they provide very little $[M+H]^+$ or $[(DAG)OOH]^+$. Also, epidioxides can be difficult to distinguish from hydroperoxides. Nevertheless, our approach allowed us to report ESI-MS mass spectra of HMW TAGOX that had not been previously reported. Still, our approach is by no means the only approach that has been demonstrated, as shown by other chapters, such as Chapter 4 in this volume.

TAG Positional Isomers

TAG P.I. by APCI-MS. Qualitative Analysis of TAG P.I. by APCI-MS. One key aspect of TAG analysis has always been determination of the positional placement of the fatty acyl chains on the glycerol backbone. Plants synthesize lipids with structural specificity, namely saturated FA are preferentially located on the *sn*-1 and -3 positions of the glycerol backbone, and polyunsaturated FA in the *sn*-2

position. TAG are metabolized by enzymes in the human digestive system with structural specificity, with FA in the *sn*-1 and -3 positions being removed from the glycerol backbone preferentially. Therefore, knowledge of the configuration of TAG is an important aspect of dietary, nutritional, metabolic, and related studies. Based purely on statistical considerations, any ABA or AAB TAG should yield twice as much of the [AB]⁺ ion as the [AA]⁺ ion, since there are two A FA available to combine with the B FA to give an [AB]⁺ ion. The statistically expected ratio of [AA]⁺ to [AB]⁺ is 1:2, or 0.50. This is the expected ratio for all ABA/AAB TAG regardless of the nature or identities of the fatty acyl chains. If a TAG exhibits abundances in a ratio other than 0.5, it is due to nonstatistical influences.

Laakso and Voutilainen (41) submitted the first article describing the effect of FA positional distribution on the fragment pattern in APCI-MS mass spectra. They noted that the DAG fragment ion formed by loss of the fatty acyl chain in the *sn*-2 position was less abundant than the DAG formed from loss of the FA in the *sn*-1 or *sn*-3 positions. These authors showed the abundances of DAG fragment ions from 10 TAG with specific FA positional distributions. Manninen and Laakso (62) later published results on the same mixture of TAG separated by using supercritical fluid/APCI-MS. Laakso (85) also published results showing differences between DAG fragment ratios exhibited by *n*-3 TAG versus *n*-6 TAG. They showed that the positions of double bonds in a fatty acyl chain, as well as the number of sites of unsaturation and the position of the fatty acyl chains on the backbone, affects the DAG fragment ratios under APCI-MS conditions.

Mottram and Evershed (39) published an article devoted to the subject of structure analysis using LC/APCI-MS and have followed up their initial work with several other works in this area. Similar to the work by Laakso and Voutilainen (41), the work by Mottram and Evershed (39) on analysis of SSO versus SOS and PPO versus POP also demonstrated that the loss of the FA from the *sn*-2 position was disfavored compared to the loss from the *sn*-1 or *sn*-3 positions, leading to a lower abundance of the *sn*-1,3 DAG fragment ion resulting from loss of the *sn*-2 FA. They further showed that a TAG with three different FA gave the lowest DAG ion abundance from the *sn*-1,3 DAG ion, from which the FA in the *sn*-2 position was lost. Manninen and Laakso (62) also showed that an ABC TAG produced the lowest DAG ion abundance from the *sn*-1,3 DAG. Kusaka *et al.* (68) noted earlier that the APCI-MS mass spectra of TAG standards showed some discrimination between positional isomers. They used mass spectra to assign likely positional isomer assignments to some of the components from perilla, corn, and olive oils. Unfortunately, numerous spurious and unexplained peaks in the mass spectra resulted in poor signal-to-noise ratios.

In a recent publication by Byrdwell and Neff (38), the authors compared the fragmentation patterns given by synthetic TAG under APCI-MS and ESI-MS conditions. They found (as others had previously) that ESI-MS mass spectra allowed discrimination between *sn*-1,3 versus *sn*-2,3 positional isomers, similar to APCI-

MS spectra. The positional isomer data from Laakso and Voutilainen (41), Mottram and Evershed (39), Laakso (85), Byrdwell and Neff (38), Hsu and Turk (19), Jakab *et al.* (88), Marzilli *et al.* (31), and Fauconnot *et al.* (86) by APCI and ESI are compiled in Table 7.2. This table highlights several important points about positional isomer determination using APCI-MS.

Trends in the nonstatistical influences on the $[AA]^+/[AB]^+$ ratio can be seen in Table 7.2. The trends in the abundances of $[AA]^+$ and $[AB]^+$ ions mentioned by the authors cited previously are clearly seen in the ratios in Table 7.2. The fact that loss of the *sn*-2 chain is energetically disfavored results in most ABA isomers reported by the majority of authors having an $[AA]^+/[AB]^+$ ratio substantially lower than the statistically expected value of 0.5. The (*n*-6) linolenic acid-containing isomer, O(*n*-6)LnO, gave a higher ratio than most other ABA isomers, including the O(*n*-3)LnO isomer, demonstrating an effect of double bond location on the $[AA]^+/[AB]^+$ ratio. Most data in Table 7.2 were obtained on FinniganMAT (now ThermoElectron Corp.) TSQ 700 or 7000 tandem quadrupole instruments.

The data reported more recently by Fauconnot *et al.* (86) were obtained by using a Micromass instrument with a Z-sprayTM interface (see Chapter 1 in this volume for a diagram); and many of the $[AA]^+/[AB]^+$ ratios reported by these authors are higher than those obtained on the TSQ instruments. This points out the importance of knowing the type of instrument used and conditions under which the $[AA]^+/[AB]^+$ ratio is obtained. The $[AA]^+/[AB]^+$ ratios reported by many authors are similar in Table 7.2. This indicates that tabulated values may be useful to assist in the determination of the composition of regioisomers in a mixture, if the tabulated values were obtained using the same or similar instrument.

The results in Table 7.2 are reasonably consistent, showing similar results for PPO and POP by HPLC/APCI-MS from all authors using TSQ instruments. A ratio of ~0.9 for PPO would allow this TAG to be identified as the *sn*-1,2 isomer, while a low value between 0.2 and 0.3 would allow the *sn*-1,3 isomer to be easily identified (the ratios produced by SFC/APCI-MS varied somewhat from those given by HPLC/APCI-MS). Similarly, for OPO, the $[OO]^+$ fragment was very much smaller than the $[OP]^+$ fragment, and the small $[OO]^+/[OP]^+$ ratio allows one to conclude that it is the *sn*-1,3 isomer. But for OOP, there is a noticeable difference between the results reported by Laakso and Voutilainen (41) and those by Byrdwell and Neff (38), by LC/APCI-MS, and those by Manninen and Laakso (62), by SFC/APCI-MS. The results by Byrdwell and Neff (38) and also Manninen and Laakso (62) for OOP were essentially indistinguishable from the statistically expected ratio of 0.50, whereas the ratio shown by Laakso and Voutilainen (41) was more indicative of a positional preference. Such results indicate, again, that a specific instrument under a specific set of conditions can affect the DAG fragment ratios (all three groups used Finnigan MAT APCI sources for HPLC-MS, but the SFC/APCI-MS source was slightly modified). To be able to employ the DAG fragment ion ratios, natural samples should be analyzed immediately after a set of standards to minimize variability. Also, it is easier to use the $[AA]^+/[AB]^+$ ratio to

TABLE 7.2

Fragment Ratios Reported by Various Authors for Regiospecific Analysis by APCI-MS and ESI-MS. Ratio of the Abundances of [AA]⁺ to [AB]⁺ in ABA and AAB TAG

| Author | APCI-MS | | | |
|--------|------------|--------------------------------------|------------|--------------------------------------|
| | AAB | [AA] ⁺ /[AB] ⁺ | ABA | [AA] ⁺ /[AB] ⁺ |
| LV | PPO | 0.89 | POP | 0.34 |
| ME | PPO | 0.95 ± 0.30 | POP | 0.20 ± 0.08 |
| BN | PPO | 0.87 | POP | 0.29 |
| ML | PPO | 0.79 | POP | 0.41 |
| FHAFD | PPO | 2.07* | POP | 0.22 |
| LV | POO | 0.70 | OPO | 0.09 |
| BN | POO | 0.51 | OPO | 0.17 |
| ML | POO | 0.48 | OPO | 0.16 |
| FHAFD | POO | 0.43 | OPO | 0.07 |
| LV | OOln (n-6) | 1.97* | OLnO (n-6) | 0.90 |
| ML | OOln (n-6) | 1.29* | OLnO (n-6) | 0.63 |
| L | | | OLnO (n-3) | 0.17 |
| L | | | OLnO (n-6) | 0.64 |
| LV | PPL | 0.76 | | |
| ML | PPL | 0.70 | | |
| FHAFD | PPL | 2.99* | PLP | 0.40 |
| FHAFD | PPS | 0.94 | PSP | 0.15 |
| LV | SSP | 0.56 | | |
| BN | SOO | 0.54 | | |
| FHAFD | SOO | 0.44 | OSO | 0.11 |
| ME | SSO | 1.07 ± 0.16 | SOS | 0.29 ± 0.12 |
| L | SSO | 1.33* | | |
| FHAFD | SSO | 1.81* | SOS | 0.26 |
| LV | | | SLS | 0.38 |
| ML | | | SLS | 0.41 |
| L | LLO | 1.24* | | |
| JJF | LLO | 0.70 | LOL | 0.23 |
| FHAFD | LLS | 1.52* | LSL | 0.37 |
| FHAFD | PPA | 10.64* | PAP | 1.56* |
| FHAFD | PAA | 0.09 | APA | 0.02 |
| ESI-MS | | | | |
| HT | PPO | 0.70 | POP | 0.34 |
| BN | PPO | 0.68 | POP | 0.23 |
| BN | POO | 0.67 | OPO | 0.24 |
| MFDV | POO | 0.50 | OPO | 0.18 |
| BN | SOO | 0.64 | | |
| MFDV | SOO | 0.50 | OSO | 0.17 |
| HT | SSO | 0.58 | SOS | 0.33 |
| MFDV | SSO | 0.91 | SOS | 0.19 |

BN: Byrdwell and Neff (38), TSQ700 or LCQ ITMS; FHAFD: Fauconnot *et al.* (86), Micromass with Zspray™ interface; HT: Hsu and Turk (19), TSQ7000; JJF: Jakab *et al.* (88), Shimadzu QP2010; L: Laakso (85), TSQ700; LV: Laakso and Voutilainen (41), TSQ700; ME: Mottram and Evershed (39), TSQ700; MFDV: Marzilli *et al.* (31), LCQ ITMS; ML: Manninen and Laakso (SFC/APCI-MS) (62), TSQ700.

*Much higher than expected statistically.

identify ABA TAG than it is to identify AAB TAG. A ratio of 0.10 to 0.40 can allow one to conclude that the TAG is highly likely to be of the ABA type, but a ratio larger than this cannot necessarily allow one to make a conclusive assignment. Unfortunately, the degree of unsaturation, and even the double bond position in the TAG also plays a role. The *n*-3 isomer of linolenic acid gave a very different ratio of $[AA]^+/[AB]^+$ than the *n*-6 isomer [Laakso (85)]. The $[AA]^+/[AB]^+$ ratios reported for $OLn(n-6)O$ were definitely not what one would expect, based on the results observed for more saturated TAG. The ratios of 0.90 or 0.64 (HPLC) or 0.63 (SFC) for this unsaturated TAG would *not* lead one to conclude that it was an ABA TAG. Therefore, it seems apparent that more work remains to be done before the DAG fragment ratios can be used systematically for reliable positional isomer identification, especially for highly unsaturated TAG. All results of ABC-type TAG indicated that the least abundant DAG fragment ion arose from the *sn*-1,3 isomer. But results by Manninen and Laakso (62) showed very little difference between the abundances given by the *sn*-1,3 versus the *sn*-2,3 DAG fragment ions. Last, the results by ESI-MS/MS appeared to be more self-consistent than the results by APCI-MS. All AAB TAG examined produced ratios of 0.6 to 0.7 using ESI-MS, while the ABA TAG gave ratios of 0.2 to 0.25. ESI-MS/MS may prove to be more reliable than APCI-MS for positional isomer determination.

Mottram *et al.* (40) went on to utilize the DAG fragment ion ratios to determine the most abundant positional isomers of a series of TAG from a range of vegetable and seed oils. They provided a qualitative assessment of the isomer identities, along with a confidence rating for the assignment. More recently, Mottram *et al.* (87) applied HPLC/APCI-MS to regiospecific characterization of TAG in animal fats (lamb, beef, pork, and chicken fats). They used the DAG fragment ratios to identify numerous regiospecific TAG molecular species, along with a confidence rating for each of the molecular species. Results were compared to the results obtained by lipase hydrolysis to determine the FA in the *sn*-2 position. Unfortunately, the results by the two very different methods were not in excellent agreement. The differences were attributed to (i) lipase specificity that led to different rates of hydrolysis for different FA, and (ii) problems with the quantification of isomers using APCI-MS. Nevertheless, APCI-MS was used to identify more molecular species in beef, pork, and chicken fats than were previously identified using ELSD detection.

Quantitative Analysis of TAG P.I by APCI-MS. Jakab *et al.* (88) recently reported the quantification of regiospecific isomers of dilinoleoyl-oleoyl glycerol (LLO and LOL), first as standards, and then in vegetable oils. (Mottram *et al.* (40) had provided qualitative estimates with confidence ratings.) In the chapter on APCI-MS in lipid analysis that also appeared in 2003, Byrdwell (3) had cited the need for this type of experiment. In discussion of the quantification of TAG positional isomers, it was stated: "A comprehensive study using the greatest possible number of positional isomers with disparate amounts of unsaturation needs to be undertaken for both

APCI-MS and ESI-MS/MS. In our initial work, we did not address this issue because we felt that it would require lengthy quantification of the abundances of DAG fragment ions from a large series of standards to address the issue adequately. We believed that the proper approach would be to perform APCI-MS of a wide range of structured lipids, determine the ratios of DAG fragment ions that are produced, and then interpolate between the ratios for the 1,2- versus the 1,3-isomers to get a quantitative estimation of the relative amounts of each of these isomers in real samples. Unfortunately only a limited number of structured lipids are commercially available, so full treatment of this subject will require synthesis of an array of structured lipids, followed by their analysis. Until then, great care must be exercised in using APCI-MS for positional isomer identification, especially for polyunsaturated TAG” (89) (as mentioned previously: DAG ratios were affected by the double bond positions in TAG containing Ln). The article by Jakab *et al.* (88) is the first example of the process described above. However, those authors simplified the complex situation by examining only the two isomers of one TAG. Nevertheless, they clearly demonstrated that the approach of determining the DAG fragment ratios for a series of standard solutions and then constructing a calibration line and interpolating the ratio of DAG fragment ions of actual samples by using the calibration line is effective for determining the relative amounts of two isomers. Of course, every TAG for which positional isomers are to be determined requires isomeric standards, and also requires multiple solutions of each standard pair of isomers to be quantified. Nevertheless, we feel that the approach taken by Jakab *et al.* (88) is the most appropriate approach for accurate quantitative estimation of the relative amounts of regioisomers.

Jakab *et al.* (88) demonstrated that the fragment ion ratio $[AA]^+/[AB]^+$ varies linearly with the percentage concentration of the individual positional isomers. The calibration curve presented by them is reproduced here as Figure 7.19. The linearity of the $[AA]^+/[AB]^+$ ratio with % ABA has important implications for the ability to quantify the relative amounts of positional isomers. They produced a line describing the $[AA]^+/[AB]^+$ fragment ratio (as a percentage) versus the percentage of the ABA species out of the total ABA+AAB. The line that they presented for the LOL/LLO isomer pair had the equation $y(\%) = -0.4906x + 69.8295$, where x was the percentage of the ABA species out of all regioisomers (LOL+LLO), and y was the $[AA]^+/[AB]^+$ fragment ratio (as a percentage, not a pure ratio). From this line, the percentage of the LOL concentration in a mixture of isomers could be calculated from the ratio $[LL]^+/[LO]^+$. This report clearly and expertly demonstrated the linear relationship between the $[AA]^+/[AB]^+$ fragment ratio and the percentage of a regioisomer. The only shortcoming of the method of Jakab *et al.* (88) was that a series of 11 solutions was required to specify the equation of the line. The question arises, then, can the same or similar information be derived from less data? We will demonstrate below that the answer is yes. Quantification of positional isomers can be accomplished with as few as two solutions (two points are required to specify a line).

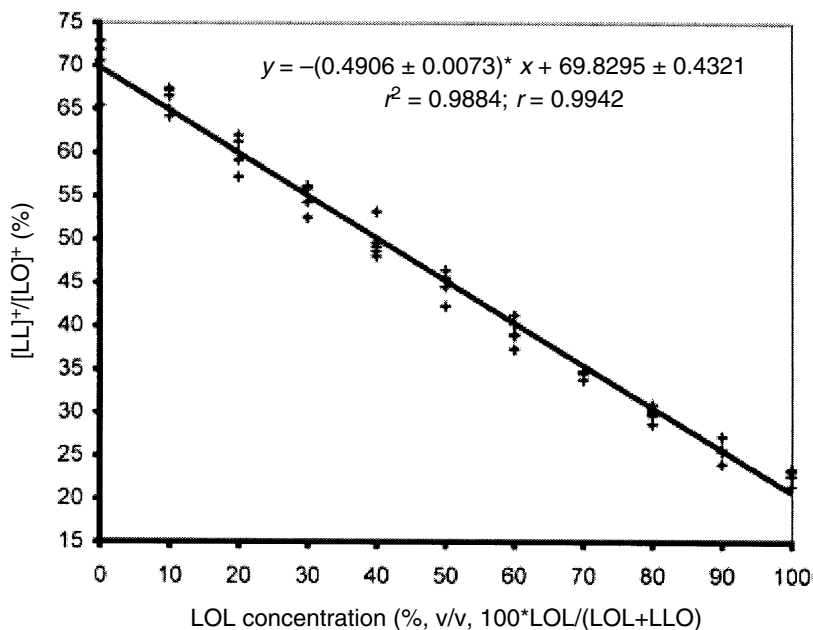


Fig. 7.19. Ratio of the $[LL]^+$ and $[LO]^+$ fragment ions (%) in mixtures of LOL and LLO at various percentages (calibration curve). *Source:* Reference 88. Reproduced with permission from John Wiley & Sons, Ltd.

The $[AA]^+ / [AB]^+$ ratio (as a ratio, not a percentage) from LLO and LOL pure positional isomers reported by Jakab *et al.* (88) was included in Table 7.2, which summarized the results of positional isomer analysis of TAG. We will show that the $[AA]^+ / [AB]^+$ ratios of the 100% pure isomers, such as those listed in Table 7.2, can be used as a good approximation to allow quantification of the relative amounts of positional isomers. When only two pure isomers are analyzed, one obtains a ratio $[AA]^+ / [AB]^+$ for each of the two isomers ABA and AAB (= BAA). The two points act as the endpoints for the range of $[AA]^+ / [AB]^+$ values, and all $[AA]^+ / [AB]^+$ of mixtures of the two isomers should fall within the range bounded by these extremes. For instance, in the data presented by Jakab *et al.* (88), the observed extremes were $[AA]^+ / [AB]^+ = 0.2289$ (average, $n = 5$) for 100% LOL and $= 0.7028$ for 100% LLO, respectively. Similarly, each set of $[AA]^+ / [AB]^+$ ratios of TAG positional isomers in Table 7.2 defines the endpoints of the range of DAG fragment ion ratios that should be encountered in APCI-MS (as well as some ESI-MS) mass spectra of TAG.

An equation of the line that approximately describes the $[AA]^+ / [AB]^+$ ratio for any combination of TAG positional isomers can be constructed from these two endpoints. If one observes the line in Figure 7.19 in the form of $y = mx + b$, then y

$= ([AA]^+/[AB]^+) = m \cdot (\% \mathbf{LOL}) + b$. In this equation, b equals the $([AA]^+/[AB]^+)$ ratio at 0% **LOL**. In terms of x and y , the coordinates of the two endpoints would be (0% **LOL**, $([AA]^+/[AB]^+)_{\text{AAB}}$) and (100% **LOL**, $([AA]^+/[AB]^+)_{\text{ABA}}$) where the subscripts represent the $([AA]^+/[AB]^+)$ ratios of pure standards of AAB and ABA, that is, **LLO** (= 0% **LOL**) and **LOL**, which would be explicitly: (0%, 0.7028), (100%, 0.2289). The equation of the line constructed from these endpoints would be: $m = ((\Delta y)/(\Delta x)) = ((y_2 - y_1)/(x_2 - x_1)) = ((([AA]^+/[AB]^+)_{\text{ABA}}) - ([AA]^+/[AB]^+)_{\text{AAB}})/(100 - 0)$ and $b = ([AA]^+/[AB]^+)_{\text{AAB}}$. In terms of the data reported by Jakab *et al.* (88), this gives: $m = ((\Delta y)/(\Delta x)) = ((y_2 - y_1)/(x_2 - x_1)) = ((([LL]^+/[OL]^+)_{\text{LOL}}) - ([LL]^+/[OL]^+)_{\text{LLO}})/(100 - 0) = ((0.2289 - 0.7028)/(100 - 0)) = ((-0.4739)/(100)) = -0.004739$; and $b = ([LL]^+/[OL]^+)_{\text{LLO}} = 0.7028$. From this line comes the relationship:

$$\left(\frac{[LL]^+}{[LO]^+} \right) = (-0.004739) \cdot (\% \mathbf{LOL}) + 0.7028$$

This is the line formed by only the two endpoint values, which can be compared to the best-fit line through all eleven points. The best-fit line had the equation:

$$\left(\frac{[LL]^+}{[LO]^+} \right) = (-0.004906) \cdot (\% \mathbf{LOL}) + 0.6983$$

This allows calculation of the expected $[LL]^+/[LO]^+$ as a pure ratio, not as a percentage. The equation formed from the endpoint values can be seen to be in the general form:

$$\left(\frac{[AA]^+}{[AB]^+} \right)_{\text{Obs}} = \left(\left(\frac{[AA]^+}{[AB]^+} \right)_{\text{ABA}} - \left(\frac{[AA]^+}{[AB]^+} \right)_{\text{AAB}} \right) \cdot \left(\frac{\% \mathbf{ABA}}{100} \right) + \left(\frac{[AA]^+}{[AB]^+} \right)_{\text{AAB}} \quad [1]$$

To get a line with a positive slope, the y values, $([AA]^+/[AB]^+)$, can be arranged from lowest to highest, which means that the x values should be put in terms of % **LLO** to make x also go from low to high as $([AA]^+/[AB]^+)$ goes from low to high. The equivalent points that would give a positive slope would be: (x_1, y_1) , $(x_2, y_2) = (0 \% \mathbf{LLO}, ([AA]^+/[AB]^+)_{\text{ABA}})$, $(100\% \mathbf{LLO}, ([AA]^+/[AB]^+)_{\text{AAB}})$, or $(0, 0.2289)$, $(100, 0.7028)$. In terms of the data by Jakab *et al.* (88), this would be a line having the equation:

$$\left(\frac{[LL]^+}{[LO]^+} \right) = (0.004739) \cdot (\% \mathbf{LLO}) + 0.2289$$

This equation can be seen to be in the general form:

$$\left(\frac{[AA]^+}{[AB]^+} \right)_{Obs} = \left(\left(\frac{[AA]^+}{[AB]^+} \right)_{AAB} - \left(\frac{[AA]^+}{[AB]^+} \right)_{ABA} \right) \cdot \left(\frac{\%AAB}{100} \right) + \left(\frac{[AA]^+}{[AB]^+} \right)_{ABA} \quad [2]$$

One can solve Equation 1 and Equation 2 for the following relationships:

One may rearrange Equation 1 to solve for the %ABA as follows:

$$(\%ABA) = \left(\frac{\left(\frac{[AA]^+}{[AB]^+} \right)_{AAB} - \left(\frac{[AA]^+}{[AB]^+} \right)_{Obs}}{\left(\frac{[AA]^+}{[AB]^+} \right)_{AAB} - \left(\frac{[AA]^+}{[AB]^+} \right)_{ABA}} \right) \times 100 \quad [3]$$

Similarly, one may rearrange Equation 2 to solve for the %AAB as follows:

$$(\%AAB) = \left(\frac{\left(\frac{[AA]^+}{[AB]^+} \right)_{Obs} - \left(\frac{[AA]^+}{[AB]^+} \right)_{ABA}}{\left(\frac{[AA]^+}{[AB]^+} \right)_{AAB} - \left(\frac{[AA]^+}{[AB]^+} \right)_{ABA}} \right) \times 100 \quad [4]$$

And these two percentages share the relationship that %ABA + %AAB (i.e., %LOL + %OLL) = 100%. Therefore, whenever one percentage is known, %ABA or %AAB, the other may be known as %ABA = 100 - %AAB or %AAB (= %AAB + %BAA) = 100 - %ABA.

Equations 3 and 4 allow the direct calculation of the percentage compositions of either: one regiospecific isomer, %ABA, or the sum of two isomers, %AAB (= %AAB + %BAA) (since the *sn*-1,2 and *sn*-2,3 isomers cannot, as yet, be distinguished without derivatization). Of course, the ([AA]⁺/[AB]⁺) ratios of pure known standards of each individual TAG must be determined for each TAG of which quantitation is sought. These ([AA]⁺/[AB]⁺) ratios of pure known standards can potentially be tabulated values. If a researcher has a similar instrument, and obtains similar ([AA]⁺/[AB]⁺) ratios of pure known standards on his/her instrument that are close to those of tabulated values, it lends credibility to the possibility that tabulated values might be helpful in assessing the percentage composition of regioisomers in a mixture of TAG. The minimal approach to linear interpolation would require the analysis of two pure regioisomeric standards, and then the ([AA]⁺/[AB]⁺)_{Obs} ratio of a mixture of unknown regioisomeric content may be interpolated between the ([AA]⁺/[AB]⁺) ratios obtained for pure isomers, and a quantitative estimate of the %ABA or %AAB can be obtained with relative ease. Assuming that current data for specific regioisomers had been determined, that is, that the

$[AA]^+/[AB]^+$ ratio has been determined for pure positional isomers on a particular instrument under specific (preferably constant) conditions, the % composition of the regioisomers for an unknown mixture of a calibrated TAG can be determined by only one piece of acquired data for each TAG in an unknown mixture, the $([AA]^+/[AB]^+)_{Obs}$ ratio. Therefore, it is worthwhile to continue to assemble tabulations of the reported ratios of as many TAG species on as many instruments as possible.

The equation made by only the two endpoint values can be compared to the best-fit line through all 11 points as follows:

The equation calculated by least-squares analysis by Jakab *et al.* (88) described the $[AA]^+/[AB]^+$ ratio versus % LOL concentration. The slope of the line produced by Jakab *et al.* was -0.4906 . Their best-fit line equation can be converted into the positive slope form of Equation 2. In Equation 2, the term $[(AA]^+/[AB]^+)_{AAB} - (AA]^+/[AB]^+)_{ABA}$ was simply the slope of the line going from endpoint 1 to endpoint 2. If the $[AA]^+/[AB]^+$ ratio is plotted versus the % LLO concentration, it would have a slope of $+0.4906$. Equation 2 reflects this positive slope. The $[AA]^+/[AB]^+$ ratio of the LOL isomer is found if one substitutes the value of 100% into the equation of Jakab *et al.* (88), which gives the value of 0.2077. Therefore, the equation of the line with a positive slope calculated from the least-squares slope and intercept of Jakab *et al.* is:

$$\frac{[AA]^+}{[AB]^+} = \left[\frac{\%AAB}{100} \times (0.4906) \right] + 0.2077$$

For 100% LLO, this equation produced a value of 0.6983 (= 69.83%), which can be seen as the y-intercept of the line in Figure 7.19. The actual average $[AA]^+/[AB]^+$ ratio obtained from mass spectra of 100% LLO was 0.7028. If the observed ratio is taken as correct, the ratio calculated using the best-fit line of Jakab *et al.* (88), and converted into positive slope form, exhibited only 0.64% relative error from the observed ratio.

Application of the positive-slope equation above to each of the 11 solution concentrations prepared by Jakab *et al.*, followed by comparison of the calculated $[AA]^+/[AB]^+$ ratios to the observed ratios (reported in their Table 7.2), resulted in an average relative error of 1.9% for the values calculated from the best-fit line versus the observed values. A similar comparison can be made for the calibration line based only on the endpoint values. Application of Equation 2, which used only the 100% positional isomer endpoint values, to each of the 11 solution concentrations prepared by Jakab *et al.*, followed by comparison of the calculated $[AA]^+/[AB]^+$ ratios to the observed ratios, results in an average relative error of 3.7%. Thus, Equation 2, which was calculated from only the endpoints, produced slightly more error than the best-fit calibration line, but both equations produced low average relative error (<5%) in the $[AA]^+/[AB]^+$ ratio calculated, compared to that

observed. The reason for the greater error is seen in Figure 7.19. The average value observed from both endpoint solutions was higher than the values calculated from the calibration line. Thus, the line calculated from just the two average endpoint values gives higher values for each interpolated point in between.

The best-fit line reported by Jakab *et al.* (88) shows that the percentage of positional isomers can be accurately calculated from an $[AA]^+/[AB]^+$ ratio, based on the equation of a line produced by analysis of numerous solutions containing varying ratios of positional isomer standards. The advantage of Equations 1 through 4 was that they can be applied with only analysis of the two pure positional isomers, without multiple solutions of intermediate concentrations. Equations 1 through 4, derived based on the work of Jakab *et al.*, demonstrate that similar results, though not quite as accurate, can be achieved with analysis of only the two 100% TAG positional isomer standard solutions.

Equations 3 and 4 can potentially be used with any pair of positional isomers for which APCI-MS mass spectra are obtained from both the *sn*-1,3 isomer and either the *sn*-1,2 or *sn*-2,3 isomer (these are not yet differentiated). The $[AA]^+/[AB]^+$ ratio is produced for each of the two isomers and these $[AA]^+/[AB]^+$ ratios can then be substituted into Equation 3 or 4. Then, the $[AA]^+/[AB]^+$ ratio observed from a TAG mixture can be input into the equation to calculate the percentage of either isomer. For instance, Table 7.2 showed the $[AA]^+/[AB]^+$ ratios for both OOP and OPO reported by Byrdwell and Neff (38) and Manninen and Laakso (62). The ratios by these separate groups agreed closely, and gave an average value of $[AA]^+/[AB]^+ = (0.51 + 0.48)/2 = 0.495$ for OOP and $[AA]^+/[AB]^+ = (0.17 + 0.16)/2 = 0.165$ for OPO. These values may be substituted into Equation 3 to yield:

$$(\%POP) = \left(\frac{0.495 - \left(\frac{[PP]^+}{[PO]^+} \right)}{0.495 - 0.165} \right) \times 100$$

Since the $[AA]^+/[AB]^+$ ratio was consistent between these two authors over a wide time range, this equation may be considered somewhat generally applicable to the OOP/OPO isomer pair under similar conditions. In other cases, where there is more disagreement or variability between values reported by various authors, the $[AA]^+/[AB]^+$ ratio should be determined by APCI-MS for the two isomers under the same conditions as any samples of unknown composition in which that isomer pair is to be determined.

The combination of the demonstration by Jakab *et al.* (88) that the $[AA]^+/[AB]^+$ varies linearly with the concentration of ABA versus AAB isomers, and the approximation equations (Equations 1 through 4) given above will allow the

quantitative estimation of the relative amounts of positional isomers in mixtures and in real samples. We would hope and expect that a wider variety of regioisomers in an increasing number of samples will be examined in this way in the coming years.

In 2004, another article appeared that describes the linear relationship between the abundances of [AA]⁺ and [AB]⁺ fragments and the compositions of known standard mixtures of TAG regioisomers. Fauconnot *et al.* (86) reported calibration curves for regioisomers of seven pairs of ABA/AAB TAG standards. The authors stated: "Identification of the major regioisomers of an AAB/ABA pair of TGs was shown to be enabled by comparing the ratios of abundances of c(AA⁺)/c(AB⁺) with the statistically expected value of 0.5."

In their calibration curves, though, they plotted what they called the "regioisomeric purity," r_{AA} , which they defined as:

$$r_{AA} = \frac{100\%c(AA^+)}{c(AA^+) + c(AB^+)}$$

This equation can be easily shown to be equivalent to

$$r_{AA} = \frac{1}{1 + \frac{1}{\frac{(AA^+)}{(AB^+)}}} \times 100$$

We find it much more convenient and useful to directly use the ratio [AA]⁺/[AB]⁺, which demonstrates a linear relationship with regioisomeric composition. This simple ratio led directly to Equations 3 and 4, which can be used to calculate the percentage composition of the regioisomers of a TAG in a mixture. The [AA]⁺/[AB]⁺ ratio was used by Jakab *et al.* (88). Nevertheless, the data by Fauconnot *et al.* (86) do indirectly demonstrate the linear relationship between the [AA]⁺/[AB]⁺ ratio and the percentage composition of the regioisomers. Fauconnot *et al.* (83) reported the [AA]⁺/[AB]⁺ ratios for nine pairs of regioisomers and their values are included in Table 7.2. Many of the values obtained by these authors were higher or much higher than statistically expected values, and were higher than the values obtained by most other authors. This is probably because Fauconnot *et al.* (86) used a Micromass mass spectrometer with an APCI head and ionization chamber that have a different design from that pictured in Chapter 1, but that also have the Zspray™ API interface pictured in that chapter. These observations point to the importance of knowing the instrument used, and the characteristics of the APCI head and API interface of the instrument, because these appear to have an impact on the ion abundances and therefore on the [AA]⁺/[AB]⁺ ratio.

One last note regarding TAG positional isomers determined by APCI-MS should be mentioned. When the chromatographic separation of TAG was optimal, the TAG positional isomers could be distinguished. Figure 7.20 shows the ion chromatograms associated with POP and OPP obtained from the synthetic 35-TAG mixture. Since this synthetic TAG mixture contained statistically predicted amounts of each TAG, both isomers were expected to be present in statistically predicted proportions. The mass spectrum across the front part of the peak in Figure 7.20E exhibited a very different $[AA]^+/[AB]^+$ ratio from the mass spectrum at the beginning of the second part of the peak, in Figure 7.20D. By comparison of the $[AA]^+/[AB]^+$ ratio to the values in Table 7.2, the ratios can be used to determine that the ABA TAG (POP) eluted before the AAB TAG (PPO). It is important to note that the greatest difference between ratios in mass spectra was observed from spectra at the very front of the peak compared to spectra in the middle (the beginning of the second portion of the peak), not between the front of the peak and the tail. The ranges over which the mass spectra showed the greatest difference in $[AA]^+/[AB]^+$ are indicated in Figure 7.20D and Figure 7.20E. The mass spectra in Figure 7.20F and Figure 7.20G had $[AA]^+/[AB]^+$ ratios of 0.31 and 0.92 for POP and PPO (see intensity lists in Fig. 7.20), respectively, in agreement with the ratios obtained from pure isomers, shown in Table 7.2. When wider ranges of spectra were averaged, intermediate ratios of $[AA]^+/[AB]^+$ were observed.

Mottram provides a complete and detailed discussion of other aspects of the use of APCI-MS for analysis of TAG positional isomers in Chapter 6 in this volume.

TAG P.I. by ESI-MS. In the first report of ESI-MS for TAG analysis in 1991, by Duffin *et al.* (13), preferential cleavages of FA due to their position on the triacylglycerol backbone were not observed. Duffin *et al.* (13) did not perform a chromatographic separation, but rather infused the sample directly into the mass spectrometer. In 1996, Myher *et al.* (14) carried out a study targeted at stereospecific analysis of TAG rich in long-chain polyunsaturated FA using liquid chromatography coupled to ESI-MS. However, this study employed derivatization of the TAG into dinitrophenylurethane (DNPU) derivatives of diacylglycerols, and so did not constitute the direct online analysis of intact stereospecific TAG. More recently, Agren and Kuksis (90) used naphthylethylurethane (NEU) derivatives for stereospecific analysis of diacylglycerols derived from TAG. Again, though, this was not direct online ESI-MS for stereospecific TAG analysis. In 1998, Cheng *et al.* (18) reported the complete structural elucidation of TAG by tandem sector mass spectrometry, from infusion of samples into the mass spectrometer. Using collisionally activated dissociation (CAD) of the $[M+NH_4]^+$ adduct ions, Cheng *et al.* reported that the positions of double bonds in fatty chains (and of course the identities of the chains) could be determined, but they reported that: "The linkage information of the three acyl groups on the glycerol backbone, however, cannot be deciphered because there is no apparent discrimination in the formation of ions in the same group" (91).

Hsu and Turk (19) were the first to report a distinct stereospecific preference in the fragmentation of TAG. These authors also employed sample infusion *via* a syringe pump. Unlike sodium adducts, which do not fragment well, the authors showed that lithium adducts underwent beneficial CAD to produce structurally indicative fragments, in ratios that could be used for determination of the stereospecific location of FA on the TAG. MS/MS mass spectra exhibited not only the normal DAG fragment ions, $[\text{DAG}]^+$ (and these could be used for stereospecific determination), but also each fragment exhibited a $[\text{DAG+Li}]^+$ adduct, larger than the $[\text{DAG}]^+$, that could also be used for stereospecific determination. Using the ABC TAG isomers PSO and POS, they showed that the $[\text{DAG}]^+$ and $[\text{DAG+Li}]^+$ ions of the *sn*-1,3 isomer had lower abundances than the *sn*-1,2 and -1,3 $[\text{DAG}]^+$ and $[\text{DAG+Li}]^+$ ion abundances, for each of the two isomers. They illustrated that “it is the position of the FA substituent on the glycerol backbone and not the identity of the FA that governs the relative abundances of ions that reflect losses of FA substituents as free FA or as lithium salts” (19). The preferential loss of the *sn*-1,2 and *sn*-2,3 positions was also seen in the appearance of lithiated monoacylglycerol (MAG) fragment ions, $[\text{M+Li-(R}_1\text{COOH)-R}'_2\text{CH=CHO}_2\text{H}]^+$ and $[\text{M+Li-(R}_3\text{COOH)-R}'_2\text{CH=CHO}_2\text{H}]^+$. The two resultant ions were of approximately equal abundance and yielded a pair of peaks separated by a difference of *m/z* value equal to the mass difference between the *sn*-1 and *sn*-3 substituents. No such peak was observed from the *sn*-1,3 isomer, which would be $[\text{M+Li-(R}_1\text{COOH)-R}'_3\text{CH=CHO}_2\text{H}]^+$ (or $[\text{M+Li-(R}_3\text{COOH)-R}'_1\text{CH=CHO}_2\text{H}]^+$).

Hsu and Turk (19) also showed ESI-MS mass spectra of lithiated SSO/SOS and PPO/POP. Just like the ABC TAG, the AAB and ABA TAG produced $[\text{M+Li-(R}_1\text{COOH)-R}'_2\text{CH=CHO}_2\text{H}]^+$ and $[\text{M+Li-(R}_3\text{COOH)-R}'_2\text{CH=CHO}_2\text{H}]^+$ fragment ions, but no $[\text{M+Li-(R}_1\text{COOH)-R}'_3\text{CH=CHO}_2\text{H}]^+$ (or $[\text{M+Li-(R}_3\text{COOH)-R}'_1\text{CH=CHO}_2\text{H}]^+$). Thus, isomer pairs can be distinguished by the ESI-MS/MS mass spectra of their lithiated adducts. Although Hsu and Turk (19) did not list the ion abundances or $[\text{AA}]^+ / [\text{AB}]^+$ ratio, these ratios could be determined by physical measurement (in mm) of the peak heights of the $[\text{M+Li-RCOO}]^+$ (= $[\text{DAG+Li}]^+$) peaks in the MS/MS mass spectra shown in their Figure 2. By doing this, it was determined that SSO and SOS had $[\text{SS}]^+ / [\text{SO}]^+$ ratios of approximately 0.58 and 0.33, respectively, while PPO and POP had $[\text{PP}]^+ / [\text{PO}]^+$ ratios of 0.70 and 0.34, respectively. These values, derived from manually measured heights, have been included in Table 7.2.

In 2001, Hvattum (21) performed non-aqueous reversed-phase HPLC of TAG with ESI-MS detection. Surprisingly, this appears to be the first application of a RP-HPLC/ESI-MS method to TAG analysis. These authors noted that, in an ABC TAG, loss of the substituent in the *sn*-2 position was energetically less favorable than loss of the FA from the *sn*-1 or *sn*-3 positions. In 2002, Dorschel (29) demonstrated RP-HPLC/ESI-MS for analysis of peanut oil, which contains a larger range of FA than most typical vegetable oils. The $[\text{M-RCOO}]^+$ fragment having the lowest abundance was assigned as the $[\text{DAG1,3}]^+$ ion and was used to give a

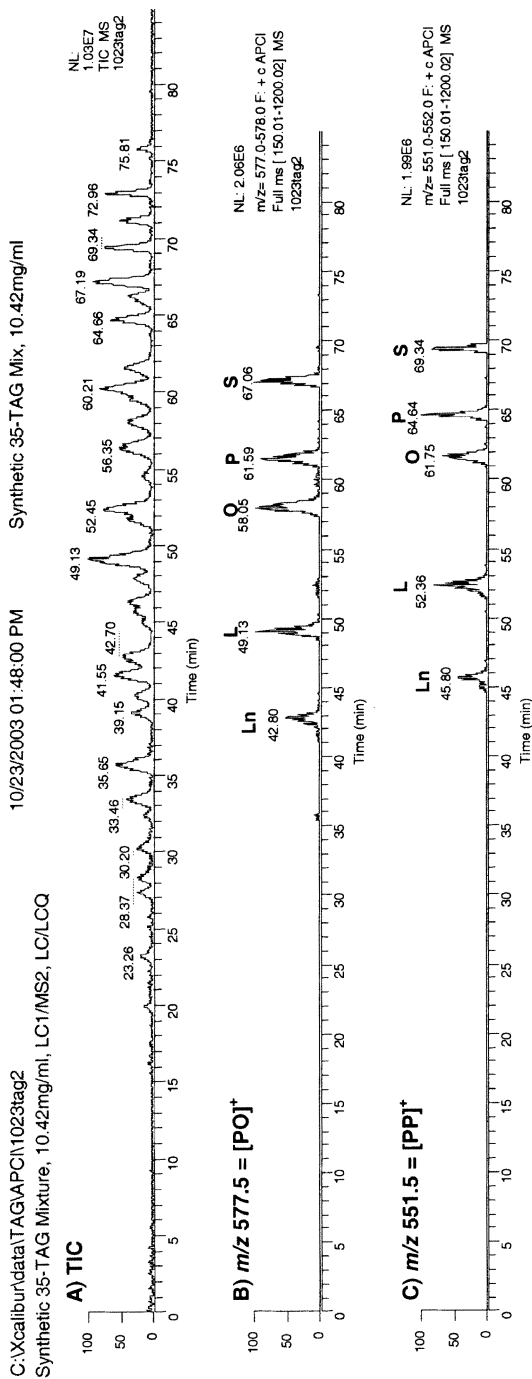


Fig. 7.20. APCI-MS total ion chromatogram, extracted ion chromatograms, and mass spectra of synthetic 35-TAG mixture showing separation of POP and PPO isomers. (A) TIC, (B) EIC of [PO]⁺ at m/z 577.5; (C) EIC of [PP]⁺ at m/z 551.5; (D) [PO]⁺ from 60 to 63 min; (E) [PP]⁺ from 60 to 63 min; (F) Average mass spectrum from 61.1 to 61.3 min (with tabulated abundances); (G) Average mass spectrum from 61.65 to 61.85 min.

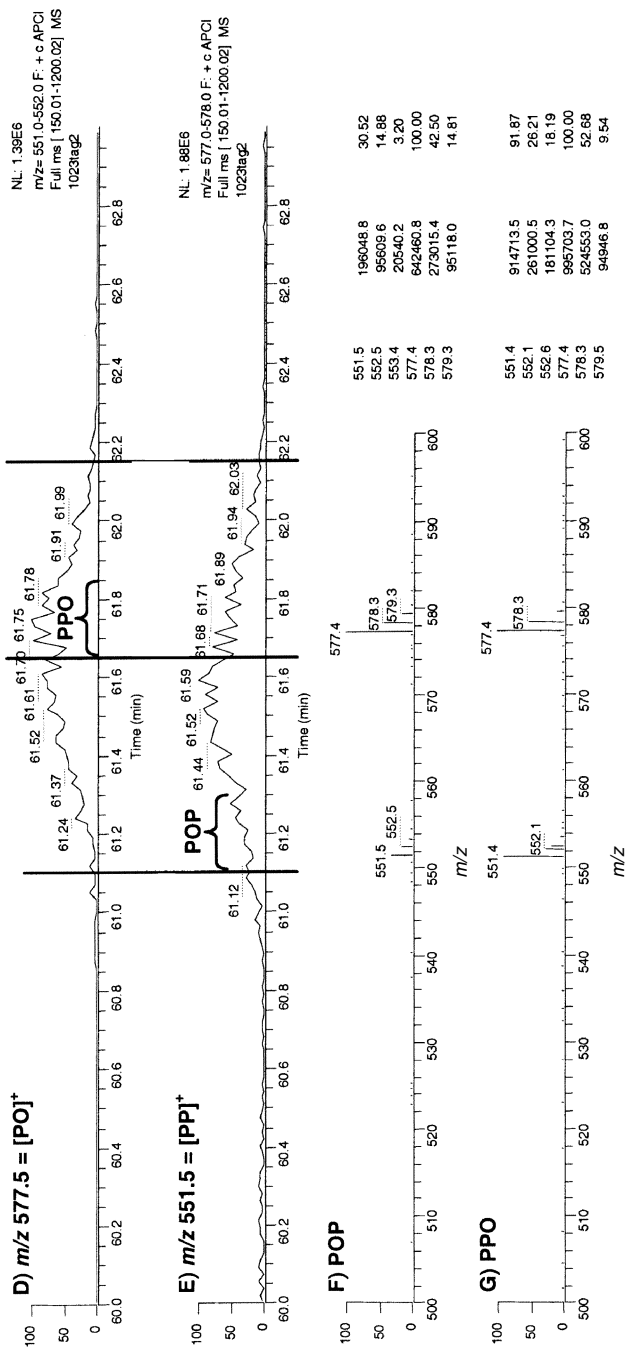


Fig. 7.20. (Continued).

confidence rating for regiospecific assignments of peanut oil TAG. Also in 2002, Byrdwell and Neff (38) reported the direct parallel comparison of $[\text{DAG}]^+$ fragment ion abundances of regiospecific isomers by both APCI-MS and ESI-MS. The preferential loss of the FA substituents in the *sn*-1 and *sn*-3 positions was observed, because loss of the *sn*-2 substituent was energetically disfavored. Byrdwell and Neff (38) reported that abundances of monoacylglycerol-related fragments depended more on the nature of the fatty acyl chains and their degree of unsaturation than on the position of the FA on the glycerol backbone. The $[\text{AA}]^+/\text{[AB]}^+$ ratios reported by Byrdwell and Neff (38) are included in Table 7.2. In 2003, two articles appeared that specifically described analysis of regioisomers of TAG. Marzilli *et al.* (31) reported the analysis of three sets of ABA/AAB isomer pairs and one ABC TAG. The results for the $[\text{AA}]^+/\text{[AB]}^+$ ratios from the report by Marzilli *et al.* (31) are included in Table 7.2. As is now familiar, these authors reported preferential loss of the *sn*-1 and *sn*-3 substituents. The $[\text{DAG}]^+$ fragment arising from loss of the *sn*-2 substituent was the fragment with the lowest abundance. Also in 2003, Kalo *et al.* (35) reported the normal-phase HPLC/ESI-MS analysis of regioisomers of short-chain TAG produced by the sodium methoxide-catalyzed interesterification of sets of short-chain TAG. The short-chain TAG molecular species were detected as their ammonium adduct ions. As expected, these authors reported that the loss of the *sn*-2 substituent was energetically less favorable, and they reported that this tendency was independent of the fatty chain length. These authors accomplished chromatographic separation of many of the isomer pairs. The regioisomers of the short-chain TAGs containing the shortest acyl chain in the secondary position were eluted first on the normal-phase HPLC column, followed by the isomers having the shortest chain in the primary positions (*sn*-1 and *sn*-3).

It is expected that the equations presented in the preceding section for calculation of the % AAB and % ABA from APCI-MS fragment ratios will be equally applicable to analysis by ESI-MS. The endpoint values of the $[\text{AA}]^+/\text{[AB]}^+$ ratios from AAB and ABA determined by ESI-MS, given in Table 7.2, may be substituted into Equation 3 or 4, above. These will allow quantitative estimation of the percentages of the two isomers from the $[\text{AA}]^+/\text{[AB]}^+$ ratio observed in ESI-MS mass spectra.

Quantitative Analysis

TAG Quantification by APCI-MS. Submitted in 1995 and published in 1996 was an article by Byrdwell *et al.* (42) that presented a novel method for accurate quantitative analysis of TAG by APCI-MS. As discussed previously, the degree of unsaturation in a TAG had a direct effect on the ratio of the protonated molecule, $[\text{M}+\text{H}]^+$, to the DAG fragment ions, $[\text{M}-\text{RCOO}]^+$. This was expected to have a strong impact on the response of TAG during quantitative analysis. Byrdwell *et al.* (42) performed analysis of a mixture of monoacid TAG, using d_{12} -PPP as an internal standard. They constructed calibration curves to show that TAG yielded linear response over concentration ranges typically encountered in vegetable oils. The cali-

bration curves exhibited the greatest sensitivity (slope of the calibration curve) for fully saturated TAG, PPP, and the least sensitivity for the most unsaturated TAG, LnLnLn. Triolein, the TAG containing monounsaturated FA, gave intermediate sensitivity. Thus, the degree of unsaturation, and therefore the fragmentation pattern, had a direct impact on the sensitivity of APCI-MS response. We deemed use of calibration curves of individual TAG to be inadequate for TAG analysis for two reasons, and therefore sought a better approach to quantitation. First, there were enough TAG molecular species in a typical natural oil that constructing calibration curves for each TAG for which quantitation was sought was simply not practical. Second, the calibration curves were not linear over several orders of magnitude. Although correlation coefficients for calibration curves were high over a limited concentration range, there was distinct roll-off of the curve at higher concentrations.

To aid in producing a better method for quantitative analysis of real samples, a complex mixture of TAG was synthesized by esterification of five FA with glycerol. The total number of TAG molecular species produced by such esterification is:

$$\# \text{ of TAG molecular species} = \frac{n^3 + 3n^2 + 2n}{6}$$

where n is the number of FA (92). For $n = 5$, the number of TAG produced is 35. This mixture contained completely randomly distributed FA, so the amount of each TAG is given by:

mono-acid:

$$\text{TAG \%} = \frac{\text{FA\%} \cdot \text{FA\%} \cdot \text{FA\%}}{10,000}$$

two FA:

$$\text{TAG \%} = \frac{(\text{FA}_1\% \cdot \text{FA}_1\% \cdot \text{FA}_2\%) \cdot 3}{10,000}$$

three different FA:

$$\text{TAG \%} = \frac{(\text{FA}_1\% \cdot \text{FA}_2\% \cdot \text{FA}_3\%) \cdot 6}{10,000}$$

Thus, the synthetic mixture had a known composition that could be used to assess the effectiveness of different approaches to quantitative analysis (42). It was

hoped that APCI-MS analysis of the 35-TAG mixture would allow a response factor to be determined for each TAG, and that the response factors could then be applied to that TAG in any other mixture of TAG. Unfortunately, this approach to producing “universal response factors” did not produce sufficiently accurate results (42).

The FA composition of the 35-TAG mixture was determined by GC with flame ionization detection (FID) of the FA methyl esters, calibrated with standards of known concentration. The mole percentage composition of the FA methyl esters (FAME) that were produced from the TAG in the 35-TAG mixture is given in Table 7.3, as well as the closely related mole percent of the FA from the FAME. The random distribution of FA had previously been confirmed by lipase hydrolysis (42). The known TAG composition was then calculated from the above equations for the statistical composition, using the mol% of the FA (not FAME) composition. The statistical composition calculated based on the FA composition is given in Table 7.4.

The basis for quantification by HPLC/APCI-MS using the method of Byrdwell *et al.* (36–38) is, first, integration of the areas under peaks (typically five to seven peaks) in each ion chromatogram that is extracted from the sum of all ions over time. The ion chromatograms that are chosen have m/z values corresponding to the $[\text{DAG}]^+$ fragment ions statistically expected based on the sum of all possible combinations of FA on the three positions of the glycerol backbone. If five FA are chosen as the quantitation set, then 35 TAG species are possible, irrespective of regioselectivity, and five peaks in most ion chromatogram will be integrated, one peak for each FA combined the $[\text{DAG}]^+$ fragment to form the TAG, as in Figure 7.20B and Figure 7.20C (APCI-MS) or Figure 7.15A–C and Figure 7.15F (ESI-MS). Of course, the combination of the chromatographic identification of the FA retention pattern based on their equivalent carbon numbers, with the identity of the $[\text{DAG}]^+$ fragment ion known by mass spectrometry, allows qualitative identification of all of the molecular species of TAG contained within the mixture. Some ion chromatograms correspond to isobaric $[\text{DAG}]^+$ fragments, such as m/z 603.5, which represents $[\text{OO}]^+$ and $[\text{SL}]^+$ fragment ions or m/z 601.5, which corresponds to $[\text{OL}]^+$ and $[\text{SLn}]^+$ fragments.

In ideal cases, the peaks corresponding to each FA lost from both isobaric $[\text{DAG}]^+$ fragments are sufficiently resolved to give readily integrated individual areas, and this will result in 10 integrated areas for the two isobaric $[\text{DAG}]^+$ fragments, having each lost each of five possible FA. This is observed in the ESI-MS spectra pictured in Figure 7.15D and Figure 7.15E. When the separation is not ideal, overlapped peaks can occur that require apportionment. We have found that apportionment is best done based on the statistical composition calculated from the FA composition determined from the raw, unadjusted unproportioned integrated EIC peak areas, to produce raw apportioned areas that reflect the trends due to the ionization method, the same as all of the unproportioned peaks exhibit. The trends seen in APCI-MS ion chromatograms (and mass spectra) are opposite the trends

TABLE 7.3
Fatty Acid Compositions Determined from Calibrated GC-FID and Calculated from TAG Compositions Determined by APCI-MS and ESI-MS

| FA | GC-FID (FAME mol%) | RSD % | GC-FID (FA mol%) | Raw LC/APCI-MS | Adjusted LC/APCI-MS | % RSD (n = 3) | Raw LC/ESI-MS | Adjusted LC/ESI-MS | % RSD (n = 4) |
|----|-----------------------|----------|---------------------|-------------------|------------------------|------------------|------------------|-----------------------|------------------|
| P | 20.43 | 0.10 | 20.36 | 25.44 | 20.43 | 0.31 | 17.09 | 20.36 | 0.28 |
| S | 21.07 | 0.05 | 21.10 | 22.42 | 21.21 | 0.51 | 19.48 | 21.23 | 0.63 |
| O | 20.42 | 0.05 | 20.44 | 21.40 | 20.45 | 0.32 | 20.65 | 20.34 | 0.22 |
| L | 19.72 | 0.13 | 19.74 | 17.25 | 19.55 | 0.87 | 21.72 | 19.65 | 0.33 |
| Ln | 18.36 | 0.08 | 18.36 | 13.50 | 18.36 | 0.24 | 21.05 | 18.45 | 0.32 |
| | 100.00 | | 100.00 | 1000.01 | 100.00 | | 99.99 | 100.03 | |

TABLE 7.4

TAG Composition Determined by APCI-MS, and Adjusted Using Response Factors Calculated from the FA Composition Obtained from the FAME Composition Determined by GC-FID^a

| TAG | ECN | R_f $t_m =$ 453 s | \pm SD | Statistical | Raw APCI- MS | Adjusted APCI- MS | \pm SD ($n = 3$) | Error |
|-----------------|-----|---------------------------|----------|------------------------|--------------------|-------------------------|-------------------------|-------|
| PPP | 48 | 7.562 | 0.006 | 0.84 | 1.46 | 0.75 | 0.01 | -0.09 |
| SSS | 54 | 9.049 | 0.014 | 0.94 | 0.98 | 0.82 | 0.07 | -0.12 |
| OOO | 48 | 6.248 | 0.023 | 0.85 | 1.01 | 0.88 | 0.04 | 0.03 |
| LLL | 42 | 3.306 | 0.008 | 0.77 | 0.52 | 0.78 | 0.12 | 0.01 |
| LnLnLn | 36 | 1.655 | 0.029 | 0.62 | 0.31 | 0.78 | 0.04 | 0.16 |
| PSP,SPP (= PPS) | 50 | 8.194 | 0.006 | 2.62 | 3.97 | 2.40 | 0.07 | -0.22 |
| POP, OPP | 48 | 7.188 | 0.003 | 2.54 | 4.06 | 2.49 | 0.08 | -0.06 |
| PLP, LPP | 46 | 5.954 | 0.015 | 2.45 | 3.92 | 2.87 | 0.02 | 0.42 |
| PLnP, LnPP | 44 | 5.075 | 0.009 | 2.28 | 2.91 | 2.53 | 0.07 | 0.25 |
| SPS, PSS | 52 | 8.668 | 0.010 | 2.72 | 3.43 | 2.44 | 0.09 | -0.28 |
| SOS, OSS | 52 | 8.417 | 0.014 | 2.73 | 2.94 | 2.48 | 0.07 | -0.25 |
| SLS, LSS | 50 | 7.772 | 0.003 | 2.64 | 2.91 | 2.96 | 0.12 | 0.32 |
| SLnS, LnSS | 48 | 6.991 | 0.026 | 2.45 | 2.28 | 2.75 | 0.19 | 0.30 |
| POP, POO | 48 | 6.699 | 0.015 | 2.55 | 3.71 | 2.72 | 0.00 | 0.16 |
| SOS, SOO | 50 | 7.580 | 0.006 | 2.65 | 3.21 | 2.76 | 0.10 | 0.12 |
| OLO, LOO | 46 | 5.161 | 0.011 | 2.47 | 2.43 | 2.54 | 0.10 | 0.06 |
| OLnO, LnOO | 44 | 4.347 | 0.021 | 2.30 | 1.83 | 2.27 | 0.19 | -0.03 |
| LPL, PLL | 44 | 4.533 | 0.009 | 2.38 | 1.91 | 2.00 | 0.08 | -0.38 |
| LSL, SLL | 46 | 5.361 | 0.015 | 2.47 | 1.86 | 2.29 | 0.09 | -0.17 |
| LOL, OLL | 44 | 4.195 | 0.011 | 2.39 | 1.86 | 2.33 | 0.12 | -0.06 |
| LLnL, LnLL | 40 | 2.644 | 0.018 | 2.15 | 1.24 | 2.21 | 0.22 | 0.06 |
| LnPLn, PLnLn | 40 | 3.028 | 0.019 | 2.06 | 1.31 | 1.94 | 0.16 | -0.12 |
| LnSLn, SLnLn | 42 | 3.751 | 0.033 | 2.13 | 1.12 | 1.96 | 0.07 | -0.18 |
| LnOLn, OLnLn | 40 | 2.763 | 0.022 | 2.07 | 1.28 | 2.26 | 0.07 | 0.19 |
| LnLLn, LLnLn | 38 | 2.099 | 0.013 | 2.00 | 1.02 | 2.15 | 0.09 | 0.16 |
| SPO | 50 | 7.896 | 0.010 | 5.27 | 7.10 | 5.11 | 0.09 | -0.16 |
| SPL | 48 | 6.966 | 0.030 | 5.09 | 6.83 | 5.89 | 0.32 | 0.80 |
| SPLn | 46 | 5.959 | 0.023 | 4.73 | 5.28 | 5.42 | 0.06 | 0.69 |
| LOP | 46 | 5.511 | 0.027 | 4.93 | 5.21 | 4.57 | 0.33 | -0.36 |
| LnOP | 44 | 4.673 | 0.017 | 4.59 | 4.42 | 4.60 | 0.21 | 0.01 |
| LnLP | 42 | 3.754 | 0.030 | 4.43 | 3.03 | 3.78 | 0.06 | -0.64 |
| LOS | 48 | 6.477 | 0.019 | 5.11 | 5.55 | 5.72 | 0.13 | 0.61 |
| OLnS | 46 | 5.496 | 0.022 | 4.75 | 3.58 | 4.38 | 0.31 | -0.37 |
| LnLS | 44 | 4.543 | 0.014 | 4.59 | 2.73 | 4.00 | 0.13 | -0.59 |
| LLnO | 42 | 3.442 | 0.024 | 4.45 | 2.82 | 4.20 | 0.33 | -0.25 |
| Sum | | | | 100.01 | 100.03 | 100.03 | Avg = | 0.25 |
| | | | | Avg. Abs. % Rel. Error | | 8.70% | | |

^aThe statistical TAG composition calculated from the FA; equivalent carbon numbers (ECN), and Retention Factors (R_f) (= the capacity factor).

observed by ESI-MS, as mentioned previously. Integrated areas under $[\text{DAG}]^+$ fragments in APCI-MS mass spectra of saturated TAG contribute to larger overall areas than the overall areas given by unsaturated TAG, and so larger response is observed from saturated TAG than unsaturated TAG by APCI-MS. Conversely, ESI-MS spectra show more response to unsaturated TAG than saturated TAG, but this is based on molecular adduct ions, rather than $[\text{DAG}]^+$ ions. Other factors that might affect integrated $[\text{DAG}]^+$ areas, such as isotopic peaks observed in ion chromatograms, are discussed further below.

In addition to $[\text{DAG}]^+$ fragments, peaks in ion chromatograms that correspond to the $[\text{M}+\text{H}]^+$ ions in APCI-MS spectra, or the $[\text{M}+\text{NH}_4]^+$ ions in ESI-MS spectra, are integrated to give areas proportional to the abundances of the molecular species, and these reflect trends associated with the method of ionization. APCI-MS and ESI-MS mass spectra both show larger abundances of the near-molecular ions for unsaturated TAG than for saturated TAG. The EIC used to obtain integrated areas of $[\text{M}+\text{H}]^+$ ions and $[\text{M}+\text{NH}_4]^+$ ions can contain several peaks arising from isobaric TAG molecular species. Under the best chromatographic conditions, these are completely resolved, and individual peak areas can be integrated, which are proportional to each $[\text{M}+\text{H}]^+$ for APCI-MS or $[\text{M}+\text{NH}_4]^+$ for ESI-MS. For instance, in the APCI-MS ion chromatogram, the $[\text{M}+\text{H}]^+$ ion at m/z 883.8 arises from OOL (see mass spectrum in Fig. 7.6B), LLS (Fig. 7.6C), and OLnS; similarly, m/z 885.8 is produced by the $[\text{M}+\text{H}]^+$ ions of OOO, LOS (Fig. 7.6D), and LnSS. In addition to the isobaric ions at a particular m/z value, peaks in an EIC can arise from the $2\text{-}^{13}\text{C}$ variant of the TAG molecular species having one more site of unsaturation. Fortunately, these isotopic peaks have shorter retention times, since they are arising from molecules having one more site of unsaturation (but two ^{13}C , which do not noticeably affect retention time). These isotopic peaks can be identified by the retention times of the parent all- ^{12}C TAG, so they can be largely ignored in EIC of the $[(\text{M}+2)+\text{H}]^+$ ions. But it is important not to misidentify and integrate these peaks as normal (all- ^{12}C) TAG, which is what are used for quantification using the reported method (42–44).

When the $[\text{DAG}]^+$ fragment ion and $[\text{M}+\text{H}]^+$ ion abundance areas have been determined, they are combined to give a total area attributable to each TAG molecular species. These total areas reflect the trends attributable to the different ionization modes. Saturates give larger total areas than unsaturates by APCI-MS, if the same molar quantities are present. Conversely, unsaturates give larger total areas than saturates by ESI-MS for equal molar amounts of species. The total areas under the fragment ion peaks and pseudomolecular ions by APCI-MS, or just the molecular adduct ions for ESI-MS, are determined for each TAG molecular species. A bar graph normalized to 100% of the integrated areas of each $[\text{DAG}]^+$ fragment ion peak and the pseudomolecular ion peak (y -axis) versus the mass of the ion (x -axis) is equivalent to the average mass spectrum averaged across the common retention window of the $[\text{DAG}]^+$ fragment ions and the pseudomolecular ion. There may be small differences from the averaged mass spectrum if the integration windows did not all start and end at the exact same time. However, small variations in the integration time windows are

insignificant, since the bulk of the area is centered around the retention time of the species, and differences at the edges of the time window represent a minimal proportion of the areas of the peaks. Regardless, there is uncertainty in the window over which any mass spectrum is averaged, since the exact range may or may not be repetitively chosen if numerous replicates by various users are considered. Furthermore, the species nearer the center of the retention time are a better representation of the population of molecules, with mass spectra at the very edges of the peaks being less typical. It can certainly be concluded that the integrated areas of the $[\text{DAG}]^+$ fragment ions and the $[\text{M}+\text{H}]^+$ ions (or adduct ions in ESI-MS spectra) provide a good representation of the mass spectrum of the population of species.

The sum of the integrated areas of the $[\text{DAG}]^+$ fragment ions and the $[\text{M}+\text{H}]^+$ ions attributable to each TAG molecular species constituted the raw, or unadjusted, TAG area by HPLC/APCI-MS, which is given in Table 7.4. For ESI-MS data, given in Table 7.5, only the $[\text{M}+\text{NH}_4]^+$ peak areas were used for quantification. From the raw TAG composition determined from either ionization method, a FA composition can easily be calculated. Then, the FA composition of the same mixture is determined by GC-FID, by comparison to authentic standards. The GC-FID signal gives the weight percentage composition of the FAME analyzed, so this must be divided by the accurate mass of the FAME and renormalized to convert them to a composition based on the molar quantities of the FAME, and then to the molar quantities of the FA. From the FA composition calculated from the TAG composition and the FA composition determined by calibrated GC-FID, a response factor can be produced for each FA, and then TAG response factors can be derived from the FA response factors.

The response factor calculations start by dividing the FA percentage determined by GC-FID by the FA percentage from the raw APCI-MS composition to get an initial ratio:

$$r_{\text{FA}} = (\text{FA}\%_{\text{GC-FID}})/(\text{FA}\%_{\text{APCI}})$$

FA response factors are then produced by normalizing the ratios to the smallest value:

$$R_{\text{FA}} = r_{\text{FA}}/r_{\text{minimum}}$$

These FA response factors express the net amount of underresponse of each FA, compared to the FA with the most sensitive response. We found that the response of the FA was reflected in the response of the TAG that contained them. Therefore, TAG response factors could be calculated by multiplying the FA response factors together:

$$R_{\text{TAG}} = R_{\text{FA1}} \cdot R_{\text{FA2}} \cdot R_{\text{FA3}}$$

All of these calculations, from summation of DAG fragment areas, to calculation of the raw FA composition, to calculation of response factors, and application of the response factors to the raw TAG composition have been incorporated into a

TABLE 7.5TAG Composition Determined by ESI-MS, and Adjusted Using Response Factors Calculated from the FA Composition Determined by GC-FID^a

| TAG | ECN | R_f $t_m =$ 453 s | \pm SD | Statistical | Raw ESI- MS | Adjusted ESI- MS | \pm SD ($n = 4$) | Error |
|----------------|-----|---------------------------|----------|-------------|------------------------|------------------------|-------------------------|-------|
| PPP | 48 | 7.577 | 0.040 | 0.84 | 0.44 | 0.74 | 0.04 | -0.10 |
| SSS | 54 | 9.060 | 0.028 | 0.94 | 1.06 | 1.36 | 0.12 | 0.42 |
| OOO | 48 | 6.273 | 0.053 | 0.85 | 1.21 | 1.17 | 0.13 | 0.32 |
| LLL | 42 | 3.327 | 0.022 | 0.77 | 1.41 | 1.06 | 0.17 | 0.29 |
| LnLnLn | 36 | 1.660 | 0.017 | 0.62 | 1.05 | 0.69 | 0.07 | 0.07 |
| PSP,SPP(= PPS) | 50 | 8.207 | 0.035 | 2.62 | 1.62 | 2.49 | 0.07 | -0.13 |
| POP, OPP | 48 | 7.203 | 0.049 | 2.54 | 2.02 | 2.84 | 0.20 | 0.30 |
| PLP, LPP | 46 | 5.979 | 0.057 | 2.45 | 1.80 | 2.32 | 0.07 | -0.13 |
| PLnP, LnPP | 44 | 5.087 | 0.042 | 2.28 | 2.73 | 3.38 | 0.34 | 1.10 |
| SPS, PSS | 52 | 8.685 | 0.029 | 2.72 | 1.74 | 2.43 | 0.11 | -0.29 |
| SOS, OSS | 52 | 8.446 | 0.030 | 2.73 | 2.44 | 2.83 | 0.12 | 0.10 |
| SLS, LSS | 50 | 7.801 | 0.039 | 2.64 | 3.54 | 3.78 | 0.25 | 1.14 |
| SLnS, LnSS | 48 | 7.034 | 0.053 | 2.45 | 2.53 | 2.59 | 0.04 | 0.14 |
| POP, POO | 48 | 6.738 | 0.051 | 2.55 | 2.39 | 2.79 | 0.19 | 0.24 |
| SOS, SOO | 50 | 7.615 | 0.033 | 2.65 | 2.36 | 2.50 | 0.04 | -0.15 |
| OLO, LOO | 46 | 5.176 | 0.043 | 2.47 | 2.95 | 2.62 | 0.04 | 0.15 |
| OLnO, LnOO | 44 | 4.365 | 0.036 | 2.30 | 3.25 | 2.78 | 0.04 | 0.48 |
| LPL, PLL | 44 | 4.545 | 0.030 | 2.38 | 1.78 | 1.75 | 0.17 | -0.63 |
| LSL, SLL | 46 | 5.377 | 0.035 | 2.47 | 3.44 | 3.08 | 0.18 | 0.61 |
| LOL, OLL | 44 | 4.211 | 0.030 | 2.39 | 3.22 | 2.64 | 0.11 | 0.25 |
| LLnL, LnLL | 40 | 2.663 | 0.024 | 2.15 | 3.04 | 2.19 | 0.09 | 0.04 |
| LnPLn, PLnLn | 40 | 3.042 | 0.020 | 2.06 | 2.86 | 2.58 | 0.13 | 0.52 |
| LnSLn, SLnLn | 42 | 3.792 | 0.030 | 2.13 | 2.26 | 1.86 | 0.12 | -0.27 |
| LnOLn, OLnLn | 40 | 2.788 | 0.021 | 2.07 | 3.09 | 2.33 | 0.07 | 0.26 |
| LnLLn, LLnLn | 38 | 2.104 | 0.015 | 2.00 | 2.76 | 1.90 | 0.05 | -0.10 |
| SPO | 50 | 7.925 | 0.041 | 5.27 | 3.28 | 4.19 | 0.10 | -1.08 |
| SPL | 48 | 7.010 | 0.060 | 5.09 | 4.11 | 4.81 | 0.13 | -0.28 |
| SPLn | 46 | 5.997 | 0.052 | 4.73 | 4.66 | 5.25 | 0.05 | 0.52 |
| LOP | 46 | 5.550 | 0.041 | 4.93 | 3.83 | 4.10 | 0.84 | -0.83 |
| LnOP | 44 | 4.706 | 0.043 | 4.59 | 4.83 | 4.98 | 0.18 | 0.39 |
| LnLP | 42 | 3.765 | 0.020 | 4.43 | 4.15 | 3.92 | 0.17 | -0.51 |
| LOS | 48 | 6.515 | 0.059 | 5.11 | 5.26 | 5.12 | 0.08 | 0.01 |
| OLnS | 46 | 5.575 | 0.051 | 4.75 | 3.32 | 3.11 | 0.21 | -1.64 |
| LnLS | 44 | 4.561 | 0.027 | 4.59 | 4.44 | 3.82 | 0.31 | -0.77 |
| LLnO | 42 | 3.469 | 0.026 | 4.45 | 5.12 | 4.02 | 0.13 | -0.43 |
| Sum | | | | 100.01 | 99.99 | 100.02 | Avg = | 0.42 |
| | | | | | Avg. Abs. % Rel. Error | | 16.32% | |

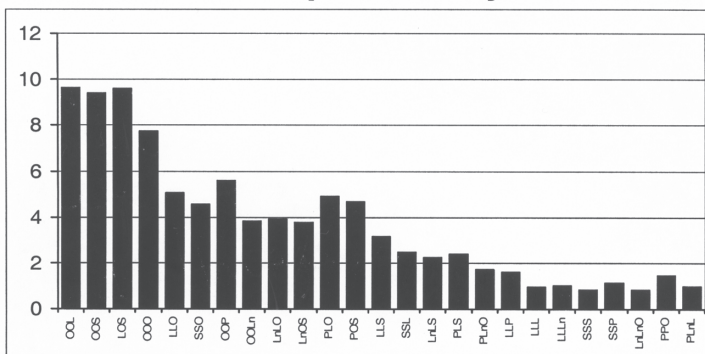
^aAlso listed are the statistical TAG composition calculated from the FA; equivalent carbon numbers (ECN); and Retention factors (R_f) = the capacity factor.

Microsoft EXCEL spreadsheet. All that is required is that the peaks are integrated manually, and the areas are imported into the spreadsheet. Then, the GC-FID composition of the mixture is entered, all calculations are automatically performed, and the final adjusted TAG composition is displayed. The process is shown graphically in Scheme 7.2. This scheme was taken from the report of Byrdwell *et al.* (44) describing the quantitative analysis of margarine basestocks. This article thoroughly described the process, and also described some of the complications involved with analysis of mixtures produced by blending a natural TAG mixture with a few specific TAG molecular species (i.e., hardstocks) to modify the physical and organoleptic characteristics of the base oil. The method for quantitative analysis was also described in our previous book chapter (43).

The process is very effective at producing a TAG composition close to the known composition for standard mixtures (such as the 35-TAG mix) and for interesterified blends, which also have a known composition. Application of the method for quantitative analysis developed by Byrdwell *et al.* (42–44) produced a TAG composition that is very close to the known composition for standard mixtures, and also showed that the FA composition calculated from the adjusted TAG composition determined by LC/APCI-MS was very close to the FA composition determined by calibrated GC-FID. The average error (either absolute or relative) in the FA composition calculated from the TAG composition using this method is lower than the average relative error given by the TAG composition determined by LC with FID detection in nearly all cases. Furthermore, if the average relative error in the FA composition determined from the adjusted TAG composition by APCI-MS is greater than ~5–7%, this is a good indication that there is substantial nonrandom distribution of TAG in the mixture. The error in the FA composition acts as a marker to be able to identify the blending of oils with specific TAG components, as well as other sample treatments. The specific TAG molecular species that are substantially nonrandom can be identified easily by comparing the APCI-MS TAG composition to the statistical TAG composition calculated from the FA composition determined by GC-FID. The calculation of the statistical composition is now a built-in function of the spreadsheet that we use for the rest of the calculations employed for quantitative analysis.

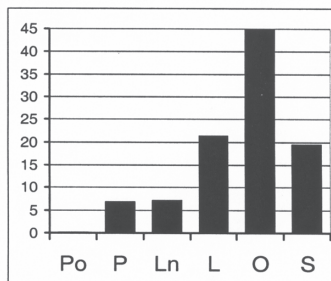
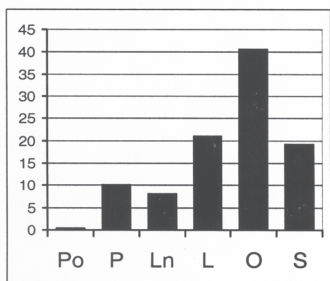
The quantitative analysis method developed by Byrdwell has some inherent characteristics that should be understood for its effective application. First, the method makes the inherent assumption that the over- or underresponse of a FA, as reflected in the calculated FA composition, results from all TAG that contain that FA. This implies that the FA are distributed throughout the TAG (not in statistically predicted proportions, just generally distributed throughout the TAG molecular species). In cases in which a FA is contributed by only a very few TAG in the mixture, this assumption is not accurate. However, in such cases, the calculated FA composition gives an average relative error greater than 5%, so it automatically alerts one to the fact that there is a significantly nonrandom distribution of the FA. So, the method includes a built-in self-check to identify cases where it may require modification.

Raw TAG Composition by APCI-MS



FA
Response
Factors

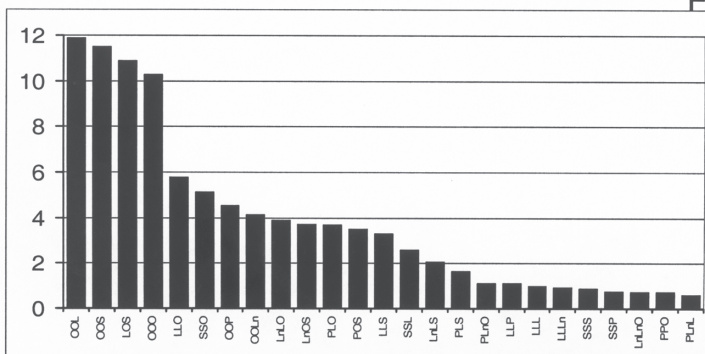
FA Comp. by GC-FID



FA Comp. from MS



TAG
Response
Factors



Adjusted TAG Composition by APCI-MS

Scheme 7.2. Quantitative analysis method, demonstrated using canola oil.

Next, there are cases of intractable overlap of two FA contributing to a peak area in the DAG fragment EIC. Such overlap does not present a great problem. The peak area can easily be apportioned by one of several methods, all of which give essentially the same results. Three methods of overlapped area apportionment may be used: First, other, nonoverlapped peaks within the EIC containing the overlapped peaks can be used to apportion the area. For instance, when the P peak of OO [1] overlapped the O peak of SL [2], the overlapped peak could be apportioned such that the O_1/O_2 and P_1/P_2 are in the same proportions as the nonoverlapped peaks, $(Ln_1 + L_1 + S_1)/(Ln_2 + L_2 + S_2)$. This method of apportionment is very effective, is easily accomplished in the spreadsheet, and keeps the FA in the proper relative proportions. A second method of apportionment is to take advantage of the fact that in every EIC, the FA are in similar proportions. By adding up all of the Ln, L, O, P, and S peak areas, one can get an overall representative ratio of Ln to L to O to P to S that does not change much from EIC to EIC, so that these general ratios could be used to apportion the peak. In this way, overlapped peak area can be divided so that the O_1/O_2 and P_1/P_2 ratios are equal to the overall ratio of O/P in the EIC. Finally, the third method for apportionment is to use the FA composition calculated from the raw, unadjusted composition (since the overlapped area is a raw area), to calculate a raw statistical TAG composition. For example, the statistical composition reflects the fact that there is more POL expected to be present than OSLn, based on the FA composition of the raw data. Thus, the statistical ratio of POL/OSLn can then be used to apportion the P_1+O_2 peak in the proper proportions. Having applied all three possible methods, we have concluded repeatedly that the results from each of the three approaches are essentially indistinguishable. This is due in major part to the fact that such overlapped peaks represent only one of several DAG peak areas that contribute to the total peak area for a particular TAG. A small amount of variation in one of the component areas in one of a large number of TAG turns out to be insignificant. If quantification were based on the areas of peaks appearing in a total ion chromatogram (TIC), instead of summing areas under peaks in specific EIC, overlapped peaks could not be readily differentiated. Using peaks in a TIC, overlapped area is not confined to only one of the several DAG fragment ions. Overall, the most important factor, by far, is adjusting for the net over- or underresponse of FA, which directly impacts the response of the TAG.

One last point is that the areas under the protonated molecules sometimes include several overlapped TAG. These are apportioned by the third approach described above. The $[M+H]^+$ areas must be apportioned based on the proportion of each TAG calculated from the raw area totals from the complete data set. Again, if there is any single TAG present in an unusually high proportion (such as in a blend), this can easily be identified by comparison of the final adjusted composition to the statistically expected composition calculated from the GC-FID FA composition. The method described produces better results for TAG mixtures of known composition than any other method (LC-FID, LC-ELSD) used for TAG quantita-

tive analysis. The method is self-consistent, and provides a built-in check of its accuracy, in the form of the FA composition calculated from the TAG composition.

Byrdwell *et al.* (42–44) did demonstrate one other approach that proved almost as effective as the method described above. If a natural mixture is interesterified (complete randomization should be confirmed by lipase analysis), its composition can be calculated and known from the statistical distribution of the FA composition determined by calibrated GC-FID. The interesterified mixture can be analyzed by HPLC/APCI-MS, and a response factor for every TAG calculated by comparison to the known (statistical) composition. The response factors thus calculated can then be applied to the natural oil. The FA compositions of the interesterified oil and the natural oil are ideally identical, and the concentration of any particular TAG in the natural sample is not radically different from the interesterified oil. This guarantees that the concentration of a TAG in the natural mixture is in the linear range of the TAG in the standard (the interesterified mix). In other words, the concentration of the TAG in the natural mixture will be close to the standard concentration, so that nonlinearity of response of the TAG will not be a problem.

With an understanding of the few caveats mentioned above, quantitative analysis by HPLC/APCI-MS is more accurate than other available methods. The method was used by Byrdwell and Neff (93) for analysis of TAG in normal, high stearic acid and high lauric acid canola oils. This method gave better results than LC with FID detection. In our previous book chapter (43) we described application of the method to the 35-TAG mixture, to normal and randomized lard samples, and to a canola oil/soybean oil saturates (hardstock) blend, with and without interesterification. The average relative error between the FA composition calculated from the APCI-MS TAG composition and the GC-FID FA composition was 0.2 to 1.4% for every sample except for the noninteresterified blend sample. The average relative error for this sample was high, indicating a significantly nonrandom distribution of TAG, as mentioned above. The two TAG responsible for the discrepancy, SSS and SSP, could easily be identified by comparing the APCI-MS TAG composition to the statistical composition. Again, an advantage of the method is that the percent relative error in the FA composition acts as an indicator of the accuracy of the method. Of course, having all of the areas for all [DAG]⁺ fragments for every TAG also allows the [AA]⁺/[AB]⁺ ratio to be constructed for any TAG and used for the determination of the composition of regioisomers.

In addition to the multiple reports by Byrdwell (42–44) *et al.*, Mottram *et al.* (40) also employed this method with good results. Mottram *et al.* (87) also applied the method of Byrdwell *et al.* to regiospecific analysis of animal fats. This method was not as effective for quantification of the FA in the *sn*-2 position as it has been shown to be for overall TAG composition. Schmeer *et al.* (94), Laakso (85), and Laakso and Voutilainen (41) reported quantitation based on the peak areas in the total ion chromatograms. This did not allow quantitative analysis of separate com-

ponents in overlapped peaks. For nonoverlapped peaks, the area under the TIC would include the areas of the DAG fragment ions and the protonated molecule peaks. This is similar to the approach of integrating the peaks in EIC of DAG fragment ions and protonated molecule peaks and adding them together, except that abundances of all background ions would also be included in the TIC area. No response factors were applied to the TIC areas to compensate for differences in response due to differences in the degree of unsaturation.

Holcapek *et al.* (65) performed quantitative analysis of a subset of TAG contained in rapeseed oil and in the mixtures produced by rapeseed oil methanolysis. Simplified quantitative analysis was performed using only three main FA: O, L, and Ln. Quantitative analysis was performed by two methods. In one method, only peaks in the EIC of DAG fragment ions were used. In the second method, peaks in the TIC in the m/z range 200–1000 were used. Both methods were external standard methods. The approach using only DAG fragment ions resulted in lower contents of TAG with high numbers of sites of unsaturation, compared to the method that used the TIC. Correction factors were determined based on the slopes of the calibration curves; however, these did not improve results.

As mentioned in the previous section on TAG regioisomers, Fauconnot *et al.* (86) performed quantitative analysis of regioisomers of TAG by plotting what they termed the “regioisomeric purity,” which was calculated as $[AA]^+ / ([AA]^+ + [AB]^+)$, versus the % AAB. The abundances used by Fauconnot *et al.* (86) were obtained from integration of the peaks in EIC of $[DAG]^+$ fragment ions, as described previously. They did not report integration of $[M+H]^+$ ions, or determination of the quantification of all molecular species in mixtures, although they did show qualitative identification of TAG in several fats and oils. Instead, they used the integrated areas under peaks in the EIC to identify specific regioisomers for which standards were available. They quantified the relative amounts of regioisomers, but not the percentage composition of the entire mixtures.

The method of Byrdwell *et al.* (42–44) appears to be the most accurate method available for current use. It does require integration of a moderate number of fragment ions and pseudomolecular ions, but this effort is rewarded with a complete composition of all TAG molecular species, and enough information to be able to identify any nonstatistical trends in the composition of molecular species. Furthermore, application of this method of quantitation provides all of the information required to allow the $[AA]^+ / [AB]^+$ ratio to be calculated and used for determination of the compositions of regioisomers for which $[AA]^+ / [AB]^+$ ratios of standards (either determined or tabulated) are known. Additionally, the quantitation method allows other ratios to be constructed that provide information that may be related to other trends in the TAG structures.

TAG Quantification by ESI-MS. As mentioned above, TAG exhibited the opposite response under ESI-MS conditions as they did by APCI-MS. Even early reports of ESI-MS for TAG analysis showed that unsaturated TAG produced more

response than did saturated TAG. Of course, when discussing the responses of TAG, observations are based on the areas under peaks in chromatograms of intact ammoniated molecules, because only a few fragments (and these having low abundances) were formed under ESI-MS conditions.

Since we had successfully demonstrated in the past that response factors calculated from FA could be combined to form response factors for TAG determined by APCI-MS, we examined whether this same approach would be successful with TAG analysis by ESI-MS. The same approach that was used for TAG analysis by APCI-MS was applied to the data obtained by ESI-MS.

Table 7.5 lists the statistical composition calculated from the FA composition determined by calibrated GC-FID of the FAME, and lists the raw, unadjusted TAG composition, and the response-factor-adjusted composition determined by using ESI-MS. Comparing Table 7.5 to Table 7.4, it can be seen that the agreement of the ESI-MS data with the statistical composition is poorer than was the agreement of the APCI-MS data. The APCI-MS data gave an average absolute value of error equal to 0.25% absolute error, compared to the statistically predicted composition. ESI-MS, on the other hand, produced 0.42% average absolute error. More importantly, the errors associated with individual TAG in the APCI-MS data, were noticeably smaller than the values for absolute error observed for individual TAG by ESI-MS. The ESI-MS data exhibited a maximum error (for LnOS) of 1.64% (absolute). Given that the percentage of LnOS that was present was 4.75%, the absolute error of 1.64% constituted 34.5% relative error. This level of error is not acceptable, and constitutes a demonstration that the approach used by Byrdwell *et al.* (42–44) for TAG quantitative analysis by APCI is not perfectly applicable to ESI-MS data.

The largest errors in the TAG composition determined by ESI-MS were exhibited by PLnP, SLS, OPS, and LnOS. Three of the four of these TAG had a common feature: the presence of two saturated FA with one polyunsaturated FA. This nonrandom characteristic will hopefully provide clues necessary to improve the method for quantitative analysis applied to ESI-MS data.

Some of the percentages observed from TAG by ESI-MS were close to the statistically expected values, but the agreement overall was poor enough to lead us to conclude that this approach is not useful for TAG quantification from ESI-MS data.

In 1998 Schuyf *et al.* (17) used silver-phase HPLC/ESI-MS for semiquantitative analysis of TAG in vegetable oils. The quantification was based on $[M+Na]^+$ ions produced by addition of 0.1 mM sodium acetate in methanol. Solutions having concentrations less than 100 μ M gave responses that appeared almost linear. These concentrations are approximately 100 times less than the concentrations commonly used for analysis by APCI-MS. This approach gives linear response only for very dilute solutions. HPLC/ESI-MS was performed with a flow rate of 30 μ L/min on samples having concentrations of 0.2 mg/mL. The authors stated that their results were in agreement with the composition obtained by Ag-HPLC-FID, and with the

calculated theoretical values based on complete randomization. The agreement of their values of the compositions of oils determined by Ag-HPLC/ESI-MS with values obtained by Ag-HPLC/ESI-FID was stated to be always better than 5%. The results in their Table 1 gave relative error percentages of 16% for OSO and higher relative error for OSL, compared to the statistically expected composition. While the agreement of some species was good, others showed substantial error. Furthermore, since $[M+Na]^+$ ions were formed for quantitative analysis, MS/MS analysis could not be performed, so additional structural information was not available. The abundances of $[M+Ag]^+$ ions of polyunsaturated TAG (no. double bonds >3) were included in the calculated areas.

Han and Gross addressed quantification of TAG as their $[M+Li]^+$ ions by ESI-MS in 2001 (20). Based on neutral loss scans from $[M+Li]^+$ ion parents, unseparated, infused mixtures of TAG were analyzed. First, they calculated sensitivity correction factors of common TAG molecular species relative to tri-17:1 TAG. These sensitivity factors were defined as the slope of a least-square regressive linear curve fitting function between the molar ratios of mixtures of prepared TAG solutions with tri-17:1 TAG, and the peak intensity ratios of the TAG and the 17:1 internal standard. These are intended to be similar to "universal response factors" for each TAG by ESI-MS. Then, the total ion counts of ions in neutral loss scans of TAG are used to assess the quantitative amounts of TAG molecular species. The standard deviations in the solutions of known composition were from 0.4 to 0.7 absolute units, or from 4 to 8% relative uncertainty. The method was then applied to a rat myocardium tissue extract. This approach remains to be further validated with complex mixtures of TAG of known composition. This approach requires neutral loss scanning on a tandem sector instrument, so it is not applicable to analysis using ion trap instruments. Also, some users prefer not to observe lithium adducts. The lack of chromatographic separation makes proper correction for the $2\text{-}^{13}\text{C}$ isotopic variant contribution essential to accurate quantitation. The $2\text{-}^{13}\text{C}$ isotopic variant contribution correction should be calculated by using the following equation (20):

$$Z = 1 - (I_{M-2}/I_M)0.011^2 m(m-1)/2 \approx 1 - 6.05 \times 10^{-5} m^2 (I_{M-2}/I_M)$$

where Z is the $2\text{-}^{13}\text{C}$ isotopic variant correction factor, m is the total carbon number in the species with lower molecular mass, and I_{M-2} and I_M are peak intensities of ions at molecular weights $M-2$ and M , respectively (20).

In 2003, Fard *et al.* (32) reported the use of high resolution ion cyclotron resonance (ICR) MS for analysis of four mixtures of macadamia nut oil representing the neat oil, the methanol extract of the oil, the esterified oil, and the esterified methanol extract. They reported the TAG compositions of the oil mixtures by infusion of the unseparated mixtures into the ESI source of the Fourier transform (FT) ion cyclotron resonance MS. The normalized percentage composition based on the sodium adducts of TAG, DAG, MAG, FA, and FAME was reported. Also, HPLC

fractions collected from the oil extract were analyzed. But no online HPLC/ESI-MS was reported by the authors. No response factors were applied.

At the time of the writing of this chapter, we must conclude, therefore, that quantitative analysis of TAG by online HPLC/ESI-MS has not yet been satisfactorily addressed. Since the signal from ESI-MS has been shown to be dependent on the degree of unsaturation in the TAG, it is obvious that quantification without response factors is not accurate, except perhaps in very dilute solutions. Peak areas under peaks in the total ion chromatogram of a mixture of TAG will certainly require response factors. A better approach to quantification of TAG by HPLC/ESI-MS remains to be reported.

Other Applications of HPLC/APCI-MS to TAG and FA Analysis

Silver ion (argention) chromatography has been used as an alternative to reversed-phase chromatography for analysis of FA based on their degree of unsaturation. Laakso and Voutilainen (41) were the first to combine Ag^+ -HPLC with detection by APCI-MS for TAG analysis. They separated oils containing high levels of α - and/or γ -linolenic acids. They found that, for pairs of isomeric TAG, the α -linolenic acid-containing TAG eluted after the γ -linolenic acid-containing TAG, due to stronger interaction of the α -isomer. They also found that, in general, the most unsaturated FA esterified in the *sn*-1 or *sn*-3 position gave rise to longer retention times than the same TAG with the most unsaturated FA esterified in the *sn*-2 position. As one would expect from the preceding discussion in this chapter, the APCI-MS mass spectra reflected the positions of the FA chains. The smaller abundance of the *sn*-1,3 DAG fragment ion was used to confirm the elution order of the regioisomeric TAG separated on the Ag^+ -loaded column. Laakso (85) also separated oils rich in α - and γ -linolenic acids using RP-HPLC/APCI-MS. In this report, they showed, among other things, that the position of the double bonds in the molecule also affects the ratio of DAG fragment ions (in addition to the positional placement of the FA chain). This trend was discussed previously in the section on APCI-MS analysis of TAG regioisomers.

As mentioned previously, in the section on quantitative analysis, Holcapek *et al.* (65) performed APCI-MS of biodiesel made from rapeseed oil methanolysis. For qualitative purposes, positive-ion APCI-MS was very effective at allowing identification of monoacylglycerols, methyl esters of FA, diacylglycerols, and triacylglycerols. Only free FA produced no signal by (+) ion APCI-MS. These were readily detected using (-) ion APCI-MS, however. The APCI-MS mass spectra exhibited all of the fragments discussed above and listed in Scheme 7.1. Holcapek *et al.* reported APCI-MS mass spectra for TAG, native intact diacylglycerols, monoacylglycerols, and methyl esters. Spectra of diacylglycerols showed a small abundance of protonated molecules, but mostly lost the glycerol hydroxy group to give DAG fragment ions as base peaks. Similarly, spectra of monoacylglycerols showed small abundances protonated molecules, but the base peaks were formed by loss of one hydroxy group to form the $[\text{RCOO}+58]^+$ (or = $[\text{RCO}+74]^+$) fragment.

It is worth mentioning one important factor concerning APCI-MS mass spectra. The accurate masses of DAG fragment ions (from 500 to 700 amu) typically have mass defects 0.5–0.6. It is very typical for m/z values determined by MS to exhibit some fluctuation, of ~ 0.1 – 0.3 amu, and this is affected by the tuning of the instrument. Thus, a mass of a DAG fragment ion, for example $[\text{OO}]^+$, commonly might fluctuate from m/z 603.4 to m/z 603.7. If masses in mass spectra are simply rounded to the nearest integer mass, the mass might appear as m/z 603 in some spectra and m/z 604 in other mass spectra. Because of this, it is best either to list m/z values to one decimal place in mass spectra, or to list nominal masses, with the mass defect subtracted. If masses are simply rounded, some DAG fragment ions end up having odd m/z values in some spectra while others end up being even. In the case of protonated molecules, the mass defect is ~ 0.7 – 0.8 for typical TAG with molecular masses under 900 amu. If the m/z values in mass spectra are simply rounded, the rounded mass ends up being even, and it is one mass unit larger than the nominal mass.

Shibayama *et al.* (66) reported the use of HPLC/APCI-MS for analysis of triacylglycerols in artists' materials. They examined TAG in the exudate from a painting in the National Gallery of Art (Mark Rothco's "Number 7"), and in extracts of oil paint films. The authors reported that the exudate was composed of palmitic and stearic acids and monoacylglycerols (MAG) and diacylglycerols containing these FA, and tristearin. The acetone extracts of four-year-old linseed oil paint films containing ivory black and Naples yellow were also analyzed, using both positive and negative ion modes. These extracts were then divided into an acetonitrile soluble fraction and a methylene chloride soluble fraction. The acetonitrile fraction contained mostly FA, MAG, and DAG, with some epoxy-FA possibly present. The methylene chloride fraction contained mostly TAG and minimally unsaturated DAG. Positive-ion APCI-MS spectra exhibited all of the fragments shown in Scheme 7.1. Negative-ion APCI-MS mass spectra showed deprotonated molecules of DAG, and fatty acyl anion fragments, as well as others. In the mass spectrum of OPO shown, the ratio of the $[\text{OP}]^+ / [\text{OO}]^+$ DAG fragment ions was ~ 0.5 . This was the statistically expected ratio when two oleoyl acyl chains are combined with one palmitoyl chain.

Boukobza *et al.* (95) have used APCI-MS interfaced directly to a maceration device, without chromatographic separation, to measure volatile components (such as hexanal, hexenal, etc.) given off by tomatoes. Linoleic and linolenic acids were added to the tomato before maceration to determine the amount of increase in the formation of volatiles caused by enzymatic degradation of the FA.

Mu *et al.* (67) reported the analysis of diacylglycerols and triacylglycerols in an interesterified TAG mixture. The authors added 50 mM ammonium acetate at 50 mL/min postcolumn to promote ammonium adduct formation. They produced ammonium adducts, even from saturated TAG, similar to the SFC/APCI-MS results previously shown by Laakso and Manninen (96). Polyunsaturated TAG in the interesterified sample gave both abundant ammoniated and protonated mole-

cules. The APCI-MS spectra of diacylglycerols were similar to those previously reported previously by Shibayama *et al.* (66), but with fewer fragments, and no noticeable protonated (or ammoniated) molecule. Mu and Hoy (97) also reported HPLC/APCI-MS for analysis of lymph TAG. Specific structured lipids were purified and administered to Wistar rats, and the changes in TAG structure due to the lipid absorption and incorporation were detected by using APCI-MS. The appearance of medium-chain (C8:0) FA in the structures of lymph TAG was confirmed.

Parcerisa *et al.* (98) used HPLC/APCI-MS for analysis of olive and hazelnut oils, and mixtures of the two. Hazelnut oil is less expensive than olive oil, and could potentially be used to adulterate olive oil, to produce a lower cost oil. The ratios of peak areas under mass chromatograms 880–884 and 850–857, [880–884]/[850–857], were determined and compared. The mass range 880–884 represented C54:5 to C54:3 (three 18-carbon chains with three to five sites of unsaturation, or ECN 44 to 48), while the mass range 850–857 represented C52:6 to C52:3 (two 18-carbon chains and one 16-carbon chain with three to six sites of unsaturation, ECN 40 to 46). One-way analysis of variance (ANOVA) showed statistically significant different ratios for these two oils. ANOVA analysis of the semiquantitative compositions determined from the TIC showed significant differences in the contents of LLL, LLO, OLnO, LLP, LOO, PLO, PLP, OOO, and POO, indicating that HPLC/APCI-MS would be an appropriate way to detect oil adulteration. APCI-MS of the trimethylsilyl ether derivatives of tocopherol and sterol components similarly revealed differences in the compositions of the original oils, although the data for the mixtures were less clear.

As mentioned in the discussion of the report on milk fat TAG using SFC/APCI-MS by Laakso and Manninen (96), the complexity of milk TAG represents a substantial analytical challenge. Mottram and Evershed (99) applied RP-HPLC/APCI-MS to the problem of milk fat TAG analysis. Prefractionation was a necessary prerequisite to HPLC separation, and two approaches were demonstrated: thin-layer chromatography (TLC) prefractionation, and preparative gel permeation chromatography (GPC). TLC produced only two bands. The first band was still too complex to allow application of RP-HPLC for definitive TAG analysis. The second band was sufficiently simple to allow 28 TAG species to be identified, most containing butyric acid (C4:0). TAG positional isomers in this relatively simple group of TAG were identified by the DAG fragment ion ratios, and it was found that butyric acid was generally not esterified in the *sn*-2 position. GLC of the milk fat TAG proved to be a better approach for prefractionation. The GLC preparative separation provided sixteen fractions that were subsequently separated by RP-HPLC/APCI-MS. Due to low abundances of [RCO]⁺ ions in APCI-MS spectra, GC-MS was also performed on 12 of the 16 fractions. In all, 120 TAG molecular species were identified by the authors, eight of which eluted in more than one peak, due to the presence of geometric isomers.

Kimpe *et al.* (100) published an application of HPLC/APCI-MS to the lipid extracts from seven ceramic oil lamps from the late Roman to early Byzantine

periods. Because triolein was present in the largest abundance in most oils, the authors concluded that olive oil was used in the oil lamps. Linoleic acid-containing TAG were also present in some extracts, leading the authors to conclude that other oils were also used. The presence of large amounts of OSS and OOP in two separate samples also led them to believe that other oils were used. In some samples, saturated TAG were present, leading the authors to conclude that some amount of animal fat was also incorporated into the lamp fuel. A group of unknown compounds eluted before the TAG in the reconstructed ion chromatogram (RIC) shown. No APCI-MS spectra of the unknown components or of TAG were shown in the report. Since the oils analyzed were well over 1,000 years old, it is reasonable to expect that some autoxidation of any sites of unsaturation would have occurred. It would be interesting to determine whether the unknown peaks had masses corresponding to epoxides, ketones, alcohols, or other TAGOX formed from TAG. If this were the case, the observed TAG composition would be that left after the TAG most susceptible to oxidation were degraded to by-products, leaving more stable components intact. There exists the possibility that the observed oils were not completely representative of the original oils, but rather represented the most stable components left after some components were degraded by autoxidation. HPLC/APCI-MS provided valuable data regarding the composition of the TAG composition of the residue, and the APCI-MS spectra of the unknown components may provide additional insight into the process of oil decomposition over the centuries. Kimpe *et al.* (101) more recently applied HPLC/APCI-MS for identification of beeswax and ruminant fat in late Roman cooking pots. Although no mass spectra were shown, the authors reported in tabular form that LC/APCI-MS of saturated monoesters produced $[M-H]^+$ deprotonated positive-ion molecules from wax esters, while unsaturated monoesters form abundant $[M+H]^+$ ions, similar to what Aichholz and Lorbeer (102) had reported by using high temperature GC/MS by chemical ionization with methane reagent gas. But while Aichholz and Lorbeer (102) reported acylium ion fragments, $[RCO]^+$, at m/z 239 (from $C_{15}H_{31}CO^+$) and $[RCOOH+H]^+$ ions at m/z 257 from monoesters. Kimpe *et al.* (101) reported $[RCOO-H_2O]^+$ ions at m/z 237 and $[RCOOH-H]^+$ ions at m/z 255. Kimpe *et al.* used the presence of a *trans* FA to deduce that ruminant fat had been in the cooking pot, and the ratio of C16 to C18 saturated fats to conclude that the fat had been sheep fat. As mentioned, however, caution must be exercised in analysis of data from archaeological samples, because a large amount of polar and/ or lower molecular weight components eluted before the wax esters and TAG in the APCI-MS chromatogram that were not mentioned or discussed. These components could arise from degraded unsaturated TAG, leaving behind only the more stable saturated species.

Other articles published in 2001 included a report by Neff *et al.* (103) describing the HPLC/APCI-MS analysis of TAG high in saturated fats often used in food formulations. Compositions of coconut oil (high in lauric acid and other medium-chain FA), cocoa butter, normal and randomized palm oil, and normal and random-

ized palm olein fractions were determined by using HPLC/APCI-MS. The physical properties of the oils were correlated with TAG composition. For instance, increased amounts of PPP at the expense of the most abundant TAG, POP, caused by interesterification of palm oil and palm olein, are probably responsible for increases in the melting points and the solid fat indices at different temperatures. HPLC/APCI-MS for quantification of TAG in other vegetable oils (corn, soybean, canola, and genetically modified soybean oils), interesterified oil, blended oils, and interesterified blends were also reported by Byrdwell *et al.* (44). This report was discussed in the section on quantitative analysis.

Several brief summaries of previous work also appeared in 2001. Holcapek *et al.* (104) published a summary of their earlier work on APCI-MS for analysis of FAME, MAG, DAG, and TAG, as previously described (65). Neff *et al.* (105,106) published brief summaries of the quantitative method previously described (42–44) for TAG analysis by using APCI-MS with response factors calculated by using the FA composition determined by GC-FID.

A 2002 article by Jakab and Forgacs (107) described the HPLC/APCI-MS analysis of peanut, pumpkin seed, sesame seed, soybean, and wheat germ oils. Two factors made this work unique: (i) The HPLC was performed on a monolithic silica column (a column composed of a single polymeric “rod” instead of packed with particles), and (ii) the authors used principal component analysis and nonlinear mapping to illustrate the differences between oils. The monolithic column produced a complete separation within eight minutes. Without EIC of critical pairs shown, it is difficult to evaluate the quality of the TAG separation on this type of column. Five runs of each of the five oils were performed, and the percent relative standard deviations in the retention times of TAG molecular species using the monolithic column were excellent. Quantitative analysis of the 11 primary TAG was performed by using the EIC of the base peaks in the APCI-MS mass spectra. This meant that the areas under the protonated molecule peaks were used for quantification of polyunsaturated TAG, while the areas of DAG fragment ions were used for quantification of TAG with few sites of unsaturation. These were combined for the total TAG composition of the 11 principal molecular species. No response factors were applied.

Evershed *et al.* (108) reported the application of HPLC/APCI-MS [as well as high temperature (HT) GC, HT-GC/MS, GC/combustion isotope ratio MS, and radiocarbon dating] to animal fats extracted from archaeological pottery, bones, soil and amorphous deposits. They reported that saturated-fat-containing TAG dominated, due to the degradation and loss of unsaturated fatty acyl chains by oxidative decay. The authors assessed the palmitic:stearic (P:S) ratio in the overall extracted fats, and in the *sn*-2 position, as determined by APCI-MS. They found that the fat believed to be of ruminant origin had a similar P:S ratio for the *sn*-2 position as modern cattle adipose fat, while the archaeological sample believed to be of nonruminant origin had a P:S similar ratio to that of modern pig adipose fat.

Another recent article, by Nichols and Davies (109), reported the use of HPLC/APCI-MS for analysis of FA phenacyl esters (FAPE) made from the total

biomass extracted from bacteria in the *Shewanella* genus. APCI-MS was shown to be clearly superior to GC-MS for identification of the PUFA chain length and degree of unsaturation. The presence of protonated molecules in APCI-MS spectra made possible the unequivocal identification of PUFA 2-oxo-phenylethyl esters. Components such as 20:5 were identified by both GC/MS of the FAME and LC/APCI-MS of the FA phenacyl esters. Other components, such as 22:5, 16:4, and 18:4, were observed only in the LC/APCI-MS data, by virtue of the presence of the protonated molecule, $[M+H]^+$, which was not present in the GC/MS data. APCI-MS/MS daughter ion spectra confirmed the presence of species such as 16:4. However, the authors reported that the extreme sensitivity of the APCI-MS technique might lead to identification of possible contaminant peaks that might not otherwise be observed. Also included in this report was analysis of the FAPE from a menhaden oil standard.

Another report in 2002 was that by Neff *et al.* (110) showing the analysis of lard and mutton tallow, which may be used in food formulations. Lard and sheep fats, as well as a mixture of these, were analyzed and quantified by using the HPLC/APCI-MS method previously described (42–44).

In 2003, Holcapek *et al.* (111) reported the characterization of TAG in 16 plant oil samples by using RP-HPLC/APCI-MS. They employed a reversed-phase separation coupled to APCI-MS, and they also reported ESI-MS and MALDI-MS of collected fractions. The authors showed the separation of mono- and diacylglycerols at shorter retention times, in the same run as triacylglycerols. Quantitative analysis was performed by determining the peak areas of TAG using a UV detector at 205 nm, with no response factors. Percentage compositions were provided for hazelnut, pistachio, poppy seed, almond, palm, brazil nut, rapeseed, macadamia, soyabean, sunflower, linseed, *Dracocephalum moldavica*, evening primrose, corn, amaranth, and *Silybum arianum* oils. The authors reported all of the trends with regard to the relationship between the fragmentation pattern and unsaturation that had previously been reported by others. They also reiterated the preferential loss of the FA from the *sn*-1 and *sn*-3 positions that had previously been reported.

Also in 2003, Stubinger *et al.* (112) reported the characterization of castor oil by positive- and negative-ion APCI-MS, and by off-line positive-ion MALDI-TOF MS. The positive-ion mass spectrum of triricinolein presented in that report was essentially identical to the APCI-MS mass spectrum that had been reported by Byrdwell and Neff (113). Stubinger *et al.* (112) identified one hydroxy-DAG and 14 hydroxy-TAG using online chloride-attachment negative-ion APCI-MS. Thirteen hydroxy-TAG were identified by off-line positive-ion MALDI-TOF MS. Several differences between this work (112) and that of Byrdwell and Neff (113) were observed. Byrdwell and Neff had reported adducts at $[M+23]^+$, $[M+39]^+$, $[M+54]^+$, and $[M+59]^+$, which they proposed were related to the acetonitrile in the solvent system. Stubinger *et al.* reported the $[M+23]^+$, but identified it as a sodium adduct, $[M+Na]^+$. No source for sodium was mentioned in the article, although it is

sometimes assumed to come from glass. The $[M+39]^+$ peak was visible in the (+) APCI-MS spectrum shown by Stubinger *et al.*, but it was not mentioned. Byrdwell and Neff had identified 18 TAG (mostly hydroxy-TAG) and 6 DAG in castor oil, as well as 44 TAG (mostly hydroxy-TAG) and 11 DAG in *Lesquerella fendleri* oil, and 47 TAG (mostly hydroxy-TAG) and 12 DAG in *Lesquerella gordonii* oil.

In 2004, van den Berg *et al.* (114) reported an analysis of the effects of traditional processing methods of linseed oil on the composition of its triacylglycerols. A freshly pressed oil and a heated oil were analyzed by using RP-HPLC/APCI-MS. The researchers reported identification of the products of both oxidation and polymerization. The presence of lead increased the degree of oxidation. Among several techniques, the authors used MALDI-TOF MS for analysis of the oligomeric oxidation products, without prior separation. They reported high molecular weight oxidation products up to the size of hexamers, with up to six oxygen atoms. They further reported analysis by ESI coupled to a Fourier transform ion cyclotron resonance mass spectrometer. The results using FTICR MS showed oligomers up to the size of trimers, with and without additional double bonds, and with and without additional oxygen atoms. These results were in complete agreement with the report of Byrdwell and Neff (8), which also came out in 2004. The number of cross-linked TAG observed by Van den Berg *et al.* (114) by MALDI-TOF-MS was 6 TAG, while the number of cross-linked TAG observed by ESI FTICR MS was 3. Van den Berg *et al.* (114) ascribed the differences in the number of cross-linked TAG to the increased sensitivity of MALDI-TOF MS compared to ESI-FTICR MS. This assumes that TAGOX cannot dimerize during MALDI ionization, as they do in an ESI source. Van den Berg *et al.* also showed a mass spectrum obtained by direct temperature resolved mass spectrometry (DTMS), which is a desorption technique.

In 2003, Morera *et al.* (115) reported the use of APCI-MS to characterize the TAG in human milk from a wide variety of subjects. They showed that some TAG were fairly consistent regardless of subject variations, and these included mostly mixed TAG composed of short- and medium-chain FA combined with normal 16 and 18 carbon FA, including (not regiospecific): CaPO, LaCaO, LaPCa LaOL, MPLn, LLO, LaOO, MPL, and MOL. Other TAG were highly variable, depending, of course, on diet and many other considerations. These TAG included PaLS, MPO, PaOO, PPP, MPS, SPP, LOO, PPO, MOS, SSP, POL, and SOS (not regiospecific). Also in 2003, Sandra *et al.* (116) reported an expansion of their earlier SFC/APCI-MS approach. They employed an automated off-line two-dimensional SFC system, using a reversed-phase column first (with UV detection), from which the fractions were collected, reconcentrated, and further separated by their degrees of unsaturation using a silver-loaded column with detection by APCI-MS (and UV detection).

In an analogous LC method that came out in 2004, Dugo *et al.* (117) reported an off-line two-dimensional liquid chromatography system for analysis of rice oil, in which reversed-phase liquid chromatography with UV detection was first performed, followed by fraction collection, reconcentration, and injection onto a sys-

tem employing a silver-loaded LC column coupled to the APCI source of a Shimadzu 2010A mass spectrometer. The first separation was by equivalent carbon number, as usual for TAG separated by RP-HPLC, while the second separation was by degree of unsaturation. Relative abundances of TAG were reported, with no response factors applied.

Dual Parallel Mass Spectrometry

Some of the results above demonstrated the capabilities and the limitations of APCI-MS mass spectra. The soft fragmentation can provide valuable structural information, but excess fragmentation can lead to an overabundance of peaks that have the potential for misinterpretation. It is often beneficial to obtain data from multiple ionization modes to provide multiple confirmatory pieces of data. Such data can take the form of running samples with no up-front CID, and then rerunning the same samples with up-front CID to elicit additional fragmentation, or changing the CID voltages between scans [such as mentioned by Rezanka (118) and used by Couch *et al.* (119)]. Or, data from multiple modes can take the form of performing APCI-MS on the sample and then performing ESI-MS on the same sample [such as done by Byrdwell and Borchman (120)]. However, run-to-run variability between chromatographic runs of complex samples can lead to some uncertainty. The best approach, therefore, is to obtain data from multiple modes of ionization simultaneously from a single chromatographic run. Byrdwell (121) was the first to perform such a “dual parallel mass spectrometer” analysis of lipids. Examples of dual parallel mass spectrometer experiments are given in Chapter 13 in this volume. Chromatograms obtained by APCI-MS during a typical dual parallel mass spectrometer experiment are shown in Figure 7.12. In 1998, this technique was first applied to phospholipids, and highlighted the complementary nature of ESI and APCI ionization methods. For instance, ESI-MS/MS spectra of phosphocholine-containing phospholipids (PC, SPM, DHS, etc.) produced only a choline head group ion, m/z 184, under ESI-MS conditions, so were not shown. Under APCI-MS conditions, on the other hand, phosphocholine phospholipids produced structurally indicative fragment ions ($[DAG]^+$ fragments, $[RCOO+58]^+$, $[RCO]^+$, etc.). For phospholipids, acquisition of both types of data can be crucial to correct identification of molecular species.

Since that first publication, other applications of multiple ionization modes have been demonstrated for lipid analysis. Siegel *et al.* (122) developed a dual ESI/APCI ionization source for use on their Micromass Platform II mass spectrometer that was capable of alternating between APCI and ESI modes, or operating in a combined mode. While an excellent concept that will probably be incorporated into source designs by others, the source did have some limitations. The optimal conditions for ESI were not the same as those for APCI, so either compromise conditions had to be used, which limited sensitivity, or a time delay had to be incorporated to allow conditions to change between the optimal conditions for the two modes. The authors reported a 30-s delay between modes to achieve desired temperatures. This

delay gave the instrument a longer duty cycle and limited the number of spectra that could be obtained in a given amount of time. Also, low flow rates of $\sim 50 \mu\text{L}/\text{min}$ were used instead of conventional analytical-scale flow rates. Of course, the use of one single mass spectrometer to obtain complementary data is the great benefit of such an approach. Siegel *et al.* (122) showed good quality positive- and negative-ion APCI and ESI mass spectra that demonstrated the proof of concept.

The advantage of the true “dual parallel MS” approach demonstrated by Byrdwell (121) is that optimal conditions can be used for both ionization modes, and the duty cycles of both mass spectrometers can be used to the greatest benefit. Positive- and negative-ion spectra can be obtained, and MS^n can be performed on an instrument dedicated to a single ionization mode. The first dual parallel MS report used a single quadrupole MS with an APCI source in parallel with a tandem mass spectrometer with an ESI source. Recently, Byrdwell and Neff (38) improved this arrangement during application of the dual parallel MS approach for analysis of TAG and TAGOX. In this report, they used a tandem mass spectrometer to perform APCI-MS and MS/MS in parallel with an ion trap mass spectrometer on which they performed ESI-MS, MS/MS, and MS/MS/MS. They employed ammonium formate as a sheath liquid, which produced abundant $[\text{M}+\text{NH}_4]^+$ ions from all TAG and TAGOX under ESI-MS conditions. This made ESI-MS more sensitive than APCI-MS for both TAG and TAGOX, and allowed HMW TAGOX oligomers to be observed intact. These large oligomers produced inadequate protonated or other near-molecular ions under APCI-MS conditions. However, the rich fragmentation patterns of smaller TAG and TAGOX ($m/z < 2000$) under APCI-MS conditions were invaluable for structural elucidation.

In the initial reports by Byrdwell *et al.*, two mass spectrometers were attached to one LC system, in a configuration now referred to as an LC1/MS2 arrangement. Most recently, Byrdwell has used dual parallel mass spectrometers in a new and unprecedented way (123). Two mass spectrometers were attached to two liquid chromatographic systems: a normal phase system and a reversed-phase system. A total lipid extract, such as that obtained using the method of Folch *et al.* (124) or Bligh and Dyer (125) contains both neutral lipids (TAG, cholesteryl esters, etc.) and polar lipids (phospholipids, etc.). Usually, if analysis of both classes is desired, these must be prefractionated into non-polar and polar components. Or, the non-polar lipids can be eluted as a bolus near the solvent front during a separation of polar lipids, or vice versa. The newest method developed by Byrdwell allows one injection of a total lipid extract to be separated by two chromatographic systems and detected by two mass spectrometers, simultaneously. This is referred to as an LC2/MS2 arrangement. The sample injection is loaded onto a polar (amine) column; see Byrdwell (121) or Byrdwell and Borchman (120). The non-polar components pass down the column essentially unretained. These are passed through a switching valve on the front of the ion trap mass spectrometer where they are diverted to a second LC system employing RP-HPLC attached to a tandem mass spectrometer having an APCI interface (alternatively, ESI-MS with ammonium formate may be used on both instruments). Typical

chromatograms from such an LC2/MS2 configuration, and thorough discussion of the results, are given in Chapter 13.

Both LC1/MS2 and LC2/MS2 configurations can be used with ESI or APCI on either instrument, along with positive- or negative-ion acquisition modes, and MSⁿ on the ion trap instrument or MS/MS on the tandem instrument. The variety of possible configurations gives a great amount of options to the analyst, and maximizes the versatility of the instrumentation. A prodigious amount of data is obtained from a dual parallel arrangement that can allow structural identification and quantitative analysis.

Acknowledgments

The help, advice, and assistance from my long-time collaborator and friend William E. Neff are gratefully acknowledged. The ongoing support and collaboration of Kathleen Warner, Sevim Erhan, and other members of the Industrial Oil Research Unit at the National Center for Agricultural Utilization Research in Peoria, IL, is gratefully acknowledged.

References

1. Byrdwell, W.C., Atmospheric Pressure Chemical Ionization Mass Spectrometry for Analysis of Lipids, *Lipids* 36: 327–346 (2001).
2. Byrdwell, W.C., APCI-MS for Lipid Analysis, *inform* 9: 986–997 (1998).
3. Byrdwell, W.C., APCI-MS in Lipid Analysis, in *Advances in Lipid Methodology—Five*, edited by R.O. Adlof, The Oily Press, Bridgwater, England, 2003, pp. 171–253.
4. Byrdwell, W.C., Liquid Chromatography/Atmospheric Pressure Chemical Ionization Mass Spectrometry for Lipid Analysis, in *HPLC of Acyl Lipids*, edited by J.T. Lin and T.A. McKeon, HNB Publishing, New York, in press (2005).
5. Laakso, P., Mass Spectrometry of Triacylglycerols, *Eur. J. Lipid Sci. Technol.* 104: 43–49 (2002).
6. Myher, J.J. and A. Kuksis, Electrospray-MS for Lipid Identification, *Inform* 6: 1068–1072 (1995).
7. Pulfer, M., and R.C. Murphy, Electrospray Mass Spectrometry of Phospholipids, *Mass Spectrom. Rev.* 22: 332–364 (2003).
8. Byrdwell, W.C., Liquid Chromatography with Electrospray Ionization Mass Spectrometry for Lipid Analysis, in *HPLC of Acyl Lipids*, edited by J.T. Lin and T.A. McKeon, HNB Publishing, New York, still in press (2005).
9. Tyrefors, L.N., R.X. Moulder, and K.E. Markides, Interface for Open Tubular Column Supercritical Fluid Chromatography/Atmospheric Pressure Chemical Ionization Mass Spectrometry, *Anal. Chem.* 65: 2835–2840 (1993).
10. Byrdwell, W.C., and E.A. Emken, Analysis of Triglycerides Using Atmospheric Pressure Chemical Ionization Mass Spectrometry, *Lipids* 30: 173–175 (1995).
11. Neff, W.E., and W.C. Byrdwell, Soybean Oil Triacylglycerol Analysis by Reversed-Phase High-Performance Liquid Chromatography Coupled with Atmospheric Pressure Chemical Ionization Mass Spectrometry, *J. Am. Oil Chem. Soc.* 72: 1185–1191 (1995).
12. Neff, W.E., and W.C. Byrdwell, Triacylglycerol Analysis by High Performance Liquid Chromatography-Atmospheric Pressure Chemical Ionization Mass Spectrometry: *Crepis alpina* and *Vernonia galamensis* Seed Oils, *J. Liquid Chromatogr.* 18: 4165–4181 (1995).

13. Duffin, K.L., J.D. Henion, and J.J. Shieh, Electrospray and Tandem Mass Spectrometric Characterization of Acylglycerol Mixtures That are Dissolved in Non-polar Solvents, *Anal. Chem.* 63: 1781–1788 (1991).
14. Myher, J.J., A. Kuksis, K. Geher, P.W. Park, and D.A. Diersen-Schade, Stereospecific Analysis of Triacylglycerols Rich in Long-Chain Polyunsaturated Fatty Acids, *Lipids* 31: 207–215 (1996).
15. Sandra, P., A. Dermaux, V. Ferraz, M.M. Dittmann, and G. Rozing, Analysis of Triglycerides by Capillary Electrochromatography, *J. Microcolumn Separations* 9: 409–419 (1997).
16. Dermaux, A., A. Medvedovici, M. Ksir, E. van Hove, M. Talbi, and P. Sandra, Elucidation of Triglycerides in Fish Oil by Packed-Column Supercritical Fluid Chromatography Fractionation Followed by Capillary Electrochromatography and Electrospray Mass Spectrometry, *J. Microcolumn Separations* 11: 451–459 (1999).
17. Schuyl, P.J.W., T. de Joode, M.A. Vasconcellos, and G.S.M.J.E. Duchateau, Silver-Phase High-Performance Liquid Chromatography-Electrospray Mass Spectrometry of Triacylglycerols, *J. Chromatogr. A* 810: 53–61 (1998).
18. Cheng, C., M.L. Gross, and E. Pittenauer, Complete Structural Elucidation of Triacylglycerols by Tandem Sector Mass Spectrometry, *Anal. Chem.* 70: 4417–4426 (1998).
19. Hsu, F.F., and J. Turk, Structural Characterization of Triacylglycerols as Lithiated Adducts by Electrospray Ionization Mass Spectrometry Using Low-Energy Collisionally Activated Dissociation on a Triple Stage Quadrupole Instrument, *J. Am. Soc. Mass Spectrom.* 10: 587–599 (1999).
20. Han, X., and R.W. Gross, Quantitative Analysis and Molecular Species Fingerprinting of Triglyceride Molecular Species Directly from Lipid Extracts of Biological Samples by Electrospray Ionization Tandem Mass Spectrometry, *Anal. Biochem.* 295: 88–100 (2001).
21. Hvattum, E., Analysis of Triacylglycerols with Non-Aqueous Reversed Phase Liquid Chromatography and Positive Ion Electrospray Tandem Mass Spectrometry, *Rapid Commun. Mass Spectrom.* 15: 187–190 (2001).
22. Sjoval, O., A. Kuksis, and H. Kallio, Reversed-Phase High-Performance Liquid Chromatographic Separation of *tert*-Butyl Hydroperoxide Oxidation Products of Unsaturated Triacylglycerols, *J. Chromatogr. A* 905: 119–132 (2001).
23. Sjoval, O., A. Kuksis, and H. Kallio, Analysis of Molecular Species of Peroxide Adducts of Triacylglycerols Following Treatment of Corn Oil with *tert*-Butyl Hydroperoxide, *Lipids* 36: 1347–1356 (2001).
24. Sjoval, O., A. Kuksis, and H. Kallio, Formation of Triacylglycerol Core Aldehydes During Rapid Oxidation of Corn and Sunflower Oils with *tert*-Butyl Hydroperoxide/Fe²⁺, *Lipids* 37: 81–94 (2002).
25. Yli-Jokipii, K., H. Kallio, U. Schwab, H. Mykkanen, J.P. Kurvinen, M.J. Savolainen, R.L. Tahvonen, Effects of Palm Oil and Transesterified Palm Oil on Chylomicron and VLDL Triacylglycerol Structures and Postprandial Lipid Response, *J. Lipid Res.* 42: 1618–1625 (2001).
26. Yli-Jokipii, K.M., U.S. Schwab, R.L. Tahvonen, J.P. Kurvinen, H.M. Mykkanen, and H.P.T. Kallio, Triacylglycerol Molecular Weight and to a Lesser Extent, Fatty Acid Positional Distribution, Affect Chylomicron Triacylglycerol Composition in Women, *J. Nutr.* 132: 924–929 (2002).
27. Yli-Jokipii, K.M., U.S. Schwab, R.L. Tahvonen, J.P. Kurvinen, H.M. Mykkanen, and

- H.P.T. Kallio, Chylomicron and VLDL TAG Structures and Postprandial Lipid Response Induced by Lard and Modified Lard, *Lipids* 38: 693–703 (2003).
28. Yli-Jokipii, K.M., U.S. Schwab, R.L. Tahvonen, X.B. Xu, H.L. Mu, and H.P.T. Kallio, Positional Distribution of Decanoic Acid: Effect on Chylomicron and VLDL TAG Structures and Postprandial Lipemia, *Lipids* 39: 373–381 (2004).
 29. Dorschel, C.A., Characterization of the TAG of Peanut Oil by Electrospray LC-MS-MS, *J. Am. Oil Chem. Soc.* 79: 749–753 (2002).
 30. Sandra, P., A. Medvedovici, Y. Zhao, and F. David, Characterization of Triglycerides in Vegetable Oils by Silver-Ion Packed-Column Supercritical Fluid Chromatography Coupled to Mass Spectroscopy with Atmospheric Pressure Chemical Ionization and Coordination Ion Spray, *J. Chromatogr. A* 974: 231–241 (2002).
 31. Marzilli, L.A., L.B. Fay, F. Dionisi, and P. Vouros, Structural Characterization of Triacylglycerols Using Electrospray Ionization-MSn Ion-Trap MS, *J. Am. Oil Chem. Soc.* 80: 195–202 (2003).
 32. Fard, A.M., A.G. Turner, and G.D. Willett, High-Resolution Electrospray-Ionization Fourier-Transform Ion Cyclotron Resonance and Gas Chromatography-Mass Spectrometry of Macadamia Nut Oil, *Aust. J. Chem.* 56: 499–508 (2003).
 33. Wu, Z.G., R.P. Rodgers, and A.G. Marshall, Characterization of Vegetable Oils: Detailed Compositional Fingerprints Derived from Electrospray Ionization Fourier Transform Ion Cyclotron Resonance Mass Spectrometry, *J. Agric. Food Chem.* 52: 5322–5328 (2004).
 34. Han, X.L., and R.W. Gross, Global Analyses of Cellular Lipidomes Directly from Crude Extracts of Biological Samples by ESI Mass Spectrometry: A Bridge to Lipidomics, *J. Lipid Res.* 44: 1071–1079 (2003).
 35. Kalo, P., A. Kemppinen, V. Ollilainen, and A. Kuksis, Analysis of Regioisomers of Short-Chain Triacylglycerols by Normal Phase Liquid Chromatography-Electrospray Tandem Mass Spectrometry, *Int. J. Mass Spectrom.* 229: 167–180 (2003).
 36. Segall, S.D., W.E. Artz, D.S. Raslan, V.P. Ferraz, and J.A. Takahashi, Ouricuri (*Syagrus coronata*) Triacylglycerol Analysis Using HPLC and Positive Ion Electrospray Tandem MS, *J. Am. Oil Chem. Soc.* 81: 143–149 (2004).
 37. Malone, M., and J.J. Evans, Determining the Relative Amounts of Positional Isomers in Complex Mixtures of Triglycerides Using Reversed-Phase High-Performance Liquid Chromatography-Tandem Mass Spectrometry, *Lipids* 39: 273–284 (2004).
 38. Byrdwell, W.C., and W.E. Neff, Dual Parallel Electrospray Ionization and Atmospheric Pressure Chemical Ionization Mass Spectrometry (MS), MS/MS and MS/MS/MS for the Analysis of Triacylglycerols and Triacylglycerol Oxidation Products, *Rapid Commun. Mass Spectrom.* 16: 300–319 (2002).
 39. Mottram, H.R., and R.P. Evershed, Structure Analysis of Triacylglycerol Positional Isomers Using Atmospheric Pressure Chemical Ionisation Mass Spectrometry, *Tetrahedr. Lett.* 37: 8593–8596 (1996).
 40. Mottram, H.R., S.E. Woodbury, and R.P. Evershed, Identification of Triacylglycerol Positional Isomers Present in Vegetable Oils by High Performance Liquid Chromatography Atmospheric Pressure Chemical Ionization Mass Spectrometry, *Rapid Commun. Mass Spectrom.* 11: 1240–1252 (1997).
 41. Laakso, P., and P. Voutilainen, Analysis of Triacylglycerols by Silver-Ion High-Performance Liquid Chromatography-Atmospheric Pressure Chemical Ionization Mass Spectrometry, *Lipids* 31: 1311–1322 (1996).
 42. Byrdwell, W.C., E.A. Emken, W.E. Neff, and R.O. Adlof, Quantitative Analysis of

- Triglycerides Using Atmospheric Pressure Chemical Ionization Mass Spectrometry, *Lipids* 31: 919–935 (1996).
43. Byrdwell, W.C., and W.E. Neff, Qualitative and Quantitative Analysis of Triacylglycerols Using Atmospheric Pressure Chemical Ionization Mass Spectrometry, in *New Techniques and Applications in Lipid Analysis*, edited by R.E. McDonald and M.M. Mossoba, AOCS Press, Champaign, IL, 1997, pp. 45–80.
 44. Byrdwell, W.C., W.E. Neff, and G.R. List, Triacylglycerol Analysis of Potential Margarine Base Stocks by High Performance Liquid Chromatography with Atmospheric Pressure Chemical Ionization Mass Spectrometry and Flame Ionization Detection, *J. Agric. Food Chem.* 49: 446–457 (2001).
 45. Dole, M., R.L. Hines, L.L. Mack, R.C. Mobley, L.D. Ferguson, and M.B. Alice, Gas Phase Macroions, *Macromolecules* 1: 96–97 (1968).
 46. Dole, M., L.L. Mack, and R.L. Hines, Molecular Beams of Macroions, *J. Chem. Phys.* 49: 2240–2249 (1968).
 47. Mack, L.L., P. Kralik, A. Rheude, and M. Dole, Molecular Beams of Macroions, II, *J. Chem. Phys.* 52: 4977–4986 (1970).
 48. Yamashita, M., and J.B. Fenn, Electrospray Ion Source—Another Variation on the Free Jet Theme, *J. Phys. Chem.* 88: 4451–4459 (1984).
 49. Yamashita, M., and J.B. Fenn, Negative Ion Production with the Electrospray Ion Source, *J. Phys. Chem.* 88: 4671–4675 (1984).
 50. Whitehouse, C.M., R.N. Dreyer, M. Yamashita, and J.B. Fenn, Electrospray Interface for Liquid Chromatographs and Mass Spectrometers, *Anal. Chem.* 57: 675–679 (1985).
 51. Iribarne, J.V., and B.A. Thomson, Evaporation of Small Ions from Charged Droplets, *J. Chem. Phys.* 64: 2287–2293 (1976).
 52. Thomson, B.A., and J.V. Iribarne, Field-Induced Ion Evaporation from Liquid Surfaces at Atmospheric Pressure, *J. Chem. Phys.* 71: 4451–4463 (1979).
 53. Bruins, A.P., T.R. Covey, and J.D. Henion, Ion Spray Interface for Combined Liquid Chromatography/Atmospheric Pressure Ionization Mass Spectrometry, *Anal. Chem.* 59: 2642–2646 (1987).
 54. Niessen, W.M.A., *Liquid Chromatography-Mass Spectrometry, Chromatographic Science Series*, edited by J. Cazes, Marcel Dekker, Inc., New York, 1999.
 55. Cole, R.B., *Electrospray Ionization Mass Spectrometry: Fundamentals, Instrumentation, and Applications*, John Wiley & Sons, Inc., New York, 1997.
 56. Horning, E.C., M.G. Horning, D.I. Carroll, I. Dzidic, and R.N. Stillwell, New Picogram Detection System Based on a Mass Spectrometer with an External Ionization Source at Atmospheric Pressure, *Anal. Chem.* 45: 936–943 (1973).
 57. Horning, E.C., D.I. Carroll, I. Dzidic, K.D. Haegele, M.G. Horning, and R.N. Stillwell, Atmospheric Pressure Ionization (API) Mass Spectrometry. Solvent-Mediated Ionization of Samples Introduced in Solution and in a Liquid Chromatographic Effluent Stream, *J. Chromatogr. Sci.* 12: 725–729 (1974).
 58. Carroll, D.I., I. Dzidic, R.N. Stillwell, M.G. Horning, and E.C. Horning, Subpicogram Detection System for Gas Phase Analysis Based upon Atmospheric Pressure Ionization (API) Mass Spectrometry, *Anal. Chem.* 46: 706–710 (1974).
 59. Carroll, D.I., I. Dzidic, R.N. Stillwell, K.D. Haegele, and E.C. Horning, Atmospheric Pressure Ionization Mass Spectrometry: Corona Discharge Ion Source for Use in Liquid Chromatography-Mass Spectrometer-Computer Analytical System, *Anal. Chem.* 47: 2369–2373 (1975).

60. Good, A., D.A. Durden, and P. Kebarle, Ion-Molecule Reactions in Pure Nitrogen and Nitrogen Containing Traces of Water at Total Pressures 0.5–4 Torr. Kinetics of Clustering Reactions Forming $H^+(H_2O)_n$, *J. Chem. Phys.* 52: 212–221 (1970).
61. Horning, E.C., M.G. Horning, D.I. Carroll, I. Dzidic, and R.N. Stillwell, New Picogram Detection System Based on a Mass Spectrometer with an External Ionization Source at Atmospheric Pressure, *Anal. Chem.* 45: 936–943 (1973).
62. Manninen, P., and P. Laakso, Capillary Supercritical Fluid Chromatography-Atmospheric Pressure Chemical Ionization Mass Spectrometry of Triacylglycerols in Berry Oils, *J. Am. Oil Chem. Soc.* 74: 1089–1098 (1997).
63. Murphy, R.C., in *Handbook of Lipid Research 7: Mass Spectrometry of Lipids*, edited by F. Snyder, Plenum Press, New York, 1993, p. 213.
64. Hsu, F.F., and J. Turk, Electrospray Ionization/Tandem Quadrupole Mass Spectrometric Studies on Phosphatidylcholines: The Fragmentation Processes, *J. Am. Soc. Mass Spectrom.* 14: 352–363 (2003).
65. Holcapek, M., P. Jandera, J. Fischer, and B. Prokes, Analytical Monitoring of the Production of Biodiesel by High-Performance Liquid Chromatography with Various Detection Methods, *J. Chromatogr. A* 858: 13–31 (1999).
66. Shibayama, N., S. Quillen Lomax, K. Sutherland, and E.R. de la Rie, Atmospheric Pressure Chemical Ionization Liquid Chromatography Mass Spectrometry and Its Application to Conservation: Analysis of Triacylglycerols, *Stud. Conserv.* 44: 253–268 (1999).
67. Mu, J., H. Sillen, and C.E. Hoy, Identification of Diacylglycerols and Triacylglycerols in a Structured Lipid Sample by Atmospheric Pressure Chemical Ionization Liquid Chromatography/Mass Spectrometry, *J. Am. Oil Chem. Soc.* 77: 1049–1059 (2000).
68. Kusaka, T., S. Ishihara, M. Sakaida, A. Mifune, Y. Nakano, K. Tsuda, M. Ikeda, and H. Nakano, Composition Analysis of Normal Plant Triacylglycerols and Hydroperoxidized *rac*-1-Stearoyl-2-oleoyl-3-linoleoyl-*sn*-glycerols by Liquid Chromatography-Atmospheric Pressure Chemical Ionization Mass Spectrometry, *J. Chromatogr. A* 730: 1–7 (1996).
69. Neff, W.E., and W.C. Byrdwell, Characterization of Model Triacylglycerol (Triolein, Trilinolein and Trilinolenin) Autoxidation Products *via* High-Performance Liquid Chromatography Coupled with Atmospheric Pressure Chemical Ionization Mass Spectrometry, *J. Chromatogr. A* 818: 169–186 (1998).
70. Byrdwell, W.C., and W.E. Neff, Non-Volatile Products of Triolein Produced at Frying Temperatures Characterized Using Liquid Chromatography with Online Mass Spectrometric Detection, *J. Chromatogr. A* 852: 417–432 (1999).
71. Byrdwell, W.C., and W.E. Neff, Autoxidation Products of Normal and Genetically Modified Canola Varieties Determined Using Liquid Chromatography with Mass Spectrometric Detection, *J. Chromatogr. A* 905: 85–102 (2001).
72. Adas, F., D. Picart, F. Berthou, B. Simon, and Y. Amet, Liquid Chromatography-Mass Spectrometry and Gas Chromatography-Mass Spectrometry of ω and (ω -1)-Hydroxylated Metabolites of Elaidic and Oleic Acids in Human and Rat Liver Microsomes, *J. Chromatogr. B* 714: 133–144 (1998).
73. Bylund, J., J. Ericsson, and E. Oliw, Analysis of Cytochrome P450 Metabolites of Arachidonic and Linoleic Acids by Liquid Chromatography-Mass Spectrometry with Ion Trap MS^2 , *Anal. Biochem.* 265: 55–68 (1998).
74. Mochida, Y., Y. Yokoyama, and S. Nakamura, Effect of Ammonia Addition to the Mobile Phase on Atmospheric Pressure Chemical Ionization Mass Spectrometry of

- Methyl Hydroperoxyoleates, *J. Mass Spectrom. Soc. Jpn.* 46: 246–249 (1998).
75. Byrdwell, W.C., Dual Parallel Mass Spectrometers for Analysis of Sphingolipid, Glycerophospholipid and Plasmalogen Molecular Species, *Rapid Commun. Mass Spectrom.* 12: 256–272 (1998).
 76. Ravandi, A., A. Kuksis, J.J. Myher, and L. Marai, Determination of Lipid Ester Ozonides and Core Aldehydes by High-Performance Liquid Chromatography with On-Line Mass Spectrometry, *J. Biochem. Biophys. Methods* 30: 217–285 (1995).
 77. Sjoval, O., A. Kuksis, L. Mairai, and J.J. Myher, Elution Factors of Synthetic Oxotriacylglycerols as an Aid in Identification of Peroxidized Natural Triacylglycerols by Reversed-Phase High-Performance Liquid Chromatography with Electrospray Mass Spectrometry, *Lipids* 32: 1211–1218 (1997).
 78. Sjoval, O., A. Kuksis, and H. Kallio, Reversed-Phase High-Performance Liquid Chromatographic Separation of *tert*-Butyl Hydroperoxide Oxidation Products of Unsaturated Triacylglycerols, *J. Chromatogr. A* 905: 119–132 (2001).
 79. Steenhorst-Slikkerveer, L., A. Louter, H.G. Janssen, and C. Bauer-Plank, Analysis of Nonvolatile Lipid Oxidation Products in Vegetable Oils by Normal-Phase High Performance Liquid Chromatography with Mass Spectrometric Detection, *J. Am. Oil Chem. Soc.* 77: 837–845 (2000).
 80. Giuffrida, F., F. Destailats, F. Robert, L.H. Skibsted, and F. Dionisi, Formation and Hydrolysis of Triacylglycerol and Sterol Epoxides: Role of Unsaturated Triacylglycerol Peroxy Radicals, *Free Rad. Biol. Med.* 37: 104–114 (2004).
 81. Giuffrida, F., F. Destailats, F. Robert, L.H. Skibsted, and F. Dionisi, Formation and Hydrolysis of Triacylglycerol and Sterol Epoxides: Role of Unsaturated Triacylglycerol Peroxy Radicals, *Free Rad. Biol. Med.* 37: 104–114 (2004).
 82. Giuffrida, F., F. Destailats, F. Robert, L.H. Skibsted, and F. Dionisi, Formation and Hydrolysis of Triacylglycerol and Sterol Epoxides: Role of Unsaturated Triacylglycerol Peroxy Radicals, *Free Rad. Biol. Med.* 37: 104–114 (2004).
 83. Dobarganes, M.C., M.C. Perezcamino, and G. Marque-Ruiz, High-Performance Size Exclusion Chromatography of Polar Compounds in Heated and Non-Heated Fats, *Fett Wissensch. Technol.* 90: 308–311 (1988).
 84. Byrdwell, W.C., and W.E. Neff. Electrospray Ionization Mass Spectrometry of High Molecular Weight Triacylglycerol Oligomers, *J. Am. Oil Chem. Soc.* 81: 13–26 (2004).
 85. Laakso, P., Characterization of α - and γ -Linolenic Acid Oils by Reversed-Phase High-Performance Liquid Chromatography-Atmospheric Pressure Chemical Ionization Mass Spectrometry, *J. Am. Oil Chem. Soc.* 74: 1291–1300 (1997).
 86. Fauconnot, L., J. Hau, J.M. Aeschlimann, L.B. Fay, and F. Dionisi, Quantitative Analysis of Triacylglycerol Regioisomers in Fats and Oils Using Reversed-Phase High-Performance Liquid Chromatography and Atmospheric Pressure Chemical Ionization Mass Spectrometry, *Rapid Commun. Mass Spectrom.* 18: 218–224 (2004).
 87. Mottram, H.R., Z.M. Crossman, and R.P. Evershed, Regiospecific Characterisation of the Triacylglycerols in Animal Fats Using High Performance Liquid Chromatography-Atmospheric Pressure Chemical Ionisation Mass Spectrometry, *Analyst* 126: 1018–1024 (2001).
 88. Jakab, A., I. Jablonkai, and E. Forgacs, Quantification of the Ratio of Positional Isomer Dilinoleoyl-Oleoyl Glycerols in Vegetable Oils, *Rapid Commun. Mass Spectrom.* 17: 2295–2302 (2003).

89. Byrdwell, W.C., APCI-MS in Lipid Analysis, in *Advances in Lipid Methodology—Five*, edited by R.O. Adlof, The Oily Press, Bridgwater, England, 2003, p. 200.
90. Agren, J.J., and A. Kuksis, Analysis of Diastereomeric DAG Naphthylethylurethanes by Normal-Phase HPLC with On-Line Electrospray MS, *Lipids* 37: 613–619 (2002).
91. Cheng, C., M.L. Gross, and E. Pittenauer, Complete Structural Elucidation of Triacylglycerols by Tandem Sector Mass Spectrometry, *Anal. Chem.* 70: 589 (1998).
92. Daubert, B.F., The Composition of Fats, *J. Am. Oil Chem. Soc.* 26: 556–558 (1949).
93. Byrdwell, W.C., and W.E. Neff, Analysis of Genetically Modified Canola Varieties by Atmospheric Pressure Chemical Ionization Mass Spectrometric and Flame Ionization Detection, *J. Liquid Chromatogr. Rel. Technol.* 19: 2203–2225 (1996).
94. Schmeer, K., G. Nicholson, S. Zhang, E. Bayer, and K. Bohning-Gaese, Identification of the Lipids and the Ant Attractant 1,2-Dioleoylglycerol in the Arils of *Commiphora guil-laumini* Perr. (Bursaceae) by Supercritical Fluid Chromatography-Atmospheric Pressure Chemical Ionisation Mass Spectrometry, *J. Chromatogr. A* 727: 139–146 (1996).
95. Boukobza, F., P.J. Dunphy, and A.J. Taylor, Measurement of Lipid Oxidation-Derived Volatiles in Fresh Tomatoes, *Postharvest Biol. Technol.* 23: 117–131 (2001).
96. Laakso, P., and P. Manninen, Identification of Milk Fat Triacylglycerols by Capillary Supercritical Fluid Chromatography-Atmospheric Pressure Chemical Ionization Mass Spectrometry, *Lipids* 32: 1285–1295 (1997).
97. Mu, H., and C.E. Hoy, Application of Atmospheric Pressure Chemical Ionization Liquid Chromatography-Mass Spectrometry in Identification of Lymph Triacylglycerols, *J. Chromatogr. B* 748: 425–437 (2000).
98. Parcerisa, J., I. Casals, J. Boatella, R. Codony, and M. Rafecas, Analysis of Olive and Hazelnut Oil Mixtures by High-Performance Liquid Chromatography-Atmospheric Pressure Chemical Ionisation Mass Spectrometry of Triacylglycerols and Gas-Liquid Chromatography of Non-Saponifiable Compounds (Tocopherols and Sterols), *J. Chromatogr. A* 881: 149–158 (2000).
99. Mottram, H.R., and R.P. Evershed, Elucidation of the Composition of Bovine Milk Fat Triacylglycerols Using High-Performance Liquid Chromatography-Atmospheric Pressure Chemical Ionisation Mass Spectrometry, *J. Chromatogr. A* 96: 239–253 (2001).
100. Kimpe, K., P.A. Jacobs, and M. Waelkens, Analysis of Oil Used in Late Roman Oil Lamps with Different Mass Spectrometric Techniques Revealed the Presence of Predominantly Olive Oil Together with Traces of Animal Fat, *J. Chromatogr. A* 937: 87–95 (2001).
101. Kimpe, K., P.A. Jacobs, and M. Waelkens, Mass Spectrometric Methods Prove the Use of Beeswax and Ruminant Fat in Late Roman Cooking Pots, *J. Chromatogr. A* 968: 151–160 (2002).
102. Aichholz, R., and E. Lorbeer, Investigation of Combwax of Honeybees with High-Temperature Gas Chromatography and High-Temperature Gas Chromatography-Chemical Ionization Mass Spectrometry II: High Temperature Gas Chromatography-Chemical Ionization Mass Spectrometry, *J. Chromatogr. A* 883: 75–88 (2000).
103. Neff, W.E., W.C. Byrdwell, and G.R. List, Triacylglycerol Structures of Food Fats High in Saturated Acids by HPLC and Mass Spectrometry, *J. Liquid Chromatogr. Rel. Technol.* 24: 837–854 (2001).
104. Holcapek, M., P. Jandera, and J. Fischer, Analysis of Acylglycerols and Methyl Esters of Fatty Acids in Vegetable Oils and in Biodiesel, *Crit. Rev. Anal. Chem.* 31: 53–56 (2001).

105. Neff, W.E., W.C. Byrdwell, and G.R. List, A New Method to Analyze Triacylglycerol Composition of Vegetable Oils, *Cereal Foods World* 46: 6–10 (2001).
106. Neff, W.E., G.R. List, and W.C. Byrdwell, New Tool for Triacylglycerol Analysis in Food Oils, *Lipid Technol.* 13: 15–17 (2001).
107. Jakab, A., and E. Forgacs, Characterization of Plant Oils on a Monolithic Silica Column by High-Performance Liquid Chromatography-Atmospheric Pressure Chemical Ionization-Mass Spectrometry, *Chromatographia* 56 (Suppl.): S69–S73 (2002).
108. Evershed, R.P., S.N. Dudd, M.S. Copley, R. Berstan, A.W. Stott, H. Mottram, S.A. Buckley, and Z. Crossman, Chemistry of Archaeological Animal Fats, *Accounts Chem. Res.* 35: 660–668 (2002).
109. Nichols, D.S., and N.W. Davies, Improved Detection of Polyunsaturated Fatty Acids as Phenacyl Esters Using Liquid Chromatography-Ion Trap Mass Spectrometry, *J. Microbiol. Methods* 50: 103–113 (2002).
110. Neff, W.E., W.C. Byrdwell, K.R. Steidley, G.R. List, and G. Snowder, Triacylglycerol Structure of Animal Tallows, Potential Food Formulation Fats, by High Performance Liquid Chromatography Coupled with Mass Spectrometry, *J. Liquid Chromatogr. Rel. Technol.* 25: 985–998 (2002).
111. Holcapek, M., P. Jandera, P. Zderadicka, and L. Hrubá, Characterization of Triacylglycerol and Diacylglycerol Composition of Plant Oils Using High-Performance Liquid Chromatography-Atmospheric Pressure Chemical Ionization Mass Spectrometry, *J. Chromatogr. A* 1010: 195–215 (2003).
112. Stubinger, G., E. Pittenauer, and G. Allmaier, Characterisation of Castor Oil by On-Line and Off-Line Non-Aqueous Reversed-Phase High Performance Liquid Chromatography-Mass Spectrometry (APCI and UV/MALDI), *Phytochem. Anal.* 14: 337–346 (2003).
113. Byrdwell, W.C., and W.E. Neff, Analysis of Hydroxy-Containing Seed Oils Using Atmospheric Pressure Chemical Ionization Mass Spectrometry, *J. Liquid Chromatogr. Rel. Technol.* 21: 1485–1501 (1998).
114. van den Berg, J.D.J., N.D. Vermist, L. Carlyle, M. Holcapek, and J.J. Boon, Effects of Traditional Processing Methods of Linseed Oil on the Composition of Its Triacylglycerols, *J. Separat. Sci.* 27: 181–199 (2004).
115. Morera, S., A.I. Castellote, O. Jauregui, I. Casals, and M.C. Lopez-Sabater, Triacylglycerol Markers of Mature Human Milk, *Eur. J. Clin. Nutr.* 57: 1621–1626 (2003).
116. Sandra, P., A. Medvedovici, and F. David, Comprehensive pSFCxpSFC-MS for the Characterization of Triglycerides in Vegetable Oils, *LC GC Eur.* 16: 32–34 (2003).
117. Dugo, P., O. Favoino, P.Q. Tranchida, G. Dugo, and L. Mondello, Off-Line Coupling of Non-Aqueous Reversed-Phase and Silver Ion High-Performance Liquid Chromatography-Mass Spectrometry for the Characterization of Rice Oil Triacylglycerol Positional Isomers, *J. Chromatogr. A* 1041: 135–142 (2004).
118. Rezanka, T., Analysis of Polyunsaturated Fatty Acids Using High Performance Liquid Chromatography-Atmospheric Pressure Chemical Ionization Mass Spectrometry, *J. High Resol. Chromatogr.* 23: 338–342 (2000).
119. Couch, L.H., M.I. Churchwell, D.R. Doerge, W.H. Tolleson, and P.C. Howard, Identification of Ceramides in Human Cells Using Liquid Chromatography with Detection by Atmospheric Pressure Chemical Ionization Mass Spectrometry, *Rapid Commun. Mass Spectrom.* 11: 504–512 (1997).

120. Byrdwell, W.C., and D. Borchman, Liquid Chromatography/Mass Spectrometric Characterization and Dihydro sphingomyelin of Human Lens Membranes, *Ophthalm. Res.* 29: 191–206 (1997).
121. Byrdwell, W.C., Dual Parallel Mass Spectrometers for Analysis of Sphingolipid, Glycerophospholipid and Plasmalogen Molecular Species, *Rapid Commun. Mass Spectrom.* 12: 256–272 (1998).
122. Siegel, M.M., K. Tabei, F. Lambert, L. Candela, and B. Zoltan, Evaluation of a Dual Electrospray Ionization/Atmospheric Pressure Chemical Ionization Source at Low Flow Rates (~50 $\mu\text{L}/\text{min}$) for the Analysis of Both Highly and Weakly Polar Compounds, *J. Am. Soc. Mass Spectrom.* 9: 1196–1203 (1998).
123. Byrdwell, W.C., Dual Parallel Liquid Chromatography/Dual Mass Spectrometry (LC2/MS2) of Bovine Brain Total Lipid Extract, *J. Liquid Chromatogr. Rel. Technol.* 26: 3147–3181 (2004).
124. Folch, J., M. Lees, and G.H. Sloane Stanley, A Simple Method for the Isolation and Purification of Total Lipides from Animal Tissues, *J. Biol. Chem.* 226: 497–509 (1957).
125. Bligh, E.G., and W.J. Dyer, A Rapid Method of Total Lipid Extraction and Purification, *Can. J. Biochem. Physiol.* 37: 911–917 (1959).

Chapter 8

Analysis of Carotenoids Using Atmospheric Pressure Chemical Ionization Mass Spectrometry

Natasa Pajkovic and Richard B. van Breemen

Department of Medicinal Chemistry and Pharmacognosy, University of Illinois College of Pharmacy, Chicago, IL 60612

Introduction

Carotenoids are naturally occurring pigments found in a wide variety of plants, algae and several lower organisms (1), and more than 600 naturally occurring carotenoids have been isolated and characterized (2). Due to an extensive conjugated polyene chain, carotenoids typically are bright yellow, orange, red, or purple with absorption maxima in the range of 400–500 nm (3). These polyisoprenoid compounds are synthesized by plants and microorganisms and interact with chlorophyll during photosynthesis to absorb light and transfer energy (4–6). Another result of their conjugated polyene chain is the ability of carotenoids to quench singlet oxygen and free radicals and thereby protect plants from photo-oxidative damage (5,6). Carotenoids have been classified into two groups, hydrocarbon carotenes and oxygenated xanthophylls (7), and the structures of carotenes and xanthophylls that are common in the human diet are shown in Figure 8.1.

In addition to their protective functions in plants, diverse biological functions in humans have been attributed to carotenoids (8,9). Approximately 50 carotenoids are precursors of vitamin A, which is essential for vision, cellular differentiation, and embryological development (10). It has been suggested that carotenoids can function in humans as antioxidants and immunoenhancers (11), as well as prevent age-related macular degeneration (12), cancer (13), and cardiovascular disease (14). Because of these clinical effects, the importance of the detection and identification of carotenoids in natural sources, biological tissues, and clinical samples has been increasing during the last 10 years.

Because of their extended system of conjugated double bonds, carotenoids are usually unstable in the presence of light, heat, or oxygen (7). Therefore, the isolation, identification, and quantitation of these pigments can be challenging (15). Complex biological samples such as human serum, tissues, and plant material often contain compounds that can interfere with the isolation of carotenoids or mixtures of carotenoids with similar structures. Therefore, the identification and quantitation of specific carotenoids requires highly sensitive and selective analytical methods (15,16).

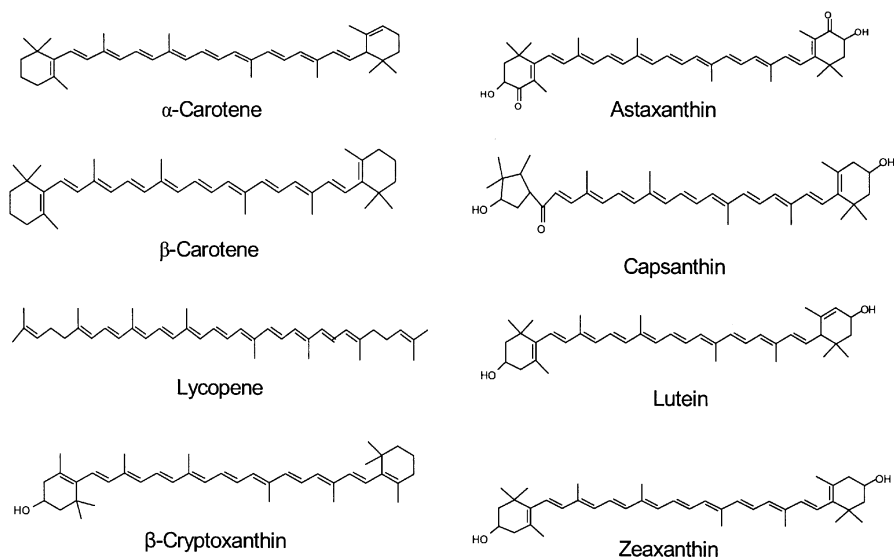


Fig. 8.1. Structures of some common dietary carotenoids.

Gas chromatography (GC) and GC-mass spectrometry (GC-MS) are unsuitable for the analysis of carotenoids because of the thermal instability of these compounds. Therefore, high-performance liquid chromatography (HPLC) with UV/visible (UV/vis) absorbance and LC-mass spectrometry (LC-MS) detection are preferred for the separation, identification, and quantitative analysis of carotenoids occurring in biological or other complex samples (16). Both normal-phase and reversed-phase HPLC have been applied to carotenoid separations, and most current methods use reversed-phase stationary supports. Reversed-phase HPLC and LC-MS of carotenoids may be performed by using C_{18} stationary phases, but C_{30} columns are often used to enhance the separation of *cis* and *trans* isomers as well as to provide efficient separation of xanthophylls and carotenes (17). Compared to C_{18} media, C_{30} stationary phases provide more interaction between carotenoids and the solid phase and provide greater chromatographic separation of carotenoids containing only small structural differences. Although isocratic mobile phases may be used, gradient elution can shorten the separation time while providing superior resolution and sharper chromatographic peaks. Typically, the polar xanthophylls elute first during reversed-phase HPLC followed by the less polar carotenoids. Interestingly, lycopene elutes after β -carotene and α -carotene on C_{30} columns but elutes before them when using monomeric C_{18} columns (17).

Since the levels of carotenoids in biological tissues are often low, highly sensitive analytical methods must be used for their analysis (18). The introduction of photodiode array (PDA) detectors has improved the sensitivity of carotenoid analyses using HPLC with UV/vis absorbance detectors. However, this method is

not specific enough for the unambiguous identification of carotenoids in complex biological matrices because of the possibility of spectral interferences from coeluting impurities and structurally similar carotenoids. Since many carotenoids have overlapping UV/vis absorbances, complete separations are crucial to avoid interferences during analysis. In addition, comparison of absorbance spectra and HPLC retention times with those of authentic standards are necessary for carotenoid identification (19).

Compared to absorbance detection for HPLC, mass spectrometry provides the advantages of higher sensitivity and selectivity for the analysis of carotenoids. High sensitivity enables the analysis of carotenoids at very low levels in small samples such as tissue biopsies, and high selectivity excludes interfering substances that might lead to misidentification or incorrect quantitative measurements. One benefit of the high selectivity of LC-MS and LC-MS/MS compared to many other analytical methods for carotenoids is that sample preparation may be streamlined (18). Rapid analysis saves time and reduces carotenoid degradation that might occur during sample preparation. Finally, the tandem combination of HPLC, in-line absorbance detection, and mass spectrometry can provide even greater selectivity than any one or two methods for the unambiguous identification of carotenoids (20,21).

Approaches to the LC-MS Analysis of Carotenoids

Five LC-MS techniques have been reported for carotenoid analysis including moving belt LC-MS, particle beam ionization LC-MS (LC/PBI-MS), continuous-flow fast atom bombardment LC-MS (LC/CF-FAB MS), electrospray ionization LC-MS (LC/ESI-MS), and atmospheric pressure chemical ionization LC-MS (LC/APCI-MS). The first LC-MS technique used for carotenoid analysis was the moving belt interface with electron impact (EI) or chemical ionization (CI) (19). In this LC-MS technique, the belt transports the HPLC effluent through a series of heated and evacuated desolvation chambers to evaporate the solvent. Solid analyte is then transported by the belt to the ion source of the mass spectrometer where it is flash evaporated and then ionized by EI or CI. Disadvantages of the moving belt interface for carotenoid analysis are loss of chromatographic separation, pyrolysis, incomplete analyte volatilization during flash evaporation, and excessive fragmentation during EI or CI. Molecular ions are of low abundance or even not detected so that the determination of molecular weight (M.W.) might be compromised (15,16). Using a moving belt system, Taylor and colleagues (19) observed the molecular ion of β -carotene in low abundance but no molecular ions for lutein. Instead, dehydrated ions, $[M-H_2O]^+$, and other fragment ions were observed in the lutein mass spectrum. This study by Taylor and colleagues (19) in 1990 was also an early application of LC-MS/MS to carotenoid analysis.

In the particle beam interface, the HPLC effluent is sprayed into a near-atmospheric pressure desolvation chamber. As the solvent evaporates, an aerosol of analyte particles is separated from the lower M.W. solvent molecules in a momentum separa-

tor. When the sample particles enter the ion source of the mass spectrometer, they strike a heated metal surface and are first vaporized before being ionized by EI or CI. To minimize fragmentation and enhance sensitivity and selectivity, negative-ion electron capture chemical ionization may be used during particle beam LC-MS analysis of carotenoids. For example, Khachik and colleagues (22–24) reported the application of particle beam LC-MS to the analysis of carotenoids in extracts of human serum and human milk (24). Carotenes formed abundant molecular anions, M^- , and xanthophylls formed abundant $[M-H_2O]^-$ ions. In another example, Kelm and colleagues (25) used particle beam LC-MS for the quantitative analyses of stable isotope-labeled and unlabeled carotenoids in plasma.

During CF-FAB, the HPLC effluent is mixed with a liquid matrix of low volatility. The mobile phase evaporates when exposed to the low pressure of the ion source, and the remaining thin film of matrix and analyte is bombarded by a beam of atoms or ions at high energy (typically xenon atoms at 3–10 kV or cesium ions at 10–20 kV). The matrix facilitates the transfer of energy from the fast atoms or ions to the analyte, which is then desorbed into the gas phase and ionized. For the analysis of carotenoids, the most effective FAB matrix has been 3-nitrobenzyl alcohol (20). Using this matrix, molecular ions, M^+ , are formed for both xanthophylls and carotenes instead of protonated or deprotonated molecules, which are characteristic of most FAB mass spectra.

In addition to LC/CF-FAB MS, van Breemen and colleagues (26) reported the use of LC-MS/MS for the analysis and identification of carotenoids in extracts of fruits and vegetables. Fragmentation during LC/CF-FAB MS was very low, and the limit of detection was comparable to PDA detection (9–28 pmol injected on-column). During LC/CF-FAB-MS/MS, molecular ions were selected for collision-induced dissociation (CID) and the resulting tandem mass spectra were analyzed for structurally significant fragment ions. In addition to fragment ions such as the elimination of toluene from the molecular ions of the isomeric carotenes such as β -carotene, α -carotene, and lycopene (i.e., m/z 444), some unique fragment ions were detected, such as m/z 467 (loss of a terminal isoprene group) that distinguished lycopene and m/z 480 (retro-Diels-Alder fragmentation) that was specific for α -carotene. An advantage of LC/CF-FAB MS compared to particle beam LC-MS for the analysis of carotenoids is the high abundance of molecular ions for both xanthophylls and carotenes. A disadvantage of CF-FAB is the high maintenance of the LC-MS interface, which results in low sample throughput.

Electrospray ionization is a unique LC-MS technique in that it removes the HPLC solvent and ionizes the analyte simultaneously instead of in discrete stages. During electrospray ionization, the HPLC effluent is sprayed through a capillary at high potential (usually 2–7 kV) relative to a surrounding electrode. The high electric field facilitates the formation of an aerosol of highly charged droplets at atmospheric pressure. This process may be facilitated by a coaxial flow of nebulizing gas. As the charged droplets move toward the opening of the mass spectrometer, they encounter a counter current of heated nitrogen gas, which accelerates the

evaporation of solvent from the droplets. As the droplets shrink in size, the electrostatic repulsion between solution phase ions probably exceeds the combined energies of solvation and surface tension so that ions are ejected from the droplets. Alternatively, the droplets might disintegrate or completely evaporate, thereby releasing analyte ions into the gas phase.

Van Breemen (27) reported in 1995 the first application of electrospray LC-MS to the analysis of carotenoids. In this study, carotenoids were separated by using C_{30} reversed-phase HPLC and both negative-ion and positive-ion electrospray ionization were evaluated. Xanthophylls such as lutein and β -cryptoxanthin formed protonated or deprotonated molecules during positive-ion or negative-ion electrospray, respectively. Carotenes like *cis* and *trans* isomers of β -carotene formed M^+ ions without fragmentation during positive ion electrospray, but no signals were observed using negative-ion mode. The limits of detection were 1 and 2 pmol for lutein and β -carotene, respectively, which were approximately 100-fold more sensitive than the PDA absorbance detector used in this study.

APCI is a two-step process beginning with nebulization of the HPLC eluate through a heated probe to form a spray of uncharged droplets at atmospheric pressure. This process is summarized in Figure 8.2. Evaporation of the droplets is facilitated by a countercurrent or crosscurrent flow of heated nitrogen gas. Once in the gas phase, solvent molecules are ionized by a continuous corona discharge to create a steady state of reagent gas ions for chemical ionization. As sample molecules eluting from the HPLC column enter the gas phase and interact with these reagent gas ions, they become ionized through various ion-molecule reactions including proton transfer or electron capture or abstraction (see Fig. 8.2). Ions are then attracted into the opening of the mass spectrometer and pass through a cross flow of dry nitrogen that prevents uncharged solvent molecules from entering the low-pressure analyzer of the mass spectrometer. Although the APCI probe and drying gas are typically heated, most of this energy is used for solvent evaporation, and thermal decomposition of sample molecules such as carotenoids is usually low. This heat energy combined with energy transferred to carotenoids during chemical ionization and acceleration of the ions into the low-pressure region of the mass spectrometer produce some in-source fragmentation. However, M.W. information is usually abundant, as described herein.

In 1996, van Breemen and colleagues (28) published the first LC/APCI-MS analysis of carotenoids. Carotenoid mixtures in plant extracts were separated. Using a C_{30} column and a solvent system consisting of a gradient from methanol (containing ammonium acetate) to methyl *tert*-butyl ether. Positive-ion and negative-ion APCI mass spectra were obtained using a quadrupole mass spectrometer. The limits of detection were similar to those obtained during ESI-MS and were determined to be 3 and 13 pmol during positive-ion APCI and 3 and 1 pmol during negative-ion mode for α -carotene and lutein, respectively. The detector response was linear over at least three orders of magnitude in both positive- and negative-ion mode APCI-MS (28).

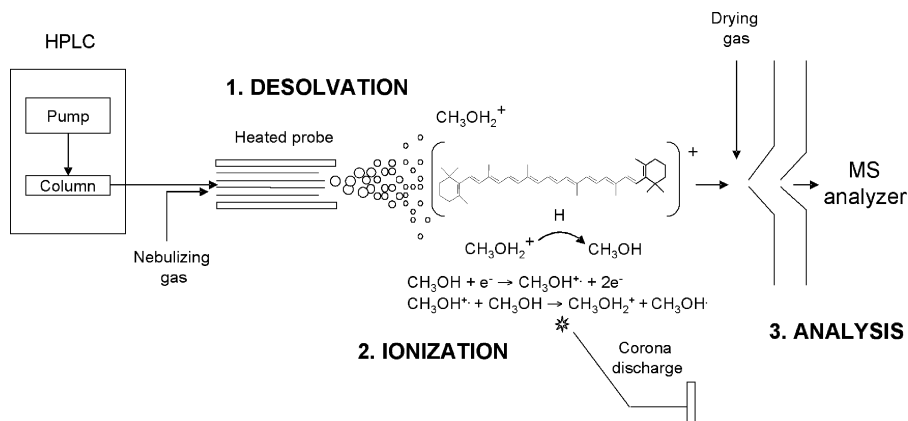


Fig. 8.2. The process of APCI desolvation and ionization of carotenoids during mass spectrometric analysis. The protonation of β -carotene is indicated by the chemical ionization reagent and HPLC solvent methanol.

Unlike previous ionization techniques that primarily produced molecular ions, protonated or deprotonated molecules, xanthophylls and carotenes form both molecular ions and protonated molecules during positive-ion APCI and molecular ions and deprotonated molecules during negative-ion APCI. The solvent composition influences the relative abundances of the molecular ions and protonated or deprotonated molecules (15). Polar solvents such as alcohols enhance the formation of protonated carotenoids, and hydrophobic solvents such as methyl *tert*-butyl ether increased the abundance of molecular ions. The presence of both protonated or deprotonated molecules and molecular ions in APCI mass spectra obtained by using gradient LC-MS may be explained by a mixture of different solvents (15).

Although the formation of M^+ ions of carotenes may be explained by dissociation of a π electron as has been observed during EI (29), electrospray (27), CI (16), and FAB (20), the observation of protonated carotenes during APCI was unexpected. One possible explanation might be that through interaction with the APCI plasma, π electrons of the carotene polyene chain are raised to excited states, and as a result, the π system of the carotene exhibits unusually high proton affinity.

During APCI, in-source fragmentation may be enhanced, if desired, by using CID in the ion source. It should be noted that CID can be used in other regions of the mass spectrometer to produce fragmentation during tandem mass spectrometry. Whether formed in the ion source or in the mass spectrometer analyzer during MS/MS, there are some typical fragment ions of protonated or deprotonated carotenoids that have been observed during APCI-MS. One unusually abundant fragment ion is the loss of water from the protonated molecule of lutein to form the ion of m/z 551 (which is usually the base peak of the positive-ion APCI-MS mass spectrum). Lutein contains an allylic hydroxyl group, which favors the elimination of a molecule of water upon

protonation since the resulting fragment ion is stabilized by mesomeric effects (30). This fragmentation pathway may be used to distinguish lutein from its isomer zeaxanthin, which differs only in the position of one double bond. Another common fragment ion is the loss of toluene, that is, $[\text{MH}-92]^+$, from the protonated molecule of β -carotene, α -carotene, lycopene, and several other carotenoids. The fragment ion at m/z 459 in the mass spectrum of lutein, corresponding to the elimination of both water and toluene, $[\text{MH}-18-92]^+$, is also a characteristic of lutein. During negative-ion APCI, loss of toluene can also occur, such as the formation of the $[\text{M}-\text{H}-92]^-$ ion from the deprotonated molecule of lutein. The fragmentation pathways of carotenoid radical cations, M^+ , are analogous to those reported by using positive-ion CF-FAB MS/MS with CID (26). For example, α -carotene forms the retro-Diels-Alder fragment ion, $[\text{M}-56]^+$ of m/z 480, and lutein, α -carotene and β -carotene eliminate toluene from the molecular ion, $[\text{M}-92]^+$.

Applications of APCI Mass Spectrometry to Carotenoid Analysis

Analysis of Foods and Natural Products

In an early application of LC/APCI-MS to the quantitative analysis of carotenoids, Clarke and colleagues (31) used positive-ion LC/APCI-MS for the determination of nine carotenoids as part of a diet survey. The carotenoids β -carotene, α -carotene, lycopene, lutein, neoxanthin, violaxanthin, antheraxanthin, zeaxanthin, and β -cryptoxanthin were separated in 14 minutes using gradient elution with a nonaqueous mobile phase system containing acetonitrile, methanol, and ethyl acetate (each solvent contained 0.05% triethylamine). Using this mobile phase, protonated molecules were formed instead of molecular ions. Selected ion monitoring (SIM) of the most abundant ions in each mass spectrum was used for quantitative analysis. These ions corresponded to the protonated molecules of each carotenoid with the exceptions of lutein and neoxanthin, which formed abundant fragment ions, $[\text{MH}-\text{H}_2\text{O}]^+$. The limits of detection were from 2 to 26 pmol on-column, and the coefficient of variation for the measurement of each carotenoid was 6–20%. In a more recent but similar study, Huck and colleagues (32) used C_{18} reversed-phase HPLC with a mobile phase containing acetonitrile, methanol, chloroform, *n*-heptane, and triethylamine for the LC/APCI-MS analysis of β -carotene, β -cryptoxanthin, lutein, and zeaxanthin in vegetable extracts. Positive-ion APCI-MS was used for the quantitative analysis of the protonated molecules of all of the carotenoids except for lutein, which was measured based on the abundance of the $[\text{MH}-\text{H}_2\text{O}]^+$ ion of m/z 551.

Hagiwara and colleagues (33) measured lycopene, α -carotene, and β -carotene in vegetable juice using LC/APCI-MS. After extraction, these carotenoids were separated using a C_{18} reversed-phase HPLC column with methanol as the eluent, and SIM was used to monitor the protonated molecules of these isomeric carotenes

at m/z 537. The limit of detection was 2 pmol injected on-column, and the coefficients of variation of repeated measurements of 60 and 300 ng of β -carotene were 3.6 and 2.6, respectively.

Another application of LC/APCI-MS for the analysis of carotenoids in vegetable juice was reported by Lacker and colleagues (34). HPLC separation was performed using a C_{30} reversed-phase column with a mobile phase consisting of a gradient from methanol to methyl *tert*-butyl ether and was similar to that reported by van Breemen and colleagues (28). Positive-ion APCI was then used to form protonated carotenoids. The identification of *cis* carotenoids was facilitated by the use of a PDA absorbance detector. The limit of detection for β -carotene was 1 pmol on-column.

LC/APCI-MS in combination with UV/vis absorbance detection was used by Davoli and Weber (35) to identify carotenoids in aeciospores of the daisy rust fungus, *Puccinia distincta*. Extracts of the aeciospores were analyzed by using reversed-phase HPLC with a C_{18} column and UV/vis detection. The presence of β - and γ -carotene was confirmed using negative-ion APCI-MS during which these compounds formed abundant molecular ions, M^+ , having m/z 536.

Zhou and colleagues (36) utilized LC/APCI-MS in combination with UV/vis absorbance detection for the identification of dipalmitoyl zeaxanthin in the berry *Gou Qi Z*. After extraction, normal-phase HPLC was used and detection was performed using UV/vis absorbance and negative-ion APCI-MS. Initially, a molecular ion was detected at m/z 1044. Following partial hydrolysis, new peaks were detected corresponding to m/z 806 (later identified as monopalmitoyl zeaxanthin) and m/z 568 (zeaxanthin). The ion of m/z 1044 was then identified as dipalmitoyl zeaxanthin.

Breithaupt and colleagues (37) reported the application of LC/APCI-MS for the identification of lutein mono- and diesters in extracts of marigold flowers and several fruits. Before extraction, partial enzymatic deesterification was used to obtain lutein monoester regioisomers. The extracts of marigold flowers and fruits were then separated using C_{30} reversed-phase HPLC with gradient elution consisting of a methanol/water/methyl *tert*-butyl ether mobile phase. Detection using positive-ion APCI mass spectrometry indicated the presence of lutein mono- and diesters as well as all-*trans* lutein. Although no protonated molecules were detected for the lutein esters, the monoesters formed abundant fragment ions resulting from the loss of water, one fatty acid, or both a fatty acid and water from the protonated molecule. The mass spectra of the lutein diesters contained fragment ions resulting from the loss of one FA or both FA from the protonated molecule. The detection limit for lutein dimyristate based on the abundance of the $[MH-FA]^+$ fragment ion was 550 pmol/mL with an injection volume of 20 μ L. Later, this group (38) used the LC-MS method to investigate the bioavailability in chickens of free and esterified lutein and capsanthin. They found that esterification of these carotenoids in chicken feed did not affect the plasma levels.

In another investigation of lutein esters in marigold flower extracts, Tian and colleagues (39) used negative-ion LC/APCI-MS with C_{30} reversed-phase HPLC.

Both molecular ions, M^+ , and fragment ions resulting from elimination of a single FA were observed for lutein diesters. In unsymmetrical diesters, elimination of the longer chain FA predominated. This approach provided both structurally significant fragment ions as well as M.W. information. In contrast, the use of positive-ion APCI-MS, as reported by Breithaupt and colleagues (37), produced no molecular ions of lutein esters. The use of negative-ion APCI-MS might provide similar benefits for the identification of other carotenoid esters.

In another study by Breithaupt and Bamedi (40), carotenoids and carotenoid esters were measured in yellow and white-fleshed potatoes by using LC/APCI-MS with the same instrument parameters as in their previous report (37). The most abundant carotenoids were violaxanthin, antheraxanthin, lutein, and zeaxanthin, while neoxanthin, β -carotene and β -cryptoxanthin were found to be minor constituents. The total concentration of the four most abundant carotenoids was in the range 58–175 $\mu\text{g}/100\text{ g}$ in yellow potatoes and from 38 to 62 $\mu\text{g}/100\text{ g}$ in white potatoes. Since triacylglycerols in these samples produced some interference with the LC-MS analysis, the triacylglycerols were hydrolyzed using lipases before analysis. Protonated molecules of the carotenoid diesters were observed in the APCI-MS mass spectra, which eliminated water $[\text{MH}-\text{H}_2\text{O}]^+$ and water plus one or the other FA, for example, $[\text{MH}-\text{H}_2\text{O}-\text{myristic acid}]^+$ or $[\text{MH}-\text{H}_2\text{O}-\text{palmitic acid}]^+$ at m/z 775. Based on these mass spectra, myristic and palmitic diesters of lutein, zeaxanthin, and violaxanthin were identified.

During studies of carotenoids in pumpkin (*Cucurbita maxima*), tomato (*Lycopersicon esculentum*), paprika (*Capsicum annuum*), brown alga (*Undaria pinnatifida*), fresh water red tide (*Peridinium bipes*), blue-green alga (*Mycrocystis* sp.), and chlorella (*Chlorella vulgaris*), Maoka (41) used positive-ion LC/APCI-MS with in-line PDA absorbance detection for their rapid identification. HPLC retention time, M.W. (based on the observation of the protonated molecule), and the presence of some structurally significant fragment ions in the APCI-MS mass spectra were sufficient for the identification of many carotenoids. For example, fucoxanthin and peridin formed fragment ions resulting from the elimination of water and the unique leaving group acetic acid, $[\text{MH}-\text{H}_2\text{O}-\text{AcOH}]^+$ and $[\text{MH}-2\text{H}_2\text{O}-\text{AcOH}]^+$. Based on the relative abundances of these fragment ions—for example, the base peak in the positive-ion APCI-MS mass spectrum of peridin was $[\text{MH}-\text{H}_2\text{O}-\text{AcOH}]^+$ but was $[\text{MH}-\text{H}_2\text{O}]^+$ in the case of fucoxanthin—these compounds could be distinguished. In the case of the isomeric carotenes α -carotene, β -carotene, γ -carotene, and lycopene, which did not form structurally significant fragment ions in the ion source, PDA absorbance data were used to confirm their identities. In a similar application, Carmona and colleagues (42) used a combination of positive-ion LC/APCI-MS and HPLC-UV/vis absorbance to identify and quantify carotenoids in the marine organism *Thraustochytrium*, CHN-1 orange-colored strain. Astaxanthin was the most abundant of the carotenoids, and echinenone, canthaxanthin, phoenicoxanthin, and β -carotene were detected at lower levels.

The work by Maoka (41) and Carmona and colleagues (42) indicates that the use of a single stage of mass spectrometry may be insufficient to identify some carotenoids and to distinguish their structural isomers during LC/APCI-MS. In these cases, another analytical technique may be used, such as PDA absorbance detection. However, the use of tandem mass spectrometry is yet another approach that may be used to solve this problem. To date, few research groups are taking advantage of MS/MS for carotenoid analysis even though many of the earliest mass spectrometric studies of carotenoids used MS/MS and LC-MS/MS; for example, see Schmitz and colleagues (20) and van Breemen and colleagues (21,26). However, some recent developments in the use of LC/APCI-MS/MS by the van Breemen group are discussed in this chapter.

Biomedical Applications of LC/APCI-MS and LC-MS/MS

In 2000, Wang and colleagues (43) reported an LC/APCI-MS method for the determination of the human bioavailability of β -carotene and its bioconversion to retinol. In this study, which focused on the bioavailability and bioconversion of β -carotene in a statistically significant group of children, ^{13}C -labeling was used to distinguish the β -carotene administered during the study from dietary or preexisting β -carotene. It should be noted that ^{13}C was used instead of deuterium because of the greater physicochemical similarity of the ^{13}C -labeled compounds to their unlabeled analogs. Physiological doses (80 μg) of [$^{13}\text{C}_{10}$]-retinyl palmitate and [$^{13}\text{C}_{10}$]- β -carotene were administered daily to children to avoid perturbation of the circulating (endogenous) levels of these compounds. The levels of [$^{13}\text{C}_{10}$]- β -carotene, [$^{13}\text{C}_{10}$]-retinol (formed from [$^{13}\text{C}_{10}$]-retinyl palmitate), and [$^{13}\text{C}_5$]-retinol (formed from [$^{13}\text{C}_{10}$]- β -carotene) were measured based on the previously published methods for carotenoids (28) and retinol (44) by this group, which included C_{30} HPLC column separations followed by positive-ion APCI mass spectrometry. A limit of detection of 0.25 pmol on-column was shown for labeled β -carotene extracted from human serum. The high sensitivity, high specificity, and wide linear dynamic range of this LC/APCI-MS method made this clinical investigation possible by facilitating the measurement of the isotopic enrichment of β -carotene and retinol in human serum in the presence of abundant unlabeled analogs.

Recently, Kurilich and colleagues (45) used the positive-ion LC/APCI-MS assay of Wang and colleagues (43) for the measurement of ^{13}C -labeled carotenoids and retinol in the serum of a single human subject after ingestion of intrinsically labeled kale (*Brassica oleracea*). SIM was used to record the $[\text{MH}-\text{H}_2\text{O}]^+$ ions of unlabeled and labeled lutein (m/z 551 and 591, respectively) and retinol, and the protonated molecules of unlabeled and labeled β -carotene and phyloquinone. The on-column detection limits were 90 fmol for lutein and β -carotene, 170 fmol for retinol, and 3 fmol for phyloquinone.

In another clinical application of LC/APCI-MS, Hagiwara and colleagues (46) modified their previously reported method for the analysis of carotenes in veg-

etable juice (33) for the analysis of carotenoids in serum. The mobile phase was changed to methanol/acetonitrile to avoid interference during SIM from coeluting serum constituents. The limit of detection for carotenoids was 5.6 pmol/mL serum with an injection volume of 30 μ L.

To identify carotenoids and distinguish their various *cis* and *trans* isomers, Dachtler and colleagues (30) and Glaser and colleagues (47) combined LC/APCI-MS with LC-nuclear magnetic resonance (LC-NMR) spectroscopy for the analysis of isomers of β -carotene, lutein, and zeaxanthin in extracts of several biological matrices including spinach, avian retina, and bovine retina. Samples were extracted using matrix solid-phase dispersion to minimize degradation and isomerization, and HPLC separation was performed using a C₃₀ reversed-phase column with a mobile phase consisting of acetone and water. During positive-ion APCI mass spectrometry, the base peaks of the β -carotene and zeaxanthin mass spectra were the protonated molecules of m/z 537 and 569, respectively, and as reported previously (28,31,32), the most abundant ion in the positive-ion APCI mass spectrum of lutein was the fragment ion $[\text{MH}-\text{H}_2\text{O}]^+$ at m/z 551. While LC/APCI-MS was useful for the separation and identification of individual carotenoids in spinach and retina extracts, LC-NMR facilitated the identification of the most abundant main geometrical isomers of carotenoids such as β -carotene, lutein, and zeaxanthin.

Van Breemen and colleagues (48) used C₃₀ reversed-phase HPLC with positive-ion APCI mass spectrometry to measure the ratios of lycopene *cis* and *trans* isomers in human serum and prostate tissue. During positive-ion APCI-MS, the protonated molecule of lycopene at m/z 537, which was the most abundant ion in the mass spectrum, was used for SIM. The limit of detection was 0.93 pmol of lycopene injected on-column. All-*trans* lycopene was identified by comparison to the authentic standard, and *cis* isomers were identified based on M.W., UV/vis absorbances, and HPLC retention times. This assay was used for the analysis of lycopene in prostate tissue and blood samples from men who consumed 30 mg of lycopene per day for 21 days in the form of tomato sauce. Although total lycopene levels could be measured using reversed-phase HPLC with absorbance detection (49), absorbance was not sensitive enough to measure the low levels of various *cis* isomers of lycopene in the prostate biopsy samples. Therefore, LC/APCI-MS was used to show that during the dietary intervention, prostate lycopene levels increased threefold, the relative amount of all-*trans* lycopene in the prostate increased from 12.4% to 22.7%, and the proportion of *cis* isomers was greater in the prostate than in the serum. This work illustrates the high sensitivity of LC/APCI-MS for the measurement of lycopene in human blood and tissue.

As noted previously, few research groups are utilizing tandem mass spectrometry with APCI for the analysis of carotenoids. Since biomedical samples are complex and often require extra sample handling measures such as additional sample preparation steps or more extensive chromatographic separation to minimize interference from the biological matrix during LC-MS, tandem mass spectrometry as an additional dimension of analytical selectivity might be used to streamline sample

preparation, minimize the potential for matrix interference, and even improve the limit of detection. Based on previous studies with FAB and tandem mass spectrometry (20,21,26) that showed how lycopene can be distinguished from isomeric α -carotene and β -carotene through the MS/MS measurement of a unique fragmentation pathway, a new LC/APCI-MS/MS assay was developed for the quantitative analysis of lycopene in human plasma and tissue (50). Unlike FAB, which produces molecular ion radicals of lycopene and then $[M-69]^+$ ions because of the loss of a terminal isoprene group during CID and MS/MS in a magnetic sector mass spectrometer, positive-ion APCI did not form these ions in abundance in a triple quadrupole mass spectrometer. This might have been the result of the lower CID energies used on the triple quadrupole instrument, lower precursor ion energies formed during APCI, or the presence of protonated molecules in the APCI source. Therefore, negative-ion APCI was investigated as an alternative to positive-ion mode.

During negative-ion APCI-MS/MS, lycopene was found to form an abundant molecular ion radical of m/z 536 that fragmented during CID in a triple quadrupole mass spectrometer to produce an abundant and unique product ion of m/z 467 (see Fig. 8.3A) (50). As in positive-ion FAB MS/MS, this product ion corresponds to loss of a terminal isoprene group $[M-C_5H_9]^-$. Although α -carotene and β -carotene also form molecular ions of m/z 536 during negative-ion APCI (see Fig. 8.3B), these compounds cannot fragment to eliminate an isoprene group from their terminal rings. In addition to lycopene, some other carotenoids with terminal isoprene groups include neurosporine, phytoene, phytofluene, and ζ -carotene. Although these carotenoids might also fragment in this manner, they will not interfere with lycopene analysis by using MS/MS because they have different M.W. Only γ -carotene and δ -carotene are both isomeric with lycopene and capable of fragmenting through the loss of a terminal isoprene group. Since these compounds are easily resolved from lycopene during HPLC (for example, see the separation of γ -carotene from lycopene in the LC-MS/MS chromatogram of a human serum extract shown in Fig. 8.4), potential interference may be avoided.

For the quantitative analysis of carotenoids by using tandem mass spectrometry, LC-MS/MS is often performed by using selected reaction monitoring (SRM). During SRM, a particular molecular ion precursor may be selected in the first stage of mass spectrometry; next, CID is used to generate fragment ions of the selected ion; and then a unique product ion is selected in the final stage of mass spectrometry. SRM enhances sensitivity by reducing the background noise and improves selectivity by eliminating potentially interfering signals. For the quantitative analysis of lycopene using SRM, our group (50) monitored the transition m/z 536 \rightarrow 467 during negative-ion LC/APCI-MS. The interassay precision of this method showed a coefficient of variation of less than 10% over the range of 0.5–50 μ M. In addition, the limits of detection and quantitation of lycopene using this method were determined to be 11 and 23 fmol injected on-column, respectively (50). For comparison, authors of a recent study who used HPLC with electrochemical detection

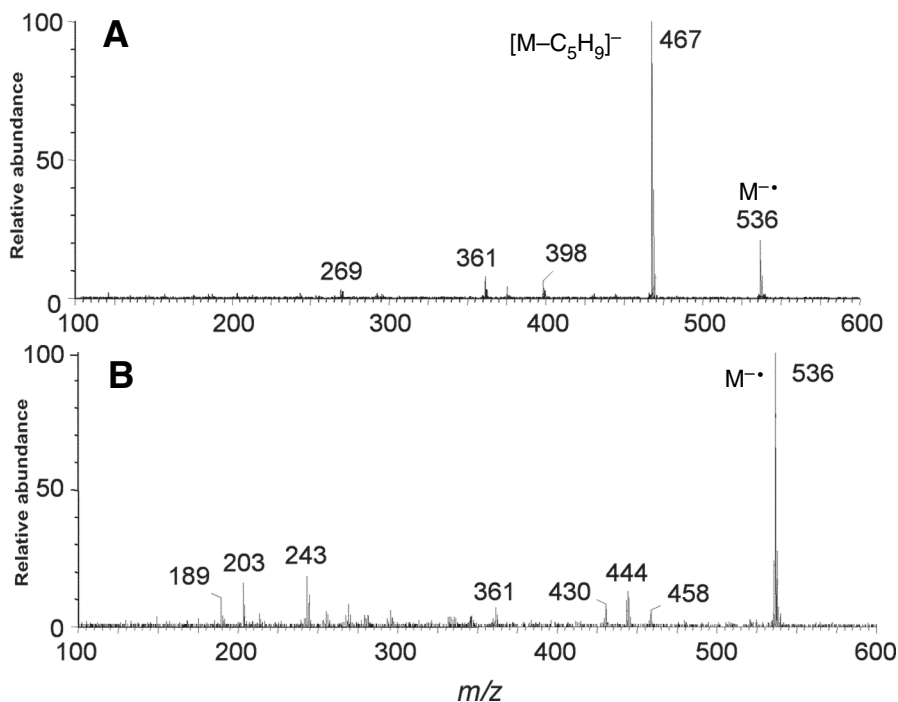


Fig. 8.3. Negative-ion APCI tandem mass spectra with CID of (A) lycopene and (B) β -carotene obtained by using a triple quadrupole mass spectrometer. Note that the fragment ion of m/z 467 (formed from the molecular ion by loss of a terminal isoprene group) is the base peak of the lycopene mass spectrum but is not detected in the tandem mass spectrum of β -carotene.

for the quantitative analysis of lycopene reported a limit of detection of 50 fmol, which was 10–100-fold more sensitive than UV/vis methods (51). This LC-MS/MS assay for the quantitative analysis of lycopene is perhaps the most sensitive and selective method currently available.

Summary

APCI has become the most popular and successful ionization method for the LC-MS and LC-MS/MS analyses of carotenoids. Both carotenes and xanthophylls may be analyzed and detected as molecular ions, protonated molecules, or deprotonated molecules, depending in part upon the solvent system being used. Either positive- or negative-ion APCI-MS may be used for carotenoid analysis. Negative-ion APCI tends to form more abundant molecular ions than does positive-ion mode, especially in the analysis of xanthophylls such as lutein and carotenoid esters, which is important for M.W. determination. Structurally significant fragment ions may be formed in the ion-

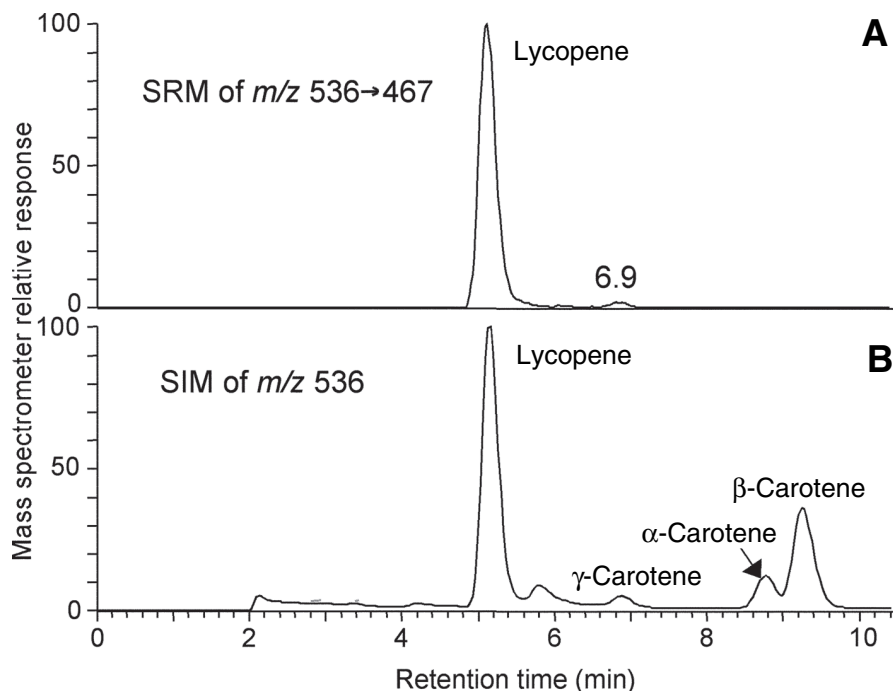


Fig. 8.4. Negative-ion APCI (A) LC-MS/MS and (B) LC-MS chromatograms of a human plasma extract showing the selective detection of lycopene by using selected reaction monitoring (SRM). When using selected ion monitoring (SIM) of the molecular ion of lycopene at m/z 536 (B), several other isomeric carotenoids were detected including β -carotene (9.3 min), α -carotene (8.8 min), and γ -carotene (6.9 min) as well as an unknown compound eluting at 5.8 minutes. Only lycopene and γ -carotene were detected during SRM. HPLC separation was performed by using a C_{18} column with isocratic acetonitrile/methyl *tert*-butyl ether (95:5, vol/vol).

ization source (i.e., using in-source CID) or during CID in combination with tandem mass spectrometry. The detection of fragment ions may be used for carotenoid identification, such as to distinguish α -carotene from isomeric β -carotene, or for the selective detection and quantitative analysis of one carotenoid, such as lycopene, in a complex matrix such as an extract of human serum. Compared to other LC-MS techniques such as electrospray, particle beam, and continuous-flow FAB ionization modes, APCI shows a linear response over a wider dynamic range and is therefore more suitable for quantitative analysis.

Compared to UV/vis absorbance detection or electrochemical detection, APCI mass spectrometry provides greater sensitivity for HPLC analyses of carotenoids. The need for high sensitivity is particularly acute when measuring carotenoids in small samples such as tissue biopsies. Another advantage of mass spectrometry, and in particular tandem mass spectrometry, over other HPLC detectors is superior selectivity,

which is essential for quantitative analysis without interference from other carotenoids or matrix compounds.

Like personal computers, the performance of mass spectrometers has been steadily increasing each year while their size and cost are decreasing. This process has facilitated the acquisition of mass spectrometers by many more laboratories than ever before so that these instruments have become more accessible to researchers working on carotenoids. Therefore, the number of applications of mass spectrometers to carotenoid analysis should be expected to grow during the next several years. Although most of the current APCI mass spectrometric applications use single-stage mass spectrometry and positive-ion mode, tandem mass spectrometry should become more popular as the enhanced selectivity of MS/MS becomes more widely recognized. New applications of LC-MS/MS that take advantage of the unique aspects of negative-ion APCI should be expected to appear during the next few years.

References

1. Olson, J.A., and N.I. Krinsky, Introduction: The Colorful, Fascinating World of the Carotenoids: Important Physiological Modulators, *FASEB J.* 9: 1547–1550 (1995).
2. Straub, O., Lists of Natural Carotenoids, in *Key to Carotenoids*, edited by H. Pfander, Birkhauser Verlag, Basel, 1987.
3. Britton, G., *UV/Visible Spectroscopy*, in *Carotenoids, 1B: Spectroscopy*, edited by G. Britton, S. Liaaen-Jensen, and H. Pfander, Birkhauser Verlag, Basel, 1995, pp. 13–62.
4. Armstrong, G.A., and J.E. Hearst, Carotenoids 2: Genetics and Molecular Biology of Carotenoid Pigment Biosynthesis, *FASEB J.* 10: 228–237 (1996).
5. Demmig-Adams, B., A.M. Gilmore, and W.W. Adams, Carotenoids 3: *In Vivo* Function of Carotenoids in Higher Plants, *FASEB J.* 10: 403–412 (1996).
6. Britton, G., Carotenoids 1: Structure and Properties of Carotenoids in Relation to Function, *FASEB J.* 9: 1551–1558 (1995).
7. Isler, O., *Carotenoids*, Birkhauser Verlag, Basel, 1971.
8. Olson, J.A., Carotenoids, in *Modern Nutrition in Health and Disease*, 9th ed., edited by M.E. Shils, J.A. Olson, M. Shike, and A.C. Ross, Williams & Wilkins, Baltimore, 1999, pp. 529–541.
9. Krinsky, N.I., The Biological Properties of Carotenoids, *Pure Appl. Chem.* 66: 1003–1010 (1994).
10. Sporn, M.B., G.H. Clamon, N.M. Dunlop, D.L. Newton, J.M. Smith, and U. Saffioti, Activity of Vitamin A Analogues in Cell Cultures of Mouse Epidermis and Organ Cultures of Hamster Trachea, *Nature (Lond.)* 253: 47–50 (1975).
11. Bendich, A., and J.A. Olson, Biological Actions of Carotenoids, *FASEB J.* 3: 1927–1932 (1989).
12. Schalach, W., *Free Radicals and Aging*, Birkhauser, Basel, 1992.
13. Ziegler, R.G., Vegetables, Fruits, and Carotenoids and the Risk of Cancer, *Am. J. Clin. Nutr.* 53: 251S–259S (1991).
14. Malone, W.F., Studies Evaluating Antioxidants and Beta-Carotene as Chemopreventives, *Am. J. Clin. Nutr.* 53: 305S–313S (1991).
15. van Breemen, R.B., Liquid Chromatography/Mass Spectrometry of Carotenoids, *Pure Appl. Chem.* 69: 2061–2066 (1997).

16. van Breemen, R.B., Innovations in Carotenoid Analysis Using LC/MS, *Anal. Chem.* **68**: 299A–304A (1996).
17. Sander, L.C., K.E. Sharpless, N.E. Craft, and S.A. Wise, Development of Engineered Stationary Phases for the Separation of Carotenoid Isomers, *Anal. Chem.* **66**: 1667–1674 (1994).
18. Barua, A.B., H.C. Furr, J.A. Olson, and R.B. van Breemen, Vitamin A and Carotenoids, in *Modern Chromatographic Analysis of Vitamins*, edited by A.P. De Leenheer, W.E. Lambert, and J.F. Van Bocxlaer, Marcel Dekker, New York, 2000, pp. 1–75.
19. Taylor, R.F., P.E. Farrow, L.M. Yelle, J.C. Harris, and I.G. Marenchic, in *Carotenoids: Chemistry and Biology*, edited by N.I. Krinsky, M.M. Mathews-Roth, and R.F. Taylor, Plenum Press, New York, 1990, pp. 105–123.
20. Schmitz, H.H., R.B. van Breemen, and S.J. Schwartz, Fast-Atom Bombardment and Continuous-Flow Fast-Atom Bombardment Mass Spectrometry in Carotenoid Analysis, *Methods Enzymol.* **213**: 322–336 (1992).
21. van Breemen, R.B., H.H. Schmitz, and J. Schwartz, Fast Atom Bombardment Tandem Mass Spectrometry of Carotenoids, *J. Agric. Food Chem.* **43**: 385–389 (1995).
22. Khachik, F., G.R. Beecher, M.B. Goli, W.R. Lusby, and J.C. Smith, Jr., Separation and Identification of Carotenoids and Their Oxidation Products in the Extracts of Human Plasma, *Anal. Chem.* **64**: 2111–2122 (1992).
23. Khachik, F., G. Englert, G.R. Beecher, and J.C. Smith, Jr., Isolation, Structural Elucidation, and Partial Synthesis of Lutein Dehydration Products in Extracts from Human Plasma, *J. Chromatogr. B Biomed. Appl.* **670**: 219–233 (1995).
24. Khachik, F., C.J. Spangler, J.C. Smith, Jr., L.M. Canfield, A. Steck, and H. Pfander, Identification, Quantification, and Relative Concentrations of Carotenoids and Their Metabolites in Human Milk and Serum, *Anal. Chem.* **69**: 1873–1881 (1997).
25. Kelm, M.A., V.P. Flanagan, R.J. Pawlosky, J.A. Novotny, B.A. Clevidence, and S.J. Britz, Quantitative Determination of ¹³C-Labeled and Endogenous Beta-Carotene, Lutein, and Vitamin A in Human Plasma, *Lipids* **36**: 1277–1282 (2001).
26. van Breemen, R.B., H.H. Schmitz, and S.J. Schwartz, Continuous-Flow Fast Atom Bombardment Liquid Chromatography/Mass Spectrometry of Carotenoids, *Anal. Chem.* **65**: 965–969 (1993).
27. van Breemen, R.B., Electrospray Liquid Chromatography-Mass Spectrometry of Carotenoids, *Anal. Chem.* **67**: 2004–2009 (1995).
28. van Breemen, R.B., C.R. Huang, Y. Tan, L.C. Sander, and A.B. Schilling, Liquid Chromatography/Mass Spectrometry of Carotenoids Using Atmospheric Pressure Chemical Ionization, *J. Mass Spectrom.* **31**: 975–981 (1996).
29. Moss, G.P., and B.C.L. Weedon, in *Chemistry and Biochemistry of Plant Pigments*, 2nd ed., edited by T.W. Goodwin, Academic Press, New York, 1976, pp. 149–224.
30. Dachtler, M., T. Glaser, K. Kohler, and K. Albert, Combined HPLC-MS and HPLC-NMR On-Line Coupling for the Separation and Determination of Lutein and Zeaxanthin Stereoisomers in Spinach and in Retina, *Anal. Chem.* **73**: 667–674 (2001).
31. Clarke, P.A., K.A. Barnes, J.R. Startin, F.I. Ibe, and M.J. Shepherd, High Performance Liquid Chromatography/Atmospheric Pressure Chemical Ionization-Mass Spectrometry for the Determination of Carotenoids, *Rapid Commun. Mass Spectrom.* **10**: 1781–1785 (1996).
32. Huck, C.W., M. Popp, H. Scherz, and G.K. Bonn, Development and Evaluation of a New Method for the Determination of the Carotenoid Content in Selected Vegetables by HPLC and HPLC-MS-MS, *J. Chromatogr. Sci.* **38**: 441–449 (2000).

33. Hagiwara, T., T. Yasuno, K. Funayama, and S. Suzuki, Determination of Lycopene, Alpha-Carotene and Beta-Carotene in Vegetable Juice by Liquid Chromatography/Atmospheric Pressure Chemical Ionization-Mass Spectrometry, *J. Food Hyg. Soc. Jap.* 38: 211–218 (1997).
34. Lacker, T., S. Strohschein, and K. Albert, Separation and Identification of Various Carotenoids by C₃₀ Reversed-Phase High-Performance Liquid Chromatography Coupled to UV and Atmospheric Pressure Chemical Ionization Mass Spectrometric Detection, *J. Chromatogr. A* 854: 37–44 (1999).
35. Davoli, P., and R.W. Weber, Identification and Quantification of Carotenoid Pigments in Aeciospores of the Daisy Rust Fungus, *Puccinia distincta*, *Phytochemistry* 60: 309–313 (2002).
36. Zhou, L., I. Leung, M.O. Tso, and K.W. Lam, The Identification of Dipalmityl Zeaxanthin as the Major Carotenoid in *Gou Qi Zi* by High Pressure Liquid Chromatography and Mass Spectrometry, *J. Ocul. Pharmacol. Ther.* 15: 557–565 (1999).
37. Breithaupt, D.E., U. Wirt, and A. Bamedi, Differentiation Between Lutein Monoester Regioisomers and Detection of Lutein Diesters from Marigold Flowers (*Tagetes erecta*, L.) and Several Fruits by Liquid Chromatography-Mass Spectrometry, *J. Agric. Food Chem.* 50: 66–70 (2002).
38. Breithaupt, D.E., P. Weller, and M.A. Grashorn, Quantification of Carotenoids in Chicken Plasma after Feeding Free or Esterified Lutein and Capsanthin Using High-Performance Liquid Chromatography and Liquid Chromatography-Mass Spectrometry Analysis, *Poultry Sci.* 82: 395–401 (2003).
39. Tian, Q., C.J. Duncan, and S.J. Schwartz, Atmospheric Pressure Chemical Ionization Mass Spectrometry and In-Source Fragmentation of Lutein Esters, *J. Mass Spectrom.* 38: 990–995 (2003).
40. Breithaupt, D.E., and A. Bamedi, Carotenoids and Carotenoid Esters in Potatoes (*Solanum Tuberosum*, L.): New Insights into an Ancient Vegetable, *J. Agric. Food Chem.* 50: 7175–7181 (2002).
41. Maoka, T., Rapid Identification of Carotenoids in a Combination of Liquid Chromatography/UV-Visible Absorption Spectrometry by Photodiode-Array Detector and Atmospheric Pressure Chemical Ionization Mass Spectrometry (LC/PAD/APCI-MS), *J. Oleo Sci.* 51: 1–10 (2002).
42. Carmona, M.L., T. Naganuma, and Y. Yamaoka, Identification by HPLC-MS of Carotenoids of the *Thraustochytrium* CHN-1 Strain Isolated from the Seto Inland Sea, *Biosci. Biotechnol. Biochem.* 67: 884–888 (2003).
43. Wang, Y., X. Xu, M. van Lieshout, C.E. West, J. Lugtenburg, M.A. Verhoeven, *et al.*, A Liquid Chromatography-Mass Spectrometry Method for the Quantification of Bioavailability and Bioconversion of Beta-Carotene to Retinol in Humans, *Anal. Chem.* 72: 4999–5003 (2000).
44. van Breemen, R.B., D. Nikolic, X. Xu, Y. Xiong, M. van Lieshout, C.E. West, *et al.*, Development of a Method for Quantitation of Retinol and Retinyl Palmitate in Human Serum Using High-Performance Liquid Chromatography-Atmospheric Pressure Chemical Ionization-Mass Spectrometry, *J. Chromatogr. A* 794: 245–251 (1998).
45. Kurilich, A.C., S.J. Britz, B.A. Clevidence, and J.A. Novotny, Isotopic Labeling and LC-APCI-MS Quantification for Investigating Absorption of Carotenoids and Phylloquinone from Kale (*Brassica oleracea*), *J. Agric. Food Chem.* 51: 4877–4883 (2003).

46. Hagiwara, T., T. Yasuno, K. Funayama, and S. Suzuki, Determination of Lycopene, Alpha-Carotene and Beta-Carotene in Serum by Liquid Chromatography-Atmospheric Pressure Chemical Ionization Mass Spectrometry with Selected-Ion Monitoring, *J. Chromatogr. B Biomed. Sci. Appl.* 708: 67–73 (1998).
47. Glaser, T., A. Lienau, D. Zeeb, M. Krucker, M. Dachtler, and K. Albert, Qualitative and Quantitative Determination of Carotenoid Stereoisomers in a Variety of Spinach Samples by Use of MSPD Before HPLC-UV, HPLC-APCI-MS, and HPLC-NMR On-Line Coupling, *Chromatogr. Suppl.* 57: S19–S25 (2003).
48. van Breemen, R.B., X. Xu, M.A. Viana, L. Chen, M. Stacewicz-Sapuntzakis, C. Duncan, *et al.*, Liquid Chromatography-Mass Spectrometry of *cis*- and All-*trans*-Lycopene in Human Serum and Prostate Tissue after Dietary Supplementation with Tomato Sauce, *J. Agric. Food Chem.* 50: 2214–2219 (2002).
49. Stacewicz-Sapuntzakis, M., P.E. Bowen, J.W. Kikendall, and M. Burgess, Simultaneous Determination of Serum Retinal and Various Carotenoids: Their Distribution in Middle-Aged Men and Women, *J. Micronutr. Anal.* 3: 27–45 (1987).
50. Fang, L., N. Pajkovic, Y. Wang, C. Gu, and R.B. van Breemen, Quantitative Analysis of Lycopene Isomers in Human Plasma Using High-Performance Liquid Chromatography-Tandem Mass Spectrometry, *Anal. Chem.* 75: 812–817 (2003).
51. Ferruzzi, M.G., M.L. Nguyen, L.C. Sander, C.L. Rock, and S.J. Schwartz, Analysis of Lycopene Geometrical Isomers in Biological Microsamples by Liquid Chromatography with Coulometric Array Detection, *J. Chromatogr. B* 760: 289–299 (2001).

Chapter 9

Analysis of Molecular Species of Plant Glycolipids by HPLC/APCI-MS

Ryo Yamauchi

Department of Applied Life Science, Faculty of Applied Biological Sciences, Gifu University, Gifu 501-1193, Japan

Introduction

Edible plant glycolipids are thought to be nutrients in the human diet. Glycolipids in higher plants consist mainly of steryl glycosides, glyceroglycolipids, and sphingoglycolipids. These glycolipids are widely distributed, if not universal, in edible plants (1,2). Plant glycolipid classes have been separated directly and quantified by normal-phase high-performance liquid chromatography (HPLC) in previous studies (3,4). However, the molecular species of each glycolipid class were not fully characterized. Ripe fruit of the red bell pepper (*Capsicum annuum* L.) are used widely as vegetables and food additives, such as ground pepper (paprika) and oleoresin, which are good sources of carotenoid pigments. Red bell peppers also contain all three of the above-mentioned glycolipid classes (5,6), and some micronutrients such as vitamins A, C, and E (7–9), but limited information is available on the content and composition of such nutrients in fresh or processed products.

Atmospheric pressure chemical ionization mass spectrometry (APCI-MS) has proven to be a very valuable technique for analysis of lipids from a variety of classes (10). This paper describes direct analyses of glycolipids from red bell pepper using HPLC coupled with on-line APCI-MS. The glycolipid classes were first separated by silica-gel column chromatography to obtain acylated steryl glucoside (ASG, **1**), steryl glucoside (SG, **2**), monogalactosyldiacylglycerol (MGDG, **3**), digalactosyldiacylglycerol (DGDG, **4**), and ceramide monoglucoside (glucocerebroside, CMG, **5**) (Fig. 9.1), and then the molecular species of each glycolipid were separated and characterized by reversed-phase HPLC/APCI-MS.

Materials and Methods

Materials

Fruit of the red bell pepper (*C. annuum* L. var. *Capia*) was supplied by a local distributor. The fruits were processed into pastes within the same day after harvest and stored at -30°C until analysis.

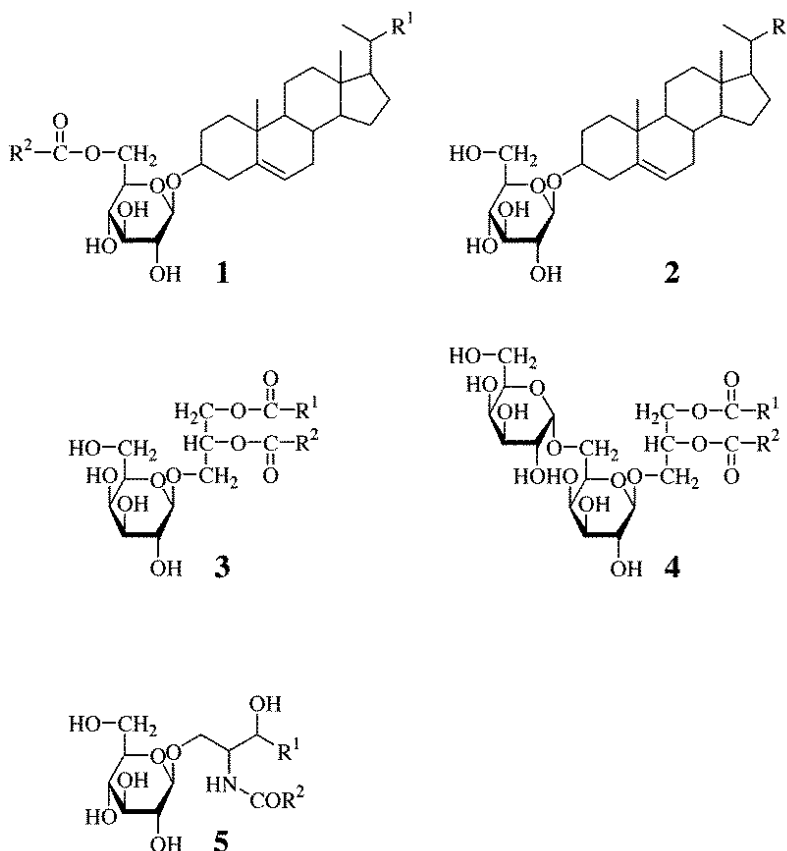


Fig. 9.1. Representative structures of acylated steryl glucoside (1), steryl glucoside (2), monogalactosyldiacylglycerol (3), digalactosyldiacylglycerol (4), and ceramide monoglucoside (5).

Isolation of Glycolipid Classes

The lyophilized fruit pastes (100 g dry weight) of red bell pepper were extracted with 600 mL chloroform/methanol (2:1, vol/vol) three times, and the total lipids were obtained following the method of Folch *et al.* (11). The total lipids (3.26 g) were dissolved in 20 mL of chloroform and subjected to silica-gel column chromatography (silica-gel BW-820MH, 70–200 mesh; Fuji Silysia Chemical Ltd., Kasugai, Japan; 4.5 × 30 cm) with sequential elutions of chloroform (1 L), acetone (2 L), and methanol (1 L). Each solvent eluate was pooled, and the solvent was removed *in vacuo* to obtain neutral lipids (1.73 g) from the chloroform, glycolipids (0.79 g) from the acetone, and phospholipids (0.63 g) from the methanol, respectively. An aliquot of the glycolipid fraction was analyzed by silica-gel thin-layer chromatog-

raphy (silica-gel 60 TLC, 0.25 mm thickness; Merck, Darmstadt, Germany) developed in chloroform/methanol (85:15, vol/vol). Six major spots, capsanthin (R_f 0.85), ASG (**1**, R_f 0.75), MGDG (**3**, R_f 0.60), SG (**2**, R_f 0.43), CMG (**5**, R_f 0.31), and DGDG (**4**, R_f 0.14), were detected on the TLC plate. The bulk of the glycolipid fraction (0.79 g) was then separated by silica-gel column chromatography (2.5 × 30 cm). Each lipid class was sequentially eluted by increasing the methanol concentration in mixtures of chloroform/methanol: a red pigment capsanthin (35 mg) was eluted with chloroform/methanol (99:1, vol/vol); ASG (43 mg), chloroform/methanol (98:2, vol/vol); MDDG (138 mg), chloroform/methanol (95:5, vol/vol); SG (171 mg), chloroform/methanol (90:10, vol/vol); CMG (76 mg), chloroform/methanol (85:15, vol/vol); and DGDG (141 mg), chloroform/methanol (80:20, vol/vol). The CMG fraction was further separated into its molecular species by preparative HPLC. Reversed-phase HPLC was done with an Inertsil Prep-ODS column (1.0 × 25 cm; GL Sciences, Tokyo, Japan) developed with methanol at a flow rate of 5 mL/min and the eluate was monitored at 205 nm. Proton nuclear magnetic resonance (^1H NMR) spectra of molecular species of CMG were recorded with a Varian Inova 400 FT-NMR spectrometer (Varian, Palo Alto, CA) with $\text{CDCl}_3/\text{CD}_3\text{OD}$ (2:1, vol/vol) as the solvent and tetramethylsilane as the internal standard.

Analysis of Components in Glycolipids

The fatty acid (FA) and sugar compositions were determined by gas-liquid chromatography (GLC) (12). The sterol composition was determined by GLC of the trimethylsilyl derivatives after saponification (12,13).

HPLC/APCI-MS

HPLC was carried out using a Shimadzu LC-10AV_{vp} pump equipped with a Shimadzu SPD-10A_{vp} ultraviolet/visible (UV/vis) detector (Shimadzu Co., Kyoto, Japan). Sample lipids were separated isocratically on a Luna 3 μ C18(2) column (2.0 × 150 mm, Phenomenex, Torrance, CA) at 40°C. The mobile phase was methanol/ethanol (3:2, vol/vol) for the analysis of ASG or methanol/water (98:2, vol/vol) for the analyses of SG, MGDG, DGDG, and CMG, with the flow rate maintained at 0.2 mL/min. On-line UV detection at 205 nm was performed before MS detection. APCI-MS was performed using a Shimadzu LCMS-QP8000 α quadrupole mass spectrometer. The MS parameters were optimized by direct infusion of polyethyleneglycol standards into the source. An APCI probe voltage of 4.5 kV and a temperature of 400°C were used. Nebulizing gas (nitrogen) was delivered at a flow rate of 2.5 L/min. The curved desolvation line (CDL) voltage was at -40 V with a temperature of 250°C. The deflector voltage was maintained at +70 V for the analysis of ASG and SG or at +80 V for the analysis of MGDG, DGDG, and CMG. Ionization was performed in the positive-ion mode for all analyses and mass spectra were acquired in the mass range m/z 200–1000 at a scan rate of 3 s.

Results and Discussion

Molecular Species of Acylated Steryl Glucoside and Steryl Glucoside

The components of ASG (**1**) and SG (**2**) were analyzed by GLC after hydrolysis. Each glucoside contained campesterol and β -sitosterol as the sterol moieties, whose percentages, respectively, were 24.3 and 75.7% for ASG, and 27.7 and 72.3% for SG. Glucose was the only sugar detected in both compounds. Furthermore, the FA composition of ASG was determined to be palmitic acid (16:0, 49.9%), stearic acid (18:0, 8.7%), linoleic acid (18:2, 33.1%), and α -linolenic acid (18:3, 8.3%).

HPLC analysis of ASG indicated at least seven molecular species, **1a–g** (Fig. 9.2). The APCI-MS mass spectrum of each peak exhibited the Na^+ adduct ($[\text{M} + \text{Na}]^+$) and fragment ions corresponding to campesterol at m/z 383.4 ($[\text{C}_{28}\text{H}_{47}]^+$), 397.4 ($[\text{C}_{28}\text{H}_{45}\text{O}]^+$), and 215.2 ($[\text{C}_{16}\text{H}_{23}]^+$), or β -sitosterol at m/z 397.4 ($[\text{C}_{29}\text{H}_{49}]^+$), 411.4 ($[\text{C}_{29}\text{H}_{47}\text{O}]^+$), and 215.2 ($[\text{C}_{16}\text{H}_{23}]^+$), and the fatty acyl moiety ($[\text{R}^2\text{CO}]^+$) at m/z 239.2 (16:0), 267.3 (18:0), 263.2 (18:2), or 261.2 (18:3). Thus, compounds **1a–g** were identified as follows: **1a**, β -sitosteryl (6'-*O*-linolenoyl)-glucoside; **1b**, campesteryl (6'-*O*-linoleoyl)-glucoside; **1c**, β -sitosteryl (6'-*O*-linoleoyl)-glucoside; **1d**, campesteryl (6'-*O*-palmitoyl)-glucoside; **1e**, β -sitosteryl (6'-*O*-palmitoyl)-glucoside; **1f**, campesteryl (6'-*O*-stearoyl)-glucoside, and **1g**, β -sitosteryl (6'-*O*-stearoyl)-glucoside. The peak area percentages of ASG **1a–g** in the total ion chromatogram in Figure 9.2 were calculated to be 7.5, 11.2, 22.4, 13.1, 31.4, 5.1 and 9.2%, respectively, which corresponded to the percentages calculated from the data of sterol and FA compositions described above.

HPLC analysis of SG showed two peaks, **2a** and **2b** (Fig. 9.3). The APCI-MS mass spectrum of each peak exhibited the Na^+ adduct ($[\text{M} + \text{Na}]^+$) and fragment ions corresponding to the sterol moiety ($[\text{RC}_{19}\text{H}_{26}\text{O}]^+$, $[\text{RC}_{19}\text{H}_{28}]^+$, and $[\text{C}_{16}\text{H}_{23}]^+$). Thus, **2a** was identified as campesteryl glucoside, having APCI-MS ions at m/z 585.4 ($[\text{M} + \text{Na}]^+$), 397.4 ($[\text{C}_{28}\text{H}_{45}\text{O}]^+$), 383.4 ($[\text{C}_{28}\text{H}_{47}]^+$), and 215.2 ($[\text{C}_{16}\text{H}_{23}]^+$); **2b** was β -sitosteryl glucoside (**2b**), with APCI-MS ions at m/z 599.4 ($[\text{M} + \text{Na}]^+$), 411.4 ($[\text{C}_{29}\text{H}_{47}\text{O}]^+$), 397.4 ($[\text{C}_{29}\text{H}_{49}]^+$), and 215.2 ($[\text{C}_{16}\text{H}_{23}]^+$). The peak area percentages of SG **2a** and **2b** in the total ion chromatogram in Figure 9.3 were calculated to be 26.1 and 73.9%, respectively, which corresponded to the sterol composition of SG determined by GLC after saponification.

Molecular Species of Monogalactosyldiacylglycerol and Digalactosyldiacylglycerol

The FA compositions of MGDG (**3**) and DGDG (**4**) were determined by GLC to be as follows: MGDG, 16:0 (3.6%), 18:0 (1.6%), oleic acid (18:1, 1.5%), 18:2 (8.6%), and 18:3 (86.0%); DGDG, 16:0 (13.9%), 18:0 (7.8%), 18:1 (1.5%), 18:2 (12.5%), 18:3 (64.3%). MGDG and DGDG were analyzed by reversed-phase HPLC. One major peak, **3a**, and five minor peaks, **3b–f**, appeared in the total ion chromatogram of MGDG (Fig. 9.4), whereas seven peaks, **4a–g**, appeared in that of DGDG (Fig. 9.5). The APCI-MS mass spectrum of each peak exhibited the Na^+ adduct ($[\text{M} +$

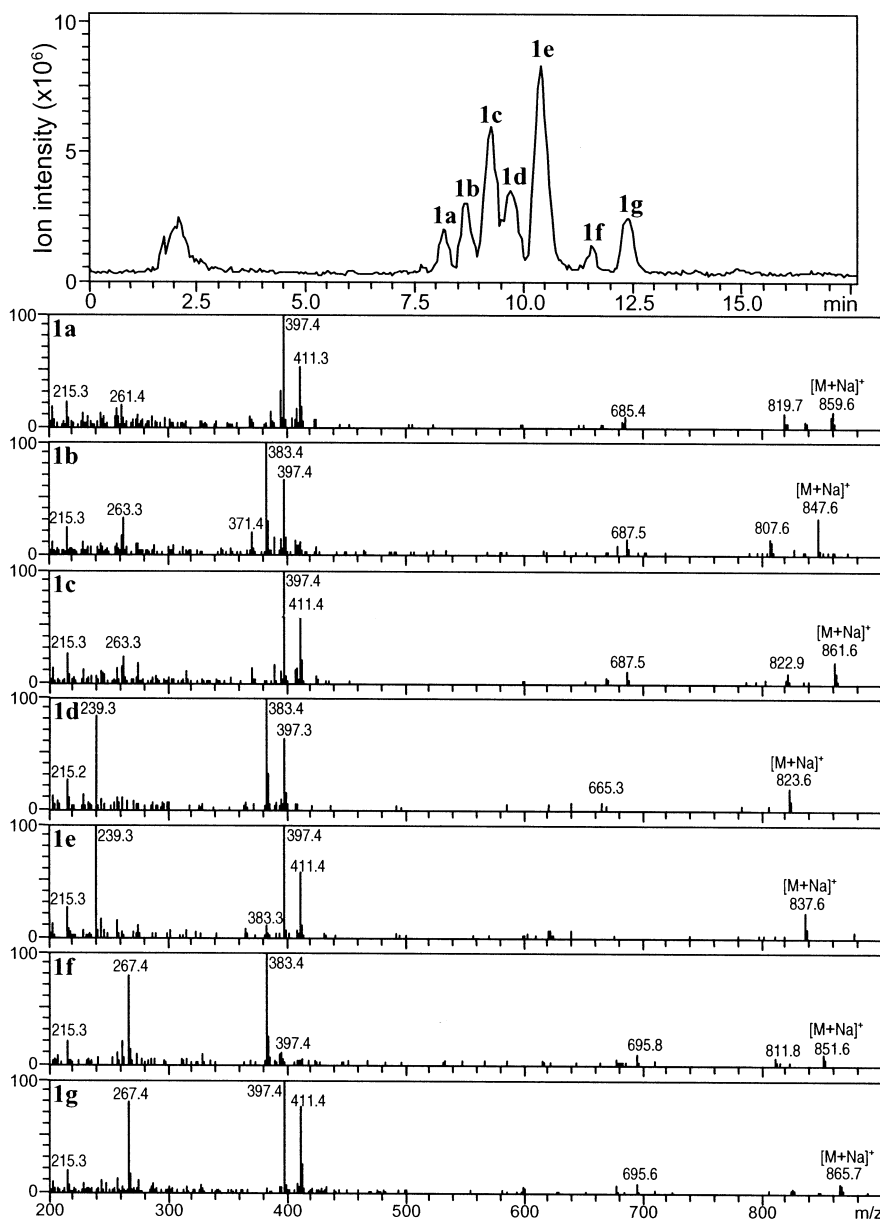


Fig. 9.2. Total ion chromatogram and mass spectra of acylated sterol glucoside from red bell pepper by HPLC/APCI-MS. Acylated sterol glucoside fraction (1) was separated on a Luna C₁₈ column (2 × 150 mm) developed with methanol/ethanol (3:2, vol/vol) at 0.2 mL/min. The eluate was monitored by total ions of APCI-MS. The mass spectra of peaks 1a–g are shown.

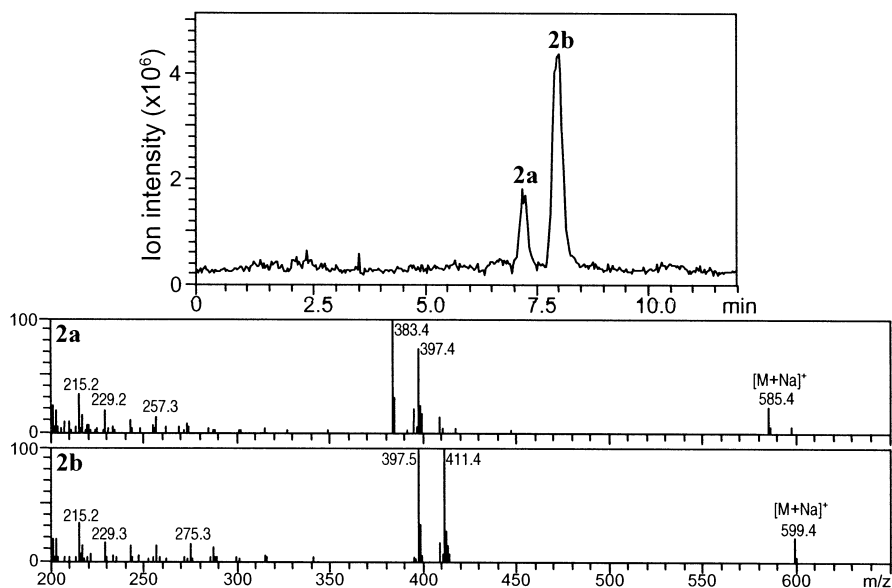


Fig. 9.3. Total ion chromatogram and mass spectra of steryl glucoside from red bell pepper by HPLC/APCI-MS. Steryl glucoside fraction (**2**) was separated on a Luna C_{18} column (2×150 mm) developed with methanol/water (98:2, vol/vol) at 0.2 mL/min. The eluate was monitored by total ions of APCI-MS. The mass spectra of peaks **2a** and **2b** are shown.

$Na]^+$) and fragment ions corresponding to diacylglycerol ($[CH_2(OCOR^1)CH(OCOR^2)CH_2OH_2]^+$ and $[CH_2(OCOR^1)CH(OCOR^2)CH_2]^+$), monoacylglycerol ($[CH_2(OCOR^1)CH(OH)CH_2]^+$ and $[CH_2(OH)CH(OCOR^2)CH_2]^+$), and fatty acyl moieties ($[R^1CO]^+$ and $[R^2CO]^+$) (Figs. 9.4 and 9.5, Tables 9.1 and 9.2). Thus, the molecular species of MGDG were found to be 18:3/18:3 (**3a**), 18:2/18:3 (**3b**), 16:0/18:3 (**3c**), 18:1/18:3 (**3d**), 16:0/18:2 (**3e**), and 18:0/18:3 (**3f**); those of DGDG were 18:3/18:3 (**4a**), 18:2/18:3 (**4b**), 16:0/18:3 (**4c**), 18:1/18:3 (**4d**), 16:0/18:2 (**4e**), 18:0/18:3 (**4f**), and 18:0/18:2 (**4g**). The molecular species compositions calculated from the total ion chromatograms indicated that the 18:3/18:3 species was predominant in MGDG, whereas the 18:3/18:3, 16:0/18:3, and 18:0/18:3 species were predominant in DGDG (Tables 9.2 and 9.3).

The reversed-phase HPLC technique has been reported to allow rapid and reproducible separations of the main molecular species of the plant galactolipids MGDG and DGDG (14,15). However, collection of the separated fractions and analysis of the component FA by GLC was required to identify molecular species. The present on-line APCI-MS technique has enabled direct identification of the molecular species of these galactolipids without such processing, although it did not give information on the *sn* positions of the two FA moieties, whether they were the same or were two different FA.

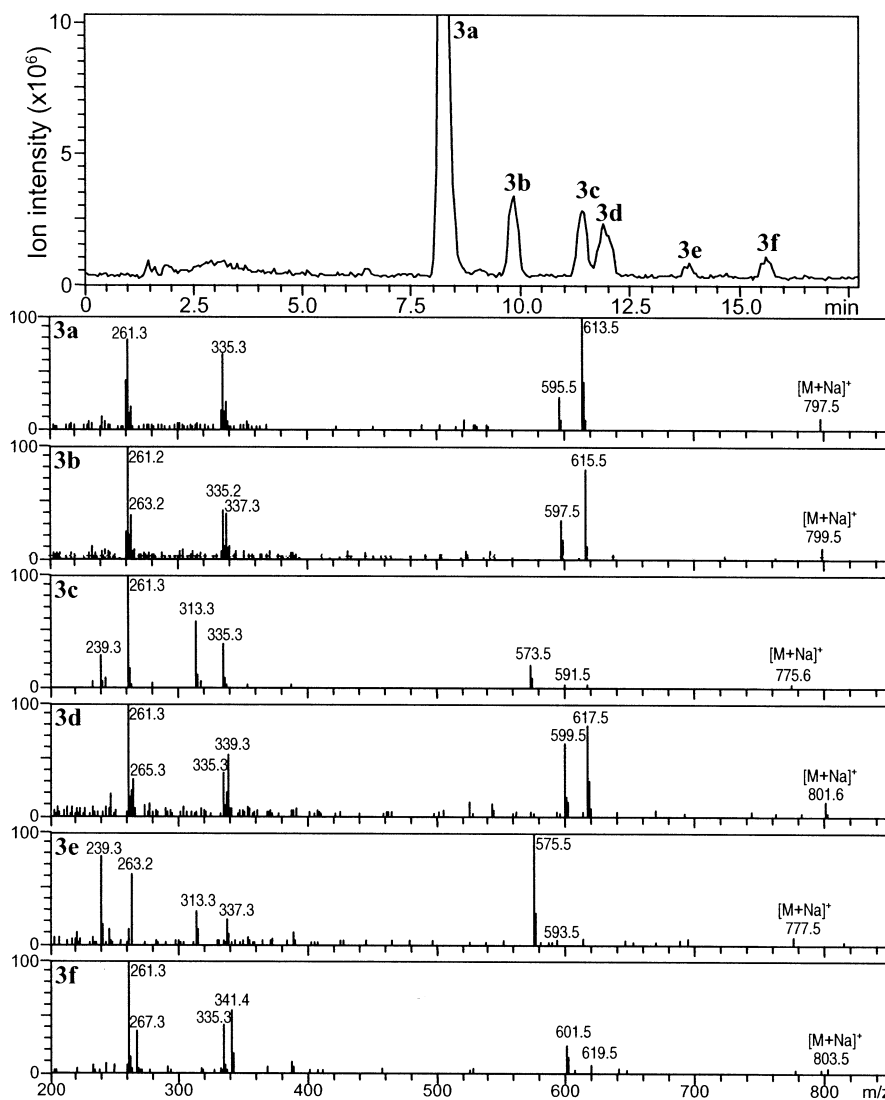


Fig. 9.4. Total ion chromatogram and mass spectra of monogalactosyldiacylglycerol from red bell pepper by HPLC/APCI-MS. HPLC conditions were the same as described in Figure 9.3. The mass spectra of peaks **3a–f** are shown.

Molecular Species of Ceramide Monoglucoside

The CMG fraction (**5**) gave seven peaks, **5a–g**, in the HPLC/APCI-MS total ion chromatogram (Fig. 9.6). Peaks **5a–g** were further separated by preparative reversed-phase HPLC, and their structures were identified by ¹H NMR (16–19) as

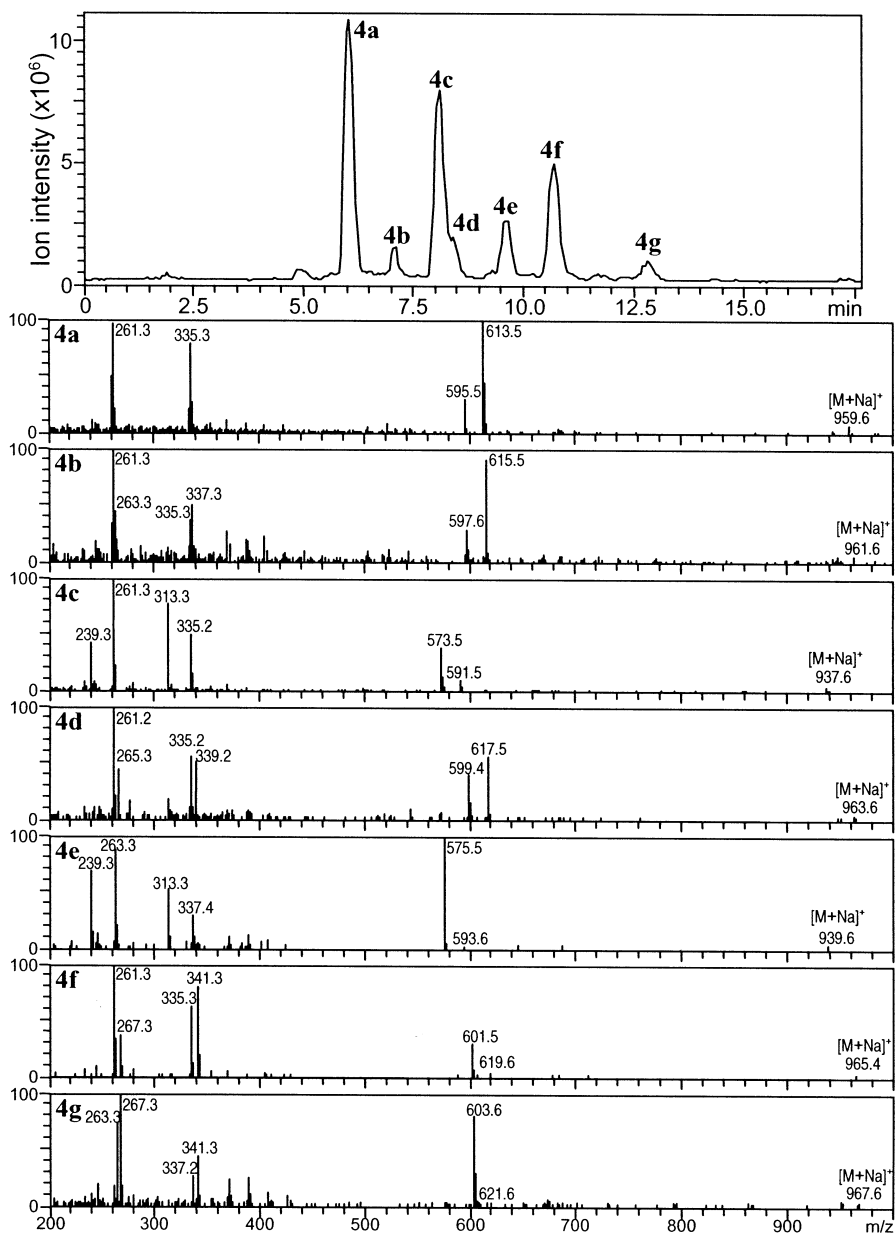


Fig. 9.5. Total ion chromatogram and mass spectra of digalactosyldiacylglycerol from red bell pepper by HPLC/APCI-MS. HPLC conditions were the same as described in Figure 9.3. The mass spectra of peaks **4a–g** are shown.

TABLE 9.1
Calculated Masses of the Molecular Species of Monogalactosyl/diacylglycerol

| Ion | Molecular species (FA/FA) ^a | | | | | |
|--|--|-----------------|-----------------|-----------------|-----------------|-----------------|
| | 18:3/18:3 | 18:2/18:3 | 16:0/18:3 | 18:1/18:3 | 16:0/18:2 | 18:0/18:3 |
| [M + Na] ⁺ | 797.5 ^b | 799.5 | 775.5 | 801.6 | 777.6 | 803.6 |
| Diacylglycerol moiety | | | | | | |
| [CH ₂ (OCOR ¹)CH(OCOR ²)CH ₂ OH ₂] ⁺ | 613.5 | 615.5 | 591.5 | 617.5 | 593.5 | 619.5 |
| [CH ₂ (OCOR ¹)CH(OCOR ²)CH ₂] ⁺ | 595.5 | 597.5 | 573.5 | 599.5 | 575.5 | 601.5 |
| Monoacylglycerol moiety | | | | | | |
| [CH ₂ (OCOR ¹)CH(OH)CH ₂] ⁺ and [CH ₂ (OH)CH(OCOR ²)CH ₂] ⁺ | 335.3 | 337.3, 335.3 | 313.3, 335.3 | 339.3, 335.3 | 313.3, 337.3 | 341.3, 335.3 |
| Acyl moiety | | | | | | |
| [R ¹ CO] ⁺ and [R ² CO] ⁺ | 261.2 | 263.2, 261.2 | 239.2, 261.2 | 265.3, 261.2 | 239.2, 263.2 | 267.3, 261.2 |
| Peak ^c | 3a | 3b | 3c | 3d | 3e | 3f |
| % ^d | 72.1 | 9.3 | 7.9 | 5.3 | 2.4 | 3.0 |

^aAbbreviations: 18:3, α -linolenic acid; 18:2, linoleic acid; 18:1, oleic acid; 18:0, stearic acid; 16:0, palmitic acid, and the sn positions of FA are not determined.
^bm/z.

^cPeak numbers correspond to those indicated in Figure 9.4.

^dValues indicate the peak percentage of total peak area measured by the total ion chromatogram described in Figure 9.4.

TABLE 9.2
Calculated Masses of the Molecular Species of Digalactosyl/diacylglycerol

| Ion | Molecular species (FA/FA) ^a | | | | | | | |
|--|--|-----------------|-----------------|-----------------|-----------------|-----------------|-----------------|-----------------|
| | 18:3/18:3 | 18:2/18:3 | 16:0/18:3 | 18:1/18:3 | 16:0/18:2 | 18:0/18:3 | 16:0/18:2 | 18:0/18:2 |
| [M + Na] ⁺ | 959.6 ^b | 961.6 | 937.6 | 963.6 | 939.6 | 965.6 | 939.6 | 967.6 |
| Diacylglycerol moiety | | | | | | | | |
| [CH ₂ (OCOR ¹)CH(OCOR ²)CH ₂ OH] ₂ ⁺ | 613.5 | 615.5 | 591.5 | 617.5 | 593.5 | 619.5 | 593.5 | 621.6 |
| [CH ₂ (OCOR ¹)CH(OCOR ²)CH ₂] ₂ ⁺ | 595.5 | 597.5 | 573.5 | 599.5 | 575.5 | 601.5 | 575.5 | 603.5 |
| Monoacylglycerol moiety | | | | | | | | |
| [CH ₂ (OCOR ¹)CH(OH)CH ₂] ₂ ⁺ and [CH ₂ (OH)CH(OCOR ²)CH ₂] ₂ ⁺ | 335.3 | 337.3, 335.3 | 313.3, 335.3 | 339.3, 335.3 | 313.3, 337.3 | 341.3, 335.3 | 313.3, 337.3 | 341.3, 337.3 |
| Acyl moiety | | | | | | | | |
| [R ¹ CO] ⁺ and [R ² CO] ⁺ | 261.2 | 263.2, 261.2 | 239.2, 261.2 | 265.3, 261.2 | 239.2, 263.2 | 267.3, 261.2 | 239.2, 263.2 | 267.3, 263.2 |
| Peak ^c | 4a | 4b | 4c | 4d | 4e | 4f | 4e | 4g |
| % ^d | 37.4 | 5.5 | 24.0 | 3.4 | 9.1 | 17.1 | 9.1 | 3.5 |

^aSee Table 9.1 for abbreviations. The *sn* positions of FA are not determined.

^b*m/z*.

^cPeak numbers correspond to those indicated in Figure 9.5.

^dValues indicate the peak percentages of total peak area measured by the total ion chromatogram described in Figure 9.5.

follows: **5a**, (8*E*)-*N*-2'-hydroxypalmitoyl-1-*O*- β -D-glucopyranosyl-4-hydroxy-8-sphinganine; **5b**, (4*E*,8*Z*)-*N*-2'-hydroxypalmitoyl-1-*O*- β -D-glucopyranosyl-4,8-sphingadienine; **5c**, (8*Z*)-*N*-2'-hydroxypalmitoyl-1-*O*- β -D-glucopyranosyl-8-sphinganine; **5d**, (8*E*)-*N*-2'-hydroxydocosanoyl-1-*O*- β -D-glucopyranosyl-4-hydroxy-8-sphinganine; **5e**, (8*E*)-*N*-2'-hydroxytricosanoyl-1-*O*- β -D-glucopyranosyl-4-hydroxy-8-sphinganine; **5f**, (8*E*)-*N*-2'-hydroxytetracosanoyl-1-*O*- β -D-glucopyranosyl-4-hydroxy-8-sphinganine; **5g**, (8*E*)-*N*-2'-hydroxypentacosanoyl-1-*O*- β -D-glucopyranosyl-4-hydroxy-8-sphinganine (Fig. 9.7).

The APCI-MS mass spectra of CMG **5a–g** exhibited the expected quasi-molecular ions ($[M + H]^+$) and fragment ions corresponding to ceramide ($[M - C_6H_9O_5]^+$, $[M - C_6H_{11}O_6]^+$, and $[M - C_6H_{13}O_7]^+$), the sphingoid moiety ($[R^1CH(OH)CH(NH_2)CH_2OH_2]^+$, $[R^1CH(OH)CH(NH_2)CH_2]^+$, $[R^1CH=CH(NH_2)CH_2]^+$, and $[sphingoid - (H_2O)_2]^+$), and the 2-hydroxy fatty acyl moiety ($[R^2CH(OH)-CONH_3]^+$) (Fig. 9.6 and Table 9.3). The mass spectra of **5a** and **5d–g** showed the same fragment ions at m/z 316.3 ($[C_{14}H_{27}CH(OH)-CH(OH)CH(NH_2)CH_2OH_2]^+$), 298.3 ($[C_{14}H_{27}CH(OH)CH(OH)CH(NH_2)CH_2]^+$), 280.3 ($[C_{14}H_{27}CH(OH)CH=CH(NH_2)CH_2]^+$), and 262.3 ($[sphingoid - (H_2O)_2]^+$), indicating the presence of 4-hydroxy-8-sphinganine as the sphingoid moiety. On the other hand, the main peak **5b** showed a different fragmentation pattern, which was characterized by intense fragment ions at m/z 696.5 ($[M - OH]^+$), 516.5 (ceramide moiety, $[M - C_6H_{13}O_7]^+$), and 262.3 (sphingoid moiety, $[C_{15}H_{27}CH=CH(NH_2)CH_2]^+$), due to the presence of 4,8-sphingadienine in the molecule. Whitaker (6) reported that reversed-phase HPLC of cerebrosides isolated from bell pepper fruits gave one major peak in addition to four minor peaks. He deduced that the structure of the major peak was (4*E*,8*Z*)-1-*O*- β -glucosyl-*N*-(2'-hydroxypalmitoyl)-4-*trans*-8-*cis*-sphingadienine, which corresponds to **5b** in our chromatogram, and aside from the assignment of sphingoid *cis/trans* double bonds, he correctly deduced the structures of **5c–f**. Our analytical methods using APCI-MS have the advantage of direct identification of almost all of the molecular species of cerebrosides in the red bell pepper without the need for hydrolysis and derivatization. However, the 1H NMR analysis was essential for the identification of the sphingoid *cis/trans* double bonds.

Edible plant glycolipids are believed to play a role in the human diet as nutrients, but little is known about their processing and absorption in the digestive tract of mammals (20,21). Since molecular species containing α -linolenic acid (18:3) were the major species in MGDG and DGDG, these glycerogalactolipids would be an important source for this *n*-3 essential FA. To clarify the nutritional roles of plant glycolipids, the average daily intake in the human body has been estimated to be 140 mg ASG, 65 mg SG, 50 mg ceramide monohexoside, 90 mg MGDG, and 220 mg DGDG (4). Fruits of red bell pepper appear to be a rich source of such glycolipids in addition to the sources of carotenoid pigments and some other micronutrients.

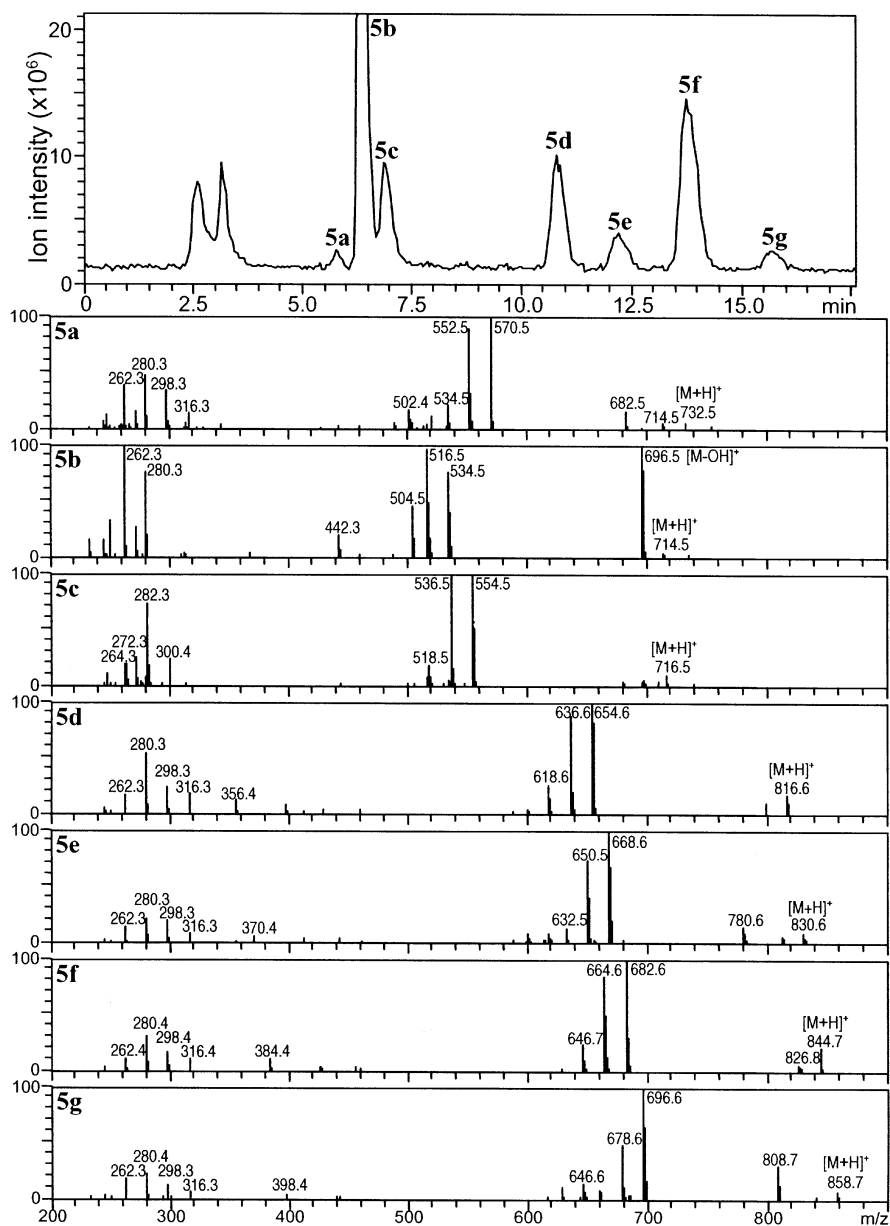


Fig. 9.6. Total ion chromatogram and mass spectra of ceramide monoglucoside from red bell pepper by HPLC/APCI-MS. HPLC conditions are the same as described in Figure 9.3. Mass spectra of peaks 5a–g are shown.

TABLE 9.3
Calculated Masses of the Molecular Species of Ceramide Monoglucoside

| Ion | Molecular species (sphingoid/2-hydroxy FA) ^a | | | | | | | |
|--|---|-----------------|-------------|-------------|-------------|-------------|-------------|--|
| | t18:1/16h:0 | d18:2/16h:0 | d18:1/16h:0 | t18:1/22h:0 | t18:1/23h:0 | t18:1/24h:0 | t18:1/25h:0 | |
| [M + H] ⁺ | 732.6 ^b | 714.6 | 716.6 | 816.7 | 830.7 | 844.7 | 858.7 | |
| [M - OH] ⁺ | 714.6 | 696.5 | 698.6 | 798.7 | 812.7 | 826.7 | 840.7 | |
| Ceramide moiety | | | | | | | | |
| [M - C ₆ H ₉ O ₅] ⁺ | 570.5 | ND ^c | 554.5 | 654.6 | 668.6 | 682.6 | 696.7 | |
| [M - C ₆ H ₁₁ O ₆] ⁺ | 552.5 | 534.5 | 536.5 | 636.6 | 650.6 | 664.6 | 678.6 | |
| [M - C ₆ H ₁₃ O ₇] ⁺ | 534.5 | 516.5 | 518.5 | 618.6 | 632.6 | 646.6 | 660.6 | |
| Sphingoid moiety | | | | | | | | |
| [R ¹ CH(OH)CH(NH ₂)CH ₂ OH] ⁺ | 316.3 | ND | 300.3 | 316.3 | 316.3 | 316.3 | 316.3 | |
| [R ¹ CH(OH)CH(NH ₂)CH ₂] ⁺ | 298.3 | 280.3 | 282.3 | 298.3 | 298.3 | 298.3 | 298.3 | |
| [R ¹ CH=CH(NH ₂)CH ₂] ⁺ | 280.3 | 262.3 | 264.3 | 280.3 | 280.3 | 280.3 | 280.3 | |
| [sphingoid - (H ₂ O) ₂] ⁺ | 262.3 | ND | ND | 262.3 | 262.3 | 262.3 | 262.3 | |
| 2-Hydroxy fatty acid moiety | | | | | | | | |
| [R ² CH(OH)CONH ₃] ⁺ | 272.3 | 272.3 | 272.3 | 356.4 | 370.4 | 384.4 | 398.4 | |
| Peak ^d | 5a | 5b | 5c | 5d | 5e | 5f | 5g | |
| % ^e | 3.2 | 47.4 | 11.7 | 11.5 | 5.0 | 18.0 | 3.2 | |

^aAbbreviations: t18:1, 4-hydroxy-8-sphingene; d18:2, 4,8-sphingadiene; d18:1, 8-sphingene; t16-25h:0, 2-hydroxy FA having carbon chain length 16–25.
^bm/z

^cND, not detected

^dPeak numbers correspond to those indicated in Figure 9.6.

^eValues indicate the peak percentage of total peak area measured by the total ion chromatogram described in Figure 9.6.

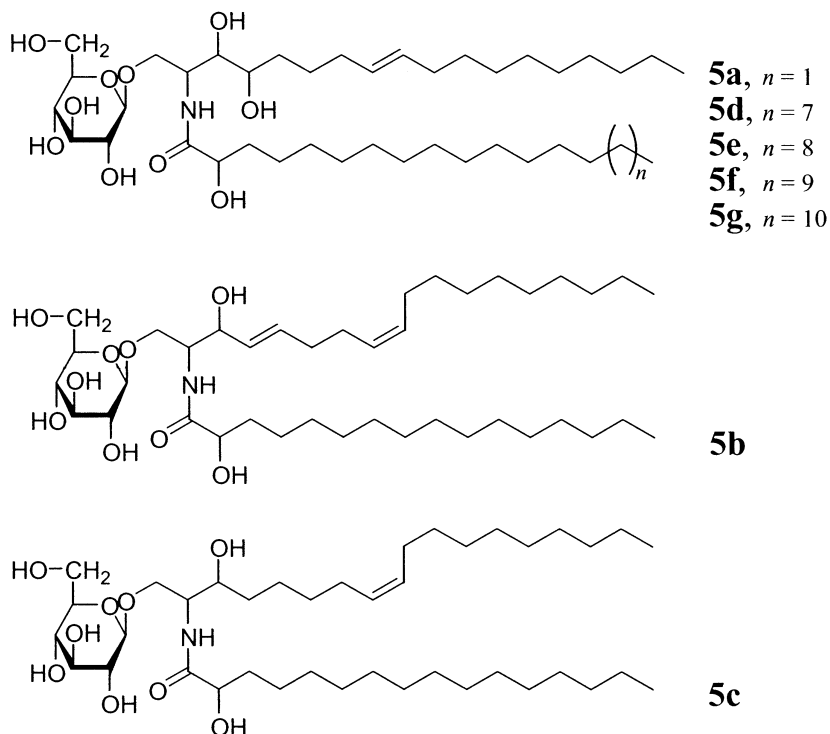


Fig. 9.7. Structures of molecular species of ceramide monoglucoside (5a–g).

Summary

Five major glycolipid classes (ASG, SG, MGDG, DGDG, and CMG) from the fruit paste of red bell pepper were separated by silica-gel column chromatography. The molecular species of each glycolipid were separated and identified by reversed-phase HPLC coupled with on-line APCI-MS. The molecular species of SG were β -sitosteryl and campesteryl glucosides, and those of ASG were their fatty acid esters. The dilinolenoyl species was predominant in MGDG in addition to small amounts of five other molecular species, whereas DGDG consisted of seven molecular species varying in their degrees of unsaturation. The CMG class contained at least seven molecular species, which were characterized by ^1H NMR. The combination of HPLC and APCI-MS is convenient and reliable for the separation and identification of the molecular species of plant glycolipids without any chemical modifications.

References

- Allen, C.F., P. Good, H.F. Davis, P. Chisum, and S.D. Fowler, Methodology for the Separation of Plant Lipids and Application to Spinach Leaf and Chloroplast Lamellae, *J. Am. Oil Chem. Soc.* 43: 223–231 (1966).

2. Mudd, J.B., and R.E. Garcia, Biosynthesis of Glycolipids, in *Recent Advances in the Chemistry and Biochemistry of Plant Lipids*, edited by T. Galliard and E.I. Mercer, Academic Press, New York, 1975, Chapter 6, pp. 161–201.
3. Picchioni, G.A., A.E. Watada, and B.D. Whitaker, Quantitative High-Performance Liquid Chromatography Analysis of Plant Phospholipids and Glycolipids Using Light-Scattering Detection, *Lipids* 31: 217–221 (1996).
4. Sugawara, T., and T. Miyazawa, Separation and Determination of Glycolipids from Edible Plant Sources by High-Performance Liquid Chromatography and Evaporative Light-Scattering Detection, *Lipids* 34: 1231–1237 (1999).
5. Kinsella, J.E., Composition of the Lipids of Cucumber and Peppers, *J. Food Sci.* 36: 865–866 (1971).
6. Whitaker, B.D., Cerebrosides in Mature-Green and Red-Ripe Bell Pepper and Tomato Fruits, *Phytochemistry* 42: 627–632 (1996).
7. Howard, L.R., R.T. Smith, A.B. Wagner, B. Villalon, and E.E. Burns, Provitamin A and Ascorbic Acid Content of Fresh Pepper Cultivars (*Capsicum annuum*) and Processed Jalapenos, *J. Food Sci.* 59: 362–365 (1994).
8. Howard, L.R., S.T. Talcott, C.H. Brenes, and B. Villalon, Changes in Phytochemical and Antioxidant Activity of Selected Pepper Cultivars (*Capsicum* species) as Influenced by Maturity, *J. Agric. Food Chem.* 48: 1713–1720 (2000).
9. Márkus, F., H.G. Daood, J. Kapitány, and P.A. Biacs, Change in the Carotenoid and Antioxidant Content of Spice Red Pepper (paprika) as a Function of Ripening and Some Technological Factors, *J. Agric. Food Chem.* 47: 100–107 (1999).
10. Byrdwell, W.C., Atmospheric Pressure Chemical Ionization Mass Spectrometry for Analysis of Lipids, *Lipids* 36: 327–346 (2001).
11. Folch, J., M. Lees, and G.H. Sloane-Stanley, A Simple Method for the Isolation and Purification of Total Lipids from Animal Tissues, *J. Biol. Chem.* 226: 497–509 (1957).
12. Christie, W.W., *Lipid Analysis. Isolation, Separation and Structural Analysis of Lipids*, 2nd ed., Pergamon Press, Oxford, UK, 1982.
13. Bortolomeazzi, R., M. De Zan, L. Pizzale, and L.S. Conte, Mass Spectrometry Characterization of the 5 α -, 7 α -, and 7 β -Hydroxy Derivatives of β -Sitosterol, Campesterol, Stigmasterol, and Brassicasterol, *J. Agric. Food Chem.* 47: 3069–3074 (1999).
14. Yamauchi, R., M. Kojima, M. Isogai, K. Kato, and Y. Ueno, Separation and Purification of Molecular Species of Galactolipids by High Performance Liquid Chromatography, *Agric. Biol. Chem.* 46: 2847–2849 (1982).
15. Demandre, C., A. Tremolieres, A.-M. Justin, and P. Mazliak, Analysis of Molecular Species of Plant Polar Lipids by High-Performance and Gas Liquid Chromatography, *Phytochemistry* 24: 481–485 (1985).
16. Kawai, G., and Y. Ikeda, Chemistry and Functional Moiety of Fruiting-Inducing Cerebrosides in *Schizophyllum commune*, *Biochim. Biophys. Acta* 754: 243–248 (1983).
17. Kawai, G., and Y. Ikeda, Structure of Biological Active and Inactive Cerebrosides Prepared from *Schizophyllum commune*, *J. Lipid Res.* 26: 338–343 (1985).
18. Kawai, G., M. Ohnishi, Y. Fujino, and Y. Ikeda, Stimulatory Effect of Certain Plant Sphingolipids on Fruiting of *Schizophyllum commune*, *J. Biol. Chem.* 261: 779–784 (1986).
19. Yamauchi, R., K. Aizawa, T. Inakuma, and K. Kato, Analysis of Molecular Species of Glycolipids in Fruit Pastes of Red Bell Pepper (*Capsicum annuum* L.) by High-Performance Liquid Chromatography–Mass Spectrometry, *J. Agric. Food Chem.* 49: 622–627 (2001).

20. Andersson, L., C. Bratt, K.C. Arnoldsson, B. Herslöf, N.U. Olsson, B. Sternby, *et al.*, Hydrolysis of Galactolipids by Human Pancreatic Lipolytic Enzymes and Duodenal Contents, *J. Lipid Res.* 36: 1392–1400 (1995).
21. Ohlsson, L., M. Blom, K. Bohlinder, A. Carlsson, and Å. Nilsson, Orally Fed Digalactosyldiacylglycerol Is Degraded During Absorption in Intact and Lymphatic Duct Cannulated Rats, *J. Nutr.* 128: 239–245 (1998).

Chapter 10

Liquid Chromatography/Mass Spectrometry Analysis of Biosurfactant Glycolipids Secreted by Microorganisms

Alberto Nuñez, Robert A. Moreau, and Thomas A. Foglia

Eastern Regional Research Center, Agricultural Research Service, U.S. Department of
Agriculture, Wyndmoor, PA 19038

Introduction

Biosurfactant glycolipids are compounds with a sugar residue linked to a lipid hydrophobic moiety by a glycosidic bond; their structures vary in size, complexity, and function and they are part of the larger family of glycoconjugates. Microorganisms such as yeasts and bacteria can secrete large amounts of simple extracellular glycolipids containing a mono- or disaccharide glycosylated to a hydroxy fatty acid (FA) (1). The amphiphilic structure of these products imparts to them surfactant-like properties that make them attractive bioemulsifiers in which there is growing commercial interest (2,3).

Although strategies have been developed for their synthesis (4), the natural products secreted by microorganisms are usually preferred for marketing reasons (5). Most of these microorganisms produce a complex mixture of glycolipids and their structural identification requires sophisticated methods of analysis. In this sense, nuclear magnetic resonance (NMR) spectroscopy is usually a good option, but this method of analysis often requires tedious sample purification. Alternatively, mass spectrometry (MS) can provide information on glycolipid structures, especially if it is associated with a chromatographic separation technique. In general, glycolipids have molecular weights that are too large for gas chromatography (GC). The introduction of high performance liquid chromatography (HPLC) associated with mass spectrometry (LC/MS), however, has opened a new dimension in the analysis of glycolipids. Mass spectral characterization using ionization techniques such as electron impact (EI) causes extensive fragmentation of glycolipids, providing little information on molecular size or structural characteristics (6). On the other hand, “soft” ionization techniques such as atmospheric pressure chemical ionization (APCI) and electrospray ionization (ESI) often permit the identification of pseudomolecular ions and a controlled degree of fragmentation. Using these two ionization methods it is often possible to obtain fine structural information. When used in combination with HPLC, this technique allows further separation and quantification of complex mixtures of glycolipids. In this chapter the discussion will focus on the analysis of simple biosurfactant glycolipids

using LC/MS methods. Since these methods were developed for the characterization of sophorolipids and rhamnolipids, other glycolipids are not included, but it should be noted that the use of this analytical approach has the potential for analyzing other classes of natural glycolipids.

Sophorolipids

Candida Species Sophorolipids

The yeasts *Candida bombicola* and *Candida apicola* produce extracellular biosurfactant-type glycolipids that contain a disaccharide sophorose residue (2-*O*- β -D-glucopyranosyl- β -D-glucopyranose) bound to a hydroxy fatty acyl moiety. The sophorose ring, usually with acetylated hydroxyl groups at carbons 6' and 6'', has a glycosidic bond between carbon 1' of the disaccharide and the ω -1 hydroxy group of the FA chain, with a minor proportion attached to an ω hydroxy fatty acyl group, as shown in Figure 10.1. The carboxylic group in the lipid portion can be either free or lactonized to carbon 4'' of the disaccharide. Depending on the carbon source used for organism growth, the FA chain length varies from 16 to 18 carbons and may or may not be unsaturated (7). The C18:1 FA sophorolipid lactone, shown as **1a** in Figure 10.1, is the main product secreted by *C. bombicola* and *C. apicola*, and is typically accompanied by a small proportion of the free acid form, **1b**. Changes in growth conditions can effectively alter sophorolipid yield and introduce modifications at the lipid portion that are related to the type of the carbon source used for growth (8,9). However, the proportion of lactonized product in the mixture also depends on the type of yeast used. It was reported that the free acid form is the only sophorolipid produced by *Rhodotorula bogoriensis* (formerly *Candida bogoriensis*) with a C22:0 hydroxy FA (10).

The industrial interest in biodegradable products has motivated many research groups to undertake enzymatic and chemical modifications of the sophorolipid structure in their search for new applications for these biosurfactants. Consequently, methods of analysis for these materials must provide structural information to follow the chemical alterations introduced either to the lipid or saccharide portion of the sophorolipid. Purification and separation of the sophorolipids have been effectively achieved by using reversed-phase HPLC methods associated with evaporative light-scattering detection (11); however, these detectors do not provide structural information. Extensive structural analysis of sophorolipids produced by *C. bombicola*, together with their enzymatically hydrolyzed products was accomplished using fast atom bombardment (FAB) ionization MS and NMR spectroscopy (12). After chromatographic fractionation of the sophorolipid molecular species, FAB-MS generated ion fragments by collision induced dissociation (CID) that allowed detailed structural elucidation.

A combination of HPLC and positive APCI-MS was first reported by Nuñez and colleagues (13). The method combined the structural information derived from

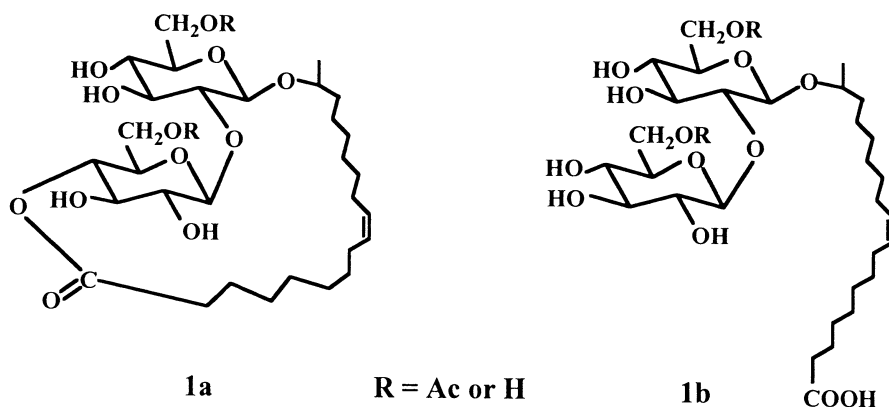


Fig. 10.1. Scheme of the sophorose ring, showing acetylated hydroxyl groups at carbons 6' and 6'', glycosidic bond between carbon 1' of the disaccharide and the ω -1 hydroxy group of the FA chain in the lactonized and free acid form.

the ionization and fragmentation associated with MS with the separation capability of reversed-phase HPLC. This analysis protocol was used for the quantification of the different sophorolipids produced by *C. bombicola* when grown on different carbon substrates. In this study, lactone **1a** (Fig. 10.1) was reported to have the APCI-MS mass spectrum shown in Figure 10.2A, where the pseudomolecular ion was formed after the addition of a proton, $[M+H]^+$, or sodium ion, $[M+Na]^+$, to give ions at m/z 689 and 711, respectively. Since the HPLC method used a gradient of H₂O-acetonitrile, the addition of 23 amu to the molecule ion might also result from solvent cluster addition, as was previously observed with the analysis of other lipids using APCI-MS (14). The most significant difference between these two types of ion addition is that the cationic adduct results in less informative structural fragmentation, as reported in a CID FAB-MS study of sophorolipids (12). The LC/APCI-MS instruments used in the authors' laboratory for sophorolipid analysis had an orthogonal probe configuration that allowed the adjustment of the position of the capillary tip in two dimensions in relationship to the corona pin that produced the ionization.

The ratio between the $[M+H]^+$ and $[M+23]^+$ ions was significantly affected by the probe position. Since the protonated molecule gives the best fragmentation information, the probe position was tuned to maximize the $[M+H]^+$. The protonated molecule showed characteristic losses of H₂O, producing ion peaks at m/z 671, 653, and 635 (Fig. 10.2A). The presence of acetyl groups on the sugar ring was evidenced by the loss of 42 amu from the ion at m/z 635, generating the ion at m/z 593, followed by another H₂O loss (ion at m/z 575). De Koster and colleagues (12) proposed the pathway shown in Figure 10.3 for the positive CID FAB-MS fragmentation and elimination of a hexose ring from lactonized sophorolipids. This mechanism initially proposed that a thermochemically favorable protonation

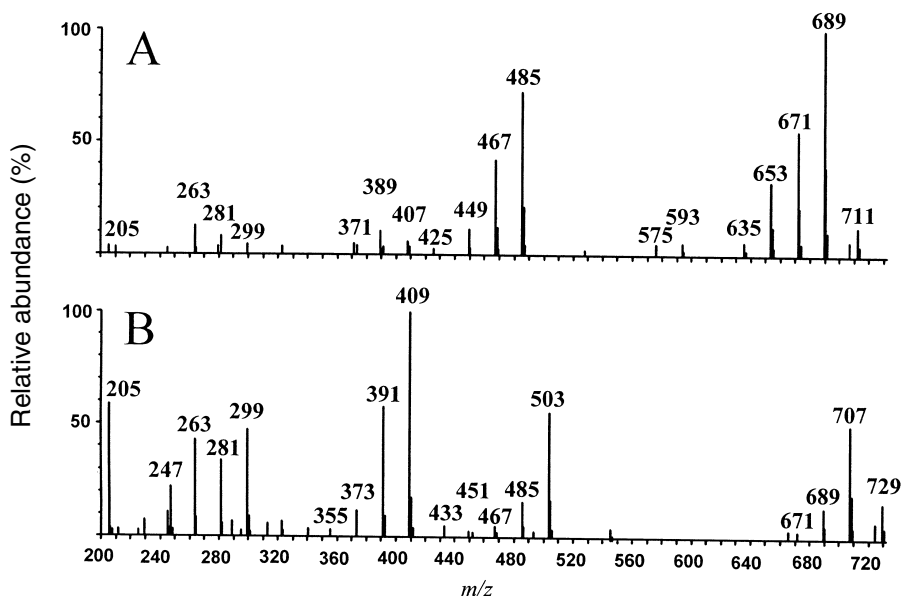


Fig. 10.2. Positive-ion APCI-MS mass spectrum of C18:1 diacetylated sophorolipids. (A) Lactone form. (B) Free acid form. *Source:* Reference 13.

process occurs at the ether oxygen, followed by cleavage of the glycosidic bond with the subsequent elimination of a hexose fragment (204 amu) from the acetylated carbon 6' (AcOC₆H₉O₅), or loss of the nonacetylated ring (C₆H₁₀O₅, 162 amu). A similar pathway can be used to explain the loss of the hexose ring that generates the second most abundant ion at *m/z* 485 in the positive APCI-MS mass spectrum of the C18:1 sophorolipid lactone (Fig. 10.2A). Subsequent loss of multiple H₂O molecules and the acetyl group from the protonated molecule (*m/z* 671) resulted in the fragmentation pattern observed in Figure 10.2A.

Direct evidence for the lipid moiety glycosylated to the sophorose was found in the spectrum of Figure 10.2A from the low intensity ion at *m/z* 299, which was assigned to a protonated C18:1 hydroxy FA that lost two H₂O molecules to produce ions at *m/z* 281 and 263. The CID FAB-MS spectrum of the lactone structure reported by de Koster and colleagues (12) lacked the corresponding ion, and its absence was taken as evidence for this sophorolipid form. The observation of the hydroxy FA ion in the spectrum indicated the presence of the free acid sophorolipid form.

The spectra in Figure 10.2 indicate that both sophorolipid forms gave the protonated hydroxy FA ion at *m/z* 299, but it is of a higher intensity in the spectrum of the molecule in the free acid form (Fig. 10.2B). Overall, the free acid form had a fragmentation pattern similar to the lactone form, but gave a characteristic ion at *m/z* 409 (base peak) that was identified as the acetylated sophorose ring after los-

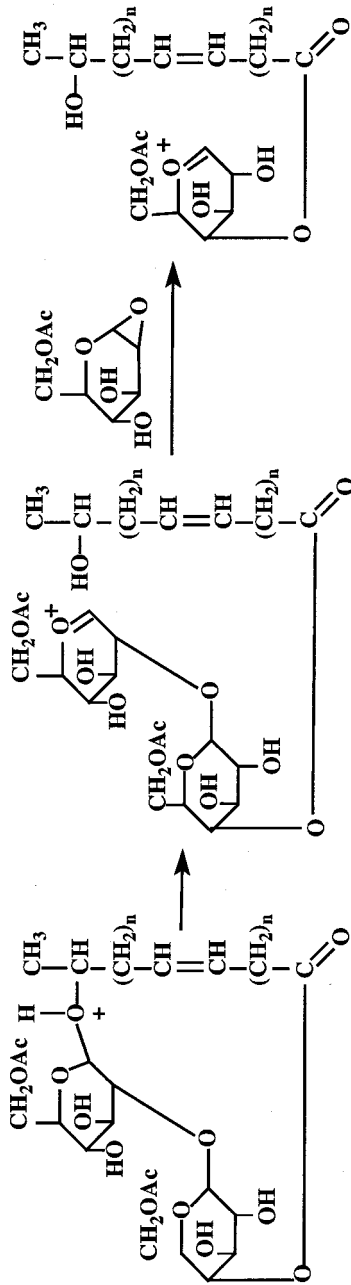


Fig. 10.3. Pathway proposed by Koster *et al.* (12) for the positive CID FAB-MS fragmentation and elimination of a hexose ring from lactonized sophorolipids.

ing the FA. The corresponding ion at m/z 409 in the spectrum of the lactonized sophorolipid is small (Fig. 10.2A); consequently its appearance at high or moderate intensity is interpreted as direct evidence for identification of the sophorolipid free acid form. However, the m/z 409 ion intensity also seems to be related to the degree of acetylation of the sophorose ring, since it diminishes with a decrease in the degree of acetylation (see later discussion).

The APCI-MS chromatogram obtained with a C18 column shows the elution of the sophorolipids produced by *C. bombicola* when grown with soybean oil as the carbon source (Fig. 10.4A), as reported by Nuñez and colleagues (13). The individual lactonized sophorolipids were identified after plotting the range of m/z 600–700 (Fig. 10.4B). Elution of the free acid sophorolipid forms was highlighted by reconstructing the chromatogram with the ion at m/z 409 (Fig. 10.4C). The LC/APCI-MS chromatograms in Figure 10.2 show second peaks for each sophorolipid, which were reported to give identical spectra but with intensities that depended fundamentally on the sophorolipid homolog (13). The C16:0 sophorolipid lactone had these second eluting chromatographic peaks with similar intensities (Fig. 10.4A and B), but the intensities of the peaks following the lactones with C18:1 or C18:0 hydroxy FA moieties were between 10–20%. Also, the authors reported the presence of two unresolved chromatographic peaks that were ascribed to the C18:2 lactone sophorolipid; however the peaks were resolved for the corresponding free acid form (Fig. 10.4C).

GC/MS and NMR analysis of the hydroxy FA obtained by hydrolysis of the sophorolipids showed that these chromatographic peaks correspond to the species that were glycosylated at the ω -1 or ω carbon positions, with the ω -1 being the dominant product for the C18:0, C18:1, and C18:2 sophorolipids (13).

The chromatogram in Figure 10.4B shows two unknown peaks denoted with question marks. These peaks were reported to have similar spectra, consistent with C17:0 hydroxy FA lactones, but they eluted too far apart to be the ω -1 and ω isomers. The presence of a C17:0 hydroxy FA was confirmed by GC/MS analysis of the hydrolyzed FA but no explanation for the structural differences between the isomers was established from the APCI-MS analysis (13). Also, the chromatogram in Figure 10.4C has a peak eluted below 3 min noted with a question mark. The spectrum associated with this chromatographic peak (not shown) had a $[M+H]^+$ at m/z 779, along with a peak at m/z 761 (the base peak) representing a loss of H_2O , and a peak at m/z 575 formed by the loss of an acetylated hexose ring. The spectrum also had ions at m/z 409 and 297, consistent with a C18:2 free acid sophorolipid form. However, an ion of significant intensity at m/z 371, which was 74 amu apart from the 297 ion in the APCI-MS spectrum, was taken as evidence of a monoglyceride ester of the C18:2 nonlactonized sophorolipid acid form (13).

Sophorolipid compositions resulting by growing *T. bombicola* on glucose as the carbon source or in combination with soybean oil or hexadecane as a secondary carbon source were analyzed by Hu and Ju (15) using negative LC/ESI-MSⁿ with an ion trap. The reversed-phase HPLC method used for separation of the sophorolipids used

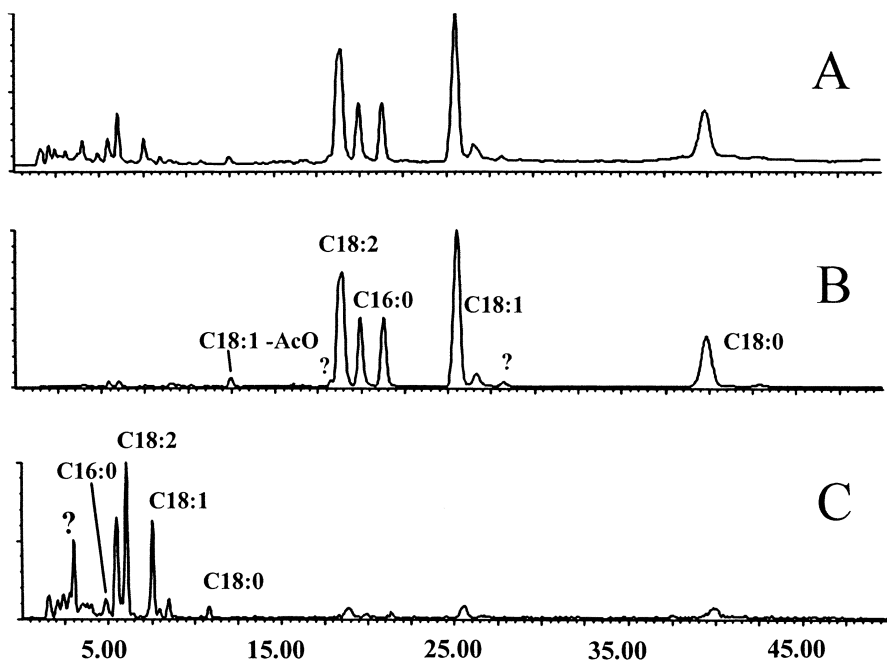


Fig. 10.4. LC/APCI-MS chromatographic profile, on a C18 column, of sophorolipids produced by *C. bombicola* when grown with soybean oil as the carbon source. (A) Total ion current chromatogram. (B) Reconstructed ion chromatogram in the mass region of m/z 600–700 showing the elution of lactonized sophorolipid forms. (C) Reconstructed chromatogram of the ion at m/z 409, showing the free acid form elution. *Source:* Reference 13.

acetonitrile/water (8:2, vol/vol) and a C18 column. In this paper, sophorolipid structural information was obtained by CID/MS-MS of selected ions using helium as the collision gas. First, the sophorolipid mixtures were infused into the mass spectrometer and the specific negative ions corresponding to individual components were trapped and fragmented in order to determine structural details. Characteristic loss of the acetyl groups and the glucose ring established the level of acetylation and provided information on the disaccharide portion of the molecule; the loss of two glucose fragments provided information on the hydroxy FA moiety. Second, the analysis was also conducted with LC/ESI-MSⁿ. Authors Hu and Ju observed the elution of two peaks with different intensities and a fragmentation pattern that indicated the same hydroxy FA residue. They concluded that the peaks corresponded to the ω and $\omega-1$ isomers, consistent with previous findings (13). The use of soybean oil as a carbon source produced a sophorolipid mixture with a dominant lactone form and a hydroxy FA profile consistent with the typical FA distribution of soybean oil, reflecting the influence of vegetable oil type on sophorolipid structure,

as was also observed previously (13). The use of hexadecane as the carbon source gave a more selective product distribution, with the C16:0 and C18:1 lactones being the main products (15).

Rhodotorula bogoriensis Sophorolipids

Early work with *R. bogoriensis* (formerly *C. bogoriensis*) demonstrated that this yeast produces a biosurfactant product with a sophorose sugar having a variable degree of acetylation on its primary alcohols, glycosylated to a C22:0 FA at carbon 13, as shown in **2**, Figure 10.6 (16). The sophorolipids produced by this yeast also were analyzed using a variation of the LC/APCI-MS method previously reported by Nuñez and colleagues (13,17). The LC chromatogram of the product had four major peaks as shown in Figure 10.5A. The spectra corresponding to these peaks had protonated molecules 42 amu apart (Fig. 10.7), indicating that the nonacetylated product **2c** eluted first, followed by two positional monoacetylated isomers, product **2b**, and the diacetylated product **2a** eluted last.

The mass spectra of **2** had fragmentation patterns similar to those reported for the sophorolipids from *C. bombicola* (Fig. 10.2). The loss of an acetylated hexose ring from the diacetylated sophorose ring was evident from the ion at m/z 561, as expected (Fig. 10.7A). The monoacetylated products, which eluted as the two intermediate peaks in the chromatogram in Figure 10.5A, have similar spectra, with the same pseudomolecular ion and showing hexose elimination by the ions at m/z 561 and 519 (Fig. 10.7B). No conclusion about the location of the acetyl group was possible from their mass spectra. Similarly, hexose ring loss from the nonacetylated sophorolipid was indicated by the ion at m/z 519 (Fig. 10.7C). The characteristic ion for the sophorose ring at m/z 409 provided evidence for the presence of the free acid form, as was observed for the sophorolipids from *C. bombicola*, discussed previously (13). The corresponding disaccharide fragment ions for the mono- and nonacetylated product were at m/z 367 and m/z 325, respectively, but their intensities decreased proportionally with the degree of acetylation, indicating a relationship between the acetyl group and the stability of the sophorose fragment.

In contrast to the hydroxy FA profile observed for the sophorolipid from *C. bombicola*, the mass spectra of all major peaks in the chromatogram in Figure 10.5A indicated the presence of a C22:0 hydroxy FA with an ion at m/z 357, followed by the subsequent loss of two H₂O molecules generating ions at m/z 339 and 321. A closer examination of the spectra in Figure 10.7 indicated the presence of two common ions, 18 amu apart, at m/z 398 and 380. This was explained as the addition of acetonitrile to the hydroxy FA with the subsequent loss of H₂O. The formation of solvent adducts is common in LC/APCI-MS methods that use acetonitrile in the mobile phase (14).

Replacement of acetonitrile with methanol eliminates the aforementioned solvent adducts as shown in Figure 10.8A for the nonacetylated C22:0 sophorolipid that was obtained after basic hydrolysis of the products secreted by *R. bogoriensis*. However,

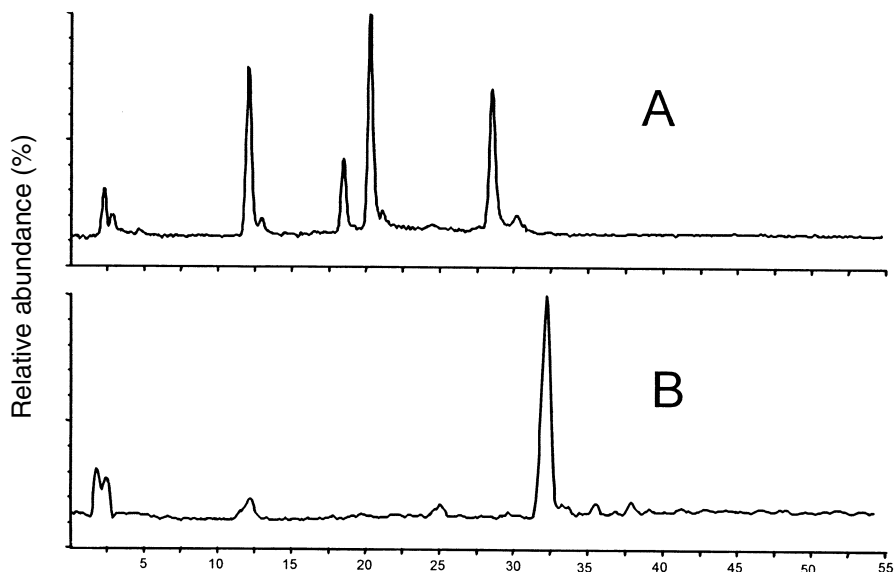


Fig. 10.5. LC/APCI-MS chromatographic elution of sophorolipids produced by *R. bogoriensis*: (A) Sophorolipid mixture of product **2** (Fig. 10.3). (B) Elution of the products of lipase activity, which produced hydrolyzed product **2c**. Source: Reference 17.

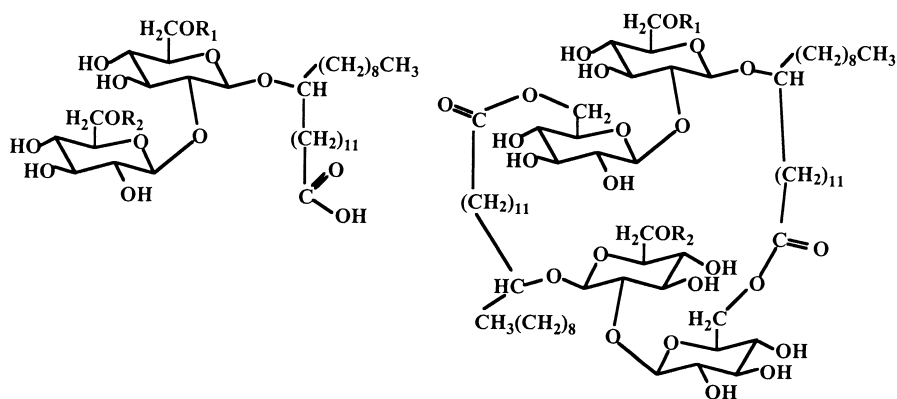
acetonitrile was the better solvent for the HPLC separation of this sophorolipid mixture (17).

The chromatogram in Figure 10.5A shows second small peaks eluted after the major peaks, but spectroscopic evidence for their identification could not be obtained from the APCI-MS spectra. After the sophorolipid mixture was hydrolyzed, the APCI-MS mass spectrum for this small secondary peak, shown in Figure 10.8B, indicated a sophorolipid structure with a $[M+H]^+$ at m/z 709 and ions at m/z 385 and 367 after losing one molecule of H_2O , consistent with a C24:0 sophoro-lipid free acid form, which was not previously reported (16).

Sophorolipid Derivatives

Oligomeric and Polymeric Sophorolipids

The primary hydroxy groups on carbon 6' and 6'' of the sophorose rings and the free carboxylic acid of the FA moiety provide two reactive centers for the derivatization of these materials. Several studies have targeted these functionalities for the introduction of polymerizable groups with the goal of producing biopolymers with potential industrial and pharmaceutical applications (12,18–20). Chemo-enzymatic modified sophorolipids with multiple functionalities on the sugar ring and the FA



2a) $\text{R}_1 = \text{R}_2 = \text{Ac}$

2b) $\text{R}_1 = \text{H}; \text{R}_2 = \text{Ac}$

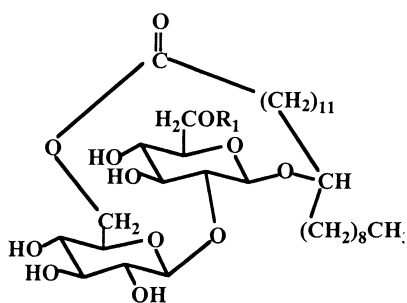
$\text{R}_1 = \text{Ac}; \text{R}_2 = \text{H}$

2c) $\text{R}_1 = \text{R}_2 = \text{H}$

3a) $\text{R}_1 = \text{R}_2 = \text{H}$

3b) $\text{R}_1 = \text{R}_2 = \text{H or Ac}$

3c) $\text{R}_1 = \text{R}_2 = \text{Ac}$



4a) $\text{R}_1 = \text{H}$

4b) $\text{R}_1 = \text{Ac}$

Fig. 10.6. Scheme of the C22:0 sophorolipids free acid form produced by *Rhodotorula bogoriensis* and the expected lipase-catalyzed esterification products.

moiety have been synthesized by Singh and colleagues (20), with the goal of making monomers for further polymerization. A structural analysis of the intermediate and final products was reported using NMR and LC/APCI-MS, but no mass spectra were presented or discussed.

Lipase-catalyzed oligomerization in tetrahydrofuran (THF) was reported for the sophorolipids produced by *C. bombicola* (21). The sophorolipid starting materials were deacetylated, ring-opened and polymerized in a lipase-mediated process using THF as solvent (21). In that study, evidence for oligomer formation was obtained by LC/ESI-MS analysis of the products. The chromatogram of the reaction product showed the conversion of the starting sophorolipid into a new material eluted at a longer retention time. The negative ion electrospray mass spectrum of

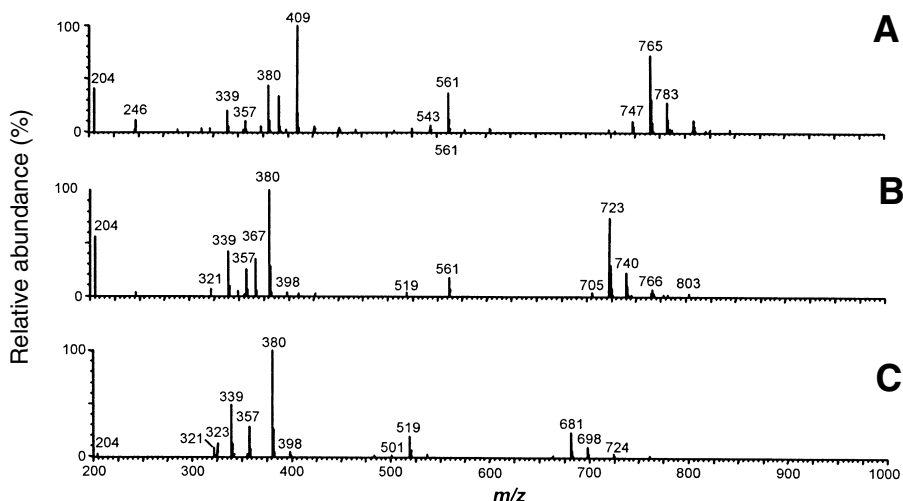


Fig. 10.7. APCI-MS mass spectra of the peaks in the chromatogram in Figure 10.5A: (A) Diacetylated sophorolipid **2a**. (B) Monoacetylated sophorolipid **2b**. (C) Nonacetylated sophorolipid **2c**. *Source:* Reference 17.

this product had ions at m/z 1240 and 2503 that were interpreted as being a cyclic dimer and a linear (ring-opened) tetramer product, respectively. However, no fragment ions were reported since the observed pseudomolecular ions were too low in intensity for further MS/MS analysis. The proposed lipase-catalyzed pathway for the formation of the products based on LC/ESI-MS analysis is shown in Figure 10.9.

Lipase-mediated dimerization was also studied for free acid sophorolipids from *R. bogoriensis* (17). The deacetylated sophorolipid **2c** (Fig. 10.6) was subjected to lipase-catalyzed interesterification in THF solvent. The isolated products were analyzed by LC/ESI-MS in both negative and positive modes. Chromatographic analysis of the products showed the conversion of the starting deacetylated sophorolipid **2c** (Fig. 10.6) to a new single peak eluted at the time shown in Figure 10.5B. The positive-ion ESI-MS spectrum of this product (Fig. 10.10, inset) had ions at m/z 1325 $[M+H]^+$, 1343 $[M+18]^+$ and $[M+23]^+$ consistent with dimer structure **3a** (Fig. 10.6) and similar to the structure reported previously (21). The pseudomolecular ions at higher masses in the negative-ion ESI-MS spectrum were also consistent with product **3a**. However, the spectrum in Figure 10.10 almost completely lacked fragments associated with the pseudomolecular ions in the higher mass region. Further investigation of the ability of lipase to form sophorolipid dimers also was investigated using a mixture of sophorolipid products **2** (Fig. 10.6).

Based on the degree of acetylation in the sophorolipid mixture starting materials, lipase catalysis should produce at least three acetylated dimer structures as shown for product **3** (Fig. 10.6). The LC/ESI-MS analysis showed a chromatogram with only two products, which was consistent with a lipase intraesterification to

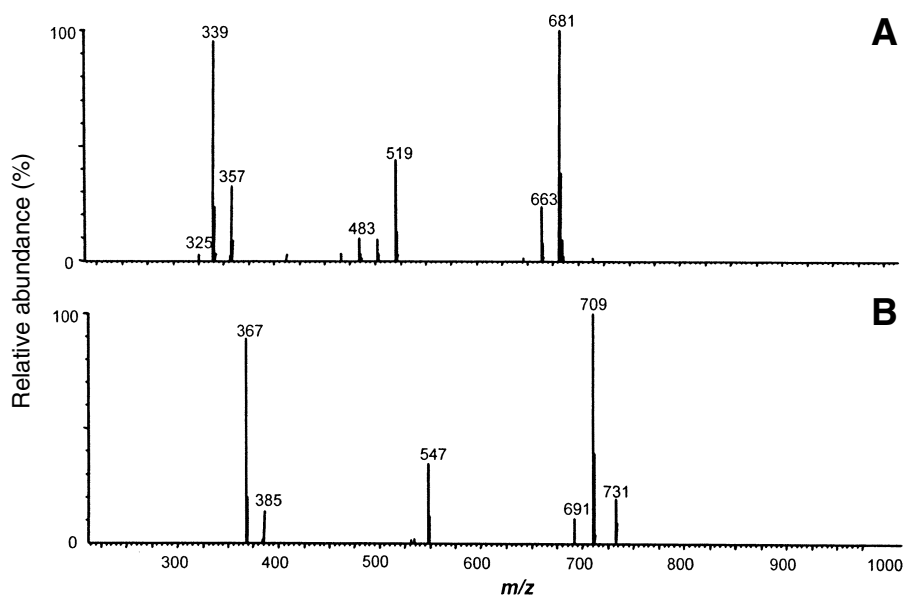


Fig. 10.8. APCI-MS mass spectrum obtained from the hydrolyzed sophorolipid produced by *C. bogoriensis* after replacing acetonitrile by methanol in the chromatographic method. (A) Main product formed after hydrolysis of **2**. (B) Minor companion peak showing a 28 amu shift in the m/z values of ions, indicating the presence of a hydroxy fatty acid with a 24-carbon chain. *Source:* Reference 17.

form lactonized product **4** (Fig. 10.6), where only two products are expected from the sophorolipids **2** used in the reaction. The ions at higher masses observed in Figure 10.10 were explained as a result of dimerization of **4a** (Fig. 10.6) in the ion source, producing the pseudomolecular ions $[2M+H]^+$ and $[2M+Na]^+$, with the corresponding formation of a solvent adduct and not a dimer product, as concluded in this study.

Galactopyranose Sophorolipids FA Ester

Nuñez and colleagues (22) reported the synthesis of sophorolipids esterified to the primary alcohol group of galactopyranose using immobilized *Candida antarctica* lipase as the catalyst. The sophorolipids produced by *C. bombicola* grown on oleic acid had a composition of 85% of C18:1 and 10% of C18:0. Figure 10.11 shows the multistep synthesis that started with the methanolysis of sophorolipid lactone **1** to the methyl ester **5**, followed by lipase-catalyzed re-acetylation of the sugar alcohols at carbon 6' and 6'' to product **6**, which avoided the cyclic intra-esterification of the carboxylic acid to the primary alcohols. The galactopyranose ketal derivative was used as a substrate in the lipase esterification with product **6** to overcome the limited organic solvent solubility of the underivatized sugar to produce **7** (Fig.

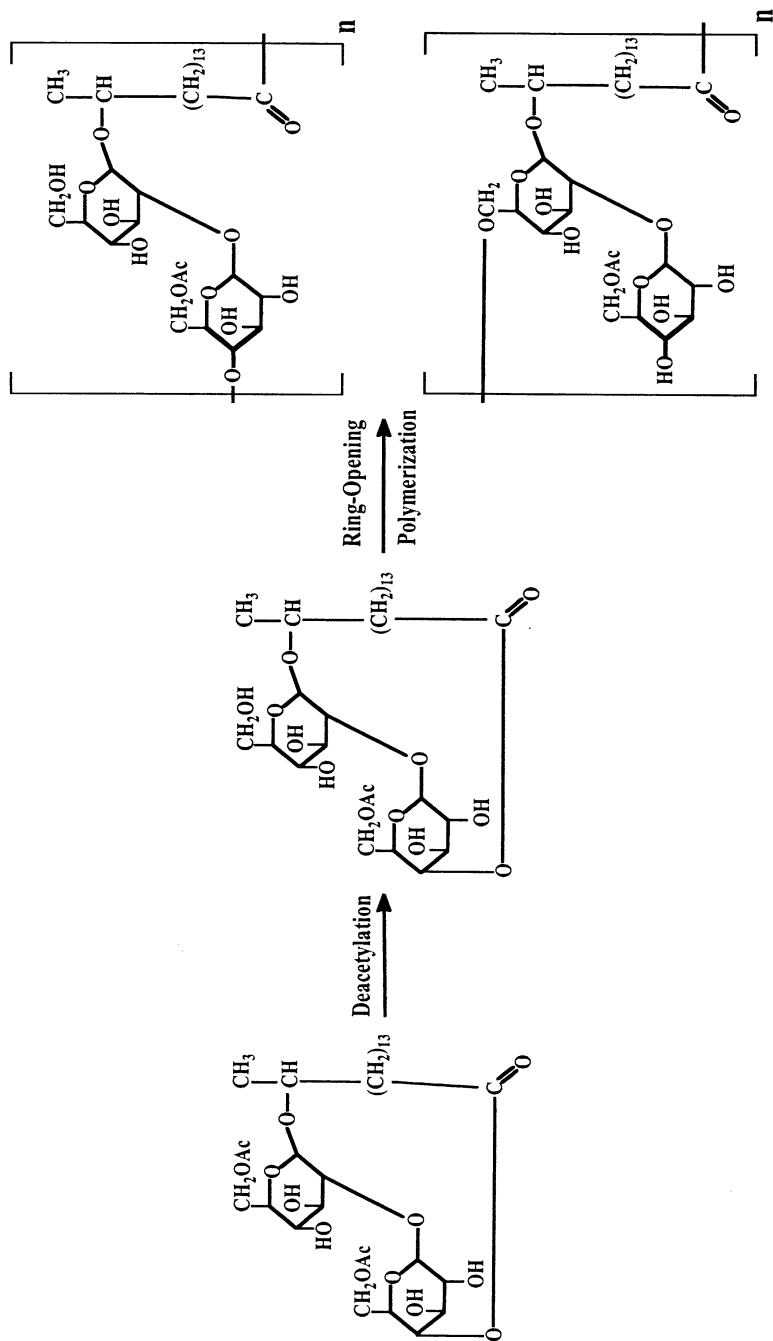


Fig. 10.9. Proposed pathway for the lipase-catalyzed oligomerization of lactone sophorolipids. Source: Reference 21.

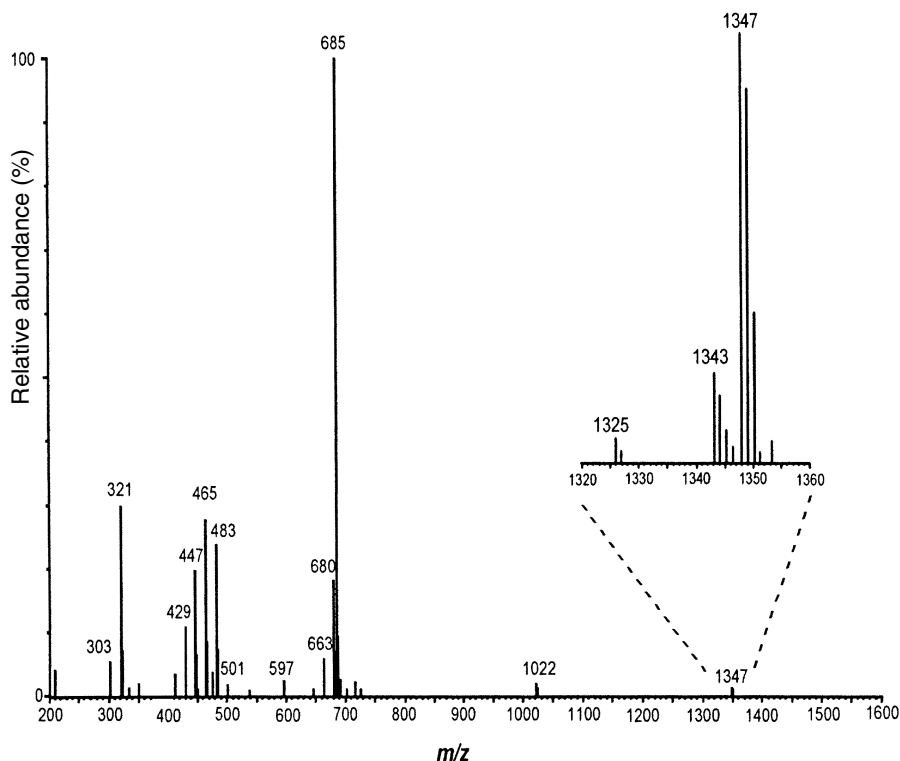


Fig. 10.10. ESI-MS mass spectrum of the lipase product with the structure **3c** in Figure 10.6, obtained by hydrolysis of the mixture of sophorolipids secreted by *C. bogoriensis*. Source: Reference 17.

10.11). Sophorolipid ester **8** was obtained after hydrolysis of **7** in $\text{HBF}_4/\text{acetonitrile}/\text{water}$ (9:1). Products formed during the different steps of this synthesis were analyzed by LC/MS.

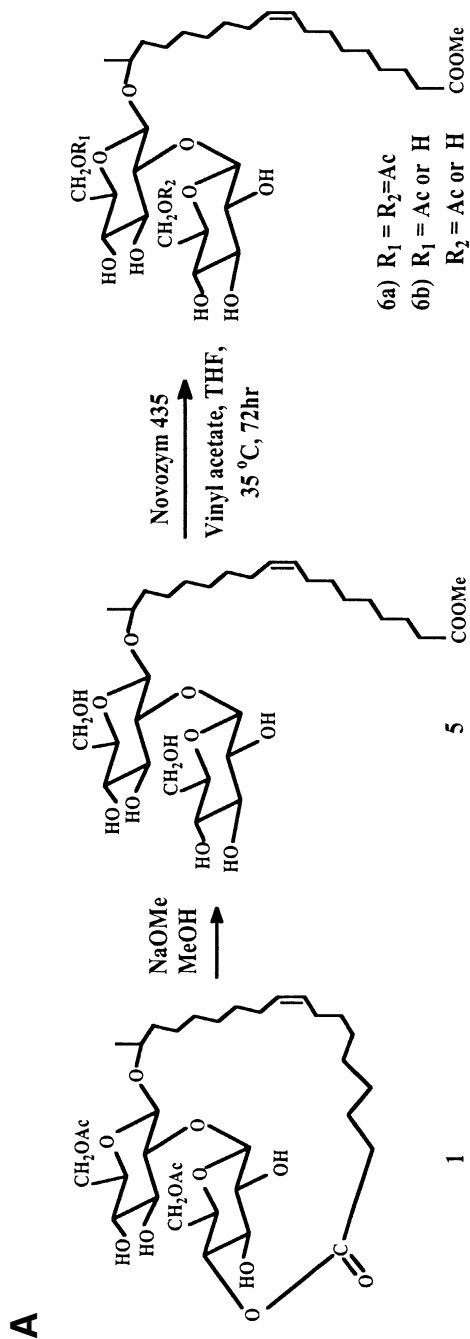
The methylated and diacetylated product **6a** had an APCI-MS mass spectrum with a protonated molecule, $[\text{M}+\text{H}]^+$, at m/z 721 (32%) and characteristic ions corresponding to methylated hydroxy FA at m/z 313 (100%) and the sophorose ring at m/z 409 (38%). The lipase-catalyzed acetylation also produced the monoacetylated product **6b** (5–10%). The APCI-MS spectrum of the latter product did not give sufficient evidence to determine whether acetylation occurred at carbon 6' or 6'', but chromatographic analysis indicated the formation of only one monoacetylated product. After acetylation, sophorolipid **6** was esterified to the ketal derivative of galactopyranose. Analysis of **7** by LC/APCI-MS, Figure 10.11, resulted in a chromatogram with four peaks associated with sugar esterification. A diacetylated product, **7a**, was assigned to the later eluting peak in the chromatographic order based on evidence in its mass spectrum. The APCI-MS mass spectrum for this product

showed a $[M+H]^+$ ion at m/z 949 (5%) and a major ion at m/z 891 (52%), consistent with the loss of acetone (58 amu) from the cyclic sugar ketal. The loss of an acetylated hexose ring from the sophorose portion, $[M+H-204]^+$, was observed as a small ion at m/z 745 (2%). This loss was more significant from the ion at m/z 891, which generated an ion at m/z 687 (28%), representing $[M+H-58-204]^+$. An ion at m/z 541 (90%) was identified as the elimination of the sophorose portion, $[M+H-204-204]^+$, with the subsequent loss of H_2O to form the base peak ion at m/z 483. The nonacetylated product **7c** eluted early, followed by two chromatographic peaks for the monoacetylated products **7b**. Despite product **6** being 90 to 95% diacetylated, the fact that a cyclic lactone structure formed between the primary alcohol at carbon 6'' on the sugar ring and the carboxylic acid was indicated in a yield of 9% for the monoacetylated and 14% for the nonacetylated products in the synthesis of **7**. The results from the LC/APCI-MS analysis of product **7** in this study suggest that the protonation of this product was occurring at the glycosidic bond rather than at the ester bond, because the loss of the galactose fragment was not observed in the spectrum.

Product **8**, produced by hydrolysis of **7** in HBF₄/acetonitrile/water (9:1), was characterized by positive and negative ESI-MS. Both ionization approaches used for characterization of product **8** resulted in LC/ESI-MS chromatograms with the same elution profile, indicating the formation of three products, as shown in Figure 10.12. The positive ESI-MS spectrum of the first eluting peak (Fig. 10.12A) had a protonated molecule at m/z 807 consistent with structure **8** (Fig. 10.11) after addition of a sodium ion to the molecule (Fig. 10.13A), but no $[M+H]^+$ was observed. Addition of ammonium acetate to the elution solvent produced an ion at m/z 802, identified as $[M+NH_4]^+$, with a small ion at m/z 785 corresponding to $[M+H]^+$. When protonated, structure **8** generated an ion at m/z 605 indicating the loss of 180 amu, corresponding to the possible loss of the galactose ring followed by the loss of H_2O (ion at m/z 587). The loss of a nonacetylated hexose ring (162 amu) from the sophorose portion generated the ion at m/z 443 with the subsequent loss of multiple H_2O molecules. Also, the ion at m/z 461 was explained as two consecutive losses of nonacetylated hexose rings from the $[M+H]^+$. Figure 10.13A and B indicate that no fragmentation occurred to the cationic adducts because the fragmentation patterns in both spectra are similar and consistent with the protonated molecule precursor.

Further confirmation of the pseudomolecular ion assigned to structure **8** was obtained from the negative ESI-MS spectrum, which had a pseudomolecular ion at m/z 783 $[M-H]^-$, (Fig. 10.13C). The base ion peak at m/z 621 in this spectrum indicated the loss of 162 amu followed by the loss of H_2O , producing the ion at m/z 603. This loss of 162 amu could happen either from the sophorose or galactose portion. To further investigate this loss, the product mixture **7** was hydrolyzed under conditions where the resulting products retained the acetylated groups on the sophorose ring.

The negative ion ESI-MS mass spectrum of the diacetylated product had an $[M-H]^-$ ion at m/z 867, with subsequent loss of 162 amu. Since the hexose ring from the acetylated sophorose portion should have a loss of 204 amu, it was concluded that in the negative mode the loss of 162 corresponded to a hexose ring



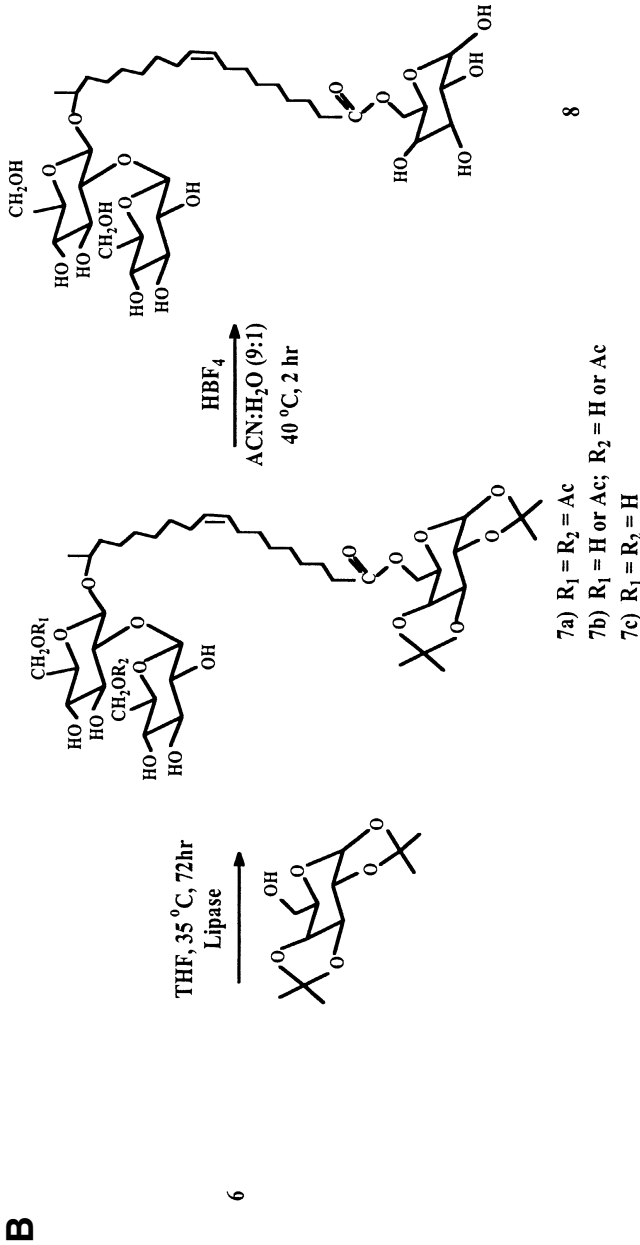


Fig. 10.11. Pathway for the synthesis of galactopyranose sophorolipid FA esters. A) Lactone ring opening and lipase acetylation of the C18:1 sophorolipids. B) Lipase esterification of the galactose derivative followed by acid hydrolysis to form the galactopyranose FA ester product. Source: Reference 22.

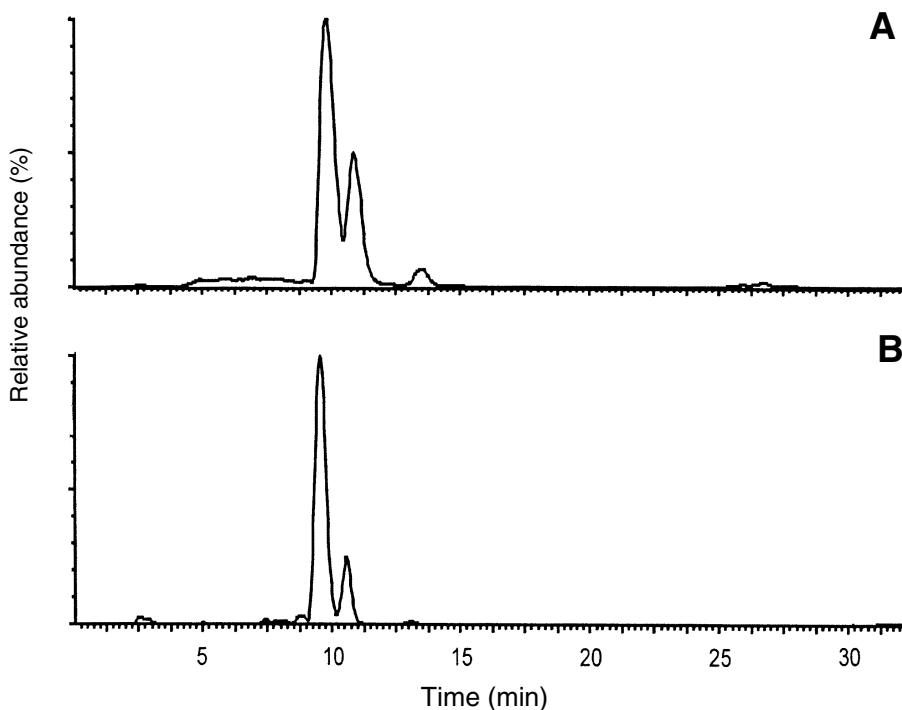


Fig. 10.12. LC/ESI-MS chromatograms of the sophorolipid product derivative **8** shown in Figure 10.5. (A) Positive ESI. (B) Negative ESI. *Source:* Reference 22.

from the galactose esterified to the sophorolipid. Characteristic losses of 60 and 90 amu from the $[M+H]^+$ in the negative-ion mode (Fig. 10.13C) were consistent with neutral losses observed in a sugar ring where the ionization takes place at the reducing end of the galactose residue (23). The second partially resolved peak eluting in the chromatograms in Figure 10.12 was identified as a C18:1 ω hydroxy FA isomer, while the ω -1 C18:0 FA isomer was assigned to the third small peak in Figure 10.12A. The ion at m/z at 263 in Figure 10.13A and B was associated with the hydroxy FA that underwent a fragmentation process to produce a C18:2 acylium ion; however, the negative ion spectrum did not provide direct evidence for the FA moiety.

Rhamnolipids

Another important class of biosurfactants is the rhamnolipids, which are secreted by several strains of *Pseudomonas aeruginosa*. These bioemulsifiers have properties similar to sophorolipids and have been subjects of numerous studies because of their potential application as antimicrobial nontoxic surfactants (3,5). However, most of the reports are associated with the intrinsic properties of these biosurfac-

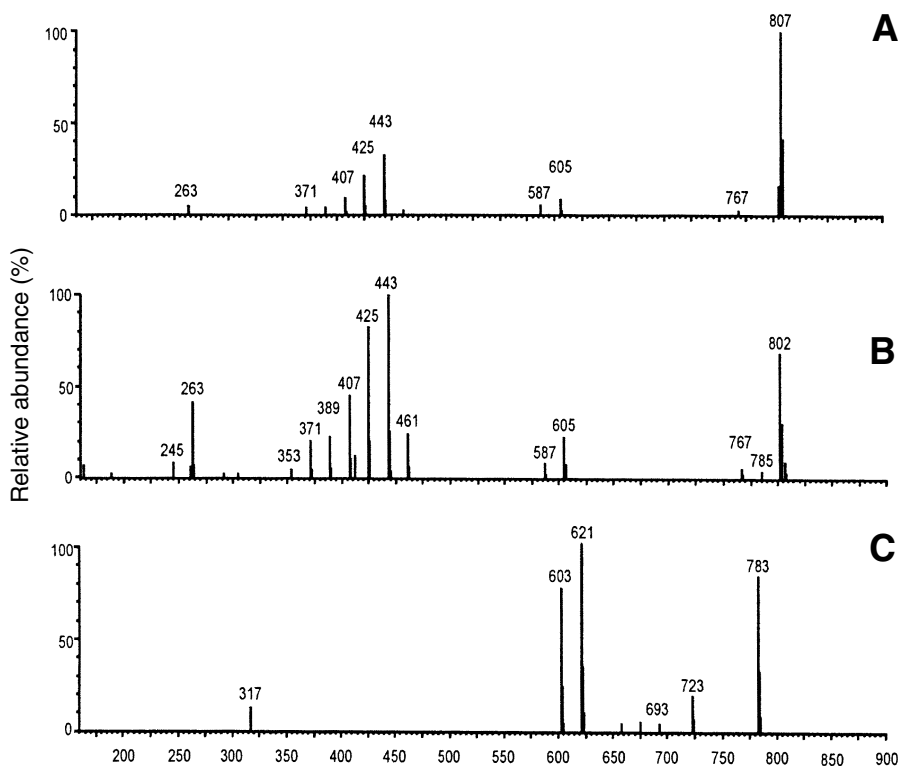


Fig. 10.13. ESI-MS spectra of **8** eluted as the main peak in Figure 10.2. (A) Positive ESI-MS mass spectrum showing the sodium addition to the molecule. (B) Positive ESI-MS spectrum showing the addition of NH₄⁺ to the molecule. (C) Negative ESI spectrum showing the [M-H]⁻ deprotonated molecule. *Source:* Reference 22.

tants and not with post-harvest chemical or enzymatic modifications. These amphiphilic surfactants are composed of a monosaccharide, α -L-rhamnopyranose (Rha), or a disaccharide, 2'-O- α -L-rhamnopyranosyl- α -L-rhamnopyranose (Rha-Rha) glycosylated to a β -hydroxycarboxylic acid that most frequently is esterified to a second β -hydroxycarboxylic acid as shown in Figure 10.14 for **9** and **10**, respectively. The β -hydroxy FA chain length varies between 8 and 14 carbons that may contain one double bond per FA chain. The fact that more than one hydroxy FA is present in the rhamnolipid structure generates a number of rhamnolipid products, referred to as "congener" isomers that have the same pair of FA but are attached in reverse order to the sugar ring. For this reason, the development of methods for analysis of these complex mixtures is an important factor in their research and development. Most chromatographic methods reported in the literature for analysis of these emulsifiers do not effectively resolve components in the

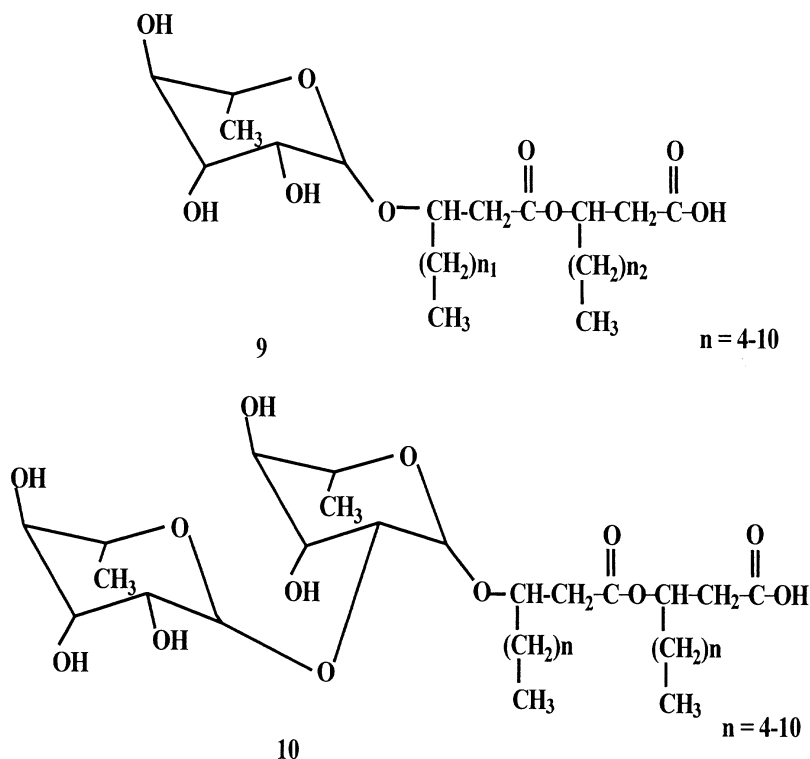


Fig. 10.14. Scheme showing rhamnolipid structures containing a monosaccharide and a disaccharide glycosylated to the β -HFA that is esterified to a second β -HFA. The HFA chain length varies between 4 and 14 carbons and might contain a single double bond.

product mixture, and require fraction collection followed by another analytical identification, such as MS, for structure determination (24,25). Recently, Déziel and colleagues reported a reversed-phase HPLC method coupled to negative-ion ESI-MS that provided complete structural identification of the rhamnolipids produced by *P. aeruginosa* (strain 57RP) grown on mannitol or naphthalene as the carbon source (26). The use of negative-ion ESI-MS was a key factor in the identification and quantification of the rhamnolipid structures since positive soft ionization techniques easily added sodium ions that produced molecular adduct ions with limited fragmentation information (see above). Figure 10.15 was the reported ESI-MS mass spectrum of two positional congener rhamnolipid structures with C_{10} - C_8 and C_8 - C_{10} FA ester moieties (26). As expected, the pseudomolecular ion, $[M-H]^-$, for both isomers was seen at m/z 475. Direct confirmation of the FA attached to the rhamnose portion of the molecule is provided by the ions at m/z 333 and 305. Evidence for the esterified hydroxy FA that remained with the carboxylic functionality could be observed from the difference between those ions and the correspond-

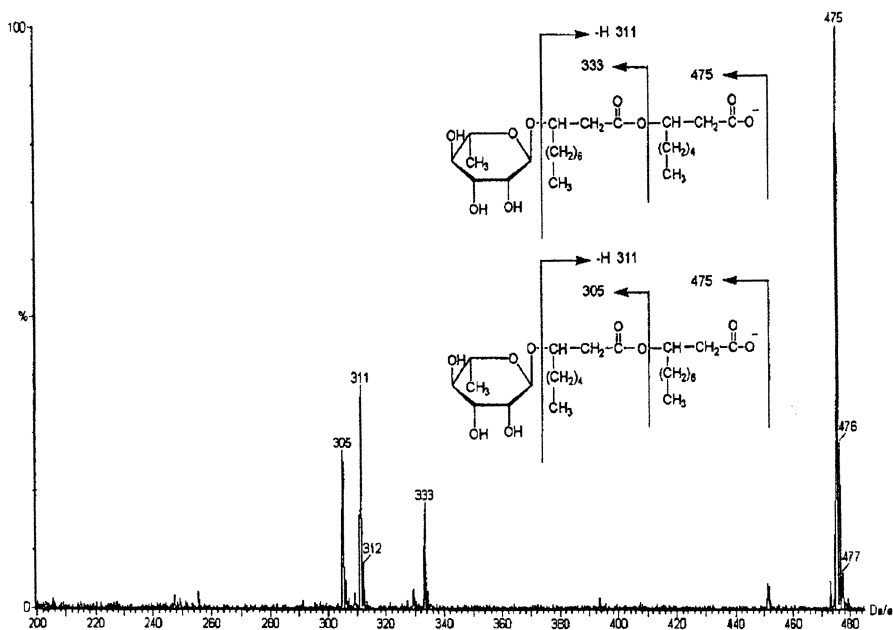


Fig. 10.15. Negative-ion ESI-MS mass spectrum of the congener isomers Rha-C₈-C₁₀ and Rha-C₁₀-C₈ showing the [M-H]⁻ ion at *m/z* 475 and proposed fragments associated with the hydroxy fatty acids that make up the rhamnolipid structures. *Source:* Reference 26.

ing dimer FA ion at *m/z* 311, or from the [M-H]⁻ ion at *m/z* 475. Successful identification of an unknown rhamnolipid, however, requires knowledge of the sugar ring glycosylated to the FA moiety. Note that the spectrum in Figure 10.15 does not have ions that represent the rhamnose portion.

To overcome this difficulty, the rhamnolipid mixture was subjected to CID-MS with argon gas. The negative ESI-CID-MS mass spectrum gave detailed information on the sugar and the FA portions, as shown in Figure 10.16. Also, in this study the molecular formula obtained from the isotopic abundance of the pseudomolecular ion was compared with the formula calculated for the individual rhamnolipids, which provided additional confirmation of the structures. As a result of using the LC/ESI-MS method in this study, 28 rhamnolipid structures were identified. Also reported were the elution times, pseudomolecular ions and relative abundances of the rhamnolipid products according to the carbon source used (Table 10.1) (26). The study provided a valuable method for the analysis of a complex mixture of rhamnolipids, establishing the benefits of using negative ESI-MS.

In a similar approach, Haba and colleagues reported an LC/MS method with a single quadrupole instrument using an ESI probe in the negative mode for the identification and quantification of the rhamnolipids produced by the *P. aeruginosa* strain

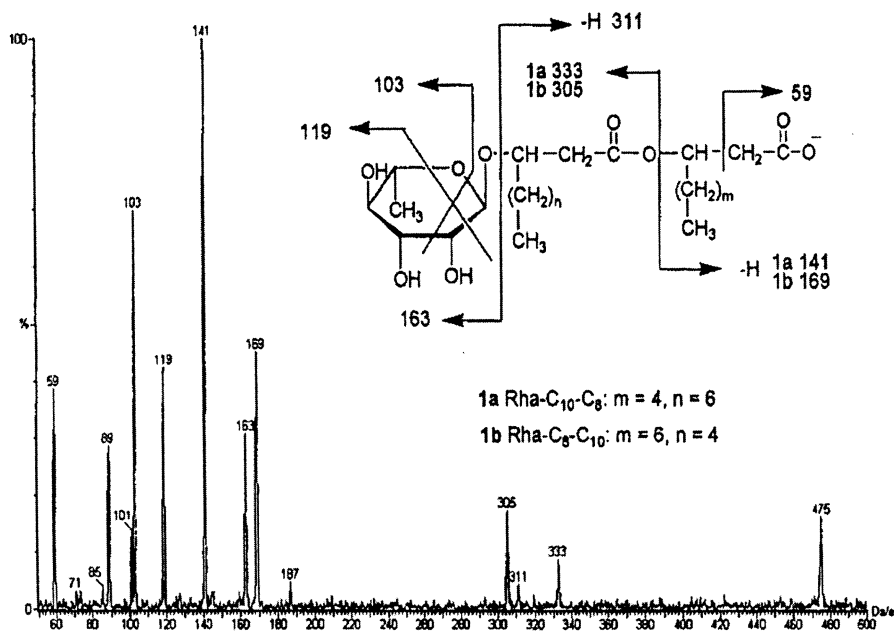


Fig. 10.16. Negative-ion ESI-CID-MS mass spectrum and proposed fragmentation of the rhamnolipids in Figure 10.15. *Source:* Reference 26.

AT10 and 47T2 (27). The rhamnolipid structures were elucidated by producing a fragmentation pattern achieved by simply changing the extraction voltage from -35 V, where the pseudomolecular ions were identified, to -75 V to increase fragmentation. In this paper the mixtures of the rhamnolipids produced from both strains were studied according to their physicochemical and biological properties. The use of LC/ESI-MS allowed the identification of 16 rhamnolipid products and allowed the study of the time course of accumulation of the homolog products secreted by *P. aeruginosa*, when grown with FA from soybean oil as the carbon source (27).

References

- Lang, S., Biological Amphiphiles (Microbial Biosurfactants), *Curr. Opin. Colloid. In.*: 12–20 (2002).
- Banat, I.M., R.S. Makkar, and S.S. Cameotra, Potential Commercial Applications of Microbial Surfactants, *Appl. Microbiol. Biotechnol.* 53: 495–508 (2000).
- Maier, R.M., and G. Soberón-Chávez, *Pseudomonas aeruginosa* Rhamnolipids: Biosynthesis and Potential Applications, *Appl. Microbiol. Biotechnol.* 53: 625–633 (2000).
- Fürstner, A., K. Radkowski, J. Grabowski, C. Wirtz, and R. Mynott, Ring-Closing Alkyne Metathesis: Application to the Total Synthesis of Sophorolipid Lactone, *J. Org. Chem.* 65: 8758–8762 (2000).

TABLE 10.1Structures and Relative Abundances of the Rhamnolipids Obtained from *P. aeruginosa* 57RP Cultured with Mannitol or Naphthalene as the Carbon Source

| Rhamnolipid | Retention time (min) | (M-H) ⁻ | Relative abundance (%) | |
|--|----------------------|--------------------|------------------------|-------------|
| | | | Mannitol | Naphthalene |
| Rha-C ₈ -C ₈ | 8.00 | 447 | 0.12 | ND |
| Rha-Rha-C ₈ -C ₁₀ | 8.00 | 593 | 0.30 | ND |
| Rha-Rha-C ₁₀ -C ₈ | 9.50 | 621 | 11.30 | 2.65 |
| Rha-Rha-C ₈ -C ₈ | 9.53 | 621 | 4.84 | 0.88 |
| Rha-C ₈ -C ₁₀ | 9.66 | 475 | 2.22 | 1.20 |
| Rha-C ₁₀ -C ₈ | 9.72 | 475 | 0.95 | 0.38 |
| Rha-Rha-C ₈ -C _{12:1} | 10.54 | 647 | 1.53 | 0.12 |
| Rha-Rha-C _{12:1} -C ₈ | 10.80 | 647 | 0.61 | 0.74 |
| Rha-Rha-C ₁₀ -C ₁₀ | 10.90 | 649 | 56.95 | 13.11 |
| Rha-C ₁₀ -C ₁₀ | 11.30 | 503 | 8.77 | 2.04 |
| Rha-Rha-C ₁₀ -C _{12:1} | 11.88 | 675 | 4.52 | 0.70 |
| Rha-C ₈ -C ₈ | 12.26 | 529 | 0.78 ^a | ND |
| Rha-C ₁₀ -C _{12:1} | 12.35 | 529 | | ND |
| Rha-Rha-C _{12:1} -C ₁₀ | 12.33 | 675 | 0.09 | ND |
| Rha-Rha-C ₁₂ -C ₁₀ | 12.35 | 677 | 1.51 | ND |
| Rha-Rha-C ₁₀ -C ₁₂ | 12.35 | 677 | 4.53 | ND |
| Rha-C ₁₂ -C ₁₀ | 12.70 | 531 | 0.10 | ND |
| Rha-C ₁₀ -C ₁₂ | 12.70 | 531 | 0.33 | ND |
| Rha-Rha-C _{12:1} -C ₁₂ | 13.00 | 703 | 0.25 ^b | ND |
| Rha-Rha-C ₁₀ -C _{14:1} | 13.00 | 703 | | ND |
| Rha-Rha-C ₁₂ -C ₁₂ | 13.50 | 705 | 0.10 | ND |
| Rha-Rha-C ₈ | 17.00 | 451 | 0.05 | 3.41 |
| Rha-Rha-C ₁₀ | 18.70 | 479 | 0.16 | 52.99 |
| Rha-C ₈ | 19.30 | 305 | ND | 1.85 |
| Rha-Rha-C _{12:1} | 20.00 | 505 | ND | 0.70 |
| Rha-Rha-C ₁₂ | 20.50 | 507 | ND | 3.33 |
| Rha-C ₁₀ | 21.58 | 333 | ND | 15.49 |
| Rha-C ₁₂ | 23.63 | 361 | ND | 0.41 |

Separation and analysis was performed by LC/MS. ND: not detected.

^aSum of the intensities of Rha-C₁₀-C_{12:1} and Rha-C_{12:1}-C₁₀.^bSum of the intensities of Rha-Rha-C_{12:1}-C₁₂ and Rha-C₁₀-C_{114:1}.

Source: Reference 26.

5. Kitamoto, D., H. Isoda, and T. Nakahara, Functions and Potential Applications of Glycolipid Biosurfactants—From Energy-Saving Materials to Gene Delivery Carriers, *J. Biosci. Bioeng.* 94: 187–201 (2002).
6. Moreau, R., and A. Nuñez, Modern Mass Spectrometry—Four Types of User Friendly Instruments and their Applications for Lipid Chemistry and Biochemistry, *inform 14*: 536–539 (2003).
7. Tulloch, A.P., and J.F.T. Spencer, Structure and Reactions of Lactonic and Acidic Sophorosides of 17-Hydroxyoctadecanoic Acid, *Can. J. Chem.* 46: 3337–3351 (1968).
8. Rau, U., S. Hammen, R. Heckman, V. Wray, and S. Lang, Sophorolipids: A Source for Novel Compounds, *Ind. Crops Prod.* 13: 85–92 (2001).

9. Casas, J.A., and F. García-Ochoa, Sophorolipid Production by *Candida bombicola*: Medium Composition and Culture Methods, *J. Biosci. Bioeng.* 88: 488–494 (1999).
10. Tulloch, A.P., and J.F.T. Spencer, A New Hydroxy Fatty Acid Sophoroside from *Candida bogoriensis*, *Can. J. Chem.* 46: 345–348 (1968).
11. Davila, A.M., R. Marchal, N. Monin, and J.P. Vandecasteele, Identification and Determination of Individual Sophorolipids in Fermentation Product by Gradient Elution High-Performance Liquid Chromatography with Evaporative Light-Scattering Detection, *J. Chromatogr.* 648: 139–149 (1993).
12. de Koster, C.G., W. Heerma, H.A.M. Pepermans, A. Groenewegen, H. Peters, and J. Haverkamp, Tandem Mass Spectrometry and Nuclear Magnetic Resonance Spectroscopy Studies of *Candida bombicola* Sophorolipids and Product Formed on Hydrolysis by Cutinase, *Anal. Biochem.* 230: 135–148 (1995).
13. Nuñez, A., R. Ashby, T.A. Foglia, and D.K.Y. Solaiman, Analysis and Characterization of Sophorolipids by Liquid Chromatography with Atmospheric Pressure Chemical Ionization, *Chromatographia* 53: 673–677 (2001).
14. Neff, W.E., and W.C. Byrdwell, Characterization of Model Triacylglycerol (Triolein, Trilinolein and Trilinolenin) Autoxidation Products via High-Performance Liquid Chromatography Coupled with Atmospheric Pressure Chemical Ionization Mass Spectrometry, *J. Chromatogr. A.* 818: 169–186 (1998).
15. Hu, Y., and L.-K. Ju, Sophorolipid Production from Different Lipidic Precursors Observed with LC-MS, *Enzyme Microb. Technol.* 29: 593–601 (2001).
16. Tulloch, A.P., and J.F.T. Spencer, A New Hydroxy Fatty Acid Sophoroside from *Candida bogoriensis*, *Can. J. Chem.* 46: 345–348 (1968).
17. Nuñez, A., R. Ashby, T.A. Foglia, and D.K.Y. Solaiman, Enzymatic Modification and LC/MS Analysis of Sophorolipids Produced by *Rhodotorula bogoriensis*, *Biotechnol. Lett.*, in press.
18. Bisht, K.S., R.A. Gross, and D.L. Kaplan, Enzyme-Mediated Regioselective Acylation of Sophorolipids, *J. Org. Chem.* 64: 780–789 (1999).
19. Lang, S., C. Sydatk, and U. Rau, Enzymatic Synthesis and Modification of Glycolipids, in *Enzymes in Lipids Modification*, edited by U.T. Bornscheuer, Wiley-VCH, Weinheim, Germany, 2000, pp. 363–393.
20. Singh, S.K., A.P. Felse, A. Nuñez, T.A. Foglia, and R.A. Gross, Regioselective Enzyme-Catalyzed Synthesis of Sophorolipid Esters, Amides, and Multifunctional Monomers, *J. Org. Chem.* 68: 5466–5477 (2002).
21. Hu, Y., and L.-K. Ju, Lipase-Mediated Deacetylation and Oligomerization of Lactonic Sophorolipids, *Biotechnol. Prog.* 19: 303–311 (2003).
22. Nuñez, A., R.D. Ashby, and T.A. Foglia, Enzymatic Synthesis of a Galactopyranose Sophorolipid Fatty Acid-Ester, *Biotechnol. Lett.* 25: 1291–1297 (2003).
23. Garozzo, D., M. Giuffrida, and G. Impallomeni, Determination of Linkage Position and Identification of the Reducing End in Linear Oligosaccharides by Negative Ion Fast Atom Bombardment Mass Spectrometry, *Anal. Chem.* 62: 279–286 (1990).
24. Mata-Sandoval, J.C., J. Karns, and A. Torrents, High-Performance Liquid Chromatography Method for the Characterization of Rhamnolipid Mixtures Produced by *Pseudomonas aeruginosa* UG2 on Corn Oil, *J. Chrom. A* 864: 211–220 (1999).
25. Déziel, E., F. Lépine, and R. Villemur, Mass Spectrometry Monitoring of Rhamnolipids from a Growing Culture of *Pseudomonas aeruginosa* Strain 57RP, *Biochim. Biophys. Acta* 1485: 145–152 (2000).

26. Déziel, E., F. Lépine, D. Dennie, D. Boismenu, O.A. Mamer, and R. Villemur, Liquid Chromatography/Mass Spectrometry Analysis of Mixtures of Rhamnolipids Produced by *Pseudomonas aeruginosa* Strain 57RP Grown in Mannitol or Naphthalene, *Biochim. Biophys. Acta 1440*: 244–252 (1999).
27. Haba, E., A. Abalos, O. Jáuregui, M.J. Espuny, and A. Manresa, Use of Liquid Chromatography-Mass Spectroscopy for Studying the Composition and Properties of Rhamnolipids Produced by Different Strains of *Pseudomonas aeruginosa*, *J. Surfactants Deterg.* 6: 155–161 (2003).

Chapter 11

Analysis of Steroids by Liquid Chromatography— Atmospheric Pressure Photoionization Mass Spectrometry

Risto Kostainen^{a,b} and Tiina J. Kauppila^b

^aFaculty of Pharmacy, Division of Pharmaceutical Chemistry, University of Helsinki, Finland, and ^bViikki Drug Discovery Technology Center, Faculty of Pharmacy, University of Helsinki, Finland

Introduction

Electrospray ionization (ESI) and atmospheric pressure chemical ionization (APCI) are the most popular ionization techniques used in liquid chromatography-mass spectrometry (LC-MS) for qualitative and quantitative analysis. In ESI, the compounds are ionized in the liquid phase and then gas-phase ions are formed by using a high electric field. Since the compounds are ionized without using thermal energy, ESI normally produces little fragmentation. The method is most suitable for ionization of polar and ionic compounds and is capable of ionizing small molecules as well as large biomolecules. In APCI, the compounds are first vaporized in a heated nebulizer, after which the vapor is ionized by a corona discharge needle. This initiates a complex ionization process, which finally leads to the ionization of the analyte. Because the compounds are vaporized by using thermal energy, only relatively small and stable compounds up to about 1,000–1,500 Da can be analyzed. On the other hand, APCI is more suitable for less polar and neutral compounds than ESI. The ionization of nonpolar compounds with ESI or APCI is often impossible, or is achieved with poor ionization efficiency.

Atmospheric pressure photoionization (APPI) has recently been introduced as a new ionization method for LC-MS (1–3). The photoionization detector (PID) has long been used as a detection method for gas chromatography (GC) (4–7), but it has also been applied to LC (8–10). Photoionization at atmospheric pressure has been described in connection with ion mobility spectrometry and mass spectrometry (11–13), but before the work of Bruins *et al.* (1), it had not been used with LC-MS. Two distinct APPI apparatuses have been described by Bruins *et al.* (1) and Syage *et al.* (2); both share the same operational principles.

Experimental

The APPI source presented by Bruins *et al.* was designed to be compatible with a PE/Sciex triple quadrupole mass spectrometer. The system includes a heated nebulizer

and housing identical to the ones used in the Sciex APCI source. Nitrogen is used as both the nebulizing and the auxiliary gas. The source is dependent on the addition of a dopant, which is added to the auxiliary gas line and vaporized, together with the solvent, by the heated nebulizer. A typical flow rate of the dopant is about 1/10 of the solvent flow rate, which in turn is usually between 100 and 300 $\mu\text{L}/\text{min}$. The vapor is swept by nitrogen gas flow into the photoionization region, which is directly at the end of the heated nebulizer probe. The photoionization lamp is a commercially available krypton discharge lamp emitting 10-eV photons (with a minor fraction at 10.6 eV). An electric potential of 1.2–1.5 kV is applied to the mounting bracket of the discharge lamp. The APPI source, described in more detail by Bruins *et al.* (1), is shown in Figure 11.1.

Syagen *et al.* have described an orthogonal APPI source, with the commercial name of PhotoMate[®], available from Agilent Technologies and ThermoFinnigan (2,3). The source is similar to the Agilent Technologies APCI source, except that the corona discharge needle is replaced by a krypton discharge lamp emitting 10-eV photons. The source was originally designed to be used without a dopant, but in many cases the sensitivity is enhanced if a dopant is used. The main difference between Bruins' and Syagen's sources is that in Bruins' source, the photoionization takes place inside a closed tube and in Syagen's source outside. A schematic diagram of the Syagen APPI source is presented in Figure 11.2.

The Ionization Mechanism

The ionization in APPI is initiated by the 10-eV photons emitted by the krypton discharge lamp. The photons can ionize molecules that possess ionization energies (IE) below 10 eV. This includes most analytes, but leaves out solvents generally used in LC, such as methanol, acetonitrile, and water (Table 11.1), as well as the

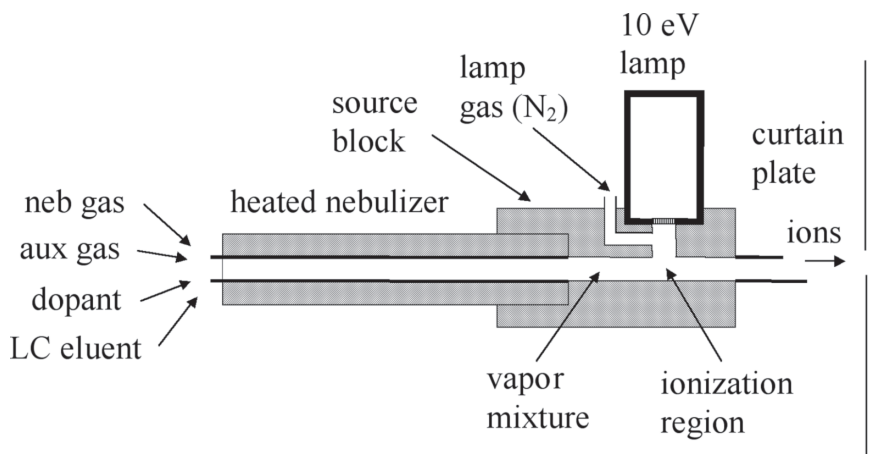


Fig. 11.1. Schematic diagram of the APPI source designed by Bruins *et al.* (1).

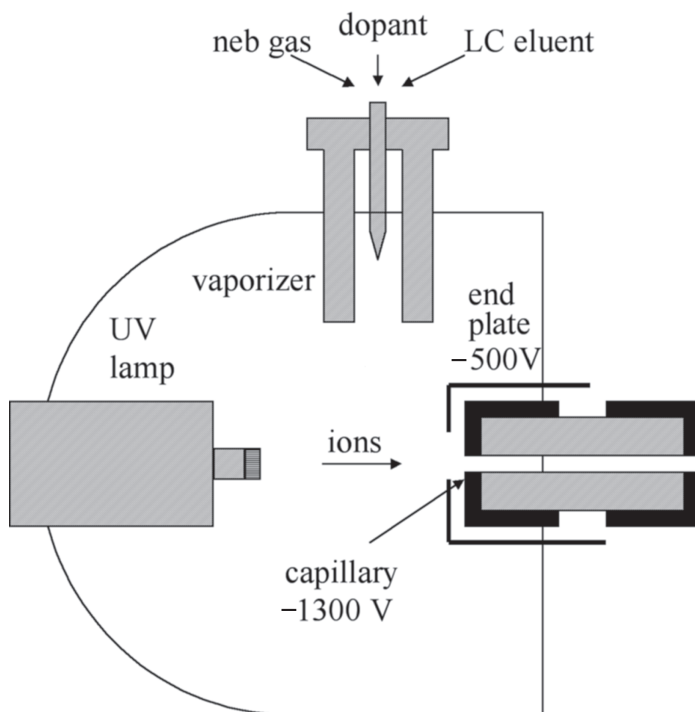


Fig. 11.2. Schematic diagram of the APPI source designed by Syage *et al.* (3).

gases used in the nebulization, or otherwise present in the atmospheric pressure ion source. In direct photoionization, that is, without dopant, the analyte forms a radical cation, M^+ (Table 11.2, reaction 1), which can further react with other gas-phase species. Possible reactions include charge exchange to species of lower ionization energy (Table 11.2, reaction 2), or abstraction of hydrogen from a protic solvent (Table 11.2, reaction 3) (2,3). Charge exchange to another species weakens the signal of the analyte, whereas the formation of a protonated molecule *via* hydrogen abstraction only transforms the analyte to another ion species and thus does not affect the overall ionization efficiency. Compounds that form protonated molecules *via* proton transfer usually possess high proton affinities (PA) and could therefore also be ionized using ESI or APCI. However, as the formation of radical cations of the analytes is dependent on the ionization energy of the compound, it makes possible the ionization of low-PA compounds, which usually are nonpolar molecules, and therefore difficult to ionize using ESI or APCI (14).

The photons typically have a short lifetime, but the ionization efficiency in photoionization techniques can be enhanced by the use of a readily ionizable substance, a dopant. Before the development of APPI, the use of a dopant had been reported with photoionization-ion mobility spectrometry (PI-IMS) (13,15) and

TABLE 11.1

Energetics of Typical Solvents, Gases, and Modifiers Used in APPI

| | IE ^a (eV) | PA ^b (kJ/mol) | EA ^c (eV) | ΔG_{acid}^d (kJ/mol) |
|------------------------------|----------------------|--------------------------|----------------------|-------------------------------------|
| Toluene | 8.83 | 784.0 | | |
| Benzyl radical | 7.2 | 831.4 | 0.912 | |
| Acetone | 9.703 | 812.0 | | |
| Anisole | 8.2 | 839.6 | | |
| Benzene | 9.243 | 750.4 | | |
| Phenyl radical | | 884.0 | | |
| O ₂ | — | — | 0.912 | — |
| HO ₂ [·] | | | — | 1451 |
| N ₂ | | | | |
| Acetonitrile | 12.2 | 779.2 | | |
| Methanol | 10.84 | 754.3 | | |
| Water | 12.6 | 691.0 | — | 1607 |
| <i>n</i> -Hexane | 10.13 | — | — | — |
| Chloroform | 11.37 | — | 0.622 | 1464 |
| Ammonia | 10.07 | 853.6 | — | — |
| Acetic acid | 10.65 | 783.7 | — | 1429 |
| Formic acid | | | — | 1415 |
| Trifluoroacetic acid | | | — | 1328 |

^aIE, ionization energy.^bPA, proton affinity.^cEA, electron affinity.^d ΔG_{acid} , gas-phase acidity.

APCI (16). Toluene, acetone, benzene, and anisole have been reported as APPI dopants (1,17), all possessing IE below 10 eV, the energy of the photons. In dopant-assisted APPI, the photons ionize the dopant first, and a radical cation (D^{·+}) of the dopant is formed (Table 11.2, reaction 4). In cases where the IE of the analyte is below that of the dopant, the dopant radical cation can then react with the analyte *via* charge exchange (Table 11.2, reaction 5). Another possibility is a proton transfer from the dopant radical cation to solvents or analytes that possess proton

TABLE 11.2

Reactions in Positive-Ion APPI

| | | | | |
|--|---|---|---|-----|
| M (analyte) + 10-eV photons | → | M ^{·+} + e ⁻ , | if IE ^a (M) < 10 eV | (1) |
| M ^{·+} + X | → | X ^{·+} + M, | if IE (X) < IE (M) | (2) |
| M ^{·+} + S (solvent) | → | MH ⁺ + [S-H]·, | if PA ^b (M ^{·+}) > PA ([S-H]·) | (3) |
| D (dopant) + 10-eV photons | → | D ^{·+} + e ⁻ | | (4) |
| D ^{·+} + M | → | M ^{·+} + D, | if IE (M) < IE (D) | (5) |
| D ^{·+} + <i>n</i> S | → | [D-H]· + S _{<i>n</i>} H ⁺ , | if PA (S _{<i>n</i>}) > PA ([D-H]·) | (6) |
| D ^{·+} + M | → | [D-H]· + MH ⁺ , | if PA (M) > PA ([D-H]·) | (7) |
| S _{<i>n</i>} H ⁺ + M | → | MH ⁺ + <i>n</i> S, | if PA (M) > PA (S _{<i>n</i>}) | (8) |

^aIE, ionization energy.^bPA, proton affinity.

affinities above that of the deprotonated dopant radical cation [D-H]. (Table 11.2, reactions 6 and 7). Protonated analyte molecules can also be formed by a proton transfer between the protonated solvent molecules and the analyte, in cases where the analyte possesses a PA above that of the solvent (Table 11.2, reaction 8) (14). In cases where the proton transfer takes place, the charge exchange reaction is suppressed as the dopant radical cations are depleted and no longer available for charge exchange reactions. Therefore, it would be desirable for the solvent to have a PA below that of the dopant in order to ionize nonpolar compounds efficiently by charge exchange.

In addition to charge exchange and proton transfer reactions, other reactions, which may complicate the ionization process, have also been reported to take place in the APPI source. When radiated with photons, acetonitrile has been reported to form a species of lower ionization energy, which can then be ionized by the 10-eV photons. The resulting species may explain the protonation of the analytes when dopant is not present (18,19). Benzene and toluene, which can be used as dopants, can react with atmospheric oxygen, forming phenol and cresol, respectively. These species have different IE and PA than the original molecules, which complicates the ionization process and can lead to an increase in the proton transfer reaction (20). Also, surface-induced reduction processes have been observed to take place in APPI (21).

Because of the nature of APPI, the reactions that take place and the ionization of the analytes can be greatly affected by the solvent. Solvents of high proton affinity promote ionization of analytes *via* proton transfer, whereas solvents of low proton affinity make possible the ionization of analytes *via* charge exchange. Acetonitrile and methanol have PA below that of the benzyl radical (deprotonated toluene radical cation), but can form solvent clusters that possess PA above the PA of the benzyl radical. Thus, they neutralize the dopant radical cations and charge exchange becomes unlikely (Table 11.2, reaction 6) (22). Instead, the proton transfer to analytes that possess PA above that of the solvent can take place with a high efficiency (Table 11.2, reaction 8). Use of solvents having low PA, such as water, hexane, and chloroform, can enhance the charge exchange reaction and increase the efficiency of the ionization of analytes of low PA (14).

Since the reactions depend on the differences in PA and IE of the reacting species, they can obviously also be affected by the choice of the dopant. The dopant should have an IE below the energy of the photons (10 eV for the krypton discharge lamp), so that it can produce radical cations. Thus far, the dopant used most often has been toluene. The deprotonated toluene radical cation, or benzyl radical, has a PA below that of methanol and acetonitrile solvent clusters and therefore gives up its proton if these solvents are present. Only in solvents such as hexane, chloroform, or water, does the toluene radical cation stay in the system and make the charge exchange reaction possible (14). In practice, this means that with reversed-phase liquid chromatography (RPLC) solvents, the ionization of the analytes *via* proton transfer is more likely than ionization *via* charge exchange. Recently, anisole, which also has a low IE (8.2 eV) and can readily be ionized by

the 10-eV photons, has been introduced as a new dopant for APPI (17). Anisole has a somewhat higher PA than toluene (Table 11.2), and therefore it does not give up its protons to solvents such as methanol or acetonitrile, but instead its radical cation lingers in the system even with these solvents. The consequence is very practical: With anisole, nonpolar compounds can be ionized through charge-exchange reaction by using reversed-phase liquid chromatography.

The ionization efficiency in APPI has been observed to be at its best at flow rates in the range 10–300 $\mu\text{L}/\text{min}$ (23,24). At flow rates above this, the ionization efficiency decreases, especially when the flow rate is increased above 500 $\mu\text{L}/\text{min}$. The situation has been found to be the same with both Agilent and Sciex ion sources, although the Agilent source seems to be less dependent on the flow rate when high-PA analytes are analyzed (24). With dopant-assisted APPI, the main reason for the signal drop for low-PA analytes was considered to be the neutralization of the dopant radical cations by solvent or solvent impurities that possess high PA. Possible reasons for the loss of high-PA analytes include neutralization of ions in recombination with electrons or ions of opposite charge, loss of photons in collisions with the increased volume of solvent, collisions with source walls, and an increasing number of competitive reactions at higher flow rate (24).

The reactions in negative-ion APPI are far less studied than the reactions in positive-ion APPI, but some phenomena are already known. In negative-ion APPI, the ionization process is started by a release of an electron by the photoionization of the dopant (Table 11.3, reaction 1) (14) or from the ion source metal surfaces due to irradiation with photons (25). These low-energy electrons may be captured by species that possess positive electron affinity, such as analytes, solvents, or gases (Table 11.3, reactions 2–5). Oxygen, which is present in the atmospheric pressure ion source, has been observed to play a critical role in the APPI source. It has a positive electron affinity and can therefore capture electrons from its surroundings, thereby forming a superoxide ion $\text{O}_2^{\cdot-}$ (Table 11.2, reaction 5). $\text{O}_2^{\cdot-}$ is

TABLE 11.3

The Reactions in Negative-Ion APPI

| | | | | |
|---|---------------|---|---|------|
| $\text{D} + h\nu$ | \rightarrow | $\text{D}^{+\cdot} + e^-$ | | (1) |
| $\text{M} + e^-$ | \rightarrow | $\text{M}^{\cdot-}$, | if $\text{EA}^a (\text{M}) > 0 \text{ eV}$ | (2) |
| $\text{M} + e^-$ | \rightarrow | $[\text{M}-\text{F}]^{\cdot-} + \text{F}^-$ | | (3) |
| $\text{S} + e^-$ | \rightarrow | $\text{S}^{\cdot-}$ | | (4) |
| $\text{O}_2 + e^-$ | \rightarrow | $\text{O}_2^{\cdot-}$ | | (5) |
| $\text{S} + \text{O}_2^{\cdot-}$ | \rightarrow | $[\text{S}-\text{H}]^{\cdot-} + \text{HO}_2^{\cdot}$, | if $\Delta G_{\text{acid}}^b (\text{S}) < \Delta G_{\text{acid}} (\text{HO}_2^{\cdot})$ | (6) |
| $\text{M} + \text{O}_2^{\cdot-}$ | \rightarrow | $[\text{M}-\text{H}]^{\cdot-} + \text{HO}_2^{\cdot}$, | if $\Delta G_{\text{acid}} (\text{M}) < \Delta G_{\text{acid}} (\text{HO}_2^{\cdot})$ | (7) |
| $\text{M} + \text{O}_2^{\cdot-}$ | \rightarrow | $\text{M}^{\cdot-} + \text{O}_2$, | if $\text{EA} (\text{M}) > \text{EA} (\text{O}_2) = 0.451 \text{ eV}$ | (8) |
| $\text{M} + \text{O}_2^{\cdot-}$ | \rightarrow | $[\text{M}-\text{X}+\text{O}]^{\cdot-} + \text{OX}^{\cdot}$, | $\text{X} = \text{H, Cl, NO}_2$ | (9) |
| $\text{M}^{\cdot-} + \text{O}_2$ | \rightarrow | $[\text{M}-\text{X}+\text{O}]^{\cdot-} + \text{OX}^{\cdot}$, | $\text{X} = \text{H, Cl, NO}_2$ | (10) |
| $\text{M} + [\text{S}-\text{H}]^{\cdot-}$ | \rightarrow | $[\text{M}-\text{H}]^{\cdot-} + \text{S}$, | if $\Delta G_{\text{acid}} (\text{M}) < \Delta G_{\text{acid}} (\text{S})$ | (11) |

^aEA, electron affinity.^b ΔG_{acid} , gas-phase acidity.

a relatively strong gas-phase base (ΔG_{acid} of $\text{HO}_2\cdot = 151$ kJ/mol, Table 11.3) and can therefore accept protons from other species and take part in the deprotonation of solvents and analytes that have higher gas-phase acidities (Table 11.3, reactions 6 and 7). In addition, it can react with solvents or analytes *via* charge exchange, in case the other species possesses an electron affinity above that of O_2 (Table 11.3, reaction 8). O_2 and $\text{O}_2^{\cdot-}$ have also been observed to react with some analytes *via* oxidation reactions (Table 11.3, reactions 9 and 10). Deprotonation of the analytes can also take place in a proton transfer between the analyte and a solvent species of lower gas-phase acidity (Table 11.3, reaction 11) (14).

Negative-ion APPI is also very dependent on the solvent composition. If solvents that possess high gas-phase acidities (e.g., formic acid, acetic acid, and trifluoroacetic acid) are introduced to the ion source, low-PA ions such as HCOO^- , CH_3COO^- , and CF_3COO^- resulting from the solvent become dominant in the system and prevent the deprotonation of analytes of low gas-phase acidity *via* reactions 6, 7, and 11 in Table 11.3. Also, they can protonate the superoxide ion, which thus cannot react *via* charge exchange with the high-EA analytes. Analytes that possess higher gas-phase acidities than the solvents can, however, be deprotonated. In fact, by the use of acidic solvents, better selectivity for these kinds of analytes may be achieved. Solvents that possess high electron affinities (chloroform, trifluoroacetic acid, etc.) have also been observed to deteriorate the signal of the analytes in negative ion APPI. They are thought to deplete the electrons from the system, thus leaving an insufficient amount for the analytes that otherwise would form ions *via* electron capture. This would also prevent the formation of superoxide ions from oxygen, and thus eliminate the possibility of proton transfer between the analytes/solvents and $\text{O}_2^{\cdot-}$. This would also explain why the formation of deprotonated analytes is decreased (26).

Applications

Because of its suitability to analysis of both nonpolar and polar analytes, APPI has been found to be an efficient ionization method for a variety of compounds. Analytes such as polyaromatic hydrocarbons (PAH) (14,27–30), pesticides (31,32), fungicides (33), explosives (34,35), quinones (36,37), nonpolar vitamins (38), flavonoids (39,40), and hydrophobic peptides (41) have been successfully analyzed using APPI as the method of ionization. Other analytes of environmental interest, such as mycotoxins (42), organic fluorine compounds (43), and harmful antibiotics (44) have also been analyzed using APPI. Problematic analytes such as mono- and disaccharides have also been analyzed successfully with APPI-MS (45). The suitability of APPI in drug discovery and drug analysis has been examined by several research groups (23,46–54). In most of the comparisons between ESI, APCI, and APPI, APPI gave equal or better sensitivity than APCI and was less susceptible to matrix effects than ESI or APCI (23,42–44,48,50,55,56). With nonpolar molecules, APPI usually showed a much higher sensitivity than ESI or APCI, but when the analyte was polar, ESI performed best (40,57).

Unlike ESI, APPI can be used under either reversed-phase or normal-phase (NP) liquid chromatographic conditions (14,28,51,58–60). The use of NP solvents can even be an advantage when the analytes are nonpolar, as the use of a nonpolar solvent promotes the charge exchange reaction and thus the ionization of nonpolar analytes (14,27). Because of the low flow rates used in APPI, it has also been found to be a suitable interface for capillary electrophoresis-mass spectrometry (CE-MS) (56) and it is more tolerant than ESI toward phosphate buffers, which are required for good CE separation (49). The newest trend in the development of APPI seems to be combining it with other atmospheric pressure ion sources, ESI (29,61) and APCI (56). Hanold *et al.* have successfully combined APPI with ESI and have been able to analyze polyaromatic hydrocarbons, proteins, peptides, and steroids, which have very different characteristics and thus could not be ionized simultaneously using ESI or APPI alone (29). Also the combination of APPI with APCI has extended the range of compounds that can be analyzed in a single run and increased the analyte signal levels (56).

APPI in the Analysis of Steroids

Steroids are a highly important class of compounds in biological systems. The most important steroids are the adrenocortical hormones, the sex hormones and the vitamin D-derived hormones. Steroids are lipid-soluble and readily pass through plasma membranes into the cytosol of target cells, causing the expression of certain genes. Corticosteroids affect the metabolism of carbohydrates (glucocorticoids) and regulate the concentrations of electrolytes in the blood (mineralocorticoids). The androgens and the estrogens are sex hormones and affect sexual development and sexual behavior. Vitamin D-derived steroid hormones regulate the uptake and metabolism of Ca^{2+} and phosphate, including the formation and mobilization of calcium phosphate in bone. The steroids that are present in the brain and whose concentration is independent of peripheral sources are called neurosteroids. They affect several types of behavior, such as anxiety (62), stress (63), and premenstrual syndrome (64). Anabolic steroids are used to treat cases of protein and bone wasting and osteoporosis, and during convalescence after chronic debilitating disease. The use of anabolic androgenic steroids (AAS) to improve athletic performance is one of the most widespread problems in sports despite the fact that it was banned in 1976.

Because steroids can exist in biological matrices at very low concentrations, highly sensitive and selective analysis methods are required. The common method for the analysis of steroids is GC-MS after a derivatization step. The analysis of steroids by LC-MS has garnered increased interest during recent years, since the method allows direct analysis without time-consuming sample pretreatment and derivatization. So far, APCI and ESI have been the most commonly used ionization techniques for LC-MS analysis of steroids. However, the ionization efficiency for less-polar steroids may be poor, especially with ESI. Recently introduced,

APPI (1,3) has been shown to be a very powerful method for the analysis of non-polar neutral compounds (65); therefore, interest in APPI as a method for analysis of steroids has increased.

Leinonen *et al.* (66) studied the applicability of LC-tandem mass spectrometry (LC-MS/MS) to the detection of free anabolic steroids in a fraction of human urine using 3'-hydroxystanozolol (HS), 6 β -hydroxy-4-chloro-dehydromethyltestosterone (HC), and oxandrolone (OX) as model compounds. Eluent composition, ion source parameters, and fragmentation were optimized for ESI, APCI, and APPI, after which the methods were compared with respect to specificity and detection limit. The use of dopant was essential for ionization in APPI, but its flow rate within a range of 5–25 μ L/min did not affect the results. Toluene as the dopant yielded approximately 20–50% higher sensitivity than acetone. All the APPI-MS spectra showed protonated analyte molecules and more extensive fragmentation than did APCI and ESI. The detection limits with LC-MS/MS using APPI and APCI were at the same level (0.08–0.9 nmol/mL), being somewhat higher than with ESI (0.06–0.5 nmol/mL).

The performance of APPI coupled to Fourier transform ion cyclotron resonance MS was compared to APCI and ESI in the analysis of six corticosteroids (67). All the APPI-MS spectra of the analytes detected without the dopant showed MH^+ and/or M^{+} , as well as fragments formed by losses of water and neutral hydrogens. The relative abundances of MH^+ and M^{+} were dependent on the solvent, M^{+} being more abundant with water than with methanol for all of the corticosteroids studied. Use of methanol as a solvent provided about five times better sensitivity than water, obviously due to better desolvation of methanol. The results obtained using toluene and acetone as dopants were similar. However, the use of dopant resulted in changes in signal that ranged from a tenfold increase to a complete signal loss. The ionization efficiency of APPI without dopant was compared to APCI and ESI using a flow rate of 8 μ L/min. In this comparison, APPI was found to ionize corticosteroids with much higher efficiency than either ESI or APCI. However, the results cannot be generalized to higher flow rates, since it has been shown that ionization efficiency of APPI is significantly better at low flow rates, but at higher flow rates APCI is a bit more efficient than APPI (68). Quenzer *et al.* compared LC-MS using ESI and APPI in the analysis of cortisol (55). The detection limit with APPI was 20 pg injected on the column, which was 2–3 times lower than with ESI. The results presented by Saba *et al.* (40) in the analysis of three glucocorticosteroids (corticosterone, prednisolone, and methylprednisolone) by APPI using toluene as the dopant were in agreement with the results presented by Greig *et al.* (67). A comparison of the analysis of corticosterone, prednisolone, and methylprednisolone by APPI and APCI is shown in Figure 11.3. The detection limits obtained for the glucocorticosteroids by analysis with LC-APPI-MS/MS were about 20 ng/mL. This was clearly lower than with LC-APCI-MS/MS, because prednisolone could be detected only at 100 ng/mL, methylprednisolone at 500 ng/mL whereas corticosterone was not detectable even at 1000 ng/mL (40).

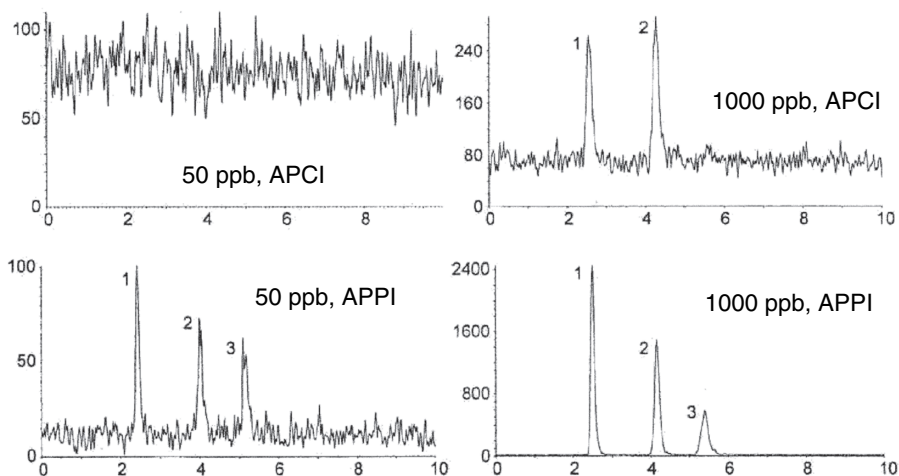


Fig. 11.3. Comparison between APPI and APCI in the detection of prednisolone (1), methylprednisolone (2), and corticosterone (3). From Saba *et al.*, 2002 (40).

Furthermore, LC-APPI-MS/MS showed good quantitative linearity for all the three glucocorticosteroids between 20 and 1000 ng/mL, with a correlation coefficient better than 0.995 (Fig. 11.4).

Alary *et al.* (59) compared APPI and APCI in the analysis of four neurosteroids (testosterone, prenelone, progesterone, and dehydroepiandrosterone) and their diacetyl-pentafluorobenzyl (Ac-PFBO) derivatives in spiked rat brain samples. The sensitivity was better with APPI for nonderivatized compounds,

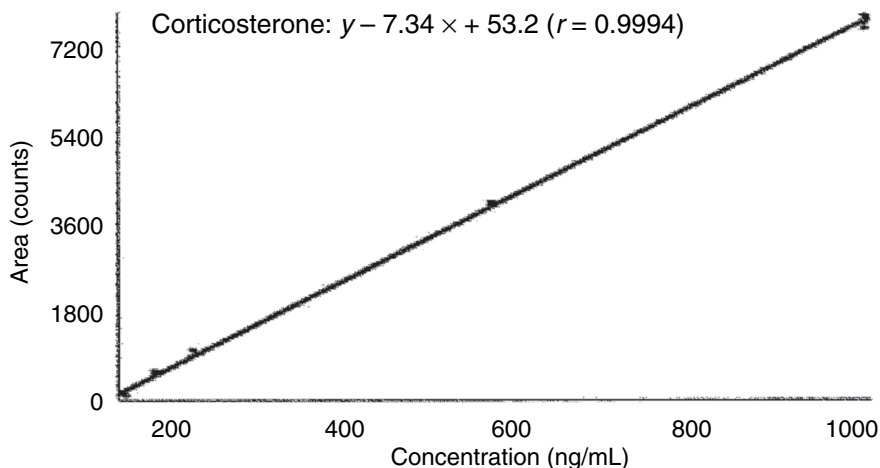


Fig. 11.4. Calibration curve obtained by atmospheric pressure photoionization for corticosterone. From Saba *et al.*, 2002 (40).

whereas APCI showed better sensitivity for Ac-PFBO derivatives. With both ion sources, the mass spectra of Ac-PFBO derivatives showed a significantly more intense protonated molecule and less fragmentation and fewer background ions than the nonderivatized neurosteroids. Limits of detection (on-column) obtained with APPI for Ac-PFBO-derivatized steroids were 90–190 fg, indicating that LC-APPI-MS/MS provides a potential new method for the analysis of neurosteroids.

The performance of APPI and APCI was compared in an LC-MS/MS analysis of 5α -androstane- $3\alpha,17\beta$ -diol, 5α -androstane- 17β -ol-3-one, testosterone, and ethynyl estradiol (58). The MS spectra measured by APPI and APCI were very similar, showing protonated analyte molecules and extensive fragmentation. The use of a dopant (toluene) in APPI was found to be essential in reversed-phase mode (MeOH/H₂O, 50/50%) to obtain an intense signal. In contrast, the photoionization process occurred with very good efficiency without any added dopant under normal-phase conditions (isooctane/isopropanol, 94/6%). The limits of detection (on-column) with normal-phase and reversed-phase LC-APPI-MS/MS were quite comparable, being between 0.1 and 10 pg, which was 3–20 times lower than with LC-APCI-MS/MS. Similarly, Fernández-Metzler showed that APPI is about 10 times more sensitive for ethynyl estradiol than APCI. However, in negative-ion mode APCI produced a fivefold more intense signal than APPI (51). Both ion sources showed similar dynamic range, precision, and accuracy.

Conclusions

APPI seems to be a very powerful and versatile ionization technique that overcomes the difficulties associated with APCI and especially with ESI in the analysis of nonpolar neutral compounds such as steroids. At this time, most of the comparative studies concerning steroid analysis by LC-MS show that the sensitivity achieved with APPI is better than, or at the same level as, APCI and is often better than the sensitivity obtained by ESI. Furthermore, APPI provides reliable quantitative analysis with a wide linear range, as well as good stability, precision, and accuracy. However, only a couple of publications concerning the analysis of steroids with APPI have been presented in refereed scientific journals (66,67). Instead, most of the studies have been presented at scientific meetings. In order to make a realistic conclusion on the performance of APPI in steroid analysis, more comparative studies should be done under carefully optimized conditions for each of the ionization techniques. On the other hand, APPI is a very young technique, which will be developed further as the understanding of the fundamentals of the APPI ionization process increases.

References

1. Robb, D.B., T.R. Covey, and A.P. Bruins, Atmospheric Pressure Photoionization: An Ionization Method for Liquid Chromatography-Mass Spectrometry, *Anal. Chem.* 72: 3653–3659 (2000).

2. Syage, J.A., and M.D. Evans, Photoionization Mass Spectrometry. A Powerful Tool for Drug Discovery, *Spectroscopy* 16: 14–21 (2001).
3. Syage, J.A., M.D. Evans, and K.A. Hanold, Photoionization Mass Spectrometry, *Am. Lab.* 12: 24–29 (2000).
4. Driscoll, J.N., Photoionization, U.S. Patent 3,933,432, January 20, 1976.
5. Driscoll, J.N., Applications of a Photoionization Detector in Gas Chromatography, *Am. Lab.* 8: 71–75 (1976).
6. Driscoll, J.N., and F.F. Spaziani, PID Development Gives New Performance Levels, *Res. Dev.*: 50–54 (1976).
7. Langhorst, M.L., Photoionization Detector Sensitivity of Organic Compounds, *J. Chromatogr. Sci.* 19: 98–103 (1981).
8. Schermund, J.T., and D.G. Locke, A Universal Photoionization Detector for Liquid Chromatography, *Anal. Lett.* 8: 611–625 (1975).
9. Locke, D.C., B.S. Dhingra, and A.D. Baker, Liquid-Phase Photoionization Detector for Liquid Chromatography, *Anal. Chem.* 54: 447–450 (1982).
10. Driscoll, J.N., D.W. Conron, and P. Ferioli, Trace Analysis of Organic Compounds by High-Performance Liquid Chromatography with Photoionization Detection, *J. Chromatogr.* 302: 43–50 (1984).
11. Baim, M.A., L. Eatherton, and H.H. J. Hill, Ion Mobility Detector for Gas Chromatography with a Direct Photoionization Source, *Anal. Chem.* 55: 1761–1766 (1983).
12. Leasure, C.S., M.E. Fleischer, G.K. Anderson, and G.A. Eiceman, Photoionization in Air with Ion Mobility Spectrometry Using a Hydrogen Discharge Lamp, *Anal. Chem.* 58: 2142–2147 (1986).
13. Spangler, G.E., J.E. Roehl, G.B. Patel, and A. Dorman, Photoionization Ion Mobility Spectrometer, U.S. Patent 5,338,931, August 16, 1994.
14. Kauppila, T.J., T. Kuuranne, E.C. Meurer, M.N. Eberlin, T. Kotiaho, and R. Kostainen, Atmospheric Pressure Photoionization. The Ionization Mechanism and the Effect of the Solvent on Ionization of Naphthalenes, *Anal. Chem.* 74: 5470–5479 (2002).
15. Döring, H.R., G. Arnold, J. Adler, T. Röbel, and J. Riemenschneider, DE Patent 19609582 C1, March 12, 1996.
16. Ketkar, S.N., J.G. Dulak, S. Dheandhanoo, and W.L. Fite, Benzene Charge Exchange at Atmospheric Pressure for Low-Level Detection of Pollutants in Ambient Air, *Anal. Chim. Acta* 245: 267–270 (1991).
17. Kauppila, T.J., R. Kostainen, and A.P. Bruins, Anisole, a New Dopant for Atmospheric Pressure Photoionization-Mass Spectrometry of Low Proton Affinity, Low Ionization Energy Compounds. *Rapid Commun. in Mass Spectrom.* 18: 808–815 (2004).
18. Marotta, E., R. Seraglia, F. Fabris, and P. Traldi, Atmospheric Pressure Photoionization Mechanisms. 1. The Case of Acetonitrile, *Int. J. Mass Spectrom.* 228: 841–849 (2003).
19. Marotta, E., and P. Traldi, On the Photo-Initiated Isomerization of Acetonitrile, *Rapid Commun. Mass Spectrom.* 17: 2846–2848 (2003).
20. Tubaro, M., E. Marotta, R. Seraglia, and P. Traldi, Atmospheric Pressure Photoionization Mechanisms. 2. The Case of Benzene and Toluene, *Rapid Commun. Mass Spectrom.* 17: 2423–2429 (2003).
21. Kertesz, V., and G.J. Van Berkel, Surface-Assisted Reduction of Aniline Oligomers, *n*-Phenyl-1,4-phenylenediimine and Thionine in Atmospheric Pressure Chemical Ionization and Atmospheric Pressure Photoionization, *J. Am. Soc. Mass Spectrom.* 13: 109–117 (2002).

22. Koster, G., and A.P. Bruins, Mechanisms for Ion Formation in LC/MS by Atmospheric Pressure Photo-Ionization (APPI), *Proceedings of the 49th ASMS Conference on Mass Spectrometry and Allied Topics*, Chicago, Illinois, May 27–31, 2001.
23. Yang, C., and J. Henion, Atmospheric Pressure Photoionization Liquid Chromatography-Mass Spectrometry Determination of Idoxifene and its Metabolites in Human Plasma, *J. Chromatogr. A* 970: 155–165 (2000).
24. Kauppila, T.J., R. Kostiainen, and A.P. Bruins, Effect of the Flow Rate on the Ionization Efficiency in Atmospheric Pressure Photoionization Mass Spectrometry, *Proceedings of the 51st ASMS Conference on Mass Spectrometry and Allied Topics*, Montreal, Quebec, Canada, June 8–12, 2003.
25. Basso, E., E. Marotta, R. Seraglia, M. Tubaro, and P. Traldi, On the Formation of Negative Ions in Atmospheric Pressure Photoionization Conditions, *J. Mass Spectrom.* 38: 1113–1115 (2003).
26. Kauppila, T.J., T. Kotiaho, A.P. Bruins, and R. Kostiainen, Negative Ion Atmospheric Pressure Photoionization, *J. Am. Soc. Mass Spectrom.* 15: 203–211 (2004).
27. Impey, G., B. Kieser, and J.-F. Alary, The Analysis of Polycyclic Aromatic Hydrocarbons (PAHs) by LC/MS/MS Using a New Atmospheric Pressure Photoionization Source, *Proceedings of the 49th ASMS Conference on Mass Spectrometry and Allied Topics*, Chicago, Illinois, May 27–31, 2001.
28. Cormia, P.H., S.M. Fischer, and C.A. Miller, Analysis of Polyaromatic Hydrocarbons by Atmospheric Pressure Photoionization LC/MS, *Proceedings of the 49th ASMS Conference on Mass Spectrometry and Allied Topics*, Chicago, Illinois, May 27–31, 2001.
29. Hanold, K.A., T. Lynn, and J.A. Syage, Evaluation of a Combined Electrospray and Photo Ionization Source, *Proceedings of the 51st ASMS Conference on Mass Spectrometry and Allied Topics*, Montreal, Quebec, Canada, June 8–12, 2003.
30. Hayen, H., U. Karst, S. van Leeuwen, and G. Zurek, HPLC/Electrochemistry/Mass Spectrometry and HPLC/Atmospheric Pressure Photoionization-Mass Spectrometry for the Determination of Polycyclic Aromatic Hydrocarbons, *The Pittsburgh Conference on Analytical Chemistry and Applied Spectroscopy*, Orlando, Florida, March 9–14, 2003.
31. Evans, M.D., B.J. Nies, and D.B. Kassel, High-Throughput Analysis of Agrochemicals by Photoionization MS, *Proceedings of the 49th ASMS Conference on Mass Spectrometry and Allied Topics*, Chicago, Illinois, May 27–31, 2001.
32. Meng, C.-K., P. Zavitsanos, and J. Zweigenbaum, Analyzing Phenyl Ureas and Carbamate Pesticides Using ESI-, APPI-, and APCI-LC/MSD, *The Pittsburgh Conference on Analytical Chemistry and Applied Spectroscopy*, Orlando, Florida, March 9–14, 2003.
33. Yoshiyoka, N., Y. Akiyama, and K. Teranishi, Rapid Simultaneous Determination of *o*-Phenylphenol, Diphenyl, Thiabendazole, Imazalil and Its Major Metabolite in Citrus Fruits by Liquid Chromatography-Mass Spectrometry Using Atmospheric Pressure Photoionization, *J. Chromatogr. A* 1022: 145–150 (2004).
34. Crescenzi, C., H. Carlsson, E. Holmgren, and C. Sanches, Analysis of Explosives in Vapor Phase Using a New Trapping Device and LC-MS Analysis with Atmospheric Pressure Photoionization, *The Pittsburgh Conference on Analytical Chemistry and Applied Spectroscopy*, Orlando, Florida, March 9–14, 2003.
35. Harkey, G.A., and D. Wichems, Comparison of Selected Explosives in LC/MS Using APPI and APCI, *The Pittsburgh Conference on Analytical Chemistry and Applied Spectroscopy*, Orlando, Florida, March 9–14, 2003.

36. Lytle, C.A., G.J. Van Berkel, and D.C. White, Comparison of Atmospheric Pressure Photoionization and Atmospheric Pressure Chemical Ionization for the Analysis of Ubiquinones and Menaquinones, *Proceedings of the 49th ASMS Conference on Mass Spectrometry and Allied Topics*, Chicago, Illinois, May 27–31, 2001.
37. Geyer, R., M. Gan, D.C. White, and G.J. Van Berkel, APPI and APCI for Analysis of Quinones as Signature Biomarker in Environmental Analysis, *Proceedings of the 51st ASMS Conference on Mass Spectrometry and Allied Topics*, Montreal, Quebec, Canada, June 8–12, 2003.
38. Miller, C.A., P.H. Cormia, and S.M. Fischer, Atmospheric Pressure Photoionization Ion Trap Analysis of Fat-Soluble Vitamins, *Proceedings of the 49th ASMS Conference on Mass Spectrometry and Allied Topics*, Chicago, Illinois, May 27–31, 2001.
39. Rauha, J.-P., H. Vuorela, and R. Kostianen, Effect of Eluent on the Ionisation Efficiency of Flavonoids by Ionspray, Atmospheric Pressure Chemical Ionisation and Atmospheric Pressure Photoionisation Mass Spectrometry, *J. Mass Spectrom.* 36: 1269–1280 (2001).
40. Saba, A., A. Raffaelli, S. Pucci, and P. Salvadori, Evaluation of a Custom Built Atmospheric Pressure Photoionization (APPI) Source, *Proceedings of the 50th ASMS Conference on Mass Spectrometry and Allied Topics*, Orlando, Florida, June 3–7, 2002.
41. Delobel, A., F. Halgand, B. Laffranchise-Gosse, H. Snijders, and O. Laprévotte, Characterization of Hydrophobic Peptides by Atmospheric Pressure Photoionization-Mass Spectrometry and Tandem Mass Spectrometry, *Anal. Chem.* 75: 5961–5968 (2003).
42. Takino, M., S. Daishima, and T. Nakahara, Liquid Chromatography/Mass Spectrometric Determination of Patulin in Apple Juice Using Atmospheric Pressure Photoionization, *Rapid Commun. Mass Spectrom.* 17: 1965–1972 (2003).
43. Takino, M., S. Daishima, and T. Nakahara, Determination of Perfluorooctane Sulfonate in River Water by Liquid Chromatography Mass Spectrometry by Automated On-Line Extraction Using Turbulent Flow Chromatography, *Rapid Commun. Mass Spectrom.* 17: 383–390 (2003).
44. Takino, M., S. Daishima, and T. Nakahara, Determination of Chloramphenicol Residues in Fish Meats by Liquid Chromatography-Atmospheric Pressure Photoionization Mass Spectrometry, *J. Chromatogr. A* 1011: 67–75 (2003).
45. Perkins, P.D., C.A. Miller, and S.M. Fischer, Acylate Anion Formation During the Analysis of Simple Sugars by Atmospheric Pressure Photoionization (APPI), *Proceedings of the 50th ASMS Conference on Mass Spectrometry and Allied Topics*, Orlando, Florida, June 3–7, 2002.
46. Keski-Hynnälä, H., M. Kurkela, E. Elovaara, L. Antonio, J. Magdalou, L. Luukkanen, J. Taskinen, and R. Kostianen, Comparison of Electrospray, Atmospheric Pressure Chemical Ionization and Atmospheric Pressure Photoionization in the Identification of Apomorphine, Dobutamide and Entacapone Phase II Metabolites in Biological Samples, *Anal. Chem.* 74: 3449–3457 (2002).
47. Plante, G., E. Tessier, and R. Guilbaud, Atmospheric Pressure Photoionization (APPI): Evaluation of an Ionization Technique for Liquid Chromatography Mass Spectrometry Using Different Compounds, *Proceedings of the 49th ASMS Conference on Mass Spectrometry and Allied Topics*, Chicago, Illinois, May 27–31, 2001.
48. Hsieh, Y., K. Merkle, G. Wang, J.-M. Brisson, and W.A. Korfmacher, High-Performance Liquid Chromatography-Atmospheric Pressure Photoionization/Tandem Mass Spectrometric Analysis for Small Molecules in Plasma, *Anal. Chem.* 75: 3122–3127 (2003).

49. Nilsson, S.L., C. Andersson, P.J.R. Sjöberg, D. Bylund, P. Petersson, M. Jörntén-Karlsson, and K.E. Markides, Phosphate Buffers in Capillary Electrophoresis/Mass Spectrometry Using Atmospheric Pressure Photoionization and Electrospray Ionization, *Rapid Commun. Mass Spectrom.* 17: 2267–2272 (2003).
50. Shen, J., H. Lin, and P.J. Rudewicz, Application of APPI Interface for High Throughput Quantitation Bioanalysis of Pharmaceutical Compounds, *Proceedings of the 51st ASMS Conference on Mass Spectrometry and Allied Topics*, Montreal, Quebec, Canada, June 8–12, 2003.
51. Fernandez-Metzler, C., A. Barrish, E. Mahan, and C. Moran, Photoionization in Drug Discovery LC-MS/MS Quantitative Analysis, *Proceedings of the 50th ASMS Conference on Mass Spectrometry and Allied Topics*, Orlando, Florida, June 3–7, 2002.
52. Hakala, K.S., L. Luukkanen, A.M. Kaukonen, J. Hirvonen, R. Kostiainen, and T. Kotiaho, Development of LC/MS/MS Methods for Cocktail Dosed Caco-2 Samples Using Atmospheric Pressure Photoionization and Electrospray Ionization, *Anal. Chem.* 75: 5969–5977 (2003).
53. Hélias, N., and S. Cepa, Characterization and Optimization of an Atmospheric Pressure Photoionization (APPI) Interface for Routine Use in Drug Discovery and Development, *Proceedings of the 51st ASMS Conference on Mass Spectrometry and Allied Topics*, Montreal, Quebec, Canada, June 8–12, 2003.
54. Hsieh, Y., K. Merkle, and G. Wang, Zirconia-Based Column High-Performance Liquid Chromatography/Atmospheric Pressure Photoionization Tandem Mass Spectrometric Analyses of Drug Molecules in Rat Plasma, *Rapid Commun. Mass Spectrom.* 17: 1775–1780 (2003).
55. Quenzer, T., B. Bolaños, M.J. Greig, J.M.R. Bylund, and C. Pham, Atmospheric Pressure Photoionization Mass Spectrometry: High Throughput Applications, *Proceedings of the 51st ASMS Conference on Mass Spectrometry and Allied Topics*, Montreal, Quebec, Canada, June 8–12, 2003.
56. Hanold, K.A., J. Horner, R. Thakur, and C.A. Miller, Dual APPI/APCI Source for LC/MS, *Proceedings of the 50th ASMS Conference on Mass Spectrometry and Allied Topics*, Orlando, Florida, June 3–7, 2002.
57. McKenzie, D.E., and L. McDermott, LC-MS Investigation of Atmospheric Pressure Photoionization Versus Electrospray Ionization and Atmospheric Pressure Chemical Ionization Using Eleven Test Compounds, *Proceedings of the 51st ASMS Conference on Mass Spectrometry and Allied Topics*, Montreal, Quebec, Canada, June 8–12, 2003.
58. Alary, J.-F., Comparative Study: LC-MS/MS Analysis of Four Steroid Compounds Using a New Photoionization Source and a Conventional APCI Source, *Proceedings of the 49th ASMS Conference on Mass Spectrometry and Allied Topics*, Chicago, Illinois, May 27–31, 2001.
59. Alary, J.-F., A. Berthemy, A. Tuong, and M.-F. Uzabiaga, Comparative LC-MS/MS Analysis of Four Neurosteroid Compounds and Their Acetyl-Pentafluorobenzyl Derivatives Using Photoionization Ion Source and a Conventional Atmospheric Pressure Chemical Ionization Source, *Proceedings of the 50th ASMS Conference on Mass Spectrometry and Allied Topics*, Orlando, Florida, June 3–7, 2002.
60. Aiello, M., Y. LeBlanc, and J.-F. Alary, Simultaneous Quantitation and Identification Using MRM Triggered MS/MS Experiments on a Hybrid Triple-Quadrupole/Linear Ion Trap with Photoionization, *Proceedings of the 51st ASMS Conference on Mass Spectrometry and Allied Topics*, Montreal, Quebec, Canada, June 8–12, 2003.

61. Dorcier, A., P.J. Dyson, and J.S. McIndoe, Analysis of Coordination and Organometallic Compounds Using Photoionization Mass Spectrometric Techniques, *Eur. J. Inorg. Chem.* 24: 4294–4297 (2003).
62. Bitran, D., M. Shiekh, and M. McLeod, Anxiolytic Effect of Progesterone Is Mediated by the Neurosteroid Allopregnanolone at Brain GABAA Receptors, *J. Neuroendocr.* 7: 171–177 (1995).
63. Purdy, R.H., A.L. Morrow, P.H.J. Moore, and S.M. Paul, Stress-Induced Elevations of γ -Aminobutyric Acid Type A Receptor-Active Steroids in the Rat Brain, *Proc. Natl. Acad. Sci. USA* 88: 4553–4557 (1991).
64. Wang, M., L. Seippel, R.H. Purdy, and T. Bäckström, Relationship Between Symptom Severity and Steroid Variation in Women with Premenstrual Syndrome: Study on Serum Pregnenolone, Pregnenolone Sulfate, 5α -Pregnane-3,20-dione and 3α -Hydroxy- 5α -pregnan-20-one, *J. Clin. Endocrinol. Metab.* 81: 1076–1082 (1996).
65. Hayen, H., and U. Karst, Strategies for the Liquid Chromatographic-Mass Spectrometric Analysis of Non-Polar Compounds, *J. Chromatogr. A* 1000: 549–565 (2003).
66. Leinonen, A., T. Kuuranne, and R. Kostiainen, Liquid Chromatography-Mass Spectrometry in Anabolic Steroid Analysis—Optimization and Comparison of Three Ionization Techniques: ESI, APCI and APPI, *J. Mass Spectrom.* 37: 693–698 (2002).
67. Greig, M.J., B. Bolaños, T. Quenzer, and J.M.R. Bylund, Fourier Transform Ion Cyclotron Resonance Mass Spectrometry Using Atmospheric Pressure Photoionization for High-Resolution Analyses of Corticosteroids, *Rapid Commun. Mass Spectrom.* 17: 2763–2768 (2003).
68. Hanold, K.A., M.D. Evans, J.A. Syage, S.M. Fischer, and P. Cormia, Atmospheric Pressure Photoionization (APPI TM) for LC/MS, *Proceedings of the 49th ASMS Conference on Mass Spectrometry and Allied Topics*, Chicago, Illinois, May 27–31, 2001.

Chapter 12

Toward Total Cellular Lipidome Analysis by ESI Mass Spectrometry from a Crude Lipid Extract

Xianlin Han^{a,b} and Richard W. Gross^{a,b,c,d}

^aDivision of Bioorganic Chemistry and Molecular Pharmacology, Departments of ^bMedicine, ^cMolecular Biology and Pharmacology, and ^dChemistry, Washington University School of Medicine, St. Louis, Missouri 63110

Introduction

Cellular lipids are important cellular molecules that have multiple distinct yet critical roles in cellular function. They form self-organizing chemical assemblies (i.e., cellular membranes) that provide an impermeable boundary layer to separate intracellular and extracellular compartments and to sequester proteins, metabolites, and nucleotides, without which life and self-renewal would be impossible. Moreover, lipids concurrently provide a matrix for the approximate interactions of membrane-associated proteins to interact with each other, as well as promote interactions of membrane proteins with their cognate intra- and extracellular binding partners. Finally, lipids act as both an energy reservoir (triacylglycerols [TAG]) and a storage depot for biologically active second messengers (eicosanoids, diacylglycerols, ceramides, etc.) that allow each cell to effectively respond to internal and external stimuli.

The inherent chemical diversity present in biological lipids is achieved through multiple discrete covalent assemblies of lipid backbones (glycerol for glycerolipids and sphingosine for sphingolipids) with linear combinations of various aliphatic chains (typically 14–22 carbons long and containing varying amounts of unsaturation), with or without polar head groups. This biological diversity facilitates the specific tailoring of individual cellular responses to alterations in cellular nutrient status, metabolic history, and signaling events. Accordingly, many groups have rigorously pursued the identification of alterations in cellular lipid constituents to identify the chemical mechanisms underlying such diverse diseases as obesity, atherosclerosis, stroke, and diabetes, all now epidemic in industrialized populations.

The precise complement of chemically distinct covalent entities in lipids of a cell or organ has been referred to as the lipidome. Lipidomics is a research field comprising the study of lipidome-lipidome, lipidome-proteome, and lipidome-genome interactions. The term describes diverse research areas, from mapping the entire profile of lipids in a biological system (a vast effort that no one is known to be attempting currently) to revealing the function and metabolism of individual

lipid molecular species. Historically, chromatography (TLC, GC, and HPLC) has played an essential role in identifying and quantifying lipid molecular species (1–7). Lipidomics is greatly facilitated by recent advances in, and novel applications of, electrospray ionization mass spectrometry (ESI-MS) and tandem mass spectrometry (8–13).

In previous work, we have used ESI-MS with specific zwitterion-reagent ion pairs to effectively resolve different classes of lipids in the ion source (8,11,13). The advantages of this ESI intrasource separation approach include, but are not limited to: (i) the complete quantitative analysis of lipid classes, subclasses, and individual molecular species, with high efficiency and without prior chromatographic separation or derivatization; (ii) a higher signal-to-noise ratio in comparison to other traditional mass spectrometric approaches; (iii) a nearly linear relationship between the relative intensities of molecular ions and the masses of individual lipids over a wide dynamic range in dilute lipid solution; (iv) ionization efficiency (within experimental error) depending only on the electrical propensity of a lipid class at low lipid concentration; and (v) excellent reproducibility of sample measurements (<5% of experimental error). Thus, through implementation of these techniques, a high throughput platform for the detailed study of lipid alterations has been developed at a time when lipid-induced disease states—diabetes, obesity, and atherosclerosis—are epidemic in industrialized nations.

In this article, we will briefly describe the principles of ESI intrasource separation techniques for lipid analysis, including principles of ESI, the classification of lipids based on their inherent electrical propensities, and our strategy for ESI intrasource separation. Then we will summarize how to fingerprint and quantify individual molecular species of each lipid class using the ESI intrasource separation technique. Finally, examples using the ESI intrasource separation technique for studies of lipid metabolism in normal and disease states will be given.

Principles of ESI

ESI is a process by which analytes present in a solution can be ionized and transferred to the gas phase. This technique was initially developed by Fenn and colleagues (14). Its application is so broad that no boundary can be defined. Although many physicochemical features of the ionization and fragmentation processes are still being actively investigated, it is clear that the effects resulting from surface tension and surface charge interactions on sprayed droplets play important roles in the ionization process (15–18). Moreover, the ions generated from analytes in the ESI source can be simply summarized in Figure 12.1. Specifically, for any compound with an ionic bond, theoretically, the cationic part of the compound can be readily analyzed by ESI-MS in positive-ion mode, while the anionic part of the compound can be analyzed in negative-ion mode. ESI can also be used for the analysis of molecules that do not possess any intrinsic ionizable site, through the formation of adduct ions.

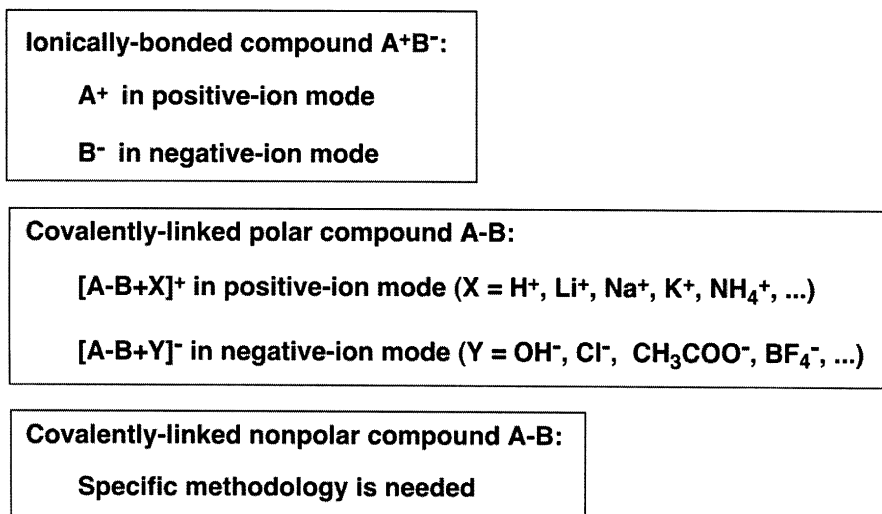


Fig. 12.1. Diagram of electrospray ionization of ionicly bonded or covalently linked compounds.

Therefore, as long as a sufficient dipole potential is present in a molecule to interact with either a small anion or cation, the molecule can be ionized during the ESI process if appropriate conditions are utilized. For example, choline glycerophospholipid (PC) molecular species do not possess a net charge but contain a very polar zwitterionic head group. Thus, these PC molecules can be ionized in positive-ion mode as small cation adducts such as protonated, lithiated, sodiated, or ammoniated pseudomolecular ions, depending on the availability of these small cations (8,19–22). Similarly, in negative-ion mode, these PC molecular species can form small anion adducts such as chlorine or acetate upon the availability and binding capability of the small anions (21,23). Although TAG containing three long-chain fatty acids (FA) belong to the class of nonpolar lipids, TAG can be ionized with a sensitivity to the low picomole range through formation of ammoniated, lithiated, or sodiated adducts chelated to the carbonyl in the infused solution (20,24–26).

Classifications of Cellular Lipids Based on Their Electrical Propensities

Cellular lipids are typically stratified into many different classes based on the covalent nature of their polar head groups. However, for the purpose and ease of presentation of the principles of ESI for lipid analyses, we have categorized lipids based on their electrical propensities and proton affinities, as shown in Table 12.1. The first category of cellular lipids is anionic lipids which contain one or more net negative charge(s) at physiological (neutral) pH. Cardiolipin, phosphatidylglycerol

TABLE 12.1Classification of Cellular Lipids Based on ESI/MS Analyses of Lipidomics^a

| Category | Lipid class | Ion form | ESI/MS mode |
|--|---------------------------------|--|--------------|
| Anionic lipids | Cardiolipin | [M-H] ⁻ or [M-2H] ²⁻ | Negation-ion |
| | PtdGro | | |
| | PTDH | | |
| | PtdIns | | |
| | PtdSer | | |
| | Sulfatide | | |
| Weak zwitterions | PE | [M-H] ⁻ (in the presence of LiOH) | Negative-ion |
| | LysoPE ^b | | |
| | PE Ceramide | | |
| Strong zwitterions Neutral polar lipids | PC | [M+H] ⁺ (in the presence of LiOH) | Positive-ion |
| | LysoPC ^b | | |
| | SM | | |
| | GalC | | |
| | TAG ^c | | |
| Nonpolar lipids | Cholesterol and its derivatives | [M'-H] ⁻ (after derivatization) | Negative-ion |
| Metabolites | NEFA | [M-H] ⁻ (in the presence of LiOH) | Negative-ion |
| | Ceramide | | |
| | Acylcarnitine | [M+H] ⁺ | Positive-ion |
| | AcylCoA | [M-2H] ²⁻ | Negative-ion |

^aAbbreviations: PtdGro, phosphatidylglycerol; PtdH, phosphatidic acid; PtdIns, phosphatidylinositol; PtdSer, phosphatidylserine; PE, ethanolamine glycerophospholipid; PC, choline glycerophospholipid; SM, sphingomyelin; GalC, galactosylcerebroside; TAG, triacylglycerol; NEFA, nonesterified fatty acid.

^bThese classes should be in the category of metabolites but they can be analyzed like their parent molecular species.

^cTAG are usually classified as nonpolar lipids but do appear in the same mass spectra as polar lipids under the stated conditions.

(PtdGro), phosphatidylinositol (PtdIns), phosphatidylserine (PtdSer), phosphatidic acid (PtdH), and sulfatide (ST) are major classes in this category. The second category of cellular lipids is the lipids which contain a phosphoethanolamine head group (linked to either the *sn*-3 position of acyl glycerides or the 1-position of sphingosine). Lipids in this category commonly include ethanolamine-containing phospholipids [ethanolamine glycerophospholipid (PE) and lysoPE]. The third category of cellular lipids is the choline-containing lipids, including PC, lysoPC, and sphingomyelins (SM), as well as glycolipids containing a nonzwitterionic polar head group, such as cerebroside. The fourth category of lipids is the nonpolar lipids [cholesterol and its derivatives, as well as TAG]. The final category of lipids to be considered is the specialized lipid metabolites which act as signaling molecules or energy transducers (or both), including lysolipids, nonesterified FA (NEFA), diacylglycerols, ceramides, long-chain acylCoA, and long-chain acylcarnitines.

Global Analysis of Cellular Lipidomes by ESI-MS and ESI-MS/MS

Anionic Lipids

As shown in Figure 12.1, all anionic lipids can be readily ionized and analyzed directly from a dilute lipid extract in the negative-ion mode by ESI-MS as their $[M-H]^-$ ions (Table 12.1, Fig. 12.2), since they all carry a net negative charge. However, cardiolipin appears as its $[M-H]^{2-}$ ion as a major pseudomolecular ion in ESI-MS mass spectra of a dilute lipid extract (Fig. 12.2). Ion peaks corresponding to PtdIns molecular species can be identified by precursor-ion scanning of m/z 241 corresponding to phosphoinositol (Fig. 12.2) (27), or by product-ion analysis (23,28). Ion peaks corresponding to PtdSer molecular species can be identified by neutral loss scanning of 87 amu corresponding to the loss of serine or by individual product-ion analyses (Fig. 12.2) (23,27). Similarly, pseudomolecular ions of PtdH, PtdGro, and cardiolipin, along with PtdIns and PtdSer, can be identified by precursor-ion scanning of m/z 153 corresponding to glycerophosphate or by individual product-ion tandem mass spectroscopic analyses (Fig. 12.2) (23). The acyl moieties, the regiospecificities, and the isobaric peak compositions can also be identified and analyzed by precursor-ion scanning of all naturally occurring FA (Fig. 12.3).

Ethanolamine-Containing Glycerophospholipids

Ethanolamine-containing glycerophospholipids contain a head group comprised of a strong phosphate anion and a weak amine cation (they are zwitterions containing a weak basic group under normal physiological conditions). Accordingly, these weak zwitterions can be coaxed into their anionic forms suitable for analysis by ESI-MS by rendering the extraction solution basic, through the addition of a small amount of LiOH. Similar to the ESI-MS of anionic lipids, these “induced” anionic ethanolamine-containing lipids can be readily analyzed in negative-ion ESI-MS as $[M-H]^-$ (Table 12.1; Fig. 12.4). The acyl chains of ethanolamine-containing lipids can be identified by precursor-ion scanning of all potential naturally occurring acyl carboxylate ions (for example, m/z 255.2 for 16:0, 279.2 for 18:2, 281.2 for 18:1, 303.3 for 20:4, and 327.3 for 22:6, etc.) (Fig. 12.4). The regiospecificity of acyl chains and the composition of molecular species under each isobaric ion peak can also be substantiated by analyzing the ion peak intensities of these acyl carboxylate ions (23).

Because of the different covalent entities connecting the aliphatic chain to the *sn*-1 hydroxy group of the glycerol backbone, there are three subclasses in the PE class. These include an acyl linkage (PtdEtn), a vinyl linkage (PlsEtn), and an alkyl linkage (AlkEtn) (Fig. 12.5). PtdEtn can be distinguished from both the PlsEtn and alkyl subclasses by ESI tandem MS as discussed above. However, PlsEtn and alkyl subclasses cannot be directly discriminated by ESI-MS techniques alone. Accordingly, to identify ion peaks corresponding to PlsEtn molecular species, a part of each lipid extract is

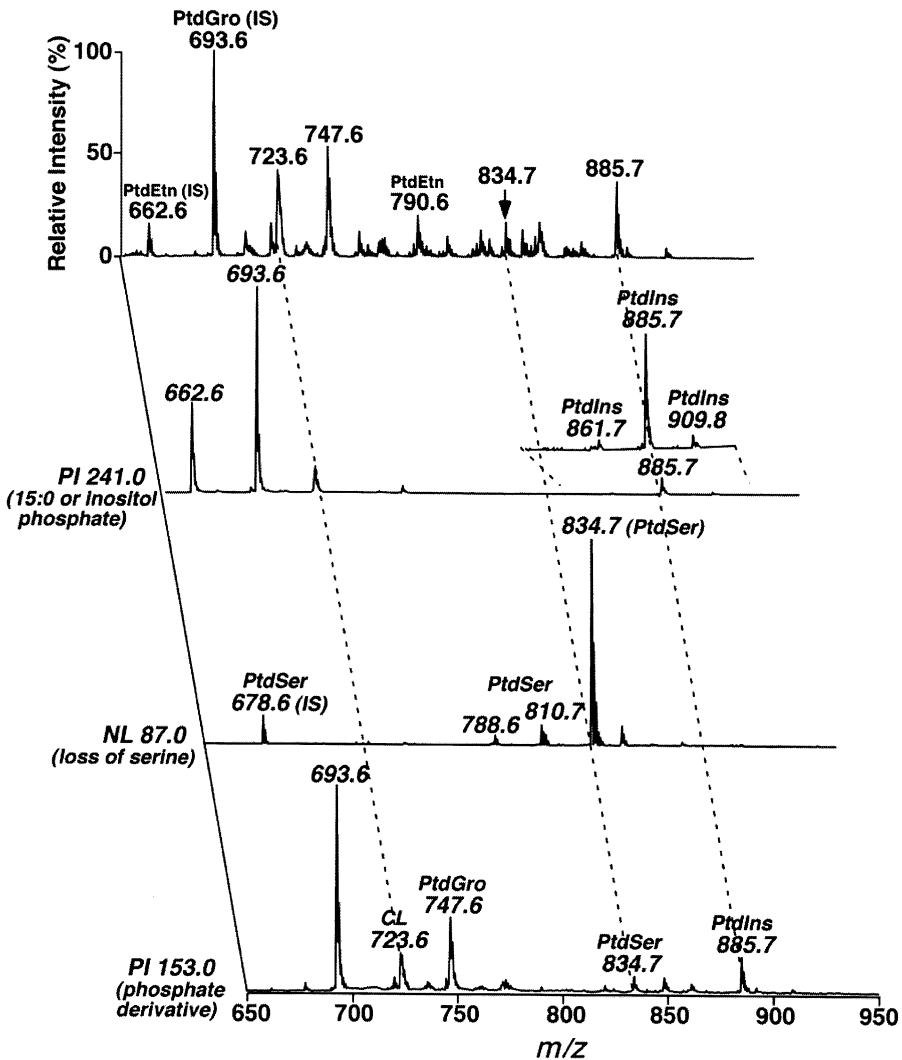


Fig. 12.2. A two-dimensional electrospray ionization (ESI) mass spectrum of mouse myocardial chloroform extract showing anionic lipid molecular species by neutral loss and precursor-ion scanning. The mouse myocardial lipids were extracted by a modified Bligh and Dyer method (58). A conventional ESI mass spectrum was acquired in the negative-ion mode prior to analysis in the second dimension by precursor-ion (PI) scanning of m/z 241.0 (inositol phosphate) or m/z 153.0 (glycerophosphate derivative). Serine glycerophospholipid molecular species were identified by the neutral loss (NL) of serine (87.0 amu). All mass spectral traces were displayed after normalization to the most intense peak in each individual spectrum. CL, doubly charged cardiolipin ion. IS, internal standard. *Source:* Han and Gross, unpublished.

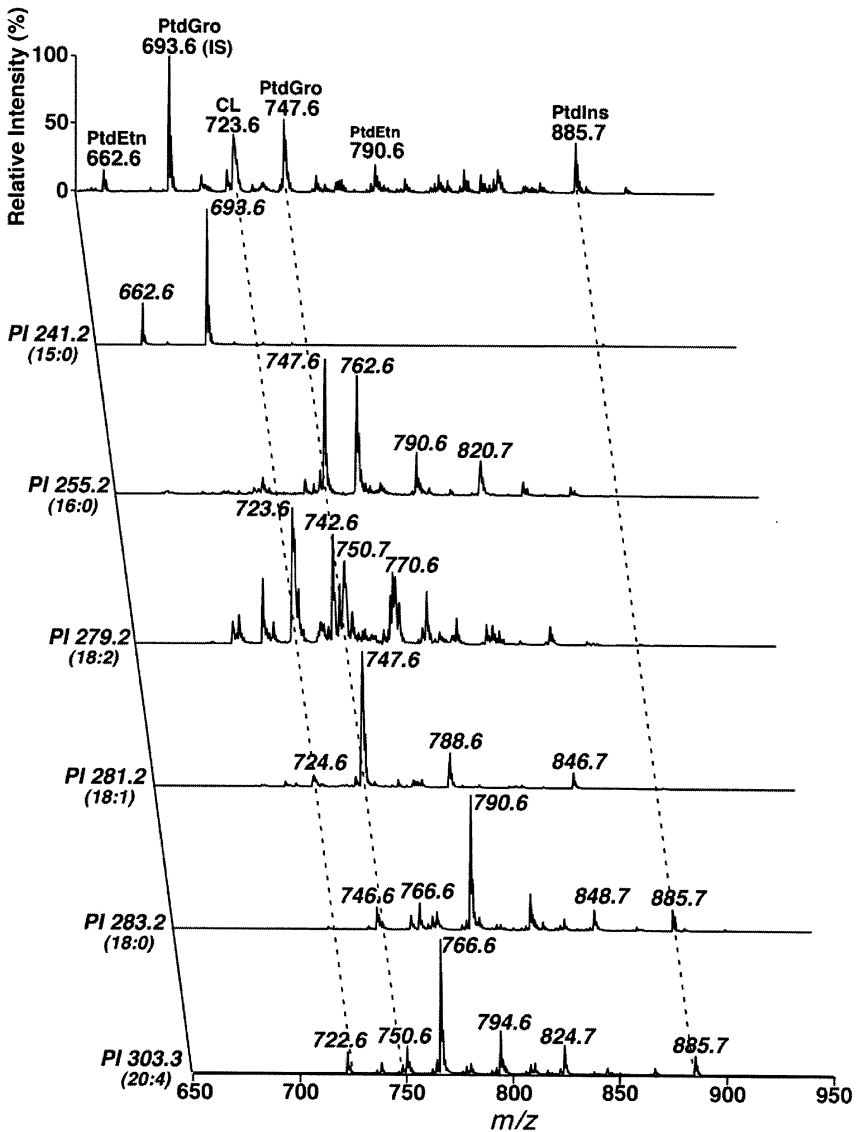


Fig. 12.3. A two-dimensional electrospray ionization mass spectrum of mouse myocardial chloroform extract in the negative-ion mode identifying the acyl chain composition of each pseudomolecular ion. The lipid extract is identical to the one used for the analysis of anionic phospholipids shown in Figure 12.2. All precursor ion (PI) mass spectral traces were displayed after normalization to the base peak in each individual spectrum. From the 2D analyses, ion peaks can be assigned, isobaric peaks can be identified, and the regiospecificity of each individual molecular species can be determined. CL, doubly-charged cardiolipin ion. IS, internal standard. *Source:* Han and Gross, unpublished.

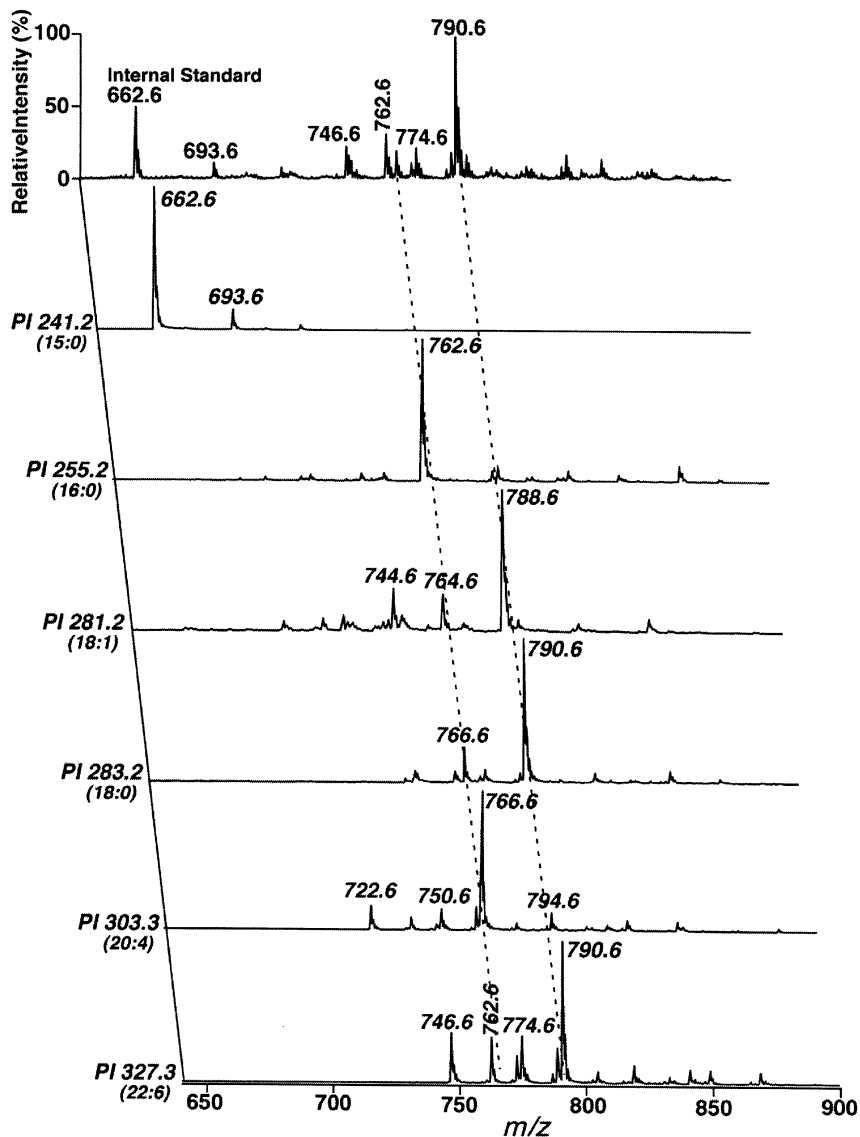


Fig. 12.4. A two-dimensional ESI mass spectrometric analysis of ethanolamine glycerophospholipid molecular species in a mouse myocardial lipid extract by precursor-ion (PI) scanning in negative-ion mode in the presence of LiOH. The lipid extract is identical to the one used for the analysis of anionic phospholipids shown in Figure 12.2. A small amount of LiOH was added prior to the mass spectroscopic analyses. All PI scans displayed are normalized to the base peak in the individual scan. From the 2D analyses, ion peaks can be assigned, isobaric peaks can be identified, and the regiospecificity of each individual molecular species can be determined. *Source:* Han and Gross, unpublished.

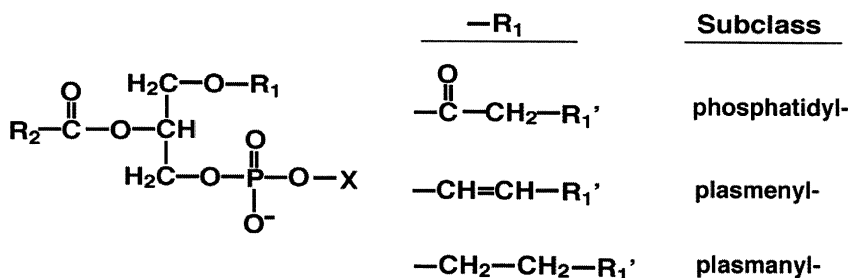


Fig. 12.5. Phospholipid subclasses. Phospholipid subclasses are categorized by the type of covalent attachment of aliphatic constituents to the *sn*-1 carbon of the glycerol backbone. The aliphatic chain of phosphatidyl, plasmeryl, or plasmanyl subclass of phospholipids contains an ester, vinyl ether, or alkyl ether bond at the *sn*-1 position, respectively.

treated with acidic vapor prior to mass spectrometric analysis as described previously (29). Through examination of PE molecular species profiles of both acid-treated and nontreated lipid extracts, PlsEtn molecular species are readily distinguished from alkyl subclass molecular species.

One may wonder whether anionic lipids in the extracts could overlap with PE molecular species and thus affect the quantitative analysis of PE molecular species. Fortunately, the mass abundances of PE molecular species are much higher than those of anionic lipid molecular species in biological samples (30). Anionic lipids are present only as minor constituents in mass spectra acquired in the presence of LiOH (Fig. 12.4). For example, comparing the top trace of Figure 12.4 to the top trace of Figure 12.2, the ion peaks corresponding to anionic lipids, including the internal standard for anionic lipids dominantly displayed in Figure 12.2, are in low abundance. Moreover, due to the differences of mass distribution between PE molecular species and anionic lipid species, only a few anionic lipid molecular species actually overlap with PE species, further minimizing errors from this approach (comparison between the top traces of Figures 12.2 and 12.4). Thus, most of these ions can be neglected in the quantitation of PE molecular species in Figure 12.4 when an experimental accuracy of $\pm 5\%$ is sufficient. Finally, because of the presence of a different number of nitrogen atoms in PE and most of the classes of anionic lipids (one nitrogen atom is present in PE and PtdSer while no nitrogen atom is present in PtdGro, PtdIns, PtdH, and cardiolipin), the nitrogen rule (31) can be utilized to deconvolute the partially overlapped anionic lipid species from the PE molecular species. However, since both PE and PtdSer molecular species possess one nitrogen atom, the nitrogen rule cannot be used to dissect the overlap, if it exists, between PE and PtdSer molecular species. Practically no overlaps between PE and PtdSer molecular species are present in the ESI-MS mass spectra under the experimental conditions, since rendering the solution alkaline by the addition of LiOH results in the production of the lithium salt of doubly charged PtdSer. It also should be noted that the abundances of hydroxy- (or other small anions such as

chlorine) associated adducts of other polar lipids such as PC are very low. For example, the hydroxy and chlorine adducts of 14:1-14:1 PtdCho (an internal standard for the quantitation of PC and SM), which have m/z at 690.6 and 708.6, respectively, are either not present or are present in very low abundances in the ESI-MS mass spectra of the lipid extract under the experimental conditions (top trace of Figure 12.4). Therefore, the effects of these adduct ions on PE analyses can be neglected with errors $<2\%$.

Choline-Containing Lipids and Nonzwitterionic Polar Lipids

The choline-containing lipids contain a strong phosphate anion and a strong quaternary amine cation (they are strong zwitterions under normal physiological conditions). As illustrated in Figure 12.1, these compounds are readily associated with small ions (both anions and cations) to form ion adducts under electrospray conditions. However, we have demonstrated empirically that they have a much higher selectivity to form adducts with small cations relative to small anions (8). Therefore, we usually analyze these choline-containing lipids in positive-ion ESI-MS (Table 12.1) as their lithiated adducts ($[M+Li]^+$) after addition of LiOH (top trace of Fig. 12.6) in conjunction with the analysis of ethanolamine-containing lipids in negative-ion ESI-MS. Note that Li^+ , but not other small cations such as Na^+ , K^+ , and NH_4^+ , is employed due to its ease in removal from the instrument and its tight association with choline-containing lipids, which aids in structural identification (22). These choline-containing lipids can be readily recognized by neutral loss scanning of 59.0, 183.0, or 189.0 amu corresponding to the loss of trimethylamine, phosphocholine, or lithium choline phosphate, respectively, in the positive-ion mode in the presence of LiOH, or neutral loss scanning of 50.0 amu corresponding to the loss of chloromethane in the negative-ion mode in the absence of LiOH (Fig. 12.6) (13). Minor sodiated choline-containing molecular ions can be readily recognized by comparison of the neutral loss mass spectra of 59.0 and 183.0 amu to those of 189.0 and 50.0 amu (Fig. 12.6). The former spectra display sodium adducts of choline-containing molecular species while the latter analyses are insensitive to sodium ions (Fig. 12.6).

An easy way to differentiate between PC and SM molecular species is to use the nitrogen rule, since there are two nitrogen atoms in SM molecular species while only one in PC molecules. The acyl chain components of each individual molecular species can be identified in either negative-ion or positive-ion tandem MS as described previously (13). Glyco(sphingo)lipids such as cerebrosides, a class of nonzwitterionic polar lipids, also show higher selectivity as their lithium adducts in comparison to hydroxy or chlorine adducts. Thus, these lipids are also analyzed by ESI-MS in the positive-ion mode (32). The pseudomolecular ions of these lipids can be easily distinguished from PC-type lipid ions by tandem MS through neutral loss scanning of 59.0 or 183.0 amu, corresponding to the loss of trimethylamine or phosphocholine, respectively.

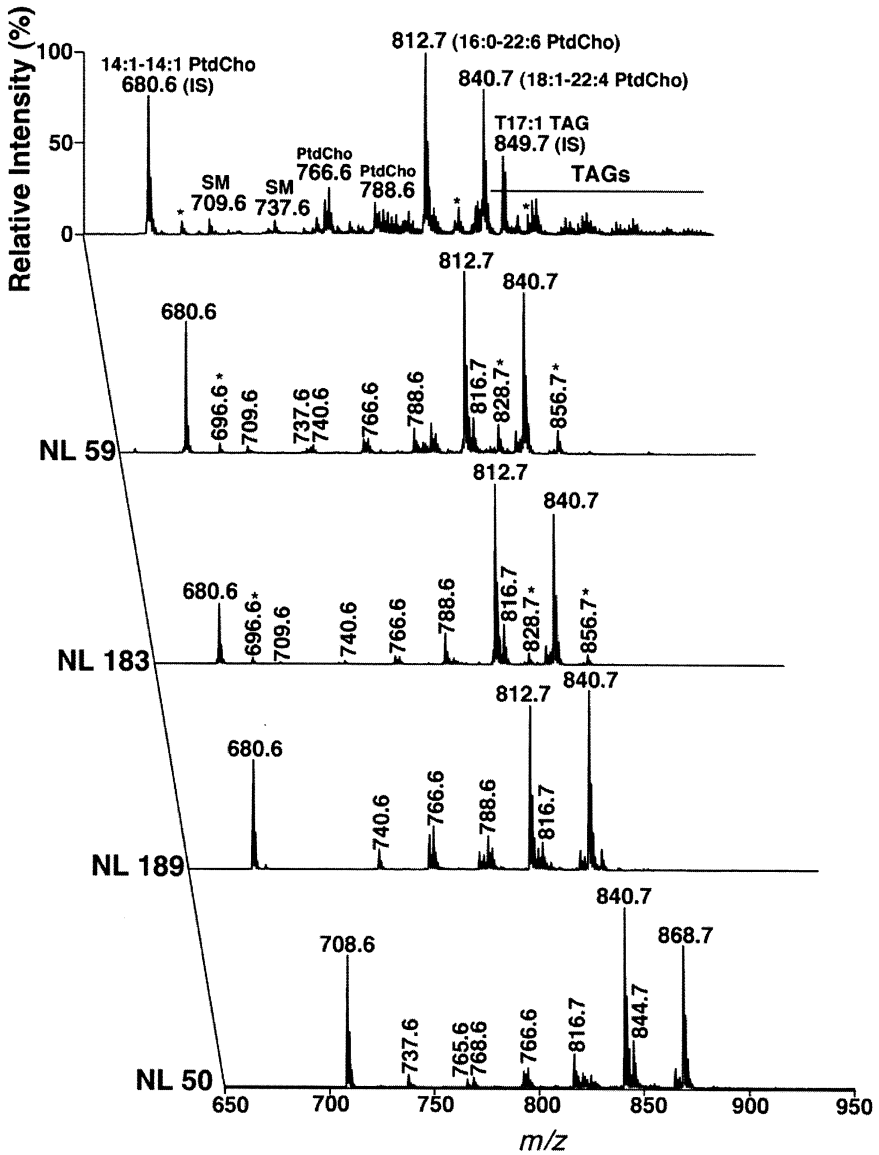


Fig. 12.6. Tandem ESI mass spectrometric analyses of choline glycerophospholipids directly from a mouse myocardial lipid extract by neutral loss scanning. The lipid extract is identical to the one used for the analysis of anionic phospholipids shown in Figure 12.2. ESI mass spectra were acquired by neutral loss scanning of 50.0 amu in the negative-ion mode in the absence of LiOH and of 59.0, 183.0, or 189.0 amu in the positive-ion mode in the presence of LiOH. IS, internal standard. *, sodiated ions. *Source:* Han and Gross, unpublished.

Nonpolar Lipids

Most nonpolar lipids in cellular extracts are comprised of TAG molecular species and cholesterol. Intriguingly, TAG (which generally are classified as nonpolar lipids) also show high selectivity as their lithium adducts (24–26). However, due to the weak coordination between the carbonyl(s) and a small cation (lithium, sodium, or ammonium), unlike polar lipids, the ionization efficiency of individual TAG molecular species varies dramatically, depending on the acyl chain lengths and the number of double bonds in the molecule (13,26). There are some overlaps between TAG molecular species and choline-containing phospholipid molecular species in the ESI-MS analyses of lipid extracts of biological samples. However, these overlaps can be readily distinguished either by applying the nitrogen rule or by tandem mass spectroscopic analyses of choline-containing phospholipids through neutral loss scanning of 183.0 amu. To quantitatively analyze TAG molecular species from a crude lipid extract of a biological sample, we have recently developed a two-dimensional mass spectrometric technique (26), which has now been routinely used in our laboratories (26,33–37).

We generally assess the content of cholesterol and its esters in lipid extracts by employing a fluorometric method (38). However, Sandhoff and his colleagues (39) have developed a method to quantitate cholesterol and its derivatives by ESI tandem MS after a simple one-step chemical derivatization of cholesterol to cholesterol-3-sulfate by a sulfur trioxide-pyridine complex. Duffin *et al.* (40) were able to profile individual molecular species of cholesterol esters by precursor-ion scanning of m/z 369.3 (corresponding to a sterol derivative) from ammoniated molecular ions.

Lipid Metabolites

Due to the low abundances of lipid metabolites in lipid extracts of biological samples, either special sample preparations or separate ESI-MS analyses typically need to be performed. LysoPC or lysoPE molecular species can be directly analyzed in either positive-ion mass spectra as their lithium adducts or in negative-ion spectra as $[M-H]^-$, respectively (as their parent molecules, as discussed above). The regioisomers of these lysophospholipids can be readily discriminated directly from lipid extracts by comparing their fragmentation patterns (41–43). Diacylglycerol molecular species may be similarly analyzed utilizing methods similar to those for TAG (26). Negative-ion neutral loss scans of mass 256.2 and 327.3 during direct infusion of crude lipid extracts in the presence of LiOH can be performed in order to identify non-hydroxyl and 2-hydroxyl ceramide molecular species in lipid extracts (44).

Acylcarnitines in lipid extracts can be readily analyzed by precursor-ion scanning of m/z 85, corresponding to a carnitine derivative, which has been used extensively for biological studies and clinical diagnoses (45–50). Long-chain fatty acyl-CoA molecular species can be analyzed directly from crude lipid extracts by precursor-ion scanning of m/z 339, corresponding to the doubly-charged CoA group (51).

After rendering the lipid extract solution basic by the addition of a small amount of LiOH in methanol, nonesterified FA in solution will be converted to their carboxylate forms and easily quantified by ESI-MS in negative-ion mode, scanning through the mass range from 200 to 400. Quantification is easily accomplished utilizing an internal standard (a FA containing an odd carbon number). The structures of NEFA can be determined in either negative- or positive-ion mode by tandem MS (52,53). Arachidonic acid can be converted into a diverse family of biologically active metabolites, including prostaglandins, leukotrienes, lipoxins, hydroxyl FA (HETE), epoxyeicosatrienoic acids (EET), etc., through enzymatic or nonenzymatic reactions. MS has been extensively employed to characterize and quantitate these numerous and complicated compounds; see Murphy *et al.* (9) for a recent review.

A Common Strategy of ESI Intrasource Separation for Major Classes of Lipids

Based on differences in lipid electrical propensities, combined with the principles of the ESI process, it is possible to perform a total cellular lipidome analysis by ESI mass spectrometric techniques directly from a crude lipid extract of a biological sample without the need for prior chromatographic separation. In combination with the appropriate front-end sample preparation, we have developed a strategy for lipidomic analyses of biological samples without the need for chromatography (Fig. 12.7). This approach has very recently been described in detail (13), and it is only discussed in brief here. Using this strategy, we have been able to fingerprint and quantify hundreds of individual lipid molecular species from most of the major lipid classes and multiple minor metabolite groups.

Specifically, the chloroform extract of a biological sample is analyzed directly at neutral pH by ESI-MS in negative-ion mode, which selects for anionic lipid species, as discussed in the previous section. Thus, the acquired mass spectrum displays a fingerprint of anionic (PtdIns, PtdGro, PtdSer, cardiolipin, and PtdH) lipid molecular ions (Fig. 12.2). These molecular ions can be further characterized by tandem MS by the analysis of the head groups and acyl moieties, as well as the isobaric molecular species (Figs. 12.2 and 12.3). The ionization efficiency of these anionic lipids is identical, within experimental error, in dilute lipid solutions as previously demonstrated (13). By comparing the intensity of each identified ion peak with an anionic lipid internal standard (or standards) and appropriate correction for ^{13}C isotope effects (13,26,44) on masses of individual molecular ions can be obtained.

Next, by the addition of a small amount of LiOH, zwitterionic ethanolamine glycerophospholipid (PE) molecular species are rendered anionic in solution by deprotonation of their quaternary amine by base. Negative-ion ESI-MS results in abundant molecular ion peaks corresponding to individual ethanolamine-containing molecular species in the mass range between m/z 600 and 900 for PE (Fig.

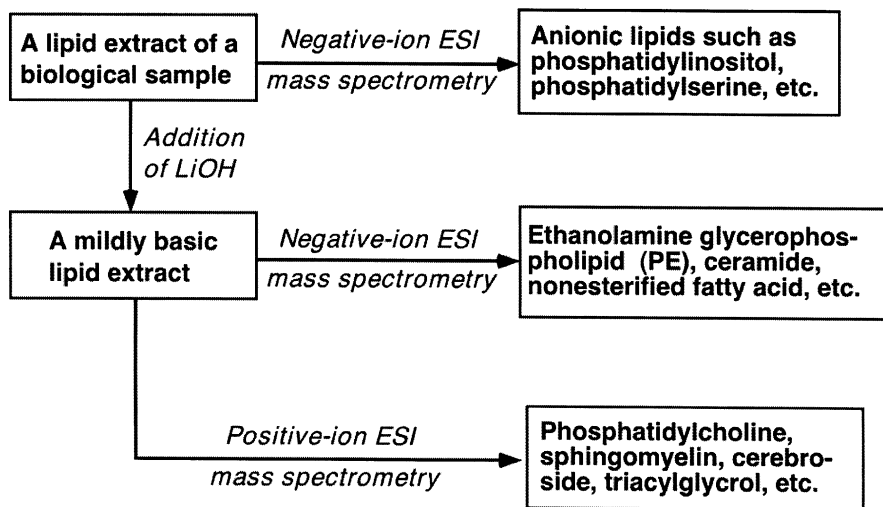


Fig. 12.7. Schematic diagram of the experimental strategy used for total cellular lipidome analyses directly from crude extracts of biological samples.

12.4) and 400 and 600 for lysoPE. These individual molecular species can be characterized by ESI-MS/MS (Fig. 12.4) and are quantified by comparison of their ion peak intensities with that of a PE internal standard. As discussed above, other classes of anionic lipids (PtdGro and PtdIns) do not overlap with PE species due to the nitrogen rule. Moreover, the amounts of each of these anionic phospholipids are quite small in comparison to the amounts of PE species and thus can introduce errors of only 2–3% in PE quantitation in extreme cases.

Similarly, NEFA exist as lithium-coordinated carboxylate anions in solution, in the presence of LiOH. Thus, abundant pseudomolecular ion peaks corresponding to NEFA molecular species are apparent in the mass range of m/z 200 to 400. These NEFA molecular species can be quantitated by comparisons of their ion peak intensities with that of a NEFA internal standard (for example, 19:0 FA or d_3 -16:0 FA) after correction for ^{13}C isotope effects. The amide proton in ceramide molecular species is partially removed in the presence of LiOH, thus allowing ceramides to be directly quantitated by comparisons with a ceramide internal standard by tandem MS as described (44).

Finally, the dilute chloroform extract at alkaline pH, as in the last step, is analyzed in the positive-ion mode. Under these experimental conditions, molecular classes that contain a negative charge (including anionic lipids and PE species) are largely prevented from forming positively charged ions during the electrospray ionization process. Molecular species of choline-containing phospholipids (PtdCho, lysoPtdCho, and SM), glycolipids, triacylglycerols and are readily ionized as lithium adducts (Fig. 12.6) (26,32,54). These pseudomolecular ions can be fur-

ther characterized by tandem MS based on the analysis of head groups (Fig. 12.6) and acyl moieties as well as isobaric molecular species (13). By comparing the intensity of each identified ion peak with an internal standard (or standards) and appropriate correction for ^{13}C isotope effects (26,44), masses of individual pseudo-molecular ions can be obtained.

Examples of Cellular Lipidome Analysis Using the Intrasource Separation Technique

Lipid Alterations in Diabetic Myocardium

Lipid alterations are associated with multiple diseases epidemic in industrialized nations, including diabetes, obesity, and atherosclerosis (55). To determine the changes in myocardial lipid metabolism linked with intrinsic cardiac dysfunction during the diabetic state, we have exploited the ESI-MS intrasource separation technique to perform detailed analysis of the lipidome in diabetic myocardium and to investigate the ability of insulin to prevent these alterations (25). Four specific alterations in lipids from rat myocardium rendered diabetic by streptozotocin treatment (a well accepted model of Type I diabetes) were demonstrated. First, dramatic alterations in TAG molecular species, including a more than five-fold increase in tripalmitin mass and a 60% decrease in TAG molecular species containing polyunsaturated acyl acids, are present in diabetic rat myocardium. Second, total PlsEtn mass content increased 44% in diabetic rat myocardium relative to the control. Third, a specific decrease in a PtdEtn molecular species (i.e., 18:0–20:4 PtdEtn) occurs in diabetic rat myocardium. Finally, a substantial increase (46 mol %) in myocardial PtdIns mass was observed in diabetic rats in comparison to normal controls. Although complete recovery of all of the diabetes-induced alterations in phospholipids were observed after insulin treatment, the dramatic alterations in TAG molecular species were not prevented by peripheral insulin treatment after induction of the diabetic state. Collectively, these results dissect alterations in myocardial lipids induced by diabetes into changes that can or cannot be remedied by routine peripheral insulin treatment alone, suggesting that peripheral insulin therapy alone might not be sufficient to correct all of the metabolic alterations occurring in diabetic myocardium.

The Role of Apolipoprotein E in the Central Nervous System

There are three common isoforms of human apolipoprotein E (apoE) (56). Numerous studies have demonstrated the role of apoE in plasma lipid metabolism in an isoform-dependent manner (see Refs. 56 and 57 for reviews). It has long been postulated that apoE may also play a role in lipid metabolism in the brain but there is no direct evidence. Therefore, by exploiting the analytical power of ESI-MS with the intrasource separation technique, we examined the effects of apoE on mouse brain lipid homeostasis, the molecular species composition and the mass of

lipids in both apoE^{+/+} and apoE^{-/-} mouse brain regions (38). For example, Figure 12.8 shows the representative ESI mass spectra of a chloroform extract from wild-type (apoE^{+/+}) mouse cortex at 12 months of age acquired in both negative- and positive-ion modes after addition of a small amount of LiOH. The mass spectrum acquired in negative-ion mode (Fig. 12.8A) demonstrated multiple abundant ion peaks corresponding to PE molecular species, accounting for a total mass of 332.4 ± 19.3 nmol/mg of protein, including 156.2 ± 9.5 nmol/mg of protein of plasmenylethanolamine. The positive-ion ESI-MS spectrum of the identical lipid extract (Fig. 12.8B) demonstrated PC, SM, and galactosylcerebroside (GalC) molecular species, accounting for 281.2 ± 8.2 , 30.5 ± 4.6 , and 118.3 ± 16.8 nmol/mg of protein of PC, SM, and GalC, respectively. Negative-ion ESI-MS analysis of the identical crude lipid extract from wild-type mouse cortex without the addition of LiOH (Fig. 12.9A) demonstrated multiple abundant ion peaks corresponding to PtdIns, PtdSer, and ST anionic lipid molecular species, accounting for 24.2 ± 1.3 , 26.4 ± 2.1 , and 12.9 ± 1.4 nmol/mg of protein of PtdIns, PtdSer, and sulfatide, respectively. The mass content of cholesterol in wild-type mouse cortex (420.7 ± 25.6 nmol/mg of protein) was obtained using a fluorometric method.

Examination of the lipid profiles and the mass of each lipid class from multiple brain regions of apoE^{-/-}, including cortex, cerebellum, and hippocampus, by ESI/MS analyses and fluorometric measurements, demonstrated no significant differences except sulfatide in all examined lipid classes in comparison with those obtained from the corresponding regions of apoE^{+/+}. Negative-ion ESI mass spectrometric analysis demonstrated an over 100% increase in sulfatide mass content in the cortex of apoE^{-/-} mice relative to that found in apoE^{+/+} at the same age (Fig. 12.9). The mass content of sulfatides in cerebellum, hippocampus, septum, striatum, and thalamus of apoE^{-/-} mice was also substantially increased relative to those found in apoE^{+/+} mice at the same age. These results indicate that apoE in some way modulates sulfatide mass levels in the central nervous system (CNS). Further study demonstrated that apoE modulates sulfatide mass levels in the CNS by the same metabolic pathways that regulate levels of apoE-containing CNS lipoproteins.

Conclusions

This article presents a new classification of lipids based on their electrical propensities, summarizes the intrasource separation technique of ESI-MS, and discusses a strategy for total cellular lipidome analyses using this technique. Two examples employing the ESI intrasource separation technique from previous studies are summarized. It can be concluded that by using the ESI intrasource separation technique in combination with other advanced technology, our knowledge of the role of lipid alterations and biochemical mechanisms underlying disease states will undoubtedly be extended. In turn, this knowledge will help us to conquer the lipid-associated epidemic diseases including diabetes, atherosclerosis, and obesity.

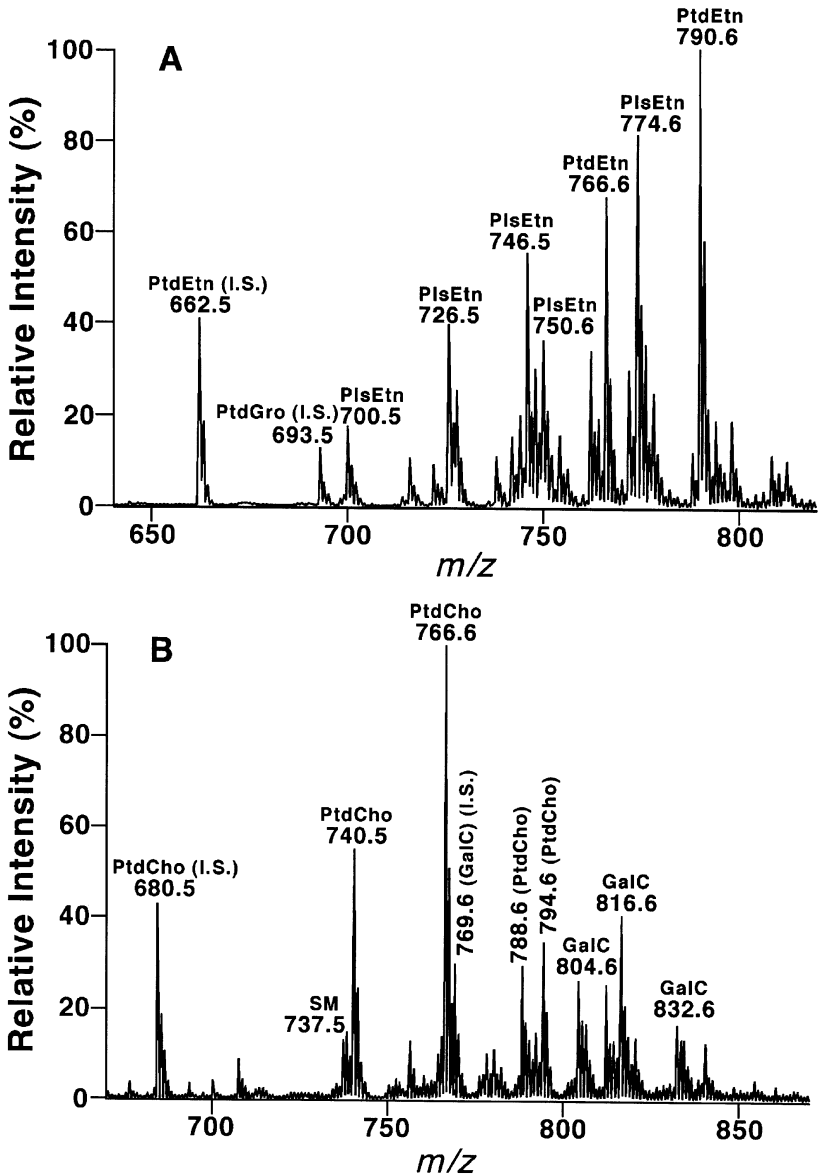


Fig. 12.8. Representative ESI mass spectra of lipid extracts from wild-type mouse cortex. Lipids of wild-type (i.e., apoE+/+) mouse cortex at 12 months of age were extracted by a modified method of Bligh and Dyer (58). Negative-ion (panel A) and positive-ion (panel B) ESI/MS of the lipid extracts were performed in the presence of a trace amount of LiOH. All major individual molecular species as indicated were identified using tandem mass spectrometry. I.S., internal standard. *Source:* Han, unpublished.

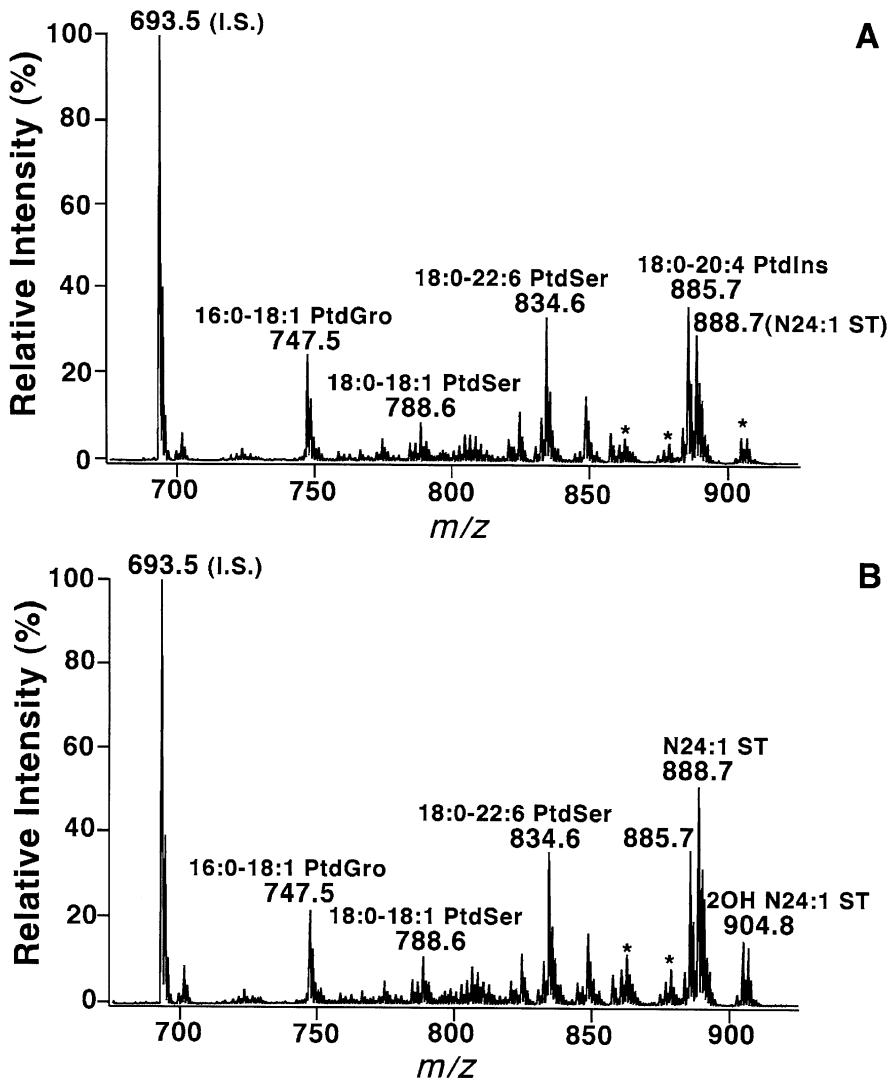


Fig. 12.9. Representative negative-ion ESI mass spectra of lipid extracts from wild-type and apoE knockout ($-/-$) mouse cortices. Lipids of wild-type (i.e., apoE $+/+$, panel A) and apoE knockout (i.e., apoE $-/-$, panel B) mouse cortice at 12 months of age were extracted by a modified method of Bligh and Dyer (58) and negative-ion ESI/MS of the lipid extracts without the presence of LiOH was performed. All major individual molecular species as indicated were identified using tandem mass spectrometry. Asterisks indicate the lower abundant ion peaks of some sulfatide (ST) molecular species present in the lipid extracts. 2OH N24:1 ST represents 2-hydroxy N24:1 ST molecular species. I.S., internal standard. Note differences in ST. *Source:* Han, unpublished.

Acknowledgments

This work was supported by NIH grant P01HL57278 and R01HL41250. Xianlin Han is the 2003 Memory Ride Prize recipient. The authors are grateful to the Washington University Mass Spectrometer Facility Center, which is supported by NIH grants P41-RR00954, P60-DK20579, and P30-DK56341, for the use of the electrospray ionization mass spectrometer.

References

1. Cooper, M.J., and M.W. Anders, High Pressure Liquid Chromatography of Fatty Acids and Lipids, *J. Chromatogr. Sci.* 13: 407–411 (1975).
2. Gross, R.W., and B.E. Sobel, Isocratic High-Performance Liquid Chromatography Separation of Phosphoglycerides and Lysophosphoglycerides, *J. Chromatogr.* 197: 79–85 (1982).
3. Gross, R.W., High Plasmalogen and Arachidonic Acid Content of Canine Myocardial Sarcolemma: A Fast Atom Bombardment Mass Spectroscopic and Gas Chromatography-Mass Spectroscopic Characterization, *Biochemistry* 23: 158–165 (1984).
4. Creer, M.H., and R.W. Gross, Separation of Isomeric Lysophospholipids by Reverse Phase HPLC, *Lipids* 20: 922–928 (1985).
5. Creer, M.H., and R.W. Gross, Reversed-Phase High-Performance Liquid Chromatographic Separation of Molecular Species of Alkyl Ether, Vinyl Ether, and Monoacyl Lysophospholipids, *J. Chromatogr.* 338: 61–69 (1985).
6. McCluer, R.H., M.D. Ullman, and F.B. Jungalwala, HPLC of Glycosphingolipids and Phospholipids, *Adv. Chromatogr.* 25: 309–353 (1986).
7. Robins, S.J. and G.M. Patton, Separation of Phospholipid Molecular Species by High Performance Liquid Chromatography: Potentials for Use in Metabolic Studies, *J. Lipid Res.* 27: 131–139 (1986).
8. Han, X., and R.W. Gross, Electrospray Ionization Mass Spectroscopic Analysis of Human Erythrocyte Plasma Membrane Phospholipids, *Proc. Natl. Acad. Sci. USA* 91: 10635–10639 (1994).
9. Murphy, R.C., J. Fiedler, and J. Hevko, Analysis of Nonvolatile Lipids by Mass Spectrometry, *Chem. Rev.* 101: 479–526 (2001).
10. Griffiths, W.J., Tandem Mass Spectrometry in the Study of Fatty Acids, Bile Acids, and Steroids, *Mass Spectrom. Rev.* 22: 81–152 (2003).
11. Han, X., and R.W. Gross, Global Analysis of Cellular Lipidomes Directly from Crude Extracts of Biological Samples by ESI Mass Spectrometry: A Bridge to Lipidomics, *J. Lipid Res.* 44: 1071–1079 (2003).
12. Pulfer, M., and R.C. Murphy, Electrospray Mass Spectrometry of Phospholipids, *Mass Spec. Rev.* 22: 332–364 (2003).
13. Han, X. and R.W. Gross, Shotgun Lipidomics: Electrospray Ionization Mass Spectrometric Analysis and Quantitation of the Cellular Lipidomes Directly from Crude Extracts of Biological Samples, *Mass Spec. Rev.* 10: 1002/MAS (2004).
14. Fenn, J.B., M. Mann, C.K. Meng, S.F. Wong, and C.M. Whitehouse, Electrospray Ionization for Mass Spectrometry of Large Biomolecules, *Science* 246: 64–71 (1989).
15. Fenn, J.B., M. Mann, C.K. Meng, S.F. Wong, and C.M. Whitehouse, Electrospray Ionization: Principles and Practice, *Mass Spectrom. Rev.* 9: 37–70 (1990).

16. Smith, R.D., J.A. Loo, C.G. Edmonds, C.J. Barinaga, and H.R. Udseth, New Developments in Biochemical Mass Spectrometry: Electrospray Ionization, *Anal. Chem.* 62: 882–899 (1990).
17. Cole, R.B., *Electrospray Ionization Mass Spectrometry*, Wiley, New York, (1997).
18. de la Mora, J.F., G.J. van Berkel, C.G. Enke, R.B. Cole, M. Martinez-Sanchez, and J.B. Fenn, Electrochemical Processes in Electrospray Ionization Mass Spectrometry, *J. Mass Spectrom.* 35: 939–952 (2000).
19. Weintraub, S.T., R.N. Pinckard, and M. Hail, Electrospray Ionization for Analysis of Platelet-Activating Factor, *Rapid Commun. Mass Spectrom.* 5: 309–311 (1991).
20. Duffin, K.L., J.D. Henion, and J.J. Shieh, Electrospray and Tandem Mass Spectrometric Characterization of Acylglycerol Mixtures that are Dissolved in Nonpolar Solvents, *Anal. Chem.* 63: 1781–1788 (1991).
21. Kerwin, J.L., A.R. Tuininga, and L.H. Ericsson, Identification of Molecular Species of Glycerophospholipids and Sphingomyelin Using Electrospray Mass Spectrometry, *J. Lipid Res.* 35: 1102–1114 (1994).
22. Hsu, F.-F., A. Bohrer, and J. Turk, Formation of Lithiated Adducts of Glycerophosphocholine Lipids Facilitates Their Identification by Electrospray Ionization Tandem Mass Spectrometry, *J. Am. Soc. Mass Spectrom.* 9: 516–526 (1998).
23. Han, X., and R.W. Gross, Structural Determination of Picomole Amounts of Phospholipids via Electrospray Ionization Tandem Mass Spectrometry, *J. Am. Soc. Mass Spectrom.* 6: 1202–1210 (1995).
24. Hsu, F.-F., and J. Turk, Structural Characterization of Triacylglycerols as Lithiated Adducts by Electrospray Ionization Mass Spectrometry Using Low-Energy Collisionally Activated Dissociation on a Triple Stage Quadrupole Instrument, *J. Am. Soc. Mass Spectrom.* 10: 587–599 (1999).
25. Han, X., A.R. Abendschein, J.G. Kelley, and R.W. Gross, Diabetes-Induced Changes in Specific Lipid Molecular Species in Rat Myocardium, *Biochem. J.* 352: 79–89 (2000).
26. Han, X., and R.W. Gross, Quantitative Analysis and Molecular Species Fingerprinting of Triacylglyceride Molecular Species Directly from Lipid Extracts of Biological Samples by Electrospray Ionization Tandem Mass Spectrometry, *Anal. Biochem.* 295: 88–100 (2001).
27. Brügger, B., G. Erben, R. Sandhoff, F.T. Wieland, and W.D. Lehmann, Quantitative Analysis of Biological Membrane Lipids at the Low Picomole Level by Nano-Electrospray Ionization Tandem Mass Spectrometry, *Proc. Natl. Acad. Sci. USA* 94: 2339–2344 (1997).
28. Hsu, F.-F. and J. Turk, Characterization of Phosphatidylinositol, Phosphatidylinositol-4-phosphate, and Phosphatidylinositol-4,5-bisphosphate by Electrospray Ionization Tandem Mass Spectrometry: A Mechanistic Study, *J. Am. Soc. Mass Spectrom.* 11: 986–999 (2000).
29. Ford, D.A., K.B. Rosenbloom, and R.W. Gross, The Primary Determinant of Rabbit Myocardial Ethanolamine Phosphotransferase Substrate Selectivity is the Covalent Nature of the *sn*-1 Aliphatic Group of Diradyl Glycerol Acceptors, *J. Biol. Chem.* 267: 11222–11228 (1992).
30. Cullis, P.R., D.B. Fenske, and M.J. Hope, Physical Properties and Functional Roles of Lipids in Membranes, in *Biochemistry of Lipids, Lipoproteins and Membranes*, edited by D.E. Vance, and J. Vance, Elsevier, New York, 1996.
31. McLafferty, F.W. and F. Turecek, *Interpretation of Mass Spectra*, University Science Books, Sausalito, California, 1993.

32. Han, X., D.M. Holtzman, D.W. McKeel, Jr., J. Kelley, and J.C. Morris, Substantial Sulfatide Deficiency and Ceramide Elevation in Very Early Alzheimer's Disease: Potential Role in Disease Pathogenesis, *J. Neurochem.* 82: 809–818 (2002).
33. Finck, B.N., J.J. Lehman, T.C. Leone, M.J. Welch, M.J. Bennett, A. Kovacs, X. Han, R.W. Gross, R. Kozak, G.D. Lopaschuk, and D.P. Kelly, The Cardiac Phenotype Induced by PPAR α Overexpression Mimics that Caused by Diabetes Mellitus, *J. Clin. Invest.* 109: 121–130 (2002).
34. Finck, B.N., X. Han, M. Courtois, F. Aimond, J.M. Nerbonne, A. Kovacs, R.W. Gross, and D.P. Kelly, A Critical Role for PPAR α -Mediated Lipotoxicity in the Pathogenesis of Diabetic Cardiomyopathy: Modulation of Phenotype by Dietary Fat Content, *Proc. Natl. Acad. Sci. USA* 100: 1226–1231 (2003).
35. Listenberger, L., X. Han, S.E. Lewis, S. Cases, R.V. Farese, Jr., D.S. Ory, and J.E. Schaffer, Unsaturated Fatty Acids Prevent Lipotoxicity Through Induction of Triglyceride Accumulation, *Proc. Natl. Acad. Sci. USA* 100: 3077–3082 (2003).
36. Mancuso, D.J., D.R. Abendschein, C.M. Jenkins, X. Han, J.E. Saffitz, R.B. Schuessler, and R.W. Gross, Cardiac Ischemia Activates Calcium-Independent Phospholipase A₂, Precipitating Ventricular Tachyarrhythmias in Transgenic Mice: Rescue of the Lethal Electrophysiologic Phenotype by Mechanism-Based Inhibition, *J. Biol. Chem.* 278: 22231–22236 (2003).
37. Newberry, E.P., Y. Xie, S. Kennedy, X. Han, K.K. Buhman, J. Luo, R.W. Gross, and N.O. Davidson, Decreased Hepatic Triglyceride Accumulation and Altered Fatty Acid Uptake in Mice with Deletion of the Liver Fatty Acid Binding Protein Gene, *J. Biol. Chem.* 278: 51664–51672 (2003).
38. Han, X., H.Cheng, D.J. Fryer, A.M. Fagan, and D.M. Holtzman, Novel Role for Apolipoprotein E in the Central Nervous System: Modulation of Sulfatide Content, *J. Biol. Chem.* 278: 8043–8051 (2003).
39. Sandhoff, R., B. Brügger, D. Jeckel, W.D. Lehmann, and F.T. Wieland, Determination of Cholesterol at the Low Picomole Level by Nano-Electrospray Ionization Tandem Mass Spectrometry, *J. Lipid Res.* 40: 126–132 (1999).
40. Duffin, K.L., M.G. Obukowicz, A. Raz, and J.J. Shieh, Electrospray/Tandem Mass Spectrometry for Quantitative Analysis of Lipid Remodeling in Essential Fatty Acid Deficient Mice, *Anal. Biochem.* 279: 179–188 (2000).
41. Han, X. and R.W. Gross, Structural Determination of Lysophospholipid Regioisomers by Electrospray Ionization Tandem Mass Spectrometry, *J. Am. Chem. Soc.* 118: 451–457 (1996).
42. Khaselev, N. and R.C. Murphy, Electrospray Ionization Mass Spectrometry of Lysoglycerophosphocholine Lipid Subclasses, *J. Am. Soc. Mass Spectrom.* 11: 283–291 (2000).
43. Hsu, F.-F., J. Turk, A.K. Thukkani, M.C. Messner, K.R. Wildsmith, and D.A. Ford, Characterization of Alkylacyl, Alk-1-Enylacyl and Lyso Subclasses of Glycerophosphocholine by Tandem Quadrupole Mass Spectrometry with Electrospray Ionization, *J. Mass Spectrom.* 38: 752–763 (2003).
44. Han, X., Characterization and Direct Quantitation of Ceramide Molecular Species from Lipid Extracts of Biological Samples by Electrospray Ionization Tandem Mass Spectrometry, *Anal. Biochem.* 302: 199–212 (2002).
45. Rashed, M.S., P.T. Ozand, M.E. Harrison, P.J.F. Watkins, and S. Evans, Electrospray Tandem Mass Spectrometry in the Diagnosis of Organic Acidemias, *Rapid Commun. Mass Spectrom.* 8: 129–133 (1994).

46. Ford, D.A., X. Han, C.C. Horner, and R.W. Gross, Accumulation of Unsaturated Acylcarnitine Molecular Species During Acute Myocardial Ischemia: Metabolic Compartmentalization of Products of Fatty Acyl Chain Elongation in the Acylcarnitine Pool, *Biochemistry* 35: 7903–7909 (1996).
47. Johnson, A.W., K. Mills, and P.T. Clayton, The Use of Automated Electrospray Ionization Tandem MS for the Diagnosis of Inborn Errors of Metabolism from Dried Blood Spots, *Biochem. Soc. Trans.* 24: 932–938 (1996).
48. Vreken, P., A.E.M. van Lint, A.H. Bootsma, H. Overmars, R.J.A. Wanders, and A.H. van Gennip, Quantitative Plasma Acylcarnitine Analysis Using Electrospray Tandem Mass Spectrometry for the Diagnosis of Organic Acidaemias and Fatty Acid Oxidation Defects, *J. Inherit. Metab. Dis.* 22: 302–306 (1999).
49. McClellan, J.E., S.T. Quarmbly, and R.A. Yost, Parent and Neutral Loss Monitoring on a Quadrupole Ion Trap Mass Spectrometer: Screening of Acylcarnitines in Complex Mixtures, *Anal. Chem.* 74: 5799–5806 (2002).
50. Moeder, M., A. Kiessling, H. Loester, and L. Brueggemann, The Pattern of Urinary Acylcarnitines Determined by Electrospray Mass Spectrometry: A New Tool in the Diagnosis of Diabetes Mellitus, *Anal. Bioanal. Chem.* 375: 200–210 (2003).
51. Kalderon, B., V. Sheena, S. Shachrur, R. Hertz, and J. Bar-Tana, Modulation by Nutrients and Drugs of Liver Acyl-CoAs Analyzed by Mass Spectrometry, *J. Lipid. Res.* 43: 1125–1132 (2002).
52. Kerwin, J.L., A.M. Wiens, and L.H. Ericsson, Identification of Fatty Acids by Electrospray Mass Spectrometry and Tandem Mass Spectrometry, *J. Mass Spectrom.* 31: 184–192 (1996).
53. Hsu, F.-F. and J. Turk, Distinction Among Isomeric Unsaturated Fatty Acids as Lithiated Adducts by Electrospray Ionization Mass Spectrometry Using Low Energy Collisionally Activated Dissociation on a Triple Stage Quadrupole Instrument, *J. Am. Soc. Mass Spectrom.* 10: 600–612 (1999).
54. Han, X., R.A. Gubitosi-Klug, B. Collins, and R.W. Gross, Alternations in Individual Molecular Species of Human Platelet Phospholipids During Thrombin Stimulation: Electrospray Ionization Mass Spectrometry-Facilitated Identification of the Boundary Conditions for the Magnitude and Selectivity of Thrombin-Induced Platelet Phospholipid Hydrolysis, *Biochemistry* 35: 5822–5832 (1996).
55. Unger, R.H., Lipotoxic Diseases, *Ann. Rev. Med.* 53: 319–336 (2002).
56. Mahley, R.W., Apolipoprotein E: Cholesterol Transport Protein with Expanding Role in Cell Biology, *Science* 240: 622–630 (1988).
57. Plump, A.S. and J.L. Breslow, Apolipoprotein E and the Apolipoprotein E-Deficient Mouse, *Annu. Rev. Nutr.* 15: 495–518 (1995).
58. Blish, E.G. and W.J. Dyer, A Rapid Method of Total Lipid Extraction and Purification, *Can. J. Biochem. Physiol.* 37: 911–917 (1959).

Chapter 13

Dual Parallel Liquid Chromatography/Mass Spectrometry for Lipid Analysis

William Craig Byrdwell

Florida Atlantic University, Department of Chemistry and Biochemistry, 777 Glades Road,
P.O. Box 3091, Boca Raton, FL 33431

Introduction

HPLC/APCI-MS for Triacylglycerol and Phospholipid Analysis

High performance liquid chromatography (HPLC) with detection by both atmospheric pressure chemical ionization (APCI) mass spectrometry (MS) and electrospray ionization (ESI) MS has been applied to both triacylglycerols (TAG) and phospholipids (PL). HPLC/APCI-MS for analysis of a mixture of TAG was first demonstrated by Byrdwell and Emken (1) in 1995. In this report, the authors showed several key features of APCI-MS spectra of TAG. First, the primary fragments that were produced were the diacylglycerol (DAG) fragment ions formed by loss of one fatty acyl chain. Second, the ratio of the protonated parent molecule to the DAG fragment ion depended on the number of sites of unsaturation in the TAG molecules. Later that year, Neff and Byrdwell (2) reported the HPLC/APCI-MS of soybean oil. Tabulated results showed that TAG having more than four sites of unsaturation had the protonated molecule as the base peak, and TAG with two or fewer sites of unsaturation had a DAG fragment ion as the base peak. TAG with either three or four sites of unsaturation could have either the protonated molecule or a DAG fragment ion as the base peak, depending on how the unsaturation was distributed. Byrdwell *et al.* (3–5) later reported how these fragmentation characteristics affected the quantitative analysis of TAG and demonstrated how response factors could be calculated. The tendency of TAG to yield simple mass spectra with structurally diagnostic fragment ions led APCI-MS to be recognized for its utility in TAG analysis. The number of publications describing HPLC/APCI-MS for TAG analysis is growing rapidly. Many of these applications have been described elsewhere in our reviews on APCI-MS for lipid analysis (6,7). The reports cited in this volume demonstrate that HPLC/APCI-MS is a valuable tool for TAG analysis.

APCI-MS has also been shown to be very effective for phospholipid analysis. Karlsson *et al.* (8) appear to have applied LC/APCI-MS to phospholipids for the first time in 1996. However, because of a lack of a protonated molecule in positive-ion mode, and no deprotonated molecule in negative-ion mode, ESI-MS was chosen for the remainder of their analyses. Soon thereafter, Byrdwell and Borchman (9) successfully applied HPLC with APCI-MS for analysis and quantification of eye lens

phospholipids. Under the conditions used by these authors, APCI-MS mass spectra of PL exhibited mostly backbone fragments, after loss of the phosphate-containing head group; but they did show small abundances of protonated molecules. In this same article, Byrdwell and Borchman (9) used ESI-MS for analysis of the same lens phospholipid mixture. The ESI-MS mass spectra showed almost exclusively protonated molecules, in positive-ion mode. Thus, this article (9) showed that these two different ionization techniques each produced valuable and complementary data. APCI-MS for analysis of phospholipids was discussed more thoroughly in our previous review articles (6,7).

HPLC/ESI-MS for Triacylglycerol Analysis

ESI-MS was applied to unseparated TAG in 1991 by Duffin *et al.* (10), by infusion of the mixture directly into the ESI-MS mass spectrometer. Sodiated ions were formed by addition of sodium acetate, and ammonium adduct ions were formed by addition of ammonium acetate. The signal obtained by these non-polar lipids was observed to be proportional to the degree of polarity of the molecules. Thus, monoacylglycerols gave more response than diacylglycerols, which gave more response than triacylglycerols. TAG containing unsaturated fatty acyl chains produced more signal than saturated TAG. These authors reported low abundances of fragment ions during MS/MS of sodiated TAG, $[M+Na]^+$, but good abundances of fragment ions and good quality MS/MS spectra from ammonium adduct ions, $[M+NH_4]^+$. In this work, the location of sites of unsaturation could not be determined from the mass spectra, due to bond migration during fragmentation.

Several years later, Schuyf *et al.* (11) demonstrated the first online LC/ESI-MS of TAG by performing argentation (silver-ion) liquid chromatography/ESI-MS of TAG. More recently, the first example of non-aqueous reversed-phase (NARP) high performance liquid chromatography with detection by ESI-MS was applied to TAG by Hvattum (12). Other applications of ESI-MS to TAG analysis are as follows: Sandra *et al.* (13) reported the use of ESI-MS of a fraction collected from capillary electrochromatography (CEC) for TAG analysis. Later, fractions from CEC following supercritical fluid chromatography (SFC) of sardine oil were analyzed by using ESI-MS (14). Cheng *et al.* (15) used ESI-MS/MS (with sample introduced by infusion, without chromatography) to distinguish the positions of double bonds on the fatty acyl chains from their fragmentation patterns. ESI-MS also allowed them to distinguish the positions of the acyl chains on the glycerol backbone. Hsu and Turk (16) used infusion of standards to analyze TAG as their lithiated adducts by ESI-MS. Fragments in the MS/MS spectra of the lithiated adducts allowed determination of the *sn*-2 fatty acid (FA) substituent. Sjovald *et al.* applied ESI-MS to TAG oxidation products (17) and dinitrophenylhydrazones of TAG oxidation products (18,19). Dorschel (20) used ESI-MS for identification of TAG in peanut oil. Sandra *et al.* (21) employed SFC/ESI-MS in which silver ions were coordinated to TAG species. In 2003, several articles appeared: Marzilli *et al.*

(22) employed ESI-MS, MS/MS, and MS³ on an ion trap mass spectrometer for analysis of TAG standards; Fard *et al.* (23) demonstrated Fourier transform ion cyclotron resonance (FI-ICR) mass spectrometry, first without prior LC separation, and then of fractions collected from an HPLC separation; and Han and Gross (24) demonstrated their technique for analysis of lipid mixtures by using positive and negative ESI-MS without prior chromatographic separation; Yli-Jokipii *et al.* (25) used HPLC/ESI-MS for analysis of chylomicron and very low density lipoprotein (VLDL) TAG to investigate the magnitude of postprandial lipemia. The previously mentioned articles demonstrated that ESI-MS was very effective at producing ions from large neutral triacylglycerols. Our applications of ESI-MS to TAG analysis have been done by using a dual parallel mass spectrometer arrangement and are discussed herein.

HPLC/ESI-MS for Phospholipid Analysis

Phospholipids are either already ionic (usually zwitterionic), or are easily charged, and so are particularly amenable to analysis by ESI-MS. For this reason, ESI-MS has been extensively applied to phospholipids in the past. A recent review article by Pulfer and Murphy (26) listed 107 references, most of which were articles describing ESI-MS for phospholipid analysis. An "ISI Web of Science" (part of the ISI Web of Knowledge) search produced more than 270 articles on ESI-MS for phospholipid analysis. Even this list of publications is not complete. It is beyond the scope of this chapter to discuss all of these articles. Only a few representative early articles will be mentioned here. Apologies are extended in advance to the many authors who are not specifically cited. The reader is encouraged to consult the recent review (26) which cites a substantial percentage of the total number of articles published.

Choline-containing phospholipids [phosphatidylcholine (PC), sphingomyelin (SPM), and dihydrosphingomyelin (DHS)] contain a charged quaternary amine in the choline moiety and are particularly amenable to positive-ion ESI-MS. Other classes of PL give excellent signal under negative-ion (NI) ESI-MS conditions. Phospholipids that have been analyzed quite successfully by NI ESI-MS include phosphatidylethanolamine (PE), phosphatidylserine (PS), phosphatidylglycerol (PG), phosphatidic acid (PA), and phosphatidylinositol (PI). As already mentioned, a prodigious number of articles have now appeared that have applied ESI-MS to PL. A few typical early examples (before 1999) of LC/MS applied to PL analyzed in NI mode are listed here. Fang and Barcelona (27) reported the use of HPLC with positive- and negative-ion ESI-MS for determination of the composition of bacterial PL. Gunnarsson *et al.* (28) described the use of LC/NI-ESI-MS for analysis of phosphatidylethanol (not PE) species in human blood samples. Hvattum *et al.* (29) showed detection of PS in human blood by LC/NI-ESI-MS. Lee *et al.* (30) described HPLC followed by positive- and negative-ion ESI-MS of PC, PE, PS, and PI. Many more examples of HPLC/ESI-MS for PL analysis are found after

1998, but the preceding examples serve as a starting point for investigation. Many examples of PL analysis performed by direct infusion of unseparated samples are also seen. Examples of NI-ESI-MS analysis of the major anionic PL classes by infusion are found in the following references: PE (31,32), PS (33), PG (34), PA (35), and PI (36), and combinations of these (22,24,27,37–42). All of these classes produced abundant $[M-H]^-$ deprotonated molecules either by loss of the proton attached to the phosphate moiety, or from the anionic head group (i.e., PS). A common element that emerges from the plethora of articles is that NI-ESI-MS/MS with collision-induced dissociation (CID) produces abundant carboxylate ions that provide information to allow the fatty acyl chains to be identified, as well as, in some cases, their regiospecific positions. These articles, while far from an exhaustive list, provide examples that demonstrate the quality and utility of NI-ESI-MS and MS/MS mass spectra.

Parallel Mass Spectrometry Techniques

The previous discussion has emphasized the important point that both APCI-MS and ESI-MS give excellent, though complementary, data for both PL and TAG. APCI-MS gives mostly carbon backbone-related ions (sphingolipids) or DAG fragment ions (TAG and most PL), whereas ESI-MS gives mostly protonated or adduct ions. In many cases, the set of fragments seen in MS/MS mass spectra obtained by ESI-MS/MS appears very similar to the set of fragments produced in the APCI source, and seen in APCI-MS full-scan (not MS/MS) mass spectra. Again, ESI-MS/MS data are often very similar to APCI-MS data. This is not always the case, however. Phosphocholine-containing PL, such as PC and SPM, usually produce only a fragment ion at m/z 184 under normal ESI-MS conditions, instead of structurally indicative DAG or ceramide backbone fragment ions. APCI-MS, on the other hand, produces abundant fragment ions that specify the nature of the backbone, whether DAG or ceramide. Furthermore, quantitative analysis using ESI-MS can be problematic for those species that undergo extensive dimer formation in the ESI source (such as PC). Thus, one type of ionization alone may not be entirely adequate for complete structural elucidation of all TAG and PL molecular species.

Because of their complementary natures, it is desirable to obtain both ESI-MS and APCI-MS data for molecules of interest, to be able to fully characterize them. Toward this end, we obtained both APCI-MS and ESI-MS data from PL in the human eye lens (9), by performing sequential runs and changing the ionization probe head between runs. After that report, we set out to accomplish the goal of obtaining both these types of MS data simultaneously from one single LC separation. In 1998, Byrdwell (43) published the first report of the use of two mass spectrometers, using two different atmospheric pressure ionization (API) techniques, for simultaneous detection of the eluate from one HPLC system. Two mass spectrometers employed APCI-MS and ESI-MS (and MS/MS), in parallel, and employed two other auxiliary detectors [an ultraviolet-visible (UV-vis) detector

and an evaporative light scattering detector (ELSD)]. This report demonstrated the “proof of concept” and showed that a prodigious amount of data is obtained from such an approach. This work will be discussed in greater detail herein.

Several years after our initial report of “dual parallel mass spectrometers” for PL analysis, we published a second report demonstrating dual parallel mass spectrometers for analysis of TAG and TAG oxidation products (44). In this series of experiments, we used a tandem mass spectrometer to obtain APCI-MS and MS/MS mass spectra, and we used an ion trap mass spectrometer to obtain ESI-MS, MS/MS, and MS³ data. The differences in response of both TAG and TAG oxidation products (TAGOX) to APCI-MS versus ESI-MS was dramatic. The benefits of acquiring both types of data simultaneously were substantial, especially for the TAGOX. These data will be discussed in detail. Shortly after our second report of dual parallel mass spectrometers, another group, working at the Merck Research Laboratories, published an example of dual parallel mass spectrometers for analysis of drug metabolites (45). These authors also used an ion trap mass spectrometer and a tandem mass spectrometer. The authors employed the same type of ionization (negative-ion ESI) on both mass spectrometers, so complementary ionization modes were not used. Instead, the authors employed the dual parallel mass spectrometer arrangement to take advantage of the different scan capabilities of the two different mass filters. ESI-MS, MS/MS, and MS³ were performed on the ion trap mass spectrometer, while neutral loss scanning and multiple reaction monitoring (MRM) experiments were performed on the tandem mass spectrometer. The complementary data obtained from the two different mass filters provided additional insight into the mechanism of metabolite formation.

Most recently, Byrdwell (46) employed two mass spectrometers in another novel way. The first two reports of dual parallel mass spectrometers employed two mass spectrometers that were connected in parallel to one HPLC system. We refer to this arrangement as an LC1/MS2 experiment. We recently reported (46) a dual parallel mass spectrometer approach in which two complementary LC systems were used, a normal-phase (NP) system and a reversed-phase (RP) system, to which were connected two mass spectrometers. One single injection was loaded onto the NP-HPLC system, and then the sample was split to divert the non-polar lipids over to the RP-HPLC system. This experiment is referred to as an LC2/MS2 arrangement. The details of the experiments mentioned, as well as other approaches for obtaining data from multiple ionization modes, will be discussed in this chapter.

Experimental

A dual parallel mass spectrometer arrangement requires no special or custom-fabricated equipment. For an LC1/MS2 experiment, the eluate from an HPLC system is simply split *via* tees placed at the end of the chromatography columns. The primary consideration is using the proper combination of tubing leading from the tees to

produce the desired flow rates from the tubing going to the mass spectrometers, compared to the flow rate to the auxiliary detector(s). We use two tees in series, with a piece of 0.005-in inside diameter (i.d.) stainless steel tubing joining them together and joining them to the outlet of the column. From the side outlet of the first tee, we attach a piece of 0.005-in i.d. polyetheretherketone (PEEK) tubing to go to the UV-Vis detector (optional) and/or the evaporative light scattering detector. A stainless steel nut and ferrule are used on this PEEK tubing, and may be tightened down to the degree necessary to produce the desired flow rate out of the tubing going to the auxiliary detector. The flow rate out the auxiliary side of the detector is typically $\sim 400 \mu\text{L}/\text{min}$. If a UV detector is used, it is nondestructive, so the analyte passes through without loss of sample. Since the ELSD is a heated and therefore destructive detector, it must be the terminal auxiliary detector. To the remaining two outlets on the second tee are connected two equal lengths (3 ft) of 0.1 mm (= 0.0039 in) i.d. deactivated fused silica capillary tubing, *via* an adapting ferrule on each. Then, the distal ends of each of these sample transfer lines are terminated by a stainless steel union (*via* an adapting ferrule), with a 5-cm-long piece of 0.005-in i.d. stainless steel tubing on the exit side of the union, which is used to connect to the mass spectrometer ionization source. The flow rate out of each of these lines is ~ 140 to $200 \mu\text{L}/\text{min}$, depending on the total system flow rate, which ranges from 0.7 to 1.0 mL/min.

Materials

The mixture of PL standards in methanol was composed of 25.3% chicken egg yolk phosphatidylethanolamine (PE), 69.4% bovine brain sphingomyelin (SPM), and 5.3% bovine brain PC, purchased from Avanti Polar Lipids (Alabaster, AL). Bovine brain whole lipid extract was also purchased from Avanti Polar Lipids. The whole extract, approximately 25 mg/ml in chloroform (CHCl_3) as received, was transferred to a tared amber vial and taken to dryness under argon. The sample was then reconstituted to a known concentration of 25.0 mg/ml in CHCl_3 . All solvents, except water, were purchased from either Aldrich Chemical Co. (St. Louis, MO) or Fisher Scientific (Fair Lawn, NJ). HPLC grade solvents were purchased and were used without further purification. Water was obtained from a Millipore (Waters, Inc., Milford, MA) Milli-Q Academic deionized water filtration system and was used without further purification.

Commercially available canola oil was purchased from a local market. The preparation of the 35-TAG mixture by the *p*-toluenesulfonic acid-catalyzed esterification of glycerol with an equimolar mixture of FA was performed by Richard Adlof and was previously discussed (3). Synthetic triolein (99+% purity) was purchased from NuChek Prep (Elysian, MN). Heated oxidation was performed by William Neff, as previously described (47). In brief, 5 g of the TAG was placed in a 12.5×2.0 -cm test tube and heated to 190°C by submersion in a temperature controlled silicone oil bath. The samples used for this report were oxidized for 6 h.

LC1/MS2 Liquid Chromatography Instrumentation

For TAG analysis using the LC1/MS2 approach, we employed an acetonitrile/dichloromethane solvent system. The HPLC pump used was a Constametric 4100MS (Thermo Separation Products, San Jose, CA). We employed a SpectraSystem membrane degasser and SpectraSystem AS3000 autosampler (both Thermo Separation Products). Two Inertsil[®] columns (25 cm × 4.6 mm, 5 μm particle size, MetaChem Technologies), either ODS-2 or ODS-3, in series were used. We have now replaced the ODS-3 columns with ODS-2 columns. The ODS-2 columns produce a better separation. The typical solvent gradient used for the TAG analysis is as follows: 30% dichloromethane (DCM)/ 70% acetonitrile (ACN) held until 20 min; linear gradient to 40% DCM/60% ACN at 40 min, held until 50 min; linear gradient to 60% DCM/40% ACN at 70 min, held until 75 min; linear to 70% DCM/30% ACN at 80 min, held until 85 min; recycle to initial conditions, 99 min. The flow rate was 0.70 ml/min. One cautionary note: insufficient recycle time between runs resulted in broadened peaks from the early-eluting TAG (polyunsaturated FA-containing TAG). Typically, a 10-μL sample of a ~10 mg/mL solution was injected. As an example, a 100-μg injection of a completely randomized TAG mixture containing 5 FA would have 35 TAG molecular species, present at levels of approximately 0.8, 2.4, or 4.8 μg (for mono-acid TAG, di-acid TAG, and TAG having three different FA, respectively), which equals 0.91 to 5.45 nmol, assuming a typical molecular weight (M.W.) of 880.

A different gradient program was used for TAG oxidation products (TAGOX). TAGOX require a lower-than-normal amount of DCM compared to unoxidized TAG initially, to keep the relatively more polar oxidized TAG monomers sufficiently retained on the non-polar stationary phase. At the end of the gradient program, it was necessary to transition to a higher-than-normal percentage of DCM, to elute the highly non-polar TAG oxidation product oligomers. The gradient used for the full range of TAG oxidation products, from monomers to oligomers is as follows: 25% DCM/75% ACN held for 20 min; linear to 30% DCM/70% ACN at 50 min (not held); linear to 70% DCM/30% ACN at 85 min; recycled to initial conditions at 99 min. The flow rate was 0.80 ml/min throughout.

LC2/MS2 Liquid Chromatography Instrumentation

For LC2/MS2 experiments, a normal-phase liquid chromatographic system was attached to the ion trap mass spectrometer, while an RP-LC system was attached to the tandem mass spectrometer. The NP-HPLC system was composed of a P4000 quaternary pump with membrane degasser, an AS3000 autosampler, and a UV 6000 photodiode array detector (Thermo Separation Products). The AS 3000 autosampler was used to make an injection of 20 μl onto the NP columns. The NP-HPLC system employed two amine columns in series, Adsorbosphere NH₂, 25 cm × 4.6 mm, 5 μm (Alltech Associates, Deerfield, IL). The gradient program used three solvents: solvent A, 40% H₂O, 60% isopropyl alcohol (IPA); solvent B, 40%

methanol (MeOH), 60% IPA; solvent C, 40% hexane (Hex), 60% IPA. Each solvent contained 0.1% NH_4OH . The gradient program used was as follows: from 0 min to 10 min, 15% A, 15% B, 70% C; from 10 min to 20 min, a linear change to 25% A, 25% B, 50% C, held until 30 min; from 30 min to 40 min, a linear change to 30% A, 45% B, 25% C; from 40 to 50 min, a linear change to 30% A, 70% B, held until 75 min; recycled to initial conditions from 75 to 85 min. The flow rate was 0.80 ml/min throughout. The outlet from the amine columns was plumbed to the diverter valve on the front of the LCQ Deca mass spectrometer described here. After the diverter valve, the flow went through the UV 6000 photodiode array detector (PDA). The flow was then split *via* a tee, with the straight-through exit connected to the ESI source on the LCQ Deca, and the 90° exit directed to waste. Splitting the flow keeps the flow rate into the ESI source at a lower level, and also allows for the future use of a fraction collector to collect PL fractions instead of sending them to waste.

The RP-HPLC system used a Constametric 4100 quaternary pump with membrane degasser (Thermo Separation Products). The RP-HPLC system employed two Inertsil ODS-3 columns in series, 25 cm \times 4.6 mm, 5 μm (MetaChem Technologies). A very different solvent program was used for the first LC2/MS2 experiment, compared to the DCM/ACN solvent system that we normally use for RP-HPLC. This was done to ensure that the solvent system on the NP-HPLC system would be fully compatible with the solvent system on the RP-HPLC system. A binary gradient was developed that used: solvent A, MeOH; solvent B, 40% Hex, 60% IPA. Both solvents contained 1 mM ammonium formate made by replacement of 1% of the pure solvent with 100 mM ammonium formate in H_2O . This was added to provide electrolyte for use in ESI mode and to promote adduct formation (this was used instead of a sheath liquid on the TSQ). The gradient program was as follows: from 0 to 15 min, 90% A, 10% B; from 15 to 30 min, a linear change to 35% A, 65% B; from 30 to 70 min, a linear change to 30% A, 70% B; from 70 to 80 min, a linear change to 10% A, 90% B; recycled to initial conditions from 80 to 90 min. The flow rate was 0.8 ml/min throughout. The effluent from the columns on LC2 was split *via* a tee, with the 90° exit of the tee delivered to an evaporative light scattering detector (ELSD), and the straight-through exit of the tee delivered to the ionization source of the tandem mass spectrometer. The ELSD data were acquired by both the tandem mass spectrometer (having low digital resolution for the auxiliary detector) and a stand-alone 24-bit data acquisition system (EZ-Chrom Elite). However, the levels of neutral lipids were below the detection limit on the ELSD under these conditions, so ELSD chromatograms are not discussed here.

The interconnections between the two liquid chromatographic systems, the two auxiliary detectors (PDA and ELSD), and the two mass spectrometers (the ion trap mass spectrometer and the tandem mass spectrometer) are shown in Figure 13.1. The outlet of the NP-HPLC columns (LC1) was connected to port 2 of the diverter valve on the LCQ Deca. Port 3 went to a tee that split flow between the PDA and the ESI source on the LCQ Deca.

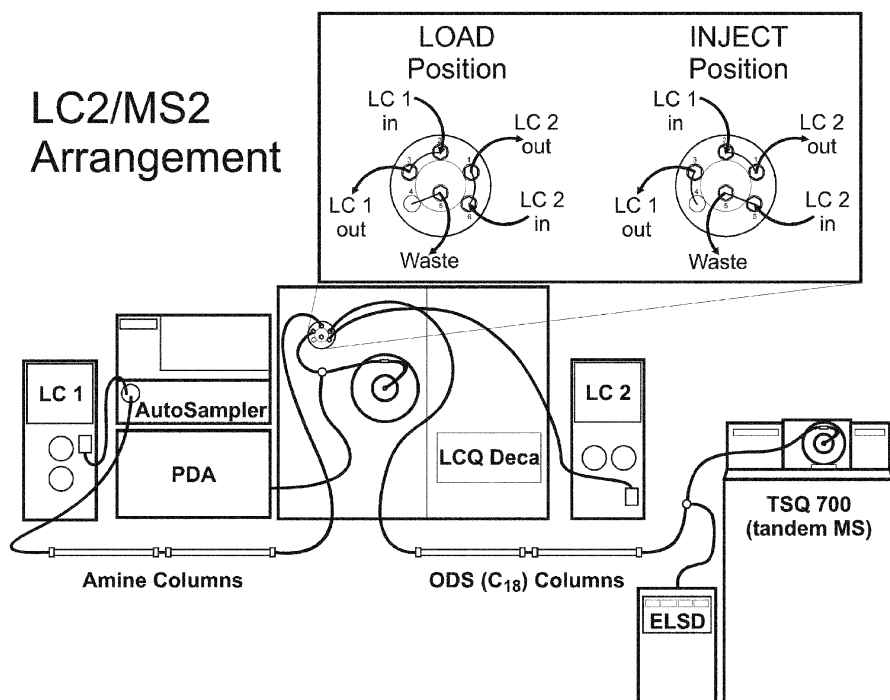


Fig. 13.1. Arrangement of instruments for dual liquid chromatography/dual mass spectrometry (LC2/MS2) experiments.

In the load position, LC1 simply flowed through the diverter valve, from port 2 to 3, and to the UV 6000 PDA and the ESI source on the LCQ. The pump of the RP-HPLC system (LC2) was attached to port 6 of the diverter valve. The line to the RP columns was attached to port 1. The RP-HPLC system was located in proximity to the diverter valve to minimize dead volume (distances in Fig. 13.1 are exaggerated for clarity). In the load position, LC2 simply flowed through the diverter valve, from port 6 to 1, and to the RP columns. In the inject position, flow from port 2 (LC1 in) was directed to port 1 (LC2 out to columns), while LC2 in was directed to waste (port 5). This arrangement allowed the neutral lipid bolus eluted from the columns on LC1 to be directed onto the columns attached to LC2, while the flow from LC2 was directed to waste. The diverter valve was open from 6.00 to 8.25 min for the bovine brain extract, and from 5.75 to 7.75 min for the sand bream total lipid extract.

LC1/MS2 Mass Spectrometry Instrumentation

A Finnigan MAT TSQ700 (ThermoQuest, Inc., San Jose, CA) was used for acquisition of APCI-MS data. The TSQ700 gave optimal signal in Q3 low mass (m/z

0–2000) mode. In full-scan mode, Q1 was set to pass ions only. The vaporizer heater was operated at 400°C, with the heated capillary set to 265°C. The corona current was set to 6.0 μ A. Sheath and auxiliary gases were set to 35 psi and 5 ml/min, respectively. The sheath gas was bubbled through methanol (~400 ml) in a 1-L bottle prior to entry into the ionization source, to minimize undesirable adduct formation in the APCI source. Spectra of normal TAG were obtained from 150 Thomson (Th) to 1200 Th with a scan time of 1.0 second. Spectra of TAGOX were obtained from 150 Th to 1200 Th with a scan time of 1.0 s up to 50 min, and thereafter the scan range was from 150 Th to 1950 Th with a scan time of 2.0 s, which was automatically changed by using a time-dependent instrument command language (ICL) procedure. Additional procedures were written for the TAGOX to allow the change in scan range at 50 min. The parameters were optimized for TAG analysis. The parent quadrupole offset was -5.0 V, the collision offset was -5.0 V in full-scan mode and -25.0 V in MS/MS mode, the daughter quadrupole offset was -5.0 V, the MS/MS correction factor was 5% throughout. Argon was used as the collision-induced dissociation (CID) gas. Four scans were obtained in full-scan mode, then the CID gas was turned on (2 mTorr) and four scans of each of MS/MS of the two most abundant parent ions were collected.

An LCQ Deca (ThermoQuest) ion trap mass spectrometer was used for acquisition of ESI-MS data. Scans were obtained from 50 to 1200 Th, in centroided positive-ion mode for normal TAG. For TAGOX, scans were obtained from 50 to 1200 Th up to 50 min, and from 50 to 2000 Th thereafter. The ion trap was set to automatically select the most abundant parent ion and perform MS/MS, and then to select the most abundant daughter ion and perform MS/MS/MS. The activation energy was 58% (arbitrary units) with a *q* factor of 0.25. The activation time was 900 ms.

LC2/MS2 Mass Spectrometry Instrumentation

LC1 was attached to an LCQ Deca ion trap mass spectrometer (Thermo Finnigan, now ThermoElectron, San Jose, CA). Scans were obtained in positive- and negative-ion modes from *m/z* 50 to 2000. The run was broken into three scan segments, with three different scan programs. In the first segment, from 0 to 25 min, the scan program was as follows: a positive MS scan, a positive MS/MS scan, a negative MS scan, and a negative MS/MS scan. In the second segment, from 25 to 55 min, the scan program was as follows: a negative MS scan, a positive MS scan, a positive MS/MS scan, and a positive MS³ scan. The third segment, after 55 min, was the same as the first segment, having a positive MS scan, a positive MS/MS scan, a negative MS scan, and a negative MS/MS scan. These segments were selected because in the first part of the run, PL that gave good positive- and negative-ion spectra eluted, so positive and negative MS/MS scans were sought. In the second segment, PL containing a quaternary amine (phosphatidylcholine, PC, sphingomyelin, SPM, and dihydrosphingomyelin, DHS) eluted. These provided excellent positive-ion spectra, but poorer negative-ion spectra, so emphasis was on posi-

tive-ion MS, MS/MS, and MS³ scans. After the sphingolipids eluted, the scan program returned to the original scan program. The heated capillary was operated at 250°C. For MS/MS and MS³ scans, the activation energy was 58% (arbitrary units) with a *q* factor of 0.25. The activation time was 900 ms; 20 mM ammonium formate solution in H₂O/ACN (1:4) was added as a sheath liquid *via* syringe pump (AB 140B, Applied Biosystems, Foster City, CA), which improved sensitivity and facilitated the formation of negative ions from the quaternary amine phospholipids, as discussed herein. Sheath liquid flow was delivered at 20 µl/min.

The tandem mass spectrometer attached to LC2 was a Finnigan MAT TSQ700 (Thermo Finnigan, San Jose, CA). The TSQ700 gave optimal signal in Q3 low mass mode. For full scans using Q3, Q1 was operated in RF-only mode. Sheath and auxiliary gases were set to 35 psi and 5 mL/min, respectively. In ESI mode, the spray voltage was 5.5 kV. ESI MS spectra were obtained from *m/z* 200 to 1200, with a scan time of 1.0 second. The heated capillary temperature was 265°C throughout. An ICL procedure was used that allowed automatic switching between MS and MS/MS modes when the signal passed a threshold. The procedure allowed real-time modification of all parameters, including the cutoff threshold, parent ion mass selection range, and others. The parent quadrupole (Q1) offset was -5.0V, the collision cell offset was -5.0V in full-scan mode and -25.0V in MS/MS mode, and the product quadrupole (Q3) offset was -5.0V. Argon was used as the CID gas. Five scans were obtained in full-scan mode, then the CID gas was turned on (~2 mTorr) and four MS/MS scans of each of the two most abundant precursor ions were collected. Data obtained on the TSQ700 were imported into the Xcalibur™ software on the LCQ computer workstation to allow the chromatograms and spectra from the two mass spectrometers to be more easily compared.

Results and Discussion

LC1/MS2 Experiments

Phospholipids. Our initial results on LC/MS of the PL of the human eye lens (9) demonstrated to us the utility of having both ESI-MS and APCI-MS results from the same samples. We therefore set out to accomplish the goal of coupling of two mass spectrometers together to act as separate detectors employing ESI and APCI simultaneously, in parallel. The first dual parallel mass spectrometer experiment (43) was performed by using a single quadrupole mass spectrometer, which employed an APCI source, and a tandem mass spectrometer, which employed an ESI source. It was felt that, since APCI produced gentle fragmentation already, it was better suited to detection by using a single quadrupole instrument. ESI, on the other hand, produced no fragments, so we felt that MS/MS on a tandem instrument was necessary to produce fragments to aid in structural identification.

The full set of chromatograms that resulted from the first dual parallel mass spectrometer experiment (43) is shown in Figure 13.2. The APCI-MS chromatogram

showed a good signal-to-noise ratio (S/N), even though some low mass peaks arising from impurities in the solvent system were present. The ESI-MS chromatogram gave a poorer S/N because of the low-mass impurity peaks. When the ESI-MS data were filtered to show only the near-molecular ion region, from m/z 700 to 850, the ion chromatogram (Fig. 13.2E) more closely resembled the peaks produced by APCI-MS. The mass spectra produced by these different ionization modes, acquired simultaneously, are shown in Figure 13.3 and Figure 13.4, for the APCI-MS and ESI-MS data, respectively. The phosphatidylethanolamine (PE) and PE plasmalogen (PE plas) molecular species produced protonated molecules by both ionization methods, with little fragmentation. All other phospholipids showed dramatic differences between the mass spectra obtained from APCI-MS versus ESI-MS. The APCI-MS mass spectra exhibited mostly $[M\text{-Headgroup}]^+$ fragments for PC and sphingolipids (SL), while ESI-MS mass spectra gave intact protonated and sodiated molecule ions. The ESI-MS instrument was more sensitive, and so produced better spectra from the phosphatidylcholine (PC) species (Fig. 13.4C and 13.4D) than did the APCI-MS instrument (PC not shown). The SL produced excellent mass spectra on both machines.

The complementary natures of APCI-MS and ESI-MS are best exemplified by comparison of the APCI-MS spectra in Figure 13.3C, 13.3D, and 13.3E to the ESI-MS spectra in Figure 13.4E, 13.4F, and 13.4G. The APCI-MS data produced mostly $[M\text{-headgroup}]^+$ fragment ions, while the ESI-MS data exhibited intact protonated molecules and sodiated molecules. Some of the $[M+\text{Na}]^+$ ions produced by ESI were isobaric with some of the $[M+\text{H}]^+$ peaks, and MS/MS of these phosphocholine-containing molecules gave only m/z 184 (representing the phosphocholine head group), which was not useful for distinguishing between isobaric molecules. Instead, the backbone fragments produced in the APCI-MS source were invaluable for distinguishing isobaric molecular species. The combination of the fragment ions by APCI-MS with the intact ions by ESI-MS allowed identification of numerous molecular species.

Triacylglycerols. In 2002, Byrdwell and Neff (44) reported the second example of dual parallel mass spectrometers. In this report, LC1/MS2 experiments were described in which TAG from canola oil and TAG oxidation products (TAGOX) were separated on a RP-HPLC system, followed by parallel MS detection by APCI-MS and MS/MS on a tandem mass spectrometer, and ESI-MS, MS/MS, and MS³ on an ion trap mass spectrometer. APCI-MS has been used extensively for analysis of TAG, as recently reviewed (6,7,48). ESI-MS has also been used extensively for TAG analysis, although it may not be a technique that first comes to mind for analysis of large neutral molecules with low proton affinities. Usually, ionic adducts with TAG are produced (adducts with ammonium or alkali or other metals) and these adducts are analyzed by ESI-MS. Early examples of ESI-MS for lipid analysis were reviewed in detail by Myher and Kuksis (49). More recently, ESI-MS for PL analysis has been reviewed by Pulfer and Murphy (26). ESI-MS

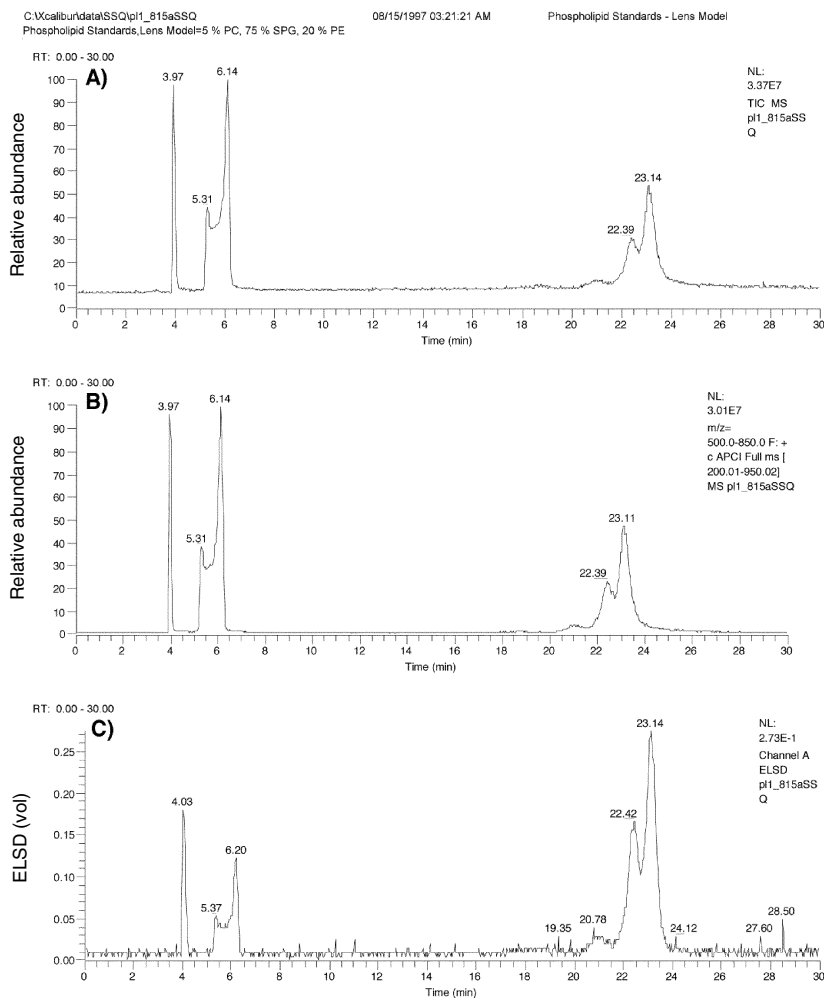


Fig. 13.2 (A–C). Chromatograms of the separation of phospholipid standards obtained from APCI-MS and ESI-MS/MS simultaneously, in parallel. (A) Total ion chromatogram by APCI-MS. (B) Ion chromatogram showing range m/z 500–850. (C) Evaporative light scattering detector (ELSD) chromatogram. (Continued →)

for analysis of oxidized lipids is covered thoroughly in the chapter in this volume by Kuksis, and ESI-MS for lipid analysis has been reviewed in the chapter by Byrdwell (50).

In our dual parallel mass spectrometer work, we employed ESI-MS with ammonium formate added as a sheath liquid, in combination with APCI-MS. Figure 13.5 shows the twin sets of chromatograms obtained by RP-HPLC/(ESI-MS

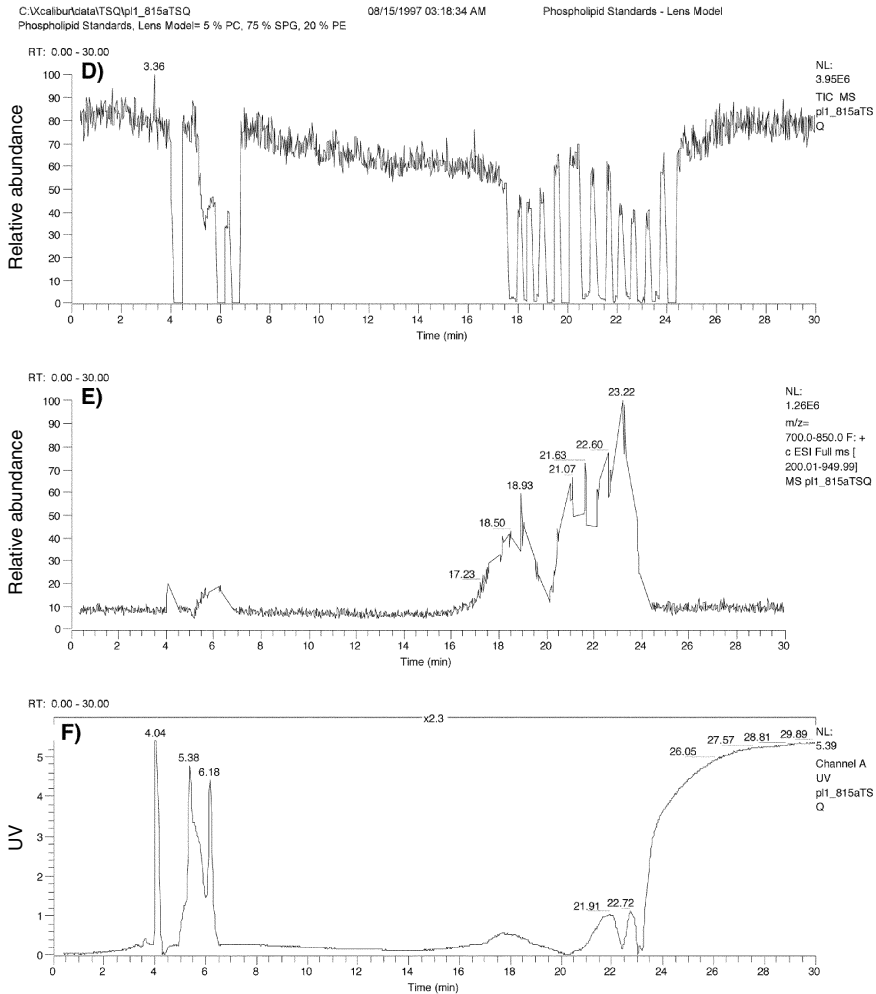


Fig. 13.2 (D–F). (D) Total ion chromatogram by ESI-MS. (E) Ion chromatogram showing only the range m/z 700–850 in full-scan mode. (F) UV chromatogram showing absorbance at 206 nm.

and APCI-MS) of canola oil. In this figure, total ion chromatograms are shown that reflect all MS, MS/MS, and MS³ scans, followed by ion chromatograms filtered to show only full-MS scans (Fig. 13.5B and 13.5E), along with the chromatogram obtained from an ELSD (Fig. 13.5C). It is evident from comparison of Figure 13.5B to 13.5E that TAG gave better response by ESI-MS of their ammonium adducts than they did by APCI-MS. Also, it is apparent from these chromatograms that TAG containing multiple sites of unsaturation, which eluted earlier in the

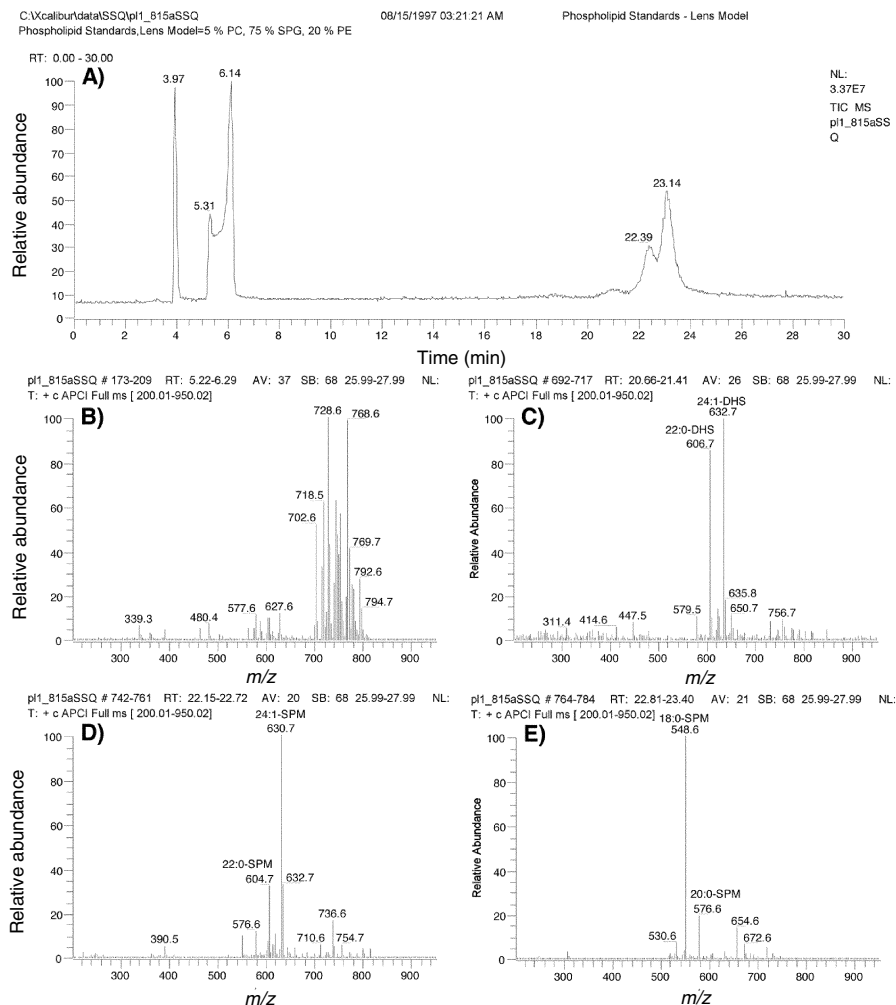


Fig. 13.3. Total ion chromatogram and APCI-MS mass spectra of phospholipid standards. (A) Total ion chromatogram. (B) Average APCI-MS mass spectrum across chromatographic peak of phosphatidylethanolamine (PE) and PE plasmalogen molecular species. (C) Average mass spectrum across first sphingolipid peak, representing long-chain dihydrosphingomyelin (DHS). (D) Average mass spectrum across second sphingolipid peak, representing short-chain DHS and long-chain sphingomyelin (SPM). (E) Average mass spectrum across third sphingolipid peak, representing short-chain SPM.

chromatographic run, gave much better response by ESI-MS than by APCI-MS. Extracted ion chromatograms (EIC) of the m/z values of diacylglycerol fragment ions, $[DAG]^+$, shown in Figure 13.6B through 13.6E, appeared very similar to EIC of TAG that have been reported extensively elsewhere (3–7). The mass spectra dis-

played similar tendencies as have been described in detail before. Specifically, highly unsaturated TAG gave protonated molecules as base peaks, with substantial abundances of $[\text{DAG}]^+$, while TAG with fewer sites of unsaturation gave DAG fragment ions as base peaks. The diacylglycerol fragment ions, $[\text{DAG}]^+$, the monoacylglycerol fragment ions, $[\text{MAG}]^+$, the acylium ions, $[\text{RC}\equiv\text{O}]^+$, and the acylium minus H_2O ions, $[\text{RC}\equiv\text{O}-\text{H}_2\text{O}]^+$ or $[\text{R}'\text{CH}=\text{CH}-\text{CH}=\text{CH}]^+$, that appeared in typical MS and MS/MS spectra of TAG are shown in Scheme 13.1. Other fragments also appeared, such as $[\text{MAG}-\text{H}_2\text{O}]^+$, that are not shown in the scheme. The region from m/z 200 to 500 in the center panel of Figure 13.6 was expanded by a factor of 20 to show that small levels of the $[\text{MAG}]^+$, $[\text{RCO}]^+$, and related ions appeared in full-scan APCI-MS spectra, at low levels. The percentage abundance of the oleoyl $[\text{MAG}]^+$ fragment ion, relative to the $[\text{DAG}]^+$ base peak, is indicated above the m/z 339 fragment in each spectrum.

In this dual parallel mass spectrometer experiment, we obtained APCI-MS/MS data, as well as full-scan data. The APCI-MS/MS spectra are shown in the right panels of Figure 13.6. The abundances of the APCI-MS/MS fragment ions were relatively low compared to the precursor ion base peaks, so magnification factors were applied to the m/z 50–500 region of the MS/MS spectra. The fragments shown in Scheme 13.1, and analogous fragments with different numbers of sites of unsaturation, can be seen in the MS/MS spectra in Figure 13.6.

The EIC and mass spectra that resulted from parallel ESI-MS, MS/MS, and MS^3 are shown in Figure 13.7. These spectra showed distinct differences compared to the APCI mass spectra in Figure 13.6. First, the full-scan ESI-MS spectra exhibited almost exclusively ammonium adduct ions, with small, but useful, abundances of $[\text{DAG}]^+$. In the full-scan spectra, magnification factors of 50 in the range m/z 200–500 showed small, but structurally informative fragments representing $[\text{MAG}]^+$ and $[\text{RCO}]^+$ fragments. The ESI-MS/MS spectra are in the center mass spectrum panel in Figure 13.7, while the MS^3 data are in the right panel. The ESI-MS/MS data appeared very similar to APCI-MS full-scan spectra. The fragmentation that occurred in the ion trap produced the same fragments as did fragmentation in the APCI ionization source, with similar abundances for $[\text{DAG}]^+$ m/z values, but dissimilar abundances for $[\text{M}+\text{H}]^+$ ions. The ESI-MS/MS mass spectra showed abundances of protonated molecule ions proportional to the number of sites of unsaturation in the molecules, similar to the behavior reported for TAG by APCI-MS. The saturates produced no $[\text{M}+\text{H}]^+$ in the ESI-MS/MS spectra, while polyunsaturated TAG produced useful abundances of these ions. The abundances of $[\text{M}+\text{H}]^+$ ions in ESI-MS/MS spectra were less than those in APCI-MS spectra. The ESI-MS/MS spectra also showed small but useful abundances of $[\text{MAG}]^+$, $[\text{RCO}]^+$, and related fragments. A magnification factor of 25 was applied to the m/z 250–400 range to show the $[\text{MAG}]^+$, $[\text{RCO}]^+$, and related fragments.

The ESI- MS^3 mass spectra, shown in the right panel of Figure 13.7, exhibited better fragmentation, with larger abundances of structurally informative fragments than did the APCI-MS/MS fragmentation of the same $[\text{DAG}]^+$ precursor ions.

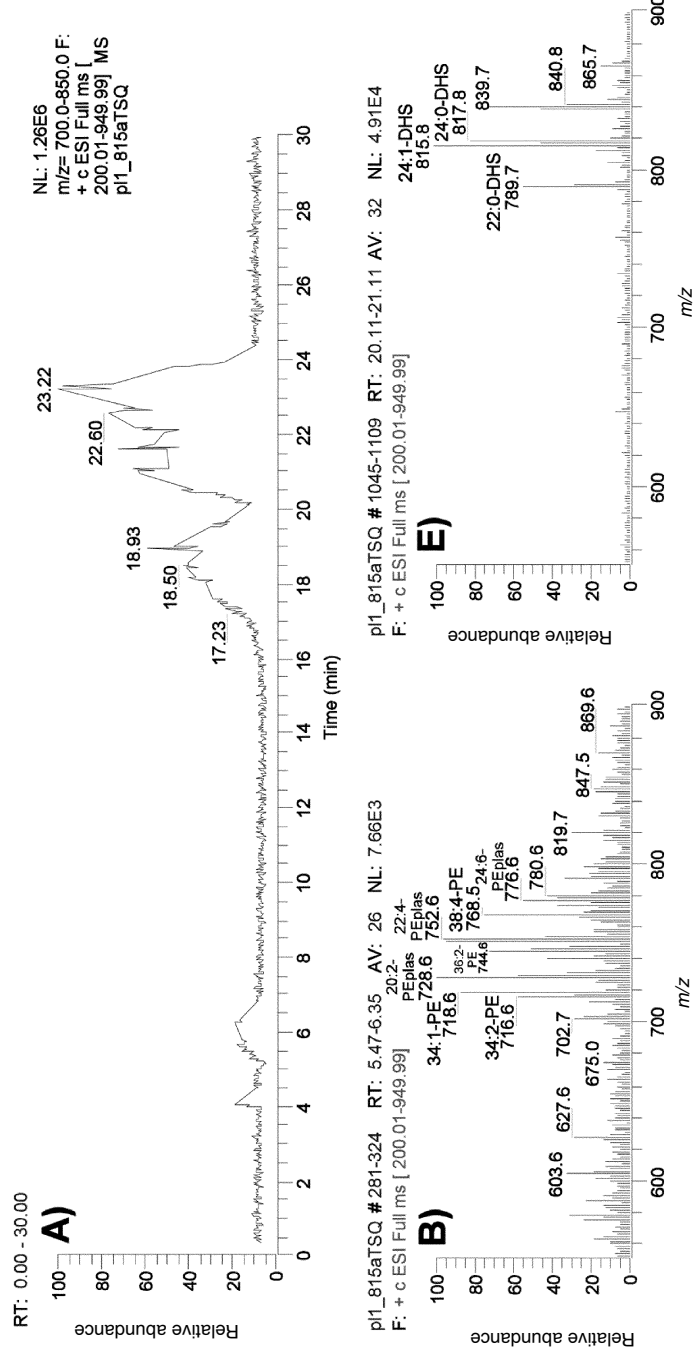


Fig. 13.4. Ion chromatogram and ESI-MS mass spectra of phospholipid standards. (A) Ion chromatogram of m/z 700–850. (B) ESI-MS mass spectrum averaged across PE + PE plasmalogen peak. (C) Average ESI-MS mass spectrum across front of PC + PC plus peak. (D) Average ESI-MS mass spectrum across middle of PC peak. (E) Average mass spectrum across first sphingolipid peak, representing long-chain dihydroshingomyelin (DHS) species. (F) Average mass spectrum across second sphingolipid peak, representing long-chain sphingomyelin (SPM) species overlapped with short-chain DHS species. (G) Average mass spectrum across third sphingolipid peak, representing short-chain SPM species.

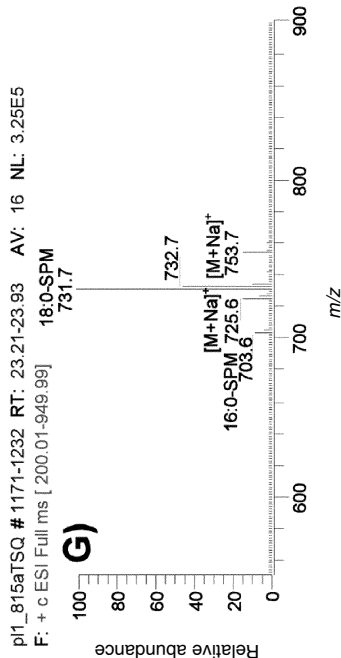
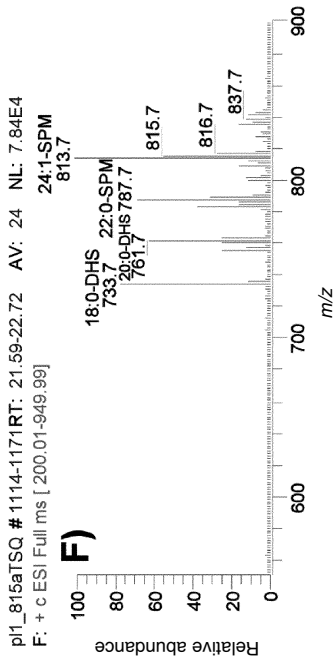
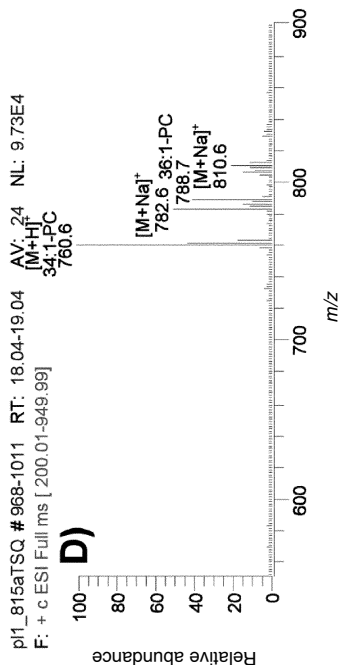
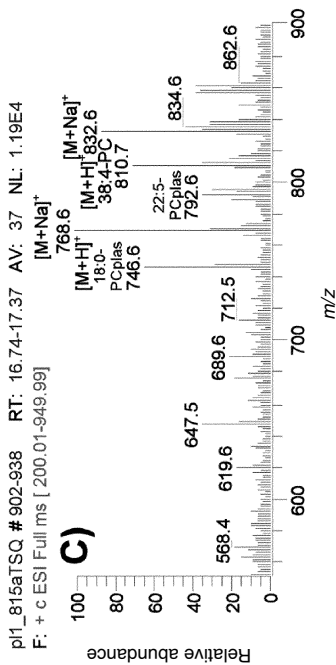


Fig. 13.4. (Continued).

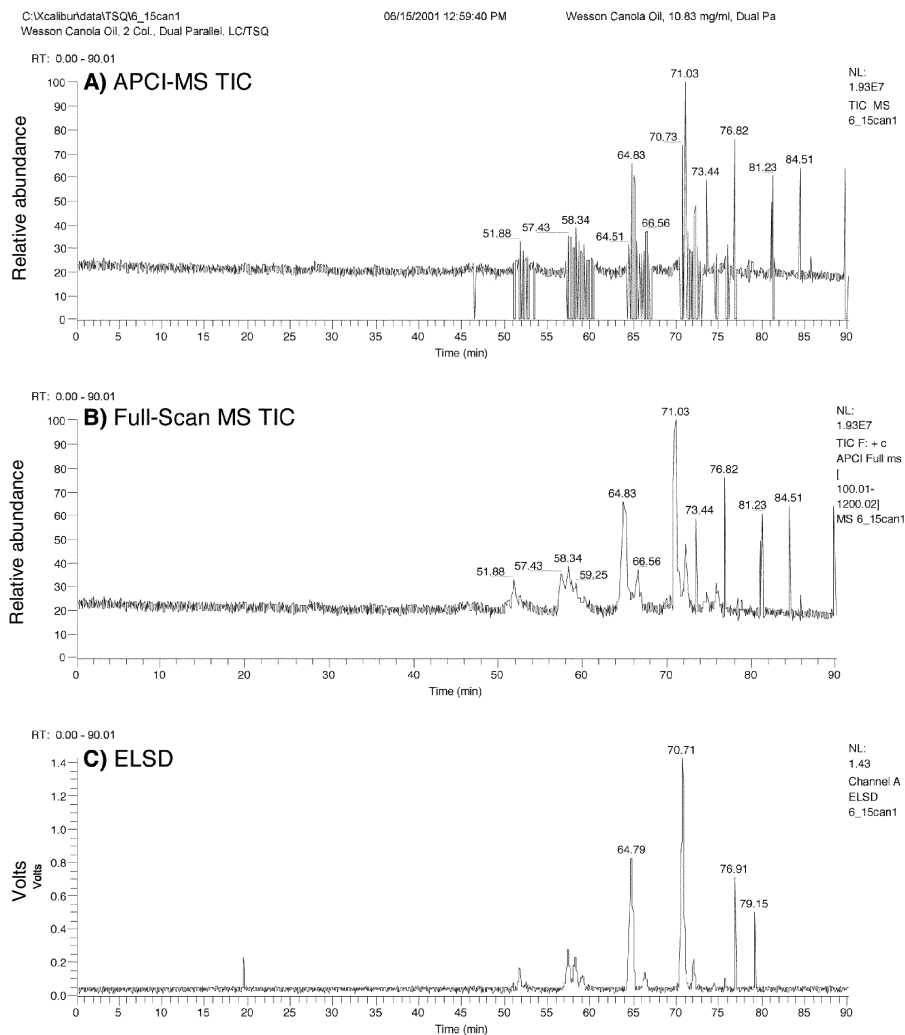


Fig. 13.5 (A–C). Twin sets of LC/MS chromatograms obtained by dual parallel liquid chromatography/mass spectrometry (LC1/MS2) of canola oil, plus an evaporative light scattering detector (ELSD). (A) APCI-MS TIC showing all MS and MS/MS on TSQ700 tandem mass spectrometer; (B) APCI-MS TIC showing scans obtained in full-scan mode; (C) ELSD chromatogram. (Continued →)

showed that the MS^3 fragmentation pattern depended to a great extent on the amount of unsaturation in the $[DAG]^+$ precursor. Linoleic acid-containing DAG fragment ions produced much more extensive charge-remote fragmentation than did the TAG that contained mostly oleic acid. The DAG fragment ions, $[DAG]^+$,

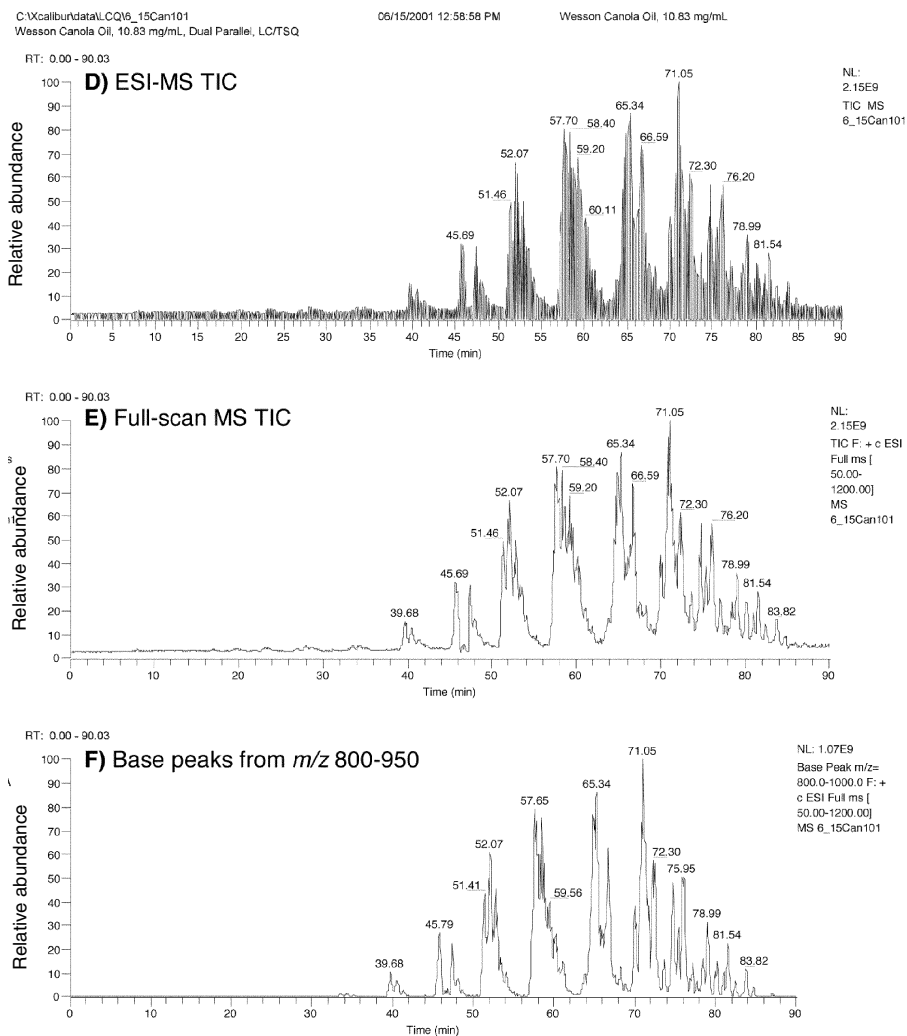


Fig. 13.5 (D-F). (D) ESI-MS TIC showing all MS/MS/MS and MS³ scans on LCQ Deca ion trap mass spectrometer. (E) ESI-MS TIC of full-scan spectra only. (F) Total ion chromatogram of all base peaks in the range m/z 800 to 950 in all spectra. All spectra obtained in (+) ion mode on both machines.

Nevertheless, the CID voltage (25 V) used on the tandem instrument for APCI-MS/MS had been optimized for maximum signal in the m/z 200–350 range.

Comparison of Figures 13.6 and 13.7 shows that ESI-MS³ produced larger abundances of useful fragments than the APCI-MS/MS spectra. Also, the ESI-MS³ mass spectra were more reproducible than APCI-MS/MS spectra. Figure 13.7 also

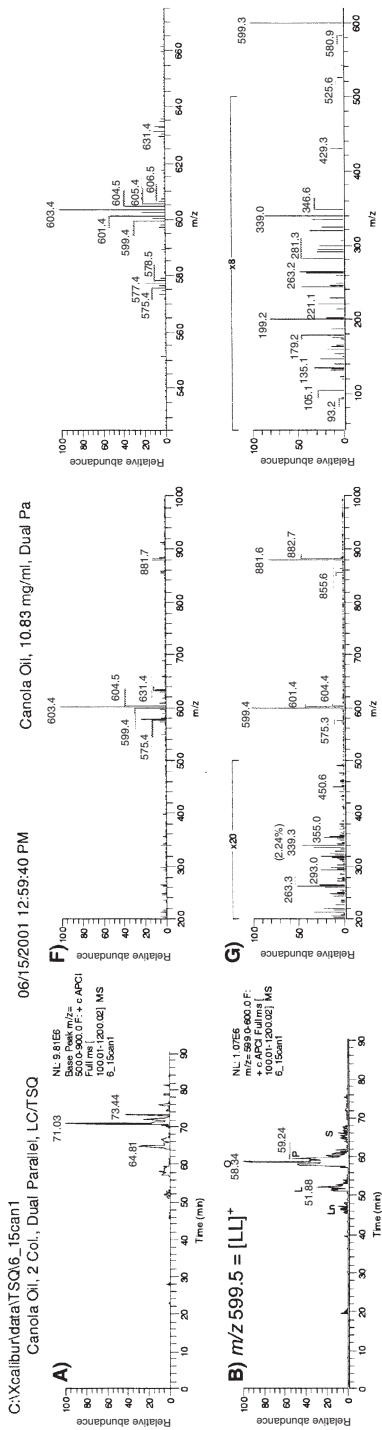


Fig. 13.6 (A–J). APCI-MS ion chromatograms, and MS and MS/MS mass spectra obtained on TSQ700 tandem mass spectrometer, in parallel with the ESI-MS data shown in Figure 13.7. (A) Ion chromatogram of all base peaks between m/z 500–900. (B) Extracted ion chromatogram (EIC) of m/z 599.5 (\pm 0.5). (C) EIC of m/z 601.5. (D) EIC of m/z 603.4. (E) EIC of m/z 605.5. (F) Average mass spectrum from 50 to 82 minutes, and expanded range from m/z 525–675. (G) Full-scan MS and MS/MS mass spectra of OOL. (H) Full-scan MS and MS/MS mass spectra of OOL; (I) Full-scan MS and MS/MS mass spectra of OOS. Precursor ion is underlined.

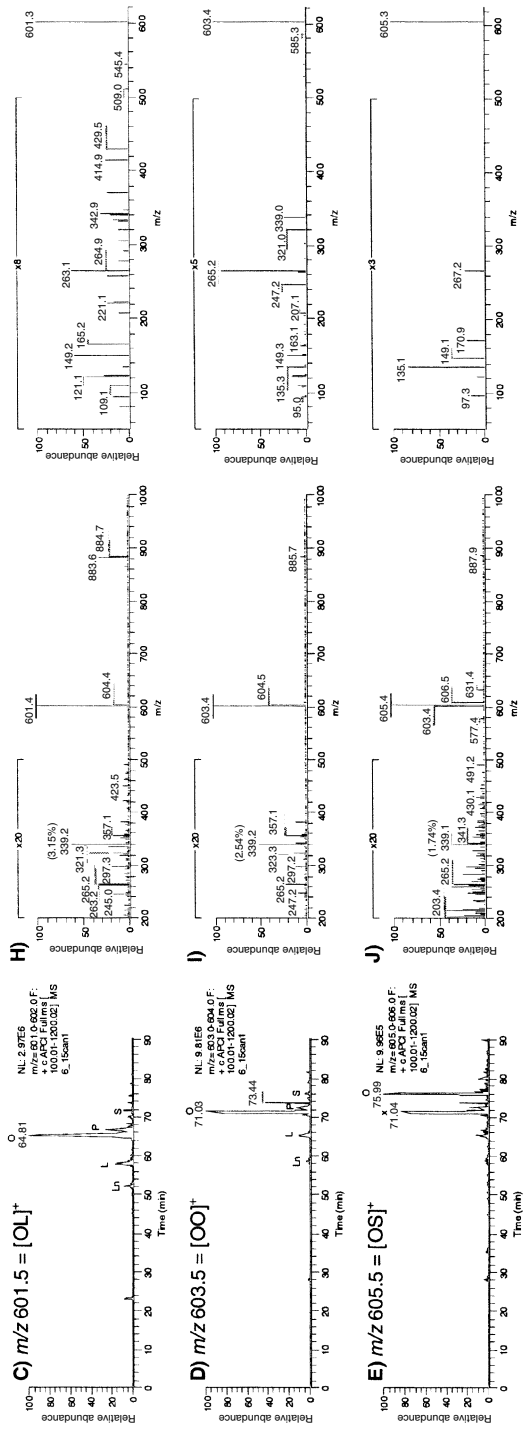


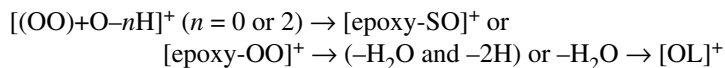
Fig. 13.6. (Continued).

MAG fragment ions, $[\text{MAG}]^+$, acylium ion fragments, $[\text{RC}\equiv\text{O}]^+$, and others that appeared in the ESI-MS² and MS³ spectra are shown in Scheme 13.1.

Triacylglycerol Oxidation Products. In the same report mentioned previously that described the APCI-MS² and ESI-MS³ analysis of TAG was also reported APCI-MS² and ESI-MS³ analysis of TAG oxidation products (44). The twin sets of chromatograms that resulted from the LC1/MS2 analysis of TAGOX are shown in Figure 13.8. In this figure, the dramatic difference in response between the APCI-MS instrument (Fig. 13.8A) and the ESI-MS instrument (Fig. 13.8D) to TAGOX were immediately apparent. By APCI-MS, triolein was the largest peak in the chromatogram, with smaller peaks arising from monomeric (containing one triolein molecule) TAGOX, and virtually no response from the higher molecular weight triolein polymers. ESI-MS, on the other hand, showed sensitive response not only from the early-eluting monomeric TAGOX, but also from late-eluting oligomeric TAGOX. Of all TAGOX, the epoxy-containing monomers were present in the greatest amounts.

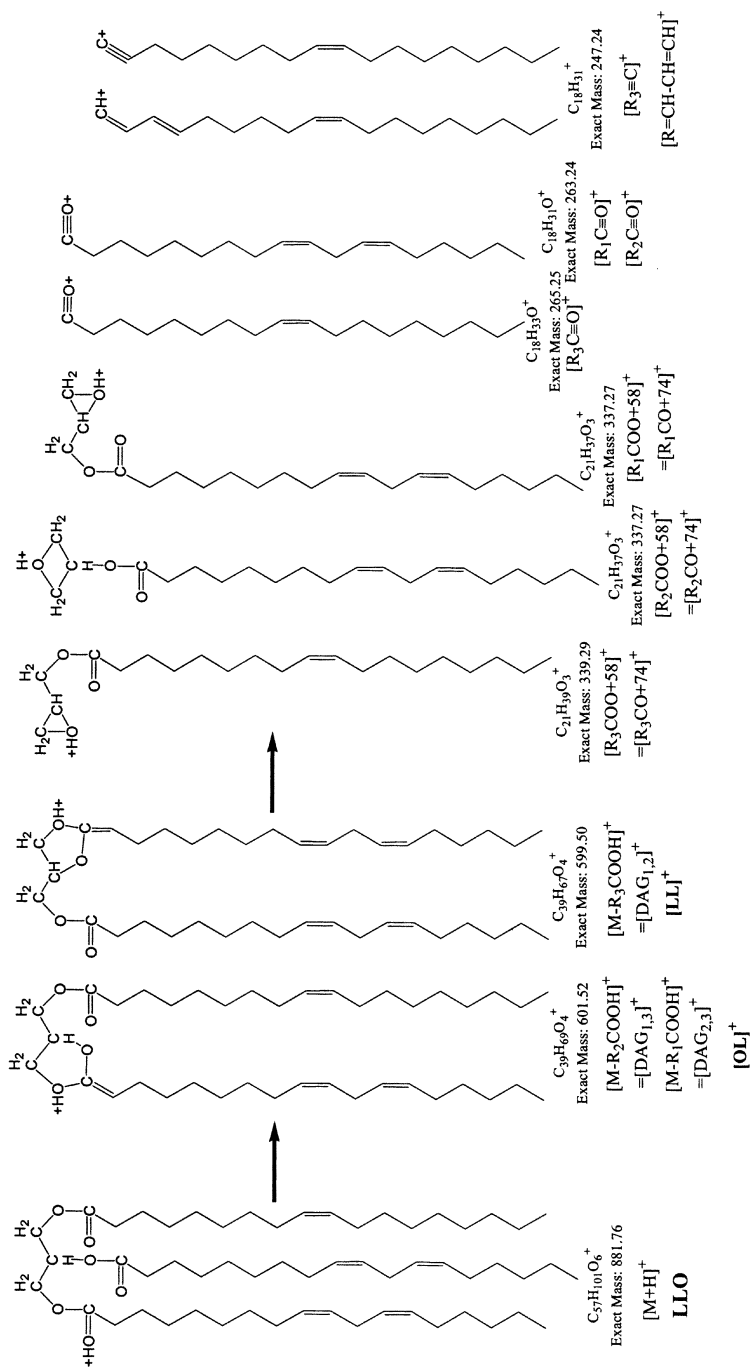
The APCI-MS mass spectra in Figure 13.9 show the characteristics of monomeric TAGOX that we have reported previously (47,51). APCI-MS of triolein monomeric TAGOX exhibited the diolein $[\text{DAG}]^+$ fragment at m/z 603.5 and also fragments from DAG with oxygen functional groups. The most abundant fragments of all triolein TAGOX monomers were DAG fragment ions, with and without additional oxygen functional groups (47,51).

The epoxides formed by oxidation occurred either across (replacing) a double bond or not across a double bond. Of those not across a double bond, they occurred both next to double bonds and not next to double bonds, and these both contributed to the fragment pattern. Epoxide fragments formed by oxidized triolein in the APCI source can be described as $[\text{DAG}+\text{O}-n\text{H}]^+$ ($= [\text{epoxy-DAG}]^+$), where n is either 0 or 2, to give either an oleoyl,epoxy-stearoyl diacylglycerol fragment ion ($[\text{DAG}+\text{O}]^+ = [\text{epoxy-SO}]^+$, m/z 619.5) or an oleoyl,epoxy-oleoyl diacylglycerol fragment ion ($[\text{DAG}+\text{O}-2\text{H}]^+ = [\text{epoxy-OO}]^+$, m/z 617.5), respectively. Another fragment produced by epoxides was the $[\text{DAG}-2\text{H}]^+$ fragment ion, equivalent to $[\text{OL}]^+$. This was produced by decomposition of an epoxide by dehydration in the APCI source, summarized as follows:



The observation that the OS-epoxide gave the $[\text{OL}]^+$ fragment required Byrdwell and Neff (51) to propose the mechanism given in their report on autoxidation. These fragments continue to be observed by APCI-MS, and the proposed mechanism continues to appear to be valid.

Both epidioxides and hydroperoxides were expected to be present in the TAGOX mixture, but these cannot be differentiated by mass. Both epidioxides and hydroperoxides gave $[\text{DAG}+2\text{O}]^+$ fragments at m/z 635.5, coming from $[(((\text{TAG})-\text{H}+\text{OOH})+\text{H})^+]$



Scheme 13.1. Common ions and fragments from triacylglycerols observed under APCI-MS.

C:\Xcalibur\data\LCQ\6_15Can101

06/15/2001 12:58:58 PM

Wesson Canola Oil, 10.83 mg/mL, Dual Parallel, LC/TSQ

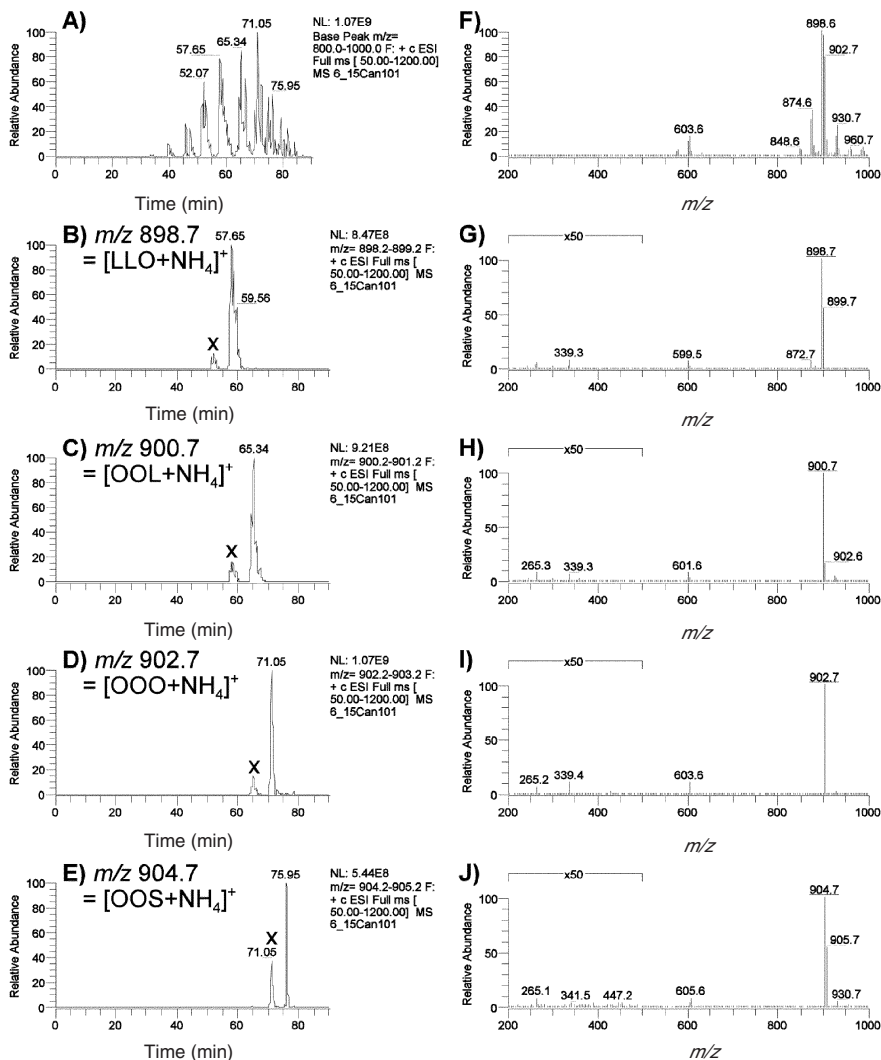


Fig. 13.7 (left). ESI-MS ion chromatograms, and MS, MS/MS, and MS³ mass spectra obtained on an LCQ Deca ion trap mass spectrometer, in parallel with the APCI-MS data shown in Figure 13.6. (A) Ion chromatogram of all base peaks between m/z 800–1000. (B) Extracted ion chromatogram (EIC) of m/z 898.7 (± 0.5). (C) EIC of m/z 900.7. (D) EIC of m/z 902.7. (E) EIC of m/z 904.7. (F) Average mass spectrum from 50 to 82 min, and expanded range from m/z 825–975 and from m/z 525–675. (G) Full-scan MS, MS/MS, and MS³ mass spectra of OLL. (H) Full-scan MS, MS/MS, and MS³ mass spectra of OOL. (I) Full-scan MS, MS/MS, and MS³ mass spectra of OOO. (J) Full-scan MS, MS/MS, and MS³ mass spectra of OOS. X: isotope peak containing 2^{13}C . Precursor ion is underlined. (Continued \rightarrow)

Wesson Canola Oil, 10.83 mg/mL

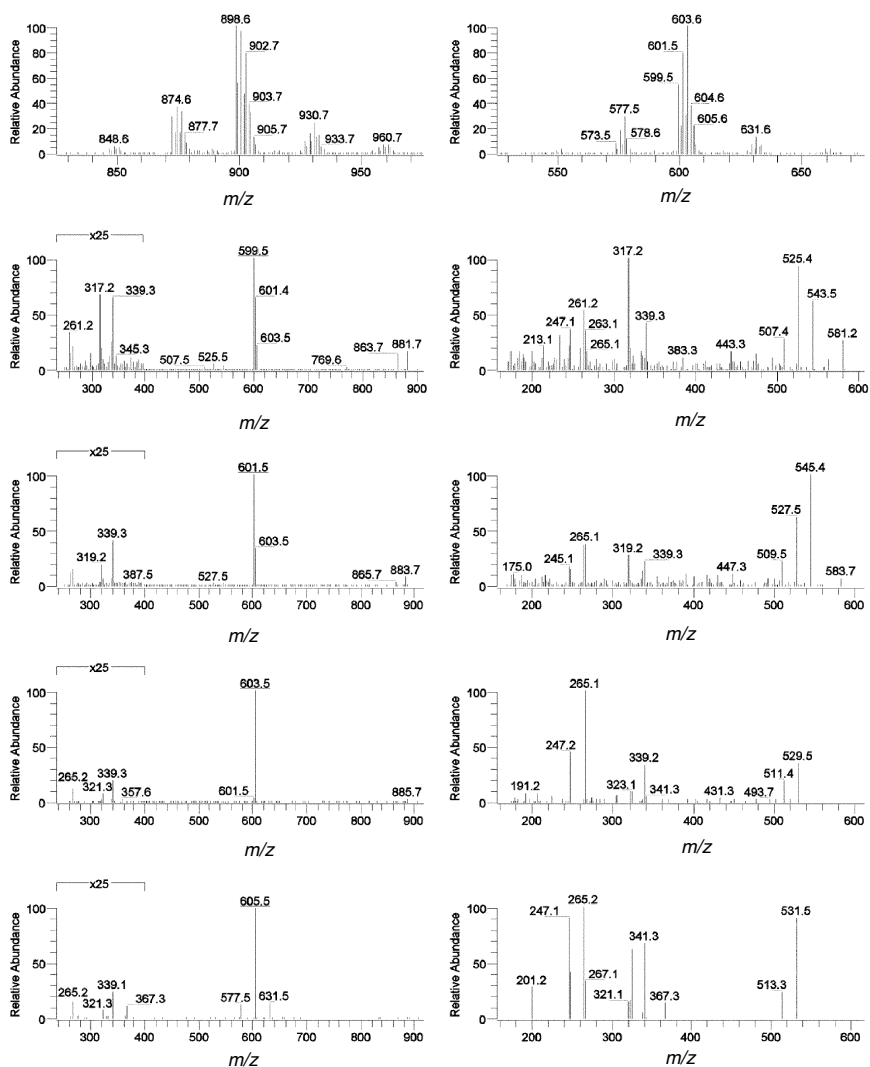


Fig. 13.7 (right). (Continued).

$\text{RCOOH}]^+$ or $[\text{(((TAG)+2O)+H}^+)-\text{RCOOH}]^+$. However, the abundance of the intact $[\text{hydroperoxy-DAG}]^+$ ion formed from OOO-hydroperoxide was small, which presents a problem for identification of the hydroperoxide. OOO-hydroperoxide readily lost H_2O to form an epoxide in the form of $[(\text{TAG})\text{OOH}-\text{H}_2\text{O}+\text{H}^+]^+$, which was equivalent to $[\text{epoxy-OOO}+\text{H}]^+$, and this gave the abundant $[\text{epoxy-DAG}]^+$ fragment ion at m/z 617.5, showing that hydroperoxides give a very abundant epoxy-DAG frag-

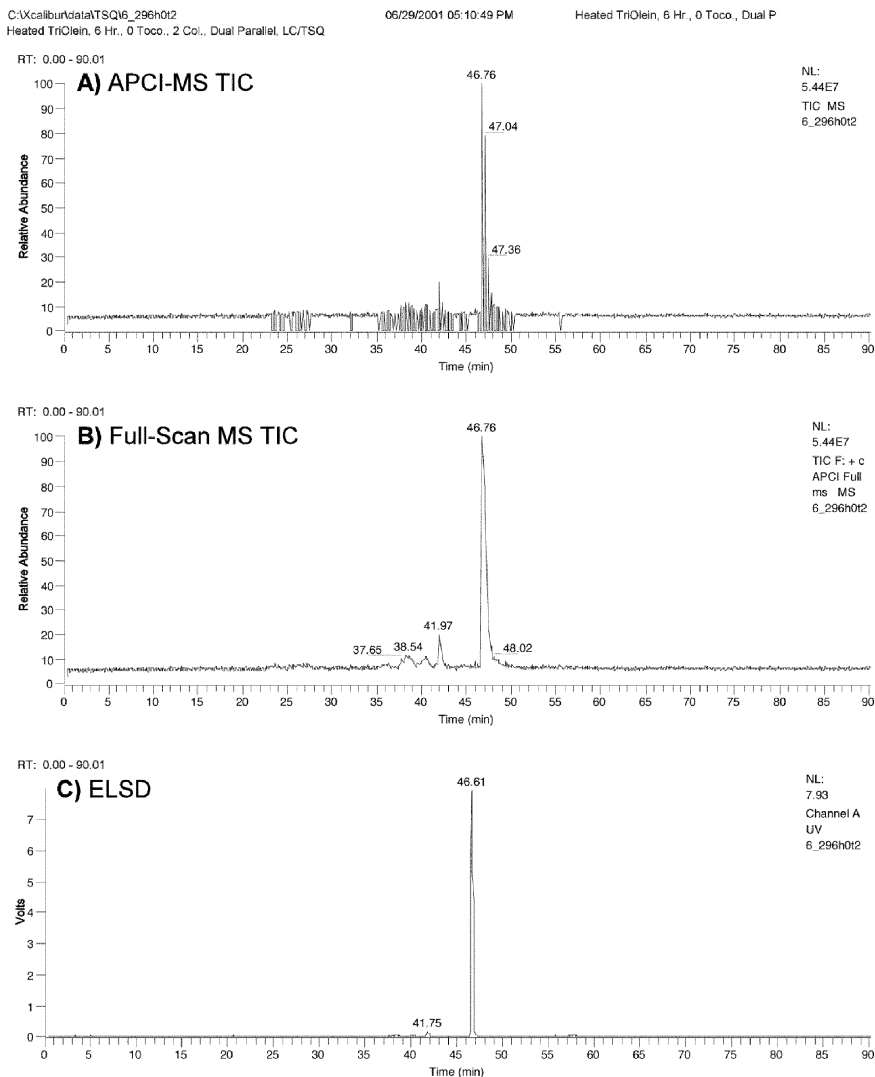


Fig. 13.8 (A–C). Twin sets of LC/MS chromatograms obtained by dual parallel liquid chromatography/mass spectrometry (LC1/MS2) of triolein oxidation products. (A) APCI-MS TIC showing all MS and MS/MS scans. (B) APCI-MS TIC showing only full scans. (C) ELSD chromatogram. (Continued →)

ment that is similar to the epoxy-DAG fragment observed from epoxy-containing TAG. Epidioxy-SOO can give rise to the [epoxy-DAG]⁺ fragment at *m/z* 619.5 ion that is equivalent to [OS-epoxide]⁺. The hydroperoxide could conceivably form a hydroxide having *m/z* 619.5, but hydroxy groups are not stable in the APCI source and

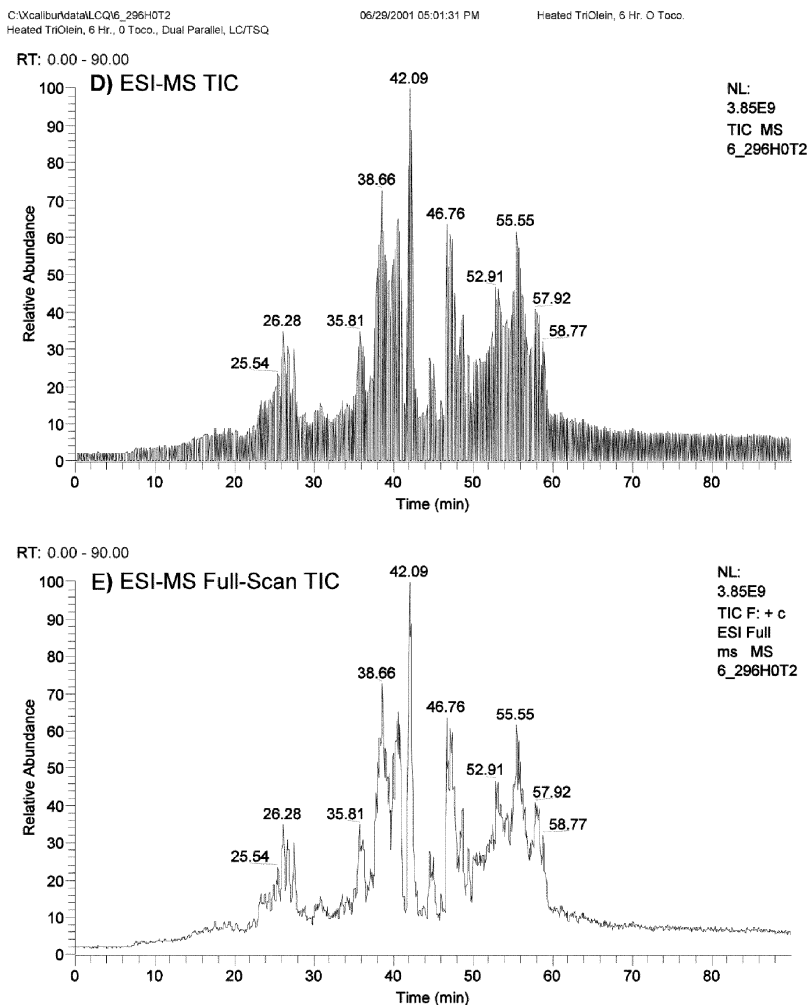


Fig. 13.8 (D–E). (D) ESI-MS TIC showing all MS, MS/MS, and MS³ scans. (E) ESI-MS TIC showing only full scans.

readily undergo further loss of H₂O, which would result in the net loss of H₂O₂ to form the [OL]⁺ fragment. The presence of a substantial abundance of *m/z* 619.5 from an abundant ion at *m/z* 635.5 is taken as an indication of the epidioxy species, while low abundances of *m/z* 635.5 and *m/z* 619.5 with a large abundance of *m/z* 617.5 produced from the *m/z* 635.5 are taken as indications of the hydroperoxy species. Thus, both epidioxides and hydroperoxides gave the same fragments as described above for epoxides: [DAG+O-*n*H]⁺ fragments (*n* = 0 or 2), and then the [DAG-2H]⁺ fragments are formed by further loss of H₂O (or H₂O and 2H).

One would expect that epidioxides would produce larger abundances of [DAG]⁺ fragment ions and [M+H]⁺ ions than hydroperoxides, because epidioxides do not have the labile hydroxy group and so cannot lose H₂O as readily as hydroperoxides. This makes them more stable and long-lived than hydroperoxides, and the additional stability should make them similar, by being cyclic, to the epoxides, which give abundant ions, so larger abundances might be expected to be observed for intact epidioxy fragments than fragments from hydroperoxy TAGOX. The molecules of which the mass spectrum is shown in Figure 13.9J are possibly epidioxides, indicated by the large abundance of the intact oxygen-containing ion at *m/z* 635.5. The difficulty in distinguishing OOS-epidioxide from OOO-hydroperoxide leads one to the conclusion that identification of hydroperoxides and epidioxides should be considered tentative until additional analytical methods, such as NMR spectroscopy, are applied to the chromatographic fractions.

APCI-MS/MS mass spectra are shown in the right-hand panel of Figure 13.9. Magnification factors were applied to the *m/z* 50–500 range to enhance the visibility of fragments in this range that were present at low relative abundances. The APCI-MS2 spectrum of OOO in Figure 13.9B showed the [DAG]⁺ precursor as a base peak, and showed the [MAG]⁺ at *m/z* 339, the [RC≡O]⁺ at *m/z* 265 and the [RC≡O-H₂O]⁺ at *m/z* 247, as expected from triolein. The epoxides formed [RC≡O+O-2H]⁺ (= [epoxy-RC≡O]⁺) acyl fragments at *m/z* 281 and 279 for the epoxy-stearoyl and epoxy-oleoyl fragments, respectively (see right panel of Fig. 13.9H and 13.9I, respectively). The epoxy-stearoyl fragment in Figure 13.9H also formed an [RC≡O+O-*n*H-H₂O]⁺ (= [epoxy-DAG-H₂O]⁺) fragment at *m/z* 263. Although the APCI-MS spectra did yield structurally useful fragmentation patterns that defined the type of oxygen-containing functional group present, the sensitivity was not as good as that observed by ESI-MS.

The ESI-MS, MS/MS, and MS³ mass spectra of triolein TAGOX are shown in Figure 13.10. The ammoniated molecules, [M+NH₄]⁺, were the base peaks in all mass spectra, even for hydroperoxides. This provided molecular weight information that was often not discernible in APCI-MS spectra. The ion chromatograms in Figure 13.10 showed much higher total signal by ESI-MS than was obtained by APCI-MS. Furthermore, the polymeric TAGOX that eluted later than triolein were clearly visible in the ESI-MS chromatograms. The ESI-MS mass spectra of the polymeric compounds yielded intact ammoniated molecules, [M+NH₄]⁺, even from dimers formed by combination of two intact triolein molecules. The ability to produce intact [M+NH₄]⁺ from high molecular weight (HMW) TAGOX represented a distinct advantage for ESI-MS over APCI-MS. In this LC1/MS2 experiment, the ion trap mass spectrometer was scanned only up to *m/z* 2000, so molecules larger than dimers were not observed. Later experiments using ESI-MS, without parallel APCI-MS, produced intact ammoniated molecules from dimers, trimers, and tetramers, with and without additional oxygen functional groups (52).

The ESI-MS/MS spectra in the third panel of Figure 13.10 exhibited the same fragments as were observed under full-scan APCI-MS conditions. The fragments that were produced included the [DAG]⁺ at *m/z* 603.5, the [DAG+O-*n*H]⁺ (= [epoxy-

DAG]⁺) at m/z 619.5 and 617.5 (for the oleoyl,epoxy-stearoyl diacylglycerol fragment ion and the oleoyl,epoxy-oleoyl diacylglycerol, respectively), and the [DAG - 2H]⁺ (from dehydration of the epoxide). Also, the dimer, [(OOO × 2)+NH₄]⁺, produced structurally informative fragments during ESI-MS/MS. Figure 13.10L showed that the ammoniated dimer ion, [(OOO × 2)+NH₄]⁺, fragmented by losing one oleoyl acyl chain, RCOO (FM 281.3), and losing the ammonium moiety: 1787.4 - 281.3 - 18 = 1488.1. This fragment was analogous to the [DAG]⁺ fragment ions shown in Scheme 13.1, except that another whole, intact triolein molecule was attached to the DAG.

The ESI-MS³ spectra of triolein oxidation products are shown in the right-hand panel of Figure 13.10. The MS³ spectra of the epoxides, Figure 13.10I and 13.10J, showed some of the same fragments as did APCI-MS/MS mass spectra (right-hand panel of Fig. 13.9), specifically: [MAG]⁺ at m/z 339 and the [RC≡O]⁺ at m/z 265. The epoxides also formed [epoxy-RC≡O]⁺ acyl fragments at m/z 281 and 279 for the epoxy-stearoyl and epoxy-oleoyl fragments, respectively. The epoxides exhibited [epoxy-MAG]⁺ ions at m/z 355 and 353 for epoxy-monostearoylglycerol and epoxy-monooleoylglycerol, respectively. Further discussion of the fragmentation of HMW TAGOX is presented in detail in our recent report (52).

In Figure 13.10K, this mass spectrum is identified as the mass spectrum of [(OOS-epidioxide)+NH₄]⁺, which is isobaric with [(OOO-hydroperoxide)+ NH₄]⁺. As with APCI-MS mass spectra, one would expect that epidioxides would produce larger abundances of [epidioxo-DAG]⁺ fragment ions and [M+H]⁺ ions, because they do not have the labile hydrogen and cannot lose H₂O as readily as hydroperoxides. This would be similar to the observation of larger abundances of epoxide fragments by ESI-MS/MS than most other fragments. The ESI-MS/MS mass spectrum of the [M+NH₄]⁺ ion in Figure 13.10K showed a substantial abundance at m/z 619.5 that would not be expected to arise from OOO-hydroperoxide, but which could easily arise from the OOS-epidioxide. Thus, the molecules of which the mass spectrum is shown in Figure 13.10K are identified as epidioxides, based on the large abundances of the intact ion at m/z 635.5, and the large fragment ion at m/z 619.5, which is equivalent to an OOS-epoxide. Furthermore, the retention time of the species shown in Figure 13.10K is just prior to the OOO-epoxides. This would be expected to be observed from the epidioxides rather than the hydroperoxides, since hydroperoxides would be even more polar, and so would be expected to elute before epidioxides, and epidioxides would elute before epoxides. Nevertheless, since the OOS-epidioxides and OOO-hydroperoxides are isobaric, any identification made based solely on mass spectrometry must be considered tentative, until confirmation is provided by an independent technique, such as NMR spectroscopy.

After our two initial reports (43,44) in 1998 and 2002 describing the first applications of LC1/MS2, Liu *et al.* (45) adopted our approach by using an LC1/MS2 system for identification of drug metabolites. Other approaches to obtaining data from complementary ionization sources have also been reported. In

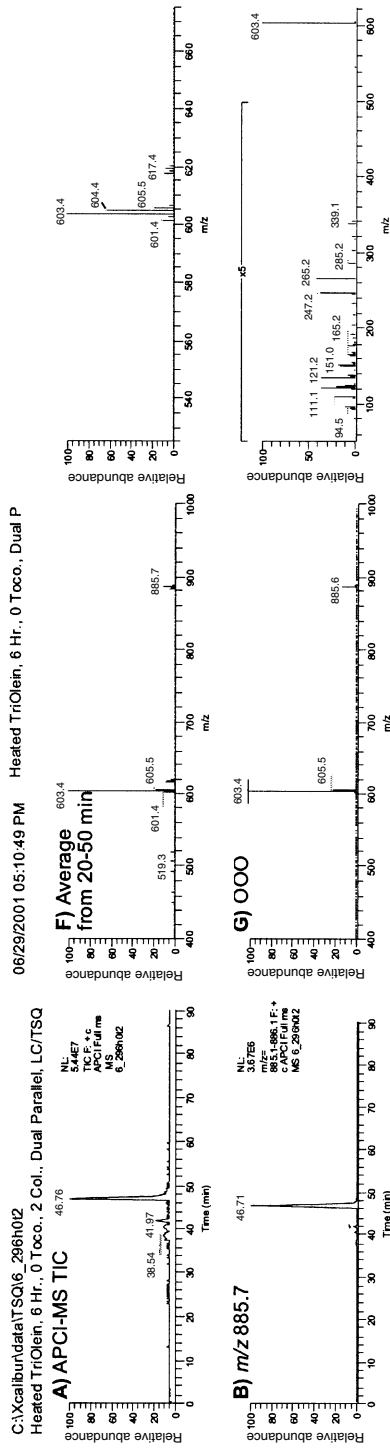


Fig. 13.9 (A-I). APCI-MS ion chromatograms, and MS and MS/MS mass spectra obtained on TSQ700 tandem mass spectrometer, in parallel with the ESI-MS data shown in Figure 13.9. (A) TIC; (B) extracted ion chromatogram (EIC) of m/z 885.6 (\pm 0.5); (C) EIC of m/z 619.4; (D) EIC of m/z 617.4; (E) EIC of m/z 635.4; (F) average mass spectrum from 20 to 50 min, and expanded range from m/z 525–675; (G) averaged full-scan MS and MS/MS mass spectra of OOO [at 46.71 min]; (H) averaged full-scan MS and MS/MS mass spectra of epoxy-OOS [at 41.97 min]; (I) Averaged full-scan MS and MS/MS mass spectra of epoxy-SOO or hydroperoxy-OOO [35.37 min].

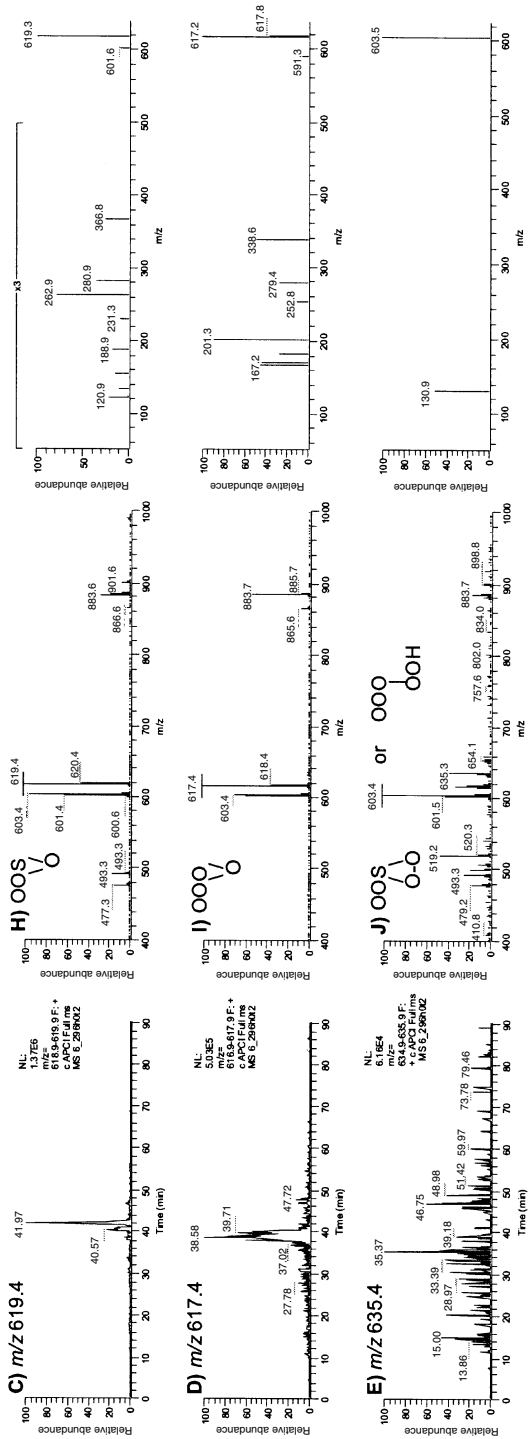


Fig. 13.9. (Continued).

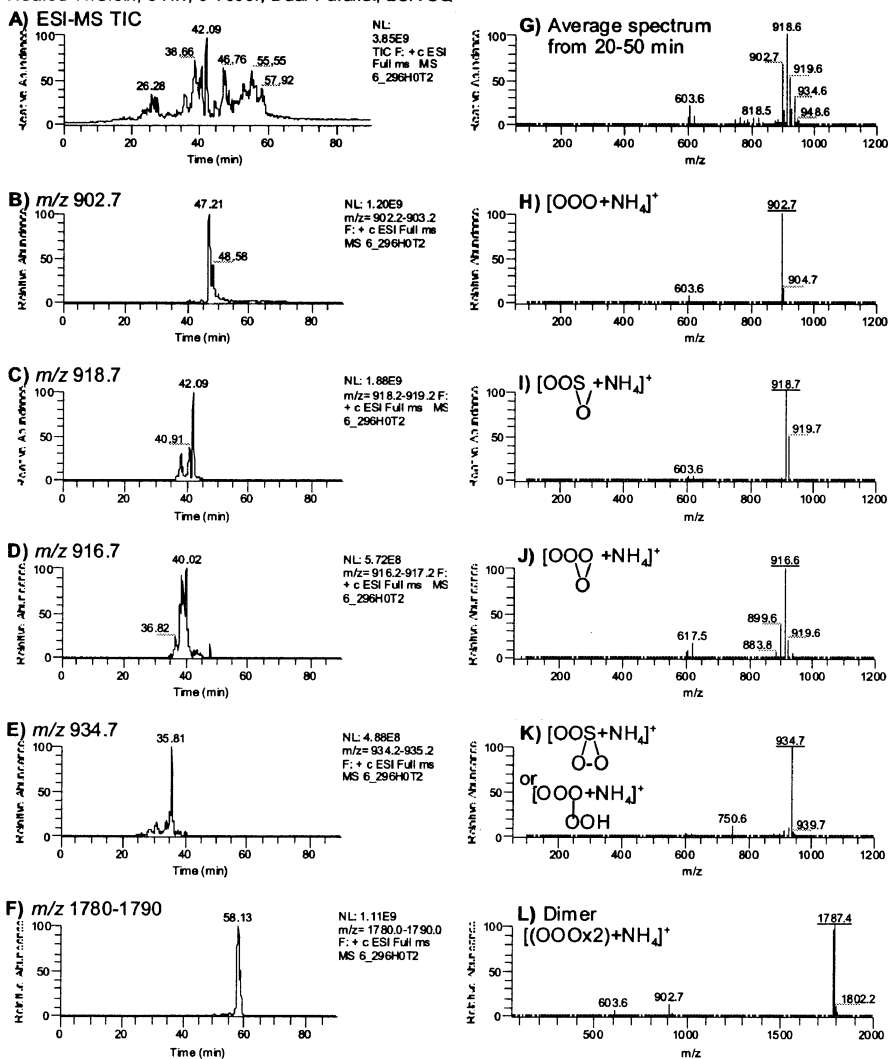


Fig. 13.10 (left). ESI-MS ion chromatograms, and MS, MS/MS, and MS³ mass spectra of triolein oxidation products, obtained on an LCQ Deca ion trap mass spectrometer, in parallel with the APCI-MS data shown in Figure 13.8. (A) TIC; (B) extracted ion chromatogram (EIC) of m/z 902.7 (± 0.5); (C) EIC of m/z 918.7; (D) EIC of m/z 916.7; (E) EIC of m/z 934.7; (F) EIC of m/z 1780–1790; (G) average mass spectrum from 20 to 50 minutes, and expanded range from m/z 850–1000 and from m/z 550–700; (H) full-scan MS, MS/MS, and MS³ mass spectra of $[\text{OOO}+\text{NH}_4]^+$; (I) full-scan MS, MS/MS, and MS³ mass spectra of $[(\text{epoxy-OOS})+\text{NH}_4]^+$; (J) full-scan MS, MS/MS, and MS³ mass spectra of $[(\text{epoxy-OOO})+\text{NH}_4]^+$; (K) full-scan MS, MS/MS, and MS³ mass spectra of $[(\text{epidioxo-SOO})+\text{NH}_4]^+$, which is isobaric with $[(\text{hydroperoxy-OOO})+\text{NH}_4]^+$; (L) full MS, MS/MS, and MS³ spectra of $[\text{dimer}+\text{NH}_4]^+$. Precursor ion is underlined. (Continued \rightarrow)

Heated TriOlein, 6 Hr. O Toco.

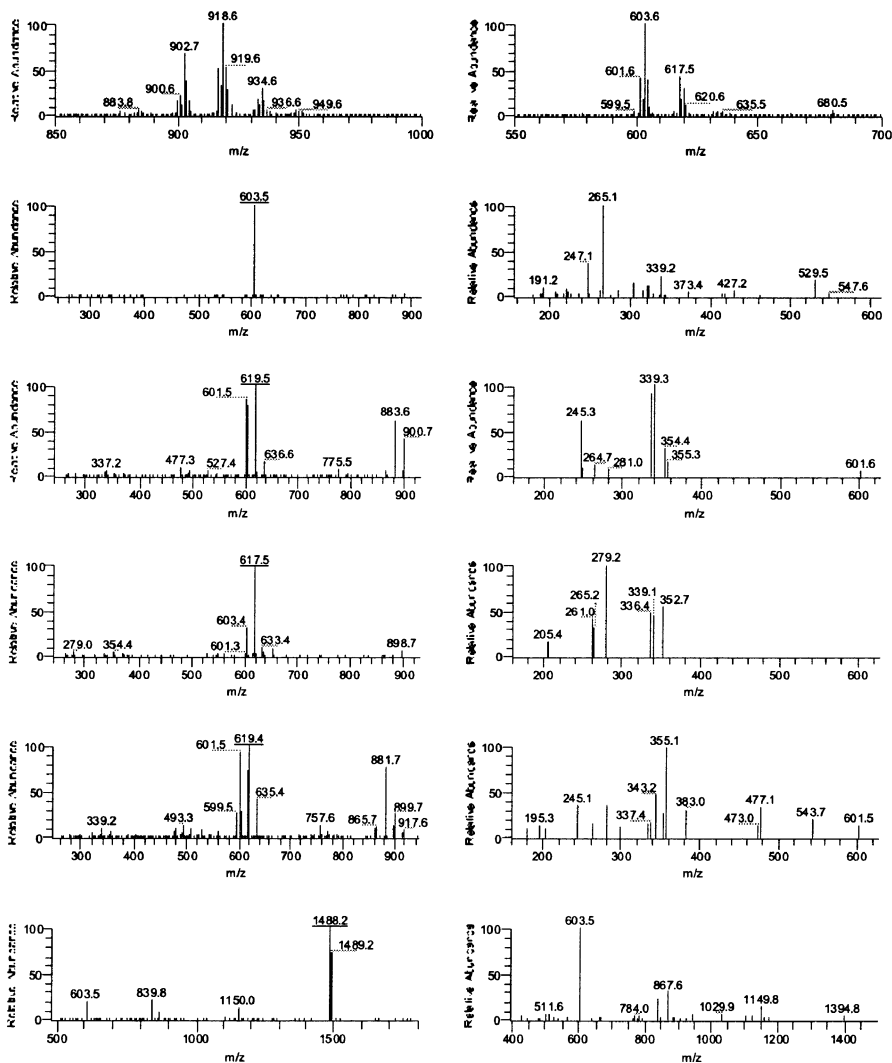


Fig. 13.10 (right). (Continued).

1998, Siegel *et al.* (53) reported the development of a combination ESI and APCI source that was capable of alternating between APCI and ESI modes, or operating in a combined mode. The optimal source conditions for ESI were not the same as those for APCI, so either compromise conditions had to be used, which limited sensitivity, or a time delay had to be incorporated to allow conditions to change between the optimal conditions for the two modes. This delay gave the instrument a longer duty cycle and limited the number of spectra that could be acquired in a given amount of time. Despite its shortcomings, the benefit of this approach was

that only one mass spectrometer was required. More recently, a combined ESI/APCI source was demonstrated for high throughput LC/MS applications (54). This source produced spectra that were very similar to the spectra obtained by conventional ESI-MS and APCI-MS. The benefit of eliminating the need for replicate runs using different ionization modes that we previously discussed (43,44) was especially important for high throughput analysis in which samples from a 96-well plate were analyzed.

Comparison of Quantitative Analysis by LC/MS2. We have previously reported an approach to calculating response factors by comparison of the FA composition calculated from the TAG composition determined by APCI-MS to the FA composition determined by calibrated gas chromatography (GC) with a flame ionization detector (FID) (3–5). In this approach, the “raw” TAG composition by LC/APCI-MS was first determined by summing the areas under every $[\text{DAG}]^+$ and $[\text{M}+\text{H}]^+$ ion belonging to each specific TAG molecular species. Next, the FA composition was calculated from this TAG composition. Then, the FA composition calculated from the LC/APCI-MS data was compared to the FA composition determined by calibrated GC-FID, and a response factor for each FA was calculated. These FA response factors (RF) were multiplied together to produce response factors for every TAG molecular species: TAG RF = $(\text{FA}_1 \text{ RF}) \times (\text{FA}_2 \text{ RF}) \times (\text{FA}_3 \text{ RF})$. The TAG RF thus produced were then multiplied by the area of each TAG to yield a response-factor-adjusted area. This was used to calculate a complete response-factor-adjusted TAG composition.

Here we report the application of the approach for quantitative analysis that we previously developed to both ESI-MS and APCI-MS. Figure 13.11 shows the twin sets of chromatograms obtained by both APCI-MS and ESI-MS from separation of a synthetic mixture of 35 TAG. Fatty acids in this mixture were completely randomly distributed through all possible TAG molecular species, so the composition was known and calculated from statistical considerations. The mol % FA composition (converted from the weight %) of the 35-TAG mixture, determined by calibrated GC-FID, is given in Table 13.1. The statistical TAG composition calculated from the FA composition is given in Table 13.2. Table 13.2 also lists the raw area percent compositions from both LC/APCI-MS and LC/ESI-MS, and the response-factor-adjusted TAG compositions.

Since APCI-MS mass spectra produced both $[\text{DAG}]^+$ and $[\text{M}+\text{H}]^+$ ions, the composition determined by APCI-MS was calculated by summing the areas under the $[\text{DAG}]^+$ and $[\text{M}+\text{H}]^+$ ions belonging to each specific TAG molecular species, and then calculating the percentage of each TAG based on its area as a percentage of the total area from all TAG. The APCI-MS ion chromatograms of several $[\text{DAG}]^+$, along with mass spectra of L_nL_nL_n, LLL, OOO, PPP, and SSS, are shown in Figure 13.12. As this figure shows, the chromatographic resolution on these columns was sufficient to avoid almost all overlapped peaks. Thus, only one APCI-MS fragment peak area had to be apportioned between overlapped isobaric

species, as we have had to do before (3–5). This occurred because the P peak in the [OL]⁺ EIC overlapped the O peak of the [SLn]⁺ EIC, at *m/z* 601.5 (not shown).

Since ESI-MS mass spectra exhibited primarily [M+NH₄]⁺ ions, the composition determined by ESI-MS was calculated from the areas under the peaks in the ion chromatograms of the [M+NH₄]⁺ ions only. Ion chromatograms of LnLnLn, LLL, OOO, PPP, and SSS are shown in Figure 13.13, along with typical ESI-MS mass spectra. There was sufficient chromatographic resolution between all species to allow the TAG composition to be determined from all [M+NH₄]⁺, without the need to apportion the areas of any of the peaks.

The response factors calculated by comparison of the FA composition determined by calibrated GC-FID to the FA compositions calculated from the TAG compositions determined by LC/APCI-MS and by LC/ESI-MS are given in Table 13.3. This table clearly demonstrated that the response of TAG under ESI-MS conditions, as reflected in the FA composition calculated from the TAG, was opposite to their response under APCI-MS conditions. Specifically, the response factors for polyunsaturated TAG were smaller than those for saturated TAG by ESI-MS, indicating that unsaturates responded better than saturates under ESI-MS conditions. The response factors of the saturated TAG were larger than the response factors for unsaturated TAG, indicating that saturated species produced less signal than unsaturates. This was opposite to the trend for APCI-MS reported previously (3–5) and shown here.

LC2/MS2 Experiments

Total lipid extracts, such as those obtained by using the methods of Folch *et al.* (55) or Bligh and Dyer (56), produce a mixture of polar and non-polar lipids. The complete set of all polar and non-polar lipids is the “lipidome” of a cellular system. A complete knowledge of the composition of all molecular species of the lipids making up the lipidome is the goal of “lipidomics.” We show here how an LC2/MS2 experiment can be used to determine the identities of numerous classes of lipids that make up most of the lipidome of a cellular extract.

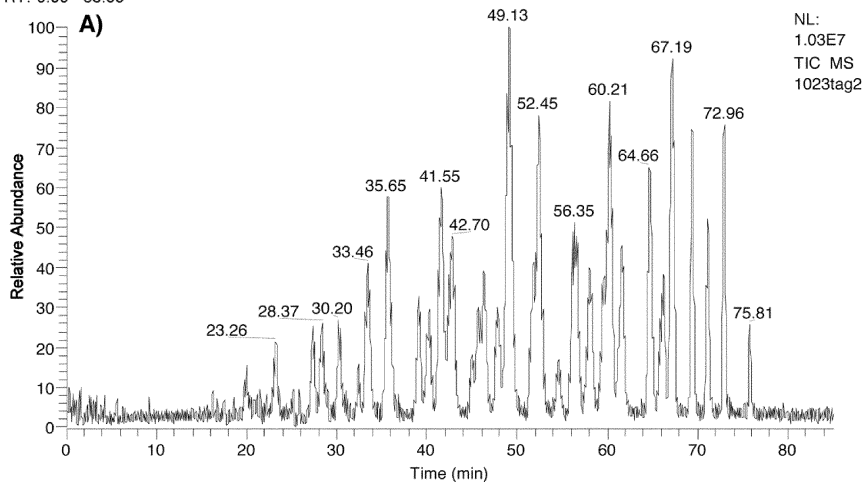
Polar lipids are comprised mostly of PL, while non-polar lipids consist of mostly triacylglycerols, diacylglycerols, cholesterol, and cholesterol esters. Often, the subject of analysis is either the class of polar lipids or the class of non-polar lipids, to the exclusion of the other. Typically, normal-phase chromatography with a silica or amine column is used for separation of the PL and other polar components. In such cases, the neutral lipids elute as a bolus near the solvent front. Conversely, reversed-phase chromatography with an octadecylsilane (C₁₈) column is typically used for separation of the non-polar components. The polar components elute as a bolus near the solvent front under reversed-phase conditions. We have previously published methods for the analysis of PL, with emphasis on SPM and DHS, using a polar amine column (9,43). In these separations, neutral lipids were eluted near the solvent front. The various classes of PL were separated into distinct peaks, and the individual molecular species within each PL class were identified by online

G:\xcalibur\1TAGL1MS2\APCI\1023tag2
 Synthetic 35-TAG Mixture, 10.42mg/ml, LC1/MS2, LC/LCQ

10/23/2003 01:48:00 PM

Synthetic 35-TAG Mix, 10.42mg/ml

RT: 0.00 - 85.00



RT: 0.00 - 85.00

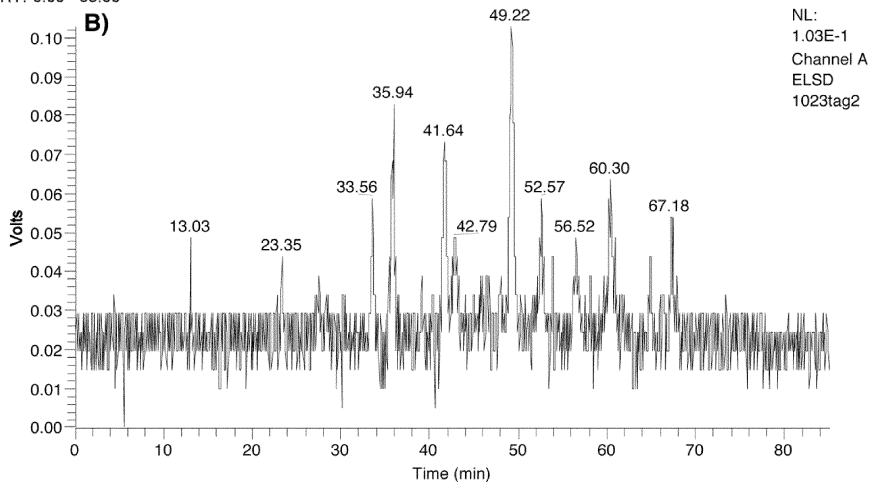


Fig. 13.11 (A–B). Twin chromatograms of a synthetic 35-TAG mixture obtained by dual parallel mass spectrometers employing (+) APCI-MS and (+) ESI-MS and MS/MS. (A) TIC obtained by APCI-MS. (B) ELSD chromatogram. (Continued →)

mass spectrometry. We were also able to use mass spectrometry to identify the major species of the non-polar components in the bolus that eluted near the solvent front (43). However, identification of the neutral lipids such as TAG without prior separation was not ideal. The bolus contained numerous isobaric TAG that were not distinguished, and also the DAG fragment ions could not be attributed to the

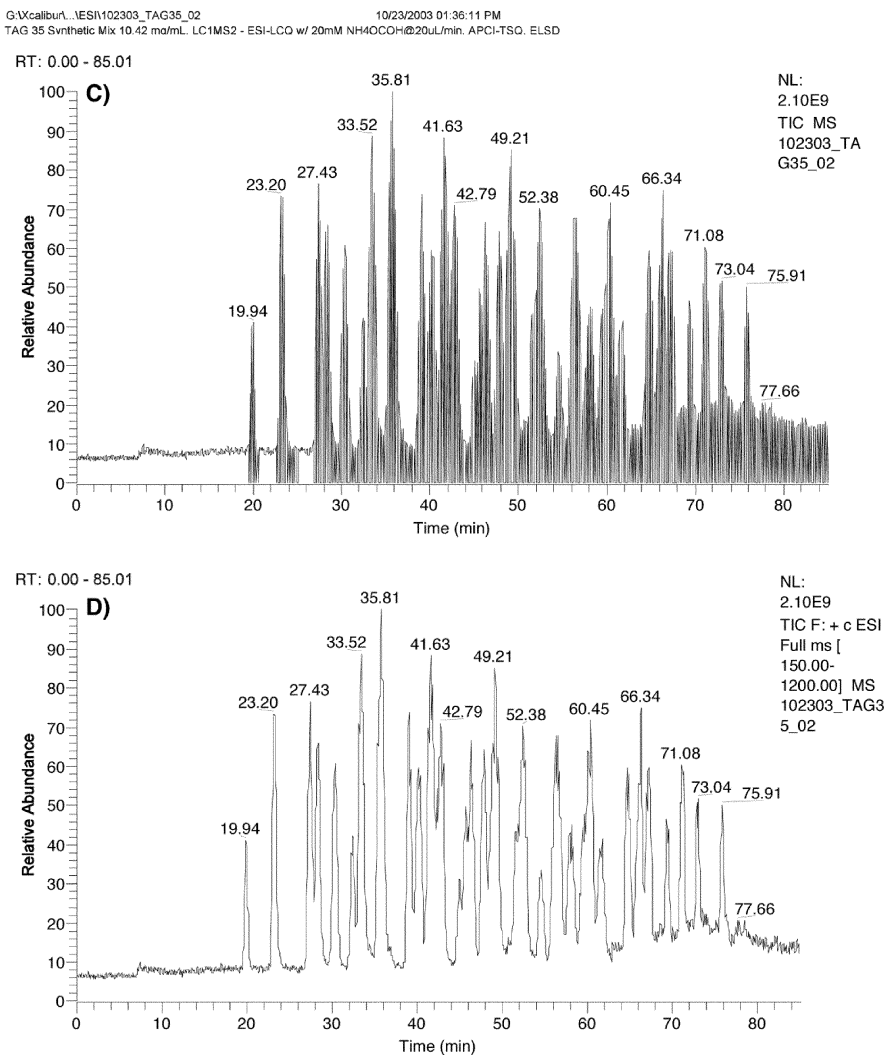


Fig. 13.11 (C–D). (C) TIC by ESI-MS and MS/MS. (D) TIC showing only full-scan ESI-MS scans.

individual parent TAG molecular species. Separation of the TAG prior to mass spectrometric analysis is preferred. Thus, one column type and solvent system is not ideal for simultaneous separation of both polar lipids and neutral lipids on one column. Given the high degree of information obtainable by mass spectrometry, in combination with the quality of separations afforded by HPLC, a single method that combines the separation of all polar and non-polar lipid classes with detection by mass spectrometry has long been sought.

TABLE 13.1
Fatty Acid Compositions Determined from Calibrated GC-FID and Calculated from TAG Compositions Determined by APCI-MS and ESI-MS

| FA | GC-FID (FAME mol%) | % RSD | GC-FID (FA mol%) | Raw LC/APCI-MS (n = 3) | Adjusted LC/APCI-MS | % RSD | Raw LC/ESI-MS (n = 4) | Adjusted LC/ESI-MS | % RSD |
|----|-----------------------|-------|---------------------|---------------------------|------------------------|-------|--------------------------|-----------------------|-------|
| P | 20.43 | 0.10 | 20.36 | 25.44 | 20.43 | 0.31 | 17.09 | 20.36 | 0.28 |
| S | 21.07 | 0.05 | 21.10 | 22.42 | 21.21 | 0.51 | 19.48 | 21.23 | 0.63 |
| O | 20.42 | 0.05 | 20.44 | 21.40 | 20.45 | 0.32 | 20.65 | 20.34 | 0.22 |
| L | 19.72 | 0.13 | 19.74 | 17.25 | 19.55 | 0.87 | 21.72 | 19.65 | 0.33 |
| Ln | 18.36 | 0.08 | 18.36 | 13.50 | 18.36 | 0.24 | 21.05 | 18.45 | 0.32 |
| | 100.00 | | 100.00 | 1000.01 | 100.00 | | 99.99 | 100.03 | |

TABLE 13.2

TAG Compositions Calculated from the FA Composition by GC-FID and Determined by APCI-MS and ESI-MS

| TAG | Statistical | Raw APCS-MS | Adjusted APCI-MS | (n=3) SD | Raw ESI-MS | Adjusted ESI-MS | (n=4) SD |
|------------------------|-------------|----------------|---------------------|-------------|---------------|--------------------|-------------|
| PPP | 0.84 | 1.46 | 0.75 | 0.01 | 0.44 | 0.74 | 0.04 |
| SSS | 0.94 | 0.98 | 0.82 | 0.07 | 1.06 | 1.36 | 0.12 |
| OOO | 0.85 | 1.01 | 0.88 | 0.04 | 1.21 | 1.17 | 0.13 |
| LLL | 0.77 | 0.52 | 0.78 | 0.12 | 1.41 | 1.06 | 0.17 |
| LnLnLn | 0.62 | 0.31 | 0.78 | 0.04 | 1.05 | 0.69 | 0.07 |
| PPS | 2.62 | 3.97 | 2.40 | 0.07 | 1.62 | 2.49 | 0.07 |
| PPO | 2.54 | 4.06 | 2.49 | 0.08 | 2.02 | 2.84 | 0.20 |
| PPL | 2.45 | 3.92 | 2.87 | 0.02 | 1.80 | 2.32 | 0.07 |
| PPLn | 2.28 | 2.91 | 2.53 | 0.07 | 2.73 | 3.38 | 0.34 |
| SSP | 2.72 | 3.43 | 2.44 | 0.09 | 1.74 | 2.43 | 0.11 |
| SSO | 2.73 | 2.94 | 2.48 | 0.07 | 2.44 | 2.83 | 0.12 |
| SSL | 2.64 | 2.91 | 2.96 | 0.12 | 3.54 | 3.78 | 0.25 |
| SSLn | 2.45 | 2.28 | 2.75 | 0.19 | 2.53 | 2.59 | 0.04 |
| OOP | 2.55 | 3.71 | 2.72 | 0.00 | 2.39 | 2.79 | 0.19 |
| OOS | 2.65 | 3.21 | 2.76 | 0.10 | 2.36 | 2.50 | 0.04 |
| OOL | 2.47 | 2.43 | 2.54 | 0.10 | 2.95 | 2.62 | 0.04 |
| OOLn | 2.30 | 1.83 | 2.27 | 0.19 | 3.25 | 2.78 | 0.04 |
| LLP | 2.38 | 1.91 | 2.00 | 0.08 | 1.78 | 1.75 | 0.17 |
| LLS | 2.47 | 1.86 | 2.29 | 0.09 | 3.44 | 3.08 | 0.18 |
| LLO | 2.39 | 1.86 | 2.33 | 0.12 | 3.22 | 2.64 | 0.11 |
| LLLn | 2.15 | 1.24 | 2.21 | 0.22 | 3.04 | 2.19 | 0.09 |
| LnLnP | 2.06 | 1.31 | 1.94 | 0.16 | 2.86 | 2.58 | 0.13 |
| LnLnS | 2.13 | 1.12 | 1.96 | 0.07 | 2.26 | 1.86 | 0.12 |
| LnLnO | 2.07 | 1.28 | 2.26 | 0.07 | 3.09 | 2.33 | 0.07 |
| LnLnL | 2.00 | 1.02 | 2.15 | 0.09 | 2.76 | 1.90 | 0.05 |
| PSO | 5.27 | 7.10 | 5.11 | 0.09 | 3.28 | 4.19 | 0.10 |
| PSL | 5.09 | 6.83 | 5.89 | 0.32 | 4.11 | 4.81 | 0.13 |
| PSLn | 4.73 | 5.28 | 5.42 | 0.06 | 4.66 | 5.25 | 0.05 |
| POL | 4.93 | 5.21 | 4.57 | 0.33 | 3.83 | 4.10 | 0.84 |
| POLn | 4.59 | 4.42 | 4.60 | 0.21 | 4.83 | 4.98 | 0.18 |
| PLLn | 4.43 | 3.03 | 3.78 | 0.06 | 4.15 | 3.92 | 0.17 |
| SOL | 5.11 | 5.55 | 5.72 | 0.13 | 5.26 | 5.12 | 0.08 |
| SOLn | 4.75 | 3.58 | 4.38 | 0.31 | 3.32 | 3.11 | 0.21 |
| SLLn | 4.59 | 2.73 | 4.00 | 0.13 | 4.44 | 3.82 | 0.31 |
| OLLn | 4.45 | 2.82 | 4.20 | 0.33 | 5.12 | 4.02 | 0.13 |
| Sum | 100.01 | 100.03 | 100.03 | | 99.99 | 100.02 | |
| Avg. Abs. % Rel. Error | | | 8.70 | | | 16.32 | |

We demonstrate here a method that employed dual parallel liquid chromatographic systems attached to dual parallel mass spectrometers for simultaneous separation and analysis of polar and non-polar lipids from (i) a commercially available total brain extract, and (ii) a total lipid extract from a sand bream filet. For the bovine brain

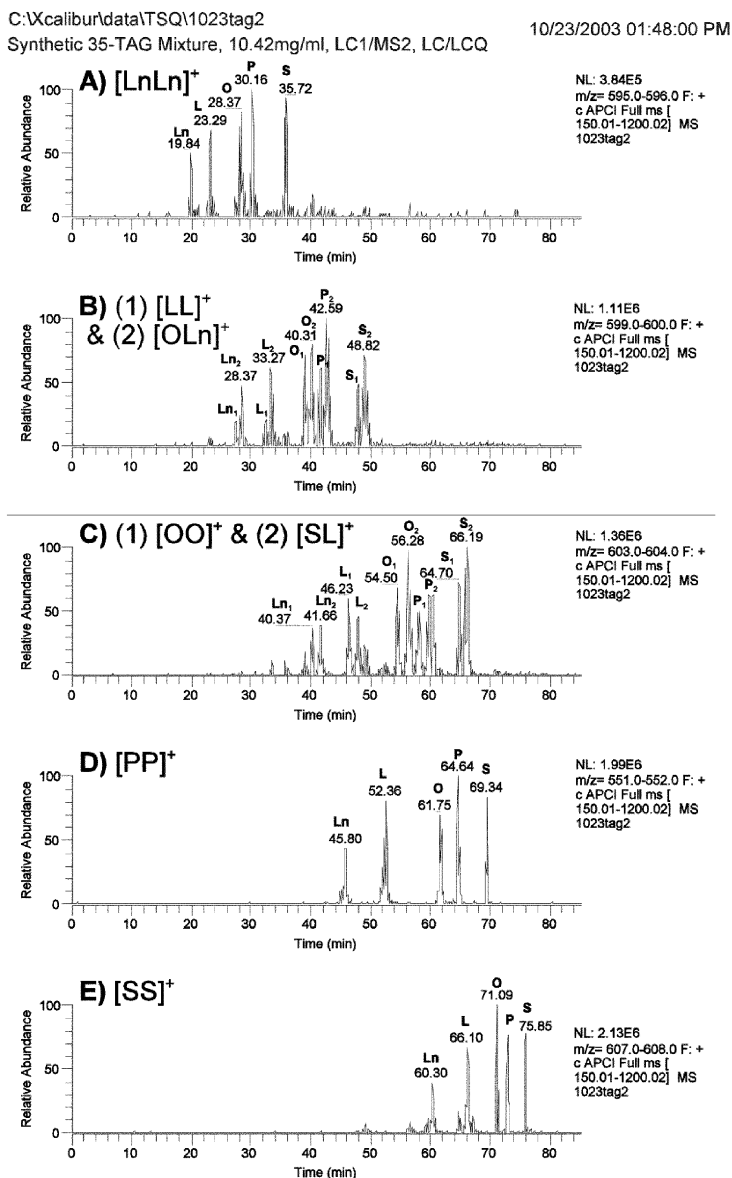


Fig. 13.12 (left). APCI-MS extracted ion chromatograms (EIC) and mass spectra of a synthetic 35-TAG mixture. (A) EIC of [LnLn]⁺ at m/z 595.5, and mass spectrum of [LnLnLn+H]⁺. (B) EIC of [LL]⁺ (= [OLn]⁺) at m/z 599.5, and mass spectrum of [LLL+H]⁺. (C) EIC of [OO]⁺ (= [SL]⁺) at m/z 603.5, and mass spectrum of [OOO+H]⁺. (D) EIC of [PP]⁺ at m/z 551.5, and mass spectrum of [PPP+H]⁺. (E) EIC of [SS]⁺ at m/z 607.5, and mass spectrum of [SSS+H]⁺. (Continued →)

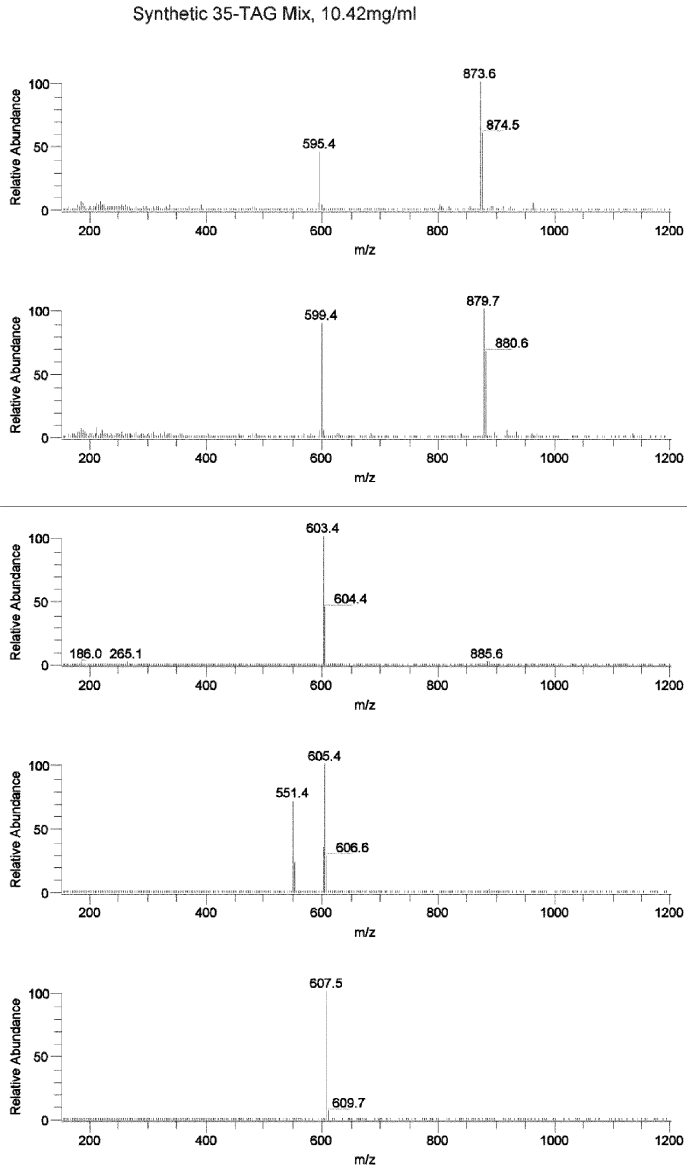


Fig. 13.12 (right). (Continued).

extract, polar lipids were separated on a normal-phase chromatographic system (LC1), with detection by positive- and negative-ion ESI ion trap mass spectrometry (MS1), MS/MS, and MS³, at the same time that neutral lipids were separated on a reversed-phase system (LC2), coupled to a second mass spectrometer (MS2) using positive-ion

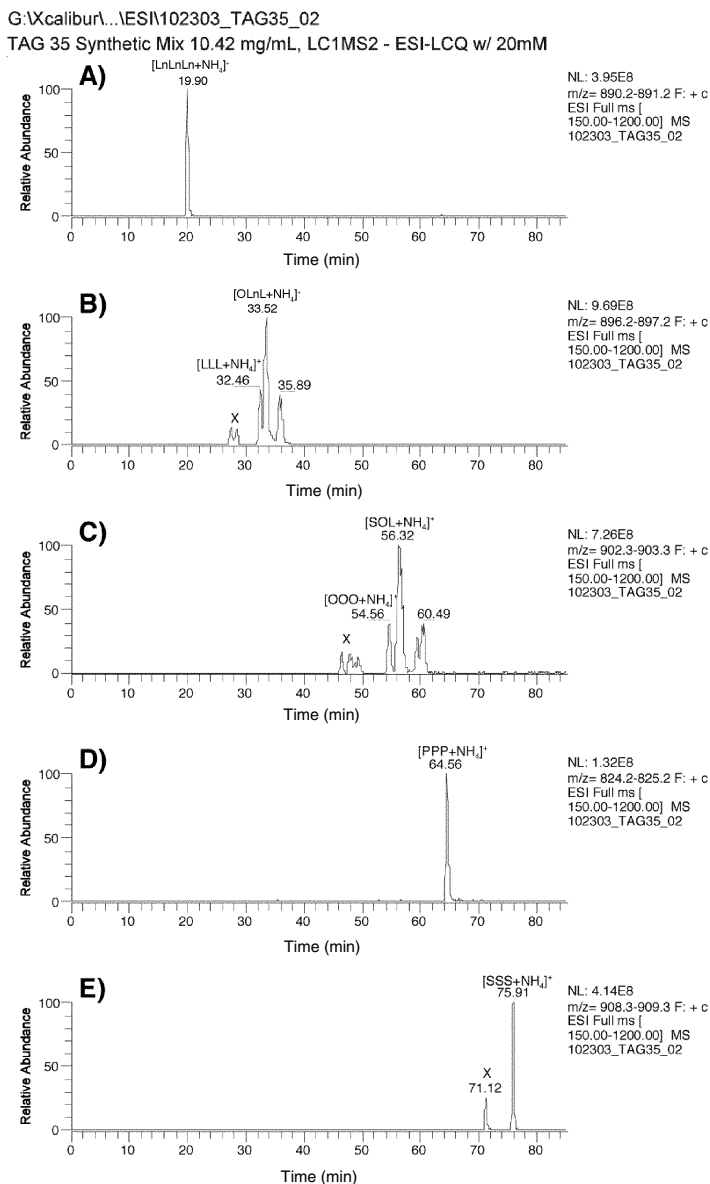


Fig. 13.13 (left). ESI-MS extracted ion chromatograms (EIC) and mass spectra of a synthetic 35 TAG mixture. (A) EIC of $[\text{LnLnLn}+\text{NH}_4]^+$ at m/z 890.7, and mass spectrum of $[\text{LnLnLn}+\text{NH}_4]^+$. (B) EIC of $[\text{LLL}+\text{NH}_4]^+$ at m/z 896.7, and mass spectrum of $[\text{LLL}+\text{NH}_4]^+$. (C) EIC of $[\text{OOO}+\text{NH}_4]^+$ at m/z 902.7, and mass spectrum of $[\text{OOO}+\text{NH}_4]^+$. (D) EIC of $[\text{PPP}+\text{NH}_4]^+$ at m/z 824.7, and mass spectrum of $[\text{PPP}+\text{NH}_4]^+$ overlapped with $[\text{OOS}+\text{NH}_4]^+$. (E) EIC of $[\text{SSS}+\text{NH}_4]^+$ at m/z 908.8, and mass spectrum of $[\text{SSS}+\text{NH}_4]^+$. X = $2\cdot^{13}\text{C}$. (Continued \rightarrow)

10/23/2003 01:36:11 PM
NH4COH@20uL/min, APCI-TSQ, ELSD

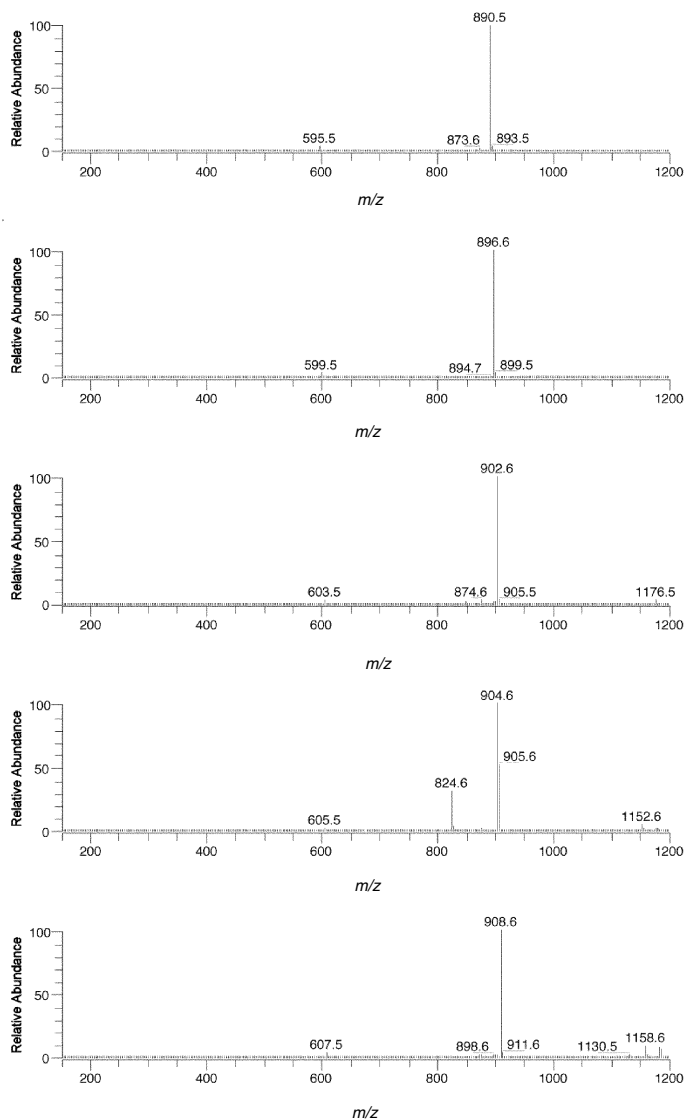


Fig. 13.13 (right). (Continued).

ESI-MS with MS/MS. For the sand bream total lipid extract, polar lipids were separated on a normal-phase chromatographic system (LC1), with detection by positive- and negative-ion ESI ion trap mass spectrometry (MS1), MS/MS, and MS³, at the same time that neutral lipids were separated on a reversed-phase system (LC2), coupled to a

TABLE 13.3

Fatty Acid Response Factors Calculated from Comparison of the FA Composition by GC-FID to the FA Composition Calculated from the TAG Composition Determined by APCI-MS and ESI-MS

| FA | GC-FID (FAME mol%) | % RSD | GC-FID (FA mol%) | Average APCI-MS response factor | Average ESI-MS response factor |
|----|-----------------------|-------|---------------------|---------------------------------------|--------------------------------------|
| P | 20.43 | 0.10 | 20.36 | 1.000000 | 1.366536 |
| S | 21.07 | 0.05 | 21.10 | 1.176775 | 1.244618 |
| O | 20.42 | 0.05 | 20.44 | 1.193762 | 1.135080 |
| L | 19.72 | 0.13 | 19.74 | 1.430737 | 1.041455 |
| Ln | 18.36 | 0.08 | 18.36 | 1.701924 | 1.000000 |
| | 100.00 | | 100.00 | | |

second mass spectrometer (MS2) using positive-ion APCI-MS with MS/MS. Both of these are examples of an LC2/MS2 configuration.

Bovine Brain Total Lipid Extract. As demonstrated above, we have employed dual parallel mass spectrometers in an LC1/MS2 configuration with ESI-MS and APCI-MS to demonstrate that ESI-MS provided increased sensitivity for the analysis of TAG compared to APCI-MS, when ammonium formate was added as a sheath liquid. Commercially available bovine brain whole extract contained a small amount of neutral lipids, so maximum sensitivity was required. Therefore, we employed dual liquid chromatography with ESI mass spectrometry on both the ion trap mass spectrometer and the tandem mass spectrometer in this experiment. In the present example, ammonium formate was used as a sheath liquid on the LCQ mass spectrometer, whereas it was incorporated into the solvent system on the TSQ. Chromatograms and mass spectra from this experimental arrangement are shown in Figure 13.14.

A commercially available bovine brain total lipid extract sample was injected onto the normal-phase columns containing an amine stationary phase, using the autosampler pictured in Figure 13.1. The neutral lipids were unretained on this polar column, and so eluted as a bolus with short retention time. The TAG and other non-polar molecules eluted between 6.00 and 8.25 min. Over this time window (labeled “diverted” in Fig. 13.14) the electronically actuated valve on the front of the LCQ Deca was set to divert the eluate (valve in the inject position) from the first columns onto the head of the second set of columns, which contained reversed-phase packing. After diverting the neutral bolus, the valve closed (valve in the load position), and the original solvent system continued to drive the polar lipids down the amine columns. At the same time, the second pump, also plumbed through the diverter valve, continued pumping a second solvent system down the reversed-phase system to perform the neutral lipid separation. Chromatograms showing elution of the polar components from the amine columns and the neutral components from the reversed-phase columns are shown in Figure 13.14A and

13.14E, respectively. Figure 13.14A through 13.14D show the ESI-MS total ion chromatogram from the ion trap mass spectrometer, a chromatogram filtered to show only positive-ion scans, a chromatogram filtered to show only negative-ion scans, and a chromatogram from the photodiode array detector. The data from the PDA are not discussed because they provided no structural information. Figure 13.14E and 13.14F show the ESI-MS total ion current chromatogram (TIC) from the tandem mass spectrometer and the TIC filtered to show only positive-ion scans. The evaporative light scattering detector was not sufficiently sensitive to produce a useful chromatogram (Fig. 13.14G). Negative-ion scans were not obtained on the tandem instrument.

Figure 13.14 shows elution of PE and its plasmalogen (PE plas), PC and the sphingolipids, as well as other polar lipids. PE and PE plasmalogen occurred at 28.5 to 32 min, PC eluted between ~35 and 39 min, and SPM came off the column between 42 and 50 min. Within these time ranges, long-chain molecular species eluted with shorter retention times, and medium- and short-chain molecular species eluted later in the peaks. The shorter molecular species of one class of PL may overlap the long-chain species of the next eluted class of PL, but the two classes were easily distinguished by mass. Other classes of polar lipids (glycosphingolipids), described herein, eluted between 10 and 25 min, and phosphatidylserine (PS) eluted near 45 to 55 min, overlapped with the sphingomyelins. The medium- to short-chain SPM species overlapped the long- to medium-chain PS species.

Figure 13.15 shows positive and negative full-scan MS mass spectra of PE, PC, and the sphingolipids. The m/z range 50–2000 is shown in the left panel of Figure 13.15, which included the range of the dimers. Dimers were formed to a substantial extent in the electrospray ionization source. Dimer formation is concentration dependent and can be greatly reduced by using a very dilute sample solution at a very low flow rate. However, at very low concentrations species present at low levels are not observed. Since neutral lipids were present at relatively low levels in this sample, a higher concentration was used to allow all possible molecular species of both neutral and polar lipids to be observed. For quantitative analysis, a dilute solution analyzed on a tandem mass spectrometer in negative-ion mode yields usable quantitative results, based on the demonstration by Han and Gross (24,37) that different molecular species of anionic PL have nearly identical ionization efficiencies, after corrections for ^{13}C isotope abundances.

The right-hand panel of Figure 13.15 shows the protonated molecule m/z region for three classes of PL. In addition to the protonated molecules and some fragments, the abundances of the m/z values of the dimers were substantial, but only in the case of the PC species were they larger than the protonated molecules. PE species produced protonated molecules, $[\text{M}+\text{H}]^+$, in positive-ion mode, and deprotonated molecules, $[\text{M}-\text{H}]^-$ in negative-ion mode, allowing facile identification of the molecular masses. The PC species and sphingolipid molecules both produced protonated, $[\text{M}+\text{H}]^+$, and sodiated molecules, $[\text{M}+\text{Na}]^+$, in positive-ion mode, while they gave almost exclusively formate adducts, $[\text{M}+45]^-$, in negative-

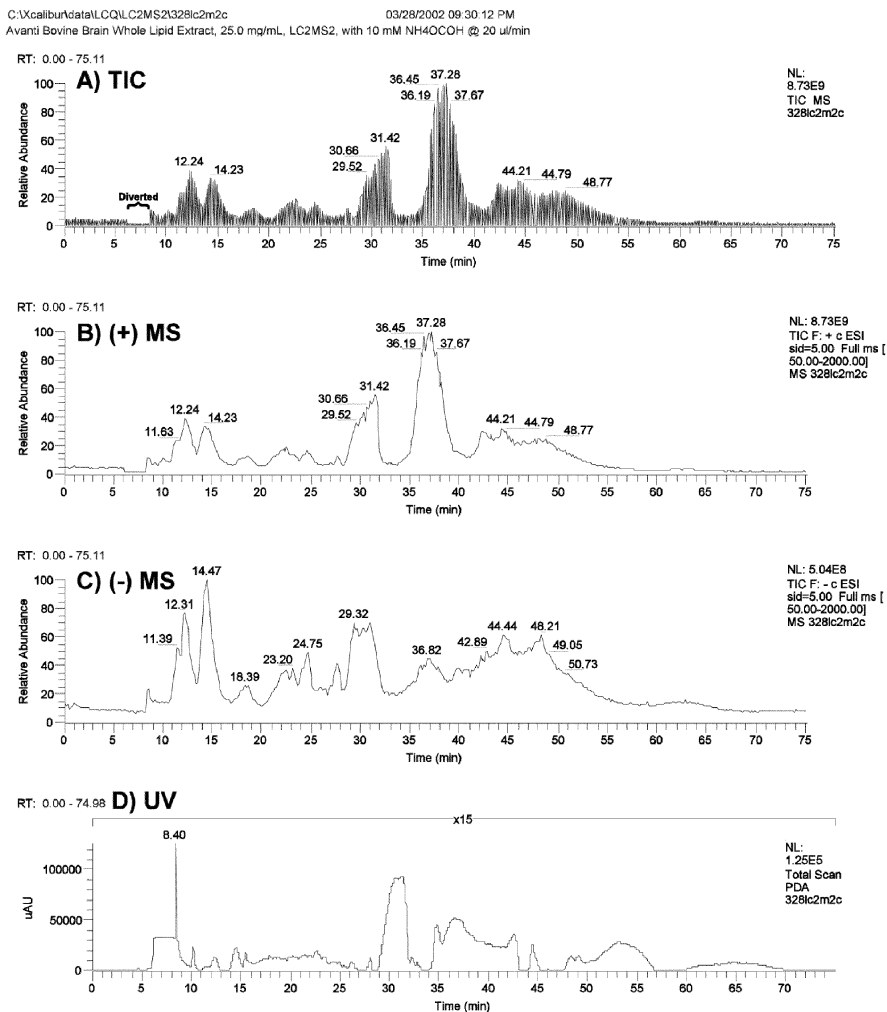


Fig. 13.14 (A–D). Chromatograms obtained from dual parallel liquid chromatography/ dual mass spectrometry (LC2/MS2) of bovine brain total lipid extract. (A) Total ion chromatogram from normal-phase separation with detection by ESI-MS on an ion trap mass spectrometer. (B) ESI-MS ion chromatogram showing only scans obtained in positive full-scan (MS) mode. (C) ESI-MS ion chromatogram showing scans obtained in negative MS mode. (D) Photodiode array total scan chromatogram.

(Continued →)

ion mode. In the mass spectra in Figure 13.15, the molecular species were most easily identified by their formate adducts, $[M+45]^-$, and then their masses confirmed by protonated and sodiated molecules.

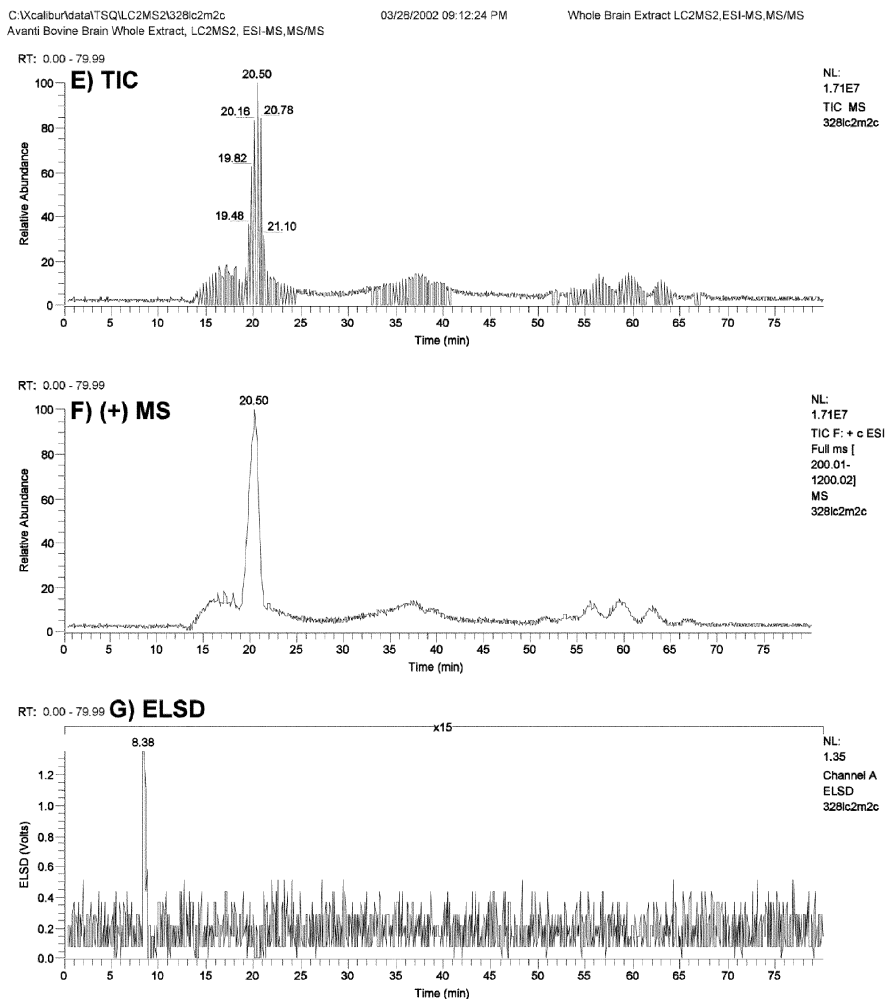


Fig. 13.14 (E–G). (E) Total ion chromatogram from reversed-phase separation with detection by ESI-MS on a tandem mass spectrometer. (F) ESI-MS chromatogram showing scans obtained in full-scan mode. (G) Evaporative light scattering detector chromatogram.

Figure 13.15C showed that the most abundant phosphatidylcholine species had m/z values of 734.7, 760.8, and 788.8. These m/z values corresponded to dipalmitoyl-PC (DPPC), palmitoyloleoyl-PC (POPC), and stearoyloleoyl-PC (SOPC), respectively. The negative-ion mass spectrum in Figure 13.15D showed m/z values that corresponded to the formate adducts, $[M+45]^-$, of each of these primary molecular species. In the positive-ion spectra, PC molecular species produced sodiated molecules having abundances that were 32 to 53% of the abundances of the protonated molecules. SPM

Avanti Bovine Brain Whole Lipid Extract, 25.0 mg/mL, LC2MS2, with 10 mM NH₄COOH @ 20 ul/min

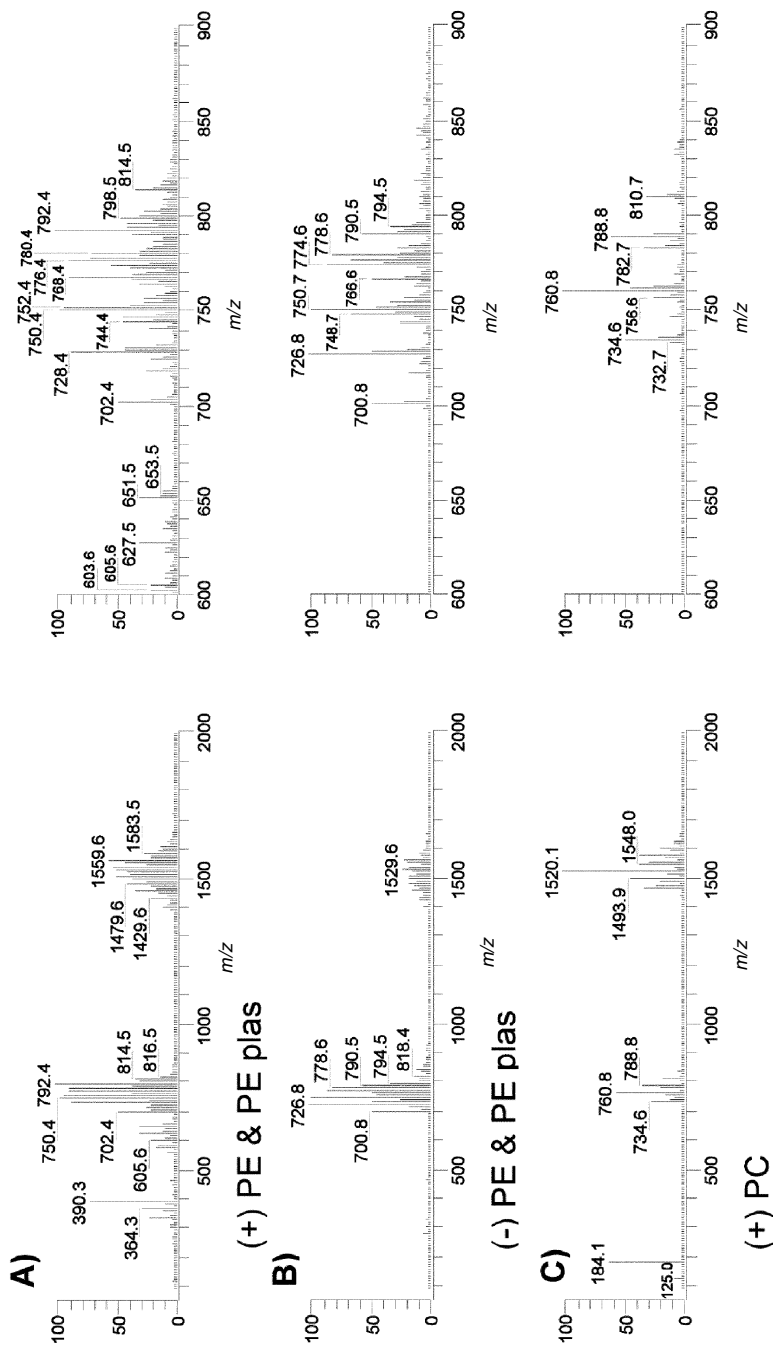


Fig. 13.15. Positive and negative averaged ESI-MS mass spectra of bovine brain phospholipids. (A) (+) ion mass spectrum of PE and PE plas. (B) (-) ion spectrum of PE and PE plas. (C) + spectrum of PC. (D) (-) ion spectrum of PC. (E) (+) ion spectrum of sphingolipids. (F) (-) ion mass spectrum of sphingolipids. Left panel, m/z 50–2000; right panel, m/z 600–900.

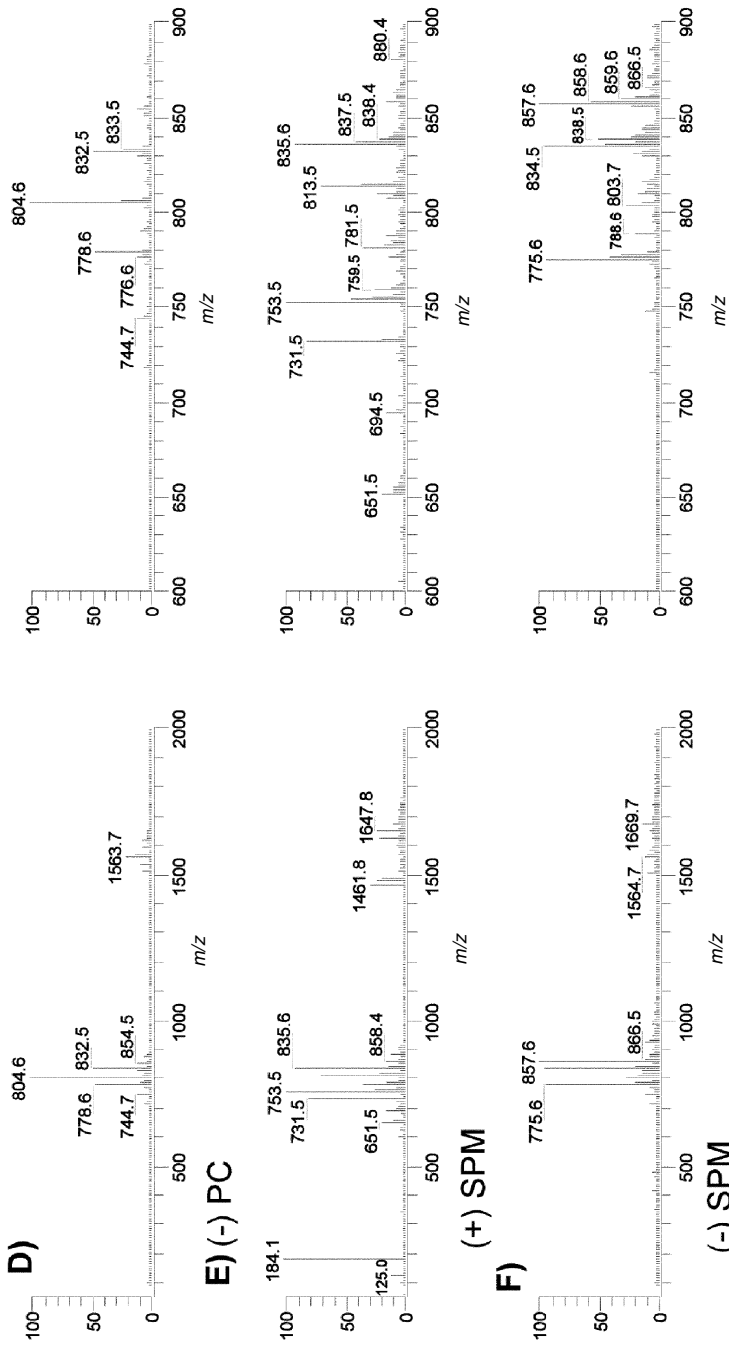


Fig. 13.15. (Continued).

species, on the other hand, gave abundances of sodiated molecules that were larger than the abundances of the protonated molecules (see Fig. 13.15E). For SPM molecular species, the protonated molecules had abundances that were 70 to 81% of the abundances of the sodiated molecules.

There were several peaks that eluted from the normal-phase system that exhibited fragments that indicated that they contained sphingosine backbones. These molecules had polar head groups, in addition to the sphingosine backbone, which caused them to be retained on the polar column instead of being diverted to the non-polar system. These sphingolipids eluted in several peaks early in the normal-phase chromatographic run, showing that they were distinctly different from SPM species. Figure 13.14 exhibited several peaks that eluted before PE (which eluted around 30 min). Ion chromatograms of prominent peaks in the mass spectra, and the average mass spectra across these peaks, are shown in Figure 13.16. Positive-ion mass spectra across the most abundant four early-eluted sphingolipid peaks exhibited base peaks of either m/z 792.5 or m/z 810.5. Because of the similar appearances of the spectra in Figure 13.16A and 13.16D, and the similar appearances of Figure 13.16B and 13.16E, the positive-ion spectra did not provide uniquely identifying peaks to allow the molecular species to be identified. However, the negative-ion mass spectra exhibited peaks arising from deprotonated molecules and from formate adducts, which allowed the molecular weights of the species to be deduced. When combined with the negative-ion mass spectra, the positive-ion mass spectra were seen to exhibit fragments that provided important structural information.

All of the early-eluted polar sphingolipid peaks exhibited m/z values of 282.3, 264.3, and 252.3 that indicated the presence of the sphingosine backbone. Furthermore, the species having the primary fragments at m/z 792.5 gave an abundant fragment of m/z 630.5 in the full mass spectra, Figure 13.16B and 13.16E, as well as in the MS/MS spectrum, Figure 13.16C. This fragment corresponded to a ceramide backbone containing a 24:1 fatty amide chain. The MS/MS mass spectrum of m/z 792.5 gave primary fragments at m/z 630.4, 612.4, and 600.3, which were the same as those observed for 24:1-ceramide that eluted at 20.50 min in the LC/APCI-MS chromatogram in Figure 13.14F.

The negative-ion ESI-MS mass spectra were necessary for identifying the molecular weights of the glycosphingolipids. The molecules fragmented minimally in negative-ion mode and so produced abundant $[M-H]^-$ peaks. The hydroxy-cerebrosides are believed to have hydroxy-fatty amide chains, according to the Avanti Polar Lipids catalog (from which the lipids were purchased), which states that brain cerebrosides eluted as two thin layer chromatography (TLC) spots, one containing nonhydroxylated FA and one containing hydroxylated FA (57).

Hsu and Turk (58) also showed mass spectra of hydroxylated glycosphingolipids, as lithium adducts. Levery *et al.* (59) had also shown ESI-MS/MS of lithium adducts of hydroxy- and nonhydroxy containing cerebrosides. Probable structures for four of the glycosphingolipids are shown in Scheme 13.2. These structures are consistent with

the mass spectra in Figure 13.16 and with the work reported by others (58,59). Further discussion of the glycosphingolipids and other classes is presented in our recent publication (46). Chromatograms and mass spectra of the non-polar lipids, including ceramide species, are also discussed in detail in that report.

The LC2/MS2 experiment required no special fabrication of components, but rather used standard commercially available instruments. Only the plumbing of the electronically actuated valve on the front of the LCQ Deca required modification. It is worth noting that the process of eluting the neutral lipid bolus from the non-polar column and then switching it through the diverter valve to the non-polar columns did not result in a dramatic degradation of peak shape and loss of resolution.

Sharp, narrow peaks could be obtained even after elution down two pairs of columns having different polarities. Nevertheless, the separation of the TAG needs to be improved to increase the resolution to the point that it is similar to what we have previously reported for this class. We have now successfully performed LC2/MS2 experiments that show that the acetonitrile/methylene chloride system, which produced a better separation of TAG, was sufficiently compatible with the normal-phase system to allow use of the better solvent pair on the reversed-phase system. We also recognize the need to modify the normal-phase system to allow the PS species to be fully resolved from the SPM species.

Sand Bream Filet Total Lipid Extract. As mentioned in the previous section, ESI-MS was chosen for the analysis of both the polar and non-polar lipids in bovine brain because the levels of neutral lipids were low, so the greater sensitivity of ESI-MS was necessary. The $\text{CHCl}_3/\text{MeOH}$ extract of sand bream filet, on the other hand, contained larger amounts of TAG and other neutral lipids. For the sand bream filet extract sample, we used APCI-MS for analysis of the components eluted from the RP-HPLC system, while ESI-MS was used for the PL. Data from the second example of an LC2/MS2 experiment are given in Figure 13.17. Only the TAG present in the largest amounts produced some signal by ELSD, shown in Figure 13.17G. The total lipid extract was obtained using the method of Bligh and Dyer (56).

As can be seen from Figure 13.17A through 13.17D, the PL profile of the fish filet was simpler than that of the bovine brain extract. Typical ESI-MS spectra from an LC2/MS2 experiment were shown in Figure 13.15, so no mass spectra of the sand bream PL are presented. The TAG that eluted from the RP-HPLC/APCI-MS system eluted between 47 and 72 min, as shown in Figure 13.17E and 17F. The RP-HPLC method that was used for the LC2/MS2 experiments was designed to allow all non-polar lipid classes to be separated and eluted, so it was not optimized just for TAG alone. Therefore, the chromatographic resolution of TAG was not as good as that obtained by the HPLC method that has been optimized for TAG separation exclusively (such as shown in Fig. 13.11). This solvent system contained 1 mM ammonium formate to promote ionization when the solvent system was used for ESI-MS. When used for APCI-MS, the ammonium formate resulted in formation of ammonium adduct molecules instead of the protonated molecules that are typical for APCI-MS mass

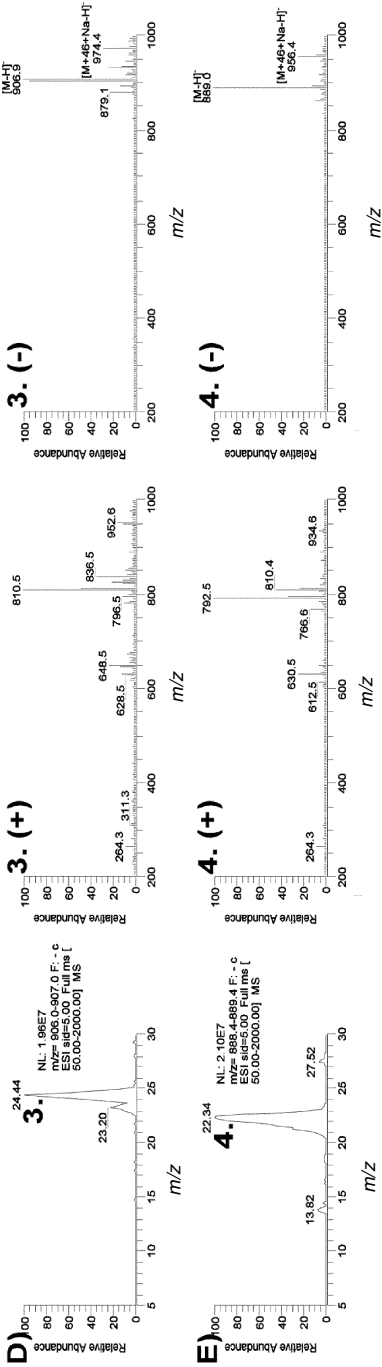
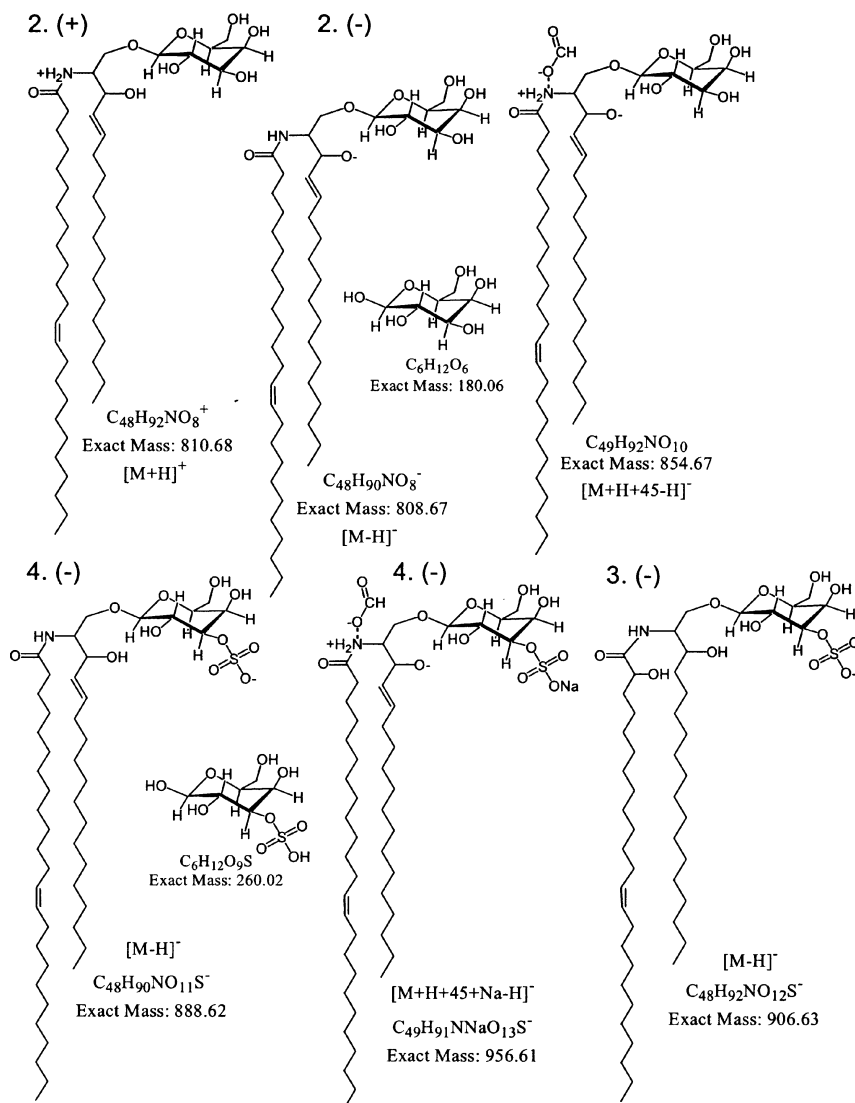
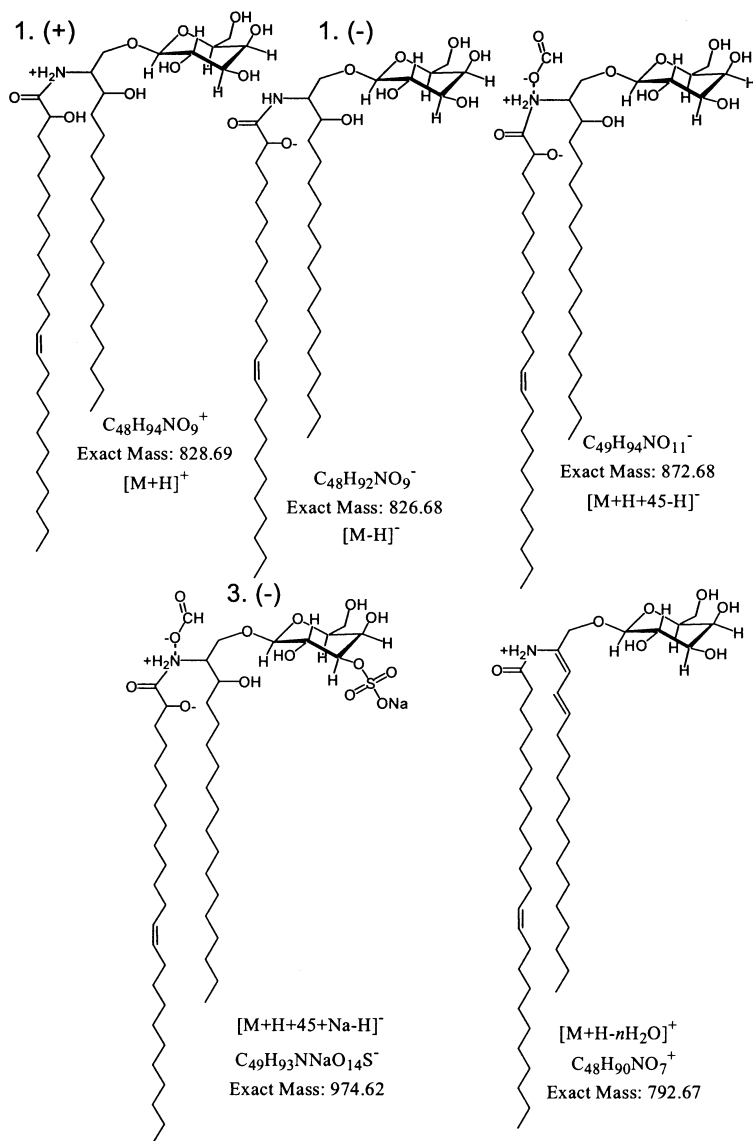


Fig. 13.16. (Continued).



Scheme 13.2 (left). Proposed identities of protonated, deprotonated and adduct ions formed from glycosphingolipids and sulfatoglycosphingolipids. Numbers refer to peaks and mass spectra in Figure 13.16. (Continued →)

spectra. APCI-MS and MS/MS mass spectra of TAG and cholesterol-related molecules are shown in Figure 13.18. As mentioned, the APCI-MS mass spectra of TAG (Fig. 13.18C and 13.18E) exhibited [M+NH₄]⁺ ions, instead of [M+H]⁺ because of the ammonium formate in the solvents. However, the fragments that were formed were



Scheme 13.2 (right).

nonammoniated. They were the typical $[DAG]^+$ fragment ions that are common to APCI-MS mass spectra. The sand bream filet extract contained numerous odd-chain FA, but these were at lower levels than normal even-carbon-chain lengths. The m/z values of odd-carbon-chain-length-containing $[DAG]^+$ can be seen between the peaks for normal (even carbon) $[DAG]^+$ in Figure 13.18C and 13.18E. The TAG containing

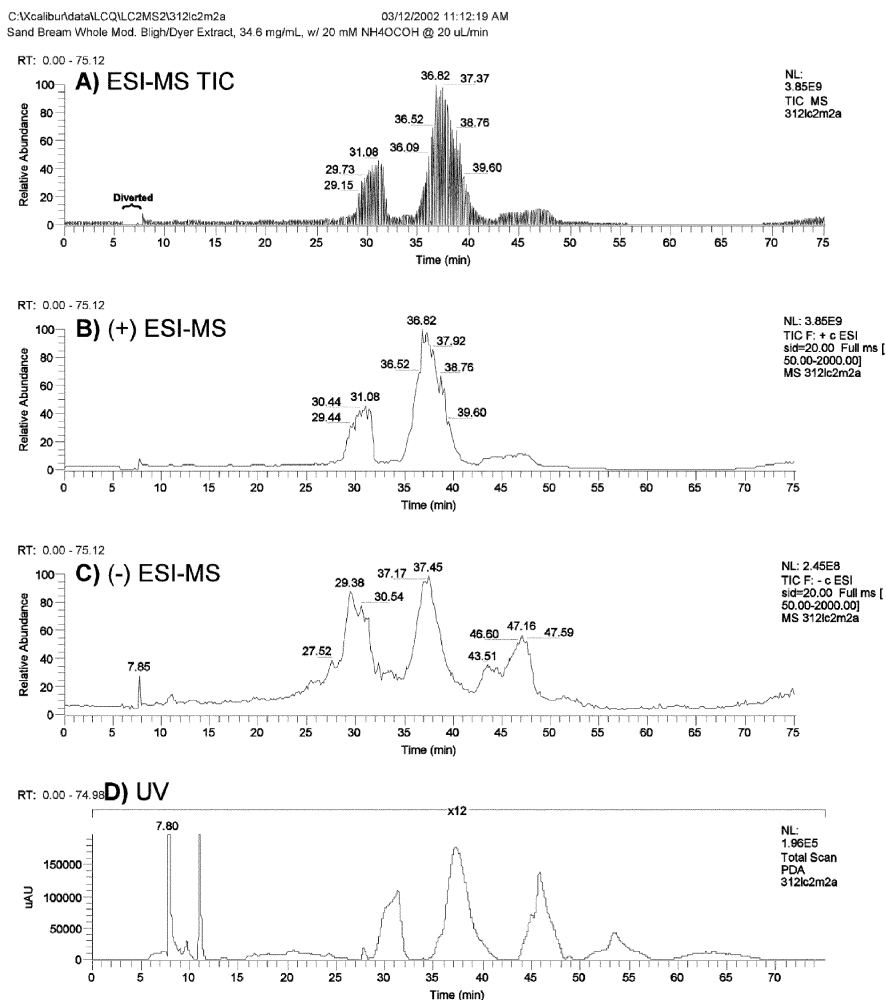


Fig. 13.17 (A–D). Chromatograms obtained from dual parallel liquid chromatography/dual mass spectrometry (LC2/MS2) of a sand bream total lipid extract. (A) Total ion chromatogram of normal-phase HPLC separation with detection by ESI-MS on an ion trap mass spectrometer. (B) ESI-MS ion chromatogram showing only scans obtained in positive full-scan (MS) mode. (C) ESI-MS ion chromatogram showing scans obtained in negative MS mode. (D) Photodiode array total scan chromatogram. (Continued →)

odd-carbon-chain lengths produced ion chromatograms that had distinctly different retention times than their even-carbon-chain-length counterparts.

The mass spectra in Figure 13.18A and 13.18B show APCI-MS and MS/MS spectra of cholesterol-related molecules. We have examined samples of pure chole-

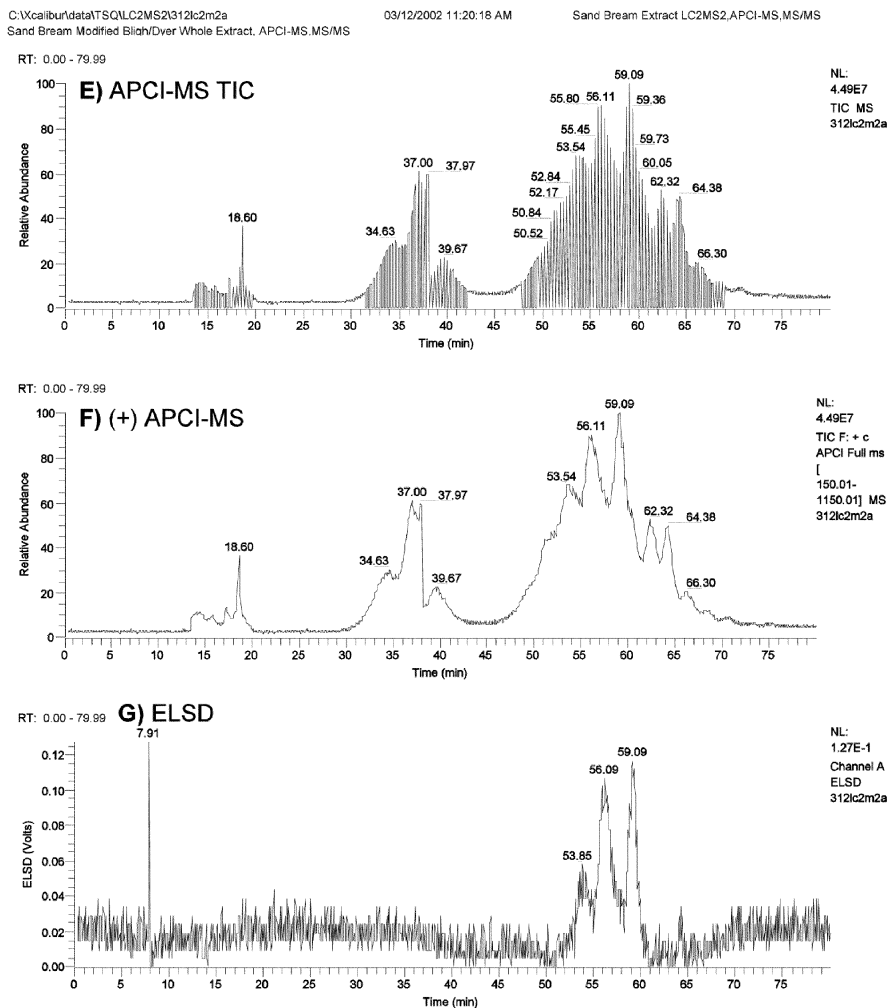


Fig. 13.17 (E–G). (E) Total ion chromatogram of reversed-phase separation with detection by APCI-MS on a tandem mass spectrometer. (F) APCI-MS ion chromatogram showing scans in positive MS mode. (G) Evaporative light scattering detector chromatogram.

terol and of several cholesterol esters (data not shown), and the mass spectrum in Figure 13.18A does not correspond to either of these classes of molecules. However, the base peak at m/z 369, and most importantly the MS/MS spectrum in Figure 13.18B indicated the presence of a cholesterol moiety. The fragment pattern in Figure 13.18B is indistinguishable from that given by pure cholesterol. The base peak at m/z 369 is the same base peak reported by Hagiwara *et al.* (60) in their report on carotenoids in vegetable juice, using cholesterol as an internal standard. This is different from the

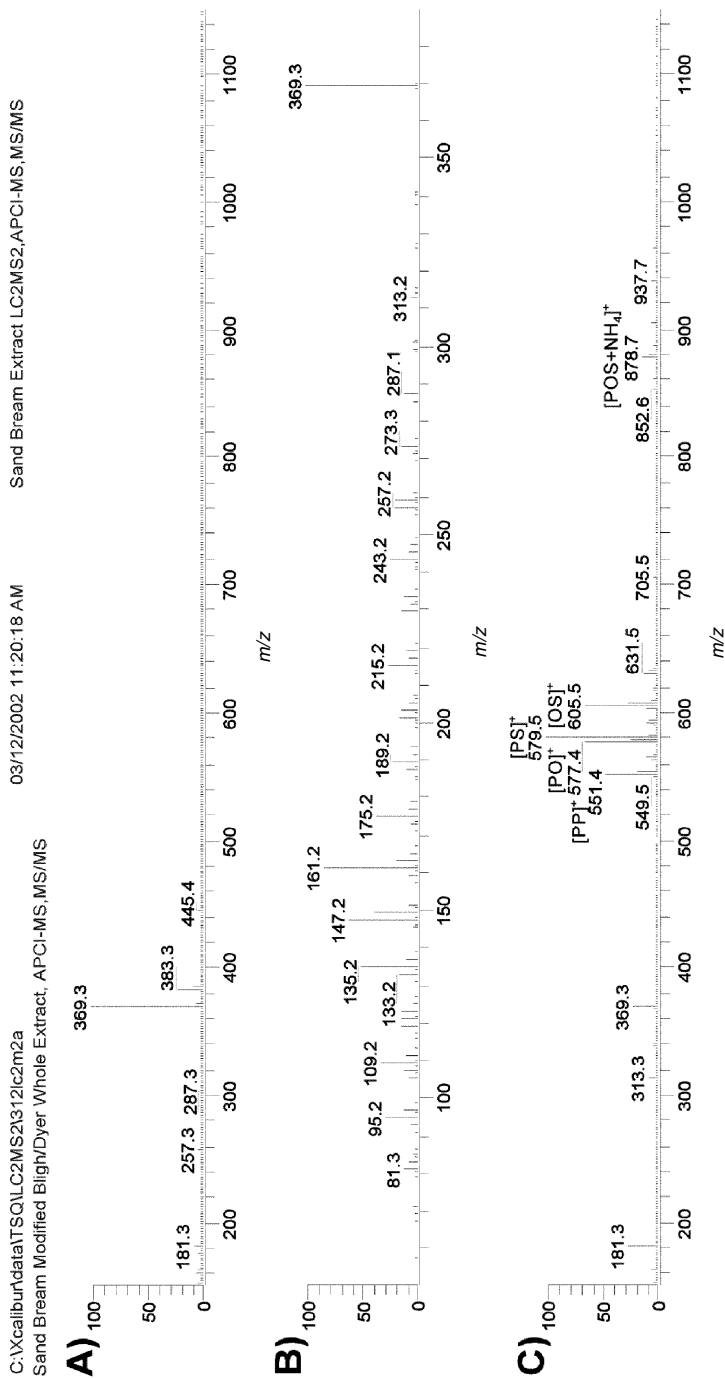


Fig. 13.18. APCI-MS and MS/MS mass spectra of neutral lipids. (A) Cholesterol molecules. (B) MS/MS of m/z 369.3. (C) MS of palmitoyl/oleoyl/stearoyl (POS) triacylglycerol and coeluted TAG. (D) MS/MS of m/z 579.5 diacylglycerol fragment ion, = [PS]⁺. (E) MS of dipalmitoyl/oleoyl (PPO) triacylglycerol and coeluted TAG. (F) MS/MS of m/z 577.5 (= [PO]⁺).

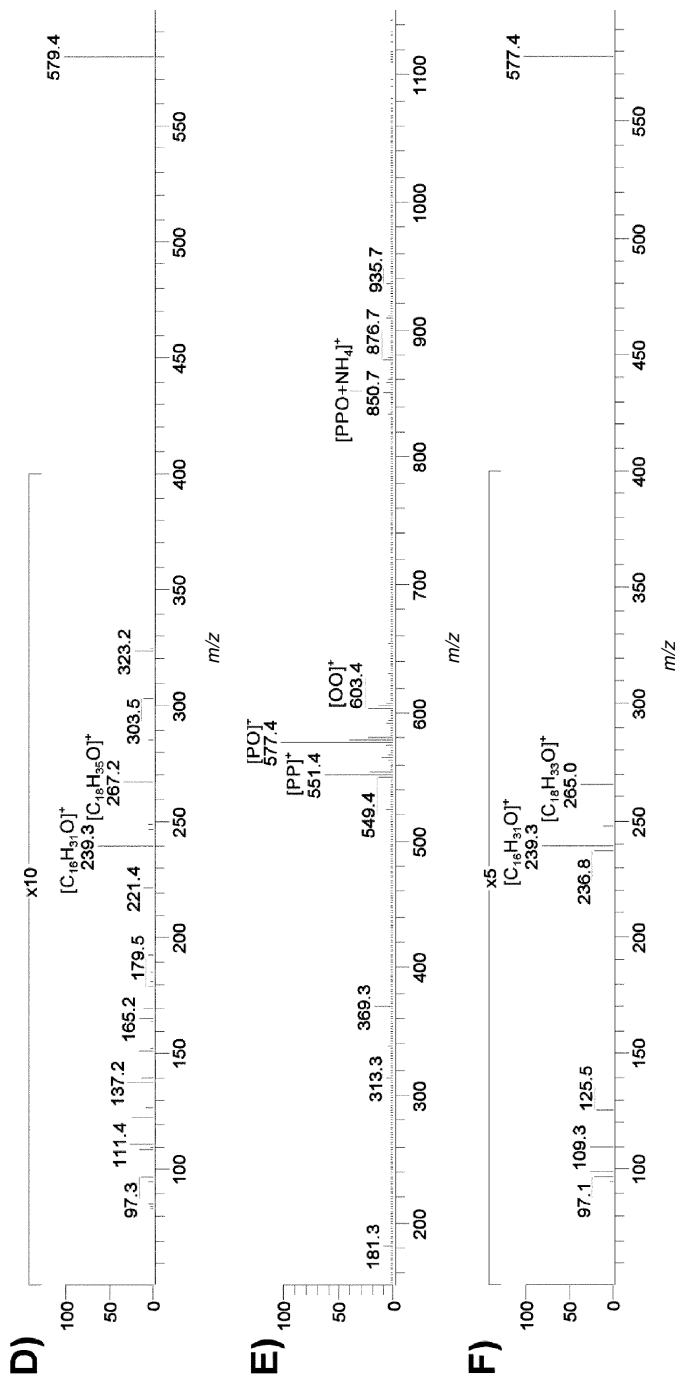


Fig. 13.18. (Continued).

mass spectra of several cholesterol oxides, reported by Razzazi-Fazeli *et al.* (61), which gave base peaks at m/z 367. Because of the uncertainty in identities of the molecules giving rise to the mass spectrum in Figure 13.18A, no further discussion of the cholesterol-related molecules will be presented here. Nevertheless, the fragments formed by APCI-MS provided information that will provide clues to the structure of this class of molecules.

Caution. A cautionary note regarding dual parallel MS runs should be mentioned. Because data is acquired on two different mass spectrometers, possibly of different vintages having different file naming conventions, extra care must be taken to ensure that the files are properly correlated. Dual parallel runs involve a higher level of complexity not encountered in normal mass spectrometric analysis, and this complexity brings with it inherent ramifications of which the user should be aware. During the preparation of this and another chapter, we found a data run in which a difference in the file naming conventions between the new and old machines caused the file names to get out of synchronization, leading to two sequential runs of dual parallel experiments having the same file name.

Since this is an inherent possibility in the new techniques of LC x /MS y runs, two steps should be taken to guard against it. First, all figures of chromatograms in dual parallel runs should include the time stamp on the chromatogram. This is commonly deleted for the sake of a cleaner appearance, but should be retained for dual parallel runs. Second, the system clocks on all machines used in LC x /MS y instruments should be synchronized to the same time, to minimize differences between the time stamps. Since the importance of synchronizing system clocks only recently became apparent, and since we mostly ignore the time clock on the legacy ICIS acquisition system, the system clock times shown on data in this chapter are not in synchronization, even though all paired runs were started simultaneously.

Conclusions

We have summarized herein all of the applications of dual parallel mass spectrometers that we have previously reported, and we have provided previously unpublished data on TAG quantitative analysis by ESI-MS and on an LC2/MS2 experiment applied to a sand bream total lipid extract. We hope to have demonstrated the tremendous value of obtaining both APCI-MS and ESI-MS data simultaneously on the same classes of molecules in an LC1/MS2 experiment. And we have demonstrated a new technique of obtaining chromatograms and spectra from two parallel HPLC separations of different polarity, directed to two mass spectrometers (LC2/MS2).

In LC1/MS2 experiments, the different ionization mechanisms of ESI and APCI resulted in complementary data from these two ionization sources. ESI-MS produced only near-molecular ions from most lipid classes, while APCI-MS produced gentle in-source fragmentation. Although ESI-MS/MS data were sometimes very similar to

APCI-MS data (as in the case of TAG), this was not always the case. In the case of phosphocholine-containing PL, ESI-MS/MS did not produce fragments that were indicative of the DAG backbone or of the individual fatty acyl chains. APCI-MS, on the other hand, did produce useful fragments in the APCI source that indicated the identities of the DAG backbone and the individual fatty acyl chains. Thus, both of these types of ionization were necessary for complete structural characterization of phosphocholine-containing PL. The dual parallel mass spectrometer approach eliminated the necessity of rerunning the chromatographic analysis to obtain data from different ionization modes. We have shown that the LC1/MS2 approach was an efficient method to obtain data from both ionization modes, simultaneously.

Some might consider it a disadvantage that our LC1/MS2 approach requires two mass spectrometers. However, older legacy instruments are quite affordable, making it comparatively inexpensive to employ two machines. Furthermore, by using two separate mass spectrometers, the scan programs and duty cycles of each instrument can be optimized to obtain more MS, MS/MS, and MS³ scans than are possible when the duty cycle of the mass filter is being divided between different ionization modes. Obviously, approximately twice as many spectra per unit time can be obtained on a dedicated instrument in LC1/MS2 mode, compared to one mass spectrometer operating in alternating APCI/ESI mode. An additional benefit of our LC1/MS2 approach is that it required no special fabrication of components, but rather used two commercially instruments without modification, joined by an inexpensive "tee." However, if two mass spectrometers were not available in a laboratory, the use of a dual APCI/ESI source (53,54) would offer distinct benefits over acquisition of only one ionization mode, and over running samples twice to obtain data from two source types. The recent developments in multiple-mode source technology are discussed further elsewhere (7). The primary disadvantage of using dual mass spectrometers for detection is the increased complexity of the experiments. Two instruments must be interlinked and coordinated to acquire data simultaneously, and two groups of conditions and parameters must be set and monitored. Although the experiments require attention to twice as many details, twice the amount of data is obtained per run. Extra care is required and extra steps must be taken to ensure that data runs are properly correlated. However, the wealth of data provided by such runs makes the extra effort well worthwhile.

The LC2/MS2 experiments demonstrated that a total lipid analysis of all classes and molecular species of both polar and non-polar lipids from one sample can be performed when two liquid chromatography systems and two mass spectrometers are combined in one analysis technique. This approach eliminated the need for duplicate sample injections on different LC systems of opposite stationary phase polarity. Our approach could allow the determination of the molecular species of all lipid classes from a single injection of a cellular extract, which is a central aim of lipidomics.

With the demonstration of the LC2/MS2 approach, an obvious opportunity presents itself. The LC2/MS2 approach used one ionization source on each mass

spectrometer. It seems obvious from the previous discussion that it would be beneficial to employ a dual ionization source, such as the APCI/ESI sources previously mentioned, on each of the two mass spectrometers used for the LC2/MS2 experiment. By doing this, both APCI- and ESI-MS mass spectra could be obtained on each instrument, for both polar and non-polar lipids in one single analysis. One would expect that it is only a matter of time before this LC2/(APCI/ESI)MS2 experiment is performed, especially given the recent commercial availability of combined sources, such as the APCI/APPI (atmospheric pressure photoionization) source from ThermoFinnigan. We expect that one of the growth areas in mass spectrometry in the next decade will be the increased availability of multiple-mode ionization sources. In addition to increased use of multiple-mode ionization sources, we expect that others will employ the LC1/MS2 and LC2/MS2 methods first demonstrated by us for lipid analysis.

As instrument manufacturers make multiple-mode ionization sources available, the software to operate the instruments will have to incorporate new functions and make possible new experiments not previously foreseen. Hopefully, manufacturers will one day incorporate features into their software to allow multiple instruments to work together and be controlled together in LC_x/MS_y experiments. In the meantime, we will continue to seek to demonstrate new modern methods for lipid analysis by using liquid chromatography/mass spectrometry. We will watch with great interest as developments in this field progress.

Acknowledgment

The work of Bill Neff at the National Center for Agricultural Utilization Research (NCAUR) to prepare and supply oxidized oil samples is gratefully acknowledged. The loan of the TSQ700 LC/(APCI and ESI)-MS and other instruments by the Industrial Oil Unit at NCAUR is gratefully acknowledged.

References

1. Byrdwell, W.C., and E.A. Emken, Analysis of Triglycerides Using Atmospheric Pressure Chemical Ionization Mass Spectrometry, *Lipids* 30: 173–175 (1995).
2. Neff, W.E., and W.C. Byrdwell, Soybean Oil Triacylglycerol Analysis by Reversed-Phase High-Performance Liquid Chromatography Coupled with Atmospheric Pressure Chemical Ionization Mass Spectrometry, *J. Am. Oil Chem. Soc.* 72: 1185–1191 (1995).
3. Byrdwell, W.C., E.A. Emken, W.E. Neff, and R.O. Adlof, Quantitative Analysis of Triglycerides Using Atmospheric Pressure Chemical Ionization Mass Spectrometry, *Lipids* 31: 919–935 (1996).
4. Byrdwell, W.C., and W.E. Neff, Qualitative and Quantitative Analysis of Triacylglycerols Using Atmospheric Pressure Chemical Ionization Mass Spectrometry, in *New Techniques and Applications in Lipid Analysis*, edited by R.E. McDonald and M.M. Mossoba, AOCS Press, Champaign, IL, 1997, pp. 45–80.
5. Byrdwell, W.C., W.E. Neff, and G.R. List, Triacylglycerol Analysis of Potential Margarine Base Stocks by High Performance Liquid Chromatography with

- Atmospheric Pressure Chemical Ionization Mass Spectrometry and Flame Ionization Detection, *J. Agric. Food Chem.* 49: 446–457 (2001).
6. Byrdwell, W.C., Atmospheric Pressure Chemical Ionization Mass Spectrometry for Analysis of Lipids, *Lipids* 36: 327–346 (2001).
 7. Byrdwell, W.C., APCI-MS in Lipid Analysis, in *Advances in Lipid Methodology—Five*, edited by R.O. Adlof, The Oily Press, Bridgwater, England, 2004, pp. 171–253.
 8. Karlsson, A.A., P. Michelson, A. Larsen, and G. Odham, Normal-Phase Liquid Chromatography Class Separation and Species Determination of Phospholipids Utilizing Electrospray Mass Spectrometry/Tandem Mass Spectrometry, *Rapid Commun. Mass Spectrom.* 10: 775–780 (1996).
 9. Byrdwell, W.C., and D. Borchman, Liquid Chromatography/Mass Spectrometric Characterization of Sphingomyelin and Dihydro-sphingomyelin of Human Lens Membranes, *Ophthalmic Res.* 29: 191–206 (1997).
 10. Duffin, K.L., J.D. Henion, and J.J. Shieh, Electrospray and Tandem Mass Spectrometric Characterization of Acylglycerol Mixtures That Are Dissolved in Nonpolar Solvents, *Anal. Chem.* 63: 1781–1788 (1991).
 11. Schuyf, P.J.W., T. de Joode, M.A. Vasconcellos, and G.S.M.J.E. Duchateau, Silver-Phase High-Performance Liquid Chromatography-Electrospray Mass Spectrometry of Triacylglycerols, *J. Chromatogr. A* 810: 53–61 (1998).
 12. Hvattum, E., Analysis of Triacylglycerols with Non-Aqueous Reversed Phase Liquid Chromatography and Positive Ion Electrospray Tandem Mass Spectrometry, *Rapid Commun. Mass Spectrom.* 15: 187–190 (2001).
 13. Sandra, P., A. Dermaux, V. Ferraz, M.M. Dittmann, and G. Rozing, Analysis of Triglycerides by Capillary Electrochromatography, *Journal of Microcolumn Separations* 9: 409–419 (1997).
 14. Dermaux, A., A. Medvedovici, M. Ksir, E. Van Hove, M. Talbi, and P. Sandra, Elucidation of Triglycerides in Fish Oil by Packed-Column Supercritical Fluid Chromatography Fractionation Followed by Capillary Electrochromatography and Electrospray Mass Spectrometry, *Journal of Microcolumn Separations* 9: 451–459 (1999).
 15. Cheng, C., M.L. Gross, and E. Pittenauer, Complete Structural Elucidation of Triacylglycerols by Tandem Sector Mass Spectrometry, *Anal. Chem.* 70: 4417–4426 (1998).
 16. Hsu, F.F., and J. Turk, Structural Characterization of Triacylglycerols as Lithiated Adducts by Electrospray Ionization Mass Spectrometry Using Low-Energy Collisionally Activated Dissociation on a Triple Stage Quadrupole Instrument, *J. Am. Soc. Mass Spectrom.* 10: 587–599 (1999).
 17. Sjoval, O., A. Kuksis, and H. Kallio, Reversed-phase High-performance Liquid Chromatographic Separation of *tert*-Butyl Hydroperoxide Oxidation Products of Unsaturated Triacylglycerols, *J. Chromatogr. A* 905: 119–132 (2001).
 18. Sjoval, O., A. Kuksis, and H. Kallio, Analysis of Molecular Species of Peroxide Adducts of Triacylglycerols Following Treatment of Corn Oil with *tert*-Butyl Hydroperoxide, *Lipids* 36: 1347–1356 (2001).
 19. Sjoval, O., A. Kuksis, and H. Kallio, Formation of Triacylglycerol Core Aldehydes During Rapid Oxidation of Corn and Sunflower Oils with *tert*-Butyl Hydroperoxide/ Fe^{2+} , *Lipids* 37: 81–94 (2002).
 20. Dorschel, C.A., Characterization of the TAG of Peanut Oil by Electrospray LC-MS-MS, *J. Am. Oil Chem. Soc.* 79: 749–753 (2002).
 21. Sandra, P., A. Medvedovici, Y. Zhao, and F. David, Characterization of Triglycerides in

- Vegetable Oils by Silver-Ion Packed-Column Supercritical Fluid Chromatography Coupled to Mass Spectroscopy with Atmospheric Pressure Chemical Ionization and Coordination Ion Spray, *J. Chromatogr. A* 974: 231–241 (2002).
22. Marzilli, L.A., L.B. Fay, F. Dionisi, and P. Vouros, Structural Characterization of Triacylglycerols Using Electrospray Ionization-MSⁿ Ion-Trap MS, *J. Am. Oil Chem. Soc.* 80: 195–202 (2003).
 23. Fard, A.M., A.G. Turner, and G.D. Willett, High-Resolution Electrospray-Ionization Fourier-Transform Ion Cyclotron Resonance and Gas Chromatography-Mass Spectrometry of Macadamia Nut Oil, *Aust. J. Chem.* 56: 499–508 (2003).
 24. Han, X.L., and R.L. Gross, Global Analyses of Cellular Lipidomes Directly from Crude Extracts of Biological Samples by ESI Mass Spectrometry: A Bridge to Lipidomics, *J. Lipid Res.* 44I: 1071–1079 (2003).
 25. Yli-Jokipii, K.M., U.S. Schwab, R.L. Tahvonen, J.P. Kurvinen, H.M. Mykkanen, and H.P. Kallio, Chylomicron and VLDL Tag Structures and Postprandial Lipid Response Induced by Lard and Modified Lard, *Lipids* 38: 693–703 (2003).
 26. Pulfer, M., and R.C. Murphy, Electrospray Mass Spectrometry of Phospholipids, *Mass Spectrom. Rev.* 22: 332–364 (2003).
 27. Fang, J., and M.J. Barcelona, Structural Determination and Quantitative Analysis of Bacterial Phospholipids Using Liquid Chromatography/Electrospray Ionization/Mass Spectrometry, *J. Microbiol. Methods* 33: 23–35 (1998).
 28. Gunnarsson, T., A. Karlsson, P. Hanson, G. Johnson, C. Alling, and G. Odham, Determination of Phosphatidylethanol in Blood from Alcoholic Males Using High-Performance Liquid Chromatography and Evaporative Light Scattering or Electrospray Mass Spectrometric Detection, *J. Chromatogr. B* 705: 243–249 (1998).
 29. Hvattum, E., A. Larsen, S. Uran, P.M. Michelsen, and T. Skotland, Specific Detection and Quantification of Palmitoyl-Stearoyl-Phosphatidylserine in Human Blood Using Normal-Phase Liquid Chromatography Coupled with Electrospray Mass Spectrometry, *J. Chromatogr. B* 716: 47–56 (1998).
 30. Lee, M.H., J.S. Yoo, and G.H. Lee, Analysis of Lecithin in Cosmetics by Reversed-Phase Liquid Chromatography Electrospray Tandem Mass Spectrometry, *Rapid Commun. Mass Spectrom.* 12: 1709–1714 (1998).
 31. Hsu, F.F., and J. Turk, Charge-Remote and Charge-Driven Fragmentation Processes in Diacyl Glycerophosphoethanolamine upon Low-Energy Collisional Activation: A Mechanistic Proposal, *J. Am. Soc. Mass Spectrom.* 11: 892–899 (2000).
 32. Brouwers, J.F.H.M., E.A.A.M. Vernooij, A.G.M. Tielens, and L.M.G. van Golde, Rapid Separation and Identification of Phosphatidylethanolamine Molecular Species, *J. Lipid Res.* 40: 164–169 (1999).
 33. Larsen, A., E. Mokastet, E. Lundanes, and E. Hvattum, Separation and Identification of Phosphatidylserine Molecular Species Using Reversed-Phase High-Performance Liquid Chromatography with Evaporative Light Scattering and Mass Spectrometric Detection, *J. Chromatogr. B* 774: 115–120 (2002).
 34. Hsu, F.F., and J. Turk, Studies on Phosphatidylglycerol with Triple Quadrupole Tandem Mass Spectrometry with Electrospray Ionization: Fragmentation Processes and Structural Characterization, *J. Am. Soc. Mass Spectrom.* 12: 1036–1043 (2001).
 35. Hsu, F.F., and J. Turk, Charge-Driven Fragmentation Processes in Diacyl Glycerophosphatidic Acids upon Low-Energy Collisional Activation: A Mechanistic Proposal, *J. Am. Soc. Mass Spectrom.* 11: 797–803 (2000).

36. Hsu, F.F., and J. Turk, Characterization of Phosphatidylinositol, Phosphatidylinositol-4-Phosphate, and Phosphatidylinositol-4,5-Bisphosphate by Electrospray Ionization Tandem Mass Spectrometry: A Mechanistic Study, *J. Am Soc. Mass Spectrom.* 11: 986–999 (2000).
37. Han, X.L., and R.W. Gross, Electrospray-Ionization Mass Spectroscopic Analysis of Human Erythrocyte Plasma-Membrane Phospholipids, *Proc. Natl. Acad. Sci. USA* 91: 10635–10639 (1994).
38. Han, X.L., R.A. Gubitosi-Klug, B.J. Collins, and R.W. Gross, Alterations in Individual Molecular Species of Human Platelet Phospholipids During Thrombin Stimulation: Electrospray Ionization Mass Spectrometry-Facilitated Identification of the Boundary Conditions for the Magnitude and Selectivity of Thrombin-Induced Platelet Phospholipid Hydrolysis, *Biochemistry* 35: 5822–5832 (1996).
39. Brugger, B., G. Erben, R. Sandhoff, F.T. Wieland, and W.D. Lehmann, Quantitative Analysis of Biological Membrane Lipids at the Low Picomole Level by Nano-Electrospray Ionization Tandem Mass Spectrometry, *Proc. Natl. Acad. Sci. USA* 94: 2339–2344 (1997).
40. Hvattum, E., G. Hagelin, and A. Larsen, Study of Mechanisms Involved in the Collision-Induced Dissociation of Carboxylate Anions from Glycerophospholipids Using Negative Ion Electrospray Tandem Quadrupole Mass Spectrometry, *Rapid Commun. Mass Spectrom.* 12: 1405–1409 (1998).
41. Fridriksson, E.K., P.A. Shipkova, E.D. Sheets, D. Holowka, B. Baird, and F.W. McLafferty, Quantitative Analysis of Phospholipids in Functionally Important Membrane Domains from RBL-2H3 Mast Cells Using Tandem High-Resolution Mass Spectrometry, *Biochemistry* 38: 8056–8063 (1999).
42. Cabrera, G.M., M.L.F. Murga, G.F. de Valdez, and A.M. Seldes, Direct Analysis by Electrospray Ionization Tandem Mass Spectrometry of Mixtures of Phosphatidylglycerols from *Lactobacillus*, *J. Mass Spectrom.* 35: 1452–1459 (2000).
43. Byrdwell, W.C., Dual Parallel Mass Spectrometers for Analysis of Sphingolipid, Glycerolipid and Plasmalogen Molecular Species, *Rapid. Commun. Mass Spectrom.* 12: 256–272 (1998).
44. Byrdwell, W.C., and W.E. Neff, Dual Parallel Electrospray Ionization and Atmospheric Pressure Chemical Ionization Mass Spectrometry (MS), MS/MS and MS/MS/MS for the Analysis of Triacylglycerols and Triacylglycerol Oxidation Products, *Rapid Commun. Mass Spectrom.* 16: 300–319 (2002).
45. Liu, D.Q., Y.Q. Xia, and R. Bakhtiar, Use of a Liquid Chromatography/Ion Trap Mass Spectrometer/Triple Quadrupole Mass Spectrometry System for Metabolite Identification, *Rapid Commun. Mass Spectrom.* 16: 1330–1336 (2002).
46. Byrdwell, W.C., Dual Parallel Liquid Chromatography/Dual Mass Spectrometry (LC2/MS2) of a Total Lipid Extract, *J. Liquid Chromatogr. Rel. Technol.* 26: 3147–3181 (2003).
47. Byrdwell, W.C., and W.E. Neff, Non-Volatile Products of Triolein Produced at Frying Temperatures Characterized Using Liquid Chromatography with Online Mass Spectrometric Detection, *J. Chromatogr. A* 852: 417–432 (1999).
48. Byrdwell, W.C., Liquid Chromatography/Atmospheric Pressure Chemical Ionization Mass Spectrometry for Lipid Analysis, in *HPLC in Lipid Analysis*, edited by J.T. Lin and T.A. McKeon, HNB Publishing, New York, in press.
49. Myher, J.J., and A. Kuksis, Electrospray-MS for Lipid Analysis, *inform* 6: 1068–1072 (1995).
50. Byrdwell, W.C., Liquid Chromatography with Electrospray Ionization Mass

- Spectrometry for Lipid Analysis, in *HPLC in Lipid Analysis*, edited by J.T. Lin and T.A. McKeon, HNB Publishing, New York, in press.
51. Neff, W.E., and W.C. Byrdwell, Characterization of Model Triacylglycerol (Triolein, Trilinolein and Trilinolenin) Autoxidation Products *via* High Performance Liquid Chromatography Coupled with Atmospheric Pressure Chemical Ionization Mass Spectrometry, *J. Chromatogr. A* 818: 169–186 (1998).
 52. Byrdwell, W.C., and W.E. Neff, Electrospray Ionization Mass Spectrometry of High Molecular Weight Triacylglycerol Oligomers, *J. Am. Oil Chem. Soc.* 81: 13–26 (2004).
 53. Siegel, M.M., K. Tabei, F. Lambert, L. Candela, and B. Zoltan, Evaluation of a Dual Electrospray Ionization/Atmospheric Pressure Chemical Ionization Source at Low Flow Rates (~50 mL/min) for the Analysis of Both Highly and Weakly Polar Compounds, *J. Am. Soc. Mass Spectrom.* 9: 1196–1203 (1998).
 54. Gallagher, R.T., M.P. Balogh, P. Davey, M.R. Jackson, I. Sinclair, and L.J. Southern, Combined Electrospray Ionization-Atmospheric Pressure Chemical Ionization Source for Use in High-Throughput LC/MS Applications, *Anal. Chem.* 75: 973–977 (2003).
 55. Folch, J., M. Lees, and G.H. Sloane Stanley, A Simple Method for the Isolation and Purification of Total Lipides from Animal Tissues, *J. Biol. Chem.* 226: 497–509 (1957).
 56. Bligh, E.G., and W.J. Dyer, A Rapid Method of Total Lipid Extraction and Purification, *Can. J. Biochem. Phys.* 37: 911–917 (1959).
 57. Avanti Polar Lipids Catalog Edition VI, Avanti Polar Lipids, Inc., Alabaster, AL, p. 60.
 58. Hsu, F.F., and J. Turk, Structural Determination of Glycosphingolipids as Lithiated Adducts by Electrospray Ionization Mass Spectrometry Using Low-Energy Collisional-Activated Dissociation on a Triple Stage Quadrupole Instrument, *J. Am. Soc. Mass Spectrom.* 12: 61–79 (2001).
 59. Lavery, S.B., M.S. Toledo, R.L. Doong, A.H. Straus, and H.K. Takahashi, Comparative Analysis of Ceramide Structural Modification Found in Fungal Cerebrosides by Electrospray Tandem Mass Spectrometry with Low Energy Collision-Induced Dissociation of Li⁺ Adduct Ions, *Rapid Commun. Mass Spectrom.* 14: 551–563 (2000).
 60. Hagiwara, T., T. Yasuno, K. Funayama, and S. Suzuki, Determination of Lycopene, α -Carotene and β -Carotene in Vegetable Juice by Liquid Chromatography/Atmospheric Pressure Chemical Ionization-Mass Spectrometry, *J. Food Hyg. Soc. Jpn.* 38: 211–218 (1997).
 61. Razzazi-Fazeli, E., S. Kleineisen, and W. Luf, Determination of Cholesterol Oxides in Processed Food Using High-Performance Liquid Chromatography-Mass Spectrometry with Atmospheric Pressure Chemical Ionisation, *J. Chromatogr. A* 896: 321–334 (2000).

Index

A

- Acylphosphatidylglycerol, 128
 - fragmentation processes, 130–131
- Adduct ions, 62, 64. *See also particular phospholipid classes*
- Amide derivatives of fatty acids, 254–258
- Anionic lipids, 490, 492, 493–494
- APCI. *See* Atmospheric pressure chemical ionization
- Apolipoprotein E (apoE), 502–503
- APPI. *See* Atmospheric pressure photoionization
- Argentation (silver-ion) chromatography, 272, 389
- Atmospheric pressure chemical ionization (APCI), 3–4, 6–8, 14–16, 242–243, 244, 280, 298–299, 415, 417, 418, 472
 - for analysis of positional isomers, 280–289, 291–292, 364–376
 - of carotenoids, 417–428
 - classes of molecules used with, 7, 8, 14, 15
 - clinical and biomedical applications of, 422–425
 - of fatty acid amide derivatives, 256–258
 - of fatty acid methyl esters, 244–248
 - of fatty acid oxidation products, 254–256
 - of fatty and resin acids, 252, 254
 - of phospholipids, 510–511
 - of plant glycolipids, 431–444
 - principles of, 304–316
 - of TAG oxidation products, 334–345
 - TAG quantification by, 380–392
 - of triacylglycerols (TAG), 299–301, 316–345, 510–511
 - of very-long-chain polyunsaturated fatty acids, 248–252, 253, 258–265
 - of vitamin metabolites, 265–267

- Atmospheric pressure ionization (API)
 - LC-MS interfaces, 8–14, 298–299.
 - See also* Atmospheric pressure chemical ionization; Electrospray ionization
- Atmospheric pressure photoionization (APPI), 6–8, 14–16, 472–478
 - applications of, 478–479
 - classes of molecules used with, 7, 8, 14, 15
 - of steroids, 479–482

B

- Biosurfactant glycolipids, LC-MS analysis of, 447–448
 - rhamnolipids, 464–468
 - sophorolipid derivatives, 455–464
 - sophorolipids, 448–455

C

- Candida* yeasts, 448
- Cardiolipin, 62, 64, 490–491
 - electrical properties, 491
 - ESI mass spectrometry of, 50, 52
 - fragmentation processes, 131, 133–136, 137
- Carotenoids, 413–415
- Ceramide monoglucoside, 431, 432, 437, 441–444
- Ceramides, 62–64, 69
 - fragmentation processes, 62, 94–109, 153, 156–157
 - metal adduct ions, 98, 105, 153, 153, 155, 157
- Cerebrosides, electrical properties of, 491
- Choline-containing lipids, 497–498
 - electrical properties of, 491
- Continuous-flow fast atom bombardment, 416

D

- Digalactosyldiacylglycerol, 431, 432, 434, 436–437, 438–440
Dimethylaminoethyl esters (DMAE), 268
Direct liquid introduction (DLI), 4
Dual parallel mass spectrometry, 402–404, 513–520

E

- Electrospray ionization (ESI), 2–3, 6–8, 14–16, 61, 301, 416–417, 472, 489–490
for analysis of apolipoprotein E (apoE), 502–503
for analysis of diabetic myocardial lipidome, 508
analysis of lipids using, 500–502
for analysis of positional isomers, 376–380
classes of molecules used with, 7, 8, 14, 15
of fatty acids and FA derivatives, 267–269
of phospholipids, 33–52, 64–65, 108, 301, 512–513
of sphingomyelins, 38
for TAG oxidation products, 349–364
TAG quantification by, 392–395
of triacylglycerols, 301–304, 345–364, 511–512
Enzymatic analysis of TAG positional isomers, 276–278
ESI. *See* Electrospray ionization
Ethanolamine-containing lipids, 492, 495–596
electrical properties of, 491

F

- Fast-atom bombardment, 415–416
Fatty acid methyl esters, 244–248

G

- Galactolipids, 431, 432, 434, 436–437, 438–440
Galactopyranose sophorolipid FA esters, 458–464
Glycerophosphocholine. *See* Phosphatidylcholine

Glycerophosphoethanolamine. *See* Phosphatidylethanolamine

Glycerophosphoglycerol. *See* Phosphatidylglycerol

Glycerophosphoinositol. *See* Phosphatidylinositol

Glycerophosphoric acid. *See* Phosphatidic acid

Glycerophosphoserine. *See* Phosphatidylserine

Glycosphingolipids, 62
fragmentation processes, 107, 158
metal adduct ions, 107–109, 158

H

High-performance liquid chromatography (HPLC) for phospholipids, 23–33

L

- Lipid metabolites, 499–500
electrical properties of, 491
Lipidomics, 488–489, 502–503
central nervous system, 502–503
LC2/MS2 experiments, 545–570
myocardial, 502
Liquid chromatography (LC). *See* High-performance liquid chromatography (HPLC)
Lithiated adduct ions, 69, 81, 85. *See also particular phospholipid classes*
Lysophospholipids, fragmentation processes, 147

M

- Matrix-assisted laser desorption/ionization (MALDI), 61–62, 301
Monodisperse aerosol generation interface for chromatography (MAGIC), 5–6
Monogalactosyldiacylglycerol, 431, 432, 434, 436–437, 438–440
Moving belt LC-MS interface, 415
Moving wire LC-MS interface, 4–5
Myocardial lipidome, diabetic, 502

N

- Neutral lipids, 395–402, 499
APCI mass spectrometry of, 299–301, 316–345

- ESI mass spectrometry for, 301–304, 345–364
 - fragmentation processes, 324, 325–334
 - oxidation products of, 196, 199–213
 - Nonpolar neutral lipids, 491
 - Normal-phase HPLC methods, 23–27
 - Nuclear magnetic resonance spectroscopy (NMR), 278–279
- O**
- Omega fatty acids, 246–247
 - Oxidation products
 - of fatty acids, 254–256, 268–269
 - of lipids, analysis of, 179–194
 - of neutral lipids, 196, 199–213
 - of polar lipids, 213–232
 - of sterols, 184–187
 - of steryl esters, 187–196, 197–198
 - of triacylglycerols, 334–345, 349–364, 532–544
 - Ozonization, 186–187, 192–196, 212–213, 228, 230–232
- P**
- Particle beam ionization, 415–416
 - Phosphatidic acid (glycerophosphoric acid), 19, 62
 - electrical properties, 491
 - ESI mass spectrometry of, 48–49
 - fragmentation processes, 68, 71, 115–120, 147
 - metal adduct ions, 64
 - Phosphatidylcholine (glycerophosphocholine), 19, 62
 - electrical properties, 491
 - ESI mass spectrometry of, 33–38
 - fragmentation processes, 65, 67–68, 70–76, 112–113, 115
 - metal adduct ions, 64, 69, 71, 73
 - Phosphatidylethanolamine (glycerophosphoethanolamine), 19, 62
 - electrical properties, 491
 - ESI mass spectrometry of, 39–44
 - fragmentation processes, 64, 65, 67–68, 79–80, 82, 122–125
 - metal adduct ions, 64, 79, 80, 82
 - Phosphatidylglycerol (glycerophosphoglycerol), 19, 62, 490–491
 - electrical properties, 491
 - ESI mass spectrometry of, 50, 51
 - fragmentation processes, 66, 68, 71, 86, 89
 - metal adduct ions, 64, 71, 89
 - Phosphatidylinositol (glycerophosphoinositol), 19, 62
 - electrical properties, 491
 - ESI mass spectrometry of, 44–46
 - fragmentation processes, 71, 86, 128, 139, 143
 - metal adduct ions, 86
 - phosphates, 136, 138–140
 - Phosphatidyl phospholipids, 496
 - Phosphatidylserine (glycerophosphoserine), 19, 62
 - electrical properties, 491
 - ESI mass spectrometry of, 46–48
 - fragmentation processes, 64, 68, 120, 122
 - metal adduct ions, 86, 88, 89
 - Phospholipids
 - APCI mass spectrometry of, 510–511
 - biological functions of, 19–22
 - classes of, 19–20, 62, 496
 - dual parallel mass spectrometry results for, 520–521
 - ESI mass spectrometry of, 33–53, 301, 512–513
 - HPLC methods for, 23–33
 - IUPAC nomenclature for, 63–64
 - with polyunsaturated FA substituents, fragmentation processes of, 150, 152
 - Photoionization, 6–7
 - Plasmanyolphospholipids, 496
 - fragmentation processes, 147
 - Plasmenylphospholipids (plasmalogens), 496
 - fragmentation processes, 147
 - Platelet activating factor (PAF), 64
 - Polar lipids, 491
 - oxidation products of, 213–232
 - Polyunsaturated fatty acids, 248–252, 253, 258–265
 - Proteomics, 301
 - Pseudomonas aeruginosa*, 464

Q

Quantitative analysis, 380–395, 544–545

R

Resin acids, 252, 254

Reversed-phase HPLC methods, 27–33

Rhamnolipids, 464–468

Rhodotorula bogoriensis, 448, 454

S

Silver-ion chromatography. *See* Argentation
(silver-ion) chromatography

Sophorolipids, 448–455

derivatives of, 455–464

Sphingolipids, 19, 62, 64

Sphingomyelins, 62, 114

APCI mass spectrometry of, 261

electrical properties of, 491

ESI mass spectrometry of, 38

fragmentation processes, 68, 70–71,
111–112,

metal adduct ions, 158

Steroids, APPI analysis of, 479–482

Sterols, oxidation products of, 184–187

Steryl esters, oxidation products of,

186–196, 197–198

Steryl glucosides, 431, 432, 434–435

Sulfatides, 62–64

electrical properties, 491

fragmentation processes, 158, 163–171

T

Tandem mass spectrometry, 62–63

Thermospray (TSP) LC-MS interface, 5

Triacylglycerols, 62, 395–402

APCI mass spectrometry of, 299–301,
316–345, 510–511

dual parallel mass spectrometry results
for, 521–532, 532–544

ESI mass spectrometry of, 301–306,
345–364, 511–512

fragmentation processes, 93–95, 324,
325–334

metal adduct ions, 94

oxidation products of, 196, 199–213,
532–544

positional isomers of, 276–280,
280–287, 364–380

quantitative analysis of, 380–395

Trimethylaminoethyl esters (TMAE), 268

V

Very-long-chain fatty acids, 248–252, 253

Vitamin metabolites, 265–267

